ISSN 0021-9673

VOL. 550 NOS. 1 + 2 JULY 26, 1991

COMPLETE IN ONE ISSUE

Lloyd R. Snyder Honour Volume

JOURNAL OF CHROMATOGRAPHY

INCLUDING ELECTROPHORESIS AND OTHER SEPARATION METHODS

SPECIAL VOLUME

ELSEVIER

JOURNAL OF CHROMATOGRAPHY

Scope. The *Journal of Chromatography* publishes papers on all aspects of chromatography, electrophoresis and related methods. Contributions consist mainly of research papers dealing with chromatographic theory, instrumental development and their applications. The section *Biomedical Applications*, which is under separate editorship, deals with the following aspects: developments in and applications of chromatographic and electrophoretic techniques related to clinical diagnosis or alterations during medical treatment; screening and profiling of body fluids or tissues with special reference to metabolic disorders; results from basic medical research with direct consequences in clinical practice; drug level monitoring and pharmacokinetic studies; clinical toxicology; analytical studies in occupational medicine.

Submission of Papers. Manuscripts (in English; *four* copies are required) should be submitted to: Editorial Office of *Journal of Chromatography*, P.O. Box 681, 1000 AR Amsterdam, The Netherlands, Telefax (+31-20) 5862 304, or to: The Editor of *Journal of Chromatography, Biomedical Applications*, P.O. Box 681, 1000 AR Amsterdam, The Netherlands. Review articles are invited or proposed by letter to the Editors. An outline of the proposed review should first be forwarded to the Editors for preliminary discussion prior to preparation. Submission of an article is understood to imply that the article is original and unpublished and is not being considered for publication elsewhere. For copyright regulations, see below.

Publication. The *Journal of Chromatography* (incl. *Biomedical Applications*) has 38 volumes in 1991. The subscription prices for 1991 are:

J. Chromatogr. (incl. *Cum. Indexes, Vols. 501–550*) + *Biomed. Appl.* (Vols. 535–572):
Dfl. 7220.00 plus Dfl. 1140.00 (p.p.h.) (total *ca.* US$ 4519.00)

J. Chromatogr. (incl. *Cum. Indexes, Vols. 501–550*) only (Vols. 535–561):
Dfl. 5859.00 plus Dfl. 810.00 (p.p.h.) (total *ca.* US$ 3604.75)

Biomed. Appl. only (Vols. 562–572):
Dfl. 2387.00 plus Dfl. 330.00 (p.p.h.) (total *ca.* US$ 1468.75).

Subscription Orders. The Dutch guilder price is definitive. The US$ price is subject to exchange-rate fluctuations and is given as a guide. Subscriptions are accepted on a prepaid basis only, unless different terms have been previously agreed upon. Subscriptions orders can be entered only by calender year (Jan.–Dec.) and should be sent to Elsevier Science Publishers, Journal Department, P.O. Box 211, 1000 AE Amsterdam, The Netherlands, Tel. (+31-20) 5803 642, Telefax (+31-20) 5803 598, or to your usual subscription agent. Postage and handling charges include surface delivery except to the following countries where air delivery via SAL (Surface Air Lift) mail is ensured: Argentina, Australia, Brazil, Canada, Hong Kong, India, Israel, Japan*, Malaysia, Mexico, New Zealand, Pakistan, PR CHina, Singapore, South Africa, South Korea, Taiwan, Thailand, USA. * For Japan air delivery (SAL) requires 50% additional charge of the normal postage and handling charge. For all other countries airmail rates are available upon request. Claims for missing issues must be made within three months of our publication (mailing) date, otherwise such claims cannot be honoured free of charge. Back volumes of the *Journal of Chromatography* (Vols. 1–534) are available at Dfl. 208.00 (plus postage). Customers in the USA and Canada wishing information on this and other Elsevier journals, please contact Journal Information Center, Elsevier Science Publishing Co. Inc., 655 Avenue of the Americas, New York, NY 10010, USA, Tel. (+1-212) 633 3750, Telefax (+1-212) 633 3990.

Abstracts/Contents Lists published in Analytical Abstracts, Biochemical Abstracts, Biological Abstracts, Chemical Abstracts, Chemical Titles, Chromatography Abstracts, Clinical Chemistry Lookout, Current Contents/Life Sciences, Current Contents/Physical, Chemical & Earth Sciences, Deep-Sea Research/Part B: Oceanographic Literature Review, Excerpta Medica, Index Medicus, Mass Spectrometry Bulletin, PASCAL-CNRS, Pharmaceutical Abstracts, Referativnyi Zhurnal, Research Alert, Science Citation Index and Trends in Biotechnology.

See inside back cover for Publication Schedule, Information for Authors and information on Advertisements.

0021-9673/91/$03.50

For Contents see p. VII

JOURNAL OF CHROMATOGRAPHY

VOL. 550 (1991)

JOURNAL of CHROMATOGRAPHY

INCLUDING ELECTROPHORESIS AND OTHER SEPARATION METHODS

SPECIAL VOLUME

ELSEVIER
AMSTERDAM — OXFORD — NEW YORK — TOKYO

J. Chromatogr., Vol. 550 (1991)

0021-9673/91/$03.50

Printed in The Netherlands

SPECIAL VOLUME

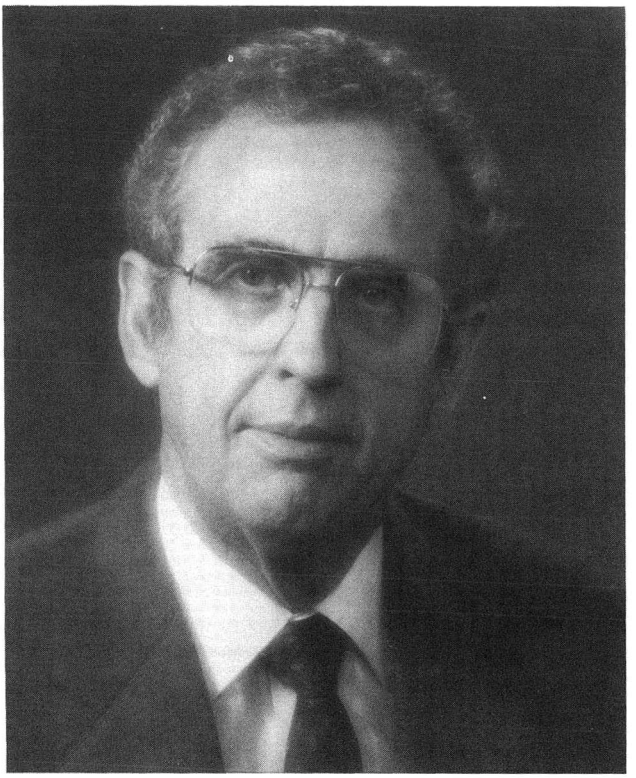

HONOUR VOLUME

on the occasion of the 60th birthday of

LLOYD R. SNYDER

VOL. 550 NOS. 1 + 2 JOURNAL OF CHROMATOGRAPHY JULY 26, 1991

CONTENTS

HONOUR VOLUME ON THE OCCASION OF THE 60TH BIRTHDAY OF LLOYD R. SNYDER

Detection

Applications

In articles with more than one author, the name of the author to whom correspondence should be addressed is indicated in the article heading by a 6-pointed asterisk (*)

Journal of Chromatography, 550 (1991) 1–4
Elsevier Science Publishers B.V., Amsterdam

PREFACE

Lloyd Robert Snyder was born on July 30, 1931 in California. He studied chemistry at the University of California at Berkeley where he graduated with highest honors in 1952. In 1954 he received a Ph.D. in physical organic chemistry from the same department and then joined Shell Oil in Houston, Texas. There he was introduced to gas chromatography (GC), and in 1955 he independently discovered the technique of column switching for the analysis of certain "key" hydrocarbons in gasoline [1]. A few years later he joined the Union Oil Company in California where he embarked on a vigorous research program that resulted in a number of major achievements over the ensuing fourteen years.

Before Snyder's seminal work commenced in the early sixties, liquid column chromatography (LC) with an adsorbent as the stationary phase was widely used —but not in the linear elution mode that was so successful in liquid–liquid partition chromatography and GC. Snyder's thorough studies published in over fifty papers during the sixties have changed this with far-reaching consequences. He provided a simple theoretical framework to account for the physico-chemical phenomena underlying separation by *linear elution adsorption chromatography*, he developed methods for reliably adjusting and standardizing adsorbent activity and he described quantitative rules for controlling mobile phase strength and selectivity. He also demonstrated the versatility, efficacy and importance of this technique by a variety of applications in the petroleum field, culminating in the first reported analysis of all of the important oxygen and nitrogen compound types in the distillate from a representative crude oil [2].

Concomitantly, Snyder began the development of a comprehensive theory of gradient elution based on his linear solvent strength (LSS) concept [3]. In retrospect, it is now eminently clear that his work at the advent of the era of high-performance liquid chromatography (HPLC) played an essential role in providing a solid foundation on which this technique has been developed. At that time there was only a handful of scientists who recognized the potential of LC as an instrumental analytical tool and advanced this technique in a major way. The accomplishments by Snyder in the first decade of his distinguished career as chromatographer, which culminated in the publication of his first book *Principles of Adsorption Chromatography* in 1968, place him in the top echelon of these pioneers.

In 1971 Lloyd Snyder accepted a position with Technicon in New York and was soon appointed Vice President of research for that organization. Despite his heavy managerial duties and responsibility for clinical chemistry R&D, he continued an active interest in many aspects of HPLC, which in those years emerged as a prime analytical tool and enjoyed meteoric growth. Lloyd continued to play a leading role in advancing the technique of HPLC while at Technicon, but in 1982 he went into business for himself in order to work exclusively with chromatography. A few years later he founded LC Resources with Dr. John Dolan, and in 1985 he returned to California as part of this organization. His company is devoted to research, education and contract services in various areas of HPLC and GC and markets the highly successful DryLab software for computer-assisted chromatographic method development.

Dr. Snyder has served on the editorial boards of many periodicals covering the fields of chromatography and analytical chemistry, as well as advisory boards for several organizations related to petroleum and clinical chemistry. Since 1987 he has been one of the editors of the *Journal of Chromatography*. He was an adjunct professor of chemistry at Pace University (1980–1986), and in 1984 he was invited to Lanzhou University in China by the ministry of education. Dr. Snyder has been bestowed with many awards for his pioneering work in chromatography. Among others he received the ACS Award in Petroleum Chemistry (1970), the Stephan Dal Nogare Memorial Award in Chromatography (1976), the ACS Award in Chromatography (1984), the Pittsburgh Society Award in Analytical Chemistry (1984), the L. S. Palmer Award in Chromatography (1985) and the A. J. P. Martin Award (1989).

The publication list of Dr. Snyder contains over 250 entries as well as several patents. This work reveals a professional career which has been closely associated with the development of modern liquid chromatography and does not show any sign of slowing down; he published nearly sixty papers in the past five years. Since 1970 he has published on almost every aspect of HPLC, and his significant contributions have made a great impact on the development of the technique at large. Many of his papers show an uncanny combination of theory and practice with the result of providing a simple framework not only for the evaluation and interpretation of chromatographic data but also for predicting and designing the separation. His treatment of gradient elution [4] based on a simple algebraic relationship has been enormously successful in making possible the prediction of separation as a function of gradient conditions. This approach has been applied to numerous practical situations and forms the basis of computer simulation (DryLab), a technique for chromatographic method development that was developed by Dr. Snyder in collaboration with John Dolan [5].

Recently, he extended his comprehensive and practicable theory of gradient elution to preparative separations with column overloading [6]. In the late 1970s Snyder refined his early results and put forward a solvent classification scheme [7] to aid mobile phase selection in HPLC. His solvent selectivity triangle has become extremely popular in many areas outside of chromatography, because it provided a simple method for data interpretation and *a fortiori* the selection of solvents in experimental design for various fields of science and technology.

The growing interest in the chromatography of biological macromolecules brought about by advances in biotechnology prompted Snyder to examine the conditions for gradient elution and preparative chromatography of such large molecules. Besides offering practical insight and guidelines for method development, his numerous papers in the middle 1980s have laid down a broad foundation for the separation of large biomolecules by gradient elution [8], which is an essential feature of biochromatography. Thus, through his lifetime involvement with adsorption chromatography and gradient elution, Snyder has also made his mark on the development of HPLC during the transition of this technique to the separation of large molecules.

Another important contribution by Dr. Snyder is his discovery of the power of "solvent strength optimization" [9] in HPLC method development. In almost all cases previously, solvent composition (%B) was varied in order to adjust retention within desirable capacity factor limits, without regard for the possible effect of solvent strength on band spacing. It is now known that such band spacing changes are quite common and important, and this phenomenon provides much of the value of DryLab

computer simulation. More recently he has demonstrated similar effects in GC [10], where changes in temperature also often provide significant variation in band spacing. In both GC and HPLC, the use of programming techniques further extends the value of this approach.

The picture would not be complete without recalling his major role as an educator who has taught the theory and practice of LC to almost two generations. His book with J. J. Kirkland, *Introduction to Modern Liquid Chromatography*, was first published in 1974 with a second edition in 1979. The book has been the "Bible" of HPLC and has sold more than 25 000 copies —a remarkable success in scientific publishing. His teaching through numerous audio and video courses dealing with various aspects of chromatography has also had a very great influence on the field. With Dr. Kirkland he has taught a very popular ACS course on HPLC since 1971; this course has been attended by over 5000 students in that period. As a prolific writer, Snyder has also contributed to the advancement of chromatography by his numerous review articles and book chapters. Some of his other books also have to be mentioned. These are: *An Introduction to Separation Science*, with Karger and Horváth (1973), *Practical HPLC Method Development*, with Glajch and Kirkland (1988) and *Troubleshooting HPLC Systems*, with John Dolan (1989).

It appears that the tumultuous years in which the edifice of modern LC as an instrumental analytical tool was erected are coming to an end. Future progress, which is expected to be quite substantial, will come about in a more orderly fashion. In honoring Lloyd Snyder at his sixtieth birthday we are paying tribute to a scientist who was one of the most influential personalities responsible for the development and wide employment of HPLC. In addition to the written work, he has exterted a great influence by his presentations at international and national meetings as well as by seminars. He has been a coveted speaker whose lectures are always very clear and substantial.

I personally feel lucky to have had many contacts with Lloyd which were particularly close in the 1970s and early 1980s when he lived near Connecticut. In fact he lured me into the world of clinical chemistry, which he quickly mastered after coming to Technicon. The twenty or so papers he published in this field manifest his versatility and inventiveness as well as his capability of treating complex problems, such as band spreading in segmented flow [11], to arrive at a simple but elegant theory of utilitarian importance. Over the years I learned to appreciate his friendship, his straightforward manner and integrity, his no-nonsense approach to problem solving, and his proficiency in writing. Lloyd has managed to make several major career changes which have provided him with fresh impetus without losing his devotion to chromatographic research, his prolificacy and creativity. This has been an enviable accomplishment and I wish him the best in his endeavors with LC Resources. After his return for the second time to California, he is likely to stay in his native state. I do not wonder. He and Barbara, his lovely wife of almost two scores of years, enjoy a beautiful home in Orinda, where it is always a pleasure to visit, and I feel fortunate to have enjoyed their hospitality.

With the contribution to this volume and in the name of his many friends, I wish Lloyd Happy Birthday and further success in coping with the challenges that chromatography apparently does not cease to offer.

New Haven, CT (USA) CSABA HORVÁTH

1 M. C. Simmons and L. R. Snyder, *Anal. Chem.*, 30 (1958) 32.
2 L. R. Snyder, *Accts. Chem. Res.*, 3 (1970) 290.
3 L. R. Snyder, *J. Chromatogr.*, 13 (1964) 415.
4 L. R. Snyder, in Cs. Horváth (Editor), *High-performance Liquid Chromatography —Advances and Perspectives*, Vol. 1, Academic Press, New York, 1980, p. 207.
5 L. R. Snyder, J. W. Dolan and D. C. Lommen, *J. Chromatogr.*, 485 (1989) 65, 91.
6 L. R. Snyder, J. W. Dolan and G. B. Cox, *J. Chromatogr.*, 540 (1991) 21.
7 L. R. Snyder, *J. Chromatogr. Sci.*, 16 (1978) 223.
8 L. R. Snyder and M. A. Stadalius, in Cs. Horváth (Editor), *High-performance Liquid Chromatography —Advances and Perspectives*, Vol. 4, Academic Press, New York, 1986, p. 195.
9 L. R. Snyder, M. A. Quarry and J. L. Glajch, *Chromatographia*, 24 (1987) 33.
10 D. E. Bautz, J. W. Dolan and L. R. Snyder, *Anal. Chem.*, 62 (1990) 1561.
11 L. R. Snyder and H. J. Adler, *Anal. Chem.*, 48 (1976) 1017, 1022.

Journal of Chromatography, 550 (1991) 5–14
Elsevier Science Publishers B.V., Amsterdam

CHROMSYMP. 2163

Computer-assisted retention prediction system for inorganic cyclic polyphosphates and its application to optimization of gradients in anion-exchange chromatography

YOSHINOBU BABA*
Kobe Women's College of Pharmacy, Kitamachi, Motoyama, Higashinada-ku, Kobe 658 (Japan)
and
GENICHIRO KURA
Department of Chemistry, Fukuoka University of Education, Akama, Munakata, Fukuoka 811-41 (Japan)

ABSTRACT

A computer-assisted technique for the retention prediction of inorganic cyclic polyphosphates under gradient elution conditions in anion-exchange chromatography is presented. A computer-assisted retention prediction system, which is an alternative to high-performance liquid chromatographic computer simulation systems, finds an optimum gradient easily in the anion-exchange separations of cyclic polyphosphates. The effect of gradient on the resolution and band spacing is illustrated by computer simulation. An increase in the initial salt concentration of the eluent is the most effective factor for the complete resolution of cyclic polyphosphates. A convex gradient is also essential for optimum resolution.

INTRODUCTION

Inorganic cyclic polyphosphates are interesting materials which have been used as multivalent electrolytes [1,2] and as phosphorylating agents for a starch and a protein [3,4]. Of these compounds, cyclo-triphosphate (P_{3m}, trimetaphosphate) has been recognized as an important material for use as a prebiotic condensing agent [5] and as an initial phosphorylating species in chemical synthesis of DNA [6]. Several authors [7–12] have investigated various chemical properties of cyclo-triphosphate as well as other cyclic polyphosphates, such as cyclo-tetra- (P_{4m}), hexa- (P_{6m}) and octa- (P_{8m}) phosphates (cyclo-penta- and cyclo-heptaphosphates are rarely available even now). However, few industrial applications for inorganic cyclic polyphosphates exists because of their difficulty of preparation and isolation.

The demand for purified synthetic cyclic polyphosphates has required the development of new methods which can rapidly purify these molecules. High-performance liquid chromatography (HPLC) provides an excellent means of rapidly and efficiently purifying synthetic cyclic polyphosphate from crude reaction mixtures. The availability of numerous anion-exchange columns makes HPLC an attractive alternative to classical methods for the purification of synthetic cyclic polyphosphates.

In 1980, the coupled system of HPLC and flow injection analysis (FIA) for the

0021-9673/91/$03.50

automatic separation and detection of inorganic polyphosphates was reported [13]. The authors applied it to the separation of inorganic cyclic polyphosphates [11,14–16] instead of classical liquid chromatography with a fraction collector and manual determination of phosphates in each fraction [17]. The HPLC–FIA system has also been successfully applied to the complete separation of complex mixtures of both linear and cyclic polyphosphates [11,18,19]. Although the HPLC–FIA system is the most suitable method of preparing and isolating cyclic polyphosphates, it remains a time-consuming and troublesome task to optimize the separation conditions of a complex mixture of cyclic polyphosphates.

In the present study, a computer-assisted retention prediction system was developed for the rapid optimization of separation conditions for inorganic cyclic polyphosphates under gradient elution conditions in anion-exchange chromatography. The authors have developed a prediction system for inorganic linear polyphosphates in isocratic [18] and gradient [19–21] anion-exchange chromatography. The system has been applied to the prediction of retention times for oligonucleotides [22] and to the optimization of isocratic [18] and gradient [19,23] elution conditions.

THEORY

Prediction of retention times, t_g, in gradient elution

The first step in the procedure for retention prediction is to determine constants a and b characteristic of each solute [20]. These constants are calculated from the relationship between the capacity factor, k', and mobile phase salt concentration, C', in isocratic ion-exchange chromatography [18,20,22]:

$$k' = aC'^{-b} \tag{1}$$

Retention time, t_g, in gradient elution is given as eqn. 2 [20–25]:

$$t_g = (1/u)\{(1/B')[(xb + 1)B'at_0u + C_i^{(xb+1)}]^{1/(xb+1)} - C_i^{1/x}/B'\} + t_0 \tag{2}$$

where u is the flow-rate (ml/min) and C_i, B', and x are adjustable parameters for the gradient profile. Constants a and b are estimated from eqn. 1.

The gradient profile [20–25] can be expressed as a function of the eluent concentration and the time:

$$\begin{aligned} C &= (C_i^{1/x} + Bt)^x \\ B &= B'u = (C_f^{1/x} - C_i^{1/x})/t_f \end{aligned} \tag{3}$$

where C is the mobile phase salt concentration at time t, C_i is the initial mobile phase salt concentration at the beginning of the gradient elution and C_f is the final salt concentration at the end of gradient elution ($t = t_f$); $B' = B/u$. The parameter x characterizes the shape of the gradient profile [20–25] as shown in Fig. 1.

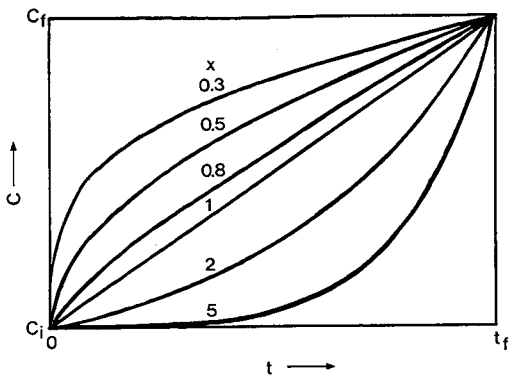

Fig. 1. Gradient profiles described by eqn. 3. (From ref. 23 with permission.)

Prediction of band widths, w_g, in gradient elution

The band width, w_g, in gradient-elution chromatography can be calculated from eqn. 4 [20–25]:

$$w_g = (4t_0/N^{1/2})\{1 + a[C_i^{1/x} + B(t_g - t_0 - t_D)]^{-xb}\} \quad (4)$$

where N is the plate number and t_D is the system dwell time between the outlet of the gradient-generating device and the column inlet. The mean value of N was measured to be 1900.

EXPERIMENTAL

Chemicals

Sodium salts of cyclo-triphosphate (P_{3m}), $Na_3P_3O_9 \cdot 6H_2O$, and cyclo-tetraphosphate (P_{4m}), $Na_4P_4O_{12} \cdot 4H_2O$, were prepared by the usual methods [26]. Sodium salts of cyclo-hexaphosphate (P_{6m}), $Na_6P_6O_{18} \cdot 6H_2O$, and cyclo-octaphosphate (P_{8m}), $Na_8P_8O_{24} \cdot 6H_2O$, were prepared according to the literature [8,9]. All other chemicals used were of reagent grade.

HPLC equipment

A Hitachi L-6200 HPLC system (Hitachi, Japan) coupled with an FIA system was used. Details of the HPLC–FIA system are described elsewhere [13,15,18].

The separations were performed on a column (500 × 4.0 mm I.D.) packed with a polystyrene-based quaternary ammonium anion exchanger (TSKgel SAX, 10 μm, Tosoh, Tokyo, Japan). The separation column was surrounded by a jacket containing circulating water at constant temperature within ± 0.1°C. The sample solution (0.5 ml) was injected into a separation column and chromatographed at a flow-rate of 1.0 ml/min. Concentrations of samples were $4 \cdot 10^{-5}$ M (P_{3m}), $3 \cdot 10^{-5}$ M (P_{4m}), $2 \cdot 10^{-5}$ M (P_{6m}), and $1.5 \cdot 10^{-5}$ M (P_{8m}). Eluent comprised appropriate concentrations of potassium chloride and 0.1% (w/v) Na_4EDTA buffered at pH 10.2.

Measurement of capacity factor

Prior to the elution of cyclic polyphosphates the column was washed with the eluent for 1 h. The column dead-time, t_0, was measured by injecting aqueous solution of $Co(NH_3)_6^{3+}$ and found to be 2.83 min. When an FIA system was used as a post-column reaction detector, extracolumn effects took place to some extent in HPLC [13,27]. The capacity factor (k'), therefore, was calculated from its retention time, allowing for the extracolumn effects.

Calculation

All predicted retention times and band widths were calculated with a PC-9801 personal computer (NEC, Tokyo, Japan). Computer simulations were carried out using software developed by the authors [20–23].

RESULTS AND DISCUSSION

Determination of constants, a and b, in isocratic elution

As described in the Theory section, constants a and b must be determined prior to the prediction of retention times. As shown in Fig. 2, the plot of $\log k'$ *vs.* $\log C'$ gave straight lines with correlation coefficients of 0.999 at a column temperature of 30°C. Constants a and b for cyclic polyphosphates were determined from the slope and intercept of the straight line in Fig. 2 and are compiled in Table I.

Fig. 2 shows that the plots for each solute are not parallel. Such irregular

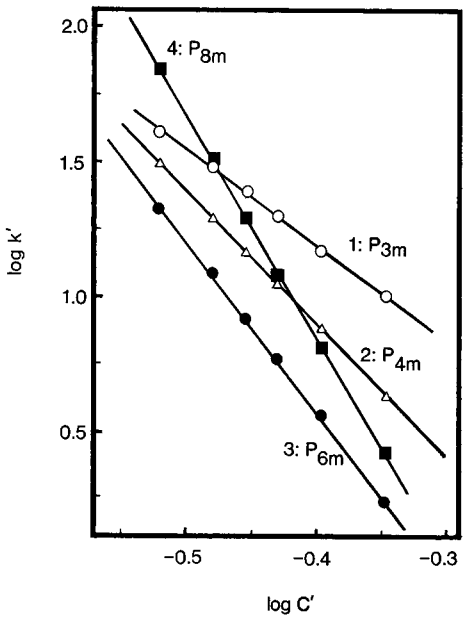

Fig. 2. Plot of $\log k'$ *vs.* $\log C'$ at pH 10.2 and a column temperature of 30°C. Eluent: potassium chloride solution with 0.1% Na_4 EDTA. Solutes are cyclo-tri- (P_{3m}), cyclo-tetra- (P_{4m}), cyclo-hexa- (P_{6m}), and cyclo-octa- (P_{8m}) phosphates.

TABLE I

VALUES OF CONSTANTS a AND b IN EQN. 1 AT A COLUMN TEMPERATURE OF 30°C

Solutes	b	a
P_{3m}	3.53	$5.91 \cdot 10^{-1}$
P_{4m}	4.88	$8.64 \cdot 10^{-2}$
P_{6m}	6.26	$1.16 \cdot 10^{-2}$
P_{8m}	8.11	$3.87 \cdot 10^{-3}$

tendencies have also been investigated by the authors through batch measurements of distribution ratio with varying salt concentration using ion-exchange resins [10].

The slope, b, corresponds to the ionic charge of cyclic polyphosphate in the exchanger phase [10]. The charge of each solute was expected to be 3 (P_{3m}), 4 (P_{4m}). 6 (P_{6m}), and 8 (P_{8m}). The b values in Table I were in rough agreement with the ionic charges of all solutes.

Prediction of retention times and band widths in gradient elution

The retention times and band widths for cyclic polyphosphates in gradient elution were predicted and compared with the observed values to test the performance of the present system. Tables II, III, and IV list the results with linear ($x = 1$), binary-convex ($x = 0.2$), and binary-convex ($x = 0.4$) gradients. The twelve observed retention times were predicted with an average error of $-2.8\% \pm 1$[relative standard deviation (R.S.D.)] and band widths with an average error of $-6.7\% \pm 7$(1 R.S.D.). Predictions reported in ion-exchange chromatography [20] were achieved in the range of errors from 1 to 10%. In comparison with the reported errors, accuracy of the retention prediction system presented here is good enough for the purpose of using computer simulations in optimizing gradients.

As an example, the simulated chromatogram displayed on the monitor screen was compared with a chromatogram observed under the gradient elution conditions in Table II, as shown in Fig. 3.

TABLE II

OBSERVED (Obs.) AND CALCULATED (Calc.) RETENTION TIMES AND BAND WIDTHS UNDER GRADIENT ELUTION CONDITIONS

$x = 1.0$; $C_i = 0.3$ M; $C_f = 0.4$ M; $t_f = 80$ min; $T = 30$°C. Error = 100 × (Calc. − Obs.)/Obs.

Solute	Retention time (min)			Band width (min)		
	Obs.	Calc.	Error (%)	Obs.	Calc.	Error (%)
P_{3m}	79.6	76.7	−3.6	6.46	6.80	5.3
P_{4m}	59.4	57.6	−3.0	5.19	5.09	− 1.9
P_{6m}	45.3	43.6	−3.8	4.51	3.79	−16
P_{8m}	71.4	68.7	−3.8	6.37	6.14	− 3.7

TABLE III

OBSERVED (Obs.) AND CALCULATED (Calc.) RETENTION TIMES AND BAND WIDTHS UNDER GRADIENT ELUTION CONDITIONS

$x = 0.2$; $C_i = 0.3$ M; $C_f = 0.4$ M; $t_f = 80$ min; $T = 30°C$. Error = 100 × (Calc. − Obs.)/Obs.

Solute	Retention time (min)			Band width (min)		
	Obs.	Calc.	Error (%)	Obs.	Calc.	Error (%)
P_{3m}	73.5	71.7	−2.3	6.37	6.33	0.10
P_{4m}	53.0	52.2	−1.5	5.01	4.59	− 8.5
P_{6m}	39.6	40.0	−2.3	4.04	3.35	−17
P_{8m}	61.7	61.3	−1.1	6.29	5.43	−14

TABLE IV

OBSERVED (Obs.) AND CALCULATED (Calc.) RETENTION TIMES AND BAND WIDTHS UNDER GRADIENT ELUTION CONDITIONS

$x = 0.4$; $C_i = 0.3$ M; $C_f = 0.5$ M; $t_f = 160$ min; $T = 30°C$. Error = 100 × (Calc. − Obs.)/Obs.

Solute	Retention time (min)			Band width (min)		
	Obs.	Calc.	Error (%)	Obs.	Calc.	Error (%)
P_{3m}	72.7	70.4	−3.2	5.95	6.26	5.2
P_{4m}	53.6	52.1	−2.8	4.55	4.59	0.88
P_{6m}	40.9	39.2	−4.2	3.99	3.40	−15
P_{8m}	61.2	59.7	−2.5	5.53	5.32	− 3.7

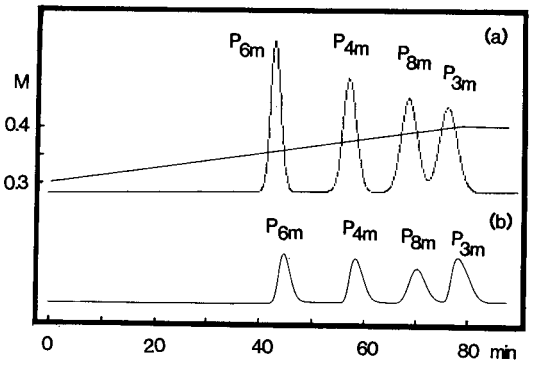

Fig. 3. Predicted (a) and observed (b) chromatograms for a mixture of four cyclic polyphosphates. (a) Gradient elution conditions as in Table II. (b) Column: TSKgel SAX (anion exchanger, 500 × 4.0 mm I.D.). Flow-rate: 1.0 ml/min. Eluents: A, 0.3 M potassium chloride +0.1% Na_4EDTA (pH 10.2); B, 0.4 M potassium chloride +0.1% Na_4EDTA (pH 10.2). Gradient elution conditions as in Table II. Column temperature: 30°C.

Optimization of gradients using computer simulation

In order to find an optimum gradient for cyclic polyphosphates, we examined effect of changes in the gradient parameters in eqn. 3 on band spacing and resolution. Gradient time, t_f, initial salt concentration, C_i, and gradient shape, x, were all taken into consideration. Gradient steepness was also considered.

Fig. 4 shows computer simulations of the separation for cyclic polyphosphates with a 0–0.5 M potassium chloride linear salt gradient and different gradient times, t_f, ranging from 50 to 400 min. An increase in gradient time corresponds to a decrease in gradient steepness, that is 0.01 M/min at 50 min (Fig. 4a), 0.005 M/min at 100 min (Fig. 4b), 0.0033 M/min at 150 min (Fig. 4c), 0.0025 M/min at 200 min (Fig. 4d), and 0.00125 M/min at 400 min (Fig. 4e). These simulations illustrated that all gradients failed to separate cyclic polyphosphates.

To improve resolution, we next examined the effect of changing initial salt concentration of eluent, C_i, from 0 to 0.4 M, while holding the gradient steepness constant. We have carried out computer simulations by varying C_i at each gradient steepness shown in Fig. 4a–e. As a result, simulations at 0.00125 M/min, which are shown in Fig. 5, gave better resolution of cyclic polyphosphates than those at any other gradient steepness.

Fig. 5 clearly demonstrates that an increase in C_i drastically improved resolution and band spacing of cyclic polyphosphates. A gradient with C_i of 0.3 M (Fig. 5c) or 0.4

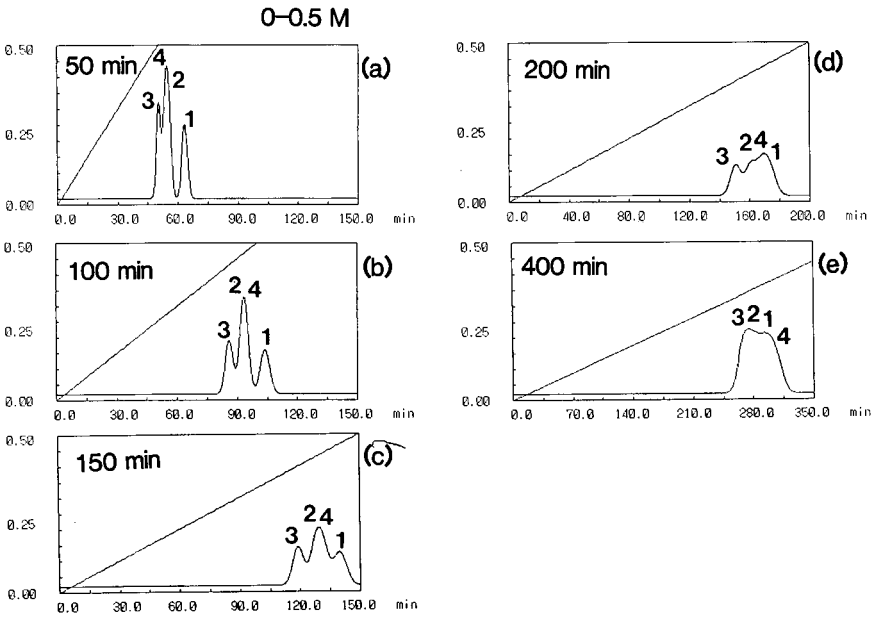

Fig. 4. Effect of gradient time, t_f, on the anion-exchange separation of cyclic polyphosphates demonstrated by computer simulations. Conditions: anion-exchange column (500 × 4.0 mm I.D.). Flow-rate: 1.0 ml/min. Gradient profile: C_i = 0.0 M potassium chloride, C_f = 0.5 M potassium chloride. Gradient shape: linear (x = 1). Gradient time: t_f = 50 min (a), 100 min (b), 150 min (c), 200 min (d), and 400 min (e). The ordinate represents molar concentration of potassium chloride solution. Peak numbers represent each cyclic polyphosphate as follows: 1, P_{3m}; 2, P_{4m}; 3, P_{6m}; and 4, P_{8m}.

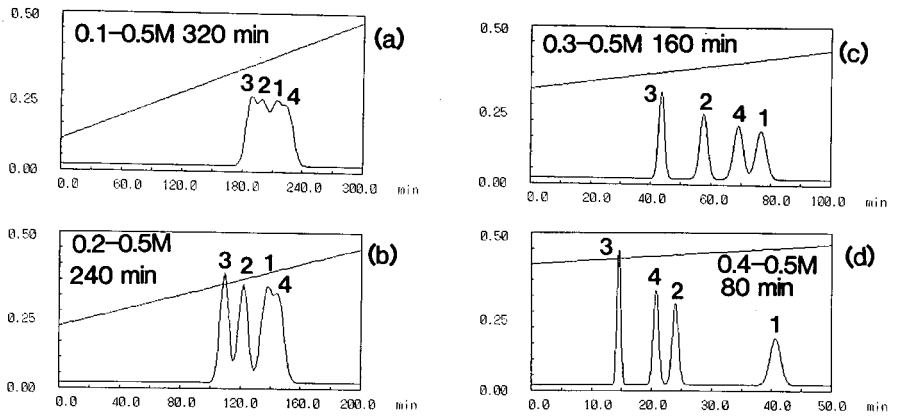

Fig. 5. Effect of initial salt concentration, C_i, on the anion-exchange separation of cyclic polyphosphates eluted with the same gradient slope as Fig. 4e demonstrated by computer simulations. Gradient profile: C_i = 0.1 *M* (a), 0.2 *M* (b), 0.3 *M* (c), and 0.4 *M* (d), C_f = 0.5 *M* potassium chloride. Gradient shape: linear (x = 1). Gradient time: t_f = 320 min (a), 240 min (b), 160 min (c), and 80 min (d). Peak numbers as Fig. 4.

M (Fig. 5d) provides adequate resolution. Additionally, an increase in C_i resulted in a decrease in analysis time. For example, all bands are eluted within only 45 min in Fig. 5d, while the last eluted band is eluted at 230 min in Fig. 5a.

A change in C_i leads to a change in band spacing, as shown in Fig. 5, where the gradient steepness is held constant. Band 4 of cyclo-octaphosphate is seen to change its position in the chromatogram as C_i changes. Similarly, an increase in gradient time seems to change the position of band 4, as seen in Fig. 4. These variations in band spacing can be understood from the isocratic plots of Fig. 2. The isocratic plots predict

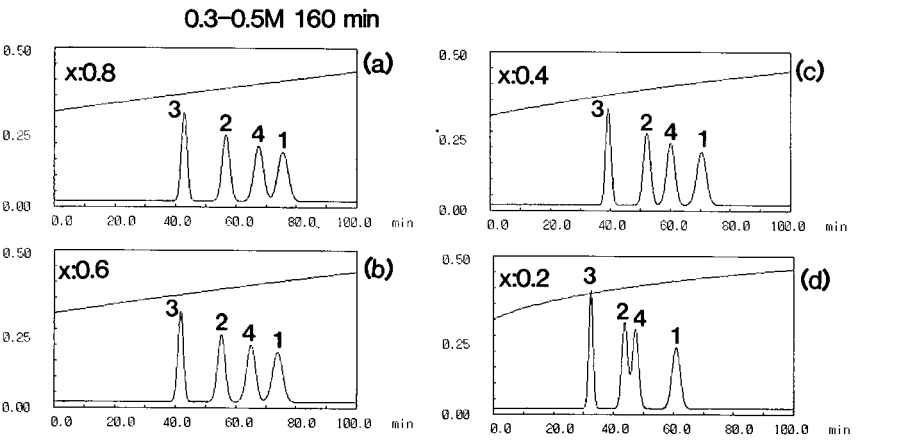

Fig. 6. Effect of gradient shape, x, on the anion-exchange separation of cyclic polyphosphates demonstrated by computer simulations. Gradient profile: C_i = 0.3 *M* potassium chloride, C_f = 0.5 *M* potassium chloride. Gradient shape: x = 0.8 (a), 0.6 (b), 0.4 (c), and 0.2 (d). Gradient time: t_f = 160 min. Peak numbers as Fig. 4.

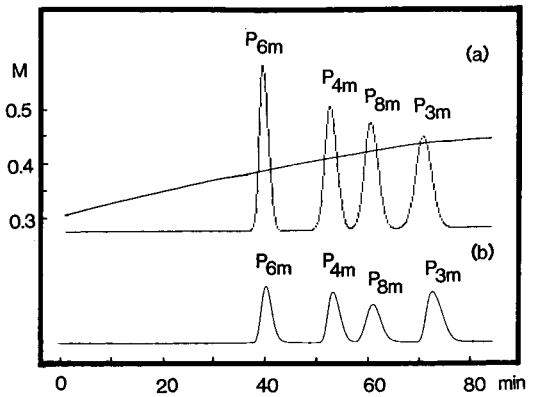

Fig. 7. Predicted (a) and observed (b) chromatograms for a mixture of four cyclic polyphosphates under an optimized gradient. (a) Gradient elution conditions as in Table IV. (b) Eluents: A, 0.3 *M* potassium chloride +0.1% Na_4EDTA (pH 10.2); B, 0.5 *M* potassium chloride +0.1% Na_4EDTA (pH 10.2). Gradient elution conditions as in Table IV.

that the relative retention of band 4 (cyclo-octaphosphate) should decrease with an increase in the salt concentration of the eluent, while the retention order of other solutes should be unchanged by changing salt concentration. Thus, an increase in C_i leads to a decrease in the relative retention of band 4, as shown in Fig. 5. On the other hand, an increase in gradient time leads to an increase in the relative retention of band 4, as shown in Fig. 4.

We further examined a fine-tuning of gradients by varying gradient shapes. Fig. 6 shows computer simulations by changing gradient shape, x, while the other gradient parameters are maintained similar to those in Fig. 5c. Fig. 6 demonstrates that a convex gradient with $x = 0.4$ (Fig. 6c) gives the best result in maximizing resolution and minimizing analysis time.

Consequently, the gradient listed in Table IV is the best choice for the rapid and complete separation of four cyclic polyphosphates. Fig. 7b demonstrates the anion-exchange separation of cyclic polyphosphates under the optimum gradient as listed in Table IV determined by computer simulations. A simulated chromatogram is also illustrated in Fig. 7a. All cyclic polyphosphates are completely resolved within 80 min. An HPLC technique using the optimum gradient presented here could become a new method of prepairing cyclic polyphosphates, such as cyclodecaphosphate, which have not yet been synthesized or prepared.

ACKNOWLEDGEMENT

The authors express their deep gratitude to Mr. Kazuki Kohkyu for his technical assistance.

REFERENCES

1 J. R. Van Wazer, *Phosphorus and Its Compounds*, Interscience, New York, 1958, Ch. 11.
2 D. E. C. Corbridge, *Phosphorus*, Elsevier, Amsterdam, 4th ed., 1990, Chap. 3.
3 A. D. F. Toy and E. N. Walsh, *Phosphorus Chemistry in Everyday Living*, American Chemical Society, Washington, DC, 2nd ed., 1987, Ch. 4.

4 M. Tsuhako, C. Sueyoshi, Y. Baba, T. Miyajima, S. Ohashi, H. Nariai, and I. Motooka, *Chem. Lett.*, (1987) 1431.
5 J. Hulshof and C. Ponnamperuma, *Origins of Life*, 7 (1976) 197.
6 K. L. Agarwal, A. Yamazaki, P. J. Cashion and H. G. Khorana, *Angew. Chem., Int. Ed. Engl.*, 11 (1972) 451.
7 E. Thilo and U. Schülke, *Z. Anorg. Allg. Chem.*, 341 (1965) 293.
8 E. J. Griffith and R. L. Buxton, *Inorg. Chem.*, 4 (1965) 549.
9 U. Schülke, *Z. Anorg. Allg. Chem.*, 360 (1968) 231.
10 G. Kura and S. Ohashi, *J. Chromatogr.*, 56 (1971) 111.
11 G. Kura, *J. Chromatogr.*, 447 (1988) 91.
12 G. Kura and H. Waki, *Polyhedron*, 9 (1990) 511.
13 Y. Hirai, N. Yoza and S. Ohashi, *Anal. Chim. Acta*, 115 (1980) 269.
14 G. Kura, T. Nakashima and F. Oshima, *J. Chromatogr.*, 219 (1981) 385.
15 G. Kura, *J. Chromatogr.*, 246 (1982) 73.
16 G. Kura, *Bull. Chem. Soc. Jpn.*, 56 (1983) 3769.
17 G. Kura, *J. Chromatogr.*, 211 (1981) 87.
18 Y. Baba, N. Yoza and S. Ohashi, *J. Chromatogr.*, 348 (1985) 27.
19 Y. Baba, N. Yoza and S. Ohashi, *J. Chromatogr.*, 350 (1985) 119.
20 Y. Baba, in J. L. Glajch and L. R. Snyder (Editors), *Computer-Assisted Method Development for High-Performance Liquid Chromatography*, Elsevier, Amsterdam, 1990, p. 143 (*J. Chromatogr.*, 485 (1989) 143).
21 Y. Baba, N. Yoza and S. Ohashi, *J. Chromatogr.*, 350 (1985) 461.
22 Y. Baba, M. Fukuda and N. Yoza, *J. Chromatogr.*, 458 (1988) 385.
23 Y. Baba and M. K. Ito, *J. Chromatogr.*, 485 (1989) 647.
24 P. Jandera and J. Churacek, *J. Chromatogr.*, 91 (1974) 207; 223.
25 P. Jandera and J. Churacek, *Gradient Elution in Column Liquid Chromatography*, Elsevier, Amsterdam, 1985.
26 G. Brauer, *Handbuch der Präparativen Anorganischen Chemie*, Ferdinand Enke Verlag, Stuttgart, 1960, pp. 494–496.
27 L. R. Snyder and J. J. Kirkland, *Introduction to Modern Liquid Chromatography*, Wiley, New York, 2nd ed., 1979.

Journal of Chromatography, 550 (1991) 15–25
Elsevier Science Publishers B.V., Amsterdam

CHROMSYMP. 2224

Multiple-criteria optimization

STANLEY N. DEMING
Department of Chemistry, University of Houston, Houston, TX 77204-5641 (USA)

ABSTRACT

In many chromatographic optimization problems, it is unusual to find only one response that must be optimized. Multiple-criteria optimization methods allow the combination of several responses into a single figure-of-merit. Origins are traced to Harringtons' "desirability functions" and Zadeh's "fuzzy sets".

INTRODUCTION

In many chromatographic optimization problems, it is unusual to find only one response that needs to be optimized. Instead, there are usually several responses that must be considered. Additionally, many of the responses must be expressed as intensive properties (*i.e.*, they should not depend on the size or throughput of the system [1]) and must be normalized by one or more factors and/or responses of the system [2]. In industrial work, for example, resolution per unit time is often of greater interest than simply resolution. Similarly, cost is often usefully measured as dollars per separation.

In all of these cases, various ratios, penalties and desirabilities can be used to specify quantitative objective functions [3].

OBJECTIVE FUNCTIONS

As stated by Beveridge and Schechter [2], "The aim of optimization is the selection, out of the multiplicity of potential solutions, of that solution which is the best with respect to some well defined criterion. The choice of this criterion, the objective, is therefore an essential step in any study... In general, economic criteria should be used, although technical forms are common".

An objective function is a mathematical relationship expressing the objective in terms of system factors and/or responses. Objective functions based on overall economic strategies tend to be highly complex [2]. Objective functions based on more restricted technical and quality considerations are usually simpler.

Consider a chromatographic system with two responses: resolution and analysis time. If the system is to be optimized, the question arises, of what the objective of the separation process is. If the separation is to be presented to an academic audience, the objective might be to make the resolution as high as possible and ignore the analysis

0021-9673/91/$03.50

time. However, if the separation is to be presented to industrial process control engineers, the objective might be to minimize the analysis time and not be purists about resolution. The sagacious laboratory manager will recognize that improving both the resolution and the analysis time (within limits) would capture the attention of both audiences.

An objective function could be used to indicate formally just how resolution and analysis time should be combined into a single figure-of-merit to be optimized. For this example, the objective function might be simply the sum of the resolution and some inverse measure of the analysis time, or, if it is desired to emphasize the resolution, the resolution might be weighted twice as much as analysis time. There might also exist target values of either or both responses: minimizing the total deviation from these target values might be the objective.

Considerations such as this illustrate an irony about objective functions: they are highly subjective. To write a proper objective function for this chromatographic example, it would be helpful to have at hand the results of a survey that measures the relative desirabilities of both resolution and analysis time for the intended customers.

OBJECTIVE FUNCTIONS BASED ON RATIOS

Ratios are often used to construct objective functions. Although ratios are simple and attractive, they can lead to unexpected results. This is well illustrated in the valuable paper by Smits *et al.* [4]; the following discussion is based on their paper.

Fig. 1 shows an incomplete liquid chromatographic separation of five inorganic ions. The vertical axis represents detector signal (arbitrary units) which is proportional to the concentration of the ions in the eluent. The horizontal axis represents the time (arbitrary units) after injection of the sample onto the chromatographic column. In many environments, the time required to elute the last ion is important: longer analysis

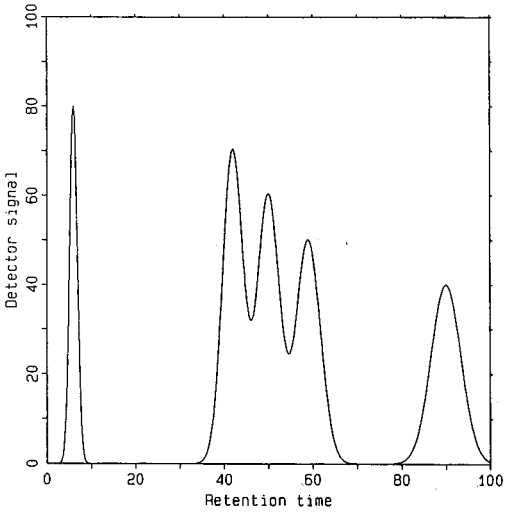

Fig. 1. Incomplete liquid chromatographic separation of five inorganic ions. Computer simulation based on ref. 4.

times mean fewer samples per day; shorter analysis times will increase the daily sample throughput, clearly an economic advantage.

The resolution/analysis time ratio could be chosen for maximization as the objective function. This seems reasonable. As the separation becomes more complete, the quantitative measure in the numerator will become larger and the objective function will become larger. As the analysis time decreases, the denominator will become smaller and again the objective function will become larger. Thus, maximizing the resolution/analysis time ratio should lead to improved separations and shorter analysis times.

Fig. 2 shows the separation that might result from the use of this optimization criterion. The objective function has been increased, but the separation of ions is now worse than when the optimization began. The denominator became small faster than the numerator became small, that is, the analysis time decreased faster than the resolution degraded. While the resolution was going from bad to worse, the analysis time was going from good to better at a faster rate. The net result was a very fast "separation" that was almost totally worthless, even though the objective function ratio (resolution/analysis time) continued to become larger.

Objective functions based on ratios must be used with caution. An alternative is to avoid ratios by basing the optimization on only one of the components (*e.g.*, resolution) and establishing a threshold and penalty function for the other component (*e.g.*, analysis time). Another alternative is to combine multiple responses into a single measure of performance that expresses the desirability of each combination.

OBJECTIVE FUNCTIONS BASED ON PENALTY FUNCTIONS

Practical considerations of sample throughput (*e.g.*, analysis per day) often dictate a maximum permissible analysis time. If an analytical laboratory must carry

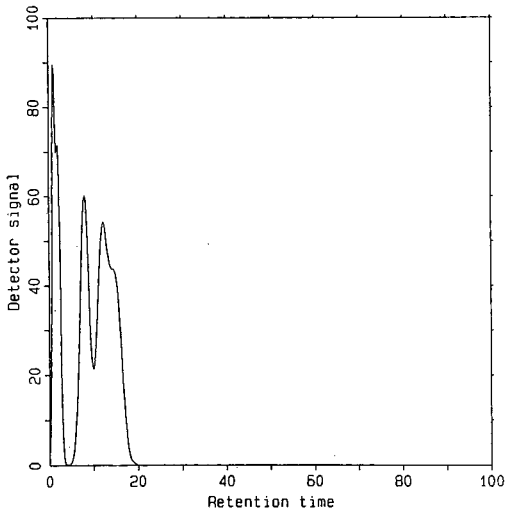

Fig. 2. Results of optimization driven by the maximization of the resolution/analysis time ratio. Computer simulation based on ref. 4.

out fifteen analyses in an 8-h day, then simple calculation suggests a maximum analysis time of *ca.* 30 min [5]. This 30-min maximum analysis time can be considered to be a threshold value: an analysis time of less than 30 min might be desirable but would not be especially beneficial, whereas an analysis time greater than 30 min would be undesirable, perhaps critically undesirable. Thus, an analysis time less than the threshold might not figure in any objective function calculations, but analysis times greater than the threshold should be taken into account: the objective function should be penalized if the analysis time exceeds the 30-min threshold.

Assuming the threshold represents an upper limit, penalty functions can be expressed mathematically is

$$\begin{aligned} p &= 0 && \text{for } y_j \leqslant y_{jt} \\ &= g(y_j - y_{jt}) && \text{for } y_j > y_{jt} \end{aligned} \tag{1}$$

where p is the value of the penalty and y_{jt} represents the threshold value associated with the response y_j. The nature of $g(y_j - y_{jt})$ is subjective but usually follows one of three well defined forms illustrated in Fig. 3. (Similar equations and figures apply to threshold values representing a lower limit.)

The first type of penalty function is an "infinite wall" illustrated at the top of Fig. 3: $g(y_j - y_{jt}) = -\infty$. Thus, violations of the threshold are considered to be infinitely bad. This type of penalty function is usually used for critical responses (those involving safety, for example).

A second type of penalty function is illustrated in the middle of Fig. 3: $g(y_j - y_{jt}) = b_j(y_j - y_{jt})$, where b_j is a slope or proportionality constant expressing the severity of the penalty ($b_j = -\infty$ is equivalent to the "infinite wall"; $b_j = 0$ is equivalent to no penalty). As the response becomes further away from the threshold value, the penalty becomes proportionally more severe. Again, the choice of b_j is often subjective.

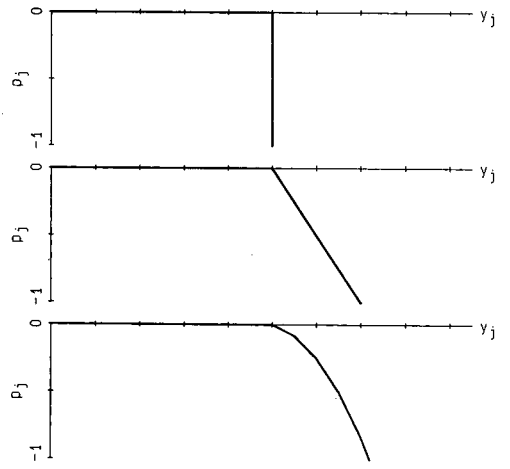

Fig. 3. Possible penalty functions for $y_j > y_{jt}$.

The third type of penalty function is illustrated at the bottom of Fig. 3: $g(y_j - y_{jt}) = b_j(y_j - y_{jt})^n$, where n is usually $\geqslant 2$. This is a power function that expresses the idea that large violations of the threshold value are much more serious than small violations. The choices of both b_j and n are subjective. This is probably the most generally useful type of penalty function and is widely used in many areas.

DESIRABILITY FUNCTIONS

It was suggested earlier that an objective function could be used that might improve both the resolution and the analysis time. But how can the "apples" of resolution and the "oranges" of analysis time be combined? Harrington [6] states the problem well: "In nearly all situations requiring human judgement, one is faced with a multiplicity of measures which must be balanced one against the other, weighted in accordance with their relative importance, compromised where these measures are mutually opposing, and variously manipulated to achieve an optimum judgement... If by some means the several properties could be measured in consistent units, or, even better, could be expressed as numbers on a dimensionless scale, then the arithmetic operations intended to combine these measures becomes feasible". Although Harrington proposed two specific forms for the "desirability function", the concepts are general and can be merged with concepts from Zadeh's field of fuzzy logic [7–11] to yield useful objective functions for optimization.

Lowe [12] proposed a simple procedure for forming desirabilities from multiple responses. If y_{ju} and y_{jd} are measures of the most undesirable and most desirable values, respectively, of a response y_j, and if it is assumed that the desirability increases linearly on going from y_{ju} to y_{jd}, then the desirability contributed by this response is calculated as

$$\begin{aligned} d_j &= 0 && \text{for } y_j < y_{ju} \\ d_j &= 1 && \text{for } y_j > y_{jd} \\ d_j &= (y_j - y_{ju})/(y_{jd} - y_{ju}) && \text{for } y_{ju} \leqslant y_j \leqslant y_{jd} \end{aligned} \tag{2}$$

where "$<$" and "$>$" represent "worse than" and "better than", respectively. Note that d_j is unitless and ranges from 0 to 1.

The concept is illustrated in Fig. 4. Along the left-hand side at the top of the figure is a desirability axis ranging from 0 (undesirable) to 1 (desirable). Along the bottom of the figure are drawn five response axes, $y_1 - y_5$ (*e.g.*, resolution, separation time, cost). The response axes have undergone zero suppression and scale expansion so that their most undesirable values are aligned vertically with the left-hand side of the figure and their most desirable values are aligned vertically with the right-hand side of the figure.

Running diagonally across Fig. 4 from left to right is a transformation line that maps values of response onto values of desirability. This line is used by reading upward from a given value of response and leftward to the corresponding values of desirability. For example, a response value of $y_5 = 4.0$ corresponds to a desirability value of $d_5 = 0.57$. Similarly, $y_4 = 15$ becomes $d_4 = 0.85$ and $y_1 = 1.2$ becomes $d_1 = 0.15$. These

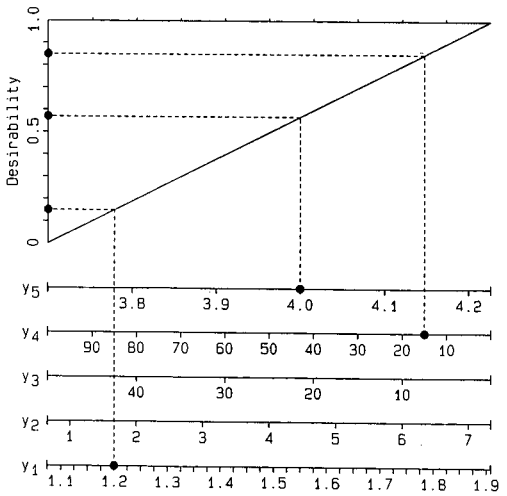

Fig. 4. Desirability as a first-order function of response. Undesirable responses at the left; desirable responses at the right.

results obtained graphically are identical with those obtained using eqn. 2:

$$d_5 = (4.00 - 3.70)/(4.23 - 3.70) = 0.57$$

$$d_4 = (15 - 100)/(0 - 100) = 0.85$$

$$d_1 = (1.2 - 1.075)/(1.908 - 1.075) = 0.15 \tag{3}$$

Responses that lie to the right of the response ranges shown in Fig. 4 would be assigned desirabilities of 1.00; responses to the left of the figure would be assigned desirabilities of 0.00.

Harrington's desirability functions [6] do not assume Lowe's [12] linear (first-order) relationship between response and desirability. Harrington's two-sided desirability function is given by

$$d_j = \exp[-(|y_j'|)^n] \tag{4}$$

where n is a positive number ($0 < n < \infty$, not necessarily integral), y_j' is a linear transform of the response variable, y_j, such that $y_j' = -1$ when y_j is equal to the lower specification limit, y_j^-, and $y_j' = +1$ when y_j is equal to the upper specification limit, y_j^+, and $|y_j'|$ is the absolute value of y_j' (the use of upper and lower specification limits comes from concerns about product quality). Any particular value of response, y_j, may be transformed into the corresponding y_j' by the relationship

$$y_j' = [y_j - (y_j^+ + y_j^-)/2]/[(y_j^+ - y_j^-)/2]$$

$$= [2y_j - (y_j^+ + y_j^-)]/(y_j^+ - y_j^-) \tag{5}$$

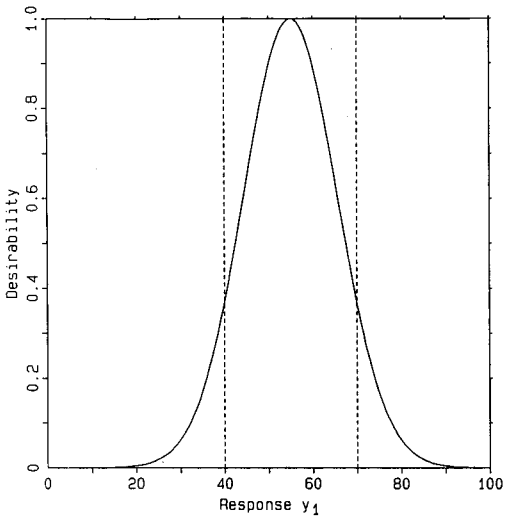

Fig. 5. Harrington's two-sided desirability function for $n = 2$.

which measures the distance of y_j from the midpoint between the upper and lower specification limits, $[(y_j^+ + y_j^-)/2]$, in units equal to half the spread between the upper and lower specification limits, $[(y_j^+ - y_j^-)/2]$. Fig. 5 illustrates this two-side desirability function for $n = 2$.

For one-sided specification limits a special form of the Gompertz growth curve is used:

$$d_j = \exp\{-[\exp(-y_j')]\} \tag{6}$$

where $y_j' = 0$ at the single spcification limit. The mapping of y_j onto y_j' is accomplished by choosing two ordered pairs of (y_j, d_j) and calculating $y_j' = -\ln[-\ln(d_j)]$. From the resulting ordered pairs of (y_j, y_j'), the straight-line equation

$$y_j' = b_0 + b_1 y_j \tag{7}$$

can be obtained, where b_0 is the intercept and b_1 is the slope. Fig. 6 illustrates this one-sided desirability function for the ordered pairs (40.0, 0.37) and (70.0, 0.90).

These desirability functions are well suited to multiple-criteria optimization work, but many alternative forms are possible. Some of the most useful versions of desirability functions are [free-form] graphical versions such as those shown in Figs. 7 and 8. Derringer and Suich [13] gave examples.

OVERALL DESIRABILITIES

There are many ways in which the individual desirabilities $d_1 - d_n$ can be combined. A simple arithmetic average is one example. However, as Harrington [6] pointed out, in any realistic situation a "basic premise is this—if any one property is so

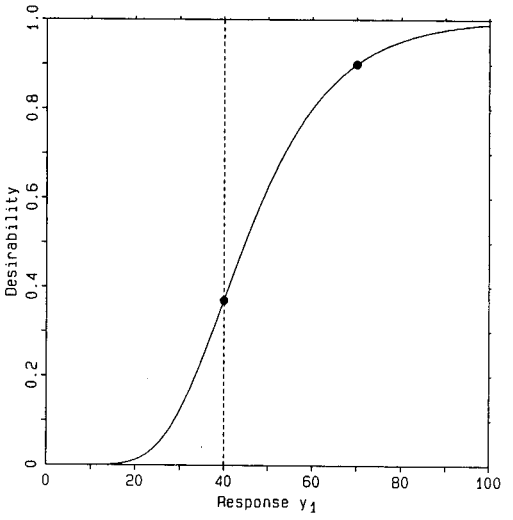

Fig. 6. Harrington's one-sided desirability function for the ordered pairs (40.0, 0.37) and (70.0, 0.90).

poor that the product is not suitable to the application, that product will not be acceptable, *regardless of the remaining properties*... customer reaction to a product is based very largely on the less desirable properties of that product because these are the focus of potential trouble".

The mathematical model analogous to these psychological reactions is the geometric mean of the component d values, or

$$D = (d_1 d_2 \ldots d_n)^{1/n} \tag{8}$$

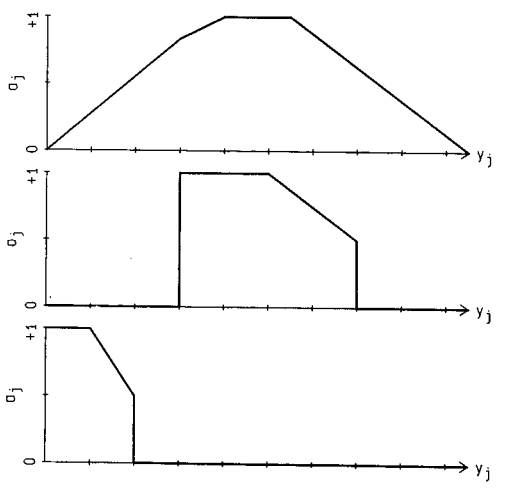

Fig. 7. Free-form desirability functions constructed from straight-line segments.

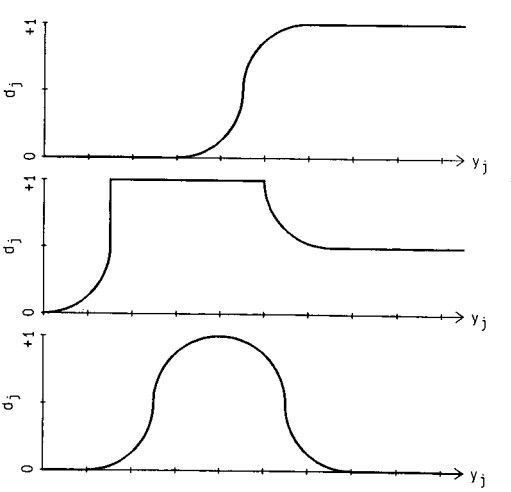

Fig. 8. Free-form desirability functions with curvature.

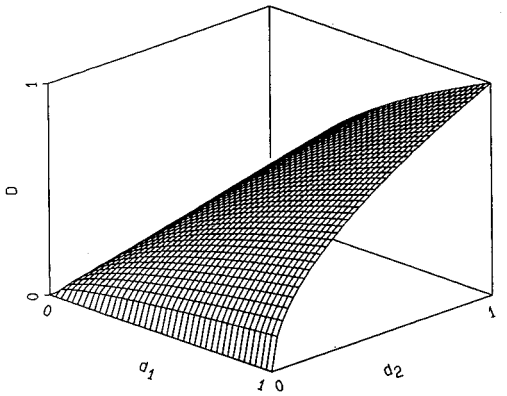

Fig. 9. Illustration of how D (the overall desirability) varies as a function of two d_j values according to eqn. 8.

where D is the overall desirability. It is clear that of any d_j is zero, the associated D will also be zero. Further, D is strongly weighted by the smaller d_j values.

Fig. 9 shows how D varies as a function of two d_j values. The nth root (square root) relationship is clear in this representation. Note again that if either d_1 or d_2 goes to zero, D is zero regardless of the value of the other d.

Fig. 10 shows individual desirabilities, d_1 and d_2, as functions of two responses, y_1 and y_2. Mapping these desirabilities through eqn. 8 gives Fig. 11, which shows how the overall desirability D is affected by the individual responses, y_1 and y_2. Figs. 12 and 13 suggest that more complicated mappings of responses onto desirabilities give rise to more complicated desirability surfaces that might contain multiple optima.

GENERAL COMMENTS

The ultimate mapping would be to show D as a function of the system factors [6], but to do so presumes a knowledge of the relationships between each y_j and all x_1 values. However, because these relationships are not usually known at the beginning of a separation project, such mappings are not usually possible initially.

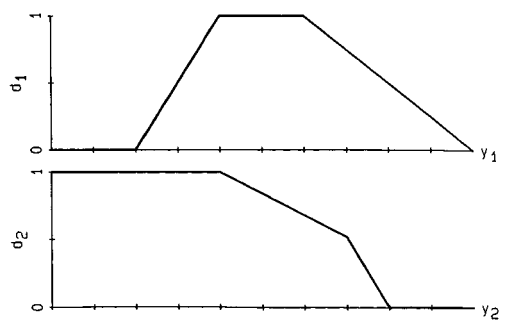

Fig. 10. Individual desirabilities, d_1 and d_2, as functions of two responses, y_1 and y_2.

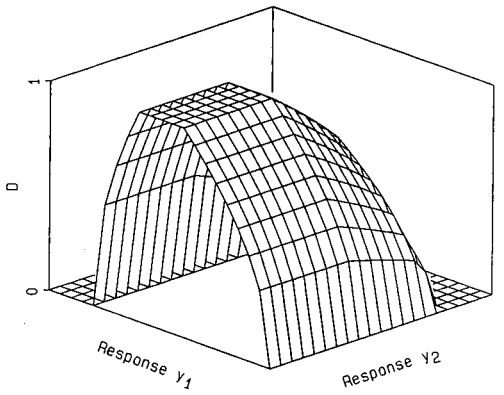

Fig. 11. Overall desirability, D, plotted as a function of the individual responses, y_1 and y_2, mapped through eqn. 8 using the individual desirabilities, d_1 and d_2, shown in Fig. 10.

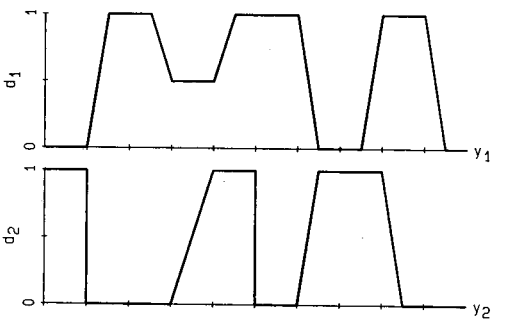

Fig. 12. Polymodal individual desirabilities, d_1 and d_2, as functions of two responses, y_1 and y_2.

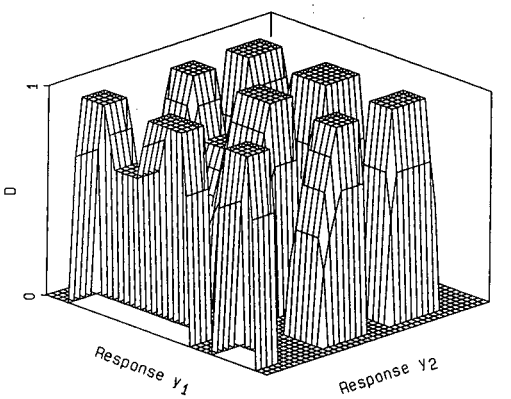

Fig. 13. Overall desirability, D, plotted as a function of the individual responses, y_1 and y_2, mapped through eqn. 8 using the individual desirabilities, d_1 and d_2, shown in Fig. 12.

Desirability functions have been used before in separation science to improve the quality of separations. The work of Glajch and Snyder [14], Laub and Purnell [15], Glajch *et al.* [16], Sachok *et al.* [17], Morgan and Jacques [18], Deming *et al.* [19], Otto and Wegscheider [20,21] and Cela *et al.* [22] may be consulted for examples.

ACKNOWLEDGEMENTS

This work was supported in part by Grant No. 003652-108 from the Applied Technology Program, Texas Higher Education Coordinating Board, Division of Research Programs.

REFERENCES

1 S. N. Deming and S. L. Morgan, *Experimental Design: A Chemometric Approach*, Elsevier, Amsterdam, 1987.
2 G. S. G. Beveridge and R. S. Schechter, *Optimization: Theory and Practice*, McGraw-Hill, New York, 1970.
3 R. E. Steuer, *Multiple Criteria Optimization: Theory, Computation, and Application*, Wiley, New York, 1986.
4 R. Smits, C. Vanroelen and D. L. Massart, *Fresenius' Z. Anal. Chem.*, 273 (1975) 1.
5 S. L. Morgan and S. N. Deming, *J. Chromatogr.*, 112 (1975) 267.
6 E. C. Harrington, Jr., *Ind. Qual. Control*, 21 (1965) 494.
7 L. A. Zadeh, *Inform. Control*, 8 (1965) 338.
8 L. A. Zadeh, *CHEMTECH*, 17 (1987) 340.
9 A. Kandel, *Fuzzy Mathematical Techniques with Applications*, Addison-Wesley, Reading, PA, 1986.
10 A. Kaufmann and M. M. Gupta, *Introduction to Fuzzy Arithmetic: Theory and Applications*, Van Nostrand Reinhold, New York, 1985.
11 C. V. Negoita, *Expert Systems and Fuzzy Systems*, Benjamin/Cummings, Menlo Park, CA, 1985.
12 C. W. Lowe, *Trans. Inst. Chem. Eng.*, 45 (1967) T3.
13 G. Derringer and R. Suich, *J. Qual. Technol.*, 12 (1980) 214.
14 J. L. Glajch and L. R. Snyder, *Computer-Assisted Method Development for High-Performance Liquid Chromatography*, Elsevier, Amsterdam, 1990.
15 R. J. Laub and J. H. Purnell, *J. Chromatogr.*, 112 (1975) 71.
16 J. L. Glajch, J. J. Kirkland, K. M. Squire and J. M. Minor, *J. Chromatogr.*, 199 (1980) 57.
17 B. Sachok, J. J. Stranahan and S. N. Deming, *Anal. Chem.*, 53 (1981) 70.
18 S. L. Morgan and C. A. Jacques, *J. Chromatogr. Sci.*, 16 (1978) 500.
19 S. N. Deming, J. M. Palasota, J. Lee and L. Sun, *J. Chromatogr.*, 485 (1989) 15.
20 M. Otto and W. Wegscheider, *J. Chromatogr.*, 258 (1983) 11.
21 M. Otto, *Chemometr. Intell. Lab. Syst.*, 4 (1988) 101.
22 R. Cela, C. G. Barroso and J. A. Pérez-Bustamante, *J. Chromatogr.*, 485 (1989) 477.

Journal of Chromatography, 550 (1991) 27–37
Elsevier Science Publishers B.V., Amsterdam

CHROMSYMP. 2329

Fully automatic high-performance liquid chromatographic optimization

N. M. DJORDJEVIC*, F. ERNI and B. SCHREIBER
Sandoz Pharma Ltd., Analytical Research and Development, Basle (Switzerland)
E. P. LANKMAYR and W. WEGSCHEIDER
Graz University of Technology, Graz (Austria)
and
L. JAUFMANN
Kontron, Munich (Germany)

ABSTRACT

A good optimization routine should correctly find the best chromatographic separation conditions for mixtures of known or unknown constituents. The chromatographer must define the number of the parameters to be optimized and their ranges. However, the more parameters to be optimized and the more they interact, the more difficult and time-consuming the optimization procedure will be. A system capable of performing fully automated optimization of mobile phase selectivity in reversed-phase liquid chromatography was built. The optimization routine searches for the best conditions (trying to maximize a chromatographic response function) and for the points, inside defined experimental borders, where the least available experimental information is available. By conducting the experiment under the predicted optimum conditions and an additional experiment under conditions corresponding to the least density of information, the system was forced not to search for a local maximum, but to approach the global optimum. Peak tracking, an important part of any optimization process in high-performance liquid chromatography, was an integral part of the optimization software and was based on fuzzy theory. This implementation of an on-line identification of the sample components made a fully automated optimization of the mobile phase composition possible. Once a suitable separation had been achieved, it was necessary to validate the procedure, special attention being focused on robustness. The robustness test appraises the outcome of small variations in method conditions on the analytical performance. An important feature of this robustness analysis was the three-dimensional representation of the data as the hypersurface which helps to relate robustness to elution characteristics.

INTRODUCTION

The use of computer-aided procedures for the optimization of separation selectivity in reversed-phase high-performance liquid chromatography (HPLC) has been extensively studied during the last decade, and various approaches are available to rationalize development and optimization. Excellent overviews on optimization techniques in chromatography can be found in the literature [1–3]. Owing to the wide variety of separation principles accessible for HPLC separations, systematic method

0021-9673/91/$03.50

development may help greatly in finding suitable experimental conditions for a given separation task. The lack of mechanistic models suitable for general application makes empirical optimization schemes the method of choice for unrestricted optimization in HPLC.

Systematic method development resulting in fully automated instrumentation is only useful if all of the variables which permit separation selectivities and retention times to be tuned effectively can be considered. Thus, a sequential approach based on a moving least-squares interpolation between experimentally obtained retention data has been proposed [4]. The moving least-squares algorithm is employed for a non-linear interpolation between experimentally obtained retention data, supplying retention curves for all sample components. The resulting data allow prediction of the separation for any intermediate experimental conditions. The resulting optimization program (OPTIM) calculates systematically the optimization hypersurface according to a preselected optimization criterion which reflects the quality of the separation.

In this study a chromatographic response function (CRF) derived from the peak separation factor [5] and generalized for multi-component analysis [6] was used with (CRF_1) and without (CRF_2) normalization on total analysis time.

$$CRF_1 = 1/t[\prod f/(g + 2n)] \quad (1)$$

$$CRF_2 = \prod f/(g + 2n) \quad (2)$$

where f and g are the separation factors according to Kaiser [5] and Wegscheider *et al.* [6], n is a baseline noise and t is analysis time, *i.e.* duration of the actual chromatogram.

The incorporation of peak separation, noise and analysis time information allows one to account for basic performance characteristics of analytical separation procedures, such as accuracy, precision, speed and ultimately also cost of analysis. Another advantage of this function is its adaptability to the actual chromatographic situation. It considers automatically the status of peak separation in the presence of peak asymmetry and at differing peak intensity ratios. The OPTIM program provides output information containing the proposed best experimental conditions and also gives the point in space which has the lowest density of experimental data. Consequently, information on the retention behavior of all analytes is accumulated in a stepwise manner to solve the apparent separation problem or to quit according to a predefined stop criterion. Owing to the sequential concept of this optimization strategy the total experimental effort needed for method development depends largely on the complexity of the separation problem itself. Simple separation tasks may call for only a few runs, whereas more complex problems may require a larger number of experiments.

For automated optimization it is necessary to keep track of the identity of the eluted signals. Typical approaches for peak identification include the separate injection of standard components and/or multi-wavelength detection with factor analysis [7]. The mere use of standard components makes the process extremely slow and can, of course, not be applied if sample components of unknown identity are analyzed. Overlapping peaks have been successfully deconvoluted using diode array detection. The use of strict statistical models for data analysis may, however, not be

adequate for fully automated peak recognition at greatly changed mobile phase compositions.

To provide a generally applicable procedure, a peak-tracking routine based on fuzzy theory has been developed. Fuzzy theory is applied sucessfully when uncertain data are to be processed for analytical reasoning, as is the case with peak data obtained during method development procedures. The incorporation of this theory allows one to account for imprecise data originating from altered experimental conditions and to assign the membership of peak data to a sample component by means of computed membership function values. This routine works with either single- or multi-channel (*e.g.* diode array) detectors and can also be used with unknown compounds, even when peak overlap occurs during the optimization runs [8,9]. Recognition of peaks is based on comparison of peak areas and elution order of the signals from a reference and a trial run. As the number of signals in the chromatograms can alter during progress of the optimization, the chromatogram showing the maximum number of signals is always chosen as a reference. In the case of peak overlap, each potentially overlapped peak is compared with all linear combinations of the reference peaks not recognized as single peaks. Fuzzy comparison results in an assignment of the peak identity by means of computed membership values. A detailed explanation of the fuzzy algorithm and the logic of the procedure is given in refs. 8 and 9.

Fully automated method development can only be achieved with modules providing peak tracking and optimization embedded in an automated HPLC system consisting at least of an autosampler, pumps, a single- or multi-channel detector and a computer-based data station. For this purpose, commercially available HPLC equipment, as described in the Experimental section, was used with an MS-DOS-based data system, which includes the possibility of running a user program from system control level. It is possible to pass control from the data acquisition/reduction level to an interface file which allows communication with the above-mentioned software modules. This provides a means of transferring the integration data, containing a list of retention times, and area data from two-channel data acquisition/reduction, to the peak-tracking routine which assigns an identity to all detected signals. A retention data/peak assignment table is produced and used by the OPTIM program to construct the optimization hypersurface. The proposed best experimental conditions for the next experiment, as well as the least-density point of experimental conditions, are then transferred from the optimization module to the system level of the data station, and again chromatographically processed. Consequently, a loop is installed into a commercial HPLC system enabling automated method optimization within the limits of HPLC equipment that was originally not designed for this specific purpose.

EXPERIMENTAL

Instrumentation and software

The fully automated HPLC system was a Kontron (Zurich, Switzerland) liquid chromatograph consisting of four D-420 pumps, a D-460 autosampler furnished with a 100-μl Hamilton dosing syringe, two M-800 mixing chambers and a Model 400 column oven. The system was controlled by a Kontron 450 PC/AT data station. The detector was a Perkin-Elmer (Norwalk, CT, USA) LC-235 diode array detector with a flow-cell path length of 10 mm and a total volume of 4 μl, coupled to a Perkin-Elmer

GR-100 graphic printer–plotter. Throughout all experiments the signals were monitored at two wavelengths (210 and 230 nm).

The software for system control and data acquisition was commercial MT2 software (Softron Munich, Germany). It was interfaced with OPTIM software (having the optimization and peak-tracking routines) developed at the Graz University of Technology (Graz, Austria). For the three-dimensional representation of the optimized hypersurface, the Statgrafics program (STCS, Rockville, MD, USA) was used.

Reagents and solvents

Acetonitrile and *tert.*-butyl methyl ether (TBME) were of HPLC grade and obtained from Rathburn (Walkerburn, UK) and Fluka Chemie (Buchs, Switzerland). Water was deionized and filtered. Separations were carried out on an Ultrasphere ODS column, 25 × 0.46 cm I.D., 5 μm particle size (Beckman Instruments, San Ramon, CA, USA).

A synthetic mixture of eight different cyclosporins (A, B, C, G, L, T, Isocyclosporin A and dihydrocyclosporin A) was prepared in house. Their full structures have been published elsewhere [10].

DISCUSSION

The system described was designed for fully automated HPLC optimization. Four pumps allow ample possibilities for the use of different combinations of organic solvents and water. Furthermore, pH and ionic strength can be very easily changed by simple variation of the mixing ratio of different buffer solutions. A mixture of different cyclosporins (cyclic undecapeptides) was used as an example for the evaluation of the computer-aided optimization. Our goal was to optimize the isocratic HPLC method (mobile phase selectivity) and to evaluate its robustness.

Generally, cyclosporins have high solubility in diethyl ether, TBME, methanol and acetonitrile, while their solubility in water is very poor. The most common mode of separation of different cyclosporins is reversed-phase HPLC [11], with a mobile phase consisting of one of the binary mixtures methanol–water or acetonitrile–water. To achieve better selectivity we have applied a ternary mobile phase consisting of TBME, acetonitrile and water. On the basis of previous knowledge regarding miscibility of this three-component liquid phase (limited miscibility of TBME with water), the upper and lower boundaries of the solvent composition were selected appropriately.

In the instrumental set-up, the sum of the flow-rates of the pumps A and B was set to be 100%. The same rule was applied to pumps C and D. To start the optimization it was necessary to define the total flow-rate resulting from all four pumps and to input the percentage of the total flow for pumps B and D. The values for the pumps A and C were adjusted automatically. Pumps A and C were delivering acetonitrile, while B and D were supplying water and TBME, respectively. For the start of the optimization four runs were selected representing the boundary conditions of the preselected variable space. The restraints were set between 60 and 80% for pump B and between 10 and 30% for pump D.

It is possible to select among several predefined stop criteria for the optimization process. Once this measure has been accomplished the program stops. A resolu-

tion of defined value can be used as one possible criterion, another being defined as the maximum number of experiments to be performed. The latter can be used in order to stop the unit before the reservoirs of the mobile phase are emptied in automated overnight operation, *e.g.* Finally, the program will stop if convergence of the optimum conditions is predicted by the optimization program. For these experiments the criterion was set to stop the procedure when five consecutive optima had been proposed within the limits of ± 3% of the variable composition.

After the four initial isocratic runs (conditions supplied by the user) had been executed, the peak-tracking routine was automatically activated and performed. The identities of the components were traced as described above, based on area measurements at the two different wavelengths and the peak elution order. This has been found to provide a reliable method for peak tracking even at conditions of signal overlap. As described in the Introduction, the routine searches first for the pure peaks. Peaks not recognized as pure are then compared with the reference run. The run with the highest number of signals is automatically selected as the reference. Linear combinations of the non-assigned reference peaks are computed in order to detect the overlapping peaks and to identify properly the peaks in the experimental run. In Table I the results of the signal identification routine are reported. Upon its completion the program proceeds to the calculation of the optimization hypersurface.

The aim of this optimization software is to find the best chromatographic attribute, which is represented by the maximum value of the CRF_2. Furthermore, the optimization routine forces the experiments to step also into the region of the least available information, to characterize systematically the entire parameter space.

After the first four runs, the conditions which provide the highest value for the CRF_2 (calculated values for pumps B and D) were computed by OPTIM, and the result was automatically transferred to the control level of the data station in order to perform the next experiment. In addition to looking for the best conditions in the predefined space, this software also determined the point with the lowest density of information, *i.e.* the least density point of experiments. Consequently, after verification of the optimum, these conditions were executed. In this way, performing consec-

TABLE I

SIGNAL ASSIGNMENT AFTER EIGHT EXPERIMENTS WITH RUN NO. 3 AS REFERENCE RUN

mf is a membership function (see text).

Signal No.	Reference signal No.	Peak area		mf Value
		210 nm	230 nm	
1	1	458.89	243.86	0.843
2	2	220.20	123.22	0.844
3	3	660.77	361.63	0.844
4	4	312.76	170.06	0.844
5	5	554.82	299.24	0.844
6	6	80.41	42.59	0.845
7	7	82.20	46.72	0.833
8	8	494.00	280.08	0.845

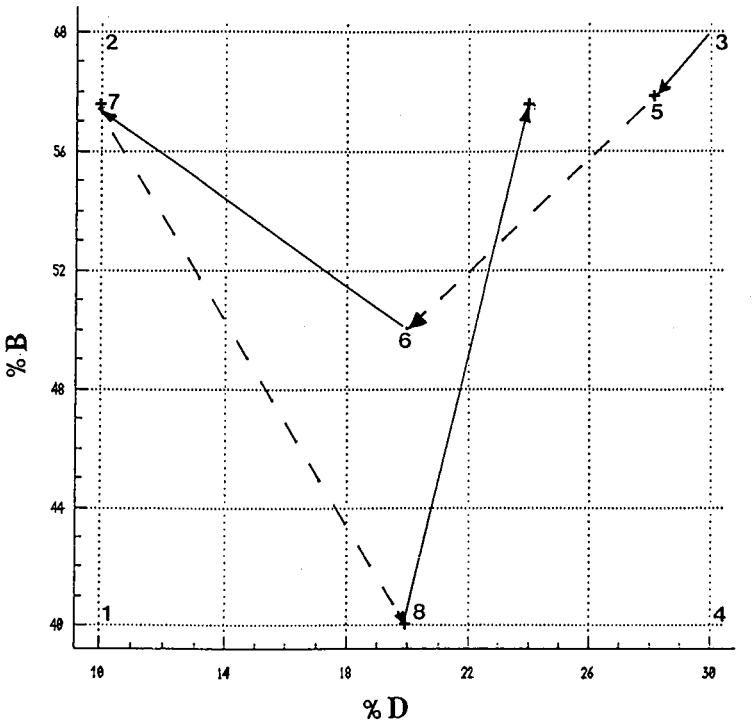

Fig. 1. Execution order of the eight optimized runs in the space defined with the percentage values for pumps B and D satisfying the conditions for a total flow for pumps A and B (A + B = 100%) and pumps C and D (C + D = 100%).

utively the best run and the experiment according to the least density of information, the program searches for a global and not for a local maximum.

Fig. 1 displays experimentally investigated points in order to visualize the order in which the experiments proceeded. As depicted in Fig. 1, after four experimental runs (labeled 1–4) experiment No. 5 was performed. This was carried out under the optimal conditions deduced from the initial four experiments. The new experimental point was used for the further optimization, but owing to the global scheme of this procedure the next chromatogram was performed under conditions corresponding to the least density point of experiments. The region of the least density information point, labeled 6, corresponds to the conditions B = 50%, D = 20%. The optimization routine then calculated new optimum conditions, marked as point 7, and the resulting experiment was executed. In a manner identical to that described above, the point with the least density information, No. 8, was performed and the refined optimum marked as + had a corresponding value of $CRF_2 = 0.9321$. To visualize more easily the development of the hypersurface, the numerical value of the CRF_2 which increases as the number of the performed experiments increases was shown in Fig. 2a, b, c and d with the hypersurfaces obtained after 4, 5, 6 and 8 performed experiments, respectively. The hypersurfaces are derived from the presently available experimentally obtained data points. Intermediate values are derived from the non-linear in-

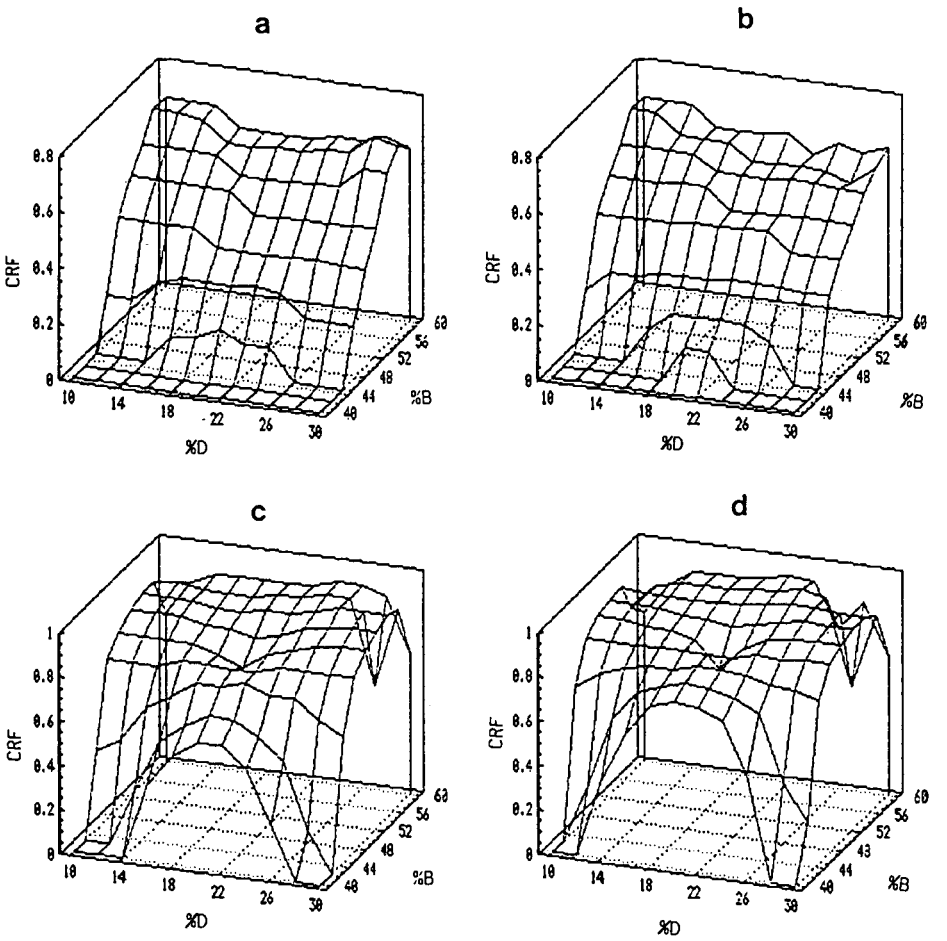

Fig. 2. Evolution of the hypersurface with increasing number of experimental points. (a) Surface derived from four experimental points; (b) five experiments; (c) six experiments; (d) eight experiments. *y*-Axis represents values for calculated CRF, while %D and %B are as in Fig. 1.

terpolation by means of the moving least-squares algorithm. It should be noted that for Fig. 2c and d, the CRF_2 axis is in the range 0–1, while for Fig. 2a and b it is from 0 to 0.8. The surface propagated to the region bounded with B = 48–60% after the five experiments. In Fig. 2c and d this increase in the CRF_2 is even more pronounced, and it is clear that the regions of previously low CRF_2 are becoming more important with increasing experimental knowledge (B = 40% and D in the region from 14–28%).

Once a proper separation quality has been accomplished, the next step is to evaluate the quantitative utilization of the procedure, *i.e.* the robustness of the chromatographic method. The robustness, being defined as a high plateau on the hypersurface, can be evaluated from the three-dimensional representation of the hypersurface. It should be emphasized that the first goal of this procedure was the optimization of the mobile phase composition with subsequent evaluation of the

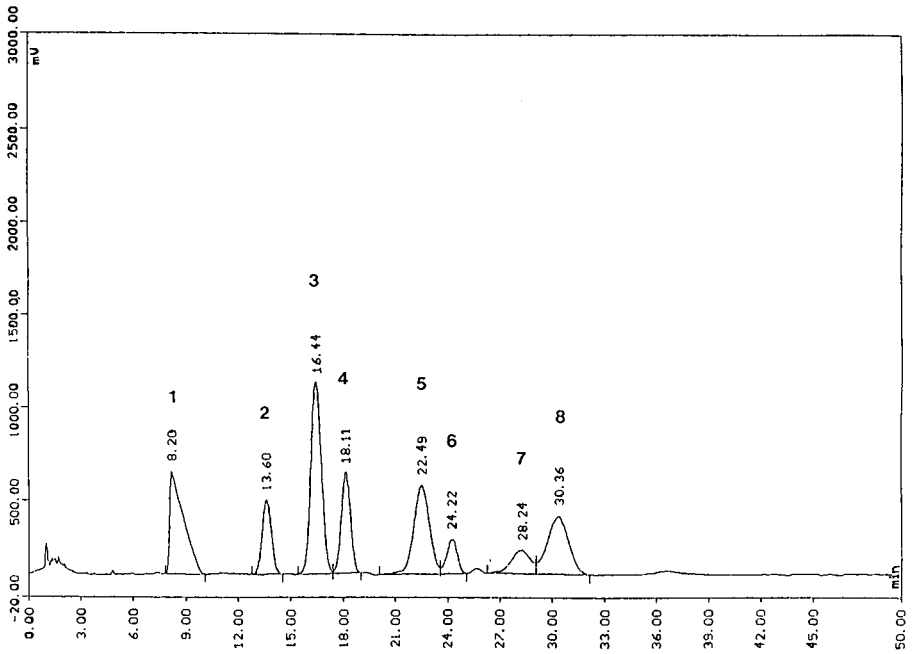

Fig. 3. Chromatogram acquired under the computed optimum mobile phase conditions: acetonitrile–TMBH–water (50.9:6.0:43.1). Total flow-rate was 2.0 ml/min. Column temperature: 353 K. Peaks: 1 = isocyclosporin A; 2 = cyclosporin C; 3 = cyclosporin B; 4 = cyclosporin L; 5 = cyclosporin A; 6 = dihydrocyclosporin A; 7 = cyclosporin T; 8 = cyclosporin G.

robustness of the newly developed chromatographic method. From Fig. 2d, it is possible to appraise the robustness of the developed method. The highest values for the CRF_2 and the best conditions concerning method robustness were limited to the region defined with the values for pump B from 52 to 60% and pump D from 16 to 26%. The experimental conditions with the highest CRF_2 were confirmed by a verification experiment under the proposed conditions (B = 57.5% and D = 24%) (Fig. 3). This demonstrates the interconnection between the quality of the chromatographic separation and the numerical value of the CRF_2. A chromatogram obtained under conditions yielding a $CRF_2 = 0.6$ is displayed in Fig. 4. It can be seen that the peak resolution is worse than that obtained under optimal conditions represented in Fig. 3. For $CRF_2 = 0$, the values for the pumps B and D were 40 and 30%, respectively. The chromatogram with overlapping peaks is presented in Fig. 5.

When the same experimental data (eight runs) were used as an input for the off-line version of the OPTIM program which includes time normalization, a new optimum was calculated at a mobile phase composition corresponding to B = 60% and D = 20%. The chromatogram in Fig. 6 clearly demonstrates that the selection of the quality criterion determines the definition of the optimum conditions. The inclusion of time normalization in the calculation of the CRF results in shorter analysis time, which may help to increase the productivity.

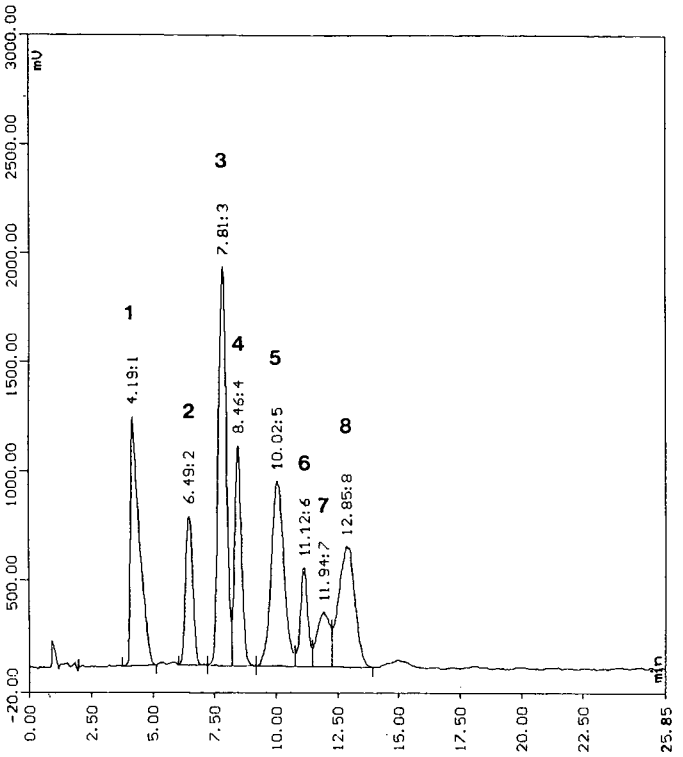

Fig. 4. Chromatogram obtained with the mobile phase conditions acetonitrile–TMBH–water (47.5:7.5:45.0). Other conditions as in Fig. 3. These conditions correspond to the point 3 in Fig. 1.

CONCLUSION

The optimization routine aimed to yield, within a precisely defined experimental framework, a preselected level of resolution for all pairs of components in a complex mixture. After an initial number of predefined experiments had been executed, the best mobile phase composition was ascertained using a strategy based on non-linear interpolation between measured retention data of the individual sample constituents and a subsequent computer construction of the optimization hypersurface. A software interface permits automatic transfer of the optimized values for the mobile phase composition to the pumps. Furthermore, to avoid reaching a local maximum, chromatographic experiments with solvent compositions representing the least density in space of variables were also performed systematically. An automated on-line identification of the solutes was accomplished using two-channel monitoring (UV absorbance at two different wavelengths) and using the recently introduced fuzzy peak-tracking approach. This peak-recognition routine was always active during the optimization process.

Robustness of the method can be judged from the optimization hypersurface. Owing to its empirical nature this approach can be applied to any chromatographic

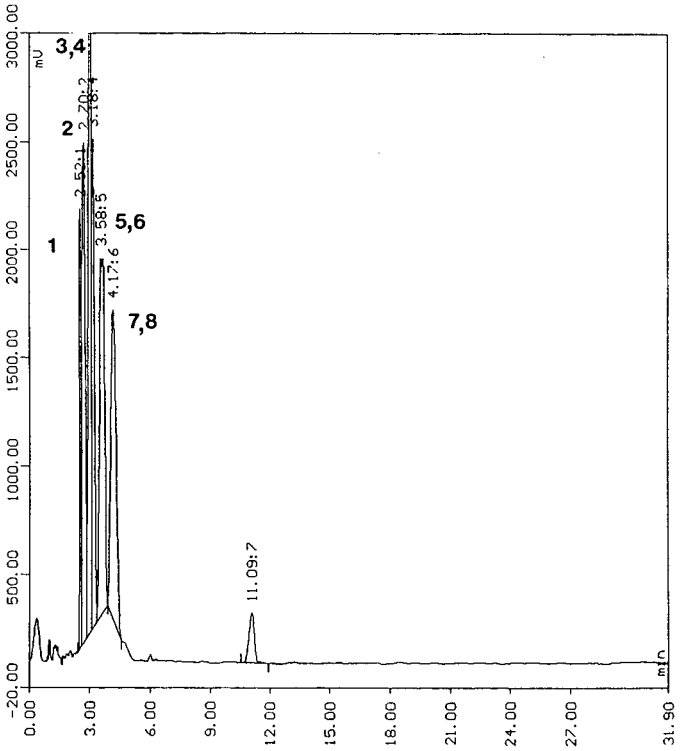

Fig. 5. Chromatogram obtained with the mobile phase conditions acetonitrile–TMBH–water (62.5:7.5:30.0). Other conditions as in Fig. 3. These conditions correspond to the point 4 in Fig. 1.

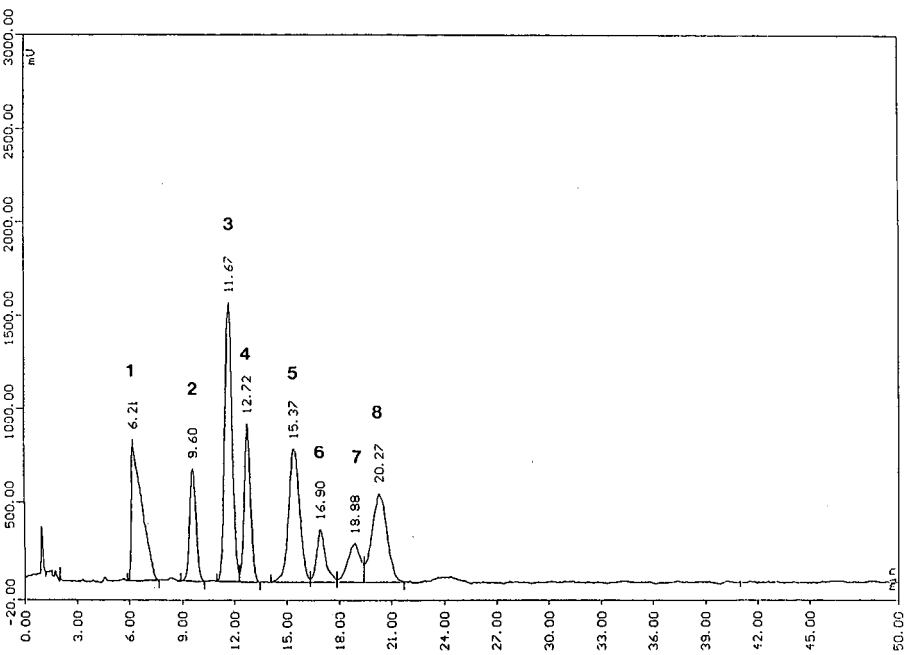

Fig. 6. Chromatogram obtained with the mobile phase conditions acetonitrile–TMBH–water (50.0:5.0:45.0). Other conditions as in Fig. 3.

separation process, even in cases where synergistic effects from separation variables are to be expected. The model is based on the real outcome of the experiment, and therefore makes it possible to obtain a more accurate interpretation on the robustness of the method. It is very flexible concerning the pick of the variables, since it does not rely on a mechanistic relationship between the chromatographic retention behavior of the sample constituents and variables, *e.g.* assuming linear or logarithmic dependence. This combination of the optimization routine, chromatographic data system and HPLC instrumentation offers a guide to higher productivity for analytical laboratories committed to HPLC method development and validation.

REFERENCES

1 P. J. Schoenmakers, *Optimization of Chromatographic Selectivity, (Journal of Chromatography Library*, Vol. 35), Elsevier, Amsterdam, 1986.
2 J. C. Berridge, *Techniques for the Automated Optimization of HPLC Separations*, Wiley, Chichester, 1985.
3 L. R. Snyder, J. L. Glajch and J. J. Kirkland, *Practical HPLC Method Development*, Wiley, New York, 1988.
4 E. P. Lankmayr, W. Wegscheider and K. W. Budna, *J. Liq. Chromatogr.*, 12 (1989) 35–58.
5 R. E. Kaiser, *Gas Chromatographie*, Geest & Portig, Leipzig, 1960, p. 33.
6 W. Wegscheider, E. P. Lankmayr and K. W. Budna, *Chromatographia*, 15 (1982) 498–504.
7 A. C. J. A. Drouen, H. A. H. Billiet and L. De Galan, *Anal. Chem.*, 57 (1985) 962–968.
8 M. Otto, W. Wegscheider and E. P. Lankmayr, *Anal. Chem.*, 60 (1988) 517–521.
9 E. P. Lankmayr, W. Wegscheider, J. Daniel-Ivad, I. Kolossvary, G. Csonka and M. Otto, *J. Chromatogr.*, 485 (1989) 557–567.
10 A. von Wartburg and R. Traber, in J. F. Borel (Editor), *Progress in Allergy*, Vol. 38, Karger, Basle, 1986, pp. 28–45.
11 M. Furlanut, M. Plebani and A. Burlina, *J. Liq. Chromatogr.*, 12 (1989) 1759–1789.

Journal of Chromatography, 550 (1991) 39–49
Elsevier Science Publishers B.V., Amsterdam

CHROMSYMP. 2232

Fast development of a robust high-performance liquid chromatographic method for *Ginkgo biloba* based on computer simulation

I. MOLNAR*
Institut für angewandte Chromatographie, Berlin (Germany)
and
K. H. GOBER and B. CHRIST
A. Nattermann & Cie GmbH, Köln (Germany)

ABSTRACT

Rapid development of robust and reliable high-performance liquid chromatographic methods for routine quality control of *Ginkgo biloba* is possible with computer simulation. The goal is to reduce method development time and to increase transparency of the complex composition of plant extracts. With only two basic experiments and a peak tracking process based on the total area ratio compared to the individual peak-area ratios a robust method with more than 50 simulated experiments was completed in 8 h. The best method has been verified experimentally. The correlation between the best simulated run and the final experiment was satisfactory.

INTRODUCTION

Extracts of the leaves of *Ginkgo biloba*, a traditional pharmaceutical product in Asiatic medicine, are used in the treatment of vascular diseases. It contains flavonoids, biflavonoids, ginkgolides (diterpenes) and the sesquiterpene bilobalid [1].

Today quality control requires modern analytical techniques to monitor all compounds in *Ginkgo biloba*. For this purpose we tried to isolate preparative amounts of some major components in *Ginkgo biloba* mixtures. In the first step a methanolic extract was separated on a Lobar RP-18 column. About 2% of the total mass of the plant extract was taken as a sharp fraction, and investigated further in a second step.

Due to differences in the origin of *Ginkgo biloba* analytical runs often reveal differences in composition. This is a time-consuming problem and often delays production of the drug. Peak overlaps especially, which depend on the amount of the organic modifier, often require a readjustment in the method for the actual sample by "trial and error".

On the other hand DryLab software, a small expert system for rapid and sys-

0021-9673/91/$03.50

tematic high-performance liquid chromatographic (HPLC) method development is able to generate a large number of data from only two sets of experiments [2]. The goal of this work was to save time, using computer simulation techniques for the rapid development of a robust HPLC separation method for the isolation of standard components from preparative fractions of *Ginkgo biloba* extracts.

EXPERIMENTAL

Equipment

The HPLC system used was a Merck-Hitachi LiChrograph with an L-4000 UV–VIS detector (Merck, Darmstadt, Germany). The dwell volume of the instrument was 5.4 ml. Chromatograms were monitored at a wavelength of 330 nm. The injection device was a Rheodyne 7125 (Cotati, CA, USA).

The software DryLab I/plus (isocratic version) and DryLab G/plus (gradient version) (LC Resources, Lafayette, CA, USA; in Europe: Molnar, Berlin, Germany) are written for use with IBM compatible personal computers and were installed on a Victor 286 with a 20-MB hard disk (Victor, Langen, Germany). Graphical simulations of chromatograms were predicted in *ca.* 0.1 s and were printed with "Grafplus" and "Graflasr" software (Jewell Technologies, Seattle, WA, USA) on a Kyocera F-800 laser printer.

Chromatographic conditions

The system was operated at 30°C or in some cases at 25°C. The column in use was packed with Nucleosil C_{18} (Macherey & Nagel, Düren, Germany) of 5 μm particle size, and of dimensions 250 × 4 mm I.D. The flow-rate was 0.8 ml/min and the column pressure was 12 MPa. The aqueous eluent A was HPLC-grade water, adjusted to pH 3.5 with concentrated ortho-phosphoric acid. The organic modifier B was HPLC-grade acetonitrile (Merck). Phosphoric acid (Merck) was of analytical grade.

Standard samples of *Ginkgo biloba* leaves were supplied by S. B. Kwon (China). A methanolic extract of the drug was separated on a Lobar RP-18 column (250 × 32 mm I.D.) (Merck). One sharp fraction, containing about 2% of the total mass of the sample extract, was especially difficult to separate. This fraction was used for computer-supported rapid method development. The injection volume was 20 μl of a 1 mg/ml solution of the fraction in methanol.

Method development with DryLab

In HPLC, computer-supported method development is becoming increasingly important [3–10]. DryLab is able to predict robust methods and conditions of equal band spacing, which are necessary for high-speed separations for small as well as for large molecules, such as ribosomal proteins [11,12]. It can generate new chromatograms under user-selected chromatographic conditions. For this purpose the software has to be supplied with two sets of experimental data.

All experimental parameters, such as dwell volume, column parameters, elution conditions, the number of components, their retention times and the peak areas of the reference run were entered into the program [3,4] (Tables I–III).

Method of peak tracking

Method development with DryLab was started using a previously developed method in isocratic mode with 27% B (Fig. 1). The separation, however, was not satisfactory, especially between the two last major peaks, which showed a strong overlap.

Next, two gradients were made from 5 to 100% B in 15 and 45 min, respectively. Both runs showed closely eluting peaks. Here we could only work with some of the major peaks when using DryLab I/plus and found an optimum at 29% B, a result which was within 2% of the routine method used previously. For the very close elution (Fig. 2) DryLab I/plus suggested less-steep gradients.

Consequently, two more gradients were run, each from 20 to 70% B, with a gradient run time (t_G) of 20 and 60 min, respectively (Fig. 3). Data from the integrator are listed in Table I.

Peak range

We first determined the range of interest in both chromatograms. In Fig. 3a, the

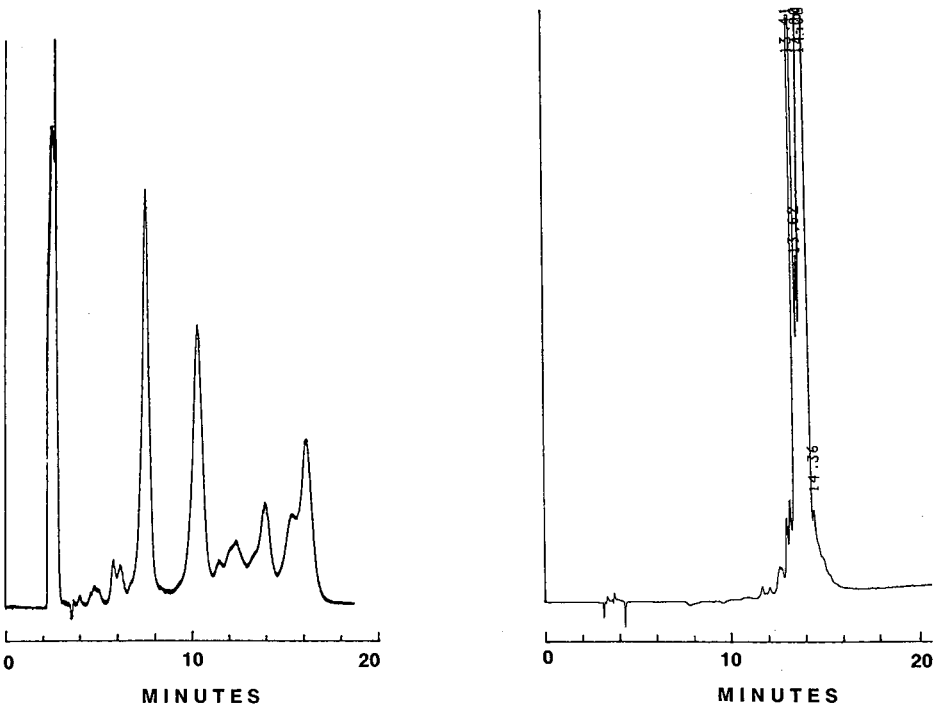

Fig. 1. Separation of a *Ginkgo biloba* extract. Elution conditions: column, Nucleosil C_{18}, 250 × 4 mm I.D., particle size, 7 μm; isocratic separation using 27% acetonitrile; temperature, 30°C. Other conditions as in Experimental.

Fig. 2. Separation of a *Ginkgo biloba* extract. Elution conditions: column, Nucleosil C_{18}, 250 × 4 mm I.D., particle size, 7 μm; gradient from 5 to 100% B in 15 min; temperature, 30°C. Other conditions as in Experimental.

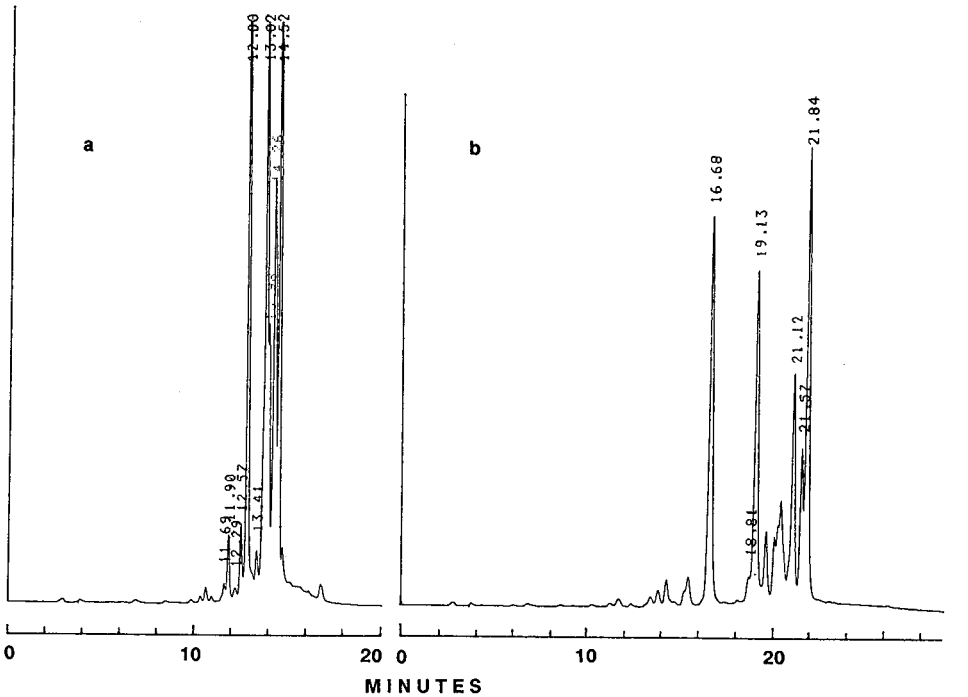

Fig. 3. Separation of a *Ginkgo biloba* extract. Elution conditions: column, Nucleosil C_{18}, 250 × 4 mm I.D., particle size, 7 μm; (a) gradient from 20 to 70% B in 20 min; (b) gradient from 20 to 70% B in 60 min; temperature, 30°C. Other conditions as in Experimental.

20-min run shows the range 8.56–16.80 min, and in Fig. 3b, the 60-min run range is 8.74–21.84 min. We observed a larger number of peaks in the 60-min run. By direct comparison we have the problem that in terms of the peak order the large peaks do not match.

Correspondence between components

The correspondence between components of the two runs had to be correctly established. The two chromatograms with their integration reports were compared as follows.

Determination of the reference run. By definition, the reference run contains the larger number of components. Using DryLab G/plus for gradient elution, the reference run is normally the one with the smaller slope, or larger gradient run time, t_G.

Trial run. We called the other chromatogram with the smaller number of peaks the trial run.

Peak assignment

This process is also called peak tracking [13,14], as our goal was to find each peak in both chromatograms. As the position of a component was changing, often unpredictably, with changing elution conditions, peak tracking was necessary for the establishment of the identity of the components.

TABLE I

INTEGRATION REPORT FOR THE 20- AND 60-min RUNS

Peak No.	Reference run (60 min)			Trial run (20 min)			$R_{i,1}$[c]
	t_R (min)	Estimated resolution values[a]	Peak area[b]	t_R (min)	Estimated resolution values[a]	Peak area[b]	
01	8.74	bl	7	8.56	bl	7	1.00
02	10.42	bl	8	9.94	bl	9	1.13
03	11.37	bl	12	10.42	bl	14	1.17
04	11.84	bl	30	10.72	bl	33	1.10
05	12.52	bl	10	11.01	bl	15	1.50
06	13.56	bl	38	11.69	0.5	51	1.34
07	13.97	1.0	52	11.90	1.1	137	2.63
08	14.40	bl	96	12.29	0.9	44	0.46
09	15.57	bl	122	12.57	0.9	156	1.28
10	16.68	bl	1112	12.88	0.8	1199	1.08
11	18.24	bl	25	13.41	0.7	127	5.08
12	18.81	0.5	79	13.82	0.5	1806	22.86
13	19.13	1.0	931	13.98	0.9	80	0.09
14	19.70	1.4	220	14.26	0.8	1015	4.61
15	20.16	0.4	149	14.52	0.6	1629	10.93
16	20.34	0.3	143	14.76	0.6	17	0.12
17	20.48	1.2	364	15.13	0.5	11	0.03
18	21.12	1.3	658	16.17	bl	4	0.01
19	21.57	0.8	352	16.80	bl	330	0.94
20	21.84	bl[d]	1207				
21	23.09	bl[d]	6				
22	26.25		3				
Total			5624			6668	1.19

[a] Resolution values are only roughly estimated.
[b] Peak-area values are given in thousands of integration units.
[c] $R_{i,1} = A_{T,i}/A_{R,i}$.
[d] bl = Baseline-separated.

RESULTS AND DISCUSSION

Peak tracking

There are 22 peaks in the 60-min run, but only 19 peaks in the 20-min run. The sum of the peak areas is, as expected with similar sample injection amounts, comparable in size. The ratio of the total peak areas is 6684:5624 = 1.19. In ideal injection and integration conditions both total peak areas should be about equal [6].

When properly assigned, individual peak-area ratios should have the same value as the total peak-area ratio. As we can observe in our case, not all peak-area ratios correspond to this number, which turned out to be 1.19. There are some strong deviations, such as at reference peak No. 7 and also at the peak group 11–19.

Resolution values can be helpful if the chromatogram is not at hand. We can see that for peaks which are baseline-separated (bl), the peak-area ratio is close to the total area ratio. Such peaks are the so-called "well behaving" ones. In overlapping

TABLE II

PEAK TRACKING PROCESS

Integration report, uncorrected						Peak tracking after corrections					
Peak No.	60 min		20 min		R_i	Peak No.	60 min		20 min		R_i
	t_R	Area	t_R	Area			t_R	Area	t_R	Area	
01	8.74	7.00	8.56	7.00	1.00	01	8.74	7.00	8.56	7.00	1.00
02	10.42	8.00	9.94	9.00	1.13	02	10.42	8.00	9.94	9.00	1.13
03	11.37	12.00	10.42	14.00	1.17	03	11.37	12.00	10.42	14.00	1.17
04	11.84	30.00	10.72	33.00	1.10	04	11.84	30.00	10.72	33.00	1.10
05	12.52	10.00	11.01	15.00	1.50	05	12.52	10.00	11.01	15.00	1.50
06	13.56	38.00	11.69	51.00	1.34	06	13.56	38.00	11.69	51.00	1.34
07	13.97	52.00	11.90	137.00	2.63	07	13.97	52.00	11.90	137.00	1.22[a]
08	14.40	96.00	12.29	44.00	0.46	08	14.40	96.00	12.29	44.00	1.22[a]
09	15.57	122.00	12.57	156.00	1.28	09	15.57	122.00	12.57	156.00	1.28
10	16.68	1112.00	12.88	1199.00	1.08	10	16.68	1112.00	12.88	1199.00	1.08
11	18.24	25.00	13.41	127.00	5.08	11	18.24	25.00	13.41	30.53	1.22
12	18.81	79.00	13.82	1806.00	22.86	12	18.81	79.00	13.41	96.47	1.22
13	19.13	931.00	13.98	80.00	0.09	13	19.13	931.00	13.82	1806.00	1.31[b]
14	19.70	220.00	14.26	1015.00	4.61	14	19.70	220.00	13.98	80.00	1.31[b]
15	20.16	149.00	14.52	1629.00	10.93	15	20.16	149.00			1.31[b]
16	20.34	143.00	14.76	17.00	0.12	16	20.34	143.00			1.31[b]
17	20.48	364.00	15.13	11.00	0.03	17	20.48	364.00			0.99[c]
18	21.12	658.00	16.17	4.00	0.01	18	21.12	658.00	14.26	1015.00	0.99[c]
19	21.57	352.00	16.80	330.00	0.94	19	21.57	352.00			1.04[d]
20	21.84	1207.00				20	21.84	1207.00	14.52	1629.00	1.04[d]
21	23.09	6.00				21	23.09	6.00	14.76	17.00	−[e]
22	26.25	3.00				22	26.25	3.00	15.13	11.00	−[e]
23						23		0.01	16.17	4.00	−[e]
24						24		0.01	16.80	330.00	
Sum		5624.00		6684.00	1.19			5624.00		6684.00	1.19
Mean (1–24)					3.02						1.19
S.D. (1–24)					5.46						0.14

[a] Bad integration causes R_i of 2.63 and 0.46. The mean value of both peak areas in both runs gives a reasonable R_i of 1.22 for both peak pairs No. 7 and 8, a value which is fairly close to the total ratio of $R_i = 1.19$.

[b] Peaks 12 and 13 of the 20-min run correspond obviously with peaks 13, 14, 15 and 16 of the 60-min run. The group ratio is 1.31, which is fairly close to 1.19.

[c] Peaks 17 and 18 of the 60-min run join to one peak in the 20-min run. The new ratio after correction is 0.99, which is fine.

[d] Similar case to note *c*. The corrected ratio is 1.04.

[e] These peaks were neglected.

groups, however, there are some "not well behaving" bands, especially in the trial (faster), but in many cases also in the reference run.

Taking a look at both chromatograms, we can distinguish five large peaks, having a distinct size ratio. On the basis of their shape and peak area we tried to match them. One of these peaks is reference peak No. 10. It has a peak-area ratio of 1.08, which is close to the statistically robust total ratio of 1.19. Other large peaks in the 20-min run are overlapping with other peaks and therefore have larger peak areas,

TABLE III

DRYLAB G, PART I INPUT VALUES

System variables: dwell volume, 5.40 ml; column length, 25.00 cm; column diameter, 0.40 cm; flow-rate, 0.80 ml/min; starting %B, 20.0; final %B, 70.0; gradient time run 1, 20.0 min; gradient time run 2, 60.0 min. Default N value for R_s calculations, 10 000. Number of bands = 13.

Band No.	Retention time (min)		Area
	Run 1	Run 2	
1	12.57	15.57	122.00
2	12.88	16.68	1112.00
3	13.41	18.24	25.00
4	13.41	18.81	79.00
5	13.82	19.13	931.00
6	13.82	19.70	220.00
7	13.82	20.16	149.00
8	13.98	20.34	143.00
9	14.26	20.48	364.00
10	14.26	21.12	658.00
11	14.52	21.57	352.00
12	14.52	21.84	1207.00
13	14.76	23.09	6.00

as expected. We have to deconvolute such peaks and this is shown in Table II. For example, it is obvious that peaks 13, 14, 15 and 16 of the reference run correspond with peak Nos. 12 and 13 of the trial run. Dividing the sum of the trial peaks 12 + 13 (1808 + 80 = 1888) by the sum of reference peaks 13–16 (931 + 220 + 149 + 143 = 1443), we have a ratio for all peaks of 1.31.

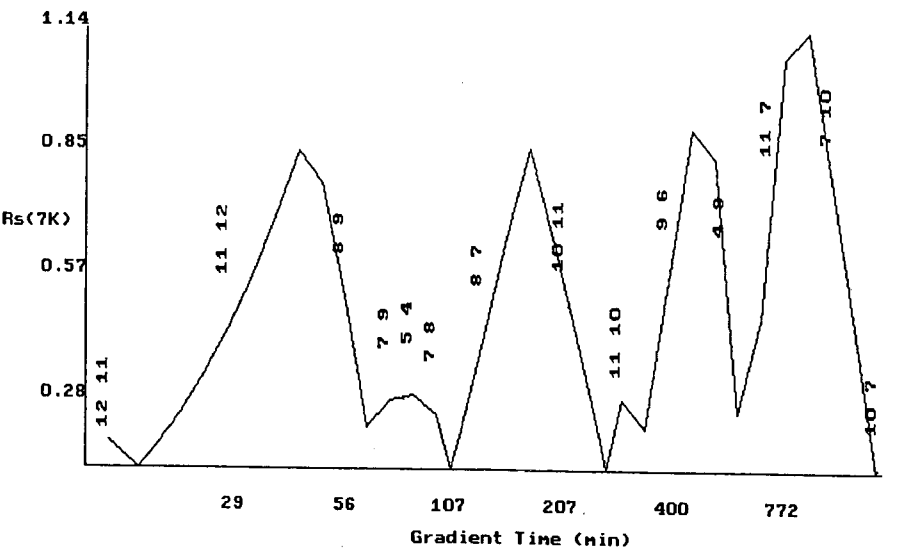

Fig. 4. Relative resolution map for the *Ginkgo biloba* sample by Dry Lab G/plus (gradient from 20 to 70% B). The highest resolution can be observed at 50 min gradient time. Other conditions as in Experimental.

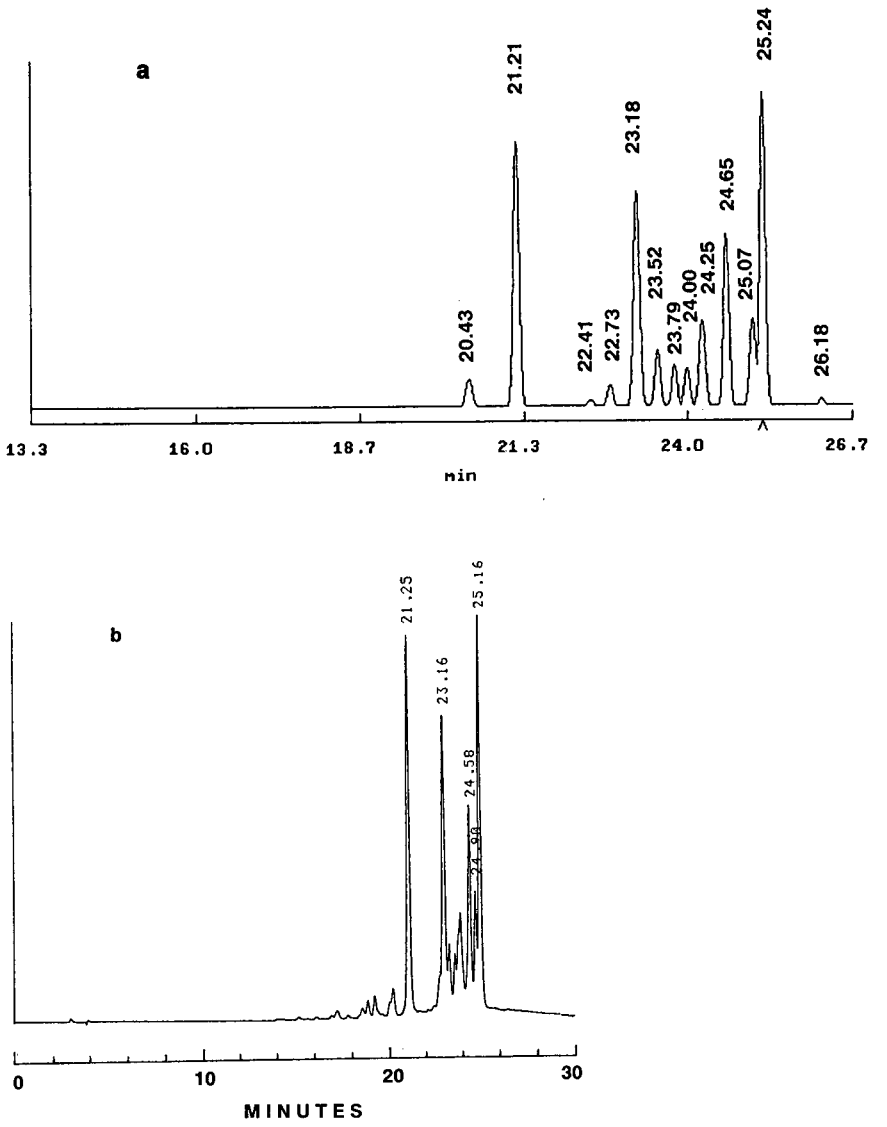

Fig. 5. Optimum gradient conditions from 15 to 40% B in 25 min by (a) simulation by DryLab G/plus and (b) the corresponding experiment. Other conditions as in Experimental.

One possible measure of the peak match is the mean value and the standard deviation of the individual peak-area ratios compared to the ratio of the sums of all peak areas [6]. As we can see in Table II, the correction of the peak identities brings the mean peak-area ratio very close to the ratio of the sums of all peak areas. As long as the uncorrected mean peak-area ratio is 3.02 with a standard deviation of 5.46, after peak tracking we have a mean peak-area ratio of 1.19, the same value as the total area ratio, 1.19. The standard deviation is now decreased to 0.14 (Table II).

TABLE IV

COMPARISON OF PREDICTED AND EXPERIMENTALLY FOUND RETENTION TIMES OF *GINKGO BILOBA* SAMPLE IN GRADIENT ELUTION FROM 15 TO 40% ACETONITRILE

Other conditions as in Fig. 1a and b.

No.	Retention time (min)		
	Predicted	Experimental	Difference
1	20.43	20.41	0.02
2	21.21	21.25	0.04
3	22.41	22.30	0.11
4	22.73	22.61	0.12
5	23.18	23.16	0.02
6	23.52	23.45	0.07
7	23.79	23.71	0.08
8	24.00	24.06	0.06
9	24.25	24.06	0.19
10	24.65	24.58	0.07
11	25.07	24.90	0.17
12	25.24	25.16	0.08
13	26.18	26.65	0.47

Average deviation < 0.4%

It has to be mentioned at this point that the quality of integration is essential for a reliable peak tracking process. The chromatographer has to be in the position to be able to change any wrong integration and to repeat integration with new data as often as necessary. This is an easy job using integration software programs such as Nelson, BarSpec's Chrom-A-Set, Maxima and many others, which are now commercially available. Stand-alone type integrators should set a mark at the start and at the end of integration, and they also should be in position to re-integrate the same data set under different baseline settings.

Simulation of chromatograms with DryLab G/plus

Following the peak assignment process, all necessary data were entered into DryLab G/plus (Table III). In accordance with the fact that the HPLC system had a low-pressure gradient mixer, an estimated dwell volume of 5.4 ml was taken.

The range of the components has been reduced to the thirteen most important peaks. For the simulation of gradient runs we started with a consideration of the relative resolution map (RRM) (Fig. 4). According to the RRM, an optimum is at a run of 50 min duration, going from 20 to 70% B. This run, however, takes rather a long time.

Another gradient is from 15 to 40% B in 25 min; this run is complete after 25 min (Fig. 5).

Reliability of the predictions

The precision of the predictions of DryLab G/plus with two other sets of samples (five benzoic acid esters and thirty ribosomal proteins) showed a coefficient of

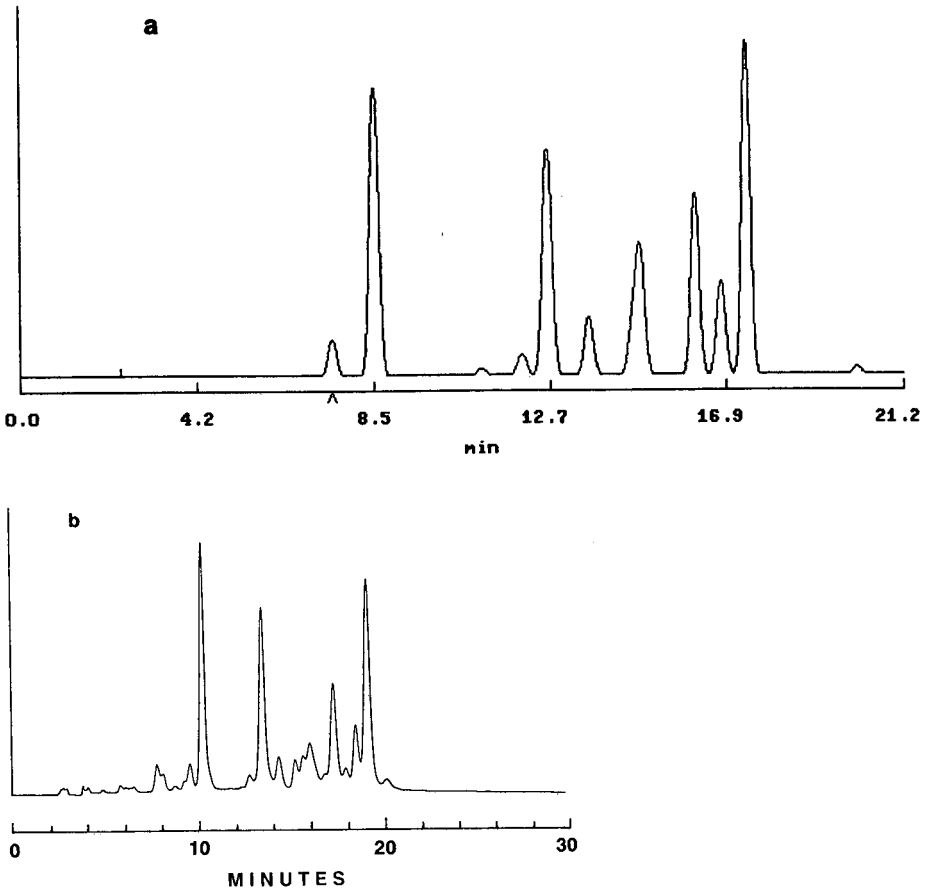

Fig. 6. Optimum gradient conditions from 25 to 30% B in 10 min by (a) simulation by DryLab G/plus (30°C) and (b) the corresponding experiment, at 25°C. Other conditions as in Experimental.

variation of less than 1% [6,11]. We expected, therefore, similar precision in the case of the *Ginkgo biloba* sample between predicted and experimentally verified values. The retention data shown in Fig. 5a were tested for correlation with the experimental values (Fig. 5b). As we can see in Table IV the reliability of the prediction is satisfactory: the average deviation between prediction and experiment is less than 0.4%.

After trying several gradients, we decided on a final run of higher peak resolution, as shown in Fig. 6a. The conditions were experimentally verified, resulting in the run shown in Fig. 6b. The correlation is also sufficient, although for better resolution the temperature in Fig. 6b was reduced from 30°C to 25°C, making the experimental retention times longer than predicted.

CONCLUSIONS

We have shown the application of computer-aided HPLC method optimization in the separation of a natural product mixture. After two initial gradient elution runs,

peaks were matched between runs using an area-ratio matching technique. Good integration software is necessary to obtain the correct peak areas. The matched peaks were input into the optimization software and the best run conditions were found using computer-based simulation tools. The predicted optimum compared well with an experimental run under the predicted conditions, with an average deviation in retention times of less than 1%. The total development time of about 1 day saved considerable time over traditional trial-and-error optimization techniques.

REFERENCES

1 H. Wagner, S. Bladt, U. Hartman, A. Daily and W. Berkulin, *Dtsch. Apoth.-Ztg.*, 129 (1989) 2421.
2 L. R. Snyder, J. W. Dolan and M. P. Rigney, *LC · GC Mag.*, 4 (1986) 921.
3 L. R. Snyder, J. W. Dolan and D. C. Lommen, *J. Chromatogr.*, 485 (1989) 65.
4 J. W. Dolan, D. C. Lommen and L. R. Snyder, *J. Chromatogr.*, 485 (1989) 91.
5 J. Schmidt, *J. Chromatogr.*, 485 (1989) 421.
6 I. Molnar, R. Boysen and P. Jekow, *J. Chromatogr.*, 485 (1989) 569.
7 R. G. Lehman and J. R. Miller, *J. Chromatogr.*, 485 (1989) 581.
8 J. Fulper, *J. Chromatogr.*, 485 (1989) 597.
9 D. J. Thompson and W. D. Ellenson, *J. Chromatogr.*, 485 (1989) 607.
10 J. D. Stuart, D. D. Lisi and L. R. Snyder, *J. Chromatogr.*, 485 (1989) 657.
11 B. F. D. Ghrist, B. S. Cooperman and L. R. Snyder, in F. E. Regnier and K. M. Gooding (Editors), *HPLC of Biological Macromolecules*, Marcel Dekker, New York, 1990, p. 403.
12 I. Molnar, R. Boysen and V. Erdmann, *Chromatographia*, 28 (1989) 39.
13 E. P. Lankmayr, W. Wegscheider, J. C. Gfeller, N. M. Djordjevic and B. Schreiber, *J. Chromatogr.*, 485 (1989) 183.
14 E. P. Lankmayr, W. Wegscheider and J. Daniel-Ivad, *J. Chromatogr.*, 485 (1989) 557.

Journal of Chromatography, 550 (1991) 51–69
Elsevier Science Publishers B.V., Amsterdam

CHROMSYMP. 2256

Resolution enhancement of chromatographic data

Considerations in achieving super-resolution with the constrained iterative relaxation method

MARK R. SCHURE

Computer Applications Research, Rohm and Haas Company, 727 Norristown Road, Spring House, PA 19477 (USA)

ABSTRACT

The consequences of numerical resolution enhancement in column chromatography are examined with respect to the increase in the number of peaks that will become recognizable for analysis as deconvolution removes peak fusion and artificially extends the peak capacity of the chromatographic system. Using computer-generated chromatograms and numerically deconvolving with the constrained iterative relaxation method (CIRM), the results suggest that under ideal conditions deconvolution lowers the average resolution necessary for singlet peak discrimination to *ca.* 0.352. This decreased resolution limit allows the number of recognizable peaks, for fairly saturated synthetic chromatograms, to increase by *ca.* 50% when the ratio of the true number of components to the peak capacity equals 1.5.

INTRODUCTION

One of the most important advancements in separation science over the last two decades has been the development and application of high-resolution chromatographic methods aimed at resolving the components of complex mixtures of biological and environmental origin. Both capillary gas chromatography (GC) and high-performance liquid chromatography (HPLC) now have the performance to achieve high-resolution separations of complex samples that a short time ago would have seemed beyond the reaches of these techniques. The requirements for stringent quality control in biotechnology, controlled substance testing, forensic applications and environmental monitoring have placed even more demands on these techniques and consequently the use of very high-resolution columns, which are capable of generating over 10^5 theoretical plates, is expanding rapidly.

Although column technology will no doubt evolve in all application areas, there are a few applications where column technology has yet to make baseline separations a commonplace occurrence. In these applications, the components of the mixture often elute at such close retention times that individual separation and determination are difficult; however, in some instances the analyst can trap the peak and use another column of different selectivity. Alternatively, the operating conditions can be changed

0021-9673/91/$03.50

to run the experiment under the highest possible resolution (by changing the column temperature and flow velocity) or to use a capillary column instead of a packed column. When available, a multi-channel detector such as a mass spectrometer (GC) or UV array detector (LC) can be used to aid in the analysis of a mixture when peaks are not well resolved. This scenario, of course, requires that the analyst has recognized that peak fusion is present and that the proper instrumentation is available for this type of analysis. It would be most convenient under these situations if the analyst could somehow increase the resolution of the column to look for other closely eluting peaks. This desire for increased resolution will probably continue until column efficiencies are high enough to resolve every component or until resolution enhancement through multi-channel detectors and computer methods is routinely available.

A number of recent driving forces have created a situation where certain aspects of numerical resolution enhancement need to be re-examined, especially with regard to the single-channel detector most commonly used in chromatographic systems. These driving forces include (1) the realization through chromatographic theory [1–13] that for samples of complex origin the resolving power needed for baseline separations has been previously underestimated, (2) the need for higher resolving power in applications where components of minor concentration may play a major role in determining some property of the sample, (3) the recent production of numerical algorithms which are capable of high-resolution deconvolution and are now, owing to the increased computational performance of laboratory computers, feasible for use in laboratory applications and (4) the renewed interest in the flame ionization detector for HPLC, an inherently single-channel detector. Not only does high resolution help the analyst in the proper assessment of peak purity, important when fractions are collected for chemical analysis or when a "hyphenated" method of analysis is used; maximum resolution is of the utmost importance when automated method development is used.

This paper addresses the question of the extent to which in theory numerical deconvolution can offer quantitative resolution enhancement for complex chromatograms. Towards this goal, one of the best numerical methods of deconvolution, namely the constrained iterative relaxation method (CIRM), is used here to examine the limit of resolution enhancement. In addition, some aspects of deconvolution implementation are discussed.

THEORY

Potential benefits of deconvolution

The broadening of chromatographic peaks, as is well known and as demonstrated in Fig. 1, causes the recognizable loss of individual components through the fusing together of closely spaced peaks. In Fig. 1, the retention time and amplitude sequence is constant between synthetic chromatograms. Only σ, the standard deviation of the Gaussian peak shapes, is varied between the chromatograms. Unless shoulders or inflection points are found in the peak shape, it is often impossible for the analyst with a single-channel detector to determine if the peak is pure or composed of two or more components. The mathematical description of this loss of identity of pure peaks was recently described [1–13] for complex chromatograms possessing random retention times (additional assumptions of this approach are contained in the references). In this

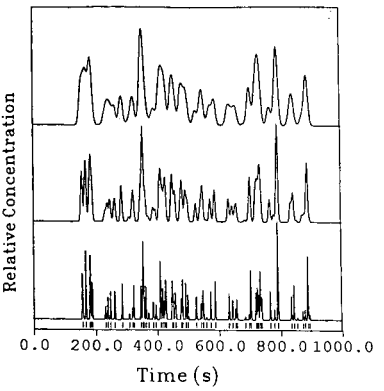

Fig. 1. Synthetic chromatograms of 80 Gaussian peaks generated with identical Poisson-distributed retention times, uniformly-distributed random peak heights (between 0.05 and 1), constant σ and no noise. Bottom, $\sigma = 1$ s; middle, $\sigma = 3$ s; top, $\sigma = 6$ s. Retention times are indicated by the bars below the bottom chromatogram.

theory the number of recognizable peaks, p, is related to the number of true components, m, via

$$p = m\exp\left(-\frac{m}{n_c}\right) \tag{1}$$

where n_c is the peak capacity [14], which is defined as the maximum number of component peaks which can be uniformly packed into a chromatographic elution profile at a stated resolution. The peak capacity, n_c, for situations such as gradient elution chromatography and programmed-temperature gas chromatography, where the peak variance, σ^2, is considered to be constant throughout the chromatographic elution profile, is given by [2,14]

$$n_c = \frac{t_{max} - t_0}{4\sigma R_s^{\ddagger}} \tag{2}$$

where t_{max} and t_0 denote the time range of the elution profile and $R_s^{\ddagger}$ is the stated critical resolution, which has been estimated for this statistical model to be 0.5 [3,11]. Other studies have suggested alternative values for the critical resolution, *e.g.*, 0.8 [9] and 0.71 [10]. For isocratic LC or constant-temperature GC, where it is assumed that the peak variance is not constant but rather increases with time [14],

$$n_c = \frac{\sqrt{N_{av}}}{4R_s^{\ddagger}} \ln\left(\frac{t_{max}}{t_0}\right) \tag{3}$$

where N_{av} is the average number of theoretical plates.

Eqns. 1–3 allow the extent of deconvolution to be related to the number of observable peaks by the realization that deconvolution increases the peak capacity by synthetically lowering $R_s^{\ddagger}$. An expression is now obtained whereby the number of

peaks visible after deconvolution of the chromatogram, p_d, is ratioed to the number of peaks visible in the native chromatogram, p. From eqn. 1:

$$\frac{p_d}{p} = \frac{m \exp\left(-\frac{mR_s^d}{n_c'}\right)}{m \exp\left(-\frac{mR_s^\ddagger}{n_c'}\right)} \tag{4}$$

where R_s^d is the critical resolution of the deconvolution technique and n_c' is the peak capacity with unit resolution, *i.e.*, $n_c' = n_c R_s$. Our use of the term resolution here is in keeping with the standard definition of resolution, $R_s = \Delta t/4\sigma$, where Δt is the difference in retention time, t_r, between two peaks whose Gaussian standard deviations are both equal to σ. Rearranging eqn. 4 yields

$$\frac{p_d}{p} = \exp\left[\frac{m}{n_c} \cdot \left(1 - \frac{R_s^d}{R_s^\ddagger}\right)\right] \tag{5}$$

where n_c is the peak capacity prior to deconvolution. Eqn. 5 gives the enhancement factor in the number of peaks that are ideally obtained by deconvolving the chromatogram as viewed by the ratio p_d/p. As can be seen from eqn. 5, this enhancement becomes greater as the ratio m/n_c increases. This ratio, m/n_c, also known as the saturation factor, α, is a measure of how crowded a chromatogram is; the efficacy of deconvolution is thus seen to increase for more crowded chromatograms. An example of the value of deconvolution is suggested by considering a chromatogram with $\alpha = 1.00$ and $R_s^d = 0.35$. We choose $R_s^\ddagger$ here to be equal to 0.5 on a purely empirical basis. Under these conditions, *ca.* 1.35 times more peaks, or an increase of 35% in the number of observable peaks, will be obtained. This suggests that a distinct beneficial gain could be obtained by considering deconvolution in the analysis of chromatograms with crowded peaks. Evaluation of eqn. 5 with a variety of α values is shown in Fig. 2. As can be seen, medium α chromatograms are predicted to benefit

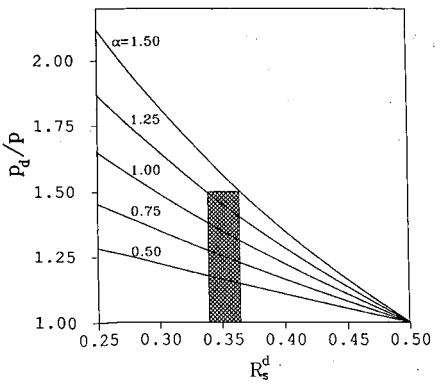

Fig. 2. The ratio p/p_d as a function of R_s^d at various saturation values, α, from eqn. 5. The critical resolution, $R_s^\ddagger$, is taken to be 0.5. The shaded bar is explained under Results and Discussion.

from deconvolution, although to a lesser extent than large α chromatograms. For relatively uncrowded chromatograms (small α), where the number of components is low or the peak capacity is high, deconvolution is known to allow better peak quantification by defusing overlapped peaks; this role of chromatographic deconvolution has been reported many times (*e.g.*, [15–20]). In addition, deconvolution has long been used in size-exclusion chromatography (SEC) where the inherently low resolution of the technique is commonly augmented by resolution enhancement [21]. In this paper, our aim is to examine super-resolution, a term commonly used in signal processing to denote the deconvolution or estimation of signals below the physically imposed broadening limit. For chromatography, the definition is broad but has recently been clarified to include the resolution of peaks separated by less than 2σ in time or alternatively with R_s less than 0.5 [22].

Problem formulation

Consider a series of Gaussian peaks composing a chromatogram of m components eluting along the time axis t so that

$$F(t) = \sum_{j=1}^{m} \frac{B_j}{\sqrt{2\pi}\sigma_j} \exp\left[\frac{-(t - t'_j)^2}{2\sigma_j^2}\right] \tag{6}$$

where $F(t)$ is the observed detector response at time t and B_j is the detector response factor of each component j with retention time t'_j and variance σ_j^2. The variance is expressed here in units of (time)^2 and the detector response factor is normalized so that $\int_0^\infty F(t)\,dt = B_j$ for the elution of the pure jth component. It is assumed here that the detector response, $F(t)$, is the linear combination of amplitudes from each component, which is an excellent assumption for detectors such as the conventional UV detector used in HPLC. The peak variance, σ_j^2, is the result of ideal intra- and extra-column broadening processes. Initially, the sample band is introduced into the column as a narrow plug which very nearly approaches a delta function, $\delta(t)$, compared with the width of a zone at the detector. Using previously developed theory [23,24], elution can be modeled as a convolution process. For ideal one-component elution with Gaussian broadening,

$$F(t) = \int_{-\infty}^{\infty} G(t - t')\delta(t)dt' \tag{7}$$

where G is the broadening operator, normalized so that eqn. 7 is independent of the measurement space, and t' is an auxiliary variable. A shortened version of eqn. 7 is often used [25,26]:

$$F(t) = G(t) * \delta(t) \tag{8}$$

where the $*$ operator denotes convolution. Using the well known commutative property of convolution [25,26]:

$$\int_{-\infty}^{\infty} G(t-t')W(t')\mathrm{d}t' = \int_{-\infty}^{\infty} G(t')W(t-t')\mathrm{d}t' \tag{9}$$

where W is some function operated on by the broadening operator, eqn. 7 can now be expressed as

$$F(t) = \int_{-\infty}^{\infty} G(t')\delta(t-t')\mathrm{d}t' \tag{10}$$

Physically, under the most ideal circumstances, this representation allows G to be a pure band broadening operator and the delta function now represents the delay time invoked by retention of the solute. Hence t' is identified as the retention time, t_r. If a mathematical inversion process were known so that given $F(t)$ and the functional form of G, t' could be determined with exact accuracy, then chromatography could be performed where all peaks in a chromatogram, regardless of the degree of fusion, could be recognized and quantified. Owing to the ill-conditioned nature of the problem, this is not possible [22]. If, in principle, eqn. 10 could be exactly solved then R_s^d would be zero because this situation corresponds to a zero critical resolution and eqn. 5 would ideally give $p_d/p = \exp(m/n_c)$, the maximum amount of resolution enhancement. This is not currently possible, and implies, in the discrete equation analogue of eqn. 10, an infinite sampling rate because the $\delta(t-t')$ term would have to lie exactly at the retention time of the peak. The presence of noise also foils this scheme. Using approximations instead of exact solutions for eqn. 10 can yield useful information if the $\delta(t-t')$ term is replaced with the function $W(t-t')$, which will now be defined as a function resembling a δ function but with finite width. Utilizing approximate solutions of eqn. 10 to solve for $W(t-t')$, as will be shown in the Results section, can give very useful information.

Numerical methodology

Although a host of numerical methods have been utilized for chromatographic and spectroscopic deconvolution, including those based on Fourier transform [15,16], least-squares solution [20], Kalman filters [27], singular value decomposition [28,29], maximum entropy methods [29], constrained iterative relaxation methods [19,30–34] and mixtures of these methods [29], a common theme that has emerged is that each method has its own advantages and disadvantages. For instance, Fourier transform methods, although fast and simple to implement, offer for most studies only a small improvement in resolution. Alternatively, the maximum entropy method (MEM) and the constrained iterative relaxation method (CIRM) offer the possibility of high deconvolution power while maintaining a reasonable baseline and peak integrity at the expense of increased computer time and increased implementation complexity. For the CIRM, high-resolution deconvolution is accomplished because the constraints of positivity and maximum value allow frequency extrapolation to occur [34], *i.e.*, the power spectral density function present in the native signal can be moved into a higher frequency domain without spurious peak generation or distortion under the best conditions. The degree to which frequency extrapolation can take place ultimately limits the minimum value that σ_d^2, the variance of the deconvolved peak, can obtain under reasonable fidelity. Fourier transform methods do not inherently allow

frequency extrapolation to occur unless constraints, such as non-negativity of solution, are combined with the method [18,35].

We now focus on the CIRM because it will be used in this paper for deconvolving synthetic chromatograms. This method is performed on a chromatogram by applying the discrete point formula:

$$W^{(k+1)}(t_i) = W^{(k)}(t_i) + r\{W^{(k)}(t_i)\}\{F(t_i) - [G * W^{(k)}]|_{t_i}\} \tag{11}$$

where the superscript denotes the iteration number, the subscript denotes the position in each vector corresponding to a unique time value and the term $r\{W^{(k)}(t_i)\}$ is the relaxation function [30]. Prior to applying this algorithm, $F(t_i)$ is scaled to between 0 and 1 and the initial values of $W^{(0)}(t_i)$ are set equal to $F(t_i)$. The functional form of the relaxation function used here is

$$r\{W^{(k)}(t_i)\} = r_0 W^{(k)}(t_i)[1 - W^{(k)}(t_i)] \tag{12}$$

where r_0 is a constant, usually equal to 2 [30]. It is easy to see how this algorithm works. The difference vector formed by $F(t_i) - [G * W^{(k)}]|_{t_i}$ is used to iteratively form each new estimate of $W^{(k+1)}(t_i)$, hence when the difference vector is small, as convergence is reached, $W^{(k+1)}(t_i) \approx W^{(k)}(t_i)$. Furthermore, the relaxation function maintains the positivity and finite constraints on $W^{(k+1)}$. Further information on this method is described by Jansson [30].

It is well known that the convolution operation can be implemented with fast Fourier transform (FFT) techniques [26]. A criticism of all numerically intensive algorithms based on convolution is that unless FFT methods are utilized for convolution, long execution times will result, which would prohibit the use of convolution on laboratory computers. This is because the computational complexity of discrete convolution, which is of the order M^2 floating-point operations (where M is the number of points in the chromatogram), grows fast with increasing M, as compared with the computational complexity of the FFT, which is of the order $M\log M$. For the utmost flexibility, however, FFT methods cannot convolve $W(t)$ with a broadening function that varies with time, because the FFT is a time-invariant operator [26].

For the case where time-varying broadening occurs across the chromatogram, for instance in isocratic LC or isothermal GC, the G term in eqn. 11 is actually composed of an M by M matrix [25] with the row number i corresponding to a unique time t in the fractogram and the column number j corresponding to a unique retention of a peak (the t' function of a peak). Each matrix entry therefore represents the broadening amplitude which occurs at time t_i when the retention time is t_j. Hence the convolution of G with W is simply a matrix multiplication [25] of the matrix G, of size M by M, with the vector W, of length M. Because these broadening response sequences contained in the matrix G are mostly zero, over the full duration of the response, there is no need to store these zeroes. In practice, an index table for the start of each column's non-sparse broadening function is utilized and the dense part of G is compressed into a banded vector. A special multiplication algorithm then forms the $G * W$ convolution. The speed and storage savings with this scheme allow relatively fast operation with minimum memory requirements. For example, a 20-min chromatogram sampled

at two points per second with a constant Gaussian response of $\sigma = 6$ s would normally require $5.76 \cdot 10^6$ entries in memory for the G matrix. If only $\pm 4\sigma$ of the Gaussian broadening curve is stored in memory, then the compressed G storage requires only 230 400 entries, a saving of a factor of 25 as compared with the full storage scheme. The speed increase with G compressed is also a factor of 25 faster than convolution with the full G matrix of size M by M. This makes the method practical to use for chromatography with fast workstations exceeding 10^6 floating point operations per second.

Implementation

The computer programs used here are written in FORTRAN-77 and run on a variety of UNIX and VMS operating system computers. Digital filtering is performed initially on $F(t_i)$ and on consecutive iterations to the convolution pair in eqn. 11 with a Kaiser filter [36] set to roll off at between 0.35 and 0.5 of the Nyquist sampling frequency. This filter has smooth roll-off characteristics and avoids the oscillatory behavior that is known to occur with the Savitsky–Golay filters in the frequency domain [37]. If filtering is not applied on every iteration, peak shapes become distorted with rectangular character as σ_d becomes small; because the filtering tends to round the rectangular edges of peaks through high-frequency attenuation, this may be only a cosmetic situation. The convergence rate appears to be little affected by the choice of cut-off frequency once filtering is performed on the original signal because the band-limiting criterion needed for convergence [34] is established. However, stability and the minimum σ_d obtainable from this method are no doubt balanced by the proper choice of the roll-off frequency and the sharpness of the filter roll off. In this regard, the digital filter used in the CIRM has to be properly chosen; in this study we chose filter conditions where stability was the primary concern.

Typically, 80 iterations of the CIRM are used for deconvolution; however, in some instances 160 iterations are used because of slow convergence. The root mean square (r.m.s.) error, computed from the difference vector, is monitored at each iteration and a smooth exponential-like decrease in the r.m.s. error is noted to occur as a function of iteration number. Typically, the discrete point density is maintained to be *ca.* 36 points over the peak (extending $\pm 4\sigma$ from the peak mean). This oversampling [15,16] promotes high accuracy in the convolution operation; preliminary experiments demonstrate reasonable peak fidelity down to 20 points over the native peak when $\sigma/\sigma_d \approx 5$.

RESULTS AND DISCUSSION

Maximum resolution deconvolution

To probe the extent of deconvolution that is possible with the CIRM, synthetic chromatograms composed of two peaks are generated with specific peak spacings and peak-height ratios and subsequently deconvolved. In the results given here only noiseless Gaussian peaks are considered; the effects of skewed peaks and noise upon deconvolution will be examined in another paper. These results are oriented towards revealing peaks that are fused in the native chromatogram, hence accuracy in peak areas is not measured here.

The result of these experiments is shown in Fig. 3, where R_s^d is given as a function

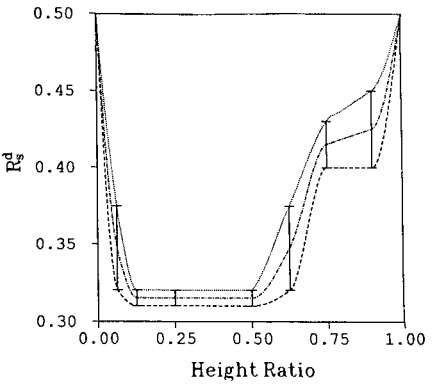

Fig. 3. Limits of deconvolution on two-component Gaussian peaks as embodied in the deconvolved peak critical resolution, R_s^d, as a function of the peak-height ratio, h_r. The bars and spline fits are explained in the text.

of the peak-height ratio, h_r. The region at the top of the bars is where the two-component peaks are easily deconvolved in 80 iterations and the peaks are resolved to within 20% of the baseline, as measured from the smallest peak height. The region at the bottom of the bars represents the threshold of deconvolution where peaks are no longer able to be separated numerically, with respect to the visual presence of two peaks. Between the bars two peaks are discernible but become increasingly difficult to differentiate as two peaks as the distance between the peaks is decreased. Most deconvolution operations in the region between the two bars requires 160 iterations for peak resolution and convergence to an r.m.s. error of $< 2 \cdot 10^{-3}$.

The three broken lines shown in Fig. 3 are calculated from spline fits [38] of the top, bottom and mean of these limit bars. The function $R_s^d(h_r)$ is extrapolated at both low and high h_r to 0.5. For a doublet of equal peak height it becomes impossible normally to distinguish two discrete peaks below $R_s = 0.5$ [39]; however, the CIRM cannot deconvolve doublet peaks of equal height at this resolution; this will be discussed below. At low h_r, the method appears to approach asymptotically the resolvability limit of $R_s^d(0) = 0.5$, although this limit is questionable because the peak-height ratio of zero has no meaning and the function $R_s^d(h_r)$ is singular at $h_r = 0$. The curve shapes outlined by the spline interpolation show that the CIRM is, on average, more effective at small than large h_r. The non-symmetrical nature of Fig. 3 is partly explained by the shape of the function describing the resolution of native peaks as a function of the height ratio, which will be discussed below. In addition, the non-symmetrical response may have its origin partly in the non-linear operation of the deconvolution method.

The spline coefficients obtained from fitting are conveniently used to compute estimates of the average critical resolution of deconvolution, $\overline{R_s^d}$, over the range $0 < h_r \leqslant 1$ by a weighted integration to find the function average value:

$$\overline{R_s^d} = \int_{0+}^{1} w(h_r) R_s^d(h_r) \mathrm{d}h_r \tag{13}$$

where the lower integration limit is set to be infinitesimally larger than zero because of the singularity mentioned previously. The term $w(h_r)$ is a weighting factor used to compensate for the non-uniform probability of height ratios sampled from exponentially distributed random variables; recent experiments have suggested that the peak area follows an exponential probability density function [7] for complex samples. Additional assumptions governing this exponential density under constant zone width and with random detector response factors have recently been discussed [5,7–10].

For most chromatographic applications, the peak height ratio, h_r, is usually defined for two peak heights, h_1 and h_2, to be $h_r = \min\{h_1,h_2\}/\max\{h_1,h_2\}$ and this convention is used throughout this paper. The normalized weighting function for the ratio of exponential density random variables has been given by Feller [40] for the case where $0 < h_r \leqslant \infty$, *i.e.*, the numerator and denominator of the ratio can take on all values except zero in the denominator. The normalized density function which we shall use for weighting is simply twice the function given by Feller (this has been verified by computer simulation):

$$w(h_r) = \frac{2}{(1 + h_r)^2} \tag{14}$$

For peaks where the height ratio density function is uniform, the weighting function, $w(h_r)$, is unity. In both the exponential and uniform density cases the values of $w(h_r)$ given here apply only to random peak heights with no serial correlation.

Evaluation of eqn. 13 for the curves displayed in Fig. 3 is given in Table I. The results in Table I and Fig. 3 indicate that the CIRM is capable of deconvolving, under zero noise and in the absence of tailing, to super-resolution ($R_s < 0.5$) with the exception of peaks with $h_r = 1$ and spaced less than $\Delta t_r = 2\sigma$. For the case of multiple peaks (triplets, quadruplets, etc.) with adjacent $h_r = 1$ and $R_s \leqslant 0.5$, where the peak shape is essentially flat at the top of the peak aggregate, the CIRM appears to be incapable of resolving any of the aggregate. This probably results because the relaxation function given in eqn. 12 is zero when $W^{(k)}(t_i) = 1$. For this extreme case, forcing the relaxation function to take on non-zero values where $W^{(k)}(t_i) = 1$ does not help because the iterative process guides the peak top to the region where the relaxation function assumes a zero value. There appears to be no easy modification to the CIRM that will maintain the top constraint and prevent this condition from occurring, short of adding noise to prevent the flat peak top condition.

Statistical chromatogram deconvolution

In an attempt to evaluate the CIRM numerical methodology on complex

TABLE I

EVALUATION OF $\overline{R_s^d}$ FOR CIRM FROM TWO-COMPONENT PEAKS

Limit	Uniform h_r weighting	Exponential h_r weighting
Low limit	0.348	0.339
High limit	0.375	0.364
Mean limit	0.362	0.352

chromatograms, synthetic chromatograms with 20–72 peaks at different α values are produced with subsequent deconvolution by the CIRM. The retention times are generated with a Poisson distribution, as has commonly been used in previous studies of statistical peak overlap [2–13], and with an exponential density of peak heights [5,7–10]. Constant peak width is used in these calculations; however as stated previously, constant peak width is not a limitation of the CIRM or the convolution algorithm used here. Because of the statistical nature of these numerical experiments, it is necessary to perform a number of calculations at each stated saturation ratio, α; random number seeds are varied within these sets to produce estimates of the ratio $\overline{(p_d/p)}$. To accommodate this requirement, five synthetic chromatograms are calculated at each α. Peak counting is performed by visible inspection of both native and deconvolved synthetic chromatograms. The presence of peak maxima and shoulders is utilized in determining the number of peaks that are present in the chromatograms.

Four cases of deconvolution at different α values are given in Figs. 4–7 using the CIRM. As can be seen, deconvolution with constant σ and in the absence of noise and tailing renders many more peaks visible than in the fused peak native chromatograms shown. As shown by the retention time markers in Figs. 4–7, the CIRM cannot remove peak fusion when retention times are very close, as explained previously. Figs. 4–7, however, clearly demonstrate that deconvolution at the super-resolution level has the potential to be an effective aid in normal chromatographic analysis.

The increase in the number of visible peaks after deconvolution, as measured by $\overline{(p_d/p)}$, the average ratio of visible deconvolved peaks to visible native peaks, is given in Table II as a function of the saturation ratio, α. As can be seen, there is a gain in the number of detectable components, with the largest increase coming from large α experiments, as predicted from eqn. 5. Table II also indicates that there is a dispersion

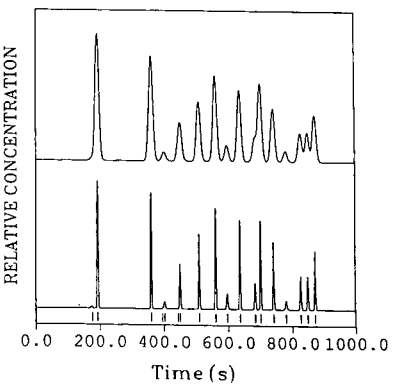

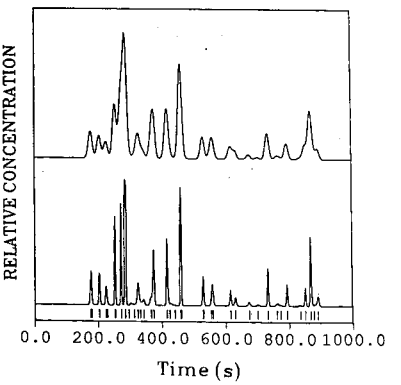

Fig. 4. Statistical chromatogram before (top) and after (bottom) deconvolution. Conditions: $\alpha = 0.513$ (with $R_s^+ = 0.8$ in n_c), $m = 20$, $\sigma = 6$ s, 80 iterations, 15 peaks detected in the native chromatogram and 16 peaks detected in the deconvolved chromatogram. Retention times are indicated by the bars below the bottom chromatogram.

Fig. 5. Statistical chromatogram before (top) and after (bottom) deconvolution. Conditions: $\alpha = 1.00$ (with $R_s^+ = 0.8$ in n_c), $m = 39$, $\sigma = 6$ s, 80 iterations, 21 peaks detected in the native chromatogram and 28 peaks detected in the deconvolved chromatogram. Retention times are indicated by the bars below the bottom chromatogram.

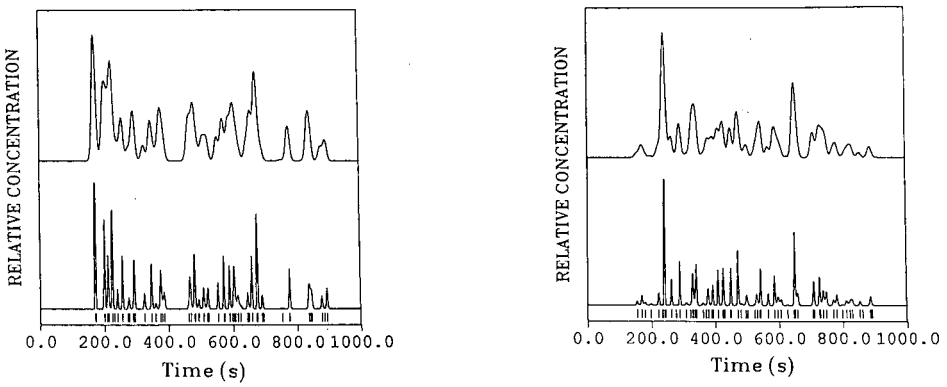

Fig. 6. Statistical chromatogram before (top) and after (bottom) deconvolution. Conditions: $\alpha = 1.49$ (with $R_s^{\ddagger} = 0.8$ in n_c), $m = 60$, $\sigma = 6$ s, 160 iterations, 22 peaks detected in the native chromatogram and 33 peaks detected in the deconvolved chromatogram. Retention times are indicated by the bars below the bottom chromatogram.

Fig. 7. Statistical chromatogram before (top) and after (bottom) deconvolution. Conditions: $\alpha = 1.85$ (with $R_s^{\ddagger} = 0.8$ in n_c), $m = 72$, $\sigma = 6$ s, 160 iterations, 25 peaks detected in the native chromatogram and 38 peaks detected in the deconvolved chromatogram. Retention times are indicated by the bars below the bottom chromatogram.

in $\overline{(p_d/p)}$, as expected, although it is not large as viewed from the relative standard deviation column. In an attempt to relate $\overline{(p_d/p)}$ from eqn. 5 to $\overline{R_s^d}$ from Table I, two different $R_s^{\ddagger}$ values are used in eqn. 5; these results are also given in Table II. It is especially important to note that $R_s^{\ddagger}$ appears in eqn. 5 explicitly as part of the ratio of critical resolutions ($R_s^d/R_s^{\ddagger}$); however, $R_s^{\ddagger}$ also appears implicitly in the n_c term in eqn. 5 through eqns. 3 and 4. For reasons that are not clear, good consistency is obtained when $R_s^{\ddagger}$, implicitly carried in n_c, is chosen to be 0.8 (consistent with [9]) and $R_s^{\ddagger}$ in the

TABLE II

EVALUATION OF $\overline{R_s^d}$ FROM STATISTICAL CHROMATOGRAMS

α^a	$\overline{(p_d/p)}$	%R.S.D.[b] in (p_d/p)	$\overline{R_s^{dc}}$	Deviation from $\overline{R_s^d} = 0.352$ (%)	$R_s^{\ddagger}$ [d]
0.513	1.13	7.23	0.383	8.91	0.539
0.794	1.28	8.77	0.346	−1.73	0.598
1.00	1.33	12.0	0.357	1.36	0.581
1.18	1.44	10.2	0.345	−2.12	0.601
1.49	1.51	8.44	0.361	2.61	0.574
1.67	1.42	6.35	0.394	12.0	0.521
1.85	1.48	9.78	0.394	11.9	0.522

[a] Calculated with $R_s^{\ddagger} = 0.8$ in n_c term.
[b] R.S.D. = Relative standard deviation.
[c] Assuming $R_s^{\ddagger} = 0.5$ in ratio term.
[d] Assuming $R_s^d = 0.352$ in ratio term, $R_s^{\ddagger}$ applied equally to ratio and n_c in α.

ratio $R_s^d/R_s^\ddagger$ is equal to 0.5 (consistent with [3] and [11]). As is noted from Table II, deviation of R_s^d from the value 0.352 is very low for the numerical experiments where $\alpha \leqslant 1.49$. In addition, R_s^d can be accepted as 0.352 and then the value of the critical resolution, $R_s^\ddagger$, can be obtained through rearrangement of eqn. 5; these values are shown in the last column in Table II. It is noted that in this instance $R_s^\ddagger$ varies over the range $0.574 \leqslant R_s^\ddagger \leqslant 0.601$ when $0.794 \leqslant \alpha \leqslant 1.49$. From the limited data given in Table II, there does not appear to be a recognizable trend which can be used in establishing one uniquely consistent value of $R_s^\ddagger$. However, the empirical use of 0.8 for $R_s^\ddagger$ internal to n_c and $R_s^\ddagger$ of 0.5 in the ratio $R_s^d/R_s^\ddagger$ serves to allow estimation of the ratio p_d/p given R_s^d from the deconvolution methodology at a stated α. The value of 0.352, from Table I, is independent of the statistical peak overlap model; hence this gives further credibility to the assignment of $\overline{R_s^d} = 0.352$ for the CIRM and suggests an independent verification for the simple statistical model of peak overlap with $R_s^\ddagger = 0.5$ [2,3,9,11]. In Table II, the lowest α result appears to be in poor agreement with $\overline{R_s^d} = 0.352$; a possible explanation is that the number of peaks in this experiment is small; only 20 peaks are used at this α value and hence the statistical sampling is poor with only five experiments contributing to the mean value. When the statistical peak overlap model is used for the estimation of the true number of peaks in both synthetic and experimental chromatograms, it is observed [11] that the accuracy of estimation degrades at $\alpha > 0.5$. It is possible that the additional mathematics needed to describe higher saturation effects (*e.g.*, the perturbation of the peak heights due to closely spaced surrounding clusters) will be less important in the application given here because the use of ratios, on which eqn. 5 is based, may tend to cancel or minimize this additional level of theory.

The results in Table II illustrate the monotonic increase in $\overline{p_d/p}$ from statistical chromatograms for $\alpha \leqslant 1.49$. Above this value, however, there is no longer an increase in p_d/p and it is at this point that the CIRM loses the ability to quantitatively remove peak fusion. A number of numerical experiments conducted with $2.0 \leqslant \alpha \leqslant 100.0$ have been used to observe that for $\alpha \geqslant 3.0$ the ratio p_d/p is consistently approximated by the value 2.1 and deconvolution gives meaningless results in this range. For the range $1.5 \leqslant \alpha \leqslant 3.0$, p_d/p asymptotically, but not monotonically, approaches 2.1 with broader deconvolved peaks than shown in Figs. 4–7. Therefore, in the absence of noise and tailing, the CIRM is observed to be effective, in the statistical sense, up to α values less than 1.5 and with the potential visible restoration of 1.5 times the number of peaks appearing in the native chromatogram. This operating range is summarized in Fig. 2 in the shaded area.

It appears from the previous discussion that deconvolution can quantitatively restore lost peak information; however, as predicted from the statistical model of peak overlap [2–13], the general performance of separation is poor as analysis is carried out at higher α conditions. This is suggested by the data in Table III, where the quantities $\overline{p/m}$ and $\overline{p_d/m}$ are given from statistical chromatogram production and deconvolution. It is noted here that although deconvolution provides an enhancement in the ratio of the number of visible peaks after deconvolution to the true number of components, this ratio is still far below unity, the value that would be obtained if deconvolution could resolve all the peaks in the chromatogram. It is seen from Table III that there is a gain, however, in that deconvolution allows working at higher α for a constant ratio

TABLE III

EVALUATION OF $\overline{p/m}$ AND $\overline{p_d/m}$ FROM STATISTICAL CHROMATOGRAMS

α^a	m	$\overline{p/m}$	$\overline{p_d/m}$
0.513	20	0.720	0.810
0.794	31	0.587	0.742
1.00	39	0.528	0.697
1.18	46	0.461	0.661
1.49	58	0.397	0.597
1.67	65	0.372	0.529
1.85	72	0.339	0.500

[a] Calculated with $R_s^{\ddagger} = 0.8$ in n_c term.

of visible peaks to true components, as compared with the native chromatogram. For example, with $\alpha = 0.513$, $\overline{p/m} = 0.720$ for the native chromatogram. With deconvolution, $\overline{p_d/m} = 0.697$ for $\alpha = 1.00$. These results suggest that CIRM deconvolution, although not capable of restoring all the peaks to a 1:1 identity with the components, can be used to perform separations at higher column saturation values than would normally be used for high-resolution separations.

Although our attention is focused on the extent of deconvolution of complex chromatograms in this paper, it is instructive to briefly examine additional $\overline{R_s^{\ddagger}}$ values for the statistical model which can be produced from the average critical resolution equation developed in this paper. As demonstrated by El Fallah and Martin [10], synthetic chromatogram methodology may be used to estimate $\overline{R_s^{\ddagger}}$ in the context of the statistical model of peak overlap. A different approach, as used here, is to find $\overline{R_s^{\ddagger}}$ independent of the statistical model.

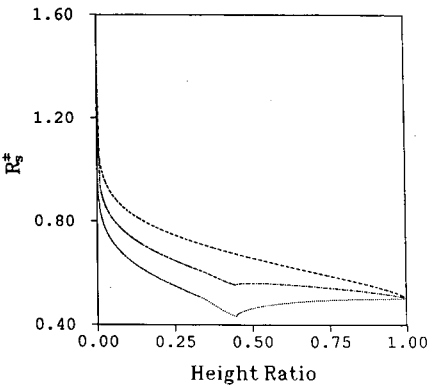

Fig. 8. Limits of resolving two-component Gaussian peaks as a function of the peak-height ratio, h_r. The top curve is the critical resolution value where valley discrimination between two peaks ceases. The bottom curve is the critical resolution value where inflection points can no longer be used to discriminate between two unique peaks. The middle curve is the average of the top and bottom curves.

In an attempt to find one uniquely consistent $\overline{R_s^\ddagger}$ value, critical resolutions for a two-component Gaussian doublet are calculated with eqns. 13 and 14 using $R_s^\ddagger(h_r)$ from two limiting systems: (1) the values of $R_s^\ddagger(h_r)$ where the valleys between fused peaks vanish as resolution is decreased and (2) the values of $R_s^\ddagger(h_r)$ where inflection points can no longer distinguish between peaks as resolution is decreased. The former case has been called the "shoulder" resolution case and the latter the "detectability" resolution case [15]. Analytical solutions for these two situations were given by Westerberg [15]. These two situations are graphically illustrated for $R_s^\ddagger$ as a function of h_r in Fig. 8 and the evaluation of these two cases using eqns. 13 and 14 is given in Table IV.

The $\overline{R_s^\ddagger}$ values for exponential weighting from Table IV are consistent with bracketing the values of $0.574 \leqslant \overline{R_s^\ddagger} \leqslant 0.601$ when $0.794 \leqslant \alpha \leqslant 1.49$ from the last column in Table II. This suggests some form of consistency in accepting the value of $\overline{R_s^\ddagger}$ of *ca.* 0.645 (the mean limit from Table IV) when eqn. 5 is formulated in a fully consistent usage of $R_s^\ddagger$. Unfortunately, this does not give insight into the proper value of $R_s^\ddagger$. Of interest, however, is the correspondence of values in Table IV with values calculated within the statistical model framework [10]. In this instance El Fallah and Martin [10] obtained values of $\overline{R_s^\ddagger} = 0.536$ for the low limit (compared with 0.558 in Table IV) and $\overline{R_s^\ddagger} = 0.796$ for the high limit (compared with 0.725 in Table IV). Although direct comparison of these numbers is not strictly valid because of differences in the definition of the measurements and because the $\overline{R_s^\ddagger}$ values estimated in Table IV only include fused doublet peaks, the correspondence is nonetheless noted. There is, however, an interesting correspondence between El Fallah and Martin's value of 0.71 ± 0.01 for the average resolution, which is suggested for use [10] in the statistical peak overlap model, and the average resolution calculated for the shoulder resolution case in Table IV of 0.725. Towards this end, further theoretical work will be needed to clarify an exactly rigorous value (if one exists) for $\overline{R_s^\ddagger}$. As was stated previously, good consistency is realized between the results in Table II and from eqn. 5 when $R_s^\ddagger$, implicitly carried in n_c, is chosen to be 0.8 and $R_s^\ddagger$ in the ratio $R_s^d/R_s^\ddagger$ is chosen as 0.5, although at this point these values must be viewed as strictly empirical.

Overview

A comparison may be made between the results given here and investigations into overlapping peak resolution with derivative methods. The derivative methods [41], tend to be noise sensitive, as is the CIRM. However, CIRM tends to be more

TABLE IV

EVALUATION OF $\overline{R_s^\ddagger}$ FOR TWO-COMPONENT PEAKS AT THE SHOULDER AND DETECTABILITY LIMITS

Limit	Uniform h_r weighting	Exponential h_r weighting
"Detectability" limit	0.529	0.558
"Shoulder" limit	0.678	0.725
Mean limit	0.605	0.645

effective in resolving severely overlapped peaks below $R_s = 0.5$. This is, of course, at the expense of computer time, where the derivative methods typically require 1 s or less of computer time and the CIRM method takes about 5 min. In addition, derivative methods require little or no information about the column response function, which is a critical matter in the use of CIRM or any other method based on convolution. If the two methods could be combined, for instance if derivative information could be used to obtain a better starting estimate of $W^0(t_i)$, the deconvolution method may be made more time efficient, requiring less iteration to reach convergence.

The response function embodied in the G matrix may be obtained experimentally by injection of individual solutes or by injection of a mixture when baseline separation is possible. In this way peak parameters can be estimated and used to form G. As stated previously, the CIRM methodology is capable of handling time-dependent broadening in the composite peak shape throughout the chromatographic elution profile. In addition, it may be possible, depending on the nature of the solutes in the test and chromatographic mixtures, to substitute similar solutes in the test mixture as long as the elution range is covered. Careful experiments must be performed, in fact, to determine whether this is feasible and to what class of substances this can be applied. In essence, this may depend on whether specific interactions are controlling the separation and whether tailing is an extra- or an intra-column effect (*e.g.*, slow desorption from the stationary phase). The reproducibility of the solvent or temperature program may also affect the accuracy of the peak response profile when gradient elution (LC) or temperature programming (GC) is used.

One of the many aspects of CIRM deconvolution not discussed in this paper is the effect that inaccurate σ values (and other peak model parameters when non-Gaussian peaks are encountered) will have on the resultant deconvolved chromatogram. Synthetic chromatograms have been produced and analyzed where the broadness is purposely reduced in the G matrix; on deconvolution no spurious peaks are recognized but there are noticeably larger σ_d values and poor overall performance. In instances where the broadening is purposely made larger than the σ value in the native singlet peak, occasional splitting into doublets has been observed, but this only happens after extensively long iteration. In this instance the rate of convergence is seen to be very slow and sometimes divergence occurs, as viewed from plot of r.m.s. error *versus* iteration number. The characterization of the broadening response of pure components in experimental chromatograms may be the accuracy-limiting step in the CIRM deconvolution process; this may also be true of any deconvolution method based on convolution.

The results given here were obtained under the limiting condition of no noise. Noise is well known to be a critical factor in limiting the ability of deconvolution algorithms to work properly [42] and this factor must be determined experimentally because of the unique nature of the noise frequency distribution in real chromatograms. Further, it has been suggested [30] that most deconvolution methods will work well on synthesized peaks but may fail when real waveforms are used. As shown in this paper, there is a finite resolving capability of the CIRM, and the purpose of this study was to find the region(s) of operation where resolution could not be restored. In addition, the Fourier method of deconvolution has been analyzed in the context of "perfect" experiments [16], where it was shown that delta function recovery was impossible and that only a small amount (compared with the CIRM) of resolution

recovery was possible. If the deconvolution methodology cannot enhance the resolution of noiseless signals, it is doubtful that high-fidelity resolution enhancement can be performed on a real noise-containing signal. There is no doubt, however, that the extent of deconvolution presented in this paper can be approached with very careful experiments, modern chromatographic equipment, and rigorous digital filtering when concentrations are adequate to permit working above the detection limit. In the context of filtering, it is known that CIRM deconvolution can be performed when the native detector signal is significantly broadened by overfiltering [34]; owing to the frequency extrapolation that occurs with CIRM, additional filtering can be deconvolved from the signal by including the filter response in the broadening operator, G.

The procedures for statistical chromatogram deconvolution presented in this paper may also be useful for evaluating other deconvolution methods in the context of chromatography. For instance, deconvolution by the maximum entropy method or the relatively new method of deconvolution by splines [43] may be evaluated by calculating $\overline{R_s^d}$, from R_s^d *versus* h_r numerical experiments, and utilizing eqn. 5 to relate α and $\overline{R_s^d}$ to p_d/p. Finally, we note that the CIRM may have application in reducing analysis time whereby the chromatographic flow velocity may be increased at the expense of losing resolution, the resolution loss being compensated by numerical deconvolution. Chromatographic experiments are in progress to determine the extent to which this is feasible.

SYMBOLS

B_j	Detector response of component j in a complex mixture
$F(t)$	Time-based concentration response of detector
$G(t), G(t,t')$	Broadening operator
h_r	Peak-height ratio
h_1, h_2	Heights of peaks 1 and 2
j	Summation index
m	Number of true components present in a mixture
M	Number of points in a digitized chromatogram
n_c	Peak capacity
n_c'	Peak capacity at unit resolution
N	Number of theoretical plates
N_{av}	Average number of theoretical plates
$\underline{p}$	Number of visible peaks in native chromatogram
p	Average number of visible peaks in native chromatograms
$\underline{p_d}$	Number of visible peaks after deconvolution
p_d	Average number of visible peaks after deconvolution
r	Relaxation function
r_0	Relaxation constant
$\underline{R_s^d}$	Critical resolution of deconvolution
$\overline{R_s^d}$	Average critical resolution of deconvolution
$\underline{R_s^\ddagger}$	Critical resolution value for peak discrimitation
$\overline{R_s^\ddagger}$	Average critical resolution value for peak discrimination
t, t_r	Time, retention time

t_{max}	Time at the end of chromatographic separation
t_0	Void time of a chromatogram
$w(h_r)$	Weighting factor for peak heights
$W^{(k)}(t_i)$	kth iterative estimate of the unbroadened peak function
α	Saturation factor, $\alpha = m/n_c$
$\delta(t)$	Delta function
σ,σ_j	Standard deviation of a Gaussian peak
σ_d	Standard deviation of a Gaussian peak after deconvolution

REFERENCES

1 K. A. Connors, *Anal. Chem.*, 46 (1974) 53.
2 J. M. Davis and J. C. Giddings, *Anal. Chem.*, 55 (1983) 418.
3 J. C. Giddings, J. M. Davis and M. R. Schure, in S. Ahuja (Editor), *Ultra-High Resolution Chromatography (ACS Symposium Series*, No. 250), American Chemical Society, Washington, DC, 1983, Ch. 2, pp. 9–26.
4 J. M. Davis and J. C. Giddings, *J. Chromatogr.*, 289 (1984) 277.
5 M. Martin and G. Guiochon, *Anal. Chem.*, 57 (1985) 289.
6 J. M. Davis and J. C. Giddings, *Anal. Chem.*, 57 (1985) 2168.
7 L. J. Nagels and W. L. Creten, *Anal. Chem.*, 57 (1985) 2706.
8 M. Martin, D. P. Herman and G. Guiochon, *Anal. Chem.*, 58 (1986) 2200.
9 W. L. Creten and L. J. Nagels, *Anal. Chem.*, 59 (1987) 822.
10 M. Z. El Fallah and M. Martin, *Chromatographia*, 24 (1987) 115.
11 S. L. Delinger and J. M. Davis, *Anal. Chem.*, 62 (1990) 436.
12 A. Felinger, L. Pasti and F. Dondi, *Anal. Chem.*, 62 (1990) 1846.
13 A. Felinger, L. Pasti, P. Reschiglian and F. Dondi, *Anal. Chem.*, 62 (1990) 1854.
14 J. C. Giddings, *Anal. Chem.*, 39 (1967) 1027.
15 A. W. Westerberg, *Anal. Chem.*, 41 (1969) 1771.
16 D. W. Kirmse and A. W. Westerberg, *Anal. Chem.*, 43 (1971) 1035.
17 M. Rosenbaum, V. Hanch and R. Komers, *J. Chromatogr.*, 294 (1984) 31.
18 G. H. Rayborn, G. M. Wood, B. T. Upchurch and S. J. Howard, *Am. Lab.*, Oct. (1986) 56.
19 P. B. Crilly, *J. Chemometr.*, 1 (1987) 175.
20 A. H. Anderson, T. C. Gibb and A. B. Littlewood, *J. Chromatogr. Sci.*, 8 (1970) 640.
21 S. T. Balke, *Quantitative Column Liquid Chromatography—A Survey of Chemometric Methods*, Elsevier, New York, 1984.
22 J. Callis, in S. Ahuja (Editor), *Ultra-High Resolution Chromatography (ACS Symposium Series*, No. 250), American Chemical Society, Washington, DC, 1983, Ch. 12, pp. 171–198.
23 J. C. Sternberg, *Adv. Chromatogr.*, 2 (1966) 205–270.
24 J. C. Giddings, *Dynamics of Chromatography, Part I, Principles and Theory*, Marcel Dekker, New York, 1965.
25 R. N. Bracewell, *The Fourier Transform and its Applications*, McGraw-Hill, New York, 2nd ed., 1978.
26 A. V. Oppenheim and R. W. Schafer, *Digital Signal Processing*, Prentice-Hall, Englewood Cliffs, NJ, 1975.
27 D. Alba and G. R. Meira, *J. Liq. Chromatogr.*, 7 (1984) 2833.
28 E. M. Rosen and T. Provder, *Sep. Sci.*, 5 (1970) 485.
29 K. Minami, S. Kawata and S. Minami, *Appl. Opt.*, 24 (1985) 162.
30 P. A. Jansson, *Deconvolution with Applications in Spectroscopy*, Academic Press, New York, 1984.
31 M. R. Schure, B. N. Barman and J. C. Giddings, *Anal. Chem.*, 61 (1989) 2735.
32 K. H. Michaelian and W. I. Friesen, *Appl. Spectrosc.*, 42 (1988) 1538.
33 P. B. Crilly, *J. Chemometr.*, 1 (1987) 79.
34 R. W. Schafer, R. M. Mersereau and M. A. Richards, *Proc. IEEE*, 69 (1981) 432.
35 S. J. Howard, *J. Opt. Soc. Am.*, 71 (1981) 819.
36 P. P. Vaidyanathan, in D. F. Elliot (Editor), *Handbook of Digital Signal Processing, Engineering Applications*, Academic Press, New York, 1987, Ch. 2, pp. 55–172.

37 K. R. Betty and G. Horlick, *Anal. Chem.*, 49 (1977) 351.
38 H. Akima, *J. Assoc. Comput. Mach.*, 17 (1970) 589.
39 L. R. Snyder, *J. Chromatogr. Sci.*, 10 (1972) 200.
40 W. Feller, *An Introduction to Probability Theory and its Applications*, Vol. II, Wiley, New York, 2nd ed., 1971.
41 E. Grushka and D. Israeli, *Anal. Chem.*, 62 (1990) 717.
42 W. E. Blass and G. W. Halsey, *Deconvolution of Absorption Spectra*, Academic Press, New York, 1981.
43 A. G. B. M. Saase, H. Wormeester and A. van Silfhout, *J. Vac. Sci. Technol.*, A7 (1989) 1535.

Journal of Chromatography, 550 (1991) 71–76
Elsevier Science Publishers B.V., Amsterdam

CHROMSYMP. 2363

Computer-aided optimization of high-performance liquid chromatographic analysis of flavonoids from some species of the genus *Althaea*

T. H. DZIDO* and E. SOCZEWIŃSKI
Department of Inorganic and Analytical Chemistry, Medical Academy, Staszica 6, 20-081 Lublin (Poland)
and
J. GUDEJ
Department of Pharmacognosy, Institute of Technology and Chemistry of Drugs, Medical Academy, Muszyńskiego 1, 90-151 Łódź (Poland)

ABSTRACT

DryLab G software was used for the optimization of gradient elution programs in reversed-phase high-performance liquid chromatography applied to the chromatographic analysis of flavonoids present in marsh-mallow (*Althaea officinalis*). The optimization experiments were carried out for a mixture of eight standard solutes (isolated previously from the plant) and then applied to an extract from the flowers of marsh-mallow. Computer simulation experiments allowed convenient analytical conditions to be chosen. The use of two modifiers, methanol and acetonitrile, made the identification of separated components more certain. Good agreement between simulated and experimental chromatograms was obtained.

INTRODUCTION

Several species of the genus *Althaea* grow in Europe [1]: in Poland the marsh-mallow (*Althaea officinalis* L.) is grown as a medicinal plant. The leaves, flowers and roots of marsh-mallow are used to prepare anti-inflammatory and mucilaginous drugs. In the USSR other *Althaea* species are also used in the production of drugs [2].

In previous papers [3,4] the content of phenolic acids, coumarins and flavonoid glycosides in several species of *Althaea* (*A. officinalis* L., *A. armeniaca* Ten., *A. cannabina* L., *A. narbonensis* Pourr. and *A. broussenetiifolia* Iljin) were investigated by means of reversed-phase high-performance liquid chromatography (RP-HPLC) and paper chromatography; other examples of separation and determination of flavonoids can also be cited [5–7]. The analysis of flavonoids is more difficult owing to the larger number of components, therefore the chromatographic systems were optimized in preliminary experiments using the DryLab G software (LC Resources, Lafayette, CA, USA; I. Molnar, Institute of Applied Chromatography, Berlin, Germany) [8,9]. The use of gradient elution is also advantageous because it rapidly removes the less polar ballast substances present in the biological sample.

0021-9673/91/$03.50

EXPERIMENTAL

DryLab G software was applied using an IBM class computer. HPLC experiments were carried out using a Hewlett-Packard (Palo Alto, CA, USA) Model 1050 liquid chromatograph with a 20-μl sample injector (Rheodyne, Cotati, CA, USA) and a spectrophotometric detector. The chromatograms were recorded at 270 nm with a 3396A reporting integrator (Hewlett-Packard). The stainless-steel column, 250 × 4.6 mm I.D., was packed with 7-μm LiChrosorb RP-18 (E. Merck, Darmstadt, Germany) with a home-made apparatus (Orlita pump). Samples of 10 μl were injected. Eluents contained 1% acetic acid in the whole composition ranges and were composed of bidistilled water and methanol or acetonitrile, chromatographic grade (E. Merck). The column dead volume, 2.3 cm^3, was determined using a pure water sample for eluent composed of methanol and water (60:40). The column efficiency was 7300 theoretical plates determined for benzene and toluene at methanol–water (60:40), flow-rate 1 cm^3/min, temperature, 20°C.

The gradient program was optimized using an artifical mixture of eight standard solutes isolated previously from the plant.

The plant material (flowers, 1.0 g), after extraction with chloroform, was extracted with boiling methanol (5 × 50 ml). Combined methanol extracts were evaporated to 100 ml *in vacuo*.

RESULTS AND DISCUSSION

According to the routine procedure [8,9] two gradient runs were carried out at different gradient steepness (gradient times for 5–100% acetonitrile–water: 20 and 60 min, Fig. 1a,b).

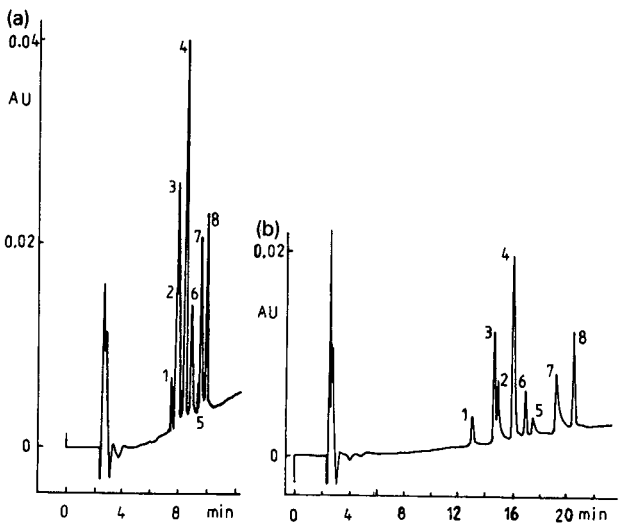

Fig. 1. Separation of the test flavonoid compounds by gradient elution with 5–100% acetonitrile–water. Peaks: 1 = dihydrokaempferol 4′-O-glucoside; 2 = hypolaetin 8-O-gentiobioside; 3 = quercetin 3-O-glucoside; 4 = kaempferol 3-O-glucoside; 5 = hypolaetin 8-O-glucoside; 6 = naryngenin 4′-O-glucoside; 7 = hypolaetin 4′-methyl ether 8-O-glucoside; 8 = tiliroside. Gradient time (a) 20 min, (b) 60 min.

TABLE I

RETENTION DATA

System variables: dwell volume, 0.45 ml; column length, 25.00 × 0.46 cm I.D.; flow-rate, 1.00 cm^3/min; starting percentage —B, 5.00%; final percentage —B, 100.00%; gradient time, first run, 20.00 min; gradient time, second run, 60.00 min. t_R = Retention time.

Band	Solute	Run 1		Run 2: t_R (min)
		t_R (min)	Area (arbitrary units)	
1	Dihydrokaempferol 4'-O-glucoside	7.64	111000.00	13.10
2	Hypolaetin 8-O-gentiobioside	7.89	334000.00	14.91
3	Quercetin 3-O-glucoside	7.99	808000.00	14.63
4	Kaempferol 3-O-glucoside	8.50	999999.00	16.03
5	Hypolaetin 8-O-glucoside	8.82	70000.000	17.47
6	Naryngenin 4'-O-glucoside	8.97	500000.00	16.92
7	Hypolaetin 4'-methyl ether 8-O-glucoside	9.65	750000.00	19.22
8	Tiliroside	10.09	690000.00	20.49

The retention data for the eight solutes, summarized in Table I, show a changed sequence of two pairs of solutes, Nos. 2–3 and 5–6, in run 2. The resolution plot calculated by the DryLab G software from the data is given in Fig. 2. It can be seen that good resolution of all solute pairs is obtained at rather long gradient times (*ca.* 80 min). Considering the long retention times of the first components (Table I), several gradient runs were simulated by means of option 6.4 (change of gradient range).

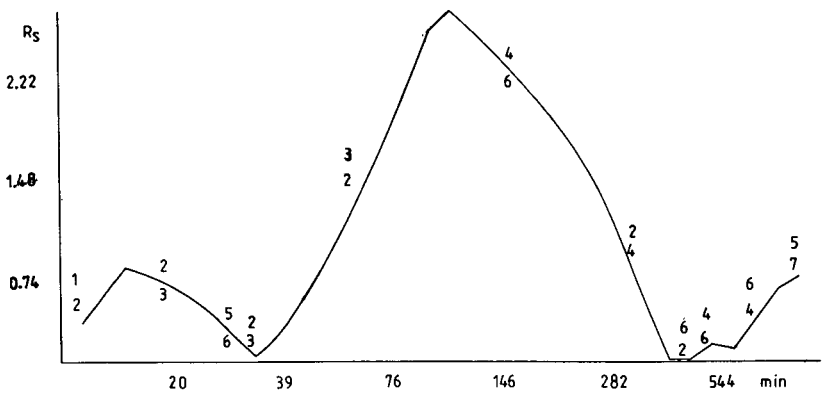

Fig. 2. Relative-resolution map for flavonoid compounds, 5–100% acetonitrile–water gradients and compounds as in Fig. 1.

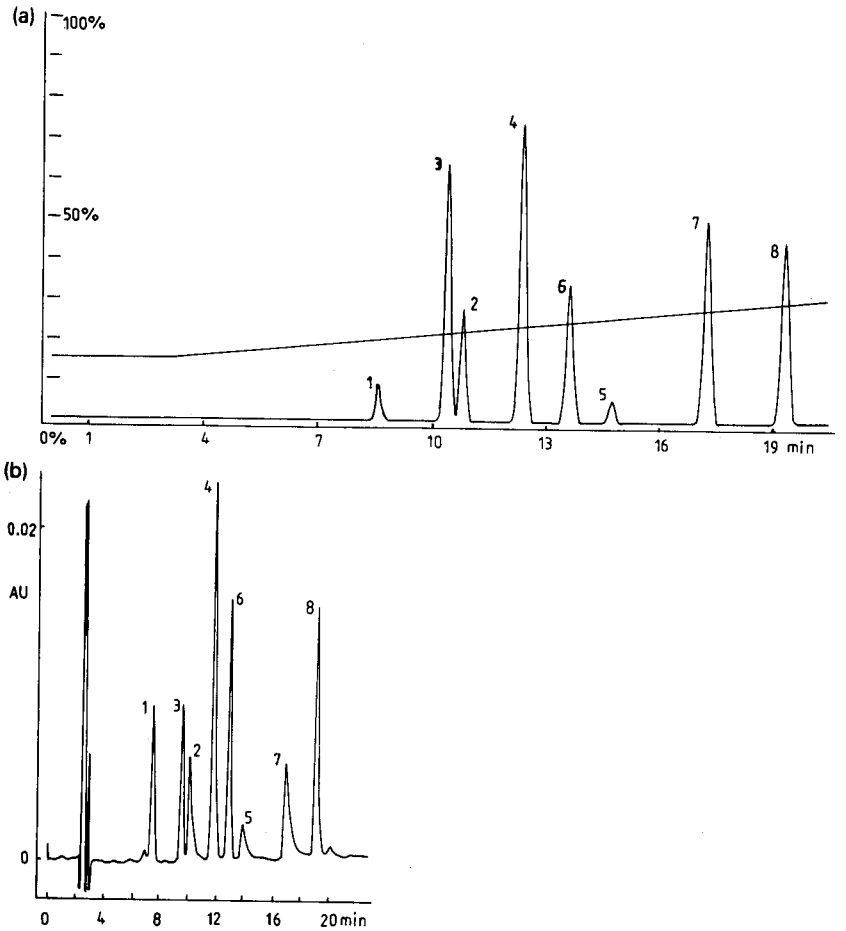

Fig. 3. (a) Computer-simulated chromatogram of the test mixture of flavonoid compounds (as in Fig. 1a), gradient elution with 16–35% acetonitrile–water, gradient time 22 min. (b) Experimental chromatogram of the mixture, sample as in Figs. 1a and 3a.

starting from a higher initial concentration of acetonitrile; good results were obtained using a 16 to 35% acetonitrile (1% acetic acid) linear gradient in 22 min. The simulated chromatogram of the eight standards, after option 7 (column optimization, assuming molecular weight, $M = 700$), is shown in Fig. 3a and the experimental chromatogram in Fig. 3b. Satisfactory separation and good agreement of simulated and experimental chromatograms can be seen.

In a similar way another solvent system, containing methanol instead of acetonitrile, was optimized. Satisfactory separation of all eight standards was obtained for a linear 29 to 65% methanol gradient (1% acetic acid) and 21 min gradient time (Fig. 4), also in good agreement with the simulated chromatogram. The separation is, however, somewhat worse than for the acetonitrile system (Fig. 3); the sequence of the solutes is quite different for the two systems, which may be advantageous for further improvement of separation by the use of ternary gradients.

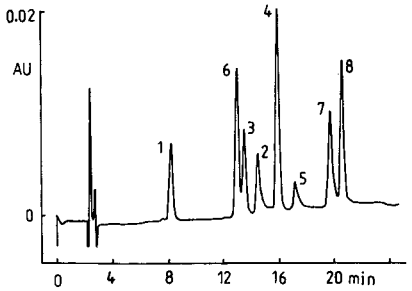

Fig. 4. Experimental chromatogram of the test mixture as in Fig. 1a, gradient elution with 29–65% methanol in water, gradient time 21 min. and compounds as in Fig. 1a.

The gradient programs were then used for the separation of actual flavonoid extracts from the flowers of *Althaea officinalis* L. (Fig. 5a acetronitrile and Fig. 5b methanol systems) and *A. cannabina* . (Fig. 6, methanol system). The flavonoid com-

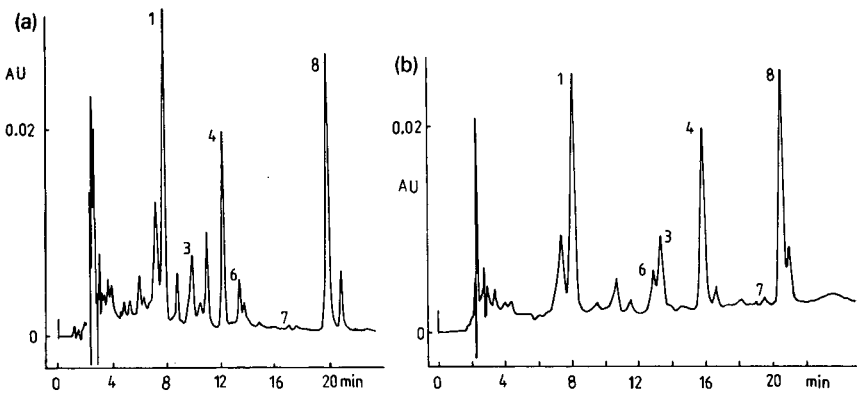

Fig. 5. Experimental chromatogram of the actual flavonoid extracts from the flowers of *Althaea officinalis* L. (a) Conditions as in Fig. 3, (b) as in Fig. 4.

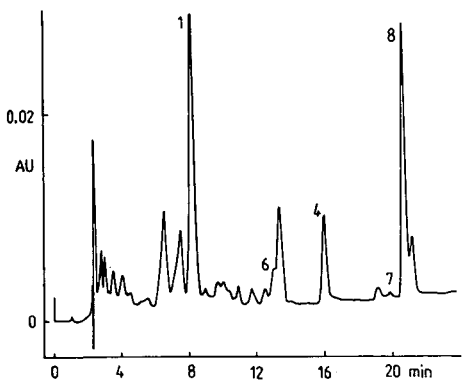

Fig. 6. Experimental chromatogram of the actual flavonoid extract from the flowers of *Althaea cannabina* L. Conditions as in Fig. 4.

position is different from the standard mixtures (Figs. 3 and 4): some new peaks are present and some of the standards occur in trace amounts. However, some compounds could be positively identified in the chromatograms of the extracts, and the identification could be more certain because of the use of two modifiers, methanol and acetonitrile, having different selectivity characteristics.

The analytical applications of the optimized systems, calibration experiments and comparison of flavonoid content in various species of the *Althaea* genus will be described in a later paper.

CONCLUSIONS

The use of DryLab G software for the optimization of gradient programs permitted the choice of convenient experimental conditions for the rapid separation and quantitation of components of complex plant extracts, basing on a few experiments. For the more reliable identification of separated components it is advantageous to use more than one eluent system (modifier).

Good agreement of simulated and experimental chromatograms was observed.

ACKNOWLEDGEMENT

The donation of a Hewlett-Packard 1050 liquid chroamtograph (Experimental section) by the Alexander von Humboldt Foundation (Bonn, Germany) to Dr. T. H. Dzido is gratefully acknowledged.

REFERENCES

1 *Flora Europea*, Vol. 2, University Press, Cambridge, 1958.
2 P. Czikov and J. Laptieva, *Rośliny Lecznicze i Bogate w Witaminy* (*Medicinal Plants and Plants Rich in Vitamins*, Polish translation from Russian), PWRiL, Warsaw, 1987.
3 J. Gudej and M. L. Bieganowska, *J. Liq. Chromatogr.*, 13 (1990) 4081.
4 J. Gudej and M. L. Bieganowska, *Chromatographia*, 30 (1990) 333.
5 F. Briancon-Scheid, A. Lobstein-Buth and R. Anton, *Planta Med.*, 49 (1983) 204.
6 K. Dalenbach-Gölke, S. Nyiredy, B. Meier and O. Sticher, *Planta Med.*, 53 (1987) 189.
7 M. Veit, F. Ch. Czygan, B. Frank, D. Hofman and B. Worliczek, *Dtsch. Apoth. Ztg.*, 129 (1989) 1591.
8 L. R. Snyder and J. W.Dolan, *DryLab G Instruction Manual*, LC Resources, Lafayette, CA.
9 J. W. Dolan, D. C. Lommen and L. R. Snyder, *J. Chromatogr.*, 485 (1989) 91; and references cited therein.

Journal of Chromatography, 550 (1991) 77–86
Elsevier Science Publishers B.V., Amsterdam

CHROMSYMP. 2160

Computer simulation of isocratic retentions of alkylketones using gradient data

JAMES D. STUART* and DIANA D. LISI
Department of Chemistry, U-60, 215 Glenbrook Road, University of Connecticut, Storrs, CT 06269-3060 (USA)

ABSTRACT

The use of computer simulation software for high-performance liquid chromatographic (HPLC) method development is considered. In particular, gradient elution data entered into DryLab G/plus are used to predict isocratic retention times. The motivation was to establish whether data generated in a research-grade, gradient environment might be used to simulate accurately isocratic HPLC conditions applicable to a process monitoring operation. Good agreement between experimentally obtained and computer-predicted retention times for a homologous series of alkylketones was found for the conversion from gradient to isocratic elution conditions.

INTRODUCTION

Many chromatographers are still reluctant to use gradient elution high-performance liquid chromatography (HPLC), even though the theory of gradient elution is now well developed [1–3]. In general, gradient elution has been regarded as a research technique and has been excluded from process monitoring work, except for special applications. This situation may have developed for several reasons, including the following [4]: (1) laboratories involved with routine separations do not always have HPLC equipment that is suitable for gradient elution methods; (2) when compared with isocratic methods, gradient elutions methods are believed to be less precise; (3) because gradient elution is a more complex technique than isocratic elution, method development is more difficult; and (4) because gradient elution procedures are instrument specific, methods developed on one gradient system often do not perform in the same way when using another instrument [5].

Gradient elution does, however, have a number of advantages over the use of isocratic experiments for method development [4]. First, when gradient elution is used, fewer trial-and-error adjustments in solvent strength are required when changing from one solvent to another. Second, since early bands overlap in isocratic separations, it is difficult to establish how the resolution changes as the solvent strength is varied. As early overlapping bands are not often encountered in gradient elution, it is possible to increase the resolution during exploratory runs. Third, gradient elution experiments make it easier to locate compounds that are eluted either very early or

0021-9673/91/$03.50

very late. With isocratic separations, early-eluted compounds are often lost in the solvent front and late-eluted compounds disappear into the baseline or overlap with the next sample. Fourth, as gradient elution method development works for both gradient elution and isocratic methods, if it turns out that the final method needed to separate a sample is gradient elution, no time will have been wasted with isocratic runs that do not work.

This paper explores the possibility of using DryLab G/plus (LC Resources) for the purpose of developing isocratic methods. DryLab G/plus is one of a group of personal computer programs available for HPLC method development [4,6–11]. Although DryLab I/plus can predict isocratic retention from either gradient or isocratic input, DryLab G/plus has the distinct advantage that it can be used to develop both gradient and isocratic methods, whereas DryLab I/plus can only be used for isocratic method development.

DryLab G has been reported to predict correctly retention times for various gradient and isocratic separations [12]. It was noted that the prediction of retention times for certain isocratic conditions was susceptible to errors in the measured dwell volume. However, the predicted resolution was not as seriously affected as resolution is a function of the difference between retention times.

To use DryLab G/plus to predict isocratic retention, the program must be "tricked". This is done by entering data for two initial gradient runs into the program and then selecting Option 6.5–Multi-Segment Gradients. When asked for the number of segments in the gradient to be predicted, one segment is entered. The percentage of organic entered for the start and finish of the gradient is the same value as the percentage of organic of the isocratic run desired. A long gradient time, here 100 min, is used to ensure that all compounds in the sample are eluted.

EXPERIMENTAL

Equipment

An LC/9533 ternary-gradient liquid chromatograph (IBM Instruments, Danbury CT, USA) was used with a Model 7125 sample injector (Rheodyne, Cotati, CA, USA) with a 20-μl loop. A circulating water-bath (Model T9; P.M. Tamson, Zoetermeer, Netherlands) was used for temperature control (23.0 ± 0.2°C) of the column compartment. A variable-wavelength UV detector (Model 9523; IBM Instruments) was used. Chromatograms were processed with a Model 3390A reporting integrator (Hewlett-Packard, Palo Alto, CA, USA); this supplied values for retention times, peak area and peak area/peak height ratio, which were used to determine the band width and column plate number when necessary.

The column dead volume, $V_m = t_o F$ (where t_o is the elution time of an unretained peak and F is the flow-rate), was measured from the retention time of sodium nitrate (70% acetonitrile as mobile phase) as $V_m = 2.16$ ml [13]. The equipment dwell volume, $V_D = t_D F$ (where t_D is the dwell time of the gradient equipment), was determined by two methods. First, a blank gradient was run without the column (see Fig. 1 in ref. 14). From this method, a value of 4.5 ml was obtained at 2.0 ml/min and 4.1 ml at 1.0 ml/min. The second method used the DryLab G/plus program. Retention data for 20- and 60-min gradients were entered into the program and retention times for an isocratic run of 73% acetonitrile were predicted and compared with values obtained

experimentally, while changing the dwell volume. The best agreement between experimental and predicted retention times was found for a dwell volume of 3.9 ml. As both methods gave similar values, 4.5, 4.1 and 3.9 ml, an average was taken, giving a dwell volume value of 4.2 ml. An extra-column band broadening of $\sigma_{ec} = 0.04$ ml was used. This value was again determined by using the DryLab G/plus software. Predicted and experimental band width values for both a flat and a steep gradient (60 and 12 min) were compared while changing the extra-column value. The best agreement was found for band width values when $\sigma_{ec} = 0.04$ ml.

Materials

Columns were 25.0 × 0.46 cm I.D., packed with octyl-bonded silica (Zorbax, 880952706; Mac-Mod Analytical, Chadds Ford, PA, USA). The column packing was a spherical silica support, 5 μm in diameter, with 100 Å pores. Columns were evaluated for plate number at frequent intervals during the study; a test mixture of uracil, acetophenone, nitrobenzene, methyl benzoate and toluene was used with methanol–water (70:30, v/v) as the mobile phase. The initial plate number for toluene was *ca.* 14 000 for a flow-rate of 0.8 ml/min.

Apart from the column test mixture described above, the following sample of a homologous series of nine alkylketones was used: 2-pentanone, 2-hexanone, 2-heptanone, 2-octanone, 2-nonanone, 2-decanone, 2-undecanone, 2-dodecanone and 2-tridecanone. These compounds were selected to be well resolved in all gradient runs, so as to allow accurate measurements of retention time and band width for every peak [15].

For the gradient separations of the alkylketones, solvent A was 0.1% phosphoric acid in distilled, deionized water and solvent B was 0.1% phosphoric acid in acetonitrile. All gradients were linear and were run from 10 to 100% B. In the isocratic separations, the percentage of organic refers to the total percentage acetonitrile content of the solvent.

Chemicals

Individual alkylketones were obtained from Aldrich (Milwaukee, WI, USA) and Fluka (Ronkonkoma, NY, USA). Acetonitrile (HPLC quality) was obtained from Fisher Scientific (Fair Lawn, NJ, USA) and methanol (HPLC quality) from Burdick and Jackson (Muskegon, MI, USA). Phosphoric acid was obtained from J. T. Baker (Phillipsburg, NJ, USA). Water used to prepare the chromatographic mobile phase was first condensed from steam, then passed through an organic removal cartridge, two mixed ion-exchange resin cartridges, followed by a 0.20-μm filter (Nanopure four-module system with pump; Sybron/Barnstead, Boston, MA, USA). The water would qualify as Type I ASTM standard water having a specific resistivity greater than 18 MΩ cm.

Computer simulations

The personal computer used to run the DryLab software was an IBM-PC/XT compatible, containing an 8087 math coprocessor chip, 640K of RAM memory, a monochrome graphics printer card, with both a 30 Mbyte hard disk and a 5.25-in. floppy disk drive (DryLab LCS Liquid Chromatography Simulator; LC Resources, Lafayette, CA, USA). Associated with this computer assembly was a high-resolution

monochrome monitor (GM-1230; Casper, Santa Clara, CA, USA) and a dot-matrix printer (MX-100; Epson-America, Torrance, CA, USA).

Predictions of band width required estimates of parameters X and Y, where X is the ratio of the volume of mobile phase outside the pores to the total volume of mobile phase and Y is the ratio of solute diffusion coefficients inside and outside the pores. Based on the use of an octyl-bonded packing of 100 Å pore size, values of X = 0.75 and Y = 0.40 were used, as suggested in the DryLab G/plus Users' Manual [16,17].

Computer predictions of band width with DryLab G/plus require a value of the Knox parameter A [16,18]. This was determined using the DryLab G/plus software in much the same way that the extra-column band broadening value was obtained. Predicted and experimental band width values for both a flat and a steep gradient (60 and 12 min) were used. The best agreement was found between predicted and experimental values for A = 0.90.

RESULTS AND DISCUSSION

Fig. 1 shows a comparison of an experimental and a simulated (DryLab G/plus) chromatogram. Tables I–X contain the results of the comparisons of experimental and predicted retention times for the isocratic separations. To generate the data in Tables I–V, retention data for nine alkylketones separated by a 20-min and a 60-min gradient with a flow-rate of 1.5 ml/min was used as input to DryLab G/plus. The program was then used as described earlier to predict the retention time for a number of different isocratic separations of the same nine ketones. In Tables VI–X, a flow-rate of 2.0 ml/min was used for both the gradient input data and the predicted isocratic runs.

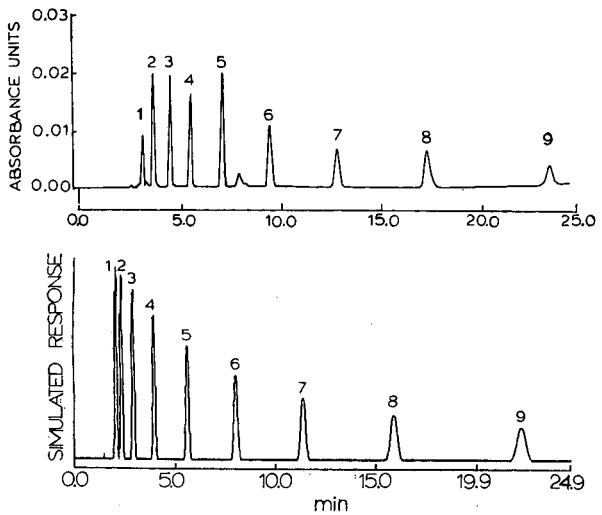

Fig. 1. Comparison of experimental and simulated (DryLab G/plus) chromatograms for an isocratic separation of nine alkylketones. Mobile phase: acetonitrile–aqueous 0.1% H_3PO_4 (70:30, v/v); flow-rate, 1.5 ml/min. Peaks: 1 = 2-pentanone; 2 = 2-hexanone; 3 = 2-heptanone; 4 = 2-octanone; 5 = 2-nonanone; 6 = 2-decanone; 7 = 2-undecanone; 8 = 2-dodecanone; 9 = 2-tridecanone.

TABLE I

EXPERIMENTAL AND PREDICTED RETENTION TIMES FOR THE ISOCRATIC SEPARATION OF ALKYLKETONES USING ACETONITRILE–AQUEOUS H_3PO_4 (70:30) AT A FLOW-RATE OF 1.5 ml/min

Solute	t_g (min)		Retention errors (±)	
	Exptl.	Calc.[a]	t_g[b]	Δt_g[c]
2-Pentanone	2.77	2.06	0.71	0.21
2-Hexanone	3.25	2.33	0.92	0.13
2-Heptanone	3.93	2.88	1.05	0.05
2-Octanone	4.91	3.91	1.00	0.30
2-Nonanone	6.28	5.58	0.70	0.42
2-Decanone	8.27	7.99	0.28	0.49
2-Undecanone	11.13	11.34	0.21	0.45
2-Dodecanone	15.19	15.85	0.66	0.38
2-Tridecanone	21.13	22.17	1.04	
Average			0.73	0.30

[a] DryLab G/plus predictions based on experimental data for 20- and 60-min gradients.
[b] Experimental minus predicted retention times (absolute values).
[c] Experimental minus predicted retention time differences, $\Delta t_g = t_2 - t_1$.

Differences in predicted and experimental retention times are expressed in two ways. The first compares experimental and predicted times directly: the absolute value of the experimental value minus the predicted value. The second uses the relationship between retention time differences, Δt_g. As R_s is proportional to the differ-

TABLE II

EXPERIMENTAL AND PREDICTED RETENTION TIMES FOR THE ISOCRATIC SEPARATION OF ALKYLKETONES USING ACETONITRILE–AQUEOUS H_3PO_4 (75:25) AT A FLOW-RATE OF 1.5 ml/min

Solute	t_g (min)		Retention errors (±)	
	Exptl.	Calc.[a]	t_g[b]	Δt_g[c]
2-Pentanone	2.60	1.91	0.69	0.22
2-Hexanone	2.98	2.07	0.91	0.11
2-Heptanone	3.45	2.43	1.02	0.07
2-Octanone	4.21	3.12	1.09	0.15
2-Nonanone	5.20	4.26	0.94	0.26
2-Decanone	6.60	5.92	0.68	0.38
2-Undecanone	8.50	8.20	0.30	0.29
2-Dodecanone	11.26	11.25	0.01	0.35
2-Tridecanone	15.09	15.43	0.34	
Average			0.66	0.20

[a-c] See Table I.

TABLE III

EXPERIMENTAL AND PREDICTED RETENTION TIMES FOR THE ISOCRATIC SEPARATION OF ALKYLKETONES USING ACETONITRILE–AQUEOUS H_3PO_4 (80:20) AT A FLOW-RATE OF 1.5 ml/min

Solute	t_g (min)		Retention errors (±)	
	Exptl.	Calc.[a]	t_g[b]	Δt_g[c]
2-Pentanone	2.48	1.80	0.68	0.18
2-Hexanone	2.76	1.90	0.86	0.16
2-Heptanone	3.15	2.13	1.02	0.07
2-Octanone	3.68	2.59	1.09	0.08
2-Nonanone	4.37	3.36	1.01	0.20
2-Decanone	5.31	4.50	0.81	0.27
2-Undecanone	6.60	6.06	0.54	0.30
2-Dodecanone	8.36	8.12	0.24	0.29
2-Tridecanone	10.84	10.89	0.05	
Average			0.70	0.19

[a-c] See Table I.

ence in retention times for two adjacent bands $(t_2 - t_1) = \Delta t_g$, errors in resolution can be related to the error in Δt_g. Because this takes into account the resolution between peaks, this method often gives a more accurate comparison of a predicted and experimental chromatogram than does the direct comparison of predicted and experimental retention times.

TABLE IV

EXPERIMENTAL AND PREDICTED RETENTION TIMES FOR THE ISOCRATIC SEPARATION OF ALKYLKETONES USING ACETONITRILE–AQUEOUS H_3PO_4 (85:15) AT A FLOW-RATE OF 1.5 ml/min

Solute	t_g (min)		Retention errors (±)	
	Exptl.	Calc.[a]	t_g[b]	Δt_g[c]
2-Pentanone	2.30	1.71	0.59	0.14
2-Hexanone	2.50	1.77	0.73	0.15
2-Heptanone	2.80	1.92	0.88	0.06
2-Octanone	3.17	2.23	0.94	0.06
2-Nonanone	3.63	2.75	0.88	0.10
2-Decanone	4.32	3.54	0.78	0.20
2-Undecanone	5.18	4.60	0.58	0.26
2-Dodecanone	6.32	6.00	0.32	0.26
2-Tridecanone	7.88	7.82	0.06	
Average			0.64	0.15

[a-c] See Table I.

TABLE V

EXPERIMENTAL AND PREDICTED RETENTION TIMES FOR THE ISOCRATIC SEPARATION OF ALKYLKETONES USING ACETONITRILE–AQUEOUS H_3PO_4 (90:10) AT A FLOW-RATE OF 1.5 ml/min

Solute	t_g (min)		Retention errors (±)	
	Exptl.	Calc.[a]	t_g[b]	Δt_g[c]
2-Pentanone	2.31	1.65	0.66	0.12
2-Hexanone	2.46	1.68	0.78	0.12
2-Heptanone	2.68	1.78	0.90	0.08
2-Octanone	2.96	1.98	0.98	0.00
2-Nonanone	3.32	2.34	0.98	0.08
2-Decanone	3.78	2.88	0.90	0.12
2-Undecanone	4.39	3.61	0.78	0.18
2-Dodecanone	5.15	4.55	0.60	0.20
2-Tridecanone	6.16	5.76	0.40	
Average			0.78	0.11

[a-c] See Table I.

The results of this study show that although the actual experimental and predicted retention times may not be exact (as indicated by the errors in predicted retention times in Table I–X), the corresponding errors in resolution are low. The errors in predicted retention times range from 0.64 to 1.05 min, with an average of 0.78 min.

TABLE VI

EXPERIMENTAL AND PREDICTED RETENTION TIMES FOR THE ISOCRATIC SEPARATION OF ALKYLKETONES USING ACETONITRILE–AQUEOUS H_3PO_4 (70:30) AT A FLOW-RATE OF 2.0 ml/min

Solute	t_g (min)		Retention errors (±)	
	Exptl.	Calc.[a]	t_g[b]	Δt_g[c]
2-Pentanone	1.98	1.52	0.46	0.22
2-Hexanone	2.32	1.64	0.68	0.17
2-Heptanone	2.81	1.96	0.85	0.11
2-Octanone	3.51	2.55	0.96	0.02
2-Nonanone	4.50	3.52	0.98	0.12
2-Decanone	5.92	5.06	0.86	0.24
2-Undecanone	7.95	7.33	0.62	0.29
2-Dodecanone	10.82	10.49	0.33	0.28
2-Tridecanone	15.03	14.98	0.05	
Average			0.64	0.18

[a-c] See Table I.

TABLE VII

EXPERIMENTAL AND PREDICTED RETENTION TIMES FOR THE ISOCRATIC SEPARATION OF ALKYLKETONES USING ACETONITRILE–AQUEOUS H_3PO_4 (75:25) AT A FLOW-RATE OF 2.0 ml/min

Solute	t_g (min)		Retention errors (±)	
	Exptl.	Calc.[a]	t_g[b]	Δt_g[c]
2-Pentanone	1.97	1.42	0.55	0.22
2-Hexanone	2.25	1.48	0.77	0.18
2-Heptanone	2.63	1.68	0.95	0.17
2-Octanone	3.18	2.06	1.12	0.11
2-Nonanone	3.93	2.70	1.23	0.04
2-Decanone	4.99	3.72	1.27	0.05
2-Undecanone	6.45	5.23	1.22	0.03
2-Dodecanone	8.49	7.30	1.19	0.01
2-Tridecanone	11.39	10.21	1.18	
Average			1.05	0.10

[a-c] See Table I.

The agreement of the corresponding error in resolution or Δt_g ranges from 0.07 to 0.30 min, with an average of 0.15 min, indicating good agreement between the experimental and predicted chromatograms.

TABLE VIII

EXPERIMENTAL AND PREDICTED RETENTION TIMES FOR THE ISOCRATIC SEPARATION OF ALKYLKETONES USING ACETONITRILE–AQUEOUS H_3PO_4 (80:20) AT A FLOW-RATE OF 2.0 ml/min

Solute	t_g (min)		Retention errors (±)	
	Exptl.	Calc.[a]	t_g[b]	Δt_g[c]
2-Pentanone	1.83	1.34	0.49	0.18
2-Hexanone	2.04	1.37	0.67	0.15
2-Heptanone	2.32	1.50	0.82	0.15
2-Octanone	2.71	1.74	0.97	0.11
2-Nonanone	3.23	2.15	1.08	0.04
2-Decanone	3.95	2.83	1.12	0.02
2-Undecanone	4.93	3.83	1.10	0.06
2-Dodecanone	6.24	5.20	1.04	0.03
2-Tridecanone	8.09	7.08	1.01	
Average			0.92	0.09

[a-c] See Table I.

TABLE IX

EXPERIMENTAL AND PREDICTED RETENTION TIMES FOR THE ISOCRATIC SEPARATION OF ALKYLKETONES USING ACETONITRILE–AQUEOUS H_3PO_4 (85:15) AT A FLOW-RATE OF 2.0 ml/min

Solute	t_g (min)		Retention errors (±)	
	Exptl.	Calc.[a]	t_g[b]	Δt_g[c]
2-Pentanone	1.75	1.28	0.47	0.15
2-Hexanone	1.91	1.29	0.62	0.13
2-Heptanone	2.12	1.37	0.75	0.12
2-Octanone	2.40	1.53	0.87	0.11
2-Nonanone	2.78	1.80	0.98	0.06
2-Decanone	3.28	2.24	1.04	0.00
2-Undecanone	3.95	2.91	1.04	0.02
2-Dodecanone	4.83	3.81	1.02	0.02
2-Tridecanone	6.03	5.03	1.00	
Average			0.86	0.08

[a-c] See Table I.

TABLE X

EXPERIMENTAL AND PREDICTED RETENTION TIMES FOR THE ISOCRATIC SEPARATION OF ALKYLKETONES USING ACETONITRILE–AQUEOUS H_3PO_4 (90:10) AT A FLOW-RATE OF 2.0 ml/min

Solute	t_g (min)		Retention errors (±)	
	Exptl.	Calc.[a]	t_g[b]	Δt_g[c]
2-Pentanone	1.71	1.23	0.48	0.11
2-Hexanone	1.83	1.24	0.59	0.11
2-Heptanone	1.98	1.28	0.70	0.09
2-Octanone	2.18	1.39	0.79	0.09
2-Nonanone	2.44	1.56	0.88	0.04
2-Decanone	2.78	1.86	0.92	0.00
2-Undecanone	3.22	2.30	0.92	0.03
2-Dodecanone	3.78	2.89	0.89	0.06
2-Tridecanone	4.51	3.68	0.83	
Average			0.78	0.07

[a-c] See Table I.

CONCLUSIONS

This study suggests that, although it was not intended for that purpose, the computer program DryLab G/plus can be used to predict isocratic retention from gradient input. Using DryLab G/plus for isocratic method development is advantageous over using DryLab I/plus, which also serves that purpose, because DryLab G/plus does not limit its user just to isocratic method development. If DryLab I/plus is used, only isocratic methods can be developed. If DryLab G/plus is used, the development of both isocratic and gradient elution method is possible.

ACKNOWLEDGEMENTS

We sincerely acknowledge the valuable suggestions and encouragement provided to us by Lloyd R. Snyder. We thank John Dolan and Thomas Jupilee of LC Resources for the gift of the DryLab software packages. We also thank U. Carterbone of Mac-Mod Analytical for the reversed-phase, octyl-bonded columns.

REFERENCES

1 L. R. Snyder, in Cs. Horvath (Editor), *High-Performance Liquid Chromatography —Advances and Perspectives*, Vol. 1, Academic Press, New York, 1980, p. 207.
2 P. Jandera and J. Churacek, *Gradient Elution in Column Liquid Chromatography —Theory and Practice*, Elsevier, Amsterdam, 1985.
3 M. A. Stadalius and L. R. Snyder, in Cs. Horvath (Editor), *High-Performance Liquid Chromatography —Advances and Perspectives*, Vo. 4, Academic Press, New York, 1986, p. 195.
4 L. R. Snyder, J. L. Glajch and J. J. Kirkland, *Practical HPLC Method Development*, Wiley, New York, 1988.
5 L. R. Snyder and J. W. Dolan, *LC · GC*, 8 (1990) 524.
6 J. W. Dolan and L. R. Snyder, *Am. Lab.*, 22 (1990) 50.
7 L. R. Snyder, J. W. Dolan and D. C. Lommen, *J. Chromatogr.*, 485 (1989) 65.
8 J. W. Dolan, D. C. Lommen and L. R. Snyder, *J. Chromatogr.*, 485 (1989) 91.
9 J. W. Dolan and L. R. Snyder, *LC · GC*, 5 (1987) 970.
10 L. R. Snyder, M. A. Quarry and J. L. Glajch, *Chromatographia*, 24 (1987) 33.
11 L. R. Snyder, J. W. Dolan and M. P. Rigney, *LC · GC*, 4 (1986) 921.
12 J. Schmidt, *J. Chromatogr.*, 485 (1989) 421.
13 M. J. M. Wells and C. R. Clark, *Anal. Chem.*, 53 (1981) 1341.
14 J. D. Stuart, D. D. Lisi and L. R. Snyder, *J. Chromatogr.*, 485 (1989) 657.
15 D. W. Hill and K. J. Langner, in D. G. Deutsch (Editor), *Analytical Aspects of Drug Testing*, Wiley, New York, 1989, p. 129.
16 R. W. Stout, J. J. DeStefano and L. R. Snyder, *J. Chromatogr.*, 282 (1983) 263.
17 *DryLab G/plus Users' Manual*, LC Resources, Lafayette, CA, 1989.
18 J. H. Knox, *J. Chromatogr. Sci.*, 15 (1977) 352.

Journal of Chromatography, 550 (1991) 87–100
Elsevier Science Publishers B.V., Amsterdam

CHROMSYMP. 2251

Prediction of initial high-performance liquid chromatographic conditions for selectivity optimization in pharmaceutical analysis by an expert system approach

GÁBOR SZEPESI*
Institute HUMAN for Serobacterological Research and Production, Budapest-Gödöllő (Hungary)
and
KLÁRA VALKÓ
Central Research Institute for Chemistry, Hungarian Academy of Sciences, Budapest (Hungary)

ABSTRACT

Initial mobile phase compositions can be selected from any physicochemical properties of solutes which can be correlated with their high-performance liquid chromatography (HPLC) retention. In this study, octanol–water partition coefficients (log P values) calculated from molecular increments are converted to HPLC retention data to achieve capacity factors (k') within a range 0.5–5. The eluent compositions are calculated to produce k' values of 0.5 (OP_{min}) and 5 (OP_{max}) for all solutes of interest. From the various eluent compositions obtained as OP_{min} values, the highest value (the strongest eluent composition, $OP_{min,ST}$) and as OP_{max} values, the lowest value (the weakest eluent composition, $OP_{max,WE}$), are chosen to calculate the optimum composition for the initial experiments (OP_{IN}). Using the suggested mobile phase composition, OP_{IN}, the k' values of each component are predicted and checked. The first guess experiment can be started with the suggested eluent composition. Pass–fail criteria have been established to evaluate the experimental data; the capacity factors of all components should be within the range 0.5–10, and the peak asymmetry factors should be between 0.8 and 1.8. For the direction of the second and third guess experiments, special rules followed by different actions are formulated. The applicability of the developed expert system is demonstrated through the separation of a model mixture containing solutes with widely different chemical structures.

INTRODUCTION

The selection of suitable experimental conditions for initial separations involves more than merely choosing an appropriate packing material to fill a tube of some prejudged dimension and a mobile phase to achieve suitable retentions. The approach suggested in this paper includes the following considerations.

Separation mode selection

The selection of phase system is a highly empirical task as a result of the unpredictable selectivity of one phase system for a new analytical problem. A single pack-

0021-9673/91/$03.50

ing material may be used in several different chromatographic modes to carry out different types of separations. The specified preknowledge regarding molecular weight, solubility and ionic properties of the solutes provide an useful source of information for the selection of the separation mode. A change in separation mode may be achieved simply by changing the composition of the mobile phase or by using various additives in the eluent. In the following discussion, only the principles relating to reversed-phase separations will be considered.

Phase system selection

Phase system selection includes decisions about two different things: stationary and mobile phase selections. All the experiments discussed here have been performed on chemically bonded octadecylsilica stationary phases with reversed-phase eluents.

The primary goal of the initialization experiments is to achieve an acceptable capacity factor (k') range and peak shape for all of the solutes of interest. Basically there are four different routes to achieve this goal.

Empirical route without any preknowledge of the sample. The experiments start using high organic concentrations in the eluent (for instance, 70–80% methanol in water at a pH of about 2.2 or 8.0 that can suppress possible ionization). The eluent composition is modified step by step on the basis of the capacity factor of the last eluting peak (a greater modification in the eluent strength is made if $k'_{last} < 1.0$; only a slight modification is made if $k'_{last} < 3$).

Empirical route considering the physicochemical properties of the solutes of interest. The mobile phase is selected according to the type of solute(s) (solubility, polarity in ion supression media and basicity). A recommended procedure has been reported by Gazdag *et al.* [1].

Application of gradient elution for the selection of initial mobile phase compositions. The application of gradient elution of initial method development has some advantages relative to the use of isocratic elution for several reasons: (1) for unknown samples, it is more likely that gradient elution will reveal the presence of compounds that might be lost due to their early elution with the solvent front or to their disappearance in the baseline as late eluting peaks under isocratic conditions; (2) the separation characteristics of sample components with a large k' range can be established more easily in a few gradient experiments (several isocratic runs would be required to obtain the same information); (3) the suitability of isocratic elution for the effective separation of a sample can be confirmed by gradient elution.

Several approaches have been described previously [2–5] to predict isocratic separations from gradient elution.

Computer-aided selection of initial mobile phase compositions. The initial mobile phase compositions can be selected on the basis of any physicochemical properties of the solutes which can be correlated with their HPLC retention. There are two different methods for this.

In the first approach (individual retention concept) suggested by Maris *et al.* [6], a calculation is carried out based on retention increments and obtaining a total retention factor for each individual solute to achieve a k' value of 3. The computer-aided selection of initial mobile phase composition is based on the calculation of the polarity of the structural fragments that are not affected by the pH (pH independent increments) and of fragments, the polarity of which strongly depends on the pH (pH

dependent increments). The mobile phase composition is given by summing all the contributions which correspond to the structural elements.

In the second approach (total retention concept), log P values (the logarithm of octanol–water partition coefficients) are calculated from molecular increments. Based on the algorithms published by Valkó [7,8] and a relatively large database, the log P data are transformed to HPLC retention data to achieve k' values within a range 0.5–5. The eluent compositions are calculated to produce a k' value of 0.5 (OP_{min}) and 5 (OP_{max}) for all solutes of interest. From the compositions obtained as OP_{min} values for all compounds in the mixture, the highest value is chosen and referred to as $OP_{min,ST}$ (the strongest eluent composition) and from the OP_{max} values the lowest value is chosen and referred to as $OP_{max,WE}$ (weakest eluent composition). From the two values the optimum composition for the initial experiments (OP_{IN}) is calculated according to the equation: $OP_{IN} = (OP_{max,WE} + OP_{min,ST})/2$.

BASIC PRINCIPLES

Fig. 1. shows the structural modules of the initialization expert system used in this study. From the initial conditions given in Fig. 1, only the mobile phase selection will be discussed here; the other conditions (column type and dimension, detection wavelength and flow-rate) were the same during the experiments. The structural elements for the prediction of the initial mobile phase composition are shown in Fig. 2.

As can be seen from Fig. 2, the input data correspond to the structural formulas of the compounds of interest. In the first step from the structural data the log P values

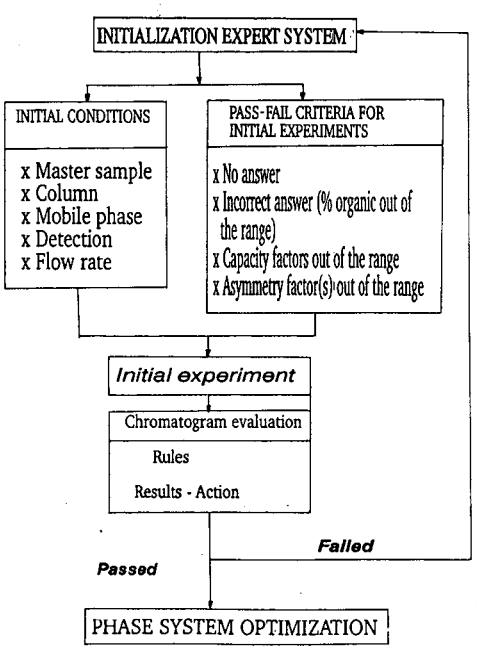

Fig. 1. Construction of the initialization expert system.

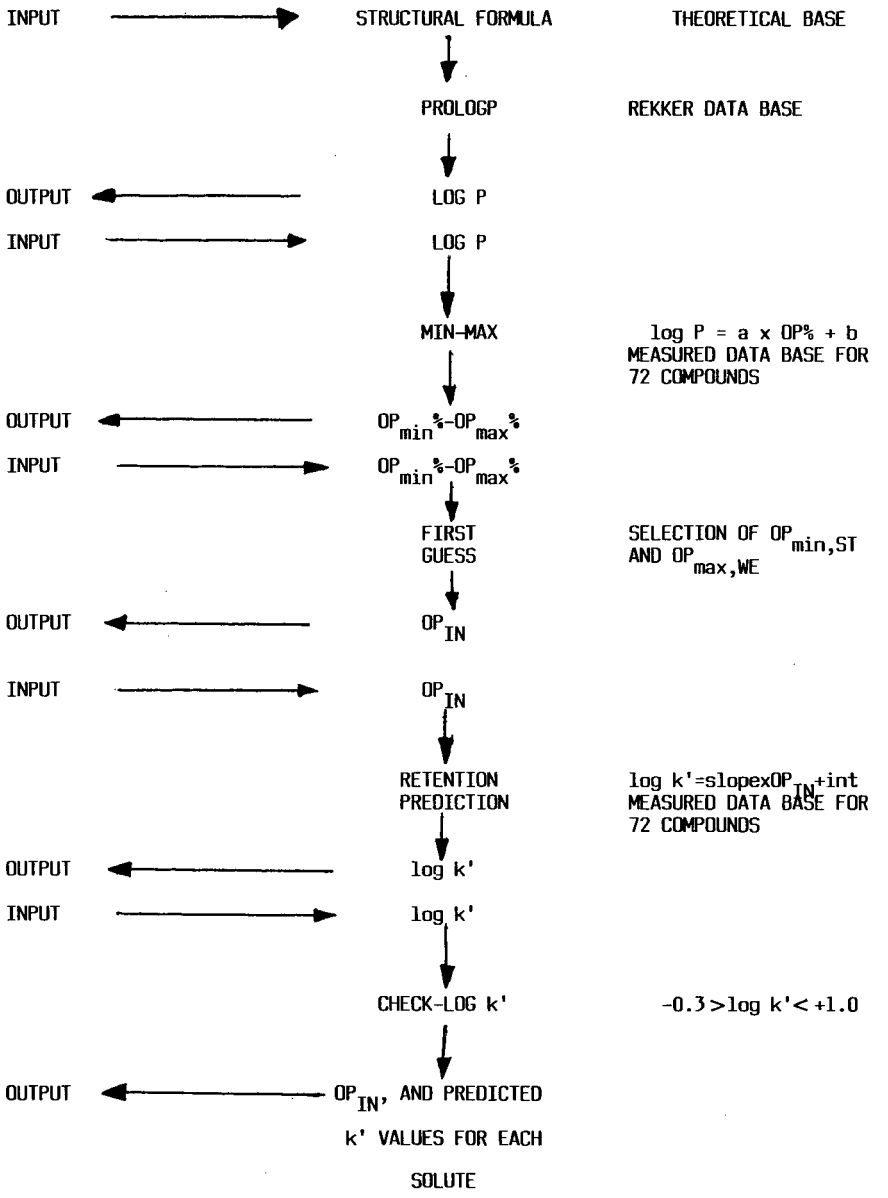

Fig. 2. Prediction of initial mobile phase composition for first guess experiment.

are calculated by the PrologP program based on the Rekker database (Compudrug, Budapest, Hungary). The calculated log P values are transformed in the next step into organic solvent concentrations in the eluent using our MinMax database, which calculates the organic solvent concentration for all components resulting in capacity factors of 0.5 (OP_{min} and 5 (OP_{max}) for each individual component. In the first guess block from the listed percentage organic solvent concentrations, the highest value of

OP_{min} (the strongest eluent composition giving $k' = 0.5$, $OP_{min,ST}$) and the lowest value of OP_{max} (weakest eluent composition giving $k' = 5$, $OP_{max,WE}$) are selected and their average is used as the first estimated eluent composition, OP_{IN}. As OP_{IN} is weaker than $OP_{min,ST}$ and stronger than $OP_{max,WE}$, the predicted values of k' for all components are estimated to be within a k' range 0.5–5. Using the suggested mobile phase composition, OP_{IN}, the k' values of each component are predicted and checked. If the predicted k' values are within the required range, the first guess experiment can be started with the suggested eluent composition.

PASS–FAIL CRITERIA FOR INITIAL EXPERIMENTS

In accordance with the main aim of the initialization experiments, criteria can be formulated for passing the experiments from the initial stage to the optimization stage. It is obvious that these criteria differ from those used for phase system optimization. In this study the following pass–fail criteria were established to evaluate the experimental data: (1) no answer (faulty operation occurs, or the PrologP program does not work); (2) capacity factors are out of range (k' of any single solute is < 0.5 or > 10); (3) peak asymmetry factor is out of the range (A_{sf} for any solute is < 0.8, or > 1.8); and (4) incorrect answer (percentage organic calculated for OP_{IN} is out of the range). If either the $OP_{min,ST}$ value or the $OP_{max,WE}$ value is out of range ($> 90\%$ or $< 1\%$ acetonitrile in the eluent are required to sufficiently elute one or more compounds in the mixture within a k' range 0.5–5), then as a first approximation the $OP_{min,ST}$ is taken as equal to 100% or $OP_{mas,WE}$ is taken as equal to zero in the OP_{IN} calculation. In this instance the predicted k' value of this particular compound will be automatically out of the range and its k' value can be adjusted to the correct value in the second or third guess experiments (see later example).

INITIAL PHASE SYSTEM: RULES

The initial mobile phase selection is based on between one and three experimental runs under predicted isocratic conditions. The first experiment is performed using a mobile phase containing acetonitrile and aqueous phosphate buffer at pH 4.5 in the suggested ratio (system I.1 in Table I). The eluent composition in the next guess experiment is dependent on the capacity factors of the first and/or the last peaks as well as on the peak asymmetry observed. The necessary steps are directed by several rules, including the change in acetonitrile concentration, using methanol in the eluent or a change in the eluent pH. The mobile phase compositions wich may be utilized in the second and third guess experiments are given in Table I.

As a general rule the following principles are used in our study: (1) if only one capacity factor criterion is out of range (k' of first eluted peak, $k'_F < 0.5$ or k' of last eluted peak, $k'_L > 10$) and the peak asymmetry factor (A_{sf}) is acceptable for each compound, the acetonitrile concentration is recalculated according to Table I (system I.1 in Table I); (2) if both capacity factor criteria are out of range, but the peak asymmetry factor is acceptable for each peak, then methanol is used in the eluent at an identical eluent strength and pH (system II.1 in Table I); (3) if only one asymmetry factor criterion is out of range, and the capacity factors are within range, the same eluent composition is used as in case (1), but the pH of the eluent is adjusted to pH 2.2

TABLE I

INITIAL PHASE SYSTEMS AND EXPERIMENTAL CONDITIONS

Column: Hypersil ODS, 5 μm, 150 × 4 mm I.D. Flow-rate: 0.85 ml/min. Detection: 254 nm.

	Mobile phases[a]	
	(I) Acetonitrile (ACN)–water	(II) Methanol (MeOH)–water
	System I.1, pH 4.5	*System II.1, pH 4.5*
(A) $k'_F < 0.05$	ACN (%) = 0.84 × ACN_I (%)	MeOH (%) = 0.80 × $MeOH_I$ (%)
(B) $k'_L > 15$	ACN (%) = 1.2 × ACN_I (%)	MeOH (%) = 1.3 × $MeOH_I$ (%)
(C) $0.05 < k'_F < 0.5$	ACN (%) = ACN_I (%)–15 log $(0.5/k'_I)$	MeOH (%) = $MeOH_I$ (%)–25 log $(0.5k'_I)$
(D) $10 < k'_L < 15$	ACN (%) = ACN_I (%) + 15 log $(k'_I/10)$	MeOH (%) = $MeOH_I$ (%) + 25 log $(k'_I/10)$
	System I.2, pH 2.2	*System II.2, pH 2.2*
(A) $k'_F < 0.05$	ACN (%) = 0.84 × ACN_I (%)	MeOH (%) = 0.80 × $MeOH_I$ (%)
(B) $k'_L > 15$	ACN (%) = 1.2 × ACN_I (%)	MeOH (%) = 1.3 × $MeOH_I$ (%)
(C) $0.05 < k'_F < 0.5$	ACN (%) = ACN_I (%)–20 log $(0.5/k'_I)$	MeOH (%) = $MeOH_I$ (%)–30 log $(0.5k'_I)$
(D) $10 < k'_L < 15$	ACN (%) = ACN_I (%) + 20 log $(k'_I/10)$	MeOH (%) = $MeOH_I$ (%) + 30 log $(k'_I/10)$
	System I.3, pH 7.8	*System II.3, pH 7.8*
(A) $k'_F < 0.05$	ACN (%) = 0.84 × ACN_I (%)	MeOH (%) = 0.80 × $MeOH_I$ (%)
(B) $k'_L > 15$	ACN (%) = 1.2 × ACN_I (%)	MeOH (%) = 1.3 × $MeOH_I$ (%)
(C) $0.05 < k'_F < 0.5$	ACN (%) = ACN_I (%)–20 log $(0.5/k'_I)$	MeOH (%) = $MeOH_I$ (%)–30 log $(0.5k'_I)$
(D) $10 < k'_L < 15$	ACN (%) = ACN_I (%) + 20 log $(k'_I/10)$	MeOH (%) = $MeOH_I$ (%) + 30 log $(k'_I/10)$

[a] Subscript I refers to the organic solvent concentration in the previous experiment.

(A_{sf} is less than 0.8, system I.2 in Table I) or to pH 7.8 (A_{sf} is higher than 1.8, system I.3 in Table I); (4) if both asymmetry factor criteria are out of range, and the capacity factors are within range, methanolic eluent is used at an identical eluent strength and pH as in case (1) (system II.1 in Table I); (5) if only one capacity factor criterion and one peak asymmetry criterion are out of range, a recalculated acetonitrile concentration with different pH (system I.2 for peak leading, or system I.3 for peak tailing) is used; (6) if both capacity factor criteria and one peak asymmetry criterion are out of range, methanol is used in the second guess experiment at an identical eluent strength but with a different pH (system II.2 for peak leading, or system II.3 for peak tailing); (7) if one capacity factor criterion and both peak asymmetry factor criteria are out of range, a recalculated methanol concentration with the same pH (system II.1 in Table I) is used; (8) if both the capacity factor and peak asymmetry factor criteria are out of range, the expert system is not able to advise on further experimental conditions. This case requires special considerations (using normal phase chromatography, ion pair chromatography or other techniques based on secondary chemical equilibria).

Table II summarizes the rules to be used for the direction of next guess experiments.

CHECKING THE EXPERT SYSTEM FOR A SELECTED MODEL MIXTURE

To control the operation of the initial expert system a model mixture (the components are shown in Fig. 3) was selected. The calculated data for log P, OP_{min}, OP_{max}, log k' and k' are also shown in Fig. 3.

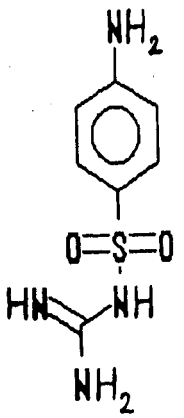

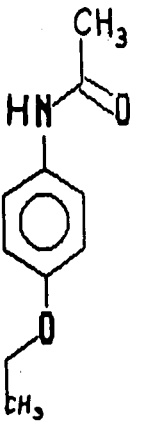

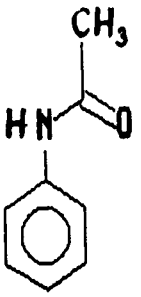

	Sulfaguanidine	Phenacetin	Acetanilide
log P	-2.384	1.128	0.529
$OP\%_{min}$	12.0%	55.7%	48.2%
$OP\%_{max}$	-16% (0)	12.4%	7.4%
log k	-0.751	0.369	0.265
k'	0.180	2.340	1.840

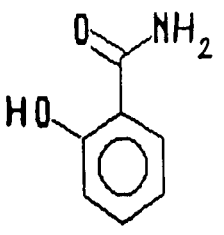

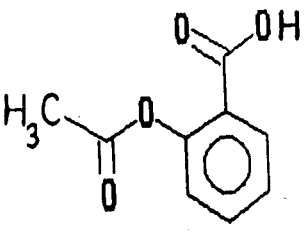

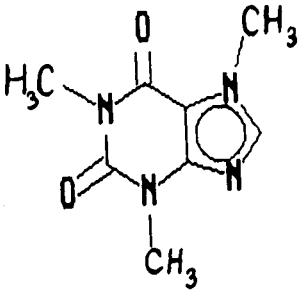

	Salicylamide	Acetylsal. acid	Caffeine
log P	0.236	1.037	-0.912
$OP\%_{min}$	44.6%	54.5%	30.2%
$OP\%_{max}$	5%	11.6%	-4.4% (0)
log k	0.157	0.315	-0.285
k'	1.435	2.067	0.519

SUGGESTED ACETONITRILE CONCENTRATION: 28%

Fig. 3. Model compounds used for checking the expert system.

As can be seen from Fig. 3, the OP_{max} values of sulphaguanidine (−16%) and caffeine (−4.4%) are out of the percentage organic range, therefore $OP_{max,WE}$ was selected to be zero. $OP_{min,ST}$ was 55.7% for phenacetin, and the calculated OP_{IN} is

TABLE II

RULES FOR DIRECTION OF NEXT GUESS EXPERIMENTS

First guess				Second guess				Third guess			
Results			Action: rule	Results			Action: rule	Results			Action: rule
Capacity factor		Peak symmetry[a]		Capacity factor		Peak symmetry[a]		Capacity factor		Peak symmetry[a]	
First peak	Last peak			First peak	Last peak			First peak	Last peak		
>0.5	<10	0.8–1.8	STOP, A.1	>0.5	<10	0.8–1.8	STOP, B.1	>0.5	<10	0.8–1.8	STOP, C.1
<0.5	<10	0.8–1.8	A.21	<0.5	<10	0.8–1.8	B.210, B.212 B.213, B.214 STOP, B.211	<0.5	<10	0.8–1.8	C.21–C.24 C.31–C.34 C.41–C.43 C.51–C.53 C.61–C.63 C.71–C.73 C.81, C.82
>0.5	>10	0.8–1.8	A.22	>0.5	>10	0.8–1.8	B.311, B.312 B.313, B.314 STOP, B.310	>0.5	>10	0.8–1.8	C.91–C.94 C.101–C.104 C.111–C.113 C.121–C.123 C.131–C.133 C.141–C.143 C.151, C.152
<0.5	>10	0.8–1.8	A.23	<0.5	>10	0.8–1.8	B.410, B.412 B.413 STOP, B.411	<0.5	>10	0.8–1.8	C.161–C.164 C.171–C.174 C.181, C. 182 C.191, C.192

>0.5	<10	<0.8 <1.8	A.31	>0.5	<10	<0.8 <1.8	B.5	Other cases:	No advise
>0.5	<10	>0.8 >1.8	A.32	>0.5	<10	>0.8 >1.8	B.6		
>0.5	<10	<0.8 >1.8	A.33	>0.5	<10	<0.8 >1.8	B.7		
<0.5	<10	<0.8 <1.8	A.411	<0.5	<10	<0.8 <1.8	B.8		
>0.5	>10	<0.8 <1.8	A.412	>0.5	>10	<0.8 <1.8	B.9		
<0.5	<10	>0.8 >1.8	A.421	<0.5	<10	>0.8 >1.8	B.10		
>0.5	>10	>0.8 >1.8	A.422	>0.5	>10	>0.8 >1.8	B.11		
<0.5	<10	<0.8 >1.8	A.431	<0.5	<10	<0.8 >1.8	B.120		
							STOP, B.121		
							STOP, B.122		
>0.5	>10	<0.8 >1.8	A.432	>0.5	>10	<0.8 >1.8	B.130		
							STOP, B.131		
							STOP, B.132		
<0.5	>10	<0.8 >1.8	STOP, A.44	<0.5	>10	<0.8 >1.8	STOP, B.14		

[a] The data refer to the investigation of a model mixture; for one peak A_{sf} should be less than 0.8, and for another one higher than 1.8.

27.9% acetonitrile. Using this eluent composition, all the predicted capacity factors with the exception of k' for sulphaguanidine are within range.

Using system I.1 with an acetonitrile–water ratio of 27.9:72.1, the chromatogram shown in Fig. 4 is obtained; a comparison of the caculated and observed values of the capacity factors is given in Table III.

From the chromatogram in Fig. 4 and data in Table III, the following important information can be drawn: (1) the predicted and observed elution orders are in good agreement; (2) the predicted and observed k' values are also in good agreement with the exception of acetylsalicylic acid and phenacetin; (3) two criteria are out of range, the k' value of sulphaguanidine is less than 0.5 (for explanation, see earlier) and the peak asymmetry factor of acetylsalicylic acid is less than 0.8.

The necessary action is directed according to rule A.411 (Table IV), suggesting a recalculation of the eluent strength and the use of system I.2 (pH 2.2). The recalculated eluent concentration is 22% acetonitrile, and the chromatogram obtained is shown in Fig. 5 (k' data are also presented in Table III).

The data presented in Table III for a 22% acetonitrile concentration show that the predicted and observed elution orders are the same; the change of eluent pH has no influence on it. Similarly, a good correlation of the predicted and observed k' values can be seen, and the peak asymmetry factors of all components are within the required range. The necessary action is directed according to rule B.213 (Table IV), leading to a recalculated acetonitrile concentration of 18%. The chromatogram obtained using this eluent is shown in Fig. 6, and the data are given in Table III.

As can be seen from Fig. 6 and Table II, if 18% acetonitrile is used a k' value of only 0.4 can be obtained for sulphaguanidine, but the phenacetin retention achieved a critical value (close to the upper limit of the k' criterion), which requires further initial experiments to stop (Table IV). Therefore this eluent composition is suggested for phase system optimization. (It should be noted that peak separation criterion as

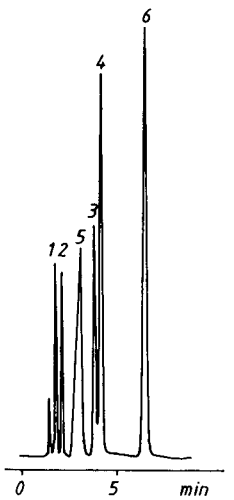

Fig. 4. Chromatogram obtained in first guess experiment. Eluent: acetonitrile–phosphate buffer (pH 4.5) (27.9:72.1). Other conditions as in Table I. Peaks: 1 = sulphaguadinine; 2 = caffeine; 3 = salycilamide; 4 = acetamide; 5 = acetylsalicylic acid; 6 = phenacetin.

TABLE III

RESULTS IN THE FIRST, SECOND AND THIRD GUESS EXPERIMENTS

Compounds	System	Capacity factors		Peak asymmetry
		Predicted	Found	
First guess	I.1. 27.9% acetonitrile			
Sulphaguanidine		0.180	0.201	1.05
Caffeine		0.519	0.400	0.95
Salicylamide		1.435	1.550	1.18
Acetanilide		1.840	1.775	1.03
Acetylsalicylic acid		2.067	1.257	0.67
Phenacetin		2.340	3.267	1.07
Second guess	I.2. 22.0% acetonitrile			
Sulphaguanidine		0.259	0.391	1.08
Caffeine		0.783	0.688	1.20
Salicylamide		2.043	2.503	1.48
Acetanilide		2.649	2.820	1.33
Acetylsalicylic acid		3.013	4.325	1.30
Phenacetin		3.197	5.879	1.43
Third guess	I.2. 18.0% acetonitrile			
Sulphaguanidine		0.324	0.400	1.05
Caffeine		1.033	1.023	1.21
Salicylamide		2.582	3.634	1.38
Acetanilide		3.428	4.049	1.18
Acetylsalicylic acid		3.864	7.105	1.32
Phenacetin		3.945	9.583	1.27

TABLE IV

RESULTS AND ACTIONS IN THE FIRST, SECOND AND THIRD GUESS EXPERIMENTS

Results	Rule	Criteria failed			Actions
		First guess	Second guess	Third guess	
First guess experiment	A.411	$k' < 0.5$ $A_{sf} < 0.8$			Use system I.2. with recalculated eluent strength for k'_F
Second guess experiment	B.213		$k' < 0.5$		Recalculate system I.2. for k'_F
Third guess experiment	C.81			$k' < 0.5$	Look for first eluting compound(s), if it is the same use B.213, if it is different use 1:1 mixture of A.411 and B.213 for optimization

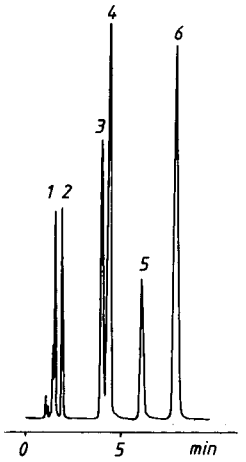

Fig. 5. Chromatogram obtained in second guess experiment. Eluent: acetonitrile–phosphate buffer (pH 2.2) (22:78). Other conditions as in Table I. For peak identification see Fig. 4.

resolution is not included in the pass–fail criteria of the initial expert system. Although practically baseline separation has been achieved for all components in the mixture during the initial experiments, in most instances two or more peaks may overlap in the initial system, therefore the separation of these overlapping compounds should be the target of further optimization steps.)

CONCLUSIONS

From the experimental data the following general conclusions can be drawn.

(1) The expert system based on the generation of solubility data (log P) from the structural formulas of compounds of interest and on their transformation to retention data on two different levels (upper boundary 10, lower boundary 0.5), resulting

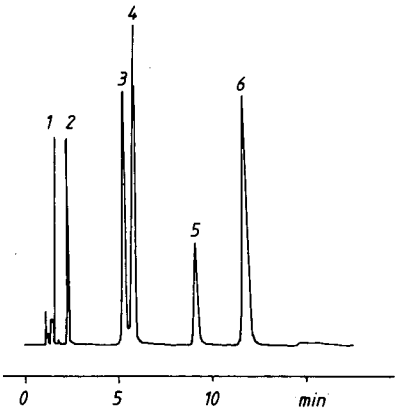

Fig. 6. Chromatogram obtained in third guess experiment. Eluent: acetonitrile–phosphate buffer (pH 2.2) (18:82). Other conditions as in Table I. For peak identification see Fig. 4.

in a suggested eluent composition for the initial experiments, can be successfully applied even if compounds differing widely in chemical structures can be separated.

(2) An acceptably good correlation to the predicted and observed elution orders has been found.

(3) The expert system can also be used in cases where one of the calculated eluent compositions for the upper or lower boundaries is out of range. In this concept zero is used for $OP_{max,WE}$ and 100 for $OP_{min,ST}$, but the experimental data also suggest using the calculated data. For a first guess experiment the expert system suggested a 16% acetonitrile concentration to achieve a k' of 5 sulphaguanidine ($OP_{max,WE}$) and 55.7% acetonitrile concentration to achieve a k' of 0.5 for phenacetine. Using these values for calculating OP_{IN}, a 19.9% acetonitrile concentration is proposed for the first guess experiment. Possibly the same k' value for sulphaguanidine should have been obtained (k' is about 0.4) in the first guess, as was obtained in the third guess.

(4) Although the main aim of the expert system concept used for the initial eluent selection in this study was to suggest a mobile phase composition providing symmetrical peaks which elute within a definite capacity factor range, a relatively good correlation between the predicted and observed capacity factors was seen. A general conclusion can be drawn from these experiments, namely, a much better correlation can be obtained for peaks with a k' value below 5 than for the peaks eluting with higher retentions. This observation possibly derives from the calculation of the first guess experiment using a k' value for the upper boundary of 5 instead of 10. However, the linearized equations between log P and OP% as well as between OP% and log k' are valid within a definite range of eluent composition; therefore according to our assumption, the calculation for the first guess experiment may give more reliable results within this narrower k' range than if it is extended to a larger k' range.

From the initial experiments some special information may be obtained, which me be a useful source of information for further optimization steps. The content of such information is also a function of the number and the necessary changes in the conditions of the initial experiments. The information obtained from the initial experiments are as follows: (1) elution order of the peaks; (2) number of peak-clusters to be resolved; (3) validity of the linear relationship of log k' *versus* the percentage organic curve; (4) dependence of elution order on the nature and concentration of organic solvents used for eluent preparation (methanol *versus* acetonitrile); (5) the dependence of solute retention on the pH of the eluent and (6) the estimation of difficulties during the optimization experiments.

ACKNOWLEDGEMENT

The authors are grateful to Dr. F. Darvas (Compudrug, Budapest, Hungary) for making the PrologP program available.

REFERENCES

1 M. Gazdag, G. Szepesi and E. Szeleczki, *J. Chromatogr.*, 454 (1988) 83.
2 J. C. Berridge, *Techniques for the Automated Optimization of HPLC Separations*, Wiley-Interscience, New York, 1985, p. 41.
3 P. J. Schoenmakers, H. A. H. Billiet and L. de Galan, *J. Chromatogr.*, 205 (1981) 13.

4 M. A. Quarry, R. L. Grob and L. Snyder, *Anal. Chem.*, 907 (1986) 907.
5 M. A. Quarry, R. L. Grob, L. Snyder, J. W. Dolan and M. P. Rigney, *J. Chromatogr.*, 384 (1987) 163.
6 F. Maris, R. Hindriks, J. Vink, A. Peeters, N. V. Driessche and L. Massart, *J. Chromatogr.*, 506 (1990) 211.
7 K. Valkó, *J. Liq. Chromatogr.*, 7 (1984) 1405.
8 K. Valkó, in H. Kalász and L. Ettre (Editors), *Chromatography, the State of the Art*, Akadémiai Kiadó, Budapest, 1985, p. 739.

Journal of Chromatography, 550 (1991) 101–134
Elsevier Science Publishers B.V., Amsterdam

CHROMSYMP. 2177

Measurement of solute dipolarity/polarizability and hydrogen bond acidity by inverse gas chromatography

JIANJUN LI, YUNKE ZHANG, ANDREW J. DALLAS and PETER W. CARR*
Department of Chemistry, University of Minnesota, Kolthoff and Smith Halls, 207 Pleasant Street SE, Minneapolis, MN 55455 (USA)

ABSTRACT

Solvatochromically based linear solvation energy relationships (LSERs) have been studied for more than ten years and been applied to the study of a very wide variety of chemical phenomena. During the past several years they have been used to explore retention processes and characterize gas chromatographic stationary phases. However, the general application of this method is limited by the complex and tedious methods needed to measure the explanatory variables and by the limited accuracy of the *a priori* parameter estimation rules. In this paper we have investigated the use of retention data for a wide variety of solutes on more than a dozen very different gas chromatographic stationary phases, including a number of extremely basic phases. These data are the basis for a method of rapidly estimating two of the explanatory variables commonly encountered in solvatochromic LSERs. Using the above approach, the polarity/polarizability parameters and the hydrogen bond donor acidity parameters for more than 200 compounds have been estimated. The results suggest that these two parameters can be estimated with a precision, and perhaps accuracy, at least as good as the more time-consuming methods. We have demonstrated that the Martin equation and LSER equations based on these parameters are compatible. Finally we have shown for the first time that the coefficients of the LSER, as required by basic theory, are proportional to the liquid phase solvatochromic parameters.

INTRODUCTION

When Kamlet and co-workers initiated their studies [1–3] of linear solvation energy relationships (LSERs), their goal was to explore how a solvent influences a property (denoted as *XYZ*) of a single solute. Their earliest studies were concerned with the effect of solvent on spectroscopic properties of a carefully chosen set of solutes. All of their initial work involved the $\pi \rightarrow \pi^*$ and $p \rightarrow \pi^*$ electronic spectra of difunctional aromatic probe solutes, N,N-dimethyl-*p*-nitroaniline being a typical solute. By choice of solute and spectroscopic methodology they hoped to elucidate the type and relative strength of the intermolecular interactions. Their solvatochromic comparison method [4–6], is based on the idea that by suitable choice of probe and reference solutes, and spectroscopic method a solvent's ability to stabilize a solute by dipolar, hydrogen bond donor, and hydrogen bond acceptor processes could be separated and measured. This work culminated in a set of three solvent parameters: the π^*, α and β values for more than 200 liquids [7]. A solvent's π^* value is a measure of its

0021-9673/91/$03.50

ability to stabilize a neighboring dipole by virtue of the dipole–dipole and dipole–induced dipole forces which exist between the dipolar solute (test probe) and the solvent. The π^* scale is defined to be zero for cyclohexane and unity for dimethyl sulfoxide (DMSO) at room temperature. The α and β scales represent the ability of a solvent to donate and accept hydrogen bonds from a solute. For various spectroscopic properties of a solute in a series of solvents Kamlet and Taft proposed the following specific LSER:

$$XYZ = XYZ_0 + s\pi^* + a\alpha + b\beta \tag{1}$$

The π^* parameter was initially proposed as a measure of the solvent's ability to interact with a solute via dipole–dipole interactions. For the class of select solvents, that is, those which are aliphatic, monodipolar and aprotic, the measured π^* values correlate with a simple function of solvent dielectric strength and is a linear function of the molecular dipole moment [8]. π^* can be used to correlate results obtained in aromatic and poly-halogenated solvents provided that it is replaced with a corrected value as shown in eqn. 2.

$$XYZ = XYZ_0 + s(\pi^* - d\delta) + a\alpha + b\beta \tag{2}$$

When modified by the $d\delta$ term, π^* can then be used to correlate a wide variety of properties, not just spectroscopic properties, of select, aromatic and polyhalogenated solvents [9].

It is now widely recognized that the correction ($d\delta$) is needed because π^* also includes considerable contributions from the solvent's own polarizability [10] and that the π^* for a very wide variety of solvents can be correlated with functions that incorporate both the dielectric strength and refractive index of the solvent [8,11,12]. As an example of the dependence of π^* on the solvent polarizability we note that π^* systematically varies from -0.08 for *n*-pentane to 0.08 for *n*-hexadecane [13] despite the fact that the dipole moments for these solvents are essentially zero. Thus, whenever the property under study results from a different "mix" of solvent dipolarity and polarizability than the spectroscopic processes used to measure π^*, a polarizability correction term ($d\delta$) is required.

The various fitting coefficients in eqns. 1 and 2 are very important. As Kamlet and co-workers pointed out very early in his work [1,2] both the signs and magnitudes must make chemical sense in order for a given regression to be accepted even if a statistically good correlation is observed. This requirement provides protection from a tendency to reach false conclusions as to the existence of causative relationships.

Since π^* represents the solvent's ability to interact with and stabilize a probe's (solute's) dipole via electrostatic interaction one expects that the coefficient s in the LSER equations should be related to the extent to which dipolar forces are involved in *XYZ*. Thus if the probe is non-polar or the process is not sensitive to dipolar interaction one expects s to be zero or small. Rutan *et al.* [14] demonstrated this for the transfer of small solutes from the gas phase to a wide variety of solvents. In that work s was observed to be linearly related to the solute's monomer π^* value (see below). Similarly if the probe is a weak hydrogen bond base or if the process under study is not sensitive to the solvent's hydrogen bond acidity (α) then the coefficient a in eqns. 1 and

2 will be zero or small. This concept was used by Kamlet *et al.* [6] in the development of solvent π^* values for very strong hydrogen bond donor solvents and was applied by Cheong and Carr [15] to measure the π^* of mobile phases used in reversed-phase liquid chromatography. Clearly if one wants to use some property to measure a solvent's α value then the probe molecule must be a strong hydrogen bond base. Conversely if one wants to measure a probe's ability to donate a hydrogen bond the solvent must be a good acceptor. As a general rule the coefficients a and b complement α and β as they appear in eqns. 1 and 2. That is the coefficient of α (a) depends on the probe's β and the coefficient of β (b) depends on the probe's α.

For present purposes among the more relevant tests of the solvatochromic LSER methodology is the investigation of gas–liquid partition equilibria [14–16]. Despite some interesting preliminary results it is now clear that the LSERs given in eqns. 1 and 2 are incomplete when applied to gas–liquid transfer processes. In the vast majority of prior LSER studies the processes involved only very minimal perturbation of the structure of the liquid. In contrast, many models of gas solubility invoke, at the outset, a "cavity formation process" [17,18] which is completely absent in eqns. 1 and 2. Second, it is generally accepted that London dispersion is invariably the major type of interaction in condensed phases [19]. Such dispersion interactions are entirely negligible in gases relative to liquids and thus there is no opportunity for them to cancel in a gas-to-liquid transfer process. Although it can be argued that London forces will be reflected to a limited extent in π^*, a single parameter simply cannot accurately model dipolar, polarizability and dispersion forces. Consequently the LSER model had to be expanded to incorporate a non-solvatochromic parameter in order to model cavity formation. The Hildebrand solubility parameter (δ_H^2) was chosen on a purely *ad hoc* basis. Qualitative and quantitative agreement was observed [14,16]. In subsequent work in which a number of polar solutes were studied in a large number of solvents the cavity term was canceled, as was some dependence on solute–solvent dispersion interactions by examining the ratio of the gas–liquid partition coefficient of the solute of interest (K_i) to that of an n-alkane of the same size (K_{alkane}). That is, the following LSER was used:

$$XYZ = \log (K_i/K_{alkane}) = XYZ_0 + s(\pi^* - d\delta) + a\alpha + b\beta \quad (3)$$

In later work Rutan *et al.* [20] showed that eqn. 3 had to be amended in order to handle protic self-associated solvents.

$$\log (K_i/K_{alkane}) = XYZ_0 + s(\pi^* - d\delta) + a\alpha + b\beta + h\alpha\beta \quad (4)$$

After the development of the above three solvent scales the fundamental concept was inverted. That is, the possibility that a conceptually similar approach could be used to assess solute-to-solute variations of some property in a fixed solvent was proposed. This is closely related to the goals of quantitative structure activity relationships (QSAR) which has found considerable currency in the design of drugs, prediction of toxicity, biological activity, environmental transport and chromatographic retention [21]. This, in fact, was a very bold step. Simply stated the measured properties of the pure bulk species were used to represent the dipolar and hydrogen bond forming interactions of the same molecule acting as a very dilute species in all environments.

This step is clearly based on the assumption that the properties in question are independent of media. One of the earliest tests of this idea was its use in correlating retention in reversed-phase liquid chromatography [22–24]. It was later used to study octanol–water partition coefficients, and solubility in water [25]. The LSER used in liquid–liquid transfer "solute" studies is:

$$XYZ = XYZ_0 + mV_2/100 + s(\pi_2^* + d\delta) + a\alpha_2 + b\beta_2 \quad (5)$$

The subscript 2 denotes a solute property and XYZ is now a solute property. Also note the incorporation of a solute size ($V_2/100$) parameter to scale the cavity formation process in the condensed phases. The V_2 term in eqn. 5 is the complement of the δ_H^2 parameter used in solvent studies.

Kamlet found that the solvatochromically defined *solvent* parameters could be used as the corresponding solute parameters provided that the species in question did not self-associate in the pure liquid state. For self-associating species, for example alcohols, the solvatochromic parameters had to be empirically modified so as to better fit the property under study. These modifications were justified based on the work of Abboud and co-workers [26,27] which shows that alcohol dimers are simultaneously both stronger hydrogen bond donors (HBD) and acceptors in the bulk phase than are alcohol monomers. While the idea that species which self-associate in the pure liquid phase should have different parameters when the same species acts as a monomeric, infinitely dilute species is chemically rational, it reveals a dilemma. The situation is best made clear with the following example. The α and β of methanol acting as a solvent are 0.93 and 0.62, respectively. In contrast, when methanol acts as a monomer (m) species, Kamlet [25] assigned the α_m and β_m as 0.35 and 0.42. Similarly Abraham established, via hydrogen bond formation equilibrium constants (see below), that the values of α_2^H and β_2^H are equal to 0.37 and 0.41 for methanol. Suppose we consider the properties of methanol as a dilute species in ethanol as a solvent. Clearly the chemical environment of a methanol monomer in ethanol is quite similar to that in pure bulk methanol. Which parameters should be used to represent the properties of a methanol monomer in this media? This suggests that even the *relative* hydrogen bond acidity and basicity scale may vary with media and thus no constant ranking is possible. A comprehensive list of solute interaction parameters and an extensive list of parameter estimation rules are available [25].

The tremendous importance of hydrogen bonding interactions in chemistry and biology has led Abraham and his co-workers [28,29] to develop a scale of relative hydrogen bond acidities (α_2^H) and basicities (β_2^H) for dilute species. These are based on measurements of hydrogen bond equilibrium constants of a wide variety of substances in carbon tetrachloride and 1,1,1-trichloroethane. With a few notable exceptions, reasonably but not completely, general scales of hydrogen bond acidity and basicity are possible [30]. This results because for many pairs of hydrogen bond donors and acceptors the ratio of electrostatic and covalent bonding in hydrogen bond formation is constant and front strain is minimal.

A series of papers [31,32] have appeared on the study of the adsorption of dilute gases in polymers, on carbon adsorbents and in gas chromatographic (GC) stationary phases. In such studies the overwhelming solute–solvent interaction is dispersion and the use of a simple dependence on solute volume inadequately represents this process.

Abraham and co-workers [33,34] have shown that dispersion interactions and cavity formation processes can be handled by using the logarithmic gas–liquid partition coefficient in *n*-hexadecane (denoted as log L^{16}) as an explanatory variable to simultaneously model both processes.

$$XYZ = XYZ_0 + l \log L^{16} + s\pi_2^* + d\delta_2 + a\alpha_2 + b\beta_2 \quad (6)$$

This approach is clearly approximate. In our recent study [35] of retention on a set of eight capillary gas chromatographic columns wherein the stationary phases ranged from a very non-polar permethyl silicone polymer to a very polar polyethylene glycol (Carbowax) phase we showed that eqn. 6 failed to accurately model retention. However, we were able to achieve a fit almost as precise as the random error in the measured property by using retention data on both a non-polar and a very polar reference column along with the solvatochromic parameters (π_2^*, δ_2, α_2, β_2) as the explanatory variables. This led us to believe the parameters we were using in that study were incorrect and that a need to develop new LSER parameter scales exists. We believe that the double reference column approach worked simply because the use of a polar reference column reduced the strength of the dependence on the interaction parameters and consequently inaccuracies in these parameters had a smaller effect on the quality of the fit.

In the present work we investigated the possibility of using eqn. 6 for the estimation of a new solute π_2^* and α_2 parameter, herein designated as $\pi_2^{*,C}$ and α_2^C. The superscript C indicates that the parameters are derived from chromatographic data. Because there are few highly acidic yet weakly basic phases in our data base we felt it premature and too complex to estimate a new β_2^C parameter. In order for this approach to work one must include chemically diverse stationary phases to obtain reliable results. Clearly it is important that retention data on as many columns as possible be linearly independent.

EXPERIMENTAL

Three different data bases (A,B,C) were used in this work. The first data base (A) is a set of capacity factors (k') for 53 highly variegated compounds that span an extremely wide range in chemical characteristics on 8 common capillary columns ranging from a methyl silicone oil to polyethylene glycol. The details of this data base have been published [35] (see the last column in Table I). The second data base (B) includes the capacity factors of 87 compounds, which includes all of the solutes in data base A, on 6 very basic phases. These basic phases are: tris-(2-ethylhexyl) phosphate (TEHP), trioctyl phosphine oxide (TOPO), N,N-diethyldodecylamide (DEDA), methyl dioctylamine (MDOA), dimethyl dodecylamine (DMDA) and 4-butylpentyl pyridine (BPP). The first three phases are oxygen bases, and the last three are nitrogen bases. These compounds were chosen because they are quite basic, have low volatility and similar molecular weights. The column temperatures were different for each phase and details of this data base will be published elsewhere. The compounds in this data base are designated as B in Table I. The third data base (C) is a part of the Patte *et al.* [36] data base used by Abraham *et al.* [37] to classify various GC phases. It includes the relative capacity factors (or specific volumes) (denoted L') for 166 compounds on

5 stationary phases. Those five phases are: Zonyl E 7 (ZE7), Carbowax 1540 (Carbowax), 1,2,3-tris(2-cyanoethoxy)propane (TCEP), polyphenyl ether 6 rings (PPE6) and diethylene glycol succinate (DEGS). The compounds included in this data base are designated as C in Table I.

COMPUTATIONAL METHODS

The computations were started by determining the regression coefficients of eqn. 6 with the best available estimates of the LSER parameters (see Table I). Thus we use π_2^*, α_2^H, and β_2^H from Abraham to initialize the first values of $\pi_2^{*,C}$ and α_2^C. In order to minimize the effect of determinate errors in the initial estimates of the parameters on the fitting coefficients (*l, s, a, b* and *d*) a zero lag adaptive Kalman filter [41] was used. This approach was chosen because it produces fitting coefficients which are much less sensitive to outliers than does conventional linear least squares analysis. However, because the Kalman filter is recursive inherently it must assume that the first few data (k', log L^{16}, π^*, α_2^H, β_2^H) in a set are accurate. This must lead to some bias in the fitting coefficients due to the initial data sequences. To minimize such bias the filter was run several times with randomized data sequences. Once the fitting coefficients were obtained for all the columns (in the three data bases) the following steps were taken to achieve the final estimates of the new $\pi_2^{*,C}$ and α_2^C parameters.

(a) Those columns with large *s* coefficient (greater than one) and small *a* and *b* coefficients were used as the basis for calculating $\pi_2^{*,C}$. Data on these columns were force-fitted to eqn. 6 by merely adjusting the π_2^* parameters. The resulting π_2^* values were normalized by setting $\pi^*_{2,\text{cyclohexane}} = 0$ and $\pi^*_{2,\text{DMSO}} = 1.00$, then the average over all columns with high *s* values was taken as a first round estimate of $\pi_2^{*,C}$.

(b) The $\pi_2^{*,C}$ parameters from step *a* were used to replace the initial π_2^*, then all the data were again regressed against eqn. 6 by using the adaptive Kalman filter procedure. The columns which gave a large *a* coefficient and a small or negligible *b* coefficient (*s* is not necessary small) were chosen as the basis for calculating α_2^C. Data on those columns were force-fitted to equation 6 by adjusting the α_2^H parameters. The α_2^C values so obtained were normalized by setting α_2^C (non-HBD compounds) = 0 and α_2^C (trifluoroethanol) = 0.57, then the average over all columns with high *a* coefficients was taken as a first round estimate of α_2^C.

(c) Steps a and b were repeated until no significant change was observed in either the coefficients or the parameters (2–3 cycles sufficed).

(d) Using the parameters from step c, a conventional linear least squares regression was performed for all columns. The fitting coefficients (*l, s, a, b, d*) for all the columns and the residuals [log k' (experimental) − log k' (calculated)] for each compound on each column were obtained. For any compound whose residual was large on most or all of the columns, a least median analysis [41] was applied to simultaneously adjust the two parameters ($\pi_2^{*,C}$ and α_2^C) for that specific compound to minimize the residuals on all the columns. These values constitute the final set of $\pi_2^{*,C}$ and α_2^C.

(e) To obtain an estimate of the standard deviation in the $\pi_2^{*,C}$ and α_2^C from different columns, the linear least squares regression coefficients for eqn. 6 were determined and sets of $\pi_2^{*,C}$ were back-calculated from the columns which were used in step a and α_2^C were back-calculated from the columns used in step b.

TABLE I

INITIAL INPUT PARAMETERS

No.	Compound	log L^{16}[a]	π_2^{*}[b]	α_2^{H}[c]	β_2^{H}[d]	δ_2[e]	Ref.[f]
1	Propane	1.050	0.00	0.00	0.00	0.0	C
2	Isobutane	1.409	0.00	0.00	0.00	0.0	C
3	Butane	1.615	0.00	0.00	0.00	0.0	C
4	Pentane	2.162	0.00	0.00	0.00	0.0	A,B,C
5	2,4-Dimethylpentane	2.841	0.00	0.00	0.00	0.0	C
6	2-Methylpentane	2.507	0.00	0.00	0.00	0.0	B,C
7	Hexane	2.662	0.00	0.00	0.00	0.0	A,B,C
8	2,2,5-Trimethylhexane	3.530	0.00	0.00	0.00	0.0	C
9	*n*-Heptane	3.173	0.00	0.00	0.00	0.0	B,C
10	3-Methylheptane	3.510	0.00	0.00	0.00	0.0	C
11	2-Methylheptane	3.480	0.00	0.00	0.00	0.0	C
12	*n*-Octane	3.677	0.00	0.00	0.00	0.0	A,B,C
13	*n*-Nonane	4.182	0.00	0.00	0.00	0.0	B,C
14	*n*-Decane	4.686	0.00	0.00	0.00	0.0	A,B,C
15	*n*-Undecane	5.191	0.00	0.00	0.00	0.0	A,B,C
16	*n*-Dodecane	5.696	0.00	0.00	0.00	0.0	B,C
17	*n*-Tridecane	6.200	0.00	0.00	0.00	0.0	B,C
18	*n*-Tetradecane	6.705	0.00	0.00	0.00	0.0	A,B,C
19	*n*-Pentadecane	7.209	0.00	0.00	0.00	0.0	A
20	Cyclopentane	2.426	0.00	0.00	0.00	0.0	B
21	Cyclohexane	2.913	0.00	0.00	0.00	0.0	A,B,C
22	Cycloheptane	3.543	0.00	0.00	0.00	0.0	B
23	Propene	0.946	0.08	0.00	0.07	0.0	C
24	1-Butene	1.491	0.08	0.00	0.07	0.0	C
25	1-Pentene	2.013	0.08	0.00	0.07	0.0	C
26	1-Hexene	2.547	0.08	0.00	0.07	0.0	A,B,C
27	1-Heptene	3.063	0.08	0.00	0.07	0.0	C
28	(*cis*)-2-Octene	3.650	0.08	0.00	0.07	0.0	C
29	2-Ethyl-1-hexene	3.510	0.08	0.00	0.07	0.0	C
30	1-Octene	3.591	0.08	0.00	0.07	0.0	C
31	α-Pinene	4.200	0.10	0.00	0.10	0.0	C
32	1-Octyne	3.480	0.20	0.13	0.20	0.0	C
33	2-Octyne	3.480	0.20	0.00	0.20	0.0	C
34	Methanol	0.922	0.40	0.37	0.41	0.0	A,B,C
35	Ethanol	1.462	0.40	0.33	0.44	0.0	A,B,C
36	1-Propanol	2.097	0.40	0.33	0.45	0.0	A,B,C
37	1-Butanol	2.601	0.40	0.33	0.45	0.0	B,C
38	2-Methyl-1-propanol	2.399	0.40	0.33	0.45	0.0	B,C
39	2-Methyl-1-butanol	3.011	0.40	0.33	0.45	0.0	C
40	Isopentanol	2.885	0.40	0.33	0.45	0.0	B,C
41	1-Pentanol	3.106	0.40	0.33	0.45	0.0	B,C
42	1-Hexanol	3.610	0.40	0.33	0.45	0.0	B,C
43	1-Heptanol	4.115	0.40	0.33	0.45	0.0	B,C
44	1-Octanol	4.619	0.40	0.33	0.45	0.0	C
45	1-Nonanol	5.124	0.40	0.33	0.45	0.0	C
46	1-Decanol	5.628	0.40	0.33	0.45	0.0	C
47	1-Undecanol	6.130	0.40	0.33	0.45	0.0	C
48	1-Dodecanol	6.640	0.40	0.33	0.45	0.0	C
49	2-Propanol	1.821	0.40	0.32	0.47	0.0	A,B,C
50	2-Butanol	2.338	0.40	0.32	0.47	0.0	B,C
51	2-Hexanol	3.340	0.40	0.32	0.47	0.0	C

(Continued on p. 108)

TABLE I *(continued)*

No.	Compound	log L^{16a}	π_2^{*b}	α_2^{Hc}	β_2^{Hd}	$\delta_2{}^e$	Ref.[f]
52	3-Hexanol	3.440	0.40	0.32	0.47	0.0	C
53	*tert.*-Butanol	2.018	0.40	0.32	0.49	0.0	A,B,C
54	3-Methyl-3-pentanol	3.277	0.40	0.32	0.49	0.0	C
55	2-Methyl-2-pentanol	3.181	0.40	0.32	0.49	0.0	C
56	2-Methyl-2-heptanol	3.990	0.40	0.32	0.49	0.0	C
57	Prop-2-en-1-ol	1.996	0.45	0.33	0.41	0.0	C
58	2-Hexenol	3.510	0.45	0.33	0.41	0.0	C
59	*trans*-2-Heptenol	4.010	0.45	0.33	0.41	0.0	C
60	*trans*-2-Octenol	4.520	0.45	0.33	0.41	0.0	C
61	Cyclopentanol	3.270	0.40	0.32	0.48	0.0	B,C
62	Cyclohexanol	3.594	0.45	0.32	0.51	0.0	C
63	Ethanethiol	2.172	0.35	0.00	0.16	0.0	C
64	*n*-Propanethiol	2.685	0.35	0.00	0.16	0.0	C
65	Isopropanethiol	2.406	0.35	0.00	0.16	0.0	C
66	Isobutanethiol	2.880	0.35	0.00	0.16	0.0	C
67	*n*-Butanethiol	3.243	0.35	0.00	0.16	0.0	C
68	*n*-Pentanethiol	3.720	0.35	0.00	0.16	0.0	C
69	Isopentanethiol	3.360	0.35	0.00	0.16	0.0	C
70	*n*-Hexanethiol	4.220	0.35	0.00	0.16	0.0	C
71	*n*-Heptanethiol	4.720	0.35	0.00	0.16	0.0	C
72	*n*-Octanethiol	5.310	0.35	0.00	0.16	0.0	C
73	*n*-Nonanethiol	5.890	0.35	0.00	0.16	0.0	C
74	*n*-Decanethiol	6.480	0.35	0.00	0.16	0.0	C
75	*tert.*-Butanethiol	2.558	0.35	0.00	0.16	0.0	C
76	Acetone	1.760	0.71	0.04	0.50	0.0	A,B,C
77	2-Butanone	2.287	0.67	0.00	0.48	0.0	A,B,C
78	2-Pentanone	2.755	0.65	0.00	0.48	0.0	A,B,C
79	3-Hexanone	3.310	0.65	0.00	0.48	0.0	C
80	2-Hexanone	3.262	0.65	0.00	0.48	0.0	C
81	2-Heptanone	3.760	0.65	0.00	0.48	0.0	C
82	2-Octanone	4.257	0.65	0.00	0.48	0.0	C
83	2-Nonanone	4.755	0.65	0.00	0.48	0.0	C
84	2-Decanone	5.260	0.65	0.00	0.48	0.0	C
85	2-Undecanone	5.760	0.65	0.00	0.48	0.0	C
86	2-Dodecanone	6.260	0.65	0.00	0.48	0.0	C
87	Carvone	5.330	0.80	0.00	0.49	0.0	C
88	Cyclopentanone	3.120	0.76	0.00	0.52	0.0	B,C
89	Cyclohexanone	3.616	0.76	0.00	0.52	0.0	B,C
90	Cycloheptanone	4.110	0.76	0.00	0.52	0.0	C
91	Cyclooctanone	4.610	0.76	0.00	0.52	0.0	C
92	Cyclononanone	5.110	0.76	0.00	0.52	0.0	C
93	Cyclodecanone	5.610	0.76	0.00	0.52	0.0	C
94	Cycloundecanone	6.110	0.76	0.00	0.52	0.0	C
95	Cyclododecanone	6.600	0.76	0.00	0.52	0.0	C
96	Acetonitrile	1.560	0.75	0.09	0.44	0.0	A,B,C
97	Propionitrile	1.978	0.63	0.00	0.43	0.0	A,B
98	1-Cyanopropane	2.540	0.68	0.00	0.44	0.0	C
99	1-Cyanobutane	3.057	0.68	0.00	0.44	0.0	C
100	Bromoethane	2.120	0.48	0.00	0.17	0.0	C
101	Iodomethane	2.106	0.40	0.00	0.18	0.0	C
102	Chlorobutane	2.716	0.37	0.00	0.10	0.5	B
103	1-Iodobutane	3.628	0.50	0.00	0.18	0.0	C
104	2-Iodobutane	3.390	0.50	0.00	0.18	0.0	C

TABLE I *(continued)*

No.	Compound	log L^{16}[a]	π_2^*[b]	α_2^H[c]	β_2^H[d]	δ_2[e]	Ref.[f]
105	1-Bromopentane	3.611	0.48	0.00	0.17	0.0	C
106	1-Chlorohexane	3.710	0.39	0.00	0.15	0.0	C
107	2-Bromooctane	5.110	0.48	0.00	0.17	0.0	C
108	Dichloromethane	1.997	0.82	0.13	0.06	0.5	B
109	1,2-Dichloroethane	2.573	0.81	0.10	0.05	0.5	B,C
110	1,1,2-Trichloroethane	2.997	0.53	0.12	0.03	0.5	C
111	Trichloromethane	2.480	0.58	0.20	0.02	0.5	B,C
112	Tetrachloromethane	2.823	0.28	0.00	0.00	0.5	A,B,C
113	Dimethyl sulfide	2.238	0.36	0.00	0.29	0.0	C
114	Diethyl sulfide	3.104	0.36	0.00	0.29	0.0	C
115	Di-*n*-propyl sulfide	4.120	0.36	0.00	0.29	0.0	C
116	Methyl-*n*-propyl sulfide	3.240	0.36	0.00	0.29	0.0	C
117	Isoamyl sulfide	5.540	0.36	0.00	0.29	0.0	C
118	Di-*n*-butyl sulfide	4.950	0.36	0.00	0.29	0.0	C
119	Diethyl disulfide	4.210	0.64	0.00	0.22	0.0	C
120	Acetic acid	1.750	0.64	0.55	0.43	0.0	A,B,C
121	*n*-Propanoic acid	2.290	0.64	0.54	0.43	0.0	B,C
122	*n*-Butanoic acid	2.830	0.64	0.54	0.42	0.0	B,C
123	3-Methylbutanoic acid	3.300	0.64	0.54	0.41	0.0	C
124	*n*-Pentanoic acid	3.380	0.64	0.54	0.41	0.0	C
125	*n*-Hexanoic acid	3.920	0.64	0.54	0.39	0.0	C
126	*n*-Heptanoic acid	4.460	0.64	0.54	0.38	0.0	C
127	*n*-Octanoic acid	5.000	0.64	0.54	0.36	0.0	C
128	*n*-Nonanoic acid	5.550	0.64	0.54	0.34	0.0	C
129	*n*-Propyl formate	2.413	0.61	0.00	0.38	0.0	C
130	Methyl acetate	1.960	0.64	0.00	0.40	0.0	B,C
131	Ethyl acetate	2.376	0.55	0.00	0.45	0.0	A,B,C
132	*n*-Propyl acetate	2.878	0.55	0.00	0.45	0.0	A,B,C
133	*n*-Butyl acetate	3.379	0.55	0.00	0.45	0.0	C
134	*n*-Pentyl acetate	3.810	0.55	0.00	0.45	0.0	C
135	Isoamyl acetate	3.740	0.55	0.00	0.45	0.0	C
136	Methyl propanoate	2.459	0.55	0.00	0.45	0.0	C
137	Propyl butanoate	3.810	0.55	0.00	0.45	0.0	C
138	Isobutyl isobutanoate	3.880	0.55	0.00	0.45	0.0	C
139	Isoamyl isopentanoate	4.580	0.55	0.00	0.45	0.0	C
140	Acetaldehyde	1.230	0.67	0.00	0.40	0.0	C
141	Propionaldehyde	1.815	0.65	0.00	0.40	0.0	A,B,C
142	Butyraldehyde	2.270	0.65	0.00	0.40	0.0	C
143	Isobutyraldehyde	2.060	0.65	0.00	0.40	0.0	C
144	3-Methylbutanal	2.620	0.65	0.00	0.40	0.0	C
145	Hexanal	3.370	0.65	0.00	0.40	0.0	C
146	Heptanal	3.860	0.65	0.00	0.40	0.0	C
147	Octanal	4.380	0.65	0.00	0.40	0.0	C
148	Propenal, acrolein	2.110	0.65	0.00	0.40	0.0	C
149	*trans*-But-2-en-1-al	2.570	0.75	0.00	0.40	0.0	C
150	Benzene	2.803	0.59	0.00	0.14	1.0	A,B,C
151	Toluene	3.344	0.55	0.00	0.14	1.0	A,B,C
152	Ethylbenzene	3.765	0.53	0.00	0.15	1.0	A,B,C
153	2-Xylene	3.937	0.51	0.00	0.17	1.0	B,C
154	3-Xylene	3.864	0.51	0.00	0.17	1.0	B,C
155	4-Xylene	3.858	0.51	0.00	0.17	1.0	A,B,C
156	Propylbenzene	4.239	0.51	0.00	0.12	1.0	A,B

(Continued on p. 110)

TABLE I *(continued)*

No.	Compound	log L^{16a}	π_2^{*b}	α_2^{Hc}	β_2^{Hd}	$\delta_2{}^e$	Ref.[f]
157	Butylbenzene	4.714	0.49	0.00	0.12	1.0	B
158	Styrene	3.908	0.55	0.00	0.18	1.0	C
159	Mesitylene	4.399	0.47	0.00	0.20	1.0	C
160	Fluorobenzene	2.785	0.62	0.00	0.07	1.0	B
161	Chlorobenzene	3.630	0.71	0.00	0.07	1.0	B
162	Bromobenzene	4.022	0.79	0.00	0.06	1.0	B
163	Iodobenzene	4.505	0.81	0.00	0.05	1.0	B
164	1,2-Dichlorobenzene	4.405	0.80	0.00	0.03	1.0	B,C
165	*p*-Dichlorobenzene	4.404	0.70	0.00	0.03	1.0	B
166	Diethylether	2.061	0.27	0.00	0.45	0.0	A,B,C
167	Dipropylether	2.971	0.27	0.00	0.46	0.0	A,B
168	Di(isopropyl) ether	2.561	0.27	0.00	0.47	0.0	B
169	Di-*n*-butyl ether	4.001	0.27	0.00	0.45	0.0	A,B,C
170	Dioxane	2.788	0.55	0.00	0.47	0.0	B
171	Nitromethane	1.892	0.85	0.12	0.25	0.0	A,B,C
172	Nitroethane	2.367	0.80	0.00	0.25	0.0	A,B,C
173	1-Nitropropane	2.850	0.79	0.00	0.25	0.0	A,B,C
174	Thiophene	2.943	0.60	0.00	0.16	1.0	C
175	2-Methylthiophene	3.302	0.40	0.0	0.14	1.0	C
176	2,5-Dimethylthiophene	3.806	0.40	0.00	0.16	1.0	C
177	Nitrobenzene	4.433	1.01	0.00	0.30	1.0	B
178	Benzyl chloride	4.290	0.71	0.00	0.31	1.0	C
179	3-Nitrotoluene	4.970	0.97	0.00	0.34	1.0	C
180	Furan	1.830	0.50	0.00	0.15	1.0	C
181	Allyl mercaptan	2.510	0.40	0.00	0.20	0.0	C
182	Tetrahydrofuran	2.521	0.58	0.00	0.51	0.0	A,B
183	Phenylethyne	3.715	0.55	0.12	0.21	1.0	C
184	Anisole	3.916	0.73	0.00	0.26	1.0	B,C
185	Pyridine	3.003	0.87	0.00	0.62	1.0	B,C
186	Benzonitrile	4.004	0.90	0.00	0.42	1.0	A,B
187	Benzaldehyde	3.985	0.92	0.00	0.42	1.0	A,B
188	Acetophenone	4.483	0.90	0.00	0.51	1.0	B,C
189	N,N-Dimethylaniline	4.753	0.90	0.00	0.35	1.0	A,B
190	Phenol	3.641	0.72	0.60	0.22	1.0	A,B
191	Aniline	3.934	0.73	0.26	0.38	1.0	A,B
192	*m*-Cresol	4.329	0.68	0.58	0.24	1.0	A
193	Benzyl alcohol	4.162	0.99	0.39	0.42	1.0	A,B
194	N-methylaniline	4.492	0.73	0.17	0.47	1.0	A,B
195	Triethylamine	3.008	0.14	0.00	0.67	0.0	A,B
196	Dimethylsulfoxide	3.110	1.00	0.00	0.78	0.0	A,B
197	Dimethylacetamide	3.357	0.88	0.00	0.74	0.0	A,B
198	Dimethylformamide	2.922	0.88	0.00	0.66	0.0	A,B
199	Trifluoroethanol	1.315	0.73	0.57	0.18	0.0	A,B
200	Hexanfluoroisopropanol	1.370	0.65	0.77	0.03	0.0	A,B
201	Ethylamine	1.677	0.32	0.00	0.70	0.0	A,B
202	Propylamine	2.141	0.31	0.00	0.69	0.0	A
203	Butylamine	2.618	0.31	0.00	0.69	0.0	A

[a] From refs. 37 and 38.
[b] From refs. 37 and 24.
[c] From refs. 37 and 39.
[d] From refs. 37 and 40.
[e] From refs. 25 and 37.
[f] Data base, see text.

RESULTS

Mutual correlation results for the different types of columns used in this work are given in Tables II and III. It is evident that quite a few of the columns are very strongly correlated. This results because they are both very non-polar and have low basicity. As expected, there are also strong correlations between the basic phases (*e.g.*, TEHP, DEDA, BPP). However, it is clear that a number of the phases are very weakly correlated. Such phases must be included in the data base to insure a numerically stable computation. Some thought indicates that the various phases can behave independently only when the common solute set, that is, those solutes which were run on all of the columns, explore a diverse set of chemical interactions. Thus, for example, if only non-polar solutes were run, all of the columns would appear to be strongly correlated.

The initial, conventional least squares regressions using the initial set of parameters given in Table I (from Abraham) gave fairly poor fits (see Table IV). The standard deviations of the fits ranged from as low as 0.052 for the low polarity phases to as high as 0.182 for the more polar and basic phases. The corresponding correlation coefficients ranged from 0.998 to 0.971. If the lack of fit were due to random experimental errors in the measured k' values then it should not be possible to systematically improve the fit on all of the columns by using a new set of adjusted parameters, however, the standard deviations of the fit are very much improved when the new parameters were used (see Table IV) indicating that the lack of fit is not random and not due to experimental errors in the k' values.

There are two distinct ways in which adjusting the parameters could improve the fit. First the initial parameter set could contain significant determinate errors which were corrected by the fitting procedures. Second, the fundamental model, that is the LSER, could be invalid or incomplete and adjusting the parameters compensated for the deficiencies in the model. We are aware of several shortcomings of the above LSER. The most serious are that it combines the dispersive interactions [19] and cavity formation processes [42,43] into a single parameter (log L^{16}) and a single fitting coefficient l; further it ignores the existence of differences in configurational entropies and free volume effects [44,45] between the various types of phases which span a very wide range in molecular weights. We also note that it may well be, as discussed above, that a solute can interact with its environment so strongly that its *relative* hydrogen bonding strength is perturbed [40].

The accuracy and indeed the validity of our entire methodology is based on the use of log L^{16} as an explanatory variable. There are two possible difficulties with this idea. First, is the relatively trivial problem that individual values of log L^{16} may be in error. This problem will propagate into an error in $\pi_2^{*,C}$ and then into an error in α_2^C. Second, far more seriously, any error in log L^{16} as a general model of the combined cavity and dispersive interaction, will complicate the interpretation of $\pi_2^{*,C}$. In order to examine this, we have done the same calculations based on retention data using a squalane column, log L^{squalane} [46], as a substitute for log L^{16}. There were no appreciable differences in the results ($\pi_2^{*,C}$) obtained. It is very likely that log L^{16} is as good, if not better, than any other single parameter used to model the gas–liquid partition process in non-polar solvents. We are still uncomfortable with the use of a single parameter that purports to represent both dispersive interaction and cavity formation processes (see below).

TABLE II

MUTAL CORRELATION BETWEEN THE PHASES (WITHIN DATA BASE A AND B) USED TO GENERATE THE NEW PARAMETERS

Phase type	Correlation coefficients[a]													
	DB-1	DB-5	DB-1301	DB-1701	DB-17	DB-210	DB-225	DB-WAX	TEHP	TOPO	MDOA	DMDA	BPP	DEDA
DB-1	1.000													
DB-5	0.998	1.000												
DB-1301	0.971	0.976	1.000											
DB-1701	0.930	0.941	0.989	1.000										
DB-17	0.941	0.957	0.979	0.986	1.000									
DB-210	0.803	0.832	0.877	0.914	0.938	1.000								
DB-225	0.745	0.772	0.868	0.930	0.923	0.929	1.000							
DB-WAX	0.604	0.636	0.743	0.827	0.822	0.832	0.964	1.000						
TEHP	0.567	0.566	0.741	0.808	0.840	0.531	0.800	0.877	1.000					
TOPO	0.619	0.632	0.709	0.765	0.762	0.632	0.809	0.870	0.936	1.000				
MDOA	0.978	0.971	0.955	0.917	0.905	0.720	0.773	0.708	0.898	0.824	1.000			
DMDA	0.814	0.805	0.889	0.892	0.880	0.661	0.806	0.792	0.958	0.883	0.989	1.000		
BPP	0.730	0.733	0.848	0.892	0.900	0.700	0.874	0.884	0.995	0.931	0.939	0.975	1.000	
DEDA	0.696	0.703	0.828	0.879	0.893	0.705	0.881	0.909	0.997	0.952	0.907	0.957	0.996	1.000

[a] For 48 compounds included in both A and B data bases.

TABLE III

MUTUAL CORRELATON BETWEEN THE PHASES (IN DATA BASE C) USED TO GENERATE THE NEW PARAMETERS

Phase Type	Correlation coefficients[a]				
	ZE7	Carbowax	TCEP	PPE	DEGS
ZE7	1.000				
Carbowax	0.947	1.000			
TCEP	0.932	0.970	1.000		
PPE6	0.962	0.920	0.861	1.000	
DEGS	0.943	0.987	0.993	0.895	1.000

[a] For all compounds ($n = 166$) in data base C.

It is well known [47] that non-polar compounds can adsorb at the gas–liquid surface of a polar stationary phase, and a polar compound will only weakly partition into a non-polar phase. How then can we use log L^{16} to simultaneously model both non-polar and polar solutes in all the phases? That is, will the parameter values vary

TABLE IV

QUALITY OF THE INITIAL AND FINAL FITS

Eqn. 6 is the regression equation employed.

Phase	Temperature	Initial		Final		n^c
		S.D.[a]	r^b	S.D.[a]	r^b	
DB-1	80	0.052	0.998	0.029	0.999	53
DB-5	80	0.065	0.997	0.034	0.999	53
DB-1301	80	0.103	0.992	0.046	0.998	52
DB-1701	80	0.114	0.991	0.030	0.999	53
DB-17	80	0.127	0.989	0.044	0.999	51
DB-210	80	0.151	0.979	0.056	0.997	53
DB-225	80	0.176	0.980	0.037	0.999	53
DB-WAX	115	0.182	0.971	0.040	0.999	74
TEHP	110	0.126	0.977	0.034	0.998	70
TOPO	100	0.159	0.984	0.058	0.998	83
MDOA	60	0.070	0.996	0.047	0.998	72
DMDA	50	0.150	0.984	0.053	0.998	75
BPP	60	0.151	0.986	0.033	0.999	77
DEDA	70	0.148	0.985	0.046	0.999	79
ZE7	120	0.125	0.984	0.101	0.990	166
Carbowax	120	0.135	0.986	0.043	0.999	166
TCEP	120	0.162	0.982	0.042	0.999	166
PPE6	120	0.112	0.990	0.050	0.998	166
DEGS	120	0.164	0.979	0.042	0.999	166

[a] Standard deviation of the fit.
[b] Correlation coefficient.
[c] Number of solutes included in the regression.

with the phase? We plotted the $\pi_2^{*,C}$ values of five very different but quite representative compounds (pentane, butylether, ethanol, 2-pentanone and nitropropane) on five very different stationary phases (DB-17, DB-225, BPP, TOPO, DEGS) (see Fig. 1). Clearly the parameters do not vary much from phase to phase. We need to point out that adsorption effects in our data set are not very important. We used several different phase loadings on the TOPO column and as expected we obtained the same coefficients (l, s, a, b, d). The intercept (XYZ_0), which does depend on the phase loadings, did vary.

The final sets of the chromatographically based $\pi_2^{*,C}$ and α_2^C parameters are given in Table V along with a measure of the uncertainty in the parameter. The uncertainty was obtained as the standard deviation in the parameter over all of the columns used to compute it. Typically, the standard deviation in $\pi_2^{*,C}$ is 0.01 to 0.02. Values for the highly acidic compounds can be as large as 0.10, but this is certainly extreme. The standard deviations in $\pi_2^{*,C}$ represent the column-to-column variations in the computed value of $\pi_2^{*,C}$. To give some idea of how good or how bad this is, we note that when π^* is determined by the original solvatochromic methodology, developed by Kamlet *et al.* [6], the variation from indicator to indicator, in select solvents, is often 0.05. In hydrogen bond donor solvents, the variation in π^* can be as large as 0.10. Thus on the whole we are pleased with the reliability of the $\pi_2^{*,C}$ values, although we do hope to improve the reliability of those solutes which are strong hydrogen bond donors.

Based on the computational procedure outlined above, the α_2^C values cannot be better defined than $\pi_2^{*,C}$ since α_2^C is computed based on the estimates of $\pi_2^{*,C}$. Thus any column-to-column variation in $\pi_2^{*,C}$ will be reflected in α_2^C. In addition the experimental error in the additional k' values on the columns used to compute α_2^C will show up in the reliability of α_2^C. Nonetheless the standard deviation in α_2^C seem to be quite acceptable.

DISCUSSION

$\pi_2^{*,C}$ *Values*

The fundamental issue is whether or not the procedure described above is merely an exercise in data fitting, that is, do the new parameters have any underlying

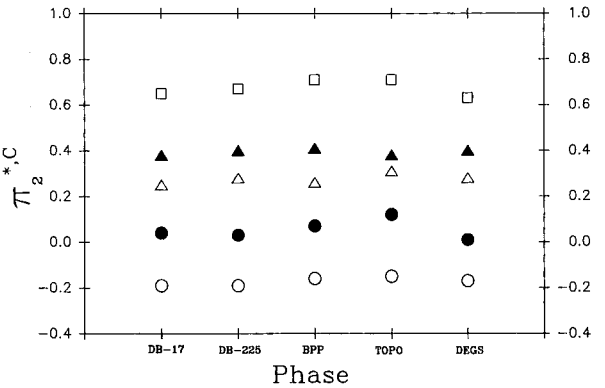

Fig. 1. $\pi_2^{*,C}$ *versus* GC phases used to compute it. ○ = Pentane; ● = butyl ether; △ = ethanol; ▲ = 2-pentanone and ■ = nitropropane.

TABLE V

FINAL SOLUTE DIPOLARITY/POLARIZABILITY AND HYDROGEN BOND ACIDITY PARAMETERS

No.	Compound	$\pi_2^{*,Ca}$	S.D.[b]	n_1[c]	n_2[d]	α_2^{Ca}	S.D.[e]	n_3[f]	n_4[g]
1	Propane	−0.17	0.01	3	0	0.00			
2	Isobutane	−0.17	0.01	3	0	0.00			
3	Butane	−0.17	0.01	3	0	0.00			
4	Pentane	−0.18	0.02	11	0	0.00			
5	2,4-Dimethylpentane	−0.18	0.05	3	0	0.00			
6	2-Methylpentane	−0.14	0.01	3	0	0.00			
7	Hexane	−0.16	0.01	11	0	0.00			
8	2,2,5-Trimethylhexane	−0.16	0.02	3	0	0.00			
9	*n*-Heptane	−0.14	0.01	7	0	0.00			
10	3-Methylheptane	−0.12	0.01	3	0	0.00			
11	2-Methylheptane	−0.13	0.01	3	0	0.00			
12	*n*-Octane	−0.12	0.01	11	0	0.00			
13	*n*-Nonane	−0.12	0.02	7	0	0.00			
14	*n*-Decane	−0.11	0.01	11	0	0.00			
15	*n*-Undecane	−0.10	0.01	11	0	0.00			
16	*n*-Dodecane	−0.09	0.01	7	0	0.00			
17	*n*-Tridecane	−0.08	0.02	7	0	0.00			
18	*n*-Tetradecane	−0.07	0.01	9	1	0.00			
19	*n*-Pentadecane	−0.06	0.01	4	0	0.00			
20	Cyclopentane	−0.07	0.02	4	0	0.00			
21	Cyclohexane	0.00	0.03	11	0	0.00			
22	Cycloheptane	0.00	0.02	4	0	0.00			
23	Propene	−0.00	0.05	3	0	0.00			
24	1-Butene	−0.02	0.04	3	0	0.00			
25	1-Pentene	−0.02	0.04	3	0	0.00			
26	1-Hexene	−0.07	0.02	10	0	0.00			
27	1-Heptene	−0.05	0.01	3	0	0.00			
28	*cis*-2-Octene	−0.02	0.01	3	0	0.00			
29	2-Ethyl-1-hexene	−0.02	0	3	0	0.00			
30	1-Octene	−0.05	0.01	3	0	0.00			
31	α-Pinene	0.07	0.02	3	0	0.00			
32	1-Octyne	0.16	0.01	3	0	0.04	0.02	3	0
33	2-Octyne	0.23	0.03	3	0	0.00			
34	Methanol	0.35	0.05	11	1	0.35	0.04	11	1
35	Ethanol	0.29	0.03	11	0	0.29	0.03	11	1
36	1-Propanol	0.30	0.02	11	0	0.32	0.03	12	0
37	1-Butanol	0.30	0.02	4	0	0.31	0.01	7	0
38	2-Methyl-1-propanol	0.30	0.03	6	0	0.31	0.01	9	0
39	2-Methyl-1-butanol	0.27	0.01	3	0	0.35	0.02	3	0
40	Isopentanol	0.28	0.01	4	0	0.34	0.01	7	0
41	1-Pentanol	0.32	0.01	7	0	0.32	0.01	10	0
42	1-Hexanol	0.33	0.01	6	0	0.34	0.01	10	0
43	1-Heptanol	0.35	0.01	5	0	0.33	0.01	7	0
44	1-Octanol	0.36	0.01	3	0	0.35	0.02	3	0
45	1-Nonanol	0.38	0.01	3	0	0.34	0.01	3	0
46	1-Decanol	0.40	0	3	0	0.32	0.01	3	0
47	1-Undecanol	0.43	0	3	0	0.33	0.01	3	0
48	1-Dodecanol	0.45	0.01	3	0	0.34	0.02	3	0
49	2-Propanol	0.21	0.02	9	0	0.29	0.03	10	0
50	2-Butanol	0.24	0.02	6	0	0.28	0.02	9	0
51	2-Hexanol	0.27	0	3	0	0.28	0.01	3	0

(Continued on p. 116)

TABLE V *(continued)*

No.	Compound	$\pi_2^{*,Ca}$	S.D.[b]	n_1[c]	n_2[d]	α_2^{Ca}	S.D.[e]	n_3[f]	n_4[g]
52	3-Hexanol	0.21	0.02	3	0	0.30	0.02	3	0
53	*tert.*-Butanol	0.19	0.03	11	0	0.25	0.04	12	1
54	3-Methyl-3-pentanol	0.19	0.02	3	0	0.27	0.03	3	0
55	2-Methyl-2-pentanol	0.16	0.02	3	0	0.29	0.03	3	0
56	2-Methyl-2-heptanol	0.25	0	3	0	0.24	0.01	3	0
57	Prop-2-en-1-ol	0.33	0.02	3	0	0.38	0.03	3	0
58	2-Hexenol	0.41	0.01	3	0	0.32	0.01	3	0
59	*trans*-2-Heptenol	0.45	0.02	3	0	0.31	0.02	3	0
60	*trans*-2-Octenol	0.45	0.01	3	0	0.33	0.02	3	0
61	Cyclopentanol	0.40	0	3	0	0.28	0.01	3	0
62	Cyclohexanol	0.37	0.04	4	0	0.31	0.03	7	0
63	Ethanethiol	0.17	0.01	3	0	0.00			
64	*n*-Propanethiol	0.19	0.01	3	0	0.00			
65	Isopropanethiol	0.15	0.01	3	0	0.00			
66	Isobutanethiol	0.20	0.01	3	0	0.00			
67	*n*-Butanethiol	0.20	0.02	3	0	0.00			
68	*n*-Pentanethiol	0.22	0.01	3	0	0.00			
69	Isopentanethiol	0.22	0.02	3	0	0.00			
70	*n*-Hexanethiol	0.24	0.01	3	0	0.00			
71	*n*-Heptanethiol	0.25	0.01	3	0	0.00			
72	*n*-Octanethiol	0.26	0.01	3	0	0.00			
73	*n*-Nonanethiol	0.26	0.02	3	0	0.00			
74	*n*-Decanethiol	0.26	0.02	3	0	0.00			
75	*tert.*-Butanethiol	0.11	0	3	0	0.00			
76	Acetone	0.38	0.03	11	1	0.01	0.01	12	0
77	2-Butanone	0.39	0.02	11	1	0.00			
78	2-Pentanone	0.40	0.02	11	1	0.00			
79	3-Hexanone	0.34	0.01	3	0	0.00			
80	2-Hexanone	0.39	0.02	3	0	0.00			
81	2-Heptanone	0.41	0.01	3	0	0.00			
82	2-Octanone	0.43	0.01	3	0	0.00			
83	2-Nonanone	0.44	0.01	3	0	0.00			
84	2-Decanone	0.45	0.01	3	0	0.00			
85	2-Undecanone	0.45	0.01	3	0	0.00			
86	2-Dodecanone	0.46	0.01	3	0	0.00			
87	Carvone	0.70	0.06	3	0	0.00			
88	Cyclopentanone	0.58	0.03	7	0	0.00			
89	Cyclohexanone	0.59	0.03	7	0	0.00			
90	Cycloheptanone	0.66	0.01	3	0	0.00			
91	Cyclooctanone	0.69	0.02	3	0	0.00			
92	Cyclononanone	0.72	0.02	3	0	0.00			
93	Cyclodecanone	0.75	0.03	3	0	0.00			
94	Cycloundecanone	0.78	0.04	3	0	0.00			
95	Cyclododecanone	0.81	0.04	3	0	0.00			
96	Acetonitrile	0.62	0.03	11	0	0.05	0.02	12	0
97	Propionitrile	0.64	0.03	8	0	0.00			
98	1-Cyanopropane	0.57	0.02	3	0	0.00			
99	1-Cyanobutane	0.57	0.02	3	0	0.00			
100	Bromoethane	0.22	0	3	0	0.00			
101	Iodomethane	0.27	0.02	3	0	0.00			
102	Chlorobutane	0.21	0.01	3	0	0.00			
103	1-Iodobutane	0.27	0	3	0	0.00			
104	2-Iodobutane	0.26	0	3	0	0.00			

TABLE V *(continued)*

No.	Compound	$\pi_2^{*,Ca}$	S.D.[b]	n_1[c]	n_2[d]	α_2^{Ca}	S.D.[e]	n_3[f]	n_4[g]
105	1-Bromopentane	0.24	0	3	0	0.00			
106	1-Chlorohexane	0.20	0.01	3	0	0.00			
107	2-Bromooctane	0.21	0.01	3	0	0.00			
108	Dichloromethane	0.34	0.04	4	0	0.06	0.02	7	0
109	1,2-Dichloroethane	0.39	0.03	5	0	0.05	0.04	8	0
110	1,1,2-Trichloroethane	0.27	0.01	3	0	0.00			
111	Trichloromethane	0.27	0.05	6	0	0.16	0.02	10	0
112	Tetrachloromethane	0.16	0.03	11	0	0.00			
113	Dimethyl sulfide	0.18	0	3	0	0.00			
114	Diethyl sulfide	0.18	0.01	3	0	0.00			
115	Di-*n*-propyl sulfide	0.18	0.01	3	0	0.00			
116	Methyl-*n*-propyl sulfide	0.18	0.01	3	0	0.00			
117	Isoamyl sulfide	0.19	0.02	3	0	0.00			
118	Di-*n*-butyl sulfide	0.22	0.02	3	0	0.00			
119	Diethyl disulfide	0.36	0.01	3	0	0.00			
120	Acetic acid	0.50	0.05	10	0	0.72	0.06	10	0
121	*n*-Propanoic acid	0.61	0.02	3	0	0.67	0.06	7	0
122	*n*-Butanoic acid	0.57	0.02	3	0	0.62	0.04	7	0
123	3-Methylbutanoic acid	0.45	0.04	3	0	0.69	0.04	3	0
124	*n*-Pentanoic acid	0.56	0.02	3	0	0.62	0.03	3	0
125	*n*-Hexanoic acid	0.60	0.05	3	0	0.52	0.06	3	0
126	*n*-Heptanoic acid	0.64	0.06	3	0	0.47	0.08	3	0
127	*n*-Octanoic acid	0.68	0.08	3	0	0.41	0.1	3	0
128	*n*-Nonanoic acid	0.72	0.1	3	0	0.35	0.12	3	0
129	*n*-Propyl formate	0.34	0	3	0	0.00			
130	Methyl acetate	0.30	0.05	7	0	0.00			
131	Ethyl acetate	0.30	0.04	11	0	0.00			
132	*n*-Propyl acetate	0.31	0.04	11	0	0.00			
133	*n*-Butyl acetate	0.33	0.01	3	0	0.00			
134	*n*-Pentyl acetate	0.35	0.02	3	0	0.00			
135	Isoamyl acetate	0.30	0.01	3	0	0.00			
136	Methyl propanoate	0.32	0.01	3	0	0.00			
137	*n*-Propyl butanoate	0.29	0.01	3	0	0.00			
138	Isobutyl isobutanoate	0.23	0.02	3	0	0.00			
139	Isoamyl isopentanoate	0.32	0.03	3	0	0.00			
140	Acetaldehyde	0.36	0.01	3	0	0.00			
141	Propionaldehyde	0.35	0.01	11	0	0.00			
142	Butyraldehyde	0.34	0.01	3	0	0.00			
143	Isobutyralodehyde	0.30	0.01	3	0	0.00			
144	3-Methylbutanal	0.31	0.02	3	0	0.00			
145	Hexanal	0.36	0.01	3	0	0.00			
146	Heptanal	0.38	0.01	3	0	0.00			
147	Octanal	0.38	0.01	3	0	0.00			
148	Propenal, acrolein	0.34	0.01	3	0	0.00			
149	*trans*-But-2-en-1-al	0.50	0.01	3	0	0.00			
150	Benzene	0.29	0.01	11	0	0.00			
151	Toluene	0.29	0.02	11	0	0.00			
152	Ethylbenzene	0.30	0.02	11	0	0.00			
153	2-Xylene	0.31	0.02	7	0	0.00			
154	3-Xylene	0.29	0.02	6	0	0.00			
155	4-Xylene	0.28	0.02	11	0	0.00			
156	Propylbenzene	0.30	0.02	8	0	0.00			

(Continued on p. 118)

TABLE V *(continued)*

No.	Compound	$\pi_2^{*,Ca}$	S.D.[b]	n_1[c]	n_2[d]	α_2^{Ca}	S.D.[e]	n_3[f]	n_4[g]
157	Butylbenzene	0.30	0.03	4	0	0.00			
158	Styrene	0.42	0.02	3	0	0.00			
159	Mesitylene	0.33	0	3	0	0.00			
160	Fluorobenzene	0.36				0.00			
161	Chlorobenzene	0.42	0.01	4	0	0.00			
162	Bromobenzene	0.48	0.02	4	0	0.00			
163	Iodobenzene	0.55	0.03	4	0	0.00			
164	1,2-Dichlorobenzene	0.57	0.01	6	0	0.00			
165	*p*-Dichlorobenzene	0.54	0.02	3	0	0.00			
166	Diethylether	0.03	0.03	11	0	0.00			
167	Dipropylether	0.03	0.03	8	0	0.00			
168	Di(isopropyl) ether	0.03	0	3	0	0.00			
169	di-*n*-butyl ether	0.04	0.04	11	0	0.00			
170	Dioxane	0.45	0.03	3	0	0.00			
171	Nitromethane	0.67	0.02	11	0	0.06	0.02	12	0
172	Nitroethane	0.66	0.03	11	0	0.00			
173	1-Nitropropane	0.65	0.03	11	0	0.00			
174	Thiophene	0.34	0.01	3	0	0.00			
175	2-Methylthiophene	0.37	0.01	3	0	0.00			
176	2,5-Dimethylthiophene	0.35	0.01	3	0	0.00			
177	Nitrobenzene	0.91	0.04	4	0	0.00			
178	Benzyl chloride	0.64	0.01	3	0	0.00			
179	3-Nitrotoluene	0.88	0.03	3	0	0.00			
180	Furan	0.26	0.01	3	0	0.00			
181	Allyl mercaptan	0.28	0	3	0	0.00			
182	Tetrahydrofuran	0.27	0.03	8	0	0.00			
183	Phenylethyne	0.47	0.02	3	0	0.09	0.02	3	0
184	Anisole	0.52	0.02	7	0	0.00			
185	Pyridine	0.60	0.04	6	0	0.00			
186	Benzonitrile	0.85	0.06	11	0	0.00			
187	Benzaldehyde	0.75	0.03	11	0	0.00			
188	Acetophenone	0.80	0.01	5	0	0.00			
189	N,N-Dimethylaniline	0.57	0.02	8	0	0.00			
190	Phenol	0.77	0.03	5	0	0.69	0.05	3	0
191	Aniline	0.76	0.04	8	0	0.20	0.05	8	0
192	*m*-Cresol	0.78	0.05	4	0	0.66	0.01	2	0
193	Benzylalcohol	0.71	0.05	6	1	0.43	0.06	9	0
194	N-Methylaniline	0.70	0.05	8	0	0.14	0.04	8	0
195	Triethylamine	0.02	0.02	6	0	0.00			
196	Dimethylsulfoxide	1.00	0.03	7	0	0.00			
197	Dimethylacetamide	0.80	0.04	8	0	0.00			
198	Dimethylformamide	0.81	0.02	8	0	0.00			
199	Trifluoroethanol	0.37	0.09	8	0	0.66	0.04	8	0
200	Hexafluoroisopropanol	0.47	0.07	5	0	1.11	0.06	6	0
201	Ethylamine	0.17	0.04	4	0	0.00			
202	Propylamine	0.22	0.02	4	0	0.00			
203	Butylamine	0.26	0.02	4	0	0.00			

[a] The final parameter value.
[b] Standard deviation in $\pi_2^{*,C}$ between all phases.
[c] Number of phases used to generate $\pi_2^{*,C}$.
[d] Number of phases for which the deviation in $\pi_2^{*,C}$ for that phase exceeds 2 S.D.
[e] Standard deviation in α_2^C between all phases.
[f] Number of phases used to generate α_2^C.
[g] Number of phases for which the deviation in α_2^C for that phase exceeds 2 S.D.

fundamental significance? As shown below the new $\pi_2^{*,C}$ and α_2^C are reasonably well correlated with the initial values used to establish them:

$$\pi_2^{*,C} = (-0.11 \pm 0.02) + (0.91 \pm 0.03)\pi_2^* \quad (7)$$
$$n = 203, \text{ S.D.} = 0.101, r = 0.919$$

$$\alpha_2^C = (-0.01 \pm 0.003) + (1.06 \pm 0.02)\,\alpha_2^H \quad (8)$$
$$n = 203, \text{ S.D.} = 0.041, r = 0.976$$

Plots of $\pi_2^{*,C}$ *versus* π_2^* and α_2^C *versus* α_2^H are shown in Figs. 2 and 3. In Fig. 2, $\pi_2^{*,C}$ is plotted against π_2^* for nine homologous series with different symbols for the different series. According to Abraham's estimation rule, within a given series, all π_2^* are the same, however, we found that their $\pi_2^{*,C}$ are not constant. This is a very significant difference, we will discuss this issue in great detail below, however, we point out here that π^* values in homologous series of solvents are different.

α_2^C Values

Abraham took α_2^H as being the same for all higher homologues. We found that within the reliability of the measurement α_2^C is the same for all homologous alcohols. Even though the column-to-column variation in α_2^C for the carboxylic acids is large (0.05) there is a definite decrease in α_2^C with homologue number (acetic acid, $\alpha_2^C = 0.72$,

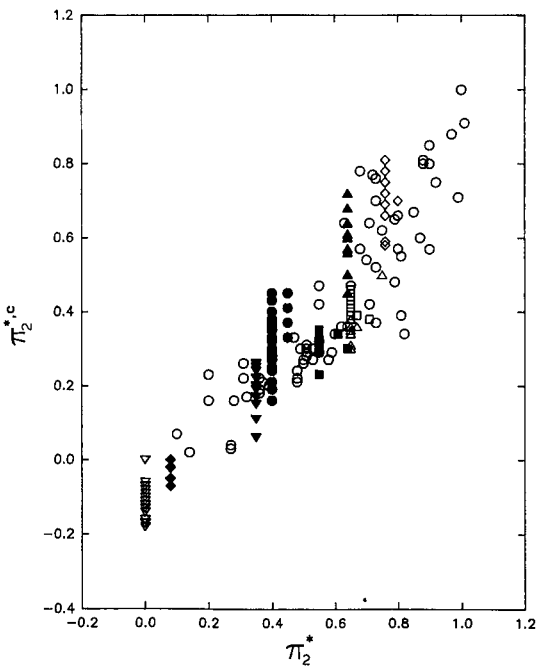

Fig. 2. $\pi_2^{*,C}$ *versus* π_2^*. ◆ = Alkenes; ◇ = cyclic ketones; ▲ = carboxylic acids; △ = aldehydes; ■ = nitriles; □ = ketones; ▼ = thiols; ▽ = alkanes; ● = alcohols and ○ = all other classes.

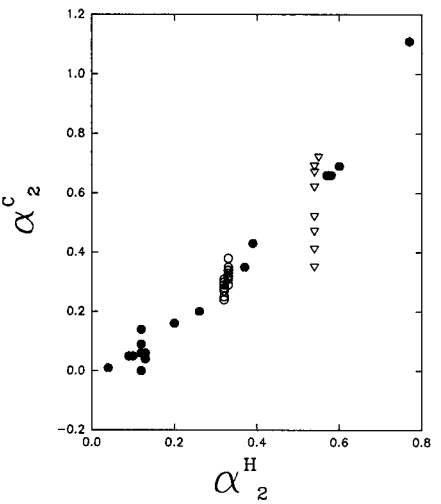

Fig. 3. α_2^C *versus* α_2^H. ○ = Alcohols; ▽ = carboxylic acids and ● = other hydrogen bond donors.

nonanoic acid $\alpha_2^C = 0.35$). Chemically it seems most unreasonable that the hydrogen bond acidity of a –COOH group would decrease so much as the number of CH_2 groups increases. Certainly we expect some tendency for propanoic acid to be a slightly weaker hydrogen bond acid than acetic acid because the ethyl group is a slightly better electron donor than a methyl group. Beyond butanoic acid we expect no further decrease in hydrogen bond acidity. At this time we believe that α_2^C values for the higher carboxylic acids may be wrong. Indeed, we are very concerned that the α_2^C values for all carboxylic acids are incorrect. There are at least four reasons why this is likely. First, carboxylic acid dimerize extensively in non-polar solvents. We are not certain that this dimerization did not occur in hexadecane which is the basis for the log L^{16} scale. Second, these are extremely polar compounds and in some of the phases gas–liquid interfacial adsorption may influence their retention. Third, carboxylates have a strong tendency to adsorb on diatomaceous earth. Finally, the carboxylic acid peaks were often asymmetric and the peak maximum shifted with the amount injected.

When the carboxylic acids were deleted from the correlation the following relationship is obtained:

$$\alpha_2^C = (-0.01 \pm 0.003) + (1.06 \pm 0.02)\,\alpha_2^H \qquad (9)$$
$$n = 194,\ \text{S.D.} = 0.032,\ r = 0.979$$

This result indicates that globally α_2^C and α_2^H are almost indistinguishable since the intercept is zero and the slope is nearly unity. The significant improvement in the fits when the two sets of parameters are replaced ($\pi_2^{*,C}$ *vs.* π_2^*, α_2^C *vs.* α_2^H, see Table IV) is due primarily to the differences between $\pi_2^{*,C}$ and π_2^*. This is evident from the fact that the correlation of $\pi_2^{*,C}$ with π_2^* is weaker than the correlation of α_2^C with α_2^H (see eqns. 7 and 8).

Test of $\pi_2^{*,C}$ as a model parameter

The above correlations show that $\pi_2^{*,C}$ and α_2^C are measuring approximately the same solute properties as are π_2^* and α_2^H. To further test the $\pi_2^{*,C}$ parameter we compared how $\pi_2^{*,C}$ and π_2^* are related to the solute dipole moment (μ) and polarizability. Our analysis is not aimed at understanding the exact dependencies but is only a comparison of the two scales for the non-HBD ($\alpha_2^C = 0$) compounds. First, we note that comparison in terms of μ^2 indicates that the $\pi_2^{*,C}$ is only slightly better than π_2^* as measured by Ehrenson's F-statistic [48].

$$\pi_2^{*,C} = (0.08 \pm 0.02) + (0.05 \pm 0.004)\,\mu^2 \qquad (10)$$
$$n = 123,\ \text{S.D.} = 0.162,\ r = 0.780$$

$$\pi_2^* = (0.25 \pm 0.02) + (0.05 \pm 0.004)\,\mu^2 \qquad (11)$$
$$n = 123,\ \text{S.D.} = 0.174,\ r = 0.768$$
$$R = 1.092 > R_{1,122,0.95} = 1.033$$

Next we added the polarizability parameter (R_2) proposed by Abraham [37],

$$\pi_2^{*,C} = (-0.04 \pm 0.02) + (0.043 \pm 0.002)\,\mu^2 + (0.49 \pm 0.04)\,R_2 \qquad (12)$$
$$n = 123,\ \text{S.D.} = 0.107,\ r = 0.911$$

$$\pi_2^* = (0.14 \pm 0.02) + (0.045 \pm 0.003)\,\mu^2 + (0.43 \pm 0.05)\,R_2 \qquad (13)$$
$$n = 123,\ \text{S.D.} = 0.138,\ r = 0.862$$
$$R = 1.285 > R_{2,121,0.95} = 1.051$$

We see that both correlations improved and the correlation of $\pi_2^{*,C}$ is statistically superior to that of π_2^*. This is an important observation. Clearly our $\pi_2^{*,C}$ and α_2^C values fit the retention data with much better precision than do π_2^* and α_2^H. However, they must do so as they are derived from the retention data. Thus the better fits to chromatographic data provide no evidence that the new parameters are in anyway superior to π_2^* and α_2^H. However, the fact that $\pi_2^{*,C}$ is better fit to a reasonable dependence on dipole moment and polarizability than is π_2^* provides independent support for its use and physical significance.

Test of the fitting coefficients

A second approach to testing the new parameters is to assess whether the coefficients (s,a) of the final regressions of log k' *versus* the explanatory variables make chemical sense. As pointed out above, according to the solvatochromic LSER method [22,24], a stationary phase with a high bulk phase π^*_{solvent} (denoted π^*) must have a high s coefficient. Smilarly a very basic stationary phase, that is, one whose bulk phase hydrogen bond basicity β_{solvent} (denoted β) is high must have a high a coefficient. To this end the bulk π^* and β parameters of the low-molecular-weight phases (in data bases B and C) were directly evaluated by the solvatochromic comparison method. Details of this work will be reported elsewhere. However, we are compelled to point out that we computed the solvent π^* by reference to the frequency of maximum

absorption of the indicator in cyclohexane and DMSO at 25°C. Since the phase s and a coefficients were measured at a variety of temperatures (often higher than 100°C), we measured π^* and β at fairly high temperatures (70–90°C) and extrapolated them to the temperature of interest. As might be expected the temperature dependence of π^* and β are difficult to define precisely, thus based on our work and that of Laurence and co-workers [49,50] we used an average temperature coefficient of -0.0017/°C for both π^* and β for all solvents. The LSER coefficients (s and a) for the phases (shown in Table VI) were plotted against the extrapolated values of π^* and β for these solvents (see Figs. 4–7) at the column temperature. Evidently there is a somewhat tighter correlation between s and π^* when we use the new solute parameters $\pi_2^{*,C}$ rather than when π_2^* was used. For $\pi_2^{*,C}$ and π_2^*, the results are as follows:

$$s\,(\pi_2^{*,C}) = (-0.04 \pm 0.09) + (2.56 \pm 0.18)\,\pi^* \qquad (14)$$
$$n = 10,\ \text{S.D.} = 0.15,\ r = 0.981$$

$$s\,(\pi_2^*) = (-0.02 \pm 0.11) + (2.25 \pm 0.22)\,\pi^* \qquad (15)$$
$$n = 10,\ \text{S.D.} = 0.18,\ r = 0.964$$
$$R = 1.220 > R_{1,9,0.90} = 1.172$$

We are very pleased to note that the intercept of these plots are quite small. As one

TABLE VI

COMPARISON OF THE INITIAL AND FINAL REGRESSION RESULTS

Eqn. 6 is the regression equation employed.

Phase			XYZ_0	l	s	b	d	a
TEHP	1	Initial	−0.014	0.580	0.880	−0.268	−0.179	2.131
	2	Final	0.304	0.521	0.889	−0.230	−0.073	1.816
TOPO	1		−1.954	0.667	0.997	−0.103	−0.136	4.103
	2		−1.564	0.608	1.158	−0.288	−0.100	3.810
DEDA	1		−1.685	0.755	1.117	−0.181	−0.198	2.917
	2		−1.348	0.706	1.176	−0.168	−0.115	2.440
DMDA	1		−1.607	0.912	0.602	−0.319	−0.197	2.845
	2		−1.365	0.859	0.558	−0.178	−0.090	2.507
MDOA	1		−1.587	0.838	0.178	0.006	−0.044	1.440
	2		−1.473	0.812	0.255	−0.095	−0.036	1.533
BPP	1		−1.863	0.817	1.031	−0.135	−0.197	2.980
	2		−1.557	0.772	1.069	−0.072	−0.126	2.523
ZE7	1		−2.093	0.434	1.161	0.599	−0.052	0.509
	2		−1.784	0.394	1.251	0.640	−0.051	0.203
Carbowax	1		−2.050	0.446	1.529	−0.142	0.056	2.066
	2		−1.624	0.388	1.676	−0.071	0.048	1.468
TCEP	1		−1.730	0.379	2.022	0.326	0.080	1.727
	2		−1.173	0.305	2.247	0.374	0.059	1.024
PPE6	1		−2.536	0.554	0.992	0.100	0.042	0.488
	2		−2.255	0.516	1.190	0.031	0.008	0.179
DEGS	1		−1.804	0.399	1.728	0.154	0.127	1.765
	2		−1.317	0.333	1.979	0.143	0.093	1.134

hopes when the π^* of the stationary phase is zero the phase s value is very small. In fact the π^* of n-hexadecane is 0.08, its s value is zero by definition. Eqn. 14 predicts its s value to be 0.16 ($\pm$ 0.15). Similarly eqn. 15 predicts its s value to be 0.16 ($\pm$ 0.18). Overall the observations reported in Figs. 4 and 5 constitute a strong qualitative verification of the basic concepts of the LSER approach.

Analysis of the correlation between a and β is more complicated. It has been shown that there is a family dependent relationship such that OH acceptors and NH acceptors act differently toward hydrogen bond donor indicators such as p-nitroaniline [49]. Based on Maria *et al.*'s work [51], this should not be surprising. We are not convinced that there is a family dependence shown in Figs. 6 and 7. The correlation results are shown as follows:

For all phases

$$a(\alpha_2^C) = (0.09 \pm 0.16) + (2.96 \pm 0.24)\,\beta \qquad (16)$$
$$n = 10,\ \text{S.D.} = 0.25,\ r = 0.974$$

$$a(\alpha_2^H) = (0.45 \pm 0.27) + (2.99 \pm 0.41)\,\beta \qquad (17)$$
$$n = 10,\ \text{S.D.} = 0.42,\ r = 0.933$$
$$R = 1.679 > R_{1,9,0.90} = 1.172$$

We note that as required by the LSER formalism the a coefficient is zero when the solvent β is zero. Again this provides excellent support for the LSER approach. We note that a based on the α_2^C scale is somewhat superior to the α_2^H scale. Given the paucity of the data we do not insist that the correlations based on $\pi_2^{*,C}$ and α_2^C are better than π_2^* and α_2^H. However, we certainly have not achieved the much superior fits of the retention data at the cost of introducing chemically meaningless values of the LSER fitting coefficients (s, a).

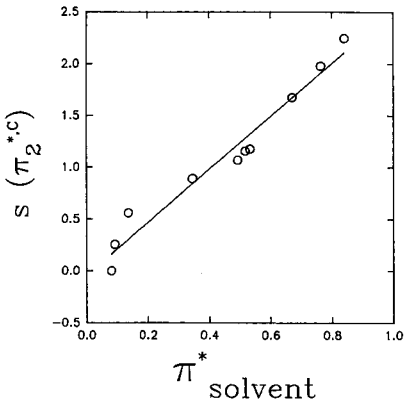

Fig. 4. $s(\pi_2^{*,C})$ *versus* $\pi^*_{solvent}$.

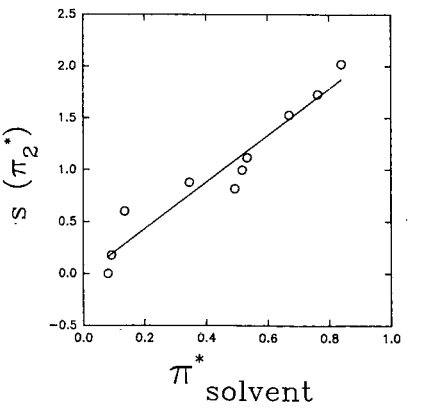

Fig. 5. $s(\pi_2^*)$ *versus* $\pi^*_{solvent}$.

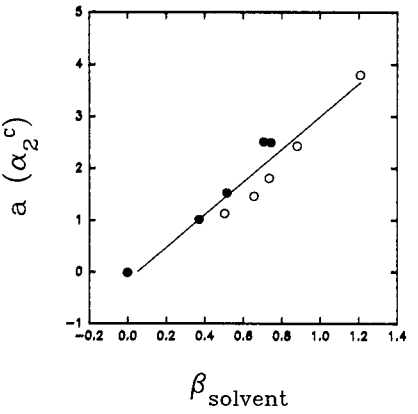

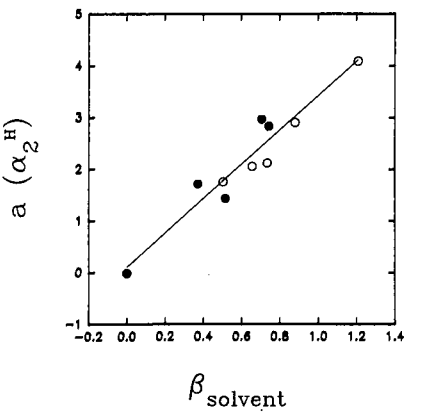

Fig. 6. $a(\alpha_2^C)$ *versus* $\beta_{solvent}$. ○ = Oxygen base and ● = nitrogen base.

Fig. 7. $a(\alpha_2^H)$ *versus* $\beta_{solvent}$. ○ = Oxygen base and ● = nitrogen base.

Generality of the new parameters

The question naturally arises as to whether the solute parameters determined here are applicable only within the context of gas chromatographic retention. Can they be used with good results in other types of correlations? The issue of the universality of solvatochromic LSER methods has been extensively discussed by Kamlet and Taft [52] and Sjöström and Wold [53]. The most extensive data set yet reported by the Kamlet group is that pertaining to the study of octanol–water partition coefficients [25]. Reexamination of this data set does not constitute a severe test of the new parameters since K_{ow} is strongly dependent on solute size and hydrogen bond basicity and only weakly dependent on dipolarity and hydrogen bond acidity. Nonetheless for the intersection of our solute sets, we obtained the following results:

Using our parameters:

$$\log K_{ow} = -0.03 + 5.72\,V_I - 0.84\pi_2^{*,C} + 0.16\delta - 4.19\beta_m + 0.44\alpha_2^C \quad (18)$$
$$n = 63,\ \text{S.D.} = 0.083,\ r = 0.9984$$

Using Abraham's parameters:

$$\log K_{ow} = 0.26 + 5.56V_I - 0.83\pi_2^* + 0.15\delta - 4.26\beta_m + 0.20\alpha_2^H \quad (19)$$
$$n = 63,\ \text{S.D.} = 0.084,\ r = 0.9984$$

Using the original Kamlet's parameters

$$\log K_{ow} = 0.25 + 5.54V_I - 0.88\pi^* + 0.20\delta - 4.18\beta_m + 0.15\alpha_m \quad (20)$$
$$n = 63,\ \text{S.D.} = 0.085,\ r = 0.9984$$

where β_m is the hydrogen bond basicity of a monomeric species and was developed by Kamlet and co-workers [54,55] to specifically fit solubility in water, K_{ow} values and

retention in reversed-phase liquid chromatography. From the above, we can see that using either Abraham's parameters (π_2^* and α_2^H) or our parameters ($\pi_2^{*,C}$ and α_2^C) give essentially the same results in terms of the goodness of fit as well as the sign and the magnitude of the regression coefficients.

We conclude that no harm will result in correlating properties related to transfer from water to less polar media, such as capacity factors in reversed-phase liquid chromatography, solubility of organic compounds in water etc., by use of the new parameters. At the same time the new parameters, in contrast to the "old" parameters, give excellent fits to GC retention data.

Test of the homologue dependence of $\pi_2^{*,C}$ and the Martin equation

Plots of $\pi_2^{*,C}$ *vs.* homologue number (HN) are shown in Fig. 8. In most cases the $\pi_2^{*,C}$ values increase more or less monotonically with the number of methylene groups in the solute. There is clearly a great deal of scatter and in one case (olefins) the $\pi_2^{*,C}$ actually decreases with increasing number of methylene groups. At this point, we are not sure if the $\pi_2^{*,C}$ for the olefins are correct. These trends in $\pi_2^{*,C}$ are somewhat disturbing. As will be shown below in any series where $\pi_2^{*,C}$ is independent of homologue number the Martin equation (see below) must be valid. In contrast it is not clear whether a monotonic or highly scattered relationship between $\pi_2^{*,C}$ and HN will be consistent with the Martin equation.

The Martin equation is a very widely accepted *experimental* observation. It indicates that the logarithmic partition coefficient or the logarithmic capacity factor is, within a homologous series, a linear function of the number of carbon atoms in the specific homologue:

$$\log k' \text{ (or } K \text{ or } L') = A + B\,\mathrm{HN} \tag{21}$$

Theoretically the Martin equation cannot be exact because of size dependent configurational contributions to the free energy of gas to liquid transfer that are not

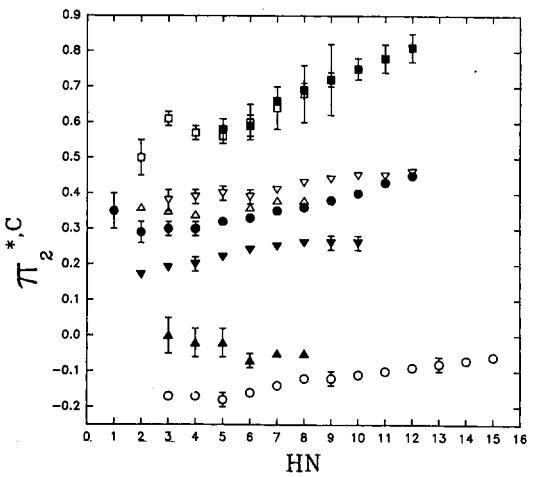

Fig. 8. $\pi_2^{*,C}$ *versus* homologue number (HN) for eight homologous series. ○ = Alkanes; ● = alcohols; ▽ = 2-ketones; ▼ = thiols; □ carboxylic acids; ■ = cycloketones; △ = aldehydes and ▲ = alkenes.

linear with HN. Relatively simple models of the solution process such as UNIFAC [56] show that there cannot be precise linearity with HN values. More advanced models such as Martire's [57,58] application of Sanchez–Lacombe lattice theory [59] to gas chromatography also show that the Martin equation is an approximate result. Any reasonable model of retention must be, at least approximately, in agreement with the Martin equation and any model which predicts significant deviations is inherently dubious.

It is easily shown that Abraham's set of solute parameters (Table I) must be in accord with the Martin equation. He assigned, in a given series, the same values to π_2^*, β_2^H and α_2^H for all higher homologues. Thus for a specific homologous series the only variable term in the LSER equation governing the variations in k' from homologue to homologue generated by Abraham's approach is the log L^{16}. Consequently, within a series the LSER can be written as:

$$\log k'_{\text{homo,Abraham}} = XYZ'_0 + l \log L^{16} \tag{22}$$

where XYZ'_0 is defined as:

$$XYZ'_0 = XYZ_0 + s\pi^*_{2,\text{homologue}} + a\alpha^H_{2,\text{homologue}} + b\beta^H_{2,\text{homologue}} \tag{23}$$

As shown in Fig. 9 log L^{16} is a linear function of HN. Thus eqn. 22 correctly predicts that log k' is a linear function of HN since as shown in Table VII for some 16 different homologous series, log L^{16} is a quite linear function of carbon number. It should be noted that for log L^{16} the slope of the homologous plot (B in eqn. 21) differs from series-to-series (see Table VII). However, these differences in slope B are small relative to the analogous differences observed on more polar columns. It follows from eqns. 22 and 23 that on any stationary phase the Abraham parameter set predicts that the differences in slope B for log L' from homologous series to homologous series will be

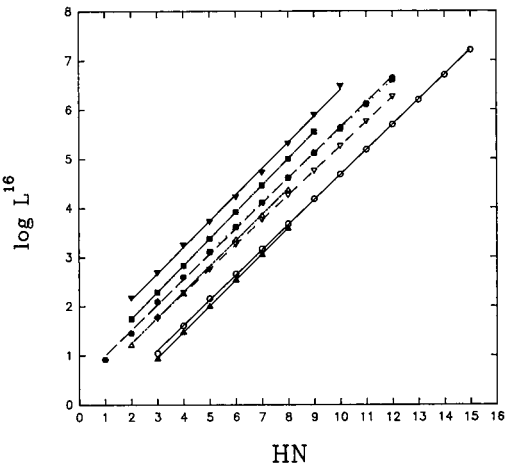

Fig. 9. log L^{16} *versus* HN for eight homologous series. ○ = Alkanes; ● = alcohols; ▽ = 2-ketones; ▼ = thiols; □ = cycloketones; ■ = carboxylic acids; △ = aldehydes and ▲ = alkenes.

TABLE VII

CORRELATION RESULTS OF LOG L^{16} *VS.* CARBON NUMBER FOR HOMOLOGOUS SERIES

Eqn. 21 is the regression equation employed.

Homologues	Series No.	n	Range	A	S.D.	r^2	B
Alkanes	1	13	3–15	−0.4144	0.0249	0.9999	0.5094
							0.0018[a]
Alcohols	2	12	1–12	0.4904	00463	0.9994	0.5150
							0.0039
2-Ketones	3	10	3–12	0.2701	0.0091	1.0000	0.4989
							0.0010
Thiols	4	9	2–10	1.0730	0.0531	0.9988	0.5330
							0.0069
Carboxylic acids	5	8	2–9	0.6631	0.0032	1.0000	0.5426
							0.0005
Cycloketones	6	8	5–12	0.6280	0.0031	1.0000	0.4980
							0.0005
Aldehydes	7	6	2–8	0.2065	0.0304	0.9995	0.5229
							0.0057
Alkenes	8	6	3–8	−0.6280	0.0078	0.9999	0.5279
							0.0019
Acetates	9	5	1–5	1.4697	0.0289	0.9989	0.4703
							0.0091
Sulfides	10	4	2–8	1.3150	0.0546	0.9986	0.4576
							0.0122
Alkylbenzenes	11	5	6–10	−0.0006	0.0296	0.9988	0.4717
							0.0094
Nitriles	12	4	2–5	0.5152	0.0460	0.9967	0.5053
							0.0206
Nitroaliphatics	13	3	1–3	1.4117	0.0033	1.0000	0.4790
							0.0023
Amines	14	3	2–4	0.7338	0.0053	0.9999	0.4705
							0.0038
Ethers	15	3	4–8	0.1010	0.0490	0.9987	0.4850
							0.0173
Cycloalkanes	16	3	5–7	−0.3903	0.0584	0.9946	0.5585
							0.0413

[a] Standard deviation of the slope.

small and in proportion to their B coefficient for log L^{16}. As shown in Fig. 10, this is not the case, that is, the ratio of the B coefficients for log L' and log L^{16} is not constant for different homologous series on any given column.

We wish to comment here on whether one should expect to see changes between different homologous series in the slopes of plots of log L^{16} *vs.* HN as shown in Fig. 9. Are these changes real or are they due to experimental problems such as interfacial adsorption? In order to assess the validity of the slopes we can compare them to slopes predicted based on a theoretical model of the solution process. Although the UNIFAC model is not highly accurate [56], it can give us a reasonable estimate especially in a system as chemically simple as these solutes in hexadecane. The partition coefficients

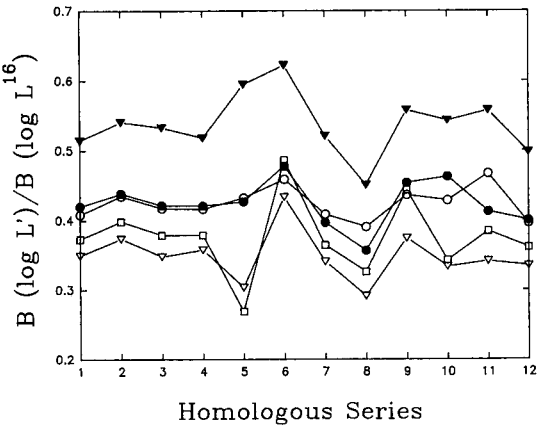

Fig. 10. Plots of the ratio of the slopes of log L' *vs.* HN and log L^{16} *vs.* HN for 12 homologous series on 5 columns. Homologous series numbers are the same as in Table VII. ▼ = PPE6; ○ = ZE7; ● = Carbowax; ▽ = TCEP and □ = DEGS.

can be computed from knowledge of the vapor pressures (P_2), estimates of the activity coefficients (γ_2^∞), molar volume (V_m) and the following equation:

$$K = RT/\gamma^\infty P_2 V_m \tag{24}$$

The slopes of computed plots of log K^{16} *vs.* HN for several homologous series and of log L^{16} are shown in Fig. 11. We also give slopes of plots of log P_2 *vs.* HN for reference purposes. From these results, it is clear that one should not expect the same slopes for plots of log L^{16} *vs.* HN for different homologous series. Plots of the logarithm of the retention volume of different compounds *versus* the number of CH_2 in their alkyl chain by Ray [60] supports this conclusion. Finally, measurement of a large number of gas–liquid partition coefficients of homologous series of solutes in hexadecane by

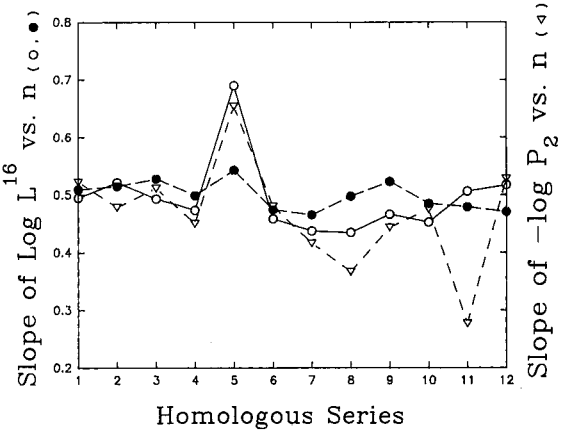

Fig. 11. Plots of UNIFAC predicted (○) and experimental (●) slopes of log L^{16} *vs.* HN and $-\log P_2$ (vapor pressure at 25°C, torr) *vs.* HN (▽) for 12 homologous series. Homologous series No.: 1 = Alkanes; 2 = alcohols; 3 = alkenes; 4 = 2-ketones; 5 = carboxylic acids; 6 = alkylbenzenes; 7 = acetates; 8 = nitriles; 9 = aldehydes; 10 = ethers; 11 = nitroaliphatics and 12 = amines.

head-space gas chromatography, which is not subject to all of the interfacial adsorption problems of the dynamic GC approach, confirm the variation in these slopes [61].

New parameters and the Martin equation

Inspection of our set of parameters (Table V) shows that in most homologous series (see, for example the alkanes, alcohols, 2-alkanones) there are significant variations in the parameters with HN. In general our parameters are neither fixed within a series nor are they strictly linear with HN. Thus we *do not* predict an *exact linear relationship* between log k' and carbon number and we are seemingly in disagreement with the Martin equation. However, this lack of agreement is only apparent (see below). It will turn out that our parameters, are, within any reasonable expectation of the experimental precision, in accord with the Martin equation. More importantly because the parameters vary within a homologous series we do not predict that all homologous series will produce the same ratio of slopes of log k' *vs.* HN relative to the slope of log L^{16} *vs.* HN (see Fig. 10).

The two different sets of parameters ($\pi_2^{*,C}$ and π_2^*) were examined by comparing the measured and computed capacity factors for a variety of homologous series of solutes on a set of phases that are chemically very distinct. We are not in a position to compare α_2^C and α_2^H because we really only have two homologous series (alcohols and carboxylic acids) of hydrogen bond donors.

First, let us show that our $\pi_2^{*,C}$ values are in good agreement with the Martin equation. To do so we will use the cycloalkanones since they show the largest change in $\pi_2^{*,C}$ of any series. Note that for a series in which the change in $\pi_2^{*,C}$ is zero exact agreement with the Martin equation is predicted so this does not constitute a useful test. Second, if the stationary phase has a small s coefficient the effect of $\pi_2^{*,C}$ on retention will be small. The Carbowax column was chosen because it is a fairly common stationary phase and has a rather high s coefficient (see Table VI). The log k' values predicted by $\pi_2^{*,C}$, by Abraham's π_2^*, and the experimental values are shown in Fig. 12. It is evident that our results, as are Abraham's, are in good agreement with the

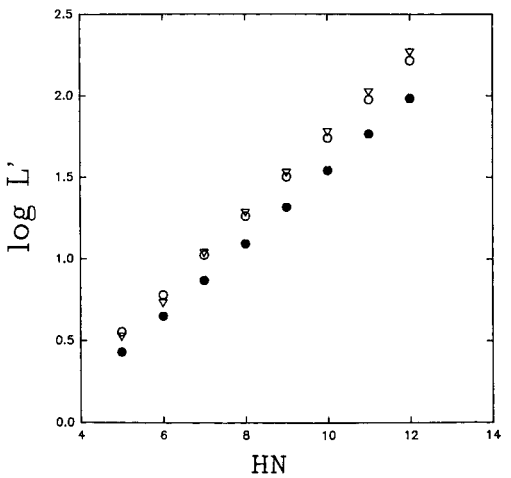

Fig. 12. Plots of experimental and predicted log L' *versus* HN for cycloketones on the Carbowax column. ○ = Experimental; ● = Abraham and ▽ = this work.

Martin equation, that is, they predict a linear dependence of log k' on HN. Clearly our results are in better agreement with the experimental data. These results are quite typical of a large number of such plots for many homologous series on a variety of stationary phases. That is, our $\pi_2^{*,C}$ parameter predicts retention variation with HN that are in better agreement with the measured k' values than are the old π_2^* parameters.

We next compare the accuracy of prediction of the slope of plots of log k' *vs.* HN for a variety of homologous series on different columns. These results are shown in Figs. 13 and 14 as the ratio of the predicted slope to the experimental slope. Obviously this ratio should be unity. The results for different columns are offset by exactly 1.0 unit. Comparison of Fig. 13 to 14 shows that, in general, $\pi_2^{*,C}$ is better than π_2^*. We conclude that the new $\pi_2^{*,C}$ is generally in better agreement with the Martin equation and the actual data than the π_2^* parameter when the data are compared either in general or when compared in terms of individual homologous series.

Although not relevant to testing concordance with the Martin equation we can also examine the intercepts predicted by the LSER approach to the experimental intercepts. This was done in the same fashion as the slopes. The results are similar to the slopes (not shown). It is clear that overall the $\pi_2^{*,C}$ parameter produces better agreement with experiment than the π_2^* parameter.

Use of the Martin equation to estimate $\pi_2^{*,C}$ values

Based on the observed consistency of the LSER approach and the Martin equation, at least for the non-hydrogen bond donor solutes, one can use the consistency to smooth the available data and estimate additional solutes in a homologous series for which some data exist. We use this idea to generate our final recommended values for $\pi_2^{*,C}$ (Table VIII). For non-hydrogen bond donor solutes on a non-acidic phase the approach is as follows. First, obtain l, s, a, b and d as above. Second, regress log k' *vs.* HN for the homologous series of interest to obtain the conventional least

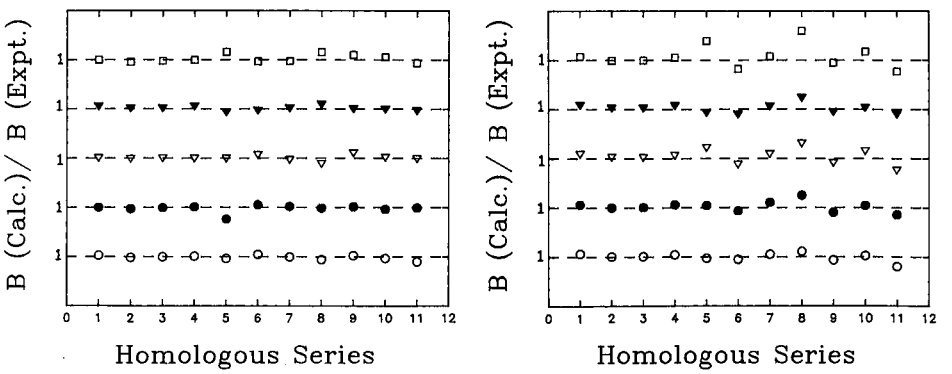

Fig. 13. Plots of the ratio of slopes of log L' *vs.* HN predicted by present work and experimental values for 11 homologous series on 5 columns. Homologous series numbers are the same as in Table VII. ○ = ZE7; ● = Carbowax; ▽ = TCEP; ▼ = PPE6 and □ = DEGS.

Fig. 14. Plots of the ratio of slopes of log L' *vs.* HN predicted by Abraham and experimental values for 11 homologous series on 5 columns. Homologous series numbers and symbols are the same as in Fig. 13.

TABLE VIII

FINAL RECOMMENDED VALUES FOR $\pi_2^{*,C}$

No.	Compound	$\pi_2^{*,C}$
24	1-Butene	−0.02
25	1-Pentene	−0.03
26	1-Hexene	−0.04
27	1-Heptene	−0.05
42	1-Hexanol	0.33
43	1-Heptanol	0.35
44	1-Octanol	0.37
45	1-Nonanol	0.39
46	1-Decanol	0.41
47	1-Undecanol	0.43
48	1-Dodecanol	0.45
68	*n*-Pentanethiol	0.22
70	*n*-Hexanethiol	0.23
71	*n*-Heptanethiol	0.24
72	*n*-Octanethiol	0.25
73	*n*-Nonanethiol	0.26
74	*n*-Decanethiol	0.27
78	2-Pentanone	0.40
80	2-Hexanone	0.41
81	2-Heptanone	0.42
82	2-Octanone	0.43
83	2-Nonanone	0.44
84	2-Decanone	0.45
85	2-Undecanone	0.46
86	2-Dodecanone	0.47
90	Cycloheptanone	0.66
91	Cyclooctanone	0.69
92	Cyclononanone	0.72
93	Cyclodecanone	0.75
94	Cycloundecanone	0.78
95	Cyclododecanone	0.81
132	*n*-Propyl acetate	0.31
133	*n*-Butyl acetate	0.33
134	*n*-Pentyl acetate	0.35
141	Propionaldehyde	0.34
142	Butyraldehyde	0.35
145	Hexanal	0.36
146	Heptanal	0.37
147	Octanal	0.38
151	Toluene	0.29
152	Ethylbenzene	0.30
156	Propylbenzene	0.31
157	Butylbenzene	0.32

squares slope and intercept for the Martin equation (A and B in eqn. 21). Third, compute the slope of $\pi_2^{*,C}$ *vs.* HN as follows:

$$B_2 = (B - lB_1)/s \tag{25}$$

where B_1 is the slope of log L^{16} *vs.* HN. Clearly this approach forces $\pi_2^{*,C}$ to be a linear

function of HN. The slope resulting from this approach is given in Table IX. Therefore, we can estimate $\pi_2^{*,C}$ by using the slope B_2 and a lower member's value as an intercept. Note we have given both the individual results based on a specific type of stationary phase and the average and standard deviation over all phases. For the alcohols, carboxylic acids and those compounds which are not a member of an homologous series the recommended $\pi_2^{*,C}$ value remain as in Table V.

Actually the above approach can be used to estimate $\pi_2^{*,C}$ for a homologous series of hydrogen bond donors provided that all higher members of the series have the same donor ability. This is always a good approximation. In this case the slope given in Table IX is used in conjunction with a $\pi_2^{*,C}$ value for a lower member of the series as obtained from Table V. The quality of the fits of gas chromatographic data is hardly affected by the above procedure (results are not given).

For all series (HN > 3), except the olefins, the average slopes of the relationship between $\pi_2^{*,C}$ and HN are positive. Within a homologous series the slope is well defined but the slopes vary rather considerably between series. As noted above the slopes of the cycloketones are quite high (+0.03, S.D. = 0.007) whereas the slope for the olefins is the lowest (−0.01, S.D. = 0.01).

The data are persuasive that $\pi_2^{*,C}$ values, as estimated from retention data, are a function of HN. In contrast we point out that measurements of dipole moments in solution are independent of HN [62]. Clearly there must be contributions to $\pi_2^{*,C}$ from factors other than the dipole moment of the species. As shown by eqns. 10 and 12 the molecular polarizability is such a factor. However, based on the fact that the change in polarizability per methylene group is virtually independent of the rest of the molecule [63] a polarizability contribution to $\pi_2^{*,C}$ cannot account for the variation in the slope of $\pi_2^{*,C}$ from series-to-series. Furthermore calculations based on the use of the Staverman–Guggenheim term of the UNIFAC method [56] show that differences in the configurational entropy per methylene groups as the homologous series is varied are much too small to be significant. We have to conclude that the $\pi_2^{*,C}$ term in this work is in part related to the inadequacy of log L^{16} to simultaneously model both dispersion interactions and the cavity formation process.

TABLE IX

SLOPE OF $\pi_2^{*,C}$ *VS.* HN

Series	B2						
	ZE7	Carbowax	TCEP	PPE6	DEGS	Avg	S.D.
Alkanes	0.006	0.010	0.010	−0.001	0.010	0.007	0.004
2-Ketones	0.009	0.010	0.010	0.007	0.012	0.009	0.001
Thiols	0.010	0.010	0.012	0.001	0.012	0.009	0.004
Cycloketones	0.026	0.027	0.028	0.044	0.039	0.033	0.007
Aldehydes	0.006	0.003	0.008	0.002	0.008	0.005	0.003
Alkenes	−0.002	−0.010	−0.003	−0.029	−0.002	−0.009	0.010
Acetates	0.016	0.018	0.014	0.016	0.026	0.018	0.004
Sulfides	0.013	0.020	0.006	0.010	0.002	0.010	0.006
Alkylbenzenes	0.028	0.007	0.008	0.017	0.012	0.014	0.008
Alcohols	0.017	0.015	0.016	0.011	0.017	0.015	0.002

CONCLUSIONS

A gas chromatographically based approach to the measurement of the dipolarity/polarizability ($\pi_2^{*,C}$) and hydrogen bond donor acidity (α_2^C) parameters has been developed. Parameters for 203 chemically very diverse species are presented. The resulting parameters naturally fit the GC retention data bases with better precision than non-chromatographically based parameters. The physical meaning of the parameters is maintained. The excellent correlations between the fitting coefficients (s and a) and the measured π^* and β parameters of the stationary phases provide a great deal of support to the legitimacy of the solvatochromic approach to the interpretation of solute–solvent interactions.

ACKNOWLEDGEMENTS

This work was supported in part by grants to the University of Minnesota from the National Science Foundation and the Petroleum Research Foundation.

REFERENCES

1 M. J. Kamlet and R. W. Taft, *J. Chem. Soc., Perkin Trans.*, 2 (1979) 337.
2 M. J. Kamlet, M. E. Jones, J.-L. M. Abboud and R. W. Taft, *J. Chem. Soc., Perkin Trans.*, 2 (1979) 342.
3 M. J. Kamlet and R. W. Taft, *J. Chem. Soc., Perkin Trans.*, 2 (1979) 349.
4 M. J. Kamlet and R. W. Taft, *J. Am. Chem. Soc.*, 98 (1976) 377.
5 R. W. Taft and M. J. Kamlet, *J. Am. Chem. Soc.*, 98 (1976) 2886.
6 M. J. Kamlet, J.-L. M. Abboud and R. W. Taft, *J. Am. Chem. Soc.*, 99 (1977) 6027.
7 M. J. Kamlet, J.-L. M. Abboud, M. H. Abraham and R. W. Taft, *J. Org. Chem.*, 48 (1983) 2877.
8 J.-L. M. Abboud and R. W. Taft, *J. Phys. Chem.*, 83 (1979) 412.
9 R. W. Taft, J.-L. M. Abboud and M. J. Kamlet, *J. Am. Chem. Soc.*, 103 (1981) 1080.
10 J. E. Brady and P. W. Carr, *Anal. Chem.*, 54 (1982) 1751.
11 J. E. Brady and P. W. Carr, *J. Phys. Chem.*, 86 (1982) 3053.
12 P. W. Carr, *J. Chromatogr.*, 194 (1980) 105.
13 J. E. Brady and P. W. Carr, *J. Phys. Chem.*, 89 (1985) 1813.
14 S. C. Rutan, P. W. Carr and R. W. Taft, *J. Phys. Chem.*, 93 (1989) 4293.
15 W. J. Cheong and P. W. Carr, *Anal. Chem.*, 61 (1989) 1524.
16 M. J. Kamlet, R. W. Taft, P. W. Carr and M. H. Abraham, *J. Chem. Soc., Faraday Trans.*, 78 (1982) 1689.
17 E. Wilhelm, R. Battino and R. J. Wilcock, *Chem. Rev.*, 77 (1977) 219.
18 R. Battino and H. L. Clever, *Chem. Rev.*, 66 (1966) 395.
19 E. F. Meyer and R. E. Wagner, *J. Phys. Chem.*, 70 (1966) 3162
20 S. C. Rutan, P. W. Carr, W. J. Cheong, J. H. Park and L. R. Snyder, *J. Chromatogr.*, 463 (1989) 21.
21 R. Kaliszan, *Quantitative Structure–Chromatographic Retention Relatonships*, Wiley, New York, 1987.
22 P. C. Sadek, P. W. Carr, R. M. Doherty, M. J. Kamlet, R. W. Taft and M. H. Abraham, *Anal. Chem.*, 57 (1985) 2971.
23 J. H. Park, P. W. Carr, M. H. Abraham, R. W. Taft, R. M. Doherty and M. J. Kamlet, *Chromatographia*, 25 (1988) 373.
24 M. J. Kamlet, M. H. Abraham, P. W. Carr, R. M. Doherty and R. W. Taft, *J. Chem. Soc., Perkin Trans.*, 2 (1988) 2087.
25 M. J. Kamlet, R. M. Doherty, M. H. Abraham, Y. Marcus and R. W. Taft, *J. Phys. Chem.*, 92 (1988) 5244.
26 B. Frange, J.-L. M. Abboud, C. Benamou and L. Bellon, *J. Org. Chem.*, 47 (1982) 4553.
27 J.-L. M. Abboud, K. Sraidi, G. Guiheneuf, A. Negro, M. J. Kamlet and R. W. Taft, *J. Org. Chem.*, 50 (1985) 2870.
28 M. H. Abraham, P. P. Duce, P. L. Grellier, D. V. Prior, J. J. Morris and P. J. Taylor, *Tetrahedron Lett.*, 29 (1988) 1587.

29 M. H. Abraham, P. L. Grellier, D. V. Prior, J. J. Morris, P. J. Taylor, C. Laurence and M. Berthelot, *Tetrahedron Lett.*, 29 (1988) 1587.
30 M. H. Abraham, G. J. Buist, P. L. Grellier, R. A. McGill, D. V. Prior, S. Oliver, E. Turner, J. J. Morris, P. Taylor, P. Nicolet, P.-C. Maria, J.-F. Gal, J.-L. M. Abboud, R. M. Doherty, M. J. Kamlet, W. J. Shuely and R. W. Taft, *J. Phys. Org. Chem.*, 2 (1989) 540.
31 M. H. Abraham, M. J. Kamlet, R. W. Taft and P. K. Weathersby, *J. Am. Chem. Soc.*, 105 (1983) 6797.
32 M. H. Abraham, G. J. Buist, P. L. Grellier, R. A. McGill, R. M. Doherty, M. J. Kamlet, R. W. Taft and S. G. Maroldo, *J. Chromatogr.*, 409 (1987) 15.
33 M. H. Abraham, P. L. Grellier and R. A. McGill, *J. Chem. Soc., Perkin Trans.*, II (1987) 797.
34 M. H. Abraham and R. Fuchs, *J. Chem. Soc., Perkin Trans.*, 2 (1988) 523.
35 J. Li, A. J. Dallas and P. W. Carr, *J. Chromatogr.*, 517 (1990) 103.
36 F. Patte, M. Etcheto and P. Laffort, *Anal. Chem.*, 54 (1982) 2239.
37 M. H. Abraham, G. S. Whiting, R. M. Doherty and W. J. Shuely, *J. Chem. Soc., Perkin Trans.*, 2 (1990) 1451.
38 Y. Zhang, A. J. Dallas and P. W. Carr, in preparation.
39 M. H. Abraham, P. L. Grellier, D. V. Prior, P. P. Duce, J. J. Morris and P. J. Taylor, *J. Chem. Soc., Perkin Trans.*, 2 (1989) 699.
40 M. H. Abraham, P. L. Grellier, D. V. Prior, J. J. Morris and P. J. Taylor, *J. Chem. Soc., Perkin Trans.*, 2 (1990) 521.
41 S. C. Rutan and P. W. Carr, *Anal. Chim. Acta*, 215 (1988) 131.
42 M. J. Kamlet, M. H. Abraham, R. M. Doherty and R. W. Taft, *J. Am. Chem. Soc.*, 106 (1984) 464.
43 R. W. Taft, M. H. Abraham, G. R. Famini, R. M. Doherty and M. J. Kamlet, *J. Pharm. Sci.*, 74 (1985) 807.
44 J. E. Brady, D. Bjorkman, C. D. Herter and P. W. Carr, *Anal. Chem.*, 56 (1984) 278.
45 J. R. Conder and C. L. Young, *Physicochemical Measurement by Gas Chromatography*, Wiley, New York, 1979.
46 Y. Zhang and P. W. Carr, unpublished data.
47 C. F. Poole and S. K. Poole, *Chem. Rev.*, 89 (1989) 377.
48 S. Ehrenson, *J. Org. Chem.*, 44 (1979) 1793.
49 C. Laurence, P. Nicolet and M. Helbert, *J. Chem. Soc., Perkin Trans.*, 2 (1986) 1081.
50 P. Nicolet and C. Laurence, *J. Chem. Soc., Perkin Trans.*, 2 (1986) 1071.
51 P.-C. Maria, J.-F. Gal, J. Franceschi and E. Fargin, *J. Am. Chem. Soc.*, 109 (1987) 483.
52 M. J. Kamlet and R. W. Taft, *Acta Chem. Scand. Ser. B*, 39 (1985) 611.
53 M. Sjöström and S. Wold, *Acta Chem. Scand. Ser. B*, 35 (1981) 537.
54 M. J. Kamlet, R. M. Doherty, J.-L. Abboud and R. W. Taft, *CHEMTECH* (1986) 566.
55 M. J. Kamlet, R. M. Doherty, M. H. Abraham and R. W. Taft, *J. Pharm. Sci.*, 75 (1986) 398.
56 J. H. Park and P. W. Carr, *Anal. Chem.*, 59 (1987) 2596.
57 D. E. Matire, *J. Chromatogr.*, 471 (1989) 71.
58 D. E. Martire and R. E. Boehm, *J. Phys. Chem.*, 91 (1987) 2433.
59 I. C. Sanchez and R. H. Lacombe, *J. Phys. Chem.*, 80 (1976) 2352.
60 N. H. Ray, *J. Appl. Chem. (London)*, 4 (1954) 21.
61 A. J. Dallas, *Ph.D. Thesis*, University of Minnesota, 1991.
62 A. L. McClellan, *Tables of Experimental Dipole Moments*, Freeman, San Fransisco and London, 1963, p. 580.
63 P. W. Carr, unpublished results.

Journal of Chromatography, 550 (1991) 135–154
Elsevier Science Publishers B.V., Amsterdam

CHROMSYMP. 2236

Effect of stationary phase on predictions of the statistical model of overlap from gas chromatograms

FRANCES J. OROS and JOE M. DAVIS*
Department of Chemistry and Biochemistry, Southern Illinois University, Carbondale, IL 62901 (USA)

ABSTRACT

The numbers of detectable components in each of four complex mixtures, which vary widely in polarity, were estimated with the statistical model of overlap from several dozen gas chromatograms. These chromatograms were generated at several heating rates and flow-rates on each of four capillary columns, with stationary phases that varied widely in polarity. For each mixture, the estimates so determined were grouped according to stationary phase. These groups then were compared by analysis of variance to establish any dependence of the model's predictions on stationary phase. These analyses show that internally consistent estimates can be calculated, unless the polarities of the mixture and stationary phase are highly mismatched or physical constraints on the chromatography prevent the establishment of random elution orders. It is also shown that the numbers of maxima detected in chromatograms generated by using a simple temperature program are comparable to those predicted by the statistical model of overlap, even when the elution order of the components is not deliberately randomized. Some problems inherent in measuring the retention times of peak maxima, which are needed to apply the model, by data processors are also addressed.

INTRODUCTION

This paper addresses the dependence on the stationary phase of parameters estimated with the statistical model of overlap (SMO) from gas chromatograms. The SMO [1] is one of several proposed statistical theories [1–6] that quantify the degree of peak overlap in chromatograms. The principal conclusions one draws from these theories is that the chromatograms of complex, multi-component mixtures contain a surprisingly large fraction of multiplet peaks and that the chromatography of such mixtures on a single column is inadequate for the resolution of the mixture components. Several applications of the SMO to both computer-generated [7–10] and experimental [9,11–15] chromatograms have been reported. In particular, the SMO has been confirmed experimentally by its application to gas chromatograms of synthetic mixtures containing known numbers of detectable components [14,15]. The theory also has been reinterpreted [16–18] and extended [19] by others.

In accordance with the Poisson statistics on which the SMO is based, the basic prerequisite to the model's application is the random elution of the various mixture components from the chromatographic column. Gas chromatographic studies have shown that, in some instances, random elution orders can be established by using

0021-9673/91/$03.50

a single linear temperature program [9,11,14]. In other instances, several contiguous linear programs (which are largely determined by trial and error) are required to force components into random elution orders [13,15]. By and large, the minimal condition necessary for the model's application can be found.

Nevertheless, several practical constraints on the model do exist. One such constraint is that the saturation, or relative component density, of the chromatogram must not exceed a certain limit, because the statistics do not account for the amplitudes of the component peaks [7–10]. (A recent statistical theory [6] shows considerable promise [20] in dealing with these amplitude effects, at least to some extent.) Another constraint, which is usually minor, is that the resolution factor, which resolves single-component peaks into separate observable peaks, depends on the signal-to-noise ratio [8]. Both of these constraints exist because the model does not address the fundamental chromatographic attributes of peak amplitude and noise. In fact, the only chromatographic attribute incorporated into the model is the peak capacity of the column [1]. In general, the basic independence of the model from specifics of the chromatography is one of its most attractive features, because the model can be applied to chromatograms of widely varying attributes. At the same time, one must be cautious in interpreting the model's predictions in cases where other chromatographic attributes, which have not been studied in detail by simulation or experiment, are or could be important.

The gas chromatographic applications of the SMO reported in the literature show the same basic trends as those determined from computer simulations [7–10]. In most of these studies, the stationary phase of the column was carefully chosen to be compatible with the mixture. In general, the compatibility of the stationary phase with a given mixture is a complex chromatographic attribute, whose influence on the predictions of the SMO has not been addressed in any detail. The only work of this kind, of which we are aware, is that of Coppi *et al.* [13], who gas chromatographed a camomile extract on an OV-1 capillary and two Carbowax 20M capillaries of different length. They found that the statistical parameters estimated from these chromatograms were internally consistent for several temperature programs. While these findings are certainly encouraging, they perhaps comprise too small a data set to be able to draw any general conclusions.

In particular, any detailed study of this attribute must answer the question of the care with which one must choose a stationary phase if one wishes to apply the SMO to a multi-component gas chromatogram. Many factors affect the interactions of mixture components with the stationary phase, but perhaps the most important is the phase polarity, which controls the solubility of the components in the phase. If one can simply match loosely the polarity of the mixture with that of the stationary phase (*e.g.*, if one can choose any polar stationary phase for the partial resolution of a polar mixture), then one can be guided by experience in the choice of that phase and can apply the SMO with little or no concern about this attribute. On the other hand, if the predictions of the model depend strongly on the stationary phase, then the utility of the SMO is called severely into question, and one will have little or no incentive to use it to characterize multi-component separations. To answer the above question more thoroughly, one must estimate statistical parameters from many chromatograms, which are generated from numerous mixture and stationary phase combinations, and check for internal consistency among the estimates.

We report here results based on the application of the SMO to several dozen gas chromatograms generated by the partial resolution of four mixtures on four capillary columns having different stationary phases. Both the various mixtures (a synthetic mixture of hydrocarbons, a coal tar extract, lime oil and peppermint oil) and the stationary phases (DB-1, DB-1701, RTX-225 and DB-WAX) span a wide range of polarity. In brief, several chromatograms were generated at several heating and flow-rates for each stationary phase–mixture combination. Several criteria were subsequently applied to evaluate the suitability of these chromatograms for analysis by the SMO. If these criteria were satisfied, then statistical parameters, including approximations to the number of detectable components, were estimated from these chromatograms. These approximations then were grouped into data sets corresponding to different stationary phase–mixture combinations. The data sets so developed from each mixture were compared by a one-way analysis of variance to determine if any statistical differences existed among them.

As an alternative to the experimental program outlined above, one could perhaps carry out a study of this type by theoretically estimating retention indices of various components on various stationary phases and constructing from these indices a series of computer-simulated chromatograms, which then could be analyzed. We chose to investigate the problem experimentally because, as observed elsewhere [15], important systematic effects, which cannot be anticipated by computer simulation, are often found in studies of this kind. Indeed, such effects are detailed below. Further, we anticipate that such a study will be more "believable" than one based on computer simulation.

THEORY

Application of the SMO

The theory underlying the SMO is detailed elsewhere [1]; only its application is reviewed here. The mean number p of detectable "peaks" in a chromatogram containing m detectable single-component peaks (SCPs) is

$$p = \bar{m} \exp(-\bar{m}/n_c) = \bar{m} \exp(-\alpha) \tag{1}$$

where $\bar{m}$ is a statistical approximation to m, n_c is the peak capacity of the chromatogram (or column) and $\alpha = \bar{m}/n_c$ is the chromatographic saturation. With this definition of α, one can express eqn. 1 in the dimensionless form

$$p/n_c = \alpha \exp(-\alpha) \tag{2}$$

By fitting data from experimental chromatograms to these expressions, one can estimate the statistical parameters $\bar{m}$ and α, which are measures of the quality of separation. Several approaches have been suggested for this fitting [1,7–10,12]. In perhaps the simplest of these, the so-called single-chromatogram method [15] by which one estimates these parameters from a single chromatogram, one expresses eqn. 1 in the equivalent form [10]

$$ln\ p = \ln \bar{m} - \bar{m}x_0/X \tag{3}$$

where x_0 is any arbitrarily chosen span, X is the span of the chromatogram to which the SMO is applied and p is interpreted as the number of gaps between adjacent chromatographic maxima which exceed x_0. In accordance with theory, a plot of ln p *vs.* x_0/X is a line whose slope $(-\bar{m})$ and intercept $(\ln \bar{m})$ yield two statistical approximations to m, which are termed m_{sl} and m_{in}, respectively [10]. By assigning the appropriate statistical weights to data in this plot, one also can calculate the standard deviations of m_{sl} and m_{in} [10]. From m_{sl}, m_{in} and their standard deviations, one then can calculate a pooled or average approximation to m [14], which is designated m_{ave}. The saturation α then can be estimated from eqn. 1 as [9]

$$\alpha = -\ln(p_m/m_{ave}) \tag{4}$$

where $p = p_m$ is the number of chromatographic maxima. The identification of the "peak" number p in eqn. 4 with the number p_m of chromatographic maxima implies that the saturation α, as defined by the minimum resolution R_s^* required to resolve adjacent SCPs, is less than about 0.5, when $R_s^* \approx 0.5$ [7–10,15].

As intimated in the Introduction, several criteria must be satisfied if one is to obtain accurate estimates of m_{ave} by using this method. These criteria are justified elsewhere [10] and are simply stated here: m_{sl} must equal m_{in} within statistical error, the graph of ln p *vs.* x_0/X must be linear, the graph of the number of chromatographic maxima eluting per unit interval of time *vs.* time must be uniformly constant and α must be less than 0.5, when $R_s^* = 0.5$. In addition, the overall appearance of the chromatogram must be consistent with this α value, as judged by a comparison of the experimental chromatogram with computer-generated chromatograms of the same saturation [11,15]. Unless noted otherwise, the results reported here were estimated from chromatograms which satisfied these criteria. The specific application of these criteria to this study is detailed below.

Analysis of variance (ANOVA)

Details on the Model I ANOVA used here can be found in appropriate references [21]. By using ANOVA, one can compare two or more groups of data and evaluate (within limitations) the statistical equivalence or non-equivalence of these groups. The basis of comparison is the Fisher ratio F_{v_1,v_2}, where v_1 and v_2 are the numbers of degrees of freedom among and within the compared groups, respectively.

In this study, each data group is composed of a series of m_{ave} values. Each value of m_{ave} in any of these groups was determined by applying the SMO to a single chromatogram of a specific mixture. This chromatogram, in turn, was developed on a specific capillary at a unique heating and flow-rate. Each group, therefore, corresponds to a specific mixture–stationary phase combination, and the various m_{ave} values comprising that group correspond to determinations made under different experimental conditions (which are detailed below). For each mixture, the groups of m_{ave} values corresponding to different stationary phases were compared by ANOVA. A schematic outline of the experimental generation and statistical comparison of such groups is depicted in Fig. 1.

We shall interpret the statistical equivalence of these groups as evidence that the m_{ave} values estimated from chromatograms of a given mixture, as developed on capillaries with different stationary phases, are identical. In other words, the stationary

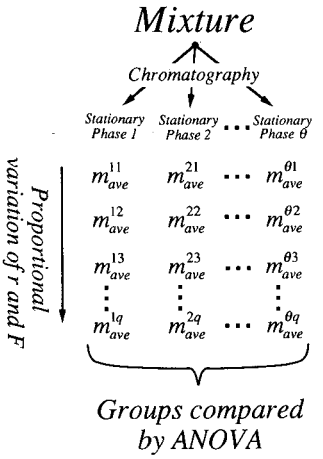

Fig. 1. Schematic outline of the experimental generation and statistical interpretation of groups of m_{ave} values in this study. Quantity $m_{ave}^{\theta q}$ is the qth member of the group of m_{ave} values corresponding to stationary phase θ. The number q of members per group can vary. Each group member is evaluated from a chromatogram generated at a unique heating rate r and flow-rate F, such that the ratio r/F is constant for all members of that group. Different groups, however, are associated with different r/F ratios.

phase has no statistically measurable effect on the estimates. This equivalence is quantitatively measured by the inequality $F_{v_1,v_2} < F^*_{v_1,v_2}$, where $F^*_{v_1,v_2}$ is a critical Fisher ratio for a given confidence level (here the 95% confidence level is used). In contrast, unless noted otherwise, we shall interpret the statistical non-equivalence of these groups (as measured by $F^*_{v_1,v_2} < F_{v_1,v_2}$) as evidence that the numbers m_{ave} depend on the stationary phase. This interpretation initially may seem too simplistic, because the dependence of these numbers on other attributes, *e.g.*, saturation α, is well established [10]. As stated above, however, extensive criteria have been developed by which to judge if these other attributes affect the estimates, and these criteria are employed in this study.

By our use of the Model I ANOVA, we are assuming implicitly that the m_{ave} values comprising each group are drawn from the same statistical population. As stated above, the m_{ave} values comprising each group were estimated from a series of chromatograms of a given mixture, as developed on a given capillary. Each chromatogram in this series, however, differs in the heating rate of, and volumetric flow-rate through, the capillary (see Fig. 1), although the ratio of these rates is held constant. Clearly, our implicit assumption that a single statistical population describes these m_{ave} values will not be valid, unless the m_{ave} values so determined are independent of these variations of heating and flow-rates. Previous studies have suggested that this independence indeed exists [9,13,15].

As an alternative to this protocol, these groups of m_{ave} values could have been generated more simply by selecting a single heating rate and flow-rate for each mixture–stationary phase combination and by generating replicate chromatograms at these fixed rates. We believe that our variation of these rates provides a significantly larger body of information for interpretation. Further, our variation of these rates enables us to confirm the independence of m_{ave} of these variations and also to discover

any unexpected trends. By and large, the results presented below verify this independence, although some subtle effects are also discovered.

EXPERIMENTAL

Preparation of mixtures

The synthetic hydrocarbon mixture, which previously was used in a detailed experimental verification of the SMO [15], was prepared from 54 C_6–C_{10} alkane and alkene standards, ethylbenzene and cyclopentanone. The preparation of this 56-component mixture is detailed elsewhere [15]; here, we note that the mean concentration of the mixture components was 1% in the solvent, tetradecane. The coal tar extract was obtained from NIST as SRM 1597 (Complex Mixture of Polynuclear Aromatic Hydrocarbons) in toluene solvent and was used as purchased. Peppermint and lime oils were kindly donated by the A. M. Todd Co. (Kalamazoo, MI, USA). One part of each of these oils was dissolved in ten parts of methylene chloride.

Chromatography

Fused-silica capillaries bonded to DB-1, DB-1701, RTX-225 and DB-WAX stationary phases were purchased from commercial sources (J & W Scientific, Folsom, CA, and Restek, Bellefonte, PA, USA). Some physical properties of these capillaries and phases are reported in Table I. The capillaries were incorporated into a Shimadzu (Columbia, MD, USA) GC9-AM modular gas chromatograph equipped with a Model SPL-9 split–splitless injector and flame ionization detector and interfaced to a Shimadzu C-R6A Chromatopac data processor. Aliquots of 1.0 μl were injected, with a 20:1 split of helium carrier gas. Helium was also passed to the detector as make-up gas at a flow-rate of 37 ml/min, except for the hydrocarbon mixture (in the latter instance, we simply did not realize that the make-up gas was turned off). The air and hydrogen flow-rates to the detector were 320 and 36 ml/min, respectively. Flow- and heating rates and injector and detector temperatures were varied for different mixture–stationary phase combinations and are reported in Table II. To minimize the possible contamination of any chromatogram by the elution of high-boiling components from previously injected mixtures (especially the coal tar extract), the oven temperature was held at the maximum temperatures reported in Table II for 30 min after the apparent completion of each chromatogram.

TABLE I

SOME PHYSICAL PROPERTIES OF THE CAPILLARY COLUMNS USED

Stationary phase	I.D. (μm)	Phase thickness (μm)	Length (m)	T_{max} (°C)[a]
DB-1	320	1.0	10; 15	325
DB-1701	320	0.25	30	280
RTX-225	320	0.25	30	220
DB-WAX	320	0.50	30	250

[a] Maximum recommended temperature for stationary phase.

TABLE II

REPRESENTATIVE r/F PROGRAMS FOR THE MIXTURE–STATIONARY PHASE COMBINATIONS IN THIS STUDY

Flow-rate ranges are reported in ml/min and were measured at ambient room temperature. Injector (I) and detector (D) temperatures are reported in °C.

Stationary phase	Mixture			
	Hydrocarbons	Coal tar extract	Lime oil	Peppermint oil
DB-WAX	Random elution order not achievable	Random elution order not achievable	Isothermal, 12.7 ml at 45°C; first ramp, 3.25°C/ml to 70°C; second ramp, 1.62°C/ml to 80°C; third ramp, 4.00°C/ml to 130°C; final ramp, 0.10°C/ml to 133°C ($2.40 < F < 9.23$; I = D = 210)	Isothermal, 0.94 ml at 35°C; first ramp, 3.03°C/ml to 100°C; second ramp, 5.27°C/ml to 130°C; third ramp, 0.21°C/ml to 133°C; final ramp, 1.34°C/ml to 170°C ($2.68 < F < 6.59$; I = D = 240)
RTX-225	Random elution order not achievable	Random elution order not achievable	Isothermal, 9.46 ml at 50°C; first ramp, 1.24°C/ml to 60°C; second ramp, 4.09°C/ml to 100°C; final ramp, 0.36°C/ml to 130°C ($1.93 < F < 6.32$; I = D = 200)	Isothermal, 10.50 ml at 55°C; first ramp, 3.70°C/ml to 100°C; second ramp, 3.32°C/ml to 113°C; final ramp, 1.49°C/ml to 115°C ($2.26 < F < 7.50$; I = D = 210)
DB-1701	Isothermal, 12.10 ml at 20°C; first ramp, 2.90°C/ml to 35°C; final ramp, 5.80°C/ml to 120°C ($1.54 < F < 5.94$; I = D = 220)	Isothermal, 12.00 ml at 100°C; ramp at 0.75°C/ml to 260°C ($3.16 < F < 12.00$; I = D = 280)	Isothermal, 9.30 ml at 65°C; first ramp, 2.20°C/ml to 95°C; second ramp, 4.45°C/ml to 120°C; final ramp, 0.75°C/ml to 140°C ($1.66 < F < 8.45$; I = D = 270)	Isothermal, 8.79 ml at 65°C; first ramp, 1.75°C/ml to 80°C; second ramp, 3.43°C/ml to 100°C; third ramp, 0.73°C/ml to 113°C; final ramp, 1.35°C/ml to 160°C ($1.78 < F < 6.00$; I = D = 230)
DB-1	Isothermal, 7.89 ml at 30°C; first ramp, 1.38°C/ml to 45°C; final ramp, 2.61°C/ml to 100°C ($2.60 < F < 12.00$; I = D = 275)[a]	Isothermal, 20.00 ml at 100°C; ramp at 0.75°C/ml to 260°C ($3.09 < F < 8.11$; I = 300; D = 310)[b]	Isothermal, 8.85 ml at 65°C; first ramp, 1.20°C/ml to 95°C; second ramp, 2.40°C/ml to 118°C; third ramp, 3.93°C/ml to 130°C; final ramp, 0.80°C/ml to 140°C ($2.45 < F < 8.00$; I = D = 260)[a]	Isothermal, 2.90 ml at 40°C; first ramp, 3.05°C/ml to 120°C; second ramp, 1.50°C/ml to 130°C; third ramp, 4.65°C/ml to 160°C; final ramp, 1.50°C/ml to 200°C ($4.11 < F < 7.14$; I = D = 240)[b]

[a] 10-m capillary.
[b] 15-m capillary.

Data acquisition and use

The voltages generated by the flame ionization detector were amplified to the same level in developing chromatograms of a given mixture on different capillaries, although this level was varied for different mixtures. Also, the threshold peak area, below which maxima were ignored by the data processor, was held constant in developing chromatograms of a given mixture on different capillaries. Both these precautions were taken to minimize the spurious detection or oversight of maxima in chromatograms of a given mixture. In addition, the flow-rate of the make-up gas was set to a relatively high value (37 ml/min) to minimize any changes in the detector response (*e.g.*, peak height) at different capillary flow-rates.

The retention times of chromatographic maxima were measured by the data processor. For reasons discussed below, the retention times of maxima in chromatograms of the coal tar extract also were measured by manually digitizing the relative positions of peak maxima with a True Grid 1011 Digitizer (Houston Instruments, Austin, TX, USA) interfaced to an Apple IIe microcomputer. Regardless of the mode of generation, the differences between adjacent pairs of retention times were calculated to generate plots of ln p *vs.* x_0/X. The procedural details underlying the generation of these plots are detailed elsewhere [11].

Ideally, all maxima should be included in span X to avoid discrepancies in comparing statistical parameters determined from one capillary to those determined from another. This ideal was achievable with the hydrocarbon mixture and oils but not the coal tar extract, because the relatively low temperature limit T_{max} of the DB-1701 capillary precluded the rapid elution of some of its high-boiling components (the temperature limits of the stationary phases are reported in Table I). These components could not be included in span X, because their slow elution rate was incompatible with the rapid elution rate of the more volatile components. In other words, their inclusion in span X would destroy an otherwise random elution order. A compromise was required, in which a common span X was chosen in the chromatograms developed on this and the DB-1 capillary. This selection was not complicate by slight shifts in the component elution orders, which were minor.

Criteria for evaluation of statistical estimates

As stated in the Introduction, the basic prerequisite for the calculation of good statistical parameters with the SMO is the random elution of mixture components from the chromatographic column. As observable maxima are not necessarily SCPs, however, this randomness cannot be determined by simply inspecting the chromatogram. Consequently, several previously developed tests were used to gauge this randomness, including the linearity of the ln p *vs.* x_0/X plot, the uniformity (or constancy) of the number of maxima eluting per unit time and the consistency between the appearance of the chromatogram and the α value predicted by eqn. 4.

The application of these tests was straightforward. Each mixture was first chromatographed on the capillary whose stationary phase most closely matched its polarity. This initial chromatography was similar to that routinely used for complex mixtures (*e.g.*, flow-rates of 2–3 ml/min and heating rates of 2–6°C/min). For the coal tar extract [22] and lime and peppermint oils [23], reference chromatograms were available for purposes of comparison. Next, the uniformity of the elution rate of the maxima in this chromatogram was evaluated by plotting the number of maxima

eluting per unit time (*i.e.*, the density of the maxima) against elution time. Computer simulations have shown that this number is fairly constant when the underlying SCP distribution is random [10]. The uniformity of this distribution was not evaluated statistically but by qualitative inspection only. The chromatography was then adjusted, if needed, to achieve the best possible compliance with this inspection. These adjustments principally consisted of changing the single heating rate into two or more rates, which were applied to the capillary at different times during the chromatography. In some instances, only partial compliance could be achieved. The lime and peppermint oils, in particular, produced small regions of maxima density which greatly exceeded that throughout the remainder of the chromatogram. These small non-uniformities do not seem to affect the prediction of statistical parameters, however, as detailed below.

Once the uniformity of the elution rate of the maxima was nearly optimum, a plot of ln p *vs.* x_0/X was constructed and checked for linearity. These plots were usually linear, because the existence of a uniform maxima density implies that the SCPs are randomly distributed in time [10]. On some occasions, however, the chromatography required some minor adjustments for one to attain linearity in these plots. Following these changes, the maxima density was again checked for its uniformity. When all necessary criteria were satisfied, then values of m_{sl}, m_{in}, m_{ave} and α were determined. In some instances, the α value for a given chromatogram exceeded the threshold value of 0.5. The statistical estimates from such chromatograms were rejected, unless noted otherwise.

Additional estimates of these four statistical parameters were then calculated from additional chromatograms of the mixture, which were generated by proportionally varying the heating rate r of, and volumetric flow-rate F through, the capillary. To a first approximation, this proportional variation maintained the retention temperatures of the mixture components [9,15,24] and consequently preserved the empirically determined elution order. For each chromatogram so developed, plots of maxima density *vs.* time and ln p *vs.* x_0/X were generated and checked for uniformity and linearity, respectively. Usually, these criteria were satisfied, although occasionally some minor changes in the chromatography were required (interestingly, these criteria were far more difficult to satisfy at low flow-rates, *e.g.*, 0.5–1.0 ml/min, than at higher values). Once these criteria were satisfied, then new estimates of m_{sl}, m_{in}, m_{ave} and α were calculated.

Some representative r/F programs are reported in Table II for the different mixture–stationary phase combinations in this study. These programs are representative only; the minor adjustments to these programs are not listed here. Only twelve programs, instead of sixteen, are reported, because random elution orders could not be established for four mixture–stationary phase combinations. The arrangement of these combinations is such that the least and most polar combinations are found in the lower left and upper right positions in the table, respectively.

A final criterion was then applied to gauge the acceptability of the calculated parameters. Each chromatogram was compared with the computer-simulated chromatograms in ref. 10 to gauge if the calculated α values were consistent with the expected appearance of the chromatogram. In almost all instances, this consistency was found. As discussed below, however, the m_{ave} values estimated from a few chromatograms were rejected because of such inconsistency.

TABLE III

STATISTICAL PARAMETERS m_{ave} AND α DETERMINED FROM, AND MAXIMA NUMBERS p_m DETECTED IN, CHROMATOGRAMS DEVELOPED FROM THE MIXTURE–STATIONARY PHASE COMBINATIONS IN THIS STUDY

F_{v_1,v_2} and $F^*_{v_1,v_2}$ ratios are reported at the bottom of the table. The numbers of chromatograms generated for each combination are reported in parentheses.

Stationary phase	Mixture			
	Hydrocarbons (m = 56)	Coal tar extract	Lime oil	Peppermint oil
DB-WAX	Random elution order not achievable	Random elution order not achievable	m_{ave}: 92 ± 6 (10) p_m: 66 ± 6 α: 0.34 ± 0.10	m_{ave}: 86 ± 8 (6) p_m: 59 ± 2 α: 0.38 ± 0.07
RTX-225	Random elution order not achievable	Random elution order not achievable	m_{ave}: 92 ± 11 (9) p_m: 68 ± 5 α: 0.30 ± 0.11	m_{ave}: 92 ± 9 (11) p_m: 59 ± 7 α: 0.44 ± 0.06
DB-1701	m_{ave}: 57 ± 5 (11) p_m: 42 ± 3 α: 0.30 ± 0.09	m_{ave}: 178 ± 13 (9) p_m: 119 ± 6 α: 0.40 ± 0.05	m_{ave}: 90 ± 4 (6) p_m: 60 ± 3 α: 0.41 ± 0.02	m_{ave}: 91 ± 4 (10) p_m: 71 ± 3 α: 0.26 ± 0.04
DB-1	m_{ave}: 56 ± 4 (15)[a] p_m: 38 ± 3 α: 0.38 ± 0.10	m_{ave}: 160 ± 10 (6)[b] p_m: 99 ± 4 α: 0.47 ± 0.06	m_{ave}: 83 ± 6 (6)[a] p_m: 58 ± 3 α: 0.34 ± 0.04	m_{ave}: 104 ± 6 (6)[b] p_m: 68 ± 5 α: 0.42 ± 0.04
	$F_{1,24}$ = 0.41 $F^*_{1,24}$ = 4.26	$F_{1,13}$ = 8.55 $F^*_{1,13}$ = 4.67	$F_{3,27}$ = 2.53 $F^*_{3,27}$ = 2.96	$F_{2,24}$ = 1.24; $F^*_{2,24}$ = 3.40 $F_{3,29}$ = 7.02; $F^*_{3,29}$ = 2.94

[a] 10-m capillary.
[b] 15-m capillary.

These procedures, with minor refinements, were then repeated to develop chromatograms of the same mixture on the other capillaries. Instead of using a simple temperature ramp to develop trial chromatograms, however, the previously developed r/F programs were used as guidelines.

Analysis of variance (ANOVA)

The estimates m_{ave} computed as detailed above for each mixture–stationary phase combination were grouped. For a given mixture, the various groups corresponding to different stationary phases were compared by one-way ANOVAs, formulae for which are given in standard references [21].

RESULTS AND DISCUSSION

Interpretation of ANOVAs

Table III reports the means and standard deviations of the statistical parameters m_{ave} and α estimated from chromatograms developed from twelve of the sixteen mixture–stationary phase combinations in this study. Also reported are the means and standard deviations of the numbers p_m of maxima detected in these chromatograms by the data processor (for reasons given below, the numbers p_m reported for the coal tar extract were determined by manual digitization and not the data processor). Several Fisher ratios F_{v_1,v_2} and $F^*_{v_1,v_2}$ (the latter for the 95% confidence level) are reported at the bottom of the table.

Four of the sixteen positions in Table III are empty, because various constraints on the chromatography prevented the establishment of random elution orders for these mixture–stationary phase combinations. For example, the lower temperature limit of the RTX-225 stationary phase (40°C) precluded sufficient cooling of the capillary to adequately retain the low-boiling constituents of the hydrocarbon mixture. In addition, the components of this mixture eluted from the DB-WAX capillary as several small clusters of maxima with large intervening gaps. Finally, the relatively low upper temperature limits, T_{max}, of the RTX-225 and DB-WAX phases (reported in Table I) prevented the rapid elution (and inclusion in a random elution order) of a substantial fraction of the high-boiling components in the coal tar extract. While our inability to develop random elution orders for these cases is disappointing, it is perhaps not surprising, because the polarities of these mixtures and stationary phases are poorly matched. Indeed, our ability to develop random elution orders for other cases of poorly matched polarities (*e.g.*, for peppermint oil on a DB-1701 phase) was more surprising than these failures.

In contrast to the above cases, the components of the hydrocarbon mixture could be forced into random elution orders on the DB-1 and DB-1701 capillaries (the chromatography of this mixture on the DB-1 capillary has been detailed elsewhere [15]). As shown by the Fisher ratios at the bottom of the second column in Table III, no statistical difference exists between the m_{ave} values estimated from the chromatograms developed on these capillaries ($F_{1,24} < F^*_{1,24}$). The estimates are not only statistically equivalent but also accurate; as reported in Table III, the mean estimates differ from the true number of detectable components [56] by $\leqslant 1$. The p_m values detected in, and the α values estimated from, chromatograms developed on the DB-1701 capillary are larger and smaller, respectively, than their DB-1 counterparts, probably because the former capillary was longer and more efficient than the latter (see Table I).

Unlike for the other mixtures considered here, the number m of detectable components in the hydrocarbon mixture, which was prepared from analytical standards [15], is known. This knowledge enables us to interpret further the data summarized in the second column of Table III. Fig. 2 is a plot of p/n_c *vs.* α constructed from these data. The solid curve is a graph of eqn. 2, whereas the points represent experimental results. A similar plot of data developed from 10- and 30-m lengths of a DB-1 capillary was presented elsewhere [15]; here, only data from the 10-m capillary are displayed. As detailed in that work [15], p was approximated as p_m, α was calculated from eqn. 4 and n_c was calculated as $56/\alpha = -56/\ln(p_m/m_{ave})$. By such calculations, an exact agreement between experiment and theory is expected only if $p = p_m$ and $m = m_{ave} = 56$ [15]. The close agreement between experiment and theory again affirms the accuracy of the statistical parameters estimated with the SMO.

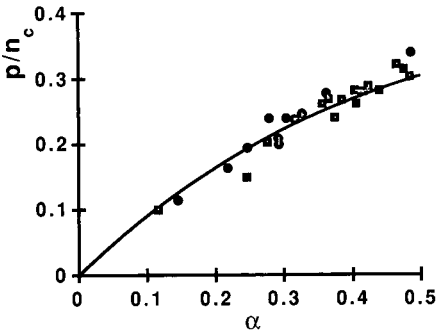

Fig. 2. Dimensionless plot of p/n_c *vs.* α ($R_s^* = 0.5$). The solid curve is a graph of eqn. 2; the data were estimated from chromatograms of the hydrocarbon mixture developed on the (■) DB-1 (10-m) and (●) DB-1701 capillaries.

In contrast to the hydrocarbon mixture, statistical parameters for the lime oil mixture were determined from chromatograms developed on all four capillaries. The Fisher ratios at the bottom of the fourth column in Table III indicate that no statistical difference exists among the various m_{ave} values determined from these capillaries ($F_{3,27} < F^*_{3,27}$), despite their marked differences in stationary phase polarity. In particular, the mean m_{ave} values estimated from the three most polar capillaries agree within the value 2. Fig. 3 depicts examples of typical chromatograms developed from this mixture on these capillaries. In each chromatogram, the span X is indicated. In contrast to one's first impressions, a substantial number of small maxima were detected in the intermediate region of the DB-1 chromatogram.

For reasons outlined above, the statistical parameters for the coal tar extract were estimated from chromatograms developed on the DB-1 and DB-1701 capillaries only. In contrast to the finding reported above, the Fisher ratios at the bottom of the third column in Table III indicate a statistical difference exists between these m_{ave} values ($F_{1,13} > F^*_{1,13}$). This finding is disquieting, because this mixture is relatively non-polar and both capillaries have low polarities. However, the finding is not crippling, because the means of the two distributions differ by only *ca.* 10%. The reason why the ANOVA is significant is that the standard deviations associated with

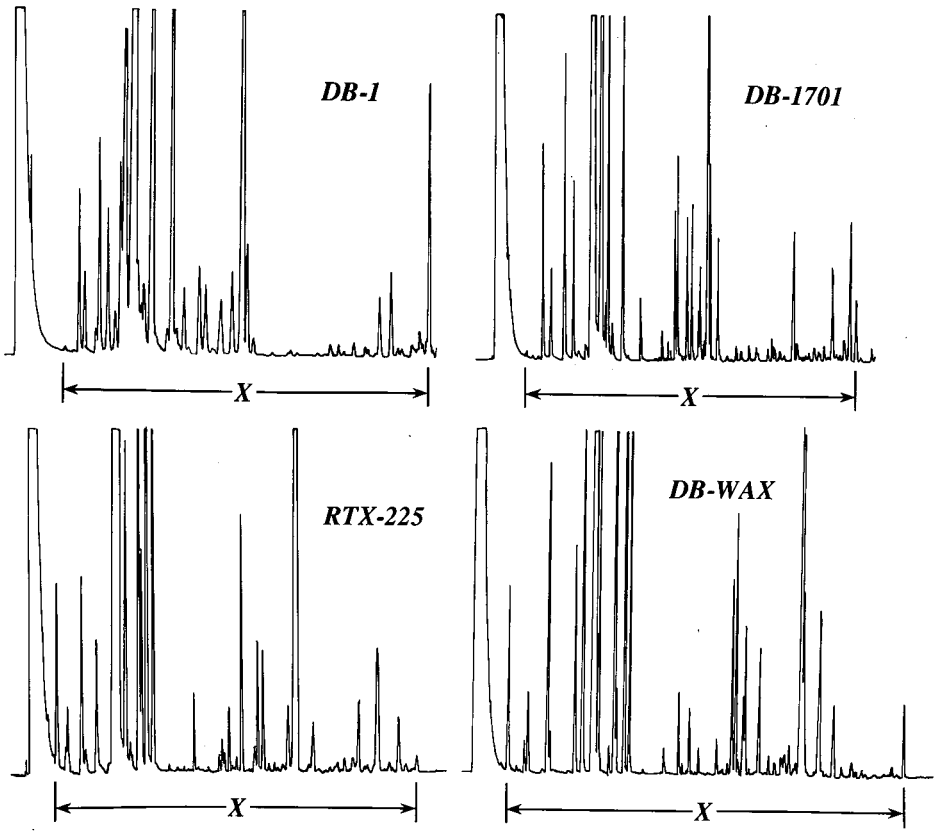

Fig. 3. Typical chromatograms of the lime oil mixture developed on the DB-1, DB-1701, RTX-225 and DB-WAX capillaries. The span X to which the SMO was applied is indicated. Flow-rates: DB-1 capillary (10-m segment), 4.11 ml/min; DB-1701 capillary, 2.78 ml/min; RTX-225 capillary, 3.39 ml/min; DB-WAX capillary, 3.57 ml/min. Representative r/F programs are reported in Table II.

these means are even smaller than the small difference between the means. For example, the coefficients of variation for the m_{ave} values determined from the DB-1 and DB-1701 chromatograms are only 6.2 and 7.3%, respectively.

In the Theory section, we argued that significant ANOVAs would indicate a dependence of m_{ave} on the stationary phase, unless other well known systematic effects were present. In this specific case, we believe that such effects are indeed present. One reason why the m_{ave} values estimated from the DB-1 chromatograms are significantly smaller than their DB-1701 counterparts is that relatively high α values ($\alpha = 0.47 \pm 0.06$), some of which clearly exceed the threshold value, $\alpha = 0.5$, are associated with the DB-1 chromatograms. As documented elsewhere, values of m_{sl} and (to a lesser extent) m_{in} are underestimated by the single-chromatogram method employed here, as α approaches this threshold [10].

To determine if this underestimation could account for the significant depression of the m_{ave} values determined from the DB-1 capillary, we reinterpreted some previously published results determined from the analysis of computer-generated

chromatograms. Table III in ref. 10 reports the means and standard deviations of the percentage errors in m_{sl} and m_{in} for the α values, 0.333, 0.500 and 0.667, as determined from the analysis of computer-generated chromatograms containing 100, 200 and 300 SCPs distributed exponentially in amplitude. By computing m_{ave} from these m_{sl} values, m_{in} values and standard deviations as detailed elsewhere [14], one can show that the quadratic polynomial which describes the pooled percentage error, *PE*, in these computer-generated chromatograms at these α values is

$$PE = 100\left(\frac{m_{ave} - m}{m}\right) = 108.8\alpha^2 - 173.1\alpha + 49.7 \quad (5)$$

This expression for PE should not be used with α values outside the range, $0.333 \leqslant \alpha \leqslant 0.667$, from which it was determined. If one now corrects for the expected percentage errors in the m_{ave} values reported in Table III by using eqn. 5 and the reported α values, one anticipates that the number m of components in the coal tar extract is 182, as determined by analysis of the DB-1701 chromatograms, and 173, as determined by analysis of the DB-1 chromatograms. These values differ by only about 5%, unlike the uncorrected values, which differ by about 10%. The close agreement between these numbers lends credence to the idea that the saturation α is too high for the estimates determined from the DB-1 chromatograms to be considered fully reliable. However, these arguments indicate a possible trend at best and cannot be interpreted as rigorous proof of deterministic error.

The statistical parameters determined from chromatograms of the highly polar peppermint oil mixture and reported in the final column in Table III are most revealing. The first set of Fisher ratios reported at the bottom of this column indicates that no statistical difference exists among the m_{ave} values determined from the DB-WAX, RTX-225 and DB-1701 capillaries ($F_{2,24} < F^*_{2,24}$), whose polarities are intermediate to high. If the m_{ave} values determined from the 15-m length of the non-polar DB-1 capillary are now included in the ANOVA, however, significant differences among the m_{ave} values are found. These differences are indicated by the second set of Fisher ratios reported at the bottom of the column ($F_{3,29} > F^*_{3,29}$). Clearly, this mixture–stationary phase combination leads to estimates which, for reasons that are not readily apparent, differ substantially from the others. Our only comfort is the realization that no experienced chromatographer would attempt to separate a mixture of this high polarity on such a non-polar capillary.

The parameter m_{ave} was also estimated from four chromatograms of this mixture, as developed on a 10-m length of DB-1 capillary. In contrast to an earlier study, which indicated that m_{ave} was fairly independent of capillary length when the polarities of the mixture and stationary phase were well matched [15], the m_{ave} values determined from the 10-m capillary ($m_{ave} = 69 \pm 3$) differ most significantly from those reported in Table III for the 15-m capillary ($m_{ave} = 104 \pm 6$). Interestingly, plots of $\ln p$ *vs.* x_0/X and maxima density *vs.* time were linear and uniform, respectively, for both capillary lengths. The only test, which suggested that the m_{ave} values determined from the 10-m capillary were spurious, was the inconsistency between the α values calculated from eqn. 4 and the subjective appearance of the chromatograms. In all instances, the chromatograms appeared to be far more saturated than indicated by the α values ($\alpha = 0.27 \pm 0.05$). The overall results determined from this mixture–stationary phase combination are puzzling.

Other findings of merit

During the course of this study, some interesting observations were made, the implications of which lie beyond the objectives outlined in the Introduction. We conclude this section with a brief description of them.

Comparison of maxima numbers developed from simple and complex r/F programs. The senior author occasionally has been criticized for portraying the chromatography of complex mixtures in too grim a light. Here, we simply wish to anticipate the objection that the overlap resulting from the use of the complex r/F programs reported in Table II may be worse than that resulting from the use of the simple temperature programs commonly used in analytical and clinical laboratories. To develop a proper perspective on these comparative degrees of overlap, each mixture for which a random elution order was developed on a given capillary was also chromatographed on that capillary by using a simple program consisting of a brief isothermal period, a single temperature ramp and a final isothermal period. Flow-rates were set slightly above the optimum value, *e.g.*, 2–3 ml/min. Table IV reports the details of these programs and the numbers of maxima, p_{ms}, detected by the data processor in these simple chromatograms (for reasons detailed below, the numbers of maxima, p_{ms}, in the coal-tar chromatograms were determined by manual digitization). In addition, the number of maxima, p_m, detected in the SMO-type chromatogram developed at the flow-rate closest to that adopted for the simple chromatogram is also reported. In all instances, the numbers p_{ms} are comparable to the numbers p_m. In other words, the gas chromatography of these mixtures, as carried out under typical conditions, generated chromatograms that were little, if any, better than those predicted by the SMO (and those are bad enough!). These findings should raise an unambiguous warning about the integrity of routine gas chromatographic separations of complex mixtures on single capillary columns.

This warning is also reinforced by the mean value of the ratio $p_m/m_{ave} = 0.69 \pm 0.05$, which was calculated from the mean values of p_m and m_{ave} reported in Table III. On average, about one SCP in three is not detectable in the SMO-type chromatograms considered here. Because the numbers p_{ms} are comparable to the numbers p_m, a similar decrease in efficiency is also found in these simple chromatograms.

Potential variation of statistical parameters with flow-rate. The numbers of maxima, p_m, detected in, and numbers of components, m_{ave}, estimated from, chromatograms of the coal tar extract developed on the DB-1 and DB-1701 capillaries were found to increase systematically with increasing flow-rate, F, when the maxima numbers were measured by the data processor. In contrast, these numbers were essentially independent of F for chromatograms of the hydrocarbon mixture and lime and peppermint oils when measured by the same processor. These trends are illustrated in Fig. 4a–d, which are graphs of p_m and m_{ave} *vs.* F, as constructed from chromatograms of all four mixtures, as developed on the DB-1701 capillary. If one were to predict any such variation, one would anticipate a decrease in p_m (but not m_{ave}) with increasing F, because of increased non-equilibrium dispersion. Indeed, one could argue that Fig. 4a–c show such a trend, although it is slight. The trend shown in Fig. 4d for the coal tar extract, however, is opposite to this expectation. Were the m_{ave} values depicted in Fig. 4d to be used in this study (they are not), this dependence would be of concern for at least two reasons. First, it would invalidate the Model I ANOVAs used here, in which one assumes that m_{ave} is independent of F. Second, and more important,

TABLE IV

SIMPLE TEMPERATURE PROGRAMS FOR THE MIXTURE–STATIONARY PHASE COMBINATIONS IN THIS STUDY AND THE NUMBERS p_{ms} OF MAXIMA DETECTED IN THE RESULTANT CHROMATOGRAMS

Maxima numbers p_m reported here are those detected in SMO-type chromatograms developed at the flow-rates closest to those used in developing the simple chromatograms. Flow-rates F are in ml/min and were measured at ambient room temperature.

Stationary phase	Mixture			
	Hydrocarbons	Coal tar extract	Lime oil	Peppermint oil
DB-WAX	Not appropriate	Not appropriate	Isothermal, 2.0 min at 45°C; 4°C/min to 180°C; isothermal, 20 min at 180°C p_{ms}: 64 (F = 3.01) p_m: 66 (F = 3.25)	Isothermal, 4.0 min at 70°C; 4°C/min to 190°C; isothermal, 20 min at 190°C p_{ms}: 63 (F = 3.01) p_m: 60 (F = 2.68)
RTX-225	Not appropriate	Not appropriate	Isothermal, 5.7 min at 50°C; 4°C/min to 200°C; isothermal, 20 min at 200°C p_{ms}: 63 (F = 3.42) p_m: 71 (F = 2.99)	Isothermal, 4.5 min at 50°C; 4°C/min to 200°C; isothermal, 20 min at 200°C p_{ms}: 56 (F = 3.42) p_m: 70 (F = 3.35)
DB-1701	Isothermal, 3.0 min at 20°C; 10°C/min to 170°C; isothermal, 10 min at 170°C p_{ms}: 45 (F = 3.14) p_m: 43 (F = 2.97)	Isothermal, 4.0 min at 100°C; 2.9°C/min to 260°C; isothermal, 30 min at 260°C p_{ms}: 127 (F = 3.82) p_m: 127 (F = 3.82)	Isothermal, 5.2 min at 75°C; 4°C/min to 200°C; isothermal, 20 min at 200°C p_{ms}: 66 (F = 3.17) p_m: 61 (F = 2.94)	Isothermal, 5.2 min at 75°C; 4°C/min to 200°C; isothermal, 20 min at 200°C p_{ms}: 65 (F = 3.16) p_m: 73 (F = 2.90)
DB-1	Isothermal, 2.9 min at 30°C; 10.4°C/min to 150°C; isothermal, 10 min at 150°C p_{ms}: 43 (F = 2.88) p_m: 44 (F = 2.60)[a]	Isothermal, 6.7 min at 100°C; 2.5°C/min to 260°C; isothermal, 30 min at 260°C p_{ms}: 98 (F = 3.00) p_m: 98 (F = 3.00)[b]	Isothermal, 4.0 min at 65°C; 4°C/min to 190°C; isothermal, 20 min at 190°C p_{ms}: 59 (F = 2.88) p_m: 61 (F = 2.50)[a]	Isothermal, 4.0 min at 75°C; 4°C/min to 200°C; isothermal, 20 min at 200°C p_{ms}: 51 (F = 3.12) p_m: 69 (F = 3.26)[b]

[a] 10-m capillary.
[b] 15-m capillary.

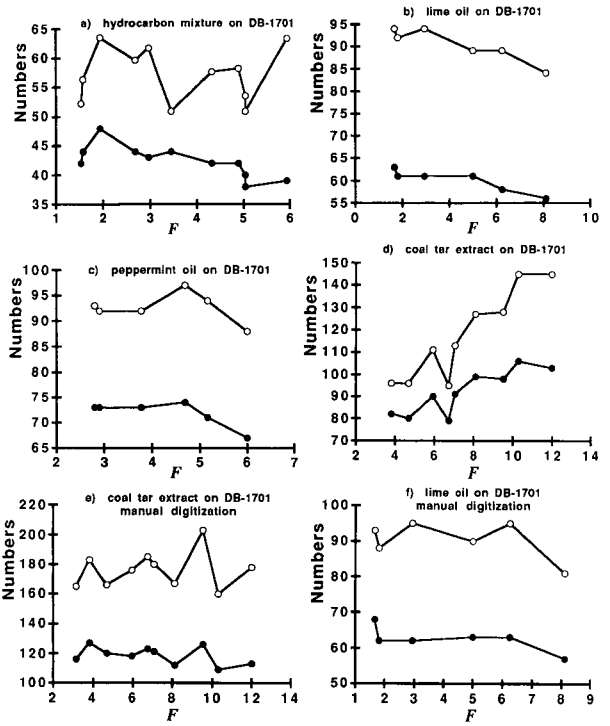

Fig. 4. Plots of maxima numbers detected in, and component numbers estimated from, chromatograms developed from various mixtures on the DB-1701 capillary *vs.* flow-rate F. Flow-rates are reported in ml/min. The maxima numbers were measured by the data processor, unless noted otherwise. ○ = m_{ave}; ● = p_m.

it would call strongly into question the integrity of statistical parameters determined for this mixture.

A close inspection of the coal tar chromatograms showed that this variation in p_m was due principally to the detection by the data processor of very small maxima at high but not at low flow-rates. This observation suggested the variation was related more to systematic errors in the detection of maxima by the data processor than to properties of the mixture. To investigate this behavior, the retention times of all maxima in chromatograms of the coal tar extract, as developed on the DB-1 and DB-1701 capillaries, were manually digitized as detailed under Experimental. From these digitized sets of retention times, new sets of statistical parameters were calculated. In contrast to the findings reported above, both the maxima numbers p_m and component numbers m_{ave} so determined were largely independent of F, as shown in Fig. 4e for results determined from the DB-1701 capillary. Fig. 4e shows the slight decrease in p_m with F that is observed in Fig. 4a–c, instead of the substantial increase in p_m with F that is observed in Fig. 4d. Further, the various m_{ave} values in Fig. 4e are scattered about a constant value, in marked contrast to their counterparts in Fig. 4d. These trends also were observed for results similarly determined from the DB-1 capillary.

The manual digitization of the retention times of maxima should be an acceptable means of data acquisition, as it was used successfully in an earlier verification of the SMO [14]. To verify this procedure further, the retention times of maxima in chromatograms of the lime oil, as developed on the DB-1701 capillary, were also manually digitized. From these retention times, a new set of statistical parameters was estimated and compared with that estimated by using the data processor. Fig. 4f depicts the p_m values and m_{ave} values so determined, which are statistically equivalent to those depicted in Fig. 4b. In other words, the maxima numbers generated by, and the component numbers estimated from, the lime oil are independent of the means by which retention times were measured. However, this independence does not extend to the coal tar extract, as shown by Fig. 4d and e.

Interestingly, both uniform plots of maxima density *vs.* time and linear plots of $\ln p$ *vs.* x_0/X were generated from chromatograms of the coal tar extract, as developed on both capillaries, regardless of the means by which the retention times were measured. This finding implies that the small peaks, which are not detected by the data processor at low flow-rates but are detected by the eye, are randomly distributed throughout the chromatogram, such that their oversight by the data processor still leaves a random (but less dense) distribution. Indeed, one should anticipate their distribution to be random, as no *a priori* reason exists to expect more small peaks in the beginning of a chromatogram than at its end.

What is the origin of this behavior? One characteristic of the coal tar extract, in comparison to the other mixtures, is the low concentration of its components. These concentration differences were so large that the signals generated by the flame ionization detector, in response to components of the coal tar extract, required substantially higher amplification (by a factor of 10 or more) than those generated by components of the other mixtures. Herein may lie the key to the behavior of the coal tar extract. We believe the most likely origin is the slope sensitivity of the data processor. The conservation of SCP area by the flame ionization detector, which is a mass-sensitive detector, requires that SCPs eluting at high flow-rates be taller and narrower than those eluting at low flow-rates [25,26]. The initial slope of a peak consequently is greater at high than at low flow-rates, and a small peak is more easily detected at high than at low flow-rates. In our system, the flow of make-up gas to the detector attenuated but did not eliminate this behavior; the highest capillary flow-rates were smaller than the make-up gas flow-rate by only a factor of *ca.* 3. If one were to expect shortcomings in the detection of maxima by a data processor, one would anticipate this behavior more from weak signals (*e.g.*, from the coal tar extract), which may or may not cross the slope-sensitivity threshold, than from strong signals (*e.g.*, from the other mixtures), which always cross the threshold.

Other than to propose this explanation, we leave the origin of this behavior unresolved here. The reason that we do so is that its resolution has no fundamental bearing on the issues raised in this particular study. The only motive for our present investigation of this behavior was to find means, which were independent of F, for estimating m_{ave} from chromatograms of the coal tar extract. The acquisition of retention times by manual digitization seems to fulfill this goal. More specifically, the use of this digitization procedure enabled us to apply the SMO to the coal-tar chromatograms and the Model I ANOVA to the m_{ave} values so determined, and the results of these analyses are reported in Tables III and IV.

Another error associated with the detection of maxima by the data processor merits brief discussion. In chromatograms of the lime oil mixture, as developed on the DB-1 and DB-1701 capillaries, and of the peppermint oil, as developed on the DB-1701 capillary, the data processor detected an off-scale signal as several maxima at low flow-rates but as only one maximum at higher flow-rates. When the attenuation was increased to bring this signal on-scale, only one maximum was observed. In our applications of the SMO, these signals at low flow-rates were interpreted as one maximum, with a retention time equal to the average of the various detected retention times. Little error was incurred by this averaging, because the m_{ave} values so determined are similar to those determined at higher flow-rates.

CONCLUSIONS

The principal conclusion of the first part of the study is that internally consistent statistical parameters can be calculated by applying the SMO to single gas chromatograms, provided that the polarity of the mixture and the stationary phase are reasonably well matched. In other words, the concern stated in the Introduction about the compatibility of the stationary phase with a mixture can largely be dismissed, if one is guided by common sense in choosing a stationary phase. This conclusion was also reached by Coppi *et al.* [13], but we have provided a substantially larger body of data to support it. Based on these data, we feel safe in proposing the general conclusion that no particular stationary phase is required to determine statistical parameters, provided that random elution orders can be established. Nor, for that matter, is a particular r/F program or flow-rate required. In some instances one can even obtain internally consistent estimates when the mixture and stationary phase polarities are not particularly well matched (*e.g.*, lime oil on the DB-1 capillary and peppermint oil on the DB-1701 capillary). As a rule of thumb, however, our results do suggest that one should avoid extreme mismatches in polarity, which can lead either to failed efforts to establish a random elution order (*e.g.*, hydrocarbon mixture on the DB-WAX capillary) or to the calculation of estimates of questionable integrity (*e.g.*, peppermint oil on the DB-1 capillary). This conclusion was not reached by Coppi *et al.* [13], principally because these behaviors were not encountered in their limited study. Certainly, these latter results emphasize the need to apply the SMO judiciously and to evaluate the estimates so calculated by several criteria.

The principal conclusion one draws from the (admittedly limited) comparison of simple and complex temperature programs is that the routine gas chromatographic separations of multi-component mixtures are relatively poor. In other words, one does not need the highly elaborate r/F programs sometimes prerequisite to the application of the SMO to develop deliberately separations of low quality. We develop these low-quality separations routinely in our laboratories, regardless of whether or not we want them. The principal conclusion one draws from the latter part of this study is that, on occasion, m_{ave} can depend strongly on the method of data acquisition. This conclusion is a simple consequence of the dependence of the SMO's predictions on what a sensor (*e.g.*, a mechanical device or the human eye) detects: the distribution of peak maxima in a chromatogram. In general, the attainment of reliable estimates may require more labor-intensive efforts than those based on the use of processor-measured retention times, especially when the mixture is composed of many trace components.

Because this method of data acquisition is highly convenient, further study of its limitations would be meritorious.

ACKNOWLEDGEMENTS

The authors thank Milton Lee of Brigham Young University for his suggestion of SRM 1597 as a test mixture, William Faas of the A. M. Todd Co. (Kalamazoo, MI, USA) for his donation of lime and peppermint oils and Lee Olszewski and Steve Roepke of Delta Instrument (Waterloo, IL, USA) for helpful discussions. This study was supported in part by the Office of Research Development and Administration at Southern Illinois University.

This study was presented at the *21st Annual Ohio Valley Chromatography Symposium, Hueston Woods State Park Lodge, OH, June 20–22, 1990*, and at *FACSS XVII, Cleveland, OH, October 7–12, 1990.*

REFERENCES

1 J. M. Davis and J. C. Giddings, *Anal. Chem.*, 55 (1983) 418.
2 K. A. Connors, *Anal. Chem.*, 46 (1974) 53.
3 D. Rosenthal, *Anal. Chem.*, 54 (1982) 63.
4 L. J. Nagels, W. L. Creten and P. M. Vanpeperstraete, *Anal. Chem.*, 55 (1983) 216.
5 M. Martin, D. P. Herman and G. Guiochon, *Anal. Chem.*, 58 (1986) 2200.
6 A. Felinger, L. Pasti and F. Dondi, *Anal. Chem.*, 62 (1990) 1846.
7 J. C. Giddings, J. M. Davis and M. R. Schure, in S. Ahuja (Editor), *Ultrahigh Resolution Chromatography (ACS Symposium Series*, No. 250), American Chemical Society, Washington, DC, 1984, p. 9.
8 J. M. Davis and J. C. Giddings, *J. Chromatogr.*, 289 (1984) 277.
9 D. P. Herman, M. F. Gonnard and G. Guiochon, *Anal. Chem.*, 56 (1984) 995.
10 J. M. Davis and J. C. Giddings, *Anal. Chem.*, 57 (1985) 2168.
11 J. M. Davis and J. C. Giddings, *Anal. Chem.*, 57 (1985) 2178.
12 F. Dondi, Y. D. Kahie, G. Lodi, M. Remelli, P. Reschiglian and C. Bighi, *Anal. Chim. Acta*, 191 (1986) 261.
13 S. Coppi, A. Betti and F. Dondi, *Anal. Chim. Acta*, 212 (1988) 165.
14 J. M. Davis, *J. Chromatogr.*, 449 (1988) 41.
15 S. L. Delinger and J. M. Davis, *Anal. Chem.*, 62 (1990) 436.
16 M. Martin and G. Guiochon, *Anal. Chem.*, 57 (1985) 289.
17 W. L. Creten and L. J. Nagels, *Anal. Chem.*, 59 (1987) 822.
18 M. R. Schure, *J. Chromatogr.*, in press.
19 M. Martin, presented at the *17th International Symposium on Chromatography, Vienna, September 25–30, 1988.*
20 A. Felinger, L. Pasti, P. Reschiglian and F. Dondi, *Anal. Chem.*, 62 (1990) 1854.
21 R. R. Sokal and F. J. Rohlf, *Biometry*, Freeman, San Francisco, 1981.
22 S. A. Wise, B. A. Benner, H. Liu and G. A. Byrd, *Anal. Chem.*, 60 (1988) 630.
23 *Chromatography Catalog*, No. 28, Supelco, Bellefonte, PA, 1990, pp. 32–33.
24 W. E. Harris and H. W. Habgood, *Programmed Temperature Gas Chromatography*, Wiley, New York, 1966.
25 I. Halasz, *Anal. Chem.*, 36 (1964) 1428.
26 N. Dyson, *Chromatographic Integration Methods*, Royal Society of Chemistry, Cambridge, 1990.

Journal of Chromatography, 550 (1991) 155–170
Elsevier Science Publishers B.V., Amsterdam

CHROMSYMP. 2290

Gas chromatography of homologous esters

XXXIV.[a] Alkyl borate and boronate esters

J. K. HAKEN* and F. ABRAHAM
Department of Polymer Science, University of New South Wales, P.O. Box 1, Kensington, NSW 2033 (Australia)

ABSTRACT

The preparation and gas chromatographic behaviour of simple alkyl borate and boronate esters is reported. Difficulties with the gas chromatography of some of these esters, the rearrangements that occur with the boronate esters and the formation of cyclic and acyclic boronates were investigated. The effect of the alkyl substituent on retention when adjacent to a boron or oxygen atom has been considered and the effects are discussed in relation to the behaviour of other ester series.

INTRODUCTION

The retention behaviour of a considerable number of series of homologous esters, including *n*-alkyl [1,2] and *n*-alkenyl [3,4] straight- and branched-chain aliphatic esters [5], keto esters [6], chlorinated aliphatic esters [7,8], aromatic [9], cycloalkyl [9] and phosphorus esters [10] has been studied previously.

The influence of the polar nature of the stationary phase on retention, the effect of the position of a substituent group, either an alkyl group, unsaturation or a chlorine atom, on retention, the increasing contribution with increasing phase polarity of carbonyl and phenyl groups on retention and the relative influence of a substituent when in the alkyl or alcohol chain (R^1) or the acyl or acid chain (R^1) according to the following convention have been reported:

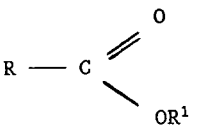

All of the series studied showed the expected increase in retention with increasing phase polarity, while the effect of a structural parameter, *e.g.*, a methylene group, an

[a] For Part XXXIII, see ref. 8.

0021-9673/91/$03.50

unsaturated linkage, an aromatic ring or chlorine atom, has been shown to exhibit a greater effect on retention when in the alkyl rather than the acyl chain, with the exception of the phosphorus esters, where the reverse effect was evident. The conclusions that have been reached [1–9] have largely been corroborated by subsequent reports using the same esters by other workers [11,12].

With phosphate esters the three substituent groups were equivalent, but the phosphinate esters are comparable to the carbonyl esters with substituents adjacent to both an oxygen atom and the parent atom. The effect with the phosphinate esters was explained on the basis that there are two OR^1 chains, and hence the inductive effect of the P = O group is split between the two and is thus reduced in magnitude. The polarity of the phosphoryl group is lower than that of the carbonyl group owing to the effects of the d electrons in the phosphorus, which tend to neutralize the electron-withdrawing effects of the O atom. The possibility of a similarity with borate and boronate esters was suggested.

The gas chromatography (GC) of borate esters has received little attention and no publications restricted to the GC of the esters seem to have appeared. The sole work employing GC–mass spectrometry (MS) is apparently that of Wada *et al.* [13], which considered triisopropyl borate. The electron impact (EI) mass spectrum of trimethyl borate was reported in 1956 [14]. Subsequently, EI mass spectra of trimethyl borate and higher trialkyl borates were reported [15–18]. Mass spectrometry has also been used to show that exchange reactions occur between mixtures of trialkyl borates [19,20]. The simple alkyl boronates have similarly attracted little attention. However, several of the acids have been extensively studied in the formation of derivatives for the identification of multifunctional compounds [21].

This paper reports the preparation and GC behaviour of simple alkyl borate and boronate esters. Difficulties with the GC of the borate and acylic boronate esters were investigated, and the effect on retention of the position of the alkyl substituent in the alkyl or acyl chain is discussed in relation to the behaviour of the other ester series reported previously.

Earlier studies of many types of homologous esters [1–10] have been reported and this work allows a study of a wider range of esters to be made using conditions relatively comparable to those in the earlier work.

Borate esters

The borate esters

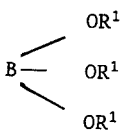

were prepared using a borane–methyl sulphide complex and alkanol under anhydrous conditions:

$$3R^1OH + BH_3S(CH_3)_2 \rightarrow B(OR^1)_3 + S(CH_3)_2 + 3H_2 \quad (1)$$

This minimizes the presence of water and reduces the susceptibility to hydrolysis.

Boronic acid esters

Two types of organoboron acids are formed: the boronic acids (I) and the borinic acids (II) with the following formulae shown below:

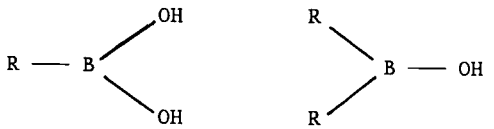

(I) (II)

The borinic acids have not been shown to have any analytical application, although the boronic acids have been extensively used for the formation of derivatives of bifunctional compounds since their introduction by Brooks and Watson [21] in 1967.

Two series of esters of alkyl boronic acid may be prepared by simple esterification. With monofunctional alcohols the acyclic dialkyl boronates are formed, whereas with bifunctional alcohols the cyclic alkyl boronates are formed:

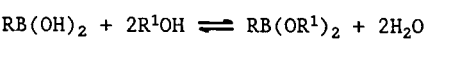

(2a)

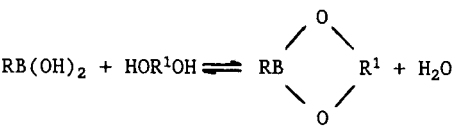

(2b)

The dialkyl boronates are of low hydrolytic stability and not usually stable to GC. The cyclic alkyl boronates have good GC properties.

The cyclic *n*-butane [21–23] and methane [24–28] boronates were first used, and subsequently also benzeneboronic acid [29–36], cyclohexaneboronic acid [23,24,26–28], *tert.*-butylboronic acid [27] and *n*-octaneboronic acid. Acylic boronates frequently occur with bifunctional compounds with isolated amino or hydroxy groups. The presence of such species has been attributed to the poor GC behaviour of some carbohydrates [27].

Cyclic boronates containing halogens [37–40] have been introduced to allow electron-capture detection. The use of boronates for derivatization and their mass spectra have been extensively reviewed [41,42].

EXPERIMENTAL

Alkyl borate esters

The esters were prepared [43] from the borane–methyl sulphide complex (10 *M*) (Aldrich, Milwaukee, WI, USA). All reactions were carried out in a dry nitrogen atmosphere, using glassware dried in an oven at 150°C. A special experimental technique was used in handling the air- and moisture-sensitive $BH_3 \cdot S(CH_3)_2$.

A dry 500-ml flask equipped with an injection port, PTFE-covered magnetic stirring bar, pressure-equallized dropping funnel and a reflux condenser connected to

an oil bubbler was purged with nitrogen. Then 7.5 ml of $BH_3 \cdot S(CH_3)_2$ were injected into the flask with a syringe through a rubber septum. While stirring and cooling in a water-bath, the alcohol was added dropwise at 25°C. Quantitative amounts of the alkyl borate esters in dimethyl sulphide were formed. The borate esters were stored under dry nitrogen, as they are extremely sensitive to moisture.

Boronic acid

The boronic acids were prepared by the hydroboronation reaction [44]:

$$RCH=CH_2 + HBr_2 \cdot S(CH_3)_2 \xrightarrow{CH_2Cl_2} RCH_2CH_2Br_2 \cdot S(CH_3)_2$$

$$\xrightarrow{H_2O} RB(OH)_2 + 2HeBr \qquad (3)$$

The *n*-butylboronic acid was obtained from Alltech (Deerfield, IL, USA) and the alkenes, the dibromoborane–dimethyl sulphide complex $HBBr_2 \cdot S(CH_3)_2$ (1 *M* in dichloromethane) and the alcohols were obtained from Aldrich.

The alkene (100 mmol) dissolved in chloromethane (100 ml) was placed in a 500-ml reaction flask. The 1 *M* $HBBr_2 \cdot S(CH_3)_2$ solution (100 ml; 100 mmol) was added slowly, using a syringe. The mixture was heated (40°C) under reflux and stirred for about 3 h. The alkyldibromoboranedimethyl sulphide formed was cooled to 0°C and transferred to a stirred, cold (0°C) mixture of water (18 ml; 1000 mmol) and diethyl ether (100 ml) through a double-ended needle. The stirring was continued for 10 min, then the water layer was separated and discarded. The organic layer was washed with cold water (2 × 30 ml) and saturated brine (1 × 50 ml) and dried over anhydrous magnesium sulphate. After evaporating the solvent, using a water aspirator, white crystals of the boronic acid were formed [45].

Alkylboronate esters

The dialkyl alkylboronate and the alkyl alkylboronate esters were formed by the esterification of the corresponding alkylboronic acids with the respective alcohols in *n*-pentane.

The alkylboronic acid (0.5 g) was suspended in 10 ml of *n*-pentane in a separating funnel. An equivalent amount of the alkanol was added, and the mixture was shaken for a few seconds. The water formed was separated. Another equivalent of the alkanol was added to the mixture and the water layer formed was separated. The pentane layer was dried with anhydrous magnesium sulphate. While the ester formed and the reacting alcohol are soluble in pentane, water and the boronic acid are not. The esters formed in pentane were stored in air-tight vials with silicone seals.

The cyclic alkylboronate esters were prepared in the same manner as outlined above, except that there was no need to add an excess amount of alkanediol.

Gas chromatography

For GC a Shimadzu GC-8A gas chromatograph fitted with a flame ionization detector and a Shimadzu Chromatopac C-RGA data processor was used. The oven temperature was 110°C and the injection port temperature was 220°C. Helium was

used as the carrier gas at a flow-rate of 30 ml/min. Three stationary phases were used: 5% SE-30 on 80–100-mesh Chromosorb W AW DMCS, 4% OV-17 on 80–100-mesh Chromosorb M AW DMCS and 3% XE-60 on 80–100-mesh Gas-Chrom Q11.

Gas chromatography–mass spectrometry

The gas chromatograph–mass spectrometer used to obtain retention times and chemical ionization mass spectra was a Finnigan 3200 quadropole instrument, interfaced with a TO.2300 Incos computer data system. The ion source was maintained at 110°C by filament emission (100 mA) and the source pressure was 0.8 Torr. Three 1.5 m × 4 mm I.D. glass columns, containing 3% OV-1, OV-17 and OV-225 as stationary phases, were used. The carrier gas was methane at a flow-rate of 20 ml/min. The oven temperature was maintained at 50 and 70°C. In one experiment with a mixture of alkyl borates, temperature programming from 35 at 6°C/min was used. The scan frequency was 1 cycle/s.

RESULTS AND DISCUSSION

The *n*-alkyl borate esters were not eluted through the gas chromatograph owing to their ease of hydrolysis, evidently assisted by traces of moisture in the carrier gas and no doubt accentuated by their limited thermal stability. This result clearly explains why minimal GC studies of the trialkyl borate esters have been published. The conditions used in the gas chromatograph–mass spectrometer with methane as carrier gas are not usually used for simple GC. However, the esters were eluted through the gas chromatograph–mass spectrometer, the hydrolysis being retarded owing to the use of both ultra-dry methane as the carrier gas and a lower column temperature. The eluted compounds exhibited very broad and unsatisfactory peaks, and the resulting peak areas were not reproducible owing to the varying degree of hydrolysis. Temperature programming when methane was the carrier gas allowed good elution of the alkyl borates. The mass spectra of the esters were readily obtained. However, it was not possible to elute the acyclic alkyl boronates, as they were readily hydrolysed to the corresponding boronic acids, but again with methane as the carrier gas satisfactory peak elution occurred.

At higher temperatures, *i.e.*, 150–200°C, it was shown by mass spectrometry that the boronic acids dehydrated to form boroxines [46]:

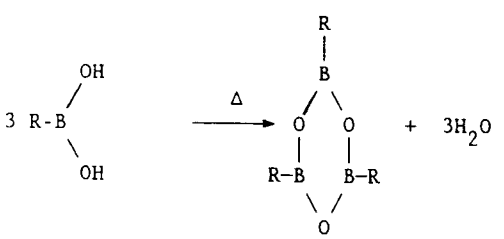

(4)

The separation of triethyl, tri-*n*-propyl and tri-*n*-butyl borates on OV-1 with temperature programming from 35°C at 6°C/min is shown in Fig. 1. Figs. 2 and 3 show the separation of the cyclic *n*-alkyl boronates. Fig. 2 shows the alcohol esters (R = C_4–C_7), separated on 3% XE-60, and Fig. 3 the acid esters (R^1 = C_2–C_4) on 3%

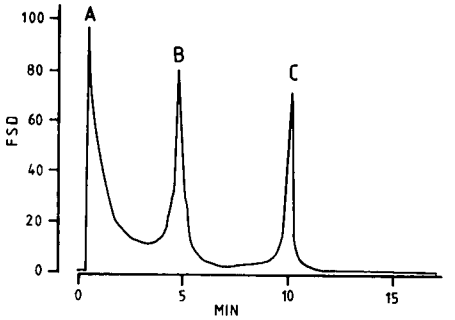

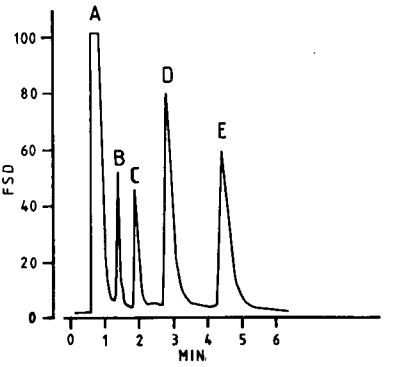

Fig. 1. Chromatogram of separation of (A) triethyl, (B) tri-*n*-propyl and (C) tri-*n*-butyl borates on OV-1 temperature programmed from 35°C at 6°C/min.

Fig. 2. Chromatogram of separation of cyclic *n*-alkyl boronates (alcohol esters, R = C_4–C_7) on XE-60 at 100°C. (A) Solvent; (B) ethyl *n*-butylboronate; (C) ethyl *n*-pentylboronate; (D) ethyl *n*-hexylboronate; (E) ethyl *n*-heptylboronate.

XE-30, with isothermal operation at 110°C in both instances. Tables I–III show retention data for the cyclic and acyclic alkyl boronate esters. Retention index plots for the cyclic alkyl boronates with both the acid (R = C_4–C_7) and alcohol (R^1 = C_2–C_4) chain as the ordinate produced linear plots on all of the stationary phases.

In a study of a sample homologous aliphatic ester series, Ashes and Haken [1] observed linearity for the acid ester series on non-polar, donor and acceptor columns. However, for the alcohol ester series they reported a loss of linearity on the acceptor column and linearity on the non-polar and donor columns. The loss of linearity for the alcohol ester series on the acceptor column was attributed to the transmission of the induced dipole in the acid chain in a geometric progression with the methylene increments, as expressed by the decreasing interaction of the carbonyl group and the

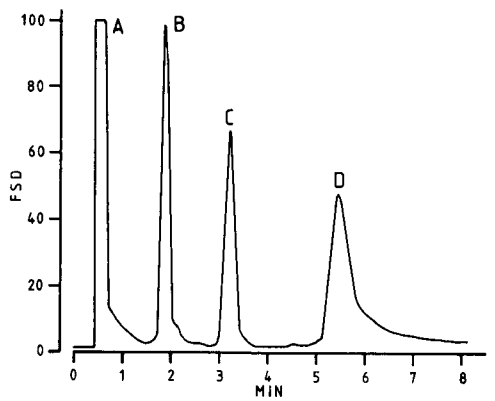

Fig. 3. Chromatogram of separation of cyclic *n*-alkyl boronates (acid esters, R^1 = C_2–C_4) on SE-30 at 110°C. (A) Solvent; (B) ethyl *n*-pentylboronate; (C) *n*-propyl *n*-pentylboronate; (D) *n*-butyl *n*-pentylboronate.

TABLE I

RETENTION DATA FOR CYCLIC *n*-ALKYLBORONATE ESTERS AT 110°C

Conditions: isothermal, 110°C; helium carrier gas at 30 ml/min; 2 m × 1/8 in. I.D. stainless-steel column.

Compound	Mol. wt.	Stationary phase								
		SE-30 (5%)			OV-17 (4%)			XE-60 (3%)		
		t_R[a] (min)	I[a]	ΔI[a] per CH_2	t_R (min)	I	ΔI per CH_2	t_R (min)	I	ΔI per CH_2
Alcohol ester series										
Ethyl *n*-butylboronate	128	1.488	914		1.22	1039		1.233	1131	
Ethyl *n*-pentylboronate	142	2.422	1020	106	1.925	1143	104	1.765	1227	96
Ethyl *n*-hexylboronate	156	4.142	1117	*97*	3.233	1242	*99*	2.697	1324	*97*
Ethyl *n*-heptylboronate	170	7.337	1214	97	5.712	1341	99	4.302	1420	96
Acid ester series										
Ethyl *n*-pentylboronate	142	2.400	1018		1.917	1141	*113*	1.757	1225	*102*
n-Propyl *n*-pentylboronate	156	4.267	1123	*105*	3.475	1254		2.733	1327	145
n-Butyl *n*-pentylboronate	170	7.447	1217	94				5.622	1472	
n-Alkane series										
Decane (C_{10})	140	2.183			1.043			0.845		
Undecane (C_{11})	154	3.745			1.578			1.110		
Dodecane (C_{12})	168	6.728			2.587			1.578		
Tridecane (C_{13})	182	12.358			4.485			2.413		
Tetradecane (C_{14})	196	23.192			8.127			3.900		

[a] t_R = Retention time; I = retention index; ΔI = retention index increment.

TABLE II

RETENTION DATA FOR CYCLIC AND ACYCLIC *n*-ALKYLBORONATE ESTER SERIES AT 70°C

Conditions: isothermal, 70°C; methane flow-rate, 20 ml/min; 1.5 m × 4 mm I.D. glass columns.

Compound	Mol. wt.	Stationary phase									
		OV-1			OV-17				OV-225			
		t_R[a]	I[a]	Δt_R[a] per CH_2	(t_R-50)[a]	t_R[a]	I	Δt_R per CH_2	(t_R-50)	t_R	I	Δt_R per CH_2
Cyclic alcohol ester series												
Ethyl *n*-butylboronate	128								(18)	68	1131	
Ethyl *n*-pentylboronate	142	(34)	1023		(33)	83	1136		(87)	137	1234	103
Ethyl *n*-hexylboronate	156	(129)	1123	*100*	(127)	176	1232	*96*	(227)	277	1332	*98*
Ethyl *n*-heptylboronate	170	(320)	1218	95	(330)	379	1330	98	(513)	563	1429	97
Cyclic acid ester series												
Ethyl *n*-pentylboronate	142	(32)	1019		(34)	84	1137		(86)	136	1233	
n-Propyl *n*-pentylboronate	156	(130)	1124	*105*	(141)	191	1247	*106*	(243)	293	1340	*107*
n-Propyl isopentylboronate	156	(49)[b]	(1044)	[b]								
n-Butyl *n*-pentylboronate	170	(299)	1210	86	(303)	353	1321	78	(568)	618	1441	101
Acyclic alcohol ester series												
Dimethyl *n*-pentylboronate	144	(6)	968									
Dimethyl *n*-hexylboronate	158	(55)	1052	84								
Dimethyl *n*-heptylboronate	172	(162)	1145	*93*								

Acyclic acid ester series									
Diethyl *n*-butylboronate	158	(13)	984						
Di-*n*-propyl isobutylboronate	186	(60)[b]	(1058)[b]						
Di-*n*-propyl *n*-butylboronate	186	(176)	1153	*84.5*					
Di-*n*-butyl *n*-butylboronate	214								
n-Alkane series									
Decane (C_{10})	140	(21)							
Undecane (C_{11})	154	(100)			(13)	63			
Dodecane (C_{12})	168	(274)			(88)	138		(0)	50
Tridecane (C_{13})	182	(640)			(274)	297		(58)	108
Tetradecane (C_{14})	196				(611)	661		(169)	219
Pentadecane (C_{15})	210							(405)	455
Hexadecane (C_{16})	224								

[a] (t_R-50) = retention time as shown on RIC chromatograms which was 50 s after injection; t_R = actual retention time; other abbreviations as in Table I.
[b] These retention times are for the isomers of the corresponding alkylboronates.

TABLE III

RETENTION DATA OF CYCLIC AND ACYCLIC *n*-ALKYLBORONATE AND *n*-ALKYLBORATE ESTER SERIES AT 50°C

Conditions: isothermal, 50°C; 20 ml/min; 1.5 m × 4 mm I.D. glass columns, 3% OV-17.

Compound	t_R[a]	I[a]	ΔI[a] per CH_2	Mol.wt.
Cyclic alcohol ester series				
Ethyl *n*-butylboronate	54	1044		128
Ethyl *n*-pentylboronate	196	1146	102	142
Ethyl *n*-hexylboronate	534	1247	*101*	156
Cyclic acid ester series				
Ethyl *n*-pentylboronate	195	1146		142
n-Propyl *n*-pentylboronate	574	1255	*109*	156
n-Butyl *n*-pentylboronate	–	–	–	170
Acyclic alcohol ester series				
Dimethyl *n*-pentylboronate	23	1002		144
Dimethyl *n*-hexylboronate	127	1108	106	158
Dimethyl *n*-heptylboronate	383	1212	*104*	172
Acyclic acid ester series				
Dimethyl *n*-butylboronate	19	995		158
Di-*n*-propyl *n*-butylboronate	285	1182	*94*	186
Di-*n*-butyl *n*-butylboronate	–	–	–	170
n-Alkyl borate esters				
Triethyl borate	2	960		146
Tri-*n*-propyl borate	148	1114	54	188

[a] Abbreviations as in Tables I and II.

TABLE IV

METHYLENE INDEX INCREMENTS FOR THE ACID AND ALCOHOL CHAINS OF THE CYCLIC ALKYLBORONATE ESTERS

Compound	Stationary phase					
	OV-1 (70°C)	OV-17 (50–70°C)	OV-225 (70°C)	SE-30 (110°C)	OV-17 (110°C)	XE-60 (110°C)
Alcohol series:	100	101 96	98	97	99	97
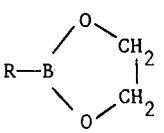						
R = C_4–C_7						
Acid series:	105	109 106	107	105	113	102
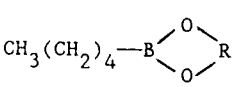						
R′ = C_2–C_4						

methyl group, resulting in an uneven relative retention for the lower and higher alcohol ester series. As the methyl group moved further away from the carbonyl group, the increase in retention became smaller, *i.e.*, as the acid chain became longer than three carbon atoms. It was reported that the expected loss of linearity for the acid ester series on the acceptor column did not occur, probably owing to the ether linkage allowing better transmission of the induced dipole, resulting in similar increases in the relative retentions of the lower and higher acid ester series.

The linear relationships for the cyclic alkylboronate alcohol ester series on the acceptor columns, in contrast to the non-linear relationship for the aliphatic alcohol ester series, may be explained as being due to the boron end of the alcohol ester series being much less polar than the carbonyl end of the aliphatic alcohol ester series. This is expected, owing to the lower polarizability of the cyclic boron–oxygen bond as compared with the carbon–oxygen double bond of the carbonyl group of the aliphatic esters. Also, boron is less electronegative than carbon [9]. Therefore, unlike the aliphatic alcohol ester series, where there was a significant but diminishing interaction between the carbonyl and the methyl groups, there seemed to be no significant interaction between the boron end and the methyl group, owing to weak polarity of the boron end of the alcohol ester. The retention index increments per methylene unit added to the alcohol or acid chain of the cyclic alkylboronate, shown in Table IV, were obtained from the differences in the successive homologous ester series.

Table IV shows that the methylene increments in the alcohol chain have a greater effect on the retention index than in the acid chain for all the stationary phases considered. This behaviour is similar to that previously observed with simple, homologous aliphatic ester series but for slightly different reasons owing to their cyclic configurations. It is also evident that in the alcohol ester series, the magnitude of the retention index increment did not change very much with increase in polarity of the stationary phases. However, with the acid ester series, there was a significant increase for OV-17, indicating a greater interaction. Ashes and Haken [1] reported a decrease in retention index increments for aliphatic esters as the polarity of stationary phase increased.

For the aliphatic ester series, Ashes and Haken [1] also reported that the greater effect in the alcohol chain was due to the ether linkage, hindering rotation of the alcohol chain, and hence an incremental change in this chain will have greater effect on molecular shape, maximizing the surface area owing to the lack of rotation and thus increasing the cohesive forces of molecules. The ether linkage was also reported to allow better transmission of the induced dipole, resulting in an increase in retention for the alcohol ester series. The same considerations also seem to explain in part the greater effect of methylene increments on the alcohol chain of the cyclic alkylboronate esters relative to the acid chain. However, the main reason for the greater effect in the alcohol chain seems to be the cyclic configuration of the alkylboronate esters. In the alcohol ester series, there is the usual increase in chain length:

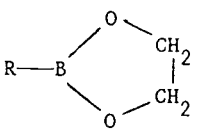

where R = C_4–C_7, without a change in the shape of the molecule. Therefore, the GC behaviour should be conventional.

In the acid ester series, 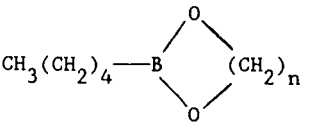

where n = 2–4, the system expands and the ring acquires a different shape. The most probable shapes for the acid ester series [47] are as follows:

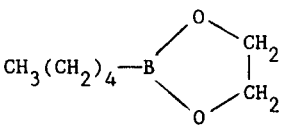

almost planar

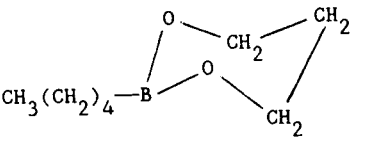

probably chair

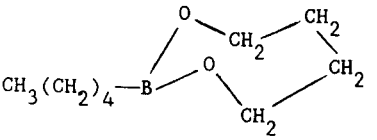

probably distorted chair

Insertion of methylene groups in the alcohol chain varies the shape of the molecule, which in turn affects the retention behaviour of the series. The variation in the ring size seems to be the main reason for the greater effect of the methylene increment in the alcohol chain rather than the acid chain.

The change in the shape of the ring (*i.e.*, steric effects) may also explain why the overall retention index increments are greater for the acid ester series than in the alcohol ester series, indicating greater interaction with the OV-17 stationary phase.

Studies with cyclic alkanes [32] and cyclic alkylboronates [47] have shown significant differences in molecular shapes with increasing size. As the size of the cyclic configuration increases from a five- to a seven-membered ring, the availability of the Pz orbital of the boron and the unpaired electrons of oxygen for interaction with the stationary phases increases.

Retention index plots for the acyclic alkylboronate ester series *versus* the number of carbon atoms in the acid or alcohol chain (retention index *versus* R or R′) were examined. For the alcohol ester series, the retention index plot was linear. However, for the acid ester series, the linear relationship is suspect, as it was only possible to obtain the retention time for two esters, and manipulation of column temperature to obtain retention times for three esters at a particular temperature did not succeed. The operating temperature for the third acid ester series, di-*n*-butyl *n*-butylboronate, was not high enough. However, the assumption that the retention index plot for the acid ester series is linear seems to be reasonable in view of the linearity of the cyclic alkylboronate esters.

Table V shows that the methylene increments in the acid chain have a greater

TABLE V

METHYLENE INCREMENTS FOR THE ACID AND ALCOHOL CHAIN OF THE ACYCLIC ALKYLBORONATE ESTER SERIES

Compound	Stationary phase	
	OV-1 (70°C)	OV-17 (50°C)
Alcohol ester series:		
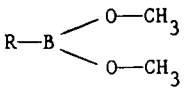	93	104
Acid ester series:		
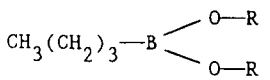	84	94

effect on the retention index than in the alcohol chain. The differences in retention index, *i.e.*, $\Delta CH_2R' - \Delta CH_2R$, was -10 units on OV-17 and -9 units on OV-1. In a similar study of aliphatic ester series [14], the retention index differences, *i.e.*, $\Delta CH_2R' - \Delta CH_2R$, of $+15$, $+7.5$ and $+11$ units on SE-30, DC-710 ($\equiv$OV-17) and Silar 5CP, respectively, were reported.

Crank and Haken [10] in a study of alkylphosphonate esters reported retention index differences, *i.e.*, $\Delta CH_2R' - \Delta CH_2R$, of -7 units on OV-17. The retention index differences of the acyclic alkylboronates, *i.e.*, $\Delta CH_2R' - \Delta CH_2R$, are similar in magnitude to those for the alkylphosphonate and aliphatic ester series. The sign is the same as that for the alkylphosphonates and opposite to that for the aliphatic ester series.

The effect with the phosphonate esters was explained on the basis that there are two $-OR'$ chains and, hence, the inductive effect of the $P=O$ group is split between the two and is thus reduced in magnitude. Also, the polarity of the phosphoryl group was reported to be less than that of the carbonyl group, owing to the effects of d electrons in phosphorus, which tend to neutralize the electron-withdrawing effect of the $=O$ atom.

Similar arguments to those for the alkylphosphonates seem also to be applicable to explain why the methylene increment on the acid chain has a greater effect on the retention index than in the alcohol chain. The structures of the acyclic alkylboronate esters in Table V indicate that there are three –OR′ ester chains bonded to the boron atom. Boron atoms usually form three bonds, involving their three sp^2 hybrid orbitals. The remaining p_z orbital is empty and accepts a pair of electrons from one of the –OR′ ester chains, making the boron–alcohol chain slightly polar. As this polarity effect is divided between the three –OR′ groups, the methylene increment on the alcohol chain will have less effect on the retention index relative to the methylene increment in the

acid chain. In addition, as indicated, the boron–alcohol chain is also less polar than the carbonyl chain.

The alkyl borate esters studied could be represented by

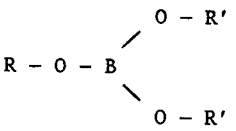

where R′ = *n*-alkyl.

Plots for both the alcohol and acid esters of the cyclic alkylboronates are shown in Fig. 4a and b, and similar plots of the acyclic esters are shown in Fig. 5, the data

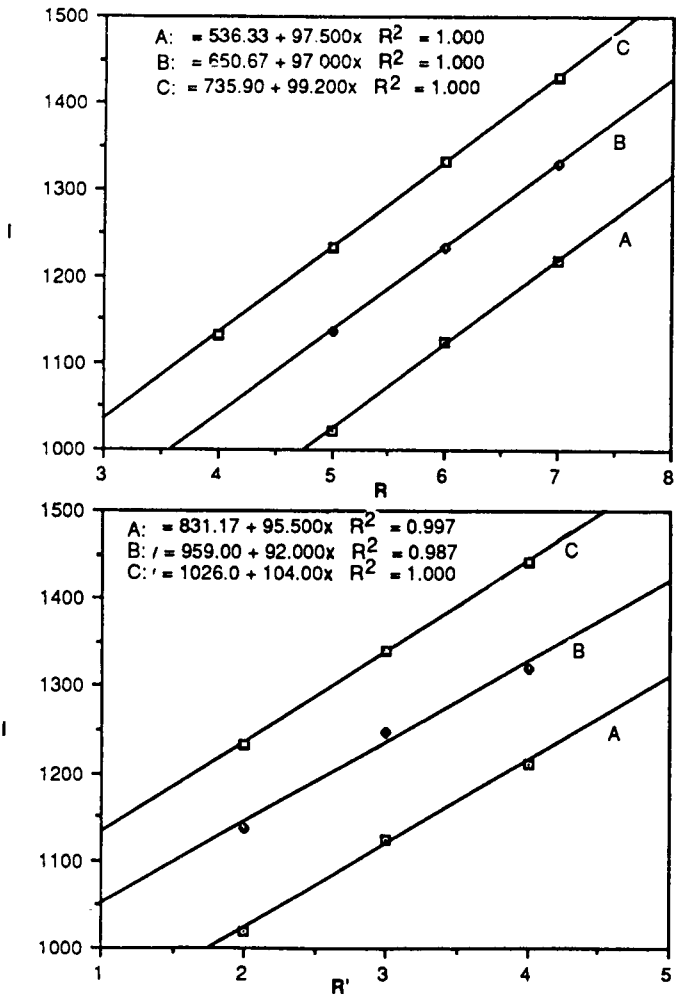

Fig. 4. Retention plots for cyclic alkylboronates: (A) alcohol ester series; (B) acid ester series. □ = OV-1; ● = OV-17; ■ = OV-225.

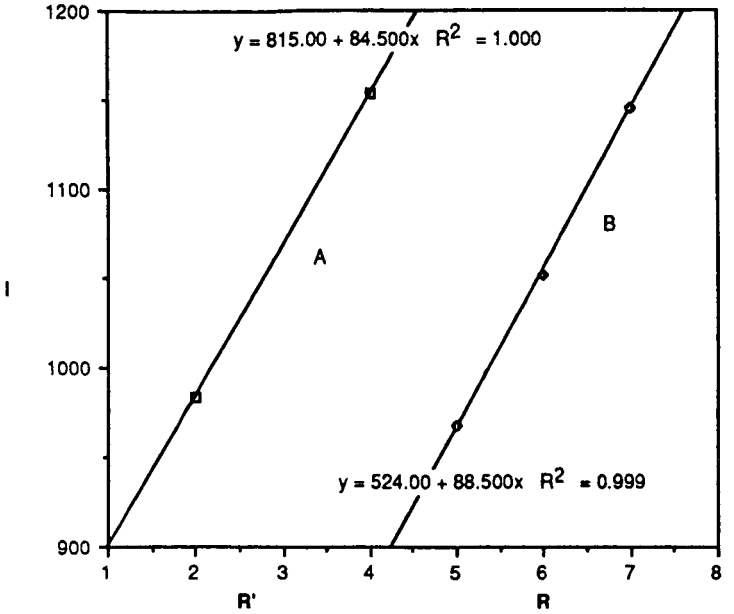

Fig. 5. Retention plots for acyclic alkylboronates: (A) acid and (B) alcohol ester series. □ and ● both OV-1.

being obtained at 70°C in all instances. Equations for the respective data on the various stationary phases are shown, and the linearity is indicated by the correlation coefficients.

The retention times and retention indices at 50°C are shown in Table III. With temperature-programmed operation the retention times are 12, 72 and 316 s for triethyl, tri-*n*-propyl and tri-*n*-butyl borate, respectively. The alkyl borates were found to be extremely sensitive to moisture, which explains the lack of GC reports in the literature. At 50°C, it was possible to achieve GC–MS elution of only two esters, *viz.*, triethyl and tri-*n*-propyl borate. Therefore, it is impossible to draw conclusions regarding the linearity or non-linearity of the data.

The retention index increments, *i.e.*, $\Delta CH_2R'$, per methylene unit in the *n*-alkyl borate ester were 54 index units, as shown in Table III. In a similar study of alkyl phosphate, Crank and Haken [10] reported about 94 retention index units on OV-17. These significant differences in retention index increments seem to be due to the borate esters being more polar than the phosphate esters. The borate esters, being more polar, will be retained less relative to the phosphate on OV-17 as the stationary phase.

The greater polarity of the alkyl borates appears to be due to its coplanar structure with sp^2 bond hybridization and ability of the empty orbital to form a dative bond by accepting the lone pairs of electrons in the OR group. This will have the effect of making the whole molecule more polar owing to the formation of three resonance structures. On the other hand, the phosphoryl group of the phosphates was reported [10] to be less polar owing to the effects of the d electrons in the phosphorus, which tend to neutralize the electron-withdrawing effect of the =O atom.

REFERENCES

1 J. R. Ashes and J. K. Haken, *J. Chromatogr.*, 60 (1971) 33.
2 J. R. Ashes and J. K. Haken, *J. Chromatogr.*, 101 (1974) 103.
3 J. R. Ashes and J. K. Haken, *J. Chromatogr.*, 62 (1971) 39.
4 J. R. Ashes and J. K. Haken, *J. Chromatogr.*, 111 (1975) 171.
5 J. K. Haken. D. K. M. Ho and M. S. Wainwright, *J. Chromatogr.*, 106 (1975) 327.
6 J. K. Haken, D. K. M. Ho and C. E. Vaughan, *J. Chromatogr.*, 106 (1975) 317.
7 J. K. Haken and I. O. O. Korhonen, *J. Chromatogr.*, 298 (1984) 89.
8 J. K. Haken and I. O. O. Korhonen, *J. Chromatogr.*, 357 (1986) 253.
9 J. K. Haken, H. N. T. Hartley and D. Srisukh, *Chromatographia*, 17 (1983) 589.
10 G. Crank and J. K. Haken, *J. Chromatogr.*, 245 (1982) 346.
11 F. S. Calisto and A. G. Raso, *Chromatographia*, 14 (1981) 143.
12 J. K. Haken, *J. Chromatogr.*, 235 (1982) 513.
13 H. Wada, S. Araki, K. Kuroda and C. Kato, *Polyhedron*, 4 (1985) 653.
14 W. Law and J. L. Margrave, *J. Chem. Phys.*, 25 (1956) 1086.
15 Y. Wada and R. W. Kiser, *J. Phys. Chem.*, 65 (1964) 1588.
16 P. J. Fallon, P. Kelly and J. C. Lockhart, *Int. J. Mass Spectrom. Ion Phys.*, 1 (1968) 133.
17 R. H. Cragg, J. F. J. Todd and A. T. Weston, *J. Chem. Soc., Dalton Trans.*, (1972) 1373.
18 H. P. Calhoun and C. R. Mason, *J. Chem. Soc., Dalton Trans.* (1980) 1282.
19 P. J. Fallon and J. C. Lockhart, *Int. J. Mass Spectrom. Ion Phys.*, 2 (1969) 247.
20 R. Heyes and J. C. Lockhart, *J. Chem. Soc. A*, (1968) 326.
21 C. J. W. Brooks and J. Watson, *J. Chem. Soc., Chem. Commun.*, (1967) 952.
22 C. J. W. Brooks and J. Watson, in C. L. A. Harbourn (Editor), *Gas Chromatography 1968: Proceedings of the Seventh International Symposium on Gas Chromatography*, Institute of Petroleum, London, 1969, p. 129.
23 G. M. Armstrong, C. J. W. Brooks, I. Maclean and I. Sangster, *J. Chromatogr. Sci.*, 7 (1969) 623.
24 C. J. W. Brooks and I. Maclean, *J. Chromatogr. Sci.*, 7 (1969) 623.
25 C. J. W. Brooks, B. S. Middleditch and G. M. Anthony, *Org. Mass Spectrom.*, 2 (1969) 1023.
26 C. J. W. Brooks and D. J. Harvey, *Biochem. J.*, 114 (1969) 15.
27 C. J. W. Brooks and D. J. Harvey, *J. Chromatogr.*, 54 (1971) 193.
28 C. J. W. Brooks, B. S. Middleditch and D. J. Harvey, *Org. Mass Spectrom.*, 5 (1971) 1429.
29 H. G. Kuivila, A. H. Keogh and E. J. Soboczenski, *J. Org. Chem.*, 19 (1954) 780.
30 J. M. Sugihara and C. M. Bowman, *J. Am. Chem. Soc.*, 80 (1958) 2443.
31 R. L. Letsinger and S. B. Hamilton, *J. Org. Chem.*, 25 (1966) 592.
32 R. Finch and J. C. Lockhart, *J. Chem. Soc.*, (1962) 3723.
33 R. L. Letsinger and S. B. Hamilton, *J. Am. Chem. Soc.*, 80 (1958) 5411.
34 E. Nyilas and A. H. Solway, *J. Am. Chem. Soc.*, 81 (1959) 2681.
35 M. Pailer and W. Fenze, *Monatsh. Chem.*, 92 (1961) 1294.
36 R. Hemming and D. G. Johnson, *J. Chem. Soc.*, (1964) 466.
37 C. F. Poole, S. Singhowangcha and A. Zlatkis, *J. Chromatogr.*, 11 (1978) 347.
38 C. F. Poole, S. Singhowangcha and A. Zlatkis, *J. Chromatogr.*, 158 (1978) 33.
39 C. F. Poole, S. Singhowangcha and A. Zlatkis, *Analyst (London)*, 104 (1979) 82.
40 C. F. Poole, *Chem. Ind. (London)*, (1976) 479.
41 W. Kosa, in R. W. Frei and J. P. Lawrence (Editors), *Chemical Derivatisation in Analytical Chemistry*, Vol. 1, Plenum Press, New York, 1981, p. 99.
42 C. F. Poole and A. Zlatkis, *J. Chromatogr.*, 184 (1980) 100.
43 C. A. Brown and S. Krishnamurthy, *J. Org. Chem.*, 43 (1978) 2731.
44 H. C. Brown, N. G. Bhat and V. Somayaji, *Organometallics*, 2 (1983) 1311.
45 F. Abrahams, *Thesis*, University of New South Wales, 1989.
46 C. J. W. Brooks, D. J. Harvey and B. S. Middleditch, *Org. Mass Spectrom.*, 3 (1970) 231.
47 H. C. Brown, R. S. Fletcher and R. B. Johnnesen, *J. Am. Chem. Soc.*, 73 (1951) 212.

Journal of Chromatography, 550 (1991) 171–179
Elsevier Science Publishers B.V., Amsterdam

CHROMSYMP. 2348

Gas chromatographic study of interaction between vinyl chloride and poly(vinyl chloride)

A. KOLIADIMA, P. AGATHONOS and G. KARAISKAKIS*
Department of Chemistry, University of Patras, GR-26110 Patras (Greece)

ABSTRACT

A reversed-flow gas chromatographic method for studying the interactions between vinyl chloride monomer (VCM) and poly(vinyl chloride) (PVC) is described. The method permits the calculation of the VCM diffusion coefficient in the gas phase and the determination of the partition coefficient of VCM between PVC and the carrier gas (nitrogen). From the variation of the partition coefficients with temperature, differential thermodynamic parameters (enthalpy and entropy) of adsorption of VCM on PVC were calculated. These are discussed in comparison with the same parameters as determined by inverse gas chromatography.

INTRODUCTION

Considerable attention has been drawn recently to the possible migration of vinyl chloride monomer (VCM) from plasticized poly(vinyl chloride) (PVC) into the contacting food phase in PVC containers, since many workers have already indicated that VCM is a carcinogenic agent [1–3]. Gilbert [4] reviewed the general topic of the migration of minor constituents from food packaging materials. Whereas at first PVC bottles were widely used as containers for beverages, including alcoholic drinks, it was soon discovered that the alcoholic drinks tasted differently, as a result of contamination by VCM. Further tests showed that VCM migrated into most foods, *e.g.*, edible oils, fats, honey.

The phenomenon of desorption or migration of VCM from PVC into a contacting phase can be considered to be a function of polymer–migrant interaction and diffusion [5]. The thermodynamics of the interaction will determine the equilibrium distribution of the migrant, while the diffusion will affect the rate of attainment of equilibrium. The "active site" hypothesis, which limits the potential migration of the monomer from the polymer into a food contacting phase, has been supported by many workers [6,7]. At very low monomer concentrations the monomer molecules are sorbed onto the most active sites. Inverse gas chromatography has also been used to determine the diffusion coefficient of VCM in PVC plasticized with dioctyl phthalate [8].

In this work reversed-flow gas chromatography, which has been used previously in the determination of various physico-chemical parameters [9], was used for the

0021-9673/91/$03.50

study of interactions between VCM and PVC. The method is based on reversing the direction of flow of the carrier gas at various time intervals. If the carrier gas contains other gases at concentrations recorded by the detector system, these flow reversals create perturbations on the chromatographic elution curve which form "extra peaks", such as those in Fig. 1.

If the concentration of a constituent in the flowing gas depends on a rate process taking place inside the chromatographic column, then, by reversing the flow, one performs a sampling of this process, for example the slow diffusion of the vapour of a liquid into the carrier gas. The equations necessary for the calculation of the rate coefficient of this slow process can be derived using suitable mathematical analysis [9]. Reversed-flow gas chromatography has been used to determine gas diffusion coefficients in binary and ternary mixtures [10–12], adsorption equilibrium constants [13], mass-transfer coefficients [14–19], activity coefficients [20,21] as well as solubility and interaction parameters [22]. An equation describing the height of the chromatographic sample peaks as a function of time was used to analyse the experimental data and calculate the values of the above coefficients. The physical separation of a rate or an equilibrium process under study from the chromatographic process itself is done keeping the former process to the diffusion column (section y in Fig. 2), while the latter occurs inside the sampling column. The flow reversals of the carrier gas at known

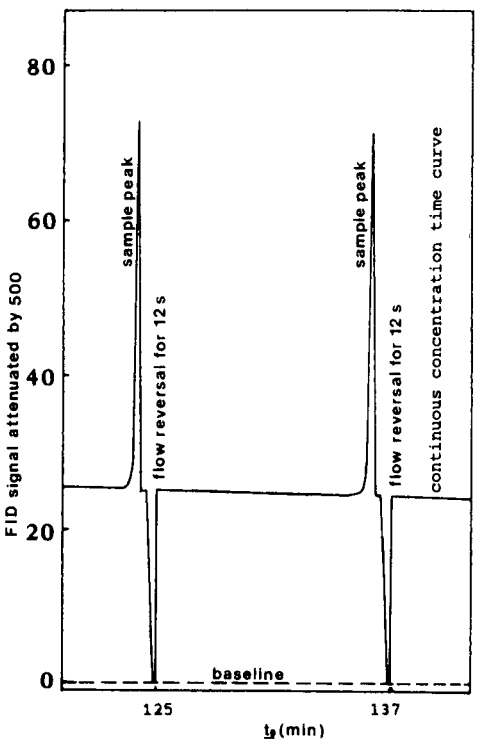

Fig. 1. Reversed-flow chromatogram showing two sample peaks for the adsorption of VCM on PVC from nitrogen at 314.2 K ($\dot{V}$ = 0.400 cm^3 s^{-1}). FID = Flame ionization detection.

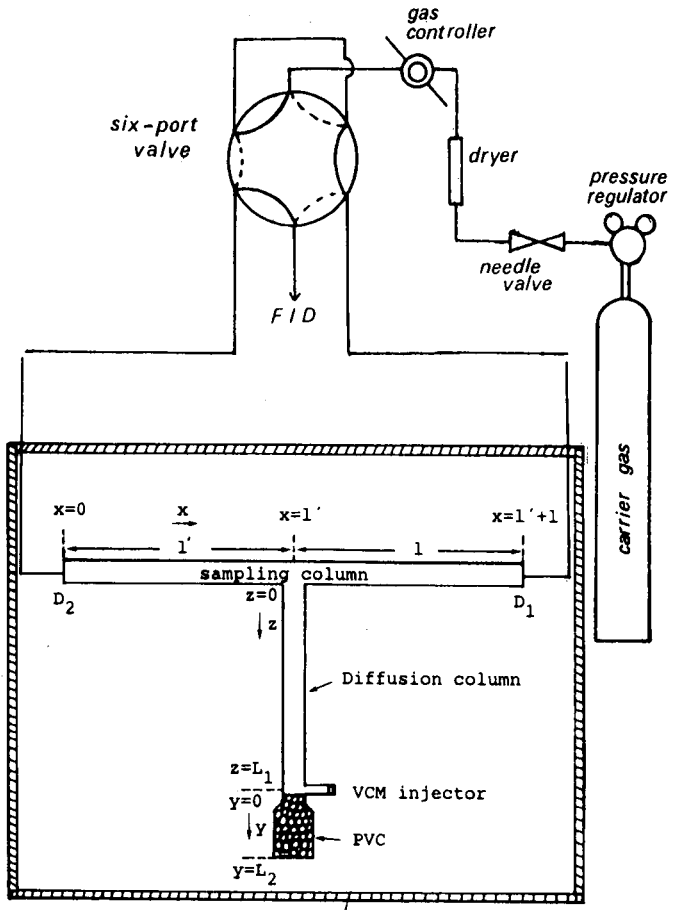

Fig. 2. Schematic representation of the reversed-flow gas chromatographic technique for studying the interactions between VCM and PVC.

times, t_0, during the experiment sample the concentration $c(l', t_0)$ of a solute vapour at the junction $x = l'$ in the form of sample peaks. The height, h, of these peaks above the ending baseline is

$$h \approx 2c(l', t_0) \tag{1}$$

The current of the carrier gas in the diffusion column is used as a carrier and the rate or equilibrium processes are superimposed on it. In this work, the diffusion band is distorted by the adsorption of VCM on PVC.

EXPERIMENTAL

Prior to use the PVC sample was essentially denuded of residual VCM by placing a limited amount of it into a wide-mouth container and placing the container under

ventilation in a hood. The PVC sample, which was treated in this manner for 2 weeks, had a molecular weight of 110 000 and was supplied by Polysciences. Vinyl chloride gas (99.99% pure) was supplied by Matheson Gas Products.

A conventional gas chromatograph (Pye Unicam Series 104) with a flame ionization detector accommodated a sampling column made from stainless-steel (4 mm I.D.) and a total length of 2 m, empty from any packing material, was connected with the diffusion column at the middle point. This column has two sections, z and y (Fig. 2). Section z (L_1) was 89 cm long (11.18 cm^3 volume) and of the same diameter as the sampling column, whilst section y (L_2) was shorter (4 cm) and with a larger diameter (18 mm I.D.). An injector between these two regions permits the introduction of a small gaseous volume (1 ml at atmospheric pressure) of solute (methane or VCM). The sampling and the diffusion columns form a "sampling cell" which must be connected to the carrier gas inlet and the detector in such a way that the direction of flow of the carrier gas (nitrogen of 99.99% purity from Linde) through the sampling column can be reversed at any time desired. This can be done using a four-port valve to connect the ends D_1 and D_2 of the sampling column to the carrier gas supply and the detector. To prevent the flame of the detector from being extinguished when the valve is turned from one position to the other, a restrictor is placed ahead of the detector.

The working temperature was in the range 29.8–52.3°C. The pressure drop along $l' + l$ was negligible and the pressure inside the whole cell was 1 atm. The carrier gas (nitrogen) flow-rate was 0.400 $cm^3\ s^{-1}$.

RESULTS AND DISCUSSION

If the diffusion column is empty and 1 ml of solute (VCM) is introduced through the injector of Fig. 2, while nitrogen flows through the sampling column $l' + l$, and fills the diffusion column, $L_1 + L_2$, a diffusion current into the carrier gas arises inside the latter column, creating a finite concentration of it at the junction $x = l'$. This is sampled as a function of time by reversing the direction of the carrier gas flow for a short interval, t', as previously described, thus giving rise to sample peaks. In curve 1 in Fig. 3 the height of the sample peaks is plotted as a function of time, t_0, of the flow reversal. This is called a "diffusion band" and is due to the longitudinal diffusion of the solute vapour into nitrogen along the diffusion column, $L_1 + L_2$. The mathematical equation describing a diffusion band as an analytical function of time has already been derived and is given by [18]

$$c(l', t_0) = \frac{\pi m D}{\dot{V} L_1^2 (1 + 1.801\ V_G'/V_G)} \cdot \exp\left(-\frac{\pi^2 D/4L_1^2}{1 + 1.801\ V_G'/V_G} \cdot t_0\right) \qquad (2)$$

where D is the diffusion coefficient of solute into the carrier gas (nitrogen), V_G and V_G' are the gaseous volumes in sections L_1 and L_2 of the diffusion column, respectively, m is the amount of solute injected and $\dot{V}$ is the volumetric flow-rate of the carrier gas in the sampling column. As the height, h, of the sample peaks is approximately equal to

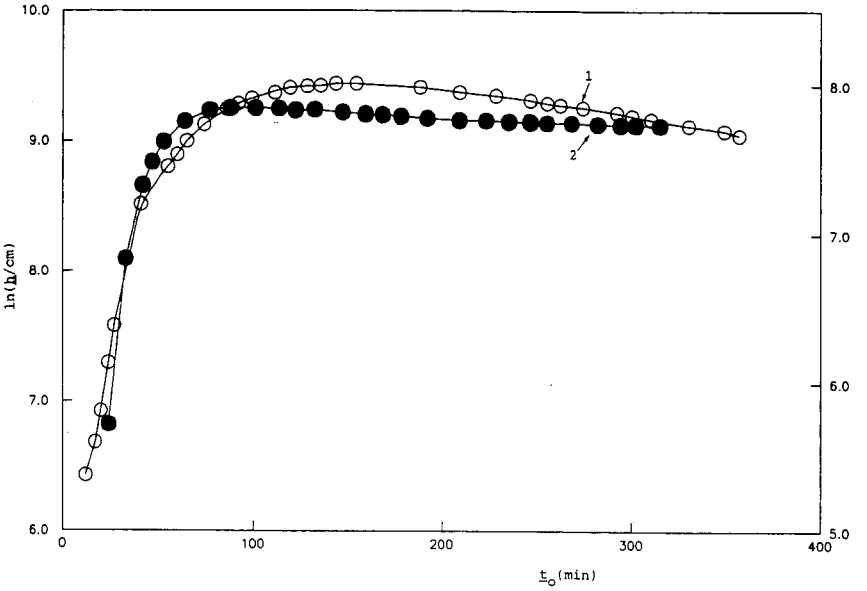

Fig. 3. Plots of ln h *vs.* t_0 for VCM and a vessel L_2, (○) empty or (●) filled with 2.94 g of PVC with molecular weight = 110 000. T = 314.2 K; $\dot{V}$ = 0.400 cm^3 s^{-1}.

$2c(l', t_0)$ according to eqn. 1, eqn. 2 describes the diffusion band (ln h *vs.* t_0) as a linear function with slope

$$b = -\frac{\pi^2 D/4L_1^2}{1 + 1.801\ V_G'/V_G} \tag{3}$$

This is valid only for the descending part of the plot after the maximum (*cf.*, Fig. 3). Knowing all the other quantities, D is easily determined from the slope of this straight line. Table I gives the experimental values of the diffusion coefficient, $D^{exp.}$, for VCM and methane into the carrier gas (nitrogen) at various temperatures. For comparison purposes Table I also gives the respective theoretical values of diffusion coefficient, $D^{theor.}$, as they were calculated from the equation of Fuller *et al.* [23]. The

TABLE I

EXPERIMENTAL DIFFUSION COEFFICIENTS, $D^{exp.}$, OF VCM VAPOUR AND METHANE, INTO THE CARRIER GAS (NITROGEN) AND THEORETICAL VALUES, $D^{theor.}$, AS CALCULATED FROM THE EQUATION OF FULLER *ET AL.* [23], AT VARIOUS TEMPERATURES

T (K)	VCM		CH_4	
	$D^{exp.}$ (cm^2 s^{-1})	$D^{theor.}$ (cm^2 s^{-1})	$D^{exp.}$ (cm^2 s^{-1})	$D^{theor.}$ (cm^2 s^{-1})
303.0	0.150	0.147	0.307	0.283
308.2	0.157	0.153	0.317	0.292
314.2	0.149	0.158	0.322	0.302
318.2	0.181	0.161	0.336	0.308
325.5	0.191	0.168	0.351	0.321

TABLE II

APPARENT DIFFUSION COEFFICIENT, $D^{app.}$, OF VCM VAPOUR AND METHANE INTO NITROGEN, IN THE PRESENCE OF PVC, AT VARIOUS TEMPERATURES

T (K)	$D^{app.}_{VCM}$ (cm^2 s^{-1})	$D^{app.}_{CH_4}$ (cm^2 s^{-1})
298.2	0.103	–
308.2	0.177	0.313
314.2	0.157	0.322
318.2	0.145	0.334
325.5	0.065	0.351

experimentally determined diffusion coefficients are in most instances very close to those calculated theoretically, and increase with increasing temperature, as the theory predicts.

If we now repeat the same experiments, but with the lower part L_2 of the diffusion column filled with solid particles of PVC (2.94 g), and we assume that the solute (VCM and methane) is not adsorbed on the solid PVC, then the descending part of the diffusion band is again described by eqn. 2, the only difference being that V'_G is now the gaseous volume of the void space in L_2, filled with the solid PVC. An example is given by curve 2 in Fig. 3. Therefore, knowing again all the other quantities in eqn. 3, one can determine the apparent diffusion coefficients, $D^{app.}$, of VCM and methane into nitrogen (*cf.*, Table II). Table II shows that, whereas the apparent diffusion coefficients of methane into nitrogen are almost identical with the true values, $D^{exp.}$, given in Table I, the apparent diffusion coefficients of VCM into nitrogen deviate significantly from the true values and, except for the $D^{app.}$ value at 298.2 K, decrease with increasing temperature, contrary to theory. This is probably due to the fact that, whereas methane is not adsorbed on the PVC particles, as is well known, VCM is adsorbed on the same particles, making possible the determination of the partition ratio, k, of the solute (VCM) between the two phases (solid and gaseous) from the relationship [24]

$$c(l', t_0) = \frac{\pi m D}{\dot{V} L_1^2 (1 + 1.801\ V'_G/V_G)} \cdot \exp\left[- \frac{\pi^2 D/4L_1^2}{1 + 1.801\ (1 + k)\ V'_G/V_G} \cdot t_0 \right] \quad (4)$$

TABLE III

PARTITION RATIOS, k, PARTITION COEFFICIENTS, K, AND ENTHALPY AND ENTROPY OF ADSORPTION OF VCM ON PVC FROM NITROGEN

T (K)	k	K	ΔH^0 (kJ mol^{-1})	ΔS^0 (J K^{-1} mol^{-1})
298.2	1.55	1.83		
314.2	0.95	1.12	-26.1 ± 0.4[a]	-148 ± 1[a]
318.2	0.85	1.01		

[a] These values are independent of temperature; derived from eqn. 8.

Eqn. 4 shows that the slope of the plot of ln h *vs.* t_0 for the VCM, in the presence of PVC particles in vessel L_2, is not that given by eqn. 3, but is equals to

$$b' = -\frac{\pi^2 D/4L_1^2}{1 + 1.801\ (1 + k)\ V'_G/V_G} \tag{5}$$

The partition ratios, k, for the adsorption of VCM on PVC from nitrogen at three temperatures, as they were determined from eqn. 5, are given in Table III. Table III also gives the partition coefficients, K, as determined from th relationship

$$K = \frac{k\varepsilon}{1 - \varepsilon} \tag{6}$$

where ε is the external porosity (void fraction) of the PVC solid bed, which can be found from [24]

$$\varepsilon = \frac{b}{b'} + \frac{b/b' - 1}{1.801} \cdot \frac{V_G}{V'_G} \tag{7}$$

where V'_G is the gaseous volume of the empty vessel L_2.

From the variation of the partition coefficients with temperature, the differential enthalpy, ΔH^0, and entropy, ΔS^0, of adsorption can be determined via the equation [13]

$$\ln (K/T) = \ln R + \frac{\Delta S^0}{R} - \frac{\Delta H^0}{R} \cdot \frac{1}{T} \tag{8}$$

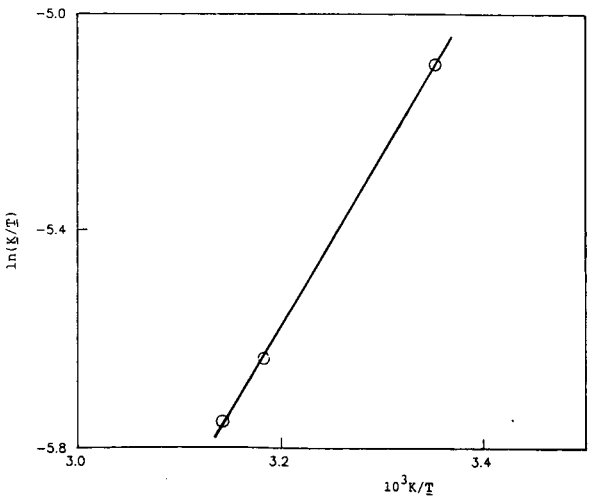

Fig. 4. Plot of ln (K/T) *vs.* $1/T$ for the adsorption of VCM on PVC.

Table III lists the enthalpies and entropies of adsorption determined by this method, and Fig. 4 gives an example of plotting the experimental results according to eqn. 8. It must be pointed out that the ΔS^0 value is a relative one, as it depends on the selected standard state for the adsorbed solute. The ΔS^0 value is negative, indicating that the polymer–monomer interaction leads to a more ordered system (binding of monomer molecules on active sites). ΔH^0 is also negative and is a measure of the exothermic nature of the interaction.

The values of ΔH^0 and ΔS^0 found in this work by the reversed-flow gas chromatographic technique are very close to those determined by other workers [6,25] using inverse gas chromatography ($-55.6 < \Delta H^0 < -29.8$ kJ mol^{-1}; $-164.9 < \Delta S^0 < -71.5$ J K^{-1} mol^{-1}).

For the experimental verification of eqns. 2 and 4, experiments were performed with a second vessel L_2, having a different volume, and thus containing a different amount (4.91 g) of PVC from that used previously. The experimental data for the diffusion coefficients and partition ratios in both cases are almost identical.

If the equilibrium state of the interaction between VCM and solid PVC is established slowly, there is a finite value for the overall mass-transfer coefficient of VCM between the gas and solid phases, and the diffusion band is no longer linear after the maximum, but distorted, as shown in Fig. 3 in ref. 18. In all of our experiments the plots of ln h *vs.* t_0 are linear (after the maximum), indicating that the monomer is either reversibly sorbed onto the polymer's "active sites" or reversibly distributed in the polymer entanglements or random coils, thus limiting the potential migration of the monomer from the polymer into a food contacting phase. Further, the thermodynamic data provide additional support for the second hypothesis, as the heat and entropy of adsorption found correspond approximately to an isosteric region of zero coverage, because the total amount of solute injected into the system was of the order of 10^{-5} mol.

It is concluded that reversed-flow gas chromatography can be used successfully for the study of interaction between VCM and PVC with obvious advantages over inverse gas chromatography, owing to the fact that the former method is a pulse technique under steady-state conditions.

ACKNOWLEDGEMENT

We are grateful to Mrs. M. Barkoula for her assistance.

REFERENCES

1 C. Maltoni, *Chem. Eng. News*, 7 (1980) 27.
2 R. M. Schaffner and P. Lombardo, *J. Assoc. Off. Anal. Chem.*, 58 (1975) 1211.
3 C. Maltoni, *Chem. Eng. News*, 25 (1974) 16.
4 S. G. Gilbert, *J. Food Sci.*, 41 (1976) 955.
5 J. R. Morano, J. R. Giacin and S. G. Gilbert, *J. Food Sci.*, 42 (1977) 230.
6 P. Demertzis, M. G. Kontominas and E. K. Voudouris, *J. Food Technol.*, 20 (1985) 419.
7 M. G. Kontominas, J. Miltz and S. G. Gilbert, *J. Food Sci.*, 47 (1982) 1208.
8 A. Y. Lazaris, T. A. Kalmykova and E. I. Konstantinova, *Vysokomol. Soedin., Ser. B*, 30 (1988) 730.
9 N. A. Katsanos and G. Karaiskakis, *Adv. Chromatogr.*, 24 (1984) 125.
10 N. A. Katsanos and G. Karaiskakis, *J. Chromatogr.*, 237 (1982) 1.
11 N. A. Katsanos and G. Karaiskakis, *J. Chromatogr.*, 254 (1983) 15.

12 G. Karaiskakis, N. A. Katsanos and A. Niotis, *Chromatographia*, 17 (1983) 30.
13 G. Karaiskakis, N. A. Katsanos and A. Niotis, *J. Chromatogr.*, 235 (1982) 21.
14 G. Karaiskakis and N. A. Katsanos, *J. Phys. Chem.*, 88 (1984) 3674.
15 E. Dalas, G. Karaiskakis, N. A. Katsanos and A. Gounaris, *J. Chromatogr.*, 348 (1985) 339.
16 G. Karaiskakis, P. Agathonos, A. Niotis and N. A. Katsanos, *J. Chromatogr.*, 364 (1986) 79.
17 N. A. Katsanos and E. Dalas, *J. Phys. Chem.*, 91 (1987) 3103.
18 N. A. Katsanos, P. Agathonos and A. Niotis, *J. Phys. Chem.*, 92 (1988) 1645.
19 P. Agathonos and G. Karaiskakis, *J. Chem. Soc., Faraday Trans. I*, 85 (1989) 1357.
20 N. A. Katsanos, G. Karaiskakis and P. Agathonos, *J. Chromatogr.*, 349 (1986) 369.
21 P. Agathonos and G. Karaiskakis, *J. Appl. Polym. Sci.*, 37 (1989) 2237.
22 A. Koliadima, P. Agathonos and G. Karaiskakis, *Chromatographia*, 26 (1988) 29.
23 E. N. Fuller, P. D. Schettler and J. C. Giddings, *Ind. Eng. Chem.*, 58 (1966) 19.
24 N. A. Katsanos, *J. Chromatogr.*, 446 (1988) 39.
25 P. Demertzis and M. G. Kontominas, *Lebensm.-Wiss. Technol.*, 19 (1986) 1.

Journal of Chromatography, 550 (1991) 181–192
Elsevier Science Publishers B.V., Amsterdam

CHROMSYMP. 2228

Homogeneous catalysis studied by reversed-flow gas chromatography

B. V. STOLYAROV
Chemistry Department, Leningrad State University, 198904 Leningrad (USSR)
and
N. A. KATSANOS*, P. AGATHONOS and J. KAPOLOS
Physical Chemistry Laboratory, University of Patras, 261 10 Patras (Greece)

ABSTRACT

The reversed-flow gas chromatography technique was used to study the kinetics of dehydration of 2-butanol in phosphoric acid solution. A combination of the mathematical analysis developed in heterogeneous catalysis, mass transfer across gas–liquid boundaries, and diffusion of gases in liquids was employed to find the relevant equations pertaining to the present problem of homogeneous catalysis in a liquid phase. The equation describing the diffusion band of the reaction product(s) was derived for both a stirred solution and a quiescent one. These equations were then used to analyze the experimental data, from which the rate constants for the first-order reaction and for transporting the products away from the solution were determined. From the latter rate constant, the overall mass transfer coefficient of butenes in the liquid phase was found. This increases with temperature, showing that mass transfer across the gas–liquid boundary is activated, with an activation energy of 60.9 kJ mol^{-1}. The diffusion coefficient of butenes in the reaction mixture, and their partition coefficient between the gas and the liquid phase, were also determined. The activation energy of the first-order reaction was found to be equal to 34.1 kJ mol^{-1}.

INTRODUCTION

The application of the reversed-flow gas chromatography (RF-GC) technique to heterogeneous catalysis is described in detail in a recently published book [1] and some newer publications [2–6]. The same technique has been used to study mass transfer of gases across gas–liquid boundaries [7] and diffusion of gases in liquids [8], both combined with partition coefficient determination in the gas–liquid interfaces. A combination of the mathematical analysis developed in the above three cases, namely catalysis, mass transfer, and diffusion in liquids, can be employed for finding the relevant equations pertaining to homogeneous catalysis in a liquid phase. This is the subject of the present work using as a probe reaction the dehydration of 2-butanol to butenes in phosphoric acid solution. The experimental arrangement was the same as that previously reported [7,8]. It is repeated schematically in Fig. 1 for the purposes of the theoretical analysis.

0021-9673/91/$03.50

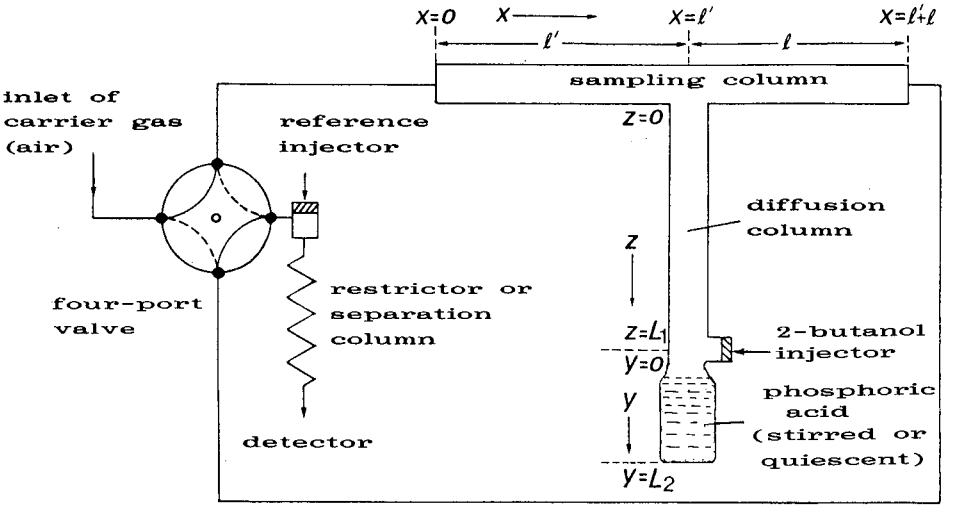

Fig. 1. Schematic representation of columns and gas connections in the reversed-flow gas chromatography technique.

THEORETICAL

The equation giving the diffusion band (plot of the logarithm of the sample peak height, ln h, *vs.* time of flow reversal, t_0) when a chemical reaction takes place inside vessel y will be derived for two cases: a stirred solution and a quiescent one.

Stirred solution

In gaseous region z the diffusion equation of a reaction product is:

$$\partial c_z/\partial t_0 = D_G \partial^2 c_z/\partial z^2 \tag{1}$$

where $c_z = c_z(z, t_0)$, and D_G is the diffusion coefficient of that product into the gaseous phase filling column z (see Fig. 1). The initial condition is $c_z(z,0) = 0$, and the boundary conditions at the junction of the sampling and the diffusion columns, *i.e.* at $x = l'$ and $z = 0$, are given by the relations:

$$c_z(0, t_0) = c(l', t_0)$$

$$D_G(\partial c_z/\partial z)_{z=0} = vc(l', t_0) \tag{2}$$

where $c(l', t_0)$ is the concentration of the solute (product) in the sampling column and v is the linear velocity of the carrier gas in that same column.

The solution of eqn. 1, subject to the boundary conditions (eqn. 2), is obtained in an analogous way as before [7,8] (the initial condition is now different), the result, in the form of Laplace transform with respect to time, being:

$$C_z = C(l', p_0)\cosh q_1 z + (v/D_G q_1)\, C(l', p_0)\sinh q_1 z \tag{3}$$

where:

$$q_1^2 = p_0/D_G \tag{4}$$

with p_0 denoting the time transform parameter. The capital letters C_z and C represent the t_0 Laplace-transformed functions c_z and c, respectively.

Going now to the other boundary of the diffusion column at $z = L_1$ and $y = 0$, the condition in this boundary is:

$$D_G a_G (\partial c_z/\partial z)_{z=L_1} = K_L a_L (c_L - c_L^*) \tag{5}$$

where a_G is the cross-sectional area in the columns z and x, a_L the free surface area of the liquid, c_L the concentration of the solute in the bulk liquid phase, c_L^* the solute concentration in a fictitious liquid in equilibrium with the real bulk gas phase, and K_L the overall mass transfer coefficient of the solute in the liquid.

The rate of change of the dissolved product is given by the relation:

$$\frac{\partial c_L}{\partial t_0} = r - \frac{K_L a_L}{V_L}(c_L - c_L^*) \tag{6}$$

where r is the rate of its formation by the chemical reaction in the liquid phase and V_L the volume of the liquid.

If one takes the t_0 Laplace transforms of all terms of eqns. 5 and 6, with initial condition $c_L(0) = 0$ (*i.e.* no solute dissolved in the liquid initially), and then combines the transformed equations to eliminate C_L, there results:

$$D_G\left(\frac{dC_z}{dz}\right)_{z=L_1} = \frac{K_L a_L}{a_G} \cdot \frac{R}{p_0 + k_{-1}} - \frac{K_G a_L}{a_G} \cdot \frac{p_0 C_z(L_1)}{p_0 + k_{-1}} \tag{7}$$

where R is the t_0-transformed reaction rate r, k_{-1} is given by the relation

$$k_{-1} = K_L a_L / V_L \tag{8}$$

and K_G is the overall mass transfer coefficient of the solute in the gas phase, related to the partition coefficient K of the solute between the two phases by the equation

$$K = c_L^*/c_z(L_1) = K_G/K_L \tag{9}$$

according to the two-film theory previously employed [7].

Finally, eqn. 3 is used to calculate both $(dC_z/dz)_{z=L_1}$ and $C_z(L_1)$ of eqn. 7, with the result, after rearrangement:

$$C(l', p_0) = \frac{K_L a_L}{D_G q_1 a_G} \cdot \frac{R}{p_0 + k_{-1}} \left[\sinh q_1 L_1 + \frac{v}{D_G q_1} \cosh q_1 L_1 + \right.$$

$$\left. + \frac{K_G a_L}{D_G q_1 a_G} \cdot \frac{p_0}{p_0 + k_{-1}} \left(\cosh q_1 L_1 + \frac{v}{D_G q_1} \sinh q_1 L_1\right) \right]^{-1} \tag{10}$$

To facilitate the inversion of this equation, we employ the same approximations as before [7,8], *viz.* omission of $\sinh q_1L_1$ compared with $(v/D_Gq_1)\cosh q_1L_1$, and also omission of $\cosh q_1L_1$ compared with $(v/D_Gq_1)\sinh q_1L_1$. Then, eqn. 10 becomes:

$$C(l', p_0) = \frac{K_L a_L}{\dot{V}} \cdot \frac{R}{p_0 + k_{-1}} \left(\cosh q_1 L_1 + \frac{K_G a_L}{D_G q_1 a_G} \cdot \frac{p_0}{p_0 + k_{-1}} \sinh q_1 L_1 \right)^{-1} \quad (11)$$

where $\dot{V} = a_G v$ is the volumetric flow-rate of the carrier gas.

A further simplification of eqn. 11 is based on the approximations:

$$\cosh q_1 L_1 \approx 1 \quad \text{and} \quad \sinh q_1 L_1 \approx q_1 L_1$$

provided L_1 is small enough. Substituting these into eqn. 11, one obtains

$$C(l', p_0) = \frac{K_L a_L R}{\dot{V}(1 + K_G L_1 a_L / D_G a_G)} \left(p_0 + \frac{k_{-1}}{1 + K_G L_1 a_L / D_G a_G} \right)^{-1} \quad (12)$$

Finally, the inversion of this transformed function depends on the form of the rate equation describing the formation of the product(s). In the simplest case of a first-order reaction, the rate equation is $r = k_2 c_R$, where c_R is the concentration of the reactant in solution and k_2 is the rate constant of the reaction. The integrated rate equation is the well-known expression:

$$r = k_2 c_R = k_2 c_0 \exp(-k_2 t_0) \quad (13)$$

c_0 denoting the initial reactant concentration. The Laplace transform of this is

$$R = \frac{k_2 c_0}{p_0 + k_2} \quad (14)$$

and the substitution of the right-hand side for R in eqn. 12 gives

$$C(l', p_0) = N_3[(p_0 + k_2)(p_0 + k_3)]^{-1} \quad (15)$$

where

$$N_3 = \frac{K_L a_L k_2 c_0}{\dot{V}(1 + K_G L_1 a_L / D_G a_G)} \quad (16)$$

and

$$k_3 = \frac{k_{-1}}{1 + K_G L_1 a_L / D_G a_G} \quad (17)$$

Taking now the inverse Laplace transform with respect to p_0 of eqn. 15, one finds the function describing the height h of the sample peaks:

$$h = 2c(l', t_0) = \frac{2N_3}{k_3 - k_2}[\exp(-k_2 t_0) - \exp(-k_3 t_0)] \tag{18}$$

This equation describes a diffusion band which depends on the competition of two phenomena: a chemical reaction forming the solute under investigation with a rate constant k_2 and its expulsion from the solution with a rate constant k_3 (*cf.* eqn. 17) depending on a_G and a_L, on K_G, D_G and K_L (*cf.* also eqn. 8), and on L_1 and V_L. By changing the length of the diffusion column L_1 and/or the volume of the liquid V_L, we can change the value of k_3, and in favorable cases decide which of the two phenomena above becomes rate-controlling.

Quiescent solution

In this case the diffusion of the product from the bulk liquid phase to the surface of the liquid must be taken into account. In the liquid region y (see Fig. 1) the diffusion equation reads:

$$\partial c_y/\partial t_0 = D_L \partial^2 c_y/\partial y^2 + r \tag{19}$$

which is similar to eqn. 7 of ref. 8, differing only in the term r due to the chemical reaction. This equation is solved in exactly the same way as before [8], the result being:

$$C_y'(0) = \left[\frac{R}{D_L q_2} - C_y(0) q_2\right] \tanh q_2 L_2 \tag{20}$$

where $C_y'(0) = (\mathrm{d}C_y/\mathrm{d}y)_{y=0}$, $C_y(0)$ is the value of the transformed function C_y at $y = 0$, D_L is the diffusion coefficient of the product in the liquid phase, and q_2 is given by a relation analogous to eqn. 4:

$$q_2^2 = p_0/D_L \tag{21}$$

Now, eqn. 20 holding in region y is linked with eqn. 3 valid in region z, using the boundary conditions at $z = L_1$ and $y = 0$:

$$K = C_y(0)/C_z(L_1) \tag{22}$$

$$a_G D_G (\partial C_z/\partial z)_{z=L_1} = a_L D_L (\partial C_y/\partial y)_{y=0} \tag{23}$$

where the equilibrium 22 is assumed to be rapidly established. Calculation of $C_z(L_1)$ and $(\partial C_z/\partial z)_{z=L_1}$ from eqn. 3 and substitution into eqns. 22 and 23, using also eqn. 20, gives:

$$C(l', p_0) = \frac{a_L R \tanh q_2 L_2}{a_G D_G q_1 q_2}\left[\sinh q_1 L_1 + \frac{v}{D_G q_1}\cosh q_1 L_1 + \right.$$

$$\left. + K\frac{a_L D_L q_2}{a_G D_G q_1}\tanh q_2 L_2\left(\cosh q_1 L_1 + \frac{v}{D_G q_1}\sinh q_1 L_1\right)\right]^{-1} \tag{24}$$

This is similar to eqn. 15 of ref. 8.

Using the same approximations as in the case of the stirred solution applied to eqn. 10, and in addition the approximation employed earlier for diffusion in liquids [8], *viz.*:

$$\frac{\coth q_2 L_2}{D_L q_2} \approx \frac{1}{L_2}\left(\frac{1}{p_0} + \frac{\pi^2}{3\beta}\right) \tag{25}$$

where:

$$\beta = \pi^2 D_L / L_2^2 \tag{26}$$

we obtain from eqn. 24 the simpler expression:

$$C(l', p_0) = \frac{a_L R}{\dot{V}(L_2/3D_L + KL_1 a_L/D_G a_G)}\left[p_0 + \frac{1}{L_2(L_2/3D_L + KL_1 a_L/D_G a_G)}\right]^{-1} \tag{27}$$

As before, the inversion of this transformed function depends on the form of the rate equation for the formation of the product(s). If this is $r = k_2 c_R$, *i.e.* a simple first-order reaction, the integrated rate equation is eqn. 13, and its Laplace transform eqn. 14. When the latter is substituted for R in eqn. 27, it gives:

$$C(l', p_0) = N_4[(p_0 + k_2)(p_0 + k_4)]^{-1} \tag{28}$$

where:

$$N_4 = \frac{a_L k_2 c_0}{\dot{V}(L_2/3D_L + KL_1 a_L/D_G a_G)} \tag{29}$$

and:

$$k_4 = \frac{1}{L_2(L_2/3D_L + KL_1 a_L/D_G a_G)} \tag{30}$$

Eqns. 28, 29 and 30 are analogous to eqns. 15, 16 and 17, respectively, applied to a stirred solution. Taking now the inverse Laplace transform with respect to p_0 of eqn. 28, the function is obtained describing the diffusion band from a quiescent solution in which a first-order reaction takes place:

$$h = 2c(l', t_0) = \frac{2N_4}{k_4 - k_2}[\exp(-k_2 t_0) - \exp(-k_4 t_0)] \tag{31}$$

This has exactly the same form as eqn. 18 for a stirred solution. The diffusion band depends again on two phenomena: a chemical reaction with a rate constant k_2 and the transport of the product(s) away from the solution, described by the rate coefficient k_4, depending on the same parameters as k_3 (see eqn. 17) except for the replacement of K_L

by $3D_L/L_2$. This is easily seen by substituting eqn. 8 for k_{-1} in eqn. 17 and dividing both terms of the fraction by $K_L a_L/V_L = K_L a_L/a_L L_2 = K_L/L_2$. The result (taking also into account eqn. 9) is:

$$k_3 = \frac{1}{L_2(1/K_L + KL_1 a_L/D_G a_G)} \tag{32}$$

Division of both terms of eqn. 16 by K_L gives:

$$N_3 = \frac{a_L k_2 c_0}{\dot{V}(1/K_L + KL_1 a_L/D_G a_G)} \tag{33}$$

A comparison of eqns. 32 and 33 with 30 and 29, respectively, indicates that stirring of the solution results in an overall mass transfer coefficient K_L equivalent to a diffusion through a liquid layer of thickness $L_2/3$, *i.e.* one-third of the total liquid height.

Summarizing the theoretical predictions, one concludes that the diffusion band must depend on three rate processes: a chemical reaction, the diffusion in the liquid, and the diffusion in the gas phase. The last-mentioned effect can be minimized by using a gas diffusion length L_1 that is as short as possible. Then, the rate constants k_3 and k_4 depend only on liquid diffusion. It is easy to distinguish whether a slope extracted from the diffusion band is $-k_2$ or $-k_3$ and $-k_4$, by increasing the height of the liquid layer L_2. If this causes a decrease in the slope, it is $-k_3$ and $-k_4$ which is measured. If, on the other hand, the slope remains unaffected by L_2, it is equal to $-k_2$.

In conclusion, various possibilities arise when the RF-GC technique is applied to homogeneous catalysis in a liquid phase, either stirred or quiescent, with or without a diffusion column. Some of these possibilities are demonstrated in the Results and discussion section.

EXPERIMENTAL

Materials

2-Butanol was obtained from BDH, and orthophosphoric acid was an 85% RPE-ACS product of Carlo Erba.

The carrier gas was nitrogen of 99.99% purity from Linde (Athens, Greece).

Apparatus

The experimental set-up is outlined in Fig. 1. The sections l, l' and L_1 of the sampling cell were $^1/_4$-in. stainless-steel tubes with lengths $l = l' = 50$ cm and $L_1 = 35$–50 cm. The reacting liquid consisted of 0.25–1.5 cm^3 of phosphoric acid, into which 0.5–15 μl of 2-butanol were dissolved. The liquid was placed in a glass vessel of 17.5 mm I.D. at its lower part and of 4 mm I.D. at its upper part, which was connected to the stainless-steel column L_1 with a 1/4-in. Swagelok union. The gaseous volume between the liquid's surface and column z was 1.67–5.80 cm^3, while the height of the liquid phase L_2 was 0.41–0.85 cm.

An additional separation column for butenes at 48–87°C was used, and this was a 2.4 m × 1/8 in. Chromosil 310 column purchased from Supelco SA. The pressure drop along this column was 44 cmHg, while that along column $l' + l$ was negligible (less than 1 mmHg).

Procedure

After placing the solution of 2-butanol in phosphoric acid in its position (see Fig. 1) and waiting for the steadily rising concentration–time curve to appear in the detector signal, the chromatographic sampling procedure was started by reversing the direction of the carrier gas flow for 6–10 s, which is a shorter time period than the gas hold-up time in both column sections l and l'. Examples of sample peaks created by the flow reversals have been given many times elsewhere [1,2,4–8].

With the additional separation column in place, two or three sample peaks were obtained after each flow reversal, whereas a single sample peak appeared without the separation column. In all cases the sample peaks were due to product butenes. No peak of 2-butanol was detected owing to its low vapour pressure at the working temperatures.

In each experimental run a long series of sample peaks was obtained. By then plotting the logarithm of the height of the peaks *vs.* the time of the respective flow reversals, the diffusion band for each run was constructed. The appearence of these bands was similar to those previously published [1,4–9].

RESULTS AND DISCUSSION

A typical diffusion band obtained in the present work is shown in Fig. 2. All bands had the same shape, as predicted by both eqn. 18 applied to a stirred solution and eqn. 31 pertaining to a quiescent liquid. From each diffusion band the two exponential coefficients k_2 and k_3 (or k_4) can be determined by means of a suitable computer program or, if these two coefficients are sufficiently different, by applying a method similar to that described elsewhere [7], *viz.* by finding first the slope $-b_1$ and the intercept $\ln h_0$ of the descending linear part of the $\ln h$ *vs.* t_0 plot (after

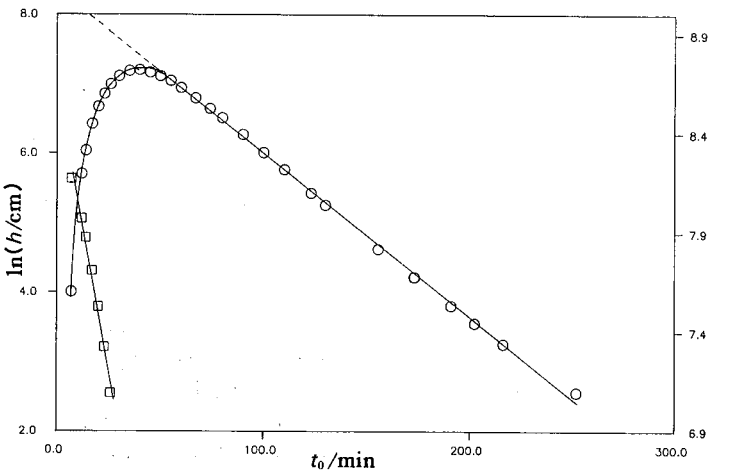

Fig. 2. A diffusion band obtained with a quiescent solution of 0.5 μl 2-butanol in 0.25 cm^3 of 85% phosphoric acid, at 408.2 K. A diffusion column L_1 of 35 cm was used and the experimental points (○) represent a mixture of all butenes (left ordinate). Points □ (right ordinate) were obtained by subtracting the experimental points before the maximum from the extrapolated (dashed line) linear descending part of the band.

the maximum), and then replotting the initial data (before the maximum) as $\ln[h_0 \exp(-b_1 t_0) - h]$ *vs.* t_0. An example is given in Fig. 2. The slope $-b_2$ of the new straight line thus obtained refers to the ascending part of the diffusion band. In experiments without a diffusion column L_1 (see Fig. 1), it was difficult to determine the slope $-b_2$ because the ascending part was very fast. When an additional separation column was employed (see Experimental section and Fig. 1) various isomeric butenes were recorded, each giving separate sample peaks and diffusion bands.

Experiments with a stirred solution

The slopes $-b_1$ (descending) and $-b_2$ (ascending) calculated from the diffusion bands, obtained with a stirred solution of 1–15 μl 2-butanol in 0.5 or 1.5 cm^3 85% phosphoric acid, and with a 50-cm diffusion column L_1 or without such a column, are collected in Table I. The following conclusions can be drawn from the data of this table, in conjunction with eqn. 17 or 32.

(1) Changing the flow-rate of the carrier gas from 30 to 13.3 cm^3 min^{-1} at the same temperature (see experiments 22 and 26) has only a small effect on the slope.

(2) The descending slopes measured must represent the rate constant k_3 for transporting the products away from the solution. This is indicated by the fact that removal of the diffusion column ($L_1 = 0$) increase this slope considerably, as predicted by eqn. 17 or 32. Moreover, eqn. 32, for $L_1 = 0$, gives $k_3 = K_L/L_2$, and, since L_2 is the known height of the liquid layer, K_L is easily calculated by simply multiplying the descending slope of Table I by L_2. For example, in experiment 22 (when 0.5 cm^3 of solution was used) L_2 was 0.52 cm and thus $K_L = 16.08 \cdot 10^{-4} \times 0.52 \cdot 10^{-2} = 8.36$ μm s^{-1}. In experiment 27 (with 1.5 cm^3 of solution) L_2 was 0.85 cm and $K_L = 8.21$ μm s^{-1}. These overall mass transfer coefficients of butenes in the liquid phase are of the same order of magnitude as those of butane in hexadecane measured earlier [7], being 2.18–2.93 μm s^{-1} at much lower temperatures (326–327 K).

(3) The increase in K_L with temperature (experiments 21–27) shows that mass transfer across the gas–liquid boundary is activated. From a plot of ln K_L *vs.* $1/T$ an activation energy of 60.9 kJ mol^{-1} is calculated. This is too high a value for a physical mass transfer phenomenon. For the transfer of propene across a gas–γAl_2O_3 surface, an activation energy of 13.8 kJ mol^{-1} was found [10]. The value of 60.9 kJ mol^{-1} determined here probably indicates that the removal of butenes from the reaction mixture is not a simple expulsion of them from the solution but involves some chemical process.

(4) The ascending slopes in Table I must represent the reaction rate constant k_2.

Experiments with a quiescent solution

The results from such experiments are listed in Table II. The slopes $-b_1$ (descending) and $-b_2$ (ascending) of the diffusion bands were determined here with five different flow-rates of the carrier gas, three lengths L_1 of the diffusion column, three different heights L_2 of the liquid solution, and at various temperatures. According to eqn. 31, these slopes give either k_2 or k_4. It remains to be decided which is which. This and other conclusions drawn from Table II are mainly based on the physical content of the rate constant k_4 as that described by eqn. 30. They are the following:

(1) Changing the flow-rate $\dot{V}$ at the same temperature (experiments 2, 9, 10) has a small effect on the slopes.

(2) Removing the diffusion column L_1 at 433.2 K (compare experiments 12 and 25) causes a big increase in the descending slope, an indication that this slope measures k_4. From eqn. 30, by setting $L_1 = 0$, we obtain $k_4 = 3D_L/L_2^2$, and from the slope $26.06 \cdot 10^{-4}$ s^{-1} and $L_2 = 0.52$ cm of experiment 25, one finds $3D_L/L_2 = 13.6$ μm s^{-1}, in acceptable agreement with $K_L = 17.2$ μm s^{-1} calculated at the same temperature from the slope of a stirred solution (see experiment 24 in Table I). Furthermore, D_L is calculated as $2.35 \cdot 10^{-8}$ m^2 s^{-1} at 433.2 K.

(3) Increasing the height of the liquid layer L_2 (experiments 38, 37 and 39) causes a decrease of the descending slope, while it leaves unaffected the ascending slope. This confirms that the first is equal to k_4, and the second to k_2, as eqns. 30 and 13 show.

Multiplying eqn. 30 by L_2 and inverting the result, one obtains the form:

$$\frac{1}{k_4 L_2} = L_1 \frac{a_L}{a_G} \cdot \frac{K}{D_G} + \frac{1}{3D_L} L_2 \tag{34}$$

According to this linear form, by plotting $1/k_4L_2$ *vs.* L_2, we find $1/3D_L$ as the slope of the plot and $L_1 a_L K/a_G D_G$ as its intercept. From the slope, D_L is calculated, while from the intercept, K/D_G is found. By then measuring the diffusion coefficient of the products in the carrier gas [9], or by calculating it theoretically [11], one finds the value of the partition coefficient K. The K/D_G value can also be found from the results with a stirred solution, by conducting two experiments at the same temperature: one with a defined length L_1 and another without a diffusion column. From the latter experiment we find K_L, since $L_1 = 0$, and then this value is used with the first experiment to calculate K/D_G.

Both procedures described above can be applied to the results of Tables I and II. Using the descending slopes from experiments 37–39 of Table II, together with the L_2

TABLE I

SLOPES OF THE DIFFUSION BANDS OF BUTENES OBTAINED WITH A STIRRED SOLUTION OF 0.5 cm^3 85% ORTHOPHOSPHORIC ACID CONTAINING 1–15 μl 2-BUTANOL

In expt. 27, 3 μl of 2-butanol was dissolved in 1.5 cm^3 of 85% orthophosphoric acid.

Expt. No.	T(K)	L_1 (cm)	$\dot{V}$ (cm^3 min^{-1})	Descending slope ($\cdot 10^{-4}$ s^{-1})				Ascending slope ($\cdot 10^{-4}$ s^{-1})	
				A[a]	B[b]	C[c]	D[d]	B[b]	C[c]
14	433.2	50	20	–	1.220	1.106	–	9.463	–
15	443.2	50	20	–	1.297	1.276	–	8.965	10.68
21	393.2	0	30	6.174	5.922	5.672	–	–	–
22	413.2	0	30	–	16.08	–	–	–	–
24	433.2	0	30	–	–	–	32.99	–	–
26	413.2	0	13.3	–	–	–	18.56	–	–
27	413.2	0	26.5	–	–	–	9.655	–	–

[a] 1-Butene + 2-methylpropene.
[b] *cis*-2-Butene.
[c] *trans*-2-Butene.
[b] Mixture of all butenes.

TABLE II

SLOPES OF THE DIFFUSION BANDS OF BUTENES OBTAINED WITH A QUIESCENT SOLUTION OF 2-BUTANOL IN 85% ORTHOPHOSPHORIC ACID

Expt. No.	T(K)	L_1 (cm)	L_2 (cm)	$\dot{V}$ (cm^3 min^{-1})	2-Butanol (μl) + orthophosphoric acid (cm^3)	Descending slope ($\cdot 10^{-4}$ s^{-1})				Ascending slope ($\cdot 10^{-4}$ s^{-1})		
						A[a]	B[b]	C[c]	D[d]	B[b]	C[c]	D[d]
2	428.7	50	0.52	30	15 + 0.5	–	–	–	3.683	–	–	15.78
9	429.2	50	0.52	17	15 + 0.5	–	–	–	1.914	–	–	14.65
10	429.2	50	0.52	10	15 + 0.5	–	–	–	2.488	–	–	–
12	433.2	50	0.52	25	15 + 0.5	–	0.6259	0.5904	–	7.383	9.348	–
16	433.2	50	0.52	20	5 + 0.5	–	1.099	1.189	–	8.151	6.957	–
18	463.2	50	0.52	20	5 + 0.5	4.168	2.206	2.486	–	–	–	–
25	433.2	0	0.52	30	1 + 0.5	–	–	–	26.06	–	–	–
38	408.2	35	0.41	30	0.5 + 0.25	–	–	–	3.920	–	–	9.509
37	408.3	35	0.52	30	1 + 0.5	–	–	–	2.751	–	–	9.234
39	408.2	35	0.64	30	2 + 1	–	–	–	2.045	–	–	9.300

[a] 1-Butene + 2-methylpropene.
[b] *cis*-2-Butene.
[c] *trans*-2-Butene.
[d] Mixture of all butenes.

values given, it is found, by plotting $1/k_4L_2$ *vs.* L_2 (with a correlation coefficient $r = 0.9973$), that $D_L = 5.41 \cdot 10^{-9}$ m^2 s^{-1} and $K/D_G = 1.066 \cdot 10^6$ m^{-2} s. This value for D_L has the correct order of magnitude for diffusion coefficients in liquids. From experiments 14 and 24 of Table I (both at 433.2 K), $K_L = 1.7155 \cdot 10^{-5}$ m s^{-1} and $K/D_G = 3.191 \cdot 10^6$ m^{-2} s. Both K/D_G values, although at temperatures differing by 25 K, have the same order of magnitude. The calculated [11] values of D_G for butenes at 408.2 and 433.2 K (at the pressure of the experiments) are $1.77 \cdot 10^{-5}$ and $1.24 \cdot 10^{-5}$ m^2 s^{-1}, respectively. Using these values, we find for K 18.9 and 39.6, respectively.

(4) From the ascending slopes of Table II, representing k_2, and the values pertaining to the mixture of all butenes (D), an activation energy for the first-order reaction is calculated. It is 34.1 kJ mol^{-1}.

CONCLUSIONS

The results presented in the previous section are by no means exhaustive for the reaction of dehydration of 2-butanol to butenes. It was simply used as a probe reaction to indicate the potentiality of the RF-GC technique for studying homogeneous catalysis. It has become obvious from the discussion of the results that some physicochemical parameters pertaining to the reaction and emerging from the theoretical treatment of the experimental data are not easily accessible by other conventional techniques. There remains to apply the theoretical analysis in other homogeneous reactions, or even to the same family of reactions, varying the experimental parameters, like L_1, L_2, T, $\dot{V}$, etc., more widely.

ACKNOWLEDGEMENT

The kind help of Mrs. Margaret Barkoula is gratefully acknowledged by the authors.

REFERENCES

1 N. A. Katsanos, *Flow Perturbation Gas Chromatography*, Marcel Dekker, New York, Basel, 1988, pp. 225–285.
2 N. A. Katsanos, *Catalysis Today*, 2 (1988) 605.
3 B. V. Ioffe, N. A. Katsanos, L. A. Kokovina, A. N. Marinichev and B. V. Stolyarov, *Kinet. Catal.*, 28 (1987) 805.
4 N. A. Katsanos, *J. Chromatogr.*, 446 (1988) 39.
5 J. Kapolos, N. A. Katsanos and A. Niotis, *Chromatographia*, 27 (1989) 333.
6 N. A. Katsanos and J. Kapolos, in M. L. Ocelli and R. G. Anthony (Editors), *Hydrotreating Catalysts, Proceedings of the Annual International AIChE Meeting, Washington, DC, 1988*, Elsevier, Amsterdam, 1989, p. 211.
7 N. A. Katsanos and E. Dalas, *J. Phys. Chem.*, 91 (1987) 3103.
8 N. A. Katsanos and J. Kapolos, *Anal. Chem.*, 61 (1989) 2231.
9 N. A. Katsanos, *Flow Perturbation Gas Chromatography*, Marcel Dekker, New York, Basel, 1988, pp. 113–142.
10 N. A. Katsanos, P. Agathonos and A. Niotis, *J. Phys. Chem.*, 92 (1988) 1645.
11 E. N. Fuller, P. D. Schettler and J. C. Giddings, *Ind. Eng. Chem.*, 58 (1966) 19.

Journal of Chromatography, 550 (1991) 193–211
Elsevier Science Publishers B.V., Amsterdam

CHROMSYMP. 2318

Review

Tandem mass spectrometry —an additional dimension of chromatography for the determination of biomarkers in fossil fuels

R. P. PHILP*
School of Geology and Geophysics, University of Oklahoma, Norman, OK 73019 (USA)
J.-N. OUNG
Chinese Petroleum Corporation, Offshore Petroleum Exploration Division, 4-7F No. 53, Jen Ai Rd., Sec 3, Taipei (Taiwan)
and
A. GALVEZ-SINIBALDI and J. ALLEN
School of Geology and Geophysics, University of Oklahoma, Norman, OK 73019 (USA)

ABSTRACT

A triple-stage quadrupole mass spectrometry (MS) system used in the MS–MS mode with both gas chromatography (GC) and direct-insertion probe as inlet systems, can provide methods alternative to GC–MS for biomarker analyses. Specific parent/daughter ion relationships can be utilized to monitor and resolve classes of biomarkers or individual components in a complex mixture. Furthermore, deuterated analogues of naturally occurring biomarkers can be utilized for quantitation purposes since the parent/daughter relationship for the standard will differ, depending on the number of deuterium atoms present, even though the relative retention times are identical.

The utilization of GC–MS–MS and the direct insertion probe MS–MS to determine biomarker distributions in crude oils both qualitatively and quantitatively are discussed in this paper. The results from the study show that it is possible to use the probe data to correlate oils on the basis of their source materials and if necessary select samples for more detailed analysis by GC–MS–MS. A major advantage of the direct insertion probe method is speed of analysis although some component resolution is lost. In an effort to minimize this problem and still maintain the rapid analysis time, the use of short columns in GC is also described. This approach permits relatively rapid analyses with limited chromatographic resolution but at relatively high levels of sensitivity.

CONTENTS

0021-9673/91/$03.50

1. INTRODUCTION

Advances in the areas or organic, petroleum, and environmental geochemistry have been rapid in the past two decades. Examination of the literature reveals two main reasons for the developments in these areas. The first of these is advances in various aspects of chromatography, particularly those in gas chromatography (GC) and the evolution of columns from the large-diameter packed columns, 2 or 3 feet in length, to the very-high-resolution and high-temperature fused-silica and aluminum-coated capillary columns available today. The second major advance is the coupling of liquid and gas chromatography to mass spectrometry (MS) that permits identification as well as separation of individual components in complex mixtures.

More recent developments in the past two or three years have provided the opportunity for further innovative advances in the above-mentioned areas. Such developments include supercritical fluid chromatography and its coupling with mass spectrometry, tandem mass spectrometry (MS–MS) and finally the combination of GC with isotope ratio MS. The complex nature of samples typically analyzed in geochemical studies make them ideal candidates for investigating and exploiting many of these new chromatographic and spectrometric techniques. Space does not permit a review of all the developments that have occurred in these areas and how they have influenced various aspects of geochemistry. The area that will be discussed in detail will be the combination of gas chromatography and tandem mass spectrometry (GC–MS–MS) for the determination of biomarker distributions in fossil fuels.

A discussion of MS–MS in a volume devoted to chromatography may seem a little out of context. However, as will be demonstrated below, the MS–MS approach provides an additional dimension of separation for extremely complex mixtures containing large numbers of co-eluting components, both isomers and homologues. In many cases even chromatographic columns with the highest levels of resolution will not totally resolve all components.

There are many designs of commercially available tandem mass spectrometers, but since this paper is more concerned with applications than instrument design it is not proposed to describe such systems in detail. For the most part all of the results described in this study have been obtained through utilization of a triple-stage quadrupole tandem mass spectrometer, where the middle quadrupole is a collision cell and operates in an R_F (radio frequency) mode only. A brief description will be given on how this instrument is used under optimum conditions for analyzing the mixtures typically encountered in various types of geochemical samples following a short review of developments in the field of tandem mass spectrometry.

MS–MS has gained rapid acceptance in the analytical community due largely to its ability to provide sensitive and selective rapid analyses of complex mixtures with minimal sample clean-up [1]. Yost and Enke [2] developed the triple-stage quadrupole mass spectrometer that made mixture analysis by MS–MS practical. MS–MS with

the direct-insertion probe (DIP) method emulates GC–MS by replacing the chromatograph with a mass separator. Whereas GC–MS is limited by the time required for chromatographic separation, the second mass separator requires only an additional ion transit time of 10^{-5}–10^{-3} s [3]. Another advantage of MS–MS with DIP is its capability of analyzing components which cannot be volatilized sufficiently in standard injection systems. The combination of GC with MS–MS further enhances the separation potential of the approach and provides a means of separating components both chromatographically and spectrometrically.

The number of papers in the literature describing the utilization of MS–MS for the analysis of geochemical samples has steadily increased. Gallegos [4] was among the first to report the measurement of appropriate metastable ion transitions in a magnetic sector mass spectrometer to study the distribution of sterane and triterpane homologues from an organic-rich sediment. Measurement of metastable ion transitions during GC–MS analysis was subsequently used to observe sterane isomer distributions without interference from unresolved sterane homologues [5] and to identify extended tricyclic terpanes up to C_{45} in crude oils [6]. The technique also permitted ready detection of the ubiquitous trace component, C_{30} desmethylsteranes, which were subsequently proposed as indicators of marine organic source material [7]. Steen [8] used high-resolution selected-metastable-ion monitoring to determine the distribution of various biomarkers present in oils and source rocks.

Ciupek *et al.* [9] presented an overview of the MS–MS capabilities and its applications to fuel-related materials, *e.g.* coal-derived liquids and diesel particulate samples, using high and low collision energy MS–MS data obtained on reversed-geometry and triple-stage quadrupole spectrometers. Wood and co-workers [10] confirmed the presence of a series of long-chain alkyl aromatic and heteroaromatic hydrocarbons in a Utah boghead coal, using a triple-stage quadrupole mass spectrometer. Summons and co-workers [11,12] have used GC–MS with multiple reaction monitoring in a number of applications to discriminate isomers of branched alkanes from ancient and modern sediments. Snowdon *et al.* [13] demonstrated the value of tandem mass spectrometry in petroleum exploration. Their study showed that GC–MS–MS provided sufficient chemical compositional detail of oils and potential source rocks to solve correlation problems.

Daughter spectra of selected molecular ions are also useful for compound identification. Chou and Wood [14] tentatively identified an alkylaromatic hydrocarbon in shale extracts with tandem mass spectrometry. Hunt and Shabanowitz [15] described the use of a triple-stage quadrupole mass spectrometer operating in the neutral-loss mode for the analysis of organosulfur compounds in crude petroleum distillates. The total analysis time per sample was under 20 min, and qualitative differences in the spectra of several crude oil samples were apparent. Tandem mass spectrometry has also been used for determination of porphyrins [16] and [17]. Complex mixtures of porphyrins present problems for GC–MS analysis due to their extreme involatility. However, with the advent of tandem mass spectrometry this obstacle can be overcome. The added specificity of MS–MS enables the individual porphyrins to be characterized directly from complex fuel matrices.

In recent studies the utilization of GC–MS–MS for the analysis of complex biomarker mixtures has been described [18] and [19]. Operation of the system in the MS–MS parent mode permits spectrometric resolution of many unresolved compo-

nents in these mixtures, greatly aiding in the utilization of the biomarker distributions for evaluation of source, maturity, migration, and characterization of depositional environments.

As mentioned above, one of the major advantages of MS–MS is its ability to resolve components spectrometrically on the basis of specific parent/daughter ion relationships. Hence, this paper describes results of studies designed to develop screening techniques for the rapid determination of biomarker distributions in crude oils, both qualitatively and quantitatively, using the DIP method. Although this does provide a rapid method for screening and significant resolution, there are still a number of components that will not be separated. For instance, hopane and gammacerane have parent ions at m/z 412 and intense daughter ions at m/z 191, and DIP-MS–MS will not resolve these components. An alternative approach for screening is to use short (3 m) GC columns to provide some chromatographic resolution, while at the same time maintaining a rapid analysis time [20]. Several examples describing the application of these techniques to the characterization of crude oils and, in particular, the utility of the approach in differentiating oils from different source rocks will be discussed. In addition to illustrating the use of DIP and short GC columns in conjunction with MS–MS, some more conventional examples of utilizing GC–MS–MS fused-silica columns will also be described. The purpose of this paper is to illustrate the application of MS–MS to various geochemical problems and the type of data obtainable from such applications.

2. EXPERIMENTAL

Samples used in this study were either unfractioned crude oil samples or oils that were fractionated by standard thin-layer chromatography techniques to provide saturate, aromatic, and polar fractions. Samples from the following areas were used in this study: Offshore Taiwan, Williston Basin, New Mexico, Gulf of Suez, Dubai, Norway, Chaidamu and Shanganning Basins, China and Monterey, California. Whole oils or selected fractions were analyzed with the Finnigan MAT TSQ70 mass spectrometer. The chromatographic column used for most of the routine analyses was a 25 m × 0.25 m I.D. aluminum-coated fused-silica capillary column (Scientific Glass Engineering), coated with a 0.1-μm film of the HT-1 phase. The column was temperature-programmed from 40 to 330°C at 2°C/min with an injector temperature of 280°C. The transfer-line temperature was set at 280°C and the ion-source temperature was 200°C. The ion source was operated in the electron impact mode at an electron energy of 70 eV. The collision gas was argon at 1 mTorr, and the collision energy was generally -10 eV. Additional experiments were also performed with short columns (3 m) for GC to show that despite the loss of GC resolution, MS–MS techniques can actually resolve many components rapidly.

For the DIP inlet system, the sample was loaded in the crucible, the solvent was evaporated and the sample was mounted on the tip of the DIP system, which was then inserted into the ion source. The DIP temperature was programmed from 50°C to 300°C in 2 min to permit distillation of the sample directly into the ion source.

The TSQ mass spectrometer was operated either as a single-stage mass spectrometer (*i.e.*, Q1MS or Q3MS) or tandem mass spectrometer in the parent mode. Selected-ion monitoring (SIM) and selected-reaction monitoring (SRM) techniques

were used for routine biomarker analysis. In the SRM techniques of tandem mass spectrometry, the parent/daughter ion pairs monitored consisted of molecular ions (parents) and characteristic base peak fragments (daughters) commonly observed in the electron-impact (EI) spectra. Each specific parent/daughter ion pair was monitored for 0.02 s before switching to the next ion pair, thus permitting a large number of experiments to be undertaken during each analysis. Introduction of deuterated standards into the sample and subsequent monitoring of the appropriate deuterated parent/daughter ion relationships, regardless of whether the undeuterated standard analogue exists in the original sample, permits absolute quantitations to be undertaken [21].

3. RESULTS AND DISCUSSION

A convenient way in which to introduce the MS–MS concept is to use the separation of steranes and diasteranes in crude oils. It is well documented that several

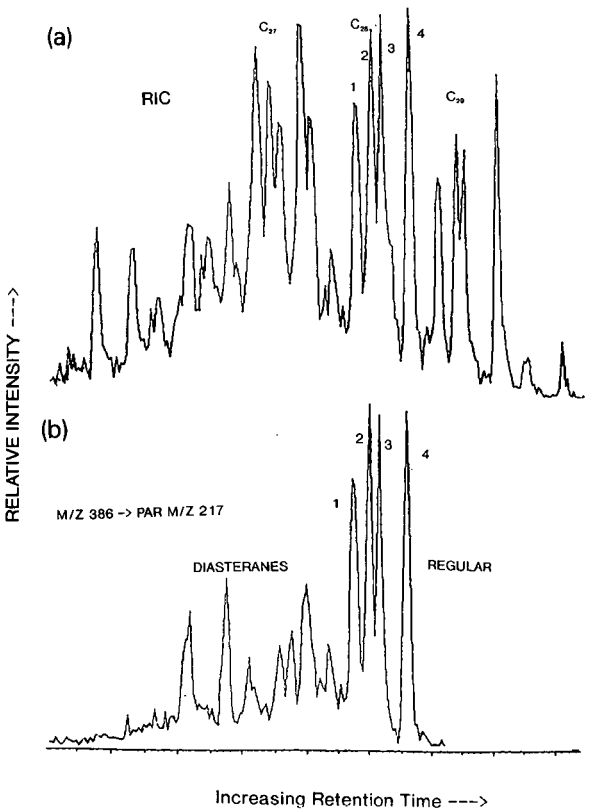

Fig. 1. (a) Reconstructed ion chromatogram (RIC) for the four parent/daughter ion reactions monitored for the C_{27}–C_{30} steranes, namely *m/z* 372/217, 386/217, 400/217 and 414/217. (b) Deconvolution of the data shown in (a) permits one to obtain distributions for the individual sterane homologues as illustrated here with the distribution of the C_{28} steranes. (In both chromatograms peaks 1 and 4 are 14α,17α-20*S*- and 20*R*-C_{28} steranes, respectively and peaks 2 and 3 are the 14β,17β-20*R*- and 20*S*-C_{29} steranes, respectively).

isomers and homologues are eluted in the C_{27}–C_{30} sterane region of a crude oil chromatogram [22]. To obtain an accurate assessment of the relative proportions of the various homologues it is desirable to resolve them completely. For most geochemical samples, such a separation is not achievable with even the best capillary columns available today. To separate the various steranes using MS–MS and GC–MS–MS it is possible to monitor the 4 parent/daughter ion pairs for the C_{27}–C_{30} steranes, namely *m/z* 372/217, *m/z* 386/217, *m/z* 400/217, and *m/z* 414/217, respectively. The result of monitoring these four parent/daughter combinations, are shown in Fig. 1a. Individual homologue distributions can now be resolved from the total sterane distributions as shown by using the C_{28} steranes (Fig. 1b). Subsequent integration of the peak areas can provide an accurate assessment of the relative proportions of the individual steranes and enable various ratios to be calculated to provide source information. Furthermore, such complete separation permits accurate calculation of commonly used maturity parameters, based on individual homologues. Each pseudohomologue distribution consists of diasteranes and regular steranes, but if necessary, diasteranes and regular steranes can be separated by monitoring the parent ions of both *m/z* 189 and 217, respectively, as shown in Fig. 2. This combination of GC and MS–MS permits complete separation of virtually all homologues and isomers of the diasteranes and steranes and can provide an accurate assessment of any maturity, source, or depositional environment, parameter based on these values. Another important application of MS–MS to sterane analyses is the ability to distinguish C_{30}-4-desmethyl and 4-methyl-steranes. The former have an intense daughter ion at *m/z* 217 and the later at *m/z* 231, and monitoring the *m/z* 414 → 217 and *m/z* 414 → 231 parent/daughter pairs provides a rapid means of distinguishing between the two types of steranes.

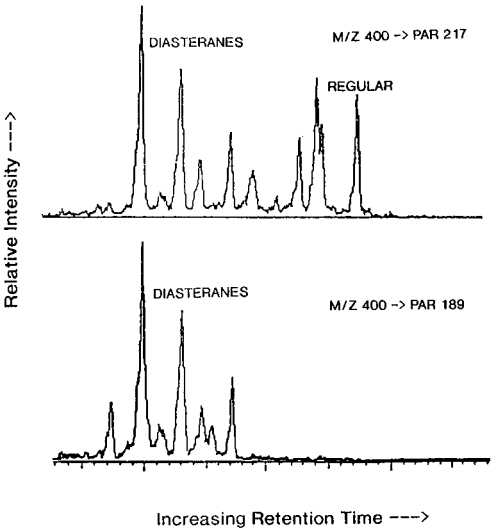

Fig. 2. Diasteranes can be resolved from the sterane–diasterane mixture by monitoring the *m/z* 400 → 189 relationship, and the *m/z* 400 → 217 relationship using the C_{29} steranes as an example.

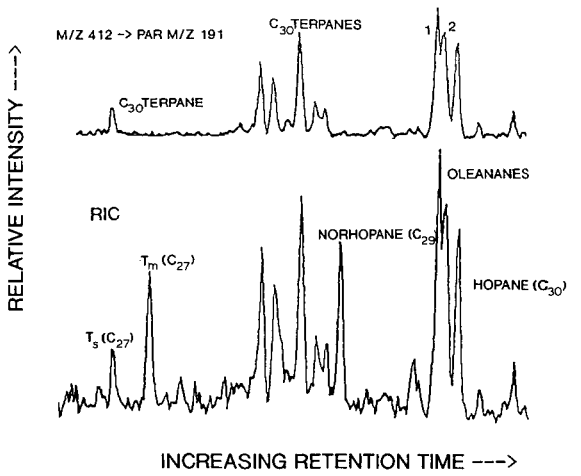

Fig. 3. Monitoring the m/z 412 → 191 parent/daughter ion relationship for an Indonesian oil sample revealed the presence of a number of C_{30} terpanes including two isomers of oleanane in this chromatogram, namely 18α(H)- and 18β(H)- oleanane (peaks 1 and 2, respectively).

3.1. Terpanes

There are many potential applications for MS–MS in the separation and characterization of the complex mixtures of terpanes found in geochemical samples. One example of this is the separation, spectrometrically, of the tricyclic terpanes from tetracyclic and pentacyclic terpanes. Although all of these compounds have an intense daughter ion at m/z 191, the parent ions for each series of terpanes differ by 2 mass units and the spectrometric separation of these three classes of terpanes is therefore possible. This is particularly useful in the region of the chromatogram where the C_{27} to C_{35} hopanes are eluted, since in this region there is also a large degree of overlap between the tricyclic and pentacyclic terpanes.

The MS–MS approach can also provide additional information on unidentified terpanes in crude oil samples, or on those incorrectly identified. An example is the identification of a C_{30}-terpane which is eluted between the two C_{27} trisnorhopanes, namely T_s and T_m (Fig. 3). Although this C_{30}-pentacyclic terpane has yet to be unequivocally identified, its relative concentration appears to be significantly higher in samples formed from higher plant material. In addition to this C_{30} terpane, there is a component which is eluted after T_m and has often been assigned as 17β(H)-trisnorhopane according to early work and simply on the basis of m/z 191 chromatograms [23]. However, repeated analyses of a variety of crude oil samples have led us to suggest that in many examples this component was not 17β(H)-trisnorhopane but rather a C_{28} pentacyclic terpane with a parent ion at m/z 384 (Fig. 4). This component shows an intense m/z 384 → 191 parent/daughter relationship and not the intense m/z 370 → 191 parent/daughter relationship shown by the T_s and T_m components which elute in the same region. In support of our tentative identification, more recent work has now established that this compound is the 17α(H),21β(H)-29,30-bisnorhopane in many oils and source rock extracts, particularly those derived from carbonate sources. T_s is the first member of this homologous series.

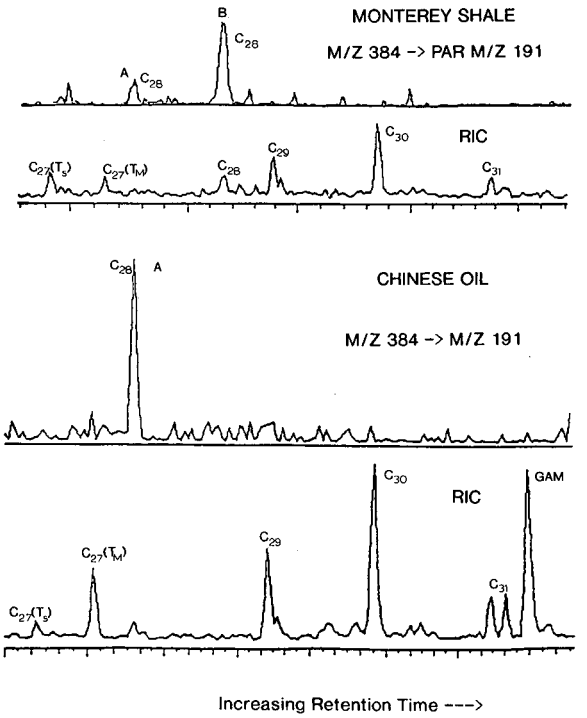

Fig. 4. The upper two chromatograms in this figure are derived from the analysis of an oil from the Monterey Formation, CA. Note the characteristically high concentrations of the 28,30-bisnorhopane (B) with the longer retention time than the 29,30-bisnorhopane (A). The bottom chromatograms are derived from a Chinese oil and unlike the Monterey sample clearly show the predominance of the early eluting 29,30-bisnorhopane (A) which elutes much closer to the C_{27}-trisnorhopanes. Other hopanes are identified by carbon number on the chromatograms along with gammacerane which is labelled GAM.

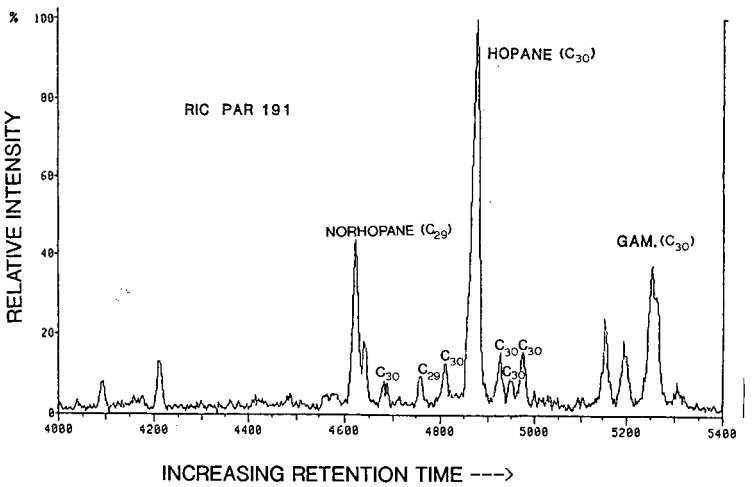

Fig. 5. Monitoring of the m/z 412 → 191 parent/daughter relationship for this Chinese oil sample provides good evidence to illustrate the presence of several C_{30}-terpanes in addition to 17α(H), 21β(H)-hopane and gammacerane (GAM).

The presence of additional terpanes, albeit in trace amounts, is relatively easy to discern in various regions of the chromatogram by use of the TSQ mass spectrometer operating in the parent mode. An example of this can be seen in Fig. 5, where a Chinese crude oil was analyzed in the parent mode with particular emphasis on the search for C_{30} terpanes, using the m/z 412 → 191 parent/daughter relationship. The presence of a significant number of C_{30}-terpanes was observed in this region of the chromatogram in addition to the C_{30} compounds hopane and gammacerane. Although their identities have still not been unambiguously established, their presence permits them to be used as correlation parameters, if necessary.

Another use of the MS–MS approach is to separate components of different molecular weights having the same daughter ion. Rinaldi *et al.* [24] commented on the presence of hexacyclic-C_{31}-hopanoids in certain oil samples which have a tendency to be inseparable from gammacerane on the chromatographic columns with particular liquid phases. Fortunately, the hexacyclic terpanes have a parent ion at m/z 424 compared to m/z 412 for gammacerane. Hence analysis of samples and simultaneous monitoring of the m/z 412/191 and m/z 424/191 parent/daughter relationships can be used to demonstrate the presence of both classes of compounds in crude oils (Fig. 6). The C_{31}-22(*S* and *R*)-homohopanes are also shown in Fig. 6 and have a parent ion at m/z 426 and daughter ion at m/z 191 but have slightly shorter retention times than the other two components mentioned above.

The preceding examples show that it is possible to obtain more additional information by the combined use of GC and MS–MS in the analysis of complex mixtures than by GC–MS and SIM. Many of the additional components observed in the mixtures may not always be immediately identifiable. This does not necessarily constitute a problem, since these components can be incorporated into maturity, source, and depositional environment parameters and their identities can be estab-

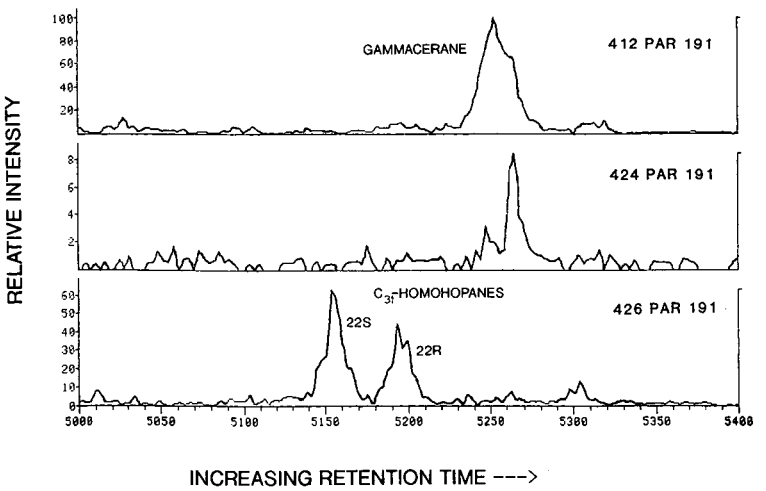

Fig. 6. Co-eluting components are readily resolved using the MS–MS approach. For example it was anticipated that this Chinese oil sample contained a C_{31}-hexacyclic hopane which co-eluted with gammacerane. Monitoring of the m/z 412 → 191 and m/z 424 → 191 parent/daughter relationship completely resolved these two components.

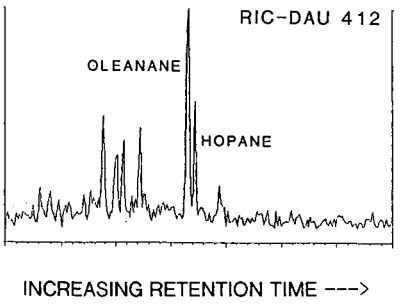

Fig. 7. In addition to obtaining parent data using the MS–MS approach it is possible to obtain daughter data on various components simultaneously. In this diagram all of the daughter spectral data for the ion at *m/z* 412 have been deconvoluted from the parent data and summed to produce this total ion current chromatogram of *m/z* 412 daughter data. The peaks labelled C_{30} are known to be pentacyclic terpanes but their precise identity remains to be established.

lished at a later date. One approach to establishing the identity of the unknown components partially is to operate the MS–MS system alternately in the parent and daughter modes. In this mode of operation, one complete set of parent experiments is performed and then a daughter experiment is performed, and this process is continually repeated throughout the analysis. The daughter experiments are performed on parent ions of components known to be eluted in various regions of the chromatogram. The sample shown in Fig. 7 was known to contain a number of previously unidentified C_{30} pentacyclic terpanes. Daughter spectra of the parent ion at *m/z* 412 were continually collected and at the end of the experiment, the parent and daughter data were deconvoluted, and complete daughter spectra for each component were obtained. Collision activated decomposition (CAD) spectra for the parent ions of two of the major components in the daughter ion chromatogram, namely 18α(H)-oleanane and hopane, are shown in Fig. 8. The collision spectra of these two components show many similarities to previously published electron-impact spectra for 18α(H)-oleanane and hopane. Similar daughter experiments could also be performed, using other parent ions throughout the GC analysis to provide a complete collection of daughter spectra. A major advantage of daughter spectra or CAD spectra over EI spectra is that the need to undertake background subtractions is virtually eliminated. The fact that only the parent ion of interest is permitted to enter the collision cell virtually eliminates all background ions from interfering components. Thus, for C_{30} pentacyclic terpanes, only the parent ions at *m/z* 412 enter the collision cell, and the daughter spectra subsequently obtained will be from that particular parent ion. This is a major improvement over EI spectra obtained with a single stage analyzer system. In such a situation it is necessary to remove interfering ions from the spectrum by carefully selecting background spectra. Poor selection can often lead to erroneous spectra being obtained.

3.2. Biomarker quantitation by tandem mass spectrometric techniques

A common feature of oils derived predominantly from the organic matter of higher plants is the relatively low proportion of steranes relative to triterpanes, as determined from the ion intensities in the *m/z* 191 and *m/z* 217 mass fragmentograms,

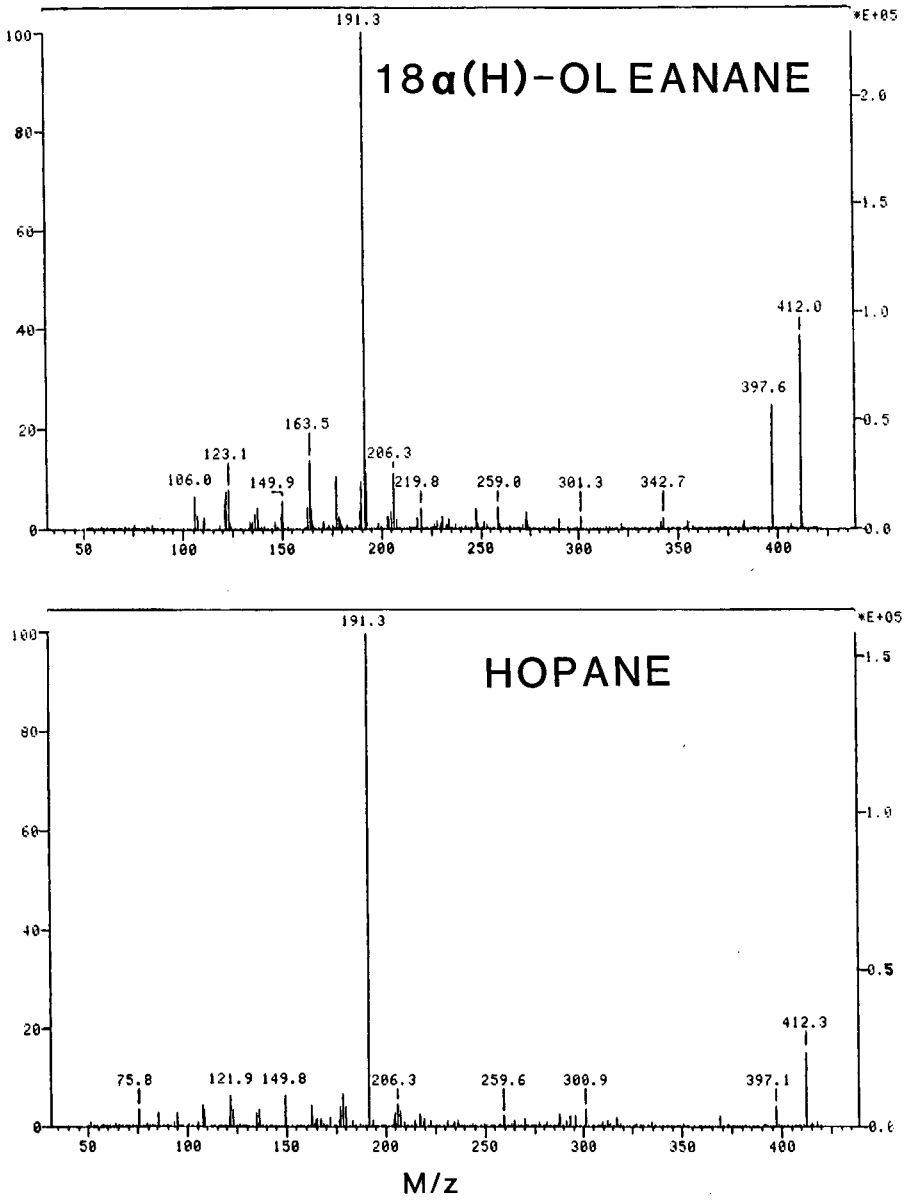

Fig. 8. Collision activated decomposition spectra of the *m/z* 412 parent ion for 18α(H)-oleanane and hopane.

respectively. For example, triterpanes in the Gippsland Basin oils, Australia, are present in approximately 3–4 times the concentration of the steranes [25], and in oils from the Mahakam Delta, Indonesia, approximately 8–10 times the concentrations of steranes [26]. For Taranaki oils from New Zealand, the ratios of hopanes to steranes were within the range 1.0–2.5. Oils from Taiwan had a ratio of triterpanes to steranes

TABLE I

QUANTITATION DATA OBTAINED FROM DIP-MS–MS ANALYSIS OF OILS DERIVED FROM TERRESTRIAL AND MARINE SOURCE MATERIALS

Concentrations of various biomarkers expressed in ng/μl using ^{2}H-cholestane as internal standard. 372, 386, 400 and 414 correspond to the C_{27}, C_{28}, C_{29} and C_{30} steranes; 398, 412 to the C_{29} and C_{30}-pentacyclic terpanes; 318-C_{23} tricyclic terpane and 330 to the C_{24}-tetracyclic terpane.

Sample location	372	386	400	414	398	412	318	330	372+386+400	372/400[a]	398/412[a]	217/191[a]	318/330[a]
Terrestrial sourced samples													
Offshore Taiwan	8.87	8.21	26.28	1.60	29.20	47.30	17.20	51.40	43.46	0.34	76.50	0.57	0.33
	12.56	8.76	37.17	3.49	24.05	47.55	11.20	103.90	58.48	0.34	71.60	0.82	0.11
	8.09	8.71	33.81	1.46	36.65	89.65	8.80	59.05	50.61	0.24	126.30	0.40	0.15
	9.27	8.35	22.00	1.43	9.25	22.05	8.60	18.85	39.62	0.42	31.30	1.27	0.46
Average	8.09	7.83	25.33	1.89	19.93	36.00	14.31	43.95	41.25	0.33	55.93	0.80	0.36
Marine sourced samples													
Williston Basin	31.28	22.03	29.51	11.38	22.29	17.26	37.89	18.49	82.82	1.06	39.55	2.09	2.05
New Mexico	66.40	31.40	42.74	8.67	11.27	19.55	29.57	25.60	140.54	1.55	30.82	4.56	1.16
Gulf of Suez	34.98	29.65	30.32	12.11	19.04	15.75	17.65	8.34	94.95	1.15	34.79	2.73	2.12
Dubai	33.13	27.67	29.16	15.18	20.13	17.28	18.96	7.56	89.96	1.14	37.41	2.40	2.51
Norway	51.35	43.00	42.00	19.48	12.38	18.38	19.45	12.53	136.35	1.22	31.23	4.37	1.55
Average	43.43	30.75	34.75	13.36	17.02	17.74	24.70	14.50	108.92	1.23	34.76	3.23	1.88

[a] These values represent ratios of the components with the various ions indicated.

ranging from 6 to 8. All of these oils are thought, or known to be produced from source rocks containing a predominance of organic matter derived from higher plants. Though the ratio of triterpanes to steranes can be derived from the GC–MS data, MS–MS provides a means to rapidly determine the absolute concentrations of terpanes and steranes in oils and differentiate between those oils derived from marine organic matter *versus* those from higher plant organic matter.

To illustrate how the MS–MS approach can be used for quantitation purposes, five oils from Taiwan produced from source rocks containing a predominance of higher plant material and five oils from other basins worldwide derived from marine source materials, were examined and characterized by MS–MS (Table I). Samples were analyzed either as whole oils or as saturate fractions. In either case, known amounts of a deuterated cholestane standard {[$^2H_2$]$C_{27}\alpha\alpha\alpha$(20R) cholestane, with a similar mode of fragmentation to $C_{27}\alpha\alpha\alpha$(20R) cholestane but a molecular weight of 374 a.m.u. and a characteristic daughter ion at *m/z* 219}, was added as an internal standard to a known amount of sample prior to fractionation. The samples containing known concentrations of the internal standard were subsequently analyzed by direct-insertion probe tandem mass spectrometry (DIP-MS–MS) operating in the parent mode. In all of these experiments the parent ions of daughter ions at *m/z* 123, 191, 217 and 219 were monitored to determine sesquiterpanes, diterpanes, tricyclic terpanes, tetracyclic terpanes, pentacyclic terpanes, steranes and the deuterated cholestane respectively.

The intensities of parent ions detected during the DIP-MS–MS analysis of these oils were summed to produce a composite spectrum showing the distribution of the various biomarkers under examination. The composite DIP-MS–MS spectra obtained from two oils analyzed in this study, one produced from higher plant source material from the Gulf of Suez, are shown in Fig. 9. For comparison, distributions of the triterpanes and steranes obtained by conventional SIM of the ions at *m/z* 191 and 217 for the oil produced from higher plant material are shown in Fig. 10. Based on the concentration of [$^2H_2$]$C_{27}\alpha\alpha\alpha$ cholestane in the original sample, absolute amounts of C_{27}, C_{28}, C_{29} and C_{30} steranes can be determined from these spectra and amounts of the terpanes relative to the internal sterane standard can also be determined from data shown in Fig. 9. The quantitative data derived from all ten oils examined in this study are summarized in Table I.

It is not possible to make a direct comparison between the biomarker distributions obtained from the DIP-MS–MS data (*e.g.* Fig. 9) *versus* the multiple ion detection (MID) data (*e.g.* Fig. 10). The DIP-MS–MS data reflect the intensity of various parent ions in the original sample, and hence each parent ion will contain a contribution from several components. However, MID data only reflect variations in intensity of the major fragments of these different compound classes and for the most part, one peak in the chromatogram represents one component. For example, the peak at *m/z* 330 in the DIP-MS–MS data is not one component but a composite of all the terpane compounds having a parent ion at m/z 330. Likewise the peak at *m/z* 372 corresponds to all the C_{27} regular and rearranged steranes. Despite the inability to resolve individual isomers, the DIP-MS–MS approach is still extremely valuable for rapid and quantitative screening of oils and source rock extracts.

Despite certain limitations still being evaluated, the data presented in Table I clearly show that oils from marine *vs.* terrestrial sources can be distinguished by using

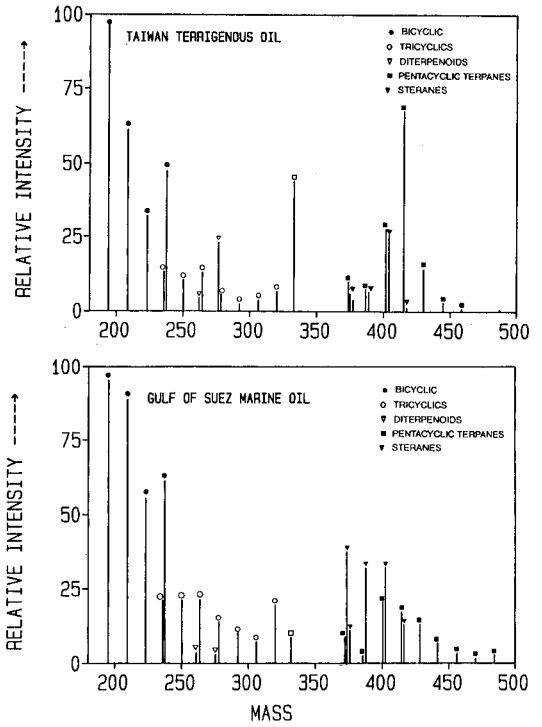

Fig. 9. Parent spectra obtained by DIP-MS–MS in parent mode. (a) A terrigenous oil from offshore Taiwan. (b) A marine oil from Gulf of Suez.

this DIP quantitation approach. Oils derived from terrestrial sources are dominated by the C_{29} steranes, with relatively low C_{30} sterane concentrations. The terrestrial oils also have high concentrations of C_{30} terpanes and C_{24} tetracyclic terpanes. In some cases, the C_{30} terpane content is relatively high, due to the presence of 18α(H)-oleanane as well as hopane in many of these samples. These two C_{30} terpanes, m/z 412 with daughter ions at m/z 191, cannot be separated by DIP-MS–MS. The marine oils generally have a higher concentration of steranes and C_{23} tricyclic terpanes than the oils from terrigenous sources. Various ratios, *e.g.* C_{27} steranes to C_{29} steranes (shown as 372/400 in Table I), steranes to terpanes (shown as 217/191 in Table I) and tricyclic terpanes to tetracyclic terpanes (shown as 318/330 in Table I) based on these quantitative data are also very different in terrigenous oils compared to marine oils and are therefore also useful for differentiating oils from different types of source materials.

3.3. GC–MS–MS analyses using short GC columns

In the preceding section, characterization of biomarker distributions with the DIP-MS–MS and deuterated cholestane used as an internal standard has been described. A major limitation of this approach is the fact that certain isomers and homologues cannot be resolved. For example, all of the C_{27} steranes with parent ions at m/z 372 and daughter ions at m/z 217 will be present as one peak in the cumulative

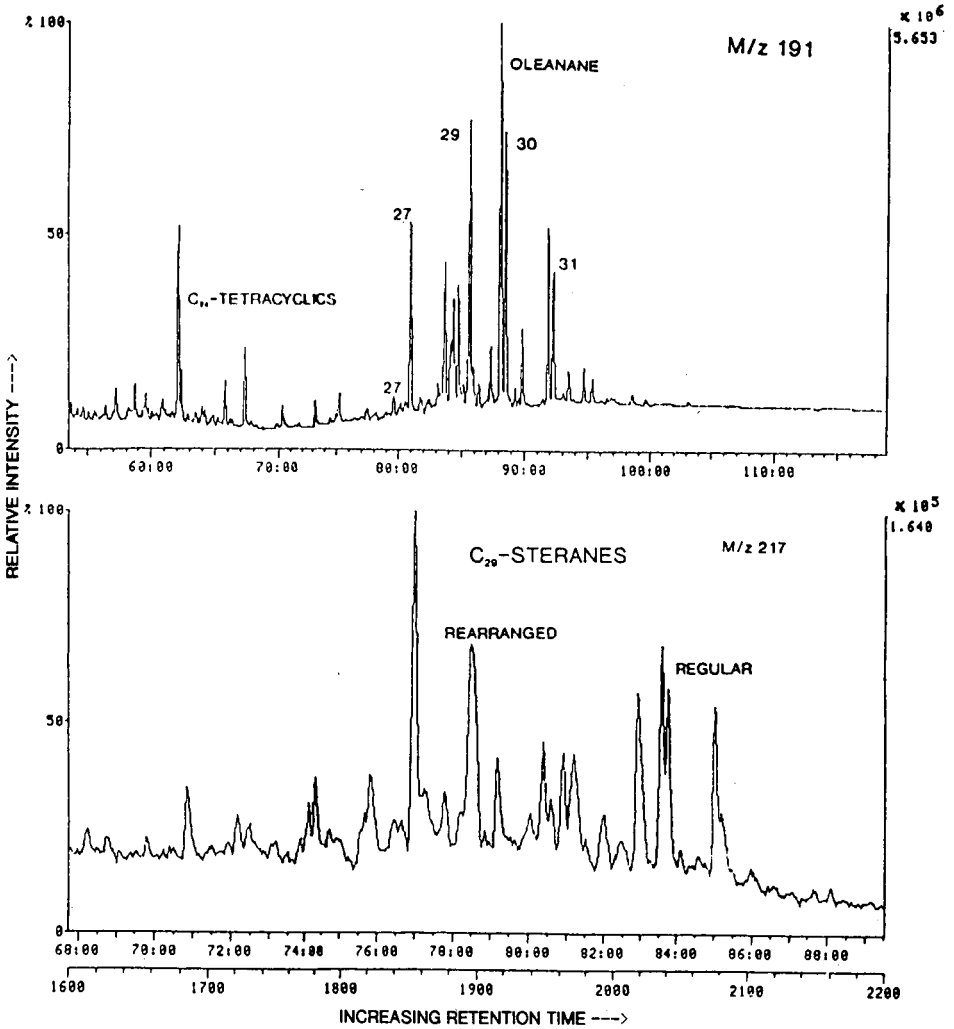

Fig. 10. The *m/z* 191 and *m/z* 217 mass fragmentograms of a terrigenous oil sample from offshore Taiwan.

spectrum. To maintain a relatively rapid analysis time whilst improving the resolution it is possible to use short chromatographic columns, 3 m in length, in conjunction with the MS–MS system [20]. This provides some separation of components with similar molecular weights, *i.e.* hopane and gammacerane with a relatively rapid analysis time and provides a better response (signal-to-noise) than the DIP method, due to better sample transfer into the ion source.

Thus, Fig. 11 shows a comparison between the direct insertion probe for 100 pg cholestane and the GC analysis of the same quantity of cholestane, demonstrating the far better signal-to-noise ratio obtained in the short-column GC analyses. Similarly, in Fig. 12 the distribution of the pentacyclic parent ions of *m/z* 191, obtained by both

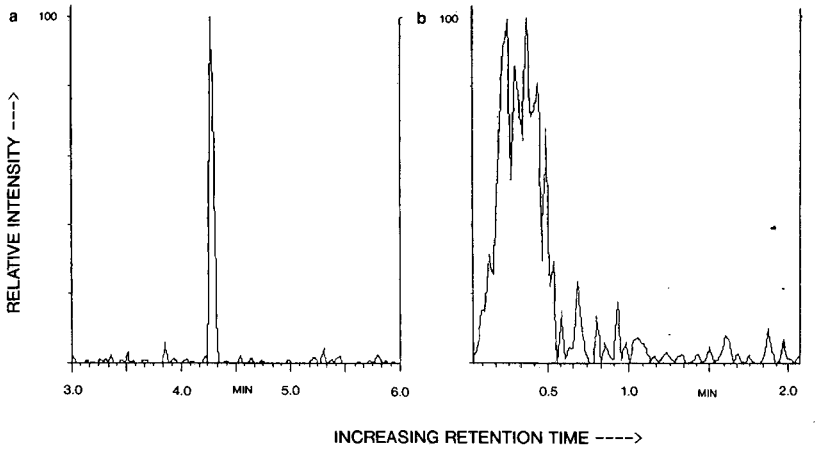

Fig. 11. A comparison between the analysis of 100 pg of 5α-cholestane in (a) GC–MS–MS mode and (b) the DIP-MS–MS mode.

techniques, are compared. Naturally the DIP method offers no resolution, but the short 7-min GC analysis time separates the various hopane homologues and starts to resolve the hopane diastereomers at C_{32}. The 22*S*- and 22*R*-C_{31}-homohopanes are not resolved on such a short column. However, when the data from these two chromatograms are used to sum the spectrum of the pentacyclic parents of *m/z* 191 from both techniques, the resultant terpane distributions, shown in Fig. 13, are virtually identical.

Another example demonstrating an advantage of the short column approach

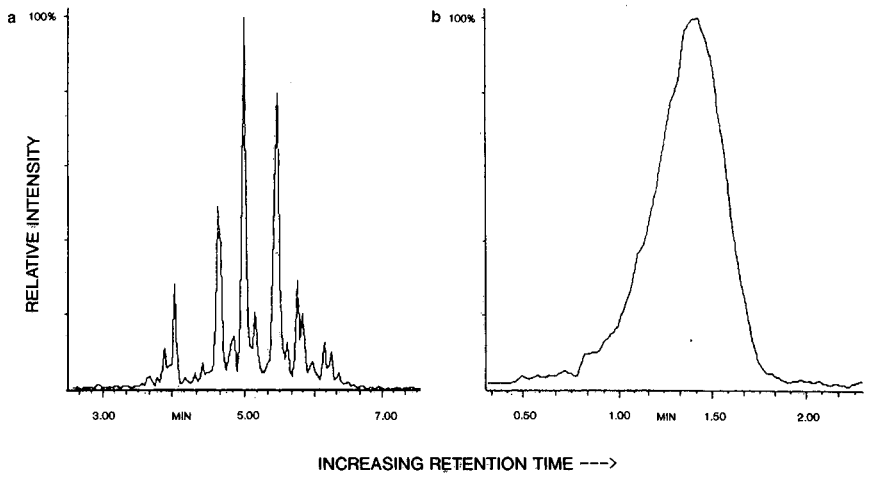

Fig. 12. Analysis of a crude oil to determine the pentacyclic terpane parent ions of *m/z* 191 in (a) the GC–MS–MS mode and (b) DIP-MS–MS mode.

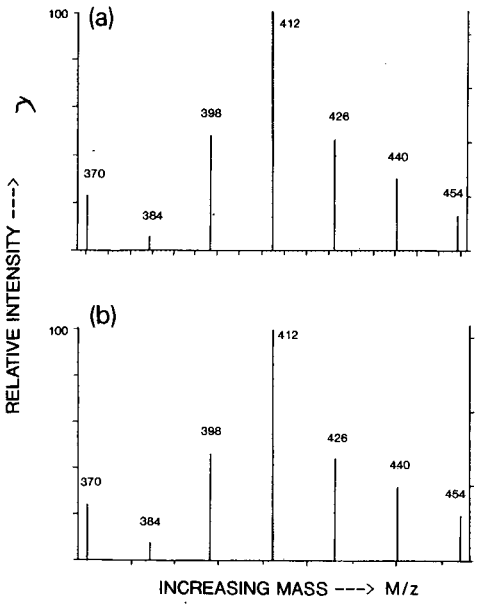

Fig. 13. Composite spectra obtained from the two data sets of Fig. 12, (a) GC–MS–MS and (b) DIP-MS–MS, showing the parent ion distribution for m/z 191.

over the direct insertion probe is shown in Fig. 14 and revolves around the ability to separate hopane and gammacerane both of which have molecular weights at m/z 412 and daughter ions at m/z 191. As mentioned above, similarities in the fragment ions produced from the m/z 412 parents of both compounds facilitate the separation of

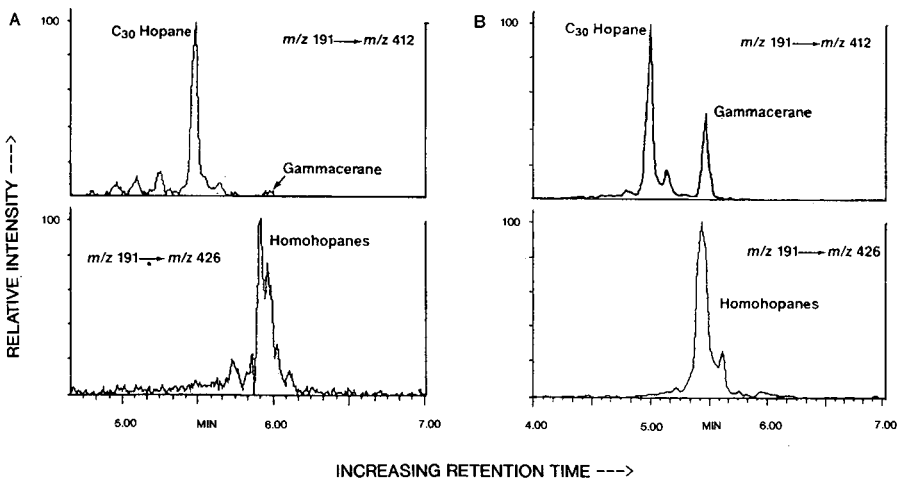

Fig. 14. Short column GC–MS–MS analysis of two oils to illustrate the rapid separation of hopanes and gammacerane resulting from the use of two different parent/daughter ion relationships. The oil for the data shown in the left hand chromatograms (A) was from the fresh-water Shanganning Basin and (B) from the moderately-saline Chaidamu Basin.

compounds with unique parent/daughter ions. Hence, although hopane and gammacerane cannot be resolved spectrometrically, the use of a short GC column will permit separation of these compounds, providing the relative gammacerane concentration in various samples rapidly. The hopane/gammacerane ratio can be used to provide us with an indication of the relative salinity of the original depositional environment [7].

4. CONCLUSIONS

This paper provides examples in which the MS–MS approach has been utilized to analyse complex geochemical samples with the system operating in either the parent or daughter mode. The resulting data may be in the form of identification of previously unidentified or tentatively identified components or it may provide information on the distribution of novel biomarkers. It is also an extremely useful technique for separating components which may have different molecular weights but are not resolved chromatographically. Operation in the daughter mode provides a novel method for obtaining collision spectra of specific parent ions which may be used to identify unknown components. Introduction of a complex mixture, *e.g.*, whole oil or hydrocarbon fractions, via the direct-insertion probe into a tandem mass spectrometer operating in the parent mode or daughter mode, or both, permits biomarker distributions to be obtained from these samples in a few minutes. Though the total separation of various isomers by the DIP-MS–MS approach is not possible, and the amount of information obtained from this technique is not as detailed as that obtained from the GC–MS–MS technique, the fingerprints derived are very valuable for the purposes of sample characterization and correlation.

DIP-MS–MS operating in the parent mode can be used for quantitative analyses of biomarkers by use of a deuterated internal standard. This technique allows the rapid quantitative determination of various biomarker classes as well as oil/oil correlations and source determinations. The present study has shown that differences in the biomarker concentrations between terrigenous oils and marine oils can be revealed by this quantitation technique.

The lack of homologues resolution by the DIP method can be overcome to some extent by the use of short GC columns. This technique partially resolved isomers and homologues that cannot be separated spectrometrically while keeping the analysis time short. Both of these approaches are therefore extremely valuable for rapid screening of a larger number of samples in order to obtain a preliminary idea of their biomarker distributions.

It should be clear from this study that tandem mass spectrometry provides a powerful alternative approach for biomarker analysis with many advantages over the conventional GC–MS approach. With the increasing availability of commercial tandem mass spectrometers, *e.g.*, triple-stage quadrupole mass spectrometers, these novel mass spectrometry techniques will be more and more important in the field of biomarker study. MS–MS provides an alternative and additional method of separating compounds which are not always separable by conventional chromatographic processes.

5. ACKNOWLEDGEMENTS

Funds to purchase the Finnigan triple-stage quadrupole mass spectrometer were obtained from the National Science Foundation Instrumentation Program (Grant No. EAR 8517312); the Sarkeys Foundation and the ARCO Foundation.

REFERENCES

1 J. V. Johnson and R. A. Yost, *Anal. Chem.*, 57 (1985) 758A–768A.
2 R. A. Yost and C. G. Enke, *Anal. Chem.*, 51 (1979) 1251A–1264A.
3 F. W. McLafferty, in F. W. McLafferty (Editor), *Introduction to Tandem Mass Spectrometry*, Wiley, New York, 1983, pp. 1–10.
4 E. J. Gallegos, *Anal. Chem.*, 48 (1976) 1348–1351.
5 G. A. Warburton and J. E. Zumberge, *Anal. Chem.*, 55 (1983) 123–125.
6 J. M. Moldowan, W. K. Seifert and E. J. Gallegos, *Geochim. Cosmochim. Acta*, 47 (1983) 1531–1534.
7 J. M. Moldowan, W. K. Seifert and E. J. Gallegos, *AAPG Bull.*, 69 (1985) 1255–1268.
8 A. Steen, *Org. Geochem.*, 10 (1985) 1137–1142.
9 J. D. Ciupek, R. G. Cooks, K. V. Wood and C. R. Ferguson, *Fuel*, 62 (1983) 829–834.
10 K. V. Wood, R. G. Cooks, Z. Mudamburi and P. H. Given, *Org. Geochem.*, 7 (1984) 169–172.
11 R. E. Summons, *Org. Geochem.*, 11 (1987) 281–289.
12 R. E. Summons, T. G. Powell and C. J. Boreham, *Geochim. Cosmochim. Acta*, 52 (1988) 1747–1764.
13 L. R. Snowdon, P. W. Brooks, G. K. Williams and F. Goodarzi, *Org. Geochem.*, 11 (1987) 529–548.
14 M. M. Chou and K. V. Wood, *Org. Geochem.*, 9 (1986) 351–356.
15 D. F. Hunt and J. Shabanowitz, *Anal. Chem.*, 54 (1982) 574–578.
16 J. V. Johnson, E. D. Britton, R. A. Yost, J. M. Quirke and L. L. Cuesta, *Anal. Chem.*, 48 (1986) 1325–1329.
17 J. S. Brodbelt, R. G. Cooks, K. V. Wood and T. J. Jackson, *Fuel Sci. Technol. Int.*, 4 (1986) 683–698.
18 R. P. Philp, J.-N. Oung and C. A. Lewis, *J. Chromatogr.*, 446 (1988) 3–16.
19 R. P. Philp and J.-N. Oung, *Anal. Chem.*, 60 (1988) 887A–896A.
20 M. E. Hail and R. A. Yost, presented at the *36th ASMS Conference on Mass Spectrometry and Allied Topics, San Francisco, CA, June, 1988.*
21 J.-N. Oung and R. P. Philp, presented at the *ACS National Meeting, Dallas, TX, April, 1989.*
22 A. S. Mackenzie, S. C. Brassell, G. Eglinton and J. R. Maxwell, *Science*, (Washington, D.C.), 217 (1982) 491–504.
23 W. K. Seifert and J. M. Moldowan, *Geochim. Cosmochim. Acta*, 42 (1978) 77–95.
24 G. G. L. Rinaldi, V. M. Leopold and C. B. Koons, in T. F. Yen and J. M. Moldowan (Editors), *Geochemical Markers*, Harwood Academic Publishers, New York, 1988, pp. 331–355.
25 R. P. Philp and T. D. Gilbert, *Org. Geochem.*, 10 (1985) 73–84.
26 C. F. Hoffmann, A. S. Mackenzie, C. A. Lewis, J. R. Maxwell, J. C. Oudin, B. Durand and M. Vandenbroucke, *Chem. Geol.*, 42 (1984) 1–23.

Journal of Chromatography, 550 (1990) 213–237
Elsevier Science Publishers B.V., Amsterdam

CHROMSYMP. 1999

Application of multivariate analysis to the selection of test solutes for characterizing stationary phase selectivity in gas chromatography

THEOPHILUS O. KOLLIE and COLIN F. POOLE*
Department of Chemistry, Wayne State University, Detroit, MI 48202 (U.S.A.)

ABSTRACT

Factors controlling the retention of 28 solutes on 23 stationary phases are identified by multivariate analysis and related to dominant intermolecular interactions. The selectivity of the stationary phases is characterized by the partial molal Gibbs free energy of solution for specific test solutes identified by principal component analysis; nitrobenzene for orientation interactions and *n*-octanol for solvent proton acceptor interactions. No test solute with acceptable certainty was identified for solvent proton donor interactions. The partial molar Gibbs free energy of solution for a methylene group is a convenient parameter for assessing dispersive interactions. For highly cohesive phases, such as OV-275, TCEP, DEGS, QACES and QTAPSO the selectivity parameters were found to be solute-size dependent. This size dependence can be removed by separating the free energy into a cavity term and an interaction term; the interaction term being independent of solute size. Using principal component analysis and cluster analysis the 23 stationary phases were classified into 5 groups based on the similarity of their capacity for specific intermolecular interactions with the phases squalane, QF-1, OV-225, OV-275 and QTAPSO behaving independently. The use of dendrograms is demonstrated to be a useful method for visualizing selectivity differences for chromatographic optimization.

INTRODUCTION

A very large number of liquid phases have been suggested for use in gas–liquid chromatography (GLC), easily exceeding the capability of any laboratory to stock all, or even a large proportion of these phases [1,2]. Among this collection of phases are many materials which simply duplicate the properties of each other or are industrial materials of poorly defined chemical composition. The bewildering number of phases and the non-standard format used to specify their separation properties has done little to aid the selection of a particular phase for a given separation problem. Even when repeating a literature separation the phase specified may not be in the collection of phases used by a particular laboratory, is not a well characterized phase (so that even if purchased it may not adequately reproduce the original separation), or the material may no longer be commercially available. In these cases, a readily available substitute phase of well defined composition would be preferred, if it could be easily identified. Consequently, there is a general need for a classification method that enables stationary phases to be grouped by their similarity, such that a smaller number of phases could be selected for general use that adequately represent the separation characteristics of all available phases. Phases of a high degree of similarity could be

0021-9673/91/$03.50

replaced by a single member of the group with the most favorable chromatographic properties (identification of duplicates) and preferred phases from groups with little similartiy (selective phases) chosen for initial exploration in optimizing a separation. This would minimize the number of phases required for general analysis to, probably, a manageable number, and given the general high efficiency of modern GLC, be quite adequate for most situations. This approach is apparent in the literature usage of fused-silica open tubular columns, although in this case selection is based on the limitations of siloxane synthesis, more so than of fundamental considerations of the type and range of intermolecular forces important in GLC [3].

In fact, numerous methods have been discussed for classifying stationary phases, and are reviewed in detail elsewhere [2–7]. Of these methods the system of stationary phase selectivity constants introduced by Rohrschneider [6] and extended by McReynolds [7] has become the most widely used. Rohrschneider published data for 30 test solutes on 23 stationary phases [8] and McReynolds data for 68 test solutes on 25 stationary phases [9] and 10 test solutes on 226 stationary phases [7]. These data sets have been analyzed by multivariate analysis techniques to determine the minimum number of test solutes required to characterize the retention properties of the stationary phases [10–13] and to classify the stationary phases into groups with similar separation properties [11,14–22]. The application of multivariate analysis to chromatography is reviewed in refs. 12 and 23 and in a wider sense to analytical chemistry in refs. 23–27. These methods of factor analysis, principal component analysis, and cluster analysis are ideally suited to deconvoluting large data sets to reveal common, independent variables and for comparing data subsets by a ranking based on similarity. The data of Rohrschneider and McReynolds are generally given in the form of retention index values or as retention index differences with respect to squalane as a reference phase. Rohrschneider suggested that 5 test solutes [6,8] and McReynolds 10 solutes [7] were required to characterize the solvent properties of the liquid phases as judged by the agreement between the predicted and experimental retention indices. Lowry *et al.* [10] suggested that three solutes chosen from the first five test solutes of McReynolds while Fernandez-Sanchez *et al.* [13] found that seven test solutes from the full set of 10 McReynolds test solutes were adequate to reproduce the retention index values with acceptable accuracy. Although the justification for the identity of the test solutes has generally been associated with particular intermolecular interactions, such as dispersion, induction, orientation, and proton donor–acceptor properties, these studies concluded that the identity of the solute was less important than the number of solutes selected for the evaluation. We believe that the two processes of characterizing the importance of specific intermolecular interactions and reproducing retention index values are different processes, since the attempt to increase the precision of the retention index values results in the addition of more test solutes than is logically needed to express the dominant intermolecular interactions.

Two factors were determined to account for about 98% of the total variance in the McReynolds data matrix by principal component analysis [3,11,15,18]. These axes were stated to be general polarity and hydrogen bonding interactions. It seems illogical that so much of the properties of the data matrix could be represented by just two factors given the general complexity of solute–solvent interactions, and therefore, other reasons must exist for the agreement found. Apart from the Rohrschneider/McReynolds data only one other study has used multivariate analysis techniques to

characterize the solvent properties of a group of common liquid phases [28]. A group of 10 chlorophenoxy acid methyl or pentafluorobenzyl esters on 10 stationary phases was used to identify similarities between phases. In this case the limited choice of test solutes provides little information about the selectivity of the phases in terms of intermolecular interactions.

The problem of identifying the relative contribution of intermolecular interactions to retention in GLC, as we see it, is not related to the choice of data analysis technique, but the unreliability of the data sets used for analysis. The data presentation of Rohrschneider/McReynolds is fundamentally flawed when used for characterizing stationary phase selectivity, in a manner which does not preclude its use for predicting retention index values [4,5,29,30]. The following problems with the McReynolds stationary phase selectivity constants for characterizing stationary phase properties have been identified:

(1) Many of the test solutes are too volatile to provide accurate retention values on a wide range of phases having different polarity. Some solutes elute at, or close to, the column dead volume [30–32].

(2) The method used to calculate retention indices ignores the contribution made by interfacial adsorption. Retention index values vary with the ratio of the stationary phase surface area/bulk volume and those parameters which effect this ratio, for example, coating efficiency, support type, etc. The retention index for polar solutes on non-polar phases depends on the degree of support deactivation. On polar phases the *n*-alkane retention index markers are retained almost exclusively by interfacial adsorption and the retention index values are meaningless [30,31,33–38].

(3) The retention index differences used as phase constants are composite terms the magnitude of which depends on both the retention of the index standards as well as that of the test solutes. Using different retention index standards results in different ranking of the phases by selectivity. The magnitude of the phase constants is determined largely by the retention of the *n*-alkanes on most phases and very good correlations exist between the magnitude of the phase constants and the partial molar Gibbs free energy of solution for a methylene group for a wide range of phases [29,30,35,39].

(4) The experimental data compiled by McReynolds are insufficiently accurate for stationary phase characterization. The stationary phase loading is not accurately determined, a wetting agent was added to each phase at the 2% (w/w) level, and several index values were determined retrospectively using an indirect method (bracketing hydrocarbons were not used) [4].

These problems preclude the further use of the McReynolds data set for evaluating stationary phase interactions. Such a data set, like the original, has many uses in GLC and we have started to generate a new data collection. Unlike those of Rohrschneider and McReynolds the data are standardized in the form of the gas–liquid partition coefficient, corrected for interfacial adsorption, and determined under experimental conditions where gas phase imperfections can be safely neglected [5,32]. Stationary phase selectivity is determined by the magnitude of the partial molal Gibbs free energy of solution for a series of test solutes chosen to express the principal intermolecular interactions. The purpose of this paper is to outline the solute selection procedure using multivariate analysis of the partial molal Gibbs free energy of solution for 28 test solutes on 23 stationary phases.

EXPERIMENTAL

Data for the partial molal Gibbs free energy of solution for the test solutes on the stationary phases identified in Table I were taken from refs. 5, 32, 40 and 41 and are summarized in Table II for the convenience of the reader. All measurements were made at 121.4°C. Multivariate analysis was performed on an Epson Apex 200 computer using Ein*Sight™ version 2.5 (Infometrix, Seattle, WA, U.S.A.) software for data analysis and pattern recognition. The data was entered via a standard spreadsheet program, VP-Planner, version 2.0 (Paperback Software International, Berkeley, CA, U.S.A.). Missing data points were added as follows: for 1,1,2,2-tetrachloroethane on OV-330 the mean, QMES the maximum, QACES the mean and QTAPSO 0.67 of the mean; for dodecafluoroheptanol on QMES the maximum, QACES the mean and QTAPSO 0.5 of the mean; and for 2,4,6-trimethylpyridine on QpTS the maximum (where the mean is the mean of all values for that test solute and the maximum is the

TABLE I

IDENTIFICATION AND ABBREVIATIONS FOR STATIONARY PHASES AND TEST SOLUTES

Stationary phases			Test solutes	
No.	Abbreviation	Name	No.	Name
1	SQ	Squalane	1	Partial molar Gibbs free energy of solution for a methylene group
2	OV-3	Poly(dimethylmethylphenylsiloxane) 10 mol% phenyl groups	2	Benzene
3	OV-7	Poly(dimethylmethylphenylsiloxane) 20 mol% phenyl groups	3	*n*-Butanol
4	OV-11	Poly(dimethylmethylphenylsiloxane) 35 mol% phenyl groups	4	1-Nitropropane
5	OV-17	Poly(methylphenylsiloxane)	5	Pyridine
6	OV-22	Poly(methylphenyldiphenylsiloxane) 65 mol% phenyl groups	6	2-Methyl-2-pentanol
7	OV-25	Poly(methylphenyldiphenylsiloxane) 75 mol% phenyl groups	7	2-Octyne
8	OV-105	Poly(cyanopropylmethyldimethylsiloxane)	8	1,4-Dioxane
9	OV-225	Poly(cyanopropylmethylphenylmethylsiloxane)	9	*cis*-Hydrindane
10	OV-275	Poly(dicyanoallylsiloxane)	10	*n*-Butylbenzene
11	OV-330	Poly(dimethylsiloxane)–Carbowax copolymer	11	1-Nitropentane
12	QF-1	Poly(trifluoropropylmethylsiloxane)	12	Nitrobenzene
13	CW20M	Poly(ethylene glycol)	13	Octanol
14	DEGS	Poly(diethylene glycol succinate)	14	Benzodioxane
15	TCEP	1,2,3-Tris(2-cyanoethoxypropane)	15	Dihexyl ether
16	PPE-5	1,3-Bis(3-phenoxyphenoxy)benzene	16	1-Dodecyne
17	QpTS	Tetra-*n*-butylammonium 4-toluenesulphonate	17	Dodecane
18	QPIC	Tetra-*n*-butylammonium 4-picrate	18	Benzonitrile
19	QMES	Tetra-*n*-butylammonium 4-morpholineethanesulphonate	19	1,1,2,2-Tetrachloroethane
20	QACES	Tetra-*n*-butylammonium 2-(2-acetamido)aminoethane-sulphonate	20	2,4,6-Trimethylpyridine
21	QTAPSO	Tetra-*n*-butylammonium 3-tris(hydroxymethyl)methyl-amino-2-hydroxy-1-propanesulphonate	21	Aniline
22	DDP	Didecylphthalate	22	N-Methylaniline
23	SE-30	Poly(dimethylsiloxane)	23	N,N-Dimethylaniline
			24	2,6-Dimethylaniline
			25	Anisole
			26	Nonanal
			27	2-Octanone
			28	Dodecafluoroheptanol

TABLE II

PARTIAL MOLAL GIBBS FREE ENERGY OF SOLUTION FOR TEST SOLUTES ON 23 STATIONARY PHASES (cal/mol)

	ΔG_k^0 (CH_2)	Dioxane	1-Butanol	Nitro-propane	Nitro-pentane	Nitro-benzene
SQ	−521	−3139	−2708	−3137	−4211	−4416
OV-3	−458	−2976	−2733	−3150	−4078	−4814
OV-7	−467	−3040	−2733	−3253	−4201	−4986
OV-11	−475	−3073	−2688	−3329	−4260	−5117
OV-17	−470	−3104	−2680	−3349	−4275	−5181
OV-22	−458	−3091	−2586	−3337	−4220	−5183
OV-25	−431	−3057	−2777	−3301	−4175	−5175
OV-105	−461	−2919	−2756	−3171	−4097	−4757
OV-225	−418	−3163	−2967	−3778	−4640	−5497
OV-275	−279	−3046	−2890	−3697	−4185	−5257
OV-330	−418	−3284	−3405	−3775	−4613	−5675
QF-1	−390	−2788	−2389	−3467	−4273	−4838
CW20M	−400	−3379	−3533	−3928	−4671	−5914
DEGS	−324	−3275	−3143	−3672	−4306	−5552
TCEP	−291	−3577	−3386	−4127	−4651	−5808
PPE-5	−487	−3420	−2888	−3604	−4578	−5714
QpTS	−377	−3300	−4632	−4319	−5062	−6234
QPIC	−411	−3439	−3439	−4136	−4965	−6049
QMES	−398	−3291	−4736	−4293	−5040	−6209
QACES	−319	−3148	−4351	−4005	−4592	−5909
QTAPSO	−274	−3007	−3809	−3722	−4261	−5576
DDP	−511	−3386	−3312	−3802	−4886	−5779
SE-30	−463	−2899	−2672	−2982	−3914	−4519

	1-Octanol	Benzo-dioxane	Dihexyl ether	Benzene	*n*-Butyl-benzene	*cis*-Hydrin-dane
SQ	−4623	−5497	−6270	−3156	−5201	−5023
OV-3	−4607	−5151	−5475	−2803	−4581	−4313
OV-7	−4643	−5333	−5472	−2814	−4622	−4317
OV-11	−4631	−5484	−5398	−2789	−4621	−4268
OV-17	−4604	−5562	−5314	−2690	−4599	−4216
OV-22	−4471	−5600	−5122	−2748	−4517	−4121
OV-25	−4393	−5630	−5034	−2816	−4497	−4061
OV-105	−4609	−5024	−5374	−2739	−4488	−4200
OV-225	−4771	−5604	−4668	−2691	−4302	−3668
OV-275	−3867	−5305	−2182	−2148	−3107	−2358
OV-330	−5198	−5970	−4958	−2897	−4566	−3968
QF-1	−3988	−4573	−4317	−2262	−3770	−3350
CW20M	−5233	−6185	−4447	−2917	−4396	−3650
DEGS	−4542	−5838	−3240	−2475	−3708	−2807
TCEP	−4611	−5957	−3215	−2703	−3766	−2751
PPE-5	−4933	−6062	−5395	−2979	−4840	−4329
QpTS	−6317	−6205	−4300	−2870	−4291	−3577
QPIC	−5177	−6009	−4407	−2916	−4426	−3654
QMES	−6406	−6172	−4316	−2837	−4267	−3537
QACES	−5738	−5878	−3123	−2543	−3652	−2868
QTAPSO	−5020	−5558	−2995	−2385	−3358	−2635
DDP	−5013	−6043	−6002	−3204	−5177	−3633
SE-30	−4554	−4944	−5468	−2772	−4538	−4332

(Continued on p. 218)

TABLE II *(continued)*

	2-Octyne	1-Dodecyne	2-Methyl-2-pentanol	Dodeca-fluoro-heptanol	Benzo-nitrile	1,1,2,2-Tetra-chloroethane
SQ	−4154	−5942	−3311	−3194	−4455	−4319
OV-3	−3677	−5256	−3023	−3220	−4348	−3968
OV-7	−3691	−5265	−3019	−3220	−4450	−4099
OV-11	−3647	−5206	−2948	−3131	−4639	−4149
OV-17	−3607	−5139	−2895	−2996	−4696	−4169
OV-22	−3526	−4950	−2847	−2969	−4711	−4139
OV-25	−3493	−4950	−2708	−2745	−4701	−4126
OV-105	−3592	−5163	−3042	−3551	−4313	−3932
OV-225	−3150	−4644	−3017	−3997	−5063	−4410
OV-275	−1940	−2439	−2371	−3391	−4897	−4043
OV-330	−3549	−5032	−3343	−4723	−5213	−4331
QF-1	−2703	−4164	−2669	−3417	−4468	−3350
CW20M	−3277	−4764	−3327	−4599	−5473	−5046
DEGS	−2560	−3824	−2946	−4077	−5090	−4449
TCEP	−2587	−3534	−3067	−4175	−5415	−4520
PPE-5	−3699	−5277	−3161	−3168	−5117	−4547
QpTS	−3052	−4703	−4198	−6992	−5791	−5606
QPIC	−2991	−4640	−3308	−4498	−5602	−4671
QMES	−2992	−4723	−4281	−6992	−5761	−5606
QACES	−2369	−3740	−3732	−3767	−5500	−4331
QTAPSO	−2009	−3257	−3323	−1883	−5179	−2902
DDP	−4008	−5829	−3598	−3767	−5267	−4396
SE-30	−3673	−5239	−3009	−3176	−4134	−3826

	Pyridine	2,4,6-Tri-methyl-pyridine	Aniline	N-Methyl-aniline	N,N-Di-methyl-aniline	2,6-Dimethyl-aniline
SQ	−3396	−4784	−4463	−5029	−5286	−5567
OV-3	−3222	−4285	−4282	−4673	−4779	−5131
OV-7	−3222	−4368	−4429	−4821	−4895	−5285
OV-11	−3366	−4416	−4549	−4938	−4984	−5406
OV-17	−3395	−4431	−4616	−4999	−5020	−5468
OV-22	−3457	−4403	−4679	−5035	−5100	−5491
OV-25	−3430	−4397	−4708	−5115	−5044	−5513
OV-105	−3159	−4195	−4281	−4635	−4689	−5079
OV-225	−3546	−4304	−5145	−5319	−5020	−5768
OV-275	−3458	−3566	−5477	−5261	−4506	−5639
OV-330	−3686	−4555	−5530	−5625	−5235	−6052
QF-1	−3071	−3646	−3977	−4264	−4276	−4665
CW20M	−3858	−4551	−5984	−5871	−5250	−6304
DEGS	−3902	−4641	−5637	−5454	−4822	−5938
TCEP	−3951	−4310	−5971	−5768	−5045	−6244
PPE-5	−3676	−4847	−5168	−5537	−5468	−6021
QpTS	−4038	−5361	−6663	−6558	−5166	−6572
QPIC	−3993	−4523	−5998	−6033	−5436	−5447
QMES	−4011	−4270	−6724	−6599	−5148	−6708
QACES	−3862	−3896	−6473	−6230	−4794	−6390
QTAPSO	−3749	−3810	−6012	−5773	−4604	−6019
DDP	−3823	−4329	−5275	−5406	−4979	−5748
SE-30	−3137	−4205	−4117	−4502	−4647	−4945

TABLE II *(continued)*

	Anisole	Nonanal	2-Octanone	Dodecane
SQ	−4364	−5178	−4608	−6025
OV-3	−3978	−4772	−4250	−5122
OV-7	−4062	−4837	−4305	−5060
OV-11	−4126	−4836	−4300	−4925
OV-17	−4150	−4805	−4257	−4800
OV-22	−4158	−4686	−4193	−5016
OV-25	−4156	−4610	−3971	−4438
OV-105	−3900	−4736	−4465	−5041
OV-225	−4149	−4763	−3867	−4006
OV-275	−3714	−3512	−3369	−1216
OV-330	−4396	−4829	−4359	−4354
QF-1	−3490	−4521	−4197	−3913
CW20M	−4484	−4648	−4217	−3816
DEGS	−4103	−4050	−3750	−2168
TCEP	−4284	−4210	−4035	−2188
PPE-5	−4514	−5089	−4555	−4755
QpTS	−4455	−4838	−4371	−3720
QPIC	−4482	−4998	−4640	−3746
QMES	−4434	−4792	−4375	−3695
QACES	−4125	−3630	−3852	−2409
QTAPSO	−3900	−3855	−3588	−2003
DDP	−4169	−4554	−4876	−5565
SE-30	−3879	−4692	−4184	−5187

largest value found for that test solute on all stationary phases). Missing values were caused by poor chromatographic properties such as adsorption at infinite dilution, irregular peak shape, excessive retention, etc., which precluded accurate determination of the partition coefficient. For similar reasons phenol and 2,4,6-trimethylphenol data from ref. 32 were not included in the data set as these test solutes were not eluted from several phases. Tetraethylammonium 4-toluenesulphonate and tri-*n*-butylammonium 4-toluenesulphonate were not included because they failed to elute, or eluted with poor peak shapes, most of the N-heterocyclic bases [32].

RESULTS AND DISCUSSION

The principal intermolecular interactions that take place in solution are dispersion, induction, orientation, and various complexation interactions, of which proton donor–acceptor interactions are the most common. Solutes and solvents show a balance of these interactions; the capacity of a solute or solvent to enter into all intermolecular interactions is characterized by its strength, or polarity, and the ratio of one particular interaction to the strength, is its selectivity. Unfortunately, no solute exhibits a single interaction for all phases, since even *n*-alkanes in a polar solvent will experience inductive as well as dispersive interactions. Those solutes that are most useful for characterizing the complementary interactions in a solvent should have a single, dominant type of interaction expressed against a weak background for other interactions. Intuitively, it would seem likely that one test solute to characterize each of

the principal intermolecular interactions should be sufficient. However, neither the number nor the identity of the test solutes required to characterize the selectivity of GLC phases can be predicted in a straightforward manner. An approach which involves the minimum number of *a priori* assumptions is multivariate analysis. In this case an undefined number of factors can be extracted from the combination of a large number of solute–solvent interactions, which hopefully can be described in terms of primary forces. Those solutes which show the strongest correlation with individual factors can be identified as suitable test solutes for defining the relative importance of a particular retention mechanism. The inverse process is also possible, and the similarity of all retention mechanisms can be used to classify stationary phases into groups with similar separation characteristics.

Since it is impractical to commence any study with the full universe of potential candidate test solutes, we used the published opinions of experts in the field of gas chromatography to preselect the 28 solutes identified in Table I [2,4–14,29–33,42]. The strength of intermolecular interactions for these solutes on 23 stationary phases was determined by the partial molal Gibbs free energy of solution [5,32,40,41]. The range of free energy values for different test solutes is quite large, so to avoid inadvertent weighting of the results by extreme values, the data was scaled, using the autoscale routine in the Ein*Sight programming environment [25–27]. This results in each variable being mean centered with a standard deviation of one. A correlation matrix of the scaled data was then produced to evaluate the relationship between individual variables. A correlation of 0.8 to 1.0 was considered to be a reasonable indication that the variables are correlated, that is, displaying the same retention mechanisms. The variables meeting this test are summarized in Table III for the three cases were it seems reasonable to assign a particular interaction as a dominant interaction. Also included are those test solutes which behave independently. Strong correlations were found for the partial molar Gibbs free energy of solution for a methylene group, ΔG_k^0 (CH_2) and dihexyl ether, dodecane, 2-octyne, 1-dodecyne, *n*-butylbenzene, *cis*-hydrindane and, to a lesser extent, nonanal. It seems reasonable to class these test solutes as dispersive probes with essentially duplicate interactions. Leaving nonanal aside, there is no additional selectivity observed for the unsaturated hydrocarbons compared to those that are fully saturated. This can be seen from the plot of 1-dodecyne against dodecane ($r = 0.97$) in Fig. 1. These test solutes have nearly identical boiling points (difference *ca.* 1.2°C) and differ insignificantly in molecular size. The two phases that are most discordant in the plot OV-275 (10) and QF-1 (12) can be explained without invoking differences in selectivity. In the case of OV-275 the test solutes have extremely small partition coefficients and are not as accurately determined as are the other values used in calculating the data for Fig. 1. QF-1 behaves anomalously for all test solutes. It is the only fluorocarbon phase in the test set and behaves independently for all probes. Fluorocarbon phases have significantly weaker dispersive interactions than hydrocarbon phases resulting in their different behavior [33,38].

The second group of highly correlated test solutes, with one exception, have fairly large dipole moments and it seems reasonable to associate these test solutes with strong orientation interactions. Dioxane would seem to be anomalous within this group and shows the lowest correlation coefficient ($r = 0.81$). Pyridine is another unexpected member of this group based on its use as a probe for stationary phase proton donor capacity. However, it has a large dipole moment (2.25 D) and shows no

TABLE III

SUMMARY OF CORRELATED VALUES ABSTRACTED FROM THE CORRELATION MATRIX

	Correlation coefficient	Dipole moment (D)
Dispersive interactions		
ΔG_k^0 (CH_2)	1.00	
Dihexyl ether	0.98	
Dodecane	0.98	
2-Octyne	0.97	
1-Dodecyne	0.96	
n-Butylbenzene	0.95	
cis-Hydrindane	0.93	
Nonanal	0.83	
Orientation interactions		
Nitrobenzene	1.00	3.97
Benzonitrile	0.99	4.08
Pyridine	0.96	2.25
N-Methylaniline	0.96	1.68
Nitropropane	0.95	3.06
Aniline	0.94	1.53
Nitropentane	0.92	3.52
Benzodioxane	0.91	1.43
2,6-Dimethylaniline	0.88	1.63
Butanol	0.84	1.78
Dioxane	0.81	0.40
Proton donor–acceptor interactions		
Octanol	1.00	1.72
2-Methyl-2-pentanol	0.98	
Butanol	0.89	1.78
N-Methylaniline	0.83	1.68
Solutes behaving independently		
Benzene		0.03–0.1
1,1,2,2-Tetrachloroethane		1.67
2,4,6-Trimethylpyridine		2.26
Dodecafluoroheptanol		
N,N-Dimethylaniline		1.59
2-Octanone		2.46
Anisole		1.25

obvious selectivity for proton donor phases over that of nitrobenzene (Fig. 2). Benzodioxan has also been used as a test solute for stationary phase proton donor capacity but again we find that its behavior is more characteristic of that of the orientation probes [5].

The third class of correlated test solutes is comprised of three alcohols and N-methylaniline, the latter is only weakly correlated with 1-octanol ($r = 0.83$). Both N-methylaniline and butanol are also correlated to nitrobenzene, the former strongly ($r = 0.96$) and the latter weakly ($r = 0.84$). We suspect that N-methylaniline is better considered representative of the orientation probes and butanol that of the proton donor probes. In fact, if the data for 1-butanol and 1-octanol are scrutinized (Fig. 3), there are two general trends that can be discerned. Those phases which are strongly

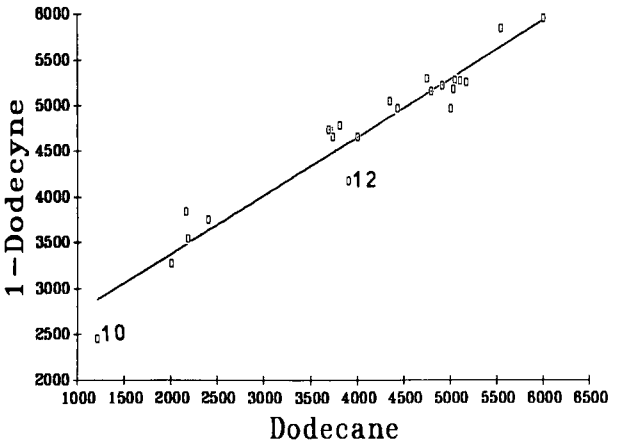

Fig. 1. Plot of the partial molal Gibbs free energy of solution for 1-dodecyne against dodecane for the 23 stationary phases identified in Table I. Phase 10 is OV-275 and 12 is QF-1.

associated (OV-275, DEGS, TCEP, QTAPSO and QACES), form one group with a correlation coefficient of 0.98 (n = 5) displaced from the remaining phases, which have a correlation coefficient of 0.97 (n = 17), QF-1 behaving independently. It seems likely that the reason for the modest correlation between butanol and 1-octanol is due to differences in the cavity term, which is important for solvent with a high degree of cohesion (see later).

The remaining seven solutes in Table III show no strong correlation with other solutes and must be considered as behaving independently. There are several reasons for this. In the case of benzene, weak retention on several phases results in a poor determination of its free energy value causing scatter in the plots against other dispersive probes with which it shows the greatest similarity. 1,1,2,2-Tetrachloro-

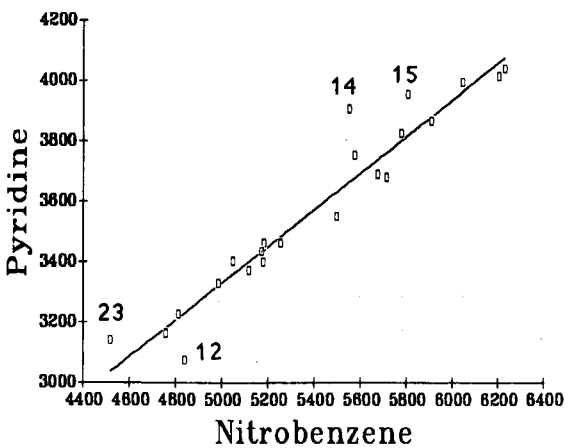

Fig. 2. Plot of the partial molal Gibbs free energy of solution for pyridine against nitrobenzene for the 23 stationary phases identified in Table I. Phase 12 is QF-1, 14 is DEGS, 15 is TCEP and 23 is SE-30.

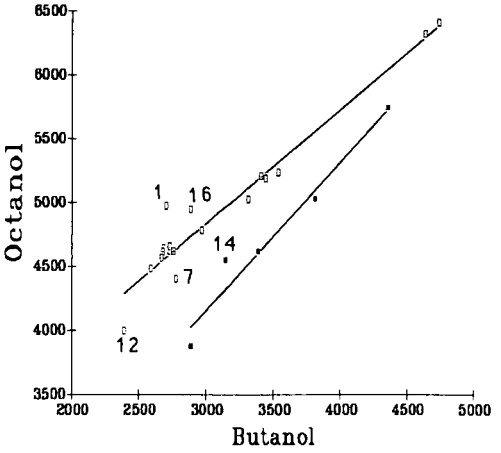

Fig. 3. Plot of the partial molal Gibbs free energy of solution for 1-octanol against 1-butanol for the 23 stationary phases identified in Table I. The strongly associated phases 10, 14, 15, 20 and 21 are displaced and separately correlated from the remaining phases. Phases identified on the figure are: 1 = SQ; 7 = OV-25; 12 = QF-1; 14 = DEGS; 16 = PPE-5.

ethane shows both orientation and proton donor capability, behaving in a mixed mode, and is not useful as a test solute for specific interactions. Dodecafluoroheptanol behaves independently because of the weak dispersive interactions of the fluorocarbon chain compared to hydrocarbon analogs. It is weakly correlated to the other alcohols ($r \approx 0.80$) if only the experimental values are considered (dodecafluoroheptanol was not eluted from all phases and approximate values were added to complete the data matrix, see Experimental). It should be a stronger acid than the alkanols but given the fact that it cannot be eluted successfully from all phases it is not a suitable test solute. 2,4,6-Trimethylpyridine is the most unique test solute and shows no correlation with any of the other solutes, including pyridine. Pyridine and 2,4,6-trimethylpyridine have similar dipole moments, and it was shown earlier that pyridine correlates very strongly with the orientation probes (Fig. 2), making the behavior of 2,4,6-trimethylpyridine the more remarkable. Further studies are required to explain the behavior of 2,4,6-trimethylpyridine. 2-Octanone correlates most strongly with the dispersive probes, with most deviation for the polar phases. 2-Octanone has a reasonable dipole moment (2.46 D), and probably shows mixed behavior, primarily dispersion with some weak orientation capacity. N,N-Dimethylaniline and anisole are most strongly correlated to each other, $r = 0.96$, and then to dioxane and benzodioxane ($r \approx 0.8$). It is likely that these test solutes are retained by a mixed retention mechanism including contributions from orientation and proton acceptor interactions.

To better define the behavior of the test solutes the autoscaled data was subjected to principal component analysis. Eigenvectors were extracted from the data such that the maximum information in the form of variance was preserved with a minimum number of eigenvectors. A summary of the results is presented in Table IV. The first three eigenvectors account for 91.45% of the total variance in the data with additional eigenvectors contributing little further useful information. The results from principal component analysis are usually presented graphically in the form of plots of the

TABLE IV

SUMMARY OF EIGENVECTOR AND PRINCIPAL COMPONENT ANALYSIS OF THE DATA MATRIX

Eigenvector	Eigenvalue	Percent variance	Percent cumulative variance
All 23 phases			
1	13.7783	49.20	49.20
2	10.3634	37.01	86.22
3	1.4652	5.23	91.45
4	0.7272	2.59	94.05
5	0.7088	2.53	96.58
18 Phases (excluding those phases that are highly cohesive)			
1	16.1629	57.72	57.72
2	7.6740	27.40	85.13
3	1.5057	5.37	90.50
4	1.2029	4.29	94.80
5	0.7788	2.78	97.58

TABLE V

SUMMARY OF THE LOADINGS FOR THE FIRST THREE PRINCIPAL COMPONENTS (× 10)

Variable	Loading 1	Variable	Loading 2	Variable	Loading 3
N-Methylaniline	0.2650	Butylbenzene	0.2989	2-Methyl-2-pentanol	0.4202
Benzonitrile	0.2641	Benzene	0.2924	Dioxane	−0.3891
Nitrobenzene	0.2634	1-Dodecyne	0.2913	Octanol	0.3655
Aniline	0.2623	2-Octanone	0.2810	N,N-Dimethylaniline	−0.3397
Pyridine	0.2600	Nonanal	0.2799	Dodecafluoroheptanol	0.3188
Nitropropane	0.2554	2-Octyne	0.2743	Butanol	0.3155
2,6-Dimethylaniline	0.2493	Dihexyl ether	0.2724	Anisole	−0.2396
Butanol	0.2425	ΔG_k^0 (CH_2)	0.2684	Benzodioxane	−0.2350
Benzodioxane	0.2385	Dodecane	0.2648	2,4,6-Trimethylpyridine	−0.1569
Nitropentane	0.2372	*cis*-Hydrindane	0.2611	Pyridine	−0.1329
Octanol	0.2121	2,4,6-Trimethylpyridine	0.2287	2-Octanone	−0.1181
Dioxane	0.2093	N,N-Dimethylaniline	0.2246	Dodecane	0.1171
2-Methyl-2-pentanol	0.1996	Anisole	0.2007	1-Dodecyne	0.0950
Dodecafluoroheptanol	0.1987	1,1,2,2-Tetrachloroethane	0.1416	Dihexyl ether	0.0718
1,1,2,2-Tetrachloroethane	0.1974	2,-Methyl-2-pentanol	0.1142	Nitropentane	0.0710
Anisole	0.1806	Octanol	0.1087	Benzene	−0.0668
N,N-Dimethylaniline	0.1330	Benzodioxane	0.0942	Nitrobenzene	−0.0633
Dodecane	−0.1314	Dioxane	0.0922	1,1,2,2-Tetrachloroethane	0.0420
cis-Hydrindane	−0.1288	Nitropentane	0.0792	*cis*-Hydrindane	0.0394
ΔG_k^0 (CH_2)	−0.1231	Dodecafluoroheptanol	0.0722	ΔG_k^0 (CH_2)	0.0394
Dihexyl ether	−0.1229	Aniline	−0.0586	Nitropropane	0.0357
2-Octyne	−0.1053	Nitropropane	−0.0459	Benzonitrile	−0.0340
2,4,6-Trimethylpyridine	0.0934	Butanol	−0.0204	2,6-Dimethylaniline	−0.0335
1-Dodecyne	−0.0793	Nitrobenzene	−0.0172	N-Methylaniline	−0.0318
Butylbenzene	−0.0605	Benzonitrile	−0.0128	Aniline	0.0290
Nonanal	−0.0441	Pyridine	−0.0023	Butylbenzene	0.0256
Benzene	0.0414	2,6-Dimethylaniline	−0.0006	Nonanal	0.0221
2-Octanone	0.0002	N-Methylaniline	−0.0003	2-Octyne	−0.0136

loadings and scores. The scores for each sample (phase) result from the projection of the sample data vector onto the principal components (eigenvectors that contain information against eigenvectors which represent noise in the data matrix). The principal component loadings are the elements of the principal components used to

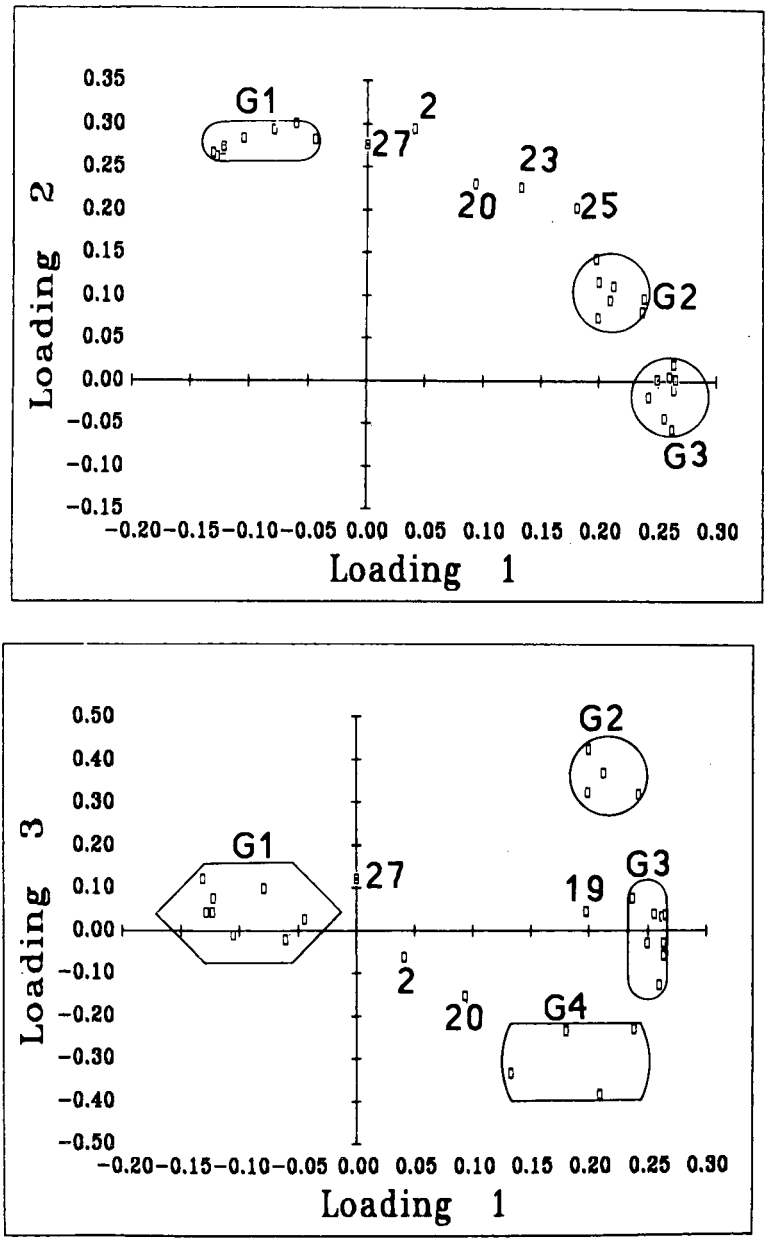

Fig. 4. Principal component plots of loading 1 against loading 2 and loading 3. The compositions of the groups (G) are identified in Tables VI and VII.

produce the scores, equivalent to the coefficients of the linear equation defining the principal components. The loadings describe how much each variable (test solute) contributes to the principal component (retention mechanism). The loadings for the first three principal components are summarized in Table V. The most highly loaded test solutes for loading 1 were previously recognized as orientation interaction probes, those of loading 2 as dispersive interaction probes, and those of loading 3 as proton donor–acceptor probes. The proton donor test solutes are characterized by a positive sign and the proton acceptor probes by a negative sign in the top half of the test solutes showing significant contributions to loading 3.

The plot of loading 1 (orientation) against loading 2 (dispersion) accounts for 86.22% of the cumulative variance (Fig. 4). The test solutes are classified into three reasonably distinct groups (Table VI), with test solutes benzene (2), 2,4,6-trimethylpyridine (20), N,N-dimethylaniline (23), and anisole (25) and 2-octanone (27) behaving independently. The classification of the test solutes into three groups seems intuitively reasonable but some obvious inconsistencies exist. For example, nitropropane and nitropentane are separated into groups 2 and 3, and so are butanol and octanol. Evaluation of the next heavily loaded principal components seem warranted. The plot of loading 1 (orientation) against loading 3 (proton donor–acceptor) is shown in Fig. 4. In this case four distinct groups are obtained (Table VII), with test solutes benzene (2), 1,1,2,2-tetrachloroethane (19), 2,4,6-trimethylpyridine (20) and 2-octanone (27) behaving independently. A more logical classification is obtained than in the previous case with group 1 test solutes containing all the dispersive probes, group 2 the proton donor test solutes, group 3 the orientation test solutes, and group 4 the proton acceptor test solutes. The group 4 test solutes are only diffusely clustered, which we believe is due to the fact that none of these test solutes exhibits a dominant proton acceptor capacity and additional test solutes, not in the current data matrix, will be required to adequately characterize this interaction. This will be the subject of an additional study, still in progress [41].

The plot of loading 1 against loading 4 accounts for almost as much of the cumulative variance (51.79%) as loading 1 against loading 3. However, the three highest weightings in loading 4 are 2,4,6-trimethylpyridine (0.7714), dodecafluoroheptanol (0.3310), and 1,1,2,2-tetrachloroethane (0.3208) which are test solutes showing the most independent behavior. The plot of loading 1 against loading 4 does not provide a good classification of the test solutes. All the dispersive probes are placed

TABLE VI

COMPOSITION OF GROUPS FROM THE CLASSIFICATION OF LOADING 1 *VS.* LOADING 2 (86.22%)

Group 1	*Group 2*	*Group 3*
1 ΔG_k^0 (CH_2)	6 2-Methyl-2-pentanol	3 Butanol
7 2-Octyne	8 Dioxane	4 Nitropropane
9 *cis*-Hydridane	11 Nitropentane	5 Pyridine
10 Butylbenzene	13 Octanol	12 Nitrobenzene
15 Dihexyl ether	14 Benzodioxane	18 Benzonitrile
16 1-Dodecyne	19 1,1,2,2-Tetrachloroethane	21 Aniline
17 Dodecane	28 Dodecafluoroheptanol	22 N-Methylaniline
26 Nonanal		24 2,6-Dimethylaniline

TABLE VII

COMPOSITION OF GROUPS FROM THE CLASSIFICATION OF LOADING 1 *VS.* LOADING 3 (54.43%)

Group 1	*Group 2*	*Group 3*	*Group 4*
1 ΔG_k^0 (CH_2)	3 Butanol	4 Nitropropane	8 Dioxane
7 2-Octyne	6 2-Methyl-2-pentanol	5 Pyridine	14 Benzodioxane
9 *cis*-Hydrindane	13 Octanol	11 Nitropentane	23 N,N-Dimethylaniline
10 Butylbenzene	28 Dodecafluoroheptanol	12 Nitrobenzene	25 Anisole
15 Dihexyl ether		18 Benzonitrile	
16 1-Dodecyne		21 Aniline	
17 Dodecane		22 N-Methylaniline	
26 Nonanal		24 2,6-Dimethylaniline	

into a tight cluster but the other test solutes are diffusely scattered with no distinction between the orientation and proton donor–acceptor probes.

In the same manner that the principal component plots of the loadings can be used to classify the test solutes, the scores plots can be used to classify the stationary phases based on their interactions with the test solutes. The scores for the four most significant principal components are summarized in Table VIII. The plots of score 1

TABLE VIII

PRINCIPAL COMPONENT SCORES FOR THE STATIONARY PHASES

Stationary phase	Scores				
	1	2	3	4	5
SQ	2.7244	−5.0862	0.2340	−0.8955	0.4778
OV-3	4.2911	−0.9711	−0.7349	−0.1927	0.3052
OV-7	3.3734	−1.4512	−0.2678	−0.1016	0.2069
OV-11	2.7235	−1.5169	0.2282	−0.0721	0.1537
PV-17	2.4245	−1.2657	0.5482	−0.0810	0.2145
OV-22	2.3366	−0.9604	0.9207	−0.2380	0.2417
OV-25	2.3235	−0.3772	1.1197	−0.6163	0.5262
OV-105	4.5357	−0.6159	−1.3660	0.2446	0.0533
OV-225	−0.1434	0.2475	0.3363	0.5857	0.2593
OV-275	0.7268	8.3215	0.8761	0.8173	0.4481
OV-330	−1.8062	−1.9728	0.2695	−0.0987	0.0225
QF-1	5.5526	4.0651	−1.7563	1.9843	−0.9096
CW20M	−3.6335	−1.3007	0.8783	0.0059	0.2769
DEGS	−1.6522	3.4658	1.3332	0.2308	1.1153
TCEP	−3.8227	2.7151	1.9583	0.7103	−0.3440
PPE-5	−0.9774	−3.7660	1.9306	−0.2435	−0.0886
QpTS	−7.3026	−2.1742	−1.8558	0.5764	1.5666
QPIC	−3.7661	−1.7816	1.0411	1.2617	−1.0996
QMES	−7.0903	−1.4666	−2.5937	0.2998	0.2683
QACES	−4.2261	3.8981	−1.2826	−1.5986	−0.5227
QTAPSO	−1.0408	6.2594	−0.3463	−2.2583	−0.8852
DDP	−1.10664	−3.8031	−0.2546	0.0281	−2.8139
SE-30	5.5558	−0.4624	−1.2160	−0.3481	0.5274

against score 2, accounting for 86.22% of the total variance, is shown in Fig. 5. Five distinct groups are obtained (Table IX), with squalane (1), OV-225 (9), OV-275 (10), QF-1 (12) and QTAPSO (21) behaving independently. OV-225 is located almost exactly at the cross hairs indicating a balance of interactions while squalane and

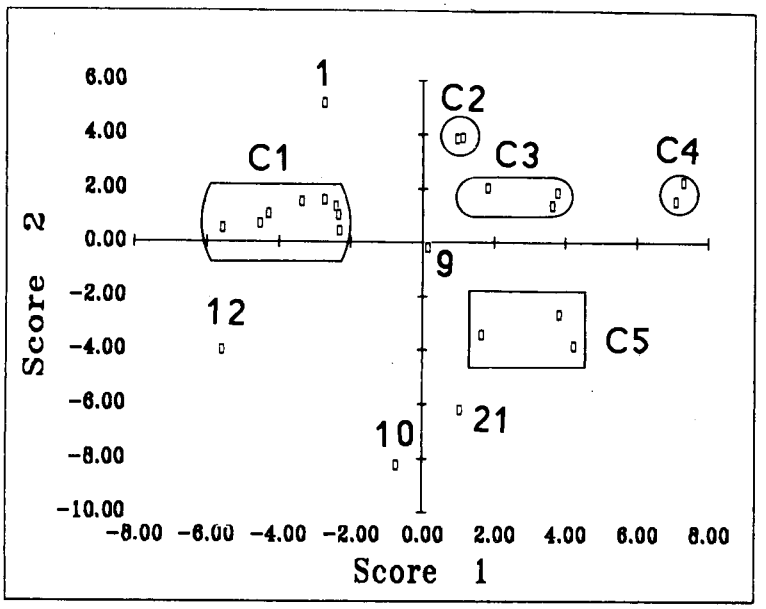

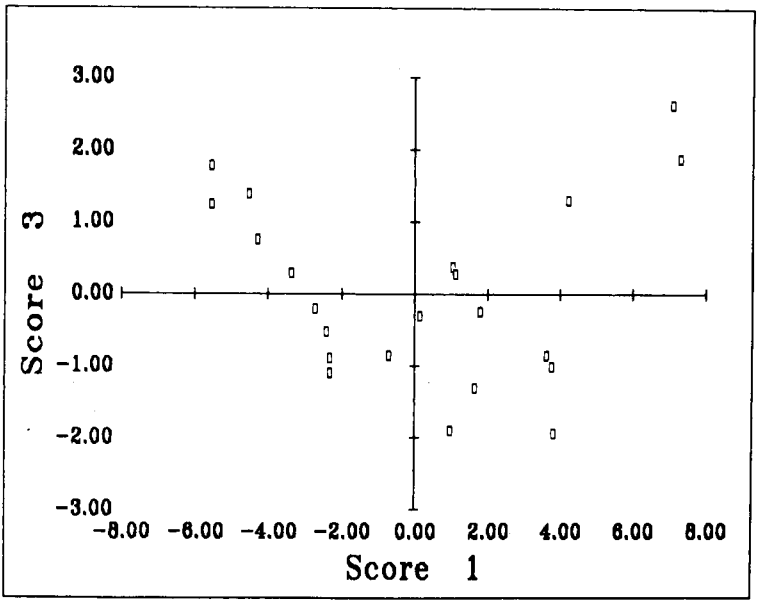

Fig. 5. Principal component plots of score 1 against score 2 and score 3. The composition of the classes (C) is given in Table IX.

TABLE IX

COMPOSITION OF THE GROUPS CLASSIFIED ACCORDING TO SCORE 1 *VS.* SCORE 2 (86.22%)

Class 1	*Class 2*	*Class 3*	*Class 4*	*Class 5*
2 OV-3	16 PPE-5	11 OV-330	17 QpTS	14 DEGS
3 OV-7	22 DDP	13 CW20M	19 QMES	15 TCEP
4 OV-11		18 QPIC		20 QACES
5 OV-17				
6 OV-22				
7 OV-25				
8 OV-105				
23 SE-30				

OV-275 are situated towards opposite edges of the figure indicating high selectivity. Few of the groups are compact indicating a transition of properties within the group. The class 1 phases show variation in both the relative contribution of orientation and dispersion interactions with a logical distribution based on increasing polarity as the mole percent of phenyl groups increases for the poly(methylphenylsiloxane) phases. The class 3 and class 4 phases are separated largely by increasing orientation interactions. The division of phases into the different classes seems to be intuitively correct. The plot of score 1 against score 3, representing 54.43% of the total variance, Fig. 5 does not produce significant clustering of the phases. The phases, as a group, vary substantially in their orientation and proton donor–acceptor capacity with little duplication among phases. The desire to have a wide selection of phases expressing different retention mechanisms to adequately test solute properties seems to have been met in the selection procedure. Score 1 against score 4 (51.79% of the total variance) and 1 against 5 (51.73% of the total variance) are somewhat similar to the results of score 1 against score 3 in that they do not lead to a general grouping of the phases into classes.

An alternative to principal component analysis for classifying samples by multivariate analysis is cluster analysis. For cluster analysis a distance matrix is formed from the original scaled (or unscaled) data matrix. The Euclidean distance between any sample (or groups of samples) to another is used as a measure of how similar the two samples are. The output for clustering algorithms are dendrograms. Ein*Sight supports seven different cluster algorithms (group average, centroid, incremental sum of squares, median, Lance and Williams flexible, single-linkage nearest neighbor, and complete-linkage farthest neighbor), all producing slightly different dendrograms for the 23 phases used in this study. The groupings are the same using farthest neighbor, Lance and Williams flexible, incremental sum of squares, centroid, and group average with only the similarity values varying. The nearest neighbor and median produces some significant differences in the position of phases within groups and intuitively are less satisfactory. Fig. 6 illustrates a dendrogram for the complete-linkage farthest neighbor method, which is representative of the other methods excepting the nearest neighbor and median methods. The phases that are most similar are next to each other and are connected. Connections at the extreme left side of the dendrogram have a similarity of 1, representing duplicates, and those at the extreme right a similarity of

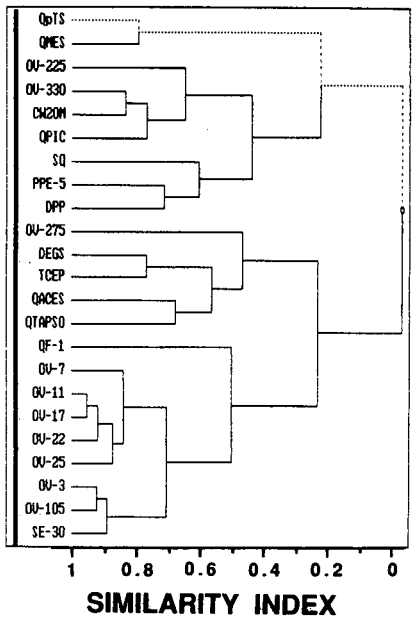

Fig. 6. Similarity of stationary phases using the complete-linkage farthest neighbor dendrogram. Similarity index for connected phases OV-11/OV-17, 0.95; OV-22/OV-25, 0.92; OV-3/OV-7, 0.91; OV-105/SE-30, 0.88; Carbowax 20M/QPIC, 0.80; QpTS/QMES, 0.78; DEGS/TCEP, 0.77; OV-225/OV-330, 0.76; PPE-5/DDP, 0.71; QACES/QTAPSO, 0.68.

zero, and have no features in common. The dendrogram classifies the phases into three basic groups consisting of QpTS, QMES, OV-225, OV-330, CW-20M, QPIC, squalane, PPE-5, and DDP; OV-275, DEGS, TCEP, QACES, QTAPSO; and QF-1, OV-11, OV-17, OV-22, OV-25, OV-3, OV-7, OV-105 and SE-30. Squalane, OV-275 and QF-1 are not connected to any other phase and are behaving independently. The major groups are then divided into subgroups of increasing similarity. A comparison of these subgroups with the classification by principal component analysis using score 1 against score 2 (Table IX) shows very good agreement. The dendrogram is a very useful device for visualizing the relative similarities between phases and for predicting phases likely to show different separation characteristics.

Originally, it was believed that test solutes could be selected by identifying solute types with the desired balance of interactions followed by selecting a homologue of the correct volatility to allow accurate determination of the gas–liquid partition coefficient at the standard measurement temperature. This simple philosophy has one failing. Considering the retention behavior of homologous test solutes in Table I (butanol and octanol, Fig. 3, benzene and *n*-butylbenzene, Fig. 7, and nitropropane and nitropentane, Fig. 8), there are two obvious types of behavior. A small group of phases (OV-275, DEGS, TCEP, QTAPSO and QACES) form a separate correlated group, displaced from the other phases. These phases are highly functionalized and are probably more cohesive than the other phases. They exhibit a marked tendency to repel alkyl groups, such that as the size of the alkyl group increases the gas–liquid partition coefficient increases very little, compared with the other phases. This

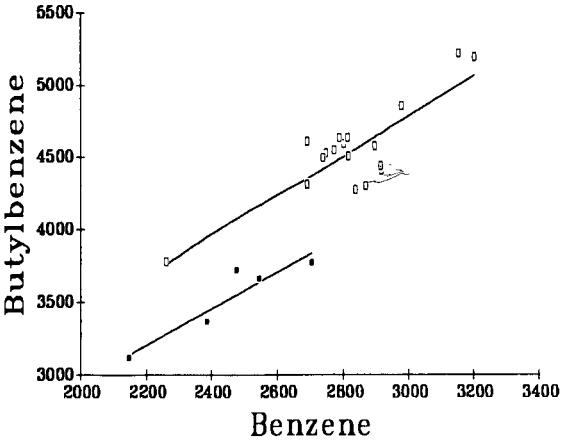

Fig. 7. Plot of the partial molal Gibbs free energy of solution for butylbenzene against benzene for the 23 stationary phases identified in Table I. The strongly associated phases 10, 14, 15, 20 and 21 (■) are displaced and separately correlated (r = 0.95) from the remaining phases (□) (r = 0.85).

difference in behavior is probably accounted for by the difference in the cavity term; the free energy required to separate the solvent molecules to provide a cavity of sufficient size to accommodate the solute molecule. The partial molal Gibbs free energy of solution (soln) for any solute X can be separated into two terms, the cavity term, and the interaction term (int), as shown in eqn. 1

$$(\Delta G_m^0 X)^{soln} = (\Delta G_m^0 X)^{cavity} + (\Delta G_m^0 X)^{int} \quad (1)$$

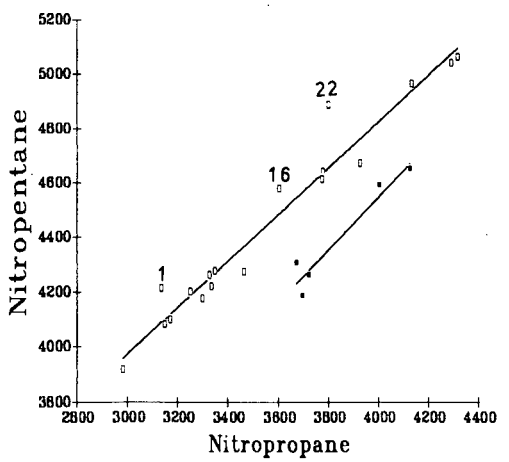

Fig. 8. Plot of the partial molal Gibbs free energy of solution for nitropentane against nitropropane for the 23 stationary phases identified in Table I. The strongly associated phases 10, 14, 15, 20 and 21 (■) are displaced and separately correlated (r = 0.96) from the remaining phases (□) (r = 0.98). Phases identified on the figure: 1 = SQ; 16 = PPE-5; 22 = DDP.

The cavity term is difficult to evaluate by itself, but the cavity term combined with the non-polar interaction term can be expressed by the free energy required to dissolve an *n*-alkane of the same size as the test solute. The interaction term now represents only polar interactions and the additional component of the free energy inadequately accounted for by using the *n*-alkane as a molecular model for the test solute. For example, pentane can be used for butanol and nonane for octanol. If $(\Delta G_m^0 X)^{int}$ for octanol is plotted against that for butanol (Fig. 9), all phases are now found to fall on the same line ($r = 0.99$) with a slope of 1.03 and a near zero intercept (-6.50). These results indicate that the polar interactions for butanol and octanol are essentially identical and independent of the molecular weight of the test solute.

In terms of estimating the capacity of a stationary phase for a particular interaction $(\Delta G_m^0 X)^{int}$ would seem to be attractive because of its clear definition. However, although physically elegant, it ignores the practice of chromatography in which solutes of different size will be routinely present in most separations. For those phases that are highly cohesive a lack of solubility of the alkyl group has just as much impact on their chromatographic properties, compared to other phases, as the strength of the polar interactions themselves. To predict the capacity of a solvent for specific intermolecular interactions a scale based on $(\Delta G_m^0 X)^{int}$ seems to be a logical next step, but to predict retention or relative retention a more complex expression that includes the influence of molecular size would be needed.

The highly cohesive phases (OV-275, DEGS, TCEP, QTAPSO and QACES) could be considered as a special case and removed from the data matrix. There is a danger in doing this in that it removes a group of phases that are generally considered among the most selective by chromatographers. Those that remain are fairly representative of orientation interactions, and the liquid organic salts are known to possess strong proton acceptor capacity, but there are probably no strong proton donor phases remaining in the matrix. The data matrix consisting of 28 solutes on 18 phases, excluding those that are highly cohesive, was reanalyzed by multivariate analysis to establish whether the conclusions reached previously are equally applicable

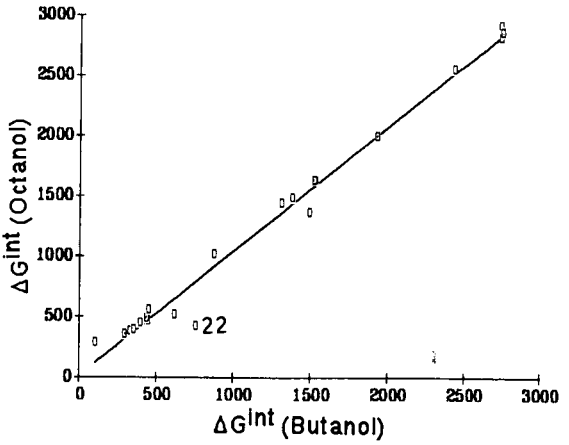

Fig. 9. Plot of the partial molal Gibbs free energy of interaction for octanol against butanol for the 23 stationary phases identified in Table I. Phase 22 is DDP.

in the absence of the highly associated phases. We will discuss this data in summary form only. There are some significant changes in the correlation matrix (Table X), compared to Table III. The dispersive probes remain well correlated except for *cis*-hydrindane, which is weakly correlated to the other test solutes in this group ($r \approx 0.8$), but otherwise could be considered to behave independently. The orientation probes remain highly correlated and likewise the proton donor solutes. However, there is now far more mixing of properties with both groups containing mainly the same test solutes with a different order of the correlation coefficients. Dodecafluoroheptanol is now well correlated to the other alcohols and 1,1,2,2-tetrachloroethane is well correlated to both the orientation and proton donor solutes. Nonanal now behaves independently and seem to have been largely decoupled from the dispersive test solutes by removal of the strongly cohesive stationary phases. Principal component analysis indicates that a greater proportion of the variance is accounted for by component 1 largely at the expense of component 2 (see Table IV). The coefficients for the loading plot remain highly weighted towards loading 1 as an orientation axis and loading 2 as a dispersion axis. Loadings 3 and 5 are now heavily weighted towards solutes that behave independently followed by solutes that are not ranked according to any expectations based on physical interactions. Loading 4 is now weighted towards proton donor–acceptor probes but not as dominantly as was loading 3 for the complete data set (Table V). The plot of loading 1 against loading 2 (Fig. 10) now provides a more obvious grouping of the test solutes than was the case for the full data set (Table VI). The group 1 solutes remain the same except that nonanal is now removed and clustered instead with 2-octanone. The proton acceptor solutes (dioxane, benzodioxane, anisole, N,N-dimethylaniline, and 2,4,6-trimethylpyridine) are now clustered into a single group. The other test solutes, except for benzene (10) are clustered into a third group consisting of the proton donor and orientation probes. The next two significant principal components 1 *vs.* 3 and 1 *vs.* 4 produce scatter plots. With the reduced data set there is a poor ability to differentiate between orientation and proton donor solutes. The scores plot of component 1 *vs.* 2 retains the original classification of stationary phases (Table IX) (Fig. 10). The scores plots of 1 *vs.* 3 and 1 *vs.* 4 are scatter plots. Removing those phases that are highly cohesive from the data matrix has primarily effected the classification of the proton donor and orientation test solutes but not the classification of phases. It is likely that at least in part, this is due to the fact that the highly cohesive phases represented the principal examples of strong proton donor–acceptor phases in the data set.

Certain general conclusions can be reached from the data presented in this work. The magnitude of the partial molal Gibbs free energy of solution for specific test solutes can be used to characterize the selectivity of stationary phases that are not highly cohesive. Since many of the test solutes are highly correlated several compounds could be identified as acceptable for this purpose. Based on experience and chromatographic behavior we suggest that the partial molar Gibbs free energy of solution for the methylene group (formally equivalent to the molal free energy since it is calculated by difference and the solvent standard state is self cancelling) be used as a measure of dispersion interactions (which must be augmented by weak induction interactions for polar phases), that nitrobenzene is a suitable test solute for orientation interactions, and that octanol is a suitable test solute for solvent proton acceptor interactions. There is less convincing evidence that any of the test solutes are

TABLE X

SUMMARY OF CORRELATED VALUES ABSTRACTED FROM THE CORRELATION MATRIX FOR 18 PHASES

	Correlation coefficient
Dispersive interactions	
ΔG_k^0 (CH_2)	1.00
Dihexyl ether	0.97
Dodecane	0.94
2-Octyne	0.92
1-Dodecyne	0.91
n-Butylbenzene	0.87
Orientation interactions	
Nitrobenzene	1.00
Benzonitrile	0.99
Pyridine	0.98
Nitropentane	0.97
Aniline	0.96
N-Methylaniline	0.96
Nitropropane	0.95
Dioxane	0.89
2,6-Dimethylaniline	0.88
1,1,2,2-Tetrachloroethane	0.88
Butanol	0.84
Octanol	0.82
Proton donor–acceptor interactions	
Octanol	1.00
Butanol	0.97
2-Methyl-2-pentanol	0.97
Dodecafluoroheptanol	0.93
N-Methylaniline	0.92
Aniline	0.91
2,6-Dimethylaniline	0.88
Pyridine	0.84
Benzonitrile	0.82
Nitrobenzene	0.82
Nitropropane	0.80
Nitropentane	0.80
Solutes behaving independently	
Benzene	
cis-Hydrindane	
2,4,6-Trimethylpyridine	
2-Octanone	
Nonanal	

acceptable for assessing solvent proton donor capacity. For highly cohesive stationary phases, which include OV-275, DEGS, TCEP, QTAPSO and QACES, the partial molal Gibbs free energy of solution for the above test solutes, by itself, is not a good method of classification since its magnitude is dependent on the size of the test solutes in a way that is not correlated with the behavior of less cohesive phases. A more logical classification in terms of solution interactions is obtained by dividing the free energy

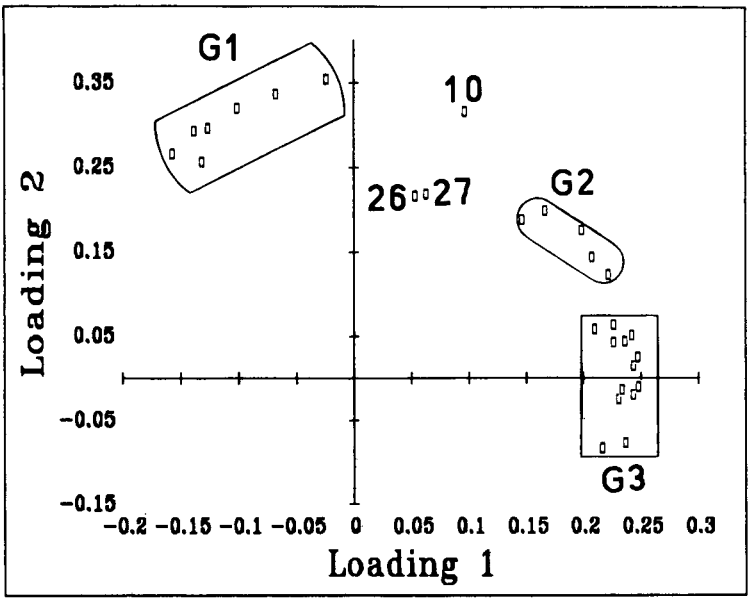

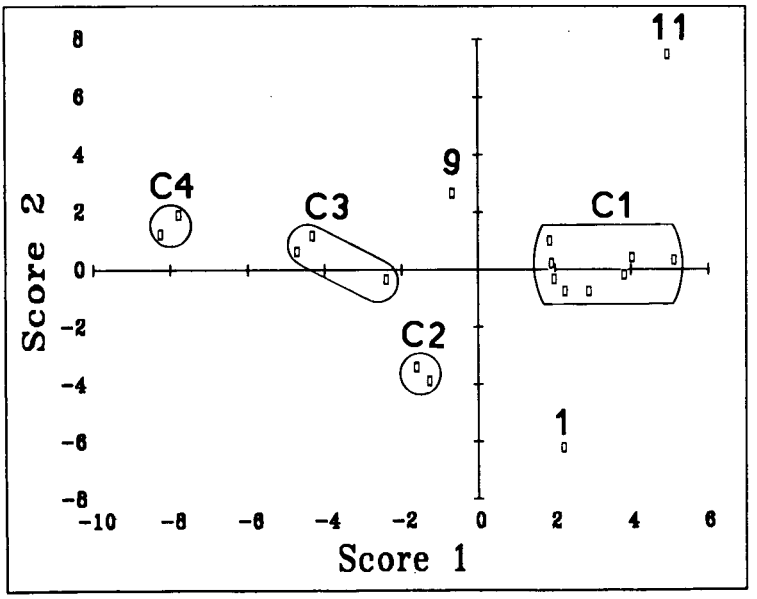

Fig. 10. Plot of loading 1 against 2 and score 1 against 2 for the 18 stationary phases identified in Table I excluding the highly associated phases 10, 14, 15, 20 and 21. See text for the composition of the identified classes (C).

term into a cavity/dispersion term and an interaction term. One method that can be used to determine the cavity/dispersion term is to represent it by the free energy required to accommodate an *n*-alkane of the same size as the test solute. This is not the

only, or necessarily the best solution to the problem [43,44]. Further studies are required to resolve this issue. The collection of test solutes combined with principal component analysis and cluster analysis provides a reasonable method for classifying stationary phases by their similarity of capacity to enter into specific intermolecular interactions. The data matrix is not sufficiently large to warrant the recommendation of a group of preferred phases but does provide useful insight into the selection of phases for initial trial separations based on maximizing the difference in chromatographic selectivity.

ACKNOWLEDGEMENTS

Acknowledgement is made to the donors of the Petroleum Research Fund administered by the American Chemical Society for support of this research. The interest in this project and a gift of OV phases by A. A. Mendicino of Ohio Valley Specialty Chemical are also gratefully acknowledged.

REFERENCES

1 G. E. Baiulescu and V. A. Ilie, *Stationary Phases in Gas Chromatography*, Pergamon Press, New York, 1975.
2 J. A. Yancey, *J. Chromatogr. Sci.*, 24 (1986) 117.
3 T. J. Stark, P. A. Larson and R. D. Dandeneau, *J. Chromatogr.*, 279 (1983) 31.
4 C. F. Poole and S. K. Poole, *Chem. Rev.*, 89 (1989) 377.
5 S. K. Poole and C. F. Poole, *J. Chromatogr.*, 500 (1990) 329.
6 L. Rohrschneider, *Adv. Chromatogr.*, 4 (1967) 333.
7 W. O. McReynolds, *J. Chromatogr. Sci.*, 8 (1970) 685.
8 L. Rohrschneider, *J. Chromatogr.*, 22 (1966) 6.
9 W. O. McReynolds, *Gas Chromatographic Retention Data*, Preston, Evanston, IL, 1966.
10 S. R. Lowry, S. Tsuge, J. J. Leary and T. L. Isenhour, *J. Chromatogr. Sci.*, 12 (1974) 124.
11 M. Chastrette, *J. Chromatogr. Sci.*, 14 (1976) 357.
12 D. L. Massart and H. L. O. De Clercq, *Adv. Chromatogr.*, 16 (1978) 75.
13 E. Fernandez-Sanchez, J. A. Garcia-Dominguez, V. Menendez, J. M. Santiuste and E. Pertierra-Rimada, *J. Chromatogr.*, 402 (1987) 318.
14 J. J. Leary, J. B. Justice, S. Tsuge, S. R. Lowry and T. L. Isenhour, *J. Chromatogr. Sci.*, 11 (1973) 201.
15 S. Wold and K. Anderson, *J. Chromatogr.*, 80 (1973) 43.
16 D. L. Massart, P. Lenders and M. Lauwereys, *J. Chromatogr. Sci.*, 12 (1974) 617.
17 S. Wold, *J. Chromatogr. Sci.*, 13 (1975) 525.
18 D. H. McCloskey and S. J. Hawkes, *J. Chromatogr. Sci.*, 13 (1975) 1.
19 S. R. Lowry, G. L. Ritter, H. B. Woodruff and T. L. Isenhour, *J. Chromatogr. Sci.*, 14 (1976) 126.
20 L. V. Semenchenko and M. S. Vigdergauz, *J. Chromatogr.*, 245 (1982) 177.
21 J. F. K. Huber and G. Reich, *J. Chromatogr.*, 294 (1984) 15.
22 J. A. Garcia-Dominguez, J. Garcia-Munoz, V. Menendez, M. J. Molera and J. M. Santiuste, *J. Chromatogr.*, 393 (1987) 209.
23 E. R. Malinowski and D. G. Howery, *Factor Analysis in Chromatography*, Wiley, New York, 1980.
24 D. L. Massart and L. Kaufman, *The Interpretation of Analytical Chemical Data by the Use of Cluster Analysis*, Wiley, New York, 1983.
25 M. A. Sharaf, D. L. Illman and B. R. Kowalski, *Chemometrics*, Wiley, New York, 1986.
26 O. Strouf, *Chemical Pattern Recognition*, Wiley, New York, 1986.
27 D. L. Massart, B. G. M. Vandeginste, S. N. Deming, Y. Michotte and L. Kaufman, *Chemometrics: A Textbook*, Elsevier, Amsterdam, 1988.
28 J. O. De Beer and A. M. Hyndrickx, *J. Chromatogr.*, 235 (1982) 337.
29 S. K. Poole, B. R. Kersten and C. F. Poole, *J. Chromatogr.*, 471 (1989) 91.
30 B. R. Kersten, C. F. Poole and K. G. Furton, *J. Chromatogr.*, 411 (1987) 43.

31 B. R. Kersten and C. F. Poole, *J. Chromatogr.*, 452 (1988) 191.
32 B. R. Kersten, S. K. Poole and C. F. Poole, *J. Chromatogr.*, 468 (1989) 235.
33 R. M. Pomaville and C. F. Poole, *Anal. Chim. Acta*, 200 (1987) 151.
34 B. R. Kersten and C. F. Poole, *J. Chromatogr.*, 399 (1987) 1.
35 R. M. Pomaville and C. F. Poole, *Anal. Chem.*, 60 (1988) 1103.
36 R. M. Pomaville, S. K. Poole, L. J. Davis and C. F. Poole, *J. Chromatogr.*, 438 (1988) 1.
37 S. K. Poole, K. G. Furton and C. F. Poole, *J. Chromatogr. Sci.*, 26 (1988) 67.
38 R. M. Pomaville and C. F. Poole, *J. Chromatogr.*, 468 (1989) 261.
39 C. F. Poole, S. K. Poole, R. M. Pomaville and B. R. Kersten, *J. High Resolut. Chromatogr. Chromatogr. Commun.*, 10 (1987) 670.
40 C. F. Poole, R. M. Pomaville and T. A. Dean, *Anal. Chim. Acta*, 225 (1989) 193.
41 T. O. Kollie and C. F. Poole, unpublished results.
42 A. Hartkopf, S. Grunfeld and R. Delumyea, *J. Chromatogr. Sci.*, 12 (1974) 119.
43 M. H. Abraham and J. C. McGowan, *Chromatographia*, 23 (1987) 243.
44 M. H. Abraham, P. L. Grellier, I. Hamerton, R. A. McGill, D. V. Prior and G. S. Whiting, *Faraday Discuss. Chem. Soc.*, 85 (1988) 107.

Journal of Chromatography, 550 (1991) 239–245
Elsevier Science Publishers B.V., Amsterdam

CHROMSYMP. 2249

Diurnal changes in plasma levels of 2-pyrrolidinone determined by isotope dilution mass spectrometry

GITA A. VAN DEN BERG*[a], BERT G. WOLTHERS, GIJS T. NAGEL and FRITS A. J. MUSKIET
Central Laboratory for Clinical Chemistry, University Hospital, P.O. Box 30.001, 9700 RB Groningen (Netherlands)
SHARON BANGHMAN[b]
Whitby Research Inc., Richmond, VA 23220 (USA)
and
ROKUS A. DE ZEEUW
Department of Toxicology, University Centre for Pharmacy, A. Deusinglaan 2, 9713 AW Groningen (Netherlands)

ABSTRACT

A new capillary gas chromatographic method with mass spectrometric detection for the determination of 2-pyrrolidinone was developed. Using quantification based on stable isotope dilution mass spectrometry by monitoring selected ions in the ammonia chemical ionization mode diurnal changes of 2-pyrrolidinone levels in plasma of three healthy adults were established. Although substantial fluctuations, ranging from 5 to 30 μg/l, occurred during a 24-h daytime period, no consistent picture related to clock time or food intake was obtained. Endogenous oscillations should be taken into consideration, for example when evaluating transdermal penetration of 2-pyrrolidinone, used as enhancer in topical drug formulation.

INTRODUCTION

2-Pyrrolidinone is a normal constituent of human plasma [1,2]. As it is formed from putrescine by rat liver homogenates [3,4], it is considered to originate from polyamine catabolism. Theoretically, it may also originate from the neurotransmitter γ-aminobutyric acid (GABA) by lactamisation. Conversion of 2-pyrrolidinone to GABA in mouse brain [5] and rat tissue [6] endorses a possible relationship between GABA and its lactam. Pharmacotherapeutically, 2-pyrrolidinone is used as a penetration enhancer for active ingredients in topical drug formulations to obtain rapid onset and sustained duration of action [7].

Several methods have been described for the quantification of 2-pyrrolidinone in plasma [1,2] and tissue homogenates [1,2,5]. These include pre-purification by

[a] Present address: Laboratory for Clinical Chemistry, P.O. Box 850, 8901 BR Leeuwarden, Netherlands.
[b] Present address: Genentech, Inc., San Francisco, CA 94080, USA.

0021-9673/91/$03.50

solvent extraction [1,2,4] or ion-exchange chromatography [5] and analyses, with [2,5] or without [1,4] previous hydrolysis to GABA, by high-performance liquid chromatography with spectrophotometric [4] or fluorometric [2] detection, and mass fragmentography [1,5].

When studying potential (side) effects of administered 2-pyrrolidinone and the extent and duration of action of 2-pyrrolidinone as a permeation enhancer of the human skin, it is obviously of importance to have knowledge of its plasma concentrations. In such studies endogenous plasma concentrations and notably its possible diurnal variation should be taken into account, as the expected increase during treatment is low and circadian rhythmicities in urinary excretion of polyamine conjugates [8] and metabolites [9] have been reported.

In our hands the previously reported isotope dilution mass fragmentographic method [1] of the N-trimethylsilyl derivative of 2-pyrrolidinone in plasma lacked the required sensitivity to reach plasma levels down to the low μg/l range that were anticipated. We therefore developed a new isotope dilution mass fragmentographic method in which 2-pyrrolidinone is converted in the N-heptafluorobutyryl-isopropyl ester derivative of GABA and analysed by monitoring the $[M+NH_4]^+$ ion in the ammonia chemical ionization mode. The method is applied for the study of diurnal variation in three healthy volunteers.

EXPERIMENTAL

Standards and reagents

2-Pyrrolidinone was obtained from Aldrich Europe (Beerse, Belgium) and 2,2,3,3,4,4-hexadeutero-γ-aminobutyric acid lactam (hexadeuterated 2-pyrrolidinone, 2-pyrrolidinone-d_6) from MSD Isotopes (Montreal, Canada). Heptafluorobutyric anhydride was from Pierce (Rockford, IL, USA) and Carbowax 1000M from Chrompack (Middelburg, The Netherlands). All other reagents were from Merck (Darmstadt, Germany) and were of analytical grade.

Study design

Three apparently healthy volunteers (two males and one female) took part in this study. They underwent extensive pre- and post-study medical checkups and gave their written informed consent. Venous blood samples were drawn in heparinised tubes from each subject at the following times: 08:00, 08:15, 08:30, 09:00, 10:00, 12:00, 14:00, 16:00, 20:00 and 08:00 (next morning). The plasma was isolated by immediate centrifugation at 800 *g*, 4°C for 10 min. The subjects received the same light breakfast (immediately after the first sample was taken at 08:00 h), hot lunch (at 13:00 h) and supper (at 19:00 h). Unlimited consumption of non-alcoholic beverages was permitted during the study. The final blood sample was taken just before breakfast.

Preparation of standard solutions

Stock solutions of 1.25 g/l 2-pyrrolidinone and 2-pyrrolidinone-d_6 in methanol were prepared. Dilutions of the stock solutions in 0.1 mol/l HCl solution resulted in a standard working solution with a final concentration of 62.5 μg/l 2-pyrrolidinone and an internal standard working solution with a final concentration of 125 μg/l 2-pyrrolidinone-d_6, respectively. Histamine was added to the internal standard and standard

working solutions as a carrier [2-pyrrolidinone-d_6/histamine ratio (mol/mol): 1:50; 2-pyrrolidinone/histamine ratio (mol/mol): 1:3.7, respectively].

Isolation and derivatization

To 0.5 ml of plasma were added 25 ng of 2-pyrrolidinone-d_6 (200 μl of the internal standard working solution, see above). After equilibration at room temperature for 30 min, the sample was mixed with 1 ml of sodium borate buffer (50 mmol/l, pH 9.0). The pH was adjusted to 9.0 by adding about three drops of 4 mol/l NaOH. 2-Pyrrolidinone and 2-pyrrolidinone-d_6 were extracted into 7 ml of dichloromethane by gently shaking for 30 min on a GLF shaker (Salm and Kipp, Breukelen, Netherlands) to avoid denaturation of proteins. The dichloromethane (lower) layer was isolated, dried by the addition of a small amount of anhydrous sodium sulphate, and subsequently evaporated to dryness at room temperature under a stream of nitrogen. Since 2-pyrrolidinone is relatively volatile, it is important to discontinue evaporation as soon as the solvent has disappeared. The residue was dissolved in 1 ml of isopropanol–HCl solution (freshly prepared by carefully adding 10 ml of acetyl-chloride to 100 ml of mechanically stirred distilled isopropanol). Conversion into the isopropyl ester of GABA was performed by heating the tightly capped tubes at 80°C for 8 h. After cooling to room temperature 1 ml of distilled water was added. The mixture was extracted with 6 ml of dichloromethane. A 900-μl aliquot of the aqueous (upper) layer was transferred to a 7-ml teflar-sealable tube and evaporated to dryness at 45°C under a stream of nitrogen. For conversion into the *N*-heptafluorobutyryl-isopropyl ester of GABA, 100 μl each of distilled acetonitrile and heptafluorobutyric anhydride were added. After heating for 30 min at 60°C the solution was evaporated to dryness at room temperature under a stream of nitrogen. The residue was dissolved in 25 μl of ethyl acetate containing 2 g/l Carbowax 1000M. A 4-μl aliquot was analysed by gas chromatography with mass spectrometric detection.

Mass spectrometry

Gas chromatography–mass spectrometry was performed with a Model 5890 gas chromatograph (Hewlett-Packard, Amstelveen, Netherlands) directly coupled to a VG Analytical 70-250 S mass spectrometer (Manchester, UK) and operated under the following conditions: mass spectrometer resolution, $M/\Delta M$, 1000; injector temperature, 250°C; splitless injection mode; helium flow-rate , 0.5 ml/min; oven temperature programme, 80°C, 15°C/min to 140°C, 5°C/min to 160°C, 30°C/min to 250°C; ammonia chemical ionization mode; ion source temperature, 150°C; ionization energy, 150 eV. The column was a 25 m × 0.2 mm I.D. CP Sil-19 CB (film thickness 0.11 μm) fused-silica capillary (Chrompak). The ions at m/z 359 and 365, corresponding to the $[M+NH_4]^+$ ions of the *N*-heptabutyryl-isopropyl ester derivatives of GABA and GABA-d_6, respectively, were monitored.

Quantification and quality control

The peak-area ratio of the ions at m/z 359 and 365 at the correct retention time was calculated using the VG Analytical 11-250 I data system. Concentrations were computed by means of linear regression analysis using a calibration graph, composed of the corresponding peak-area ratios of various amounts of 2-pyrrolidinone (0–37.5 ng) added to a fixed amount (25 ng) of its deuterated analogue and subjected to the same extraction and derivatisation procedure as described above.

For quality control, we analysed in each series a 0.5-ml aliquot of a pooled serum sample, together with the same aliquot enriched with 12.5 ng of 2-pyrrolidinone (200 μl of the standard working solution, see above).

RESULTS AND DISCUSSION

Methodology and quality control

As, in general, the selectivity of mass fragmentographic assays of low-molecular-weight compounds increases with the selection of ions with increasing m/z, the isolated 2-pyrrolidinone (m/z of the $[M + NH_4]^+$ ion = 103) was subsequently converted into the N-heptafluorobutyryl-isopropyl ester of GABA (m/z of the $[M + NH_4]^+$ ion = 359). Fig. 1 shows the ammonia chemical ionization mass spectra of the *N*-heptafluorobutyryl-isopropyl ester derivatives of GABA (top) and its hexadeuterated analogue (bottom), resulting from their respective 2-pyrrolidinones. The most prominent peaks at m/z 359 and 365, corresponding to their $[M + NH_4]^+$ ions, account for about 30% of the total ion current and proved suitable for selected ion monitoring.

Derivatisation of 2-pyrrolidinone results to some extent in exchange of one or two deuterium atoms for hydrogen atoms. The amount of the hexadeuterated compound was about 89% of the sum of the intensities of the ions at m/z 365, 364 and 363, corresponding to hexa-, penta- and tetradeuterated GABA, respectively. As the purity of the deuterium used in the synthesis of 2-pyrrolidinone-d_6, was 98.5%, the calculated amount of the hexadeuterated compound was 91.3%. In each series the percentage of the hexadeuterated derivative of 2-pyrrolidinone was checked by additional monitoring at m/z 364 (penta) and 363 (tetra) and was shown to be consistent.

Separation between the relatively apolar 2-pyrrolidinone and polar GABA was achieved by selective extraction of the former into dichloromethane at pH 9.0. Addition of GABA up to 3 μg/ml in plasma did not result in increased plasma values for 2-pyrrolidinone with the present method.

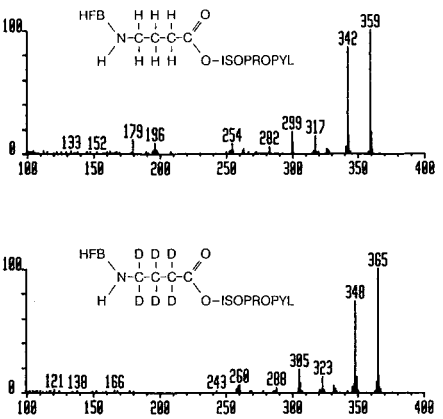

Fig. 1. Ammonia chemical ionization mass spectra of the N-heptafluorobutyryl-isopropyl ester derivatives of GABA and its hexadeuterated analogue, resulting from 2-pyrrolidinone (top) and hexadeuterated 2-pyrrolidinone (bottom), respectively. D = Deuterium.

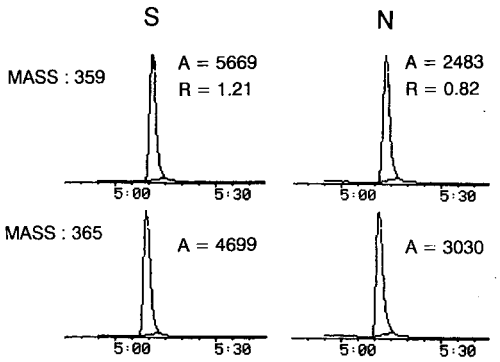

Fig. 2. Mass fragmentograms of the N-heptafluorobutyryl-isopropyl ester derivatives of GABA (*m/z* 359) and its hexadeuterated analogue (*m/z* 365), resulting from 2-pyrrolidinone and hexadeuterated 2-pyrrolidinone, respectively, in a standard (S) containing a mixture of 12.5 ng 2-pyrrolidinone and 25 ng 2-pyrrolidinone-d_6, and a plasma sample of a healthy adult (N) with a concentration of 12.4 μg/l. Time scale in minutes. A, peak area in arbitrary units (counts); R, peak-area ratio of the ions at *m/z* 359 and 365. Time scale in min:s.

Plastic materials may give rise to contamination with 2-pyrrolidinone [1]. Therefore, glass vessels and tubes were used for the storage of all chemicals and standards. All procedures were performed in glassware. However, 2-pyrrolidinone exhibits the peculiar property of adsorption onto silica at neutral and alkaline pH. Therefore, histamine, showing the same property [10], was added to the internal standard solution as a carrier to minimize losses of endogenous 2-pyrrolidinone and its stable isotopically labelled internal standard by this process.

For plasma samples a post-esterification clean-up procedure (*i.e.* extraction with dichloromethane, see Experimental) proved necessary to remove apolar substances that gave rise to interference with naturally occurring 2-pyrrolidinone at *m/z* 359.

Fig. 2 shows mass fragmentograms of 2-pyrrolidinone and its deuterated internal standard for a standard and a plasma sample of a healthy adult.

Table I gives the within- and between-series quality-control data for the endogenous concentration of 2-pyrrolidinone in a pooled serum, together with results of analytical recovery studies. The detection limit for this method (peak/background ratio = 6:1) is about 2 μg/l 2-pyrrolidinone in plasma.

TABLE I

WITHIN- AND BETWEEN-SERIES PRECISION AND RECOVERY FOR DETERMINATION OF 2-PYRROLIDINONE IN POOLED SERUM FROM ADULTS

	n	Concentration (μg/l) (mean ± S.D.)		Recovery (%) (mean ± S.D.)	
Within series	6	18.2	1.1	94.3	4.5
Between series	8	17.4	3.1	102.4	7.3

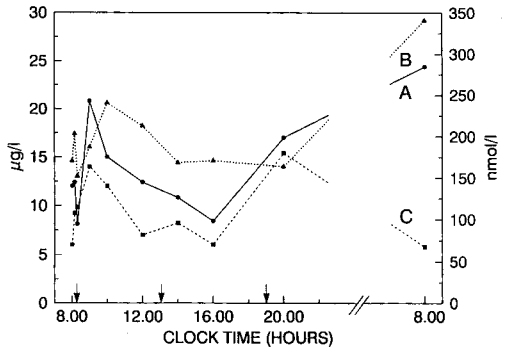

Fig. 3. Diurnal changes in plasma levels of 2-pyrrolidinone, established for two healthy men (A,B) and one woman (C). The arrows indicate the times at which meals were taken.

Diurnal changes

Fig. 3 depicts the results of the study on diurnal changes in plasma levels of 2-pyrrolidinone for three healthy adults. The plasma levels of 2-pyrrolidinone obtained in this study are mostly higher than previously reported for human plasma [1,2]. Although substantial oscillations during a 24 h daytime period occurred, no consistent picture relating to clock time or food intake was obtained.

It is, however, conceivable that fluctuations in the supply of putrescine contribute to fluctuations in circulating levels of 2-pyrrolidinone. Sources of exogenous putrescine are the diet, notably microbially fermented food products [11], and the microbial flora in the colon. The latter produces putrescine, by decarboxylation of ornithine, to counteract a drop in pH caused by carbohydrate fermentation [11,12]. In the small intestine dietary putrescine is likely to become oxidatively deaminated by the locally high activity of diamine oxidase [13], leading to production of Δ'-pyrroline, GABA and possibly 2-pyrrolidinone [14]. Absorption of microbially produced putrescine in the colon, which is low in diamine oxidase activity [13], may increase the levels of circulating putrescine. The latter is, at least partly, degraded to GABA [15], and possibly Δ'-pyrroline and 2-pyrrolidinone. Whether excessive intake of putrescine and consumption of poorly absorbable carbohydrates lead to increases of circulating 2-pyrrolidinone remains to be established.

In conclusion, the average plasma levels of endogenous 2-pyrrolidinone and its diurnal fluctuation should be taken into consideration when evaluating transdermal penetration of 2-pyrrolidinone.

ACKNOWLEDGEMENTS

We thank Mrs. A. W. Kingma and A. W. de Ruyter-Buitenhuis and Mr. H. Elzinga for their technical assistance. We thank Mrs. L. B. D. and G. J. J. B., and Mrs. I. A. M. for their voluntary participation in this study.

REFERENCES

1 E. F. Bandle, G. Wendt, U. B. Ranalder and K.-H. Trautmann, *Life Sci.*, 5 (1984) 2205.
2 D. Dell, G. Wendt, F. Buchelli and K.-H. Trautmann, *J. Chromatogr.*, 344 (1985) 125.
3 D. W. Lundgren and J. Hankins, *J. Biol. Chem.*, 253 (1987) 7130.
4 D. W. Lundgren, H. Teresz and E. A. Krill, *Anal. Biochem.*, 148 (1985) 462.
5 P. S. Callery, M. Stogniew and L. A. Geelhaar, *Biomed. Mass Spectrom.*, 6 (1979) 23.
6 C. Fasolato, A. Bertazzon, A. Previero and L. Galzigna, *Pharmacology*, 36 (1988) 258.
7 D. Southwell and B. W. Barry, *J. Invest. Dermatol.*, 80 (1983) 507.
8 W. J. M. Hruskesky, J. Merdink and M. M. Abel-Monem, *Cancer. Res.*, 43 (1983) 3944.
9 F. A. J. Muskiet, G. A. van den Berg, A. W. Kingma, D. C. Fremouw-Ottevangers and M. R. Halie, *Clin. Chem.*, 30 (1984) 687.
10 J. J. Keyzer, B. G. Wolthers, F. A. J. Muskiet, H. Breukelman, H. F. Kauffman and K. de Vries, *Anal. Biochem.*, 139 (1984) 474.
11 A. E. Pegg and H. G. Williams-Ashman, in D. R. Morris and L. J. Marton (Editors), *Polyamines in Biology and Medicine*, Marcel Dekker, New York, 1981, Ch. 1, p. 3.
12 D. R. Morris and R. H. Fillingame, *Annu. Rev. Biochem.*, 43 (1974) 303.
13 T. Bieganski, J. Kusche, W. Lorenz, R. Hesterberg, C.-D. Stahlknecht and K.-D. Feussner, *Biochim. Biophys. Acta*, 756 (1983) 196.
14 N. Seiler, F. N. Bolkenius and O. M. Rennert, *Med. Biol.*, 59 (1981) 334.
15 G. A. van den Berg, H. Elzinga, G. T. Nagel, A. W. Kingma and F. A. J. Muskiet, *Biochim. Biophys. Acta*, 802 (1987) 175.

Journal of Chromatography, 550 (1991) 247–255
Elsevier Science Publishers B.V., Amsterdam

CHROMSYMP. 2283

Equilibrium elution chromatography

The column-origin boundary condition

PAUL J. KAROL
Department of Chemistry, Carnegie Mellon University, Pittsburgh, PA 15213 (USA)

ABSTRACT

Linear, equilibrium chromatography on a finite column has been re-examined using the rate model. Unlike most previous descriptions, the boundary condition at the column origin is treated as reflective. The development of the band profile on the column behaves in a physically and mathematically reasonable fashion. In this regard, long-standing disagreements on this fundamental issue are finally eliminated. For almost all practical situations, the use of Gaussian profiles for theoretical descriptions of on-column equilibrium chromatography appears valid.

INTRODUCTION

Developments in theories, applications and instrumentation of elution chromatography continue unabated. The interdependence of these three attributes was well illustrated by Snyder and Kirkland [1]. Among the many theoretical approaches are efforts to extract physico-chemical parameters from experimental elution curves [2–7]. A requirement in these efforts is that the relationship between the peak profile and the various parameters be both accurate and well understood. Along these lines, we have been re-examining [8,9] some of the most elementary aspects of column chromatography in order to explore the effects of approximations that have been routinely imposed, over the years, in modeling the chromatographic process. Our long-term goals are either to justify the use of these approximations or to alter theory accordingly.

We begin by restricting our considerations to only the hypothetical case of linear, two-phase equilibrium chromatography. This is usually the starting point for more complete theories that incorporate non-linearities and non-equilibrium considerations. For our current objectives, therefore, we assume fast mass transfer, that the density of the mobile phase remains constant over the length of the column, that the sorption isotherm is linear and that the velocity of the mobile phase is well represented by its constant average. Under these simplifying conditions, the chromatographic

0021-9673/91/$03.50

process, what Snyder [10] termed column development, is modeled according to the partial differential equation of diffusion with forward drift [11,12]:

$$\frac{\partial c_m}{\partial t} = -u \cdot \frac{\partial c_m}{\partial z} + D \cdot \frac{\partial^2 c_m}{\partial z^2} + \frac{1}{\varepsilon} \cdot \frac{\partial c_s}{\partial t}$$

$$\frac{\partial c_s}{\partial t} = -k_1 c_s + k_2 c_m$$

where D is an effective dispersion constant of the solute in the mobile phase, u is the velocity of the mobile phase in the axial (z) direction, ε is the fraction void volume and k_1 and k_2 are the rate constants for transfer between phases. For a linear isotherm and fast interphase kinetics, these equations reduce to the rate expression for linear, equilibrium chromatography:

$$\frac{\partial c}{\partial t} = -u_e \cdot \frac{\partial c}{\partial z} + D_e \cdot \frac{\partial^2 c}{\partial z^2} \tag{1}$$

where $u_e = u/(1 + k')$, $D_e = D/(1 + k')$ and k' is the capacity factor or equilibrium mass distribution ratio. This paper focuses entirely on the solution to the latter hypothetical system and on its relevance to chromatographic theory and, to a lesser extent, practice.

Traditionally, there has been more than one scheme for solving eqn. 1. By and large, the reasons for the choices have been a combination of mathematical convenience and justifiability under certain operating conditions. A very general discussion, not restricted to chromatographic systems, has been developed by Kreft and Zuber [13]. Some schemes involve solving for the on-column profile $c(z,t)$ and others for the elution profile $P(t)$. Further, the boundary conditions employed in these situations have been one of two types: the infinite column in which $-\infty < z < +\infty$ and the semi-infinite column in which $0 \leqslant z < +\infty$. The true column is neither of these, but rather is finite, a fact that can subtly influence the form of the solution to eqn. 1. The present discussion begins with a brief description of the conventional models: infinite, semi-infinite and finite.

The infinite column

Grubner [14], Grushka [15], Kučera [16] and Jönsson [17], among others, have treated the column as if it were infinite. The initial conditions are such that at time zero, the sample is only at the z-origin. The column extends without limit in the positive and negative directions. Eqn. 1 can then be solved and gives exactly the Gaussian curve for the on-column profile at any fixed time $t > 0$, regardless of the magnitude of either the diffusion constant or the mobile phase velocity. The solution can be expressed as the fractional concentration per unit length at time t and axial position z as

$$c(z,t) = \frac{1}{\sqrt{4\pi D_e t}} \cdot \exp\left[-\frac{(z - u_e t)^2}{4 D_e t} \right] \tag{2}$$

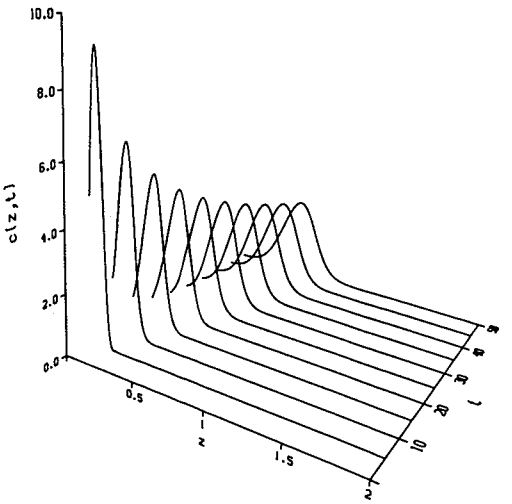

Fig. 1. On-column concentration probability profile for the infinite column. The sample is initially at $z = 0$ at time zero in which $-\infty < z < \infty$, $u_e = 0.01$ (in the positive z-direction), $D_e = 0.0002$. The figure has not been extended into the negative column coordinate region. Time is in units of D_e/u_e^2.

An example set of curves is shown in Fig. 1. Kučera [16] assigned the elution profile to be the function $c(L,t)$, where L is the fixed column length. Kreft and Zuber [13] referred to the use of $c(L,t)$ as "detection in resident fluid".

In contrast, Jönsson [17] argued that the elution profile is more appropriately obtained by what Kreft and Zuber termed "detection in flux", having units of fractional concentration per unit time:

$$P(t) = \int_L^\infty \frac{\partial c(z,t)}{\partial t} \cdot dz$$

As a consequence, Kučera and Jönsson obtained different predictions for elution chromatograms which we shall distinguish by subscripts K and J, respectively. Jönsson presented an analytical expression for the detection in flux elution curve:

$$P_J(t) = \left(\frac{u_e}{2} + \frac{L}{2t}\right) \cdot \frac{1}{\sqrt{4\pi D_e t}} \cdot \exp\left[-\frac{(L - u_e t)^2}{4D_e t}\right] \quad (\text{time}^{-1})$$

For comparison, Kučera's detection in resident fluid elution curve may be written as

$$P_K(t) = c(L,z) = \frac{1}{\sqrt{4\pi D_e t}} \cdot \exp\left[-\frac{(L - u_e t)^2}{4D_e t}\right] \quad (\text{length}^{-1})$$

Jönnson noted the apparent inappropriateness of the dimensionality of $P_K(t)$ for an elution profile. Kreft and Zuber's more thorough consideration shows that normaliza-

tion taking into account the dimensional difference between flux and concentration accounts for the seeming conflict.

The semi-infinite column

Kubin [18] and Yamaoka and Nakagawa [19] used a semi-infinite column in their derivations. The boundary conditions in this case correspond to a column which is infinite only in the positive z-direction. At time zero, the concentration of solute is zero everywhere but at the origin. At the origin, the concentration is unity at time zero and zero thereafter; that is, $c(0,t) = \delta(t)$, the Kronecker delta. This boundary condition produces a profile solution expressed as the fractional concentration per unit time at time t and axial position z. Jönsson gave the following expression for the on-column profile in this case:

$$c(z,t) = \frac{z}{\sqrt{4\pi D_e t^3}} \cdot \exp\left[-\frac{(z - u_e t)^2}{4D_e t} \right] \tag{3}$$

although as quoted, $c(z,t)$ has not been correctly normalized for $0 \leqslant z < \infty$. Fig. 2 shows normalized (semi-infinite) $c(z,t)$ for a set of conditions comparable to those in Fig. 1. At constant time $t > 0$, the on-column profile in eqn. 3 is non-Gaussian. This is in contrast to the profile on the fully infinite column, eqn. 2. Jönsson pointed out that the $\delta(t)$ boundary condition for the semi-infinite column gives the unrealistic result that the profile develops an instantaneous node at the origin when the separation begins as Fig. 2 shows. This happens even in the limit of zero mobile phase velocity, an extreme condition which should reproduce the on-column profile at the diffusion-only limit: broadening downstream from the origin.

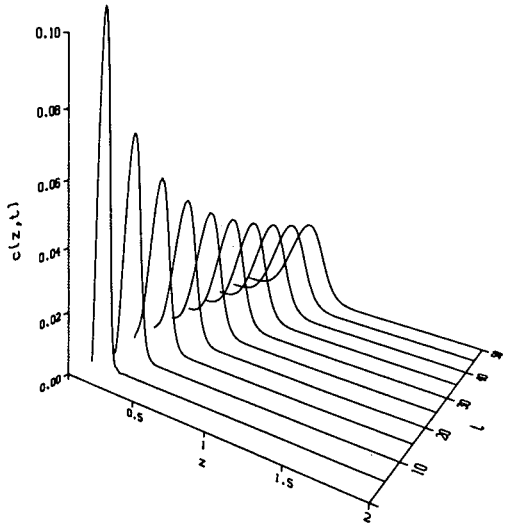

Fig. 2. On-column concentration probability profile for the semi-infinite column. Conditions as in Fig. 1, except $0 \leq z < \infty$.

The finite column

The aforementioned contradictory solutions purposely avoid any end effect by invoking a column that is infinite in the $+z$ direction. One should bear in mind that the end effect has also been neglected in theories that do incorporate mass transfer and other non-equilibrium effects. No chromatographic theory based on the rate equation has invoked boundary conditions associated with a truly finite column. However, in another study, we did address the finite column using the plate model of chromatography in a way that is valid at high capacity factors [9]. In addition, for a column semi-infinite in the negative direction, the influence of just the end effect on statistical moments in equilibrium chromatography was the subject of an earlier report [8].

THEORY

The boundary condition we invoke at the column origin differs from that used by Kubin and others that was described above, whether for equilibrium or non-equilibrium systems. In recognition that a solute molcule at $z = 0$ cannot retreat backward from that point to $z < 0$ since the column doesnot exist there, we have what is referred to as a reflecting barrier at the origin [20]. In the mathematics of heat-transfer studies, this is equivalent to an insulation boundary condition [21,22]. In fact, Sommerfeld used, as an heuristic illustration of reflection, diffusion in a cylindrical column. At the bottom of the column at time zero is a small amount of concentrated $CuSO_4$ solution and above that is a layer of pure water extending to infinite height and into which the colored solution diffuses [22]. The phenomenon is easily demonstrated and also easily pictured mentally. This reflecting barrier boundary condition in chromatographic terms may be written as [20,23]

$$\left(D_e\frac{\partial c}{\partial z} - u_e c\right)_{z=0} = 0$$

Cox and Miller [20], following Smoluchowski [24] and Sommerfeld [22], solved the diffusion equation with drift, that is, eqn. 1 with a reflecting barrier at the origin. The solution corresponds to the concentration profile of the solute as a function of position and time while the solute is on a semi-infinite column. This, in turn, approximates the behavior of a band that has been appropriately dealt with at the origin and that has not yet approached the elution point L where the end effect applies. In the early stages of chromatography then, the on-column profile is well represented by Cox and Miller's expression (after correction for some typographical errors):

$$c(z,t) = \frac{1}{\sqrt{\pi D_e t}}\left\{\exp\left[-\frac{(z-u_e t)^2}{4D_e t}\right]\right\} - \frac{u_e}{D_e}\left[1 - \Phi\left(\frac{z+u_e t}{\sqrt{2D_e t}}\right)\right]\exp\left(\frac{zu_e}{D_e}\right)$$

$$\text{for } t \ll \frac{L}{u_e} \qquad (4)$$

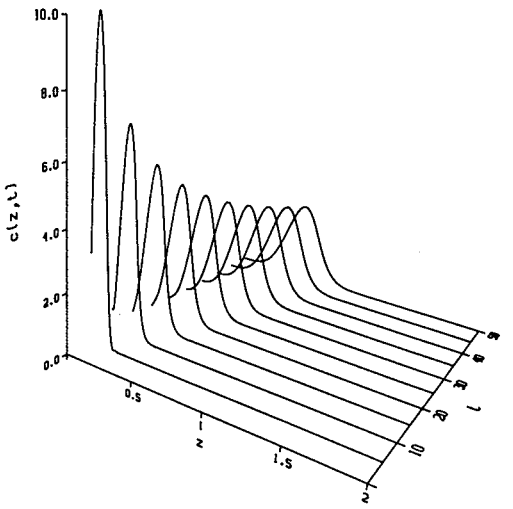

Fig. 3. On-column concentration probability profile for the semi-infinite column with a reflection boundary condition at the origin. Other conditions as in Figs. 1 and 2.

where $\Phi(x)$ is the standard normal integral:

$$\Phi(x) = \frac{1}{\sqrt{2\pi}} \int_{-\infty}^{x} \exp\left(-\frac{y^2}{2}\right) dy$$

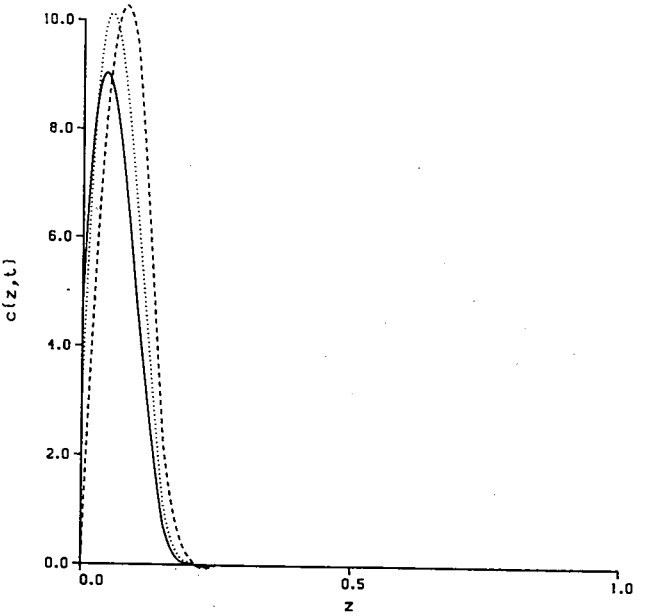

Fig. 4. Comparison of the on-column profiles at $t = 5.0\ D_c/u_e^2$, a representative short time for the infinite (solid line), semi-infinite (dashed line) and semi-infinite with reflection (dotted line) systems in Figs. 1–3.

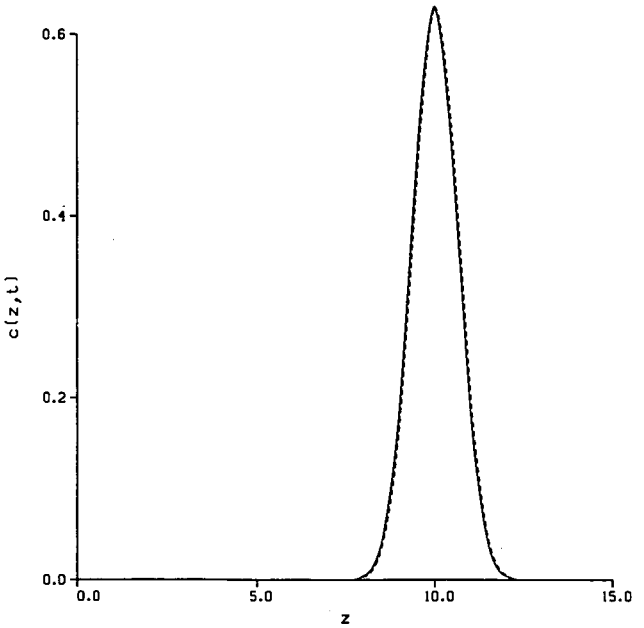

Fig. 5. Comparison of the on-column profiles at $t = 1000.0\ D_e/u_e^2$, a representative long time for the three sets of boundary conditions as in Fig. 4. The dotted line cannot be easily distinguished from the solid line (infinite column result).

Eqn. 4 is identical with Kreft and Zuber's equation for a semi-infinite bed with injection in flux and detection in resident fluid. Fig. 3 illustrates the effect of introducing reflection at the origin. Fig. 4 compares the various calculated on-column profiles at short times. Note that the profile with reflection at the origin "leads" the peak from the infinite model profile. For long times, all three profiles converge, as shown in Fig. 5, becoming indistinguishable from a common Gaussian profile. This can be verified mathematically. For long chromatography times, we can use an approximation for the second term on the right in eqn. 4. From Abramowitz and Stegun [25], the asymptotic expansion for $x > 0$

$$1 - \Phi(x) = \frac{Z(x)}{x}\left(1 - \frac{1}{x^2} + \ldots\right)$$

enables us to show that

$$\frac{u_e}{D_e}\left[1 - \Phi\left(\frac{z + u_e t}{\sqrt{2D_e t}}\right)\right]\exp\left(\frac{zu_e}{D_e}\right) \rightarrow \frac{1}{\sqrt{4\pi D_e t}}\left\{\exp\left[-\frac{(z - u_e t)^2}{4D_e t}\right]\right\}\left[1 + \frac{(z - u_e t)}{u_e t} + \ldots\right] \qquad (5)$$

Exploring eqn. 4 graphically as in Fig. 5 demonstrates that for long times, $z - u_e t$ is nearly normally distributed about zero with a standard deviation that is *ca.* $\sqrt{2D_e t}$. In that case, the first-order term in the series expansion is negligible when $\sqrt{2D_e t}/u_e t \ll 1$. Consequently, eqn. 4 reduces to eqn. 2, the Gaussian distribution, at times $t \gg 2D_e/u_e^2$.

At least as far as equilibrium chromatography is concerned, we see that behavior at the column origin ultimately has a negligible effect on band development provided that we are not dealing with very short columns or unusually fast effective diffusion relative to peak migration rate.

DISCUSSION

With regard to one of the two column boundaries, the origin, Jönsson had dismissed the semi-infinite model of Kubin as physically unrealistic. The justification was that it gave a node in the on-column profile at the origin at all times other than $t = 0$, as can be seen in Fig. 2. However, the infinite models are equally unrealistic because they allow diffusion of solute into a non-existent part of the column, $z < 0$. It is apparent, though, that in the high velocity limit, these conflicts lose their impact. The awkwardness of both of these physical situations is completely vitiated when it is recognized that the boundary condition at the column origin corresponds to a reflection, that is, the probability flux through the origin is zero. At the very least, it is gratifying that as a direct consequence of using a reflection at the origin of the column, the on-column profile neither extends to negative column coordinates nor bears a node at the origin.

In a recent note [8], we drew attention to the end effect associated with elution at the column terminus. This involves another boundary condition necessary for solving the differential eqn. 1 under physically appropriate restraints. That is, the realistic cessation of diffusion and drift that occurs at the column terminus results in an elution profile that does not generally correspond to previous versions, although it does under certain limiting conditions. In that work, we had derived statistical moments of the equilibrium chromatogram on a column in which $-\infty < z \leq L$. The end effect was mathematically determined by incorporating an absorbtion sink at $z = L$. In this way, solute reaching the elution coordinate is removed and cannot reappear on the column via dispersive effects. The drawback with those results might have been that the column was viewed as semi-infinite, extending towards $-\infty$. However, we have demonstrated in this work that, except in highly unusual circumstances, the effect of this oversight on the developing profile and consequently on the elution profile should be non-essential. The technique for addressing the end effect in the above reference should be valid.

The developments presented here seem very satisfactory when applied to linear equilibrium chromatography. It is our hope next to explore what changes, if any, arise when using these boundary conditions where kinetic effects have also been included.

ACKNOWLEDGMENT

The author thanks the Samuel and Emma Winters Foundation for its support of this research.

REFERENCES

1 L. R. Snyder and J. J. Kirkland, *Introduction to Modern Liquid Chromatography*, Wiley, New York, 2nd ed., 1979.
2 C. Vidal-Madjar and G. Guiochon, *J. Chromatogr.*, 142 (1977) 61.
3 K. P. Li and Y. Y. H. Li, *Anal. Chem.*, 48 (1976) 737.
4 J. R. Conder and C. L. Young, *Physicochemical Measurements by Gas Chromatography*, Wiley, New York, 1979.
5 Cs. Horváth and H.-J. Lin, *J. Chromatogr.*, 149 (1978) 43.
6 F. H. Arnold and H. W. Blanch, *J. Chromatogr.*, 355 (1986) 13.
7 E. D. Katz and R. P. W. Scott, *J. Chromatogr.*, 270 (1983) 29.
8 P. J. Karol, *J. Chromatogr.*, 445 (1988) 207.
9 P. J. Karol, *Anal. Chem.*, 61 (1989) 1937.
10 L. R. Snyder, *Principles of Adsorption Chromatography*, Marcel Dekker, New York, 1968.
11 L. Lapidus and N. R. Amundson, *J. Phys. Chem.*, 56 (1952) 984.
12 J. J. van Deemter, F. J. Zuiderweg and A. Klinkenberg, *Chem. Eng. Sci.*, 5 (1956) 271.
13 A. Kreft and A. Zuber, *Chem. Eng. Sci.*, 33 (1978) 1471.
14 O. Grubner, *Adv. Chromatogr.*, 6 (1968) 173.
15 E. Grushka, *J. Phys. Chem.*, 76 (1972) 2586.
16 E. Kučera, *J. Chromatogr.*, 19 (1965) 237.
17 J. Å. Jönsson, *Chromatographia*, 18 (1984) 427.
18 M. Kubin, *Collect. Czech. Chem. Commun.*, 30 (1965) 1104.
19 K. Yamaoka and T. Nakagawa, *J. Chromatogr.*, 93 (1974) 1.
20 D. R. Cox and H. D. Miller, *The Theory of Stochastic Processes*, Wiley, New York, 1965.
21 R. V. Churchill, *Modern Operational Mathematics in Engineering*, McGraw-Hill, New York, 1944.
22 A. Sommerfeld, *Partial Differential Equations in Physics*, Academic Press, New York, 1949.
23 N. S. Goel and N. Richter-Dym, *Stochastic Models in Biology*, Academic Press, New York, 1974.
24 M. V. Smoluchowski, *Phys. Z.*, 17 (1916) 585.
25 M. Abramowitz and I. Stegun (Editors), *Handbook of Mathematical Functions*, Dover, New York, 1968, p. 935.

Journal of Chromatography, 550 (1991) 257–266
Elsevier Science Publishers B.V., Amsterdam

CHROMSYMP. 2094

Expert system for repeatability testing of high-performance liquid chromatographic methods

M. MULHOLLAND*[a] and N. WALKER
Philips Scientific, Cambridge (UK)
F. MARIS and H. HINDRIKS
Organon International, Oss (Netherlands)
L. BUYDENS
University of Nijmegen, Nijmegen (Netherlands)
T. BLAFFERT
Philips Research Laboratories, Hamburg (Germany)
and
P. J. SCHOENMAKERS
Philips Research Laboratories, Eindhoven (Netherlands)

ABSTRACT

A repeatability test is performed as part of the validation of the precision of a high-performance liquid chromatographic method. The purpose of the test is to establish the random errors of the method with respect to various method features. It is usual to test the repeatability of the sample preparation and the injection procedure by a number of repetitions. The number of repetitions depends on the application of the method. For instance, a quality control method is expected to analyse up to and over 50 samples in a single run. The repeatability test of the injection process therefore needs to reflect this number, in order to identify fully potential errors. These errors could be due to the instrument error or to drifting factors such as temperature. The expert system described provides the necessary expertise to identify the required tests and interpret the results. It also contains a diagnosis module which can identify sources of unacceptable errors. The diagnosis module is linked to a reoptimization process which can modify the method to improve the resolution between a critical pair of peaks. This expert system was built as part of the ESCA project, which is a 3-year project investigating the application of expert systems to analytical chemistry.

A repeatability test requires both heuristic and algorithmic knowledge and therefore provides a good challenge for expert system technology. The system is implemented in a multiple windows software environment and uses workstation hardware. This software has been evaluated in practical laboratory environments and some of the results and conclusions are described. The major advantage of an expert system implementation appears to be that it can give advice when problems occur. It also ensures that the statistics are used and interpreted correctly. This is not possible using conventional algorithmic software.

INTRODUCTION

High-performance liquid chromatography (HPLC) is usually applied as a quantitative technique, where the relative concentrations of components in a mixture

[a] Present address: University of New South Wales, Sydney, Australia.

0021-9673/91/$03.50

are determined. Each sample application requires a unique combination of chemical and instrumental conditions. The development of a method is a complex series of choices and optimizations which consider features of both the chemistry of the sample and its application. When developing a method, the analyst has certain expectations of its quantitative performance. These include accuracy, sensitivity, specificity and precision. To ascertain whether the new method achieves the expected levels of performance requires a series of validation experiments. Each validation test can be defined in four stages:

(1) The method characteristic is defined; this could be accuracy, precision or any other performance characteristic which is important to the application.

(2) The actual test is defined; for precision this could be repeatability, reproducibility of ruggedness.

(3) An experimental procedure with which to test these characteristics is then selected and carried out. This includes the measurement of various method characteristics.

(4) The final stage in a method validation test is to diagnose the results. This requires pass/fail criteria and a method for identifying and curing problems. It may sometimes require the reoptimization of the method if it fails to meet the specified performance levels.

HPLC method validation is thus an integral part of process of method development. Links back to method optimization are often required. It is also necessary to be aware of the performance requirements during the method development process. For instance, a method developed on a delicate microbore column would not be suitable for multiple usage throughout busy quality control laboratories.

This paper describes an expert system built to tackle these problems and create these links for a repeatability test. The system is built as part of a research project investigating the use of expert systems in analytical chemistry, ESCA.

A small expert system was initially built as a test case for the expert system development tool Goldworks. It used a combination of spreadsheets and expert system facilities such as frames and rules [1]. However, as the work of ESCA progressed it became clear that analysts did not just need stand-alone packages but communication links throughout the method development process. It was therefore decided to build a system which could perform a repeatability test and also communicate with the method optimization process. Three expert systems have been built which tackled the various stages in the method development process: first guess [2], selectivity optimization [3] and optimization of the instrumentation [4,5]. Links to the latter system looked most promising for the purpose of re-optimizing methods which had failed a method validation test. However, links or other systems would eventually be required in order to form a complete picture [6].

STRUCTURE OF THE EXPERT SYSTEM

The structure of the system is illustrated in Fig. 1. The system starts by consulting the system optimization module. This module optimizes the physical parameters such as flow-rate, column dimensions and detector flow cell. The aim of the optimization is to provide the fastest analysis time within the required resolution. In the stand-alone system the optimization limits consist of the hard physical limits on the

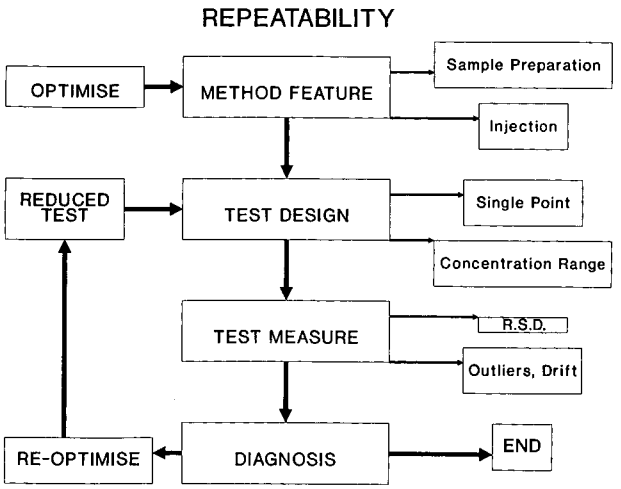

Fig. 1. Overview of the repeatability test expert system.

instrument capability, the available sample volume, with user-defined ranges for the resolution and signal-to-noise ratio of the analysis. The role of these limits changes when they are applied to optimizing a method which has predefined constraints on its repeatability. The limits need to specify ranges within which an optimized method should be repeatable. Some of these limits are shown in Table I. They are divided into three categories: the possible range, the reliable range and the robust range. The range is selected by examining the method application. Some examples are shown in Table I. When the required range is specified the system optimizes for the fastest analysis time. The results include the following information: (1) the selected column dimensions; (2) the selected detector flow cell; (3) the value of the time constant; (4) the flow-rate and pressure drop of the instrument; (5) the projected analysis time, resolution and signal-to-noise ratio for the analysis; and (6) the selected values for the

TABLE I

RANGE REQUIREMENTS FOR THE OPTIMIZATION

Parameter	Possible range	Reliable range	Robust range[a]
Flow-rate	0.01–10 ml/min	0.1–5 ml/min	0.3–3 ml/min
Pressure	0–400 bar	5–250 bar	5–200 bar
Resolution	1	2	3
Signal-to-noise ratio	10	100	200
Column I.D.	0.25–25 mm	2–8 mm	4–8 mm
Examples:			
Sample No.	<25	25	25
Lab. No.	1	>1	>2

[a] The range of values within which the method is likely to be robust, *i.e.*, not affected much by small changes.

TABLE II

AN EXAMPLE OF A PEAK TABLE

Peak No.	Retention time (s)	Peak height (mm)	Peak area	Asymmetry	Plate count	Relevant: yes/no
0	79	20	1000	1	23 000	yes
1	91	70	1000	1	23 900	yes
2	145	100	1000	1	21 700	yes
3	180	20	1000	1	24 900	yes

sample concentration and injection volume. The user can interact with these results by selecting from several options. When one is satisfied with the optimization, the repeatability test can begin.

The method features to be tested are then defined as the sample preparation and the injection procedure. The analyst inputs a description of the HPLC method together with information on the expected usage. With this information an experimental design can be recommended. Originally, the system recommended a number of repetitions of the sample preparation and the injection procedure at a single concentration point. However, during the evaluation this was found to be inadequate. Therefore, designs were added to deal with multiple concentration levels.

After the design has been recommended, the user carries out the experiments and collects data for retention times, peak areas, peak heights and concentration. These data are input to the system using peak tables; an example is shown in Table II. The user is only allowed to proceed to the next stage if all the peak tables are entered and all have the same number of peaks.

The test measure is now made on these data. For each peak, the relative standard deviation (R.S.D.) of each value is calculated [1]. These measurements are then used to diagnose the repeatability of the method.

The diagnosis is performed in several stages:

(1) The concentration variations are measured against a pass/fail criterion, usually 1%. If they pass then the diagnosis ends here and the method is concluded to be repeatable. However, if it fails it then proceeds to the next stage.

(2) A Grubbs test for outliers is performed and the user is allowed to remove any outliers identified.

(3) The results can be viewed graphically to determine any drifting conditions.

(4) Potential problems are diagnosed and a cure is suggested.

TABLE III

CLASSIFICATION OF R.S.D. VALUES

Classification	Height R.S.D. (%)	Area R.S.D. (%)	Retention time R.S.D. (%)
Small	0	0	0
Medium	1	1	0.5
Large	2	2	1

The R.S.D. values are used to identify possible problems. The R.S.D.s are first classified as small, medium or large according to Table III. The combined behaviour of these values can indicate specific problems. For instance, if multiple injections of the same sample gives rise to large variations in peak height and area, but not in the retention times, then this could be due to a variation in injection volume or possibly degradation of the sample. The diagnosis section of the repeatability test gives a list of possible problems with the method. It does this in four stages.

(1) The classifications of small, medium and large are used to create lists of possible problems for each peak. Each problem within a list has a priority or weight. A value of zero means that the problem is not possible. Two lists are formed, one for sample preparation problems and the other for injection problems.

(2) The individual lists of problems are combined into two overall lists by summing the priorities of each problem over the peaks.

(3) The list of problems are then checked. Certain problems, although diagnosed, can be discounted if the chromatographic method contains the correct features. For instance, if pH variation is diagnosed but the method is utilizing a buffer then this problem can be discounted.

(4) The list of problems with injection and sample preparation are combined into one complete ordered list. The list of problems with injection is considered to be more important than those for sample preparation, so are given a higher priority. If a problem occurs in both lists then the higher of the two priorites is taken. Once the problem list has been established the system goes on to recommend corrective actions.

Each possible problem diagnosed has a list of actions that can be taken to try to solve the problem. These actions can be divided into two categories: actions that involve changing the method, such as the re-optimization of resolution, and actions that involve checking or maintaining the chromatograph. The expert system provides suggested actions to the user based on their priority score and checking and maintenance cures are always performed first. If a certain action does not solve the problem, this is measured by performing a reduced test, then the next highest priority is suggested. If the method cannot perform after any recommended checking or maintenance cures then some reoptimization is suggested. If the resolution between a pair of peaks falls below a predefined level throughout repeatability test, then the user is routed to the system optimization module. This causes the resolution to be increased to a larger value. Fig. 2 shows a graphical representation of the diagnosis process.

The software is implemented using Pascal in a multiple windows environment. A fuller description of the software and hardware environment is given elsewhere.

This system was evaluated using several pharmaceutical examples. The results for the analysis of ethinylestradiol are presented here.

EXPERIMENTAL

Sample preparation

Samples are prepared by adding a formulated tablet containing ethinylestradiol to 2.0 ml of an internal standard solution of estradiol. This is then shaken and sonicated until the tablet is completely dispersed. The mixture is centrifuged and 10 μl of the supernatant are injected onto the column.

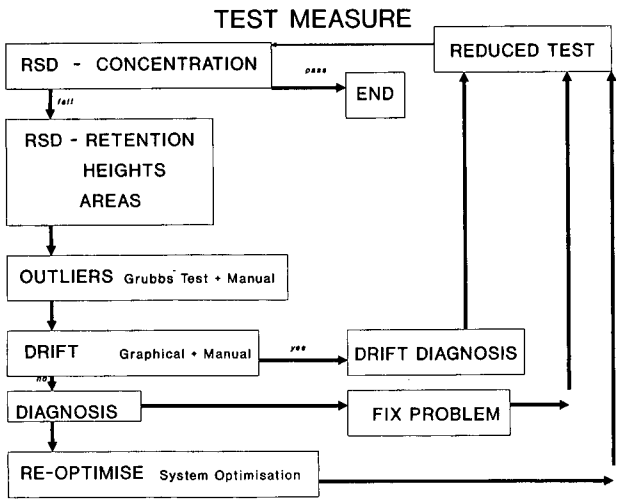

Fig. 2. Overview of the measurement and diagnosis modules.

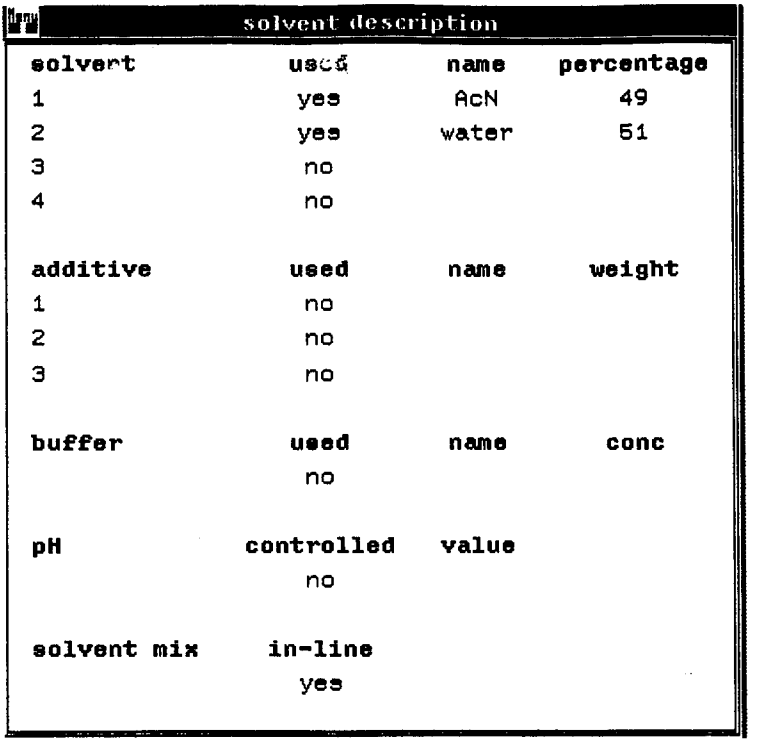

Fig. 3. Chromatogram of ethinylestradiol (latest eluting peak) with estradiol as the internal standard.

Chromatographic conditions

The sample is eluted from a 100 × 5 mm I.D. Novapak C_{18} column with a mobile phase of acetonitrile–methanol–phosphoric acid (60:40:0.05) at a flow-rate of 2 ml/min. The column temperature is ambient and the sample is detecting using a UV detector at 205 nm.

RESULTS

Fig. 3 shows as an example a chromatogram of ethinylestradiol together with estradiol. This method is input to the system using a number of tables reserved for this information, an example of the solvent description is shown in Fig. 4. The recommended experimental design involves a total of 98 injections. This includes the injection of standards to calibrate the instrument.

Fig. 5 shows the conclusions obtained from the diagnosis of these results. The calculated values for the R.S.D. are shown for each of the sample preparation tests and the injection procedure test. For the injection procedure test no problems are found and all the R.S.D.s have values below the medium classification shown in Table III. However, for the sample preparation a small problem is observed in the variation of peak heights and areas for peak 2. The problem is diagnosed as due to either sample degradation or inadequate sample preparation. For this example the sample degradation is considered the priority problem. The suggested action is to

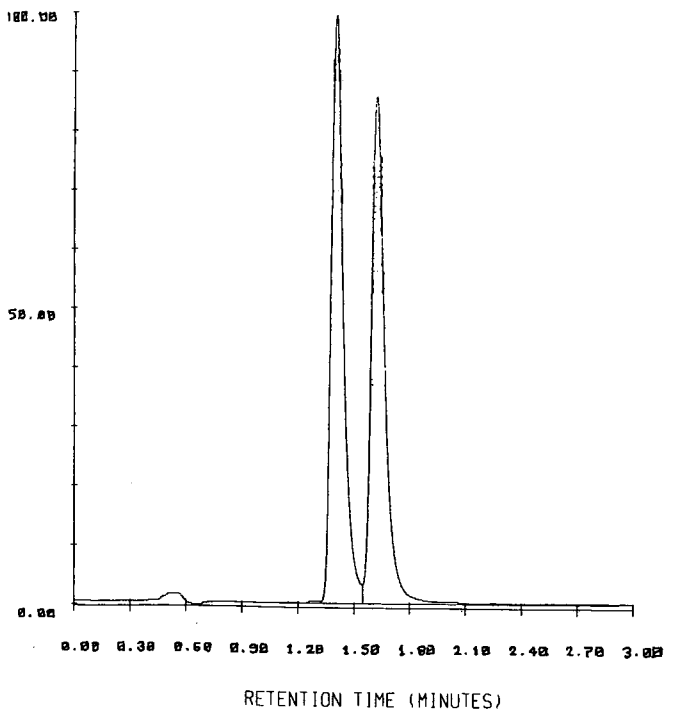

Fig. 4. Example input window for the solvent description.

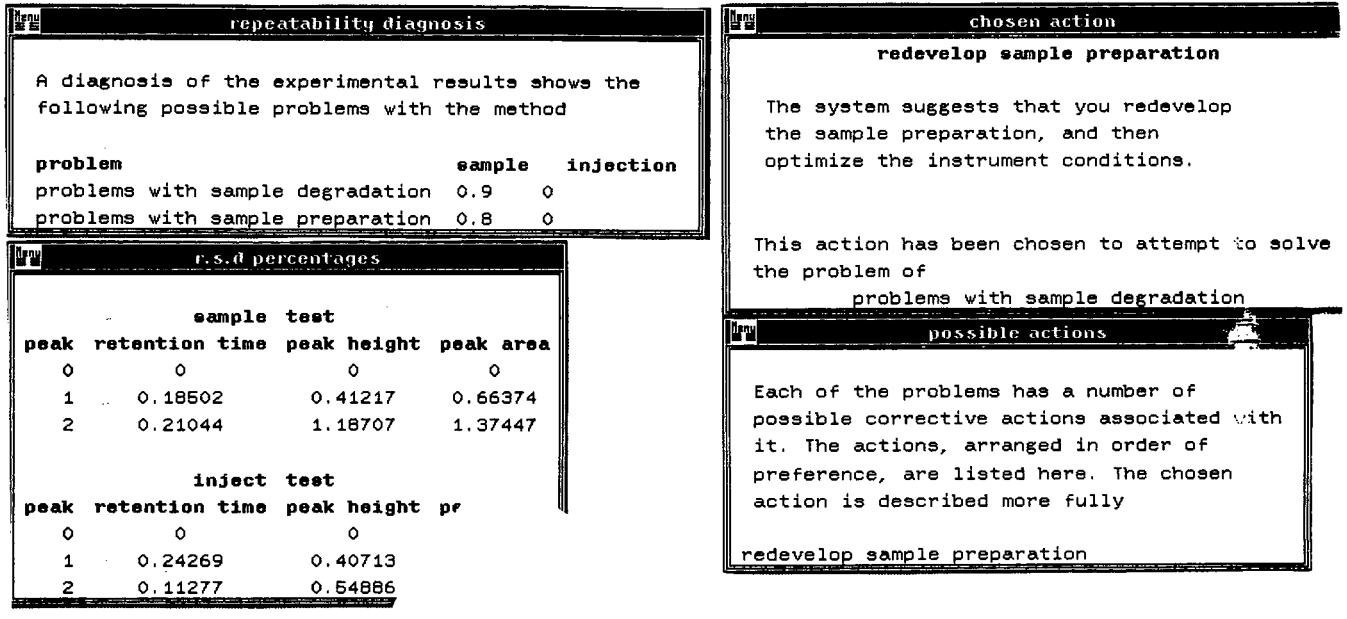

Fig. 5. Screens resulting from the diagnosis of the method for ethinylestradiol.

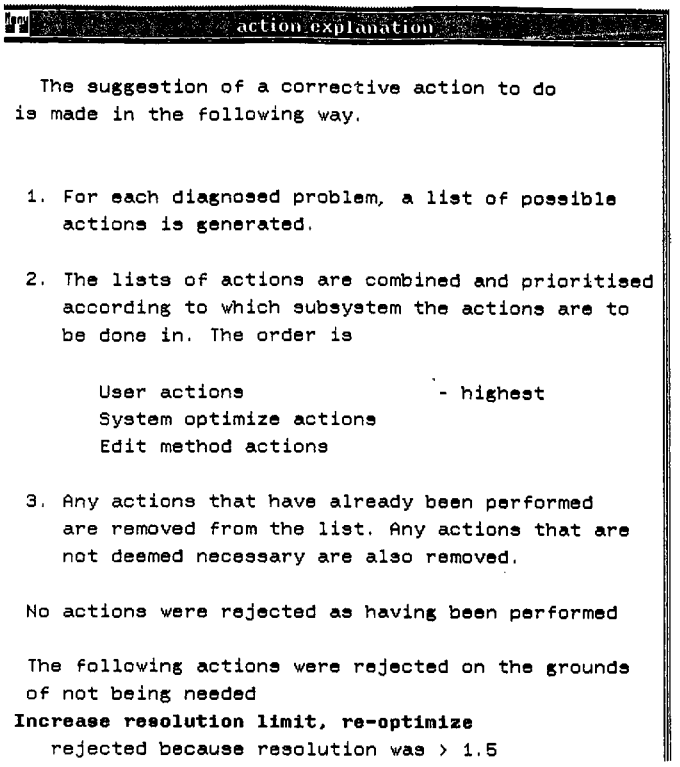

Fig. 6. Explanation provided for the suggested corrective actions.

re-develop the sample preparation. Fig. 6 shows the explanation available for this corrective action.

It is interesting that the evaluators felt that the measured performance is acceptable for this method, but were pleased to find the system suggesting actions that could further improve the method. This is a typical advantage of expert systems over conventional software packages.

CONCLUSIONS

The use of expert system technology to develop a repeatability test package is considered successful. The approach allows the use of both algorithmic and heuristic knowledge. Algorithmic knowledge, such as that required for R.S.D. calculation, can be implemented in a conventional equation, whereas heuristic knowlegde, such as that required for problem diagnosis, can be implemented as rules.

The evaluation of this system proved extremely valuable as it resulted in several additions which enhanced the software considerably. The software was shown to give good advice and even suggested improvements to methods that were previously considered acceptable.

However, several additions could still be made to complete the repeatability test

system. It could be integrated with a chromatography data station to improve the efficiency of data transfer within the software. To complete the picture the system would need to be linked with the remainder of the method development process. This would allow any problems identified to be cured by re-developing the method.

REFERENCES

1 M. Mulholland, J. A. van Leeuwen and B. G. M. Vandeginste, *Anal. Chim. Acta*, 223 (1989) 183–192.
2 H. Hindriks, F. Maris, J. Vink, A. Peeters, M. de Smet, D. L. Massart and L. Buydens, *J. Chromatogr.*, 485 (1989) 255–265.
3 A. Peeters, L. Buydens, D. L. Massart and P. J. Schoenmakers, *Chromatographia*, 26 (1988) 101–109.
4 P. J. Schoenmakers, N. Dunand, A. Clelland, G. Musch and T. Blaffert, *Chromatographia*, 26 (1988) 37–44.
5 P. J. Schoenmakers and N. Dunand, *J. Chromatogr.*, 485 (1989) 219–236.
6 P. Conti, H. Pityns, N. Vanden Driessche, M. de Smet, T. Hamoir, F. Maris, H. Hindriks, P. J. Schoenmakers and D. L. Massart, *Chromatographia*, submitted for publication.

Journal of Chromatography, 550 (1991) 267–283
Elsevier Science Publishers B.V., Amsterdam

CHROMSYMP. 2167

Role of π-π interactions in reversed-phase liquid chromatography

GÉRALDINE THÉVENON-EMERIC[a], ALAIN TCHAPLA[b] and MICHEL MARTIN*[,c]
École Polytechnique, Laboratoire de Chimie Analytique Physique, 91128 Palaiseau (France)

ABSTRACT

The retention of various saturated and unsaturated solutes in reversed-phase liquid chromatography (RPLC) was investigated for various saturated and unsaturated packings in mobile phase mixtures of various compositions of methanol and acetonitrile. Non-aqueous eluents containing acetonitrile have a lower solvent strength than eluents containing methanol for saturated alkanes, alcohols and triglycerides, as expected from the solvophobic theory of retention. Very peculiar retention behaviours are observed when unsaturated solutes are analysed on aromatic stationary phases and/or when mobile phase containing acetonitrile is used with either an aromatic stationary phase or with unsaturated solutes or both. All these observations can be rationalized by taking into account the effect of π-π interactions between the π-electron systems of the solute, the stationary phase and the mobile phase. The influence of the residual silanols on silica-based RPLC supports on the retention of alcoholic solutes in pure acetonitrile is demonstrated. The influence of the concentration of a charge-transfer complexing agent (silver nitrate) in the mobile phase on the retention of unsaturated triglycerides was studied in a methanolic eluent and compared with that in a mobile phase containing acetonitrile.

INTRODUCTION

The optimization of a separation in reversed-phase liquid chromatography (RPLC) is helped by an understanding of all the different interactions involved in the system [1–3]. In the past, much work has been carried out towards understanding and quantifying the effect of the mobile phase on the retention of the solutes.

The theory of the solvophobic effect [4,5] provides a good model of the retention behaviour when the stationary phase is not involved in specific interactions with either the solutes or the solvent. In this situation the elution is mostly controlled by interactions in the mobile phase and the retention is closely related to the eluent properties. Various classifications of solvents based on different parameters, which

[a] Present address: Department of Medicinal Chemistry, Pharmacy Building, Purdue University, West Lafayette, IN 47907, USA.
[b] Present address: IUT Orsay I, LETIAM, B.P. 127, 91403 Orsay Cedex, France.
[c] Present address: Ecole Supérieure de Physique et Chimie Industrielles, Laboratoire de Physique et Mécanique des Milieux Hétérogènes (URA CNRS 857), 10 Rue Vauquelin, 75231 Paris Cedex 05, France.

0021-9673/91/$03.50

may serve as guidelines for the selection of a chromatographic eluent, are available [6–8].

However, the prediction of retention can be effective only if all the interactions between the three species involved in the chromatographic process, *i.e.* the solutes, eluent and stationary phase, are considered at the same time. Tanaka and co-workers [9,10] and Colin *et al.* [11] studied the influence of the organic modifier on retention and selectivity for a large number of solutes by looking at their retention in methanol *versus* that in acetonitrile. The investigations were performed with *n*-alkyl-bonded phases. These supports only give non-specific interactions, except for undesirable hydrogen bonding as a result of the residual free silanol groups present on the surface of the silica-based packing materials. However, many supports now in use in RPLC can exhibit interactions other than non-specific, rendering the prediction of retention more complex. Studies of retention, selectivity and/or peak shape have been performed on some of these supports, such as phenyl-bonded silica-based phases [12,13] or polymeric supports such as poly(styrene–divinylbenzene) [14]. These were usually carried out in aqueous mobile phases and focused mainly on the effect of the organic modifier on the retention of the solutes.

These supports contain π-electron systems which, in presence of other π-electron systems in either the mobile phase or the solutes, may give rise to π–π interactions. These rather specific interactions, which are one form of the more general electron donor–electron acceptor type of interactions [15], are expected to influence the retention behaviour. They may also occur between the solutes and the mobile phase.

To better understand the retention mechanism in RPLC when these interactions occur in the chromatographic system, their effect has been investigated somewhat systematically. Their influence on retention was first studied when π-electron systems are present in the mobile phase and in the solutes, then in the mobile and stationary phases, then in the solutes and in the stationary phase, and then simultaneously in these three species. For each of these cases, a comparison with similar systems in which π–π interactions are absent allows the specific influence of these interactions to be isolated as much as possible. In addition, the influence of the presence of a charge-transfer complexing agent (silver ion) with π-electron systems in the mobile phase is studied.

This investigation took place in the framework of a more general study on the separation by RPLC of homogeneous triglycerides [16]. Therefore, the solutes used in this work are mainly selected from within this family of compounds. In fact, they constitute good probes for studying the influence of π–π interactions as they can contain a relatively large number of double bonds for a fixed number of carbon atoms. Furthermore, the separation of the triglycerides according to the number of carbon atoms and to the number and position of double bonds is one of the present challenges for the analysis and characterization of fats.

EXPERIMENTAL

Reagents

All solvents were of HPLC grade (Carlo Erba, Milan, Italy). All were filtered through a Millipore GF/C 1.2-μm filter, then mixed as required and briefly sonicated. All solutions were freshly prepared. All mobile phase mixtures were prepared using a 100-ml burette.

The triglycerides were purchased from Interchim (Montluçon, France). The alkanes and alcohols were from various manufacturers.

Equipment

The LC system consisted of a Beckman Model 112 pump (San Ramon, CA, USA), a Rheodyne 7125 injection valve (Cotati, CA, USA) with a 20-μl loop and a Waters R-401 refractive index detector (Milford, MA, USA). The pre-column, column and injection valve were all thermostated using a laboratory-made water jacket. The bath temperature was controlled by a Huber HS thermostat (Offenburg-Elgersweier, Germany) with a precision of 0.1°C.

Four columns were used: an Ultrasphere ODS (an octadecyl-bonded silica-based material), 5 μm, 80 Å, 15 × 0.46 cm, from Beckman; a Zorbax *n*-propylphenyl 6 μm, 80 Å, 25 × 0.46 cm, from DuPont (Wilmington, DE, USA); a Hamilton PRP-1 (styrene–divinylbenzene polymeric material), 10 μm, 80 Å, 15 × 0.46 cm (Hamilton, Reno, NV, USA); and a laboratory-made column packed with LiChrosorb RP-18 (an octadecyl-bonded silica-based material), 10 μm, 80 Å, 20 × 0.46 cm from Merck (Darmstadt, Germany).

Methods

All retention values are reported in terms of the capacity factor, k'. The calculation of this parameter requires the determination of the void volume of the column used. The weighing method was as described previously [16]. Each k' value reported results from at least three reproducible injections.

RESULTS AND DISCUSSION

Relative solvent strength of methanol and acetonitrile for saturated solutes on an octadecyl-silica support

This study of the role of π–π interactions in RPLC involves the comparison of the retention of solutes in mobile phases containing acetonitrile *versus* that in eluents containing methanol. It is therefore interesting to compare first the eluotropic strengths of acetonitrile and methanol when π–π interactions are not present in the chromatographic system. There is a huge amount of data on the retention of various series of solutes in acetonitrile–water and methanol–water mixtures.

It is commonly accepted that acetonitrile is a stronger eluent than methanols, as at a given, not low, water percentage, retention in methanol–water mixtures is usually larger than in acetonitrile–water mixtures. However, it has already been observed that pure methanol or methanol–water mixtures with a low water content are stronger eluents than pure acetonitrile or acetonitrile–water mixtures with the same low water content; this was considered to be an "abnormal" behaviour of the acetonitrile–

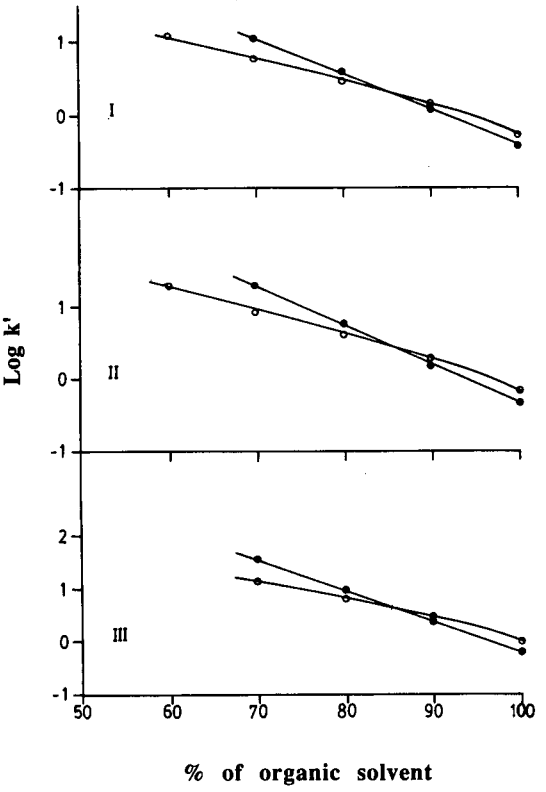

Fig. 1. Retention of *n*-hexane (I), *n*-heptane (II) and *n*-octane (III) *versus* percentage of organic modifier in water. Mobile phase: (○) water–acetonitrile; (●) water–methanol. Column: LiChrosorb RP-18. (Compilation of data from refs. 17 and 18).

water mixtures with a low water content [17]. The explanation of this contradiction can be found in the theory of the solvophobic effect. It is well documented that this effect is one of the most important phenomena governing retention in RPLC. This theory predicts that the retention increases with the surface tension of the mobile phase. The surface tension of acetonitrile (29.3 dyne/cm at 20°C) is higher than that of methanol under the same conditions (22.6 dyne/cm), whereas the surface tension of methanol–water mixtures exceeds that of acetonitrile–water mixtures when the water content is larger than about 28% (v/v). Accordingly, in the absence of water, and if no phenomena other than hydrophobic interactions are involved in the retention process, methanol must be a stronger eluent than acetonitrile. This can be verified from Fig. 1, which represents the logarithms of the capacity factors (k') of three *n*-alkanes *versus* the percentage of both methanol and acetonitrile in water, compiled from data in refs. 17 and 18. The retention of the alkane solutes, which were selected as they give only non-specific interactions, becomes lower in methanol–water than in acetonitrile–water when the amount of the organic component of the mobile phase exceeds 85% (v/v). This finding confirms the validity of the solvophobic theory for

describing the retention of non-polar solutes in RPLC. The slight difference in the water content of the cross-over points of the surface tension and retention *versus* eluent composition curves (28 and 15%, respectively) may arise from differences between the microscopic value of the surface tension of the eluent, which controls the retention, and the measured macroscopic value.

It can be noted that, although the solvophobic theory does not account for the change in retention arising from a modification of the stationary phase configuration by the mobile phase, such an influence is likely to be negligible in either pure organic eluents or those containing a low amount of water as the mechanism of penetration of the solute chains into the stationary phase, investigated previously [16], demonstrates that in these environments the alkyl chains of the bonded phase, attached to the solid surface, can move more or less freely in the mobile phase.

Influence of the presence of π-electron systems in the solutes and mobile phase with an octadecyl-silica support

In RPLC on *n*-alkyl-bonded phases, the decrease in retention of a linear solute due to the replacement of a saturated bond by an unsaturated bond in the hydrocarbon chain is well known. This phenomenon, which is observed in the presence of double or triple carbon–carbon bonds can be explained by the fact that these bonds

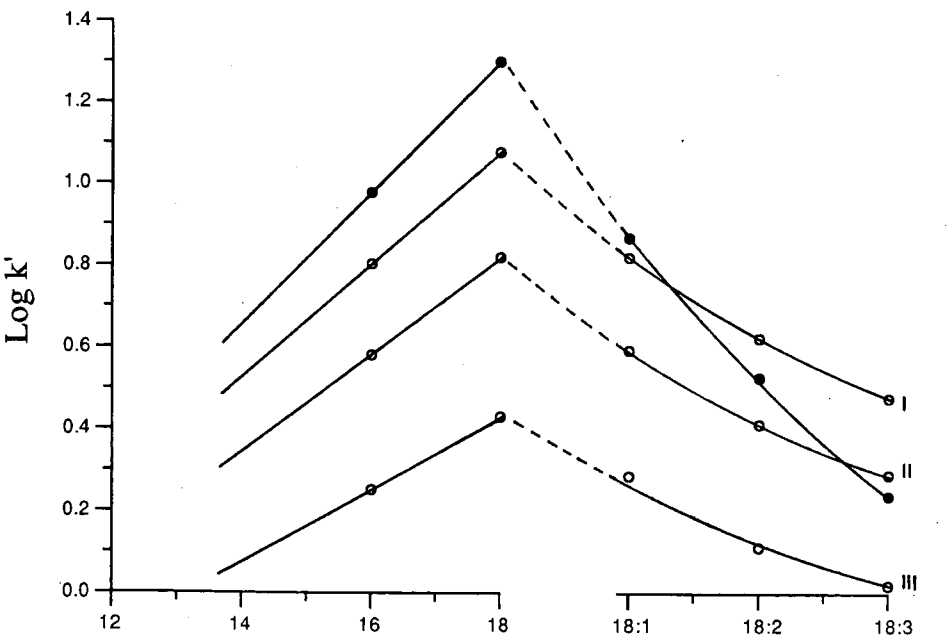

Fig. 2. Retention of homogeneous triglycerides. Left panel, retention *versus* number of carbon atoms in each chain of saturated compounds (tripalmitin and tristearin); right panel, retention *versus* number of double bonds contained in each chain with eighteen carbon atoms (18 = tristearin; 18:1 = triolein; 18:2 = trilinolein; 18:3 = trilinolenin). Column, LiChrosorb RP-18; temperature, 29°C; mobile phase: (●) acetonitrile–chloroform (75:25, v/v), (○) I = methanol–chloroform (80:20, v/v), II = methanol–chloroform (75:25, v/v), III = methanol–chloroform (65:35, v/v).

destroy the conformational similarity between the ligands (the bonded octadecyl moieties) and the linear chain of the solute. This results in a weaker interaction between the hydrocarbon chains of the solute and the ligand and in a greater surface area of contact of the solute–ligand complex with the eluent and, hence, in a weaker retention according to the solvophobic theory. However, the consideration of interactions between the solute and the stationary phase alone provides only a partial explanation of the retention phenomenon. Interactions between all species present in the chromatographic system must be taken into account. The decrease in retention associated with the presence of unsaturated bonds also arises from interactions between the solute and the eluent. Thus the greater polarizability of the unsaturated solutes leads to a greater interaction with polar solvents and contributes to lowering the retention.

This phenomenon is illustrated in Fig. 2, which shows the retention of homogeneous saturated triglycerides (tripalmitin and tristearin) and of unsaturated triglycerides containing eighteen carbon atoms in each of their ester chains (triolein, trilinolein and trilinolenin) on an *n*-octadecyl-bonded phase on silica (ODS). On the left-hand part of the figure, it is seen that, whatever the nature of the organic modifier, $\log k'$ of the saturated solutes increases with the number of carbon atoms of the alkyl chains. It has been previously observed that this increase is linear [16].

It is also noted that, in mixtures with 25% chloroform, methanol is a stronger eluent than acetonitrile for saturated solutes on an ODS stationary phase. This confirms the observations made in pure methanol and acetonitrile mobile phases as well as in acetonitrile–water and methanol–water eluents with a low water content and indicates that, in the chloroform-containing eluents, the solvophobic effect remains the dominating factor controlling the retention, in spite of the varying degree of hydrogen bonding interactions of chloroform with acetonitrile and methanol.

On the right-hand part of Fig. 2 are reported, for binary eluents of a different nature and composition, the retention of saturated and unsaturated homogeneous triglycerides with eighteen carbon atoms in each chain. In all instances a decrease is observed in the retention factor when one or more double bonds are inserted into the carbonaceous skeleton of the solute. Several conclusions can be deduced from these observations.

(1) Whatever the nature of the solvents in the binary eluents or the composition of the mobile phase, the retention drop increases when the number of double bonds in each chain is increased.

(2) The amount of chloroform in the mobile phase does not significantly affect the magnitude of the decrease in retention due to the unsaturated bonds. This is clear from Fig. 1 where the right-hand parts of the curves for three different compositions of the methanol–chloroform mixture are nearly parallel.

(3) The magnitude of the decrease in retention is much larger in an acetonitrile–chloroform mixture than in a methanol–chloroform mobile phase. This can be interpreted by specific interactions occurring between the π-electrons of the solutes and those of the mobile phase. Indeed, acetonitrile, with its cyano group, possesses a site rich in electrons, as do unsaturated compounds. The interaction of these sites results in a high affinity of the unsaturated solutes for the mobile phase. Consequently, in the presence of such interactions, the solute retention is reduced.

(4) The decrease of $\log k'$ and, hence, of the standard free enthalpy (Gibbs

function) of transfer of the solute from the mobile phase to the stationary phase, *versus* the number of double bonds is not linear. This probably results, according to the solvophobic theory, from the non-linearity of the variation between the number of double bonds of the solute and reduction of the surface area of contact of the solute and the ligand with the eluent when forming the solute–ligand complex. In addition, the polarizability of the solutes may not be a linear function of the number of double bonds. Accordingly, Fig. 2 shows that for triglycerides possessing eighteen carbons in each of their three chains, the presence of one, two or three ethylenic bonds has the same effect as the withdrawal of 2.6, 4.8 or 6.5 methylene groups, respectively, from each chain of the solute in acetonitrile–chloroform eluents or the withdrawal of 1.9, 3.3 or 4.2 methylene groups from each solute chain in methanol–chloroform mixtures. These results show that parameters such as the partition number (NP), or the equivalent carbon number (ECN) must always be given with well defined chromatographic conditions. The NP number has been defined by Goiffon *et al.* [19] to relate the retention of triglycerides to their number of carbon atoms and double bonds. The ECN has been introduced by Podlaha and Toregard [20] and represents the number of carbon atoms of a hypothetical saturated triglyceride which would elute at the same time as the unsaturated triglyceride in question.

Another illustration of the influence of the nature of the mobile phase mixture

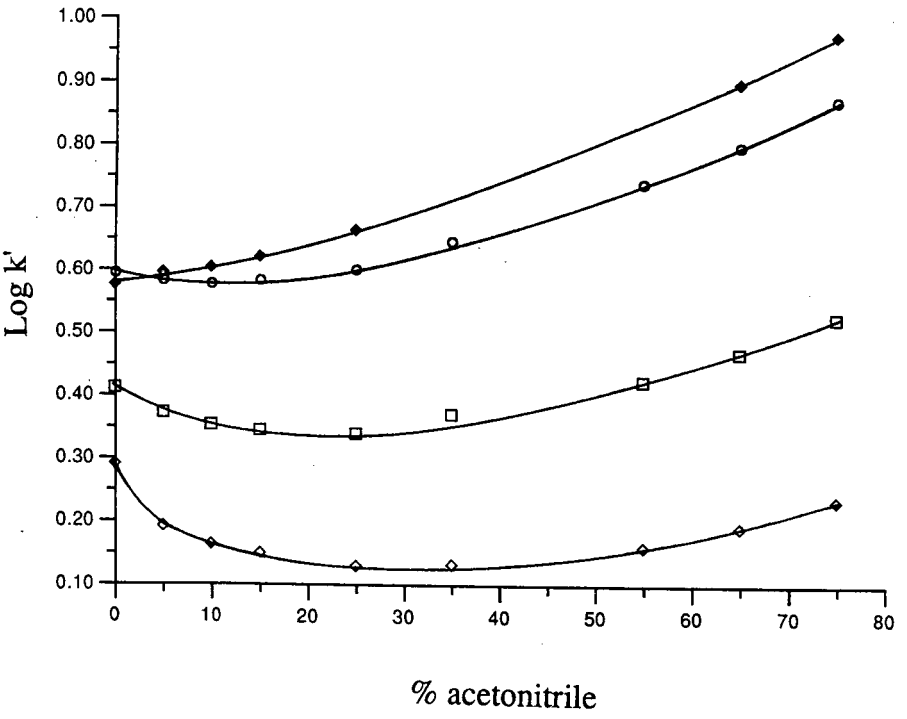

Fig. 3. Retention of homogeneous triglycerides *versus* amount (x) of acetonitrile in the mobile phase. Column, LiChrosorb RP-18; temperature, 29°C; mobile phase, methanol–acetonitrile–chloroform ($75-x$:x:25, v/v/v). Triglycerides: (◆) tripalmitin; (○) triolein; (□) trilinolein; (◇) trilinolenin.

and of the presence of alkene bonds in the solutes on retention is shown in Fig. 3. This represents the variation of log k' of homogeneous saturated and unsaturated triglycerides with the composition of a ternary methanol–acetonitrile–chloroform mobile phase. The amount of chloroform is fixed (25%, v/v) and the percentage composition of the acetonitrile–methanol mixture varies from 0:75 to 75:0. For the saturated solute, the only effect of the addition of increasing amounts of acetonitrile is the decrease of the eluotropic strength of the mobile phase, resulting in an increase in solute retention, as observed for tripalmitin. Another parameter affects the retention of unsaturated solutes. Indeed, the addition of acetonitrile favours the interaction between the solute and solvent due to the presence of the π-electron systems. Consequently, two opposite phenomena compete: the increased solvophobicity of the eluent due to the addition of acetonitrile, which results in an increase in the retention, and a stronger interaction between the solutes and the solvent, which results in a decrease in the retention. Classically, such a competition between two effects leads to an optimum in the curves. In this case, a minimum is observed for the retention of unsaturated compounds *versus* the amount of acetonitrile. The addition of the first aliquots of acetonitrile results in a drop in the retention because the solutes interact with the mobile phase. A further increase in the amount of acetonitrile causes a continuous decrease in retention up to the point where the π–π interaction cannot compensate for the higher solvophobicity of this solvent compared to methanol. This then results in an increase in retention. That a minimum rather than a maximum is observed in Fig. 3 can be qualitatively understood from the variation of the magnitude of the two effects with the amount of acetonitrile added to the mobile phase. The variation of the solvophobicity of the eluent with composition is rather monotonous, as is the variation of the eluent surface tension according to the solvophobic theory of retention in RPLC [4]. In contradiction to this, the variation in the effect of π–π interactions with the eluent composition is expected to be largest for the smallest percentages of acetonitrile in the eluent as once the amount of acetonitrile has reached the point where each solute molecule is surrounded by one or two acetonitrile molecules, the intensity of the π–π interactions will not change significantly with a further addition of acetonitrile in the mobile phase. Consequently, the solvophobic effect is predominant for large percentages of acetonitrile whereas the π–π interaction effect dominates at low percentages. The strength of the interaction between acetonitrile and the solute depends on the number of unsaturated bonds in the solute chains. Therefore, the amount of acetonitrile for which the solvophobic effect becomes the predominant phenomenon is also dependent on the number of unsaturated bonds in the solutes. This is why the decrease in the retention and the percentage of acetonitrile corresponding to the minimum of the curves increase from triolein to trilinolein to trilinolenin.

It is interesting to note in Fig. 3 that the acetonitrile–chloroform (75:25) binary solvent is a stronger eluent for trilinolenin than the methanol–chloroform (75:25) mobile phase, whereas the opposite is true for tripalmitin, triolein and trilinolein. This reflects the fact that the intensity of the π–π interactions between acetonitrile and trilinolenin, which is the most strongly unsaturated of these four triglycerides, overcomes the greater solvophobicity of acetonitrile compared to methanol. Similarly, it can be seen from an analysis of the retention data of Stalcup *et al.* [21] that the four polyaromatic hydrocarbons investigated are retained more in pure methanol than in pure acetonitrile, except, perhaps, the phenanthrophenanthrene.

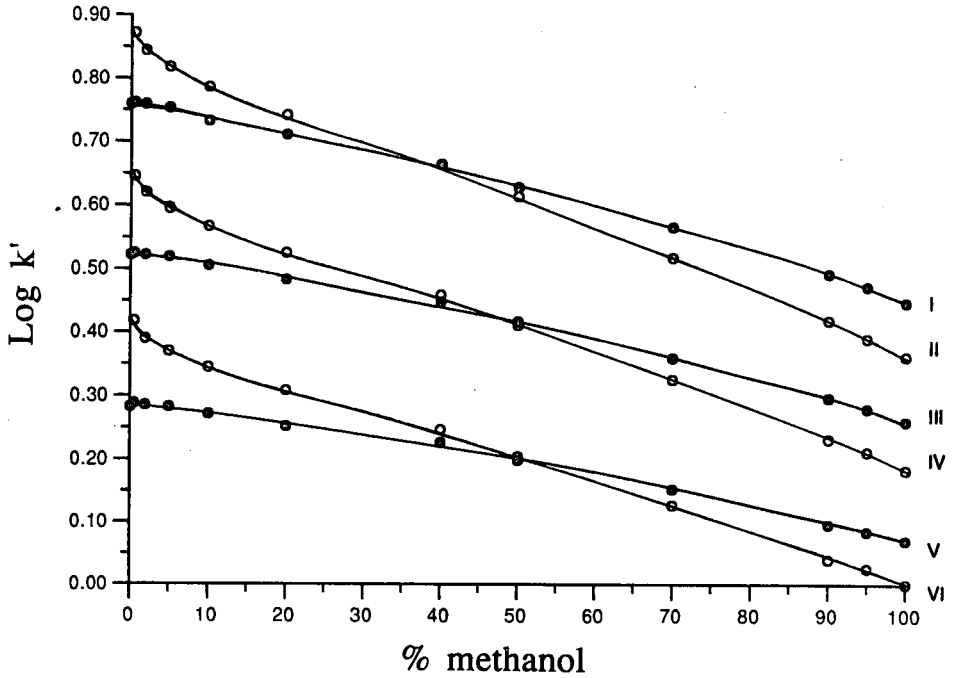

Fig. 4. Retention of *n*-alkanes (●) and *n*-alcohols (○) *versus* the amount of methanol (v/v) in the acetonitrile–methanol mobile phase. Column, Ultrasphere ODS; temperature, 25°C. Solutes: (I) *n*-dodecane, (III) *n*-decane, (V) *n*-octane, (II) *n*-octadecanol, (IV) *n*-hexadecanol, (VI) *n*-tetradecanol.

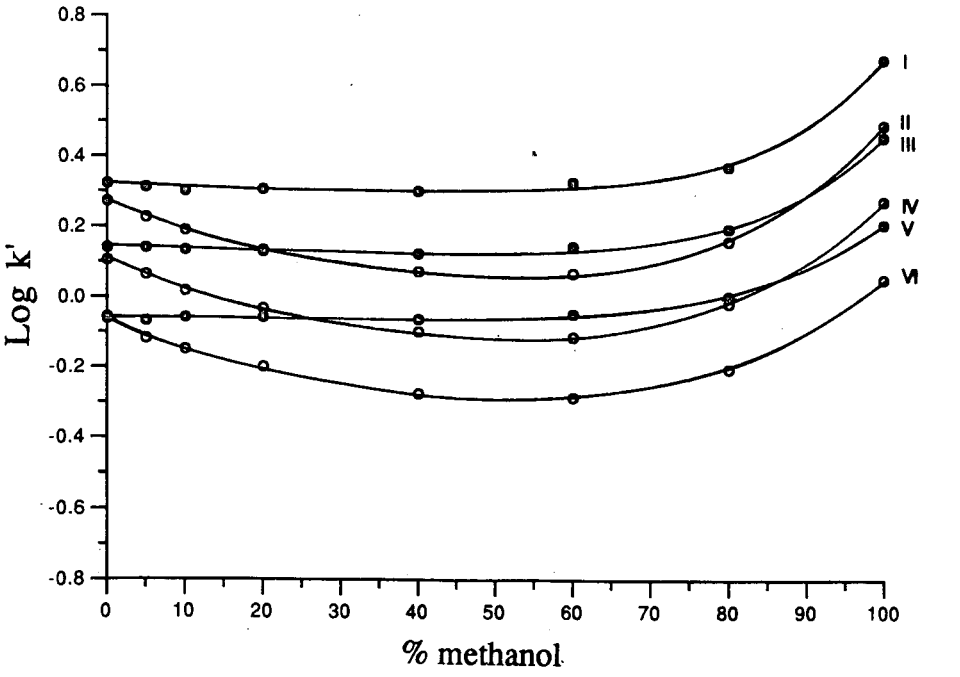

Fig. 5. Retention of *n*-alkanes (●) and *n*-alcohols (○) *versus* the amount of methanol, (v/v) in the acetonitrile–methanol mobile phase. Column, Hamilton PRP-1; temperature, 20°C. Solutes: (I) *n*-decane, (III) *n*-octane, (V) *n*-hexane, (II) *n*-hexadecanol, (IV) *n*-tetradecanol, (VI) *n*-dodecanol.

Influence of the presence of π-electron systems in the mobile and stationary phases with saturated solutes

The effect of the presence of ethylenic bonds in the solute on the retention on the ODS support in various eluents has revealed the essential influence of the π–π interactions between the solute and the eluent. It is interesting to examine these interactions when only the mobile and stationary phases are involved. To do this, a study of the retention of saturated small molecules as a function of the relative amount of methanol and acetonitrile was considered. Owing to its larger retention characteristics for these solutes, a poly(styrene–divinylbenzene) support was preferred to a bonded phenylpropyl silica for this purpose.

To increase the understanding of the results, similar experiments were also performed on the ODS support. The purpose of this comparative study was to unravel the individual effects of π–π interactions and the difference in solvophobicity of the methanol and acetonitrile eluents. The results are reported, in terms of log k' *versus* percentage methanol, in Fig. 4 for the ODS phase and in Fig. 5 for the poly(styrene–divinylbenzene) support. The curves on Fig. 4 for three *n*-alkanes and three *n*-alcohols confirm the results presented in the first part of the Results and Discussion section: the retention of these solutes decreases when the proportion of methanol increases. Pure acetonitrile is more solvophobic than pure methanol and is thus a weaker eluent when solvophobic interactions dominate the retention.

It is interesting to note the rapid decrease in retention for the alcohols when the first aliquots of methanol are added to acetonitrile. This rapid decrease is not observed for the *n*-alkanes. It can be explained by the hydrogen bond interactions occurring in the mobile phase between the alcoholic solutes and the methanol. In addition, the significant peak tailing which is observed with acetonitrile as the eluent for the alcohols, but not for the alkanes, disappears when the amount of methanol in the mobile phase exceeds 0.5% (data not shown). This phenomenon is most likely to be related to competition between the alcoholic solutes and methanol for the interactions, through hydrogen bonds, with the free silanol sites present on the surface of the support. The competition is displaced in favour of the eluent with increasing amounts of methanol. It is important to be aware of this phenomenon when working with non-aqueous mobile phases. It indicates that, although acetonitrile can form hydrogen bonds through its free electron pair on the nitrogen atom [22,23], this bonding is not strong enough to hinder the interaction of the alcoholic solutes with the silanol groups. Obviously, these effects (hydrogen bond interactions in the mobile phase and silanol interactions) contribute simultaneously to the rapid decrease in retention of the alcohols noted at low percentages of methanol in the eluent.

The results obtained on poly(styrene–divinylbenzene) are reported in Fig. 5. Surprisingly, the retention of the *n*-alkanes remains nearly constant when acetonitrile is replaced by methanol. It would have been expected that, as a result of the higher solvophobicity of acetonitrile, the retention of these compounds would decrease when the amount of methanol increased, as was observed on the ODS support. However, another effect has to be taken into consideration in this instance. Acetonitrile can interact by means of π–π interactions with the aromatic rings of the poly(styrene–divinylbenzene) support, whereas methanol does not. The addition of methanol to the mobile phase weakens the interaction of the eluent with the support. Consequently, interactions of the solute with the stationary phase are favoured when methanol is

added. This should result in an increase in the retention of the solutes. The two phenomena, lower solvophobicity and lower eluent interaction with the stationary phase with increasing methanol amount in the mobile phase, have antagonistic effects on the retention. The direction of the retention variation will depend on which phenomenon is the stronger. For the alkanes, these effects are nearly equivalent. The retention is approximately constant over a wide range of methanol–acetonitrile mixtures. It is noticeable that the point is never reached at which the higher eluent strength of methanol is predominant. The decrease in retention is never observed for the alkanes. Conversely, when the amount of methanol is greater than 60%, an increase in retention is observed. This indicates that when the amount of acetonitrile is high enough, a solvent layer is formed at the surface of the stationary phase, rendering the interaction of the solute with this phase more difficult. When the percentage of acetonitrile is low enough, the poly(styrene–divinylbenzene) becomes more accessible to the solutes and their retention increases. For the alcohols, the same phenomenon occurs, except that the retention decreases with the addition of the first aliquots of methanol. This is attributed to the interaction between these solutes and methanol, through hydrogen bonds between their polar heads, which is strong enough to compensate for the increased accessibility of the surface of the stationary phase.

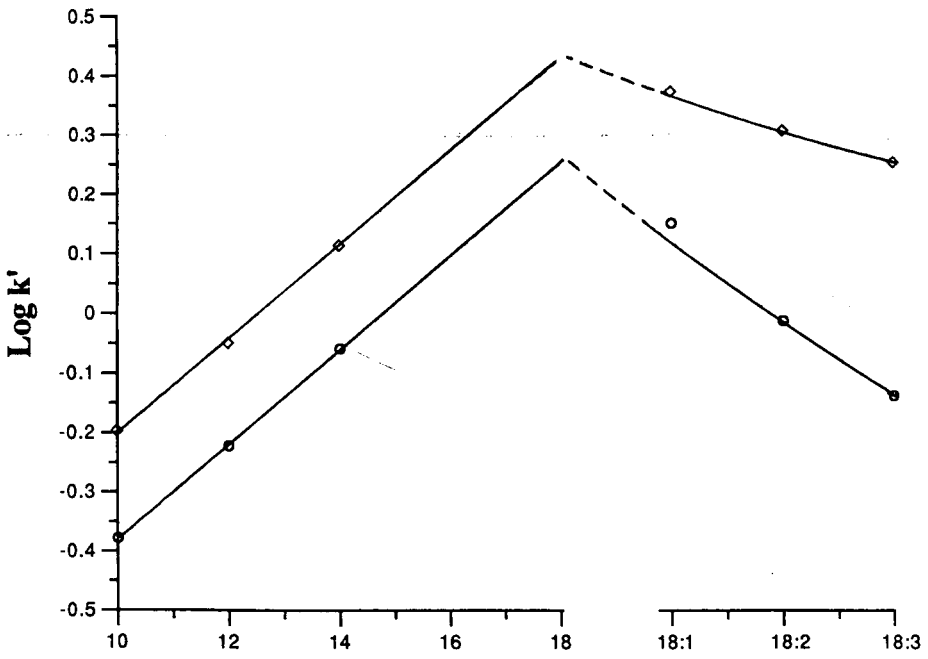

Fig. 6. Retention of homogeneous triglycerides. Left panel, retention *versus* number of carbon atoms in each chain of saturated compounds (tricaprin, trilaurin and trimyristin); right panel, retention *versus* number of double bonds contained in each chain with eighteen carbon atoms (18:1 = triolein; 18:2 = trilinolein; 18:3 = trilinolenin. Column, Zorbax *n*-propylphenyl; temperature, 20°C; mobile phase, (◇) methanol, (○) acetonitrile.

Influence of the presence of π-electron systems in the solutes, stationary phase and mobile phase

The π–π interactions discussed above were taking place between the mobile phase and the solute or the stationary phase. However, these interactions can simultaneously involve these three species. Fig. 6 shows the retention results obtained for saturated and unsaturated triglycerides with a silica support bonded with a propylphenyl phase, which can lead to π–π interactions through the π-electrons of the phenyl groups. This figure can be described in exactly the same way as Fig. 2 for an ODS phase: on the left-hand part of the figure, the logarithms of the capacity factors of the saturated solutes increase linearly with the number of carbon atoms of the solute chains. This phenomenon does not depend on the nature of the organic modifier. As for the ODS support, the right-hand part of the figure shows that the presence of unsaturated bonds in the molecular structure of the solute decreases the retention. The higher the number of unsaturated bonds, the more important is the decrease in retention. Again, the decrease of log k' is not proportional to the number of double bonds.

When comparing the two curves corresponding to the phenyl phase in Fig. 6, it is noted that, as in the case of the ODS support, the magnitude of the decrease in retention due to an unsaturated bond is larger with acetonitrile than with methanol as

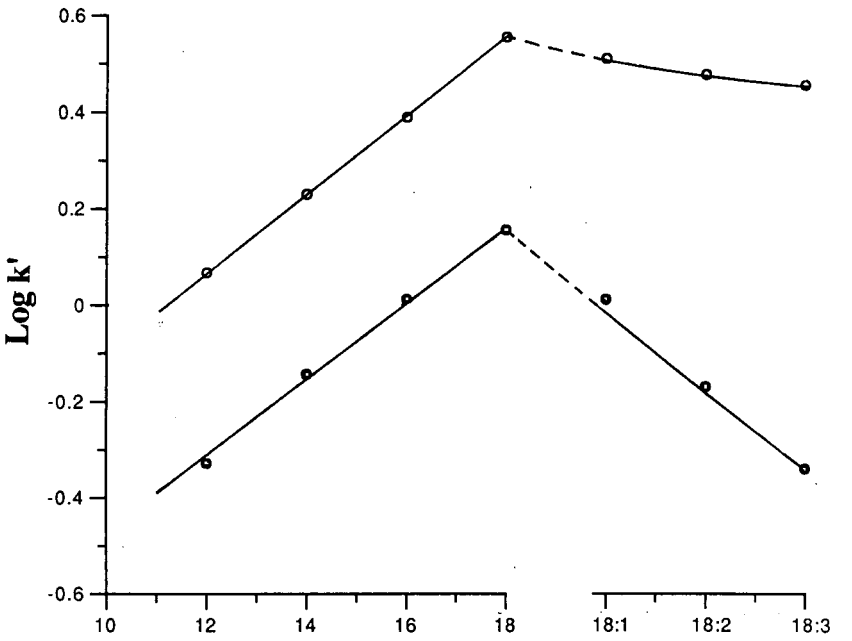

Fig. 7. Retention of homogeneous triglycerides. Left panel, retention *versus* number of carbon atoms in each chain of saturated compounds (trilaurin, trimyristin, tripalmitin and tristearin); right panel, retention *versus* number of double bonds contained in each chain with eighteen carbon atoms (18 = tristearin; 18:1 = triolein; 18:2 = trilinolein; 18:3 = trilinolenin). Column, Hamilton PRP-1. (○) Mobile phase, methanol–chloroform (70:30, v/v); temperature, 20°C. (●) Mobile phase, acetonitrile–chloroform (70:30, v/v); temperature, 15°C.

the mobile phase. This, as with the ODS support, can be explained by the fact that acetonitrile interacts with the π-electrons of the solutes, which decreases their retention.

Fairly similar results are observed on the poly(styrene–divinylbenzene) support, as seen in Fig. 7. The main difference between Figs. 6 and 7 is that, to obtain moderate retention levels with the polymeric support, stronger eluents have to be used. For this reason acetonitrile and methanol are mixed with 30% chloroform. However, as was observed in Fig. 2, the only effect of chloroform is to control the overall solvophobicity of the mobile phase as curves with various percentages of chloroform are parallel for both saturated and unsaturated solutes.

It is interesting to compare the curves obtained in methanolic mobile phase on the three supports shown in Figs. 2, 6 and 7. The decrease in retention due to the replacement of an alkane bond by an alkene bond in the solute chains is larger on the ODS support than on the phenylic phases. Indeed, on the *n*-alkyl-bonded phase, the presence of one, two or three ethylenic bonds in each chain of a triglyceride gives the same retention as that which would be obtained by withdrawing, respectively, 1.9, 3.3 and 4.2 methylene groups in each chain. On the aromatic supports, the corresponding numbers of methylene units to be withdrawn are much lower and are equal to 0.5, 1.6 and 2.2 for the propylphenyl phase and 0.45, 0.9 and 1.2 for the polymeric support, respectively. It can be seen in Fig. 2 that the presence of chloroform in the mobile phase does not affect these numbers. Clearly, these large differences between the ODS phase and the aromatic supports result from π–π interactions between the aromatic sites of the support and the ethylenic bonds of the solute. Indeed, when adding a double bond to a solute, its retention is favoured because of the π–π interaction of the double bond with the support, but the solvophobic effect overcomes this effect so that the retention decreases. However, it decreases less strongly on the aromatic stationary phase than on the ODS support. Consequently, the relative retention difference between triolein, trilinolein and trilinolenin is lower on the aromatic support than it is on the ODS support when methanol or a methanol–chlorofom mixture is used as the eluent.

In contradiction with what is found on the ODS support, in Figs. 5–7, acetonitrile appears to be a stronger eluent than methanol on the two aromatic supports [propylphenyl phase bonded on silica and poly(styrene–divinylbenzene)]. This can be explained by the interaction occurring between the π-systems of the acetonitrile and of the support. Such an interaction lowers that of the solute with the stationary phase. Indeed, the solute has to displace the solvent molecules to interact with the stationary phase. The π–π interaction between the support and the acetonitrile renders this displacement more difficult. Consequently, the solutes interact less strongly with the support, making their retention lower in such an eluent. This effect is fairly significant as it largely overcomes the intrinsically lower solvent strength of the acetonitrile, for both saturated and unsaturated solutes.

It is interesting to determine the effect of acetonitrile on the retention of unsaturated solutes with the stationary phases containing π-electrons, in terms of the numbers of methylene units to be withdrawn to an unsaturated solute to obtain the same retention as a saturated compound of the same series. For homogeneous triglycerides with one, two or three double bonds in each chain, these numbers per chain are 1.3, 3.3 and 5.0 for the propylphenyl silica, 1.8, 4.2 and 6.4 for the polymeric PRP-1

support and equal to 2.6, 4.8 and 6.5 for the ODS support, respectively. These numbers are larger with acetonitrile than with methanol, which is explained by the π–π interactions between the solutes and the eluent. However, the relative differences in these numbers between the ODS support and the aromatic supports is much lower in acetonitrile than in methanol, especially for the polymeric support, which probably reflects the effect of the π–π interactions between the acetonitrile and the aromatic stationary phases.

The data shown in Figs. 1–6 clearly reflect the competitive interactions occurring among the three species engaged in the chromatographic retention process: the stationary phase, mobile phase and the solute. When at least two of these are involved in π–π interactions, the relative strength of these interactions, compared to the other interactions associated with the solvophilic or solvophobic eluent properties which affect the retention in RPLC, can drastically change the selectivities of the separations. If the elution order of the saturated triglycerides is never affected, whatever the nature of the support and the eluent used, the relative retention of the saturated and unsaturated triglycerides is strongly affected by the nature of these phases. Accordingly, great care must be taken, when using partition numbers or equivalent carbon numbers for triglycerides, to specify all the parameters pertaining to the nature of the mobile and stationary phases.

Influence of the addition of a π-complexing agent in the mobile phase on the retention of saturated and unsaturated solutes

The charge-transfer interactions of silver salts with unsaturated compounds is well known [24,25]. This type of interaction is, like the π–π interactions discussed herein, one form of the more general electron donor–electron acceptor group of interactions [26]. It was used to separate unsaturated triglycerides according to their number of double bonds by liquid chromatography with the silica stationary phase loaded with silver nitrate [27]. Separations of unsaturated compounds by RPLC were also performed by adding silver nitrate to the mobile phase [28].

The influence of the addition of silver nitrate to the mobile phase on the retention of saturated and unsaturated triglycerides in RPLC with an ODS support was studied and the results are given in Fig. 8 as a function of the concentration of silver nitrate in methanol–chloroform (75:25) and acetonitrile–chloroform (75:25) eluent mixtures. For both the methanol- and acetonitrile-containing mobile phases, the retention of the saturated compounds slightly increases with an increasing concentration of the salt. This behaviour can be understood from the solvophobic theory as the addition of a salt to a solvent increases its surface tension and thus contributes to an increase in the retention.

In contrast, the retention of the unsaturated triglycerides decreases when the amount of silver ion in the methanolic eluent is increased. This results from the complexation of the ethylenic solutes by the silver salt which, as it occurs in the mobile phase, contributes to the decrease in the retention. This effect largely overcomes the solvophobic effect and is larger for polyunsaturated than for monounsaturated compounds.

However, in the acetonitrile–chloroform eluent, this effect is not observed and the retention of the unsaturated compounds is seen to increase slightly, with an increasing concentration of the salt in the eluent. The behaviour is then fairly similar

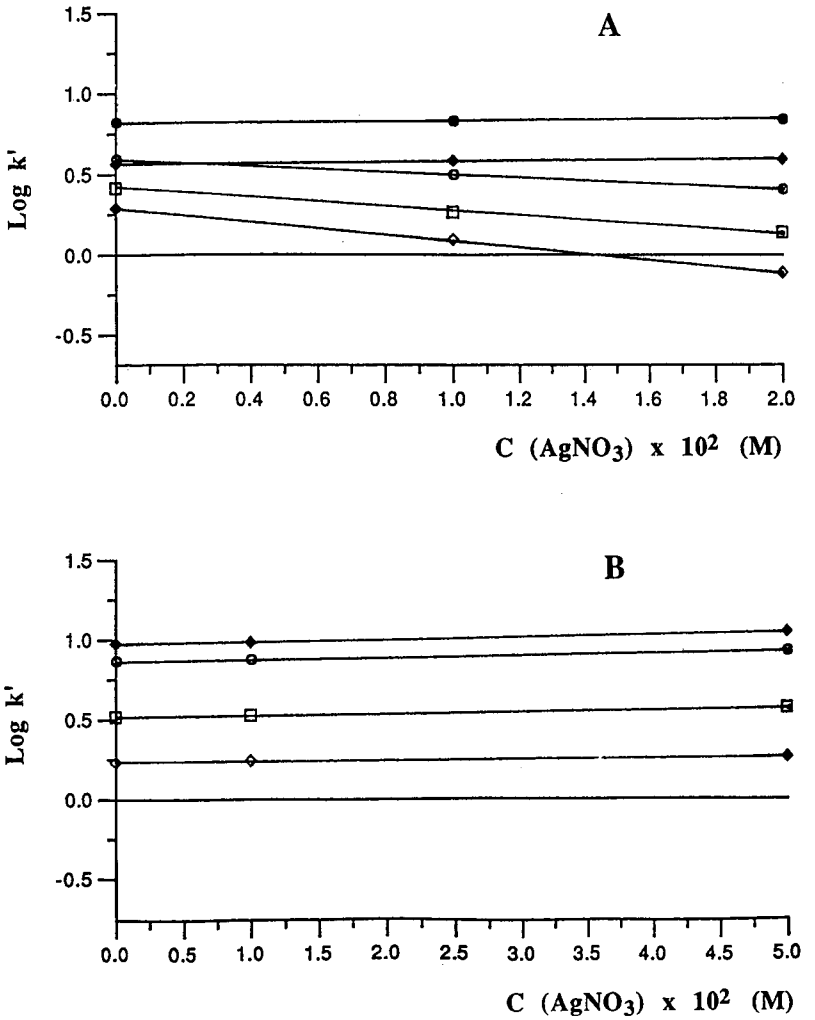

Fig. 8. Retention of homogeneous triglycerides *versus* molar concentration of silver nitrate in the mobile phase. Column, LiChrosorb RP-18; temperature, 29°C. Mobile phase: (A) methanol–chloroform (75:25, v/v); (B) acetonitrile–chloroform (75:25, v/v). Solutes: closed symbols, saturated triglycerides (●, tristearin; ◆, tripalmitin); open symbols, unsaturated triglycerides (○, triolein; □, trilinolein; ◇, trilinolenin).

to that of saturated compounds. Thus, acetonitrile hinders the complexation of the silver ion with the double bonds of the triglycerides, which can be explained by the fact that a charge-transfer complex is formed between the silver ion and the electron-rich cyano group of the acetonitrile. As the amount of acetonitrile in the mobile phase is much larger than that of the triglycerides and largely exceeds that concentration required to complex the silver ions, these ions cannot interact with the double bonds of the triglycerides.

CONCLUSIONS

This investigation of the retention of various saturated and unsaturated solutes in RPLC has shown evidence of the following effects.

(1) In non-aqueous mobile phases, eluents containing acetonitrile have a lower eluotropic strength for saturated compounds than eluents containing methanol. This is in agreement with the solvophobic retention theory of RPLC, but in contradiction with the common belief based on extrapolation of the retention behaviour in water–organic eluents with relatively large amounts of water.

(2) The solvophobic effect is not the major retention-controlling mechanism in RPLC when relatively strong specific interactions occur in the chromatographic system. In some instances, this results in the inversion of the eluting power of eluents containing methanol and acetonitrile, as shown for the highly unsaturated trilolenin.

(3) The study of the relative retention of saturated and unsaturated homogeneous triglycerides on an ODS based material with acetonitrile–methanol mixtures has revealed the significant influence on retention of the π–π interactions occurring between the double bonds of the solutes and the cyano group of acetonitrile.

(4) A similar study on small molecules such as *n*-alcohols revealed the inability of acetonitrile to hinder the formation of hydrogen bonds between the solute and the free silanol groups remaining on the surface of the support. The addition of a very small amount of methanol to the non-aqueous mobile phase is enough to prevent significant peak tailing.

(5) Experiments performed with stationary phases possessing unsaturated sites, such as the poly(styrene–divinylbenzene) or phenylpropyl-bonded silica-based supports, have clearly demonstrated the large influence on retention of π–π interactions when only the stationary phase and the mobile phase are involved. The presence of unsaturated bonds in the support tremendously influences the rate of change of retention when replacing acetonitrile by methanol in the mobile phase.

(6) A comparison of the effect of the presence of double bonds in the solutes on their retention on an ODS support and on aromatic supports has shown that π–π interactions can exist simultaneously among the three species of the system, solute–stationary phase–mobile phase, and that their interplay tremendously influences the selectivity of the separation.

(7) π–π interactions occurring between π-electron-containing molecular systems are one kind of the more general electron donor–electron acceptor group of interactions, as are charge-transfer interactions. Is is shown that such interactions between unsaturated solutes and silver ions present in the mobile phase can be removed by the complexation of the ions with acetonitrile.

This investigation was mainly concerned with the effects of π–π interactions on the retention of saturated and unsaturated solutes. These effects are rather complex as π–π interactions can occur between the components of the chromatographic system, *i.e.* the solute, mobile phase and stationary phase. Although the above discussion is only qualitative, this study shows that taking these π–π interactions into account when at least two of these components possess π-electron bonds allows a coherent description of the various retention effects observed.

This study has particularly illustrated the difference in eluting power between methanol and acetonitrile when double bonds are present either in the solute molec-

ular structure or in the stationary phase. Much work has been devoted over the past few years and is still devoted to the problem of finding the mobile phase composition which gives the best separation of a given sample mixture by RPLC. Usually, two binary aqueous mobile phases (acetonitrile–water and methanol–water) with the same eluotropic strength, *i.e.* providing the same k' range, are selected for the elution of the sample components. Optimization procedures are then used to find the composition of the mixture of these two binary solvents which provides the best separation of the mixture. Sometimes quaternary solvents, generally including tetrahydrofuran as a mobile phase component, are used instead of ternary eluents for this purpose. These results suggest that one of the major effects of modifying the relative content of acetonitrile–methanol in the mobile phase is to affect the relative retentions of the various pairs of sample components due to the interplay of π–π interactions between acetonitrile and the solutes. A proper quantitative treatment of these interactions is expected to greatly facilitate the search for the optimum mobile phase composition.

ACKNOWLEDGEMENTS

The authors gratefully acknowledge J. L. Azemar and M. Anselme for the loan of the Utrasphere ODS column, S. Rabiet and F. Sarlin for the loan of the Hamilton PRP-1 column and J. P. Moissonnier and P. Saint-Martin for the loan of the propylphenyl column. The authors also thank Carla Desilets for her assistance in the preparation of this manuscript.

REFERENCES

1 L. R. Snyder, M. A. Quarry and J. L. Glach, *Chromatographia*, 24 (1987) 33.
2 L. De Galan, D. P. Herman and H. A. H. Billiet, *Chromatographia*, 24 (1987) 108.
3 P. Jandera, *J. Chromatogr.*, 352 (1986) 111.
4 Cs. Horváth, W. Melander and I. Molnár, *J. Chromatogr.*, 125 (1976) 129.
5 B. L. Karger, J. R. Gant, A. Hartkopf and P. H. Weiner, *J. Chromatogr.*, 128 (1976) 65.
6 L. R. Snyder, *J. Chromatogr.*, 92 (1974) 223.
7 J. G. Dorsey and B. P. Johnson, *J. Liq. Chromatogr.*, 10 (1987) 2695.
8 W. J. Cheong and P. W. Carr, *J. Liq. Chromatogr.*, 10 (1987) 361.
9 N. Tanaka, H. Goodell and B. L. Karger, *J. Chromatogr.*, 158 (1978) 233.
10 N. Tanaka, K. Sakagami and M. Araki, *J. Chromatogr.*, 199 (1980) 327.
11 H. Colin, A. M. Krstulovic, G. Guiochon and Z. Yun, *J. Chromatogr.*, 255 (1983) 295.
12 W. R. Melander, J.-X. Huang, Cs. Horváth, R. W. Stout and J. J. DeStefano, *Chromatographia*, 20 (1985) 641.
13 T. Hanai and J. Hubert, *J. Chromatogr.*, 291 (1984) 81.
14 R. M. Smith and D. Garside, *J. Chromatogr.*, 407 (1987) 19.
15 L. Nondek, *J. Chromatogr.*, 373 (1986) 61.
16 M. Martin, G. Thévenon and A. Tchapla, *J. Chromatogr.*, 452 (1988) 157.
17 H. Colin, G. Guiochon, Z. Yun, J. C. Diez-Masa and P. Jandera, *J. Chromatogr. Sci*, 21 (1983) 179.
18 Z. Yun, *University Doctorate Thesis*, University of Paris VI, Paris 1982.
19 J. P. Goiffon, C. Réminiac and D. Furon, *Rev. Fr. Corps Gras*, 4 (1981) 167.
20 O. Podlaha and B. Toregard, *J. High Resolut. Chromatogr. Chromatogr. Commun.*, 5 (1982) 553.
21 A. M. Stalcup, D. E. Martire and S. A. Wise, *J. Chromatogr.*, 442 (1988) 1.
22 E. Tesarova and V. Pacakova, *Chromatographia*, 17 (1983) 269.
23 S. M. Staroverov, G. V. Lisichkin and E. L. Styskin, *Chromatographia*, 21 (1986) 165.
24 S. Winstein and H. J. Lucas, *J. Am. Chem. Soc.*, 60 (1938) 836.
25 M. A. Muhs and F. T. Weiss, *J. Am. Chem. Soc.*, 20 (1962) 4697.
26 R. Foster, *Organic Charge-transfer Complexes*, Academic Press, London, 1969.
27 E. C. Smith, A. D. Jones and E. W. Hammond, *J. Chromatogr.*, 188 (1980) 205.
28 B. Vonach and G. Schomburg, *J. Chromatogr.*, 149 (1978) 417.

Journal of Chromatography, 550 (1991) 285–300
Elsevier Science Publishers B.V., Amsterdam

CHROMSYMP. 2137

Reversed-phase liquid chromatographic study of excess and absolute sorption isotherms of acetonitrile–water mixtures

A. ALVAREZ-ZEPEDA and D. E. MARTIRE*
Department of Chemistry, Georgetown University, Washington, DC 20057 (USA)

ABSTRACT

The retention volumes of the disturbance peak, $V_{r,(1,2)}$, and the isotopically labeled counterparts, $V_{R,1^*}$ and $V_{R,2^*}$, of the components of acetonitrile–water mixtures were determined over a wide composition range at 25, 35, 45 and 55°C. An explicit, model-independent, self-consistency equation relating $V_{R,(1,2)}$ and the composition derivatives of $V_{R,1^*}$ and $V_{R,2^*}$ derived and succesfully tested. Also derived were equations that lead to the evaluation (from the same data set) and linkage of the excess and absolute sorption isotherms of the components. The latter isotherms are based on an internally consistent model which permits the determination of the mobile phase volume.

INTRODUCTION

In an attempt to understand the solute retention mechanism(s) in reversed-phase liquid chromatography (RPLC), a large number of papers have been devoted to the surface characterization of *n*-alkyl-bonded phases [1,2]. Sander and Wise [2] reviewed various types of substrates, stationary bonded phases, their methods of characterization and chromatographic properties. In addition to the characterization of the *n*-alkyl-bonded chain and the residual silanols on the silica surface, Knox and Pryde [3] were among the first to propose the importance of the uptake of the organic modifier in the stationary phase. Soon thereafter, this was experimentally demonstrated by Scott and Kucera [4,5] and others [6,7].

Introduction in the column of a very small amount of an isotopically labelled solute (ILS) (*e.g.*, ^2H_2O) in a binary system causes a finite "minor disturbance peak" or disturbance peak (DP) [8,9], in addition to the elution peak of the ILS [10–16]. The elution data of the ILS have been used to investigate the distribution of organic modifiers in reversed-phase columns [11,12,16,17], as a method for the determination of surface excess isotherms [12–14,17–19] and the determination and interpretation of the column dead volume [11,13–16].

We review here some aspects of previous work relevant to this paper. McCormick and Karger [11] studied the elution behavior of the ILS in three organic modifiers mixed with water: methanol, acetonitrile (ACN) and tetrahydrofuran (THF). The interpretation of the elution data of the ILS and the DP was based on

0021-9673/91/$03.50

Helfferich's equation for the finite band migration in liquid chromatography [20,21]. A generalized distribution isotherm was proposed to explain the elution behavior of the ILS and DP or "vacancy band". The enrichment of the stationary phase by the organic modifier was also considered. Slaats *et al.* [12] used various experimental methods to measure the surface excess isotherms of ACN and CH_3OH with aqueous binary mixtures. Two models were proposed to calculate the volume of the adsorbed layer in the stationary phase. Zhu [16], using the ILS elution data in ACN–water mixtures, determined an absolute adsorption isotherm of ACN and defined the column dead volume as the difference between the maximum column hold-up volume and the volume of the adsorbed solvent (ACN). Based on his absolute isotherm of ACN, Zhu attempted to explain the chromatographic behavior of the DP, ^2H_2O and deuterated acetonitrile (ACN-d_3).

The work of Riedo and Kováts [13] is particularly noteworthy. From the differential equation of the material balance in the column, they found an analytical solution for the retention volume of a solute in isocratic, isothermal liquid chromatography. This equation, which has general validity for a binary mixture and is independent of any specific model, determines the retention volume of a solute introduced in the column as an infinitesimal perturbation of the eluent mixture composition or "the concentration vector" [13]. The retention volume of the solute depends on the changes occurring in the column eluent composition caused by the introduction of the solute(s). This equation can be expressed in terms of mass, moles or volumes [14,19].

The purpose of this paper is two-fold. First, we shall derive a set of equations that describe quantitatively the elution behavior of the ILS and DP in terms of absolute quantities (*i.e.*, absolute sorption isotherms). An explicit, self-consistency relationship is derived that relates the retention volumes of the ILS to the retention volume of the DP. The retention of the DP can be determined in terms of absolute quantities or excess quantities. We show that they are equivalent and that the surface excess isotherm can be calculated from the absolute sorption isotherms. A second purpose is to propose and test a simple model for the sorbed water ($V_{1,s}$) and the sorbed ACN ($V_{2,s}$) in the stationary phase (*i.e.*, the absolute sorption isotherms). We have investigated this problem because of the need for a model of the stationary phase in RPLC, *i.e.*, its volume, composition and structure [22]. A consequence of this model is the determination of the mobile phase volume, V_m.

EXPERIMENTAL

Equipment and materials

The liquid chromatograph consisted of a Beckman Model 112 pump, a Valco injector with a 0.5-μl internal sample loop, a differential refractive index detector (Model R401, Waters Assoc., Milford, MA, USA) and a Perkin-Elmer Model 56 strip-chart recorder. The column used was a C_{18} chemically bonded phase, purchased from ES Industries (Marlton, NJ, USA). The column (25 cm × 4.6 mm I.D.) was packed with 4.7 g of *n*-octadecyl-bonded amorphous silica. The packing specifications reported by the manufacturer were mean particle diameter 5 μm, nominal pore diameter 300 Å, surface area 100 m^2/g and carbon content 5.5%. The high-performance liquid chromatographic-grade eluents, acetonitrile and water, were obtained

from Fisher Scientific (Fair Lawn, NJ, USA). Deuterium oxide and deuterated ACN were obtained from MSD Isotopes, a division of Merck Frosst Canada (Montreal, Canada).

Procedures

The solvent mixtures were prepared by measuring separately and then mixing known volumes of ACN and water. Every mixture was degassed prior to use by applying a vacuum for at least 10 min while stirring with a magnetic bar. The column was thermostated by putting it inside a water-jacket, the temperature of which was controlled to within ± 0.1°C. The nominal flow-rate was 1 ml/min. The actual flow-rate of (collected) eluent under ambient conditions was measured with a timer and a 5-ml calibrated volumetric flask. The correction for isothermal compressibility was found to be insignificant. However, a necessary correction from ambient temperature was made using the equation

$$F_c = F_a(\rho_a/\rho_c)$$

where F_c and F_a are the corrected and measured (ambient) flow-rates and ρ_a and ρ_c are the densities of the eluent at ambient temperature and at the column temperature. Retention volumes (V_R) were calculated using the equation

$$V_R = F_c\, t_r$$

where t_r is the retention time. The retention volumes were corrected for the extra-column volume. Each retention time was recorded at least three times. Retention times were obtained by injecting pure ILS or eluent (water or ACN). Injection of an ILS generally generates two peaks, one for the elution of the ILS and the other corresponding to the DP. The retention time of the DP was separately corroborated by injecting pure water or ACN. Four temperatures were investigated, 25, 35, 45 and 55°C.

THEORY

We start with the Riedo–Kováts basic equation [13,19]. The retention volume of a solute ($V_{R,i}$), in a binary solvent mixture, under isothermal and isocratic conditions, when an infinitesimal amount of solute i is injected, is given by

$$V_{R,i} = \left(\frac{\partial V_i}{\partial \theta_i}\right)_{\theta^0} - \theta_i^0 \left(\frac{\partial V_t}{\partial \theta_i}\right)_{\theta^0} \tag{1}$$

where V_i represents the volume of component i in the column (*i.e.*, its partial volume in the column), θ_i is the volume fraction of component i in the column, V_t is the total volume of the liquid mixture in the column, θ^0 is the isocratic composition of the equilibrated mixture prior to the injection of solute i and θ_i^0 is the composition of i in the column prior to the injection of solute i. If the solute i is not present in the column liquid mixture, its retention volume is given by

$$V_{R,i} = \left(\frac{\partial V_i}{\partial \theta_i}\right)_{\theta^0} \tag{1a}$$

From material balance, V_i can be expressed as

$$V_i = V_{i,s} + \theta_i V_m \tag{2}$$

where $V_{i,s}$ represents the volume of i sorbed on the modified surface (*i.e.*, the stationary phase) and $\theta_i V_m$ represents the volume of i in the mobile phase with a volume V_m.

Retention volume of the disturbance peak (DP)

The retention volume of the DP in a binary mixture is analyzed as follows. Consider a mobile phase consisting of water (component 1) and ACN (component 2) (*i.e.*, i is 1 or 2). If a very small perturbation in the composition of the mobile phase is caused by injecting an infinitesimal amount of component 1 or 2, the overall column liquid composition remains the same. The total liquid volume in the column (V_t) in this case is

$$V_t = V_1 + V_2 \tag{3}$$

Using eqn. 2 in eqn. 3, we obtain

$$V_t = V_m + V_{1,s} + V_{2,s} \tag{4}$$

where s refers to the stationary phase and m refers to the mobile phase. The substitution of the derivatives of eqns. 2 ($i = 1$) and 4 with respect to θ_1 into eqn. 1 gives the retention volume of component 1 as

$$V_{R,1} = V_m + \left(\frac{\partial V_{1,s}}{\partial \theta_1}\right) + \theta_1\left(\frac{\partial V_m}{\partial \theta_1}\right) - \theta_1^0\left[\left(\frac{\partial V_m}{\partial \theta_1}\right) + \left(\frac{\partial V_{1,s}}{\partial \theta_1}\right) + \left(\frac{\partial V_{2,s}}{\partial \theta_1}\right)\right] \tag{5}$$

where we have dropped the subscript θ^0 in the partial derivative notation. As the amount of component 1 injected is very small, $\theta_1 = \theta_1^0$, and eqn. 5 reduces to

$$V_{R,1} = V_m + \left(\frac{\partial V_{1,s}}{\partial \theta_1}\right) - \theta_1\left[\left(\frac{\partial V_{1,s}}{\partial \theta_1}\right) + \left(\frac{\partial V_{2,s}}{\partial \theta_1}\right)\right]$$

Similarly for component 2, we obtain

$$V_{R,2} = V_m + \left(\frac{\partial V_{2,s}}{\partial \theta_2}\right) - \theta_2\left[\left(\frac{\partial V_{1,s}}{\partial \theta_2}\right) + \left(\frac{\partial V_{2,s}}{\partial \theta_2}\right)\right]$$

and using the relationship $\partial\theta_1 = -\partial\theta_2$, we obtain

$$V_{R,1} = V_{R,2} = V_{R,(1,2)} = V_m + \theta_1\left(\frac{\partial V_{2,s}}{\partial \theta_2}\right) + \theta_2\left(\frac{\partial V_{1,s}}{\partial \theta_1}\right) \tag{6}$$

where $V_{R,1}$, $V_{R,2}$ and $V_{R,(1,2)}$ are the retention volumes of component 1, component 2 and the DP, respectively. Elution volumes of the DP are described by eqn. 6, in terms of the absolute quantities V_m, $V_{1,s}$ and $V_{2,s}$; however, the evaluation of eqn. 6 requires a model that relates these quantities to the mobile phase composition.

Retention volume of the isotopically labeled solutes (ILS)

The elution volumes of the ILS, deuterium oxide (^2H_2O or 1*) and deuterated ACN (ACN-d_3 or 2*) are found as follows. As the ILS are not present in the column prior to the injection of either i*, eqn. 1a applies and substitution of eqn. 2 in eqn. 1a gives

$$V_{R,i*} = V_m + \theta_{i*}\left(\frac{\partial V_m}{\partial \theta_{i*}}\right) + \left(\frac{\partial V_{i*,s}}{\partial \theta_{i*}}\right)$$

Also, as a very small amount of the ILS is injected, $\theta_{i*} \approx 0$ and the previous equation reduces to

$$V_{R,i*} = V_m + \left(\frac{\partial V_{i*,s}}{\partial \theta_{i*}}\right) \tag{7}$$

where $V_{R,i*}$ is the retention volume of ILS component i.

If isotopic exchange is ignored [23], and one considers only the thermodynamic distribution (*i.e.*, partition by dilution) of the ILS into the corresponding non-labeled eluent (water or ACN) between the mobile phase and the stationary phase, the dilution partition constant (K_*) is

$$K_* = \frac{C_{1*,s}}{C_{1*,m}} = \frac{v_{1*}n_{1*,s}V_{1,m}}{v_{1*}n_{1*,m}V_{1,s}} = 1 \tag{8a}$$

or

$$V_{1*,s} = V_{1*,m}\left(\frac{V_{1,s}}{V_{1,m}}\right) \tag{8b}$$

where $C_{1*,s}$ and $C_{1*,m}$ are the concentrations of 1* in the stationary and mobile phases, respectively, v and n represent the molar volume and number of moles of the ILS, respectively, and V represents volume. The substitution of $V_{1,m} = \theta_1 V_m$ in eqn. 8b gives

$$V_{1*,s} = \theta_{1*,m}\left(\frac{V_{1,s}}{\theta_1}\right) = \theta_{1*}\left(\frac{V_{1,s}}{\theta_1}\right) \tag{9}$$

where $\theta_{1*,m}$ is the volume fraction of 1* in the mobile phase, which is equal to θ_{1*}. Taking the derivative of eqn. 9 with respect to θ_{1*} and substituting the result into eqn. 7, we obtain

$$V_{R,1*} = V_m + \frac{V_{1,s}}{\theta_1} \tag{10a}$$

Similarly,

$$V_{R,2*} = V_m + \frac{V_{2,s}}{\theta_2} \tag{10b}$$

where $V_{R,1*}$ and $V_{R,2*}$ are the retention volumes of ^2H_2O and ACN-d_3, respectively. Eqns. 10 can be derived in an alternative manner [16,22].

The substitution of eqns. 10a and 10b into eqn. 4 gives

$$V_t = \theta_1 V_{R,1*} + \theta_2 V_{R,2*} = \langle V_{R,(1*,2*)} \rangle \tag{11}$$

which is the total or "hold-up" column volume of the liquid solvent mixture [13,19,22].

The derivative of $V_{1,s}$ with respect to θ_1 in eqn. 10a is

$$\left(\frac{\partial V_{1,s}}{\partial \theta_1}\right) = V_{R,1*} + \theta_1\left(\frac{\partial V_{R,1*}}{\partial \theta_1}\right) - V_m - \theta_1\left(\frac{\partial V_m}{\partial \theta_1}\right) \tag{12}$$

The derivative of V_m with respect to θ_2 in eqn. 10b is

$$-\left(\frac{\partial V_m}{\partial \theta_2}\right) = \left(\frac{\partial V_m}{\partial \theta_1}\right) = -\left(\frac{\partial V_{R,2*}}{\partial \theta_2}\right) + \frac{1}{\theta_2}\left(\frac{\partial V_{2,s}}{\partial \theta_2}\right) - \frac{V_{2,s}}{(\theta_2)^2} \tag{13}$$

Utilizing eqns. 6 and 10–13 we obtain the following equivalent forms:

$$V_{R,(1,2)} = \theta_1 V_{R,2*} + \theta_2 V_{R,1*} + \theta_1\theta_2\left[\frac{\partial (V_{R,2*} - V_{R,1*})}{\partial \theta_2}\right] \tag{14a}$$

$$V_{R,(1,2)} = \theta_2\left[\frac{\partial (\theta_1 V_{R,1*})}{\partial \theta_1}\right] + \theta_1\left[\frac{\partial (\theta_2 V_{R,2*})}{\partial \theta_2}\right] \tag{14b}$$

$$V_{R,(1,2)} = \langle V_{R,(1*,2*)} \rangle + \left\{\frac{\partial [\theta_1\theta_2 (V_{R,2*} - V_{R,1*})]}{\partial \theta_2}\right\} \tag{14c}$$

Eqn. 14, which relates the retention volumes of the DP and ILS peaks, is an important, model-independent, self-consistency equation (see below).

Finally, we relate surface excess volumes (V_i^E) to the absolute volumes $V_{1,s}$ and $V_{2,s}$. We adopt the convention "nothing is adsorbed in terms of volumes, VNA" [14,19]. From the relationships

$$V_2^E = V_{2,s} - \theta_2(V_{1,s} + V_{2,s}) = \theta_1 V_{2,s} - \theta_2 V_{1,s} \tag{15}$$

and

$$V_1^E = V_{1,s} - \theta_1(V_{1,s} + V_{2,s}) = \theta_2 V_{1,s} - \theta_1 V_{2,s} \tag{16}$$

one obtains

$$V_2^E = -V_1^E \tag{17}$$

From eqns. 10a, 10b, 15 and 17, we obtain

$$V_2^E = -V_1^E = \theta_1\theta_2(V_{R,2*} - V_{R,1*}) \tag{18}$$

The substitution of eqn. 18 in eqn. 14c gives

$$V_{R,(1,2)} = \langle V_{R,(1*,2*)} \rangle + \left(\frac{\partial V_2^E}{\partial \theta_2}\right) = \langle V_{R,(1*,2*)} \rangle + \left(\frac{\partial V_1^E}{\partial \theta_1}\right) \tag{19}$$

which is equivalent to eqn. 7 in ref. 19.

RESULTS AND DISCUSSION

Temperature dependence

Four temperatures were investigated, 25, 35, 45 and 55°C. Elution volumes of the ILS ($V_{R,1*}$ and $V_{R,2*}$) and the DP [$V_{R,(1,2)}$] are listed in Tables I–III. $V_{R,(1,2)}$ is calculated as the average of the retention volumes of water and ACN. The average difference between the retention volumes of water ($V_{R,1}$) and ACN ($V_{R,2}$) is 0.005 ml, which is within the experimental error. Tables I–III show temperature effects, which

TABLE I

RETENTION VOLUMES OF ^2H_2O

Volume fraction of ACN	$V_{R,1*}$ (ml)			
	25°C	35°C	45°C	55°C
0.15	3.066	3.050	3.049	3.040
0.20	3.041	3.011	3.020	3.017
0.25	3.001	2.990	2.989	2.994
0.30	2.967	2.965	2.975	2.985
0.35	2.945	2.943	2.970	2.967
0.40	2.925	2.927	2.958	2.957
0.45	2.906	2.904	2.934	2.942
0.50	2.893	2.887	2.915	2.931
0.55	–	2.896	2.916	2.936
0.60	2.921	2.930	2.937	2.957
0.65	–	2.964	2.986	2.980
0.70	2.987	2.992	3.006	3.006
0.75	–	3.018	3.034	3.040
0.80	3.054	3.037	3.047	3.062
0.85	–	3.093	3.123	3.126
0.90	3.214	3.182	3.199	3.222
0.95	–	3.255	3.252	3.271

TABLE II

RETENTION VOLUMES OF ACN-d_3

Volume fraction of ACN	$V_{R,2*}$ (ml)			
	25°C	35°C	45°C	55°C
0.15	3.835	3.788	3.767	3.752
0.20	3.777	3.692	3.663	3.622
0.25	3.708	3.639	3.593	3.573
0.30	3.652	3.562	3.528	3.493
0.35	3.590	3.512	3.480	3.463
0.40	3.500	3.443	3.421	3.381
0.45	3.461	3.393	3.379	3.360
0.50	3.408	3.354	3.329	3.319
0.55	–	3.316	3.285	3.275
0.60	3.323	3.288	3.256	3.257
0.65	–	3.249	3.235	3.226
0.70	3.267	3.232	3.220	3.204
0.75	–	3.213	3.205	3.197
0.80	3.205	3.177	3.169	3.177
0.85	–	3.172	3.170	3.160
0.90	3.208	3.160	3.169	3.162
0.95	–	3.153	3.150	3.148

TABLE III

RETENTION VOLUMES OF THE SOLVENT DISTURBANCE PEAK

Volume fraction of ACN	$V_{R,(1,2)}$ (ml)			
	25°C	35°C	45°C	55°C
0.15	3.536	–	3.458	3.407
0.20	3.517	3.427	3.383	3.353
0.25	3.445	3.362	3.309	3.270
0.30	3.358	3.274	3.233	3.212
0.35	3.273	3.199	3.184	3.142
0.40	3.143	3.080	3.047	3.053
0.45	3.027	2.995	2.991	2.975
0.50	2.928	2.917	2.917	2.932
0.55	–	2.846	2.865	2.896
0.60	2.810	2.814	2.840	2.865
0.65	–	2.813	2.837	2.860
0.70	2.801	2.836	2.865	2.883
0.75	–	2.857	2.889	2.904
0.80	2.889	2.892	2.925	2.932
0.85	–	2.955	2.989	2.967
0.90	3.030	3.000	3.067	3.023
0.95	–	3.054	3.081	3.066

TABLE IV

SOLVENT HOLD-UP VOLUMES

Volume fraction of ACN	V_t^a (ml)			
	25°C	35°C	45°C	55°C
0.15	3.181	3.161	3.157	3.147
0.20	3.188	3.148	3.149	3.138
0.25	3.178	3.152	3.140	3.139
0.30	3.172	3.144	3.141	3.138
0.35	3.171	3.142	3.148	3.141
0.40	3.155	3.133	3.143	3.127
0.45	3.155	3.124	3.134	3.130
0.50	3.150	3.120	3.122	3.125
0.55	–	3.127	3.119	3.122
0.60	3.162	3.145	3.128	3.137
0.65	–	3.149	3.148	3.140
0.70	3.183	3.160	3.156	3.145
0.75	–	3.164	3.162	3.158
0.80	3.175	3.149	3.145	3.154
0.85	–	3.160	3.163	3.155
0.90	3.209	3.162	3.172	3.168
0.95	–	3.158	3.155	3.154

[a] Calculated from eqn. 11 and the results in Tables I and II.

appear to be relatively small; however, the effect of temperature is clearly noticeable in the absolute and excess quantities to be discussed. Also, listed in Table IV are the solvent hold-up volumes, which, as expected, are virtually independent of temperature.

Retention of the disturbance peak

The retention volume of the disturbance or "vacancy" peak has an interesting behavior as a function of mobile phase composition (Fig. 1). It passes through

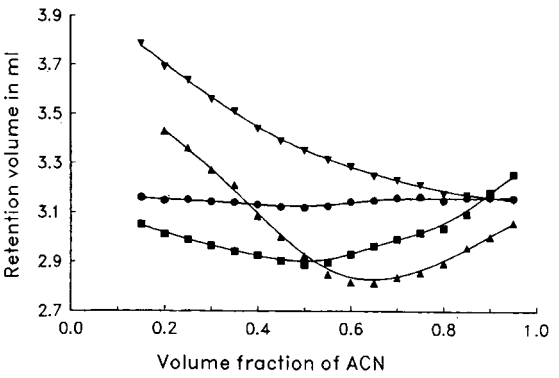

Fig. 1. Dependence of (■) $V_{R,1}*$, (▼) $V_{R,2}*$, (▲) $V_{R,(1,2)}$ and (●) V_{total} on θ_2 at 35°C.

a minimum, and both the water-enriched band and the ACN-enriched band essentially co-elute. Similar behavior has been observed in other binary systems. McCormick and Karger [11] explained this behavior by proposing a convex-type distribution isotherm, which has a maximum, with positive and negative slopes. Depending on the sense of the slopes (positive or negative), the vacancy velocity would decrease or increase with respect to the mobile phase velocity [21]. Zhu [16] proposed an absolute Langmuir-type adsorption isotherm for ACN, which we believe is essentially correct. However, it only partially explains the overall retention behavior of the DP. It does not consider the water adsorption isotherm contribution to the retention of the DP.

Eqn. 6 describes the retention volume of the DP as function of V_m, mobile phase composition and the derivatives (slopes) of the absolute isotherms of the solvent components. This relationship clearly indicates that the overall retention of the DP depends on the slopes of both isotherms (components 1 and 2). Eqn. 6 involves no approximations and any model that one proposes has to be consistent with it. We use eqn. 6 (with eqns. 10) to test our model for the absolute sorption isotherms, which provide insight into the changes occurring in the stationary phase due to changes in the mobile phase composition. Retention of the DP can also be expressed in terms of the hold-up volume and the derivative of the surface excess isotherm by eqn. 19. This relationship is exact and model independent, but does not provide a means of determining the individual contributions of components 1 and 2 to the overall retention of the DP. Note that eqns. 6 and 19 are essentially equivalent, though, in that they are related through the self-consistency relationship, eqn. 14, and eqns. 10 and 15–18.

Retention of the isotopically labeled solutes

Retention of the ILS is described by eqns. 10a and 10b, and their validity can be tested through eqns. 14. If $V_{R,(1,2)}$ can be reproduced by means of eqns. 14, then retention of the ILS is correctly described by eqns. 10 (in fact, the assumed absence of isotopic effects in the derivation of eqns. 10 also applies to eqns. 14 and 18, which derive from eqns. 10). Similarly, the reproduction of $V_{R,(1,2)}$ by means of the surface excess isotherm [19] is an equivalent way of testing eqns. 10. Accordingly, $V_{R,(1,2)}$ values were calculated using eqn. 14a. The derivative of the difference, $V_{R,2}* - V_{R,1}*$, in eqn. 14a was evaluated by first fitting this difference to a third-order polynomial in θ_2. The coefficients of the equation and the correlation coefficients are displayed in Table V. The absolute average differences of the $V_{R,(1,2)}$ values calculated using

TABLE V

COEFFICIENTS OF THE THIRD-ORDER POLYNOMIAL FIT OF $V_{R,2}* - V_{R,1}*$ TO θ_2

$V_{R,2}* - V_{R,1}* = a + b\theta_2 + c\theta_2^2 + d\theta_2^3$.

Temperature (°C)	a	b	c	d	R^2
25	0.839	−0.401	−0.443	−0.169	0.999
35	0.885	−1.154	1.035	−0.960	0.998
45	0.912	−1.600	1.781	−1.289	0.998
55	0.946	−2.069	2.769	−1.879	0.997

eqn. 14a and the results in Tables I, II and V, and the experimental values of $V_{R,(1,2)}$ are 0.040, 0.034, 0.028 and 0.036 ml at 25, 35, 45 and 55°C, respectively, or an overall average difference of about 1%. Fig. 2 compares the calculated and experimental values at 35°C, revealing both negative and positive deviations. We believe that these differences can be further minimized with a more elaborate curve fitting of $V_{R,2}* - V_{R,1}*$ to the mobile phase composition [19]. These results indicate that eqns. 10, 11 and 18 are essentially valid for the ACN–water mixtures in RPLC.

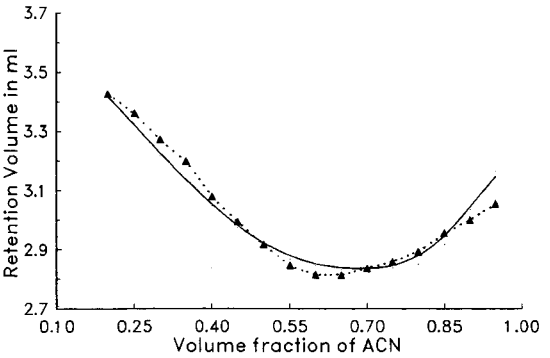

Fig. 2. Comparison of (▲) experimental $V_{R,(1,2)}$ values and (solid line) calculated $V_{R,(1,2)}$ values from eqn. 14a at 35°C.

Model for the absolute isotherms

Here we develop a model for the absolute volumes of ACN ($V_{2,s}$) and water ($V_{1,s}$) sorbed on the stationary phase, based on two experimental observations. Water adsorption from the gas phase on trimethylsilylated surfaces is weak and completely reversible at low pressures [24]. The wettability of reversed-phase packing materials is a simple way to test their hydrophilic character. Wettability is defined as the organic composition (v/v) in an aqueous–organic mixture at which floating particles in the mixture sink to the bottom of the vessel [25,26]; non-wettable particles float on the surface of the solution. It has been observed that an RP-C_{18} packing is wetted if the ACN concentration is greater than 40% (v/v) [25]. Wettability has been demonstrated to be highly dependent on the characteristics of the RP materials [26], *i.e.*, the length and population of alkyl chains, the amount of residual silanols, etc.

We begin by first assuming that water is not sorbed below 0.40 volume fraction of ACN. From eqns. 10, if $V_{1,s} = 0$, then $V_m = V_{R,1}*$ and $V_{2,s} = (V_{R,2}* - V_{R,1}*)\theta_2$. $V_{2,s}$ is then fitted to a Langmuir-type form:

$$V_{2,s} = (a\theta_2)/(1 + b\theta_2) \tag{20}$$

From eqn. 20, $V_{2,s}$ values are generated for all eluent compositions and V_m is then calculated from eqn. 10b and $V_{1,s}$ from eqn. 10a. Through successive iterations, the best fit to eqn. 20 is eventually found by assuming that there is no sorption of water for $\theta_2 \leq 0.50$. Table VI shows the values of the parameters a and b for the temperatures studied here.

TABLE VI

COEFFICIENTS OF THE CURVE FITTING OF EQN. 20

It is assumed that $V_{1,s}$ is zero for $\theta_2 \leq 0.50$.

Temperature (°C)	a	Standard error	b	Standard error
25	1.063	0.066	2.041	0.293
35	1.016	0.031	2.358	0.155
45	1.058	0.030	3.102	0.170
55	1.065	0.079	3.518	0.471

Fig. 3 illustrates that effect of temperature on the absolute isotherm of ACN and shows the absolute isotherm of water at 35°C, as obtained from the model. As expected, the volume of sorbed ACN decreases with increasing temperature at all compositions. The calculated $V_{2,s}$ values at $\theta_2 = 1$, for example, are 0.350, 0.303, 0.258 and 0.236 ml at 25, 35, 35 and 55°C, respectively. The volume of sorbed water, which is

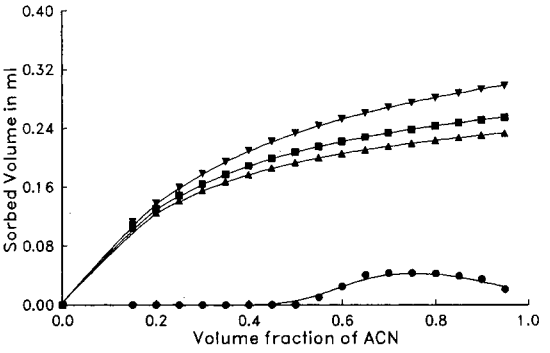

Fig. 3. Absolute sorption isotherms of ACN at (▼) 35, (■) 45 and (▲) 55°C and (●) absolute sorption isotherm of H_2O at 35°C.

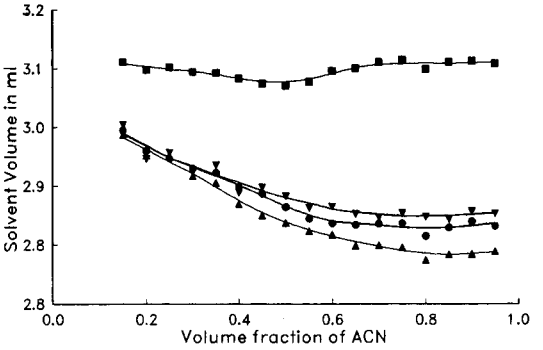

Fig. 4. Comparison of (■) the total solvent volume, V_t, at 35°C and the mobile phase volume, V_m, which is illustrated at (▲) 35, (●) 45 and (▼) 55°C.

much smaller than that of ACN, has a parabolic-like dependence on θ_2 for $\theta_2 \geq 0.50$. At 35°C a maximum value of $V_{1,s} = 0.043$ ml is found at $\theta_2 \approx 0.75$, decreasing to 0.037 and 0.034 ml at 45 and 55°C, respectively, and increasing to 0.050 ml at 25°C. We believe that, at high θ_2, the water is initially driven onto the stationary phase by the already sorbed ACN, which renders the C_{18} stationary phase somewhat hydrophilic. Then, consistent with the wetting studies [25,26], the volume of sorbed water starts to decrease with decreasing θ_2 and reaches negligible levels below $\theta_2 \approx 0.50$. This also suggests that the structure of the stationary phase may be altered by the sorbed solvent [22].

Fig. 4 and Table IV show that the hold-up volume (V_t) is only slightly dependent on the composition of the eluent. V_t has been shown to be equivalent to the column void volume [14,19,22]. A consequence of this model is the determination of the mobile phase volume, which, according to eqn. 4, is the difference between the total or hold-up volume and the volume of the solvent sorbed in the stationary phase (*i.e.*, water + ACN). Fig. 4 shows that the values of V_m obtained from this model vary with mobile phase composition and temperature, in the opposite direction of the corresponding variation of $V_{2,s}$ with the same variables (Fig. 3).

Test of the model

As was mentioned before, this model or any other model of absolute isotherms for a binary solvent mixture in liquid chromatography has to satisfy eqn. 6. Therefore, we tested our model by generating the values of $V_{R,(1,2)}$ from the V_m values and the absolute isotherms, utilizing eqn. 6. We evaluated the derivatives in eqn. 6 by first fitting the values of $V_{2,s}$, in terms of θ_2, to a third-order polynomial (correlation coefficient in excess of 0.999) and $V_{1,s}$, in terms of θ_1, to a fourth-order polynomial, in the composition range $0.50 \leq \theta_2 \leq 0.95$ (correlation coefficient 0.99). The evaluation of the derivative of $V_{1,s}$ with respect to θ_1 is especially difficult in the vicinity of $\theta_2 = 0.95$ and $\theta_2 = 0.50$, because the slopes are changing rapidly in these regions. In the vicinity of $\theta_2 = 0.60$, there appears to be an inflection point (see Fig. 3). We assume that the rate of change of this function in the vicinity of this point is symmetrical with respect to the inflection point. Fig. 5 shows a comparison of the experimental $V_{R,(1,2)}$

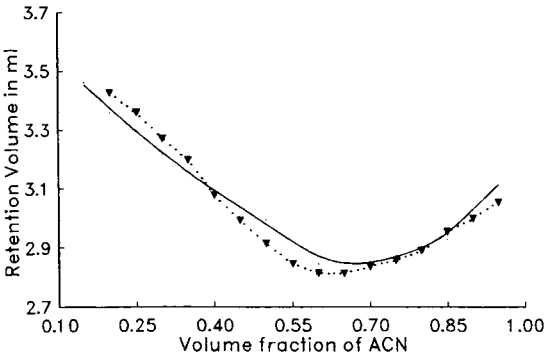

Fig. 5. Comparison of (▼) the experimental $V_{R,(1,2)}$ values and (solid line) calculated $V_{R,(1,2)}$ values from the absolute isotherms and eqn. 6 at 35°C.

TABLE VII

COMPARISON OF EXPERIMENTAL AND CALCULATED $V_{R,(1,2)}$ VALUES AT 35°C

Volume fraction of ACN	Experimental $V_{R,(1,2)}$ (ml)	V_m	$\theta_1(\partial V_{2,s}/\partial\theta_2)$	$\theta_2(\partial V_{1,s}/\partial\theta_1)$	Calculated $V_{R,(1,2)}$[a] (ml)
0.15	–	3.038	0.425	0.000	3.463
0.20	3.427	3.002	0.359	0.000	3.361
0.25	3.362	3.000	0.300	0.000	3.300
0.30	3.274	2.967	0.249	0.000	3.216
0.35	3.199	2.956	0.205	0.000	3.161
0.40	3.080	2.920	0.167	0.000	3.087
0.45	2.995	2.900	0.135	0.000	3.035
0.50	2.917	2.887	0.108	0.000	2.995
0.55	2.846	2.873	0.086	−0.037	2.922
0.60	2.814	2.867	0.068	−0.089	2.846
0.65	2.813	2.848	0.053	−0.089	2.812
0.70	2.836	2.849	0.041	−0.037	2.853
0.75	2.857	2.846	0.032	−0.001	2.877
0.80	2.892	2.825	0.024	0.032	2.880
0.85	2.995	2.834	0.018	0.078	2.929
0.90	3.000	2.834	0.012	0.157	3.003
0.95	3.054	2.839	0.006	0.295	3.140

[a] Calculated from eqn. 6.

TABLE VIII

MODEL-INDEPENDENT SURFACE EXCESS VOLUMES OF ACN

V_2^E was calculated from eqn. 18 and the results in Tables I and II.

Volume fraction of ACN	V_2^E (ml)			
	25°C	35°C	45°C	55°C
0.00	0.000	0.000	0.000	0.000
0.15	0.098	0.094	0.092	0.091
0.20	0.118	0.109	0.103	0.097
0.25	0.132	0.122	0.113	0.109
0.30	0.144	0.125	0.116	0.106
0.35	0.147	0.130	0.116	0.113
0.40	0.138	0.124	0.111	0.102
0.45	0.137	0.121	0.110	0.103
0.50	0.129	0.117	0.104	0.097
0.55	–	0.104	0.091	0.084
0.60	0.096	0.086	0.077	0.072
0.65	–	0.065	0.056	0.056
0.70	0.059	0.050	0.045	0.042
0.75	–	0.036	0.032	0.029
0.80	0.024	0.022	0.019	0.018
0.85	–	0.010	0.006	0.004
0.90	0.000	−0.002	−0.003	−0.005
0.95	–	−0.005	−0.005	−0.006

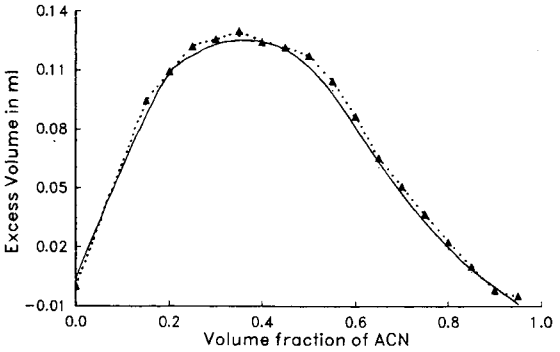

Fig. 6. Comparison of (▲) the surface excess isotherm determined from eqn. 18 and (solid line) the surface excess isotherm determined from the absolute isotherms and eqn. 15 at 35°C.

and calculated $V_{R,(1,2)}$ values at 35°C. It can be seen that the greatest differences occur around $\theta_2 = 0.50$ and $\theta_2 = 0.95$, where $V_{1,s}$ is changing rapidly with solvent composition. The average difference between the experimental and calculated $V_{R,(1,2)}$ values is 0.037 ml, which is about 1%. Table VII shows the partial contributions to the calculated $V_{R,(1,2)}$ values. From Table VII it can be seen that this model explains and predicts the behavior of the DP.

The absolute isotherms can be tested in a second way. The surface excess volumes can be directly determined from the results in Tables I and II, and eqn. 18, which is model independent. The values of V_2^E, so determined, are listed in Table VIII. These results can then be compared with those obtained from eqn. 15, using the absolute volumes, $V_{1,s}$ and $V_{2,s}$, previously determined from our model. Fig. 6 illustrates this comparison at 35°C. The average difference between the two sets of V_2^E results is about 0.002 ml at 25 and 35°C and about 0.001 ml at 45 and 55°C. This clearly demonstrates the consistency of our model.

An independent check of the physical reasonableness of the results for $V_{1,s}$ and $V_{2,s}$ can be achieved by determining the maximum volume available to the solvent within the chain structure of the chemically bonded phase (CBP), *i.e.*, the volume which would be obtained if the alkyl chains were fully extended [22]. From the quoted total mass and carbon content of the packing material, and from available densities [27], the volume of the CBP chains, *per se*, is estimated to be about 0.39 ml. In addition, using the quoted specific surface area of the packing, a surface coverage of 2.47 μmol/m^2 is calculated, corresponding to a specific occupancy of one CBP chain per 66.7 Å^2. With a close-packed arrangement of the CBP, each chain would occupy about 25 Å^2. Therefore, the fractional chain coverage is about 0.375, leaving the remaining 62.5% of potential space, or *ca.* 0.65 ml, available for sorbed solvent. Accordingly, there is sufficient volume available for the sorbed solvent to be accommodated wholly within the milieu of the CBP chains.

We plan to use the results for the ACN–water mixtures and the same general model to analyze other organic modifier–water mixtures and to investigate the solute retention mechanism in RPLC in more quantitative and molecular-level detail [22].

ACKNOWLEDGEMENTS

This material is based on work supported by the National Science Foundation under Grant CHE-8902735. The authors extend their best wishes to Lloyd R. Snyder, one of the pioneers in liquid chromatography, on the occasion of his 60th birthday.

REFERENCES

1 D. E. Leyden, *Silanes, Surfaces and Interfaces*, Gordon and Breach, New York, 1986.
2 L. C. Sander and S. A. Wise, *CRC Crit. Rev. Anal. Chem.*, 18 (1987) 299, and references cited therein.
3 J. H. Knox and A. Pryde, *J. Chromatogr.*, 112 (1975) 171.
4 R. P. W. Scott and P. Kucera, *J. Chromatogr.*, 142 (1977) 213.
5 R. P. W. Scott and P. Kucera, *J. Chromatogr.*, 175 (1979) 51.
6 D. Westerlund and A. Theodorsen, *J. Chromatogr.*, 144 (1977) 27.
7 A. Tilly-Melin, Y. Askemark, K. G. Wahlund and G. Schill, *Anal. Chem.*, 51 (1979) 976.
8 J. F. K. Huber and R. G. Gerritse, *J. Chromatogr.*, 58 (1971) 137.
9 P. Valentin and G. Guiochon, *J. Chromatogr. Sci.*, 14 (1976) 56, 132.
10 R. M. McCormick and B. L. Karger, *J. Chromatogr.*, 199 (1980) 259.
11 R. M. McCormick and B. L. Karger, *Anal. Chem.*, 52 (1980) 2249.
12 E. H. Slaats, W. Markovsky, J. Fekete and H. Poppe, *J. Chromatogr.*, 207 (1981) 299.
13 F. Riedo and E. sz. Kováts, *J. Chromatogr.*, 239 (1982) 1.
14 N. L. Ha, J. Ungváral and E. sz. Kováts, *Anal. Chem.*, 54 (1982) 2410.
15 J. H. Knox and R. Kaliszan, *J. Chromatogr.*, 349 (1985) 211.
16 P. L. Zhu, *Chromatographia*, 20 (1985) 425.
17 K. Tani and Suzuki, *J. Chromatogr. Sci.*, 27 (1989) 698.
18 J. J. Kipling, *Adsorption from Solutions of Non-Electrolytes*, Academic Press, New York, 1965.
19 G. Foti, C. de Reyff and E. sz. Kováts, *Langmuir*, 6 (1990) 759.
20 F. J. Helfferich, *J. Chem. Educ.*, 41 (1964) 410.
21 D. L. Peterson and F. J. Helfferich, *J. Phys. Chem.*, 69 (1965) 1283.
22 D. E. Martire and R. E. Boehm, *J. Phys. Chem.*, 87 (1983) 1045.
23 G. Foti and E. sz. Kováts, *Langmuir*, 5 (1989) 232.
24 A. C. Zettlemoyer and H. H. Hsing, *J. Colloid Interface Sci.*, 58 (1977) 263.
25 H. Engelhardt and D. Mathes, *J. Chromatogr.*, 142 (1977) 311.
26 T. Welsch, H. Frank and G. Vigh, *J. Chromatogr.*, 506 (1990) 97.
27 W. Cheng, *Anal. Chem.*, 57 (1985) 2409.

Journal of Chromatography, 550 (1991) 301–312
Elsevier Science Publishers B.V., Amsterdam

CHROMSYMP. 2280

Stationary phase effects in reversed-phase liquid chromatography under overload conditions

N. T. MILLER
Research & Development Center, The PQ Corporation, Conshohocken, PA 19428 (USA)

ABSTRACT

Stationary phase parameters that influence the performance of silica-based reversed phases under overload conditions were examined. High concentrations of the solute 2-phenylethanol were eluted from a variety of C_{18} packings differing in particle diameter and surface area (pore size). Apparent efficiency and retention factors of the solute bands resulting from concentration overload in these systems were measured and compared. In agreement with the literature, beyond a certain solute load and depending on the initial efficiency of the system, the dependence of column efficiency on load is less influenced by the stationary phase particle diameter. Smaller pore (*i.e.*, nominal 100 Å) C_{18} packings showed a slightly greater efficiency and less retention loss with an increase in sample load than larger pore (*i.e.*, nominal 200 Å) sorbents. The small-pore silicas also showed a greater decrease in pore volume relative to large-pore silicas when used as substrates for C_{18} bonding. The chromatographic data could also be used to calculate coefficients of the Langmuir adsorption isotherm. Changes in total porosity of the column greatly influence the determination of the dominant coefficient in the Langmuir equation.

INTRODUCTION

Preparative liquid chromatography continues to develop, as evidenced by increasing interest in international symposia and consolidation of commercial activity. Key advances in the theory of large-scale chromatography [1–4] complement basic studies [5–7]. In particular, the development of a theoretical framework (*i.e.*, the ideal and semi-ideal models) has revealed under-appreciated effects in the elution behavior of large-concentration bands (*i.e.*, competitive adsorption, sample self-displacement [8] and tag-along phenomena [9]), which play a significant role in the optimization of throughput, mass yield and purity. Practical guidelines for optimized preparative separations also exist to benefit the user [10].

The availability of preparative chromatographs and column technology for use with modern microparticulate packings has made the technique more acceptable. Preparative columns now employ compression technology such that 10-μm diameter porous silicas and bonded phases can be used routinely [11,12].

From a practical point of view, much work remains to be done on the optimized use of stationary phases in preparative chromatography, for example, to establish what compromise should be struck between sorbent surface area for sample capacity and sorbent mechanical strength. Although several reports have discussed the role of

0021-9673/91/$03.50

particle characteristics in preparative liquid chromatography, confusion still exists in the literature [13,14]. Sorbent reproducibility and stability will continue to be a concern, as will economics of packing use and reuse.

In this paper, we examine several characteristics of column packings for the elution of a single-solute band at high concentration, including the effect of C_{18} reversed-phase particle diameter and surface area.

EXPERIMENTAL

Equipment

A Perkin-Elmer (Norwalk, CT, USA) liquid chromatograph consisting of a Series 410 solvent delivery pump, a Model ISS-100 autosampler and a Model LC-95 variable-wavelength UV detector was used to obtain elution band profiles. Data were recorded on a Chromatopac C-R6A integrator (Shimadzu, Columbia, MD, USA) and on an IBM-AT computer (IBM, Boca Raton, FL, USA) using Nelson Analytical (Cupertino, CA, USA) chromatography software.

Materials

High-coverage and end-capped IMPAQ reversed-phases were obtained from PQ (Conshohocken, PA, USA) and are listed in Table I with characteristics. The sorbents were slurry-packed into 15 cm × 0.46 cm I.D. columns using a pneumatic-amplifier pump (Haskel, Burbank, CA, USA). Uracil and 2-phenylethanol were obtained from Sigma (St. Louis, MO, USA). Polystyrene of molecular weight $1.8 \cdot 10^6$ was purchased from Supelco (Bellefonte, PA, USA). High-performance liquid chromatographic grade water was prepared in-house. Other solvents were obtained from EM Science (Cherry Hill, NJ, USA).

Procedures

Solutions of 2-phenylethanol in the range 1–600 mg/ml were prepared by weighing the solute into volumetric flasks and diluting to volume with methanol or with the mobile phase ($\leqslant$30% aqueous methanol). Injections of variable sample volumes for a fixed sample concentration were made to determine the onset of volume overloading for a given column. Thereafter, in concentration overload studies, fixed sample volume injections (*e.g.*, 5–20 μl) well under that needed for volume overloading were employed. The detector response was calibrated using step gradients of known solute concentration [15] or a linear solute concentration gradient. Solute concentrations of the peak maxima could then be obtained for use in the Langmuir isotherm plots (see later). Proper detector wavelength selection also ensured reliable detector calibration.

Uracil was used as an unretained solute for determination of the column void volume, V_m. Polystyrene of molecular weight $1.8 \cdot 10^6$ was used with dichloromethane as mobile phase to measure the interstitial porosity, ε_0. Retention factors (k') were determined from the peak maxima of the large concentration bands. Apparent efficiency (N) was obtained using the width of the band at half-height ($W_{0.5}$) according to the equation

$$N = 5.54(t_R/W_{0.5})^2 \quad (1)$$

and following the guidelines of Golshan-Shirazi and Guiochon [16].

RESULTS AND DISCUSSION

It has been shown that for optimum productivity, the peparative liquid chromatographic technique should be operated under conditions of significant concentration overload such that peak overlap can occur [17]. Hence column efficiency can in large part be determined by the thermodynamic contribution (isotherm linearity) to band broadening rather then by axial dispersion and mass-transfer kinetics [1]. Under these conditions, optimization of the stationary phase characteristics in large-scale liquid chromatography is of interest.

In this paper, we examine the influence of stationary phase characteristics on the elution behavior of single-component (2-phenylethanol) bands of high concentration with mobile phases of $\leqslant 30\%$ aqueous methanol. First, we shall summarize measured characteristics of the packings used in this work. Second, various parameters (*i.e.*, injection size, k', flow-rate) are explored for a given system, followed by a study of the influence of C_{18}-bonded phase particle diameter and pore size. Lastly, Langmuir adsorption coefficients can be determined from the experimental data collected. These results should provide a further insight into the role of stationary phase properties in large-scale liquid chromatography.

Table I summarizes the stationary phases examined and their characteristics. Nitrogen BET surface areas of the sorbents and bonded-phase surface area per column are listed. Surface area is decreased by about 60% in the C_{18}-bonded 100 Å silica relative to the *ca.* 44% loss in the C_{18}-bonded 200 Å silica. The unbonded silicas show no micropores, so the decrease in surface area due to bonding affects the pores accessible to the solute. Thus, the *ca.* 50% excess surface-area advantage of the 100 Å silica is decreased to 15% owing to C_{18}-bonding and increased to about 30% after the sorbents have been packed into columns.

We also measured the interstitial volume, V_0, of each column by elution of

TABLE I

CHARACTERISTICS OF REVERSED-PHASES STUDIED

Stationary phase[a]	Surface area[b]			ε_0	ε_p	$\varepsilon_p/\varepsilon_0$	$\frac{\varepsilon_p}{1-\varepsilon_0}$
	Silica (m^2/g)	Bonded phase (m^2/g)	Bonded phase[c] (m^2)				
RG1010-C_{18}	366	152	170	0.44	0.24	0.55	0.43
RG1020-C_{18}	366	152	198	0.40	0.25	0.63	0.42
RG1040-C_{18}	385	160	192	0.38	0.26	0.68	0.42
RG1080-C_{18}	381	169	207	0.40	0.25	0.63	0.42
RG2010-C_{18}	246	139	163	0.44	0.36	0.82	0.64
RG2020-C_{18}	240	135	135	0.40	0.34	0.85	0.57

[a] The nomenclature RG_{xxyy}-C_{zz} indicates a silica of nominal *xx* nm pore diameter with *yy* μm particle diameter and bonded with C_{zz} alkyl chains. The C_{18} columns were 15 × 0.46 cm I.D.

[b] Surface area measured by the N_2 BET method.

[c] These values represented the total surface area in the column and are obtained from the bonded phase surface area and the packed density (g packing per column) of the column.

high-molecular-weight polystyrene in dichloromethane and the column pore volume, V_p, from the difference between V_0 and V_m, the column void volume (retention volume of uracil). V_0 and V_p are expressed as percentages of the empty column volume (*i.e.*, ε_0 and ε_p, respectively). The ε_0 value is roughly constant within experimental error (about 5% relative standard deviation) from column-to-column, reflecting a consistent packing procedure. Pore volume, ε_p, values however, increase by about 40% from the 100 Å to the 200 Å sorbent, reflecting less consumption of pore volume in the 200 Å silica by the C_{18} chains. Values for the ratio of pore volume to interstitial volume ($\varepsilon_p/\varepsilon_0$) and the fractional empty space of the particle [$\varepsilon_p/(1 - \varepsilon_0)$] are in agreement with the above results and the literature [18].

Effect of sample concentration

Fig. 1 summarizes the dependence of the apparent efficiency on sample load applied to the column containing 200 Å pore-size C_{18}-bonded silica of 20-μm particle diameter (*i.e.*, RG2020-C_{18} in Table I) with methanol–water (30:70) as mobile phase. Injections of 10 μl of 1–600 mg/ml (0.01–6 mg) 2-phenylethanol were injected onto the column and the resulting band widths measured. For solute concentrations $\leqslant$25 mg/ml, 2-phenylethanol is soluble in methanol–water (30:70) and volume overloading occurs at >250 μl injected for the solute peak at k' = 5.3 [19]. For concentrations >25 mg/ml, 2-phenylethanol is less soluble in methanol–water (30:70) and these solutions were made up in methanol. Large-volume injections of these solutions produced a significant V_m peak, possibly due to partial elution of the band. The 10-μl injections and variable-sized injections of 5, 10 and 25 mg/ml of 2-phenylethanol in methanol–water (30:70) produce a single curve with a plateau of about 1000 plates followed by a decrease in efficiency at higher loads. Increased and

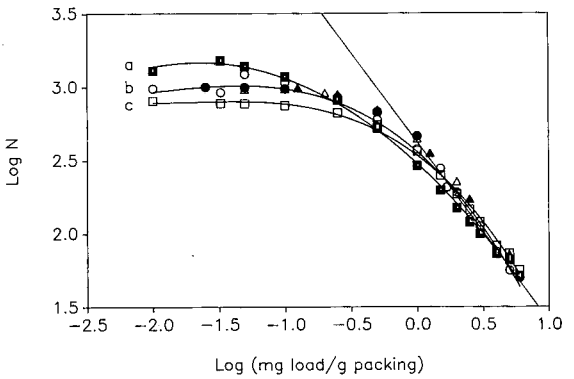

Fig. 1. Column efficiency as a function of 2-phenylethanol load on the RG2020-C_{18} column. A mobile phase of methanol–water (30:70, v/v) was used to obtain a k' of 5.3. A flow-rate of 1 ml/min was used, except where noted. ○ = 10-μl injections of variable concentration (1–600 mg/ml) 2-phenylethanol; ● = variable size injections (10–200 μl) of 5 mg/ml 2-phenylethanol; △ = variable size injections (10–200 μl) of 10 mg/ml 2-phenylethanol; ▲ = variable size injections (10–200 μl) of 25 mg/ml 2-phenylethanol; □ = 10-μl injections of 1–600 mg/ml 2-phenylethanol at a flow-rate of 1.5 ml/min; ■ = 10-μl injections of 1–600 mg/ml 2-phenylethanol at a flow-rate of 0.5 ml/min. (a) Curve through the ■ data points at flow-rate of 0.5 ml/min; (b) curve through the ○ data points at a flow-rate of 1 ml/min; (c) curve through the □ data points at a flow-rate of 1.5 ml/min.

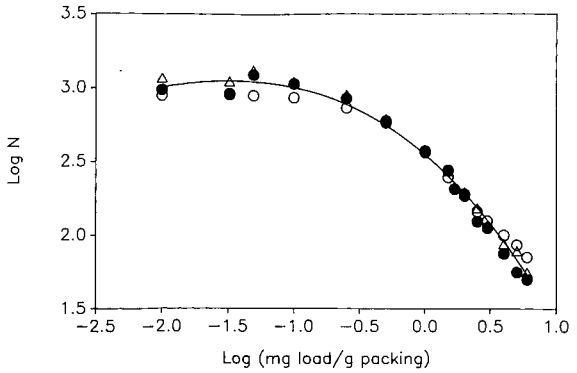

Fig. 2. Column efficiency as a function of 2-phenylethanol load at different k' values on the RG2020-C_{18} column. Injections of 10 μl of 1–600 mg/ml 2-phenylethanol were made into the column. Mobile phase composition of methanol–water adjusted to obtain the particular k' at a flow-rate of 1 ml/min. k': ○ = 2.3; ● = 5.2; △ = 9.3.

decreased volumetric flow-rates produce decreased (about 800 plates) and increased (1500 plates) efficiency, respectively, in the front half of the curve. The data points come together in the final portion of the curve to define a line of slope −1.1. This portion of the curve represents the greater contribution of isotherm non-linearity to the efficiency obtained in the system [16].

Fig. 2 shows data for efficiency *versus* load as a function of solute k' in the range 2–9. The points describe a single line with some scatter in the first part of the curve. The results in Figs. 1 and 2 are in good agreement with the literature [13,20].

Effect of particle diameter

We next studied the elution behavior of 2-phenylethanol on columns differing in particle size of the C_{18} 100 Å pore reversed-phase. Fig. 3 shows efficiency *versus* sample

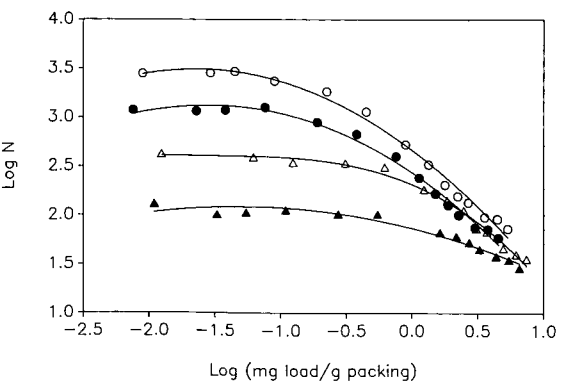

Fig. 3. Column efficiency as a function of 2-phenylethanol load for C_{18} columns of different particle diameter. Injections of 10 μl of 1–600 mg/ml 2-phenylethanol were made on each column operated with a methanol–water (30:70) eluent at 1 ml/min. ○ = RG1010-C_{18}, 10-μm particle diameter; ● = RG1020-C_{18}, 20 μm; △ = RG1040-C_{18}, 40 μm; ▲ = RG1080-C_{18}, 80 μm.

load for the four C_{18} sorbents of nominal particle diameter 10, 20, 40 and 80 μm. A mobile phase of methanol–water (30:70) was used to obtain an average solute k' of *ca.* 5.8 (4.5% relative standard deviation) in each system. The front portion of the

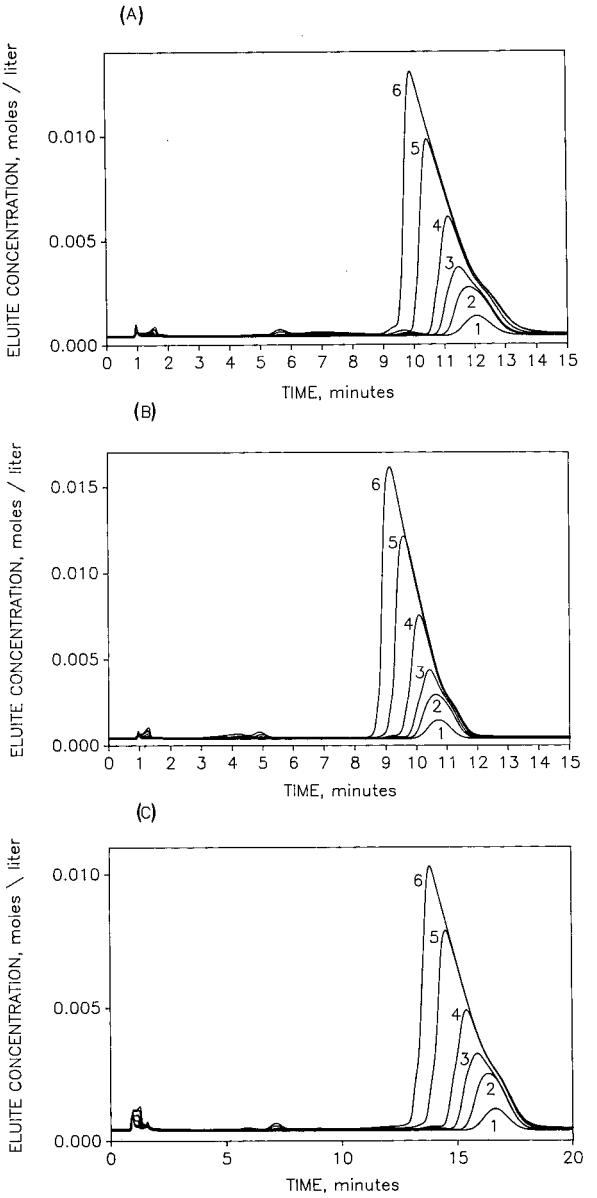

Fig. 4. Elution of high concentrations of 2-phenylethanol from C_{18} columns of different pore size. Each 15 × 0.46 cm I.D. column was operated at 1 ml/min. The chromatograms result from a 10-μl injection of the following 2-phenylethanol concentrations: 1 = 5 mg/ml (0.4 μmol solute injected); 2 = 25 mg/ml (2.0 μmol); 3 = 50 mg/ml (4.1 μmol); 4 = 100 mg/ml (8.2 μmol); 5 = 200 mg/ml (16.4 μmol); 6 = 300 mg/ml (24.6 μmol). (A) RG2020-C_{18}, k' = 5.3; (B) RG1020-C_{18}, k' = 5.4; (C) RG1020-C_{18}, k' = 8.9.

curves are determined by the efficiency of the column, *i.e.*, about $N = 3000$ plates for 10-μm, $N = 1000$ for 20-μm, $N = 425$ for 40-μm and $N = 130$ for 80-μm particles. The point at which the plots become non-linear at larger sample loads increases with increasing particle diameter. The slopes of the final portions of the curves are similar, with the exception of the 80-μm system, which still shows curvature. Although smaller particles always produced higher efficiency, beyond a certain sample load the rates of decrease in efficiency with load are similar. However, columns packed with smaller particles can be used at higher flow-rates with the advantage of a large production rate relative to the same efficiency obtained on the larger particle columns. Golshan-Shirazi and Guiochon [14] have detailed the optimization of efficiency via column length and particle size (d_p^2/L) and flow-rate compromises in a recent comprehensive study; the results of Fig. 3 are in agreement with these studies [8,13,20,21].

We now turn to a study of the influence of porosity on the efficiency/load behavior observed in Figs. 1–3.

Surface area effects

For this study, we examined 2-phenylethanol elution on four C_{18} reversed-phase columns: 10- and 20-μm particles in each of 100 and 200 Å pore sizes (RG1010-C_{18}, RG2010-C_{18}, RG1020-C_{18} and RG2020-C_{18} in Table I). The gain in surface area (based on nitrogen BET measurements) using the smaller pore-size packing is about 30% owing to the presence of C_{18} chains on the surface and the packed bed density in the column. The mobile phase conditions were adjusted to normalize k' to *ca.* 5 to examine in a straightforward manner the influence of increased pore diameter. In one case, methanol–water (30:70) was used to obtain 2-phenylethanol elution at $k' = 8.9$ and 5.3 on the RG1020-C_{18} and RG2020-C_{18} columns, respectively.

Fig. 4A–C show chromatograms for several sample loads of 2-phenylethanol on the 20-μm columns. In each chromatogram, the detector response at 254 nm was converted to solute concentration (M) in the mobile phase using the detector calibration graph constructed previously (see Experimental). Solute injections of 8 mM–2.5 M 2-phenylethanol solutions result in band elution with peak maxima of <15 mM concentration in the mobile phase. For the same k', the 2-phenylethanol peak in the RG2020-C_{18} (200 Å) system shows slightly increased broadening and decreased retention at high load relative to the RG1020-C_{18} (100 Å) system. All of the chromatograms show peak tailing at high sample load, suggesting that a convex-shaped adsorption isotherm is operable. We have no explanation for the inflection point on the trailing side of the higher concentration peaks.

Fig. 5 details the efficiency–load relationship for the chromatograms in Fig. 4. In this plot we have not normalized sample load to mass of packing in the column. Plotting log N against log(mg sample load/g packing) yields curves for these data that are superimposed. Note that at the second data point (0.25 mg injected) in Fig. 5, the efficiency on the 200 Å system has decreased to 80% of the initial value relative to 95% of initial value for the 100 Å system. The points come together as the load is increased. Interestingly, increased k' on the RG1020-C_{18} column plays no role in the observed influence of sample load on efficiency.

One approach to studying the above experimental data is to apply the ideal and semi-ideal models developed for high solute concentration conditions by Golshan-

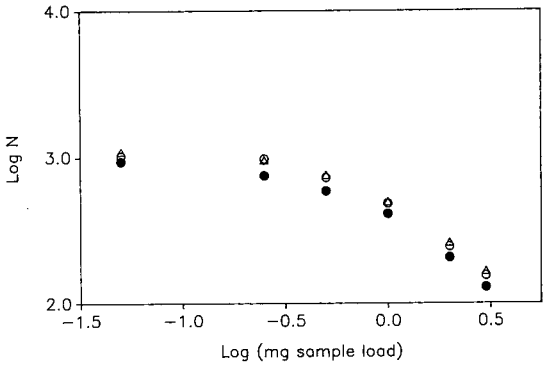

Fig. 5. Column efficiency as a function of 2-phenylethanol load on C_{18} columns. Conditions as in Fig. 4. ○ = RG1020-C_{18}, k' = 5.4; ● = RG2020-C_{18}, k' = 5.3; △ = RG1020-C_{18}, k' = 8.9.

Shirazi and Guiochon [16]. Using this approach, a loading factor, L_f, can be defined according the equation

$$L_f = \{1 - [(t_f - t_m - t_p)/(t_{R,0} - t_m)]^{0.5}\}^2 \quad (2)$$

where t_f is the retention time of the high concentration solute band, t_m the column void volume, t_p the injected pulse width and $t_{R,0}$ the retention time of a very small sample. Thus, L_f is proportional to k'_f/k'_0, *i.e.*, the decrease in band k' when the solute load is increased. Fig. 6 illustrates this relationship and shows that the 100 Å C_{18} sorbent provides less retention loss as the sample size increases relative to the larger pore size system. Note that even at larger values of L_f (*i.e.*, *ca.* 3%), the slopes of the curves are non-zero.

The plot of log N *vs.* log L_f in Fig. 7 shows a steeper slope for the RG1020-C_{18} system due not to a faster decrease in efficiency (see Fig. 5), but rather to a more

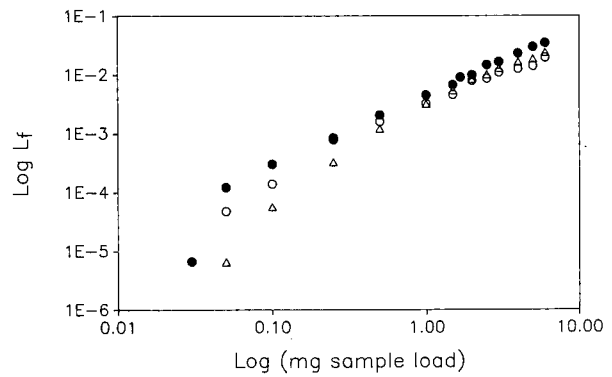

Fig. 6. Loading factor for 2-phenylethanol on C_{18} columns as a function of sample load. Conditions as in Fig. 4, except sample concentrations up to 600 mg/ml were investigated. Loading factor is defined in the text. ○ = RG1020-C_{18}, k' = 5.4; ● = RG2020-C_{18}, k' = 5.3; △ = RG1020-C_{18}, k' = 8.9.

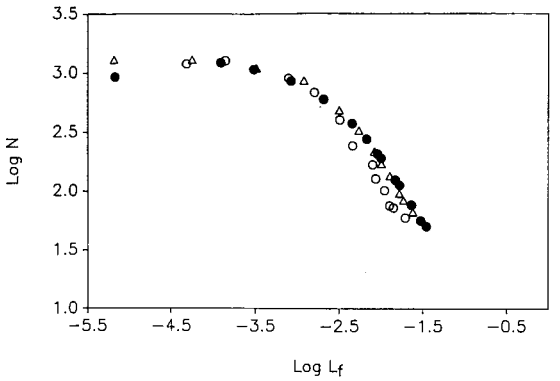

Fig. 7. Column efficiency as a function of loading factor for 2-phenylethanol on C_{18} columns. Conditions as in Fig. 4, except sample concentrations up to 600 mg/ml were investigated. Loading factor defined in the text. ○ = RG1020-C_{18}, k' = 5.4; ● = RG2020-C_{18}, k' = 5.3; △ = RG1020-C_{18}, k' = 8.9.

gradual change in L_f as sample size increases. From this point of view, the small pore size packing resists changes in k' (by virtue of a greater working surface area to accommodate solute) relative to the wider pore system. Employing the same solvent system as for k' = 5.3 on RG2020-C_{18} results in k' = 8.9 on RG1020-C_{18} and the resulting curve in Fig. 7 is shifted toward that for the wide-pore packing. This result reflects the dependence of L_f on solute load shown in Fig. 6 and is in agreement with the literature [16]. Similar conclusions can be drawn for the RG1010-C_{18} and RG2010-C_{18} systems.

Langmuir isotherm estimation

The L_f calculation and the chromatographic data at very small sample size provide a convenient means of calculating the coefficients of the Langmuir isotherm in accordance with the model of Golshan-Shirazi and Guiochon [16]. The Langmuir isotherm can be written as

$$Q = aC/(1 + bC) \tag{3}$$

where Q and C are the equilibrium concentrations of the solute in the stationary and mobile phases, respectively. The coefficient a is given by

$$a = \frac{(t_{R,0} - t_m)\varepsilon_T}{t_m(1 - \varepsilon_T)} \tag{4}$$

The total porosity, ε_T, is equal to $\varepsilon_0 + \varepsilon_p$, values of which are given in Table I. The coefficient b is defined as

$$b = \frac{L_f F(t_{R,0} - t_m)}{n_m} \tag{5}$$

TABLE II

LANGMUIR ISOTHERM CHARACTERISTICS OF C_{18} REVERSED-PHASES

All results obtained at $k' \approx 5$ except where noted.

Stationary phase	a	L_f (%)	b (l/M)	Q_{lim} (M)
RG1010-C_{18}	11.5	0.96 1.87	4.05 3.94	2.9
RG1020-C_{18}	12.3	1.26 1.94	4.14 4.27	2.9
RG1040-C_{18}	11.4	1.27 1.70	2.66 2.85	4.1
RG1080-C_{18}	11.2	1.69 2.07	2.74 2.72	4.1
RG2010-C_{18}	21.7	1.40 2.78	6.15 6.08	3.6
RG2020-C_{18}	15.4	1.47 3.47	7.22 7.10	2.2
RG1020-C_{18}[a]	27.0	0.98 2.8	10.6 10.0	3.1

[a] These results were obtained at $k' = 8.9$.

where F is the volumetric flow-rate and n_m the number of moles of solute injected. At high mobile phase solute concentration, C, the limiting stationary phase solute concentration, Q_{lim}, becomes equal to a/b, which in turn is proportional to n_m/V_s, where V_s is the volume of the stationary phase.

The assumption is made that the Langmuir equation can approximate the adsorption behavior of 2-phenylethanol in our studies. This assumption can be

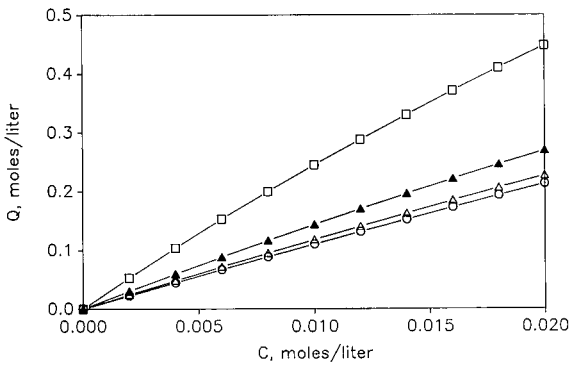

Fig. 8. Langmuir isotherm plot for 2-phenylethanol on C_{18} columns of different pore diameter. See text for explanation. ○ = RG1010-C_{18}, $k' = 5.6$; △ = RG1020-C_{18}, $k' = 6.1$; ▲ = RG2020-C_{18}, $k' = 5.5$; □ = RG1020-C_{18}, $k' = 8.9$.

checked by determining the constancy of b over several values of L_f [16]. Moreover, several studies using 2-phenylethanol in reversed-phase systems with methanol–water eluents utilized Langmuir isotherms for the description of solute adsorption [22,23].

Table II lists the a and b values for the columns studied, and Fig. 8 reconstructs selected isotherms over the mobile phase solute concentration used. The isotherms for the RG10 (100 Å) series differing in particle size were clustered together, as expected. For clarity, only the RG1010-C_{18} and RG1020-C_{18} curves are shown in Fig. 8. The RG2020-C_{18} plot lies above the 100 Å curves. Increasing k' to *ca.* 9 causes the isotherm for the RG1020-C_{18} column to rise above that for the RG10 system at $k' = 5$ and the 200 Å column. In the mobile phase solute concentration range studied in Fig. 8, the isotherm equation is dominated by a. In turn, a is influenced greatly by the total porosity of the system, *i.e.*, increasing ε_T from 0.65 to 0.8 increases a from 9.3 to 20 for a fixed k' of 5.0. Hence the C_{18} chains serve to modulate the effect of decreased pore diameter (*i.e.*, greater surface area) because they occupy a greater portion of the pore volume. Preliminary results suggest a 100 Å C_4-bonded phase can produce a larger a value owing to an increased ε_T, assuming that the mobile phase can be manipulated to achieve comparable retention. The limiting stationary phase solute concentration is shown in Table II as Q_{lim} and is in the range 2–4 M. On average, Q_{lim} is lower in the RG20 columns and reflects the decreased bonded-phase surface area in this system (see Table I).

CONCLUSIONS

We have examined the loading behavior of 2-phenylethanol in methanol–water eluents on C_{18} reversed-phase columns differing in particle size and pore size. As the solute concentration at a fixed injection volume onto the column is increased, the apparent efficiency at first remains constant and then decreases. The onset of efficiency loss depends on the magnitude of the initial column efficiency. In these studies, larger particles (*e.g.*, 80 μm) maintained their efficiency over a wider range of solute load relative to smaller particles (*e.g.*, 10 μm). Of course, the 10-μm column always provided more plates than the 80-μm column. Retention factors in the range 2–9 did not influence the dependence of efficiency on solute load. The loading factor, L_f, proportional to the decrease in band k' when the sample load was increased, showed a dependence on the pore size of the C_{18} sorbent used. Using the retention time method of Golshan-Shirazi and Guiochon [16], plots of efficiency *versus* loading factor reveal that the small-pore (100 Å) C_{18} sorbents showed slightly greater efficiency and less loss in k' as the solute load is increased relative to the large-pore (200 Å) C_{18} stationary phase. Langmuir isotherm coefficients could be estimated from the experimental data for the adsorption of 2-phenylethanol in these systems. The a value plays a dominant role in the range of mobile phase solute concentrations studied and is greatly affected by the total porosity of the column. Separate measurements of bonded-phase surface area and column pore volume revealed that the C_{18} bonding on 100 Å silica consumes proportionately more (about 60%) pore volume than on the 200 Å silica (*ca.* 44% consumed), and serves to diminish the advantageous higher surface area of the small-pore silica.

ACKNOWLEDGEMENTS

This paper is dedicated to Dr. Lloyd R. Snyder on the occasion of his sixtieth birthday.

The author thanks J. T. Kowalewski for the packing of several columns and B. P. Wilson for assistance with the chromatographic experiments. M. R. Derolf is thanked for numerous valuable discussions.

REFERENCES

1 J. H. Knox and H. M. Pyper, *J. Chromatogr.*, 363 (1986) 1.
2 A. Jaulmes, C. Vidal-Madjar, H. Colin and G. Guiochon, *J. Phys. Chem.*, 90 (1986) 207.
3 J. E. Eble, R. L. Grob, P. E. Antle and L. R. Snyder, *J. Chromatogr.*, 384 (1987) 25.
4 Cs. Horváth, A. Nahum and J. H. Frenz, *J. Chromatogr.*, 218 (1981) 365.
5 F. Eisenbeiss, S. Ehlevding, A. Wehrli and J. F. K. Huber, *Chromatographia*, 20 (1985) 657.
6 H. Poppe and J. C. Kraak, *J. Chromatogr.*, 255 (1983) 395.
7 G. Cretier and J. L. Rocca, *Chromatographia*, 20 (1985) 461.
8 J. Newburger, L. Liebes, H. Colin and G. Guiochon, *Sep. Sci. Technol.*, 22 (1987) 1933.
9 S. Golshan-Shirazi and G. Guiochon, *J. Phys. Chem.*, 93 (1989) 4341.
10 L. R. Snyder, G. B. Cox and P. E. Antle, *Chromatographia*, 24 (1987) 82.
11 J. N. Little, R. L. Cotter, J. A. Prendergast and P. D. McDonald, *J. Chromatogr.*, 126 (1976) 439.
12 H. Colin, P. Hilaireau and J. de Tournemire, *LC · GC*, 8 (1990) 302.
13 A. W. J. De Jong, H. Poppe and J. C. Kraak, *J. Chromatogr.*, 209 (1981) 432.
14 S. Golshan-Shirazi and G. Guiochon, *Anal. Chem.*, 61 (1989) 1368.
15 S. Golshan-Shirazi, S. Ghodbane and G. Guiochon, *Anal. Chem.*, 60 (1988) 2630.
16 S. Golshan-Shirazi and G. Guiochon, *Anal. Chem.*, 61 (1989) 462.
17 A. Katti and G. Guiochon, *Anal. Chem.*, 61 (1989) 982.
18 B. W. Sands, Y. S. Kim and J. L. Bass, *J. Chromatogr.*, 360 (1986) 353.
19 P. Gareil and R. Rosset, *J. Chromatogr.*, 450 (1988) 13.
20 H. Colin, *Sep. Sci. Technol.*, 22 (1987) 1851.
21 S. Golshan-Shirazi and G. Guiochon, *Anal. Chem.*, 60 (1988) 2364.
22 Z. Ma, A. Katti, B. Lin and G. Guiochon, *J. Phys. Chem.*, 94 (1990) 6911.
23 G. B. Cox and L. R. Snyder, *J. Chromatogr.*, 483 (1989) 95.

Journal of Chromatography, 550 (1991) 313–324
Elsevier Science Publishers B.V., Amsterdam

CHROMSYMP. 2302

Review

Structure–retention correlation in liquid chromatography

T. HANAI
International Institute of Technological Analysis, Health Research Foundation, Institute Pasteur de Kyoto 5F, Hyakumanben, Sakyo-ku, Kyoto 606 (Japan)

ABSTRACT

The analysis of retention mechanisms and the prediction of retention time in liquid chromatography were examined by physico-chemical parameters. The basic parameters used for the calculation were the octanol–water partition coefficient (log P), the Van der Waals volume, the dissociation constant and Hammett's sigma constant. The log P values were calculated by Rekker's method and the Van der Waals volumes were calculated by Bondi's method. The dissociation constants were calculated by the modified Hammett's equation. A method for the prediction of retention time in reversed-phase liquid chromatography is proposed and demonstrated from these calculated values and the retention was analysed by the measured enthalpy and proposed selectivity.

CONTENTS

1. INTRODUCTION

The optimization of chromatography and the characterization of solutes under different chromatographic conditions are important in solving purification problems in various fields of chemistry. Chromatographic results indicate the relative differences in the nature of the solutes. If, therefore, solutes can be characterized by physico-chemical parameters in addition to their relative retention times, chromatographic

0021-9673/91/$03.50

conditions may be optimized and the nature of the solutes can be determined from chromatographic retention times.

Retention differences related to chemical structure have been discussed in normal-phase liquid chromatography (adsorption liquid chromatography, including thin-layer chromatography), where hydrogen bonding and π–π interactions are dominant. This approach is extended here to analyse the retention mechanisms in aqueous-phase liquid chromatography, including reversed-phase and ion-exchange liquid chromatography.

The molecular interactions which occur are probably related to solubility. A relative solubility in water expressed as an octanol/water partition coefficient has been proposed mathematically as Hansch's π-constant, and this was later summarized as Rekker's hydrophobic fragmental constant. Rekker's hydrophobic fragmental constant is used to optimize reversed-phase liquid chromatography, and Hammett's equation is used to predict the retention time of ionizable compounds. However, Hansch's π-constant and Rekker's hydrophobic fragmental constant are relative values and do not explain the meaning of solubility properties. To characterize the solutes from a basic knowledge about molecules, their capacity ratios based on their Van der Waals volume (VWV) calculated by Bondi's method is analysed here. The chromatographic behaviour of alkanes is used to provide standard values in both reversed-phase liquid chromatography and gas chromatography. The difference of the logarithm of capacity ratio ($\Delta\log k'$) was found to be related to the delocalization energy of polyaromatic hydrocarbons (PAHs). The value $\Delta\log k'$ was first described as a π-energy effect related to delocalization energy, and was later referred to as a selectivity R^* as a result of a common explanation for the effect of different substitutes. A quantitative structure relationship in liquid chromatography is described as well as solubility properties.

2. SOLUBILITY PROPERTIES AS A FUNCTION OF RETENTION IN LIQUID CHROMATOGRAPHY

The analysis of the retention mechanism and the prediction of retention time have been examined by several methods. Computer-aided analysis is difficult as the retention mechanism is not well understood and the analysis is carried out by trial and error. How are the solutes held on, or in, a support? This must depend on the physico-chemical interaction between the solutes and the stationary phase [1]. When a strong solvent in which the solute dissolves is used, the solute is eluted very quickly from the column. In this case, the forces holding the substance on the stationary phase should be similar to those responsible for dissolution in a solvent. Eight solubility properties are recognized: Van der Waals (London dispersion) forces, dipole–dipole, ion–dipole, Coulombic and repulsion forces, charge transfer complexes, hydrogen bonding and co-ordination bonds [2]. An attempt has been made to explain the retention mechanisms based on solubility properties, and a possible mechanism was analysed by nuclear magnetic resonance (NMR) and electron spectroscopy for chemical analysis (ESCA) [3]. The molecular interactions which are probably involved in retention are summarized in Table 1.

The molecular interactions in liquid chromatography can be explained by the solubility properties listed in Table 1 [4,5]. The retention of a single molecule is not due

TABLE I

CLASSIFICATION OF LIQUID CHROMATOGRAPHY

Symbols: ● = important; ○ = considerable; △ = considerable on a packing.

	Van der Waals	Repulsion	London dispersion	Hydrophobic	Dipole–dipole	Charge-transfer	Hydrogen-bonding	Coulomb (ion–ion and ion–dipole)	Ligand formation	Complex formation	Salting-out	Steric effect
Size-exclusion	●	○	○									
Reversed-phase	○	○	○	●	△		△					
Reversed-phase ion-par	○	○	○	●	△			●				
Ion-pair partition	○	○	○				○	●				
Ion-exchange	○	○	○	○	○		△	●			○	
Normal-phase (adsorption)	○	○	○		●	○	●			△		○
Charge-transfer	○	○	○		○	●		○				
Salting-out	○	○	○	○	○			○			●	
Ligand-exchange	○	○	○					○	●			
Chelation	○	○	○			○		○		●		
Affinity	○	○	○	○	○	○	○	○	○	○		●
Chiral separation	○	○	○		○	○	○		○			●

to only one property, but to a combination of several different properties. However, one typical property can usually be determined experimentally. The probable interactions can be estimated from the chemical structure of the analytes and packing materials.

One packing can be used for several different types of liquid chromatography by suitable selection of the eluent components. As an example, a column packed with octadecyl-bonded silica gel was used for size-exclusion liquid chromatography in tetrahydrofuran, for normal-phase liquid chromatography in *n*-hexane and for reversed-phase liquid chromatography in acetonitrile. The chromatograms obtained are shown in Fig. 1.

The elution volumes of polystyrene, decylbenzene and toluene were 1.05, 1.57 and 1.64 ml, respectively (Fig. 1A). This means that size-exclusion liquid chromatography can be achieved with an elution volume between 1.05 and 1.64 ml in this system. The elution volumes of decylbenzene and toluene were 1.70 and 1.84 ml, respectively, in *n*-hexane (Fig. 1B) and the elution volumes of dodecane, heptane, hexane, pentane and butylbenzene were 1.69, 1.73, 1.77, 1.77 and 1.77 ml, respectively. This type of chromatography is called adsorption or non-aqueous reversed-phase liquid chromatography. The elution order of alkylbenzenes was reversed in acetonitrile, as shown in Fig. 1C. The elution volumes of toluene and octylbenzene were 2.18 and 4.66 ml,

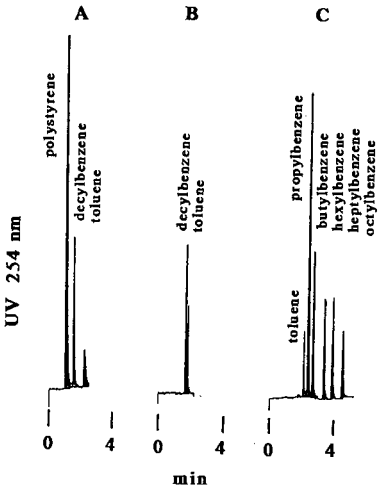

Fig. 1. Chromatograms obtained on one column using different solvents. Column: 15 cm × 4.6 mm I.D., packed with 5-μm Develosil ODS. Eluents: A, tetrahydrofuran; B, *n*-hexane; C, acetonitrile.

respectively. The elution volume increased with the addition of water into the acetonitrile. These elution orders are based on the solubility of solutes, except for size-exclusion liquid chromatography.

The digitization of solubility properties from chemical structures will be required for the further development of the optimum system based on solubility properties.

3. OPTIMIZATION OF REVERSED-PHASE LIQUID CHROMATOGRAPHY BY PARTITION COEFFICIENT

The determination of the solubility of drugs is very important in the field of pharmaceuticals. One method measures this solubility in terms of the partition coefficient between octanol and water. The mathematical calculation of an octanol/water partition coefficient was first proposed by Leo *et al.* [6] as Hansch's π-constant, and was later proposed by Rekker [7] as a hydrophobic fragmental constant (log P). Attempts have been made to measure such an octanol/water partition coefficient by liquid chromatography [8–12]. It is possible to correlate the elution order in reversed-phase liquid chromatography with the octanol/water partition coefficient (log P). The log k' of standard compounds was correlated with log P calculated by Rekker's method [13]. An organic modifier effect on log P in reversed-phase liquid chromatography has been described, and a method for the qualitative analysis of free fatty acids was proposed [13–15]. Hanai *et al.* [16] reported the prediction of retention time in a given eluent from log P for aromatic hydrocarbons. The log k' values of phenols [17] and nitrogen-containing compounds [18] were also related to their log P value, and the calculated log P was used for the qualitative analysis of urinary aromatic acids by reversed-phase liquid chromatography [19,20]. The inclusion of the dissociation constant in the calculation makes it possible to predict the retention times of

ionized aromatic acids [21,22]; the dissociation constant was calculated by the method proposed by Perrin *et al.* [23].

3.1. Prediction of retention time from the partition coefficients (log P) in reversed-phase liquid chromatography

Various methods have been used for the prediction of retention time in reversed-phase liquid chromatography. The number of carbon atoms of the aliphatic chain was used for alcohols [14] and phenols [24–26], and this method was further improved by the use of molecular connectivity [27].

Another approach is the use of a quantitative structure–activity relationship, where Hansch's π-constant [6] and Rekker's hydrophobic fragmental constant [7] are derived from the octanol/water partition coefficients and the partition coefficient is measured by liquid chromatography. The partition coefficient calculated by Rekker's method has a linear relationship with log k' measured in reversed-phase liquid chromatography [13]:

$$\log k' = y\log P + m \tag{1}$$

where y and m are constant in a given system. An example of this relationship is given in Fig. 2.

A good correlation coefficient was obtained in 20–80% acetonitrile–water mixtures. The standard compounds used to evaluate the columns were 2-hydroxyacetophenone, coumarin, acetophenone, indole, propiophenone, butyrophenone, isopropylbenzoate, butylbenzoate and isopentylbenzoate. A polynomial regression between the slope (y) and the percentage concentration (x) of acetonitrile in water was calculated from eqn. 2:

$$y = \sum_{i=0}^{i=n} a_i x^i \qquad n = 2\text{–}8 \tag{2}$$

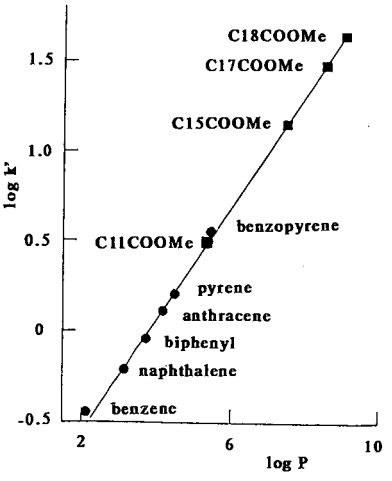

Fig. 2. Relationship between hydrophobicity (log P) and the logarithm of the capacity ratio (log k'). Column: 25 cm × 4.0 mm I.D., packed with Partisil ODS. Eluent: 95% ethanol–water (1:1).

A fourth-degree polynomial was calculated by regression from the log k' values of standard compounds measured in five acetonitrile–water mixtures.

An optimization of the organic modifier concentration for the separation of known compounds has been proposed. When the value of the actual column plate number, the resolution and log P of pairs of compounds a and b are known, the percentage concentration (x) required for their separation is calculated from eqns. 3–5 [15,16]:

$$R_s = (\alpha - 1)\, N_{\text{eff}}^{\frac{1}{2}}/4\alpha \tag{3}$$

$$y = [\log N_{\text{eff}}^{\frac{1}{2}} - \log (N_{\text{eff}}^{\frac{1}{2}} - 4R_s)]/(\log P_a - \log P_b) \tag{4}$$

$$x = \sum_{j=0}^{j=n} b_j y^j \tag{5}$$

The difference between the log k' values measured and predicted by eqns. 1 and 2 from the log P values calculated by Rekker's hydrophobic fragmental constant is within 5%. An example of log P values obtained experimentally compared to those calculated by Rekker's method is shown in Fig. 3.

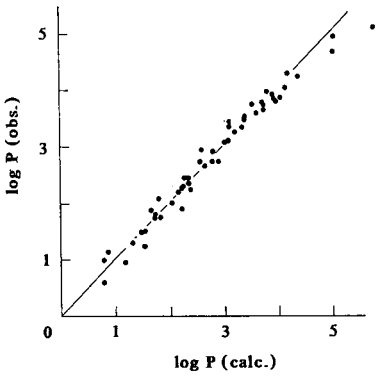

Fig. 3. Comparison of calculated and observed log P values. Column: 25 cm × 4.1 mm I.D., packed with Unisil QC_{18}. Eluent: 60% aqueous acetonitrile. Column temperature: 30°C.

The values of log P obtained from eqn. 1 using measured log k' values of 54 compounds, including alkyl alcohols, alkyl phenones, alkyl benzoates, PAHs and halogenated benzenes, were related to the log P values calculated according to Rekker [7]. The average difference was within 0.16 log P unit. The correlation coefficient was 0.981 [16].

3.2. Prediction of retention time from the partition coefficients and dissociation constants in reversed-phase liquid chromatography

The retention time of the molecular form of compounds can be predicted by the above calculation method, but the retention times of ionized compounds is also very

important. The dissociation constant (pK_a) was therefore added to the calculation to predict the retention time of aromatic acids [21]:

$$k' = \frac{k'_m + k'_i(K_a/[H^+])}{1 + K_a/[H^+]} \tag{6}$$

where k'_m is the capacity ratio of molecular form of the acid and can be obtained from log P, and k_i is the capacity ratio of the 100% ionized acid. Unfortunately, k'_i cannot be obtained mathematically at present, and the value is close to zero.

Eqn. 6 was further modified to improve the precision at low pH, where the strong acid used for pH control eliminates the retention of weak acids from the hydrophobic surface of packings [22]. The modified eqn. 7 is given in the following form, and a slight modification of constant A improves the precision:

$$k' = A\frac{k'_m - k'_i}{2}\tanh(pK_a - pH) + \frac{k'_m + k'_i}{2} \tag{7}$$

The dissociation constant can be mathematically calculated by Hammett's equation [23], and the organic solvent effect on pK_a was also examined [22]. The modified values are: benzoic acids, $4.20–1.00\Sigma\sigma$; 2-hydroxybenzoic acids, $4.20–1.13\Sigma\sigma$; phenylacetic acids, $4.30–0.35\Sigma\sigma$; cinnamic acids, $4.38–0.66\Sigma\sigma$; and mandelic acids, $3.38–0.454\Sigma\sigma$, where σ = Hammett's sigma constant.

An example of the relationship between the predicted and observed log k' values at pH 4.26 is shown in Fig. 4.

The agreement between the observed and predicted k' values of aromatic acids is within 10%. An error greater than 10% for 3-hydroxy-2-naphthoic acid [3(OH)NA] and 2-hydroxybenzoic acid [2(OH)BA] was attributed mainly to the error in K_a [21]. In Fig. 4, IPA, CA, 3MeOCA and NA are indole-3-propionic acid, cinnamic acid, 3-methoxycinnamic acid and 2-naphthoic acid, respectively. The partition coefficient, log P, and the dissociation constant, pK_a, can be obtained by simple calculation, and the retention time can be predicted from reversed-phase liquid chromatography.

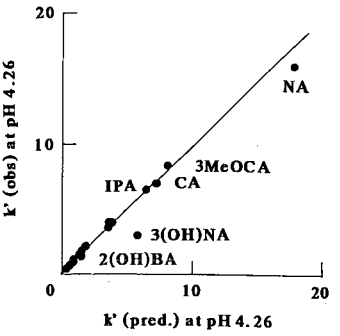

Fig. 4. Relationship between observed and predicted capacity ratio at pH 4.26. Column: 15 cm × 4.1 mm I.D., packed with 5-μm polystyrene gel (Hitachi 3013). Eluent: 30% aqueous acetonitrile with 0.05 M sodium phosphate. Column temperature: 55°C.

However, each group of compounds requires individual standard compounds to obtain the constants for the equations which were used for the calculation of retention time, resolution and concentration of the acetonitrile organic modifier. This means that if a compound had two or more different types of substituted groups, then the retention time predicted from one set of equations was often far from the observed value. The system based on the partition coefficient between octanol and water was therefore not adequate for producing an optimized system for mixtures of different types of compounds. Log P is a relative quantity obtained by experiment; it is not a solubility property. A further optimization of liquid chromatography was therefore attempted using a basic physico-chemical property, the VWV, calculated by Bondi's method [28].

4. USE OF VAN DER WAALS VOLUME AS A BASIC VALUE IN REVERSED-PHASE LIQUID CHROMATOGRAPHY

A system was examined in which only the size and the π-energy of the molecules may be involved in their retention by reversed-phase liquid chromatography using octadecyl-bonded silica gels as the packing. If the hydrogen bonding and Coulombic forces are negligible, the retention of the molecules depends upon their size, and the presence of π-electrons enhances the selectivity. The molecular size, *i.e.*, th VWV, was calculated by Bondi's method [28]. The delocalization energy was obtained from the literature as a property of the π-electrons [29–31]. An example of the relationship between VWV and log k' is shown in Fig. 5.

The maximum log k' values were obtained from the relationship between the retention of n-alkanes and the VWVs [32]. Values for $\Delta\log k'$ were calculated as the difference between this maximum log k' and the observed log k' values of PAHs. The results for PAHs were applied to other compounds, the standard compounds used being benzene, naphthalene, phenanthrene, chrysene and tetrasene. The selectivity was derived from the relationship between the $\Delta\log k'$ values and the delocalization energy. The retention is given by the following equation:

$$\log k'(\text{PAH}) = \log k'(\text{VWV}) - \Delta\log k' \tag{8}$$

where log k'(VWV) is related to molecular size.

The selectivity obtained on some octadecyl-bonded silica gels in acetonitrile–water mixtures was very similar, so an optimization in reversed-phase liquid chromatography can be carried out from the VWV and selectivity. This approach was also applied to alkyl alcohols whose $\Delta\log k'$ values were also related to the delocalization energy, even if they did not have a double bond in their structure, and the values were therefore referred to as a hydrogen bonding effect [32]. The retention of alcohols is given by eqn. 9:

$$\log k'(\text{alcohol}) = \log k'(\text{VWV}) - \log k'(\text{hydrogen bonding}) \tag{9}$$

This hydrogen bonding effect was later renamed as selectivity. This prediction system for the retention time in reversed-phase liquid chromatography was applied to evaluate the selectivity of a phenyl-bonded silica gel in acetonitrile–water and

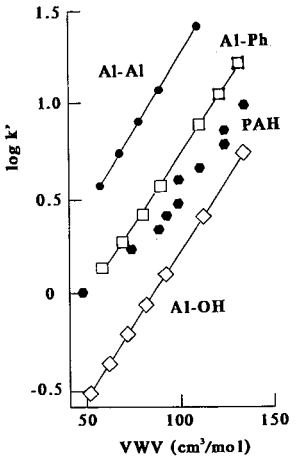

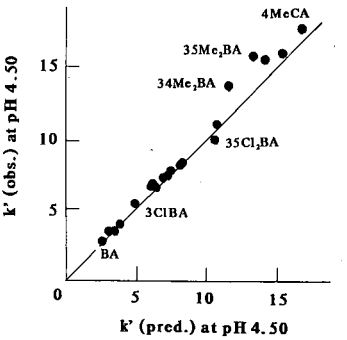

Fig. 5. Relationship between Van der Waals volume (VWV) and the logarithm of the capacity ratio (log k'). Column: 15 cm × 4.6 mm I.D., packed with 5-μm Develosil ODS. Eluent: 80% aqueous acetonitrile. Column temperature: 30°C. Al-Al = Alkanes (pentane–decane); Al-Ph = alkylbenzenes (toluene–octylbenzene); PAH = polyaromatic hydrocarbons (benzene–benzopyrene); Al-OH = alkyl alcohols (butyl alcohol–dodecyl alcohol).

Fig. 6. Predicted and observed capacity ratios (k') of aromatic acids at pH 4.50. Column: 15 cm × 6.0 mm I.D., ERC-1000 (ODS). Eluent: 25% aqueous acetonitrile with 0.05 M sodium phosphate. Column temperature: 40°C. BA = Benzoic acid; 3ClBA = 3-chlorobenzoic acid; $35Cl_2BA$ = 3,5-dichlorobenzoic acid; $34Me_2BA$ = 3,4-dimethylbenzoic acid; $35Me_2BA$ = 3,5-dimethylbenzoic acid; 4MeCA = 4-methylcinnamic acid.

tetrahydrofuran–water mixtures. The selectivity of the phenyl-bonded silica gel was clearly observed in the chromatographic behaviour of chlorobenzenes as a selectivity difference [33]. This approach was applied to the analysis of the liquid chromatographic behaviour of phenols [34] and aromatic acids [35]. The retention of the molecular form of phenols and aromatic acids was predicted from eqns. 10 and 11:

$$\log k'(\text{ArOH}) = \log k'(\text{VWV}) - \log k'(\text{Ph}) - \log k'(\text{OH}) \quad (10)$$

$$\log k'(\text{ArCOOH}) = \log k'(\text{VWV}) - \log k'(\text{Ph}) - \log k'(\text{COOH}) \quad (11)$$

where $\log k'(\text{ArOH})$ and $\log k'(\text{ArCOOH})$ are the capacity ratios of a substituted phenol and aromatic acid, respectively. $\text{Log}\, k'(\text{VWV})$ is obtained from their VWV, and $\log k'(\text{Ph})$ is the selectivity of the phenyl group. $\text{Log}\, k'(\text{OH})$ and $\log k'(\text{COOH})$ are the selectivity of a hydroxyl and carboxyl group conjugated with phenyl, respectively. The retention times of ionized aromatic acids were also predicted from their VWVs, selectivity and dissociation constants by eqn. 6 where the maximum capacity ratios (k'_m) were calculated from their VWVs and selectivity instead of from their log P values [35]. An example is shown in Fig. 6.

The difference between the predicted and observed capacity ratio was within 10%. The error for 3,4- and 3,5-dimethylbenzoic acids (3,4-Me_2BA and 2,5-Me_2BA) was more than 10%, but the error for 3,4-Me_2BA should depend on the value of selectivity, but not the dissociation constant. The correlation coefficient was 0.990 (n = 21).

5. ENTHALPY RELATED TO RETENTION IN REVERSED-PHASE LIQUID CHROMATOGRAPHY

The higher the enthalpy (ΔH), the longer the retention time, and log k' has a linear correlation to enthalpy [36]. As seen in Fig. 7, each group of compounds exhibits such a linear relationship between enthalpy and log k', although it is not perfect. The ΔH values are also independent of the VWVs as seen in Fig. 8.

The $\Delta\Delta H$ value of a methylene unit of alkyl alcohols is fairly constant, and the hydrogen-bonding energy can therefore also be considered as constant [33]. Substituted benzenes with longer alkyl groups have a larger selectivity constant. This result seems unreasonable because alkylbenzenes with a larger alkyl group must lose their aromaticity even if their selectivity difference becomes smaller. The $\Delta\Delta H$ value of a methylene unit alkylbenzenes is, however, not constant and larger molecules have a higher $\Delta\Delta H$ value than the average $\Delta\Delta H$ value of a methylene unit. The larger $\Delta\Delta H$ value may be due to dimerization between solutes, as described by Ben-Neim [37], and/or to the strong direct interaction between alkylbenzene and the octadecyl group of the packing.

In contrast, the isomeric effect of the $\Delta\Delta H$ value of substitutes of chlorobenzenes is very small. This means that the molecular size of isomers is almost the same under these conditions. The $\Delta\pi$ values of isomers are very large, the difference in the log k' values of the isomers being due mainly to the selectivity and not to the enthalpy.

The selectivity of PAHs is about twice the ΔH of these compounds. This result supports the assumption that retention is mainly due to selectivity. Furthermore, the Δlog k' values of tetrasene and chrysene, which are four-ring PAHs, can be related to their ΔH values but not to their selectivity. This means that, although the calculated molecular size obtained using Bondi's method is the same, the actual size is not the same under these chromatographic conditions [38].

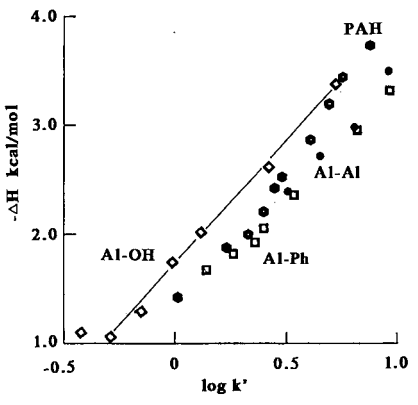

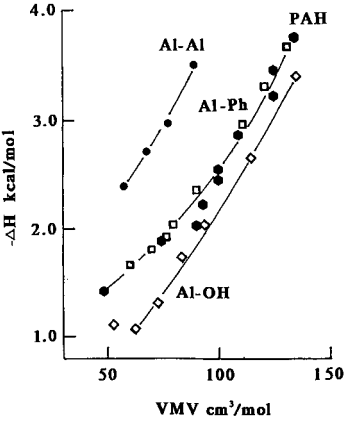

Fig. 7. Relationship between enthalpy ($-\Delta H$) and logarithm of capacity ratio (log k'). Column: 10 cm × 6.0 mm I.D., ERC-ODS. Eluent: 80% aqueous acetonitrile. Al-Al = Alkanes (pentane–octane); Al-Ph = alkylbenzenes (toluene–octylbenzene); PAH = polyaromatic hydrocarbons (benzene–benzopyrene); Al-OH = alkyl alcohols (butyl alcohol–dodecyl alcohol).

Fig. 8. Relationship between enthalpy ($-\Delta H$) and Van der Waals volume (VWV). Experimental conditions as in Fig. 7.

The selectivity (R^*, former energy effect) of alkyl- and chlorophenols varied from 7.9 to 10.1 and from 7.9 to 7.4, respectively. The enthalpy of methylphenols was about 2.0 kcal/mol, and that of chlorophenols varied from 2.0 to 2.4 kcal/mol in the case of pentachlorophenol. This means that the retention difference depended not on the size but on the π-electron density [39]. A similar result was obtained for alkylated and halogenated aromatic acids whose enthalpies were nearly equal, and their selectivity values varied [40]. The ΔH values may depend on the type of packing used and the water content of an eluent [41].

Carbon loading and the end-capping effect of octadecyl-bonded silica gels were studied. The enthalpy was highest on non-end-capped high-carbon octadecyl-bonded silica gels, and slightly higher on high-carbon end-capped gels than low-carbon end-capped gels. There was, however, a selectivity difference in the retention between alkyl alcohols and other hydrophobic compounds depending on the end-capping treatment applied [42]. The order of enthalpies of phenols showed no direct relationship to the capacity ratio or the hydrophobicity of octadecyl-bonded silica gels with a different carbon content [43]. In addition, enthalpy was not directly related to the log k' values nor to the alkyl chain length of bonded-silica gels, even if the retention behaviour of one group of compounds, such as PAHs, and especially the retention of smaller size polar compounds, appeared to indicate this [44].

6. CONCLUSIONS

The qualitative analysis of retention behaviour in liquid chromatography is now well established. However, quantitative analysis is still difficult, *i.e.*, the prediction of retention time and the optimization of separation conditions from physico-chemical properties is not completely successful. One reason is lack of an ideal packing material. The packing has to be stable as part of an instrument, and this is very difficult to achieve in normal-phase liquid chromatography because the humidity of the organic solvent ages the silica gel.

Several packings have been synthesized for reversed-phase liquid chromatography. One possible material is a vinyl alcohol co-polymer gel. This packing is fairly polar and very stable, however, it demonstrates a strong retention capacity for PAHs [45–49]. Although silica gel-based stable octadecyl- and octyl-bonded packings have been synthesized from pure silica gel [50], such an optimization system has not yet been built. Further experiments are required to elucidate the retention mechanism and to systematize it within the context of instrumentation.

REFERENCES

1 L. R. Snyder, *Principles of Adsorption Chromatography*, Marcel Dekker, New York, 1968.
2 K. Shinoda, *Yoeki To Yokaido*, Maruzen, Tokyo, 1969.
3 W. Funasaka and T. Hanai, presented at the *Annual Autumn Symposium of Chubu Kagaku Karenkyokai, October 1974*, paper IE04.
4 T. Hanai and K. Fujimura, *J. Chromatogr. Sci.*, 14 (1976) 140.
5 T. Hanai and H. Hatano (Editors), *Shin. Khosoku Ekitai Kuromatogurafi (New HPLC)*, Nankodo, Tokyo, 1978, p. 35 (in Japanese).
6 A. Leo, C. Hansch and D. Elkins, *Chem. Rev.*, 71 (1971) 525.
7 R. F. Rekker, *The Hydrophobic Fragmental Constant*, Elsevier, Amsterdam, 1977.

8 W. J. Haggerty and E. A. Murrill, *Res. Dev.*, 25 (1974) 30.
9 R. M. Calson, *J. Chromatogr.*, 107 (1975) 219.
10 J. M. McCall, *J. Med. Chem.*, 18 (1975) 549.
11 M. S. Mirrless, S. T. Moulton, C. T. Murphy and P. J. Taylar, *J. Med. Chem.*, 19 (1976) 615.
12 K. Miyake and H. Terada. *J. Chromatogr.*, 157 (1978) 386.
13 T. Hanai, *Chromatographia*, 12 (1979) 77.
14 M. D'Amboise and T. Hanai, *J. Liq. Chromatogr.*, 5 (1982) 229.
15 T. Hanai, S. Hara, S. Mori and T. Hanai (Editors), *Kuromatogurafi, Bunri Shisutemu (Chromatography, the Separation System)*, Maruzen, Tokyo, 1981, p. 138 (in Japanese).
16 T. Hanai, K. C. Tran and J. Hubert, *J. High Resolut. Chromatogr. Chromatogr. Commun.*, 4 (1981) 454.
17 T. Hanai and J. Hubert, *J. High Resolut. Chromatogr. Chromatogr. Commun.*, 6 (1983) 20.
18 T. Hanai and J. Hubert, *J. Liq. Chromatogr.*, 8 (1985) 2463.
19 T. Hanai and J. Hubert, *J. Chromatogr.*, 239 (1982) 527.
20 T. Hanai and J. Hubert, *J. High Resolut. Chromatogr. Chromatogr. Commun.*, 4 (1981) 500.
21 T. Hanai, K. C. Tran and J. Hubert, *J. Chromatogr.*, 239 (1982) 385.
22 T. Hanai and J. Hubert, *J. High Resolut. Chromatogr. Chromatogr. Commun.*, 7 (1984) 524.
23 D. D. Perrin, B. Dempsey and E. P. Serjeant, *pKa Prediction for Organic Acids and Bases*, Chapman and Hall, London, 1981.
24 K. Calmmer, L.-E. Edholm and B. E. F. Smith, *J. Chromatogr.*, 136 (1977) 45.
25 J. F. Schabron, R. J. Hurtubise and H. F. Silver, *Anal. Chem.*, 50 (1980) 1911.
26 N. Nomura, *Toyama Univ. Kyoikugakubu-Kiyo*, 27 (1979) 1.
27 B. L. Karger, J. R. Gant, A. Harkopt and P. H. Weiner, *J. Chromatogr.*, 128 (1976) 65.
28 A. Bondi, *J. Phys. Chem.*, 68 (1964) 441.
29 C. A. Streuli and M. Orloff, *J. Chromatogr.*, 62 (1971) 73.
30 W. Ecknig, B. Trung, R. Radeglia and U. Gross, *Chromatographia*, 16 (1982) 178.
31 A. Streitwieser, Jr., *Molecular Orbital Theory for Organic Chemistry*, Wiley, New York, London, 1961, p. 241.
32 T. Hanai and J. Hubert, *J. Chromatogr.*, 290 (1984) 197.
33 T. Hanai and J. Hubert, *J. Chromatogr.*, 291 (1984) 81.
34 T. Hanai and J. Hubert, *J. Chromatogr.*, 302 (1984) 89.
35 T. Hanai, *J. Chromatogr.*, 332 (1985) 189.
36 W. Melander, D. E. Campbell and Cs. Horváth, *J. Chromatogr.*, 158 (1978) 215.
37 A. Ben-Neim, *Hydrophobic Interaction*, Plenum Press, New York, London, 1980.
38 T. Hanai, A. Jukurogi and J. Hubert, *Chromatographia*, 19 (1984) 266.
39 Y. Arai, M. Hirukawa and T. Hanai, *J. Chromatogr.*, 384 (1987) 279.
40 Y. Arai, J. Yamaguchi and T. Hanai, *J. Chromatogr.*, 400 (1987) 21.
41 H. Colin, J. C. Diez-Mesa, G. Guiochon, T. Czaikowska and I. Miedziak, *J. Chromatogr.*, 167 (1978) 41.
42 J. Yamaguchi, T. Hanai and H. Cai, *J. Chromatogr.*, 441 (1988) 183.
43 J. Yamaguchi and T. Hanai, *J. Chromatogr. Sci.*, 27 (1989) 710.
44 J. Yamaguchi and T. Hanai, *Chromatographia*, 27 (1989) 371.
45 T. Hanai, Y. Arai, M. Hirukawa, K. Noguchi and Y. Yanagihara, *J. Chromatogr.*, 349 (1985) 323.
46 Y. Arai, M. Hirukawa and T. Hanai, *Nihon Kagaku Kaishi*, (1986) 969.
47 Y. Arai, M. Hirukawa and T. Hanai, *J. Liq. Chromatogr.*, 10 (1987) 635.
48 M. Hirukawa, Y. Arai and T. Hanai, *J. Chromatogr.*, 395 (1987) 481.
49 Y. Arai, M. Hirukawa and T. Hanai, *J. Chromatogr.*, 400 (1987) 27.
50 T. Hanai, M. Ohhira and T. Tamura, *LC · GC*, 6 (1988) 922.

Journal of Chromatography, 550 (1991) 325–334
Elsevier Science Publishers B.V., Amsterdam

CHROMSYMP. 2114

Retention prediction for polymer additives in reversed-phase liquid chromatography

KIYOKATSU JINNO* and YUUICHI YOKOYAMA
School of Materials Science, Toyohashi University of Technology, Toyohashi 441 (Japan)

ABSTRACT

A retention prediction approach for polymer additives has been investigated. The relationship between retention and hydrophobicity can be useful in predicting the retention of polymer additives in reversed-phase liquid chromatography. Peak identification is possible using both a retention matching process based on this prediction scheme and an ultraviolet spectral matching process with a photo-diode array, multi-wavelength ultraviolet detection system.

INTRODUCTION

The selection of satisfactory separation conditions is still a major problem in liquid chromatography (LC). At present, trial-and-error experiments are usually performed to find the best optimal separation conditions, but this approach is a very difficult, tedious and time-consuming task. A recent improvement proposed by Berridge [1,2] and Snyder and co-workers [3–5] involved systematic computer techniques which are gradually becoming more popular although still in the developmental stage. A unique computer technique which we have proposed is the retention prediction approach [6–10]. Retention predicted by this concept can be useful in the optimization of procedures to obtain faster analysis times and better separations [7,10].

In order to predict the retention of solutes, a clear understanding of the retention mechanism is required. Consideration of the basis of the retention mechanism of reversed-phase LC makes it possible to predict a component's physicochemical parameters such as surface area, partition coefficient between two immiscible phases and aqueous solubility which might correlate with retention. In practice, such correlations between retention and physicochemical parameters exist and some of these parameters have been determined based on these relationships. This is the basic idea of the approach termed QSRR (quantitative structure–retention relationships) [11,12]. QSSR can be useful in predicting retention in reversed-phase LC, based on the premise that relationships exist between the physicochemical parameters representing the molecular properties of the solute such as structure, shape and/or electronic state, etc., and its retention, if such parameters are available. Using log P (the partition coefficient between 1-octanol and water proposed by Hansch and Leo [13]),

0021-9673/91/$03.50

Baker and co-workers [14–16] and Smith [17,18] have also attempted to predict retention index in LC.

The basic concept of retention prediction can be described as

$$k' = \mathrm{f}(Pi) \tag{1}$$

where k' is the capacity factor of a solute and Pi is a physicochemical parameter of the solute. To generalize the retention description in eqn. (1) for n different chromatographic conditions such as mobile phase compositions, temperature or pH of the mobile phase, the following n equations should be obtained by the same procedures with multiple regression analysis. In this instance, we assume two parameters are the most dominant for the retention:

$$\begin{aligned} X = X_1 \quad & \log k' = a_1 P_1 + b_1 P_1 + c_1 \\ X = X_2 \quad & \log k' = a_2 P_2 + b_2 P_2 + c_2 \\ \vdots \quad & \quad \vdots \\ X = X_n \quad & \log k' = a_n P_n + b_n P_n + c_n \end{aligned} \tag{2}$$

where X is the experimental condition, a and b are coefficients corresponding to the descriptors P_1 and P_2, respectively, c is the intercept, and n is the number of experimental conditions examined.

If a, b and c can be expressed as functions of X, namely, if X–a, X—b and X–c are highly correlated, the following three equations can be obtained from the multiple regression analyses:

$$a = \mathrm{f}_1(X) \tag{3}$$

$$b = \mathrm{f}_2(X) \tag{4}$$

$$c = \mathrm{f}_3(X) \tag{5}$$

and then

$$\log k' = \mathrm{f}_1(X) P_1 + \mathrm{f}_2(X) P_2 + \mathrm{f}_3(X) \tag{6}$$

should be obtained by several experiments. This equation means that, if X, P_1 and P_2 are given, the logarithm of the capacity factor, $\log k'$, can be determined for any chromatographic condition. This is the basic concept of our retention prediction approach. Predicted k' can then be useful in optimizing the separation conditions in which the conditions (X in this case) will be optimized by the calculation [7,10].

In this paper, the retention prediction approach for polymer additives is described as an extention of our work in this field. The analysis (determination and identification) of polymer additives is one of the most important practical analytical problems because of the number of additives existing in commercially available polymer materials, the quantities and species of which are very important in the quality control of polymer products.

EXPERIMENTAL

The LC system used consisted of a Jasco 880-PU pump (Tokyo, Japan), Rheodyne 7125 20-μl loop injector (Cotati, CA, USA) and a Jasco MULTI-320 photodiode array multiwavelength UV detector. The column for the separation of polymer additives was a Capcell Pak C_{18} (250 mm × 4.6 mm I.D., Shiseido, Yokohama, Japan) with mobile phases consisting of methanol and water. The flow-rate of the mobile phase was 1 ml/min and the column temperature was maintained at 40°C in a Jasco TU-100 column oven. The column dead volume was determined by the sodium nitrite peak.

Data handling, retention prediction and identification by the UV spectral matching process were performed with a NEC 9801 Series 16-bit microcomputer.

The polymer additives used in this work can be separated into two groups, Irganox and Tinuvin. Structures of which are shown in Fig. 1.

RESULTS AND DISCUSSION

The first step towards retention prediction for polymer additives is to establish which descriptor can best describe retention. Basic consideration of the retention mechanism of reversed-phase LC suggests that hydrophobicity should be the dominant physicochemical parameter in describing retention [11], as many authors have reported the possibility of retention prediction using log P in reversed-phase LC [14–18]. Although there are a number of methods proposed by Hansch and Leo [13] and Rekker [19] for calculating the hydrophobicity of these polymer additives, the values determined in the laboratory provide better accuracy for retention prediction. Therefore, we have attempted to determine the hydrophobicity of the additives using a common LC method [20–22]. In order to determine hydrophobicity, we used alkylbenzenes as the standard because alkylbenzenes have phenyl rings and alkyl chains, as do the polymer additives. Of course this selection is not completely appropriate for the accurate determination of the hydrophobicity of polymer additives because the compounds have polar substituents such as $-$OH or hetero atoms in their structures and the structural similarities between the additives and alkylbenzenes are restricted. However, it is also true that finding the best standard compound groups suitable for additives which have a variety of structures is difficult. Alkylbenzenes are simple and convenient for this purpose. Using methods described in the literature [20–22], the log P values for the polymer additives obtained with this LC system are summarized in Table I. These values will change if a different LC system is used for the determination and thus it is very important to note that the log P values in Table I are not universally applicable.

In order to obtain a retention prediction equation, we divided the standard additives into two groups, Irganox and Tinuvin, because of their greatly differing structures.

Four of the additives selected as standards were injected into the LC system with mobile phase compositions of methanol–water in the ratios 95:5, 90:10, 88:12 and 85:15. The measured capacity factors are listed in Table II. The relationships between log P and log k' were obtained by regression analysis for each data set with different mobile phase compositions, using

$$\log k' = A_x \log P + B \tag{7}$$

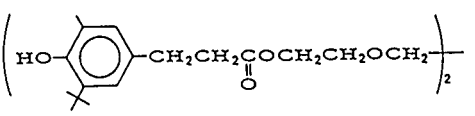

Irganox 245

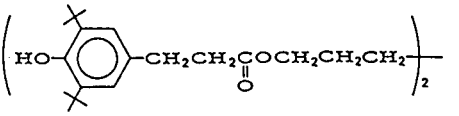

Irganox 259

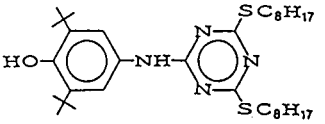

Irganox 565

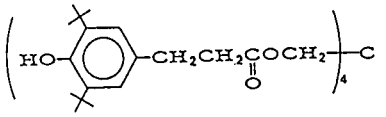

Irganox 1010

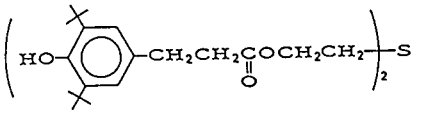

Irganox 1035

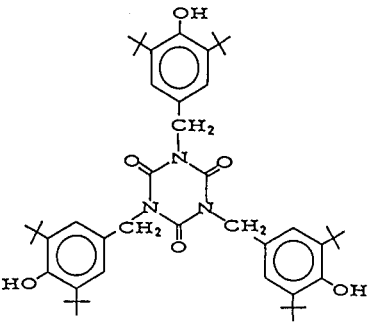

Anox 3114

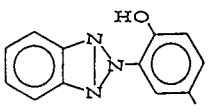

Tinuvin P

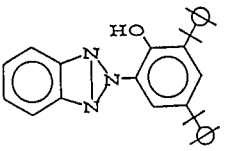

Tinuvin 234

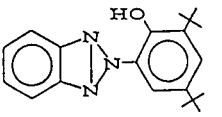

Tinuvin 320

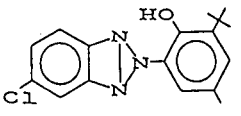

Tinuvin 326

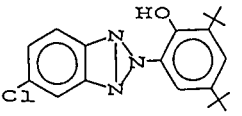

Tinuvin 327

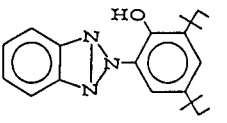

Tinuvin 328

Fig. 1. Structures of the polymer additives used.

The values of A, B and the correltion coefficients are given in Table II.

The relationships between the mobile phase composion X (in this case methanol volume percentage in the mobile phase), and A and B were then subjected to regression analysis to obtain the equations. They are:

$$\text{for Irganox } A = 6.55\,X^2 - 12.2\,X + 5.93 \qquad r = 0.998 \tag{8}$$

$$B = -48.3\,X^2 + 78.6\,X - 32.5 \qquad r = 0.999 \tag{9}$$

TABLE I

DETERMINED LOG *P* VALUES OF THE POLYMER ADDITIVES USED

Log *P* values cited here were determined by the LC system used in this work, based on alkylbenzenes as the standard.

Compound	Log *P*
Irganox 245	2.34
Tinuvin P	4.38
Irganox 1035	5.78
Irganox 259	6.47
Anox 3114	7.12
Tinuvin 320	7.46
Tinuvin 234	7.73
Tinuvin 326	7.79
Tinuvin 328	8.34
Tinuvin 327	8.46
Irganox 1010	9.84
Irganox 565	10.1

TABLE II

RETENTION DATA OF SELECTED POLYMER ADDITIVES WITH VARIOUS MOBILE PHASE COMPOSITIONS AND REGRESSION DATA FOR EQN. 7

Compound	Capacity factor			
	Volume fraction of methanol in the mobile phase			
	$X=0.95$	$X=0.90$	$X=0.88$	$X=0.85$
Irganox				
Irganox 245	0.117	0.450	0.624	1.08
Irganox 259	1.22	4.16	6.76	13.9
Anox 3114	1.55	5.93	10.0	22.1
Irganox 565	6.93	28.9	51.2	122
A^a	0.229	0.233	0.247	0.272
B^a	−1.44	−0.89	−0.775	−0.605
r^b	0.999	1.000	1.000	1.000
Tinuvin				
Tinuvin P	0.763	1.35	1.68	2.22
Tinuvin 320	3.24	7.84	11.1	18.5
Tinuvin 328	4.40	11.4	16.7	29.0
Tinuvin 327	4.68	12.2	17.9	31.3
A	0.193	0.234	0.252	0.282
B	−0.961	−0.895	−0.878	−0.888
r	1.000	1.000	1.000	1.000

[a] Regression coefficients for eqn. 7.

[b] Correlation coefficient.

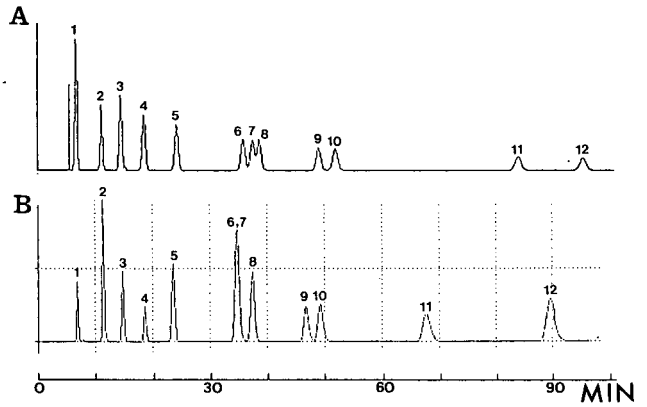

Fig. 2. Comparison of (A) the predicted and (B) the observed (254 nm) chromatograms. Mobile phase: methanol–water (92:8); flow-rate: 1 ml/min; column temperature: 40°C.

$$\text{for Tinuvin } A = 1.46\,X^2 - 3.52\,X + 2.26 \qquad r = 1.000 \qquad (10)$$

$$B = -13.0\,X^2 + 22.6\,X - 10.7 \qquad r = 0.999 \qquad (11)$$

Using these retention descriptions one can predict the retention of various polymer additives at appropriate conditions. The actual trial was performed at $X = 0.92$ and the chromatogram obtained is compared with the predicted chromatogram in Fig. 2, with the retention data compared in Table III. The agreements between the measured and predicted retention times are very good except for peak 11, Irganox 1010. This

TABLE III

COMPARISON OF THE OBSERVED AND THE PREDICTED RETENTION TIMES OF TWELVE POLYMER ADDITIVES

Peak number	Retention time (min)		Relative error [a] (%)
	Observed	Predicted	
1	6.92	7.06	2.0
2	11.1	11.6	4.5
3	14.7	14.9	1.4
4	18.7	18.9	1.1
5	23.5	24.4	3.8
6	34.7	36.4	4.9
7	34.7	37.8	8.9
8	37.5	38.8	3.5
9	46.6	49.3	5.8
10	49.3	52.1	5.7
11	67.7	84.0	24.1
12	89.7	95.5	6.5

[a] Relative error (%) = [(observed − predicted)/observed] × 100.

deviation might arise from the bulkiness of the solute. In this prediction scheme, log P was used as the descriptors of equivalent molecular size, shape and three-dimensional structure. As in reversed-phase LC the three-dimensional structure of solutes strongly influences retention.

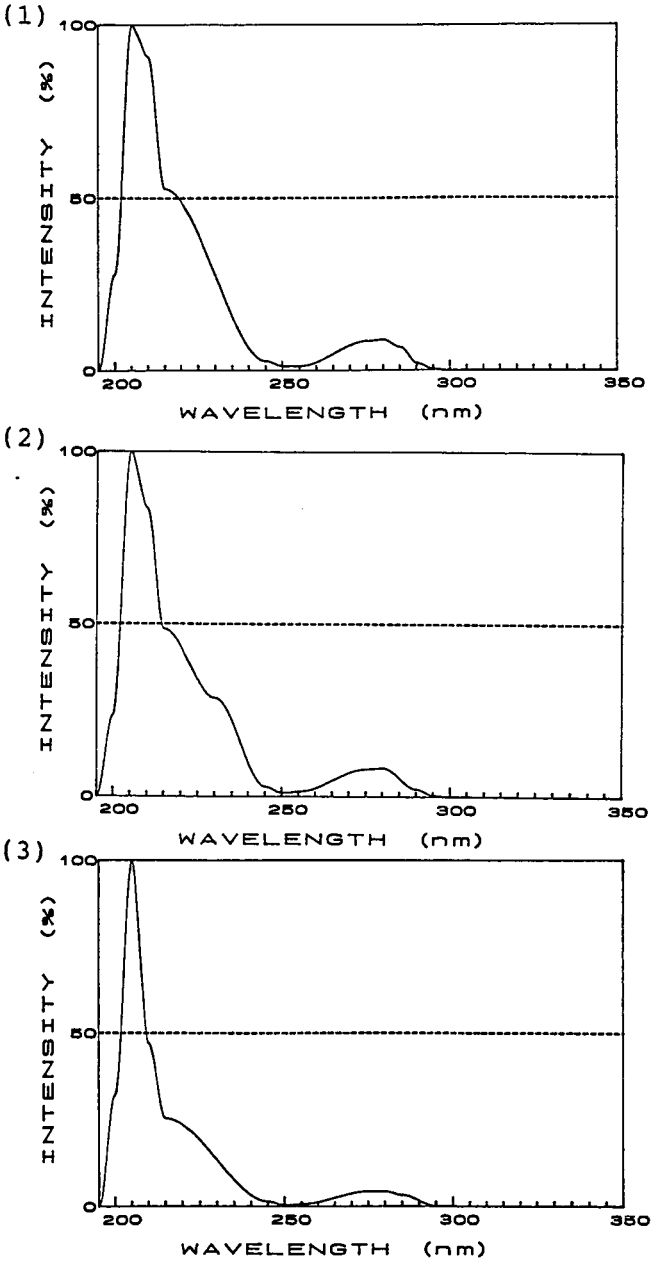

Fig. 3. UV spectra of the observed and the top two candidates found by UV spectral matching. (1) Observed UV spectrum of peak 3. (2) UV spectrum in the spectral data base for Irganox 1035. (3) UV spectrum in the spectral data base for Irganox 259.

TABLE IV

RESULTS OF THE IDENTIFICATION PROCESSES FOR PEAK 3 IN THE CHROMATOGRAM SHOWN IN FIG. 2

Rank	Sample name	Matching rate
UV spectrum matching process		
1	Irganox 1035	1.000
2	Irganox 259	1.000
3	Irganox 1010	0.999
4	Irganox 245	0.999
5	Anox 3114	0.979
6	Tinuvin 234	0.363
7	Irganox 565	0.345
8	Tinuvin 328	0.088
9	Tinuvin 327	0.088
10	Tinuvin P	0.087
Retention matching process		
1	Irganox 1035	0.918

In order to identify the peaks in the chromatogram two approaches can be applied [18–20]: (1) retention match between measured and predicted values or (2) UV spectral match between measured spectra and stored spectra. For the first approach, one can use the retention prediction scheme established in our laboratory and for the second approach, one can use the diode-array detection system where the UV spectra of polymer additives are stored.

As an example of this identification scheme, we attempted the identification of peaks 3 and 12 in the chromatogram shown in Fig. 2. The results are summarized in Tables IV and V and Fig. 3. In the identification process for peak 3, identification by UV spectral match, as shown in Table IV, is difficult because at least five candidates

TABLE V

RESULTS OF THE IDENTIFICATION PROCESSES FOR PEAK 12 IN THE CHROMATOGRAM SHOWN IN FIG. 2

Rank	Sample name	Matching rate
UV spectrum matching process		
1	Irganox 565	1.000
2	Irganox 1010	0.372
3	Irganox 245	0.359
4	Irganox 259	0.352
5	Irganox 1035	0.351
6	Anox 3114	0.302
7	Tinuvin 327	0.080
8	Tinuvin 326	0.068
9	Tinuvin 320	0.067
10	Tinuvin 328	0.062
Retention matching process		
1	Irganox 1010	0.779
2	Irganox 565	0.766

TABLE VI

RESULTS OF PEAK IDENTIFICATION FOR THE CHROMATOGRAM IN FIG. 2

Peak No.	Correlation coefficient		Identified polymer additives
	UV spectrum matching	Retention matching	
1	1.000	0.468	Irganox 245
2	1.000	0.718	Tinuvin P
3	1.000	0.918	Irganox 1035
4	1.000	0.945	Irganox 259
5	1.000	0.843	Anox 3114
6	0.988	0.796	Tinuvin 320
7	0.979	0.633	Tinuvin 234
8	1.000	0.873	Tinuvin 326
9	1.000	0.783	Tinuvin 328
10	1.000	0.787	Tinuvin 327
11	1.000	0.129	Irganox 1010
12	1.000	0.766	Irganox 565

are listed as possible, because of their similarity, as shown in Fig. 3, where the UV spectra of the top two candidates are illustrated in comparison to the observed UV spectrum. However, using the retention prediction approach, one can identify that this peak is Irganox 1035 as none of the other candidates from the UV spectral matching also matched retention time. For the determination of the peak 12, as shown in Table V, the situation was reversed. By UV spectral matching only one candidate was identified, however, retention matching provided two candidates. The top candidate from both processes, Irganox 565, can thus be identified as peak 12.

Every peak in the chromatogram in Fig. 2 has been retrieved and the final identification results are summarized in Table VI. The identified solutes agree well with the injected components.

In conclusion, the approach described in this paper can open a new dimension in the identification and quantitation of polymer additives by LC. We have shown that identification of compounds is made possible by retention matching based on retention prediction in addition to UV spectral matching. Further studies of other groups of compounds will make this approach of great practical use.

REFERENCES

1 J. C. Berridge, *Techniques for the Automated Optimization of HPLC Separations*, Wiley, Chichester, 1986.
2 J. C. Berridge, *Trends Anal. Chem.*, 3 (1984) 5.
3 B. F. D. Ghrist, B. S. Cooperman and L. R. Snyder, *J. Chromatogr.*, 459 (1988) 1.
4 B. F. D. Ghrist and L. R. Snyder, *J. Chromatogr.*, 459 (1988) 25.
5 B. F. D. Ghrist and L. R. Snyder, *J. Chromatogr.*, 459 (1988) 43.
6 K. Jinno and K. Kawasaki, *J. Chromatogr.*, 316 (1984) 1.
7 K. Jinno and K. Kawasaki, *J. Chromatogr.*, 298 (1984) 326.
8 K. Jinno, Y. Saigusa, M. Kuwajima, M. Atomura and M. Okamoto, *Chromatographia*, 21 (1986) 24.
9 K. Jinno and M. Kuwajima, *Chromatographia*, 21 (1986) 541.

10 K. Jinno, *A Computer-Assisted Chromatography System*, Hüthig, Heidelberg, 1990.
11 R. Kaliszan, *Quantitative Structure Chromatographic Retention Relationships*, Wiley-Interscience, New York, 1987.
12 Cs. Horváth, W. Melander and I. Molnár, *J. Chromatogr.*, 125 (1976) 129.
13 C. Hansch and A. Leo, *Substituted Constants for Correlation Analysis in Chemistry and Biology*, Wiley, New York, 1979.
14 J. K. Baker and C.-Y. Ma, *J. Chromatogr.*, 169 (1979) 107.
15 J. K. Baker, *Anal. Chem.*, 51 (1979) 1693.
16 J. K. Baker, R. E. Skelton, T. N. Riley and J. R. Bagley, *J. Chromatogr. Sci.*, 18 (1980) 153.
17 R. M. Smith, *Anal. Chem.*, 56 (1984) 256.
18 R. M. Smith, *J. Chromatogr.*, 236 (1982) 313.
19 R. F. Rekker, *The Hydrophobic Fragmental Constants*, Elsevier, Amsterdam, 1977.
20 M. S. Mirrless, S. J. Moulton, C. T. Murphy and P. J. Taylor, *J. Med. Chem.*, 19 (1976) 615.
21 G. L. Biagi, A. M. Barbaro, M. C. Guerra, G. Hakein, G. C. Solaini and P. A. Borea, *J. Chromatogr.*, 177 (1979) 35.
22 K. Jinno, *Chromatographia*, 15 (1982) 667.
23 K. Jinno and M. Kuwajima, *Chromatographia*, 21 (1986) 622.
24 K. Jinno, M. Kuwajima, M. Hayashida, T. Watanabe and T. Hondo, *J. Chromatogr.*, 436 (1988) 11.
25 K. Jinno and M. Kuwajima, *J. Chromatogr. Sci.*, 27 (1989) 57.

Journal of Chromatography, 550 (1991) 335–356
Elsevier Science Publishers B.V., Amsterdam

CHROMSYMP. 2180

Retention prediction of analytes in reversed-phase high-performance liquid chromatography based on molecular structure

VI.[a] Disubstituted aromatic compounds

ROGER M. SMITH* and CHRISTINA M. BURR
Department of Chemistry, Loughborough University of Technology, Loughborough, Leics. LE11 3TU (UK)

ABSTRACT

As part of the development of a model for retention prediction based on molecular structure, the effects of interactions between substituents on the retention of aromatic analytes in reversed-phase high-performance liquid chromatography were examined, using 73 *ortho*-, *meta*- and *para*-disubstituted aromatic compounds. The interactions can be expressed empirically as eluent-dependent interaction terms. A more general expression was also examined that includes elements for electronic interactions, dependent on the Hammett constants of the substituents and their susceptibility, *ortho*-steric effects and hydrogen bonding.

INTRODUCTION

A number of computer-based methods have been devised to aid the development of separations in high-performance liquid chromatography (HPLC) [1]. The most common approach has been optimization methods, which rely on the combination of experimental observation with calculations, and require no knowledge of the structure of the analyte. In contrast, relatively few methods have been proposed that estimate the retention from the molecular structure of the analyte, although a number of groups have worked within restricted groups of compounds [2,3], or on more specialized separations, such as ion-exchange chromatography [4,5]. Close correlations have also been drawn between structure-based molecular connectivity calculations and retentions [6]. The structure or partial structure of the analyte is frequently known or the structural differences between related compounds, such as isomers or metabolites, are known and it should be possible to use this information as the basis of a prediction system.

[a] For Part V, see ref. 10.

0021-9673/91/$03.50

The aim of this project has been to develop a retention prediction method for reversed-phase liquid chromatography based on the molecular structure of the analyte [7]. The intention is to calculate the retention index as the summation of a series of terms:

$$I = I_P + I_{S,R} + \sum I_{S,Al-X} + \sum I_{S,Ar-X} + \sum I_{I,Y-Z} \quad (1)$$

These represent the retention index of a parent compound (I_P), a contribution for saturated alkyl chains ($I_{S,R}$), contributions for substituents on saturated aliphatic carbons ($I_{S,Al-X}$), contributions for aromatic substituents ($I_{S,Ar-X}$) and terms to account for any interactions between substituents ($I_{I,Y-Z}$) caused by electronic, hydrogen bonding and steric effects. Each of these terms will be sensitive to eluent composition and the organic modifier in the eluent and will be related to the percentage of modifier (x) using a quadratic equation ($I = ax^2 + bx + c$). Benzene was selected as the parent compound as its substituted derivatives can be readily detected. Retention indices based on the alkyl aryl ketones were used as the basis of the study as they are more robust than capacity factors and can be more readily transferred between systems. So far the terms for individual aromatic [7] and aliphatic [8] substituents and structural isomerization [9] have been determined. The coefficients of the regression equations are held in a database, which can be interrogated by an expert system program (CRIPES; Chromatographic Retention Index Prediction Expert System) for the calculation of predicted retention indices [10].

This model for retention prediction resembles the methods used by Hansch and others to calculate octanol–water partition coefficients (log P) [11] and in the early stages of this study it was shown that the retention substituent indices for groups on an aromatic ring were closely related to the Hansch substituent contributions (π) [7]. Hansch found that for disubstituted aromatic compounds containing polar groups, simple summation of the π terms to calculate log P was not very successful [12]. This was assumed to be due to interactions between the substituents and led initially to individual sets of π_Y values for each parent substituent. However, this approach was clearly unsatisfactory as it leads to multiple sets of π values and a proliferations of data.

For the *meta* and *para* isomers it was found that the difference between the π value of a substituent X with benzene as the parent compound and that with phenol as the parent could be described using the Hammett constant σ of the substituent [12]. This led to a more general equation, which attempted to quantify the effect of a group Y on the Hansch constant of a substituent X in terms of their "susceptibility" constants (ρ) and Hammett constants (σ) [12–14].

$$\pi_{X(PhY)} - \pi_{X(PhH)} = \rho_Y \sigma_X + \rho_X \sigma_Y \quad (2)$$

where ρ_X and ρ_Y are the susceptibilities of X and Y to the modifying effects of Y and X, respectively. Values for the susceptibility constants were derived experimentally using multiple regression analysis. This approach was extended to *ortho* substituents by adding additional terms to account for the proximity effects [14]:

$$\Sigma_{o\text{-}XPhY} = a\pi_{XPhY} + \rho_Y \sigma^0_{o-X} + \rho_X \sigma^0_{o\text{-}Y} + f_Y F_X + f_X F_Y + \delta_Y E_S^X + \delta_X E_S^Y + c \quad (3)$$

where $a\pi$ = the additive π, E_S = Taft steric effect value, F = Swain–Lupton field-effect constant, f = the susceptibility for the F constants and δ the susceptibility for the Taft E_S values. The E_S term was found to be insignificant for phenols and anilines (in the absence of intramolecular hydrogen bonding).

In a similar study, Leo [15,16] developed a simplified model to facilitate the rapid estimation of the interaction terms. The sigma/rho interaction term (F_σ) was calculated in the same way as by Fujita [14] but closely related substituents were assigned a common σ value and the same σ and ρ values were used for *ortho, meta* and *para* substituents. He also considered that for many groups one factor or the other was so small as to be safely ignored. The substituents were divided into three classes, either inducers (electron withdrawing) with $\rho = 0$ (*e.g.*, CN, NO_2, halogen), responders (electron releasing) with $\sigma = 0$ (*e.g.*, OH, NH_2) or bi-directional with $\rho > 0$ and $\sigma > 0$ (*e.g.*, CHO, CO_2CH_3 and OR), whose overall effect would be governed by the second substituent present in the compound. Additional terms were included to account for intramolecular hydrogen bonding (F_{HB}), the negative *ortho* effect (F_o) and the presence of alkyl–aryl systems ($F_{\alpha\varphi}$). Linear regression analysis gave the following correlation with experimental partition coefficients:

$$\log P = \Sigma\pi + F_\sigma - 0.29F_o + 0.63F_{HB} - 0.15F_{\alpha\varphi} \quad (4)$$

in which

$$F_\sigma = \rho_Y\sigma_X + \rho_X\sigma_Y$$

With the exception of the electronic effects each of the terms was quantized taking values 0, 1, 2, etc. Although a single intramolecular hydrogen bonding term was suggested, this was found to be insufficient to account for the observed hydrogen bonding effects between *ortho*-hydroxyl and amide groups.

This paper describes the examination of the retentions of a number of isomeric substituted toluenes and phenols in methanol–buffer and acetonitrile–buffer eluents. These studies have led to a set of coefficients for empirically based interaction indices (I_I), which have been used in the retention prediction system. However, because the applicability of these terms is limited to these specific substituent pairs, the results were also examined to determine if a model similar to that developed by Leo (eqn. 4) would be appropriate, which would have general applicability to any pair of substituents.

EXPERIMENTAL

Chemicals, equipment and procedures were as described previously [7].

Calculation of interaction indices

The retention index increments for each interaction (δI) were calculated as the difference between the retention index of the disubstituted compound (I_{Expl}) and the calculated retention index (I_{Sum}) for the same eluent based on the summation of the parent index value of benzene and the individual contributions for the substituents derived earlier [7].

DISCUSSION

In order to study the interactions, 73 *ortho*-, *meta*- and *para*-substituted toluenes and phenols were examined. The former compounds would be expected to show only minor effects, mainly due to steric or electronic interactions, whereas the phenols are likely to demonstrate stronger electronic effects and many are capable of intramolecular hydrogen bonding. The capacity factors of the compounds were determined in a range of eluents from 40–80% methanol–pH 7 buffer and 30–80% acetonitrile–pH 7 buffer (Tables I and II). In each instance the retentions of the homologous alkyl aryl

TABLE I

CAPACITY FACTORS OF SUBSTITUTED TOLUENES

Compound	Capacity factor (k')										
	Methanol (%)					Acetonitrile (%)					
	40	50	60	70	80	30	40	50	60	70	80
2-Bromotoluene	105.99	39.60	15.27	6.54	2.63	72.19	24.95	10.61	5.24	2.88	1.67
3-Bromotoluene	106.98	39.79	15.39	6.48	2.59	75.32	25.59	10.59	5.20	2.83	1.62
4-Bromotoluene	104.87	38.94	15.02	6.34	2.54	74.98	25.27	10.53	5.16	2.80	1.61
2-Chlorotoluene	83.81	32.24	12.82	5.48	2.31	64.45	21.19	9.16	4.73	2.56	1.50
3-Chlorotoluene	–	31.77	12.72	5.42	2.27	65.48	21.29	9.13	4.68	2.51	1.45
4-Chlorotoluene	76.31	32.55	12.47	5.26	2.20	65.56	21.45	9.07	4.64	2.48	1.44
1,2-Dimethylbenzene	60.72	26.61	11.34	5.11	2.25	54.74	18.27	8.16	4.16	2.34	1.37
1,3-Dimethylbenzene	70.30	29.85	12.57	5.53	2.38	63.40	20.43	8.99	4.54	2.52	1.47
1,4-Dimethylbenzene	72.19	30.35	13.17	5.63	2.41	63.64	20.73	9.11	4.60	2.56	1.47
2-Methylacetophenone	13.35	5.76	2.92	1.55	0.87	12.59	6.02	2.96	1.77	1.07	0.76
3-Methylacetophenone	15.04	5.81	2.98	1.56	0.84	12.50	5.91	2.89	1.73	1.05	0.75
4-Methylacetophenone	14.81	5.82	2.94	1.54	0.83	11.70	5.56	3.04	1.66	1.02	0.74
2-Methylanisole	34.63	14.72	7.06	3.43	1.68	33.85	14.67	7.01	3.32	1.82	1.18
3-Methylanisole	28.90	11.76	5.80	2.92	1.47	26.81	11.94	5.84	2.84	1.58	1.04
Methyl 2-methylbenzoate	28.70	11.62	5.02	2.47	1.22	25.82	8.29	4.10	2.29	1.37	0.88
Methyl 3-methylbenzoate	32.83	12.72	5.37	2.58	1.24	27.57	8.60	4.19	2.35	1.40	0.89
Methyl 4-methylbenzoate	32.90	12.58	5.35	2.58	1.24	26.78	8.44	4.16	2.32	1.40	0.90
2-Nitrotoluene	16.72	7.60	3.53	1.83	0.94	21.20	7.15	3.49	1.94	1.14	0.71
3-Nitrotoluene	19.99	8.93	4.24	2.14	1.08	24.82	8.41	3.92	2.14	1.25	0.77
4-Nitrotoluene	18.53	8.45	3.96	2.02	1.05	21.72	7.67	3.74	2.06	1.21	0.75
2-Phenyltoluene	–	105.96	34.17	14.71	4.21	–	77.11	22.18	9.09	4.12	2.31
3-Phenyltoluene	–	125.14	38.49	13.72	4.87	–	83.16	23.70	9.60	4.32	2.40
4-Phenyltoluene	–	141.24	42.17	11.65	5.37	–	87.94	24.83	10.02	4.49	2.49
2-Tolualdehyde	10.70	4.87	2.47	1.41	0.84	10.73	5.43	2.89	1.70	1.11	0.58
3-Tolualdehyde	11.00	4.88	2.47	1.37	0.83	11.26	5.62	2.98	1.73	1.14	0.58
4-Tolualdehyde	10.16	4.57	2.33	1.32	0.81	10.18	5.15	2.77	1.65	1.10	0.57
2-Toluamide	1.43	0.97	0.49	0.39	0.28	1.35	0.74	0.52	0.41	0.33	0.34
3-Toluamide	2.40	1.19	0.67	0.48	0.33	1.70	0.92	0.62	0.46	0.36	0.33
4-Toluamide	2.44	1.14	0.66	0.47	0.33	1.90	1.01	0.61	0.47	0.36	0.35
2-Toluidine	3.39	1.91	1.09	0.72	0.45	4.65	2.30	1.44	0.97	0.65	0.48
3-Toluidine	3.52	1.98	1.10	0.71	0.44	4.87	2.33	1.43	0.96	0.64	0.47
4-Toluidine	3.77	2.04	1.12	0.70	0.45	4.85	2.30	1.43	0.96	0.66	0.48
2-Toluonitrile	10.81	5.28	2.32	1.29	0.71	11.43	5.08	2.67	1.58	0.98	0.65
3-Toluonitrile	11.88	4.82	2.52	1.36	0.73	13.03	5.65	2.91	1.68	1.04	0.66
4-Toluonitrile	11.39	5.04	2.43	1.31	0.70	12.21	5.33	2.77	1.61	0.99	0.65

ketones, acetophenone–heptanophenone, were also measured and these were used to calculate the retention indices (I) of the analytes (Tables III and IV). A few of the compounds were eluted too rapidly for accurate measurement ($k' < 0.2$) and the corresponding indices are given in parentheses as they may be unreliable [10]. In some instances, such as with the hydroxybenzamides and dihydroxybenzenes, the retention index scale required considerable extrapolation and these values may also be less reliable.

Although the capacity factors changed significantly with eluent composition, the retention indices were usually relatively constant across the composition range. For most of the substituents the retention indices of the *meta* and *para* isomers were similar (± 50 units) but frequently that of the *ortho* isomer was significantly different (up to 400 units). Both the capacity factors and retention indices for 4-nitrophenol (pK_a = 7.1) [17] appeared to be abnormally low, particularly in methanol–buffer eluents, and it was suspected that this acidic phenol was significantly ionized in the mobile phase. Subsequently it appeared that 4-hydroxybenzaldehyde (pK_a = 7.6), 2-cyanophenol (pK_a = 6.9), 4-cyanophenol (pK_a = 7.7–7.9) and 2-nitrophenol (pK_a = 7.2) [17] might also be partially ionized, particularly with high proportions of methanol in the eluent. The results from these compounds were therefore regarded as potential outliers and were excluded from any correlation studies.

Because of the close relationship between octanol–water partition coefficients ($\log P$) and $\log k'$, which has often been used in QSAR studies [18], the retention indices in methanol–buffer (60:40) were compared with reported $\log P$ values [11,15] (Tables III and IV, Fig. 1). Although there was a good correlation for the substituted toluenes, there were systematic differences between the toluenes and many of the phenols. This difference agrees with the contribution of the phenolic group to the retention index ($I_{S,ArOH}$), which was about 90 units more negative than that predicted [7] from a linear relationship between I_S and π. Similar marked differences for ionizable compounds were also reported by Miyake *et al.* [19].

However, phenols with an *ortho*-carbonyl substituent capable of strong intramolecular hydrogen bonding ($COCH_3$, CO_2CH_3, $CONH_2$ and NH_2) behaved similarly to the toluenes, suggesting that the effect of the hydroxy group was largely masked in these compounds. The retentions of the compounds suspected of being ionized were all lower than the correlation curve for the non-ionized phenols.

Interaction increments

In order to study the interactions between the substituents, estimated retention indices (I_{Sum}) for each eluent were calculated by the summation of the previously determined parent index values for benzene and the substituent indices (I_S) for the individual groups [7] (Table V). These sums do not contain a contribution for interactions between the substituents so that the *ortho*, *meta* and *para* isomers have the same values. The interaction increments for each pair of substituents were then calculated as $\delta I = I_{Expt} - I_{Sum}$ (Tables VI and VII).

In order to represent these values in the retention prediction program [10], the relationship between the increment for each pair of substituents and the elucnt composition was expressed as a quadratic expression (Tables VIII and IX). These coefficients can then be used to calculate the interaction increments ($I_I = ax^2 + bx + c$). For many substituted toluenes the interaction increments for each eluent

TABLE II

CAPACITY FACTORS OF SUBSTITUTED PHENOLS[a]

Compound	Capacity factor (k')										
	Methanol (%)					Acetonitrile (%)					
	40	50	60	70	80	30	40	50	60	70	80
2-Aminophenol	0.78	0.66	0.42	0.30	0.26	1.08	0.79	0.63	0.54	0.42	0.44
3-Aminophenol	0.35	0.28	0.25	(0.19)	(0.18)	0.63	0.52	0.38	0.30	0.23	0.26
4-Aminophenol	0.25	0.22	(0.19)	(0.16)	0.21	0.40	0.38	0.29	0.24	0.20	0.26
2-Bromophenol	6.12	3.34	1.70	0.86	0.45	5.82	3.06	1.60	0.97	0.61	0.45
3-Bromophenol	9.38	4.82	2.17	1.11	0.56	7.85	3.77	1.84	1.08	0.66	0.48
4-Bromophenol	8.80	4.56	2.14	1.10	0.57	7.49	3.60	1.77	1.05	0.65	0.49
2-Chlorophenol	4.86	2.72	1.36	0.74	0.42	4.69	2.75	1.43	0.89	0.56	0.44
3-Chlorophenol	7.38	3.95	1.85	0.93	0.51	6.98	3.26	1.64	0.99	0.61	0.47
4-Chlorophenol	6.94	3.65	1.76	0.91	0.51	6.39	3.04	1.57	0.94	0.59	0.45
1,2-Dihydroxybenzene	0.96	0.64	0.43	0.31	0.25	0.85	0.78	0.53	0.42	0.31	0.41
1,3-Dihydroxybenzene	0.53	0.37	0.27	(0.19)	(0.18)	0.55	0.55	0.38	0.29	0.22	0.25
1,4-Dihydroxybenzene	0.31	0.27	0.20	(0.18)	(0.18)	0.35	0.43	0.32	0.25	0.21	0.24
2-Hydroxyacetophenone	9.02	4.33	2.21	1.25	0.84	7.57	4.51	2.16	1.52	0.84	0.65
3-Hydroxyacetophenone	2.02	1.02	0.58	0.39	0.34	1.70	1.31	0.67	0.55	0.29	0.32
4-Hydroxyacetophenone	1.55	0.78	0.44	0.29	(0.19)	1.15	0.88	0.53	0.46	0.27	0.29
2-Hydroxybenzaldehyde	4.99	2.52	1.41	0.83	0.53	6.86	5.56	2.39	1.34	0.94	0.56
3-Hydroxybenzaldehyde	1.64	0.89	0.54	0.37	0.25	1.77	1.11	0.74	0.50	0.35	(0.19)
4-Hydroxybenzaldehyde	1.00	0.51	0.27	(0.14)	(0.07)	1.20	0.78	0.54	0.40	0.29	(0.16)

2-Hydroxybenzamide	1.57	0.84	0.50	0.31	0.20	1.52	0.95	0.76	0.47	0.35	0.21
4-Hydroxybenzamide	0.32	0.22	(0.16)	(0.13)	(0.11)	0.27	0.23	(0.19)	(0.17)	(0.14)	(0.01)
2-Hydroxybenzonitrile	1.31	0.74	0.34	(0.18)	–	1.51	1.02	0.66	0.48	0.30	0.22
3-Hydroxybenzonitrile	2.17	1.26	0.68	0.42	0.21	2.50	1.47	0.87	0.58	0.38	0.33
4-Hydroxybenzonitrile	1.48	0.89	0.47	0.26	(0.07)	1.74	1.18	0.73	0.49	0.34	0.26
2-Methoxyphenol	2.95	1.49	0.92	0.59	0.37	3.12	1.90	1.12	0.77	0.51	0.41
3-Methoxyphenol	2.63	1.29	0.78	0.50	0.31	2.73	1.62	0.97	0.64	0.42	0.32
4-Methoxyphenol	1.93	0.99	0.63	0.42	0.29	2.05	1.30	0.82	0.56	0.38	0.29
Methyl 2-hydroxybenzoate	19.60	10.09	4.65	2.31	1.16	14.59	7.29	3.41	2.00	1.18	0.82
Methyl 3-hydroxybenzoate	3.72	1.96	0.99	0.58	0.34	3.10	1.67	0.95	0.61	0.41	0.36
Methyl 4-hydroxybenzoate	3.39	1.88	0.88	0.49	0.25	2.44	1.48	0.88	0.61	0.40	0.33
2-Methylphenol	4.75	2.76	1.42	0.78	0.47	5.26	2.55	1.41	0.89	0.58	0.41
3-Methylphenol	4.41	2.44	1.29	0.72	0.44	4.45	2.28	1.28	0.81	0.53	0.25
4-Methylphenol	4.86	2.51	1.31	0.73	0.45	5.10	2.28	1.28	0.82	0.54	0.24
2-Nitrophenol	3.56	1.96	0.91	0.40	(0.08)	5.27	2.59	1.57	1.07	0.65	0.36
3-Nitrophenol	3.38	1.96	1.00	0.53	0.23	4.23	2.03	1.12	0.71	0.45	0.35
4-Nitrophenol	1.27	0.69	0.29	(0.13)	–	2.12	1.06	0.67	0.49	0.28	(0.19)
2-Phenylphenol	33.87	10.73	4.48	1.97	0.90	31.39	10.51	4.15	1.98	1.04	0.67
3-Phenylphenol	35.87	11.35	4.53	1.92	0.92	27.91	9.01	3.63	1.76	0.93	0.62
4-Phenylphenol	35.74	11.52	4.12	1.98	0.96	27.59	8.86	3.36	1.72	0.99	0.63

[a] Values in parentheses in this and subsequent tables are for analytes with capacity factors less than 0.20 and may be unreliable.

TABLE III

RETENTION INDICES OF SUBSTITUTED TOLUENES

Compound	Retention index (I)											Log P^a
	Methanol (%)					Acetonitrile (%)						
	40	50	60	70	80	30	40	50	60	70	80	
2-Bromotoluene	1134	1157	1179	1205	1244	1140	1152	1168	1183	1202	1223	–
3-Bromotoluene	1135	1157	1180	1203	1240	1145	1156	1167	1181	1197	1211	–
4-Bromotoluene	1132	1154	1176	1199	1235	1145	1154	1166	1178	1194	1208	–
2-Chlorotoluene	1107	1129	1150	1174	1207	1115	1126	1138	1151	1168	1182	3.42
3-Chlorotoluene	–	1127	1149	1172	1202	1117	1126	1137	1149	1162	1171	3.28
4-Chlorotoluene	1096	1130	1144	1166	1192	1117	1128	1136	1146	1159	1168	3.33
1,2-Dimethylbenzene	1071	1103	1130	1159	1199	1085	1102	1115	1125	1141	1150	3.12
1,3-Dimethylbenzene	1088	1118	1147	1179	1215	1104	1120	1134	1147	1163	1174	3.20
1,4-Dimethylbenzene	1091	1121	1155	1180	1219	1104	1122	1137	1150	1168	1176	3.15
2-Methylacetophenone	894	896	895	898	902	888	887	886	889	892	892	–
3-Methylacetophenone	900	900	899	900	903	887	884	881	882	886	887	–
4-Methylacetophenone	898	900	897	896	899	879	875	873	874	879	882	2.10
2-Methylanisole	1003	1026	1044	1063	1090	1014	1024	1030	1037	1043	1046	2.74
3-Methylanisole	974	996	1011	1030	1055	985	992	996	1001	1003	1002	2.66
Methyl 2-methylbenzoate	984	991	997	999	1019	976	974	976	977	985	985	2.75
Methyl 3-methylbenzoate	1000	1003	1008	1008	1025	984	980	980	984	991	991	–
Methyl 4-methylbenzoate	1000	1001	1007	1009	1025	981	977	979	980	990	993	–
2-Nitrotoluene	922	933	938	942	945	952	950	943	935	932	905	2.30
3-Nitrotoluene	942	955	969	976	985	971	976	967	960	959	937	2.45
4-Nitrotoluene	934	948	957	963	977	955	961	957	950	949	926	2.42
2-Phenyltoluene	–	1296	1303	1318	1340	–	1274	1273	1274	1276	1277	–
3-Phenyltoluene	–	1322	1336	1352	1379	–	1286	1286	1287	1289	1291	–
4-Phenyltoluene	–	1334	1351	1367	1397	–	1294	1295	1297	1300	1304	–
2-Tolualdehyde	869	873	877	881	894	868	871	870	880	893	879	2.26
3-Tolualdehyde	872	873	876	876	890	873	877	876	884	901	877	–
4-Tolualdehyde	863	865	866	868	883	861	863	862	873	890	872	–
2-Toluamide	628	655	617	609	589	621	584	561	550	568	631	–
3-Toluamide	688	682	668	654	638	650	619	594	581	597	625	1.18
4-Toluamide	689	677	664	651	639	664	633	592	582	594	642	1.18
2-Toluidine	728	747	747	742	730	765	766	764	762	769	761	1.32
3-Toluidine	732	751	748	739	731	771	769	763	761	762	754	1.41
4-Toluidine	740	755	750	745	722	770	767	763	761	770	760	1.39
2-Toluonitrile	871	872	870	863	860	898	895	889	884	886	874	–
3-Toluonitrile	882	884	884	873	869	914	912	906	900	905	880	–
4-Toluonitrile	877	878	878	865	857	906	903	897	890	891	871	–

[a] Values from refs. 11 and 15.

TABLE IV

RETENTION INDICES OF SUBSTITUTED PHENOLS

Compound	Retetion index (I)											Log P^a
	Methanol (%)					Acetonitrile (%)						
	40	50	60	70	80	30	40	50	60	70	80	
2-Aminophenol	576	592	580	562	569	586	589	600	618	635	711	0.52
3-Aminophenol	483	477	492	(467)	(474)	519	522	496	474	468	519	0.15
4-Aminophenol	446	446	(449)	(429)	515	463	471	445	423	424	516	0.04
2-Bromophenol	813	810	809	777	734	821	805	786	765	749	723	2.35
3-Bromophenol	862	860	849	830	793	859	838	815	792	772	743	2.63
4-Bromophenol	855	852	847	829	799	853	831	807	785	765	747	2.65
2-Chlorophenol	786	783	772	753	708	786	788	764	744	724	714	2.19
3-Chlorophenol	834	833	823	803	767	836	815	792	769	749	731	2.48
4-Chlorophenol	827	822	815	798	768	825	804	783	758	739	717	2.40
1,2-Dihydroxybenzene	599	589	583	570	568	577	587	565	558	553	687	1.01
1,3-Dihydroxybenzene	531	516	506	(483)	(476)	522	532	498	467	453	495	0.77
1,4-Dihydroxybenzene	469	474	461	(451)	(467)	467	492	461	433	435	493	0.50
2-Hydroxyacetophenone	853	860	867	875	888	849	867	853	854	855	857	1.90
3-Hydroxyacetophenone	679	661	641	619	614	663	669	616	605	588	597	1.39
4-Hydroxyacetophenone	649	624	594	551	(428)	615	606	569	562	556	562	1.30
2-Hydroxybenzaldehyde	782	783	783	769	771	862	875	834	822	845	867	1.81
3-Hydroxybenzaldehyde	656	641	623	600	571	648	630	610	592	571	(510)	1.38
4-Hydroxybenzaldehyde	600	565	507	(396)	(243)	600	577	550	537	513	(462)	1.35
2-Hydroxybenzamide	651	636	605	563	518	629	608	616	577	568	540	1.28
4-Hydroxybenzamide	463	454	(418)	(384)	(350)	420	393	(356)	(336)	(324)	(251)	0.33
2-Hydroxybenzonitrile	634	608	547	(447)	–	648	630	608	589	542	463	1.60
3-Hydroxybenzonitrile	693	678	658	625	510	711	688	665	639	610	606	1.70
4-Hydroxybenzonitrile	649	632	599	529	(196)	666	653	628	597	575	520	1.60
2-Methoxyphenol	715	711	705	698	682	720	712	697	693	682	678	1.32
3-Methoxyphenol	701	692	678	663	635	704	688	668	653	625	593	1.58
4-Methoxyphenol	666	656	643	628	606	668	654	636	622	601	565	1.39
Methyl 2-hydroxybenzoate	947	959	975	989	1006	931	944	940	945	941	940	2.55
Methyl 3-hydroxybenzoate	755	738	720	700	654	738	707	681	652	633	635	1.89
Methyl 4-hydroxybenzoate	744	733	701	666	565	708	688	667	649	622	608	1.96
2-Methylphenol	783	785	779	766	746	788	776	761	745	732	714	1.96
3-Methylphenol	775	768	764	748	725	772	758	741	722	708	691	1.96
4-Methylphenol	777	772	766	752	733	774	758	741	723	713	700	1.94
2-Nitrophenol	750	739	706	622	(228)	781	778	783	789	766	641	1.79
3-Nitrophenol	744	739	721	685	543	754	739	716	688	659	623	2.00
4-Nitrophenol	631	597	519	(379)	–	669	635	611	598	518	(395)	1.91
2-Phenylphenol	992	981	969	947	922	984	973	939	916	884	847	3.09
3-Phenylphenol	1007	989	973	943	918	985	950	914	888	854	822	3.23
4-Phenylphenol	1006	991	970	949	929	984	947	910	879	853	816	3.20

[a] Values from refs. 11 and 15.

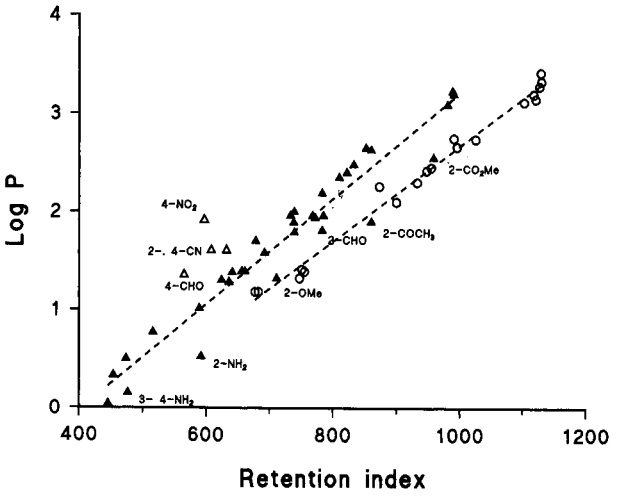

Fig. 1. Relationship of log P and retention indices for derivatives based on Tables III and IV. Analytes: ○ = substituted toluenes; ▲ = phenols; △ = suspected ionized phenols. Me = Methyl.

TABLE V

ESTIMATED RETENTION INDICES CALCULATED AS THE SUM OF PARENT INDEX AND SUBSTITUENT INDICES[a]

Groups	I_{Sum}										
	Methanol (%)					Acetonitrile (%)					
	40	50	60	70	80	30	40	50	60	70	80
$I_P + I_{S,CH_3} + I_{S,Br}$	1128	1148	1168	1188	1210	1137	1154	1167	1178	1185	1190
$I_P + I_{S,CH_3} + I_{S,Cl}$	1099	1118	1136	1153	1171	1108	1125	1138	1149	1156	1161
$I_P + I_{S,CH_3} + I_{S,CH_3}$	1085	1113	1138	1161	1182	1110	1127	1140	1151	1158	1163
$I_P + I_{S,CH_3} + I_{S,COR} + I_{S,CH_3}$	900	900	900	900	900	900	900	900	900	900	900
$I_P + I_{S,CH_3} + I_{S,OR} + I_{S,CH_3}$	985	1001	1019	1036	1054	1000	1008	1012	1016	1015	1014
$I_P + I_{S,CH_3} + I_{S,CO_2R} + I_{S,CH_3}$	1000	1003	1006	1010	1015	990	993	994	996	996	996
$I_P + I_{S,CH_3} + I_{S,NO_2}$	950	959	966	971	976	969	973	971	964	952	936
$I_P + I_{S,CH_3} + I_{S,Ph}$	1306	1318	1332	1349	1368	1300	1298	1295	1295	1294	1295
$I_P + I_{S,CH_3} + I_{S,CHO}$	875	875	876	878	883	880	886	888	888	885	880
$I_P + I_{S,CH_3} + I_{S,CONH_2}$	704	692	679	666	653	679	636	613	614	636	681
$I_P + I_{S,CH_3} + I_{S,NH_2}$	749	759	760	755	741	795	797	796	796	795	793
$I_P + I_{S,CH_3} + I_{S,CN}$	876	879	877	871	861	913	918	914	910	901	890
$I_P + I_{S,OH} + I_{S,NH_2}$	443	430	402	363	310	484	454	427	405	385	370
$I_P + I_{S,OH} + I_{S,Br}$	822	819	810	796	779	825	811	798	787	776	767
$I_P + I_{S,OH} + I_{S,Cl}$	793	789	778	761	740	796	782	769	758	747	738
$I_P + I_{S,OH} + I_{S,OH}$	474	455	423	380	320	486	441	401	368	339	317
$I_P + I_{S,OH} + I_{S,COR} + I_{S,CH_3}$	594	571	542	508	469	588	557	530	508	492	477
$I_P + I_{S,OH} + I_{S,CHO}$	569	546	518	486	452	568	543	518	497	476	457
$I_P + I_{S,OH} + I_{S,CONH_2}$	398	363	321	274	222	367	293	244	223	227	258
$I_P + I_{S,OH} + I_{S,CN}$	570	550	519	479	430	601	575	545	519	492	467
$I_P + I_{S,OH} + I_{S,OR} + I_{S,CH_3}$	679	673	661	644	623	688	665	643	624	606	591
$I_P + I_{S,OH} + I_{S,CO_2R} + I_{S,CH_3}$	694	674	648	618	583	678	650	625	605	586	573
$I_P + I_{S,OH} + I_{S,CH_3}$	779	784	780	769	751	798	784	771	760	749	740
$I_P + I_{S,OH} + I_{S,NO_2}$	644	630	608	579	545	657	630	601	573	543	513
$I_P + I_{S,OH} + I_{S,Ph}$	1000	989	974	957	937	989	955	926	903	884	872

[a] Values of I_P and $I_{S,X}$ derived from ref. 7.

TABLE VI

INTERACTION INCREMENTS FOR SUBSTITUTED TOLUENES

Substituent pairs	Interaction increment (δI)										
	Methanol (%)					Acetonitrile (%)					
	40	50	60	70	80	30	40	50	60	70	80
CH_3 + 2-Br	6	9	11	17	34	3	−2	1	5	17	33
CH_3 + 3-Br	7	9	12	15	30	8	2	0	3	14	21
CH_3 + 4-Br	4	6	8	11	25	8	0	−1	0	9	18
CH_3 + 2-Cl	8	11	14	21	36	7	1	0	2	12	21
CH_3 + 3-Cl	–	9	13	19	31	9	1	−1	0	6	10
CH_3 + 4-Cl	−3	12	8	13	21	9	3	−2	−3	3	7
CH_3 + 2-CH_3	−14	−10	−8	−2	17	−25	−25	−25	−26	−17	−13
CH_3 + 3-CH_3	3	5	9	18	33	−6	−7	−6	−4	5	11
CH_3 + 4-CH_3	6	8	17	19	37	−6	−5	−3	−1	10	13
CH_3 + 2-$COCH_3$	−6	−4	−5	−2	2	−12	−13	−14	−11	−8	−8
CH_3 + 3-$COCH_3$	0	0	−1	0	3	−13	−16	−19	−17	−14	−13
CH_3 + 4-$COCH_3$	−2	0	−3	−4	−1	−21	−25	−27	−26	−21	−18
CH_3 + 2-OCH_3	18	25	25	27	36	14	16	18	21	28	32
CH_3 + 3-OCH_3	−11	−5	−8	−6	1	−15	−16	−16	−15	−12	−12
CH_3 + 2-CO_2CH_3	−16	−12	−9	−11	4	−14	−19	−18	−19	−11	−11
CH_3 + 3-CO_2CH_3	0	0	−2	−2	10	−6	−13	−14	−12	−5	−5
CH_3 + 4-CO_2CH_3	0	−2	−1	−1	10	−9	−16	−15	−16	−6	−3
CH_3 + 2-NO_2	−28	−26	−28	−29	−31	−17	−23	−28	−29	−26	−31
CH_3 + 3-NO_2	−8	−4	3	5	9	2	3	−4	−4	7	1
CH_3 + 4-NO_2	−16	−11	−9	−14	1	−14	−12	−14	−14	−3	−10
CH_3 + 2-Ph	–	−22	−29	−31	−28	–	−24	−22	−21	−18	−18
CH_3 + 3-Ph	–	4	4	3	11	–	−12	−9	−8	−5	−4
CH_3 + 4-Ph	–	16	19	18	29	–	−4	0	2	6	9
CH_3 + 2-CHO	−6	−2	1	3	11	−12	−15	−18	−8	8	−1
CH_3 + 3-CHO	−3	−2	0	−2	9	−7	−9	−12	−4	16	−3
CH_3 + 4-CHO	−12	−10	−10	−10	0	−19	−23	−26	−15	5	−8
CH_3 + 2-$COHN_2$	−76	−33	−62	−57	−64	−58	−52	−53	−64	−68	−50
CH_3 + 3-$CONH_2$	−16	−10	−11	−12	−15	−29	−17	−20	−33	−39	−56
CH_3 + 4-$CONH_2$	−15	−15	−9	−15	−14	−15	−3	−22	−32	−42	−39
CH_3 + 2-NH_2	−21	−12	−12	−13	−11	−30	−31	−32	−34	−26	−32
CH_3 + 3-NH_2	−17	−8	−12	−14	−9	−24	−28	−33	−35	−33	−39
CH_3 + 4-NH_2	−9	−4	−10	−10	−19	−25	−30	−33	−35	−25	−33
CH_3 + 2-CN	−5	−7	−7	−8	−1	−15	−23	−26	−26	−15	−16
CH_3 + 3-CN	6	5	7	2	8	1	−6	−9	−10	4	−10
CH_3 + 4-CN	1	−1	1	−6	−4	−7	−15	−18	−20	−12	−19

TABLE VII

INTERACTION INCREMENTS FOR SUBSTITUTED PHENOLS

Substituent pairs	Interaction increment (δI)										
	Methanol (%)					Acetonitrile (%)					
	40	50	60	70	80	30	40	50	60	70	80
OH + 2-NH_2	133	162	178	199	259	102	135	173	213	250	341
OH + 3-NH_2	40	47	90	(104)	(164)	35	68	69	69	83	149
OH + 4-NH_2	3	16	(47)	(66)	205	−21	17	18	18	39	146
OH + 2-Br	−9	−9	−1	−19	−45	−4	−6	−12	−22	−27	−44
OH + 3-Br	40	41	39	34	14	34	27	17	5	−6	−24
OH + 4-Br	33	33	37	33	20	28	20	9	−2	−11	−20
OH + 2-Cl	−7	−6	−6	−8	−32	−10	6	−5	−14	−23	−24
OH + 3-Cl	41	44	45	42	27	40	33	23	11	12	−7
OH + 4-Cl	34	33	37	37	28	29	22	14	0	−8	−21
OH + 2-OH	125	134	160	190	248	91	146	164	190	214	370
OH + 3-OH	57	61	83	(103)	(156)	36	91	97	99	114	178
OH + 4-OH	−5	19	37	(71)	(147)	−19	51	60	65	96	176
OH + 2-$COCH_3$	259	289	325	367	419	261	310	323	346	363	380
OH + 3-$COCH_3$	85	90	99	111	144	75	112	86	97	96	120
OH + 4-$COCH_3$	55	54	52	43	(−41)	27	49	39	54	64	88
OH + 2-CHO	213	237	265	283	319	294	332	316	325	369	410
OH + 3-CHO	87	95	105	114	119	80	87	92	95	95	(53)
OH + 4-CHO[a]	31	19	−11	(−90)	(−209)	32	34	32	40	37	(5)
OH + 2-$CONH_2$	253	273	284	289	296	262	315	372	354	341	282
OH + 4-$CONH_2$	65	91	(97)	(110)	(128)	53	100	(112)	(113)	(97)	(−7)
OH + 2-CN[a]	64	58	28	(−32)	–	47	55	63	70	50	−4
OH + 3-CN	123	128	139	146	80	110	113	120	120	118	139
OH + 4-CN[a]	79	82	80	50	(−234)	65	78	83	78	83	53
OH + 2-OCH_3	36	38	44	54	59	32	47	54	69	76	87
OH + 3-OCH_3	22	19	17	19	12	22	23	25	29	19	2
OH + 4-OCH_3	−13	−17	−18	−16	−17	−14	−11	−7	−2	−5	−26
OH + 2-CO_2CH_3	253	285	327	371	423	253	294	315	340	355	367
OH + 3-CO_2CH_3	61	64	72	82	71	60	57	56	47	47	62
OH + 4-CO_2CH_3	50	59	53	48	−18	30	38	42	44	36	35
OH + 2-CH_3	4	1	−1	−3	−5	−10	−8	−10	−15	−17	−26
OH + 3-CH_3	−4	−16	−16	−21	−26	−26	−26	−30	−38	−41	−49
OH + 4-CH_3	−2	−12	−14	−17	−18	−24	−26	−30	−37	−36	−40
OH + 2-NO_2[a]	106	109	98	43	(−317)	124	148	182	216	223	128
OH + 3-NO_2	100	109	113	106	−2	97	109	115	115	116	110
OH + 4-NO_2[a]	−13	−33	−89	(−200)	–	12	5	10	25	−25	(−118)
OH + 2-Ph	−8	−8	−5	−10	−15	−5	18	13	13	−2	−25
OH + 3-Ph	7	0	−1	−14	−19	−4	−5	−12	−15	−32	−50
OH + 4-Ph	6	0	−4	−8	−8	−5	−8	−16	−24	−33	−56

[a] Compounds considered to be partially ionized.

TABLE VIII

REGRESSION EQUATIONS RELATING CHANGE IN INTERACTION INCREMENT TO ELUENT CONCENTRATION FOR SUBSTITUTED TOLUENES

$I_{1,Y-Z} = ax^2 + bx + c$ (x = % modifier).

Substituent pairs	Coefficients of regression equation					
	Methanol			Acetonitrile		
	a	*b*	*c*	*a*	*b*	*c*
CH_3 + 2-Br CH_3 + 3-Br CH_3 + 4-Br CH_3 + 2-Cl CH_3 + 3-Cl CH_3 + 4-Cl	0.0150	−1.230	31	0.0209	−2.079	51
CH_3 + 2-CH_3	0.0243	−2.214	37			−22
CH_3 + 3-CH_3 CH_3 + 4-CH_3	0.0200	−1.670	40			0
CH_3 + 2-$COCH_3$			0			−11
CH_3 + 3-$COCH_3$ CH_3 + 4-$COCH_3$			0 0			−19
CH_3 + 2-OCH_3			26			21
CH_3 + 3-OCH_3			0			−14
CH_3 + 2-CO_2CH_3			−11			−15
CH_3 + 3-CO_2CH_3 CH_3 + 4-CO_2CH_3			0 0			−10
CH_3 + 2-NO_2			−28			−26
CH_3 + 3-NO_2			0			0
CH_3 + 4-NO_2			0			−11
CH_3 + 2-Ph			−28			−21
CH_3 + 3-Ph CH_3 + 4-Ph			0 21			0
CH_3 + 2-CHO CH_3 + 3-CHO CH_3 + 4-CHO			0 0 0	0.0060	−0.286	−1?
CH_3 + 2-$CONH_2$	−0.0471	5.657	−219			−58
CH_3 + 3-$CONH_2$ CH_3 + 4-$CONH_2$			−13	−0.0148	0.972	−33
CH_3 + 2-NH_2 CH_3 + 3-NH_2 CH_3 + 4-NH_2			−12			−31
CH_3 + 2-CN			0			−20
CH_3 + 3-CN			0			0
CH_3 + 4-CN			0			−15

TABLE IX

REGRESSION EQUATIONS RELATING CHANGE IN INTERACTION INCREMENT TO ELUENT CONCENTRATION FOR INTERACTIONS OF SUBSTITUENTS WITH PHENOLIC HYDROXYL

Substituent pairs	Coefficients of regression equation					
	Methanol			Acetonitrile		
	a	*b*	*c*	*a*	*b*	*c*
OH + 2-NH_2	0.0479	−2.853	176	0.0510	−1.103	94
OH + 3-NH_2	0.0550	−3.550	93[a]	0.0387	−2.505	88
OH + 4-NH_2	0.1714	−16.031	378[a]	0.0759	−5.774	102
OH + 2-Br	−0.0557	5.868	−157	−0.0127	0.614	−11
OH + 2-Cl	−0.0371	3.937	−107	−0.0137	1.038	−23
OH + 3-Br OH + 4-Br OH + 3-Cl OH + 4-Cl			35	−0.0002	−0.968	63
OH + 2-OH	0.0728	−5.723	238	0.0945	−5.748	199
OH + 3-OH	0.0686	−5.828	181[a]	0.0144	0.640	19
OH + 4-OH	0.0857	−6.726	132[a]	0.0246	0.475	−36
OH + 2-CHO	0.0100	1.380	143	0.0455	−3.008	355
OH + 3-CHO	−0.0050	1.430	37			90
OH + 4-CHO[b]			–			35
OH + 2-$COCH_3$	0.0357	−0.305	214	−0.0257	5.048	138
OH + 3-$COCH_3$	0.0421	−3.667	166	0.0062	−0.150	85
OH + 4-$COCH_3$			50[c]	0.0161	−0.725	40
OH + 2-$CONH_2$	−0.0229	3.763	140	−0.1500	16.957	−114
OH + 4-$CONH_2$	−0.0064	2.221	−11[a]			–[d]
OH + 2-CN[b]			–	−0.0753	7.537	−118
OH + 3-CN	−0.1043	11.834	−191			120
OH + 4-CN[b]			–	−0.0384	4.080	−23
OH + 2-OCH_3	−0.0071	−0.237	33	−0.0036	1.470	−8
OH + 3-OCH_3			18	−0.0246	2.402	−30
OH + 4-OCH_3			−16	−0.0264	2.801	−77
OH + 2-CO_2CH_3	0.0300	0.660	178	−0.0302	5.542	176
OH + 3-CO_2CH_3			70			55
OH + 4-CO_2CH_3			53[e]			38
OH + 2-CH_3			0			−14
OH + 3-CH_3	0.0093	−1.544	43	−0.0064	0.227	−26
OH + 4-CH_3						−32
OH + 2-NO_2[b]			–	−0.1255	14.60	−217
OH + 3-NO_2			107			111
OH + 4-NO_2[b]			–			–
OH + 2-Ph			0	−0.0482	4.846	−105
OH + 3-Ph OH + 4-Ph	−0.0007	−0.606	28	−0.0204	1.317	−26

[a] Includes all data points including those based on capacity factors <0.2.
[b] Compound suspected of ionization particularly in methanol–buffer.
[c] Excludes increments based on capacity factors <0.2.
[d] Only two data points based on capacity factors >0.2.
[e] Mean excludes 80% methanol values as it appears to be an outlier.

composition were < 10 units, which is within the experimental errors of measurement [7], and they were assigned coefficients of zero. Changes in the increments across the eluent composition range of less than 20 units were regarded as insignificant and were assigned a single coefficient equal to the mean value. The halotoluenes were unusual as they all showed a systematic (although still relatively small) increase in interaction increment with the proportion of organic modifier. All six halo isomers were fitted to a common regression relationship. Similarly, the *meta* and *para* isomers of a number of the other substituents could be linked in a common equation.

The only significant toluene interactions were found for 2-methylbenzamide and in earlier work Clark *et al.* [20] reported that this compound was eluted more rapidly than the 3- and 4-isomers. They considered this difference to be due to a steric interaction causing the amide group to be less coplanar with the aromatic ring and hence more polar.

Most of the substituted phenols showed much larger interaction increments, which changed significantly with eluent composition (Table VII). The smallest effects were found for the methyl-, methoxy- and phenyl-substituted phenols, a number of which were assigned zero or constant regression coefficients (Table IX). Some of the *meta* and *para* substituents could again be linked in a common relationship. In developing the relationships for the other substituents, it was considered reasonable to include a number of the values which were possibly "unreliable" if these followed a steady trend. However, because there was a marked jump with 80% methanol for the 4-carbomethoxyl substituents, this value was thought to be an outlier and was excluded from the correlation.

The largest interactions were observed with the carbonyl substituents capable of hydrogen bonding, such as 2-hydroxyacetophenone (Fig. 2) and 2-hydroxybenzamide, which also differed markedly from the 4- and 3-isomers. These differences reflect those reported by Clark and co-workers [21,22] for the same or closely related compounds. Smaller but still significant interactions were also found for the *ortho*-dihydroxybenzenes and aminophenols.

When these quadratic expressions and constants for the toluenes and phenols were incorporated in the expert system program CRIPES, it was able to demonstrate

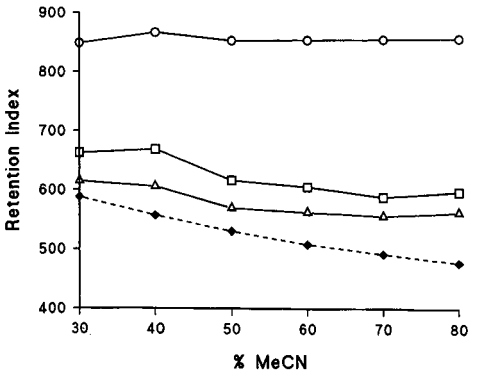

Fig. 2. Comparison of (◆) calculated (I_{Sum}) and experimental retention indices for (○) 2-, (□) 3- and (△) 4-hydroxyacetophenone. MeCN = Acetonitrile.

a reasonably successful ability to predict the retention indices and capacity factors of further substituted benzenes [10]. However, these interaction increments can really only be applied if values for the corresponding pairs of substituents are in the database. As a general prediction method this approach is very limited because a separate regression expression would have to be measured experimentally for each isomer of every possible pair of substituents. Additional terms would probably also be needed for multiple substitution. It was recognized, therefore, that the present form of the expert system database had only a limited application [10] and that a more general approach based on substituent susceptibilities would be needed.

General prediction model

For a more versatile prediction system, it is necessary to develop a model in which each substituent is associated with a set of terms that can reflect their mutual interactions in a similar manner to the σ and ρ terms used by Leo for the calculation of log P values [15,16]. Based on eqn. 4, an equation can be derived for $I_{I,X-Y}$:

$$I_{I,X-Y} = (\sigma_X\rho_Y^* + \sigma_Y\rho_X^*) + F_{HB}^* + F_o^* \tag{5}$$

where ρ^*, F_{HB}^* and F_o^* correspond to the terms in eqn. 4 but are expressed in retention index units. It is hoped that in each instance they could be directly related through a common regression equation for the eluent composition, *e.g.*, $\rho^* = \rho(ax^2 + bx + c)$, although the concept may need to be refined as more data becomes available. Leo [15] has noted that σ constants are valid for up to 80% organic modifier in aqueous solutions and so should be applicable in the present eluents. In preliminary calculations it appeared that the *meta* and *para* interactions differed so that instead of common σ values as suggested by Leo [15,16], published σ_{meta} and σ_{para} values [11] were used (Table X). The term for alkyl–aryl substitution has been omitted as it is thought that this effect may already be covered by an interaction term introduced earlier for alkyl substitution on a benzylic carbon [8].

Tsantili-Kakoulidou *et al.* [22] examined a very similar relationship between log k'_w values for a number of substituted phenols and anilines with sigma/rho correction values and *ortho* effects using linear regression analysis. Their results suggested that the approach was feasible but the weightings of the *ortho*-factors were quantized. They assigned ρ^* values but these often had large error ranges (*e.g.*, OH = 0.93 $\pm$ 0.30) and, unlike the Leo ρ values [15] some were negative (*e.g.*, Cl = -0.28 ± 0.21 and $NO_2 = -0.43 \pm 0.31$).

Meta and para groups

In order to determine the relationship between ρ and ρ^* in this study, the increments for the substituted phenols were examined. The phenolic group is a responder group ($\rho = 1.06$, σ relatively small) so that if σ is assumed to be zero (by analogy with Leo [15]), eqn. 5 for *meta* and *para* substituents can be redefined as

$$I_I = \sigma_X\rho_{OH}^* = \sigma_X\rho_{OH}(ax^2 + bx + c) \tag{6}$$

TABLE X

VALUES OF σ AND ρ USED IN CALCULATIONS OF INCREMENTS

Substituent	σ_{meta}[a]	σ_{para}[a]	ρ[b]
CH_3	−0.07	−0.17	0.00[c]
Phenyl	0.06	−0.01	0.00[c]
Inducers			
CN	0.56	0.66	0.00
NO_2	0.71	0.78	0.00
Br	0.39	0.23	0.00
Cl	0.37	0.23	0.00
Bi-directional			
CHO	0.35	0.42	0.44
CO_2CH_3	0.37	0.45	0.27
$COCH_3$	0.38	0.50	0.27
$CONH_2$	0.28	0.36	0.72
OCH_3	0.12	−0.27	0.50
Responders			
OH	0.12	−0.37	1.06
NH_2	−0.16	−0.66	1.08

[a] Ref. 11.
[b] Ref. 15.
[c] Ref. 14.

Thus in each eluent there should be a close relationship between the empirical interaction increments δI (from Table VII) and σ_X (from Table X). In methanol–buffer (50:50) a good linear correlation was found for the inducer and bi-directional substituents (*para*, Fig. 3a; *meta*, Fig. 3b). However, the amino and hydroxyl substituents, which are responder groups, (and the formyl and nitro substituents which gave ionized compounds) were clearly outliers. The σ values also correctly forecast the sign of the increments. Negative values of σ_{para} for methyl, methoxy and phenyl groups and of σ_{meta} for the methyl group were matched with negative retention increments and the positive value of σ_{meta} for the methoxyl group was matched by a positive increment (Table VII). Although σ_{meta} for the phenyl group gave the wrong indication, its influence was very small.

To determine the values of the coefficients *a*, *b* and *c* in eqn. 6, the ratios $\delta I_X/\rho_{OH}\sigma_X$ were then calculated for each substituent (using $\rho_{OH} = 1.06$ but excluding the hydroxyl and amino groups) and were correlated with the proportion of modifier (x). The phenyl and methyl groups were omitted as their σ values are very small and gave erratic ratios. The mean values of the ratios from the different substituents were virtually independent of the percentage of methanol (Fig. 4a for *para* substituents) and suggested that the relationship for methanol–buffer eluents could be represented by a single value rather than a quadratic expression, hence $\rho^*_{para\text{-}X} = 100\rho_X$ and $\rho^*_{meta\text{-}X} = 170\rho_X$. The results for most substituents in acetonitrile–buffer eluents were also similar so that $\rho^*_{para\text{-}X} = 105\rho_X$ and $\rho^*_{meta\text{-}X} = 190\rho_X$ (*e.g.*, for *meta* substituents see Fig. 4b). The exceptions were the bromo and chloro groups, whose ratios changed systematical-

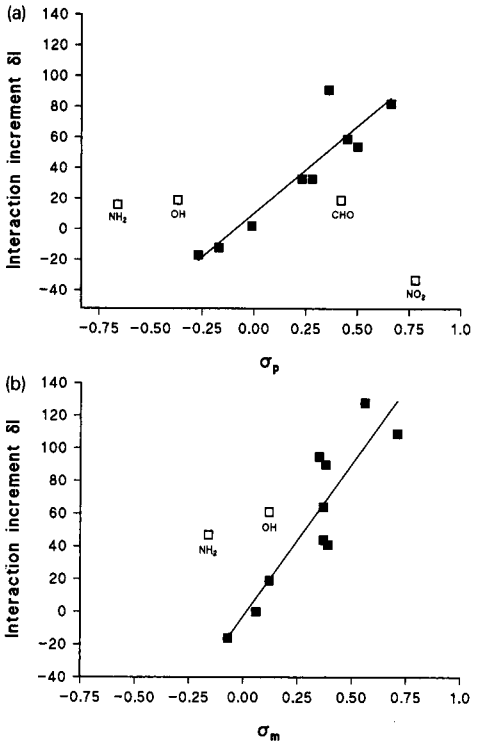

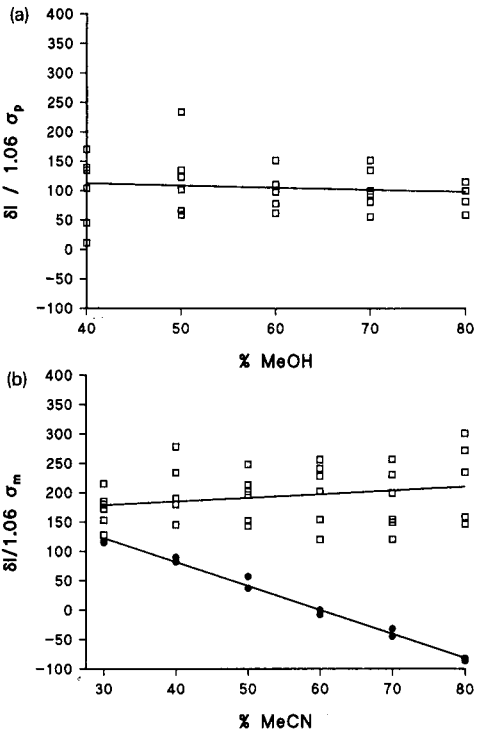

Fig. 3 (left). Relationship between interaction index (δI) and σ values in methanol–buffer (50:50). Open symbols were not used in the correlation. (a) *para*-Substituted phenols; (b) *meta*-substituted phenols.

Fig. 4 (right). Relationship between $\delta I_X/1.06\sigma_X$ and percentage of organic modifiers in eluents. (a) *para* Substituents in methanol (MeOH)–buffer; (b) *meta* substituents in acetonitrile (MeCN)–buffer, ● = bromo and chloro substituents.

ly with eluent composition so that $\rho^*_{para\text{-halogen}} = \rho_{halogen}(244-4x)$ and $\rho^*_{meta\text{-halogen}} = \rho_{halogen}(175-2.6x)$. A similar but smaller systematic change in the interaction increments also occurred with the halotoluenes (Table VIII).

Except for the halogens, these correction ratios suggest that for most substituents the interaction increment (I_I) can be assumed to be a constant irrespective of the proportion of modifier. This corresponds well to the empirical interaction increments (Table VII), many of which were almost constant across the eluent ranges for *para* and *meta* isomers. Using these ratios, the predicted interactions increments in methanol–buffer (60:40) and acetonitrile–buffer (60:40) were calculated using eqn. 5 (F^*_{HB} and $F^*_o = 0$) and compared with the values from Table VII. In this case the reported values of σ for 3- and 4-hydroxyl were used with the bi-directional substituents [11]. In most instances the predicted I_I and experimental values corresponded reasonably closely with differences of less than 30 units (Table XI). However, the values from hydroxyl and amino groups showed large and erratic errors and in their regression studies Fujita [14] found that these groups had to be regarded as

TABLE XI

PREDICTED INTERACTION INDEX VALUES FOR *PARA*- AND *META*-SUBSTITUTED PHENOLS

Substituent	Interaction terms[a]			
	Methanol		Acetonitrile	
	I_1	δI (60%)	I_1	δI (60%)
OH + 3-NH_2	−9	90	−32	69
OH + 4-NH_2	−110	(47)	−73	18
OH + 3-Br	70	39	8	5
OH + 4-Br	24	37	1	−2
OH + 3-Cl	67	45	7	11
OH + 4-Cl	24	37	1	0
OH + 3-OH	42	83	24	99
OH + 4-OH	−78	37	−41	65
OH + 3-$COCH_3$	74	99	82	97
OH + 4-$COCH_3$	43	52	46	54
OH + 3-CHO	72	105	80	95
OH + 4-CHO	28	−11[b]	30	40[b]
OH + 4-$CONH_2$	12	(97)	12	(113)
OH + 3-CN	101	139	113	120
OH + 4-CN	70	(80)[b]	73	78[b]
OH + 3-OCH_3	32	17	35	29
OH + 4-OCH_3	−47	−18	−49	−2
OH + 3-CO_2CH_3	73	72	80	47
OH + 4-CO_2CH_3	38	53	40	44
OH + 3-CH_3	−13	−16	−14	−38
OH + 4-CH_3	−18	−14	−19	−37
OH + 3-NO_2	128	113	143	115
OH + 4-NO_2	83	−89[b]	87	25
OH + 3-Ph	11	−1	12	−15
OH + 4-Ph	−1	−4	−1	−24

[a] I_1 calculated using eqn. 5. δI from Table VII.
[b] Suspected ionized analyte.

outliers. Further studies will be needed to determine the best way to approach analytes containing two strong responder groups.

Using the same ratios for ρ^*/ρ it is also possible to predict the increments for the substituted toluenes using eqn. 5 (Table XII). In this instance ρ_Y^* for the methyl group is zero so that $I_1 = \rho^*\sigma_Y$. Again, the predicted increments are constants irrespective of eluent composition and show a good correlation with the empirical values in methanol–buffer (60:40) or acetonitrile–buffer (60:40). In particular they reflect the high values for the amido substituent.

TABLE XII

PREDICTED INTERACTION INDEX VALUES FOR *PARA*- AND *META*-SUBSTITUTED TOLUENES

Substituent	Interaction terms[a]			
	Methanol		Acetonitrile	
	I_1	δI (60%)	I_1	δI (60%)
CH_3 + 3-Br	0	12	0	3
CH_3 + 4-Br	0	8	0	1
CH_3 + 3-Cl	0	13	0	0
CH_3 + 4-Cl	0	10	0	−3
CH_3 + 3-CH_3	0	9	0	−6
CH_3 + 4-CH_3	0	17	0	−3
CH_3 + 3-$COCH_3$	−3	−1	−4	−17
CH_3 + 4-$COCH_3$	−5	−3	−5	−26
CH_3 + 3-OCH_3	−6	−8	−6	−15
CH_3 + 4-OCH_3	−8	–	−1	–
CH_3 + 3-CO_2CH_3	−3	−2	−4	−12
CH_3 + 4-CO_2CH_3	−5	−1	−5	−16
CH_3 + 3-NO_2	0	3	0	−4
CH_3 + 4-NO_2	0	−9	0	−14
CH_3 + 3-Ph	0	4	0	−8
CH_3 + 4-Ph	0	19	0	2
CH_3 + 3-CHO	−5	0	−6	−4
CH_3 + 4-CHO	−7	−10	−8	−15
CH_3 + 3-$CONH_2$	−8	−11	−9	−33
CH_3 + 4-$CONH_2$	−13	−9	−13	−32
CH_3 + 3-NH_2	−13	−12	−14	−35
CH_3 + 4-NH_2	−18	−10	−13	−35
CH_3 + 3-CN	0	7	0	−10
CH_3 + 4-CN	0	1	0	−20

[a] I_1 calculated using eqn. 5. δI values from Table VI.

Ortho substituents

For the *ortho*-substituents it is assumed that the σ/ρ electronic interactions are the same as those for the *para*-substituents and that $\sigma_{ortho} = \sigma_{para}$. Therefore, to determine the magnitude of any extra negative *ortho* interactions (F_o) the interaction increments of the *ortho*-substituents were compared with those for the *para*-substituents.

Only small differences (+10 to −30 units) were observed for most of the *ortho*-substituted toluenes (Table VI). Acetyl and cyano groups had a negligible *ortho* effect, bromo, chloro, formyl, amino and hydroxyl groups showed small positive effects and methyl, carbomethoxy and nitro groups showed small negative effects.

Only the bulky phenyl and amido groups (−21 to −61 units) showed a significant change which agreed with Leo's observation [15] that the *ortho* effect was greatest with $CONH_2$ > halogen > NO_2 > OH, NH_2, but his rankings contained anomalies and differed depending on the parent substituent.

Examination of those substituted phenols which do not undergo hydrogen bonding (Table VII) suggested that negative *ortho* effects are present for the bromo and chloro groups. These varied with eluent composition, rising sharply with increasing proportion of methanol but less markedly with acetonitrile. The phenyl group gave a small negative effect in methanol but a positive effect in acetonitrile and the methyl group was positive in both eluents. The assignment of negative *ortho* interaction indices for retention prediction will be difficult because insufficient examples are available in the present study for a detailed analysis. Leo [15] suggested a number of quantized assignments but many of his values were interpolations and he suggested that Taft steric effect constant, E_s, and field effects, F, might play a role.

The largest *ortho* interaction increments for the phenols were apparently due to hydrogen bonding and the substituents could be divided into three groups, weak interactions from methoxyl and possibly from nitro substituents, medium interactions with hydroxyl and amino groups and strong interactions with the carbonyl-containing substituents. In each instance the effect was very dependent on the eluent composition and could change by over 150 units. Leo [15] suggested that for a limited set of compounds a single F_{HB} factor could be used, although for some combinations an additional term was required. A more limited interaction (150–250 units) occurs between OH + OH and OH + NH_2 groups, which was very dependent on the eluent composition. To isolate the F_{HB} effect the σ/ρ increment (from Table XI) should first be subtracted from the interaction increments; however, as seen above, the predicted values for the hydroxyl and amino substituents are unreliable.

Until further examples have been studied it seems that it will be difficult to develop general rules for these pairs of substituents and they are best described by the empirical relationships determined earlier (Table IX). Because the structural features causing these interactions are well defined, in any prediction system it will be possible to make specific rules to accounts for these effects.

The interaction between nitro and hydroxyl groups is unclear. Leo suggested that no hydrogen-bonding correction was needed for 2-nitrophenol, but in the present study the changes were large and because of possible ionization direct comparison with the 4-nitro isomer is difficult. The predicted *para* interaction (Table IX) in methanolic eluents of 83 is close to the empirical *ortho* interaction in methanol–buffer (60:40) of 98, but deviates more in acetonitrile–buffer (60:40) with a predicted value of $I_1 = 87$ compared with the observed value $\delta I = 216$. Further studies at a lower pH will be needed to avoid ionization effects.

CONCLUSIONS

The model compounds show a number of interactions between substituents on an aromatic ring. These have been incorporated as empirical relationships into a retention scheme. It appears that a more widely applicable model can be based on the use of the sigma/rho corrections for *meta* and *para* interactions but that *ortho* effects, such as hydrogen bonding and steric effects, may need to be incorporated as specific

interaction terms for individual pairs of substituents. There were particular problems with compounds that could be ionized. Further model compounds will need to be examined to test the general model and specifically a method is needed to deal with analytes containing more than one electron-releasing group.

REFERENCES

1 J. L. Glajch and L. R. Snyder (Editors), *Computer-Assisted Method Development for High-Performance Liquid Chromatography*, Elsevier, Amsterdam, 1990.
2 M. De Smet, G. Musch, A. Peeters, L. Buydens and D. L. Massart, *J. Chromatogr.*, 485 (1990) 237.
3 R. Hindriks, F. Maris, F. Vink, A. Peeters, M. De Smet, D. L. Massart and L. Buydens, *J. Chromatogr.*, 485 (1990) 255.
4 Y. Baba, *J. Chromatogr.*, 485 (1990) 143.
5 T. Sasagawa, Y. Sakamoto, T. Hirose, T. Yoshida, Y. Kobayashi and Y. Sato, *J. Chromatogr.*, 485 (1990) 533.
6 P. Härmälä, H. Vuorela, P. Lehtonen and R. Hiltunen, *J. Chromatogr.*, 507 (1990) 367.
7 R. M. Smith and C. M. Burr, *J. Chromatogr.*, 475 (1989) 57.
8 R. M. Smith and C. M. Burr, *J. Chromatogr.*, 481 (1989) 71.
9 R. M. Smith and C. M. Burr, *J. Chromatogr.*, 481 (1989) 85.
10 R. M. Smith and C. M. Burr, *J. Chromatogr.*, 485 (1989) 325.
11 C. Hansch and A. Leo, *Substituent Constants for Correlation Analysis in Chemistry and Biology*, Wiley-Interscience, New York, 1979.
12 T. Fujita, J. Isawa and C. Hansch, *J. Am. Chem. Soc.*, 86 (1964) 5177.
13 T. Fujita, *J. Pharm. Sci.*, 72 (1983) 285.
14 T. Fujita, *Prog. Phys. Org. Chem.*, 14 (1983) 75.
15 A. Leo, *J. Chem. Soc., Perkin Trans. 2*, (1983) 825.
16 A. J. Leo, in W. J. Dunn, J. H. Block and R. S. Pearlman (Editors), *Partition Coefficient. Determination and Estimation*, Pergamon Press, New York, 1986, p. 61.
17 E. P. Serjeant and B. Dempsey, *Ionisation Constants of Organic Acids in Aqueous Solutions*, Pergamon Press, Oxford, 1979.
18 T. Braumann, *J. Chromatogr.*, 373 (1986) 191.
19 K. Miyake, N. Mizuno and H. Terada, *J. Chromatogr.*, 439 (1988) 227.
20 C. R. Clark, M. J. M. Wells, R. T. Sansom, J. L. Humerick, W. B. Brown and B. J. Commander, *J. Chromatogr. Sci.*, 22 (1984) 75.
21 M. R. Clark, L. E. Garcia-Roura and C. R. Clark, *J. Liq. Chromatogr.*, 11 (1988) 3213.
22 C. R. Clark and L. E. Garcia-Roura, *J. Chromatogr. Sci.*, 27 (1989) 11.
23 A. Tsantili-Kakoulidou, N. El Tayar, H. van de Waterbeemd and B. Testa, *J. Chromatogr.*, 389 (1987) 33.

Journal of Chromatography, 550 (1991) 357–382
Elsevier Science Publishers B.V., Amsterdam

CHROMSYMP. 2079

Review

Chiral stationary phases derived from tyrosine

MARCEL CAUDE*

Laboratoire de Chimie Analytique, École Supérieure de Physique et Chimie Industrielles de Paris, 10 Rue Vauquelin, 75231 Paris Cedex 05 (France)

ANDRÉ TAMBUTÉ

Direction des Recherches et Études Techniques, Centre d'Études du Bouchet, B. P. No. 3, Le Bouchet, 91710 Vert-le-Petit (France)

and

LAURENT SIRET

Laboratoire de Chimie Analytique, École Supérieure de Physique et Chimie Industrielles de Paris, 10 Rue Vauquelin, 75231 Paris Cedex 05 (France)

ABSTRACT

Numerous chiral stationary phases (CSPs) have been developed in the last decade to provide an efficient and economic means for separating optical isomers. Among them, Pirkle-type CSPs have been designed according to a rational investigation of chiral recognition mechanisms. Following a similar approach, new CSPs possessing specific properties were designed starting from tyrosine.

The special features of CSPs derived from tyrosine are surveyed. These CSPs are characterized by the way in which the chiral selector (CS) is grafted onto silica gel, which allows the preparation of an entire family of CSPs based on the same starting material. This entails a wide scope of application including numerous racemates such as phosphine oxides, sulphoxides, lactams, benzodiazepinones and amino acid derivatives. This is reviewed either for analytical or preparative purposes. Chiral recognition mechanisms involved with tyrosine-derived CSPs are discussed.

Owing to the high stability of their grafting mode, tyrosine-derived CSPs are suited for all types of mobile phase nature, either liquid (LC) (reversed- or normal-phase), or supercritical fluid chromatography (SFC). A convenient method for optimizing the mobile phase (suitable for all Pirkle-type and related CSPs) is proposed. By using SFC, very high resolutions per unit of time are achieved, either on an analytical or on a preparative scale.

CONTENTS

0021-9673/91/$03.50

1. INTRODUCTION

In the last decade, chromatographic enantioseparations have given rise to widespread interest, directly connected with the growing attention paid to stereochemistry in drug design. Chiral high-performance liquid chromatography (HPLC) provides a powerful tool for monitoring enantiomeric ratios (analytical scale) and/or for preparing highly optically pure enantiomers (preparative scale).

Accordingly, there has been a tremendous increase in the design and synthesis of chiral stationary phases (CSPs) [1–4]. They are usually divided into two classes according to the chiral recognition process they are assumed to involve [5]. Independent CSPs (class 1) [6] are obtained by grafting an optically pure moiety (chiral selector, CS) on an achiral matrix (modified silica gel such as γ-aminopropyl, γ-glycidyloxypropyl or γ-mercaptopropyl [2]). Each CS operates independently in distinguishing the solute enantiomers. The chiral discrimination results from the formation of transient CSP–solute enantiomer diastereoisomeric complexes differing in internal energy [7]. They are opposed to cooperative CSPs (class 2), for which chiral entities are acting in concert to achieve chiral discrimination through complex chiral recognition mechanisms (inclusion phenomena). Class 2 includes natural [8–11] (cellulose derivatives, proteins) or synthetic polymers [8,12]. Cyclodextrin-bonded CSPs [13] are located between the two previous classes as each oligosaccharide acts independently and inclusion complex formation is required.

The major contribution to the design of class 1 CSPs was given by Pirkle and co-workers, who proposed a rational approach starting from NMR studies of diastereomeric solvates [14]. The grafting of 2,2,2-trifluoro-1-(9-anthryl)ethanol (initially used as a chiral solvating agent for NMR investigations) onto silica gave rise to the first Pirkle-type CSP (CSP A, Fig. 1) [15,16]. The elucidation of CSP A–solute chiral recognition mechanisms led to the development of a second generation of Pirkle-type CSPs. Numerous 3,5-dinitrobenzoyl (3,5-DNB) derivatives of amines, alcohols and related compounds have been resolved on CSP A [16,17]. The 3,5-DNB group provides both a π-acid (suitable for interacting through a π–π interaction with the strong π-basic 9-anthryl group of CSP A) and a proton acceptor site. By grafting N-(3,5-DNB) amino acids *via* an amidic linkage onto γ-aminopropyl silica, π-acid CSPs were prepared. According to the "reciprocality concept" [17] (if an optically active entity A resolves the enantiomers of B, then optically active B is expected to resolve the enantiomers of A), secondary aromatic alcohols were early resolved. A wide range of π-basic racemates (naturally occurring or prepared after derivatization) were also separated on these CSPs. The most popular π-acid CSPs were prepared from phenylglycine (DNBPG; CSP B, Fig. 1) [17–19] and leucine (DNBLeu; CSP C, Fig. 1) [18,20]. Their early commercialization has extended their scope of application, especially among pharmaceutical compounds.

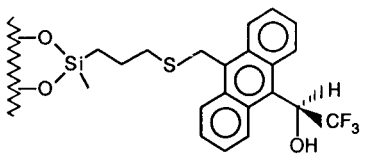

CSP A

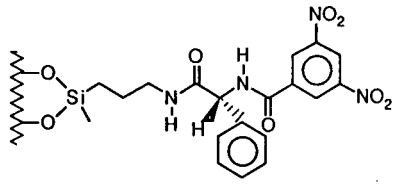

CSP B
(R)-DNBPG

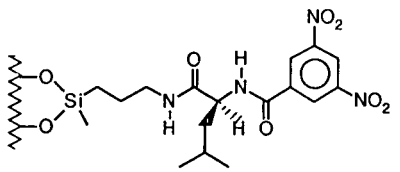

CSP C
(S)-DNBLeu

Fig. 1. Structures of Pirkle-type CSPs.

The rational design success of class 1 CSPs has prompted many researchers to develop new π-acid CSPs (*e.g.*, [21–24]). Although their scopes of application did not greatly differ, their chemical structure has resulted in specific chromatographic behaviours. The chiral recognition ability of a chromatographic system (CSP–solute–mobile phase) requires to a large extent a balance between the potential attractive interactions (π–π interactions, hydrogen bondings or dipole stackings) and steric hindrance, closely related to the conformational rigidity [25]. Hence, in order to extend the scope of application of Pirkle-type CSPs and to improve the knowledge of chiral recognition mechanisms, the development of new concepts is required. Literature data [1–4] indicate that π-basic CSPs are more frequently prepared and studied than the π-acid type, even if their scope of application is narrower (natural enantiomers scarcely show a π-acid character). Hence, the design and preparation of π-acid CSPs still remain a challenge.

For a few years, our laboratories have been involved in the synthesis and evaluation of CSPs derived from tyrosine. Their design is based on a rational approach taking into account the additional functional group of tyrosine (hydroxyl group) with regard to conventional Pirkle-type CSP precursors (phenylglycine, leucine, valine, etc.). This paper is organized into six sections, each emphasizing the originality and the properties of tyrosine-derived CSPs.

2. DESIGN

The design of CSPs derived from tyrosine results from the "reciprocality concept" introduced by Pirkle and House [17]. Our experience with Pirkle-type CSPs started with the enantiomeric separation of a series of tertiary phosphine oxides by Pescher and co-workers [26,27]. These solutes were easily resolved on a preparative scale [28] using a DNBPG CSP. In that manner, chiral aromatic tertiary phosphine oxides were prepared and grafted onto silica in order to provide π-basic CSPs with a chiral phosphorus atom [29,30].

For this purpose, one enantiomer of 1-(4-methoxynaphthyl)methylphenylphosphine oxide was chosen as chiral selector for the following reasons: the racemic mixture was well resolved on the DNBPG CSP (α = 1.61 [27]) and thus could easily be prepared as a single enantiomer with a high enantiomeric purity. Further, the absolute configuration of each enantiomer could readily be deduced by chemical correlation from those of methylnaphthylphenylphosphine oxide enantiomers, which had previously been established by Luckenbach [31].

The methoxy substituent was of great interest. Indeed, after treatment with boron tribromide, the resulting phenol could react either with various electrophilic reagents such as ethyl bromoacetate, allyl bromide or epibromohydrin (Fig. 2). In this way, starting from one chiral selector, three CSPs differing in the grafting mode were obtained [29,32]. The way of coupling 2, previously described by Rosini *et al.* [33], avoids generating a polar linkage in the spacer far from the chiral centre (amino alcohol in way 1 and amide in way 3, Fig. 2); such polar groups may induce non-stereoselective interactions. Accordingly, this grafing mode was selected for synthesizing tyrosine-derived CSPs [34].

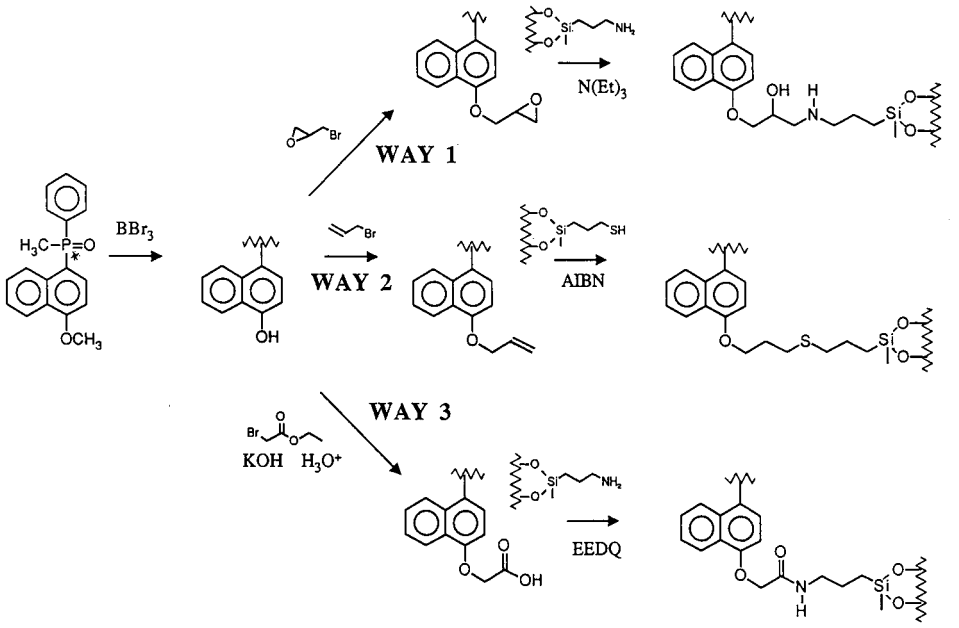

Fig. 2. The three different grafting modes investigated for the CSPs derived from phosphine oxides.

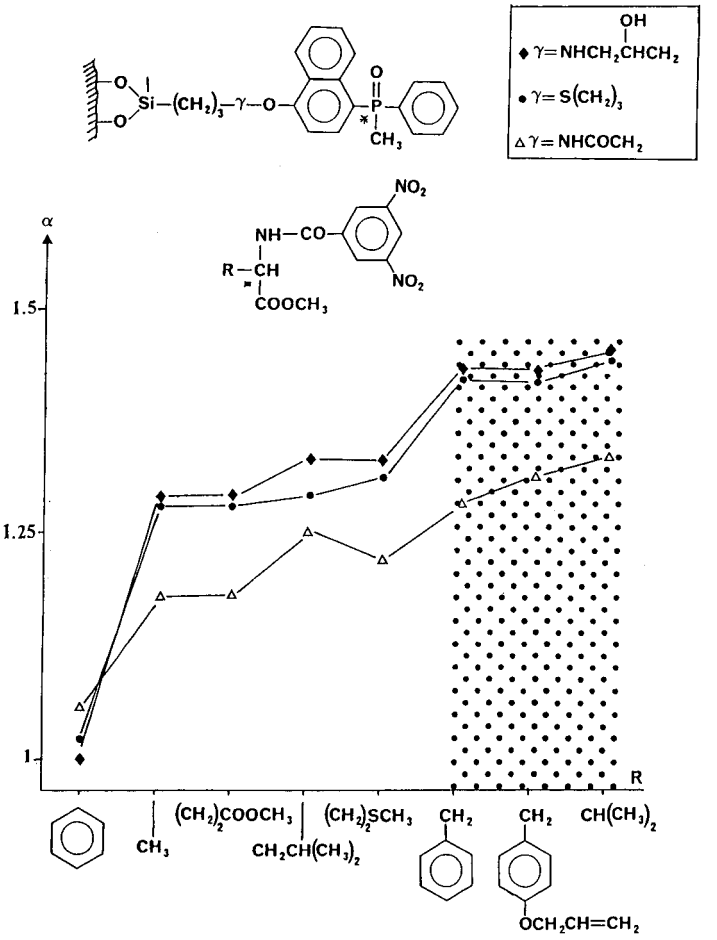

Fig. 3. Enantiomeric separation of 3,5-DNB amino esters on π-basic CSPs derived from phosphine oxides. Operating conditions: column, 150 × 4.6 mm I.D.; mobile phase, *n*-hexane–ethanol [(◆) 83:17; (●) 78:22; (△) 90:10, v/v]; flow-rate, 2 ml/min; temperature, 40°C; UV detection at 254 nm.

The enantiomeric separation of a series of 3,5-DNB amino methyl ester racemates (Fig. 3) was investigated on these CSPs [29,32]. Although the 3,5-DNB derivative of phenylglycine was the reciprocal precursor of these CSPs, it was surprising that this compound was the worst resolved (Fig. 3). This result illustrated the limitations of the "reciprocality concept" insofar as it does not take into account the chiral selector environment (spacer arm, silica matrix, mobile phase nature).

On the other hand, 3,5-DNB derivatives of valine [35], phenylalanine [21,35] and O-allyltyrosine were among the best resolved amino methyl ester derivatives (Fig. 3). Tyrosine was chosen because of its hydroxyl group, which could conveniently be turned into an allylic ether (site 1 in Fig. 4). This was suitable for reaction according to an anti-Markownikoff addition with the thiol group of a γ-mercaptopropyl-modified silica (way 2 in Fig. 2). In this manner, the chiral centre is removed from the silica matrix (with regard to the DNBPG CSP), the steric hindrance of which is minimized.

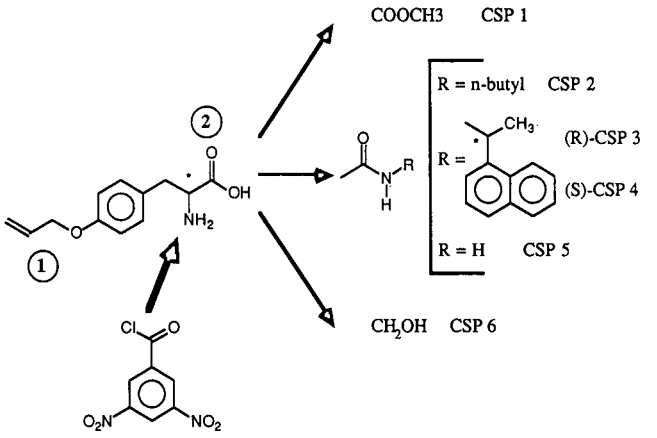

Fig. 4. Design of CSPs derived from tyrosine. The allylic functional group is employed for grafting the CS onto silica. The remaining carboxylic acid group is then converted into ester (CSP 1), amide (CSPs 2–5) or alcohol (CSP 6).

Moreover, supercritical fluid chromatographic (SFC) experiments indicated significant leaching of chiral grafts for CSPs displaying an amidic grafting mode [25]. This was related to the presence of unstable ionically bonded CSs. Such leaching was never evidenced with CSs grafted with a mercapto linking group, thus emphasizing their high stability.

Above all, using the hydroxyl group as the anchorage point, the carboxylic acid group (site 2 in Fig. 4) remains free for further derivatization. It can be converted into various functional groups (ester, amide, alcohol), allowing numerous interaction opportunities. Thus, two CSPs were early prepared [25,34,36,37]: CSP 1 (Fig. 4) for which the carboxylic acid group has been conveniently converted into a methyl ester and CSP 2 bearing an *n*-butyl amide group. They were termed (*S*)-thio-DNBTyr-E and (*S*)-thio-DNBTyr-A, respectively. Then, while keeping the amidic function and the 3,5-DNB group of CSP 2, the additional introduction of a π-basic moiety was considered. The replacement of the *n*-butylamine reagent (CSP 2) with chiral (*R*)- or (*S*)-1-(1-naphthyl)ethylamine afforded two novel "mixed" (*i.e.*, bearing both π-acid and π-basic moieties) CSPs [38] (CSP 3 and 4 in Fig. 4). Although mixed CSPs had been described previously [39,40], these CSPs were the first examples of CSPs suitable for the simultaneous separation of π-basic and π-acid racemates. Finally, very recently two novel CSPs bearing a primary amide (CSP 5 in Fig. 4) or a primary alcohol (CSP 6 in Fig. 4) were prepared [41].

3. SYNTHESIS

Syntheses of CSPs 1 and 2 [34], 3 and 4 [38] and 5 and 6 [41] were reported previously.

The starting material [(*S*)-Boc-tyrosine] belongs to the chiral pool. It is commercially available in large amounts and is fairly cheap. The various steps leading to CSPs 1–6 (Fig. 5) are classical and give satisfactory overall yields. The grafting rates

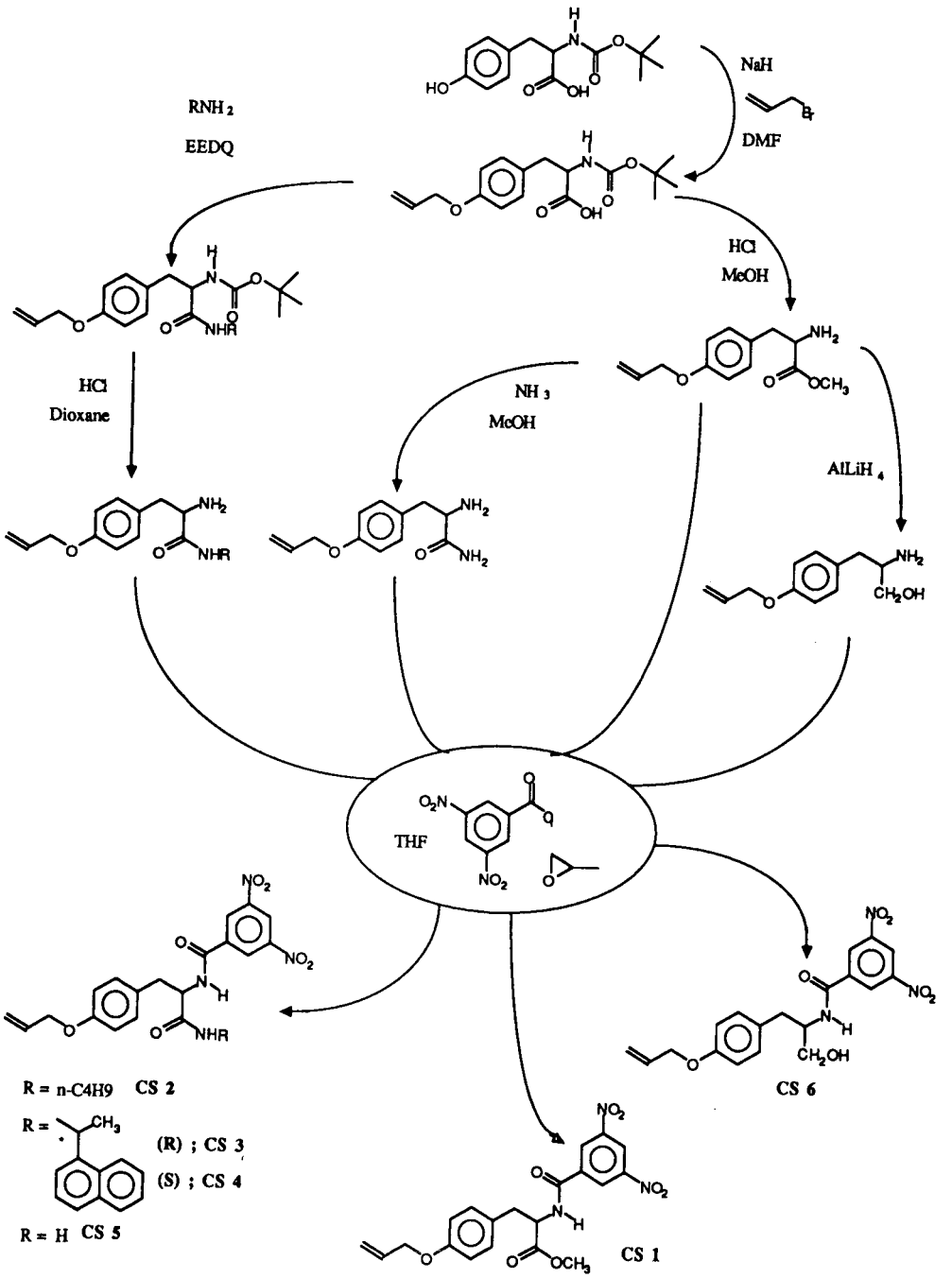

Fig. 5. The various pathways used for the synthesis of CSs derived from tyrosine.

are in the region of 0.2 mmol per gram of modified silica, corresponding to a 20% coverage of the initial mercaptopropyl groups.

4. MOBILE PHASE OPTIMIZATION

Normal-phase (NPLC) and reversed-phase (RPLC) modes are used with CSPs derived from tyrosine. Although the NPLC mode is far more used, recent separations have been carried out under RPLC conditions (Fig. 6) [42]. Recently, super- and sub-critical fluid chromatography (SFC and SubFC) were introduced and a section will be devoted to this new technique.

4.1. Influence of solvent nature in NPLC

n-Hexane is a typical apolar solvent used in the mobile phase and generally polar modifiers are chosen according to their selectivity parameters (χ_e, χ_d, χ_n, which reflect the ability of a solvent to act mainly as a proton acceptor, a proton donor or a strong dipole, respectively) as defined and calculated by Snyder [43,44] from solubility data reported by Rohrschneider [45].

4.1.1. Binary mixtures. From our experience with Pirkle-type and related CSPs the main effective polar modifiers can be classified into two groups: alcohols and chlorinated solvents. Retention times and selectivity values cannot be directly related to the mobile phase polarity (P') but rather depend on the polar modifier chemical structure and selectivity group. For an equivalent mobile phase polarity, differences observed in k' and α values when using alcohols belonging to the same selectivity group can be ascribed to the relative bulkiness of their alkyl moiety. Bulky alcohols give the highest selectivities and retentions, whereas a small linear alcohol such as ethanol exhibits both efficiency (plate number) and solvent strength [27].

Chlorinated solvents exhibit a greater selectivity than alcohols but a lower

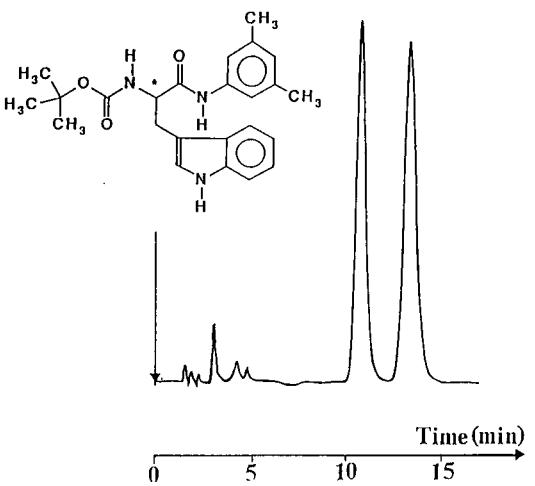

Fig. 6. Reversed-phase separation of the 3,5-dimethylanilide derivative of N-*tert.*-Boc-tryptophan on CSP 2. Operating conditions: column, 150 × 4.6 mm I.D.; mobile phase, methanol–water (80:20, v/v); flow-rate, 1 ml/min; room temperature; UV detection at 230 nm.

efficiency [46]. These characteristics may be correlated with the fact that alcohols can be considered as both proton donors and acceptors. Hence they may interact through hydrogen bondings with the basic and/or the acid site of the CSP amide dipoles. In contrast, chloroform (proton donor) and methylene chloride (strong dipole) only interact with a single site. Therefore, CSP–solute interactions are maximized when using chlorinated solvents (resulting in a higher selectivity) but the adsorption–desorption kinetics of solutes on CSP are slower (resulting in a weaker efficiency). Consequently, it is of interest to use a mixture of both a chlorinated solvent (in order to achieve a high selectivity) and a linear alcohol (in order to obtain a high efficiency and eluting strength) as polar modifier.

4.1.2. Ternary mixtures. Very often, a ternary mixture, *n*-hexane–alcohol–chlorinated solvent, turns out to be the optimum mobile phase for the resolution of enantiomers on Pirkle-type and related CSPs. Pescher *et al.* [27] first observed that phosphine oxides were much more soluble in chloroform than in an isoeluotropic *n*-hexane–alcohol mixture, predicting stronger solute–mobile phase interactions. Plotting α and k' values *versus* the concentration of binary mixture B (*n*-hexane–chloroform) in the ternary mixture A–B (A = *n*-hexane–alcohol), they obtained curves as shown in Fig. 7, displaying a concave profile for k'_2 and a regular increase in α from alcohol to chloroform.

This profile can be explained as follows: the capacity factor, k', can be expressed as

$$k' = \Sigma \text{ CSP–solute interactions} / \Sigma \text{ mobile phase–solute interactions}$$

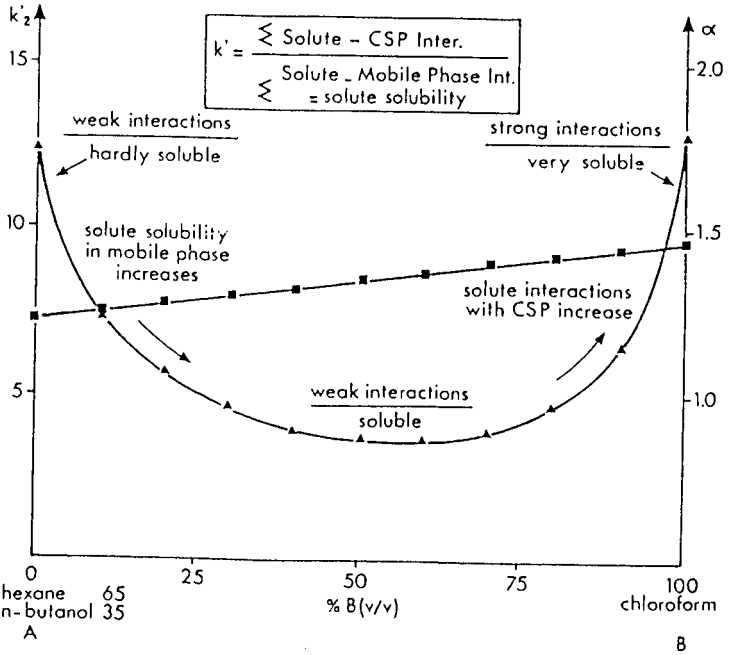

Fig. 7. Dependence of (▲) the capacity factor k' [for the most retained enantiomer of methyl(9-phenanthryl)phenylphosphine oxide] and (■) selectivity α on the chloroform content in the ternary mobile phase *n*-hexane–alcohol–chloroform (%B). Schematic explanation of the concave profile of k' *versus* %B.

To a first approximation, the solute solubility can be considered as a measure of the solute–mobile phase interactions. When the solubility of methyl(9-phenanthryl)-phenylphosphine oxide is plotted *versus* the chloroform content in *n*-hexane–chloroform–alcohol mixtures, a linear increase is observed. Consequently, in these mixtures, two phenomena may be assumed: (a) a higher solubility of solute molecules in the mobile phase when chloroform is added; and (b) the substitution of some alcohol molecules (which are strongly adsorbed on CSP) by chloroform molecules (which are easily displaced from CSP by solute molecules). At first, the CSP–solute interactions can be considered as weak with *n*-hexane–alcohol mobile phases because of the strong adsorption of alcohol molecules on the CSP. When a small amount of chloroform is added to the mobile phase, the solubility of the solute increases according to (a); with regard to (b), the chloroform can displace only a few alcohol molecules fixed on the CSP; the increase in solubility overshadows the phenomenon (b), leading to a decrease in k' values. This accounts for the descending left-hand part of the curve. Alternatively, at higher chloroform contents, phenomenon (b) becomes predominant (mass law). This entails an increase in the CSP–solute interactions and consequently in k', yielding the ascending right-hand part of the curve. In the concave minima region of the k' curve, the selectivity and the resolution per unit of time are significantly increased.

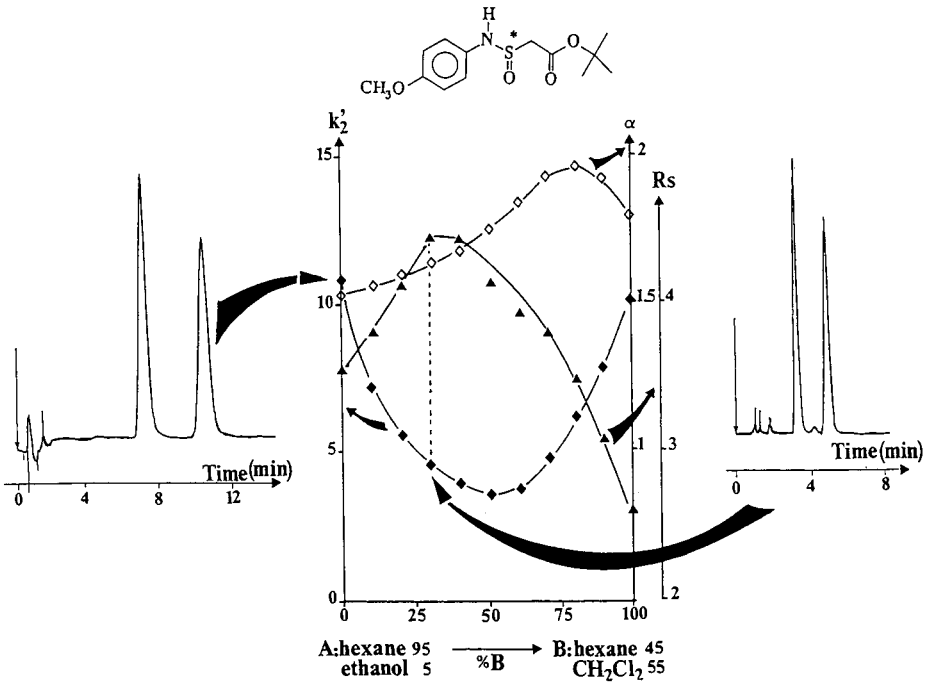

Fig. 8. Ternary optimization for *tert.*-butyl-N-(4-methoxyphenyl)sulphinamoyl acetate on CSP 3 using *n*-hexane–ethanol (95:5, v/v) (solvent A) and *n*-hexane–methylene chloride (45:55, v/v) (solvent B) as eluents. The capacity factor of the most retained enantiomer k'_2 (◆), the selectivity value α (◇) and the resolution factor R_s (▲) are plotted *versus* the content of solvent B in the ternary mobile phase A–B. Operating conditions: column, 150 × 4.6 mm I.D.; flow-rate, 2 ml/min; room temperature; UV detection at 254 nm.

This mobile phase optimization is now currently used [38,46]. As an example, Fig. 8 shows the ternary optimization of the enantiomeric separation of *tert.*-butyl N-(4-methoxyphenyl)sulphinamoyl ester on CSP 2.

In one instance, reversal of the elution order of the enantiomers using an *n*-hexane–ethanol–methylene chloride (or chloroform) ternary mixture as mobile phase has been reported (Fig. 9) [47]. Such a phenomenon is very difficult to explain. The reversal of elution order between ethanol and methylene chloride (or chloroform) can be ascribed to a change in the dominant interaction nature during the transient diastereomeric complex formation. The solvatation of both the solute and the CSP polar groups is affected by the nature of the solvent and is partly responsible for their conformation. The reversal of elution order can be the consequence of two separate causes: (a) both the solute and CSP contain too many sites of interaction of the same nature (two amide dipoles) and a low steric hindrance at the asymmetric centre; and (b) the lack of a strong driving force (such as a π–π overlapping) which could orientate the two molecules preferentially inside the diastereomeric complex, whatever the mobile

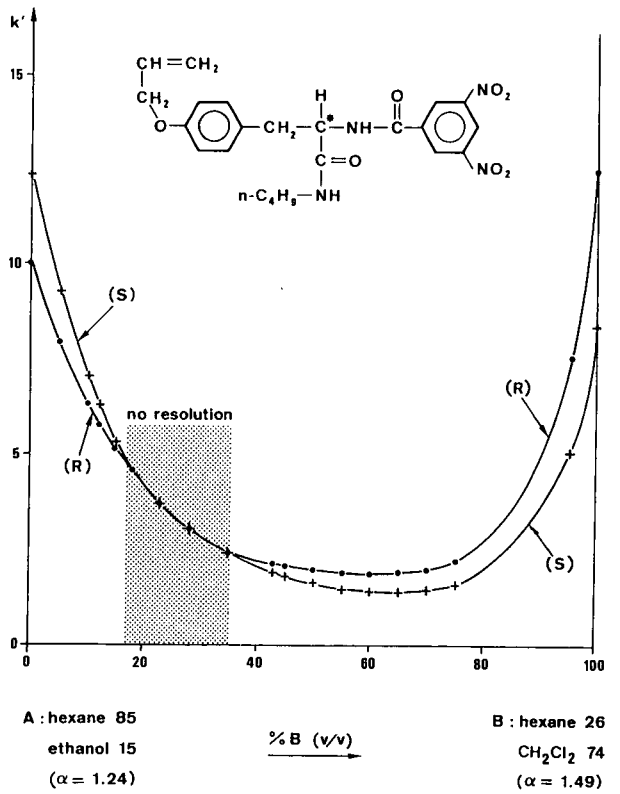

Fig. 9. Reversal of elution order of solute **20a** enantiomers (Table II) on CSP 2 on changing from *n*-hexane–ethanol (85:15, v/v) (solvent A) to *n*-hexane–methylene chloride (26:74, v/v) (solvent B) binary mixtures. The capacity factors *k'* of (+) (*S*)-**20a** and (●) (*R*)-**20a** are plotted *versus* the content of binary mixture B in the ternary mixture A–B. Operating conditions: column, 150 × 4.6 mm I.D.; flow-rate, 2 ml/min; temperature, 25°C; UV detection at 254 nm.

phase nature. As no driving, planar π–π attraction can be advocated, the solute can approach the CS in various orientations; multiple chiral recognition processes can thus be expected, some of them even working in opposite stereochemical senses and involving deeply conformational criteria directly connected to the mobile phase nature. We consider that ethanol favours dipole stacking mechanisms whereas chlorinated solvents rather favour hydrogen bondings.

4.1.3. Influence of the water content in the mobile phase. Generally, the addition of a small amount of water to the mobile phase does not lead to a significant increase in selectivity but gives an improvement of efficiency, leading to a higher resolution (Fig. 10). We assume that the water molecules are preferentially adsorbed on the residual silanols, thus cancelling non-stereoselective silica-solute interactions and leading to better kinetics of exchange [48].

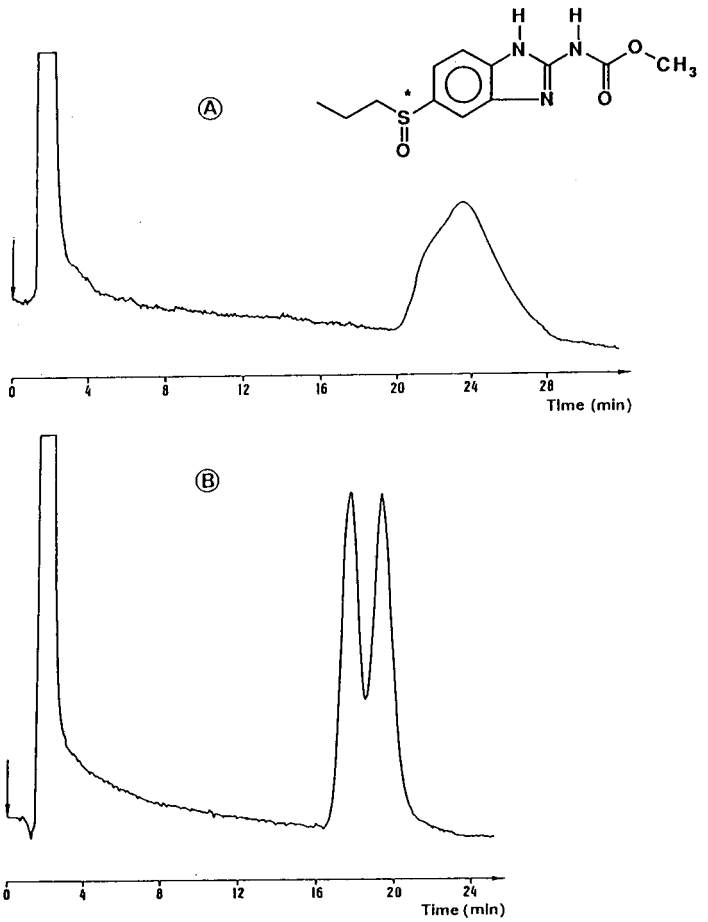

Fig. 10. Influence of the addition of water to an *n*-hexane–2-propanol mobile phase on the resolution of albendazole sulphoxide (solute 13, Table II). Mobile phase: (A) *n*-hexane–2-propanol (80:20, v/v); (B) *n*-hexane–2-propanol containing 2% of water (80:20, v/v). Column: CSP 1 (250 × 4.6 mm I.D.; d_p = 5 μm); flow-rate, 2 ml/min; temperature, 25°C; UV detection at 220 nm.

4.2. Supercritical fluid chromatography

As stated previously, chiral recognition on CSPs derived from tyrosine is mainly based on the setting of polar attractive CSP–solute interactions. Hence, the polarity of carbon dioxide (the main fluid used in SFC) is not sufficient to elute the enantiomers. Accordingly, polar modifiers should be added to the mobile phase. Their properties emphasized in NPLC are equivalent in SFC (modifiers which usually induce a high selectivity such as methylene chloride or chloroform also display a lower efficiency). No significant influence of the average column pressure on selectivity has been observed, meaning that carbon dioxide does not play a major role in the chiral recognition process. For a given racemate, LC and SFC afford the same elution order and a similar stereoselectivity. Similar chiral recognition processes can then be proposed for LC and SFC [49].

Further, the inherent advantages of SFC over LC are maintained (diffusion coefficients, D_m, and thus optimum velocities are 5–10 times greater in SFC than in LC). Consequently, the resolution per unit time in SFC is greater than that in LC. The superiority of SFC is twofold: for a given analysis time resolutions are significantly improved, and for a given resolution, analysis times are greatly reduced (Fig. 11)

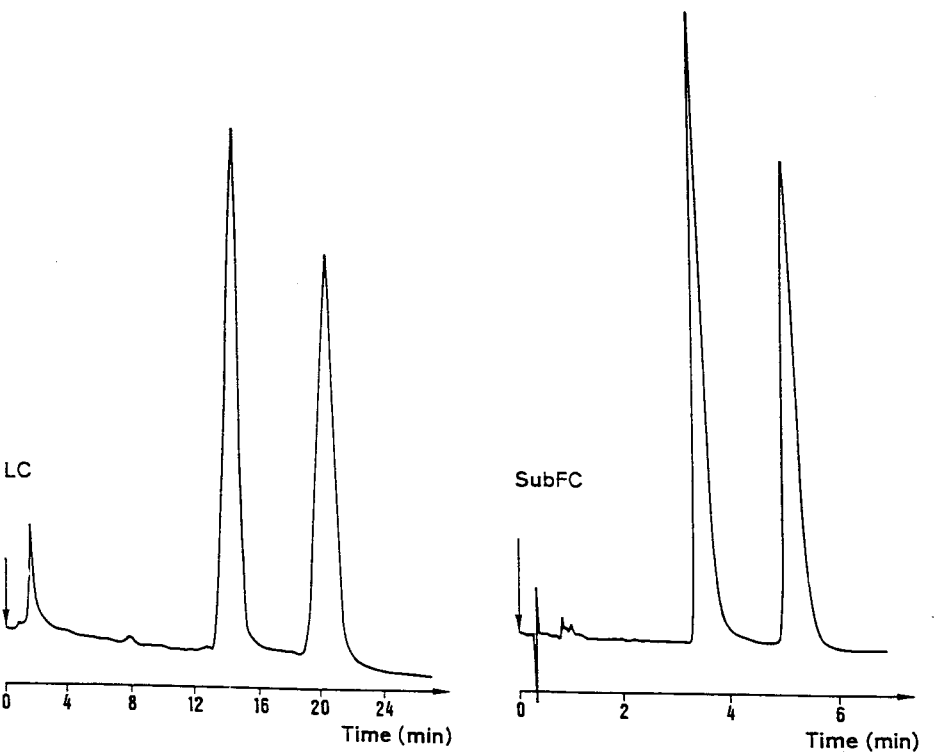

Fig. 11. Comparison of the analysis times measured at constant resolution factor in LC and SFC for oxazepam (solute **10**, Table II). Column: CSP 2 (150 × 4.6 mm I.D.; 5 μm). LC: mobile phase, *n*-hexane–ethanol (90:10, v/v); flow-rate, 2 ml/min; temperature, 25°C. SFC: mobile phase, carbon dioxide–ethanol (92:8, w/w); flow-rate, 6 ml/min at 0°C; average pressure, 200 bar; temperature, 25°C; UV detection at 229 nm.

[50,51]. All these results are valid for the resolution of π-basic solutes on π-acid CSPs, *i.e.*, in the case where a driving π–π interaction occurs in the CSP–solute diastereomeric complex formation. When this planar interaction does not exist, several chiral recognition processes may occur and carbon dioxide, owing to its induced dipolar character, behaves similarly to methylene chloride [47].

5. CHIRAL RECOGNITION MECHANISMS

CSPs derived from tyrosine belong to class 1 CSPs. Each modified tyrosine graft operates independently towards the solute enantiomers through the formation of transient CSP–solute bimolecular complexes.

According to the three-point rule proposed by Dalgliesh [7], to achieve chiral recognition the mechanism requires a minimum of three simultaneous interactions, one of which is stereochemically dependent. Nevertheless, one- or two-contact point models have been proposed to account for chiral discrimination [52–54]. The CSP–solute complex formation results from the occurrence of attractive CSP–solute interactions (π–π interaction, hydrogen bonding, dipole stacking).

In the case of tyrosine-derived CSPs the sites of interaction (amide or ester dipoles and 3,5-dinitrophenyl) are located only in two directions from the asymmetric centre. Accordingly, two-contact-point chiral recognition processes may be advocated for tyrosine-derived CSPs. The two CSP sites of interaction may interact with either two (Fig. 12A) or three (Fig. 12B) solute sites of interaction according to an M1 or M2 mechanism. These mechanisms are referred to as (2–2) or (3–2) mechanisms, respectively, according to Finn [55] (classified by the number of the four groups of the chiral tetrahedral centres involved in the chiral recognition process). For the M1

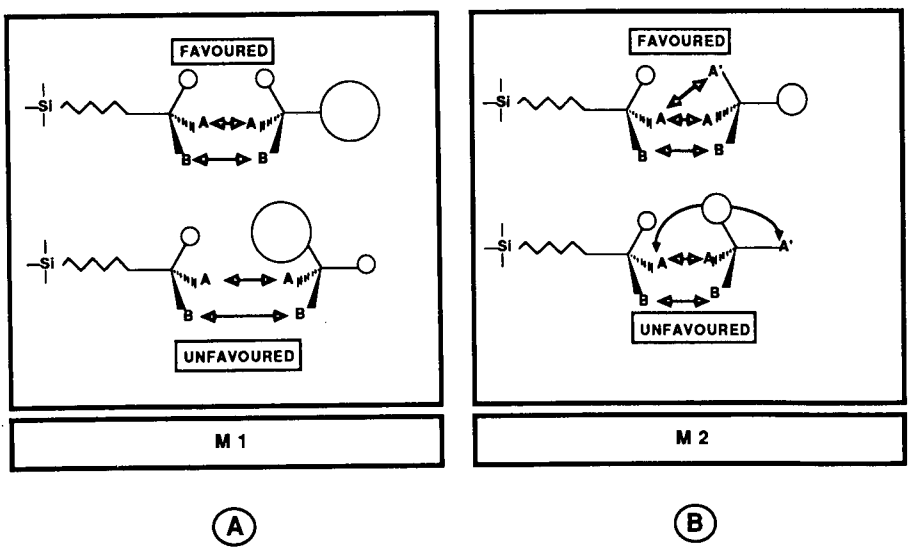

Fig. 12. Schematic representation of the most frequently encountered mechanisms with tyrosine-derived CSPs.

mechanism, equivalent attractive interactions are advocated for the two complexes, and the difference in stability results from the sterically unfavoured conformation of one CSP–solute complex (according to Topiol [54], this may be related to a difference in the distance matrices of the two complexes). This mechanism is frequently encountered [25,48], but higher selectivities are usually achieved with the M2 mechanism. Thus, the enantiomeric separation of N-aryl sulphinamoyl acetates which leads to high selectivity values on CSP 2 effectively obeys an M2 mechanism [46]. This is depicted in Fig. 13. The π–π interaction was evidenced by correlating the selectivity value with the π-acidity of the solute (expressed by means of its Hammet σ value) [46]. The hydrogen bonding HB 3 was evidenced by correlating the retention with the proton donor character of the CSP (CSPs 1, 2, 5 and 6 were tested) [41].

The conformational state of CSPs 3 and 4 results from a potential intra-

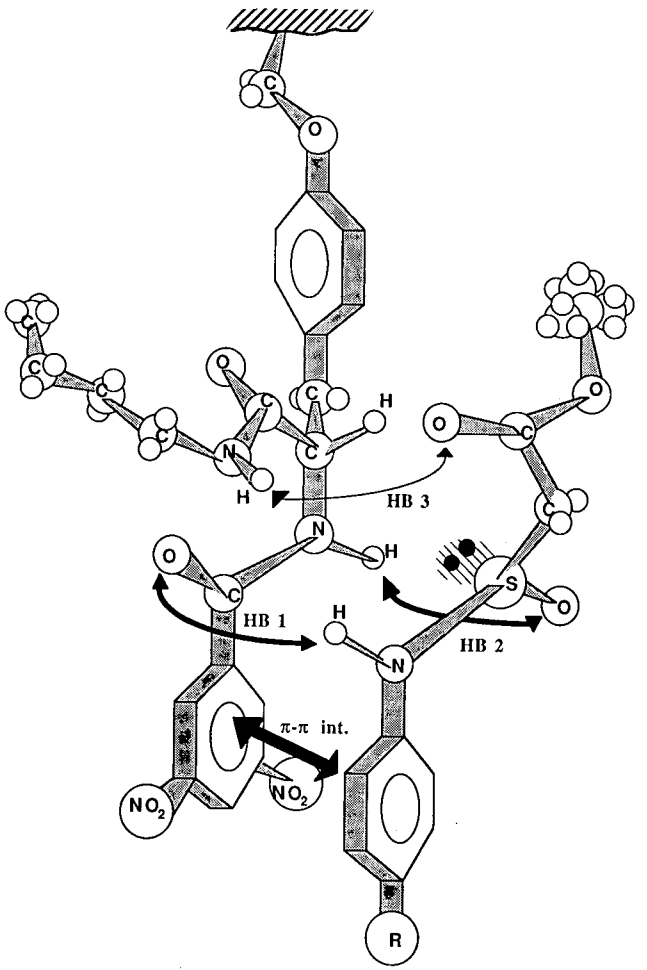

Fig. 13. Proposed chiral recognition model for N-aryl sulphinamoyl esters on CSP 2.

molecular π–π interaction strengthened by an intramolecular dipole stacking [38]. These CSPs bear two asymmetric centres, each located in the vicinity of either a π-basic or a π-acid centre. Accordingly, they may generate π–π complexes either with π-acid or π-basic solutes. So far, no indication had been given of the possibility of such a "mixed" CSP acting independently according to either a π-acid or a π-basic mode. Indeed, the resulting CSPs 3 and 4 display two distinct moieties: the π-acid moiety, in the vicinity of the 3,5-DNB moiety, is structurally similar to CSP 2 and thus exhibits a similar chromatographic behaviour toward π-basic racemates. Nevertheless, lower selectivities are generally observed as the intramolecular π–π interaction weakens to a certain extent the π-acceptor properties of the dinitrophenyl moiety. Further, the presence of the π-basic moiety allows the separation of π-acid racemates. It has been shown that both π-acid and π-basic modes do not interfere with each other [38]. For instance, the separation mechanism of 3,5-dinitroanilide derivatives of substituted 2-arylpropionic acid (APA) and related compounds only involves the π-basic moiety of CSP 3. This is shown in the Fig. 14 (the most retained enantiomer is represented). For APA derivatives (X = H), a typical M1 mechanism may be advocated; the chiral discrimination results from the aromatic group steric hindrance which prevents the

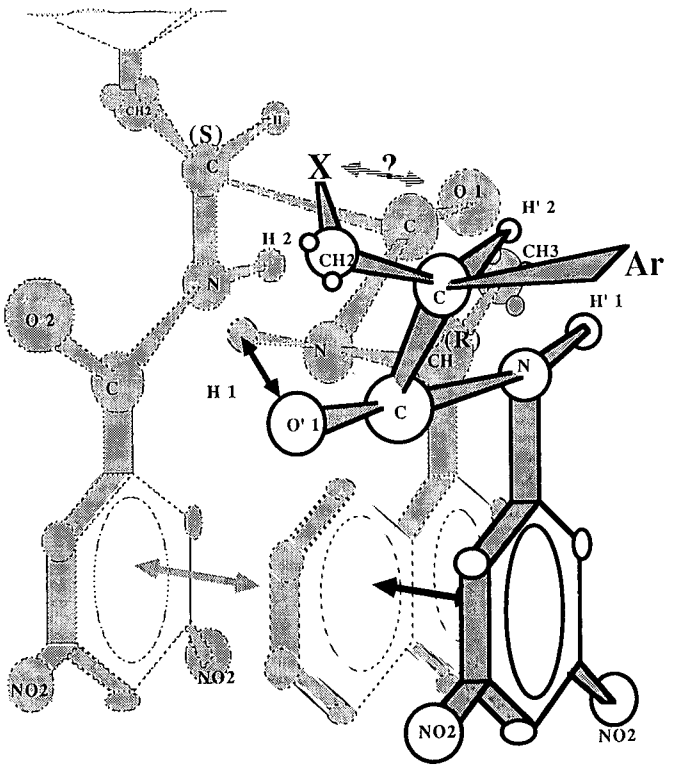

Fig. 14. Proposed chiral recognition mechanism for 3,5-dinitroanilide derivatives of aryl-2-propionic acids (APAs, X = H) and tropic acid (X = OH) on CSP 3. The most retained enantiomer is represented (according to chromatographic data), *S*-form for the APA derivative and *R*-form for the tropic acid derivative.

R enantiomer from approaching the CSP closely. For the tropic acid derivative (X=OH), the occurrence of a third interaction (hydrogen bonding between the hydroxyl group of the solute and the oxygen atom O-1 of the CSP) results in an M2 mechanism. The methyl substituent of the CSP hinders hydrogen bonding with the *S*-enantiomer and thus leads to chiral discrimination.

6. SCOPE OF APPLICATION

Numerous racemates of medium polarity containing aromatic substituents can be resolved on tyrosine-derived CSPs. So far, no racemate containing strong polar groups such as carboxylic acid or amine groups has been resolved. Such functional groups should be converted into functional groups of lower polarity (ester or amide) prior to injection. The scope of application of tyrosine-derived CSPs is focused on racemates containing asymmetric centres (carbon, phosphorus or sulphur). Nevertheless, some atropoisomers such as binaphthol derivatives may also be resolved [34]. Some specific functional groups of medium polarity are required in the vicinity of the asymmetric centre: amide or ester dipoles, carbamate, urea or hydroxyl groups. The chirality may also be borne by a dipole such as phosphine oxide, sulphoxide or sulphinamoyl.

Table I illustrates the scope of application of CSP 1. The main application of CSP 1 lies in the separation of solutes **3** enantiomers. These compounds play a prominent role in asymmetric catalysis [56]. So far, only CSP 1 allows the enantiomeric preparative-scale separation of such compounds [56,57], which are not or only poorly resolved on commercially available Pirkle-type CSPs (DNBPG and DNBLeu). Other miscellaneous racemates are resolved on CSP 1 (solutes **4**–**7**).

CSP 2 and the DNBPG CSP possess a complementary scope of application (Table II). Some typical Pirkle-type solutes such as the 2,2,2-trifluoro-1-(9-anthryl)-ethanol (TFAE, solute **8**), binaphthol (solute **9**) and oxazepam (solute **10**) are also resolved on CSP 2. Like DNBPG CSP, CSP 2 displays high selectivity values towards N-naphthylamino esters, previously described by Pirkle and Pochapsky [58] (solutes **15**). In addition, CSP 2 allows the enantiomeric separation of compounds of pharmaceutical or biological interest which were not or only poorly resolved on DNBPG CSP. This is the case for the anthelmintic drug albendazole sulphoxide (SOABZ) [48] (solute **13**), α-methylene γ-lactam cytotoxic agents [34] (solutes **18**) and sulphinamoyl CADH inhibitors [46] (solutes **11**). Contrary to all expectations, CSP 2 is also suitable for the separation of some π-acid derivatives of amino amides and esters (solutes **20**) [47]. This phenomenon has been taken into account in order to monitor the enantiomeric purity of CSs 1 and 2 prior to grafting them onto silica. Owing to the mild operating conditions, the racemization of CSs 1 and 2 had never occurred during their multi-step synthesis. A similar behaviour was expected for the other CS 3–6 candidates.

With CSPs 3 and 4, the scope of application of CSP 2 is extended from π-basic to π-acid racemates [38]. The initial scope of application of CSP 2 is maintained, but with lower selectivity owing to an intramolecular π–π interaction occurring within CSPs 3 and 4. Therefore, the CSP–solute π–π interaction is weakened, leading to lower selectivity (about a 10% decrease on average). Nevertheless baseline resolution are still achieved for compounds **8**–**19** [38]. In addition to their ability to resolve π-basic

TABLE I

SCOPE OF APPLICATION OF CSP 1

The selectivity values indicated for each solute were obtained with *n*-hexane–ethanol mobile phases, otherwise the polar modifier is specified. Ref. 34 for solutes 1, 3, 4, 5 and 6; ref. 42 for solutes 2 and 7.

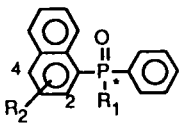

1 Phosphine oxides

R_1 = methyl	R_2 = H
a R_2 = H 1.24	**h** R_1 = H 1.11
b R_2 = 2-methyl 1.22	**i** R_1 = methoxy 1.05
c R_2 = 4-methyl 1.32	**j** R_1 = *n*-propyl 1.23
d R_2 = 2-methoxy 1.27	**k** R_1 = allyl 1.26
e R_2 = 4-methoxy 1.23	
f R_2 = 2-OH 1.11	
g R_2 = 4-OH 1.26	

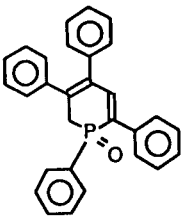

2 1.11

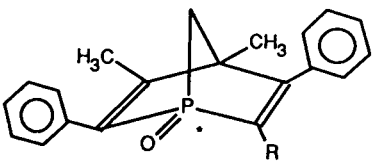

3 Phosphonorbornadiene oxides
a R = H 1.09
b R = methyl 1.33
c R = phenyl 1.07
d R = $COOC_2H_5$ 1.24

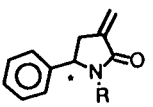

4 **a** R = phenyl 1.06
b R = 2-ethoxyphenyl 1.15
c R = 2,4-dimethoxyphenyl 1.24

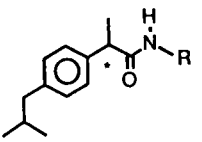

5 Ibuprofen derivatives
a R = *p*-anisyl 1.10
b R = naphthyl 1.12

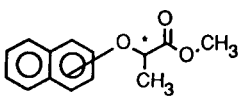

6 **a** 1-naphthyl 1.21 (CH_2Cl_2)
b 2-naphthyl 1.15 (CH_2Cl_2)

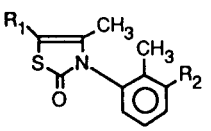

7 **a** R_1 = H, R_2 = methyl 1.08
b R_1 = H, R_2 = H 1.07
c R_1 = methyl, R_2 = H 1.07
d R_1 = methyl, R_2 = methyl 1.09

TABLE II

SCOPE OF APPLICATION OF CSP 2

Mobile phase conditions as in Table I. Ref. 34 for solutes 8, 9, 10, 14, 16 and 18; ref. 46 for solutes 11; ref. 42 for solutes 12, 15 and 19; ref. 48 for solute 13; ref. 63 for solutes 17; ref. 47 for solutes 20.

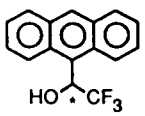

8 TFAE 1.26

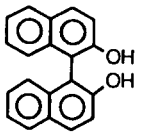

9 Binaphthol 1.13

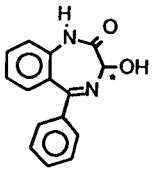

10 Oxazepam 1.53

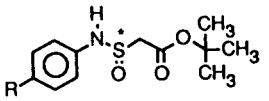

11 N-Aryl sulphinamoyl acetates
- **a** R = NO_2 1.72
- **b** R = CF_3 2.00 ($CHCl_3$)
- **c** R = Cl 2.00 ($CHCl_3$)
- **d** R = OCH_3 2.00 ($CHCl_3$)

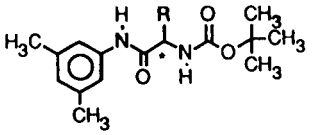

12 3,5-Dimethylanilide derivatives of *tert.*-Boc-amino acids
- **a** Alanine 1.31
- **b** Phenylalanine 1.35
- **c** Tryptophan 1.30
- **d** Tyrosine 1.32

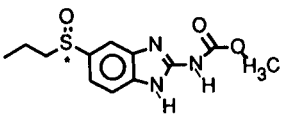

13 Albendazole sulphoxide (anthelmintic) 1.18

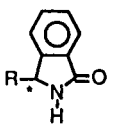

14 Lactams
- **a** R = *p*-anisyl 1.45
- **b** R = 1-naphthyl 1.07
- **c** R = isopropyl 1.07
- **d** R = cyclohexyl 1.15

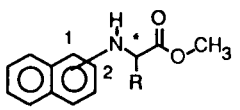

15 N-Naphthyl amino esters
- **a** 2-naphthylphenylalanine 8.83 (CH_2Cl_2)
- **b** 2-naphthylvaline 7.24 (CH_2Cl_2)
- **c** 1-naphthylvaline 9.69 (CH_2Cl_2)

(Continued on p. 376)

TABLE II *(continued)*

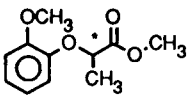

16 *o*-Anisyloxypropionic methyl ester
1.10 (CH_2Cl_2)

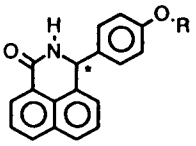

17 **a** R = methyl 1.57
b R = H 1.47
c R = glycidyloxy 1.61

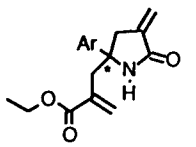

18 α-Methylene γ-lactams (cytotoxic agents)
a Ar = phenyl 1.35
b Ar = 3,4,5-trimethoxyphenyl 1.24

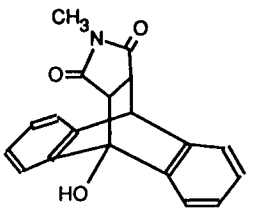

19 1.25

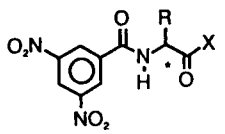

20

X = NH-*n*-C_4H_9 3,5-DNB derivatives of amino *n*-butylamides	X = OCH_3 3,5-DNB derivatives of amino methyl esters
a O-allyltyrosine 1.51 ($CHCl_3$)	**f** leucine 2.01 (CH_2Cl_2)
b phenylalanine 1.40	**g** O-allyltyrosine 1.71 (CH_2Cl_2)
c phenylglycine 3.43 ($CHCl_3$)	**h** phenylglycine 1.18
d methionine 1.35	
e leucine 1.51	

racemates, CSPs 3 and 4 afford good selectivity toward numerous π-acid racemates (Table III). It has been shown that the conformations of CSPs 3 and 4 result in CSPs displaying two distinct moieties (π-acid and π-basic), each suitable for discriminating enantiomers bearing a complementary π-character: a reversal of elution order occurred between CSP 3 and 4 (the absolute configuration of the asymmetric centre bearing the naphthyl group is inverted) for π-acid solutes, whereas no inversion occurred for π-basic racemates [38].

CSPs 5 and 6 were designed in order to obtain further insight into chiral recognition mechanisms [41]. With regard to CSP 1 and 2, these CSPs differ only in one potential site of interaction: the functional group directly bound to the asymmetric centre. The chromatographic data obtained with CSPs 1, 2, 5 and 6 allow the determination of the nature of the CSP–solute interaction occurring at this functional group [41].

TABLE III

SCOPE OF APPLICATION OF CSPs 3 AND 4

Mobile phase conditions as in Table I. Ref. 38 for all solutes.

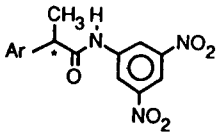

CSP 3

21 3,5-Dinitroanilide derivatives of 2-arylpropionic acids (anti-inflammatory drugs)
- **a** 2-phenylpropanoic acid 1.52
- **b** ibuprofen 1.80
- **c** naproxen 1.48
- **d** flurbiprofen 1.49
- **e** ketoprofen 1.29

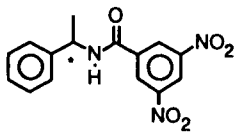

22 3,5-Dinitrobenzoyl derivative of phenylethylamine 1.32

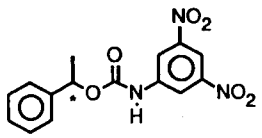

23 3,5-Dinitrophenylcarbamate derivative of phenylethanol 1.17

CSP 4

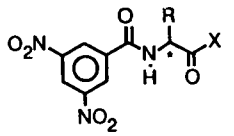

24 X = OCH_3
3,5-Dinitrobenzoyl derivatives of amino methyl esters
- **a** alanine 1.21
- **b** leucine 1.17
- **c** methionine 1.27
- **d** phenylalanine 1.34
- **e** tyrosine 1.31
- **f** valine 1.24

25 X = NH-*n*-C_4H_9
3,5-Dinitrobenzoyl derivatives of amino *n*-butyl amides
- **a** phenylalanine 1.15
- **b** phenylglycine 2.14

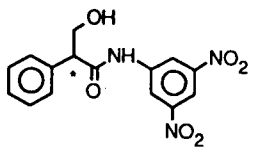

26 3,5-Dinitroanilide derivative of tropic acid 2.10

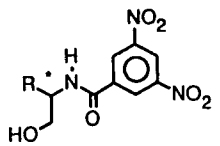

27 3,5-Dinitrobenzoyl derivatives of amino alcohols
- **a** R = phenyl 1.48
- **b** R = ethyl 1.13

(Continued on p. 378)

TABLE III *(continued)*

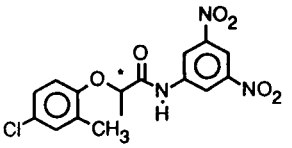	**28**	3,5-Dinitroanilide derivative of CMPP (herbicide) 1.13

7. PREPARATIVE-SCALE CHROMATOGRAPHY

The direct preparative resolution of enantiomers by LC using chiral stationary phases provides a useful alternative to enantioselective synthesis or fractional crystallization of diastereomeric salts. Pirkle-type CSPs, owing to their easy preparation from readily available chiral materials and their good mechanical properties, are attractive candidates for use in large-scale preparative systems [59,60].

Preparative scale separations were carried out on CSPs 1 and 2 according to a linear behaviour [61,62], corresponding to the usual injection conditions in analytical chromatography. This method was chosen for difficult separations ($\alpha < 1.2$) where it is necessary to use a small particle size ($d_p = 7$ μm) to maintain the column efficiency. The main preparative applications performed in our laboratories are given in Table IV. An example of a preparative-scale separation is given in Fig. 15 [57].

The relatively low sample capacity of these CSPs (with respect to microcrystalline cellulose triacetate for instance) is expected to be partly overcome by using SFC. The high diffusion coefficients allow a satisfactory production rate to be maintained.

8. CONCLUSION

Starting from tyrosine, an entire family of CSPs was synthesized. Their properties mainly result from their specific grafting mode:

(1) With regard to conventional π-acid Pirkle-type CSPs (amidic grafting mode), the asymmetric centre of tyrosine is removed further from the silica matrix, thus limiting its unwanted steric hindrance contribution. Accordingly, the scopes of application of tyrosine-derived CSPs are different from those of DNBPG or DNBLeu, but these CSPs display the same type of interaction. It can be assumed that solutes bearing bulky groups are generally better resolved on tyrosine-derived CSPs than on DNBPG, which however displays a higher enantiorecognition ability toward small molecules. This can be closely related to the conformational flexibility–enantiorecognition ability relationships proposed by Lienne *et al.* [25].

(2) The carboxylic acid moiety of the amino acid, which was previously conventionally used for grafting the CS onto γ-aminopropylsilica remains free for further derivatization. Thus, so far six different CSPs have been prepared and evaluated [34,38,41]. This entails a wide potential scope of application: so far, more than twenty different families of solutes have been resolved. Further, a specific functional group may be readily introduced in the CSP in order to maximize the

TABLE IV

PREPARATIVE-SCALE APPLICATIONS OF CSPs 1 and 2

Solute	CSP	Injection	Ref.
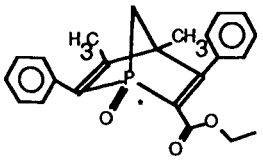	CSP 1 (200 g)	150 mg	56, 57
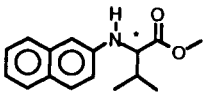	CSP 2 (200 g)	1 g enrichment, initial S/R ratio = 92:8	42
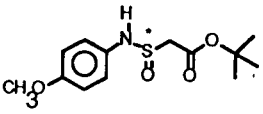	CSP 2 (200 g)	200 mg	46
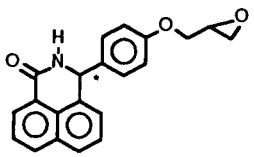	CSP 2 (200 g)	300 mg	63
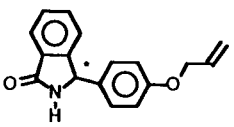	CSP 2 (200 g)	300 mg	57
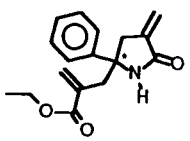	CSP 2 (200 g)	120 mg	25
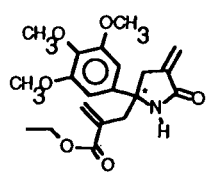	CSP 2 (200 g)	150 mg	57

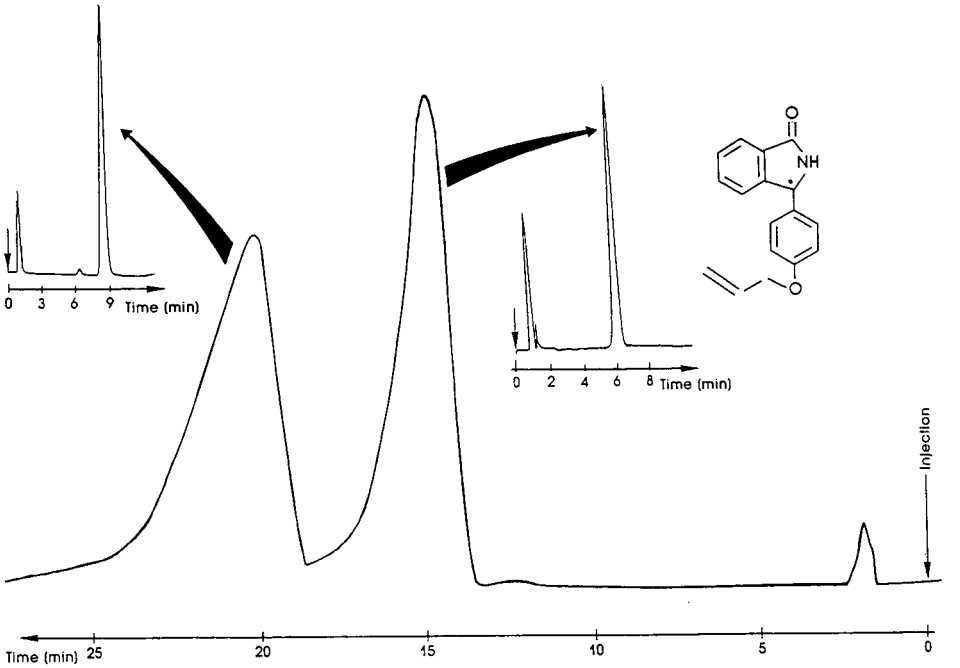

Fig. 15. Preparative-scale resolution of 300 mg of a derivative of solute **14a** (Table II) on 200 g of CSP 2, d_p = 7 μm. Operating conditions: mobile phase, *n*-hexane–ethanol (90:10, v/v); flow-rate, 42 ml/min; UV detection at 254 nm. The enantiomeric purity was checked on an analytical column (CSP 2) using the same mobile phase at 2 ml/min.

resolution of a given racemate. Thus, the introduction of chiral 1-(1-naphthyl)ethylamine has allowed the scope of application of earlier π-acid tyrosine-derived CSPs to be extended to π-acid racemates while keeping their enantiorecognition ability toward π-basic racemates [38].

(3) Very often, a ternary mobile phase optimization results in high resolutions per unit time. This can be very useful for decreasing retention times and increasing the throughput in preparative LC.

(4) Owing to the high stability of their grafting mode, tyrosine-derived CSPs are suited to classical mobile phases used with a silica matrix. The direct reversed-phase separation of pharmaceutical molecules is now under investigation in our laboratories. In addition, the use of modified carbon dioxide SFC allows higher resolutions per unit time to be achieved than with LC.

(5) The high efficiency and stability of tyrosine-derived CSPs allow their use for preparative-scale separations. Enantiomers of high purity have been prepared in the gram range by LC. Preparative applications using SFC are under investigation.

9. ACKNOWLEDGEMENTS

The authors are grateful to Mrs. Arlette Bégos (Centre d'Etudes du Bouchet) for the synthesis of tyrosine-derived chiral stationary phases and to Michelle Lienne for helpful advice concerning this paper.

REFERENCES

1 M. Zief and L. J. Crane (Editors), *Chromatographic Chiral Separations (Chromatographic Science Series*, Vol. 40), Marcel Dekker, New York, 1988.
2 A. M. Krstulovic (Editor), *Chiral Separations by HPLC: Applications to Pharmaceutical Compounds*, Ellis Horwood, Chichester, 1989.
3 S. G. Allenmark, *Chromatographic Enantioseparation: Methods and Applications*, Ellis Horwood, Chichester, 1988.
4 W. J. Lough (Editor), *Chiral Liquid Chromatography*, Blackie, Glasgow, 1989.
5 M. Lienne, M. Caude, A. Tambuté and R. Rosset, *Analusis*, 15 (1987) 431.
6 W. H. Pirkle and J. M. Finn, in J. D. Morrisson (Editor), *Asymmetric Synthesis, Vol. 1, Analytical Methods*, Academic Press, New York, 1983, p. 87.
7 C. E. Dalgliesh, *J. Chem. Soc.*, (1952) 3940.
8 G. Blaschke, *J. Liq. Chromatogr.*, 9 (1986) 341.
9 T. Shibata, Y. Okamoto and K. Ishii, *J. Liq. Chromatogr.*, 9 (1986) 313.
10 J. Hermansson and M. Eriksson, *J. Liq. Chromatogr.*, 9 (1986) 621.
11 S. G. Allenmark, *J. Liq. Chromatogr.*, 9 (1986) 425.
12 Y. Okamoto and K. Hatada, *J. Liq. Chromatogr.*, 9 (1986) 369.
13 T. J. Ward and D. W. Armstrong, *J. Liq. Chromatogr.*, 9 (1986) 407.
14 W. H. Pirkle and D. L. Sikkenga, *J. Org. Chem.*, 40 (1975) 3430.
15 W. H. Pirkle and D. L. Sikkenga, *J. Chromatogr.*, 123 (1976) 400.
16 W. H. Pirkle and D. W. House, *J. Org. Chem.*, 44 (1979) 1957.
17 W. H. Pirkle, D. W. House and J. M. Finn, *J. Chromatogr.*, 192 (1980) 143.
18 W. H. Pirkle and J. M. Finn, *J. Org. Chem.*, 46 (1981) 2935.
19 W. H. Pirkle, J. M. Finn, J. L. Schreiner and B. C. Hamper, *J. Am. Chem. Soc.*, 103 (1981) 3964.
20 W. H. Pirkle and C. J. Welch, *J. Org. Chem.*, 49 (1984) 138.
21 L. Oliveros and M. Cazau, *J. Chromatogr.*, 409 (1987) 183.
22 G. Gargaro, F. Gasparrini, D. Misiti, G. Palmieri, M. Pierini and C. Villani, *Chromatographia*, 24 (1987) 505.
23 J. Kip, P. Van Haperen and J. C. Kraak, *J. Chromatogr.*, 356 (1986) 423.
24 N. Oi, M. Nagase, Y. Inda and T. Doi, *J. Chromatogr.*, 265 (1983) 111.
25 M. Lienne, P. Macaudière, M. Caude, R. Rosset and A. Tambuté, *Chirality*, 1 (1989) 45.
26 P. Pescher, M. Caude, R. Rosset, A. Tambuté and L. Oliveros, *Nouv. J. Chim.*, 9 (1985) 621.
27 P. Pescher, M. Caude, R. Rosset and A. Tambuté, *J. Chromatogr.*, 371 (1986) 159.
28 A. Tambuté, P. Gareil, M. Caude and R. Rosset, *J. Chromatogr.*, 363 (1986) 81.
29 A. Tambuté, A. Bégos, M. Lienne, M. Caude and R. Rosset, *J. Chromatogr.*, 396 (1987) 65.
30 M. Lienne, A. Tambuté, M. Caude and R. Rosset, presented at the *International Symposium on Chiral Separations, Guilford, U.K., September 3–4, 1987.*
31 R. Luckenbach, *Phosphorus*, 1 (1972) 223.
32 M. Lienne, *Thèse de Doctorat*, Université Pierre et Marie Curie (Paris VI), 1989.
33 C. Rosini, C. Bertucci, D. Pini, P. Altemura and P. Salvadori, *Tetrahedron Lett.*, 26 (1985) 3361.
34 A. Tambuté, A. Bégos, M. Lienne, P. Macaudière, M. Caude and R. Rosset, *New J. Chem.*, 13 (1989) 625.
35 W. H. Pirkle and R. Däppen, *J. Chromatogr.*, 404 (1987) 107.
36 M. Lienne, P. Macaudière, M. Caude, R. Rosset, A. Tambuté and A. Bégos, presented at the *1st International Symposium on Separation of Chiral Molecules, Paris, May 31–June 2, 1988.*
37 M. Lienne, P. Macaudière, M. Caude, R. Rosset, A. Tambuté and A. Bégos, presented at the *12th International Symposium on Column Liquid Chromatography, Washington, DC, June 19–24, 1988.*
38 A. Tambuté, L. Siret, M. Caude, A. Bégos and R. Rosset, *Chirality*, 2 (1990) 106.

39 M. Ho Hyun and W. H. Pirkle, *J. Chromatogr.*, 393 (1987) 357.
40 N. Oi, H. Kitahara, Y. Matsumoto, H. Nakajima and Y. Horikawa, *J. Chromatogr.*, 462 (1989) 382.
41 L. Siret, A. Tambuté, M. Caude and R. Rosset, *J. Chromatogr.*, 540 (1991) 129.
42 L. Siret, A. Tambuté and M. Caude, unpublished results.
43 L. R. Snyder, *J. Chromatogr. Sci.*, 16 (1978) 223.
44 L. R. Snyder, *J. Chromatogr.*, 92 (1974) 223.
45 L. Rohrschneider, *Anal. Chem.*, 45 (1973) 1241.
46 L. Siret, A. Tambuté, M. Caude and R. Rosset, *J. Chromatogr.*, 498 (1990) 67.
47 P. Macaudière, M. Lienne, M. Caude, R. Rosset and A. Tambuté, *J. Chromatogr.*, 467 (1989) 357.
48 M. Lienne, M. Caude, R. Rosset, A. Tambuté and P. Delatour, *Chirality*, 1 (1989) 142.
49 P. Macaudière, A. Tambuté, M. Caude, R. Rosset, M. A. Alembik and I. W. Wainer, *J. Chromatogr.*, 371 (1986) 177.
50 P. Macaudière, M. Caude, R. Rosset and A. Tambuté, *J. Chromatogr. Sci.*, 27 (1989) 383.
51 P. Macaudière, M. Caude, R. Rosset and A. Tambuté, *J. Chromatogr. Sci.*, 27 (1989) 583.
52 S. Topiol, M. Sabio, W. B. Caldwell and J. Moroz, *J. Am. Chem. Soc.*, 110 (1988) 8367.
53 S. Topiol and M. Sabio, *J. Chromatogr.*, 461 (1989) 129.
54 S. Topiol, *Chirality*, 1 (1989) 69.
55 J. M. Finn, in M. Zief and L. J. Crane (Editors), *Chromatographic Chiral Separations* (*Chromatographic Science Series*, Vol. 40), Marcel Dekker, New York, 1988, p. 61.
56 A. Brèque, J. M. Alcaraz, L. Ricard, F. Mathey, A. Tambuté and P. Macaudière, *New J. Chem.*, 13 (1989) 369.
57 A. Tambuté, F. Guir and L. Siret, presented at the *2nd International Conference on Heteroatom Chemistry, Albany, NY, July 17–22, 1989.*
58 W. H. Pirkle and T. C. Pochapsky, *J. Org. Chem.*, 51 (1986) 102.
59 W. H. Pirkle and J. M. Finn, *J. Org. Chem.*, 47 (1982) 4037.
60 W. H. Pirkle, T. C. Pochapsky, G. S. Mahler, D. E. Corey, D. S. Reno and D. M. Alessi, *J. Org. Chem.*, 51 (1986) 4991.
61 P. Gareil, L. Personnaz, J. P. Feraud and M. Caude, *J. Chromatogr.*, 192 (1980) 53.
62 P. Gareil and R. Rosset, *Analusis*, 10 (1982) 397.
63 M. Sallé, A. Tambuté and A. Bégos, *J. Chromatogr.*, 475 (1989) 153.

Journal of Chromatography, 550 (1990) 383–395
Elsevier Science Publishers B.V., Amsterdam

CHROMSYMP. 2066

High-performance liquid chromatography of amino acids, peptides and proteins

CIX[a]. Investigations on the relation between the ligand density of Cibacron Blue immobilized porous and non-porous sorbents and protein-binding capacities and association constants[b]

H. J. WIRTH, K. K. UNGER[c] and M. T. W. HEARN*
Department of Biochemistry, Monash University, Clayton, Victoria 3168 (Australia)

ABSTRACT

A porous silica of nominal 5 μm particle diameter and 30 nm pore size (Nucleosil 300-5) and a non-porous silica of nominal 1.5 μm particle diameter were activated with 3-mercaptopropyltriethoxysilane (MPTS), followed by the immobilization of the triazine dye, Cibacron Blue F3GA. Various biomimetic dye sorbents with graduated ligand densities between 1 μmol/m^2 and 0.01 μmol/m^2 were prepared. The capacities and the association constants associated with the binding of lysozyme to these sorbents were determined by frontal analysis experiments [*J. Chromatogr.*, 476 (1989) 205–225].

Due to the ability of the Cibacron Blue F3GA-modified silicas to act as mixed mode coulombic and hydrophobic interaction sorbents and the highly charged nature of the surface structure of lysozyme (p*I* 11), two mobile phase conditions were examined. In one case a 0.1 *M* phosphate buffer, pH 7.8, was used as the equilibration and loading buffer, in the second case 1 *M* sodium chloride –0.1 *M* phosphate buffer, pH 7.8 was employed as the equilibration and loading buffer to monitor the influence of ionic interactions. The elution was performed in each case with a 2.5 *M* potassium thiocyanate solution.

With the porous silica dye sorbents and 1 *M* NaCl present in the loading buffer, the highest capacity was achieved when Cibacron Blue F3GA was immobilised to the level of 0.1 μmol/m^2. In the case of the non-porous silica dye sorbents, the maximum protein capacity was achieved when 0.5 μmol/m^2 dye were immobilised onto the support. Evaluation of the frontal breakthrough curves confirmed that the kinetics of adsorption of lysozyme onto the non-porous sorbent were substantially faster than the adsorption of lysozyme onto the porous sorbent due to the absence of pore diffusion effects in case of the non-porous

[a] For Part CVIII, see ref. 20.

[b] It is a great pleasure for the authors to dedicate this publication to Lloyd Snyder. As a towering influence over the chromatographic science, Lloyd has provided an incisive and rigorous scientific focus to many areas of research development throughout his distinguished career. His insight has been a catalyst to innumerable conceptual and practical developments some of which the authors have employed in their own studies. The authors warmly acknowledge Lloyd's monumental scientific accomplishments, his stringent advice and generous friendship.

[c] On Sabbatical leave from: Institut für Anorganische Chemie und Analytische Chemie, Johannes Gutenberg-Universität, 6500 Mainz, Germany.

0021-9673/91/$03.50

support. Furthermore, the adsorption of lysozyme on both sorbents was faster when no salt was added to the loading buffer, indicating that there is either conformational or reorientation effects operating during the specific binding of the protein to the dye ligand, or that the interaction is proceeding through the participation of a second class of binding sites.

The magnitude of the association constants, K_a, for the lysozyme–Cibracron Blue F3GA systems were found to be dependent on the ligand density of the sorbent. With decreasing ligand density, the protein–ligand interaction became stronger, *e.g.* K_a values became larger. These results confirm earlier observations on the effect of ligand steric compression on the affinate–ligand association constant, *e.g.* the protein needs sufficient space to interact with the ligand in an optimum way. This phenomenon was particularly evident in case of the non-porous silica dye sorbents where no pore diffusion effects can occur to obscure or restrict the interaction between the protein and its ligand.

INTRODUCTION

The increasing use of natural and genetically engineered proteins as pharmaceuticals demands the development of high performance separation techniques, which are able to purify the specific protein rapidly and to a very high purity without destroying its biological activity. In order to achieve product efficiencies at process scale, these purification methods must be able to cope with multistage procedures operating under volume and/or concentration overload conditions. At the other end of the separation spectrum, the analytical separation of specific proteins or other bioproducts at trace levels represent the constant challenge for advanced modes of quality control procedures.

Recently, affinity chromatography based on mechanically stable supports has emerged as a powerful tool for the separation of biopolymers under both analytical- as well as preparative-scale conditions. Traditionally, soft polymeric gels such as agarose, cellulose, or polymethacrylate have been used to prepare affinity sorbents. During the last few years however a growing number of investigators [1–8] have turned their attention to the application of microparticulate porous silicas as supports for the development of high-performance affinity sorbents.

The maintenance of the biological activity of a protein during the separation is the essential objective of affinity chromatography as well as all other modes of adsorption chromatography. Preservation of bioactivity can be achieved by ensuring that the contact time between the support material and the protein of interest in the biological sample is minimized. One way this can be achieved is to employ very rapid separation times based on non-porous sorbents. In our previous studies [6,7] the advantages in analytical and semi-preparative biospecific affinity chromatography of monodisperse, non-porous silicas compared with porous silica-based supports or soft gels were documented.

In conventional laboratory scale biomimetic and biospecific affinity chromatography, separation selectivity is traditionally optimised, *i.e.* a ligand of requisite association constant, K_a, is selected, in preference to the optimisation of separation efficiency. In both process applications and ultramicroanalytical applications, the consequences of inappropriate ligand characteristics are very apparent. However, kinetic considerations [9,10] arising from an analysis of mass transport effects associated with the capture rate, the desorption rate, and the zone broadening due to the component diffusion processes, indicate considerable advantages of non-porous sorbents, once a suitable ligand and ligand density has been selected.

In this paper the influence of the ligand density on the kinetics of adsorption, the binding capacities and the association constants of a protein–biomimetic dye sorbent system has consequently been investigated with porous and non-porous silica support particles. In order to evaluate the binding capacity and the association constant of the adsorbate–ligand complex, frontal analysis was used which, as previously documented from this and other laboratories (see, for example, refs. 6, 7, 11–14) represents an accurate method to quantitatively compare different chromatographic adsorption systems. The biomimetic ligand employed was Cibacron Blue F3GA, a triazine dye which has been widely used for the fractionation of NAD-dependent enzymes and many other proteins.

EXPERIMENTAL

Preparation of the sorbents

In the following investigations, a porous silica of nominal 5 μm particle diameter (d_p) and 30 nm pore size (Nucleosil 300-5, Macherey-Nagel, Düren, Germany) and a non-porous silica of nominal $d_p = 1.5$ μm, prepared as described previously [15], were employed.

The modification of the silicas were performed in two steps. In the first step the support was activated [6] with 3-mercaptopropyltriethoxysilane (MPTS), while in the second step the Cibacron Blue F3GA dye molecule was bound to the thiol group of the immobilized silane. The amount of silane needed for the reaction was calculated from the surface area of the support and the concentration of silanol groups on the surface of about 8 μmol/m^2. Since only half of the silanol groups are accessible to the immobilzation ligand, this procedure ensured that the silanating reagent was always added in excess. The silanating reaction was carried out in water, adjusted to pH 3.5 with nitric acid. The silica supports were suspended in the solvent, the silane added and the suspension agitated (inversion shaker) at 363 K for 3 h. After the reaction had finished, the silica was washed with water, followed by methanol and dried.

TABLE I

CONDITIONS TO IMMOBILIZE CIBACRON BLUE F3GA ON MERCAPTO-ACTIVATED SILICAS

In case of a ligand density of 1 μmol/m^2 the dye was added to the reaction mixture in 0.5 mole equivalents excess to ensure a maximum ligand density.

Silica	Ligand density (μmol/m^2)	Amount of immobilized dye (mg/g silica)
Nucleosil 300-5	1	160
	0.1	8
	0.01	0.8
Non-porous silica 1.5 μm	1	3.0
	0.5	1.1
	0.2	0.44
	0.1	0.22
	0.01	0.023

The conditions used for the immobilization of Cibacron Blue F3GA are given in Table I. In brief, the MPTS-silicas were suspended in a 0.1 *M* sodium carbonate buffer, pH 8.2 containing 0.5 *M* sodium chloride. The dye (1.5 mole equivalents in the case of the maximally covered sorbent and adjusted as appropriate for the sorbents of lower ligand density) was then added and the mixture shaken (inversion shaker) for 24 h at 333 K. Depending on porosity of the support and the final prepared ligand density, the color of the resulting sorbent ranged from deep blue, aquamarine, to a very faint shade of sky blue in colour. Ligand densities were determined as described previously [6,11,12].

The sorbents were packed by the slurry procedure into LiChroCart cartridge columns, which were 19 mm × 4 mm I.D. All frontal analysis experiments were performed at 282 K with an eluent flow-rate of 0.5 ml/min. Protein frontal breakthrough was monitored spectrophotometrically at a detector wavelength of 276 nm.

Equipment and instrumental procedures

The equipment used for the frontal analysis experiments (Fig. 1) consisted of two HPLC pumps (Waters Model 6008; Millipore, Bedford, MA, USA). The first HPLC pump (1) delivered the protein solution while the second pump (2) delivered the elution and the washing buffer. The column (3), a LiChroCart cartridge column 19 × 4 mm, supplied by Merck (Darmstadt, Germany) was connected to the pumps by a 6-way valve (6). The column outlet was attached to a variable-wavelength Waters Model 450 detector (4) and to a Shimadzu chart recorder (5). A LKB Multitemp 2209 thermostat was used to keep the column at a defined temperature.

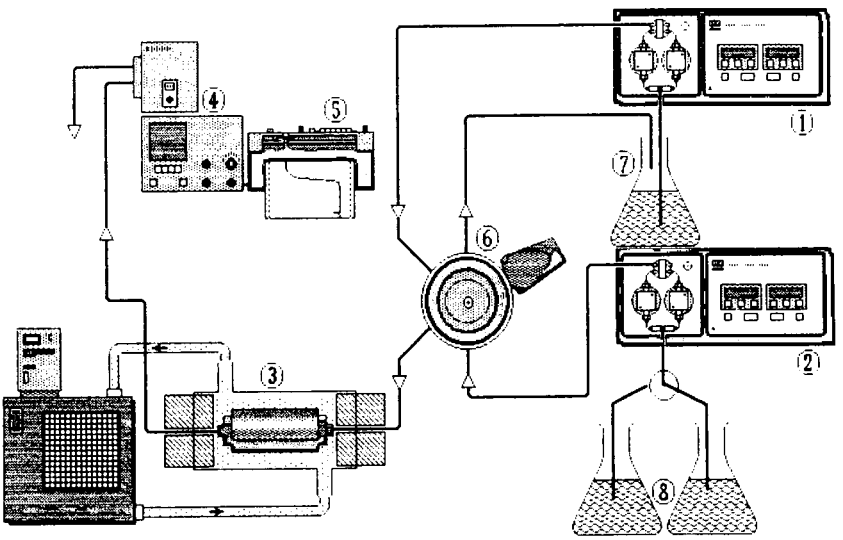

Fig. 1. High-performance liquid chromatography (HPLC) equipment used for frontal analysis experiments. 1 = Pump for the protein solution; 2 = pump for elution and washing buffer; 3 = thermostated column; 4 = UV detector; 5 = chart recorder; 6 = Rheodyne valve; 7 = protein solution; 8 = elution and washing buffer.

Each frontal analysis experiment consisted of three steps. In the first step, the protein solution was pumped through the column until all binding sites were saturated and a constant breakthrough plateau was achieved. In the second step, the protein bound to the column was eluted by adding a competitive ligand or a chaotropic salt to the mobile phase, or by changing the pH value. The elution conditions were designed to be as gentle as possible to retain the biological activity of the protein. In the third step, the column was washed with the reequilibration buffer to remove all components introduced during the elution step. The whole procedure was repeated as multiple replicates ($n > 4$) with the same and different protein concentrations.

Evaluation of the frontal analysis data

Frontal analysis is a method which can evaluate the accessible ligand concentration on the surface of a sorbent as well as the value of the association constant (K_a) between the ligand and the protein. To calculate the breakthrough volume, V_e, the following integral under the breakthrough curve has to be solved.

$$V_e = \frac{1}{M} \int_0^M V \, dm$$

where

M = initial adsorbate concentration
m = momentary adsorbate concentration at the column outlet
V = volume

The calculation of this integral was done numerically with an "in-house" programme written in Turbo-C for an IBM-compatible personal computer.

The association constant and the accessible ligand concentration were evaluated according to the methods of Nichol *et al.* [16]. The following expression was employed together with appropriate input values derived from the results of the frontal analysis experiments:

$$\frac{1}{V_e - V_0} = \frac{1}{V_0[L]K_a} + \frac{[A]}{V_e[L]}$$

where

V_e = breakthrough volume
V_0 = elution volume of the adsorbate without interaction
K_a = association constant of the adsorbate–ligand complex
[A] = average adsorbate concentration
[L] = accessible ligand concentration

This treatment assumes a first order dependency between the average adsorbate concentration and the reciprocal breakthrough volume. The value for V_0 was determined from the elution volume of non-retarded proteins and was found with the systems used in the present study to be independent of the protein concentration. With the knowledge of V_0 the accessible ligand concentration was then calculated from the slope of the dependency whilst the association constant, K_a, was evaluated from the y-axis intercept.

RESULTS AND DISCUSSION

Studies with the immobilized Cibacron Blue F3GA Nucleosil 300-5 system

Three experimental systems of different ligand density were examined with the surface-modified Nucleosil 300-5 support, namely a dye sorbent with maximal coverage equivalent to 1 μmole/m^2, and two dye sorbents with partial coverage of 0.1 and 0.01 μmole/m^2, respectively.

In the case where the porous Nucleosil 300-5 silica was modified with the maximum amount of Cibacron Blue F3GA, experimental breakthrough curves were obtained by using a loading buffer with and without 1 *M* NaCl added in order to examine the difference in protein–ligand interactions due to non-specific ionic effects and the effects due to specific biomimetic affinity interactions. The isotherms, corresponding to these experiments, are shown in Fig. 2. In case of the dye sorbents with ligand densities corresponding to 10% and 1% coverage only the loading buffer condition with 1 *M* NaCl added was used to accumulate data on the specific interactions. The adsorption isotherms for these experiments are shown in Figs. 3 and 4.

The values for the accessible ligand concentrations and the association constants for the lysozyme–Cibacron Blue F3GA interactions for these four different experimental conditions were calculated by methods adapted from Nichol *et al.* [16], and are listed in Table II. When 1 *M* sodium chloride was added to the loading buffer in case of the Nucleosil 300-5 dye sorbent with maximum ligand density, the accessible ligand concentration, *i.e.* the amount of immobilised dye ligands which are accessible to lysozyme and which determine the effective binding capacity, q_m, for this adsorbate–ligand system, was decreased by about 48% compared to the salt-free loading buffer condition. For the Nucleosil 300-5 dye sorbent with a ligand density of 0.1 μmole/m^2, it is noteworthy that the accessible ligand concentration increased by about 50% compared to the sorbent with 1 μmole/m^2 coverage although 1 *M* salt was again added to depress ionic interactions. With further decrease in ligand density to 0.01 μmole/m^2,

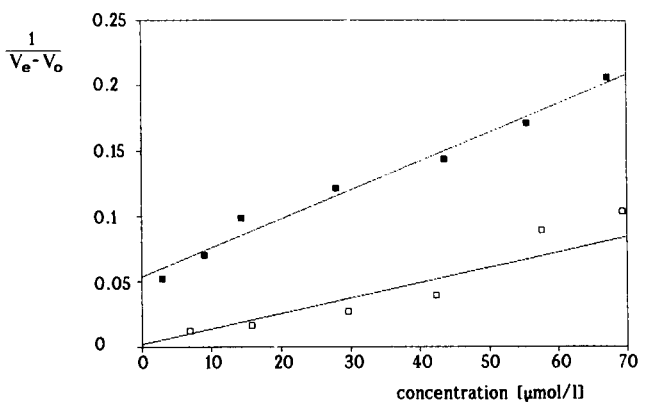

Fig. 2. Adsorption isotherm of lysozyme on Cibacron Blue F3GA-modified Nucleosil 300-5 with maximum ligand density. Mobile phases: □ = 0.1 *M* phosphate buffer pH = 7.9; ■ = 0.1 *M* phosphate buffer with 1 *M* NaCl.

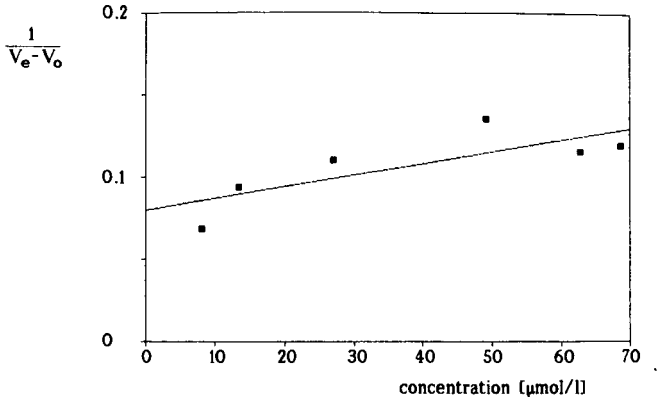

Fig. 3. Adsorption isotherm of lysozyme on Cibacron Blue F3GA-modified Nucleosil 300-5 with 0.1 μmol/m^2 ligand density. Mobile phase: 0.1 *M* phosphate buffer with 1 *M* NaCl.

the accessible ligand concentration and thus the capacity decreased as expected to *ca.* 12% of these initial values.

Studies with Cibacron Blue F3GA-immobilized 1.5 μm non-porous silica–lysozyme system

As in the preceeding experiments with the porous Nucleosil 300-5 support, the frontal analysis experiments were performed with the non-porous sorbents with and without 1 *M* sodium chloride added to the loading buffer and sorbents of varying ligand coverage ranging from maximum ligand density, equivalent to 1, 0.5, 0.2, 0.1 and 0.01 μmole/m^2. The adsorption isotherm of lysozyme on the support with 1 μmole/m^2 and a loading buffer without salt added is shown in Fig. 5. When 1 *M* salt was added to the loading buffer, no specific binding could be observed. By decreasing the ligand density to 0.5 μmol/m^2, the isotherms shown in Fig. 6 were obtained. Here

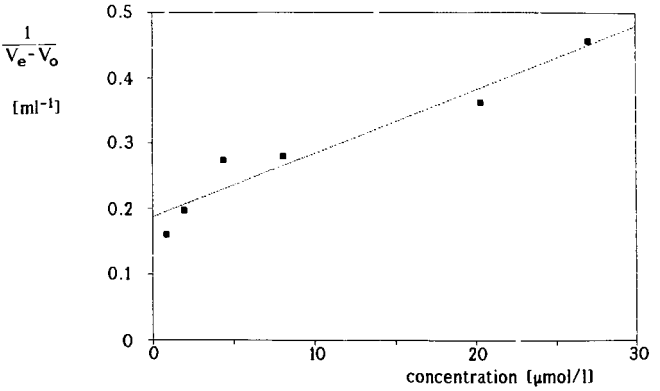

Fig. 4. Adsorption isotherm of lysozyme on Cibacron Blue F3GA-modified Nucleosil 300-5 with 0.01 μmol/m^2 ligand density. Mobile phase: 0.1 *M* phosphate buffer with 1 *M* NaCl.

TABLE II

ACCESSIBLE LIGAND CONCENTRATION AND ASSOCIATION CONSTANT OF CIBACRON BLUE-MODIFIED NUCLEOSIL 300-5 AND LYSOZYME AS SUBSTRATE

Ligand concentration[a] (μmol/m^2)	Accessible ligand concentration (μmol)	Association constant ($\cdot 10^7$ mol^{-1})
1	1.77 ± 0.41	36.3 ± 8.4
1	0.91 ± 0.11	4.2 ± 0.5
0.1	1.71 ± 0.41	1.5 ± 0.3
0.01	0.21 ± 0.04	5.2 ± 1.1

[a] Mobile phase: 0.1 *M* phosphate buffer pH 7.8 + 1 *M* sodium chloride.

the accessible ligand density was in the same range for both specific and non-specific interactions. In Fig. 7 the adsorption isotherms of lysozyme on Cibacron Blue F3GA-modified non-porous silica with a 0.2 μmol/m^2 ligand density is plotted. The upper curve corresponding to the frontal analysis experiments with 1 *M* NaCl added to the mobile phase, shows a non-ideal behaviour of adsorption.

In the frontal analysis experiments with the non-porous dye sorbent with a 0.1 μmole/m^2 ligand density only the loading buffer condition of 1 *M* NaCl was used. The adsorption isotherm for these experiments is shown in Fig. 8. The dye sorbent with 0.01 μmole/m^2 of Cibacron Blue F3GA bound to the silica surface showed a very low capacity. Because of the extremely small differences in the values between V_0 and V_e over the corresponding range of protein concentrations, not surprisingly, calculation of the association constant and the accessible ligand concentrations showed significant systematic experimental errors. Nevertheless, the trend of these data showed that the capacity decreased at these very low densities of dye ligands immobilised at the surface of the support, indicating that non-specific interactions with unreached thiol groups were not occurring.

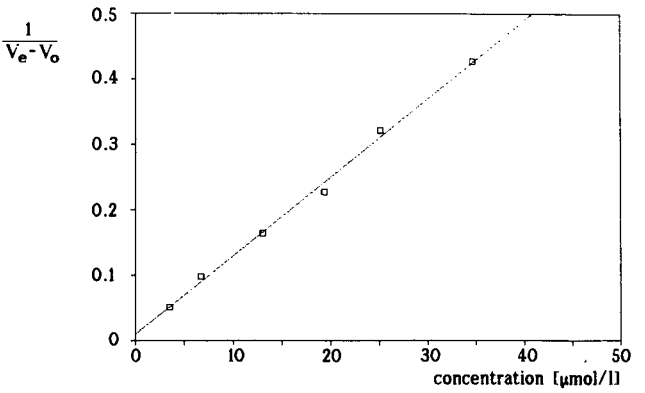

Fig. 5. Adsorption isotherm of lysozyme on Cibacron Blue F3GA-modified non-porous silica with maximum ligand density. Mobile phase: 0.1 *M* phosphate buffer pH 7.9 without salt added.

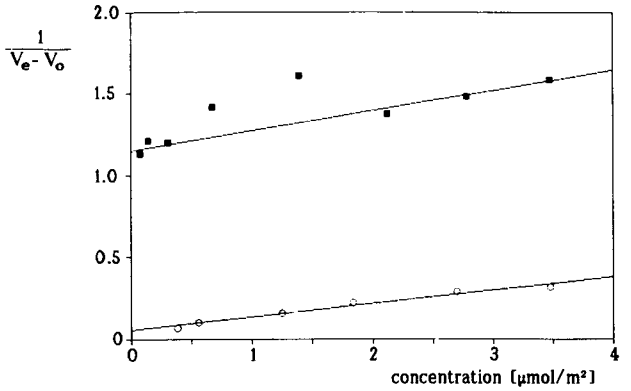

Fig. 6. Adsorption isotherm of lysozyme on 1.5 μm non-porous silica with 0.5 μmol/m² Cibacron Blue F3GA immobilized. Mobile phases: ■ = 0.1 *M* phosphate buffer pH 7.9; ○ = 0.1 *M* phosphate buffer pH 7.9 with 1 *M* NaCl.

Effects of accessible ligand density and ionic strength on association constants and kinetics

In Table III, the accessible ligand concentrations and association constants, calculated from the adsorption isotherms plotted in Figs. 5–8, are tabulated. These data in particular provided comparative information on the effect of high ionic strength conditions on the adsorption process.

The higher capacities, as revealed from the frontal analysis breakthrough curves and isotherm plots for the interaction of lysozyme with the Cibacron Blue F3GA dye sorbents when no salt was added to the loading buffer, reflect the interplay of (at least) three processes occurring during adsorption, namely (i) specific binding involving biomimetic interactions between the dye and unique structural regions of the protein, (ii) non-specific binding involving interaction of the protein to other classes of binding

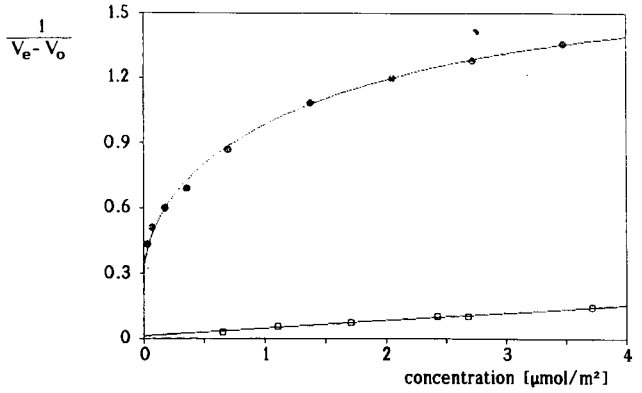

Fig. 7. Adsorption isotherm of lysozyme on 1.5 μm non-porous silica with 0.2 μmol/m² Cibacron Blue F3GA immobilized. Mobile phases: □ = 0.1 *M* phosphate buffer pH 7.9; ● = 0.1 *M* phosphate buffer pH 7.9 with 1 *M* NaCl.

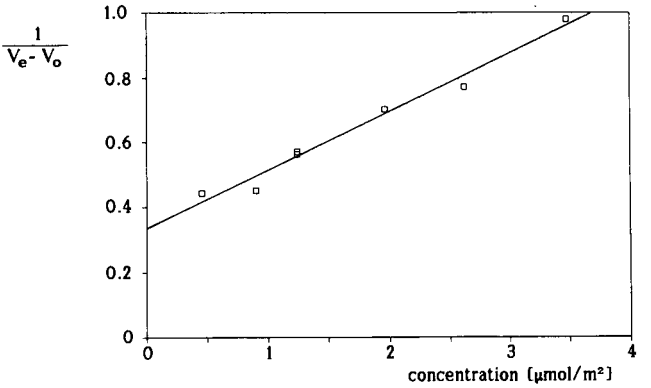

Fig. 8. Adsorption isotherm of lysozyme on 1.5 μm non-porous silica with 0.1 μmol/m^2 Cibacron Blue F3GA immobilized. Mobile phase: 0.1 *M* phosphate buffer pH 7.9 with 1 *M* NaCl.

sites on the sorbent, and (iii) protein–protein interactions involving conformational or aggregational effects. Protein–protein aggregation is usually interpreted in terms of hydrophobic interactions which increase with increasing ionic strength. Involvement of these hydrophobic effects leads to self-condensation and fractal network formation of proteins in the presence of high salt concentrations. Since a decrease in capacity was observed with increasing salt concentrations, it can be concluded that the origin of these differences in capacity with the low ionic strength loading conditions reside in coulombic, not hydrophobic, effects predominately associated with the silica surface itself. When these non-specific ionic interactions are depressed, the protein prefers to bind via its biomimetic site(s) to the dye ligand. These experimental data further indicate that the kinetics of adsorption become slower under conditions where, in relative terms, fewer of the ligands are utilised, *i.e.* the effective capacity decreases with dye sorbents when the ligand density is high due to steric hindrances.

The decrease in the adsorption kinetics when high salt concentrations are employed in the eluent is particularly evident when the breakthrough curves for the

TABLE III

ACCESSIBLE LIGAND CONCENTRATION AND ASSOCIATION CONSTANT CALCULATED FROM THE ADSORPTION ISOTHERMS USING THE NON-POROUS, 1.5 μm d_p SILICA AS SUPPORT

Ligand concentration (μmol/m^2)	Accessible ligand concentration (μmol)	Association constant ($\cdot 10^6$ mol^{-1})
1[b]	0.33 ± 0.02	1.33 ± 0.07
0.5[b]	0.043 ± 0.006	45.6 ± 6.8
0.5[a]	0.034 ± 0.003	0.10 ± 0.01
0.2[b]	0.11 ± 0.01	3.81 ± 0.6
0.2[a]	0.015 ± 0.002	0.46 ± 0.07
0.1[a]	0.023 ± 0.003	0.53 ± 0.06

[a] Mobile phase: 0.1 *M* phosphate buffer pH 7.8 + 1 *M* sodium chloride.
[b] Mobile phase: 0.1 *M* phosphate buffer pH 7.8.

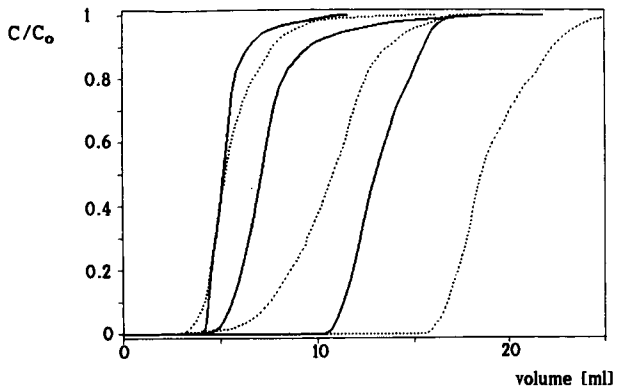

Fig. 9. Comparison of breakthrough curves with specific and non-specific interactions. Breakthrough curves are shown with specific interactions (·····) and ionic interactions (———) for the non-porous dye sorbents of ligand density 1 (right), 0.5 (middle) and 0.2 μmol/m² (left). C_0 = Inlet concentration; C = instantaneous concentration.

non-porous silica dye sorbents are compared for specific and non-specific binding. When no salt is added to the mobile phase, the slope of the breakthrough curve becomes substantially steeper (see Fig. 9). A reason for the slower kinetics for the specific binding when salt is present might be the requirement for the protein to undergo a re-orientation or minor conformational change during the binding step. Similar conformational changes have been documented [17,18] for enzyme–substrate binding, antibody–antigen interactions and protein–DNA interactions. This effect is not evident with the porous Nucleosil 300-5 silica sorbents. With these porous sorbents kinetic effects associated with protein transport within the porous structure ("pore" diffusion effects) are superimposed upon the adsorption kinetics. Pore diffusion restrictions represent [19] with these porous sorbents, the rate limiting step for binding with proteins with molecular weights larger than 20 000. The experimental data further confirm the requirement to minimise ligand crowding, *e.g.* surface space is needed for the protein to bind in an optimum way to the immobilised dye. Similar results have been reported [11] for immunoaffinity sorbents. The fact that the value of the association constant increases with decreasing ligand density (see Fig. 10), suggests

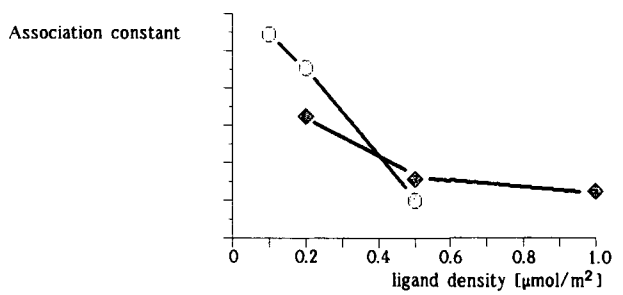

Fig. 10. Relation between the ligand density and the association rate constant with the 1.5-μm non-porous silica modified with Cibacron Blue F3GA. Mobile phase: 0.1 *M* phosphate buffer with 1 *M* NaCl added (◆) and without salt added (○).

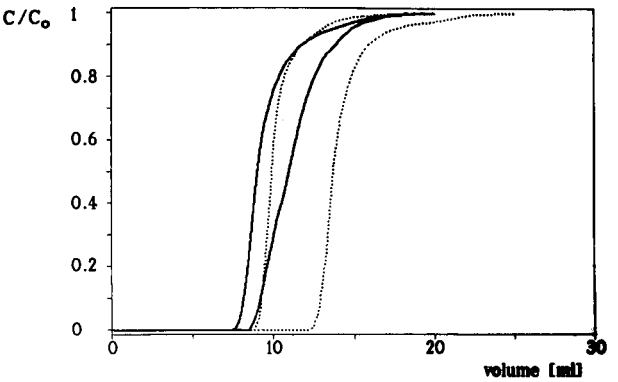

Fig. 11. Comparison of breakthrough curves on porous and non-porous supports. Breakthrough curves are shown for the non-porous (·····) and porous supports (———) eluted with a mobile phase of 0.1 *M* phosphate buffer containing 1 *M* NaCl (right) or without 1 *M* NaCl (left). C_0 = Inlet concentration; C = instantaneous concentration.

that as more space is made available for the protein to bind, in general, the stronger will become the association between the adsorbate and ligand.

Another result evident from these studies is the advantage in using a non-porous compared to a porous silica support for very rapid ultramicroanalytical dye affinity separations. This advantage is easily seen, when the breakthrough curves using the non-porous silica are compared with those using the porous silica (see Fig. 11). When the non-porous silica sorbents were used, the breakthrough curves were much steeper, indicative of faster overall binding kinetics, compared to the corresponding porous silica, whilst all other experimental condition remain unchanged. Although the present study has examined the adsorption behaviour of only a single protein —hen eggwhite lysozyme— similar trends have been observed [10,12] with other proteins and multicomponent protein mixtures in analogous dye affinity systems. These results highlight further the necessity to discriminate the factors which contribute to the adsorption rate. For example, kinetics effects due to additional mass transport mechanisms are operating when a porous support is used, with the kinetic effects due to adsorption often overwhelmed by the mass transfer effects due to pore diffusion. Procedures to discriminate the contributions from film, pore and adsorption transport effects have been reviewed [19] recently. As also noted previously [8–11], and confirmed in this study, examination of the relationship between ligand density and the effective capacity of a sorbent is necessary to optimize an affinity system. This requirement has been found to be especially important when expensive ligands, *e.g.* monoclonal antibodies, are used in biospecific affinity chromatography [11].

ACKNOWLEDGEMENTS

These investigations were supported by Grants from the Australian Research Council and the Monash University Research Excellence Committee.

REFERENCES

1 P. O. Larsson, *Methods Enzymol.*, 104 (1984) 212.
2 J. Turkova, K. Blaha and K. Adamamova, *J. Chromatogr.*, 236 (1982) 375.
3 R. R. Walters, *J. Chromatogr.*, 249 (1982) 19.
4 M. T. W. Hearn, *Methods Enzymol.*, 135 (1987) 102.
5 K. Nilsson and K. Mosbach, *Methods Enzymol.*, 135 (1987) 65.
6 F. B. Anspach, H. J. Wirth, K. K. Unger, P. Stanton, J. R. Davies and M. T. W. Hearn, *Anal. Biochem.*, 179 (1989) 171.
7 F. B. Anspach, A. Johnston, H. J. Wirth, K. K. Unger and M. T. W. Hearn, *J. Chromatogr.*, 476 (1989) 205.
8 T. Miron and M. Wilchek, *Methods Enzymol.*, 135 (1987) 84.
9 A. I. Liapais, B. Anspach, M. E. Findley, J. Davies, K. K. Unger and M. T. W. Hearn, *Biotech. Bioengin.*, 34 (1989) 467.
10 M. T. W. Hearn, Q. Mao and A. Johnston, submitted for publication.
11 M. T. W. Hearn and J. D. Davies, *J. Chromatogr.*, 512 (1990) 23.
12 A. Johnston and M. T. W. Hearn, *J. Chromatogr.*, 512 (1990) 101.
13 J. Jacobsen, J. Frenz and Cs. Horváth, *J. Chromatogr.*, 316 (1984) 53.
14 K. I. Kasai, Y. Oda, M. Nishikata and S. I. Ishii, *J. Chromatogr.*, 376 (1986) 33.
15 G. Jilge, R. Janzen, K. K. Unger, J. N. Kinkel and M. T. W. Hearn, *J. Chromatogr.*, 397 (1987) 71.
16 L. W. Nichol, A. G. Ogsten, D. J. Winzor and W. H. Sawyer, *Biochem. J.*, 143 (1974) 435.
17 W. F. DeGrado, *Adv. Protein Chem.*, 39 (1988) 51.
18 D. M. Brems and H. A. Havel, *Proteins*, 5 (1989) 93.
19 A. Johnston, Q. M. Mao and M. T. W. Hearn, *J. Chromatogr.*, 548 (1991) 127.
20 R. Janzen, K. K. Unger, W. Muller and M. T. W. Hearn, *J. Chromatogr.*, 520 (1991) 77–93.

Journal of Chromatography, 550 (1991) 397–410
Elsevier Science Publishers B.V., Amsterdam

CHROMSYMP. 2347

Multivariate characterization of solvent strength and solvent selectivity in reversed-phase high-performance liquid chromatography

P. M. J. COENEGRACHT*, A. K. SMILDE, H. BENAK, C. H. P. BRUINS, H. J. METTING, H. DE VRIES and D. A. DOORNBOS

Chemometrics Research Group, University Centre for Pharmacy, A. Deusinglaan 2, NL-9713 AW Groningen (Netherlands)

ABSTRACT

Principal component analysis was used to determine the dimensionality and structure of three data sets consisting of the capacity factors of eleven to twenty different solutes measured in nine different mobile phase compositions consisting of water and methanol and/or acetonitrile on three reversed-phase columns. Principal component analysis showed that two principal components could account for the total variance in the data and that the percentage variance explained by the first principal component (about 80–95%) was much greater than the percentage explained by the second principal component, but that the percentage depended strongly on the choice of solutes for the sample. The first principal component could be associated with solvent strength and solvent strength selectivity and the second principal component with modifier selectivity. Solutes that showed strong modifier selectivity could be distinguished from solutes that have almost zero modifier selectivity, which could be useful for the definition of an empirical solvent strength scale.

INTRODUCTION

Solvent strength and selectivity

In reversed-phase (RP) chromatography strong interactions occur between the polar mobile phase and the molecules of the sample. The mobile phase consists of water and one to three organic solvents or modifiers. Solvent properties have been classified by Snyder [1] in terms of solvent polarity and selective interactions.

The eluting power of the mobile phase in RP chromatography depends on the strength of the pure organic solvent, which is related to the coefficient S by the following equation:

$$\log k' = \log k_w - S\varphi \quad (1)$$

Here k_w refers to the isocratic capacity factor (k') of the solute for pure water as the mobile phase and φ is the volume fraction of organic modifier in the binary mobile phase [2]. S is a constant which is not only characteristic of a given modifier, but

0021-9673/91/$03.50

depends also on the molecular size and structure of the solute [3]. Eqn. 1 is applicable for a limited range of k' values ($1 < k' < 10$), and S values also depend on the RP packing material [4]. For typical samples consisting of benzene derivatives, the average variation of S was considered small enough to assign an unique solvent strength value to a given solvent [4]. This approach makes it possible to calculate the composition of iso-eluotropic mobile phases consisting of water and different organic modifiers using transfer rules [5,6]. These rules allow the substitution of one organic solvent for another, whereas the sample k' values remain roughly constant.

This substitution changes the selectivity of the mobile phase and exploits the ability of a solvent to exhibit different selective interactions with different solutes to separate solutes of a similar polarity [7].

"The strength of a mobile phase is a major factor in controlling the retention and is a function of its quantitative composition, *i.e.* the water-to-modifier ratio, but the selectivity depends on its qualitative composition, *i.e.* the type of modifier" [8]. Descriptions of this kind and statements that it is possible to change the ratio of the carrier (water) to organic modifier with the net result that the strength of the mobile phase changes while the selectivity remains constant [5], treat the solvent strength and solvent selectivity as two independent properties of the mobile phase. Changing the solvent strength would alter the capacity factors of all the solutes of a sample but not effect the ratios of the capacity factors of the solutes so that the relative peak positions in the chromatogram would remain the same. This would mean that strength is a solvent property that has an equally strong proportional effect on all solutes and is therefore almost independent of the individual solute properties, while selectivity depends on solvent–solute interactions that also depend on the properties of the solute.

It has been shown, however, that if the water fraction of a binary, ternary or quaternary mobile phase changes, not only the strength, but also the selectivity changes [9]. The simultaneous variation of selectivity and strength is the basis of the solvent strength selectivity optimization of binary systems according to Snyder *et al.* [10] and was realized in a ternary solvent system by the combination of a statistical mixture design technique and multicriteria decision making [11].

The solvent strength concept stresses that the fraction of water in an eluent determines the range of the capacity factors of all the solutes of a sample. The solvent selectivity alters to a lesser degree the capacity factors of the individual solutes and does not significantly change the range of the capacity factors.

The empirical transfer rules for calculating the iso-eluotropic mobile phase compositions are based on retention data collected for a large number of solutes at different mobile phase compositions. The transfer rules are found by regression analysis [12] and represent an averaged solute retention behaviour. The selectivity refers to the deviation of a given solute from the average retention behaviour. This means that a good transfer rule should depend on a representative sample, *i.e.* a sample consisting of solutes that contribute equally to different selective interactions.

This paper describes the use of principal component analysis (PCA) for the determination of the number of uncorrelated factors (dimensions) that account for the total variation in the retention data of solutes in different mobile phase compositions. In addition, the contribution of each factor to the total variation is estimated and this is related to the solute composition of the sample and the selective interac-

tions of each solute. This allows an approximately quantitative estimate of the effect of solvent strength and modifier selectivity and indicated a method for the choice of solutes which are a good measure of "pure" solvent strength.

Principal component analysis

PCA constructs linear combinations of the original variables that account for as much of the total variation in the data as possible. The successive linear combinations are not correlated with each other and account for successively smaller amounts of variation. The principal components are the basic dimensions of the data necessary to define their total variance [13].

Mobile phases composed of water and methanol (MeOH) and/or acetonitrile (ACN) with different ratios of water and modifier(s) are characterized chromatographically by differences in solvent strength and selectivity. These differences can be measured by the capacity factors of the sample solutes, *i.e.*, the mobile phases are the objects and the solutes are the variables of the data matrix.

If solvent strength and solvent selectivity are different properties of the objects, then PCA should reveal at least two dimensions in the data. That is, PC1 is that linear combination of the observed variables $X_j, j = 1, 2, ..., p$

$$PC1 = wl_1X_1 + wl_2X_2 + ...wl_pX_p \quad (2)$$

where the loadings wl_1, wl_2, $...wl_p$ have been chosen to maximize the ratio of the variance of PC1 to the total variation. Component loading wl_i is a measure of the contribution of the ith variable to PC1; it measures the contribution of the ith solute to the variance explained by PC1.

The second principal component, PC2, is that weighted linear combination of the variables which is not correlated to the first PC1 and which accounts for the maximum amount of the remaining total variation. The goal of PCA is to account for most of the total variation with as few principal components as possible [13].

The principal components are statistical descriptors and do not represent physical properties, but they can be used to test hypotheses about qualitative distinctions in the data. PCA was used for the classification and selectivity characterization of different RP high-performance liquid chromatography (HPLC) packings [14–17], but not for the characterization of the strength and selectivity of RP mobile phases.

EXPERIMENTAL

General set-up

Three data matrices were investigated. The choice of the mobile phase compositions was made according to a constrained mixture design. The design aims at a regular spread of the design points in a constrained area of design space [18]. The first data matrix consisted of nine mobile phases. The solvent strength was varied at three levels and at each level two different binary and one ternary mobile phase were composed of water, MeOH and /or ACN (Fig. 1). Fifteen solutes were used to characterize the nine objects (Table I).

The second data matrix consisted of eight mobile phases. The solvent strength

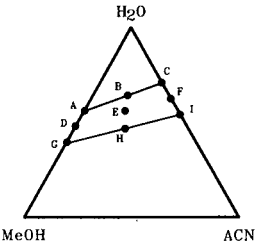

Fig. 1. Design points corresponding to the mobile phase compositions A–I of Table I.

was varied at two levels (Fig. 2). At each level the solvent strength was kept constant by experimental adjustment of the eluent composition so that the variation of the mean capacity factor of the sample solutes was smaller than 5%. At each level two different binary and two different ternary mobile phases were composed of water, MeOH and ACN (Table II). The eleven solutes used were essentially a subset of the previous sample, but an octadecylsilane (ODS) column of a different brand was used. The third data matrix was published by Weyland [19] and consisted of four binary eluents of water and MeOH, three binary eluents of water and ACN and two ternary

TABLE I

MOBILE PHASE COMPOSITIONS AT THE DESIGN POINTS A–I AND MEASURED CAPACITY FACTORS OF THE SOLUTES

Mobile phase component	A	B	C	D	E	F	G	H	I
Water	0.550	0.625	0.700	0.467	0.541	0.617	0.383	0.459	0.533
Methanol	0.450	0.225	0.000	0.533	0.267	0.000	0.617	0.308	0.000
Acetonitrile	0.000	0.150	0.300	0.000	0.192	0.383	0.000	0.233	0.467
Solute	Capacity factor								
Acetophenone (ACP)	2.747	3.960	4.030	1.534	2.237	2.437	0.910	1.262	1.692
Acetanilide (ACT)	1.145	1.450	1.111	0.683	0.871	0.729	0.435	0.525	0.571
Anisole (ANS)	5.912	8.147	9.606	3.316	4.722	5.406	1.970	2.515	3.373
p-Cresol (CRE)	2.815	3.950	3.424	1.574	2.178	2.000	0.920	1.202	1.373
Ethylaminobenzoate (EAB)	2.640	4.245	4.121	1.356	2.158	2.229	0.702	1.101	1.439
Nitrobenzene (NBZ)	3.650	5.999	7.444	2.118	3.425	4.218	1.267	1.868	2.681
Toluene (TOL)	14.213	19.735	21.909	7.683	10.237	11.218	4.198	5.090	6.395
2-Phenylethanol (PE)	2.368	2.754	1.848	1.346	1.534	1.156	0.782	0.888	0.868
Propylhydroxybenzoate (PHB)	11.038	15.147	10.090	4.722	6.445	4.343	2.217	2.818	2.395
Ethylhydroxybenzoate (EHB)	4.689	6.254	4.454	2.227	2.990	2.250	1.148	1.464	1.406
Methylhydroxybenzoate (MHB)	2.126	2.764	2.151	1.108	1.465	1.239	0.623	0.797	0.868
Dimethylphthalate (DMP)	3.310	5.745	5.414	1.603	2.811	2.947	0.851	1.454	1.890
Phenobarbital (PBL)	1.980	2.960	1.747	1.009	1.495	1.072	0.544	0.757	0.747
Prednisone (PRE)	5.592	7.058	2.242	2.158	2.653	0.947	0.960	1.181	0.593
Prednisolone (PRS)	8.213	8.343	2.060	3.227	3.217	0.812	1.465	1.414	0.505
Mean	4.830	6.568	5.444	2.378	3.230	2.867	1.267	1.623	1.787

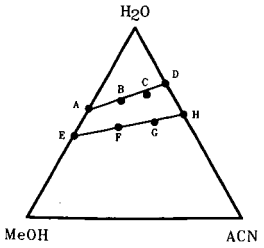

Fig. 2. Design points corresponding to the mobile phase compositions A–H of Table II.

eluents with the same modifiers. The retention times of the sample solutes, twenty sulphonamides (*p*-aminobenzoic acid analogues, Table III), were measured on a 15.0 cm × 4.6 mm stainless-steel column packed with Nucleosil C_8, particle size 5 μm.

Measurements were collected as k' values and transformed to ln k' values to obtain a constant variance of the data. The ln k' data matrix was transformed to a covariance matrix prior to PCA. Standardization was not performed because the variables are measured in the same ln k' units.

Instrumentation and chemicals

The experiments for the first data set were performed on an HPLC apparatus consisting of an automatic sampler (KA 9209, sample loop 20 μl), a solvent delivery system (KA 9208), a fixed-wavelength UV detector (KA 9202, 254 nm) and a Model B40 Kipp recorder. Stainless-steel columns, 15 cm × 4.6 mm I.D., slurry-packed with ODS Hypersil, 5 μm particle diameter, number of plates (N) = 8000 (fluoranthene in

TABLE II

MOBILE PHASE COMPOSITIONS AT THE DESIGN POINTS A–H AND MEASURED CAPACITY FACTORS OF THE SOLUTES

Mobile phase component	A	B	C	D	E	F	G	H
Water	0.560	0.590	0.640	0.700	0.420	0.460	0.490	0.540
Methanol	0.440	0.310	0.150	0.000	0.580	0.380	0.200	0.000
Acetonitrile	0.000	0.100	0.210	0.300	0.000	0.160	0.310	0.460
Solute	Capacity factor							
Acetophenone (ACP)	2.431	2.730	2.984	3.262	0.983	1.031	1.186	1.316
Acetanilide (ACT)	0.891	1.065	0.969	0.958	0.454	0.442	0.447	0.443
Aniline (AN)	1.431	1.425	1.328	1.847	0.593	0.578	0.707	0.860
p-Cresol (CRE)	2.492	2.835	2.738	2.836	1.000	1.094	1.103	1.053
Ethylaminobenzoate (EAB)	1.977	2.708	3.008	3.258	0.731	0.884	1.009	1.070
Nitrobenzene (NBZ)	3.023	3.957	4.953	6.067	1.403	1.558	1.825	2.035
Toluene (TOL)	13.538	14.357	15.308	18.607	5.085	4.800	5.190	5.193
2-Phenylethanol (PE)	2.094	2.108	1.828	1.574	0.850	0.813	0.772	0.667
Propylhydroxybenzoate (PHB)	9.453	10.258	9.297	7.656	2.417	2.620	2.368	1.789
Phenobarbital (PBL)	1.662	1.966	1.708	1.459	0.567	0.625	0.627	0.526
Prednisolone (PRS)	7.369	6.942	3.531	1.557	1.600	1.516	0.847	0.386
Mean	4.353	4.683	4.400	4.462	1.457	1.470	1.505	1.481

TABLE III

MOBILE PHASE COMPOSITIONS AT THE DESIGN POINTS A-I AND MEASURED CAPACITY FACTORS OF THE SOLUTES

Mobile phase component	A	B	C	D	E	F	G	H	I
Water	0.80	0.75	0.70	0.60	0.90	0.80	0.70	0.70	0.80
Methanol	0.20	0.25	0.30	0.40	0.00	0.00	0.00	0.15	0.10
Acetonitrile	0.00	0.00	0.00	0.00	0.10	0.20	0.30	0.15	0.10
Solute	Capacity factor								
Sulphanilamide	0.41	0.32	0.24	0.15	0.52	0.38	0.32	0.36	0.51
Sulphacetamide	1.54	1.12	0.81	0.43	1.97	0.95	0.59	0.80	1.44
Sulphapyridine	3.19	2.18	1.40	0.69	3.41	1.31	0.71	1.11	2.27
Sulphadiazine	2.76	1.92	1.26	0.62	3.00	1.25	0.69	1.02	2.06
Sulphamerazine	4.31	3.01	1.87	0.92	4.41	1.71	0.93	1.40	2.92
Sulphadimidine	5.94	4.14	2.52	1.19	5.98	2.02	1.07	1.72	3.76
Sulphamethoxydiazine	6.85	4.68	2.78	1.23	8.40	2.83	1.31	1.94	4.71
Sulphisomidine	1.75	1.24	0.73	0.33	1.87	0.51	0.21	0.50	1.19
Sulphadimethoxine	37.78	21.98	12.51	4.37	45.64	10.35	3.57	6.51	20.77
Sulphametopyrazine	8.16	5.71	3.44	1.52	10.02	3.29	1.57	2.36	5.65
Sulphamethoxypyridazine	6.54	4.56	2.78	1.20	7.27	2.32	1.07	1.79	4.26
Sulphathiazole	3.13	2.39	1.35	0.60	3.81	1.28	0.60	0.99	2.32
Succinylsulphathiazole	8.47	5.29	2.73	1.03	8.96	1.63	0.52	1.41	4.32
Phthalylsulphathiazole	27.83	15.05	8.15	2.53	34.36	5.28	1.58	3.84	13.72
Sulphafurazole	11.41	7.44	4.50	1.75	19.28	6.33	2.66	3.70	9.55
Sulphaguanidine	0.33	0.26	0.18	0.09	0.34	0.17	0.06	0.19	0.34
Sulphamethylthiodiazole	6.41	4.24	2.76	1.12	7.65	2.39	1.09	1.79	4.18
5-Methylsulphadiazine	5.71	3.87	2.50	1.08	6.44	2.35	1.21	1.76	3.84
Sulphaphenazole	26.16	13.99	8.86	3.04	44.84	12.02	4.34	6.34	19.17
Sulphamoxole	5.18	3.58	2.15	0.90	5.66	1.71	0.80	1.39	3.28

water–ACN = 3:1) were used. The mobile phase flow-rate was 1 ml/min. The dead time was measured by the injection of uracil. The capacity factors were calculated from at least duplicate injections. The reproducibility was estimated by three repetitions of all measurements at one mobile phase composition regularly spaced in the mobile phase series. The mean relative standard deviation of all retention times was 2.74%. Data sampling was performed by a Digital Minc 11 minicomputer and in-house developed software (SIP). The test solutes were used as purchased (Merck, Darmstadt, Germany, "zur Synthese"). MeOH was of analytical-reagent grade and ACN was of chromatographic quality.

The experiments for the second data matrix were performed with a Waters 6000A HPLC pump, a Shimadzu SPD-6a UV detector and an injection loop of 10 μl. Glass columns, 10 cm × 3.0 mm I.D., filled with Chromspher C_{18}, 5 μm particle diameter, were used. The mobile phase flow-rate was 0.5 ml/min. The dead time was measured by the injection of uracil. The capacity factors are usually the result of one measurement of the retention time. To estimate the repeatability, the retention times of three solutes were measured twice at every mobile phase composition. The relative standard deviation of the capacity factor was 2.4%. The reproducibility was estimated by three repetitions of all measurements at one mobile phase composition regu-

larly spaced in the mobile phase series. The mean relative standard deviation of all the capacity factors was 4.75%. Data sampling was performed by an Olivetti M24 personal computer and in-house developed software (CODA). The test solutes and chemicals were of the same quality as for the first data set.

Software

The calculations were performed on an IBM-compatible AT personal computer with a mathematical co-processor using the Unscrambler program (Camo, Norway) for PCA and the in-house developed POEM (predicting optimal eluent mixtures) package for response surface modelling by multiple linear regression and statistical model validation.

RESULTS AND DISCUSSION

First data set

The fifteen solutes of he first sample consisted of twelve benzene derivatives of different functionality often used in studies of solvent strength and selectivity [2,3,6,12], of which three formed a homologous series of increasing hydrophobicity, *i.e.* MHB, EHB and PHB (for abbreviations see Table I). The remaining three solutes were phenobarbital, PBL, and two larger molecules, the steroids PRE and PRS.

The mobile phases of the design were selected so that the capacity factors of the solutes would lie in the range 0.5–20. The solvent strength of the mobile phases A, B and C is about 1.0, of the mobile phases D, E and F 1.3, and of mobile phases G, H and I 1.5 (according to the transfer rules of Glajch and Kirkland [5]) with relative standard deviations of 11.4, 7.4 and 4.9% at each solvent strength level (Fig. 1). The capacity factors of the fifteen solutes measured at the nine mobile phase compositions are given in Table I.

The results of the PCA of these data are shown in Fig. 3a and b. The first PC accounts for 82% of the variance of the data and the second PC for 17%. This means that, given a repeatability of about 1.4% and a reproducibility of 2.74%, two principal components are sufficient to account for the variation in the data and the data have two intrinsic dimensions that are not correlated.

Parallel to PC1 in the scores plot (Fig. 3a) are three groups of mobile phase compositions for which the solvent strength decreases from left to right: G, D, A; H, E, B; and I, F, C. The water-to-modifier ratio increases in each group in the aforesaid sequence (Fig. 1) and in each group the mean capacity factor of all solutes in a given mobile phase composition increases in the same order (Table I). The mobile phase composition G has the lowest mean k' value of 1.27 and mobile phase A has the highest mean k' value of 4.83 in the first group. Therefore PC1 can be associated with a varying water fraction of the mobile phase and with a change of the mean k', *i.e.* a change in solvent strength. The scale of PC1 units does not, however, correspond quantitatively with the values of the mean k': the distance between mobile phases G and A is five PC1 units (Fig. 3a) and corresponds with a difference of 3.56 mean k' units, while for mobile phases H and B a distance of about 5.2 in PC1 units corresponds with 4.95 units of the mean k'.

Parallel to PC2 the modifier type of the mobile phases changes; mobile phases G, D and A are composed of MeOH and water and mobile phases I, F and C of ACN

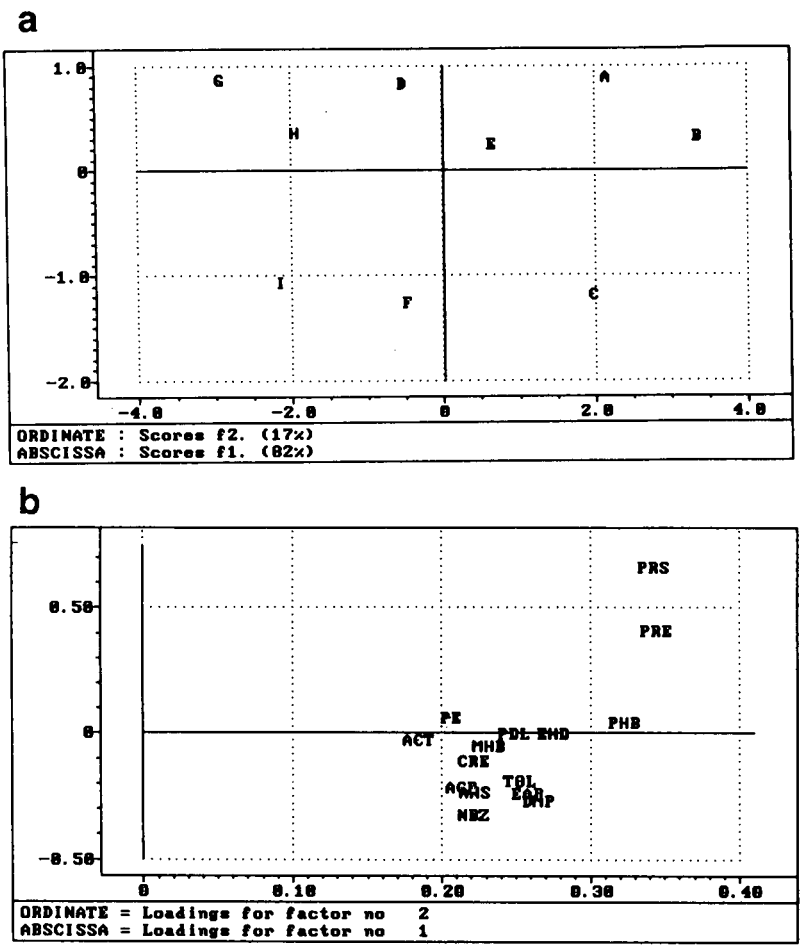

Fig. 3. (a) Scores and (b) loadings on the first two principal component axes of the data of Table I.

and water. The ternary mobile phases H, E and B contain about 40% more MeOH than ACN and are found above the PC1 axis, which does not lie in the middle between the group of MeOH-containing mobile phases (G, D, A) and the ACN-containing groups (I, F, C). This means that PC2 is associated with the substitution of ACN by MeOH, but that the magnitude of this substitution in percentages by volume is not linearly proportional to units of the PC2 axis. In addition, the units of the PC2 axis cannot be related to a change of mean k' values. The respective mean k' values of mobile phases G, D and A are 1.27, 2.38 and 4.83, and these different values all project onto the same point, about 0.8, on the PC2 axis. The same argument applies to mobile phases of the groups H, E, B and I, F, C that project different mean k' values for each group on to the points 0.3 and -1.2 of the PC2 axis, respectively. This means that along the PC2 axis a source of variation in the capacity factors is described that is not related to an increase or decrease of the mean k' value of all the

solutes in a given mobile phase, but to a variation of the capacity factor of the individual solutes. These observations indicate that PC2 can be related to modifier selectivity.

The plot of loadings (Fig. 3b) shows that ACT contributes the least to PC1 and that the loadings of PHB, PRE and PRS are highest on PC1. This means that the k' of ACT changes less along the PC1 axis, while the k' of PHB changes the most. ACT is compared with PHB and not with PRE and PRS, because these latter compounds also have high loadings on PC2. If the change in capacity factor of ACT is compared with the change in the capacity factor of PHB when the solvent strength is decreased, then the k' of ACT increases by 263% and the k' of PHB increases by 498% on going from mobile phase G to A. On going from mobile phase I to C the corresponding increase of k' is 195% for ACT and 421% for PHB. An increase of the water fraction (Table I, Fig. 1) decreases the solvent strength of the binary mobile phase and should cause a proportionally equal increase of k' for all solutes. The difference in the degree of change of k' between ACT and PHB for the same change in solvent strength can be called a solvent strength selectivity effect. This difference is not caused by modifier selectivity, because the modifier type remains the same. Both compounds also have low loadings on PC2, which represents the modifier selectivity.

The compounds MHB, EHB and PHB form a homologous series of increasing hydrophobicity. Their loadings on PC1 increase and this was reflected by a corresponding increase of their log k_w values, that were calculated from eqn. 1 using their capacity factors in water–MeOH (A, D, G) and in water–ACN (C, F, I) mobile phases, respectively. Their positions in Fig. 3b lie on a line that forms a small angle with PC1, which means that the PC1 axis problaby represents not pure hydrophobicity, but has a strong correlation with hydrophobicity. NBZ and PRS have the lowest and highest loading on PC2, respectively. This will be discussed in the next section.

Second and third data sets

In the second data set (Table II) anisole (ANS) was replaced by aniline (AN), MHB, EHB and PRE were omitted and a different brand of ODS packing material was used.

The solvent strength was adjusted at two levels (Fig. 2). The mean capacity factor of the solutes was used as a measure to adjust the solvent strength. Iso-eluotropic mobile phases have equal mean k' values according to this definition. At the first level the relative standard deviation of the mean capacity factors of all solutes measured in mobile phases A, B, C and D is 3.27%. At the second level the relative standard deviation is 1.40% among the mobile phases for the mean k' of all solutes measured in mobile phases E, F, G and H. The purposes of this experiment were firstly to see if the results obtained with the first data set could be confirmed on another packing material. The second purpose was to investigate whether the experimental adjustment of the composition of the mobile phases, to give an approximately constant mean k' value at each level of solvent strength, would lead to a better correspondence of PC1 with differences in the mean k'. Stated differently: do the scores on the PC1 axis quantitatively represent solvent strength values defined by the mean k' of all solutes measured in a given mobile phase composition?

From the scores plot (Fig. 4a) it can be concluded that this is not the case. The mean score of the mobile phases with the lower solvent strength (A, B, C, D) is 1.75

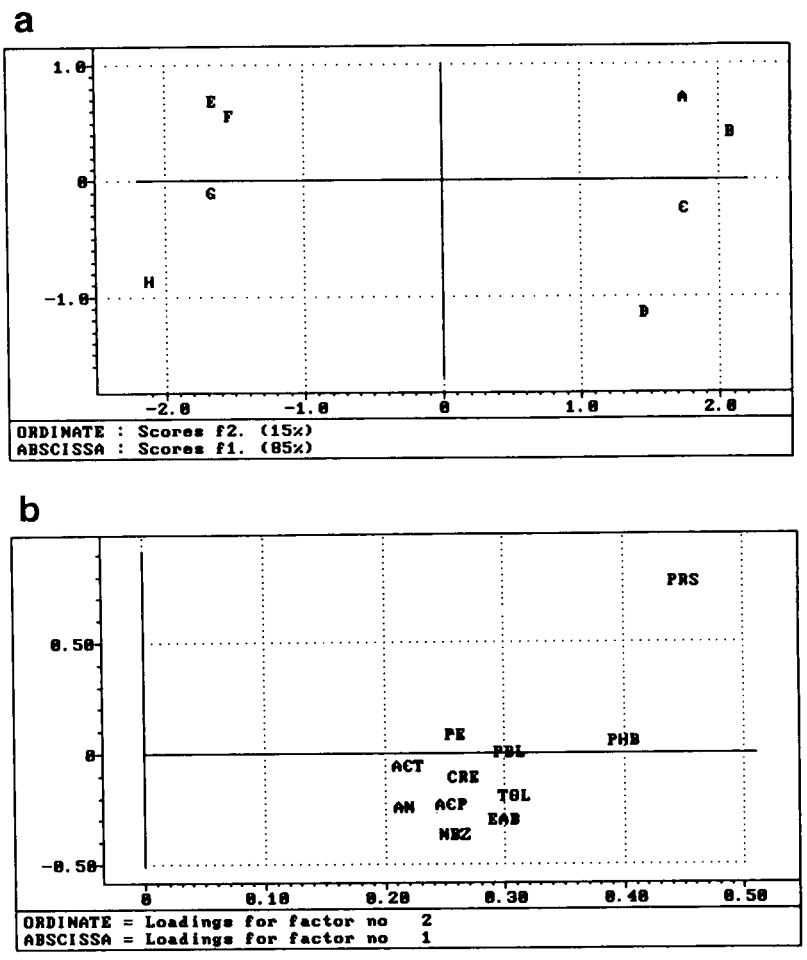

Fig. 4. (a) Scores (b) loadings on the first two principal component axes of the data of Table II.

on PC1 and the overall mean k' is 4.47; the mean score of the mobile phases E, F, G and H is -1.75 and their mean k' is 1.48. So a distance of 3.5 PC1 units corresponds to a difference of 2.99 mean k' units. This confirms that the PC1 axis can be associated with increasing mean k' values of the mobile phases. The difference in mean k' of mobile phases H and G is only 0.01 k units, but the corresponding distance in PC1 units is 0.46. This means that the PC1 scale does not correspond quantitatively with a mean k' scale and does not correspond exactly to the solvent strength defined by the mean k' of a sample. The reason is that variations in k' of the individual solutes due to selectivity effects also contribute to the mean k' value, but the variance explained by the PC1 axis is not confounded by modifier effects because they are associated with the PC2 axis.

This hypothesis is corroborated by the fact that compared with the first data set PC1 now accounts for 85% of the variance of the data and PC2 for 15%. The main

difference between the first and second data set is the presence of PRE in the first data set (see Figs. 3b and 4b), because the other solutes that have been changed have smaller loadings. By removing PRE from the data set, which has a high loading on PC2 (Fig. 3b) and is very sensitive to a change of modifier type, the variance accounted for by PC2 decreases from 17 to 15%. An even stronger confirmation can be obtained by performing a new PCA on the second data set after the removal of PRS, the solute of this data set that has the highest loading on PC2 (Fig. 4b). The results of the PCA of the data after the removal of PRS are shown in Fig. 5. The scores plot (Fig. 5a) again shows two groups of mobile phases with different solvent strength. The loadings plot (Fig. 5b) shows that the relative positions of the remaining solutes are similar to those of Fig. 4b. (The sign reversal of PC2 is irrelevant for this analysis). The variance accounted for by PC1 has been increased to 94%, whereas the variance explained by PC2 has been decreased to 5%.

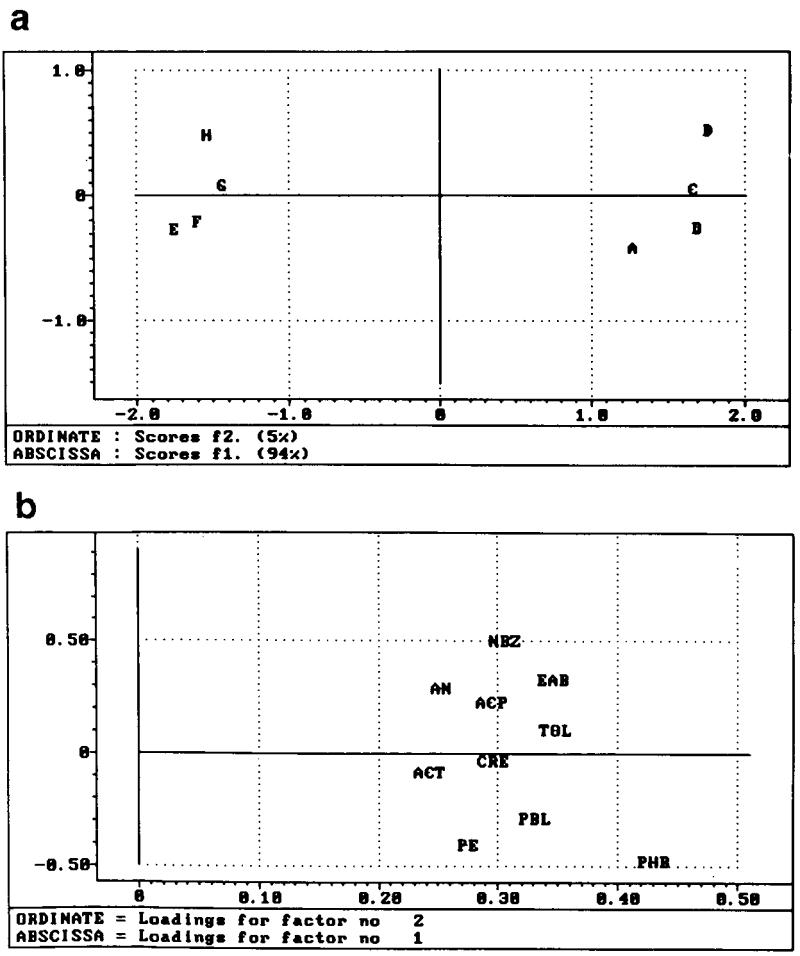

Fig. 5. (a) Scores and (b) loadings on the first two principal component axes of the data of Table II after removal of prednisolone.

This also shows that the amount of variation that is accounted for by each PC strongly depends on the selection of the variables or solutes. To obtain another impression of these amounts a third data set consisting of twenty sulphonamide derivatives was analysed and it was found that the first principal component accounted for 96% and the second for 2% of the total variance of the data. These figures suggest that for samples consisting of structurally related compounds PC1 accounts for about 95% and PC2 for about 4% of the total variance.

The PCA suggests the possibility of an unequivocal definition of solvent strength by the use of compounds that are not sensitive to a change of modifier type, *i.e.* markers of which the capacity factor remains constant when MeOH in the binary water–MeOH mobile phase is replaced by a different modifier without a change in eluotropic strength. Positive selectivity indicates a specific acceleration of the solute by the modifier [20]. Therefore if a solute has zero modifier selectivity, then changes in the capacity factor by varying the water fraction of the binary mobile phase are due to solvent strength and solvent strength selectivity.

The ideal solvent strength marker should have a zero modifier selectivity and an average solvent strength selectivity. Zero modifier selectivity means that the capacity factor of the marker is not affected by a change of modifier type provided that the solvent strength of the binary mobile phase does not change. Average solvent strength selectivity ensures that the capacity factor of the marker decreases in an average manner if the water content of a binary mobile phase is increased.

PRS has a high loading on PC2 (Fig. 4b) and is very sensitive to a change of modifier type, as is shown in Fig. 6, the contour plot of the capacity factor of PRS in the design space. The contour plot was obtained by fitting a quadratic model to the capacity factors of PRS measured at the mobile phase compostions A to H. The

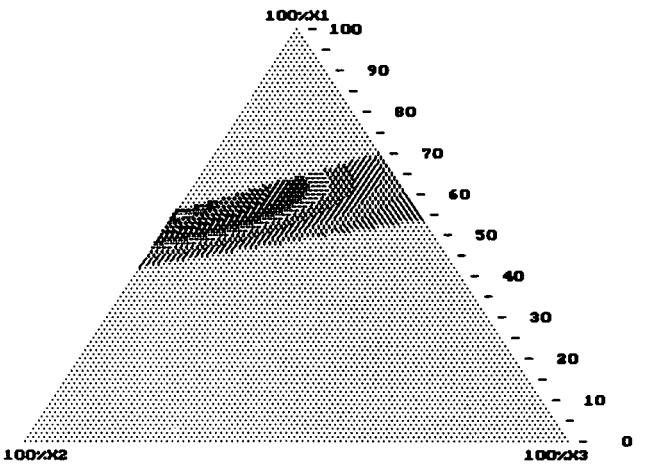

Fig. 6. Contour plot of the capacity factor of prednisolone based on the data of Table II. The capacity factor varies from 0.4 to 7.6. The different symbols correspond to ten different ranges of values of k'. The highest range from 6.9 to 7.6 is indicated by black squares (upper left corner of the design space). The lowest range of 0.4–1.1 is indicated by back-slashes (lower right corner of the design space). X_1 is water, X_2 is methanol and X_3 is acetonitrile.

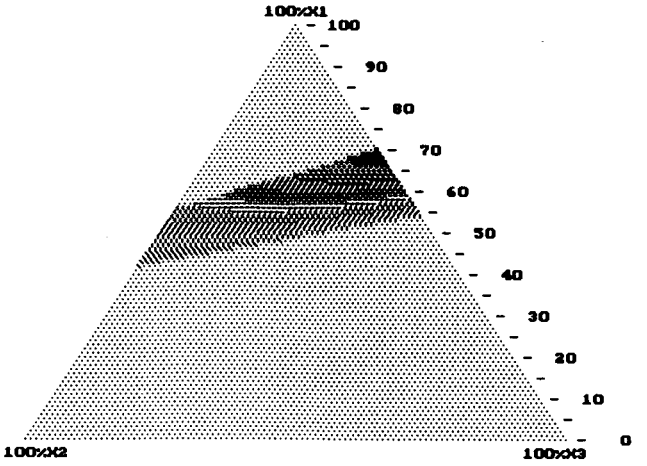

Fig. 7. Contour plot of the capacity factor of nitrobenzene based on the data of Table II. The capacity factor varies from 1.4 to 6.1. Different symbols correspond to ten different ranges of values of k'. The highest range from 5.6 to 6.1 is indicated by black squares (upper left corner of the design space). The lowest range of 1.4–1.8 is indicated by back-slashes (lower right corner of the design space). X_1 is water, X_2 is methanol and X_3 is acetonitrile.

contour lines are strongly curved and indicate that the capacity factor of PRS for a water–MeOH binary mobile phase is considerably greater than for the corresponding iso-eluotropic water–ACN binary mobile phase, for example, mobile phases A and D of Fig. 2.

The contour plots illustrate very well the sensitivity of a compound to a change of modifier type and the meaning of loading on the PC2 axis. PRS has the highest loading on PC2 and NBZ the lowest (Fig. 4b). The contour lines of the plot of NBZ (Fig. 7) indicate that the capacity factor of NBZ in a water–MeOH binary mobile phase is smaller than for the corresponding iso-eluotropic water–ACN binary mobile phase. So if a 50% water–MeOH binary mobile phase is replaced by a water–ACN binary mobile phase in such a way that the capacity factors of PRS and of NBZ remain constant, then the water–ACN binary mobile phase for PRS will contain less ACN than the water–ACN binary mobile phase for NBZ. The fraction of ACN in a water–ACN binary mobile phase that gives the same capacity factor as a 50% water–MeOH phase has been calculated for a number of solutes of the second data set, and the results are given in Table IV. The results clearly show that the fraction of ACN necessary to keep the capacity factor constant in both binary mobile phases strongly

TABLE IV

PERCENTAGE OF ACETONITRILE EQUIVALENT TO 50% METHANOL INDICATED BY A CONSTANT CAPACITY FACTOR OF A SOLUTE

Solute	PRS	PE	PHB	PBL	ACT	CRE	TOL	ACP	NBZ
Percentage ACN	20[a]	31	35	37	40	39	39	42	45

[a] Extrapolated.

correlates with the loading on PC2 (Fig. 4b). Solvent strength markers should have low absolute loadings on PC2 and as such ACT, CRE and TOL are good possible choices for a sample without steroids (Fig. 5b). The ACN fraction of these solutes corresponds well with the percentages calculated by the transfer rules of refs. 6 and 12, which are 36.5 and 40.0% of ACN, respectively.

The definition of an empirical solvent strength scale of reversed-phase mobile phases seems to be possible once the markers have been selected from the correct set of test compounds. Further research on this subject is in progress.

CONCLUSIONS

PCA of a data set of mobile phases consisting of water and different percentages of MeOH and/or ACN characterized by capacity factors of different solutes shows that there are two intrinsic dimensions in the data set. The variance in the data is caused by two independent effects that are described by two principal components.

The first principal component accounts for about 82–96% of the total variance and the second for about 17–2%. The amount of variance explained by each principal component depends strongly on the selection of the solutes that constitute the test sample. The first principal component can be associated with the water fraction of the mobile phase and is interpreted in terms of solvent strength and solvent strength selectivity. The second principal component can be associated with the modifier type of the mobile phase and is interpreted in terms of modifier selectivity.

PCA enables the selection of solutes from a sample that are the most critical test compounds for the characterization of solvent strength and modifier selectivity, and could be used for the definition of an empirical solvent strength scale of reversed-phase mobile phases.

REFERENCES

1 L. R. Snyder, *J. Chromatogr. Sci.*, 16 (1978) 223.
2 L. R. Snyder, J. W. Dolan and J. R. Gant, *J. Chromatogr.*, 165 (1979) 3.
3 P. Jandera, *J. Chromatogr.*, 314 (1984) 13.
4 J. W. Dolan, J. R. Gant and L. R. Snyder, *J. Chromatogr.*, 165 (1979) 31.
5 J. L. Glajch and J. J. Kirkland, *Anal. Chem.*, 54 (1982) 2593.
6 P. J. Schoenmakers, H. A. H. Billiet and L. de Galan, *J. Chromatogr.*, 205 (1981) 13.
7 S. R. Bakalyar, R. McIllwrick and E. Roggendorf, *J. Chromatogr.*, 142 (1977) 353.
8 H. B. Patel and T. M. Jefferies, *J. Chromatogr.*, 389 (1987) 21.
9 P. M. J. Coenegracht, H. J. Metting, A. K. Smilde and P. J. M. Coenegracht-Lamers, *Chromatographia*, 27 (1989) 135.
10 L. R. Snyder, M. A. Quarry and J. L. Glajch, *Chromatographia*, 24 (1987) 33.
11 A. K. Smilde, A. Knevelman and P. M. J. Coenegracht, *J. Chromatogr.*, 369 (1986) 1.
12 D. P. Herman, H. A. H. Billiet and L. de Galan, *J. Chromatogr.*, 463 (1989) 1.
13 W. R. Dillon and M. Goldstein, *Multivariate Analysis*, Wiley, New York, 1984, p. 23.
14 B. Walczak, M. Dreux, J. R. Chretien, K. Szymoniak, M. Lafosse, L. Morin-Allory and J. P. Doucet, *J. Chromatogr.*, 353 (1986) 121.
15 J. R. Chretien, B. Walczak, M. Dreux and M. Lafosse, *J. Chromatogr.*, 371 (1986) 253.
16 B. Walczak, L. Morin-Allory, M. Lafosse, M. Dreux and J. R. Chretien, *J. Chromatogr.*, 395 (1987) 183.
17 M. F. Delaney, A. N. Papas and M. J. Walters, *J. Chromatogr.*, 410 (1987) 31.
18 J. A. Cornell, *Experiments with Mixtures*, Wiley, New York, 1981.
19 J. W. Weyland, *Ph.D. Thesis*, State University of Groningen, Groningen, 1986, p. 56.
20 P. J. Schoenmakers, H. A. H. Billiet and L. de Galan, *J. Chromatogr.*, 218 (1981) 262.

Journal of Chromatography, 550 (1991) 411–424
Elsevier Science Publishers B.V., Amsterdam

CHROMSYMP. 2334

Dependence of retention on the organic modifier concentration and multicomponent adsorption behavior in reversed-phase chromatography

FIROZ D. ANTIA and CSABA HORVÁTH*
Department of Chemical Engineering, Yale University, New Haven, CT 06520 (USA)

ABSTRACT

A three-parameter equation is derived to express the dependence of the logarithmic retention factor, κ, on the volume fraction of the retention modulator, φ, in a binary eluent (such as the organic modifier in the hydro-organic eluents used in reversed-phase chromatography). It is based on the competitive binary adsorption isotherm of the eluite and the modulator generated by employing the ideal adsorbed solution (IAS) method. The equation is found to describe adequately the trends in the κ–φ relationship experimentally observed in reversed-phase systems. Furthermore, the expression affords an estimation of the single-component adsorption isotherm of the eluite from the corresponding κ *versus* φ plot and thus provides a simple means to gather data of importance in the design of separations by non-linear chromatography. For instance, the method can be used to determine whether a pair of eluite isotherms cross one another, a situation that could lead to difficulties in preparative separations. The inherent limitations of the IAS approach may restrict the usefulness of the expression in specific cases. Nevertheless, the approach presented here establishes an explicit, thermodynamically consistent link between the eluite–modulator multicomponent isotherm and corresponding plots and allows a rational description of the generally observed retention behavior in reversed-phase chromatography. The results of this work also illustrate the limitations of the competitive Langmuir isotherm, which is most frequently used to treat competitive adsorption, in the study of the κ–φ relationship specifically and in investigating and modeling non-linear chromatography at large.

INTRODUCTION

Recent interest in industrial separations by preparative/process liquid chromatography has given renewed impetus to the study of adsorption from multicomponent liquid solutions. In such applications, feed components are usually present at concentrations high enough to render their adsorption behavior non-linear and competitive so that they interfere with one another as they traverse the column. The main features of the separation process are dictated by the non-linear multicomponent isotherm function, which describes the simultaneous adsorption of the different feed components. For this reason the process is called non-linear chromatography and it has been the subject of several recent reviews [1–3].

On the other hand, in linear elution chromatography, which is most commonly

0021-9673/91/$03.50

used in analytical work, the sample components are at such low concentrations that their adsorption isotherms are linear and the interference between them is insignificant. Nevertheless, in order to control retention of the eluites in linear elution chromatography, modifiers (retention modulators) are often added to the eluent at such high concentrations that their adsorption isotherms are non-linear and they compete with the eluites for binding sites. For this reason, multicomponent competitive adsorption can be important, not only in preparative applications, but also in analytical chromatography.

The relationship between the eluite retention factor and the modulator concentration is the key to the selection of the optimum eluent strength or gradient profile for a given separation. Since this relationship depends on the competitive adsorption of the modulator and eluite, it ought to be possible to describe it using an appropriate multicomponent isotherm. Yet, save in the case of electrostatic interaction chromatography [4,5], none of the current treatments of this important relationship make any explicit reference to multicomponent adsorption. In reversed-phase chromatography, where hydro-organic eluents are employed, empirical expressions [6,7] or theories of extra-thermodynamic origin [8] have been used to relate the logarithmic retention factor, κ, to the modulator volume fraction, φ. Treatments of chromatography with polar stationary phases have taken into account the adsorption isotherm of the modulator [9,10], but no connection has been made with either the multicomponent or the eluite isotherm.

The reasons for this lacuna become apparent when one considers that it is the multicomponent Langmuir equation that is almost exclusively employed to describe competitive adsorption behavior. Whereas this isotherm allows for great mathematical simplifications when modeling non-linear chromatography, it is thermodynamically inconsistent, except under special conditions, and more than often fails to reflect real behavior. For this reason, many of the simulations carried out with the multicomponent Langmuir isotherm formalism are likely to be of dubious value. The ideal adsorbed solution (IAS) method provides a thermodynamically consistent framework for generating multicomponent equilibrium relationships from arbitrary single component isotherms [11,12]. Due to its simplicity, the IAS method has serious limitations and is not expected to be universally applicable. Nevertheless, it represents a significant advance over the multicomponent Langmuir isotherm.

In this work we test whether the thermodynamically consistent multicomponent isotherm so generated provides a realistic description of the relationship between retention and modulator concentration (the κ–φ relationship). Concomitantly, we study the influence of the modulator on the isotherms of the eluites and examine whether estimates of the eluite adsorption isotherms can be made from κ–φ plots. The terminology of reversed-phase chromatography is employed and reference is made to data obtained in such systems. The general principles, however, are applicable to all non-electrolyte chromatographic systems.

THEORY

In general, the amounts of components adsorbed from liquid solutions cannot be quantitatively determined. It is therefore necessary to introduce the concept of excess adsorbed quantities and to adopt a convention for their definition [13–15]. In

analytical liquid chromatography the concentrations of the feed components in the mobile phase are much lower than that of the solvent; thus no distinction has to be made between excess and absolute adsorbed amounts. The concentration of the mobile phase modulator, however, may vary in a wide range so that the treatment of its adsorption necessitates the choice of a suitable convention.

For this case, the most convenient is the "solvent-not-adsorbed" convention where the most weakly bound component is considered to be absent from the adsorbed phase [13,16]; the adsorbed amounts of other components are then represented by "relative excess" quantities. In the literature, the "molar reduced excess" is frequently used to express the adsorption of modulators [9,17–21], and for binary eluents this can be easily converted to the relative excess upon dividing by the mole fraction of the reference, or principal, solvent [13,14,19].

We will employ the "solvent-not-adsorbed" convention and consider only binary eluents containing a modulator and the principal solvent. The single component isotherms of the modulator, or of the individual feed components, determined in the presence of the principal solvent alone, are called "principal" isotherms.

Single component isotherms

For an eluite e, it is convenient to express the amount adsorbed per unit mass of sorbent, q_e^0, as a function of its molar concentration in the mobile phase, c_e^0, where the superscript 0 denotes that only a single component is being considered. For the modulator, m, q_m^0 represents the relative excess per unit sorbent mass, and mole fractions, x_m^0, rather than molar concentrations, are the appropriate units for the mobile phase composition. (For the rigorous derivation of adsorption isotherms in liquid systems, mole fractions are the required units [22]: molar concentrations are acceptable for eluites present at low concentrations, since, to a good approximation, they are linearly related to their mole fractions.) In this work, we still distinguish between feed components and modulator by employing molar concentrations for the former and mole fractions for the latter.

The single component, or principal, isotherms of feed components are most simply expressed by the Langmuir equation [23]

$$q_e^0 = \frac{\lambda_e^0 b_e^0 c_e^0}{1 + b_e^0 c_e^0} \tag{1}$$

where λ_e^0 and b_e^0 are the pertinent isotherm parameters for the eluite e; λ_e^0 represents the largest possible value for q_e^0 and is therefore called the saturation capacity of the sorbent for that eluite. Experimentally determined single-component isotherms of small and large molecular weight eluites in liquid chromatographic systems have been fit reasonably, with a few exceptions, to eqn. 1 [24–28].

Similarly, the simplest form for the relative excess isotherm of the modulator is given by (*cf.* ref. 22)

$$q_m^0 = \frac{\lambda_m^0 \beta_m^0 x_m^0}{1 + \beta_m^0 x_m^0} \tag{2}$$

where use of the symbol β_m^0 denotes that its units (dimensionless) are distinct from those of b_e^0 (molar concentration $^{-1}$) in eqn. 1. Even though q_m^0 is not equal to λ_m^0 at $x_m^0 = 1$, the parameter λ_m^0 does represent the saturation capacity of the sorbent for the modulator, as may be verified by applying Schay's method for determining the maximum adsorption capacity to eqn. 2 [29].

The molar reduced excess form of eqn. 2 —obtained by multiplying it by $(1 - x_m^0)$— yields an inverted U-shaped curve. This is the simplest of the several possible types of isotherms for binary miscible systems [19,30,31]. Molar reduced excess isotherms of modulators in reversed-phase systems have been experimentally determined [13,17,20,21,32], and often display a maximum and a minimum in the water-rich and organic-rich regions, respectively. For simplicity we assume that the modulator adsorption is well described by eqn. 2; later we will discuss briefly how other isotherm shapes can also be accommodated. With the parameters $\lambda_m^0 = 2.0$ mmol/g sorbent and $\beta_m^0 = 3.7$, eqn. 2 approximates the isotherm of methanol in water on μBondapak C_{18} [20], and these values are used in the calculations except where otherwise mentioned.

Multicomponent isotherms

The simultaneous adsorption of more than one component, at a given temperature, is described by multicomponent isotherm functions. In general, the multicomponent function must be fit to equilibrium adsorption data obtained over the entire composition range of interest. However, only a few measurements have been made of multicomponent adsorption in liquid chromatographic systems [25,28]; for the most part, simple formalisms are employed to predict multicomponent adsorption using parameters obtained from single component data. We will outline here two formalisms for multicomponent isotherms when the principal isotherms of the eluite and modulator are well represented by eqns. 1 and 2: the competitive Langmuir isotherm and the multicomponent isotherm derived using the IAS theory. The results will then allow us to link the plots of the logarithmic retention factor of the eluites *versus* the modulator volume fraction to the principal isotherms of the eluites and the mobile phase modulator.

For brevity, the multicomponent isotherm equations will be written here in terms of concentrations; it is understood that for the modulator m, the term $b_i^0 c_i$ is replaced by $\beta_m^0 x_m$ and for the eluite e by $b_e^0 c_e$ —the absence of a superscript on the concentrations denotes that multicomponent systems are being considered. Furthermore, it is assumed that the mole fraction of the modulator is unaffected by the presence of the feed components.

The competitive Langmuir isotherm is given by [33]

$$q_i = \frac{\lambda_i^0 b_i^0 c_i}{1 + \sum_{j=1}^{N} b_j^0 c_j} \qquad i = 1,2,\ldots,N \tag{3}$$

where N is the total number of adsorbed components and the subscripts i and j refer to all the components including the eluites and the modulator. As mentioned before, a severe shortcoming of eqn. 3 is that it fails to satisfy the Gibbs' adsorption equation

and is therefore thermodynamically inconsistent except in the rare case when [34,35]

$$\lambda_1^0 = \ldots = \lambda_i^0 = \ldots = \lambda_N^0 = \lambda \tag{4}$$

i.e., the saturation capacity of the system is the same for all components.

The Gibbs' adsorption equation relates adsorbed amounts to the spreading pressure, defined as the difference of the interfacial tensions between the multicomponent solution–sorbent and the pure principal solvent–sorbent systems. The ideal adsorbed solution (IAS) method provides a framework to generate from any set of single-component isotherms a multicomponent isotherm that satisfies Gibbs' equation [11,12]. We are interested in using the IAS approach to obtain such multicomponent isotherms from principal Langmuir isotherms. In this case the calculation proceeds in two steps [12,35]. First, the reduced spreading pressure, Π, is determined for the given set of Langmuir isotherm parameters and concentrations from the following implicit equation

$$\sum_{j=1}^{N} \frac{b_j^0 c_j}{\exp\{\Pi/\lambda_j^0\} - 1} = 1 \tag{5}$$

Next, for a known value of Π, the multicomponent isotherm is calculated from the following relationship

$$q_i = \frac{b_i^0 c_i/(\exp\{\Pi/\lambda_i^0\} - 1)}{\sum_{j=1}^{N} b_j^0 c_j \exp(\Pi/\lambda_j^0)/\{\lambda_j^0[\exp(\Pi/\lambda_j^0) - 1]^2\}} \qquad i = 1,2,\ldots,N \tag{6}$$

Eqn. 6 represents a multicomponent isotherm obtained from Langmuirian parent isotherms and we call it the IAS/L isotherm. In the case where eqn. 4 is satisfied, eqn. 6 reduces to the competitive Langmuir isotherm, eqn. 2, which is therefore a special case of the IAS/L model.

Relationship between logarithmic retention factor, κ, and modulator volume fraction, φ

In linear elution chromatography the eluite is present in a trace amount so that its retention factor, k', is given by its mass distribution ratio in the stationary and mobile phases at vanishing eluite concentration as follows

$$k' = \phi\left(\lim_{c_e \to 0} \frac{q_e}{c_e}\right) \tag{7}$$

where ϕ is the phase ratio, which for simplicity is assumed here to be unity. In order to examine the dependence of the retention factor, or more conveniently, that of the logarithmic retention factor, κ, on the modulator concentration, we combine eqn. 7 with the IAS/L expression. In the limit $c_e \to 0$, eqn. 5 becomes explicit since there is no longer any need for the summation, and Π is found to be

$$\Pi = \lambda_m^0 \ln(1 + \beta_m^0 x_m) \tag{8}$$

If eqn. 8 is substituted into eqn. 6, applying eqn. 7 and taking logarithms yields the result:

$$\kappa = \kappa_L + \log\left[\frac{\Lambda\beta_m^0 x_m}{(1 + \beta_m^0 x_m)^\Lambda - 1}\right] \tag{9}$$

where Λ is the ratio λ_m^0/λ_e^0. The term κ_L is the logarithmic retention factor of the eluite when $\Lambda = 1$, *i.e.*, the IAS/L isotherm reduces to the competitive Langmuir isotherm, and is given by the expression

$$\kappa_L = \log a_e^0 - \log(1 + \beta_m^0 x_m) \tag{10}$$

where $a_e^0 = \lambda_e^0 b_e^0$ is the initial slope of the eluite isotherm in the absence of the modulator.

In the practice of reversed-phase chromatography the volume fraction of the organic modifier, φ, rather than its mole fraction, is most commonly used. For binary eluents, the modulator mole fraction, x_m is related to φ by the expression

$$x_m = \frac{\varphi}{\varphi + (1 - \varphi)\Omega} \tag{11}$$

Here $\Omega = \bar{v}_m/\bar{v}_s$, where $\bar{v}_m$ and $\bar{v}_s$ are the partial molar volumes of the modulator and the principal solvent, respectively. In eqn. 11 it is assumed that in hydro-organic eluents the ratio Ω is constant even though $\bar{v}_m$ and $\bar{v}_s$ usually depend on the composition [36]. Eqns. 9–11 together give the expression for κ *versus* φ. For a given value of Ω, eqns. 9–11 represent a relationship with three parameters: a_e^0, the initial slope of the eluite isotherm measured in the principal solvent proper; Λ, the ratio of the saturation capacities for the single component (parent) isotherms of the modulator and the eluite; and β_m^0.

RESULTS AND DISCUSSION

The most widely used branch of modern liquid chromatography is reversed-phase chromatography, carried out with aqueous eluents containing an organic modifier and it offers an eminently suitable means to examine the applicability of the derived equations for the dependence of κ on φ. Because of the importance of this chromatographic technique, the κ–φ relationships for eluites of widely different molecular weight and various modulators have been extensively documented; the plots are quasi linear and have negative slopes [37–45]. The negative slope of the κ *vs.* φ plot is termed the S value in the literature of gradient elution. The sign of the slope is due to the fact that the excess adsorbed amount of the modulator is positive [16]. Generally, in a given chromatographic system, it is found to increase with the molecular weight of eluites of similar chemical structure [42] and believed to be proportional to the area of contact between the bound eluite and sorbent [8,45]. The ordinate intercept of the plot, $\log a_e^0$, represents the κ value for the eluite in neat water; for sets of related molecules, it is also thought to increase with the area of contact [42,44].

As it shares a common physico-chemical basis with reversed-phase chromato-

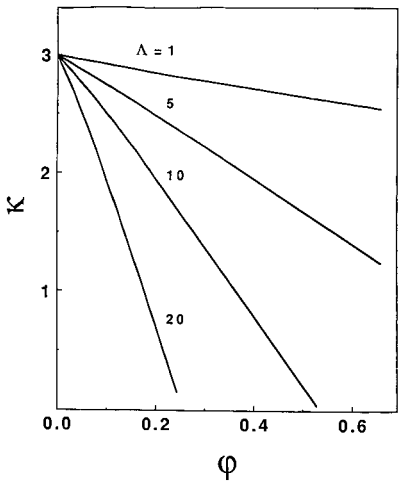

Fig. 1. Plots of the logarithmic retention factor, κ, *versus* modulator volume fraction, φ, for different values of the parameter Λ according to the IAS/L isotherm model. The data were calculated from eqn. 9 with fixed values of $a_e^0 = 1000$ and $\beta_m^0 = 3.68$ (dimensionless), $\phi = 1$ g sorbent/ml mobile phase.

graphy, hydrophobic interaction chromatography (HIC) exhibits similar behavior for κ *versus* salt molality plots [46–49]. In HIC, however, the relative excess adsorption of the salt with respect to water is a negative quantity [50], and thus the slopes of the quasi-linear plots of κ *versus* salt molality are positive. Application of the Gibbs' adsorption equation shows that negative excess adsorption of salt in HIC implies an increase in the corresponding interfacial tension with salt concentration; the opposite is true for positively adsorbing organic modifiers in reversed-phase systems. This viewpoint is thus consistent with the solvophobic theory that is used to describe both HIC and reversed-phase chromatography [8,47]. Our treatment is therefore expected to be applicable to HIC *mutatis mutandis*.

As the Langmuir multicomponent equation has already been proved to be inadequate [51], the equation derived from the IAS/L isotherm will be used to interpret the κ–φ relationship in terms of the adsorption isotherms of the eluite and modulator. Although other thermodynamically consistent multicomponent isotherm models could conceivably found for the same purpose, here we consider only the IAS/L formalism. We have found no complete set of data that includes not only the isotherms of the modulator and eluites, but also the corresponding κ–φ plots. Therefore, we refrain from verifying the accuracy of eqn. 9. However, the general properties of the κ *versus* φ plots should allow us to evaluate the ability of eqn. 9 to describe, at least qualitatively, the experimentally observed behavior.

Our first concern is the linearity of the κ *versus* φ relationship. It is found that with β_m^0 values in the practical range, the equation gives rise to quasi-linear plots over the region $1 < \Lambda < 20$. Further investigations showed that the curvature depends on the ratio of molar volumes, Ω, and changes from slightly concave upward (positive second derivative) to slightly convex (negative second derivative) over $1 < \Omega < 3$, which covers the practical range for most modifiers. Despite the small changes in curvature, the dependence of the linearity on Ω is fairly weak in this region; all the plots

can be fit reasonably with straight lines. In the calculations, we have used the value $\Omega = 2$, which is close to the value of 2.2 calculated for methanol–water systems from density data at 20°C [52].

As is evident from eqn. 10, the κ–φ relationship derived from the competitive Langmuir isotherm alone is unrealistic, in agreement with earlier observations [51]. The derivative of eqn. 10 with respect to x_m (or φ), and hence the slope of the corresponding κ–φ plot, depends solely on the parameter β_m^0, implying that for a given modulator, the κ–φ plots of all eluites, regardless of their isotherm parameters, would have the same slope. This absurdity reveals the limitations of one of the properties of the competitive Langmuir isotherm that makes it mathematically attractive, *viz*, constant separation factor (or selectivity, $\alpha_{21} = q_2c_1/q_1c_2 = a_2^0/a_0{}^1$, for any two components).

In contradistinction, according to the relationship derived from the IAS/L multicomponent isotherm, eqn. 9, the slopes of the plots, *i.e.* the S values, depend on the ratio of the saturation capacities of the modulator and eluite single component isotherms, Λ, and the parameter β_m^0. An approximate relationship for the dependence of S on these parameters is derived in the Appendix. Fig. 1 shows plots of κ *versus* φ for fixed values of β_m^0 and the intercept $\log a_e^0$. The slope increases with increasing values of Λ. As the IAS/L isotherm correctly describes a wider range of behavior it offers a marked improvement in simulating dynamic adsorption behavior over the multicomponent Langmuir expression. In particular, in a given chromatographic system, the IAS/L model allows for eluites having different S values and thus separation factors that vary with changes in the modulator concentration. The slope also increases with increasing values of β_m^0 (not shown in Fig. 1), corresponding to the use of a more strongly sorbed modulator, other factors remaining constant.

The increase in the S values with the molecular contact area upon adsorption at

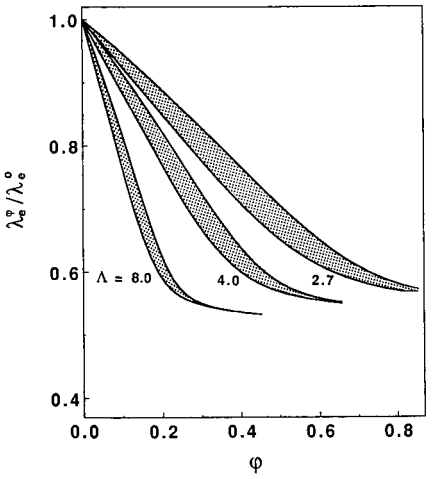

Fig. 2. Plots of the normalized apparent saturation capacity of eluite isotherms, $\lambda_e^\varphi/\lambda_e^0$, *versus* the modulator volume fraction φ, for different values of the parameter Λ. The curves representing the lower and upper envelopes of the shaded regions were calculated from eqn. 6 with $b_e^0 = 1000$ and 4000, respectively. Note that $\Lambda = \lambda_m^0/\lambda_e^0$ and $b_e^0 = a_e^0/\lambda_e^0$. Conditions: $\lambda_m^0 = 2$ mmol/g sorbent, β_m^0 and ϕ as in Fig. 1.

the chromatographic surface in reversed-phase chromatography can also be inferred from the IAS/L isotherm. Eluite molecules having larger contact areas when bound to the stationary phase would be expected to occupy larger area at the surface and consequently to have smaller values for the molar saturation capacity, λ. The larger A values then result in greater S values as illustrated in Fig. 1. A similar conclusion can be drawn for the dependence of S on the molecular weight of the eluites.

Influence of the modulator on the eluite adsorption isotherm

So far we have considered only the principal isotherm of the eluite, *i.e.* the single-component eluite isotherm measured in principal solvent in the absence of the modulator. Here we turn our attention to the effect of the modulator concentration measured by its volume fraction, φ, on the isotherm of the eluite measured at a fixed value of φ in the eluent. Since the dependence on φ of the initial slope of the resulting isotherm is described by the κ–φ relationship discussed before, our concern here is the effect of the modulator on the observed saturation capacity, λ_e^φ, that differs from the saturation capacity of the eluite in neat principal solvent, λ_e^0. As shown in the Appendix, λ_e^φ can be found as a function of φ from eqn. 6. In Fig. 2, the normalized observed saturation capacity, $\lambda_e^\varphi/\lambda_e^0$, is plotted against the modulator volume fraction, φ, for different values of the parameters A and b_e^0. As seen in Fig. 2 the observed saturation level decreases with increasing φ in agreement with experimental findings [24]. The rate of the decrease, or suppression rate, increases with A, but is only a weak function of b_e. Since the slopes of κ–φ plots also increase with A, both the initial slope and the saturation capacity of the isotherm are suppressed more strongly with increasing values of A. This conclusion is in agreement with the observed sharp drops in the retention factor and in the saturation capacity of large molecules with small changes in modulator concentration [53].

Estimation of the eluite isotherm from the κ–φ plot

In the design of process scale separations by chromatography, there is a significant need to estimate the isotherms of the components to be separated in the chromatographic system under consideration. Since κ–φ plots can be conveniently determined from a few gradient runs [45,54], a method using such data for even a crude estimate of the parameters of the principal eluite isotherm could be of importance because of the considerable saving in time with respect to the tedious conventional methods. Unfortunately, as mentioned before, the expression derived from the competitive Langmuir isotherm, eqn. 10, contains only the initial slope and therefore does not provide sufficient information to estimate the two isotherm parameters. On the other hand, the dependence of κ on φ, eqn. 9, derived from the IAS/L multicomponent isotherm entails both parameters of the principal eluite isotherm and provides an opportunity to estimate them from a κ–φ plot. If the parameters of the modulator isotherm, λ_m^0 and β_m^0, and Ω are known independently, $\lambda_e^0 (= \lambda_m^0/A)$ can be determined from the S value (*vide* eqn. A2) and a_e^0 from the intercept. Knowing λ_e and a_e^0, b_e^0 $(= a_e^0/\lambda_e^0)$ is readily obtained. If the modulator isotherm is not Langmuirian, the IAS method can still be used to generate multicomponent isotherms, as discussed briefly later.

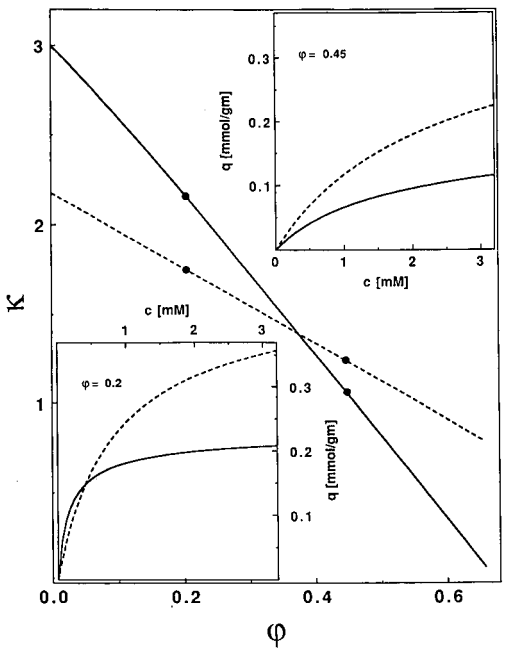

Fig. 3. Intersecting κ *versus* φ plots calculated from eqn. 9. The corresponding eluite isotherms were calculated from eqn. 6 with $\varphi = 0.2$ and $\varphi = 0.45$ and are shown in the lower and upper insets respectively. (– – –) $\lambda_e^0 = 0.5$ mmol/g sorbent, $\Lambda = 4$, $b_e^0 = 300\ M^{-1}$; (———) $\lambda_e^0 = 0.25$ mmol/g sorbent, $\Lambda = 8$, $b_e^0 = 4000\ M^{-1}$. Other conditions as in Fig. 2.

Convergent κ–φ plots and crossing isotherms

Consider a pair of eluites whose κ–φ plots converge and intersect at modulator concentrations of practical interest, as shown in Fig. 3. According to eqn. 9, the eluite with the steeper slope, *i.e.* the greater S value, must have the higher value of Λ, and hence a lower saturation capacity, λ_e^0. On the other hand this eluite also has a higher intercept, and consequently a greater value for the initial slope of its principal isotherm, a_e^0. As a result, the principal isotherms of the two eluites, *i.e.* their single-component isotherms measured in the absence of the modulator, must cross at a certain concentration when viewed in the same plane. Several recent reports have stressed the adverse effects of such isotherm crossing in non-linear chromatography [55–59], and therefore a simple method for diagnosing such behavior can be helpful in the design of a preparative separation.

If the principal isotherms of both the modulator and the eluites are known, the isotherms of the eluites in solutions containing various concentrations of the modulator can be calculated from eqn. 6. Such isotherms, determined separately for each of the two eluites under consideration at two different values of φ are plotted in the insets of Fig. 3. Recent advances in this area of research [60] allow us to generalize the results: for values of φ less than that corresponding to the intersection of the κ–φ plots, the isotherms cross, whereas at φ values beyond this point, the isotherms no longer intersect. Since the isotherm of the eluite with the greater Λ value is more

strongly suppressed by increasing modulator concentration than the other, it lies completely below the latter isotherm at sufficiently high values of φ. It is seen that the initial slopes and apparent saturation capacities of both isotherms are lower at the higher φ values; thus addition of a modulator uncrosses the offending isotherms at the cost of lowering the retention of the eluites and adsorption capacity of the system. The practical benefit of adding a modulator to uncross the isotherms depends on the κ value of the intersection point, κ^*. If it is sufficiently large, the uncrossing can be accomplished with modest reduction of the retention and saturation capacity of the components. If, on the other hand, κ^* is too low, the retention and adsorption capacity are likely to be suppressed to unacceptable levels, and other means to uncross isotherms, such as changing the modifier, pH, temperature, or even the stationary phase itself, might be necessary.

In what circumstances might isotherms of eluites be expected to cross? Let us consider, as an example, a series of homologous compounds; each successive homologue binds more tightly to the stationary phase, therefore having a higher initial isotherm slope and thus a greater value for the intercept of its respective κ–φ plot. Since higher homologues are likely to occupy a larger area on the surface of the adsorbent, they would have smaller values, on a molar basis, for the saturation capacity, λ_e. Consequently the single-component isotherms of homologues are expected to cross. Since, in a given system, lower λ_e values correspond to greater A and consequently larger S values, the κ–φ plots of the homologues would intersect as well. Experimental observations indeed bear out this prediction for the κ–φ plots [42–44].

Non-Langmuirian isotherms

In principle, the IAS method can be employed with all types of single-component isotherms: therefore, κ–φ plots can be calculated, combining eqn. 7 with the guidelines given in the Appendix of ref. 12, for any type of modulator and eluite principal isotherms, even those that are fitted to experimental data by a polynomial or other suitable function. If isotherm parameters of eluites are to be estimated from the κ–φ plots, an *a priori* postulate for the form of the principal eluite isotherm is required; the Langmuir form is usually adequate, but again, in principle, any appropriate function may be employed. The practicability of using the approach, however, may be limited because small errors in the experimental data may give inaccurate results due to the sensitivity of the complicated calculations. Indeed, unless great care is taken in the measurement and appropriate fitting of the data to suitable functions representing all the isotherms involved, substantial errors may be introduced [61].

Eqn. 2 is expected to describe adsorption of the modulator only in the water rich region *i.e.* up to about $\varphi = 0.7$. At higher φ values, the reduced molar excess of modifier is often observed to be negative [9,17–21]. Under such circumstances, the IAS theory would predict positive slopes for κ–φ plots. This is consistent with an increase in retention with increasing modifier concentration in the eluent as observed sometimes with organic-rich mobile phases in reversed-phase chromatography [62,63].

CONCLUSIONS

On the basis of its ability to describe qualitatively the observed trends in the relationship between logarithmic retention factor and modulator concentration in

reversed-phase chromatography, the IAS/L isotherm should be viewed as a distinct improvement over the more restrictive, and more than often thermodynamically inconsistent, competitive Langmuir isotherm. Indeed, the competitive Langmuir isotherm, which is seen to be a special case of the IAS/L equation, fails to describe all but the most rudimentary cases; in this light its indiscriminate use in the past to model the dynamics of non-linear chromatography calls for criticism.

The IAS/L multicomponent isotherm itself, however, is far from perfect and for this reason the literature is replete with elaborate schemes to incorporate liquid and adsorbed-phase activity coefficients into the fundamental IAS formalism [12,15,22, 64–66]. As mentioned above it is also sensitive to small errors in the measurement of single-component isotherms. Nevertheless, for sets of related compounds having commensurate activity coefficients, it is likely that the trends predicted by the IAS/L isotherm provide a reasonable picture of reality. Indeed the simple expression, eqn. 9, derived from the IAS/L multicomponent isotherm to describe the κ–φ relationship, embodies much of the experimentally observed behavior. In particular, it not only provides the missing link between κ–φ plots and the eluite isotherms, but also offers a rapid means to diagnose isotherm crossing, a source of potential difficulties in preparative separations. In general the approach presented here offers a method to treat the effect of non-linear adsorption in linear elution chromatography on the basis of thermodynamically sound multicomponent isotherms.

ACKNOWLEDGEMENTS

This work was supported by Grant No. GM20993 from the National Institutes of Health, U.S. Department of Health and Human Resources and by the National Foundation for Cancer Research.

APPENDIX

Dependence of the S value on isotherm parameters

For a given value of the ratio Ω ($= \bar{v}_m/\bar{v}_s$) the negative slope, S, of the nearly linear κ–φ plots can be determined from

$$S \approx (\kappa_{\varphi=0} - \kappa_{\varphi=0.5})/0.5 \tag{A1}$$

where $\kappa_{\varphi=0}$ (given by $\log a_e^0$) and $\kappa_{\varphi=0.5}$ are κ values evaluated at $\varphi = 0$ and $\varphi = 0.5$ respectively. Since at $\varphi = 0.5$, $x_m = 1/(1 + \Omega)$ (*vide* eqn. 11), substitution of eqn. 9 into eqn. A1 yields

$$S \approx S_L + 2\log\left[\left(1 + \frac{\beta_m^0}{1+\Omega}\right)^A - 1\right] - 2\log\left[\frac{A\beta_m^0}{(1+\Omega)}\right] \tag{A2}$$

where S_L is the slope obtained with the multicomponent Langmuir isotherm, given by

$$S_L \approx 2\log\left(1 + \frac{\beta_m^0}{1+\Omega}\right) \tag{A3}$$

which is a function only of β_m^0. The value of S reduces to S_L when $A = 1$ which is a condition unlikely to have practical significance.

Calculation of the apparent saturation capacity of the eluite isotherm at fixed φ

For the dependence of the apparent saturation capacity of the eluite isotherm on φ (or x_m) no explicit relationship has been found. Therefore we fitted the isotherms generated using eqn. 6 at fixed values of φ to a single component Langmuir expression (*vide* eqn. 1) using a Scatchard diagram, *i.e.* a plot of q_e/c_e *vs.* q_e. The intercept of the straight line thus obtained with the q_e axis yields the apparent saturation capacity, λ_e^φ, plotted in Fig. 2.

REFERENCES

1 A. L. Lee, A. Velayudhan and Cs. Horváth, in G. Durand, L. Bobichon and J. Florent (Editors), *8th International Biotechnology Symposium*, Société Française de Microbiologie, Paris, 1989, pp. 593–610.
2 F. D. Antia and Cs. Horváth, *Ber. Bunsenges. Phys. Chem.*, 93 (1989) 961.
3 G. Guiochon and A. Katti, *Chromatographia*, 24 (1987) 165.
4 A. Velayudhan and Cs. Horváth, *J. Chromatogr.*, 367 (1986) 160.
5 A. Velayudhan and Cs. Horváth, *J. Chromatogr.*, 443 (1988) 13.
6 P. J. Schoenmakers, H. A. H. Billiet, R. Tijssen and L. de Galan, *J. Chromatogr.*, 149 (1978) 519.
7 L. R. Snyder, in Cs. Horváth (Editor), *High-Performance Liquid Chromatography —Advances and Perspectives*, Vol. 1, Academic Press, New York, 1980, pp. 208–316.
8 Cs. Horváth, W. R. Melander and I. Molnár, *J. Chromatogr.*, 125 (1976) 129.
9 M. Jaroniec and B. Oscik-Mendyk, *J. Chem. Soc. Faraday Trans. 1*, 77 (1981) 1277.
10 G. H. Findenegg and F. Köster, *J. Chem. Soc. Faraday Trans. 1*, 82 (1986) 2691.
11 A. L. Myers and J. M. Prausnitz, *AIChE. J.*, 11 (1965) 121.
12 C. J. Radke and J. M. Prausnitz, *AIChE. J.*, 18 (1972) 761.
13 F. Riedo and E. sz. Kováts, *J. Chromatogr.*, 239 (1982) 1.
14 Z. Kiraly and I. Dekany, *Colloid. Polym. Sci.*, 266 (1988) 663.
15 A. L. Myers, in A. I. Liapis (Editor), *Fundamentals of Adsorption*, Engineering Foundation, New York, 1987, pp. 3–25.
16 W. R. Melander, J. F. Erard and Cs. Horváth, *J. Chromatogr.*, 282 (1983) 211.
17 E. H. Slaats, W. Markovski, J. Fekete and H. Poppe, *J. Chromatogr.*, 207 (1981) 299.
18 N. L. Ha, J. Ungvárai and E. sz. Kováts, *Anal. Chem.*, 54 (1982) 2410.
19 K. László, L. G. Nagy, G. Fóti and G. Schay, *Periodica Polytechnica*, 29 (1985) 73.
20 C. S. Koch, F. Köster and G. H. Findenegg, *J. Chromatogr.*, 406 (1987) 257.
21 M. C. Hennion and R. Rosset, *Chromatographia*, 25 (1988) 43.
22 O. G. Larionov and A. L. Myers, *Chem. Eng. Sci.*, 26 (1971) 1025.
23 I. Langmuir, *J. Am. Chem. Soc.*, 38 (1916) 2221.
24 J. M. Jacobson, J. H. Frenz and Cs. Horváth, *J. Chromatogr.*, 316 (1984) 53.
25 J. M. Jacobson, J. H. Frenz and Cs. Horváth, *Ind. Eng. Chem. Res.*, 26 (1987) 43.
26 J.-X. Huang and Cs. Horváth, *J. Chromatogr.*, 406 (1987) 276.
27 J.-X. Huang and Cs. Horváth, *J. Chromatogr.*, 406 (1987) 285.
28 J.-X. Huang and G. Guiochon, *J. Coll. Interface Sci.*, 128 (1989) 577.
29 G. Schay, L. G. Nagy and G. Fóti, *Acta Chim. Acad. Sci. Hung.*, 100 (1979) 289.
30 L. G. Nagy, G. Schay and T. Szekrényesy, *Acta Chim. Hung.*, 53 (1967) 145.
31 G. Schay and L. G. Nagy, in B. Csákvári (Editor), *A kémia újabb eredményei*, Vol. 18, Akadémiai Kiadó, Budapest, 1974, pp. 7–181.
32 R. M. McCornick and B. L. Karger, *Anal. Chem.*, 52 (1980) 2249.
33 G. M. Schwab, *Ergebnisse der exacten Naturwissenschaften*, Vol. 7, Julius Springer, Berlin, 1928, p. 276.
34 D. B. Broughton, *Ind. Eng. Chem.*, 40 (1948) 1506.
35 D. M. LeVan and T. Vermeulen, *J. Phys. Chem.*, 85 (1981) 3247.
36 N. L. Ha and E. sz. Kováts, *Chromatographia*, 15 (1982) 61.
37 S. Terabe, H. Nishi and T. Ando, *J. Chromatogr.*, 212 (1981) 295.

38 L. R. Snyder and M. A. Stadalius, in Cs. Horváth (Editor), *High-Performance Liquid Chromatography: Advances and Perspectives*, Vol. 4, Academic Press, New York, 1986, pp. 195–312.
39 B. P. Johnson, M. G. Khaledi and J. G. Dorsey, *Anal. Chem.*, 58 (1986) 2354.
40 A. Ooperhuizen, T. L. Sinnige, J. M. D. van der Steen and O. Hutzinger, *J. Chromatogr.*, 388 (1987) 51.
41 M. T. W. Hearn and M. I. Aguilar, *J. Chromatogr.*, 392 (1987) 33.
42 L. R. Snyder, M. A. Quarry and J. L. Glach, *Chromatographia*, 24 (1987) 33.
43 K. Valkó, I. Fellegvári, A. Katti and L. Ötvös, *J. Liq. Chromatogr.*, 11 (1988) 833.
44 K. Valkó, T. Cserháti, I. Fellegvári, J. Sági and A. Szemő *J. Chromatogr.*, 506 (1990) 35.
45 S. Lin and B. L. Karger, *J. Chromatogr.*, 499 (1990) 89.
46 J. L. Fausnaugh and F. E. Regnier, *J. Chromatogr.*, 359 (1986) 131.
47 W. R. Melander, D. Corradini and Cs. Horváth, *J. Chromatogr.*, 317 (1984) 67.
48 A. Katti, Y.-F. Maa and Cs. Horváth, *Chromatographia*, 24 (1987) 646.
49 J. Gehas and D. B. Wetlaufer, *J. Chromatogr.*, 511 (1990) 123.
50 T. Arakawa and S. N. Timasheff, *Biochemistry*, 21 (1982) 6545.
51 F. D. Antia and Cs. Horváth, *J. Chromatogr.*, 484 (1989) 1.
52 R. H. Perry and C. H. Chilton (Editors), *Chemical Engineers Handbook*, 5th ed., McGraw Hill, New York, 1973, p. 3–83.
53 K. Kalghatgi and Cs. Horváth, *J. Chromatogr.*, 398 (1987) 335.
54 M. A. Quarry, R. L. Grob and L. R. Snyder, *Anal. Chem.*, 58 (1986) 907.
55 Cs. Horváth, A. L. Lee, A. Velayudhan and G. Subramanian, presented at *Dal Nogare Symposium at the Pittsburgh Conference, Atlantic City, NJ, March 9–13, 1987.*
56 A. Lee, *Ph.D. Thesis*, Yale University, 1990.
57 A. Velayudhan, *Ph.D. Thesis*, Yale University, 1990.
58 G. Subramanian and S. M. Cramer, *Biotechnol. Progress*, 5 (1989) 92.
59 G. Vigh, G. Quintero and G. Farkas, *J. Chromatogr.*, 506 (1990) 481.
60 F. D. Antia and Cs. Horváth, *J. Chromatogr.*, 556 (1990) in press.
61 E. Richter, W. Schütz and A. L. Myers, *Chem. Eng. Sci.*, 44 (1989) 1609.
62 A. Nahum and Cs. Horváth, *J. Chromatogr.*, 203 (1981) 53.
63 K. E. Bij, Cs. Horváth, W. R. Melander and A. Nahum, *J. Chromatogr.*, 203 (1981) 65.
64 A. L. Myers, *AIChE. J.*, 29 (1983) 691.
65 O. Talu and I. Zwiebel, *AIChE. J.*, 32 (1986) 1263.
66 G. Gamba, R. Rota, G. Storti, S. Carra and M. Morbidelli, *AIChE. J.*, 35 (1989) 959.

Journal of Chromatography, 550 (1991) 425–447
Elsevier Science Publishers B.V., Amsterdam

CHROMSYMP. 2260

Review

Gradient elution methods for predicting isocratic conditions

PETER J. SCHOENMAKERS*
Philips Research, P.O. Box 80 000, 5600 JA Eindhoven (Netherlands)
ÁKOS BARTHA
Astra Pharmaceutical Production AB, S-15185 Södertälje (Sweden)
and
HUGO A. H. BILLIET
Department of Biotechnology, Delft University of Technology, De Vries van Heystplantsoen 2, 2628 RZ Delft (Netherlands)

ABSTRACT

Gradient elution methods can elegantly be used for rapidly establishing the appropriate isocratic elution conditions for newly chromatographed samples. In comparison with the conventional approach of running a number of isocratic chromatograms on a trial-and-error basis, gradient elution methods can be much more efficient and yield more consistent results. Key factors are a description of the retention behaviour of the solutes under isocratic conditions as a function of the programmed parameters and an accurate knowledge of the actual gradient profile, *i.e.*, the variation of the programmed parameters with time. Reasonably simple calculation procedures are facilitated by the use of simple (*e.g.*, linear) programmes and instrumentation that affects the actual profile as little as possible. For non-ionic solutes two different gradient scans suffice in principle. In certain cases a single gradient scan may be adequate. A combination of one gradient scan and one isocratic verification experiment can often be used for the accurate prediction of optimum isocratic conditions. For ionic solutes a larger number of scanning experiments are needed than for non-ionic solutes, but in comparison with the time needed for trial-and-error optimization the potential benefits of gradient scanning methods are much greater. For characterizing the ionic solutes in unknown samples two things are needed. First, the solutes need to be classified according to their type (weak or strong; acids or bases) and charge. Next, the optimum isocratic conditions should be established. The concentration of organic modifier, the pH and the type and concentration of ion-pair reagent are the most important parameters to be considered in the process. Using linear gradients at two different pH values in combination with "pulse injection" of ion-pairing reagents, four scanning experiments form the basis of an efficient classification procedure. Once the solutes have been classified, simple, stepwise procedures can be used to establish optimum isocratic conditions.

CONTENTS

0021-9673/91/$03.50

1. INTRODUCTION

Even for compounds of known chemical structure it is usually not possible to predict chromatographic conditions (mobile phase, stationary phase, temperature, pH, etc.) at which elution as sharp peaks in the optimum range of retention times can be achieved. Thus, some experimental data are almost always needed to establish appropriate conditions for elution. One way to elute a wide variety of samples under approximately optimum conditions in high-performance liquid chromatography (HPLC) is to apply solvent programming or gradient elution techniques. This implies that the mobile phase is somehow varied during the chromatographic run. Solvent programming may involve stepwise ("step gradients") or continuous (linear, convex or concave gradients) variations in the concentration of solvent components, the pH or the ionic strength. Combinations (multi-segment gradients) are also possible. Varying the stationary phase is not practical in LC, but temperature programming is. The latter technique, however, is much less powerful in HPLC than it is in gas chromatography, because the retention of solutes cannot be varied by several orders of magnitude within the practical temperature range. Such large variations can be realized with the most widely applied gradient elution methods, *i.e.*, the programming of the mobile phase composition (or "solvent strength") for neutral solutes, ionic strength for ionic solutes and pH for ionogenic solutes. Aspects of these various gradient elution methods will be considered in this paper.

Gradient elution methods may be used in several different ways:

(1) for the elution of samples of which the individual components require vastly different elution conditions;

(2) for scanning unknown samples for the presence of a wide variety of components; and

(3) for predicting suitable non-programmed (*i.e.*, isocratic, isoprotic, etc.) elution conditions for unknown samples.

The purpose of this paper is to review the application of gradient elution techniques for the third purpose. Several advantages of gradient elution methods can be identified:

(i) potentially, all components of the sample can be eluted in a single experiment, including unexpected contaminants;

(ii) no *a priori* information on suitable non-programmed elution conditions is needed; and

(iii) approximately constant resolving power and sensitivity can be maintained throughout the run.

These advantages need to be balanced against the following disadvantages:

(i) the detection techniques used need to be compatible with gradient elution methods and thus need to be selective; as a consequence, certain sample components may be overlooked;

(ii) the accuracy of the predictions is limited by experimental errors and non-idealities, assumptions regarding the (approximate) behaviour of solutes and imprecise calculation procedures.

1.1. Optimum isocratic elution range

If it is our aim to predict conditions under which retention times in the optimum range can be obtained, then this optimum range should be defined. For separating two compounds, the optimum capacity factor can be found from the equation describing resolution ($R_{s,ji}$) as a function of retention (the average capacity factor $\bar{k} = \frac{1}{2}k_i + \frac{1}{2}k_j$), selectivity ($\alpha_{ji} = k_j/k_i$) and efficiency (plate count, N) [1]:

$$R_{s,ji} = \left(\frac{\bar{k}}{1+\bar{k}}\right)\left(\frac{\alpha_{ji}-1}{\alpha_{ji}+1}\right)\frac{\sqrt{N}}{2} \tag{1}$$

The efficiency can be related to the column length (L) and the height equivalent to one plate (H) by $N = L/H$. The column length is the product of the linear velocity (u) and the time (t_0) needed for an unretained solute to pass through the column ($L = ut_0$). The average time needed for solutes i and j is $\bar{t} = \frac{1}{2}t_i + \frac{1}{2}t_j = t_0(1 + \bar{k})$. Substitution of these relationships in eqn. 1 yields an expression for the required (average) retention time of the two solutes:

$$\bar{t} = 4R_{s,ji}^2\left[\frac{(1+\bar{k})^3}{\bar{k}^2}\right]\left[\frac{(\alpha_{ji}+1)^2}{(\alpha_{ji}-1)^2}\right]\frac{H}{u} \tag{2}$$

From the derivative of $\bar{t}$ with respect to $\bar{k}$, we find that two peaks can be separated most rapidly if the average capacity factor equals 2. The capacity factor of the first peak can be found from

$$k_1 = \bar{k} - \frac{2R_s(\bar{k}+1)}{\sqrt{N}} = 2 - \frac{6R_s}{\sqrt{N}} \tag{3}$$

whereas for the second peak

$$k_2 = \bar{k} + \frac{2R_s(\bar{k}+1)}{\sqrt{N}} = 2 + \frac{6R_s}{\sqrt{N}} \tag{4}$$

For separating more than two peaks a broader range of capacity factors will need to be covered. For three peaks we may calculate the optimum values, assuming that the resolution between the two pairs of peaks is the same (*i.e.*, $R_{s,32} = R_{s,21}$) and that the values of the function $(1 + \bar{k})^3/\bar{k}^2$ are equally far from the optimum value of 6.75 for each pair of peaks. These criteria are met if $k_2 = 1 + \sqrt{1 - 4R_s/N}$. This means that

the centre peak will remain located very close to the "optimum value" of 2. The capacity factor of the first peak can be found from

$$k_{j-1} = \frac{k_j(\sqrt{N} - 2R_s) - 4R_s}{\sqrt{N} + 2R_s} \tag{5}$$

whereas for the last peak

$$k_{j+1} = \frac{k_j(\sqrt{N} + 2R_s) + 4R_s}{\sqrt{N} - 2R_s} \tag{6}$$

Using eqns. 5 and 6 the positions of series of peaks can be calculated assuming the middle peak [number $\frac{1}{2}(n + 1)$ in the case of n peaks] to be eluted at $k = 2$. In the case of an even number of peaks the average k value of the two peaks in the middle (numbers $\frac{1}{2}n$ and $\frac{1}{2}n + 1$) can be taken to equal 2. The resulting peak positions can be used to establish suitable capacity factor ranges for multi-component mixtures. Values under two different sets of conditions, *i.e.*, $R_s = 2$, $N = 10^4$ and $R_s = 5$, $N = 5000$, are listed in Table 1.

Obviously, more peaks can be separated in a certain interval if the mutual distances become smaller (*e.g.*, $R_s = 2$ instead of $R_s = 5$). In the example in Table 1 in which the peaks are more widely spread, it appears not to be possible to elute more than eight peaks in the range $1 < k < 20$ with the middle peak(s) around $k = 2$.

Allowing capacity factors all the way down to zero is usually not advisable. Some system peaks or just baseline disturbances are always likely to be present close to $k = 0$, and the presence of solvent peaks may force us to aim to elute all relevant peaks with capacity factors above a certain value (*e.g.*, $k = 0.5$ or $k = 1$). If the k value for the first peak suggested by Table 1 (or by the repeated use of eqn. 5) falls below this threshold, then the following equation may be used to establish a desirable range of k values:

$$k_\omega = (1 + k_\alpha) \exp\left[\frac{4R_s(n-1)}{\sqrt{N}}\right] - 1 \tag{7}$$

where k_ω is the capacity factor of the last peak, k_α the (desired) capacity factor of the first peak and n the number of peaks. This equation may, for example, be used to establish that ten peaks can be eluted with $R_s = 5$ and $N = 10^4$ between $k_\alpha = 1$ and $k_\omega \approx 11$.

Both in Table 1 and in eqn. 7, it has been assumed that all peaks are distributed evenly thoughout the chromatogram. Of course, this is unlikely to be the case for "new" samples, *i.e.*, early in the development of chromatographic methods. Assuming that the peaks are distributed randomly, the required peak capacity (n_p) for resolving n peaks can be estimated [2]. In this case, Table 1 and eqn. 7 can be used by using n_p instead of the actual number of peaks n.

Often, once the components in a sample have been eluted within the optimum range of k values, the selectivity of the separation will subsequently be optimized. If this is the case, the assumption of a random distribution of the peaks becomes

TABLE 1

OPTIMUM CAPACITY FACTORS FOR SEPARATING GIVEN NUMBERS OF PEAKS

Data calculated using eqns. 5 and 6, assuming the middle peak to be located at $k = 2$ for odd numbers of peaks or around $k = 2$ for even numbers of peaks. Values of k above 20 (and below 0) are not given.

Odd numbers of peaks			Even numbers of peaks		
No. of peaks	$R_s = 2$, $N = 10^4$	$R_s = 5$, $N = 5000$	No. of peaks	$R_s = 2$, $N = 10^4$	$R_s = 5$, $N = 5000$
21	0.35	–	20	0.40	–
19	0.46	–	18	0.52	–
17	0.58	–	16	0.64	–
15	0.71	–	14	0.78	–
13	0.86	–	12	0.93	–
11	1.01	–	10	1.09	–
9	1.18	–	8	1.27	0.10
7	1.36	0.28	6	1.45	0.46
5	1.56	0.70	4	1.66	0.94
3	1.77	1.26	2	1.88	1.58
1	2.00	2.00			
3	2.25	2.99	2	2.12	2.42
5	2.52	4.30	4	2.38	3.55
7	2.81	6.05	6	2.66	5.05
9	3.13	8.37	8	2.97	7.05
11	3.48	11.46	10	3.30	9.70
13	3.85	15.56	12	3.66	13.22
15	4.25	–	14	4.04	17.90
17	4.69	–	16	4.46	–
19	5.17	–	18	4.92	–
21	?	–	20	5.41	–

unrealistic. A typical series of actions in developing HPLC separations is to perform retention optimization, selectivity optimization and system optimization. In modern software for system optimization [3,4] the required resolution can be specified. This required resolution refers to the lowest value for R_s between any two peaks of which at least one is relevant. All other (relevant) values for R_s in the chromatogram will be higher. Therefore, the required range of capacity factors will be broader than suggested by Table 1 or eqn. 7. The required value for N depends very much on the results of the selectivity optimization. However, if an HPLC separation is successfully developed, the required plate count should not exceed *ca.* 10 000. A reasonable practical estimate for the required capacity factor range may be obtained by using twice the value for R_s that will be specified during the system optimization stage, a reasonable value for the required number of plates (*e.g.*, $N = 10^4$) and eqns. 5–7 or Table 1. An optimization process in which the required capacity factor range is adapted based on the results obtained during the selectivity optimization stage may seem attractive, but one should be aware that most methods used to affect the capacity factors will also have an effect on the selectivity.

1.2. Principles of gradient scanning methods

The use of gradient elution techniques for predicting isocratic elution conditions is based on the ability to describe the retention of solutes under gradient conditions from known data on their isocratic behaviour [5–8] and, most important for the present application, *vice versa*. Let us assume that the capacity factor $k(x)$ is some function of the parameter x, which is programmed during the chromatographic run. The gradient elution programme is described by the function f:

$$x = \mathrm{f}(t) \tag{8}$$

A gradient programme will need a certain time (the so-called delay time, τ) to reach the top of the column and a further time z/u, with u being the linear velocity of the mobile phase ($u = L/t_0$), to reach a certain point z in the column. Assuming that the function f itself is not affected by the process (*i.e.*, no significant deformations occur due to the instrumentation and connections, or due to selective retention of solvent components on the column; see section 1.3), we find

$$x(z,t) = \mathrm{f}\left(t - \frac{z}{u} - \tau\right) \tag{9}$$

and, after introducing the inverse function f^{-1},

$$t = \frac{z}{u} + \tau + \mathrm{f}^{-1}(x) \tag{10}$$

or

$$\mathrm{d}t = \frac{\mathrm{d}z}{u} + \mathrm{df}^{-1}(x) \tag{11}$$

The migration velocity of the solute is given by

$$\frac{\mathrm{d}z}{\mathrm{d}t} = \frac{u}{1 + k(x)} \tag{12}$$

Eliminating $\mathrm{d}t$ from eqns. 11 and 12 yields

$$\frac{\mathrm{df}^{-1}(x)}{k(x)} = \frac{\mathrm{d}z}{u} \tag{13}$$

Eqn. 13 can be integrated if we realize that z varies between 0 and the column length L and the inverse function f^{-1} (see eqn. 10) varies between a value of $-\tau$ at $t = 0$ and $t_R - t_0 - \tau = t'_R - \tau$ when the solute elutes from the column ($z = L$). Until the solute is overtaken by the gradient programme at the time $t = \tau + z/u$ (or $\mathrm{f}^{-1} = 0$), the programming parameter will maintain its initial value x_0 and the capacity factor will likewise remain constant [$k = k(x_0)$]. We now find

$$\int_{-\tau}^{0} \frac{\mathrm{df}^{-1}(x)}{k(x_0)} + \int_{0}^{t'_R-\tau} \frac{\mathrm{df}^{-1}(x)}{k(x)} = \int_{0}^{L} \frac{\mathrm{d}z}{u} = t_0 \tag{14}$$

or

$$\int_{0}^{t'_R-\tau} \frac{\mathrm{df}^{-1}(x)}{k(x)} = t_0 - \frac{\tau}{k(x_0)} \tag{15}$$

The two vital ingredients of eqn. 15 are the function f describing the gradient programme and the relationship $k(x)$ between the capacity factor and the programmed parameter. Once these two functions are known, the integral equation can always be solved numerically to yield a value for t'_R. In a number of instances analytical solutions can be found. For a summary of these, the reader is referred to the literature [7]. Here we shall just consider one particularly important example, namely that of a linear composition gradient in reversed-phase liquid chromatography (RPLC). Over a limited range of composition, the function $k(\varphi)$ that describes the variation of the solute capacity factor with the volume fraction φ of the organic modifier in the mobile phase can be approximated by

$$\ln k(\varphi) = \ln k_0 - S\varphi \tag{16}$$

where k_0 is the extrapolated capacity factor in pure water and S is the slope of the logarithmic plot. A linear gradient can be described by

$$\varphi = a + bt \tag{17}$$

so that the inverse function becomes

$$\mathrm{f}^{-1}(\varphi) = \frac{\varphi - a}{b} \tag{18}$$

Substitution of eqns. 16 and 18 into eqn. 15 yields

$$\int_{0}^{t'_R-\tau} \frac{\mathrm{d}\,\dfrac{\varphi - a}{b}}{k_0 \mathrm{e}^{(-S\varphi)}} = t_0 - \frac{\tau}{k(a)} \tag{19}$$

or

$$\frac{1}{bk_0} \int_{a}^{a+b(t'_R-\tau)} \mathrm{e}^{S\varphi}\,\mathrm{d}\varphi = t_0 - \frac{\tau}{k(a)} \tag{20}$$

which yields

$$t'_R = \frac{1}{Sb} \ln \left\{ 1 + Sbk(a) \left[t_0 - \frac{\tau}{k(a)} \right] \right\} + \tau \tag{21}$$

If the solute is eluted after completion of the gradient, *i.e.*, after the final composition y has been reached at the end of the column [$t'_R \geqslant (y - a)/b + \tau$], then

$$t'_R = k(y) \left[t_0 - \frac{\tau}{k(a)} \right] + \frac{k(y)}{Sb} [k(y) - k(a)] - \frac{a - y}{b} + \tau \tag{22}$$

These equations can be simplified if the sample is injected at the time at which the gradient programme reaches the top of the column, *i.e.*, at $t = \tau$. In that case we find

$$t'_R = \frac{1}{Sb} \ln [1 + Sbt_0k(a)] \tag{23}$$

and

$$t'_R = k(y)t_0 + \frac{k(y)}{Sb} [k(y) - k(a)] - \frac{a - y}{b} \tag{24}$$

for elution prior to and after completion of the gradient, respectively.

1.2.1. Ionogenic solutes. With the exception of ion-exchange chromatography [10], the description of gradient elution experiments using eqn. 15 is more difficult for ionogenic solutes. This is due to both experimental [controlling the inverse gradient function $f^{-1}(x)$] and fundamental [the function $k(x)$] difficulties. In many cases gradients are used to obtain qualitative (charge, type) rather than quantitative information.

Based on theoretical considerations from an equilibrium retention model, Foley and May [11] suggested that pH gradients in the reversed-phase mode could potentially be useful for the separation of multi-component mixtures of weak acids or weak bases. The problem of running linear gradients over a broad pH range with good buffer capacity was satisfactorily tackled [12,13]. Linear gradients from pH 3 to 9 were generated by using two pumps and mixing a 0.05 *M* "universal buffer" (consisting of acetic, phosphoric and boric acids) and a 0.1 *M* sodium hydroxide solution. The flow-rate of the two pumps had to be controlled by a special computer programme [13], which is not readily available for others. The difficulty of realizing linear or otherwise well characterized pH gradients may be the main reason why the usefulness of pH gradients for predicting suitable initial conditions for optimization procedures has not been evaluated.

In contrast, organic modifier gradients at constant eluent pH have been found extremely useful for classifying the components of more or less unknown samples according to their charge and "type" (see section 3.2.). In this context, the type of a solute refers to whether it is neutral, strongly or weakly acidic, or strongly or weakly basic.

The use of micellar mobile phases for gradient elution in reversed-phase

chromatography has been demonstrated. Micellar gradients, in which the concentration of micelles increases with time, can be used to elute sample mixtures covering a broad polarity range [14] and are compatible with electrochemical detection [15]. In principle, micellar gradients may be used to determine initial mobile phase conditions prior to the optimization of micellar chromatographic separations.

1.3. Potential complications

From eqn. 14 it is apparent that there are two fundamental sources of error in predicting retention times under gradient conditions: errors in the inverse gradient function $f^{-1}(x)$ and errors in the relationship between the capacity factor and the programmed parameter $k(x)$. Errors in the gradient function generally reflect differences between the desired gradient programme $x(t)$, as entered by the user, and the actual variation $x_{obs}(t)$ of the programmed parameter with time [16,17]. One such variation is the gradient delay time τ, which has been accounted for in the mathematics in the previous section. However, there it was assumed that the function $x(t)$ was otherwise left unchanged. The programmed function is affected by instrumental factors: mixing volumes, inaccurate or imprecise mixing, pump efficiency, etc. Generally, the actual gradient function will therefore differ from the programmed function. If the deviations are (quantitatively) known, they can be accounted for mathematically [16]. However, in practical situations this is often not the case. Steeper gradients, lower flow-rates and higher pressures tend to cause greater differences between $x(t)$ and $x_{obs}(t)$. It is important to select instrumentation that is as good as possible for the purpose, *i.e.*, that shows the smallest possible differences between the desired and the actual gradients. Certain pieces of instrumentation, such as sample loops with very large internal volumes, are not recommended for use in the present application.

Another source of variations is the deformation of the gradient programme by the column itself [18], most importantly because of preferential adsorption of solvent components by the stationary phase, an effect sometimes referred to as "solvent demixing". In some instances, *e.g.*, in ion-pair chromatography, this effect can be so large as to impair the practical application of gradient elution techniques. In many other instances it is a significant factor.

The second major category of complications is formed by variations in the relationship between k and x. Only a reasonable description of this relationship is needed to predict retention times under gradient conditions [9,18]. This implies that the reverse process, obtaining information on the $k(x)$ relationship from gradient elution retention data, will be sensitive to errors. Assumptions made about the relationship between k and x and about the parameters involved, for example assuming retention in RPLC to vary with composition according to $\ln k = \ln k_0 - S\varphi$ with $S = p + q \ln k_0$ (see section 2), can significantly affect the outcome of calculation procedures.

The accuracy of prediction methods based on gradient elution will be considered in the relevant sections below.

1.4. Alternative scanning methods

At the beginning of this paper the advantages and disadvantages of gradient scanning techniques were summarized. The main disadvantages, limited accuracy and restricted detection possibilities, could possibly be overcome by using other scanning

techniques. One obvious improvement is to follow the gradient experiment by the (predicted) non-programmed run and to improve the conditions if necessary. In such a second experiment both of the major disadvantages of gradient scanning methods disappear and therefore this method is to be preferred over the use of two different gradient elution experiments.

Instead of a single gradient experiment, a number of isocratic runs may be used to establish optimum retention conditions [19]. The obvious disadvantage of this method is the number of experiments required. It is important to do a first experiment with a strong eluent, *e.g.*, 100% organic modifier in RPLC, so that relevant solutes will not adhere to the column. The solvent strength can then be lowered in a carefully considered manner, *e.g.*, by using large steps first, followed by "fine tuning" of the eluent.

If thin-layer chromatography (TLC) is used as a scanning technique, the risk of non-migrating solutes is eliminated. Therefore, an experiment on a TLC plate in support of a column experiment is often worth considering. However, TLC is much more attractive as a method for finding an appropriate stationary phase than for establishing the optimum mobile phase composition. In the latter instance the technique is much more time consuming and much less easily automated than column LC.

A final way to predict conditions under which retention times in the optimum range can be achieved is to make use of existing data on known (related) compounds and to predict the behaviour of unknown (*e.g.*, newly synthesized) solutes. Many studies on so-called "quantitative structure–retention relationships" have been performed. In all instances, vast amounts of data are needed on very closely related compounds. A potential way to improve this situation is by the use of expert systems. These allow heuristic knowledge and experience from a chromatographer to be captured in a computer programme. In one recent system optimum conditions are predicted for basic drugs. The predictions are verified experimentally and subsequently improved [20].

2. NEUTRAL SOLUTES

2.1. Two gradient scans

Assuming that the variation of retention with composition can be described by eqn. 16, we need to determine two coefficients, $\ln k_0$ and S, to characterize the behaviour of a solute. In principle, we need two data points to determine the two unknown coefficients. More generally, this will be the case in any situation in which two parameters define the relationship between retention under non-programmed conditions and the programmed parameter, in other words, in any situation in which a straight line can be obtained by plotting some known function of the capacity factor *vs.* some known function of the programmed parameter. In applying two different gradients, the analyst can be reasonably assured that all detectable compounds actually appear in the chromatogram. Thus, running two different gradient programmes is an effective way to obtain the two required data points. This strategy is, for example, applied in the DryLab programme developed by Snyder *et al.* [21,22].

When the solutes elute before the completion of the gradient, and assuming for simplicity that the solutes are injected after a delay time τ, *i.e.*, when the gradient

actually reaches the top of the column, we may write for the retention times of a solute i subjected to two different linear gradients

$$t'_{R_{i,1}} = \frac{1}{S_i b_1} \ln [1 + S_i b_1 t_0 k_i(a_1)] = \frac{1}{S_i b_1} \ln (1 + S_i b_1 t_0 k_{0,i} e^{-S_i a_1}) \quad (25)$$

and

$$t'_{R_{i,2}} = \frac{1}{S_i b_2} \ln [1 + S_i b_2 t_0 k_i(a_2)] = \frac{1}{S_i b_2} \ln (1 + S_i b_2 t_0 k_{0,i} e^{-S_i a_2}) \quad (26)$$

Knowing the starting conditions (a_1 and a_2, respectively) and the slopes (b_1 and b_2) of the two gradient programmes, the coefficients k_0 and S can be established using eqns. 25 and 26. The more different the slopes of the gradients (b_1 and b_2) are chosen, the more precise will be the estimate for S [23]. There is no analytical solution to the set of two equations, but when using a computer numerical methods are rapid and convenient [23].

While the use of two gradients may potentially provide more accurate estimates of the parameters describing the isocratic retention behaviour of a solute, there are also some additional problems [24]. The most significant of these is the need to match correctly the peaks of the individual solutes in the two chromatograms. Reversals in peak orders form a complication for methods based on two gradient scans. However, when single-scan methods are used the same effect causes inaccurate predictions.

2.2. Single gradient scan

In the previous section we investigated the possibility of characterizing the isocratic retention behaviour of solutes based on two gradient runs. If only one parameter is needed to characterize the isocratic elution behaviour of a solute, then a single gradient would suffice. Suggestions have been made for "rules of thumb" that provide an estimate of suitable isocratic elution conditions based on a single gradient scan. For example, Snyder *et al.* [5] suggested that for a component eluting after a time t_R under gradient conditions, the composition at the column inlet at a time $t_R - 2.5t_0$ would be a good starting point for isocratic elution. However, it is a prerequisite for successful gradient elution experiments that the programmed parameter has a strong effect on retention, and at least two parameters (and thus two experimental data points) are normally needed to characterize such an effect. One experimental data point (*i.e.*, one gradient scan) would only suffice if there is some known relationship between the two parameters (slope and intercept). The most significant example of a situation in which this is the case occurs in RPLC when using methanol (and to some extent THF) as the organic modifier [25].

The theoretical basis for the rapid determination of suitable isocratic conditions from a single linear gradient in RPLC originates from a study of more than 50 different solutes eluted under isocratic conditions from an ODS stationary phase using binary methanol–water mixtures [9]. Over a limited range ($1 < k < 10$) the retention behaviour of a solute in such systems could be accurately described by eqn. 16.

Moreover, the slope S and the intercept $\ln k_0$ were shown to be highly correlated. The equation

$$S = p + q \ln k_0 \tag{27}$$

has been found to be approximately valid, at least for well defined groups of solutes. The values obtained for the parameters in ref. 9 were $p = 2.86$ and $q = 0.77$. The generality of these coefficients has been disputed by Berridge [26], who argued that p and q were likely to depend on the type of the column, in addition to the hold-up time (t_0) and the flow-rate. The stationary phase must doubtlessly have some effect, but k values (and thus p and q values, which are derived from these) are principally independent of the flow-rate. When a consistent method is used to determine or estimate t_0, errors in its value should not greatly affect k values, at least not for capacity factors larger than 1 (eqn. 16 is assumed to be valid only over the range $1 < k < 10$).

Hafkenscheid and Tomlinson [27] compared values of p and q from four different sources, obtained from large numbers of data on three different columns (Hypersil-ODS, Nucleosil 10RP-18, and LiChrosorb RP-18). They found good agreement between the different values for p and (especially) q and proposed to use the average values to obtain the most reliable estimates for S. The suggested values were where $p = 3.592$ and $q = 0.74$. Calculations based on both sets of parameters (*i.e.*, those of Schoenmakers *et al.* [25] and those of Hafkenscheid and Tomlinson [27]) show a maximum difference in the predicted optimum mobile phase composition of 2.5% (see Table 2). This illustrates that in applying eqn. 27 for gradient scanning purposes the values of p and q are not a major source of error.

If eqn. 27 holds, eqn. 23 (again, for reasons of simplicity, assuming the sample to be injected at $t = \tau$) can be written explicitely in terms of either k_0 or S. The latter, simpler, equation is

TABLE 2

PREDICTED ISOCRATIC METHANOL–WATER BINARY ELUENT COMPOSITIONS (φ) AND CAPACITY FACTORS FOR THE FIRST PEAK (k_α) ON THE BASIS OF HYPOTHETICAL GRADIENT DATA

t'_α = net retention time of first peak under gradient conditions; t'_ω = gradient elution retention time of last peak. Gradient programme, 0–100% methanol in water in 15 min; $t_0 = 2$ min. Isocratic capacity factor for the last peak, $k_\omega = 10$. Coefficients in eqn. 27 were taken from Schoenmakers *et al.* [25] ($p = 2.86$, $q = 0.77$) and from Hafkenscheid and Tomlinson [27] ($p = 3.592$, $q = 0.74$).

t'_α (min)	t'_ω (min)	Ref. 25		Ref. 27	
		φ	k_α	φ	k_α
4	6	0.044	3.9	0.067	3.6
4	8	0.217	1.9	0.232	1.7
4	10	0.371	1.0	0.383	0.8
4	12	0.521	0.6	0.531	0.4
4	14	0.673	0.3	0.683	0.2
4	16	0.833	0.2	0.841	<0.1

$$t'_{R_i} = \frac{1}{S_i b} \ln \left[1 + S_i b t_0 e^{\frac{S(1-qa)-p}{q}} \right] \quad (28)$$

Although eqn. 28 cannot be made explicit in S, it can easily be solved graphically or numerically [25]. In this respect, an important characteristic of the equation is that it is monotonous, *i.e.*, t'_{R_i} always increases with increasing S.

Fig. 1 can be used to estimate graphically the optimum binary composition of a methanol–water mixture based on the net retention times of solutes under standard gradient conditions (0–100% linear gradient in 15 min; $t_0 = 125$ s). Fig. 1 incorporates eqns. 16, 27 and 28. Non-ideal processes (instrumental and chromatographic) can reduce the accuracy of the above equations and thereby lead to errors in the estimated binary composition. Deviations of eqn. 16 or 27 are specific to the physical and chemical properties of the solute. Instrumental and experimental problems, such as malfunctioning of equipment, should be taken care of by the operator instead of being included in the procedure. The gradient delay time can be taken into account mathematically, but in drawing Fig. 1 it has been assumed that $\tau = 0$, which corresponds to injection of the sample a time τ after starting the gradient programme.

The desired capacity factor range ($k_\alpha^* \leqslant k \leqslant k_\omega^*$, where k_α^* is the minimum desirable capacity factor for the first peak and k_ω^* the maximum desirable capacity factor for the last peak) can be taken into account in a gradient scanning procedure. De Galan *et al.* [28] calculated the peak capacity from

$$N_c = \frac{\sqrt{N}}{4R_{s,req}} \ln \left(\frac{1 + k_\alpha}{1 + k_\omega} \right) + 1 \quad (29)$$

where N_c is the peak capacity, $R_{s,req}$ is the required resolution and N is the plate count. The statistical approach developed by Herman *et al.* [29] can be used to determine the peak capacities needed to achieve a separation with a given probability of success. This can be used to determine which capacity factor range should be aimed for. The following data are needed: how many solutes are present, how many of these are of analytical interest, what is the polarity range of the sample, what is the actual plate

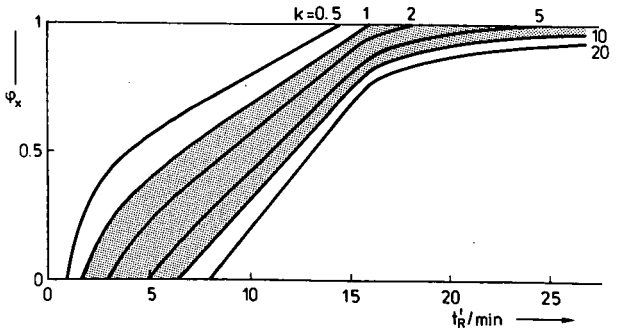

Fig. 1. Graphical presentation of the relationship between gradient elution (net) retention times and isocratic composition. Lines represent the required composition to achieve the indicated capacity factor. Linear gradient from 0 to 100% of methanol in water, $t_0 \approx 2$ min. Column, ODS. Reprinted from ref. 25 with permission.

count of the column and what resolution will be required for the peaks of interest? In this procedure, interpreting the result of a gradient scan becomes very important. The total number of components in the mixture, the number of components which are of analytical interest, the lowest k value which is allowed for the first-eluting peak and the required minimum resolution all need to be estimated. If the number of components is not known, but gradient data are available, the total number can be estimated from the statistical theory of component overlap devised by Martin *et al.* [30].

2.2.1. Transfer to other solvents. A useful addition to the above procedure is the possibility of transferring to an alternative organic modifier after satisfactory retention conditions have been established for the methanol–water system. Empirical transfer rules [25] can be used to estimate the appropriate compositions of binary acetonitrile–water and THF–water mixtures. These so-called iso-eluotropic mixtures are expected to yield approximately the same retention times, in combination with different (hopefully improved) selectivity. The equations were obtained for an "average" solute, based on experimental data for a large number of aromatic compounds. Within the range $1 < k < 10$ the following equations can be applied:

$$\varphi_{ACN} = 0.32\varphi^2_{CH_3OH} + 0.57\varphi_{CH_3OH} \tag{30}$$

where ACN is acetonitrile, and

$$\varphi_{THF} = 0.66\varphi_{CH_3OH} \tag{31}$$

The use of eqns. 30 and 31 may lead to differences in the experimentally observed capacity factors of up to 50% between the methanol–water system and the acetonitrile–water system and of up to 100% between methanol–water and THF–water. If the entire group of solutes in the sample is either eluted too early or too late, additional isocratic measurements can be performed as described by Herman *et al.* [31] and by Haddad and Sekulic [32]. Patel and Jefferies [33] have explored the possibility of using the octanol–water partition coefficient of the mobile phase as a solvent strength parameter. In their studies, the predicted iso-eluotropic compositions were in good agreement with those predicted by the above transfer rules (eqns. 30 and 31).

In Fig. 2 a graphical comparison is given for the equations derived by Schoenmakers *et al.* [25], Herman *et al.* [31] and Patel and Jefferies [33]. In the lower range of organic modifier concentrations (up to 40 or 50% methanol) all the equations predict similar iso-eluotropic eluent compositions. At high concentrations of organic modifier the transfer rules given by Schoenmakers *et al.* [25] are seen to yield values between the other two.

2.3. Single gradient scan plus isocratic correction

Because eqn. 27 will only be approximately valid, the predicted isocratic elution conditions may differ from those observed experimentally in a subsequent experiment. Deviations of up to a factor of two have been recorded, although the errors are usually less. The combination of the gradient elution retention data and those obtained in the first isocratic experiment allow a more accurate characterization of the isocratic retention behaviour. If we again use RPLC as our example and assume eqn. 16 to be valid, we have for the capacity factor (k_c) at the predicted isocratic composition (φ_c)

$$\ln k_c = \ln k_0 - S\varphi_c \tag{32}$$

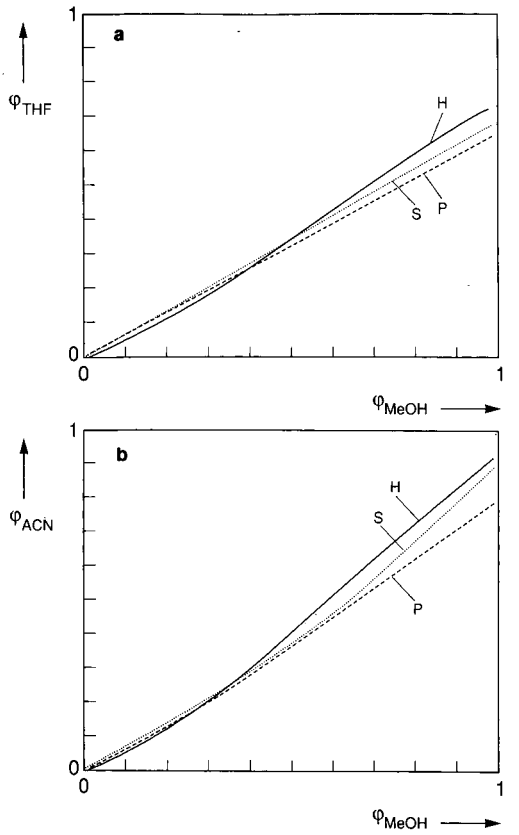

Fig. 2. Comparison of the transfer rules given by Schoenmakers *et al.* [25], Herman *et al.* [31] and Patel and Jefferies [33]. (a) Transferring from methanol to THF; (b) transferring from methanol to acetonitrile. MeOH = methanol.

and

$$\ln k_a = \ln k_0 - S\varphi_a = \ln k_c - S(\varphi_a - \varphi_c) \tag{33}$$

Substitution of eqn. 33 in eqn. 23 (injecting the sample at $t = \tau$) yields

$$t'_{R_i} = \frac{1}{Sb} \ln [1 + Sbt_0 k_c e^{-S(\varphi_a - \varphi_c)}] \tag{34}$$

Again, this equation cannot be made explicit in S, but it can easily be solved numerically. Once knowing S, the intercept $\ln k_0$ can readily be obtained by rearranging eqn. 32. A correction procedure based on this principle has been described by Herman *et al.* [31]. The practical correction method described by Haddad and Sekulic [32] for ionogenic solutes (see section 3.3) can also be used. Still more pragmatic approaches have been reported by Snyder *et al.* [34], based on the so-called linear solvent strength theory, and by De Smet *et al.* [35], who used expert systems.

3. IONIC SOLUTES

3.1. Selecting the optimum elution range

The optimization of the separation of sample mixtures containing ionic and/or ionogenic and neutral compounds represents a complex task owing to the large number of (often interrelated) mobile phase variables which affect solute retention and selectivity. In RPLC the separation of non-charged solutes involves almost exclusively the manipulation of the type and/or concentration of the organic modifier(s) in the aqueous eluents. The separation of samples containing ionic solutes usually needs the variation or correct selection of eluent pH, ionic strength, type and concentration of the ion-pairing reagent and the organic modifier(s).

An important feature of sample mixtures containing ionic solutes is that at a given (isocratic) concentration of the organic modifier the retention of all solutes, thus including the first- and the last-eluting ones, may be considerably influenced by the eluent pH or by the addition of ion-pairing reagents. When a sample contains only neutral compounds, a very large difference in the gradient retention times of the first- and the last-eluting peaks may clearly indicate that isocratic elution of the sample is not possible. On the other hand, when the first- and last-eluting compounds are different with respect to charge or type, varying the pH or adding a pairing ion may bring the first and last peaks closer together so as to make isocratic elution of the sample possible.

It must be pointed out that the charge and type of the components play an important role in the selection of the optimum capacity factor range and the corresponding organic modifier concentration of the isocratic eluent. Let us consider a four-component mixture of two neutral solutes and two strong bases, with a large difference in the retention times between these two groups of solutes. The hypothetical $\ln k$ *vs.* organic modifier concentration (φ) behaviour for the four components is shown in Fig. 3a. If the strong bases elute as the last two peaks in the chromatogram, then the two groups of peaks can be brought closer by decreasing the retention of the late-eluting peaks. This may be achieved by adding a similarly (positively) charged pairing ion (see Fig. 3b). The organic modifier concentration must be fixed at a level (φ_1) which results in reasonable retention times for the two hydrophilic neutral solutes. If the sample contains two hydrophilic strong bases and two late-eluting neutral components (see Fig. 3c), then the organic modifier concentration must be high enough (φ_2) to elute the last peaks within an acceptable analysis time. The retention of the early eluting strong bases can be increased by the addition of an oppositely (negatively) charged ion-pairing reagent.

In both instances, the cluster of the neutral solutes must be considered in selecting the optimum k range. The retention of the ionic compounds may be out of the optimum range in this initial chromatogram, but it can be increased or decreased by at least one order of magnitude by adding a pairing ion of the appropriate hydrophobicity and concentration [36]. Once the retention of all components falls within the desired range, systematic selectivity optimization can be carried out (*e.g.*, by varying the type of the organic modifier [37]).

Obviously, these two hypothetical samples represent different separation problems and require different initial isocratic concentrations of organic modifier for a successful optimization of the separation, even though the $\ln k$ *vs.* φ behaviour (and

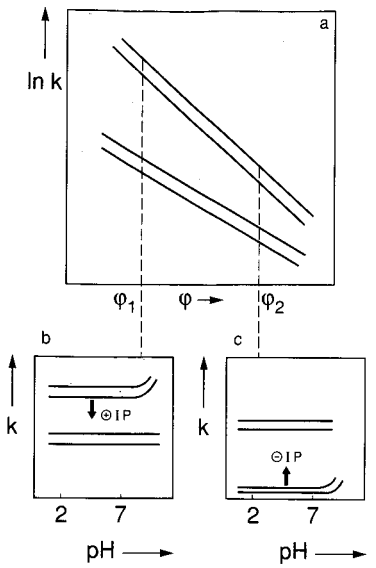

Fig. 3. (a) Schematic k *vs.* φ behaviour of a four-component sample mixture; (b) schematic k *vs.* pH behaviour of a sample mixture containing two hydrophobic strong bases (SB) and two hydrophilic non-charged (N) solutes at a constant organic modifier concentration (φ_1); (c) schematic k *vs.* pH behaviour of a sample mixture containing two hydrophobic non-charged (N) solutes and two hydrophilic strong bases (SB) at a constant organic modifier concentration (φ_2). Arrows indicate the direction of retention changes when an ion-pairing reagent (IP) is added to the eluent.

the gradient retention times) in the two cases may be identical. Therefore, the information on the charge and type of the solutes and the retention times of both the first- and the last-eluting solute peak(s) must always be carefully considered when deciding upon a suitable isocratic composition from gradient data.

When the sample contains components of other types (*e.g.*, weak acids or bases), the effect of the eluent pH must also be considered. For complex sample mixtures practical parameter selection rules [36–38] and expert systems [39–41] are valuable tools for guiding the analyst in the selection of suitable initial experimental conditions.

In order to make sound decisions, information is needed about the charge and type and the relative hydrophobicity (relative retention) of the components. When the nature of the sample components is not known *a priori*, the information can be determined from a number of specifically designed organic modifier gradients.

3.2. Classification according to charge and type

In the early 1980s, Berry and Shansky [42–44] introduced the technique of "pulse injection" of ion-pairing reagents in combination with linear solvent strength gradients at constant eluent pH. The basis of this technique is to deposit a concentrated plug of ion-pairing reagent on the top of the reversed-phase column before sample injection and the start of the gradient. The hydrophobic ion-pairing reagent adsorbs on the column and alters the retention of the ionic sample components through ionic attraction or repulsion. As a result, the retention time of solutes with a charge opposite

to the ion-pairing reagent increases relative to the non-charged solutes and that of similarly charged solutes decreases.

The pairing-ion pulse-injection technique has been used for the separation of several complex sample mixtures [45]. Although its potential for obtaining information about the charge and type of the sample components has been recognized [26], until recently the method has not been used as a systematic scouting procedure prior to selectivity optimization.

Low *et al.* [38] developed a strategy to establish the types and charges of solute ions from the retention shifts of the sample components that were observed in four successive 0–90% (v/v) methanol–buffer gradients run at pH 2.5 and 7.5. In two of the runs pairing-ion plugs, containing octanesulphonate (pH 2.5) or tetrabutylammonium (pH 7.5), respectively, were injected prior to sample injection. By tracking the shifts of the peaks in the different chromatograms, type assignments can be made by comparing the observed shifts with the expected (ideal) behaviour of charged solutes [38,46,47]. A typical example of solute-type determination by the above strategy is presented in Fig. 4 [47]. Four gradient chromatograms of a reaction mixture of pyrroloquinoline-quinone (PQQ) and cyclopropanol were recorded at different combinations of pH and pairing-ion pulse injection. It is important to note that only PQQ and its 5-(3-propanal) adduct (PQQ-M) were known in the sample mixture, and that no reliable information on the number and type of the other reaction products was available.

When the two gradients at pH 2.5 without (Fig. 4a) and with (Fig. 4b) octanesulphonate pulse injection are compared, no significant retention shifts are seen, indicating that all solutes are in a non-charged form at this eluent pH. In the gradient

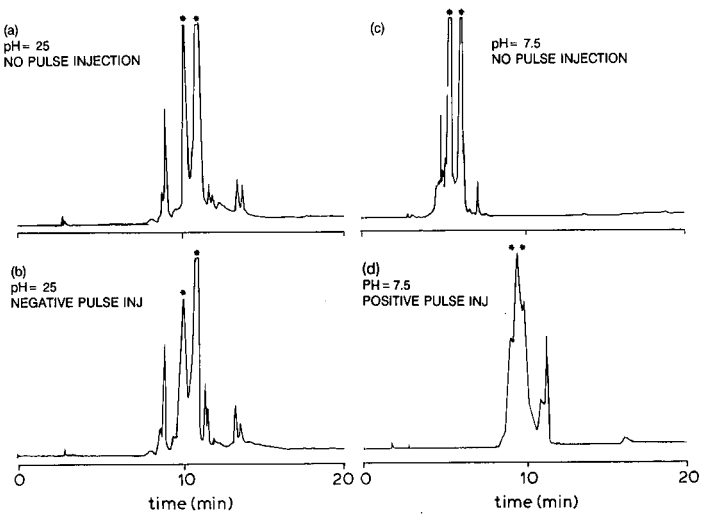

Fig. 4. Gradient elution chromatograms of a PQQ reaction mixture. Linear gradients of 0–90% methanol–triethylamine phosphate buffer in 15 min. (a) pH 2.5 without pulse injection ; (b) pH 2 with pulse injection of negatively charged octanesulphonate (as sodium salt); (c) pH 7.5 without pulse injection; (d) pH 7.5 with pulse injection of positively charged tetrabutylammonium (as bromide). Column, 20 cm × 4.6 mm I.D., packed with 5-μm Hypersil ODS. Flow-rate, 1.0 ml/min (t_0 = 2.05 min); UV detection at 320 nm. Asterisks indicate positions of PQQ and PQQ-M. Reprinted from ref. 47 with permission.

chromatogram at pH 7.5 without pulse injection (Fig. 4c) the retention times of all peaks are shorter by about 50%. The last peak observed with the pH 7.5 gradient even appears before the first one in the pH 2.5 gradient. This can be explained only by a lower hydrophobic retention of the ionized (dissociated) form of weakly acidic groups. Therefore, after examining three gradients we already know that all solutes are weak acids. However, we do not know whether all contain the same number of charged groups, as one or two negative charges may cause equally early elution in the gradient at pH 7.5. The pulse injection of a positively charged pairing-ion at pH 7.5 (Fig. 4d) results in a collective shift of all peaks to higher retention, indicating that all solutes have equal negative charge(s). Based on the information obtained from these scouting experiments, the relevant optimization parameters were selected and a successful iterative optimization was performed (see ref. 47 for details).

The main advantage of this experimental strategy is that it allows a rapid re-equilibration of the chromatographic system and a flexible variation of experimental conditions with different pH and pairing-ion combinations. Berry [45] has also shown that with sufficient purity of the mobile phase components and pairing-ions, gradients can be run using "near-universal" detection, *i.e.*, UV absorption at wavelengths down to 210 nm. There are two experimental factors which have to be carefully adjusted in order to classify the solutes based on the four gradients. First, the behaviour of non-charged compounds, strong acids and strong bases must be approximately ideal, *i.e.*, retention must be largely independent of variations in the pH and the buffer composition. This can usually be achieved by a careful selection of the stationary phase and by using a triethylamine–phosphate buffer [38,48,49]. Second, retention shifts induced by the pairing-ion must occur for all ionic solutes, irrespective whether they elute early or late in the gradient run. However, the adsorbed pairing-ion is increasingly removed from the column in the later part of the organic modifier gradient. Therefore, its effect diminishes for the late-eluting solute ions. In order to avoid early elution of the pairing-ion plug, multi-component pairing-ion mixtures can be applied [50].

When the retention shifts of the individual sample components can be established from the different chromatograms, classification of the solutes is straightforward [38,46]. However, peak tracking by injecting standards is either impractical or even impossible in the case of unknown samples. Peak tracking based on UV spectra (using a diode-array detector) is hampered by the sometimes dramatic variations in the spectral properties of ionogenic compounds with eluent pH [38]. Therefore, an extended design of seven linear gradients (run at pH 2.5, 5 and 7.5, with and without pulses of positively and negatively charged pairing-ions) in combination with an "artificial intelligence"-type computer programme has been proposed for establishing solute types without peak tracking. It has been demonstrated that solute classification can be carried out by this strategy for totally unknown sample mixtures [50].

3.3. Isocratic conditions for ionic solutes

Once the sample components are classified (either on the basis of *a priori* information or by means of a gradient scouting procedure) the results of gradient scans can be used to define non-programmed mobile phase compositions, where the sample mixture can be eluted in the selected optimum range. This is a vital step in the

application of various selectivity optimization procedures, *e.g.*, those described by Goldberg *et al.* [48], Coenegracht *et al.* [49] and Billiet *et al.* [51].

In reversed-phase chromatography the translation of the results of the gradient scans into isocratic eluent compositions is often based on some general assumptions for the approximate value of the slope (S) of the relationship between retention ($\ln k$) and the volume fraction of organic modifier (φ; see section 2.2). However, the gradient scouting procedures used for non-charged solutes often fail to provide good estimates of isocratic eluent compositions for ionic solutes [46,47]. Limited sets of data [52,53] suggest that in water-rich eluents and with comparable retention the slope of the $\ln k$ *vs.* φ relationship is generally steeper for ionic solutes than it is for non-charged solutes. In Fig. 5 the $\ln k$ data of fully ionized strong acids, bases and non-charged solutes are plotted as a function of the concentration of methanol and acetonitrile in an aqueous phosphate buffer eluent (see ref. 53 for experimental details). The differences in the slopes for ionic (solid lines) and non-charged (dashed lines) solutes might at least in part be responsible for the failure of conventional methods to predict suitable isocratic conditions for the elution of sample mixtures containing ionic solutes. Thus, one should expect large deviations between the observed k values of ionic solutes and the predicted values in the first isocratic binary eluent. Rules of thumb given by Snyder *et*

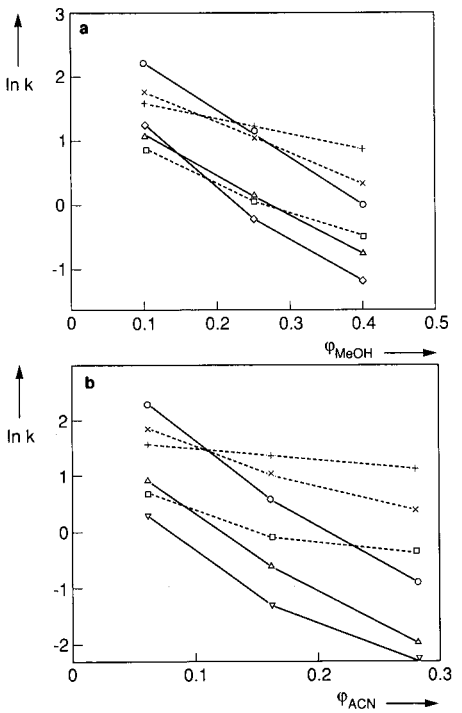

Fig. 5. Retention (k) of non-charged (dashed lines) and ionic (solid lines) solutes as a function of the concentration of (a) methanol and (b) acetonitrile in an aqueous 50 mM phosphate buffer eluent (pH 2.1) on a Hypersil ODS (5-μm) column. Solutes: + = methyl iodide; □ = 2-butanone; × = phenol; ○ = 2-naphthalenesulphonic acid; △ = phenylalanine; ◇ = morphine; ▽ = isoprenol. See ref. 53 for further details.

al. [34] or experimental procedures, such as that described by Haddad and Sekulic [32], can be applied to readjust the concentration of the organic modifier and to elute the sample mixture within the required retention limits.

The method suggested by Haddad and Sekulic [32] is based on a simple stepwise approximation of the capacity factor of the last-eluting peak using experimental isocratic retention data. The advantage of this procedure is that it can easily be extended [54] to estimate the retention of both the first- and the last-eluting sample components. A schematic illustration of this extended method is shown in Fig. 6. First, one should decide on the target capacity factors for the first (k_α^*) and the last (k_ω^*) eluting peaks. Maximum acceptable differences between the required and the actual solute retentions (*e.g.*, 20%; indicated by the horizontal dashed lines in Fig. 6) can also be defined. Next, the capacity factors of the first (k_{α_1}) and the last (k_{ω_1}) peaks obtained with the first isocratic eluent (φ_1) are compared with the target values. If the measured values fall outside the shaded area, an estimate is made of a new organic modifier concentration (φ_2) by assuming a linear ln k *vs.* φ relationship and a steep slope (*e.g.*, $S = 20$ in the reversed-phase mode). The sample mixture is chromatographed again at φ_2, and the capacity factors of the first (k_{α_2}) and the last (k_{ω_2}) peaks are determined. These are compared again with the target values (k_α^* and k_ω^*). If the deviations still exceed the predefined limits, the k values from the two isocratic measurements can be used to calculate new slope values and to estimate a new mobile phase composition (φ_3). This can be done so as to obtain the target value for the first- or for the last-eluting peak using either of the following equations:

$$\varphi_3^{<\alpha>} = \left(\frac{\varphi_1 - \varphi_2}{\ln k_{\alpha_1} - \ln k_{\alpha_2}}\right)(\ln k_\alpha^* - \ln k_{\alpha_1}) + \varphi_1 \tag{35}$$

or

$$\varphi_3^{<\omega>} = \left(\frac{\varphi_1 - \varphi_2}{\ln k_{\omega_1} - \ln k_{\omega_2}}\right)(\ln k_\omega^* - \ln k_{\omega_1}) + \varphi_1 \tag{36}$$

The next isocratic composition will be a compromise (often the average) between the values of $\varphi_3^{<\alpha>}$ and $\varphi_3^{<\omega>}$.

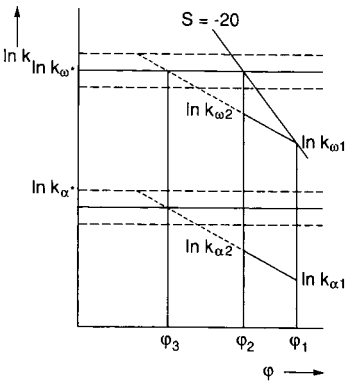

Fig. 6. Schematic representation of the stepwise approximation procedure of Haddad and Sekulic [32], extended to estimate the retention of both the first- and the last-eluting components of the sample.

4. CONCLUSIONS

Gradient-elution methods can elegantly be used for rapidly establishing the appropriate isocratic elution conditions for newly chromatographed samples. In comparison with the conventional approach of running a number of isocratic chromatograms on a trial-and-error basis, gradient-elution methods can be much more efficient and yield more consistent results.

Key factors are (i) a description of the retention behaviour of the solutes under isocratic conditions as a function of the programmed parameters and (ii) accurate knowledge of the actual gradient profile, *i.e.*, the variation of the programmed parameters with time. Reasonably simple calculation procedures are facilitated by the use of simple (*e.g.*, linear) programs and instrumentation that affects the actual profile as little as possible.

For non-ionic solutes two different gradient scans suffice in principle. In certain cases a single gradient scan may be adequate. A combination of one gradient scan and one isocratic verification experiment can often be used for the accurate prediction of optimum isocratic conditions.

For ionic solutes a larger number of scanning experiments is needed than for non-ionic solutes, but in comparison to the time needed for trial-and-error optimization the potential benefits of gradient-scanning methods are much greater. For characterizing the ionic solutes in unknown samples two things are needed. First, the solutes need to be classified according to their type (weak or strong; acids or bases) and charge. Next, the optimum isocratic conditions should be established. The concentration of organic modifier, the pH, and the type and concentration of ion-pair reagent are the most important parameters to be considered in the process. Using linear gradients at two different pH values in combination with "pulse injection" of ion-pairing reagents, four scanning experiments form the basis of an efficient classification procedure. Once the solutes have been classified, simple, stepwise procedures can be used to establish optimum isocratic conditions.

REFERENCES

1 P. J. Schoenmakers, *The Optimization of Chromatographic Selectivity —A Guide to Method Development*, Elsevier, Amsterdam, 1986.
2 J. M. Davis and J. C. Giddings, *Anal. Chem.*, 55 (1983) 418.
3 P. J. Schoenmakers, N. Dunand, A. C. Cleland, G. Musch and T. Blaffert, *Chromatographia*, 26 (1988) 37.
4 P. J. Schoenmakers and N. Dunand, *J. Chromatogr.*, 486 (1989) 219.
5 L. R. Snyder, J. W. Dolan and J. R. Gant, *J. Chromatogr.*, 165 (1979) 3.
6 L. R. Snyder, in Cs. Horváth (Editor), *High-Performance Liquid Chromatography —Advances and Perspectives*, Vol. 1, Academic Press, New York, 1980, p. 207.
7 P. Jandera and J. Churácek, *Gradient Elution in Column Liquid Chromatography —Theory and Practice*, Elsevier, Amsterdam, 1985.
8 P. J. Schoenmakers, H. A. H. Billiet, R. Tijssen and L. de Galan, *J. Chromatogr.*, 148 (1979) 519.
9 P. J. Schoenmakers, H. A. H. Billiet and L. de Galan, *J. Chromatogr.*, 185 (1979) 179.
10 Y. Baba, *J. Chromatogr.*, 485 (1989) 143.
11 J. P. Foley and W. E. May, *Anal. Chem.*, 59 (1987) 102.
12 R. V. Perkins, V. J. Nau and A. McPartland, *LC · GC*, 5 (1987) 419.
13 K. Ravichandran, J. J. Lewis, I.-H. Yin, M. Koenigbauer, C. R. Powley, P. Shah and L. B. Rogers, *J. Chromatogr.*, 439 (1988) 213.

14 J. S. Landy and J. G. Dorsey, *J. Chromatogr. Sci.*, 22 (1984) 68.
15 M. G. Khaledi and J. G. Dorsey, *Anal. Chem.*, 57 (1985) 2190.
16 M. A. Quarry, R. L. Grob and L. R. Snyder, *J. Chromatogr.*, 285 (1984) 1.
17 H. A. H. Billiet, P. D. M. Keehnen and L. de Galan, *J. Chromatogr.*, 185 (1979) 515.
18 M. A. Quarry, R. L. Grob and L. R. Snyder, *J. Chromatogr.*, 285 (1984) 19.
19 V. V. Berry, *J. Chromatogr.*, 199 (1980) 219.
20 R. Hindriks, F. Maris, J. Vink, A. Peeters, M. de Smet, D. L. Massart and L. Buydens, *J. Chromatogr.*, 485 (1989) 255.
21 L. R. Snyder, J. W. Dolan and D. C. Lommen, *J. Chromatogr.*, 485 (1989) 65.
22 J. W. Dolan, D. C. Lommen and L. R. Snyder, *J. Chromatogr.*, 485 (1989) 91.
23 M. A. Quarry, R. L. Grob and L. R. Snyder, *Anal. Chem.*, 58 (1986) 907.
24 J. W. Dolan, L. R. Snyder and M. A. Quarry, *Chromatographia*, 24 (1987) 261.
25 P. J. Schoenmakers, H. A. H. Billiet and L. de Galan, *J. Chromatogr.*, 205 (1981) 13.
26 J. C. Berridge, *Techniques for the Automated Optimization of HPLC Separations*, Wiley, Chichester, 1985, p. 45.
27 T. L. Hafkenscheid and E. Tomlinson, *J. Chromatogr.*, 264 (1983) 47.
28 L. de Galan, D. P. Herman and H. A. H. Billiet, *Chromatographia*, 24 (1987) 108.
29 D. P. Herman, H. A. H. Billiet and L. de Galan, *Anal. Chem.*, 58 (1986) 2999.
30 M. Martin, D. P. Herman and G. Guiochon, *Anal. Chem.*, 58 (1986) 2200.
31 D. P. Herman, H. A. H. Billiet and L. de Galan, *J. Chromatogr.*, 463 (1989) 1.
32 P. R. Haddad and S. Sekulic, *J. Chromatogr.*, 392 (1987) 65.
33 H. B. Patel and T. M. Jefferies, *J. Chromatogr.*, 389 (1987) 21.
34 L. R. Snyder, J. L. Glajch and J. J. Kirkland, *Practical HPLC Method Development*, Wiley, New York, 1988, p. 30.
35 M. de Smet, G. Hoogewijs, M. Puttemans and D. L. Massart, *Anal. Chem.*, 56 (1984) 2662.
36 Á. Bartha, Gy. Vigh and J. Ståhlberg, *J. Chromatogr.*, 485 (1989) 403.
37 Á. Bartha, Gy. Vigh and Z. Varga-Puchony, *J. Chromatogr.*, 499 (1990) 423.
38 G. K. C. Low, Á. Bartha, H. A. H. Billiet and L. de Galan, *J. Chromatogr.*, 478 (1989) 21.
39 M. de Smet, A. Peeters, L. Buydens and D. L. Massart, *J. Chromatogr.*, 457 (1989) 25.
40 Y. Hu, A. Peeters, G. Musch and D. L. Massart, *Anal. Chim. Acta*, 182 (1989) 1.
41 M. de Smet, A. Peeters, L. Buydens and D. L. Massart, *J. Chromatogr.*, 457 (1988) 25.
42 V. V. Berry, *J. Chromatogr.*, 236 (1982) 279.
43 V. V. Berry and R. E. Shansky, *J. Chromatogr.*, 284 (1984) 303.
44 V. V. Berry, *J. Chromatogr.*, 290 (1984) 143.
45 V. V. Berry, *J. Chromatogr.*, 321 (1985) 33.
46 J. K. Strasters, F. Coolsaet, Á. Bartha, H. A. H. Billiet and L. de Galan, *J. Chromatogr.*, 499 (1990) 523.
47 Á. Bartha, H. A. H. Billiet and L. de Galan, *J. Chromatogr.*, 464 (1989) 225.
48 A. P. Goldberg, A. Nowakowska, P. E. Antle and L. R. Snyder, *J. Chromatogr.*, 316 (1984) 241.
49 P. M. J. Coenegracht, N. V. Tuyen, H. J. Metting and P. M. J. Coenegracht-Lamers, *J. Chromatogr.*, 389 (1987) 351.
50 Á. Bartha and Gy. Vigh, *J. Chromatogr.*, 485 (1989) 383.
51 H. A. H. Billiet, J. Vuik, J. K. Strasters and L. de Galan, *J. Chromatogr.*, 384 (1987) 153.
52 T. L. Hafkenscheid, *J. Chromatogr. Sci.*, 24 (1986) 307.
53 Á. Bartha, Gy. Vigh, H. A. H. Billiet and L. de Galan, *J. Chromatogr.*, 303 (1984) 29.
54 Á. Bartha, H. A. H. Billiet and L. de Galan, unpublished results.

Journal of Chromatography, 550 (1991) 449–459
Elsevier Science Publishers B.V., Amsterdam

CHROMSYMP. 2122

Standardization of a multi-wavelength UV detector for liquid chromatography-based toxicological analysis

S. R. BINDER*, A. K. ADAMS, M. REGALIA and H. ESSIEN
Bio-Rad Laboratories, Clinical Systems Division, 1000 Alfred Nobel Drive, Hercules, CA 94547 (USA)
and
R. ROSENBLUM
BarSpec Systems Inc., P.O. Box 560, Rehovot 76103 (Israel)

ABSTRACT

The performance of a multi-wavelength UV detector for automated drug identification following liquid chromatographic separation was evaluated. The ability of selected wavelength ratios to distinguish two closely related drugs was considered at different concentrations. Calibration of the detector based on wavelength ratios was then utilized to standardize two different detectors and to evaluate instrument-to-instrument variation of a series of detectors. Reproducibility of the second-derivative zero intercept for these drug spectra was also evaluated. Standardization of detector performance by reference to these two parameters permitted the transfer of UV spectral libraries stored on one instrument to another without compromising the reliability of qualitative data.

INTRODUCTION

The use of multi-wavelength detectors (MWDs) in liquid chromatographic (LC) systems was actively explored 15 years ago [1–4] and their use in analysis of drug mixtures has been demonstrated [5]. The introduction of commercial instruments within the last decade [6–8] has permitted numerous investigations, primarily in the fields of pharmaceutical analysis and analytical toxicology.

Evaluation of peak purity has emerged as the most common application of LC–MWD, owing to regulatory requirements governing drug purity and stability testing. It is not uncommon that impurities and breakdown products have near-identical retention times and spectra, compared with the parent. Three different techniques have been used to validate peak homogeneity: (1) wavelength ratios, either one or several ratios; (2) multi-point spectral comparison, using either normalized spectra or transformed data; and (3) evaluation of spectral derivatives, especially the second derivative.

Numerous evaluations of the usage and comparative utility of these approaches have been published [9–14]. In most instances, the ability of the technique to detect impurities of 1% or less has been shown.

MWDs have also been used to monitor the location of peaks during mobile

0021-9673/91/$03.50

phase optimization experiments. The three techniques listed above can be successfully employed for this purpose [15,16], but is is also possible to utilize a stored spectral library for peak matching, as the spectra of all components are known [16,17]. Multi-parameter techniques have also been employed [18].

In contrast to these applications, the use of LC–MWD for the qualitative analysis of toxicological samples always requires the use of a spectral library. Although dual-wavelength ratios have been applied with moderate success [19,20], increased computerization has permitted the development of a variety of algorithms for drug identification. The most straightforward approaches rely on only one parameter (in addition to the retention time). The fraction of total absorbance at λ_{max} (FTA) [21,22] has been proposed, in addition to a normal vector produced by a Fourier transform [23]. However, for forensic work an algorithm which utilizes multiple parameters is desirable for increased confidence in the degree of matching between a library and unknown spectra. The use of multi-parameter identification can be compared with the use of multiple ion ratios (with retention data) in gas chromatographic–mass spectrometric (GC–MS) identification of drugs [24] and the use of multiple solvent systems in thin-layer chromatography [25]. Accordingly, many investigators have reported multi-parameter identification schemes, combining wavelength ratios, spectral maxima and minima and comparisons of normalized spectra or other transformed data [26–31].

The widespread availability of an LC toxicology system would provide a useful supplement to existing screening methods. This has not been possible for several reasons. First, the succesful application of library searching algorithms has been demonstrated [20,22,29,32,33] but each of the investigators developed an in-house spectral library. No reports have demonstrated the successful transfer of stored spectral data from one chromatographic system to another. As common MWDs utilize a multi-element diode array, it is likely that spectra from different instruments will show variation. Difficulties associated with the transfer of GC–MS libraries have been reported previously [25,34]. Further, the robustness of search algorithms could be affected, at both high and low concentrations, by deviations of detectors from linearity. A recent report by Dose and Guichon [35] indicates that bias and non-linearity are commonly observed and are affected by both the shape of the spectrum and the detector bandwidth. Published validations of search algorithms have generally employed samples at only one concentration, generally with high absorbance.

We recently described a multi-column LC–MWD that permits on-line purification and reproducible separation of basic drugs [36]. In this work, the calibration of a scanning detector for that analytical system was investigated, using wavelength ratios and second derivatives to establish linearity and reproducibility. Finally, the calibration scheme was tested on a larger series of instruments, demonstrating the reproducibility of this approach.

EXPERIMENTAL

Apparatus

The computer-controlled multi-column apparatus has been described previously [36]. Briefly, urines or sera initially pass through two clean-up cartridges, where proteins, salts and hydrophobic acids and neutral endogenous compounds are re-

moved. A 2-ml fraction containing basic drugs reaches a coupled 25 × 3.2 mm I.D. reversed-phase cartridge (Shandon, Runcorn, UK) and 150 × 4.6 mm I.D. silica cartridge (Machery, Nagel & Co., Düren, Germany), where the analytical separation occurs. In this study, only the conditions for the final separation are of interest, so the system can be considered equivalent to an isocratic analysis using cation-exchange chromatography. The flow-rate was 1.5 ml/min and the temperature was maintained at 35°C.

In place of the Hewlett-Packard Model 1040A diode-array detector used in the previous work, we monitored absorbance with a Chrom-A-Scope detector (BarSpec, Rehovot, Israel). This detector utilizes a rotating holographic grating, which permits the collection of ten scans per second. After wavelength selection light passes through the flow cell to a single diode sensor. The collected analog data from the diode are digitized and integrated with the velocity and acceleration data from the scanning assembly to produce three-dimensional array consisting of time, wavelength and absorbance. The wavelength accuracy of the detector is specified as ± 1 nm, with repeatability better than 1 nm. Repeatability is maintained by monitoring a "null point" which is used to calibrate the grating drive mechanism with each rotation. Although it is a single-beam system, all spectra are corrected continuously for dark current. Also, all the spectra taken for each peak are corrected by subtraction of a background spectrum, collected after the conclusion of the peak.

For the experiments described below, the wavelength range was 193–305 nm and the spectral bandwidth was 5 nm. The baseline noise was less than 1 mAU at 205 nm. The flow cell had a 9-μl volume and 5-mm path length.

Software for calculation of wavelength ratios, similarity factor (*SF*) and second derivative zero intercepts (2DI) was written at BarSpec. Wavelength ratios were calculated from absorbance readings which were the average of five scans; thus each data point corresponded to a 0.5-s segment of the peak. All of the absorbance ratios from upslope mid-point to downslope mid-point of the chromatographic peak were considered in the determination of a median ratio (typically 16–24 values). Except for the lowest concentrations, the range of values about the median ratio was no more than ± 5%. Similarity factors were calculated after comparison of spectra normalized from 205 to 250 nm so that the maximum absorbance value for each spectrum was 1.00. The sum of squares of the normalized differences at each wavelength yielded a parameter (*SF*) which was typically 0.020 or less for repetitive injections of the same drug. An *SF* value greater than 0.150 is evidence of an unsatisfactory spectral match. The 2DI and *SF* were each determined at the apex of the chromatographic peak. For most of the drugs evaluated, more than one 2DI was observed, but only the value between 215 and 245 nm was considered.

Chemicals

J. T. Baker high-performance liquid chromatographic (HPLC)-grade acetonitrile was obtained from VWR (Brisbane, CA, USA); Each batch was checked for conformity with the manufacturer's absorbance specification (less than 0.02 absorbance units at 200 nm); HPLC-grade potassium dihydrogen phosphate was from Fisher (Santa Clara, CA, USA) and N,N-dimethyloctylamine from Aldrich (Milwauke, WI, USA). All other laboratory chemicals were of analytical-reagent grade. Water was purified using an in-house ion-exchange system and was equivalent to

HPLC grade. Drugs were obtained from Alltech (State College, PA, USA) or Sigma (St. Louis, MO, USA).

After preliminary washing and cleaning steps, drugs were eluted from the cation-exchange column with a mobile phase consisting of 6 m*M* phosphate buffer containing 2 m*M* dimethyloctylamine (adjusted to pH 6.35 with phosphoric acid)–acetonitrile (2:1, v/v).

A 1 g/l stock solution of each drug was prepared in methanol and stored at −20°C. Working solutions of the drugs (0.3–20 mg/l) were prepared by dilution with urine from healthy individuals receiving no medication.

RESULTS AND DISCUSSION

Identification of amphetamine abuse by analysis of urine samples requires the differentiation of this drug from several closely related analogues. Some of these compounds are available without prescription for diet control (*e.g.*, phenylpropanolamine) or as decongestants (*e.g.*, pseudoephedrine). Others have no established medical usage but are illegally distributed, including the 'designer drugs' (*e.g.*, methylenedioxyamphetamine).

We evaluated the properties of amphetamine and several related drugs using our chromatographic system (Table I). The parent compound, methamphetamine, elutes well after amphetamine and is readily distinguished from it, but it must in turn be differentiated from phendimetrazine and other analogues. All of these drugs have a λ_{max} near 209 nm, which is of no value for differentiation. It is evident that retention time data alone can readily distinguish amphetamine from ephedrine, a contaminant often seen in methamphetamine preparations. Methoxyamphetamine and methylenedioxyamphetamine have spectra which are readily distinguished from amphetamine, as the *SF* value is well above our cut-off (0.150). Phenmetrazine, which is a secondary amine with a heterocyclic ring, has a spectrum that does not differ greatly from amphetamine (*SF* = 0.043) but has a different 2DI (221 *vs.* 223 nm). If the 2DI could be determined with high reproducibility, it would aid in the differentiation of phen-

TABLE I

RELATIVE RETENTION TIMES (RRT) AND SIMILARITY FACTORS (*SF*) FOR AMPHETAMINE AND RELATED DRUGS

Similarity factors were calculated by comparison with amphetamine. The internal standard was chlorpheniramine. For retention data, each drug was analyzed five times over a 4-month period.

Compound	RRT ± S.D.	2DI	*SF*
Phenylpropanolamine	0.298 ± 0.008	223	0.049
Chlorphentermine	0.320 ± 0.010	235	8.747
Methylenedioxyamphetamine	0.327 ± 0.013	227	3.505
Methoxyamphetamine	0.335 ± 0.009	241	12.156
Phentermine	0.343 ± 0.007	223	0.007
Amphetamine	0.349 ± 0.013	223	–
Phenmetrazine	0.384 ± 0.005	221	0.043
Ephedrine	0.385 ± 0.007	223	0.001
Pseudoephedrine	0.402 ± 0.008	223	0.002

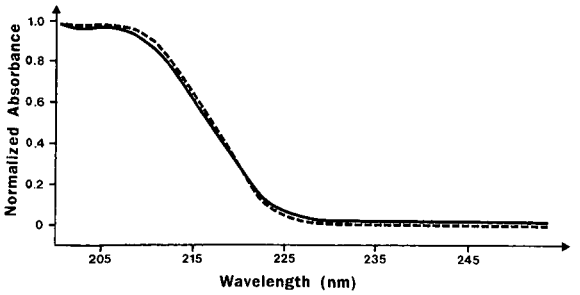

Fig. 1. Normalized spectra of (solid line) amphetamine and (dashed line) phentermine. For the data shown, $SF = 0.007$.

metrazine from amphetamine, ephedrine and pseudoephedrine. Finally, phentermine (α,α-dimethylphenethylamine) differs by only one α-methyl group from amphetamine (α-methylphenethylamine); the two compounds have very similar spectra (Fig. 1) and cannot be distinguished on the basis of relative retention times, 2DI or *SF*.

The very slight difference in the spectra in Fig. 1 was further evaluated as a test of detector reproducibility. The wavelength ratios at 5 nm intervals were calculated after duplicate analysis of each drug (Table II). The maximum difference in wavelength ratios (about 7%) was observed from 211:216 to 215: 220 nm. Although the largest differences were obtained at the highest wavelength ratio, the actual absorbances were less, which would limit sensitiviy. On the other hand, the baseline noise and background due to mobile phase increases at lower wavelengths. The 213:218 nm ratio was chosen as a compromise; the absorbance at 218 nm is about 50% of the maximum absorbance at 209 nm.

TABLE II

EVALUATION OF DIFFERENCES FOR WAVELENGTH RATIOS OF AMPHETAMINE AND PHENTERMINE

5 mg/l solutions were analyzed in duplicate.

Wavelength ratio (nm)	Phentermine	Amphetamine	Difference (%)
200:205	1.075	1.038	3.4
201:206	1.018	1.012	0.6
202:207	1.002	1.000	0.2
203:208	1.002	1.008	−0.6
204:209	1.014	1.025	−1.1
205:210	1.020	1.046	−2.5
206:211	1.069	1.089	−1.8
207:212	1.114	1.142	−2.4
208:213	1.169	1.210	−3.4
209:214	1.235	1.282	−3.7
210:215	1.313	1.385	−5.2
211:216	1.392	1.489	−6.5
212:217	1.499	1.601	−6.4
213:218	1.624	1.744	−6.9
214:219	1.796	1.942	−7.5
215:220	1.996	2.151	−7.2

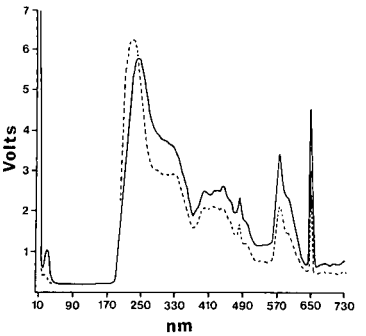

Fig. 2. Plot of the output of the deuterium lamp, collected in two different detectors. Solid line, unit 1; dashed line, unit 2.

Next, the ratio studies were used to evaluate the effect of calibration on detector performance. The detector manufacturer provides software for wavelength calibration, based on the output of the deuterium lamp. Although the maximum output is near 235 nm, this peak is a very broad line (Fig. 2). Further, exact location of this line may be affected by the characteristics of the quartz flow cell, the diode sensor and the aluminized mirror, which have different transmittance features. In contrast, the line at 651 nm is very sharp. A sharp emission peak is of little value for detection purposes, but is very useful for calibration. Therefore, the autocalibration software assigns 651 nm to this peak, with a stated accuracy of ± 1 nm. It may be observed in Fig. 2 that calibration on the 651-nm line is straightforward and that the observed lamp output from 200 to 250 nm showed variation between the two detectors.

The operating software permits reassignment of the calibration peak. The effect of this type of adjustment is shown in Table III. The 205:209 and 209:213 nm are shown for comparison. A shift of even 1 nm has a significant effect on all detection parameters. The 213:218 nm ratio is located at a point on the curve where absorbance changes rapidly, and it is profoundly affected by calibration. It is clear that any inaccuracy in calibration will alter this ratio.

To study variations between detectors, wavelength ratios for amphetamine and phentermine were collected using two different detectors, at concentrations that

TABLE III

RELATIONSHIP BETWEEN LAMP CALIBRATION AND AMPHETAMINE IDENTIFICATION CRITERIA

Calibration peak (nm)	Ratio 205:209 nm	Ratio 209:213 nm	Ratio 213:218 nm	2DI	Similarity factor, 205:250 nm
649	1.112	1.371	2.307	221	0.316
650	1.071	1.291	2.083	221	0.116
651	1.041	1.221	1.885	223	0.015
652	0.997	1.114	1.570	225	0.143
653	0.996	1.070	1.436	225	0.400

TABLE IV

WAVELENGTH RATIOS FOR TWO DIFFERENT DETECTOR UNITS

Each ratio is the mean of four values collected from analyses on four consecutive days.

Compound	Concentration (mg/l)	Unit 1			Unit 2		
		Ratio 205:209 nm	Ratio 209:213 nm	Ratio 213:218 nm	Ratio 205:209 nm	Ratio 209:213 nm	Ratio 213:218 nm
Amphetamine	20.0	1.035	1.228	1.906	1.020	1.202	1.828
	10.0	1.034	1.223	1.885	1.020	1.201	1.804
	5.0	1.035	1.220	1.871	1.026	1.198	1.802
	2.0	1.038	1.216	1.850	1.037	1.203	1.784
	1.0	1.045	1.206	1.872	1.067	1.197	1.786
	0.5	1.060	1.231	1.805	1.068	1.237	1.736
	0.3	1.074	1.195	1.854	1.057	1.267	1.811
	Mean	1.046	1.217	1.876	1.042	1.215	1.793
Phentermine	20.0	1.018	1.190	1.805	1.012	1.157	1.638
	10.0	1.020	1.184	1.736	1.014	1.156	1.615
	5.0	1.021	1.180	1.713	1.019	1.146	1.605
	2.0	1.022	1.172	1.671	1.065	1.144	1.612
	1.0	1.027	1.168	1.666	1.059	1.150	1.590
	0.5	1.037	1.170	1.666	1.101	1.203	1.630
	0.3	1.045	1.158	1.663	1.074	1.204	1.535
	Mean	1.027	1.175	1.703	1.049	1.166	1.604

ranged from 0.3 to 20 mg/l. The absorbance range covered by these concentrations was 10–600 mAU. Each drug was analyzed on four successive days at each concentration (Table IV).

All of the wavelength ratios showed slight changes with respect to changes in concentration. The 205:209 nm ratio decreased in response to an increase in concentration, whereas the 209:213 nm and 213:218 nm ratios increased. The instrument-to-instrument difference was 1–2% at 205:209 nm and 209:213 nm, but at 213:218 nm the mean amphetamine ratios differed by 4.6% and the mean phentermine ratios differed by 6.2%. As the previous study (Table III) had suggested that a 1-nm change in wavelength could produce on the average a 13% change in this ratio, the observed differences are consistent with very good agreement in wavelength accuracy between the detectors. On the other hand, the instrument-to-instrument variation is similar in magnitude to the amphetamine–phentermine differences observed in Table II. Overlap of the reported 213:218 nm ratios may be observed between amphetamine on unit 2 and phentermine on unit 1.

The within-instrument data for the 213:218 nm ratio for unit 1 are shown in Fig. 3. Although the mean ratios drift slightly downward and are slightly less precise at the lowest concentrations, the ± 2 S.D. ranges do not overlap at any concentration. Therefore, this ratio would be of considerable value in the differentiation of amphetamine and phentermine.

Several limitations of this technique for qualitative analysis should be apparent.

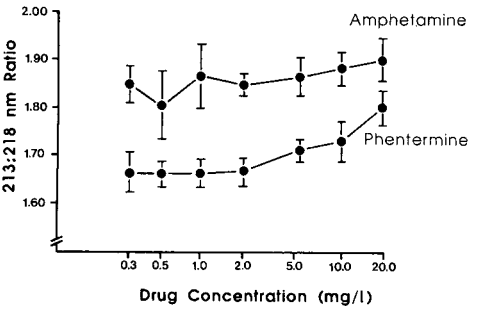

Fig. 3. Mean ± 2 S.D. ranges for the 213:218 nm ratio of amphetamine and phentermine (n = 4). The data were collected on four successive days on unit 1.

First, in a toxicological examination, the concentration of drugs is not known. In practice, solutions containing amphetamine and phentermine yielding peak heights similar to the unknown should be prepared and analyzed. Second, this approach could not be incorporated in any automated search routine owing to the instrument-to-instrument differences. The purpose of this investigation was to document a measurement that is highly reproducible on a single detector unit but showed variability between units and could be used for assessment of instrument differences.

From each of the analyses reported in Table IV, a corresponding set of 2DI data were collected (Table V). It may be observed that the reproducibility was very high. In no instance did the 2DI differ by more than 2 nm from 223 nm; the outlier values were seen at both high and low drug concentrations. We have confirmed this reproducibility in many other studies and propose that the location of 2DI can be used to corroborate small differences in normalized spectra (*SF*), *e.g.*, with phenmetrazine and ephedrine. Because 2DI is reported as an integer, any slight calibration difference between units 1 and 2 could not be detected; there was in fact no difference in the reported 2DI statistics for amphetamine.

We further tested the reproducibility of 213:218 nm ratios for amphetamine

TABLE V

SECOND-DERIVATIVE INDEX (2DI) DATA FOR TWO DIFFERENT DETECTOR UNITS

Concentrations and number of analyses as in Table IV.

Compound	Parameter	Unit 1	Unit 2
Amphetamine	Mean 2DI ± S.D.	222.93 ± 0.38	222.92 ± 0.39
	Lowest result	221	221
	Highest result	223	223
	223 nm as % of all results	96	96
Phentermine	Mean 2DI ± S.D.	222.93 ± 0.38	223.32 ± 0.90
	Lowest result	221	221
	Highest result	223	225
	223 nm as % of all results	96	75

TABLE VI

VARIATION IN AMPHETAMINE IDENTIFICATION PARAMETERS BETWEEN DETECTOR UNITS

Unit No.	Calibration peak (nm)	213:218 nm ratio	2DI
1	651	1.871	223
2	651	1.802	223
3	652	1.777	223
4	651	1.892	223
5	651	1.853	223
6	652	1.894	223
7	651	1.745	223
Mean ± S.D.		1.833 ± 0.059	223 ± 0

using five additional detectors (Table VI). Unit 2 was chosen as a reference system. If the ratio was not between 1.71 and 1.91, the location of the calibration peak was adjusted by 1 nm to achieve the desired result. This acceptance range would produce a difference of no more than 12% between any two detectors, which corresponds to less than 1 nm, according to Table III. For two of the additional five units, a calibration adjustment was required. After adjustment, the 2DI for amphetamine on these units was 223 nm and normalized spectra (*SF*) compared with unit 2 gave values of 0.015 or less. Additional drugs were analyzed and compared with library spectra collected on unit 2, including methamphetamine, imipramine, morphine, methadone and codeine. In all instances, excellent agreement was observed for normalized spectral data and 2DI.

Several investigators have proposed algorithms that can be used to calculate optimum wavelength ratios for distinguishing library entries [37,38]. Choosing ratios in a toxicological setting is not easy, as hundreds of drugs and metabolites may be encountered. It is more practical to recognize that different regions of the spectra can be used to characterize certain drugs [27] and employ tests that focus on that spectral region. In this study similarity factors for normalized spectra covering the range 205–250 nm were considered, because this range is generally useful for amphetamines and opiates. Although most drugs show increased absorbance between 200 and 205 nm, the deuterium energy from the lamp is reduced and the mobile phase absorbance is increased in this region, resulting in high background noise. Selection of a 2DI between 215 and 245 nm yielded a distinct value for each drug. These two features, coupled with retention time data, provide a powerful multi-parameter approach for library matching. Because each is determined at the peak apex, they are minimally affected by incomplete resolution from other peaks, and they are not concentration dependent. Wavelength ratios are highly characteristic for many drugs but do show some concentration dependence, in agreement with a published study [35]. On the other hand, a carefully chosen ratio may be useful for judging wavelength calibration.

The use of an isocratic separation, rather than a gradient, eliminates a major source of variability which affected several earlier studies. However, the composition of the isocratic mobile phase must be tightly controlled with respect to pH and organic solvent concentration. Very small pH changes can produce significant spectral shifts for phenothiazines, barbiturates and other drugs. In practice, the pH has

been maintained within 0.02 pH unit and the acetonitrile concentration has been controlled to within 0.5%.

CONCLUSIONS

We have compared the performance of two spectral parameters, the wavelength ratio at 213:218 nm and the zero intercept of the second derivative, for amphetamine and phentermine. Using a multi-wavelength detector that employs a rotating holographic grating and a single diode sensor, we have shown the high reproducibility of each measurement, with minimum dependence on concentration. Because each measurement was dramatically altered by a change in calibration, we were able to compare the agreement in wavelength accuracy between several detectors. After proper calibration, the observed differences in the 213:218 nm ratio were consistent with a difference of less than 1 nm between any two instruments. The agreement between normalized spectra collected on different instruments after this calibration was excellent.

REFERENCES

1 D. A. Yates and T. Kuwana, *Anal. Chem.*, 48 (1976) 510.
2 M. J. Milano, S. Lam and E. Grushka, *J. Chromatogr.*, 125 (1976) 315.
3 R. E. Dessy, W. D. Reynolds, W. G. Nunn, C. A. Titus and G. F. Moler, *J. Chromatogr.*, 126 (1976) 347.
4 M. S. Denton, T. P. DeAngelis, A. M. Yacynych, W. R. Heineman and T. W. Gilbert, *Anal. Chem.*, 48 (1976) 20.
5 A. E. McDowell, R. S. Harner and H. P. Pardue, *Clin. Chem.*, 22 (1976) 1862.
6 A. F. Fell, H. P. Scott, R. Gill and A. C. Moffat, *Chromatographia*, 16 (1982) 69.
7 S. A. George and A. Maute, *Chromatographia*, 15 (1982) 419.
8 S. A. Borman, *Anal. Chem.*, 55 (1983) 836A.
9 A. F. Fell, H. P. Scott, R. Gill and A. C. Moffat, *J. Chromatogr.*, 282 (1983) 123.
10 A. Grant and P. K. Bhattacharyya, *J. Chromatogr.*, 347 (1985) 219.
11 A. A. Fasanmade and A. F. Fell, *Anal. Chim. Acta*, 187 (1986) 233.
12 P.C. White, *Analyst* (London), 113 (1988) 1625.
13 M. S. F. Ross, O. Leisten and Y. Bar-Shad, *Am. Lab.*, June (1989) 64.
14 T. D. Wilson, W. F. Trompeter and H. F. Gartelman, *J. Liq. Chromatogr.*, 12 (1989) 1231.
15 A. C. J. H. Drouwen, H. A. H. Billiet and L. de Galan, *Anal. Chem.*, 56 (1984) 971.
16 A. C. J. H. Drouwen, H. A. H. Billiet and L. de Galan, *Anal. Chem.*, 57 (1985) 962.
17 T. P. Bridge, M. H. Williams, G. G. R. Seaton and A. F. Fell, *Chromatographia*, 24 (1987) 691.
18 J. K. Strasters, H. A. H. Billiet, L. de Galan, B. G. M. Vandeginste and G. Kateman, *J. Liq. Chromatogr.*, 12 (1989) 3.
19 J. K. Baker, R. E. Skelton and C.-Y. Ma, *J. Chromatogr.*, 168 (1979) 417.
20 P. C. White and T. Catterick, *J. Chromatogr.*, 402 (1987) 135.
21 D. W. Hill, T. R. Kelley and K. J. Langner, *Anal. Chem.*, 59 (1987) 350.
22 D. W. Hill and K. J. Langner, *J. Liq. Chromatogr.*, 10 (1987) 377.
23 C. W. Brown and S. M. Donahue, *Appl. Spectrosc.*, 42 (1988) 347.
24 R. C. Baselt, *Analytical Procedures for Therapeutic Drug Monitoring and Emergency Toxicology*, PSG, Littleton, MA, 2nd ed., 1987, p. 67.
25 R. A. De Zeeuw, *J. Pharm. Biomed. Anal.*, 1 (1983) 435.
26 H-J. Boessenkool, P. Cleij, C. E. Goewie, H. H. van den Broek and H. A. van 't Klooster, *Mikrochim. Acta*. 2 (1986) 75.
27 T. Alfredson, T. Sheehan, T. Lenert, S. Aamodt and L. Correia, *J. Chromatogr.*, 385 (1987) 213.
28 E. I. Minder, R. Schaubhut and C. E. Minder, *J. Chromatogr.*, 419 (1987) 135.

29 D. M. Demorest, J. C. Fetzer, I. S. Lurie, S. M. Carr and K. B. Chatson, *LC · GC*, 5 (1987) 128.
30 H. Engelhardt and Th. Konig, *Chromatographia*, 28 (1989) 341.
31 K. Jinno and M. Kuwajima, *J. Chromatogr. Sci.*, 27 (1989) 57.
32 M. Bogusz, M. Klys, R. A. De Zeeuw and J. P. Franke, *Symp. Biol. Hung.*, 34 (1985) 647.
33 V. H. Kaferstein and G. Sticht, *Beitr. Gerichtl. Med.*, 44 (1986) 253.
34 V. A. Soo, R. J. Bergert and D. G. Deutsch, *Clin. Chem.*, 32 (1986) 325.
35 E. V. Dose and G. Guiochon, *Anal. Chem.*, 61 (1989) 2571.
36 S. R. Binder, M. Regalia, M. Biaggi-McEachern and M. Mazhar, *J. Chromatogr.*, 473 (1989) 325.
37 P. C. Thijssen, L. J. P. Vogels, H. C. Smit and G. Kateman, *Fresenius' Z. Anal. Chem.*, 320 (1985) 531.
38 F. V. Warren, Jr., B. A. Bidlingmeyer and M. F. Delaney, *Anal. Chem.*, 59 (1987) 1890.

Journal of Chromatography, 550 (1991) 461–494
Elsevier Science Publishers B.V., Amsterdam

CHROMSYMP. 2331

Review

Gas chromatographic detectors for use in column liquid chromatography

Ch. E. KIENTZ

Prins Maurits Laboratory TNO, P.O. Box 45, 2280 AA Rijswijk (Netherlands)

G. J. DE JONG

Duphar BV, Research Laboratories, Analytical Development Department, P.O. Box 2, 1380 AA Weesp (Netherlands)

and

U. A. Th. BRINKMAN*

Department of Analytical Chemistry, Free University, De Boelelaan 1083, 1081 HV Amsterdam (Netherlands)

ABSTRACT

Gas chromatographic detectors are increasingly used in order to obtain sensitive and selective detection in both conventional-size and miniaturized column liquid chromatography. A critical review of the literature is given, with suitable emphasis on instrumental design, optimization of interfaces and applications. Future trends are discussed.

CONTENTS

0021-9673/91/$03.50

1. INTRODUCTION

In recent years, continuing research in instrumental chromatographic techniques has led to many interesting developments in capillary gas chromatography (GC) and column liquid chromatography (LC). With the introduction of supercritical fluid chromatography (SFC), three sophisticated complementary separation techniques are now available for the analytical chemist who, today, is increasingly faced with complex trace-level analyses in the fields of environmental, industrial and biomedical chemistry. With the complex samples often under investigation, extensive off-line or on-line sample clean-up and/or trace enrichment are generally necessary. To simplify these sometimes complicated and time-consuming procedures, a more direct approach using a highly sensitive and selective detector system is often desirable. Good examples of selective and sensitive detection in trace analysis, illustrating an approach that does not require extensive sample clean-up, are mentioned by Hutte *et al.* [1] in a review on the development of chemiluminescence detection for GC. Generally, detection is a strong point of GC, where sensitive and selective detectors such as those for electron-capture (ECD), flame photometric (FPD), thermionic (TID) and nitrogen–phosphorus (NPD) detection are commercially available.

Today, LC with its wide range of separation procedures is the most versatile chromatographic technique. With the use of normal-phase, reversed-phase, ion-pair, ion-exchange or gel-permeation LC, a separation can be achieved for almost any class of compounds. With the introduction of miniaturized LC, *i.e.*, the use of microbore (0.5–1 mm I.D.), micro (0.1–0.5 mm I.D.) and capillary (0.05–0.1 mm I.D.) columns, in the late 1970s, new detection modes became available. Recently, Novotny [2] reviewed the advantages of several types of detection systems (and their miniaturization) in microcolumn LC. Not surprisingly, the combination of the separation power of LC and the sophisticated detector systems currently being used in GC is an area of increasing interest. This paper reviews the developments in coupling LC on-line with GC detectors. Combining LC with, *e.g.*, mass spectrometry, nuclear magnetic resonance or Fourier transform infrared detectors is not covered in this survey. For comprehensive reviews in this area, the reader should consult, *e.g.*, refs. 3 and 4.

2. GAS CHROMATOGRAPHIC DETECTORS USED IN LIQUID CHROMATOGRAPHY

A survey of GC detectors compiled from information sent by the manufacturers and/or distributors of GC instrumentation was recently published in *European*

Chromatography News [5]. This survey and other reviews on GC [6–8] show that increasing numbers of GC detector types are being used today. The following types of GC detector are frequently mentioned: flame ionization, photoionization, electron-capture, flame photometric, microcoulometric, thermal conductivity, chemiluminescence, electrolytic conductivity and thermionic.

A survey of the literature, including the database of *Chemical Abstracts* up to January 1990, was performed, combining the keywords "liquid chromatography" or "LC" with the above GC detector types. In the case of GC and LC detection techniques based on similar detection principles, only gas-phase detection was included in the overview. As a result, electrolytic conductivity and microcoulometry had to be excluded, because both techniques are based on detection in an electrolyte solution after combustion or hydrogenolysis. Most papers on chemiluminescence and photoionization had to be discarded for similar reasons. Fig. 1 shows the result of the literature search.

Since the early years of LC, there has been a need for a universal mass-sensitive detector. Therefore, in the early history of coupling LC to GC detectors, *i.e.*, in the period 1968–73, most work was devoted to the use of flame ionization detection (FID), as shown in Fig. 1. Fig. 1 also shows the application of other GC detectors, such as those for chemiluminescence (CLD), electron-capture (ECD), flame photometric (FPD), thermionic (TID) and photoionization (PID) detection, which have become increasingly important in more recent years. In the past decade, many papers have been published which deal with CLD and, especially, the use of thermal energy analysis (TEA) in combination with conventional LC. The use of ECD for selective LC detection has also become popular in the past decade. PID is a rather novel detection technique in GC, which may explain why only a few papers have appeared up to now on LC–PID. Only two papers have been published on LC with thermal conductivity detection (TCD), both originating from the period 1968–71. An explanation may be that TCD, although widely applied in GC, is less suitable for coupling to LC because of the variation of its response depending on the compound and detector operating conditions. Finally, Fig. 1 demonstrates the increased use of GC detectors in miniaturized LC systems since the early 1980s.

3. INTERFACING LC TO GC DETECTORS

Interfacing LC to GC detectors or, more specifically, introducing the analytes dissolved in a liquid phase into a heated detection zone or flame is a difficult problem. Key parameters are the LC effluent flow-rate and composition, and also the type of GC detector to be interfaced. Ideally, an interface should be able to introduce all analytes into the detection zone or flame independently of their physical properties, while the GC detector should be able to accept the total LC effluent and maintain its main characteristics as a GC detector, such as linearity and sensitivity. Unfortunately, these demands have not yet been fully met in any published set-up. The present developments are interesting and promising, however, as will be shown below.

3.1. Transport systems

To solve the problems encountered when introducing a liquid mobile phase into a GC detector, LC effluent transport systems were designed based on the work of

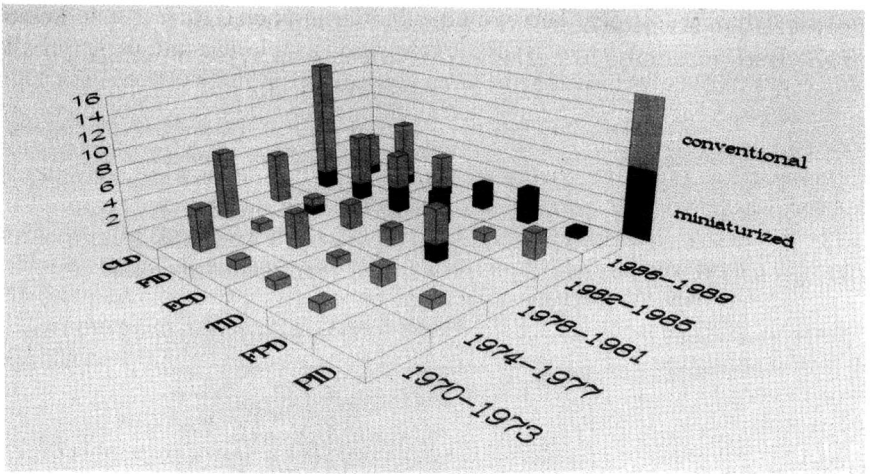

Fig. 1. Number of papers on LC systems coupled with GC detectors during the period 1970–1990.

Haahti and Nikkari [9] and James *et al.* [10]. A transport system consists of a carrier, which can be a metal chain, wire or disc, or another similar device which is continuously rotating between the LC effluent introduction point, an evaporation unit and the detector. The liquid LC effluent is loaded on the moving part of the system and, subsequently, removed by evaporation. Next, the non-volatile analytes are either brought into a pyrolysis furnace or directly into a flame, depending on the detector system used. Most transport systems are applied in FID and they will be discussed in more detail in the pertinent section below.

In 1984, Yang *et al.* [11] presented a new transport system based on thermospray vaporization coupled to a PID or an ECD instrument. A schematic diagram of their system is shown in Fig. 2. The transport device is similar to earlier systems in that a moving surface is required, the sample being detected after the solvent has been removed. The unique feature of the approach is that the sample is vaporized and the solvent removed without being deposited as a liquid on the moving surface. This is

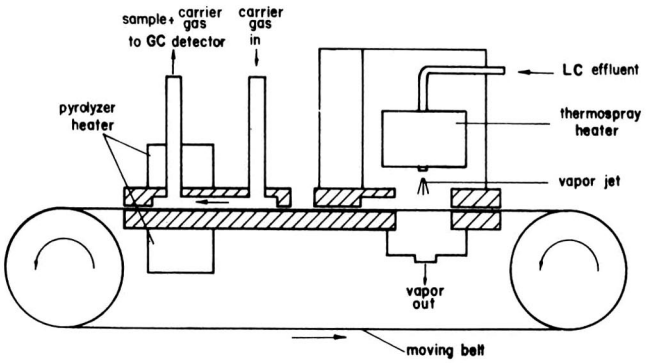

Fig. 2. Schematic diagram of LC detector employing thermospray deposition of the sample onto a moving belt and sample detection by vaporization or pyrolysis of the sample into standard GC detector [11].

accomplished by using a heated thermospray vaporizer, which creates a superheated mist carried in a supersonic jet of vapour. Non-volatile molecules are preferentially retained in the droplets of the mist. When the droplets deposit on the moving surface, which is placed perpendicular to the vapour jet, under optimized temperature and flow conditions, most of the effluent will be vaporized. The analytes are then carried into a pyrolyser chamber and, after pyrolysis, are transported into the GC detector by means of a carrier gas.

3.2. Direct introduction systems

A transport system can be considered as an indirect way of interfacing LC systems and GC detectors. With direct introduction, the analytes dissolved in the LC effluent are transported into the detection zone or flame as a liquid, for example as fine droplets or an aerosol. This approach involves the use of a nebulizer or spraying device. An example of an aerosol interface is shown in Fig. 3. Another, but less direct, way of interfacing is to use an evaporation interface. In this instance the liquid effluent is totally evaporated via a heated capillary or desolvation chamber and then introduced into the detection zone as a gas. Interfacing by direct introduction or via evaporation places special demands on the GC detector. Selective GC detectors are to be preferred in this instance. Recently, Brinkman and Maris [12] reviewed the use of selective GC detectors in LC. As regards the LC mobile phase, the relatively high flow-rates of 0.5–3 ml/min in conventional-size LC seriously limit one's choice if total introduction of the LC effluent is aimed for. Successful attempts appear to be restricted to coupling with ECD [77–89] or FPD [52–59], which will be discussed in detail below. When using reversed-phase eluents, generally only a small part of the LC effluent is introduced, which often results in seriously reduced sensitivity. On the other hand, direct interfacing of LC with GC detectors has become distinctly more popular with the advent of miniaturized LC with its flow-rates of, typically, 1–50 μl/min.

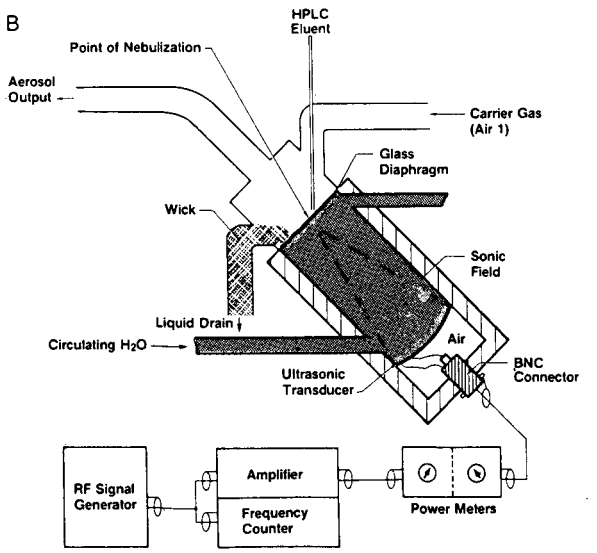

Fig. 3. Schematic diagram of the micronebulizer [62].

4. FLAME IONIZATION DETECTION

In his book on liquid chromatographic detectors, Scott [13] extensively described the development of transport systems for FID, and reported on the then commercially available Pye Unicam LCM2 system which was introduced in the late 1970s. Published applications of this and other of LC–FID systems are summarized in Table 1.

More recently, another transport FID has become available, *viz.*, the Tracor Model 945 LC–FID system, which was introduced at the 1983 Pittsburgh Conference and was described in detail by Dixon [14].

The detector (Fig. 4) consists of a fibrous quartz belt at the periphery of rotating

TABLE 1

APPLICATIONS OF TRANSPORT LC–FID SYSTEMS

Class of compounds	Detector type[a]	Ref.
Lipids	b, b, b	18, 19, 20
	e, e	35, 36
Triglycerides	b, c, b, b	27, 33, 19, 20
	b, e, f, a	21, 15, 23, 38
Sterols	c, a, b, e	27, 29, 19, 15
	e, e	14, 37
Phospholipids	c, b, e	27, 19, 15, 39
Albumin	c, b	28, 18
Hydrocarbons	e, d, e	17, 34, 16
Squalane	f, d, f	30, 31, 32
Carbohydrates	b, f, e, e	18, 24, 14, 37

[a] a = Moving wire [29]; b = moving belt [18]; c = moving chain [27]; d = rotating disc [31]; e = Tracor 945; f = Pye Unicam LCM 2.

disc enclosed in a heated-air-swept housing. The total LC column effluent is applied as a fine stream onto the rotating porous quartz belt. As the disc rotates, the solvent is vaporized while the non-volatile analytes are carried to the FID. A second, much hotter flame is used to clean the belt. Using the Tracor LC–FID system, Maxwell *et al.*

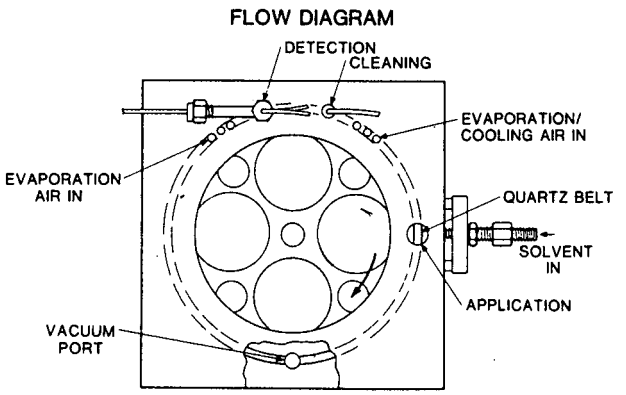

Fig. 4. Flow diagram of the Tracor LC–FID [14].

[15] performed linearity studies on sterols, glycerides and phospholipids. Each of the lipid classes gave a linear response over the tested range of 6–200 μg with correlation coefficients, r, of over 0.9978. By modifying the system, which allowed a reduction of the evaporation block temperature from 150 to 68°C, Pearson and Gharfeh [16,17] were able to extend the use of the system to the lower molecular weight alkanes, *i.e.*, from C_{32} to C_{24}.

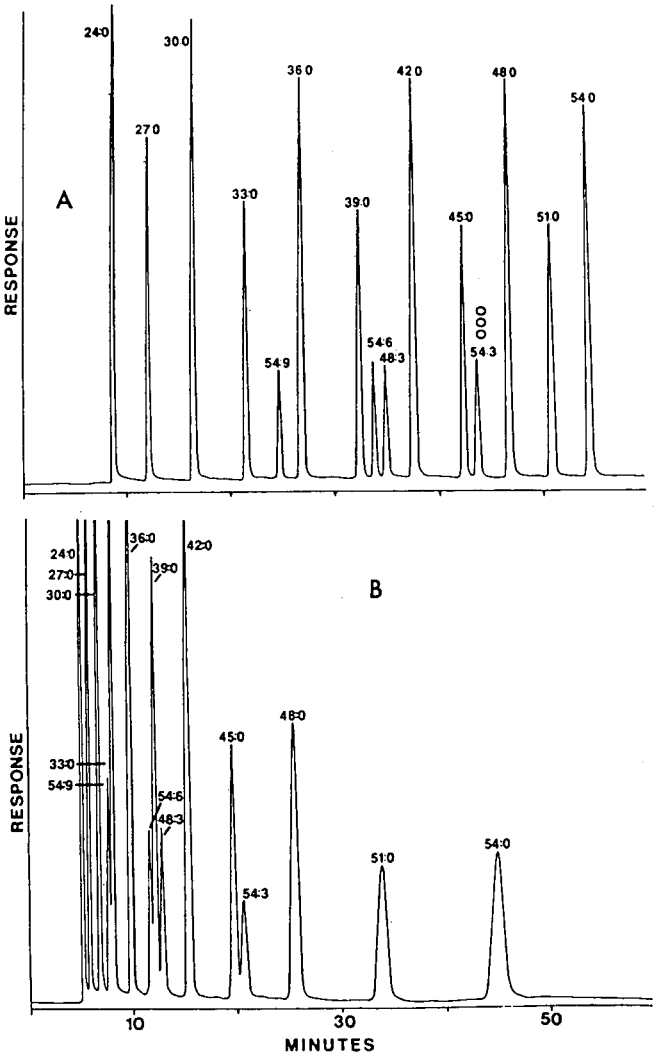

Fig. 5. Separation of triglyceride mixture HPLC G-1. Column, 250 × 4.6 mm I.D., 5 μm, Zorbax C_{18} ODS with 15% carbon content (column 1). (A) Mobile phase, 60-min linear gradient from 15 to 55% methylene chloride in acetonitrile; flow-rate, 0.8 ml/min; sample size, 40 μg; detector, flame ionization. (B) Isocratic elution with 45% methylene chloride in acetonitrile. Peaks: number before colon = number of carbon atoms in acyl chains and number after colon = number of double bonds in acyl chains: 24:0 = Tricaprylin; 27:0 = trinonanoin; 30:0 = tricaprin; 33:0 = triundecanoin; 54:9 = trilinolenin; 36:0 = trilaurin; 39:0 = tritridecanoin; 54:6 = trilinolein; 48:3 = tripalmitolein; 42:0 = trimyristin; 45:0 = tripentadecanoin; 54:3 = triolein; 48:0 = tripalmitin; 51:0 = triheptadecanoin; 54:0 = tristearin [21].

Parallel to the development of commercial LC–FID systems, Privett and Erdahl [18] improved an earlier laboratory-made LC–FID design. Their system is based on the use of a perforated stainless-steel belt for the collection and transport of the LC column effluent. After evaporation of the solvent, the analytes are converted to hydrocarbons in a stainless-steel reactor and detected by FID. Privett and co-workers used this system for the determination of albumin, glucose and lipids [19,20]. A recent application [21] to the determination of triglyceride species present in vegetable oils is shown in Fig. 5.

Recently, a different type of transport device was developed by Malcolme-Lawes and Moss [22]. It consists of a number of 1-mm diameter drawn quartz rods mounted on a two-part disc. When liquid LC effluent (under normal operating conditions *ca.* 10 μl) is deposited on a rod, the rod moves through a three-step air-flow evaporation system. After the end of the third step the rod is placed in the centre of the flame of an unmodified flame ionization detector. During the operation, the system is under computer control. First studies on normal-phase LC gave a repeatability of better than 2% for four successive injections of 10 μg of pyrene and good linearity for 1–10 μg of injected sample. For the lower molecular weight alkanes, the system can be used down to about C_{22}, which is comparable to the results of Pearson and Gharfeh [16,17]. The limit of detection for both pyrene and C_{36} alkane was of the order of 100 ng.

4.1. Miniaturized LC

The advantage of transport systems is that the volatile constituents of the LC column effluent are removed completely. The limitation is that only a small fraction of the effluent is coated onto the moving surface of the transport system. This is due to the relatively high flow-rates used in conventional LC. If, however, miniaturized LC systems are employed, the entire column effluent can be deposited on a suitable matrix for FID. Tsuda *et al.* [23] were the first to combine micro-LC with a commercially available system, *viz.*, the Pye Unicam wire-transport flame ionization detector, as shown in Fig. 6. This wire-transport detector was not modified except for the loading system, which consisted of a micro glass capillary tube (20 mm × 50 μm I.D. × 0.65 mm O.D.) inserted into the end of the LC column, which was constructed of PTFE tubing (I.D. 0.5 mm). The entire effluent of 2–12 μl/min was fed into the glass capillary and loaded onto the moving wire. A detection limit of 10–20 ng for triolein was reported but a non-linear relationship was found in the range 1–1000 ng. In 1986, Veening *et al.* [24] also reported on the use of the Pye Unicam moving-wire flame ionization detector in combination with microbore LC (1.2 mm I.D. columns). The system was compatible with the low flow-rates (60–100 μl/min) of microbore LC. For a series of carbohydrates, the limits of detection ranged from 160 ng for xylose to 400 ng for lactose. Linear calibration graphs were recorded for xylose, glucose, sucrose and maltose between 0.3 and 13 μg.

Krejci and co-workers [25,26] described a special burner designed for the on-line coupling of capillary LC columns (5–34 μm I.D.) to GC detectors, which was used for flame ionization and thermionic detectors. The burner (Fig. 7) consists of a quartz tube into which the tip of the capillary column is inserted. The temperature at the end of this column can be varied from room temperature up to *ca.* 700°C. The authors claimed an identical transfer velocity into the detector for analytes with boiling points in the range 80–320°C. The FID system can be used with mobile phases that contain methanol;

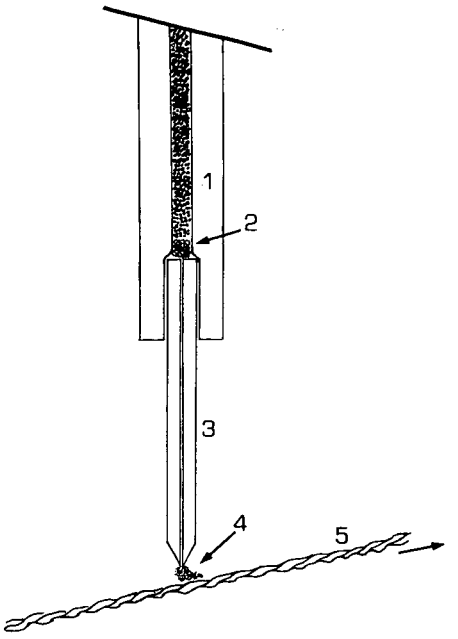

Fig. 6. Schematic diagram of total effluent loading system. 1 = Micro-column (I.D. 0.5 mm, O.D. 2 mm); 2 = quartz-wool; 3 = microglass capillary tubing (I.D. 50 μm, O.D. 0.65 mm); 4 = effluent; 5 = twisted steel wire (I.D. *ca.* 0.2 mm) consisting of three strands [23].

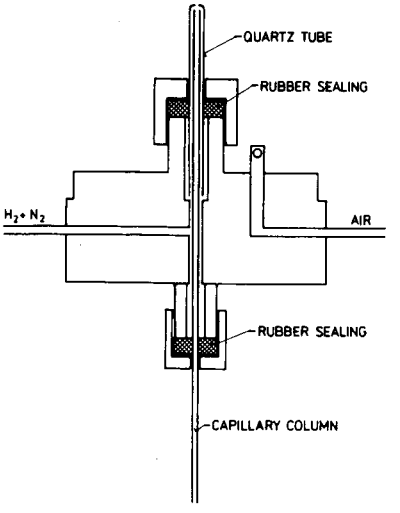

Fig. 7. Diagram of the flame ionization burner [25].

however, a decrease in response has to be accepted, depending on the methanol content. An example of a capillary LC–FID application is shown in Fig. 8. The minimum detectable mass flow-rate for the detector was 1 pg/s for *m*-cresol.

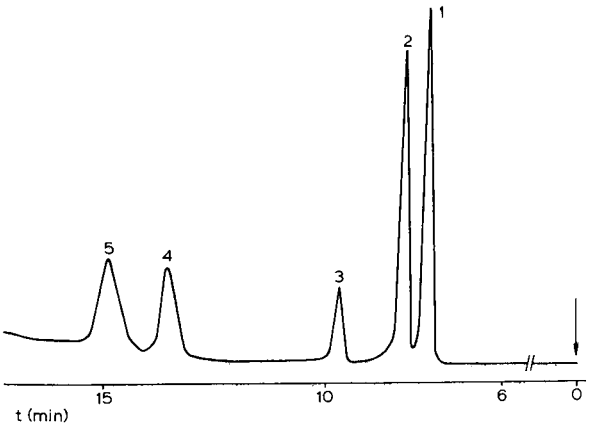

Fig. 8. Example of a chromatogram with flame ionization detection. Column, 3 m × 14 μm I.D.; stationary liquid, OV-101; mobile phase, water. Solutes: 1 = triethylene glycol; 2 = *m*-cresol; 3 = 2,4-dimethylphenol; 4 = 2 methyl-4-ethylphenol; 5 = 2-isopropylphenol [25].

5. THERMIONIC DETECTION

Thermionic detection (TID) is extensively used in gas chromatography because of the excellent sensitivity for phosphorus- and nitrogen-containing substances. For this reason the technique is also known as nitrogen-phosphorus detection (NPD).

TID/NPD was first coupled to LC in 1973 [40]. Here, as in several later instances [41–43], modified transport FID systems were used in combination with conventional-size LC set-ups. In coupling LC to GC-type detectors there has been a trend towards the miniaturization of column dimensions to reduce solvent introduction, which results in better compatibility with selective detection. On-line LC–TID is a good example to demonstrate the benefits of miniaturized LC and here all further work has been carried out with narrow-bore or even smaller columns.

5.1. Flame-based thermionic detection

In 1983, McGuffin and Novotny [44] described a dual-flame thermionic detector for on-line use with micro-LC (Fig. 9). The total microcolumn effluent was concentrically nebulized and aspirated into the primary flame. The combustion products from the primary flame were combined with additional fuel and transported into the analytical flame. The best response and lowest background were obtained when combustion was carefully controlled in the region near the rubidium bead without ignition of the analytical flame. In principle, the system operates as a flameless thermionic detector with liquid introduction and combustion in the primary flame. The optimization of the system was performed in the phosphorus mode with trimethyl phosphate as the model compound. The detector was compatible with organic solvents such as methanol, acetone, ethyl acetate and hexane. A substantial increase in

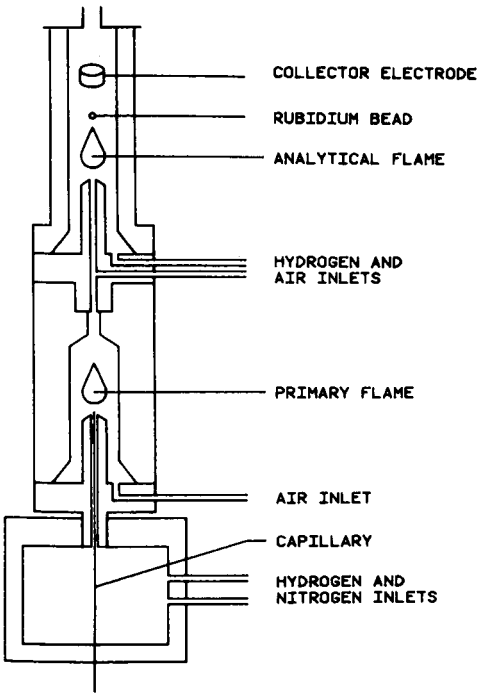

Fig. 9. Schematic diagram of the dual-flame thermionic detector for microcolumn chromatography [44].

background current was observed, however, when using water, acetonitrile or dichloromethane. The minimum detectable amount of phosphorus was found to correspond to 0.5 ng of analyte, and the corresponding average mass flux at the peak maximum was 22 pg/s. The calibration graph was linear over at least three decades of concentration.

With a new version of the thermionic detector [45], the column effluent was orthogonally nebulized and aspirated directly into the primary air–hydrogen diffusion flame. With this approach, the nebulizing efficiency was significantly increased for larger molecules; organophosphorus species having molecular weights >500 could now be detected. As more (organic) effluent was introduced into the flame compared with concentric nebulization, the flame temperature increased, which caused an increase in the background signal. As a result, the detection limits remained similar to those obtained with the former version of the thermionic detector. For the less volatile dimethylthiophosphinic ester of estradiol (MW = 456) the detection limit was ten times higher than for trimethyl phosphate. A linear dynamic range of two decades, instead of the earlier three, was obtained owing to a bipolar orientation at high concentrations.

The LC–TID system has also been optimized for nitrogen sensitivity. In this case, Gluckman and Novotny [46] returned to concentric nebulization directly into the diffusion flame. Detection limits of 14 pg of nitrogen per second at the peak maximum were achieved, with the linearity spanning three orders of magnitude. The applicability

of the system was demonstrated for compounds rather different in molecular weight and tested with microcolumns (0.2 mm I.D.) in addition to open-tubular columns (30–60 μm I.D.). An example of the analysis of underivatized barbiturate standards is shown in Fig. 10.

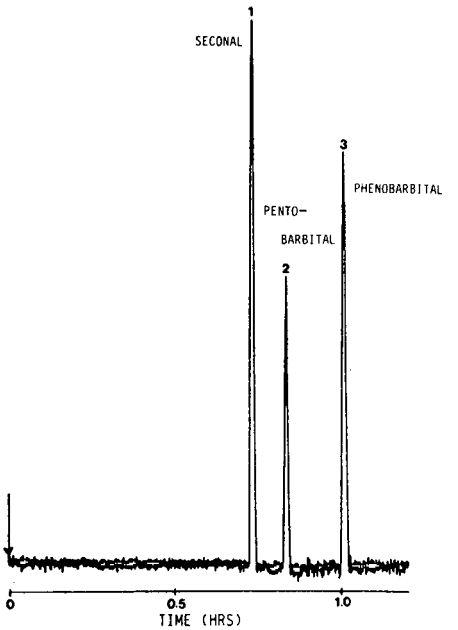

Fig. 10. Chromatogram of three barbiturate standards in their free acid form. Column, 1.8 m × 200 μm I.D., packed with Spherisorb (5 μm) C_8 packing; mobile phase, methanol (1.3 μl/min); injected amount, 20 ng nitrogen per compound [46].

In 1983, Krejci *et al.* [26] demonstrated the use of TID in capillary LC. They stated that when using capillary columns with extremely low flow-rates of 0.001–1 μl/min of organic eluent, the corresponding amount of organic compound introduced is of the same order of magnitude as encountered as a background in GC (column bleeding) when using high temperatures in combination with liquid stationary phases. That is, the detector is operating under average GC conditions, which is very attractive from the point of coupling to LC. However, the interfacing problem still remains. The authors mentioned that the temperature at the end of the capillary column is not too critical for volatile compounds, but should be kept sufficiently high for low-volatile substances. Too high a temperature, however, resulted in clogging of the capillary column due to decomposition of the solutes. The minimum detectable mass flow-rates are 0.1 pg of solute per second for all solutes which are transferred to the detector.

Recently, the use of micro-LC with thermionic detection was extended to the determination of non-volatile polar compounds (see Fig. 11) [47]. An interface, originally developed for the coupling of micro-LC with a flame photometric detector [62], was adapted to TID. Optimization of the detector parameters were studied using the polar non-volatile methylphosphonic acid and its volatile ester dimethyl methylphosphonate as analytes. The system has also been used for the determination of phosphorus-containing pesticide enantiomers [48].

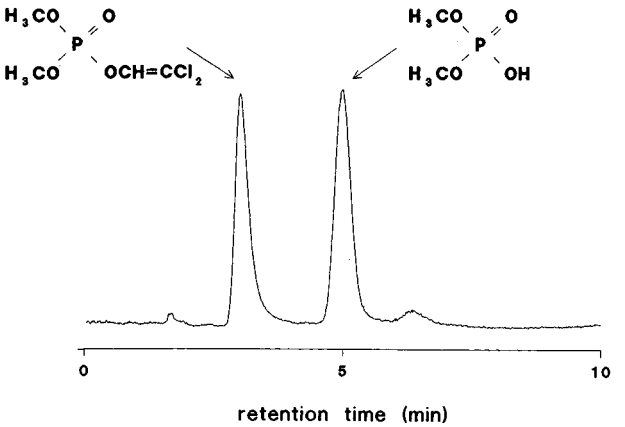

Fig. 11. Micro-LC–TID separation of dichlorvos and its major acidic metabolite dimethylphosphoric acid. Column, PRP-X100, 200 × 0.32 mm I.D.; eluent, 7% ammonium acetate (0.5 *M*) in methanol; flow-rate, 10 μl/min [47].

5.2. Flameless thermionic detection

Flameless thermionic detection was coupled on-line to microbore LC by Maris *et al.* [49]. A commercial GC–flameless TID unit was used in combination with 0.7 mm I.D. columns. The set-up allows easy switching from the GC–TID to the LC–TID mode. The evaporation-type interface is a modified version of an earlier developed LC–ECD interface [94], and consists of an aluminium block containing a 150 mm × 0.25 mm I.D. stainless-steel capillary. The temperature of the interface was kept at 300°C. The detection limit was of the order of 5 pg P/s; linear calibration graphs were obtained over at least three orders of magnitude and the selectivity was 10^5 g C/g P.

In a later design [50] (Fig. 12), the vaporized effluent is directed into the base of a GC–TID system via a heated fused-silica capillary. The effluent is swept into the detector using a low flow-rate of nitrogen. With the improved interface, detection limits of 0.2–0.5 pg P/s were obtained for a variety of phosphorus-containing compounds, including several polar pesticides.

The repeatability of the system proved to be good with relative standard deviations (R.S.D.) (n = 9) varying from 2% (ethyl-paraoxon and ethylparathion) to 5% (fenitrothion). The performance of this system was further evaluated in a subsequent study [51]. The band broadening of the system proved to be dependent on the volatility of the solutes and on the LC flow-rate. An increased effluent flow-rate decreased the volumetric band broadening considerably for less volatile compounds. This indicates that the type of connection of the capillary between the column and the heated interface is very critical: a thermal gradient existing in the connection capillary should be avoided. This conclusion illustrates the difficulty of vaporizing low-volatility or high-molecular-weight compounds and may well indicate the limitation of evaporation interfaces. In the quoted papers [49–51], trace-level applications to tomato, onion and sediment samples are presented. One such example is shown in Fig. 13.

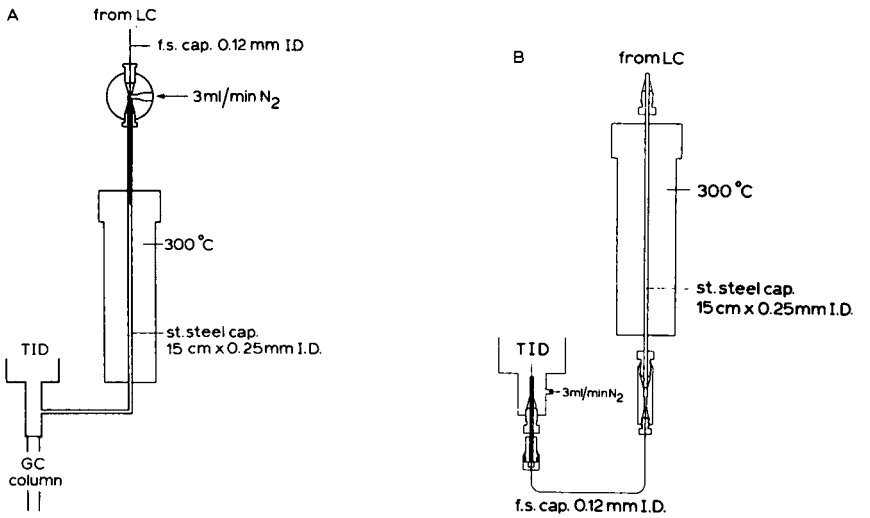

Fig. 12. Schematic diagrams of (A) the original and (B) the modified evaporation interface (ref. 50).

6. FLAME PHOTOMETRIC DETECTION

As early as 1969, Oster [52] reported on the development of a selective detector for LC in the patent literature. The organic LC effluent was evaporated before introduction into a flame photometric detector. In 1975, Freed [53] and, in more detail, Julin *et al.* [54], reported on the on-line combination of ion-exchange chromatography and FPD. The latter group used right-angle pneumatic nebulization and a burner design that allowed the introduction of the mobile phase up to a flow-rate of 5 ml/min. The application of the detector was limited to systems with aqueous mobile phases, because the addition of organic modifiers significantly reduced the detector sensitivity. At 1% methanol, the emission intensity for phosphorus decreased by about 50%. The presence of alkali and alkaline earth metal ions in the mobile phase caused both negative chemical interferences and positive spectral interferences. The system permits the detection of about 0.02 and 0.2 μg/ml of phosphorus and sulphur, respectively. The paper reported interesting applications to non-volatile monophosphate nucleotides and phosphoric acids.

In 1980, Chester [55] also described a flame photometric detector coupled to conventional-size LC. The system utilizes a primary air–hydrogen flame with an inverted configuration, *i.e.*, with air flowing into a hydrogen atmosphere to eliminate solvent interferences, and a secondary flame to measure the molecular HPO emission. In another paper [56] the inverted configuration of the primary flame was compared with the normal configuration. The quenching of the HPO emission by organic compounds is greatly reduced by burning the air–hydrogen flame inside out and the dual-flame configuration has the same advantages as the dual-flame GC detector described by Patterson *et al.* [57,58]. Chester reported an excellent selectivity ratio of about 28 000, a linear dynamic range of 50 000 and a detection limit for trimethyl phosphate of 50 ng of injected compound. The system was used for non-ionic

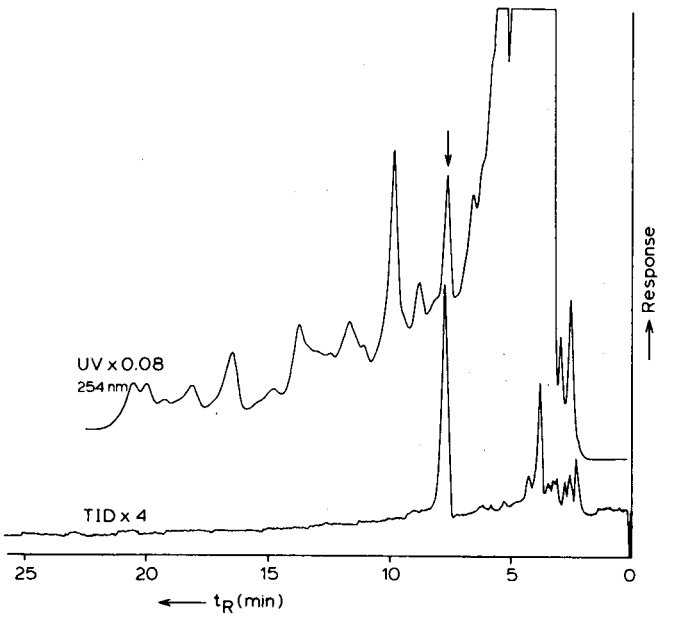

Fig. 13. Reversed phase LC–UV and LC–TID of the extract of an onion spiked with 3.6 ppm of diazinon using LiChrosorb RP-18 with methanol–water (80:20) as eluent; flow-rate, 20 μl/min; UV detection (254 nm), attenuation ×0.08; TID, i_{bc} = 1.6 pA, attenuation ×4 [49].

phosphoric compounds and for ionic species. More recently, Chester *et al.* [59] reported the determination of ortho-, pyro- and tripolyphosphates in detergents; the results agreed closely with values obtained by ion-exchange–autoanalyser systems.

6.1. Miniaturized LC–FPD

The above results indicate that FPD can, to a certain extent, handle reversed-phase LC eluents. One major disadvantage of the commonly used nebulizing interfaces is the low nebulizing efficiency of 15–25%. For a further improvement in the efficiency the introduction of miniaturized LC is recommended: the combination of flame-based detection and micro-LC permits effluent introduction close to or even directly into the flame.

An example of total effluent nebulization into a cool hydrogen–air diffusion flame was first presented by McGuffin and Novotny [60,61]. In principle, the mobile phase introduction was the same as in the micro-LC–TID combination (see Fig. 9). The detector can be used with aqueous mobile phases, while mobile phases containing as much as 50% of methanol, ethanol or acetone (flow-rates of 1–10 μl/min) do not cause a decrease in signal intensity. However, acetonitrile greatly increases the background noise and causes quenching even at low percentages (1–5%). The detector response is linear over two orders of magnitude, with a detection limit of 71 pg/s at the peak maximum for trimethyl phosphate under non-retained (t_0) conditions. Optimum response was obtained with flow-rates below 5 μl/min. Several mixtures of organophosphorus pesticides and dimethylthiophosphinyl derivatives were separated.

In 1987, an interesting alternative was published by Karnicky *et al.* [62] using microbore (1 mm I.D.) and micro (0.32 mm I.D.) LC columns and a virtually unmodified dual-flame photometric detector. Effective nebulization of 2–20 μl/min was obtained using a sophisticated ultrasonic micro-nebulizer. Depending on the mobile phase composition, the flow-rate and radiofrequency power, 10–70% of the LC effluent is nebulized at the excitation point. Droplets less than 10 μm in diameter are swept out of the nebulizing chamber and transported into the detector via the aerosol transport tube and condenser. The authors separated non-volatile phospholipid and sugar phosphate mixtures (Fig. 14). Mobile phases containing buffers caused variations in the nebulizing efficiency; therefore, dual-beam detection was used to improve signal-to-noise ratios and to reduce baseline shifts. With water a detection limit of 50 pg P/s was obtained with a dynamic range of three orders of magnitude. Addition of organic solvents to the mobile phase increased the detection limit to 200–1000 pg P/s, mainly as a result of quenching of the HPO emission.

Folestad and co-workers [63,64] described a chlorine-selective flame-based detector for microbore (1 mm I.D.) LC, in which the total column effluent (20–70 μl/min) is introduced into a heated oven via a spray induced by an electrically heated

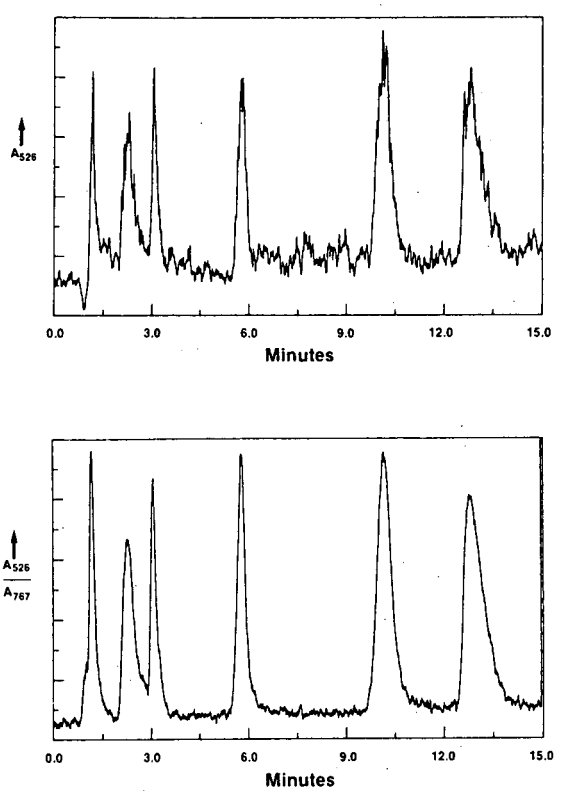

Fig. 14. Illustration of the effect of dual-beam operation. Column, 170 × 0.32 mm I.D. Micropak SP IP-5; mobile phase, 1% *n*-butyl alcohol–0.06% tetrabutylammonium hydroxide–0.12% acetic acid–0.008% perchloric acid; pressure, 304 atm; split flow operation; sample, 0.2 μg each of CMP, 5-AMP, 3-AMP, 2-AMP and cAMP, in order of elution [62].

capillary tip. After pyrolysis in a hydrogen stream, chlorinated compounds are converted into indium(I) chloride in a cool hydrogen diffusion flame and subsequently measured by FPD. The detection limit is 9 pg/s for 1,1,2-trichloroethane in water. In an aqueous mobile phase containing 15% of methanol a linear response was obtained for 5–70 ng of this solute. However, owing to quenching effects the detection limit increased to 115 pg/s. Compounds such as chlorinated uracils, guanine and guanosine could be selectively detected.

Kientz and Verweij [65] coupled a commercially available flame photometric detector to microcolumn (0.32 mm I.D.) LC using an evaporation interface and total effluent introduction. This system was limited to the detection of relatively volatile organophosphorus compounds. In a recent paper, Kientz *et al.* [66] described an improved interface suitable for the detection of non-volatile organophosphorus acids. The total effluent is introduced close to the reaction zone of the hydrogen diffusion flame. For a series of organophosphorus acids, plots of peak area *vs.* amount injected are linear ($r > 0.9998$) in the 0.5–4000 ng range. The repeatability is better than 6% ($n = 148$). The LC–FPD system shows a detection limit of 20 pg P/s when using aqueous solutions containing ammonium formate or acetate, or nitric acid solutions as eluent. With the use of on-line trace enrichment, injection volumes could be increased from 60 nl to 500 μl (Fig. 15), which means that organophosphorus compounds can be detected at concentrations of 5–50 ppb [67].

7. PHOTOIONIZATION DETECTION

Because of the high sensitivity and linearity and also a certain degree of selectivity, photoionization detection (PID) has become an important detection technique in GC. Its potential for GC has been reviewed by Driscoll [68] and Verner [69]. Generally, detection limits are 10–50 times better than those obtained with FID; in addition, PID can detect certain inorganic species and phosphorus- or sulphur-containing compounds. For sulphur-containing compounds, PID is about ten times more sensitive than FPD, with the advantage that linear calibration graphs are obtained.

The ionization of the analytes occurs as a result of the absorption of photon energy, which must exceed the analyte's ionization potential. The photon energy is normally supplied by a suitable UV light source. The ionization potentials for LC solvents typically range from 10.17 eV for hexane, via 10.48 eV for ethanol, 10.85 eV for methanol and 12.22 eV for acetonitrile to 12.59 eV for water. Proper choice of the UV lamp allows the photoionization of many organic compounds, which often have ionization potentials of below 10 eV, with a low background contribution from the LC effluent. Unfortunately, in the liquid state the ionization potential of water is reduced to 6.05 eV [70], that is, with liquid-phase photoionization the use of reversed-phase LC is ruled out and application is limited to normal-phase LC. The use of gas-phase PID after evaporation, *i.e.*, coupling LC to a gas-phase PID system, is therefore interesting.

Preliminary work on LC–PID was carried out by Schmermund and Locke [71]. In their set-up, the normal-phase effluent (1 ml/min) was completely vaporized in a modified Hamilton injection port. Solvents such as *n*-pentane, diethyl ether, methanol and their mixtures could be used. No signal was obtained with these solvents when a lithium fluoride (11.9 eV) window was used on the discharge tube. The

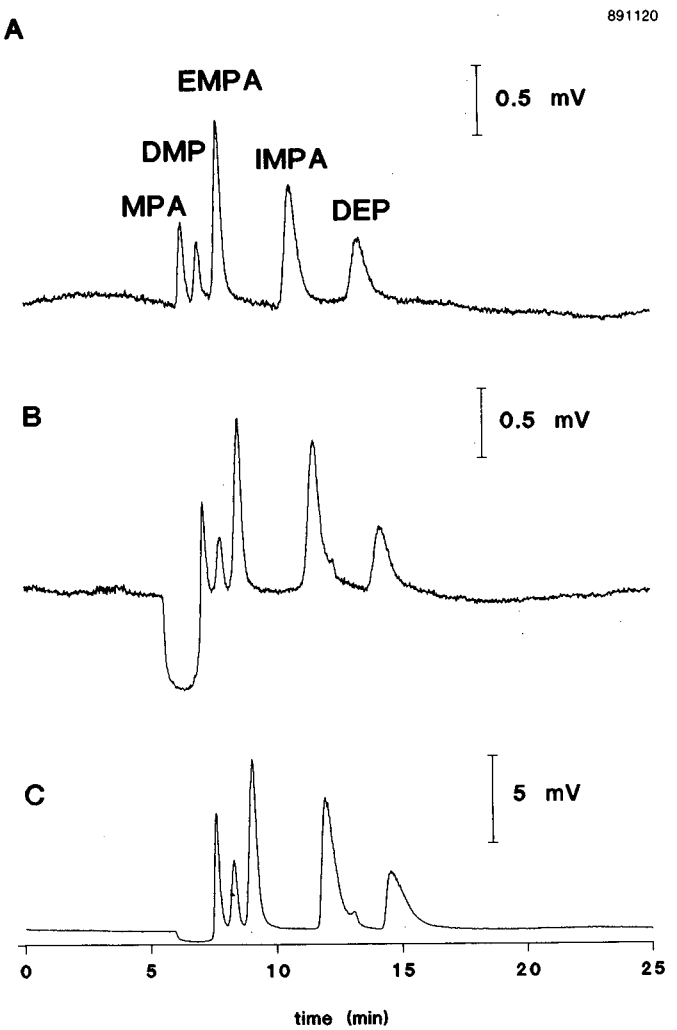

Fig. 15. Trace enrichment of organophosphorus acids with (A) direct injection of 60 nl of test mixture (0.5–3 mg/ml), (B) and (C) 60 and 500 μl, respectively, injection of the 1000-fold diluted test mixture via a precolumn. Eluent, 0.5 *M* ammonium acetate (pH 5); flow-rate, 6 μl/min; column, 700 × 0.32 mm I.D. fused-silica capillary packed with 10-μm PRP-1. Precolumn (4 × 1 mm I.D.) packed with 10-μm MA-100 polymeric anion exchanger. MPA, methylphosphonic acid; DMP, dimethylphosphoric acid; EMPA, ethylmethylphosphonic acid; IMPA, isopropylmethylphosphonic acid; DEP, diethylphosphoric acid [67].

relatively low maximum temperature of 80°C limited the use of solvents with higher boiling points. From the mass flow-rate of methylaniline producing a peak twice the noise level, a detection limit of 10 pg/s was calculated. The linear dynamic range was 10^4. More recently, Locke *et al.* [72] compared results obtained with liquid-phase and gas-phase PID. With regard to gas-phase PID, they concluded that the great advantage is the ability to accept reversed-phase effluents; the real applications will probably be found in miniaturized LC with flow-rates below 10 μl/min.

In 1984, Driscoll *et al.* [73] evaluated the applicability of LC–PID for the determination of specific classes of analytes, using reversed-phase eluents. A schematic diagram of their system is shown in Fig. 16. The separations were carried out on conventional C_8- or C_{18}-bonded silica columns, with acetonitrile–water or methanol–water mixtures at flow-rates of 0.5–2.5 ml/min as mobile phase. The liquid effluent was led into a heated interface oven providing complete evaporation of the mobile phase; after (variable) splitting of the vaporized effluent and addition of helium carrier gas, the gas stream was transported to the detector. The heated interface allows the introduction of both aqueous and organic mobile phases. The system was tested with analytes such as aromatic and aliphatic amines and substituted hydrocarbons. The detection limits varied from 3 to 700 ng, and were determined by the nature of the analytes, the carrier gas and the applied lamp energy. The lowest detection limits were observed for analytes having electronegative groups, and when working at relatively low flow-rates of 0.5 ml/min, with helium as carrier gas. Compounds with ionization potentials in the range 7–8 and 8.5–9.5 eV, showed a response improvement of one order of magnitude when 9.5-eV (instead of 10.2-eV) and 10.2-eV (instead of 9.5-eV) lamps were used, respectively.

Yang *et al.* [11] coupled PID to a transport system based on thermospray vaporization, as discussed above in the section on interfacing. Their system was used for the detection of amino acids and peptides, with water as mobile phase, in both a flow-injection and an LC separation system. The detection limit for phenylalanine was 2 ng and the linear dynamic range was $>10^4$.

7.1. Capillary chromatography

Recently, De Wit and Jorgenson [74] reported on the coupling of vapour-phase PID to open-tubular LC. The three major processes, vaporization, ionization and ion collection, could be studied separately owing to the special detector design (Fig. 17). The vaporization of the LC effluent is accomplished by a fine heating wire placed over the column end. To prevent plugging caused by extensive heating of the column end, the wire is pulse-heated ohmically so that the effluent vaporizes as it leaves the column. Cooling was facilitated by an additional helium carrier gas flow. A 10.02-eV krypton discharge lamp was used as the light source. Parameters such as the electrical potential, helium flow-rate and detector temperature were optimized using toluene as a test solute [ionization potential (*IP*) = 8.82 eV] and acetonitrile (*IP* = 12.20 eV) as mobile

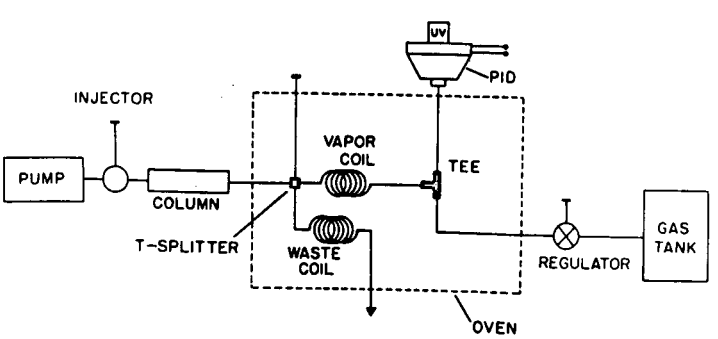

Fig. 16. Schematic diagram of the LC–PID system [73].

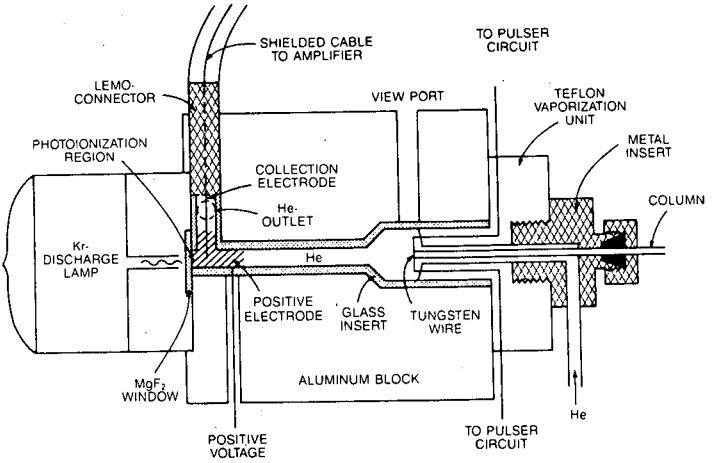

Fig. 17. Schematic diagram of the photoionization detector [74].

phase so that toluene was ionized without ionization of the acetonitrile. An example of the analysis of a mixture of pesticides is shown in Fig. 18. The response of four analytes *versus* their concentration showed good linearity (slope of log–log response >0.9986); the detection limit for toluene was 5 μM.

8. ELECTRON-CAPTURE DETECTION

As early as 1968, Maggs [75] published the first results on LC–ECD coupling. The author used the Pye Unicam moving-wire system which had recently become commercially available, and replaced the flame ionization detector by a Pye Unicam electron-capture detector. He obtained a high detection limit of 10 ng/ml after the separation of lindane and dieldrin on alumina using hexane–ethanol (95:5) as eluent. Since these early attempts, it has been convincingly shown that the low response of

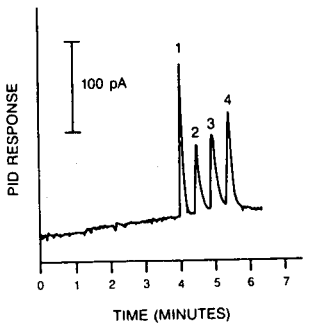

Fig. 18. Chromatogram of a mixture of pesticides. The separation was carried out on a 1 m × 10 μm I.D. fused-silica column coated with OV-17-V. The mobile phase was acetonitrile–water (50:50) at a flow-rate of *ca.* 100 nl/min. The pulsed heating wire was used, and the detector block was operated at 200°C. The helium flow-rate was 20 ml min. Peaks: 1 = metribuzin; 2 = fenthion; 3 = ametryn; 4 = prometryn; all at a concentration of 1 mg/ml [74].

ECD towards various types of LC mobile phases permits a more direct on-line set-up. This will be discussed in the next section.

8.1. Direct introduction LC–ECD

In 1971, Nota and Palombari [76] presented an on-line LC–ECD system using a nebulizer interface. The effluent is nebulized continuously and part (*ca.* 10 μl/min) is admitted into the detector. The following effluents could be used without serious problems: lower alcohols, benzene, hexane, cyclohexane, pyridine, diethyl ether and acetone. The significant additional band broadening due to the nebulizer was probably the reason why no follow-up of this work has been published. However, the basic design is interesting, as it is the most direct type of LC–ECD interfacing reported so far.

In most of the work published since 1974 vaporizing interfaces were used, based on the work of Willmott and Dolphin [77]. The total LC effluent is vaporized in a stainless-steel tube mounted in an oven maintained at 300–350°C; from this, the vapour is forced by an additional nitrogen purge through the electron-capture detector and, finally, into a metal condenser which acts as a trap for radioactive material. This approach was applicable with normal-phase LC using conventional columns. The system has been commercially available for several years through Philips (Eindhoven, Netherlands). A successful application was the development of an automated instrument for the determination of pesticides in milk [78]. The detection limits of the pesticides in milk fat were below 0.1 mg/kg. Another application was presented by Demeter and Heyndrickx [79] for the determination of the relatively polar pesticide endosulfan in serum and urine samples (Fig. 19). A detection limit of 200 pg of α-endosulfan and linearity within a range of 500 agreed within the manufacturer's specifications.

As regards the mobile phase, which, in the initial stages, almost invariably was isooctane or hexane and, more recently, also toluene, there was of course a strong need for dry solvents completely free from electron-capturing impurities. The initial problems in this area were solved by refluxing the solvents for 1 h with a 45% dispersion of finely divided sodium in solid paraffin, which resulted in a much reduced background noise [80]. It was also shown that the addition to the mobile phase of 10–15% of a polar modifier such as dioxane or a few percent of a lower alcohol can be tolerated with only a marginal increase in the background [81]. Several interesting applications were published on LC–ECD in the normal-phase mode. Krull and co-workers [82,83] interfaced a conventional liquid chromatograph to an electron-capture detector using the GC system as vaporization unit. They used their system for the trace-level determination of explosives such as 2,4,6-trinitrotoluene, 2,4-dinitrotoluene, pentaerythritol tetranitrate and 1,3,5-trinitro-1,3,5-triazacyclohexane in post-blast residues. With a splitting ratio of 10:1, the detection limits (signal-to-noise ratio = 3) are 0.1–1 ng with a linear response over four orders of magnitude.

Further optimization of LC–ECD interfacing was studied by De Kok *et al.* [84]. They designed a new (shorter and smaller bore) coiled evaporation-type interface which fits snugly in the grooves of a cylindrical metal block; this results in improved heat transfer. The advantages of the new interface design compared with the commercial one were an improved performance, allowing the detection of higher boiling halogenated aromatics, and a reduction in additional band broadening.

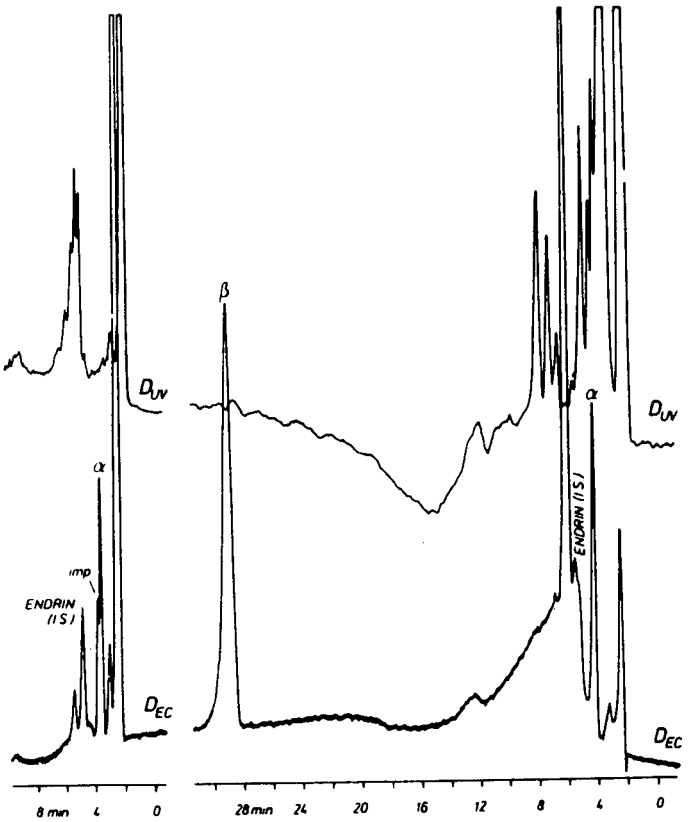

Fig. 19. Liquid chromatogram of a spiked liver extract containing 50 ng of α- and 200 ng of β-endosulfan. Right: no clean-up by liquid–liquid partitioning. Left: preliminary clean-up by liquid–liquid partitioning [79].

Detection limits for diverse types of halogenated compounds were in the 5–100 pg range and the system proved to be linear over three orders of magnitude. In further work, the authors extended the application range of LC–ECD to more polar compounds such as substituted anilines, chlorophenols and hydroxylated polychlorobiphenyls, and also to phenylurea herbicides, by applying derivatization with heptafluorobutyric anhydride (HFBA) [85]. The detection limits of the phenylurea herbicides in surface water were far below the 1 ppb level [86]. Further applications are the determination of chloroxuron as its HFB derivative in strawberries, with a detection limit of 20 ppb [87], and the determination of pentachlorophenol in wood samples [88] and, down to 5–10 ppb, in liver samples [89].

An interesting development to make conventional reversed-phase LC compatible with ECD was published by Maris *et al.* [90]. They designed a post-column extraction module in order to be able to use aqueous LC eluents containing non-volatile ion-pairing agents, with hexane, toluene and their mixtures (generally 1:1) as extraction solvents. The general set-up is shown in Fig. 20. Using methanol–water mixtures at an (LC) flow-rate of 1 ml/min, a detection limit of 500 pg was found for

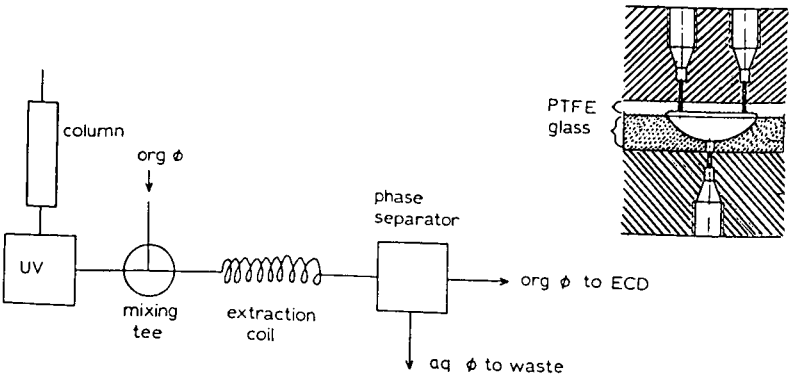

Fig. 20. Schematic design of the reversed-phase LC–ECD system, coupled via a post-column extraction module. The detailed construction of the phase separator is shown as an inset [90].

pentachlorophenol, with an acceptable total post-column band broadening compared with the contribution of the evaporation interface. As a follow-up, a paper was presented on the separation of nitroaromatics and chlorinated pesticides [91]. Combination of this set-up with on-line trace enrichment has allowed the determination of pentachlorophenol in urine samples at the 4 ppb level (see Fig. 21) [90].

Improved detection limits in LC–ECD were reported by Krull and Bushee [82] when applying very low flow-rates. In addition, the early results of Nota and Palombari [76] indicated that small amounts of solvents typically used in reversed-phase chromatography can be tolerated in LC–ECD. In other words, reduction of the flow-rate by applying miniaturized LC is a promising approach to extend the application range of LC–ECD.

8.2. Miniaturized LC–ECD

In 1983, Brazhnikov *et al.* [92] used ECD to test the performance of microbore (1 mm I.D.) columns in the normal-phase LC mode. They coupled the detector directly to the LC column and compared their results on extra-column band broadening with results obtained with a UV detector having a 1-μl cell volume. They found an acceptable extra-column band broadening of 1.4 μl at an eluent flow-rate of 30 μl/min. The loss in efficiency at flow-rates of 30–50 μl/min did not exceed 5%.

In 1984, Brinkman *et al.* [93] showed the applicability of miniaturized LC–ECD (0.7–1 mm I.D. columns; flow-rates of *ca.* 50 μl/min) for both normal- and reversed-phase LC. This was an important step forward in on-line LC–ECD coupling, because in this instance reversed-phase LC was combined with ECD using total effluent introduction. For reversed-phase LC a Hypersil ODS column (1 mm I.D.) was used with methanol–water (85:15) at a flow-rate of 50 μl/min as the mobile phase. The mobile phase was evaporated at 300°C using a miniaturized interface, *viz.*, a 300 mm × 40 μm I.D. nickel capillary. A linear calibration graph was obtained for 2,6,2′,6′-tetrachlorobiphenyl over 2–3 orders of magnitude with a detection limit of 100 pg. Subsequently [94], the same group studied the mobile phase composition. Methanol and dioxane are clearly preferable to acetonitrile as organic modifiers; considerable noise reduction can be obtained by thoroughly degassing the eluent.

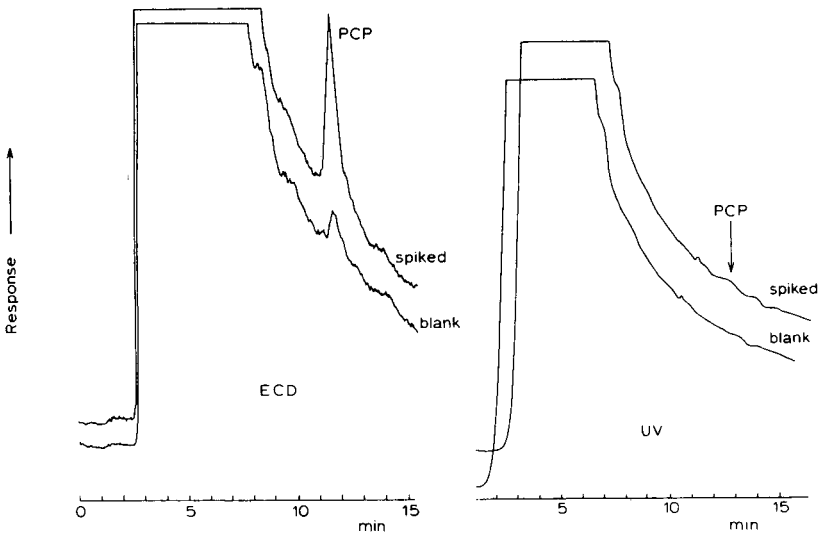

Fig. 21. Reversed-phase LC–extraction module–ECD and reversed-phase LC–UV detection for a urine sample spiked with 10 ppb PCP and a blank urine sample, both obtained after on-line preconcentration of 2.3 ml (onto the column); 25% of the extraction solvent was directed to the electron-capture detector [90].

Surprisingly, the LC–ECD system can even be used with pure water (at 20 μl/min) as eluent. Several successful separations have been reported; an example is given in Fig. 22. It was also shown that the addition of acids such as acetic or formic acid or of triethylamine to the mobile phase can be tolerated. However, under acidic conditions peak distortion was occasionally observed, probably owing to the use of nickel tubing in the interface. In a later stage [95], the nickel tubing was replaced with a fused-silica capillary, which gave an acceptable extra band broadening (including the detector) of 1 μl^2 at an effluent flow-rate of 25 μl/min. The system was applied in the normal-phase mode and was the first to be used for gradient elution with hexane–toluene mixtures. The baseline stability is high and the detection limits of suitable electron-capturing compounds are of the order of 1 pg; calibration graphs are linear over three orders of magnitude. The LC–ECD applications published in the literature are summarized in Table 2.

9. GAS-PHASE CHEMILUMINESCENCE DETECTION

When chemical reactions result in the formation of compounds that are electronically or vibrationally excited, the resulting photon emission is called chemiluminescence. In the past decade, GC detectors based on this principle have been developed and their high selectivity has repeatedly been demonstrated [1]. For the determination of nitrosamines and nitrosamides, a GC detector, the thermal energy analyser (TEA), has been developed by Fine and co-workers [97–99] (see Fig. 23). This instrument is commercially available from Thermo Electron (Waltham, MA, USA). Subsequently, the use of TEA in combination with LC was demonstrated [100,101]. The LC effluent which may contain both volatile and non-volatile N-nitroso

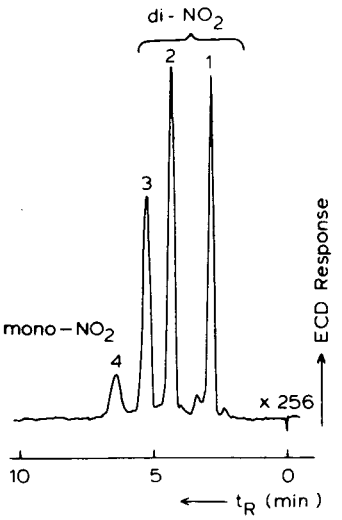

Fig. 22. Reversed-phase LC–ECD for injection of 6 ng of nitroaromatics using LiChrosorb RP-18 with methanol–water (80:20) as eluent. Flow-rate, 35 μl/min; attenuation, × 256. Solutes: 1 = 2,4-dinitrophenol; 2 = 2,4-dinitroaniline; 3 = 1,3-dinitrobenzene; 4 = 4-nitrotoluene [90].

TABLE 2

APPLICATIONS OF LC–ECD

Class of compounds	Matrix	Ref.
Pesticides	Milk	78
	Serum, urine	79, 91
Explosives	Post-blast residue	82, 83
Nitroaromatics	Urine	91
Phenylurea herbicides	Surface water	84
	Strawberries	87
Pentachlorophenol	Wood, liver	88, 89
Chlorophenols	River water, urine	96

compounds, is led into a pyrolysis oven together with a flow of argon or nitrogen carrier gas. In the oven catalysed pyrolysis of N-nitroso compounds takes place and nitric oxide is formed according to

$$R^1R^2N\text{–}NO \rightarrow NO^{\bullet} + R^1R^2N^{\bullet} \quad (1)$$

The heated gas and vapours subsequently pass two cold traps; the first trap serves to liquefy the effluent and the second to remove all remaining solvent vapours and decomposition products. Owing to its high vapour pressure, even at −150°C, nitric oxide passes through the second cold trap, whereas most potentially interfering organic compounds are retained. In the reaction chamber, chemiluminescence is induced according to the following reactions:

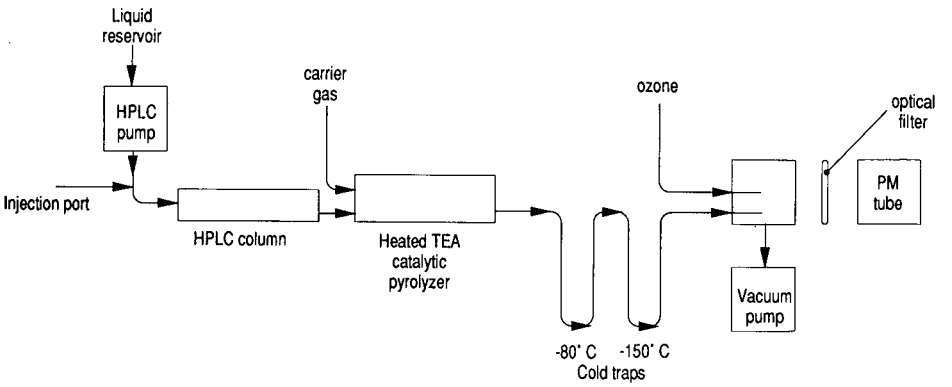

Fig. 23. Schematic diagram of the LC–TEA interface [101].

$$NO^{\cdot} + O_3 \rightarrow NO_2^{*} + O_2 \quad (2)$$

$$NO_2^{*} \rightarrow NO_2 + h\nu \quad (3)$$

The intensity of the emitted light is proportional to the number of nitrosyl radicals present and is measured by an infrared-sensitive photomultiplier. If the pyrolysis oven is kept at 500°C, the system is highly selective for N-nitroso compounds.

In GC, when applying temperatures of up to 800°C, nitro compounds decompose and form nitric oxide; this extends the use of the TEA to aromatic nitro compounds and explosives. Unfortunately, in the LC mode the operating temperature of the pyrolysis oven has an upper limit of 550°C because of baseline noise. Therefore, LC–TEA is always operated in the nitroso mode. The dead volume of both solvent traps (see Fig. 20) is less than 10 μl of mobile phase. This is accomplished by reducing the pressure inside the traps from 760 mmHg (100 kPa) to less than 4 mmHg (0.5 kPa), thus reducing the 300-ml trap volume to less than 1.7 ml. The linearity of the system is over four orders of magnitude, and the sensitivity is *ca.* 1 ng/ml for N-nitroso compounds with the use of 40-μl injections.

The characteristics of LC–TEA were described by Baker and Ma [102]. They found that the response of the TEA detector is highly dependent on the operating temperature of the furnace and on the flow applied to purge it. The response also depends on the volatility of the nitroso compounds, which results in different operating conditions for low- and high-volatile nitroso compounds. Under optimum conditions a minimum concentration sensitivity of 3–5 μg/ml was found for these compounds, which is *ca.* 100 times poorer than levels obtained by others [100,101,112, 127]. One limitation of the LC–TEA system is that the considerable amounts of LC effluent require a constant cleaning of the cold traps, which implies repeated interruption of the analyses. In 1981, Widmar and Grolimund [103] solved this problem by using a secondary vacuum system to empty the cold traps. LC–TEA cannot be operated with aqueous effluents or inorganic buffer solutions.

As was stated above, nitroaromatics are not readily detected at a pyrolysis oven temperature of 550°C. This is due to the significantly higher bond energy (292 kJ/mol) of the C–NO_2 bond of nitroaromatics compared with the N–N bond energy (159

kJ/mol) of nitrosamines and the O–N bond energy (175 kJ/mol) of nitrate esters. In order to improve the detection of nitrotoluenes, in 1987 Selavka *et al.* [104] introduced photolytically assisted thermal energy analysis (LC–PAT). They used UV irradiation to induce C–NO_2 bond cleavage, releasing NO_2 which is suitable for TEA detection. The release of NO_2 was confirmed using batch irradiation followed by LC–TEA, which resulted in the identification of mono-, di- and trinitrotoluenes. In order to reduce the band broadening, a knitted open-tubular photochemical reaction detector design was used, with a 0.6 mm I.D. knitted PTFE tube having a volume of 6 ml. The use of LC–PAT improved the TEA detectability of tri- and dinitrotoluene by a factor of 30 and 16, respectively. The former compound now had a detection limit of 0.5 ng; its response was linear over three orders of magnitude (0.1–100 ppm). Mononitrotoluene could be detected at the sub-nanogram level in the LC–PAT mode, whereas 60 ng of this compound could not be detected when the UV lamp was turned off.

The applications of LC–TEA reported in the literature are listed in Table 3. Krull *et al.* [105] have reviewed the determination of N-nitroso contaminants in biological samples.

In 1988, Robbat *et al.* [133] coupled a gas-phase chemiluminescence detector, which was originally developed for the GC of polycyclic nitroaromatics [134], to LC. The operating principle is based on the well known nitric oxide–ozone reaction. In GC the pyrolysis chamber is kept at 1000°C in order to form nitrosyl radicals. In contrast to results on LC–TEA mentioned above, the pyrolysis oven temperature is kept at a relatively high value of 900°C without baseline instability. In addition, the use of aqueous eluents is allowed. The system was used for the reversed-phase LC of nitroaromatics utilizing a 2.1 mm I.D. column and relatively low flow-rates of 0.2–0.5 ml/min. The detection limit increased from 30 ng of injected 1-nitronaphthalene in

TABLE 3

APPLICATIONS OF LC–TEA ANALYSIS

Class of compounds	Matrix	Ref.
N-Nitroso	Water	106
	Food	107, 108
	Blood	109
	Animal	110
Nitrosamines	Food	125
	Cutting fluid	114, 137
	Cosmetics	112, 126, 127 128, 129, 116
	Rubber	132, 124
Nitrate esters	Explosives	126, 122, 121, 131
Nitroglycerine	Plasma	111, 118, 122, 132
Isosorbide dinitrate	Plasma	113, 132
Pentaerythritol	Plasma	132
Methylated N-nitroso acids and dipeptides		130
Nitrotoluenes	Explosives	104

pure acetonitrile to 250 ng of injected analyte in acetonitrile–water (50:50). Linearity was observed between 70 and 1000 ng for ten nitroaromatics using a reversed-phase linear gradient.

9.1. Miniaturized LC–chemiluminescence detection

In 1982, Massey *et al.* [135] used microbore (1 mm I.D.) LC–TEA to permit work with aqueous eluents and ion-pair reagents, in order to be able to determine polar and ionic nitrosamines. The LC effluent, methanol–water (70:30) containing 0.1 *M* ammonium heptanesulphonate at a flow-rate of 20 μl/min, was mixed with acetone (2 ml/min) and introduced into the pyrolyser oven operated at 650°C. Fig. 24 shows the chromatogram recorded for the ionic nitrosamine N-nitroso-N^1,N^1-dimethylpiperazinium iodide.

In 1985, Rühl and Reusch [123] used microbore LC–TEA to determine N-nitrosamines by means of normal-phase LC; the pyrolyser oven was operated at 500°C. Flow-rates of 60–80 μl/min allowed the system to be operated continuously. They compared their results on the analysis of nitrosatable compounds in rubber nipples with those of GC–TEA, and found good agreement.

For the detection of organosulphur compounds, a gas-phase chemiluminescence detector has been developed by Mishalanie and Birks [136]. Detection is based on the chemiluminescence reaction that occurs when certain sulphur-containing compounds react with molecular fluorine:

$$R_1\text{–}S\text{–}R_2 + F_2 \rightarrow X^* \rightarrow \text{products} + h\nu \qquad (4)$$

where X* is an electronically or vibrationally excited species which, based on spectroscopic studies, can be HF, CH_2S, HCF or FCS. The emission is viewed through

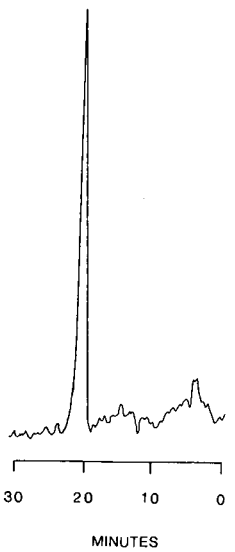

Fig. 24. Reversed-phase ion-pair LC–TEA of N-nitroso-N^1,N^1-dimethylpiperazinium iodide (105 ng). TEA attenuation, × 16 [135].

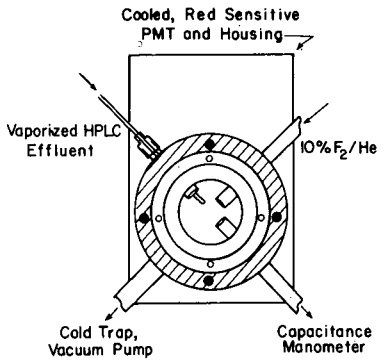

Fig. 25. Front view of the detector cell [136].

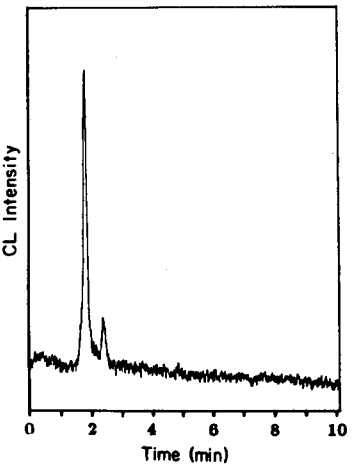

Fig. 26. Chromatogram of a filtered beer sample. The peak at 1.8 min corresponds to about 1 ng of dimethyl sulphide. Chromatographic conditions: acetonitrile–water (70:30) at a flow-rate of 80 μl/min; sample, 1 μl [136].

quartz windows and measured by a cooled red-sensitive photomultiplier using a filter accessible to wavelengths between 659 and 800 nm. The front view of the detector cell is shown in Fig. 25. The microbore LC column is interfaced to the detector cell by means of a 100 × 0.254 mm I.D. stainless-steel capillary which is wrapped with heating take and maintained at 300°C to vaporize the column effluent. The system was used to detect a number of sulphides, disulphides, thiols, the sulphur-containing pesticides malathion and parathion and dimethyl selenide and dimethyl diselenide. For most organosulphur compounds the detector response is linear over three orders of magnitude and detection limits are from 50 pg to 3 ng of analyte. Fig. 26 shows the determination of dimethyl sulphide in a filtered beer sample.

10. CONCLUSIONS AND FUTURE PROSPECTS

The present literature research revealed that, especially in the past decade, much attention has been devoted to the on-line coupling of column LC and GC-type detectors. Use of GC-type detectors will often lead to increased sensitivity and, even more important, increased selectivity of the LC procedure. As is to be expected in every situation in which two more or less incompatible systems or system parts have to be coupled in an on-line mode, much effort has gone into the design and construction of proper types of interfaces which, obviously, cannot be the same for every type of GC detector studied. In many instances, successful solutions to the various problems have been found, miniaturization of the LC part of the system frequently having been introduced to promote the viability of the on-line coupling approach. The real success of the column LC–GC-type detector coupling is probably read best from the many real applications that have been published and from the notable success of LC–ECD coupling in both normal- and reversed-phase LC.

A series of more detailed comments on the present state and future prospects of the various column LC–GC-type detector systems discussed so far is given below.

10.1. Interfacing

Transport systems and the (often fairly simple to construct) vaporizing devices share the disadvantage of possible loss of analytes, *viz.*, of volatile and non-volatile compounds, respectively. Although further development of these devices should not be neglected, total LC effluent introduction from miniaturized LC systems or by using spraying devices, induced by gas flow or thermal effects, is probably a more interesting alternative, because the complete transport of all analytes into the detection zone is now being achieved. Admittedly, with miniaturized LC an important practical problem is the low sensitivity in terms of concentration units, which is a direct result of the small injection volume. Except for those instances where sample volumes are limited, the development of suitable on-line trace enrichment techniques should therefore be given priority: most of today's real LC applications require a sensitivity at the ng/ml level.

An interface-related problem that often is not recognized is the solubility of the silica column packing materials in aqueous eluents with pH values higher than 5–6 [67]. Even before a distinct decrease in separation efficiency and/or baseline instability are observed, clogging of the interface can occur. The introduction of pressure-resistant and efficient polymer-based packing materials may well provide a solution here.

10.2. LC–FID

For this combination, transport systems have been improved significantly over the years. Miniaturized LC, in combination with transport systems, permits total effluent introduction and, thus, better sensitivity. On-line interfacing of capillary LC to FID has shown that the detector can handle a total solvent flow of about 1 μl/min. When water-containing effluents are used, miniaturized on-line LC–FID may be a promising technique for the determination of ionic and polar organic species. Organic effluents, unfortunately, induce an increased base current and reduced sensitivity, which makes them less desirable. In other words, for the use of universal solute detection using organic LC eluents, the transport flame ionization detector is still the best solution.

10.3. LC–TID/NPD

Both dual-flame TID and flameless TID have been discussed in the literature. On-line coupling of both detectors to miniaturized LC systems has resulted in the detection of trace amounts of both phosphorus- and nitrogen-containing compounds. A reliable comparison of the two systems is difficult, because inherently different interface principles, such as direct liquid introduction and evaporation, have been used. The main limitations are that neither system can be used with LC effluents containing inorganic buffers or salts and that most non-volatile analytes cannot, as yet, be handled.

10.4. LC–FPD

When coupling FPD on-line to a conventional LC system, the sensitivity is low; in addition, the use of organic modifiers dramatically reduces the sensitivity. The influence of the flame configuration on the quenching effect, which, *e.g.*, reduced quenching when burning the flame "inside out" [56], should be further investigated. With microbore LC (1–0.7 mm I.D.) and micro-LC (0.5–0.1 mm I.D.), total LC

effluent introduction is possible. The sensitivity distinctly increases and even non-volatile organophosphorus compounds can now be analysed. The use of micro-LC is most promising because the effluent flow of, typically, less than 5 μl/min also permits the use of organic modifiers because of the reduced total amount of carbon introduced per second.

10.5. LC–PID

Only a few papers have been published on on-line LC–PID. However, the further development of this technique, especially when using miniaturized LC, may well yield a promising alternative to LC–FID. By using a UV source with a photon energy output below the ionization potentials of water and acetonitrile, which are relatively high in the gas phase, it should be possible to determine a substantial number of organic compounds with a minimum background contribution.

10.6. LC–ECD

On-line LC–ECD is the combination that has been discussed most frequently and a number of interesting applications have been published; these mainly deal with normal-phase LC. However, distinct successes have also been reported in the area of reversed-phase LC. For example, when using microbore LC columns, total effluent introduction was permitted even with mainly aqueous LC eluents. Further studies in this direction certainly are of great interest. Such studies should include further work on interface design. At present, the interface principle in LC–ECD generally is based on vaporizing the total effluent; this limits the possibility of handling relatively non-volatile and/or polar compounds.

10.7. LC–chemiluminescence detection

In the past, LC–TEA has clearly proved its importance in the determination of N-nitroso compounds which are potential carcinogens. Recent developments, such as utilizing miniaturized LC and working with photolytically assisted TEA, are extending the application range to more polar and ionic nitrosamines and nitroaromatics and the use of aqueous buffer solutions.

Miniaturized LC combined with gas-phase chemiluminescence, with its excellent sensitivity and selectivity, may well turn out to become an important tool in environmental analysis.

REFERENCES

1 R. S. Hutte, R. E. Sievers and J. W. Birks, *J. Chromatogr. Sci.*, 24 (1986) 499.
2 M. Novotny, *Anal. Chem.*, 60 (1988) 500A.
3 R. E. Majors, F. E. H. G. Barth and C. H. Lochmuller, *Anal. Chem.*, 56 (1984) 300R.
4 H. G. Barth, W. E. Barber, C. H. Lochmuller, R. E. Majors and F. E. Regnier, *Anal. Chem.*, 58 (1986) 211R.
5 Editorial, *Eur. Chromatogr. News*, 1 (1988) 20.
6 F. W. Karasek, F. I. Onuska, F. J. Yang and R. E. Clement, *Anal. Chem.*, 56 (1984) 174R.
7 R. E. Clement, F. I. Onuska, F. J. Yang and G. A. Eiceman, *Anal. Chem.*, 58 (1986) 321R.
8 H. V. Drushel, *J. Chromatogr. Sci.*, 21 (1983) 20.
9 E. O. A. Haahti and T. Nikkari, *Acta Chem. Scand.*, 17 (1963) 2565.
10 A. T. James, J. R. Ravenhill and R. P. W. Scott, *Chem. Ind. (London)*, (1964) 746.
11 L. Yang, G. J. Fergusson and M. L. Vestal, *Anal. Chem.*, 56 (1984) 2632.

12 U. A. Th. Brinkman and F. A. Maris, *LC·GC Int.*, 1 (1987) 45.
13 R. P. W. Scott, *Liquid Chromatography Detectors*, Elsevier, Amsterdam, 1977, p. 19.
14 J. B. Dixon, *Chimia*, 38 (1984) 3.
15 R. J. Maxwell, E. H. Nungesser, W. N. Marmer and T. A. Foglia, *LC·GC Int.*, 1 (1987) 56.
16 C. D. Pearson and S. G. Gharfeh, *J. Chromatogr.*, 329 (1985) 142.
17 C. D. Pearson and S. G. Gharfeh, *Anal. Chem.*, 58 (1986) 307.
18 O. S. Privett and W. L. Erdahl, *Anal. Biochem.*, 84 (1978) 449.
19 F. C. Phillips, W. L. Erdahl and O. S. Privett, *Lipids*, 17 (1982) 992.
20 F. C. Phillips, W. L. Erdahl, J. D. Nadenicek, L. J. Nutter, J. A. Schmit and O. S. Privett, *Lipids*, 19 (1984) 142.
21 F. C. Phillips, W. L. Erdahl, J. A. Schmit and O. S. Privett, *Lipids*, 19 (1984) 880.
22 D. J. Malcolme-Lawes and P. Moss, *J. Chromatogr.*, 482 (1989) 53.
23 T. Tsuda, A. Nago, G. Nakagawa and M. Maseki, *J. High Resolut. Chromatogr. Chromatogr. Commun.*, 6 (1983) 694.
24 H. Veening, P. P. H. Tock, J. C. Kraak and H. Poppe, *J. Chromatogr.*, 352 (1986) 345.
25 M. Krejci, K. Tesarik, M. Rusek and J. Pajurek, *J. Chromatogr.*, 218 (1981) 167.
26 M. Krejci, M. Rusek and J. Houdkova, *Collect. Czech. Chem. Commun.*, 48 (1983) 2343.
27 A. Karmen, *Sep. Sci.*, 2 (1967) 387.
28 R. H. Stevens, *J. Gas Chromatogr.*, 6 (1968) 375.
29 B. M. Lapidus, A. Karman, *J. Chromatogr. Sci.*, 10 (1972) 103.
30 J. H. van Dijk, *J. Chromatogr. Sci.*, 10 (1972) 31.
31 H. Dubsky, *J. Chromatogr.*, 71 (1972) 395.
32 V. Pretorius and J. F. J. van Rensburg, *J. Chromatogr. Sci.*, 11 (1973) 355.
33 A. Stolyhwo, O. S. Privet and W. L. Erdahl, *J. Chromatogr. Sci.*, 11 (1973) 263.
34 J. J. Szakasits and R. E. Robinson, *Anal. Chem.*, 46 (1974) 1648.
35 L. A. Smith, H. A. Norman, S. H. Cho and G. A. Thomson, *J. Chromatogr.*, 346 (1985) 291.
36 H. A. Norman and J. B. St. John, *J. Lipid Res.*, 27 (1986) 1104.
37 G. Simmonite, *Int. Analyst*, 1 (1987) 38.
38 K. V. V. Nurmela and L. T. Satama, *J. Chromatogr.*, 435 (1988) 139.
39 M. D. Grieser and J. N. Geske, *J. Am. Oil. Chem. Soc.*, 66 (1989) 1485.
40 A. A. Balaukin, B. C. Utorov, O. I. Kalmanouskii and A. A. Chernokozhin, *Russ. Pat.*, 370 520 (1973).
41 K. Slais and M. Krejci, *J. Chromatogr.*, 91 (1974) 181.
42 B. J. Compton and W. C. Purdy, *J. Chromatogr.*, 169 (1979) 39.
43 V. V. Brazhnikov, V. M. Poshemansky, K. I. Sakodynskii and V. N. Chernjakin, *J. Chromatogr.*, 175 (1979) 21.
44 V. L. McGuffin and M. Novotny, *Anal. Chem.*, 55 (1983) 2296.
45 J. C. Gluckman and M. Novotny, *J. Chromatogr.*, 314 (1984) 103.
46 J. C. Gluckman and M. Novotny, *J. Chromatogr.*, 333 (1985) 291.
47 Ch. E. Kientz, A. Verweij, G. J. de Jong and U. Th. Brinkman, to be published.
48 Ch. E. Kientz, J. P. Langenberg, G. J. de Jong and U. A. Th. Brinkman, to be published.
49 F. A. Maris, R. J. van Delft, R. W. Frei, R. B. Geerdink and U. A. Th. Brinkman, *Anal. Chem.*, 58 (1986) 1634.
50 J. C. Gluckman, D. Barcelo, G. J. de Jong, R. W. Frei, F. Maris and U. A. Th. Brinkman, *J. Chromatogr.*, 367 (1986) 35.
51 D. Barcelo, F. A. Maris, R. W. Frei, G. J. de Jong and U. A. Th. Brinkman, *Int. J. Environ. Anal. Chem.*, 30 (1987) 95.
52 H. Oster, *Ger. Offen.*, DE 1 965 547 (1971), p. 9.
53 D. J. Freed, *Anal. Chem.*, 47 (1975) 186.
54 B. G. Julin, H. W. Vandenborn and J. J. Kirkland, *J. Chromatogr.*, 112 (1975) 443.
55 T. L. Chester, *Anal. Chem.*, 52 (1980) 1621.
56 T. L. Chester, *Anal. Chem.*, 52 (1980) 638.
57 P. L. Patterson, R. L. Howe and A. Abu-Shumays, *Anal. Chem.*, 50 (1978) 339.
58 P. L. Patterson, *Anal. Chem.*, 50 (1978) 345.
59 T. L. Chester, C. A. Smith and S. Culshaw, *J. Chromatogr.*, 287 (1984) 447.
60 V. L. McGuffin and M. Novotny, *Anal. Chem.*, 53 (1981) 946.
61 V. L. McGuffin and M. Novotny, *J. Chromatogr.*, 218 (1981) 179.
62 J. F. Karnicky, L. T. Zitelli and S. van der Wal, *Anal. Chem.*, 59 (1987) 327.

63 S. Folestad and B. Josefsson, *J. Chromatogr.*, 203 (1981) 173.
64 S. Folestad, B. Josefsson and P. Martorp, *Anal. Chem.*, 59 (1987) 334.
65 Ch. E. Kientz and A. Verweij, *Int. J. Environ. Anal. Chem.*, 30 (1987) 255.
66 Ch. E. Kientz, A. Verweij, H. L. Boter, A. Poppema, R. W. Frei, G. J. de Jong and U. A. Th. Brinkman, *J. Chromatogr.*, 467 (1989) 385.
67 Ch. E. Kientz, A. Verweij, G. J. de Jong and U. A. Th. Brinkman, *J. High Resolut. Chromatogr.*, 12 (1989) 793.
68 J. N. Driscoll, *J. Chromatogr. Sci.*, 23 (1985) 488.
69 P. Verner, *J. Chromatogr.*, 300 (1984) 249.
70 M. Anbar, G. A. St. John, H. R. Gloria and R. I. Reinsch, in H. H. G. Jellinek (Editor), *Water Structure at the Water–Polymer Interface*, Plenum Press, New York, 1972.
71 J. T. Schmermund and D. C. Locke, *Anal. Lett.*, 8 (1975) 611.
72 D. C. Locke, B. S. Dhingra and A. D. Baker, *Anal. Chem.*, 54 (1982) 447.
73 J. N. Driscoll, D. W. Conron, P. Ferioli, I. S. Krull and K. H. Xie, *J. Chromatogr.*, 302 (1984) 43.
74 J. S. M. de Wit and J. W. Jorgenson, *J. Chromatogr.*, 411 (1987) 201.
75 R. J. Maggs, *Column*, 2, No. 4 (1968) 5.
76 G. Nota and A. Palombari, *J. Chromatogr.*, 62 (1971) 153.
77 F. W. Willmott and R. J. Dolphin, *J. Chromatogr. Sci.*, 12 (1974) 695.
78 R. J. Dolphin, F. W. Willmott, A. D. Mills and L. P. J. Hoogeveen, *J. Chromatogr.*, 122 (1976) 259.
79 J. Demeter and A. Heyndrickx, in A. Frigerio and M. McCamish (Editors), *Recent Developments in Mass Spectrometry in Biochemistry and Medicine, 6*, Elsevier, Amsterdam, 1980, p. 317.
80 U. A. Th. Brinkman, P. M. Onel and G. de Vries, *J. Chromatogr.*, 171 (1979) 424.
81 A. T. Chamberlain and J. S. Marlow, *J. Chromatogr. Sci.*, 5 (1977) 29.
82 I. S. Krull and D. Bushee, *Anal. Lett.*, 13A (1980) 1277.
83 I. S. Krull, E. A. Davis, C. Santasania, J. Kraus, A. Basch and Y. Bamberger, *Anal. Lett.*, 14A (1981) 1363.
84 A. de Kok, R. B. Geerdink and U. A. Th. Brinkman, *J. Chromatogr.*, 252 (1982) 101.
85 A. de Kok, R. B. Geerdink and U. A. Th. Brinkman, *Chromatographia*, 16 (1982) 237.
86 U. A. Th. Brinkman, A. de Kok and R. B. Geerdink, *J. Chromatogr.*, 283 (1984) 113.
87 F. A. Maris, R. B. Geerdink, R. van Delft and U. A. Th. Brinkman, *Bull. Environ. Contam. Toxicol.*, 35 (1985) 711.
88 C. E. Goewie, R. J. Berkhof, F. A. Maris, M. Treskes and U. A. Th. Brinkman, *Int. J. Environ. Anal. Chem.*, 26 (1986) 305.
89 F. A. Maris, *Ph.D. Thesis*, Free University, Amsterdam, 1988.
90 F. A. Maris, M. Nijenhuis, R. W. Frei, G. J. de Jong and U. A. Th. Brinkman, *Chromatographia*, 22 (1986) 235.
91 F. A. Maris, M. Nijenhuis, R. W. Frei, G. J. de Jong and U. A. Th. Brinkman, *J. Chromatogr.*, 435 (1988) 297.
92 V. V. Brazhnikov, L. M. Yakushina, E. M. Syanava and Sh. A. Karapetyan, *J. High Resolut. Chromatogr. Chromatogr. Commun.*, 6 (1983) 451.
93 U. A. Th. Brinkman, R. B. Geerdink and A. de Kok, *J. Chromatogr.*, 291 (1984) 291.
94 F. A. Maris, R. B. Geerdink and U. A. Th. Brinkman, *J. Chromatogr.*, 328 (1985) 93.
95 F. A. Maris, A. van der Vliet, R. B. Geerdink and U. A. Th. Brinkman, *J. Chromatogr.*, 347 (1985) 75.
96 F. Maris, J. A. Stab, G. J. de Jong and U. A. Th. Brinkman, *J. Chromatogr.*, 445 (1988) 129.
97 D. H. Fine, F. Rufeh and B. Gunther, *Anal. Lett.*, 6 (1973) 731.
98 D. H. Fine, F. Rufeh, D. Lieb and D. P. Rounbehler, *Anal. Chem.*, 47 (1975) 1188.
99 D. H. Fine, D. Lieb and F. Rufeh, *J. Chromatogr.*, 107 (1975) 107.
100 P. E. Oetinger, F. Huffman, D. H. Fine and D. Lieb, *Anal. Lett.*, 8 (1975) 411.
101 D. H. Fine, D. P. Rounbehler, A. Sivergleid and R. Ross, in B. J. Tinbergen and B. Krol (Editors), *Proceedings of the 2nd International Symposium on Nitrite in Meat Products, Zeist, The Netherlands*, Cent. Agric. Publ. Documentation, Wageningen, The Netherlands, 1976, p. 191.
102 J. K. Baker and C.-Y. Ma, *IARC. Sci. Publ.*, 19 (1978) 19.
103 H. M. Widmar and K. Grolimund, *Chemia*, 35 (1981) 156.
104 C. M. Selavka, R. E. Tontarski and R. A. Strobel, Jr., *J. Forensic Sci.*, 32 (1987) 941.
105 I. S. Krull, T. Y. Fau, H. Wolf, R. Ross and D. H. Fine, *J. Chromatogr. Sci.*, 10 (1979) 443.
106 D. H. Fine, F. Huffman, D. P. Rounbehler and N. M. Belcher, *IARC Sci. Publ.*, 14 (1976) 43.
107 D. H. Fine, R. Ross, D. P. Rounbehler, A. Silvergleid and L. Song, *J. Agric. Food Chem.*, 24 (1976) 1069.

108 N. P. Sen and S. Seaman, *IARC Sci. Publ.*, 57 (1984) 137.
109 D. H. Fine, R. Ross, D. P. Rounbehler, A. Silvergleid and L. Song, *Nature (London)*, 265 (1977) 753.
110 D. P. Rounbehler, R. Ross, D. H. Fine, Z. M. Igbal and S. S. Epstein, *Science*, 197 (1977) 917.
111 R. J. Spanggord and R. G. Keck, *J. Pharm. Sci.*, 69 (1980) 444.
112 I. L. Ho, H. H. Wisneski and R. L. Yates, *J. Assoc. Off. Anal. Chem.*, 64 (1981) 800.
113 J. Maddock, P. A. Lewis, A. Woodward, P. R. Massey and S. Kennedy, *J. Chromatogr.*, 272 (1983) 129.
114 U. Goff, *IARC Sci. Publ.*, 45 (1983) 389.
115 T. Y. Fan, J. Morrison, D. P. Rounbehler, R. Ross, D. H. Fine, W. Miles and N. P. Sen, *Science*, 196 (1977) 70.
116 D. H. Fine, *IARC Sci. Publ.*, 45 (1983) 309.
117 S. S. Hecht, I. P. Adams, D. Hoffman, *IARC Sci. Publ.*, 45 (1983) 429.
118 A. J. Woodward, P. A. Lewis, M. Aylward, R. Rudman and J. Maddock, *J. Pharm. Sci.*, 73 (1984) 1838.
119 D. D. Fine, W. C. Yu and E. U. Goff, in *Proceedings of International Symposium on the Analytical Detection of Explosives, 1983*, Fed. Bur. Invest., Washington, DC, p. 169.
120 E. C. Bender, in *Proceedings of International Symposium on the Analytical Detection of Explosives, 1983,* Fed. Bur. Invest. Washington, DC, p. 309.
121 A. L. Lafleur, B. D. Morriseau and D. H. Fine, in *Proceedings of New Concepts Symposium and Workshop on Detection and Identification of Explosives*, National Technical Information Service, Springfield, VA, 1978, p. 597.
122 S. H. Curry, G. Algozzine and W. Yu, *Methodol. Surv. Biochem. Anal.*, 14 (1984) 367.
123 C. Rühl and J. Reusch, *J. Chromatogr.*, 328 (1985) 362.
124 N. P. Sen, S. W. Seaman and S. C. Kushwaha, *J. Chromatogr.*, 463 (1989) 419.
125 R. C. Massey, P. E. Key, D. J. McWeeny and M. E. Knowles, *IARC Sci. Publ.*, 57 (1984) 131.
126 M. D. Erickson, D. B. Lakings, A. D. Drinkwine and I. L. Spigarelli, *J. Soc. Cosmet. Chem.*, 36 (1985) 213.
127 M. D. Erickson, D. B. Lakings, A. D. Drinkwine and I. L. Spigarelli, *J. Soc. Cosmet. Chem.*, 36 (1985) 223.
128 D. Klein, A. M. Girard, J. De Smedt, Y. Fellion and G. Debry, *Food Cosmet. Toxicol.*, 19 (1981) 233.
129 T. Y. Fan, U. Goff, L. Song and D. H. Fine, *Food Cosmet. Toxicol.*, 15 (1977) 423.
130 S. J. Kubacki, D. D. Havery and T. Fazio, *IARC Sci. Publ.*, 57 (1984) 131.
131 A. L. Lafleur, B. D. Morriseau, *Anal. Chem.*, 52 (1980) 1313.
132 W. C. Yu and E. U. Goff, *Anal. Chem.*, 55 (1983) 29.
133 A. Robbat, Jr., N. P. Corso and T. Y. Lin, *Anal. Chem.*, 60 (1988) 173.
134 A. Robbat, Jr., N. P. Corso, P. J. Doherty and M. H. Wolf, *Anal. Chem.*, 58 (1986) 2078.
135 R. C. Massey, C. Crews, D. J. McWeeny and M. E. Knowles, *J. Chromatogr.*, 236 (1982) 527.
136 E. A. Mishalanie and J. W. Birks, *Anal. Chem.*, 58 (1986) 918.
137 D. H. Fine, *IARC Sci. Publ.*, 45 (1983) 319.

Journal of Chromatography, 550 (1991) 495–506
Elsevier Science Publishers B.V., Amsterdam

CHROMSYMP. 2197

Possibilities of enhancing the sensitivity of the determination of UV-absorbing compounds in high-performance liquid chromatography

PAVEL JANDERA* and BOŘIVOJ PROKEŠ
Department of Analytical Chemistry, Institute of Chemical Technology, Nám. Legií 565, 532 10 Pardubice (Czechoslovakia)

ABSTRACT

The signal-to-noise ratio and the detection limits in high-performance liquid chromatographic (HPLC) analysis using UV detection depend on the design of the detector and on the detector settings. For the best sensitivity, the detector should be operated at a wavelength as close as possible to the absorption maximum, with a spectral band width as narrow as possible and with a frequency of the detector signal storage between 10 to 20 data per chromatographic peak. However, variations of the detector setting parameters, except for the detection wavelength, do not affect the sensitivity and the detection limits very significantly. In high-speed HPLC, computerized accumulation of several complete chromatograms from repeated runs can be used to enhance the sensitivity and to improve the detection limits. As has been verified on the example of reversed-phase chromatography of three chlorobenzenes with UV detection, this approach can be used with good accuracy to obtain detection limits below 100 ppb with an analysis time of 20–25 min. These are still considerably higher than the detection limits that can be obtained using on-line sample enrichment techniques with solid-phase extraction, but the chromatogram accumulation approach may be useful in those trace analysis problems where sample enrichment is difficult or tedious and where selective derivatization techniques or sensitive detectors are not available.

INTRODUCTION

In spite of generally poorer detection possibilities than in gas chromatography, the number of applicatons of high-performance liquid chromatography (HPLC) in the trace analysis of organic compounds is increasing steadily. On-line and off-line precolumn derivatization techniques in connection with sensitive, selective detectors are the most efficient approaches to improving the sensitivity of determination and the detection limits [1], but they are often not available or not readily applicable for some less reactice compounds or very dilute samples. Consequently, less sensitive UV detection should be still used in many applications.

Both the precision of the integrated peak areas and the limits of detection improve with increasing signal-to-noise ratio [2]. The detection limits are usually defined as the concentration of the sample solute that gives a signal-to-noise ratio of two [3] or three [4]. The signal-to-noise ratio can be improved either by enhancing the

0021-9673/91/$03.50

detector signal or by limiting the noise originating from the detector and the pumps of the instrument. The baseline noise is affected by fluctuations in the flow-rate, pressure and temperature [2] and depends on the design of the detector; signal processing may also contribute to the noise [5,6].

The useful signal, *i.e.*, the height or the integrated area of a chromatographic peak, can be enhanced by using a sensitive detector with optimized parameter settings, an efficient chromatographic column with a small dead volume, a chromatographic system allowing a low retention and simultaneously a sufficient separation selectivity and sample volumes as large as possible without deteriorating the column efficiency. The flow-rate of the mobile phase also affects the heights and areas of the peaks, which usually increase with decreasing flow-rate.

Computerized processing of the digitized detector signal offers a possibility of "bunching" and averaging several successive signal readings to be stored in the computer memory. In addition, diode-array spectrophotometric detectors make it possible to "bunch" simultaneous signals from several photodiodes in a spectral segment of a preselected width. This method of data processing can also affect the reproducibility, sensitivity and detection limits.

The signal-to-noise ratio can also be enhanced by using a filter to reduce the noise amplitude, but this approach is limited by the requirement to retain accurate peak shapes [5]. Fourier transformation of the chromatographic signal can be utilized for improving the signal-to-noise ratio by discriminating and cutting off the high-frequency noise from the useful signal [7]. Smoothing procedures have been suggested that allow one also to filter the noise with frequencies close to that of the signal [8].

High-speed HPLC employing short columns packed with a material of small particle diameter (3 μm) [9] is especially suitable for trace analysis, as the lower column dead volume means a lower dispersion of the solute band and an increased mass sensitivity in comparison with conventional columns [10,11]. High-quality separations of simpler sample mixtures can be obtained in 1–2 min using this technique [9], which suggests a possibility of using the accumulation of several chromatograms from repeated runs to enhance the signal-to-noise ratio and to reduce the limits of detection. Although this approach has been widely used in various spectroscopic techniques, its application to chromatographic analysis has not previously been reported, to our knowledge.

It was the objective of this work to investigate the practical feasibility of applying computerized accumulation of chromatograms from the repeated high-speed runs to enhance the sensitivity and to decrease the detection limits in HPLC analyses using UV detection and to compare this approach with other possibilities, such as the "bunching" and averaging of signal readings in preselected time and wavelength intervals and with the on-line sample enrichment technique using column switching, which has been widely used in the reversed-phase chromatography of aqueous samples [12–18]. For this investigation, a relatively simple reversed-phase separation of a mixture of chlorobenzenes was used.

EXPERIMENTAL

An HP 1090M liquid chromatograph equipped with an automatic sample injector, a column-switching valve, a 3DR solvent-delivery system, a thermostated col-

umn compartment, a Series 7994A workstation and an HP 2225 Think-Jet printer (Hewlett-Packard, Avondale, PA, USA) was used in connection with three UV spectrophotometric UV detectors. Unless stated otherwise, the chromatographic experiments were performed with a built-in standard UV diode-array detector (detector A). The other two detectors were connected to the column outlet by a 280 mm × 0.12 mm I.D. stainless-steel capillary and to the chromatographic workstation via a 760 Series analog/digital converter (Nelson Analytical): an HP 1050 wavelength programmable UV detector, equipped with a monochromator (detector B) and an HP 1050 multiple-wavelength (diode-array) UV detector (detector C), both from Hewlett-Packard. The detectors were operated at wavelengths of 223 or 230 nm.

Two conventional stainless-steel columns (250 × 4 mm I.D.) were packed with octadecylsilica Separon SGX C18, particle size (a) 5 μm and (b) 7 μm, using a high-pressure slurry technique. A high-speed column (60 × 4 mm I.D.), prepacked with Hypersil ODS, 3 μm, (c) was purchased from Hewlett-Parckard. A sample-enrichment octadecylsilica column, (40 × 2 mm I.D.) was dry-packed with Separon SGX C18, 60 μm (d). The bulk Sepharon SGX C18 materials were purchased from Tessek (Prague, Czechoslovakia).

1,4-Di-, 1,2,3,4-tetra-, 1,2,3,5-tetra- and pentachlorobenzene standards were obtained from Lachema (Bohumín, Czechoslovakia). Methanol (spectroscopic grade), purchased from Lachema (Brno, Czechoslovakia), and water, deionized and doubly distilled in glass with addition of potassium permanganate, were filtered through a 0.45-μm filter (Millipore) and used to prepare the mobile phases (90 and 80% aqueous methanol) by mixing directly in the liquid chromatograph with continuous degassing by stripping with helium. The flow-rate of the mobile phase was 1 ml/min in the experiments with the conventional columns and 3 ml/min in those with the high-speed column.

The peak areas (A) and heights (h) were measured as the arithmetic means from three repeated experiments. The detector sensitivities, S_A, S_h, were evaluated from the plots of A and h *versus* concentrations of chlorobenzenes in the range 0.5–1000 ppm (six data points) using linear regression. The baseline noise (N) was determined as the difference between the upper and lower readings of the baseline signal during a 2-min period; the minimum detectable concentrations (MDC) corresponding to the peak heights equal to twice the peak-to-peak noise were evaluated from the concentration plots of S_h for the individual solutes.

For the experiments with on-line sample enrichment using solid-phase extraction, the sorption precolumn (d) was connected to the analytical column (b) in the HP 1090M chromatograph via a standard switching valve. A U6K injector (Waters–Millipore, Milford, MA, USA) was inserted between the autosampler and the precolumn. In the sorption step, 2 ml of the aqueous sample were pushed from the sample loop through the precolumn by water pumped using channel A of the chromatographic pump. After washing the precolumn with water, the column switching valve was switched to the position directing the eluate from the precolumn to the analytical column and to the detector. Aqueous methanol (80%) as the mobile phase was then pumped using channels B and C of the chromatographic pump to elute the enriched sample from the precolumn and to accomplish the chromatographic separation on the analytical column. To test the recovery in this technique, artificial aqueous samples containing 0.01–1 ppm of each of the chlorobenzenes tested were injected in this

way and the peak areas were compared with the experiments where 20-μl samples containing equal masses of chlorobenzenes as in the enrichment experiments (concentrations 1–100 ppm) dissolved in the mobile phase were injected directly into the analytical column using the autosampler.

RESULTS AND DISCUSSION

Effects of the construction and parameters of a UV detector on the sensitivity and limits of detection

The limits of detection can be conveniently characterized as the concentration of a sample solute resulting in a detector signal, S, equal to twice the baseline noise, N, at the maximum of the chromatographic peak. The suitability of various experimental conditions to provide the best limits of detection can be tested by comparing the corresponding signal-to-noise ratios, S/N.

The results of the comparison of three different variable-wavelength UV detectors under the same experimental conditions summarized in Table I suggest that the most important factors for the detector performance are the length of the detector cell and the baseline noise. At a comparable noise level, the sensitivity of detection is higher and the detection limits are lower for detector B with a longer optical path length of the cell (10 mm) in comparison with detector C (6 mm). Because of the construction differences, detector A showed a higher sensitivity (S_A *ca.* 120%, S_h *ca.* 30-50%), but a *ca.* 2.5 times higher noise level than detector C with the same optical path length, which resulted in a 1.8 times lower S/N and higher detection limits for the chlorobenzenes tested. Although these results could be expected on the basis of the Lambert-Beer law, only qualitative estimates can be made *a priori* because of other important design parameters, such as the volume and shape of the detector cell and of the connecting tubing.

TABLE I

NOISE (N), INTEGRATED PEAK AREA (S_A) AND PEAK HEIGHT (S_h) SENSITIVITIES AND MINIMUM DETECTABLE CONCENTRATIONS (*MDC*) CORRESPONDING TO PEAK HEIGHTS EQUAL TO TWICE THE BASELINE NOISE CALCULATED FROM N AND S_h FOR DETECTORS A–C

Compounds: 1 = 1,4-dichlorobenzene; 2 = 1,2,3,4-tetrachlorobenzene; 3 = 1,2,3,5-tetrachlorobenzene. Wavelength, 230 nm; band width, 4 nm.

Parameter	Compound	Detector		
		A	B	C
N (mV)		0.015	0.006	0.006
S_A (area units · cm^3 · g^{-1} × 10^{-5})	1	47.60	42.97	21.38
	2	38.32	31.44	16.92
	3	38.38	33.25	17.54
S_h (mV · cm^3 · g^{-1} × 10^{-5})	1	4.67	7.50	3.16
	2	2.24	3.41	1.83
	3	2.05	3.06	1.47
MDC (ppm)	1	0.064	0.016	0.038
	2	0.13	0.035	0.066
	3	0.15	0.039	0.082

It is well known that the detection wavelength should be set to the spectral absorption maximum to obtain the highest detection sensitivity. Also, the spectral band width affect S/N and the detection limits. In contrast to spectrophotometric detectors equipped with a monochromator that usually operate with a fixed width of the monochromator exit slit, diode-array detectors allow the spectral band width to be controlled by "bunching" together the signals from all the photodiodes within a preselected spectral range. We tested different spectral band width settings of detector A from 4 to 60 nm. In this range, the baseline noise was approximately constant (0.1–0.14 mV), with no systematic dependence on the spectral band width. With the detection wavelength set to the maximum of the absorption band of 1,4-dichlorobenzene, *i.e.*, 223 nm, both the area and the height of the chromatographic peak of this solute decreased with increasing spectral band width, as expected (Figs. 1 and 2). More interesting were these dependencies for the two tetrachlorobenzenes having absorption maxima below 190 nm, so that the detection wavelength could be set only at the slope of the absorption band. Here, flat maxima of the integrated peak areas were observed between spectral band widths of 30 and 50 nm. However, the increase in the integrated peak areas and in the peak heights with increasing spectral band width represents only a marginal improvement (Figs. 1 and 2), so that the selection of the detection wavelength as close as possible to the adsorption maximum and of the spectral band width as narrow as possible in agreement with common spectroscopic practice, can be recommended for obtaining the best sensitivity and detection limits, even for compounds lacking absorption maxima in the near-UV spectral region.

Another variable detection parameter is the frequency with which the detector signal is digitized and stored in the computer memory during the elution of a chromatographic peak. Several subsequent "readings" of the detector signal may be

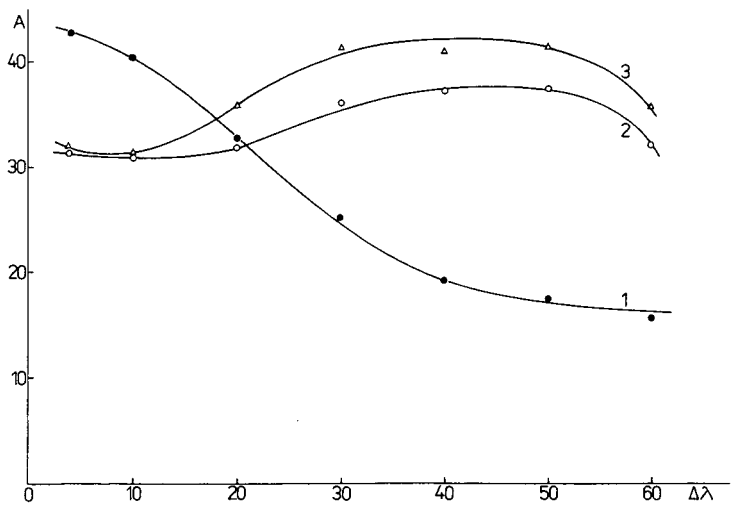

Fig. 1. Dependence of the peak areas A (in integrator units) on the spectral band width $\Delta\lambda$ (in nm) for (1) 1,4-dichlorobenzene, (2) 1,2,3,4-tetrachlorobenzene and (3) 1,2,3,5-tetrachlorobenzene. Column, Hypersil ODS, 3 μm, 60 × 4 mm I.D.; mobile phase, 80% methanol in water, 3 ml/min: sample volume, 5 μl; detector A, λ = 223 nm, 0.32 s data storage period.

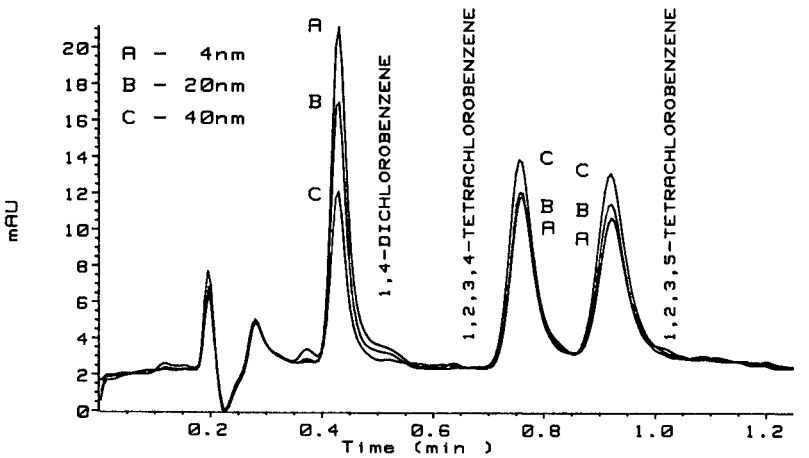

Fig. 2. Overlayed chromatograms for a mixture of three chlorobenzenes at different spectral band widths. Conditions as in Fig. 1.

"bunched" and averaged within the signal storage period, which results in reduced baseline noise. For example, the experimental noise of detector A at 223–230 nm, with 90% methanol as the mobile phase, was reduced from 0.11 mV at a signal storage period of 0.32 s to 0.025 mV at a signal storage period of 1.28 s. However, the signal storage frequency should not fall below the minimum required to give 10–20 signals stored per chromatographic peak, otherwise the peak shape is not reconstructed accurately and poor reproducibility of quantitation may result. To achieve the best S/N, this minimum signal storage frequency should not be exceeded.

Computer-assisted accumulation of chromatograms

The computerized accumulation of spectrograms is a well known approach to increase the sensitivity of various spectroscopic methods, such as NMR, Fourier transform IR and mass spectrometry, but to our knowledge this technique has not previously been applied to the improvement of sensitivity and detection limits in chromatography. Unlike the signal "bunching" and averaging during a single chromatographic run discussed earlier, several chromatograms from the subsequent repeated runs are added to the contents of a single raw data memory register so that the register eventually contains the sum of all the chromatograms from the repeated runs. In the final accumulated chromatograms reconstructed from the contents of the register, the chromatographic signal is amplified proportionally to the number of individual repeated chromatographic runs, but because of the random character of the baseline noise, the final noise after the accumulaton is expected to increase proportionally to the square root of the number of accumulations, yielding an increase in S/N and a decrease in the detection limits proportional to the square root of the number of accumulations, as in the accumulated spectrograms.

The technique of computerized accumulation of chromatograms is practically feasible only in connection with high-speed separations, to avoid excessive analysis times. It can be speculated that good reproducibility of the retention times is also

required for this approach, otherwise both the leading and the trailing edges of the small peaks of trace compounds in some of the subsequent individual chromatograms could be shifted outside the integration area of the accumulated peak, resulting in a negative error in the integrated peak area in the final reconstructed chromatogram.

The main objective of this work was to investigate the practical feasibility of applying computerized accumulation of chromatograms in high-speed HPLC. The same three chlorobenzenes were used as sample compounds as in the previous section, with a high-speed Hypersil ODS column. In 80% methanol as the mobile phase, the separation of the three solutes could be accomplished in 1.2 min at a flow-rate of 3 ml/min. This means that twenty individual chromatograms could be accumulated in *ca.*. 24 min, which is the analysis time commonly accepted for many separations on conventional analytical columns. For this investigation, detectors B and C were no longer available to us, so that detector A had to be used. On the basis of the results reported in the previous section, we adjusted the detection parameters to the optimum settings: a detection wavelength of 223 nm and a spectral band width of 4 nm were the optimum values for 1,4-dichlorobenzene (Figs. 1 and 2) and a signal storage period of 0.32 s provided 13–18 data stored during the elution of a peak for the three sample compounds, which is in the aformentioned optimum signal storage frequency range.

Fig. 3 shows a non-accumulated chromatogram from one of the subsequent repeated runs with the sample containing 0.1 ppm of each of the three chlorobenzenes. According to Table I, this concentrations is sligthly above the detection limit for 1,4-dichlorobenzene and below the detection limits for the two tetrachlorobenzenes, whose peaks could be only tentatively attributed in the baseline noise on the basis of the retention times of the more concentrated standards. The peak heights and areas for the 0.1 ppm sample are necessarily subject to significant errors (relative standard deviations 35–60%, Table II).

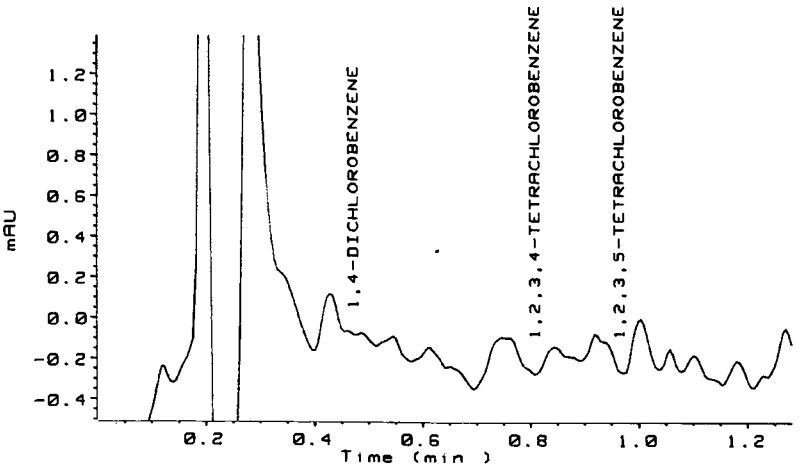

Fig. 3. Single chromatogram for 5 μl of 0.1 ppm methanolic solution of chlorobenzenes. Conditions as in Fig. 1; spectral band width 4 nm.

TABLE II

EFFECT OF THE COMPUTERIZED ACCUMULATION OF CHROMATOGRAMS ON SENSITIVITY AND DETECTION LIMITS

Column, Hypersil ODS, 3 μm, 60 × 4 mm I.D.; mobile phase, 80% methanol in water, 3 ml/min; 5 μl of methanolic solutions of 1,4-dichlorobenzene (1), 1,2,3,4-tetrachlorobenzene (2) and 1,2,3,5-tetrachlorobenzene (3); detector A, 223 nm, spectral band width 4 nm, data storage period 0.32 s. A_i, A_a, h_i and h_a, integrated peak areas (in integrator area units) and peak heights (in mAU) for an unaccumulated chromatogram (*i*) and for the chromatogram reconstructed after 20 acumulations (*a*). *MDC* = minimum detectable concentration (ppm).

Compound	Concentration (ppm)	A_i[a]	ΣA_i[b,*]	A_a*	h_i	h_a*	MDC_i	MDC_a
1	10	43.85 ± 1.0	876.9	869.2	14.2	300	0.3	0.06
	1	3.34 ± 0.83	66.8	69.9		36		
	0.1	0.39 ± 0.14	7.8	6.4	0.2	4.1		
2	10	31.36 ± 1.05	627.2	619.3	7.2	150	0.6	0.12
	1	3.61 ± 1.11	72.1	59.0		18		
	0.1	0.36 ± 0.15	7.2	4.6	0.1	2.2		
3	10	34.42 ± 1.14	688.3	688.0	6.2	125	0.7	0.15
	1	3.20 ± 1.01	64.1	60.0		15		
	0.1	0.37 ± 0.22	7.4	5.1	0.1	2.2		

[a] Arithmetic means from twenty repeated experiments ± standard deviaton.

[b] Sum of the areas evaluated from the individual non-accumulated chromatograms.

* Regression equations for the concentration dependences (concentrations c in ppm; R = correlation coefficient):

Solute: 1 $A_a = -9.803 + 87.830c$; $R = 0.9999$
2 $A_a = -2.341 + 62.153c$; $R = 0.9999$
3 $A_a = -5.349 + 69.303c$; $R = 0.9999$
1 $\Sigma A_i = -0.550 + 88.692c$; $R = 0.9998$
2 $\Sigma A_i = 0.262 + 62.244c$; $R = 0.9999$
3 $\Sigma A_i = -0.104 + 69.014c$; $R = 0.9999$
1 $h_a = 3.611 + 29.664c$; $R = 0.9987$
2 $h_a = 1.889 + 14.823c$; $R = 0.9999$
3 $h_a = 1.778 + 12.330c$; $R = 0.9999$.

Fig. 4 shows a reconstructed accumulated chromatogram after the summation of twenty individual chromatograms such as that shown in Fig. 3. Comparison of Figs. 3 and 4 shows that the peaks of the chlorobenzenes are clearly distinguished from the baseline noise in the accumulated chromatogram, with the peak heights amplified *ca.* 20-fold. Should there be other trace impurities in the sample, their peaks would be amplified in the same ratio as the peaks of the chlorobenzenes. However, the amplitudes of all the other "peaks" in Fig: 4 were 0.9 mAU or lower, in comparison

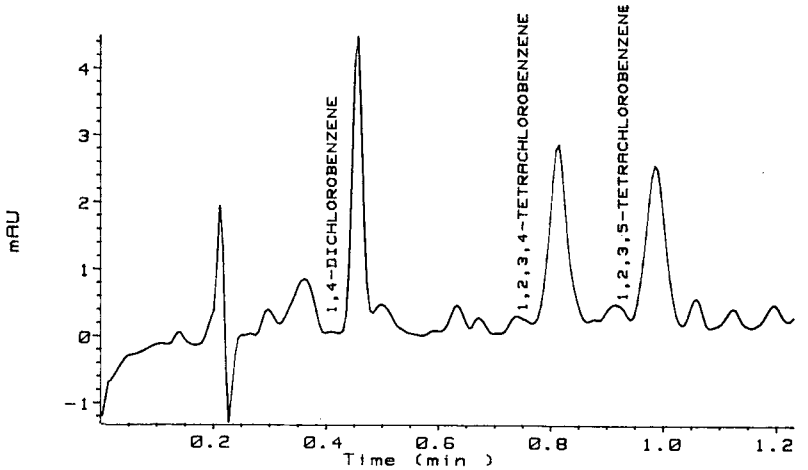

Fig. 4. Chromatogram for 5 μl of 0.1 ppm methanolic solution of chlorobenzenes after twenty accumulations of repeated experiments. Conditions as in Figs. 1 and 4.

with the maximum amplitude of the baseline noise in the non-accumulated chromatogram of 0.22 mAU (Fig. 3). This is only a 4.1-fold increase after the acculumation, corresponding well with the expected noise increase of $\sqrt{20} = 4.5$-fold, which allows us to conclude that no impurities were present in the sample in concentrations comparable to those of the sample solutions and to attribute all the small "peaks" in Fig. 4 to the baseline noise.

To test the accuracy of the accumulation approach, the peak areas and heights before and after the accumulation were compared for three different concentrations of the solutes tested (Table II). The areas of the peak in the accumulated chromatograms, A_a, differ from the sum of the peak areas in the original twenty chromatograms, A_i, by *ca.* 1% for 10 ppm samples and 10–20% for 1 ppm samples. The differences between A_a and A_i relative to A_a were less than the relative standard deviation of a single experiment. Also, the dependences of both A_a and A_i on the concentration of the sample solutes, c, showed good linearities, with the slopes differring by less than 1%. The increased absolute values of the intercepts of the A_a *versus* c plots can possibly be attributed to the accumulation of the noise.

The heights of peaks in the accumulated chromatograms are slightly greater than the sums of the peak heights in the individual non-accumulated chromatograms (*ca.* 1–5% for 10 ppm samples and 3–10% for 0.1 ppm samples). The plots of the peak heights in the accumulated chromatograms *versus* the concentrations of chlorobenzenes in the samples analysed were linear, like the plots of the peak areas *versus c*. The miminum detectable concentrations corresponding to the peak heights twice the baseline noise were 0.3–0.7 ppm for non-accumulated chromatograms and decreased to 0.06–0.15 ppm after twenty accumulations, *i.e.*, *ca.* 5-fold, in agreement with the theoretical prediction ($\sqrt{20} = 4.5$).

On the basis of the present results, it can be concluded that the technique of computerized accumulation of chromatograms in high-speed HPLC can be perform-

TABLE III

LINEARITY AND RECOVERY TESTS OF THE ON-LINE ENRICHMENT TECHNIQUE FOR AQUEOUS SAMPLES OF CHLOROBENZENES

Analytical column, Separon SGX C18, 7 μm, 250 × 4 mm I.D.; enrichment precolumn, Separon SGX C18, 60 μm, 40 × 2 mm I.D.; mobile phase, 80% methanol in water, 1 ml/min; sample volume, 2 ml; solutes, as in Table I; detector A, 230 nm. A = Integrated areas in integrator units; c = concentrations of sample solutes; R = correlation coefficient; recovery as % of areas determined in the experiments with direct injection of 20-μl samples containing equal amounts of sample solutes as in the enrichment experiments.

Regression equations for the concentration dependences

Solute	Equation	R
1	$A = -6.41 + 3357\ c$	0.998
2	$A = 12.1 + 3639\ c$	0.999
3	$A = 26.7 + 3423\ c$	0.999

Concentration dependences of recoveries

c (ppm)	Recovery (%)		
	Solute 1	Solute 2	Solute 3
1	83.0	84.7	80.8
0.5	86.5	78.0	78.2
0.1	82.8	75.7	80.0
0.05	86.8	65.4	76.2
0.02	58.5	76.3	87.1
0.01	70.7	67.2	94.8

ed with adequate accuracy. It allowed the detection limits of the chlorobenzenes tested to be decreased about 5-fold to the 100 ppb level in a tolerable time of analysis of 24 min.

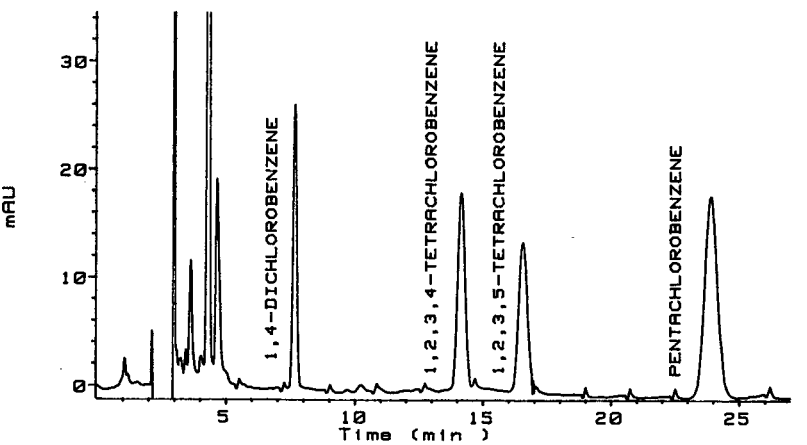

Fig. 5. Chromatogram for 2 ml of aqueous sample containing 0.1 ppm of each of the chlorobenzenes using the on-line sample enrichment technique. Conditions as in Table III.

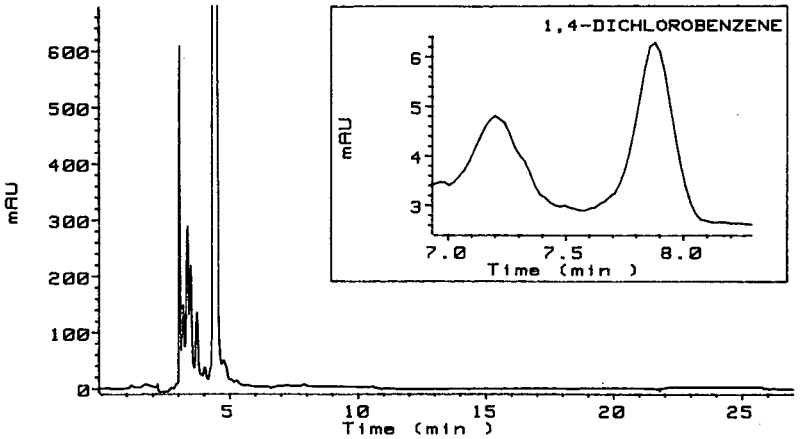

Fig. 6. Chromatogram for 2 ml of a sample of waste water from an industrial plant, containing 14 ppb of 1,4-dichlorobenzene, using the on-line sample enrichment technique. Conditions as in Table III.

On-line sample enrichment using solid-phase extraction

The tests of the on-line sample enrichment technique in reversed-phase HPLC of the three chlorobenzenes, summarized in Table III, showed good linearity of the calibration graphs in the range 50–1000 ppb with average recoveries of 80%. Fig. 5 shows the chromatogram for 2 ml of an artificial sample containing 0.1 ppm of each of the chlorobenzenes in water. The chromatogram of a practical sample of waste water from an industrial plant, containing 14 ppb of 1,4-dichlorobenzene (identified on the basis of both the retention time and the UV spectrum), is shown in Fig. 6. The detection limits for the 2-ml samples are in the range 2–5 ppb, *i.e.*, approximately 30 times lower than those achieved with 5-μl samples using high-speed HPLC with twenty accumulations of the repeated experiments. The amount of 1,4-dichlorobenzene in the sample in Fig. 6 is below the detection limits of the chromatogram accumulation technique.

A combination of computerized accumulation of chromatograms with the on-line sample enrichment technique could possibly further decrease the limits of detection. However, (1) it would require a low inner-volume switching valve suitable for work with high-speed columns (such a valve was not available to us), (2) longer analysis times should be tolerated and (3) the detection limits in on-line sample enrichment techniques are likely to be controlled by the "chromatographic" noise originating from trace impurities in the sample or in the components of the mobile phase rather than by the baseline noise; this "chromatographic" noise, of course, cannot be reduced by the technique of computerized accumulation of chromatograms. On the other hand, the chromatogram accumulation approach may offer a means of increasing the sensitivity and decreasing the limits of determination for analyses where the application of sample enrichment techniques would be tedious of where there is no adequate sorbent for solid-phase extraction.

CONCLUSIONS

The computerized accumulation of subsequent repeated chromatograms in high-speed HPLC makes it possible to increase the signal-to-noise ratio and to decrease the minimum detectable concentrations approximately in proportion to the square root of the number of accumulations with good accuracy of quantification. A compromise between the time of analysis and the detection limits should be chosen; however, the accumulation of the data from twenty repeated simple high-speed HPLC separations at 100 ppb levels may take no longer than 20–30 min, which is a time comparable to those for many single-run analyse on conventional columns.

To obtain low detection limits using the accumulation approach it is important to use a detector designed to yield a high signal-to-noise ratio. The UV detector set to the wavelength of the absorption maximum should use a narrow spectral band width setting and a signal acquisition frequency of 10–20 signal readings during the elution of a chromatographic peak.

On-line sample enrichment techniques based on solid-phase extraction result in detection limits at least one order of magnitude lower than those achievable using computerized accumulations of repeated chromatograms, but the latter approach may be a useful option for analyses where no adequate sorbent is available or where the sample enrichment techniques are too tedious.

ACKNOWLEDGEMENT

Dr. Hans Peter Schiefer of the East-European Office of Hewlett-Packard, Vienna, Austria, is thanked for the loan of detectors B and C.

REFERENCES

1 J.F. Lawrence, *Organic Trace Analysis by Liquid Chromatography*, Academic Press. New York, 1981.
2 E. Grushka and I. Zamir, in P. R. Brown and R. A. Hartwick (Editors), *High Performance Liquid Chromatography*, Wiley, New York, 1989, p. 552.
3 R. P. W. Scott, in E. Katz (Editor), *Quantitative Analysis Using Chromatographic Techniques*, Wiley, Chichester, 1987, p. 25.
4 ACS Committee on Environmental Improvement, *Anal. Chem.*, 52 (1980) 2242.
5 K. Ogan, in E. Katz (Editor), *Quantitative Analysis Using Chromatographic Techniques*, Wiley, Chichester, 1987, Ch. 2.
6 S. Ahuja, *Selectivity and Detectability Optimization in HPLC*, Wiley, New York, 1989, Ch. 13.
7 G. J. de Groot, *Trends Anal. Chem.*, 4 (1986) 134.
8 T. Hevesi, J. Krupčík, E. Benická, D. Repka and J. Garaj, *8th International Symposium on Advances and Applications of Chromatography in Industry, Bratislava, 1989*, Abstract No. B52.
9 R. C. Simpson, in P. R. Brown and R. A. Hartwick (Editors), *High Performance Liquid Chromatography*, Wiley, New York, 1989, p. 375.
10 S. van der Wal, *J. Chromatogr. Sci.*, 23 (1985) 341.
11 G. Guiochon and H. Colin, in P. Kucera (Editor), *Microcolumn High Performance Liquid Chromatography*, Elsevier, Amsterdam, 1984, Ch. 1.
12 K. Ogan, E. Katz and W. Slavin, *J. Chromatogr. Sci.*, 16 (1978) 517.
13 R. W. Frei, *Int. J. Environ. Anal. Chem.*, 5 (1978) 143.
14 C. E. Werkhoven-Goewie, U. A. Th. Brinkman and R. W. Frei, *Anal. Chem.*, 53 (1981) 2072.
15 R. P. W. Scott and P. Kucera, *J. Chromatogr.*, 169 (1979) 51.
16 M. C. Harvey and S. D. Stearns, *Am. Lab.*, 14, No. 5 (1982) 68.
17 P. Jandera, L. Svoboda, J. Kubát, J. Schvantner and J. Churáček, *J. Chromatogr.*, 292 (1984) 71.
18 S. van der Wal, *J. Liq. Chromatogr.*, 9 (1986) 1815.

Journal of Chromatography, 550 (1991) 507–517
Elsevier Science Publishers B.V., Amsterdam

CHROMSYMP. 2082

Chromatographic characterization of some dideoxyribonucleosides

NAN-IN JANG and PHYLLIS R. BROWN*
Department of Chemistry, University of Rhode Island, Kingston, RI 02881 (U.S.A.)
and
ELI GRUSHKA
Department of Inorganic and Analytical Chemistry, Hebrew University, Jerusalem (Israel)

ABSTRACT

Selectivity and retention surfaces were developed for the rapid high-performance liquid chromatographic separation of dideoxyribonucleosides which are promising antiretroviral agents. In this study, the dideoxyribonucleosides 2′,3′-dideoxyadenosine, 2′,3′-dideoxyinosine, 2′,3′-dideoxycytidine and 3′-deoxythymidine were used as model compounds and 2′-azido-3′-deoxythymidine (AZT) and AZT-5′-phosphate (AZT-5′-P) as experimental test compounds. The interdependence of the experimental variables, column temperature, mobile phase pH and percentage of methanol, and the effects of these variables on the reversed-phase liquid chromatographic (RPLC) behavior of the dideoxy compounds were investigated. The conditions for optimal resolution of these compounds, as determined from the surfaces, were mobile phases of pH 5.0 and either 14% methanol at 40°C or 15% methanol at 30°C. These surfaces served as guidelines in determining conditions for preparative and analytical scale RPLC separations of AZT from AZT-5′-P.

INTRODUCTION

Dideoxyribonucleosides (ddNs) have been shown to be inhibitors of the human immunodeficiency virus (HIV) *in vitro* [1–7]. At present, 3′-azido-3′-deoxythymidine (AZT), a ddN, is approved for use in the treatment of the acquired immunodeficiency syndrome (AIDS). Other ddNs, which are promising antiretroviral drugs, include 2′,3′-dideoxycytidine (ddCyd), 2′,3′-dideoxyinosine (ddIno), 3′-deoxythymidine (dThd) and 2′,3′-dideoxyadenosine (ddAdo). However, because these ddNs as well as AZT have serious toxic side-effects [8,9], new analogues, which have the potential for the same or greater efficacy but lower toxicity, are being synthesized.

Since high-performance liquid chromatography (HPLC) has been succesfully used for the past two decades for the separation of nucleotides and nucleosides [10,11], it is the method of choice for the separations of ddNs. In the past, we have investigated structure–retention relationships in reversed-phase liquid chromatography (RPLC) of nucleotides, nucleosides and their bases [12,13], and we have developed retention and selectivity surfaces for deoxyribonucleotides [14] and deoxyribonucleosides [15], which

0021-9673/91/$03.50

can be used to determine the conditions for various HPLC separations of these compounds. With these surfaces, optimal resolution and retention times can be obtained by two or more sets of experimental conditions; thus the best conditions for difference scale separations (*e.g.*, analytical, preparative) can be readily chosen.

In this study, we applied the results of our previous work [12–15] to the separation of the ddNs. First, we used structure–retention relations to determine the initial experimental conditions, retention and selectivity surfaces of the deoxyribonucleosides to find the approximate conditions for the separations of ddNs and the surfaces of the ddNs to fine-tune these separations. Finally, we used AZT and AZT-5′-phosphate (AZT-5′-P) as model compounds to test experimentally our predictions for the conditions needed both on the analytical and preparative scale to separate AZT-5′-P from its precursor AZT in the synthesis of the monophosphate [16]. Large amounts of the AZT-5′-P are needed to synthesize new analogues of AZT for animal studies and clinical trials.

EXPERIMENTAL

Instrumentation

The chromatographic system was equipped with a Waters 6000A pump (Waters Division, Millipore, Milford, MA, U.S.A.), a Rheodyne 7125 injector (Rheodyne, Berkeley, CA, U.S.A.) and a Waters M440 absorbance detector at 254 nm. Retention times were recorded on an HP 3390A integrator (Hewlett-Packard, Avondale, PA, U.S.A.) and an Omniscribe recorder (Houston, TX, U.S.A.). The column was a 110 mm × 4.70 mm I.D. cartridge packed with 5-μm C_{18} packing material (Whatman, Clifton, NJ, U.S.A.). A guard column (30 mm × 2.0 mm) packed with Whatman pellicular C_{18} glass beads was installed between the injector and the column.

Materials

The dideoxyribonucleosides ddAdo, ddCyd, ddIno and dThd, which were of the highest purity, were purchased from ICN Biochemicals (Cleveland, OH, U.S.A.). The dideoxyribonucleoside AZT (Sigma, St. Louis, MO, U.S.A.) and AZT-5′-P (synthesized in the Medicinal Chemistry Laboratory at URI) were used to test the optimization schemes. Stock solutions (20 m*M*) were prepared and stored at −20°C. Working standards, which were diluted to $2 \cdot 20^{-5}$ *M*) with doubly distilled, deionized water before injection into the chromatograph, were kept at 4°C. The pH of each solution was adjusted to 5.6 with potassium hydroxide (KOH). For the mobile phase, HPLC-grade potassium dihydrogenphosphate (KH_2PO_4) and methanol were obtained from Fisher Scientific (Fairlawn, NJ, U.S.A.).

Procedures

The mobile phase consisted of a solution of 10 m*M* KH_2PO_4 and methanol. The pH of the mobile phase was adjusted with phosphoric acid or KOH before the methanol had been added to the buffer. All experiments were carried out by changing one condition systematically while holding constant the two remaining conditions. The temperatures were 30, 35, 40, 45 and 50°C. The pH values were 3.5, 4.5, 5.0, 5.5 and 6.0. The methanol content (v/v) was 13.0, 13.5, 14.0, 14.5 or 15.0%. The flow-rate was 1 ml/min and the chart speed was 0.5 cm/min. The absorbance units of the detector were 0.02 absorbance units full scale.

Calculations

The void volume was determined using sodium nitrate as a void volume marker. The capacity factors (k') were the average of three measurements. The selectivity factors (α) were determined for adjacent peaks: ddAdo/dThd, ddIno/ddCyd, dThd/ddIno. The retention and selectivity surfaces were plotted by using Turbo Basic (Borland, CA, U.S.A.).

RESULTS AND DISCUSSION

Temperature effects

Capacity factors are related inversely to the temperature. The relationship is obtained from the following equation:

$$\ln k' = -\Delta H/RT + \Delta S/R + \ln \varphi \quad (1)$$

where ΔH and ΔS are the enthalpy and entropy of transfer of the solute between the phases, respectively, T is the absolute temperature, φ is the column phase ratio and R is the gas constant. By using the linear regression of the equation, the values of the slope ($-\Delta H/R$) and the intercept ($\Delta S/R + \ln \varphi$) were obtained. The slopes of all the ddNs in the plots of $\ln k'$ *versus* $1/T$ were positive, thus indicating that the capacity factors decrease with increasing column temperature (Fig. 1). Although these slopes were the same for the pyrimidine ddNs, they were different from those of the purine ddNs. Moreover, the capacity factors of ddAdo and ddIno decreased at different rates. Therefore, temperature can be utilized to manipulate retention time and to optimize the separation of ddAdo from its nearest neighbor dThd, ddIno from dThd as well as ddAdo from ddIno.

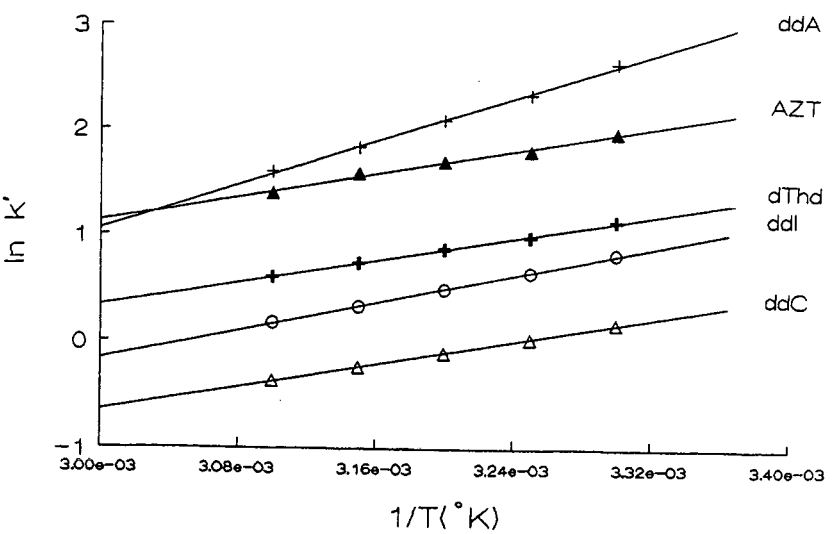

Fig. 1. Plots of ln k' values of ddAdo, ddCyd, ddIno, dThd and AZT as a function of the reciprocal of temperature at pH 5.0 and 14.0% methanol.

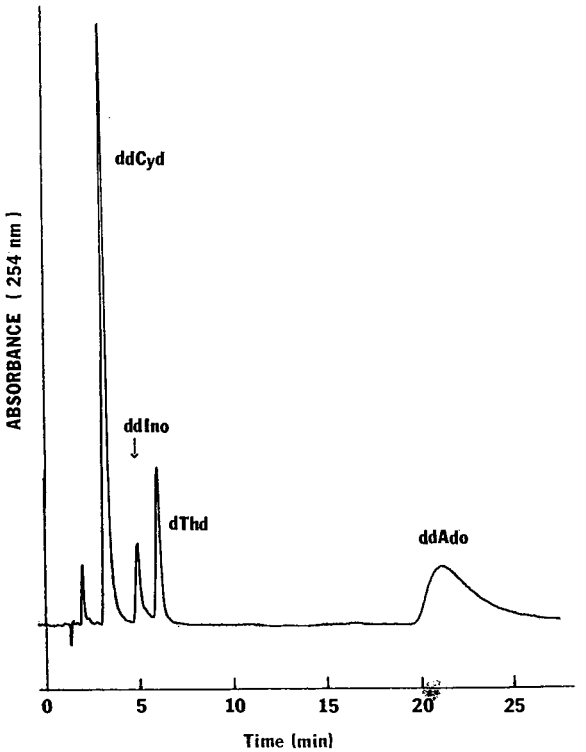

Fig. 2. Chromatogram of the four dideoxyribonucleosides in order of retention times: ddCyd, ddIno, dThd, ddAdo. Conditions: temperature, 30°C; pH, 5.0; methanol concentration, 14%; flow-rate, 1 ml/min.

With ddAdo, elevation of temperature not only decreased the capacity factor but also improved the peak shape as is shown in chromatograms obtained at 30°C (Fig. 2) and at 40°C (Fig. 3). With ddCyd, however, higher temperatures have an adverse effect on retention behavior because this compound had such a small capacity factor ($k' < 1$) at the lowest temperature (30°C) that it was eluted in the void volume at temperatures higher than 40°C.

The selectivity of two neighboring solutes is important in the determination of resolution. The selectivity (α) for any two solutes can be expressed as a function of changes in temperature:

$$\ln \alpha = (\Delta H_1 - \Delta H_2)/RT + (\Delta S_2 - \Delta S_1)/R \quad (2)$$

where subscript 2 indicates the more retained compound and subscript 1 is the less retained compound. The values of the slope, $(\Delta H_1 - \Delta H_2)/R$, and the intercept, $(\Delta S_2 - \Delta S_1)/R$, for all three pairs of ddNs (ddAdo/dThd, ddIno/ddCyd, and dThd/ddIno) are obtained by the linear regression of ln α *versus* $1/T$. The selectivities of both ddAdo/dThd and ddIno/ddCyd decreased with increases in the temperature; however, the selectivity of dThd/ddIno increased as the temperature increased (Fig. 4).

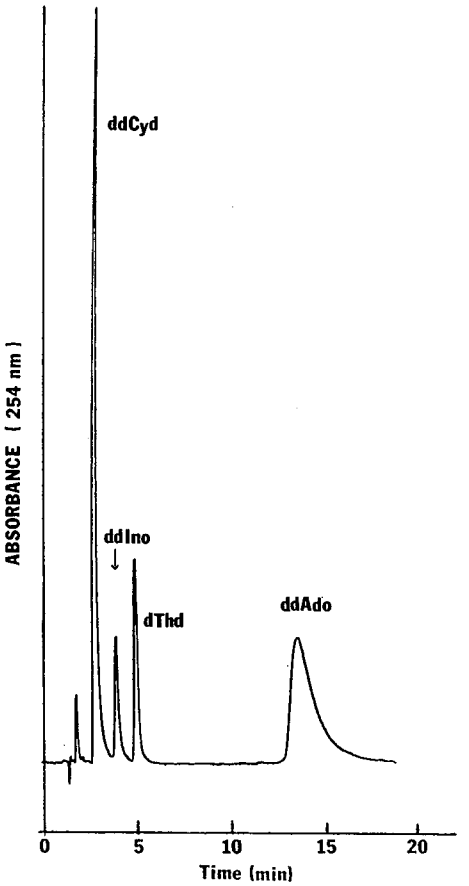

Fig. 3. Chromatogram of the four dideoxyribonucleosides in order of retention times (see Fig. 2). Conditions: temperature, 40°C; pH, 5.0; methanol concentration, 14%; flow-rate, 1 ml/min.

pH effects

The N-1 site in the purine ring of ddAdo has a pK value of 3.8 and the N-3 site in the pyrimidine ring of ddCyd has a value of 4.3. When the pH is 3.5, these two solutes are charged, thus it was predicted that their retention times would be lower than those at pH values of 4.5 and higher [12]. Experimentally it was found that at all temperatures and methanol contents, the capacity factors of ddAdo were at a maximum at pH 5.0 (Fig. 5). The capacity factors of ddCyd decreased slightly with a change of pH from 4.5 to 3.5 and the retention behavior of ddIno and dThd was not influenced by a change of pH in the range studied since the pK of ddIno is 8.9 and of dThd is 9.8.

Effects of methanol content

Based on structure–retention relationships [12], the elution order of a mixture of deoxyribonucleotides, deoxyribonucleosides and ddNs on a reversed-phase column can be predicted. Since deoxyribonucleotides contain phosphate groups which are ionic at all the pH values studied, they will be eluted first on reversed-phase columns;

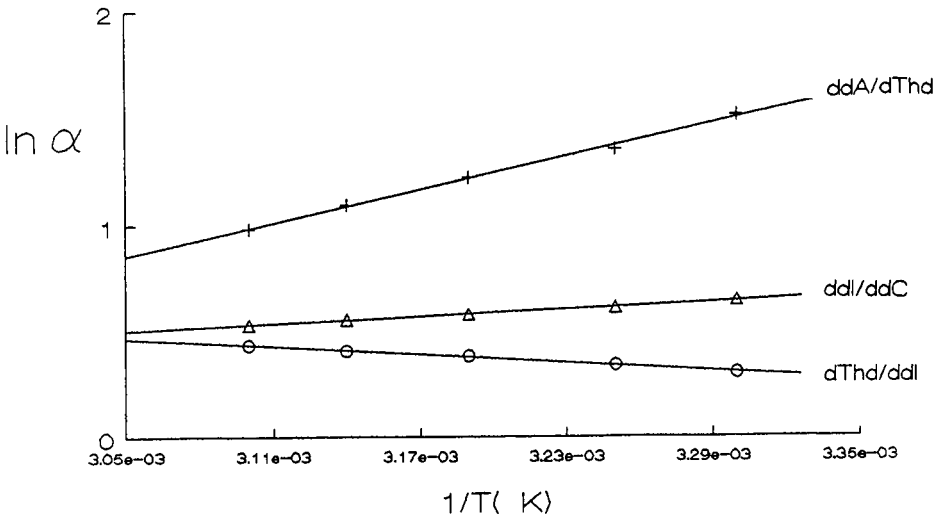

Fig. 4. Plots of ln α values of ddAdo/dThd, ddIno/ddCyc, dThd/ddIno as a function of the reciprocal of temperature at pH 5.0 and 14.0% methanol.

ddNs, which are less polar than deoxyribonucleosides, have the longest retention times. Therefore, it was predicted that a mobile phase containing more than 9% methanol, the maximum percentage of methanol used for the deoxyribonucleosides studies, would be needed in the separation of ddNs. It was also predicted from the work on deoxyribonucleosides [15] that the higher methanol concentrations will cause decreased retention of the ddNs without causing significant changes in their selectivities.

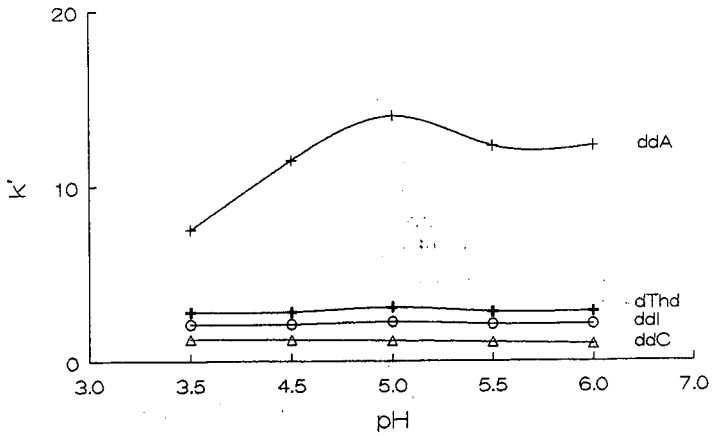

Fig. 5. Plot of k' values of ddAdo, ddCyd, ddIno and dThd as a function of the pH of the mobile phase at 30°C and 14% methanol.

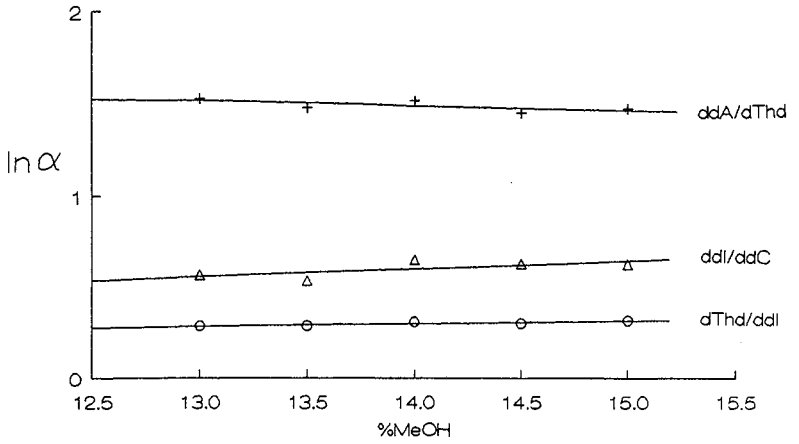

Fig. 6. Plot of ln α values of ddAdo/dThd, ddIno/ddCyd, dThd/ddIno as a function of the methanol content in the mobile phase at pH 5.0 and 30°C.

The dependence of selectivity on the percentage of organic modifier in the mobile phase (X) can be written as follows:

$$\ln \alpha = (a_1 - a_2)X + (b_2 - b_1) \tag{3}$$

where a and b are constants and the subscripts identify the solutes. The values of $(a_1 - a_2)$ and $(b_2 - b_1)$ were calculated by linear regression. The negative values of $(a_1 - a_2)$ for ddAdo and dThd indicated that the selectivity of ddAdo/dThd would

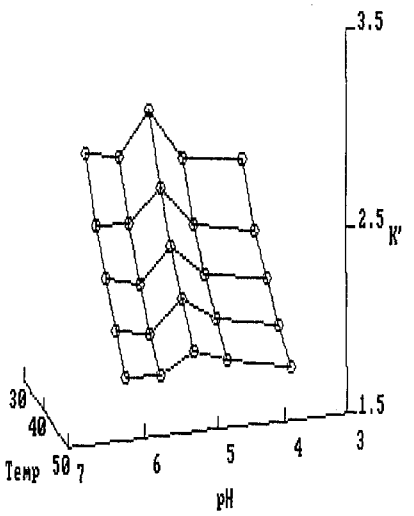

Fig. 7. Retention surface generated by plotting k' values of dThd as a function of the temperature (°C) and pH of the mobile phase that contains 14% methanol. Each circle on an intersection of two or more lines represents an experimentally determined k' value (average of triplicate determinations).

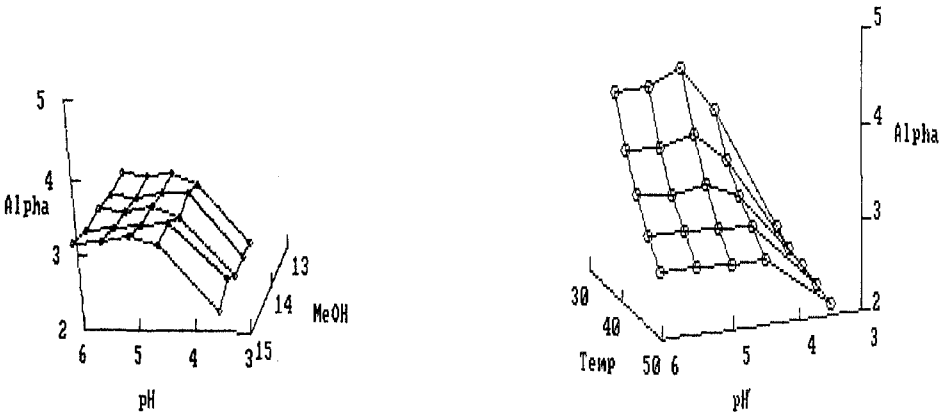

Fig. 8. Selectivity surface generated by plotting α values of ddAdo/dThd as a function of the methanol content and pH in the mobile phase at 40°C. Each circle on an intersection of two or more lines represents an experimentally determined α value (average of triplicate determinations).

Fig. 9. Selectivity surface generated by plotting α values of ddAdo/dThd as a function of temperature and pH of the mobile phase that contains 14.0% methanol. Each circle on an intersection of two or more lines represents an experimentally determined α value (average of triplicate determinations).

decrease with increasing methanol concentration (Fig. 6). However, with dThd/ddIno, since the values of $(a_1 - a_2)$ did not change, the selectivity for this pair of compounds would remain constant even with increases in the methanol content.

Selectivity and retention surfaces

The pH–temperature retention surfaces of ddAdo, ddIno and dThd have a maximum at pH 5.0 at all methanol concentrations. An example of this type of

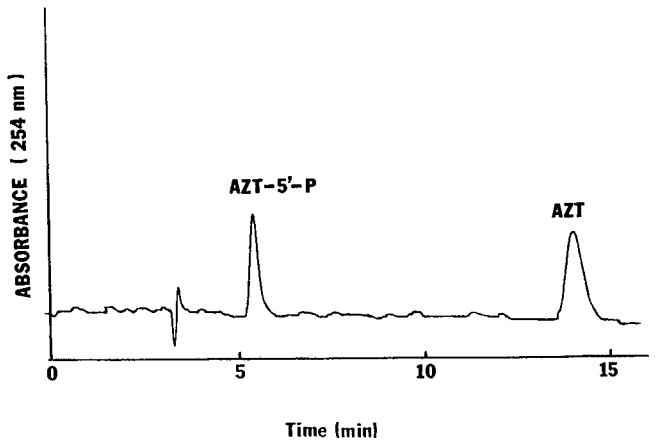

Fig. 10. Chromatogram of analytical separation of AZT and AZT-5′-P. Conditions: Waters μBondapak C_{18} column (30 cm × 4.6 mm I.D., 10 μm particle size); temperature, 26°C; pH, 5.0; methanol concentration, 15%; flow-rate, 1 ml/min.

surface is the pH–temperature retention surface (at 14% methanol) of dThd as shown in Fig. 7.

In the pH–methanol selectivity surface for ddAdo/dThd, the lowest α values are at the edge of pH 3.5 and there is a flat surface when the pH is higher than 4.5 (Fig. 8). In the pH–temperature selectivity surface plot of ddAdo/dThd, there is a maximum between pH 4.5 and 5.0 (Fig. 9), and the selectivity improves with increasing temperature.

The selectivity surface of dThd/ddIno is flat. However, the surface of ddIno/ddCyd at 13 and 13.5% methanol has a minimum at pH 4.5 and as the pH increases from 4.5 to 6.0, the selectivity increases.

These retention and selectivity surfaces show no interdependence of the experimental variables (*e.g.* pH, temperature and methanol content) in the ranges studied. However, if a certain analysis time or selectivity is desired, it can be achieved by selecting two or more sets of conditions from the surfaces. Using the surfaces, it was predicted that the best conditions for analyzing ddNs are a mobile phase of pH 5.0 and either 14% methanol and 40°C or 15% methanol and 30°C. A chromatogram of a separation of the ddNs using a mobile phase of pH 5.0 with 14% methanol at 40°C is shown in Fig. 3.

Discussion

From the guidelines we developed for the RPLC structure–retention relationships of purines, pyrimidines, their nucleosides and nucleotides [12], we predicted that the order of retention by groups would be deoxyribonucleotides prior to deoxyribonucleosides, and the ddNs would have the longest retention times. This order of retention was verified experimentally. Therefore, 13–15% methanol rather than the 7–9% used for the deoxyribonucleosides was needed to obtain k' values of 1–10 for the ddNs.

The experimental conditions necessary for good resolution of the ddNs differed from those of their deoxy analogues in several ways. With the deoxyribonucleosides the slopes in plots of ln k' *versus* percentage methanol (Fig. 2 in ref. 15) were steeper than the slopes of the dideoxy compounds; thus the percentage methanol had a larger effect on the separation factors of the deoxyribonucleosides than those of the ddNs. Within each group of compounds, the slopes of the four solutes were approximately the same; thus methanol concentration could be used to decrease the retention times without affecting the selectivity. Therefore, for the separation of a ddN from its parent deoxy compound, methanol can be a very effective parameter to manipulate the selectivity as the slopes of the methanol–capacity factor plots for the two groups of compounds differed.

In optimizing a separation, temperature can be used effectively to optimize selectivity, especially in the separation of purines frm pyrimidines (Fig. 1 in ref. 15) [17–19]. Although the slopes of all the pyrimidines are the same, these slopes are different from the slopes of the purines (ddIno and ddAdo) which also differ from each other. Therefore, temperature can be used to improve the separation of purines from pyrimidines as well as of ddIno from ddAdo. Since ddIno is a metabolite of ddAdo, this separation is an important one for pharmacokinetic studies of ddAdo. In addition, as can be seen from Figs. 2 and 3, an increase in temperature can be used not only to decrease the retention time but also to improve peak shape of the adenosine analogues. Although higher temperature also improved the resolution of thymidine from

2′-deoxyguanosine, it did not affect the excellent resolution of the three ddN peaks which were eluted first (Figs. 2 and 3).

The effects of pH are largely dependent on the structures of the solutes. The most pronounced effects of structure were observed with deoxyribonucleotides (Fig. 2 of ref. 14) and least pronounced with the dideoxyribonucleosides (Fig. 5). Thus, even through all the deoxyribonucleotides have the same charge on the phosphate group, the extent of influence of this charged moiety is dependent on the structure of the base and the presence or absence of a 3′-hydroxyl group on the ribose ring.

An important advantage of the use of retention surfaces is that if we wish to hold k' constant for isochronal analyses, we can find two or more sets of conditions which will give good separation of the ddNs.

Our work to date involved deoxy- and dideoxyribonucleosides in which there was no substitution on either the heterocyclic base or ribose rings. To test whether these retention and selectivity surfaces together with our structure–retention guidelines were valid in predicting the conditions that would give us good separation of substituted ddNs, we applied our work to the separation of AZT from AZT-5′-P. This separation is needed since AZT-5′-P is a precursor used in the synthesis of new AZT analogues. Based on retention surfaces and our structure–retention guidelines, we predicted that AZT would be eluted after dThd and before ddAdo in the RPLC separation of dideoxynucleosides using the conditions given in Fig. 3. All five compounds were well resolved. The AZT eluted at 14 min and was separated cleanly from both neighboring peaks, dThd and ddAdo. We also predicted that AZT-5′-P would be eluted quickly prior to Thd. This prediction was also verified experimentally.

Using the retention surfaces generated for the deoxyribonucleotides, deoxyribonucleosides and the ddNs, the conditions for analytical, method development and preparative separations of AZT from AZT-5′-P were chosen. Although the column length or diameter and/or particle size accounted for differences in actual retention times of AZT from AZT-5′-P [16], the relative retention times and orders were analogous.

From the pH–methanol and pH–temperature surfaces, it was indicated that a pH of 5.0 gave optimal selectivity. Since our ultmate objective was to optimize the conditions for a preparative separation, we chose ambient temperature as it was easier to work at room temperature with a preparative system. According to our surfaces, at pH 5.0, 14% methanol and a temperature of 30°C, good selectivity would be obtained. However, since room temperature was 26°C, the surfaces indicated that a higher concentration of methanol would compensate for the lower temperature, thus it was predicted that 15% methanol in an eluent of pH 5.0 would give the desired separation at 26°C. Experimentally these conditions gave excellent separations of the AZT and AZT-5′-P both on the analytical scale (Fig. 10) and preparative scale.

In conclusion, using our structure–retention guidelines together with retention and selectivity surfaces of the parent compounds, the ddNs, we found that we could optimize the conditions for the separations of analogues of these compounds as illustrated by the analytical and preparative separations of AZT and AZT-5′-P. We are applying these predictions to separations of other analogues of AZT from precursors and impurities in synthetic mixtures and will report on this work in the near future.

ACKNOWLEDGEMENTS

We thank Dr. Joseph Turcotte for AZT and AZT-5'-P and for his discussions with us on this work. We also acknowledge a Fulbright Fellowship to Israel to P.R.B.

REFERENCES

1 E. De Clercq, A. Van Aeroschot, P. Herewijn, M. Baba, R. Pauwels and J. Balzarini, *Nucleosides Nucleotides*, 8 (1989) 659.
2 H. Mitsuya and S. Broder, *Proc. Natl. Acad. Sci. U.S.A.*, 83 (1986) 1911.
3 J. Balzarini, R. Pauwels, P. Herdewijn, E. De Clercq, D. A. Cooney, G.-J. Kand, D. G. Johns and S. Broder, *Biochem. Biophys. Res. Commun.*, 140 (1986) 735.
4 M. Baba, R. Pauwels, P. Heredwijn, E. De Clercq, J. Desmyter and M. Vandeputte, *Biochem. Biophys. Res. Commun.*, 142 (1987) 128.
5 F. Sanger, S. Nicklen and A. R. Coulson, *Proc. Natl. Acad. Sci. U.S.A.*, 74 (1977) 5463.
6 H. Mitsuya and S. Broder, *AIDS Res. Hum. Retroviruses*, 4 (1988) 107.
7 R. Yarchoan, H. Mitsuya, R. V. Thomas, J. M. Pluda, N. R. Heartman, C. F. Perno, K. S. Marczyk, J. P. Allain, D. G. Johns and S. Broder, *Science (Washington, D.C.)*, 245 (1989) 412.
8 D. D. Richman, A. M. Fischl, M. H. Grieco, M. S. Gottlieb, P. A. Volberding, O. L. Laskin, J. M. Leedom, J. E. Groopman, D. Mildvan, M. S. Hirsch, G. G. Jackson, D. T. Durack, D. Phil, S. Nusinoff-Lehrman and The AZT Collaborative Working Group, *N. Engl. J. Med.*, 317 (1987) 192.
9 R. Yarchoan, H. Mitsuya and S. Broder, *Sci. Am.*, 259 (1988) 110.
10 P. R. Brown (Editor), *HPLC in Nucleic Acid Research*, Marcel Dekker, New York, 1984.
11 N.-I. Jang and P. R. Brown, in E. Heftmann (Editor), *Chromatographia*, Elsevier, Amsterdam, 5th ed., 1990, Ch. 17, in press.
12 P. R. Brown and E. Grushka, *Anal. Chem.*, 52 (1980) 1210.
13 S. Assenza and P. R. Brown, *J. Chromatogr.*, 282 (1983) 477.
14 E. Grushka, N.-I. Jang and P. R. Brown, *Anal. Chem.*, 60 (1988) 2104.
15 E. Grushka, N.-I. Jang and P. R. Brown, *J. Chromatogr.*, 485 (1989) 617.
16 C. W. Gehkre, K. C. Kuo and R. Zumwalt, *J. Chromatogr.*, 188 (1980) 129.
17 C. Yi, J. L. Fasching and P. R. Brown, *J. Chromatogr.*, 352 (1986) 221.
18 M. Mesbah and W. B. Whitman, *J. Chromatogr.*, 479 (1989) 279.
19 J. G. Turcotte, N.-I. Jang, P. E. Pivarnik, H. H. Singh, D. E. MacBride and P. R. Brown, *J. Chromatogr.*, 499 (1990) 56.

Journal of Chromatography, 550 (1991) 519–537
Elsevier Science Publishers B.V., Amsterdam

CHROMSYMP. 2155

Chromatographic separation and examination of carbohydrate and phenolic components of the non-tannin fraction of black wattle (*Acacia mearnsii*) bark extract

SHIRLEY C. CHURMS* and ALISTAIR M. STEPHEN
Department of Chemistry, University of Cape Town, Rondebosch, Cape Town 7700 (South Africa)

ABSTRACT

Commercial black wattle extract, from which most of the tannin had been removed with organic solvents (so being enriched with "non-tannins") and low-molecular-weight constituents by dialysis, was fractionated by chromatography on polyvinylpolypyrrolidone (PVPP). Steric-exclusion chromatography (SEC) then yielded a polysaccharide–protein conjugate, two polysaccharide fractions and two minor fractions containing both carbohydrate and phenolic components. Examination of each by SEC, gas–liquid chromatographic analysis of the carbohydrate and thin-layer chromatography of the fractions and derivatives thereof demonstrated the main structural features of the carbohydrate components and an association between carbohydrate and phenolic moieties in the minor fractions (as shown also for a dialysate). Chromatographic methods also afforded information on the behaviour of the non-dialysable "non-tannins" on fractionation by use of solvents, lead precipitation and the standard hide-powder technique.

INTRODUCTION

Extract from the bark of black wattle (*Acacia mearnsii*), which is widely used in the manufacture of leather, contains a high proportion of tannins, which are concentrated by extraction into acetone [1]. This tannin fraction has been shown [2–4] to consist of a mixture of condensed tannins having molecular structures based on *ar*-hydroxylated flavan-3,4-diol nuclei; a molecular weight range from 350 to *ca.* 3000 has been reported [5]. Some phenolic components of lower molecular weight, such as the phloroglucinol derivative fisetin, have also been isolated [6].

The acetone-insoluble fraction of wattle bark extract has been found [2,7] to contain sugars, mainly sucrose, with traces of glucose and fructose, and the cyclitol (+)-pinitol, which are removed, with some tannin, by further fractionation with 95% ethanol and by dialysis. Gummy polysaccharides of high molecular weight constitute a major component of the material remaining after such treatment, and protein is present in significant proportions, but the so-called "non-tannin" fraction also contains phenolic components [8] in high proportion (*ca.* 40%). The polysaccharides are known to associate strongly with tannins, owing to occlusion and/or adsorptive effects [6]. Similar strong interaction of starch with condensed tannins in the hot-water

0021-9673/91/$03.50

extract from the bark of Ponderosa pine has been reported [9]. No evidence has been obtained for covalent bonding between carbohydrate and tannin in these cases, although a polymer believed to be a covalently bonded flavologlycan, flavolan chains of various degrees of polymerization being linked to a galacturonoglycan chain of high molecular weight, has been isolated from mangrove leaves [10].

The incomplete separation of carbohydrate and tannin components of wattle bark extract, due to this strong interaction, presents problems in some of the commercial applications of this material. The presence of carbohydrate is beneficial in leather manufacture, tempering the astringency of the phenolic tanning solution, but is deleterious in the preparation of adhesives formed by condensation of the phenolic components with, for example, methanal. It is, therefore, of industrial interest to examine more closely the association of carbohydrate and tannin in fractions derived from wattle bark extract.

Adsorbents of the polyamide type have proved invaluable in both column [10,11] and planar [11,12] chromatographic separations of tannins and highly hydroxylated flavonoids, and paper chromatography [3,13] and steric-exclusion chromatography (SEC) are useful in fractionating both condensed tannins [11] and carbohydrates [14]. This paper describes the use of these methods, individually and in combination, in the isolation of the components of the "non-tannin" fraction of wattle bark extract, and the investigation of these components and of fractions obtained by classical methods of purification and analysis.

EXPERIMENTAL

Chromatographic materials and methods

Preparative-scale fractionation of the non-tannin fraction of the wattle bark extract was performed by chromatography on a glass column (22 cm × 3.5 cm I.D.) packed with polyvinylpolypyrrolidone (PVPP) (Sigma, St. Louis, MO, USA). Elution with water until no further carbohydrate was detected (phenol–sulphuric acid colorimetric assay [15]) in the column effluent was followed by elution with redistilled formamide and then with 8 *M* aqueous urea [10]. The portion eluted with water was further fractionated by preparative SEC on a glass column (84 cm × 3.3 cm I.D.) packed with the agarose gel Sepharose 4B (Pharmacia, Uppsala, Sweden), which was eluted with water at a flow-rate of 40 ml/h. The same column, eluted with 0.5 *M* pyridinium acetate buffer solution (pH 5.0) at a flow-rate of 50 ml/h, was used to purify the fraction obtained from the PVPP column by elution with formamide.

Analytical SEC was performed with 1 *M* sodium chloride as the eluent in all instances. Three different columns were used: (i) acrylic plastic, 60 cm × 9 mm I.D. (Pharmacia column K 9/60), packed with Sepharose 4B, eluted at 15 ml/h; (ii) borosilicate glass, 90 cm × 15 mm I.D. (Pharmacia column K 15/90), packed with Sephacryl S-300 Superfine (Pharmacia; allyldextran cross-linked with N,N′-methylenebisacrylamide), eluted at 25–30 ml/h; and (iii) glass, 50 cm × 15 mm I.D., packed with Bio-Gel P-10, 100–200 mesh (Bio-Rad Labs., Richmond, CA, USA; polyacrylamide cross-linked with N,N′-methylenebisacrylamide), eluted at 20 ml/h. Fractions (1–1.5 ml) were monitored for protein or tannin by UV spectrophotometry (220 or 280 nm) and for carbohydrate by the phenol–sulphuric acid assay [15]. Estimates of relative, average molecular weights ($\bar{M}_w$) of carbohydrate components from SEC elution volumes were based on calibrations with characterized dextran fractions (Pharmacia).

Thin-layer chromatography (TLC) was performed on plastic strips (Polygram, 20 cm × 5 cm) precoated with Polyamide-6 UV_{254} (0.1-mm layer) (Macherey-Nagel, Düren, Germany). The strips, cut to lengths of 8–10 cm, were developed with formamide. Phenolic components were detected on these plates by their UV absorbance. Spray reagents used for detection were (a) freshly mixed iron(III) chloride–potassium hexacyanoferrate(III) (1:1, v/v), both 0.1 *M*; (b) 3 *M* sulphuric acid, followed by heating at 110°C for 5 min.

For TLC of acetylated derivatives, Kieselguhr plates were used, prepared by coating glass plates (10 cm × 5 cm) with Kieselguhr G (particle diameter 10 μm; E. Merck, Darmstadt, Germany), layer thickness *ca.* 0.5 mm. The plates were developed with chloroform–acetic acid (1:1, v/v) and the detection reagent was *p*-anisaldehyde–sulphuric acid–ethanol (1:1:18, v/v).

Paper chromatography of hydrolysates was carried out by the descending method on Whatman No. 1 paper, with the following solvent systems (all v/v/v): (A) ethyl acetate–pyridine–water (8:2:1); (B) 1-butanol–acetic acid–water (2:1:1); and (C) upper phase of 1-butanol–ethanol–water (4:1:5) (for methylated sugars). Spots were revealed by spraying with 3% (w/v) *p*-anisidinium chloride in aqueous 1-butanol, or ammoniacal silver nitrate (5%, w/v), followed by heating at 110°C for 5–10 min.

Gas–liquid chromatography (GLC) of sugars in hydrolysates, as the alditol acetates [16], was performed on a Carlo Erba 4200 or (for capillary columns only) a Carlo Erba GC 6000 Vega Series 2 instrument, each with a flame ionization detector coupled to a Spectra-Physics SP4290 integrator. Another Carlo Erba 4200 gas chromatograph was coupled through a jet separator to a VG Micromass 16F mass spectrometer. The columns used were (1) a glass column, 2 m × 3 mm I.D., packed with 3% OV-225 on Chromosorb W HP (80–100 mesh); (2) a glass capillary (surface-coated open tubular, SCOT) column, 30 m × 0.35 mm I.D., coated with OV-225; and (3) a fused-silica capillary column, 30 m × 0.32 mm I.D., with OV-225 (0.25 μm thickness) as a bonded phase (Durabond DB-225; J & W Scientific, Folsom, CA, USA). The carrier gas was helium in all instances.

Peracetylated alditols were analysed on column 1, isothermally at 210°C, and on column 2, with cold on-column injection and temperature programming from 100 to 250°C at 4°C/min. Partially methylated alditol acetates were analysed on column 1, isothermally at 175°C and column 3 at 195°C; for GLC–mass spectrometry (MS) column 2, with temperature programming from 100 to 230°C at 5°C/min, or column 3, isothermally at 210°C, were used. For quantitative analyses of partially methylated alditol acetates, the molar response factors calculated by Sweet *et al.* [17], were applied to the peak areas obtained in GLC. Empirically determined molar response factors were used in GLC analysis of mixtures of peracetylated alditols, to which *myo*-inositol was added as an internal standard.

Analytical methods

GLC of the alditol acetates derived from carbohydrate components was preceded by hydrolysis in 2 *M* trifluoroacetic acid at 100°C, under nitrogen in a sealed tube, for 6 h for neutral carbohydrates and for 18 h for those containing acid-resistant aldobiouronic acid linkages and for methylated derivatives. In order to compensate for losses due to decomposition of the free sugars under the hydrolytic conditions used (pentoses being especially labile [18,19]), correction factors [20], obtained by

analysis of standard mixtures of sugars heated under the same conditions prior to derivatization, were applied in the GLC analyses of sugar mixtures in hydrolysates. For samples containing tannin these factors were not valid, as destruction of the free sugars was greatly increased. An attempt was made to apply appropriate response factors, obtained by analysis of standard sugar mixtures to which free wattle bark tannin was added, in a proportion similar to that in the sample, before heating under the conditions used in acid hydrolysis, but the reproducibility of these factors was poor. Precise quantitative analysis of sugar ratios in this manner was, therefore, impossible for fractions containing both carbohydrate and tannin.

In methylation analysis of carbohydrate components samples were methylated by the Hakomori procedure [21], as modified by Phillips and Fraser [22], followed by several treatments by Purdie and Irvine's method [23]. Those containing uronic acid, which was determined spectrophotometrically on the polysaccharide by Blumenkrantz and Asboe-Hansen's method [24], were further examined by carboxylate reduction with lithium aluminium deuteride [25] and by base-catalysed β-elimination [26] of portions of the per-O-methylated derivatives. All methylated samples were hydrolysed as described above, prior to GLC–MS of the derived alditol acetates. Use of 2,3,4-tri-O-methylgalactose as an internal standard showed a very low recovery of partially methylated alditol acetates in the presence of tannin, so that the precision of methylation analysis must also be adversely affected for samples containing tannin together with carbohydrate.

Tannin was determined by UV spectrophotometry, at 280 nm as recommended by Roux [27] or, in the absence of protein, at 220 nm. The latter wavelength was preferred in monitoring eluates from columns, owing to the greater sensitivity resulting from the higher molar absorptivity. The sensitive, specific spectrophotometric method using *p*-nitobenzenediazonium tetrafluoroborate (Brentamine Fast Red 2G; Sigma), which has been applied successfully in the determination of polyphenols in seaweeds [28,29], was also used in the analysis of samples of low tannin content ($\leqslant 10\%$ by weight). In all of these determinations, a sample of wattle bark tannin isolated from the acetone-soluble fraction of the extract (see Fig. 1) served as a calibrant. The same sample was used to establish correction curves applied to determinations of carbohydrate by the phenol–sulphuric acid method in the presence of tannin, which interferes, giving an appreciable colour response with the reagents [30]. This response was found to be lower in 1 *M* sodium chloride than in water.

The nitrogen content of some fractions obtained from the wattle bark extract indicated the presence of protein in significant proportions. A sample of such a fraction (see below) was hydrolysed under the conditions (6 *M* hydrochloric acid, 110°C, 24 h) required for cleavage of peptide linkages and the hydrolysate was injected into an amino acid analyser (Model 420; Waters Assoc., Milford, MA, USA). Hydroxyproline, an important amino acid in many glycosylated proteins from plant sources [31,32], was determined independently by the Leach spectrophotometric method [33].

Isolation of "non-tannin" fraction from wattle bark extract

The sample of commercial wattle bark extract (donated by Wattle Industry Centre, Pietermaritzburg, South Africa) that was used in this study had been prepared by hot-water extraction of stripped bark from *Acacia mearnsii*. Isolation of carbohydrate-rich material was carried out at room temperature by steeping the

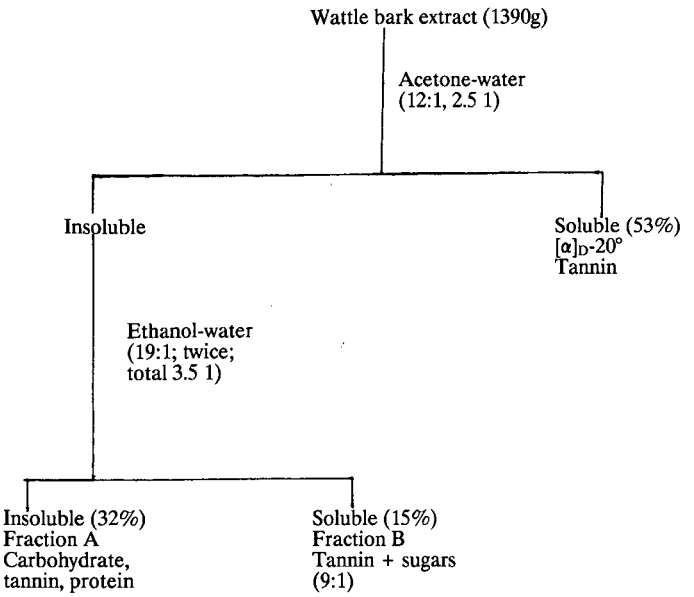

Fig. 1. Solvent fractionation of wattle bark extract.

brown, glassy material in acetone (containing some water), recovering the insoluble fraction by filtration and repeating the extraction twice with 95% ethanol. The yields and composition of the various fractions are shown in Fig. 1. The residue, fraction A, was dried *in vacuo* at 40°C and a portion was hydrolysed for GLC analysis of the sugar constituents (Table I). The ethanol-soluble fraction, B, was found (paper chromatography) to contain the sugars sucrose, glucose and fructose, together with tannin.

Dialysis of a sample (20 g) of A in Spectra/Por 1 tubing (Spectrum Medical Industries, Los Angeles, CA, USA; 32 mm diameter, molecular-weight cut-off 6000–8000) against distilled water (2 l, changed twice) for 6 days resulted in passage of a high proportion (70% by weight) into the pooled dialysate, D1. The tannin content of the retentate R1 was, however, not greatly diminished (see Table I). A larger sample of A was dialysed in preparative tubing (120 mm diameter, molecular-weight cut-off 12 000–14 000) in three stages (Fig. 2), yielding retentate R2 and final dialysate D2, which was not pooled with those removed at earlier stages of dialysis. An appreciable proportion (14% by weight) of the sample was irreversibly adsorbed by the dialysis membrane, the porosity of which was decreased by interaction with the tannin. The sugar ratios in D1, D2, R1 and R2 were determined (Table I), and the retentates R1 and R2 were used in subsequent experiments as "non-tannin" fractions of the wattle bark extract.

Fractionation of R1 on PVPP and agarose columns

The bulk of R1 was fractionated by chromatography on PVPP followed by sub-fractionation on Sepharose 4B, as described above. The yields and composition

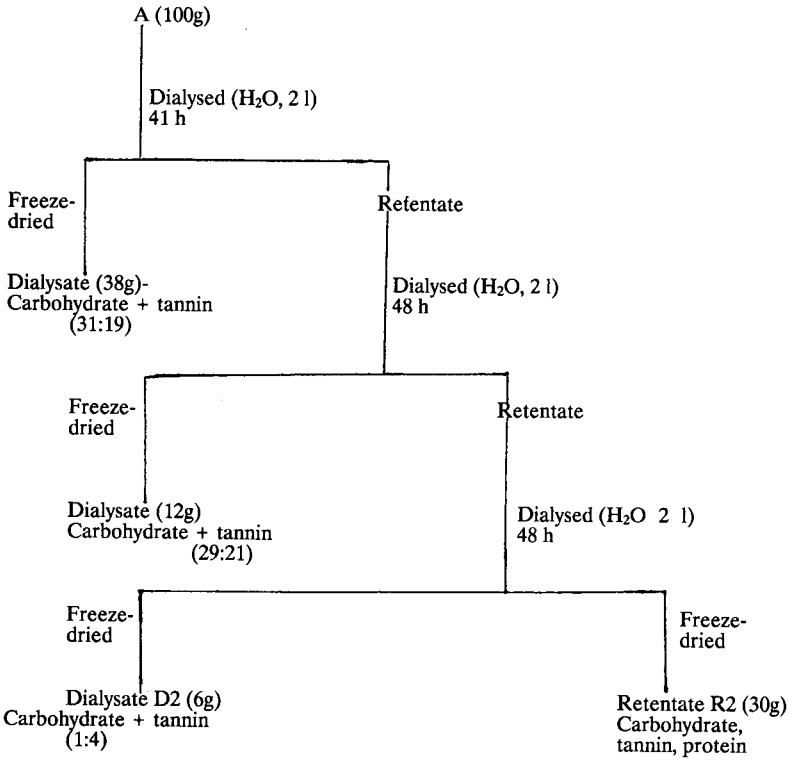

Fig. 2. Preparative-scale dialysis of fraction A.

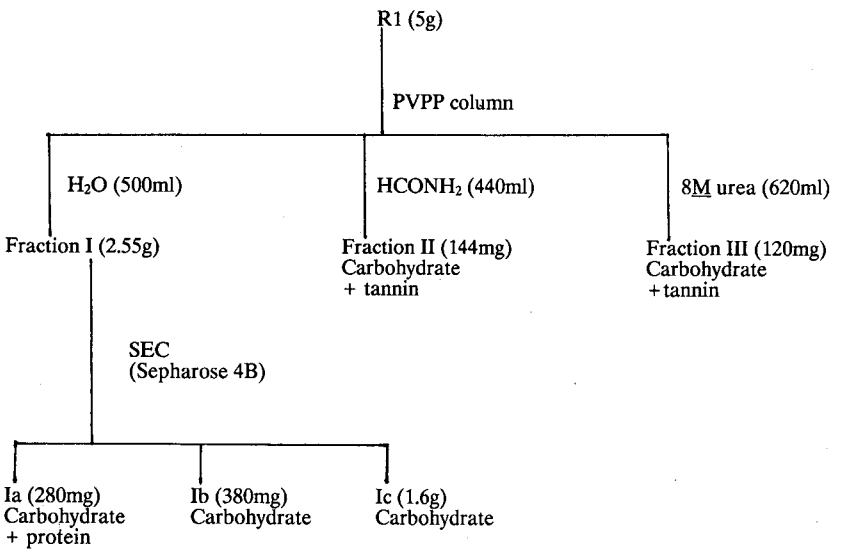

Fig. 3. Fractionation of R1 on PVPP and agarose columns.

of the fractions obtained are shown in Fig. 3. A high proportion (over 40%) of R1, including nearly all of the tannin, was retained on the PVPP column. Fractions Ia, Ib and Ic were recovered by freeze-drying the aqueous eluate from the agarose column, after pooling of fractions corresponding to different zones in the chromatogram (see Fig. 4). The formamide eluate from the PVPP column was concentrated by vacuum distillation (b.p. 60°C at 1 mmHg) and the remaining solvent removed by continuous extraction, first with diethyl ether and then with ethyl acetate; the residue was purified by SEC as described and the eluate freeze-dried to yield fraction II. The aqueous urea eluate, after concentration by freeze-drying, was fractionated with ethanol (2 volumes), which gave a brown precipitate that was dissolved in water and freeze-dried, yielding fraction III.

All fractions were examined by GLC analysis of the sugar components (Table I), analytical SEC, methylation analysis and TLC. Portions were acetylated, fractions Ia–Ic by the method of Carson and Maclay [34], with formamide as a dispersing agent, and fractions II and III with acetic anhydride–sodium acetate, for TLC on Kieselguhr. Polyamide plates were used in TLC of the tannin-containing fractions II and III, and products of partial acid hydrolysis (2 *M* trifluoroacetic acid, 100°C, 1 h) of these and of de-O-acetylation (sodium methoxide, 20°C, 16 h) of their acetylated derivatives. A portion of the proteinaceous fraction Ia was analysed for amino acids as described.

Fractionation of D2 and R2 by precipitation with lead

A portion (3 g) of freeze-dried dialysate D2, dissolved in water (50 ml), was treated at pH 5.0 with 1 *M* lead acetate solution until precipitation was complete. After centrifugation, lead was removed from both the centrifugate and precipitate by reaction with 1 *M* oxalic acid (neutralized by addition of $NaHCO_3$) and the solutions thus obtained were freeze-dried to give fractions C (centrifugate; 1.2 g) and P (precipitate; 1.6 g). The latter consisted almost entirely of tannin, with only a trace of carbohydrate, but C contained carbohydrate and tannin, in a mass ration (9:11) comparable with that in fractions II and III from the PVPP column (Table I). Fraction C was examined by GLC, SEC, TLC and methylation analysis as described for II and III.

A sample (10 g) of R2, dissolved in water (200 ml), was similarly fractionated by precipitation with 1 *M* lead acetate solution (30 ml), the uptake of Pb^{2+} being monitored by back-titration of the excess with standard 0.05 *M* EDTA, with xylenol orange as indicator. After centrifugation and removal of Pb^{2+} from the centrifugate and precipitate by leaching with oxalate as described, the two fractions were purified by addition of 1 *M* barium acetate to remove excess of oxalate, treatment with H^+-form cation-exchange resin to remove Ba^{2+} and freeze-drying. The precipitated fraction R2 P (80% of R2) contained 35% of carbohydrate in addition to tannin, whereas the centrifugate fraction R2 C contained only 4% of phenolics, consisting almost entirely of carbohydrate; protein was totally removed from R2 by this treatment. The two fractions were examined by SEC and TLC, and the distribution of neutral and acidic sugars in each was investigated by paper chromatography of hydrolysates.

The behaviour of R2 on treatment with lead was compared, by model experiments conducted under the same conditions, with that of pure tannin, L-arabinose, an arabinan isolated from apple juice [35], a neutral arabinogalactan of low molecular

weight ($\bar{M}_w$ 3600) obtained from the gum of *Acacia difformis* by Smith degradation [36] and the acidic polysaccharide isolated from the gum exudate of *A. mearnsii* [37,38].

Fractionation of R2 with aqueous acetone

A portion (5 g) of R2 was dissolved in water and acetone (3 volumes) was added, precipitating about 50% of the sample. The acetone-insoluble and acetone-soluble fractions, recovered by freeze-drying, were examined by SEC and TLC and hydrolysates by paper chromatography. The phenolic content of the acetone-insoluble fraction (R2 I) was below 5%, the main component being polysaccharide, with some protein. The acetone-soluble portion (R2 S) was sub-fractionated by further treatment with aqueous acetone, which gave another insoluble fraction (54% of R2 S), containing 13% of tannin, and a soluble fraction (58% tannin). The former gave no precipitate with lead acetate, but most of the latter was precipitated.

Fractionation of R2 and A by adsorption on hide powder

Samples of R2 and A were shaken in the conventional way with hide powder (donated by the Leather Industries Research Institute, Grahamstown, South Africa), which had been lightly chrome-tanned [39]. The "non-tannins", recovered by freeze-drying the supernatant solution, constituted 53% by weight of R2, 64% of A. The non-tannins from A gave no precipitate with Pb^{2+}, but a small gelatinous, colourless precipitate was formed on addition of lead acetate to R2 non-tannins. Both reacted positively with the iron(III)–hexacyanoferrate(III) reagent and spectrophotometric assay [28,29] indicated the presence of 4–5% of phenolics in each. The molecular-weight distribution of the carbohydrate in these fractions was determined by SEC on Sephacryl S-300.

Tests with gelatin reagent and surfactant

A solution containing gelatin (1%, w/v) in 2 *M* sodium chloride, in an acetate buffer (pH 4.7), was added dropwise to solutions (0.1%, w/v) of each of the various fractions obtained from wattle bark extract. Dense precipitates were given immediately by the pure tannin, A, R1, R2, D1, D2 and R2 S; precipitation occurred more slowly with II, III, C and R2 P, and with R2 C only a slight turbidity was observed. As expected, there was no reaction with the tannin-free fractions Ia, Ib and Ic, and there was none with the non-tannins from hide-powder fractionation of A and R2.

The inhibition of interaction between tannin and protein by surfactants such as cetyltrimethylammonium bromide (Cetavlon) has been reported [40,41]. The presence of cetavlon (1%, w/v) was found to suppress precipitation of tannin, R2 S, II and C by the gelatin reagent. A sample of II that had been left for 24 h in the Cetavlon solution was re-examined by TLC, to ascertain whether association in the tannin–carbohydrate conjugate was affected by competitive interaction of tannin with the surfactant.

RESULTS AND DISCUSSION

Isolation and chromatographic fractionation of R1

It is evident (Table I) that despite repeated solvent fractionation (Fig. 1) and

TABLE I

ANALYTICAL DATA FOR FRACTIONS FROM WATTLE BARK EXTRACT

Fraction	$[\alpha]_D$ (°)	Composition (%, w/w)			Sugar proportions[b] (mol%)						
		Carbo hydrate	Tannin	Protein[a]	Uronic acid	Ara	Glc	Gal	Rha	Xyl	Man
A	+10	54	41	5	7	46	28	7	4	4	4
R1	+14	56	35	9	8	47	21	7	10	3	4
R2	+15	55	33	12	10	50	13	12	9	3	3
D1	0	58	42	–	–	39	39	9	2	5	6
D2	−7	20	80	–	–	44	36	5	7	3	5
Ia	+51	65	–	35	15	50	3	20	10	1	1
Ib	+84	100	–	–	15	36	16	16	12	tr	5
Ic	+22	100	–	–	18	42	15	7	10	4	4
II	+3	40	60	–	–	76	13	5	2	2	2
III	−2	46	54	–	–	26	51	5	11	2	5
C		45	55	–	–	25	52	5	7	4	7

[a] Calculated from nitrogen content.

[b] For fractions containing tannin, ratios of neutral sugars serve only to indicate the distribution pattern in the carbohydrate component, as replicate analysis showed standard deviations of the order of 20–60%, owing to variable destruction of sugars.

prolonged dialysis (Fig. 2), an appreciable proportion of tannin persists in the so-called non-tannin fraction from wattle bark extract. Dialysis had a minimal effect on the carbohydrate: tannin ratio of the retentates, although it should be noted that adsorption of phenolic material by the cellulose membrane, which was considerably darkened and hardened during the dialysis process, must have influenced progressively its permeability to the various components of the extract. Carbohydrate and phenolic components were found in both retentates and dialysates, only protein being totally retained. The material recovered from the dialysates consisted of carbohydrate of relatively low molecular weight ($\bar{M}_w \leqslant 30\,000$), co-eluted with some phenolic components at the total (maximum) volume, V_t, in SEC on the analytical Sepharose 4B column. Much of the phenolic fraction was retarded by adsorptive interaction with the gel matrix and was eluted after V_t, with pronounced tailing; some was irreversibly adsorbed. This behaviour is illustrated in Fig. 4 for the phenolic components of retentate R1. There was some overlap with the major carbohydrate component, $\bar{M}_w$ 70 000, which was, however, well separated from a minor fraction containing polysaccharide of high molecular weight together with protein, eluted at the void volume, V_0, of the column.

The polysaccharide fraction of R1 was separated from the phenolic material by elution with water from the PVPP column, which retained all the phenolic components under these conditions (Fig. 3). The fraction (I) recovered from the aqueous eluate consisted mainly of carbohydrate with some protein (6% by weight). On sub-

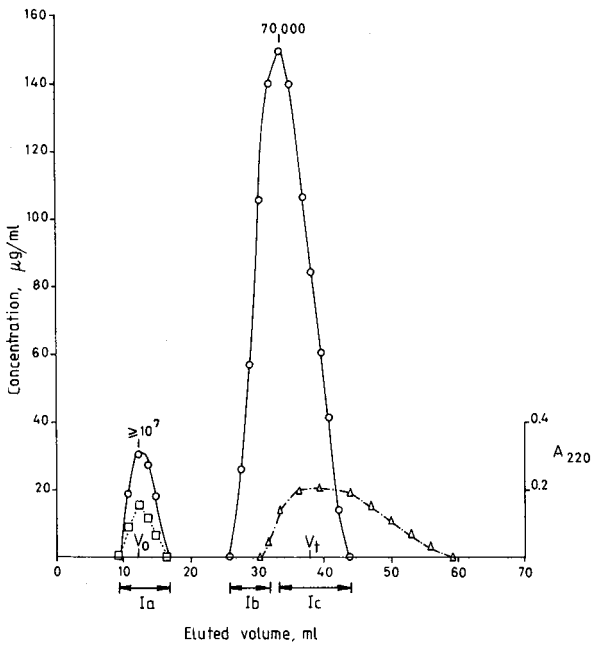

Fig. 4. Analytical SEC of retentate R1 on Sepharose 4B. Conditions as given in the text. Absorbance at 220 nm (A_{220}) plotted for protein only; concentrations plotted for other components. Zones from which fractions Ia, Ib and Ic were isolated on preparative SEC are indicated. ○ = Carbohydrate; △ = tannin; □ = protein.

fractionation on the preparative column of Sepharose 4B, three polysaccharide fractions, Ia–Ic, were isolated. All of the protein appeared in fraction Ia, together with the polysaccharide ($\bar{M}_w \geqslant 10^7$) eluted at V_0 from the analytical column (Fig. 4). The major polysaccharide component was resolved on the larger column into discrete fractions, Ib ($\bar{M}_w$ 150 000) and Ic ($\bar{M}_w$ 50 000). The sugar constituents of Ia–Ic (Table I) were, in general, typical of acidic arabinogalactans from plant sources [42], and their composition differed from that of the gum exudate of *Acacia mearnsii* [37,38] only in the presence of glucosyl residues in significant proportion in Ib and Ic.

Polysaccharides Ia–Ic also differed from the gum polysaccharide of *A. mearnsii* in their positive specific rotations (Table I), that of the gum being negative ($[\alpha]_D - 33°$) [38]. The modes of glycosidic linkage in Ia–Ic, determined by methylation analysis, were generally similar in all three and constituted another point of resemblance between these and the gum polysaccharide. Terminal arabinofuranosyl (Ara*f*), rhamnopyranosyl (Rha*p*) and galactopyranosyl (Gal*p*) residues, → 5)-linked Ara*f*, and → 3)-, → 4)- and → 6)-linked Gal*p* were structural features common to bark polysaccharides and gum, though some Rha*p* was present as → 2,4)-linked branch-points, which was unusual. The glucopyranosyl residues (Glc*p*) were → 3)- and → 4)-linked, a characteristic of cell-wall polysaccharides, not gums [42]. Fraction Ic differed from the others in containing terminal Glc*p* and → 3)-linked Ara*f* in significant proportions.

GLC–MS after reduction of the carboxylate ester groups in methylated Ia–Ic with lithium aluminium deuteride [25] showed, from the presence in the hydrolysates of 2,3-di-O-methylglucose and 2-O-methylglucose deuterated at C-6, that the glucuronic acid (GlcA) residues occurred both as → 4)-linked chain units and as → 3,4)-linked branch-points, in equal proportions. There was no evidence for terminal GlcA, found in the gum [43,44]. A significant increase in the proportion of 2,3,4,6-tetra-O-methylgalactose, with concomitant disappearance of 2,3,4- and 2,3,6-tri-O-methylgalactose, in the hydrolysate after portions of methylated Ia–Ic had been submitted to base-catalysed β-elimination [26] showed the attachment of GlcA to Gal at O-6 or O-4. The former mode of linkage was also indicated by the detection of the aldobiouronic acid GlcAβ1–6Gal on paper chromatography (solvent B) of the products of partial acid hydrolysis (0.5 *M* trifluoroacetic acid, 100°C, 6 h) of Ia–Ic. All Rha was lost by base-catalysed β-elimination of methylated Ia–Ic, which suggested the location of these residues immediately exterior to → 4)-linked GlcA, as in many *Acacia* gum polysaccharides [26,42]. There was also loss of Glc in this reaction, but this may have been due to alkaline degradation ("peeling") [45] from the reducing end of a glucan component, rather than an indication of the location of Glc exterior to GlcA in the acidic polysaccharides.

The main amino acid constituents of the protein component of Ia were aspartic acid (15% of total amino acids), glutamic acid (12%), serine (11%), glycine (10%) and alanine (10%). Hydroxyproline was present in very low proportion (< 1%). In this respect, therefore, the protein in Ia resembles that associated with the seed galactomannans guar and locust bean gum [46], rather than that in some *Acacia* gums [18,47].

Elution of the PVPP column with formamide and then with 8 *M* aqueous urea yielded two further fractions, II and III, in low yields (each 2–3% of starting material; see Fig. 3). These contained both carbohydrate and phenolic components, the latter

preponderating. Carbohydrate and phenolic components were co-eluted at V_t on SEC on the analytical Sepharose 4B column. When the Sephacryl S-300 column was used, II and III were eluted at K_{av} 0.90 and 0.87, respectively; in both instances carbohydrate and tannin were co-eluted, each giving a single, sharp peak, and there was no broad, tailing peak extending beyond V_t, as given by free tannin. This suggested very strong association, perhaps covalent linkage, between carbohydrate and phenolic moieties in II and III. The carbohydrate was evidently of relatively low molecular weight, but it was impossible to estimate actual values as the relationship between V_e and $\bar{M}_w$ must obviously be different from that for dextrans, used to calibrate the column, and the retarding effect of the phenolic component will be superimposed on the normal SEC mechanism.

The carbohydrate components of II and III differed from Ia–Ic in containing no uronic acid. Arabinose and glucose were the main neutral sugar constituents, Ara preponderating in II, whereas Glc appeared to be the major constituent of III (but analyses of III were particularly seriously affected by variable destruction of sugars when heated in the presence of tannin and therefore must be interpreted with caution). Methylation analysis showed the same glycosidic linkages as were found in Ia–Ic, with terminal and → 5)-linked Ara*f*, → 3) and → 4)-linked Glc*p* preponderant. A high proportion of terminal groups, without a corresponding number of sugar residues present as branch points, suggests attachment of short chains of sugar residues, or single units, to non-carbohydrate components and may thus be indicative of covalent linkage between carbohydrate and phenolic moieties.

Further evidence for very strong association between carbohydrate and tannin in II and III was afforded from their behaviour on TLC, on both Kieselguhr and polyamide plates. Acetylated samples moved as discrete spots ($R_F \approx 0.75$) on the Kieselguhr plates, in contrast to acetylated Ib, Ic and tannin, which streaked (methylated Ia remained at the origin). Acetylated tannin gave a characteristic blood-red colour with the anisaldehyde–sulphuric acid spray reagent, but no such colour was produced by acetylated II or III, which turned dark grey with this reagent, as did the acetylated polysaccharide fractions. On the polyamide plates free tannin streaked from the origin to $R_F \approx 0.6$, but II and III moved as compact spots ($R_F \approx 0.9$). With the Fe^{3+}–$Fe(CN)_6^{3-}$ spray reagent (a) the tannin streak gave the characteristic Prussian blue colour, whereas the spots due to II and III did not react unless the plate was subsequently sprayed with 3 *M* sulphuric acid (b) and heated as described. The blue coloration produced under these conditions was confined to the area of the spots (as indicated by examination under UV), suggesting release of free tannin *in situ* by the action of the acid spray. Spraying with b alone turned the spots brown, and the tannin streak pink. On polyamide TLC of samples of II and III that had been submitted to partial acid hydrolysis the streaking shown by free tannin was observed and the Prussian blue coloration was produced by spray reagent a. The acid spray gave a corresponding pink streak, together with a brown streak closer to the solvent front, which was ascribed to free carbohydrate. The same behaviour was shown on similar TLC of the products of de-O-acetylation of acetylated II and III in base. These results indicate production of free tannin and carbohydrate from II and III only after cleavage of bonds (of whatever type) by treatment with acid or base, and supplement the evidence from SEC for complexation between carbohydrate and phenolic moieties in these minor fractions from R1.

Fractionation by precipitation with lead

The precipitated fraction, P, obtained on treatment of dialysate D2 with lead acetate behaved as free tannin on polyamide TLC, whereas C, the fraction isolated from the centrifugate, behaved as described for fractions II and III, only the products of partial acid hydrolysis, and of de-O-acetylation of acetylated C, showing the presence of free tannin. The carbohydrate portion of C, which was co-eluted with the phenolic component at V_t on SEC on the analytical Sepharose 4B column, appeared to resemble fraction III with respect to sugar ratios (Table I), but the reproducibility of the analytical results was as poor as that for III. Methylation analyses showed the distribution of glycosidic linkages found in II and III.

In contrast to the behaviour of D2, treatment of R2 with lead acetate resulted in the coprecipitation of a high proportion of carbohydrate (over 50% of the total carbohydrate) with tannin, which was also precipitated to a greater extent than that in D2. The uptake of Pb^{2+} by R2 corresponded to 1 mol per 880 g; for pure tannin the uptake of Pb^{2+} under similar conditions was 1 mol per 520 g. The precipitated fraction, R2 P, $[\alpha]_D$ +45°, was found, by paper chromatography (solvents A and B) of the hydrolysate, to contain glucuronic acid in appreciable proportion, together with the neutral sugar constituents of R2, whereas the centrifugate fraction, R2 C, which had $[\alpha]_D$ −36°, consisted almost entirely of the neutral sugars, with only a trace of glucuronic acid.

SEC of R2 P on Sepharose 4B gave a peak for carbohydrate of $\bar{M}_w$ 70 000 but most of the sample was co-eluted with tannin at V_t. Use of the Bio-Gel P-10 column resulted in the co-elution of tannin and carbohydrate, mainly at V_0, although in a model experiment tannin that had not been treated with lead was eluted from the column, as expected, in a broad peak at and after V_t. Owing to adsorptive interaction with the polysaccharide gel matrix, the recovery of tannin was low (*ca.* 20%) in the model experiment, but over 80% of that in the lead precipitate was recovered from the column. The best resolution of the carbohydrate components was achieved by SEC on Sephacryl S-300 (Fig. 5A), but again there was overlap with the tannin, which was eluted (recovery *ca.* 70%), in a sharp peak at K_{av} 0.54, within the range at which carbohydrate emerged (K_{av} 0.29–0.84). In a model experiment tannin not subjected to lead precipitation was eluted in a broad peak in the region of V_t, with low recovery from this column as from Bio-Gel P-10. These results indicate that tannin removed from lead precipitates by leaching with oxalic acid undergoes self-condensation or other chemical change, reducing its affinity for polyacrylamide and allyldextran gels.

No such effect was observed on SEC of R2 C on Sephacryl S-300 (Fig. 5B), the phenolic components (which may not be tannins) being eluted in the region of V_t, with only slight overlap with the carbohydrate components of lowest molecular weight. The carbohydrate in this fraction had a broader molecular weight distribution than that in R2 P (Fig. 5A), which suggests a certain optimum size range for precipitation with tannin.

Fractions R2 P and R2 C behaved similarly on polyamide TLC. The phenolic components were detected as streaks, turning blue when sprayed with reagent a; this was very faint for R2 C. Further spraying with acidic reagent b, after reagent a, had no effect (*cf.*, II and III).

In model experiments designed to investigate the factors governing coprecipitation of carbohydrate with tannin on treatment with lead, it was found that arabi-

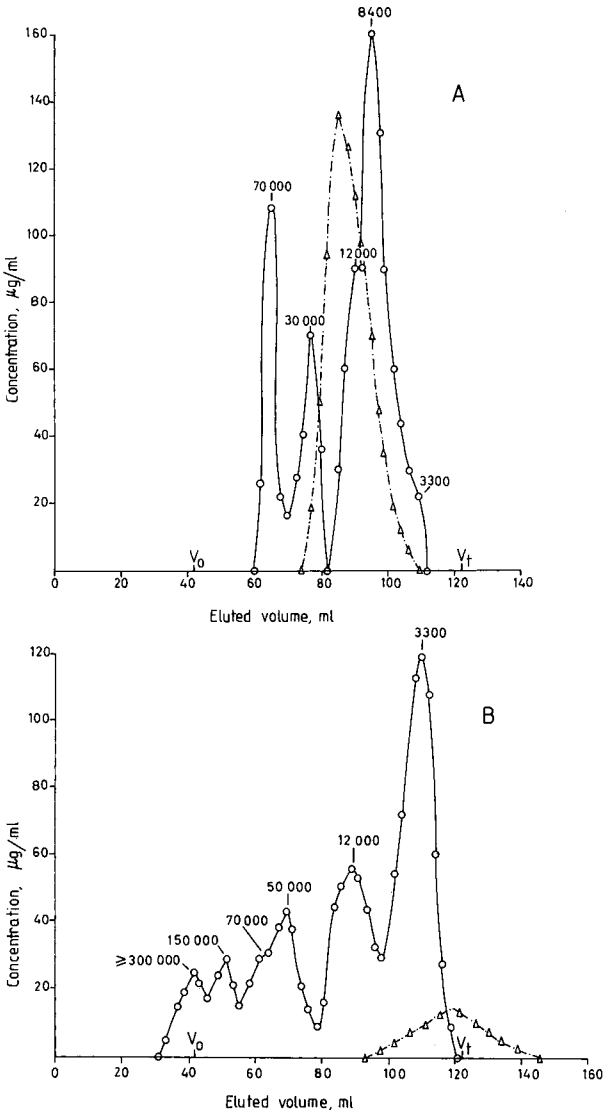

Fig. 5. SEC on Sephacryl S-300 of (A) lead-precipitated fraction (R2 P) of R2 and (B) fraction R2 C from centrifugate. Conditions as given in the text. (A) ○ = Carbohydrate; △ = tannin. (B) ○ = Carbohydrate; △ = phenolics.

nose, the apple juice arabinan, and the Smith-degraded arabinogalactan from *Acacia differmis* gum did not coprecipitate. However, the acidic arabinogalactan from *A. mearnsii* gum, which was 10% precipitated by lead alone, was 90% precipitated in the presence of an equal weight of tannin. The gum contains components in the molecular-weight range of the carbohydrate fraction of R2, whereas the other carbohydrates tested were of much lower molecular weight (below 10 000). The fact that the

carbohydrate in dialysate D2, which was of low molecular weight, did not coprecipitate is also significant here. Further, D2 and the other carbohydrates that did not coprecipitate contained no uronic acid, but the *A. mearnsii* gum polysaccharide is similar to R2 with respect to uronic acid content. It has been noted that the uronic acid in R2 was concentrated into R2 P. Thus, both uronic acid content and molecular size appear to be important in determining whether or not carbohydrates will coprecipitate with tannin in the presence of lead.

In these model experiments, the behaviour of tannin on SEC on Bio-Gel P-10 and Sephacryl S-300 was altered after recovery from the lead precipitate, as has been described for R2, whether the tannin was precipitated alone or together with the *A. mearnsii* gum polysaccharide. This demonstrated that the change in the tannin was a consequence of the chemical processes involved rather than any interaction with the carbohydrate.

Fractionation with aqueous acetone

Fractionation of R2 with aqueous acetone resulted in precipitation of all carbohydrate components having molecular weight of 8000 or above, together with the protein. The small amount of tannin found in the acetone-insoluble fraction, R2 I, was probably coprecipitated by adsorption to the polysaccharide. SEC of R2 I on Sepharose 4B separated the polysaccharide–protein conjugate (corresponding to fraction Ia isolated from R1), which was eluted at V_0, from the bulk of the carbohydrate, which emerged as a single, broad peak ($\bar{M}_w$ 70 000; *cf.*, fractions Ib and Ic), overlapping with the phenolic component, eluted in the region of V_t. The carbohydrate in the acetone-soluble fraction, R2 S, was co-eluted with the tannin at V_t on this column. With the Bio-Gel P-10 column, all carbohydrate and protein in R2 I were eluted at V_0, well removed from the phenolic component at V_t. Optimum resolution of the polysaccharide components of R2 I was given by Sephacryl S-300, which also separated these from the phenolic material (Fig. 6A). SEC of R2 S on this column showed the presence of two carbohydrate components, the major one eluting at K_{av} 0.84 (corresponding to $\bar{M}_w$ 3300) and the minor one at K_{av} 0.90 ($\bar{M}_w$ 2400). The latter peak coincided with one due to phenolic material, which was resolved from the main tannin fraction, eluted (with low recovery) at V_t. Further fractionation of R2 S with aqueous acetone distinguished the two types of phenolic component, that eluting at K_{av} 0.90 being precipitated with most of the carbohydrate in a sub-fraction that did not react with lead acetate.

Paper chromatography (solvents A and B) of hydrolysates of R2 I and R2 S showed that all the uronic acid was recovered in R2 I, but the neutral sugar constituents of both fractions were the same. In TLC on polyamide, R2 I was not detectable by spray reagent a, but R2 S showed the characteristic blue streak given by free tannin. When the plate was subsequently sprayed with acid reagent b and heated, a further component of R2 S was revealed as a blue spot ($R_F \approx 0.9$), not seen with R2 I. This behaviour and the absence of reaction with lead suggests strong association between carbohydrate and phenolic moieties in the minor component (7% by weight) of R2 S, this component corresponding to fractions II and III from R1.

Hide-powder fractionation

The "non-tannins" recovered after fractionation of R2 with hide powder were

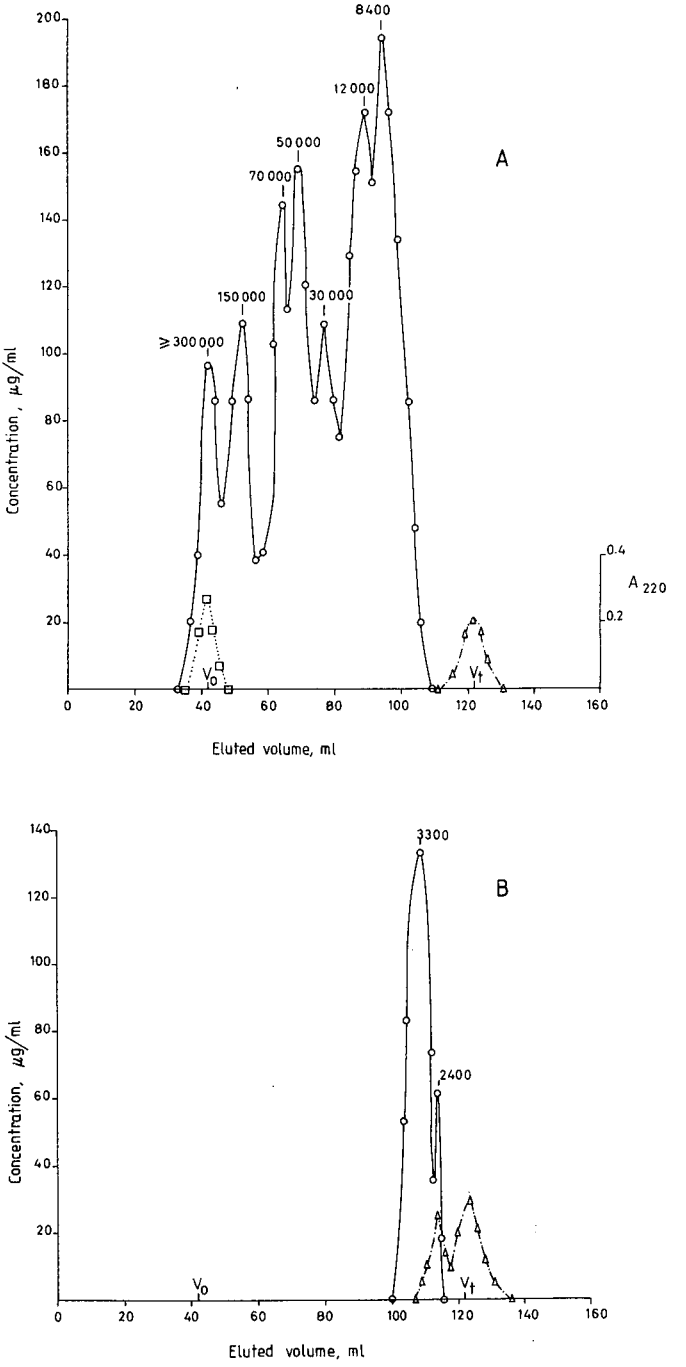

Fig. 6. SEC on Sephacryl S-300 of (A) acetone-insoluble fraction (R2 I) of R2 and (B) acetone-soluble fraction (R2 S). (A) ○ = Carbohydrate; △ = phenolics; □ = protein, (B) ○ = Carbohydrate; △ = tannin.

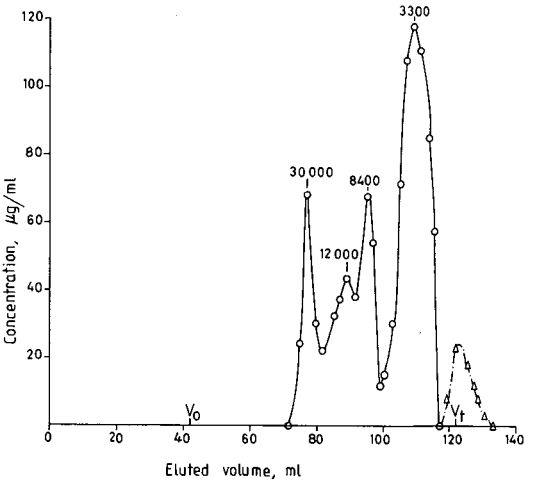

Fig. 7. SEC on Sephacryl S-300 of "non-tannins" from hide-powder fractionation of R2. ○ = Carbohydrate; △ = phenolics.

found, by SEC on Sephacryl S-300, to contain carbohydrate components having molecular weights in the range 3000–30 000 (Fig. 7), which were completely separated on the column from the residual phenolic material (probably not tannin). The corresponding fraction from A gave a similar elution profile, but with more carbohydrate of lower molecular weight and some overlap between this and UV-absorbing material at V_t. These results show that all carbohydrate having molecular weight $>30\,000$ is adsorbed with tannin on hide powder. There is no evidence for carbohydrate–tannin complexes (such as fractions II, III and R2 S) in the non-tannins from R2; these conjugates are apparently also adsorbed by the hide powder.

Behaviour of fractions with gelatin and surfactant

The gelatin reagent, which gives a dense precipitate immediately when added to solutions containing free tannins, reacted less readily with fraction R2 P, in which the chemical nature of the tannin had been changed, and with II and III, in which the tannin appears to be strongly associated with carbohydrate. Addition of cetavlon was found to suppress the interaction of tannin and gelatin by strong competitive interaction (believed to be hydrophobic [41]) with the tannin. Nevertheless, the behaviour on polyamide TLC of a sample of II that had been exposed to Cetavlon was unchanged, there being no indication of free tannin unless the plate was sprayed with acid and heated after pre-spraying with a. This persistence of complexation between carbohydrate and tannin in II, despite the presence of the strongly competing surfactant, is further evidence for very close association, perhaps covalent linkage, between these two components in such fractions.

CONCLUSIONS

The problem of separating carbohydrate from phenolic components in wattle

bark extract is emphasized by this investigation, and the heterogeneity of the products obtained by accepted methods of fractionation has been clearly demonstrated by chromatographic methods, mainly SEC. Neither solvent fractionation nor dialysis is effective in separating tannin from carbohydrate, and strong interaction between the polyphenolic material and the acidic polysaccharides of intermediate molecular weight in the retentate from the non-tannin fraction causes these to coprecipitate on addition of lead (Fig. 5A) or ethanol (Fig. 1), and to be adsorbed together on hide powder (Fig. 7). The coprecipitation of polysaccharide in the molecular weight range 8000–70 000 with tannin on treatment with lead acetate has been clearly demonstrated and quantified by SEC, as has the adsorption by hide powder of polysaccharides of molecular weight above 30 000. The limitations of the hide-powder method have been described [8].

Polysaccharide of molecular weight above 8000 is precipitated by addition of acetone to an aqueous solution (Fig. 6A), but the presence of carbohydrate of lower molecular weight together with tannin in the acetone-soluble fraction has been shown by SEC (Fig. 6B). There is some evidence, mainly from TLC, of the presence of a carbohydrate–tannin complex in the acetone-soluble fraction, as in the material eluted with formamide and with aqueous urea on PVPP column chromatography of a similar retentate from the non-tannin fraction. These are, however, minor components and, if compounds of carbohydrate and tannin are present, they may be artefacts produced in the initial process of extraction of the bark with hot water. Methylation analysis of these fractions suggests that the carbohydrate moiety consists of single sugar units (mainly Ara*f*) and short chains (2 or 3 units).

More complex carbohydrate components, containing uronic acid, have been isolated from the aqueous eluate obtained on PVPP column chromatography of the retentate of the non-tannin fraction. The polysaccharide of highest molecular weight is associated with protein (covalent attachment has not been proved). This and the other polysaccharides thus isolated ($\bar{M}_w$ 150 000 and 50 000) were the only fractions completely freed of tannin, possibly because their molecular size was above the optimum range, as suggested by SEC, for interaction with the phenolic components of wattle bark extract.

ACKNOWLEDGEMENTS

The financial support of the University of Cape Town and the Foundation for Research Development of the South African Council for Industrial Research is gratefully acknowledged. We are indebted to Dr. N. P. Slabbert, Mr. Carl Knauff and Mr. Gerald Tarboton of the Wattle Industry Centre, Pietermaritzburg, for gifts of wattle bark extract and for discussions that initiated this research, and to Dr. D. R. Cooper and staff of the Leather Industry Research Institute, Grahamstown, for a gift of hide powder and for providing library and laboratory facilities to one of us (A.M.S.). We thank Associate Professor W. F. Brandt (Department of Biochemistry, University of Cape Town) for performing the amino acid analysis, Dr. W. T. Mabusela for the uronic acid analysis and Ms. J. Burger and Ms. H. van der Straaten for technical assistance with the GLC–MS analyses.

REFERENCES

1 A. M. Stephen, *J. Chem. Soc.*, (1949) 3082.
2 D. G. Roux, S. E. Drewes and H. M. Saayman, *J. Soc. Leather Trades Chem.*, 49 (1965) 416.
3 D. G. Roux, *ChemSA*, 4 (1978) 90.
4 J. P. Steynburg, J. A. Steenkamp, J. F. W. Burger, D. A. Young and D. Ferreira, *J. Chem. Soc., Perkin Trans. 1*, (1990) 235.
5 D. G. Roux and S. R. Evelyn, *Biochem. J.*, 69 (1958) 530.
6 D. G. Roux, *J. Soc. Leather Trades Chem.*, 36 (1952) 274.
7 A. M. Stephen, *J. Sci. Food Agric.*, 3 (1952) 37.
8 D. G. Roux, *J. Soc. Leather Trades Chem.*, 41 (1957) 287.
9 M. D. Rahman and G. N. Richards, *J. Wood Chem. Technol.*, 8 (1988) 111.
10 M. J. Neilson, T. J. Painter and G. N. Richards, *Carbohydr. Res.*, 147 (1986) 315.
11 J. B. Harborne, in E. Heftmann (Editor), *Chromatography, Part B, Applications (Journal of Chromatography Library*, Vol. 22B), Elsevier, Amsterdam, 1983, pp. 407–433.
12 S. G. Shuttleworth, A. E. Russell and D. A. Williams-Wynn, *J. Soc. Leather Trades Chem.*, 52 (1968) 486.
13 K. S. Kirby, E. Knowles and T. White, *J. Soc. Leather Trades Chem.*, 35 (1951) 338.
14 S. C. Churms, in E. Heftmann (Editor), *Chromatography, Part B, Applications (Journal of Chromatography Library*, Vol. 22B), Elsevier, Amsterdam, 1983, pp. 224–286.
15 M. Dubois, K. A. Gilles, J. K. Hamilton, P. A. Rebers and F. Smith, *Anal. Chem.*, 28 (1956) 350.
16 P. Albersheim, D. J. Nevins, P. D. English and A. Karr, *Carbohydr. Res.*, 5 (1967) 340.
17 D. P. Sweet, R. H. Shapiro and P. Albersheim, *Carbohydr. Res.*, 40 (1975) 217.
18 S. C. Churms and A. M. Stephen, *Carbohydr. Res.*, 133 (1984) 105.
19 C. J. Biermann, *Adv. Carbohydr. Chem. Biochem.*, 46 (1988) 251.
20 A. M. Stephen, S. C. Churms and D. C. Vogt, in P. M. Dey (Editor), *Methods in Plant Biochemistry*, Vol. 2, Academic Press, London, 1990, pp. 496–498.
21 S. Hakomori, *J. Biochem. (Tokyo)*, 55 (1964) 205.
22 L. R. Phillips and B. A. Fraser, *Carbohydr. Res.*, 90 (1981) 149.
23 T. Purdie and J. C. Irvine, *J. Chem. Soc.*, 83 (1903) 1021.
24 N. Blumenkrantz and G. Asboe-Hansen, *Anal. Biochem.*, 54 (1973) 484.
25 P. Åman, L.-E. Franzén, J. E. Darvill, M. McNeil, A. G. Darvill and P. Albersheim, *Carbohydr. Res.*, 103 (1982) 77.
26 G. O. Aspinall and K.-G. Rosell, *Carbohydr. Res.*, 57 (1977) C23.
27 D. G. Roux, *J. Soc. Leather Trades Chem.*, 35 (1951) 322.
28 M. A. Ragan and A. Jensen, *J. Exp. Mar. Biol. Ecol.*, 30 (1977) 209.
29 S. Tugwell and G. M. Branch, *J. Exp. Mar. Biol. Ecol.*, 129 (1989) 219.
30 M. D. Rahman and G. N. Richards, *Carbohydr. Res.*, 170 (1987) 112.
31 A. E. Clarke, R. L. Anderson and B. A. Stone, *Phytochemistry*, 18 (1979) 521.
32 G. B. Fincher, B. A. Stone and A. E. Clarke, *Annu. Rev. Plant Physiol.*, 34 (1983) 47.
33 A. A. Leach, *Biochem. J.*, 74 (1960) 70.
34 J. F. Carson and W. D. Maclay, *J. Am. Chem. Soc.*, 68 (1946) 1015.
35 S. C. Churms, E. H. Merrifield, A. M. Stephen, D. R. Walwyn, A. Polson, K. J. van der Merwe, H. S. C. Spies and N. Costa, *Carbohydr. Res.*, 113 (1983) 339.
36 S. C. Churms, E. H. Merrifield and A. M. Stephen, *Carbohydr. Res.*, 55 (1977) 3.
37 A. M. Stephen, *J. Chem. Soc.*, (1951) 646.
38 S. C. Churms, E. H. Merrifield, A. M. Stephen and E. W. Stephen, *S. Afr. J. Chem.*, 31 (1978) 115.
39 *Official Methods of Analysis*, Society of Leather Trades Chemists, Redbourn, 4th rev. ed., 1965, Sect. 2/3.
40 J. L. Goldstein and T. Swain, *Phytochemistry*, 4 (1965) 185.
41 H. I. Oh, J. E. Hoff, G. S. Armstrong and L. A. Haff, *J. Agric. Food Chem.*, 28 (1980) 394.
42 A. M. Stephen, in G. O. Aspinall (Editor), *The Polysaccharides*, Vol. 2, Academic Press, New York, 1983, pp. 97–193.
43 M. Kaplan and A. M. Stephen, *Tetrahedron*, 23 (1967) 193.
44 G. O. Aspinall, J. J. Carlyle and R. Young, *Carbohydr. Res.*, 7 (1968) 421.
45 G. O. Aspinall, *Pure Appl. Chem.*, 49 (1977) 1105.
46 D. M. W. Anderson, in G. O. Phillips, D. J. Wedlock and P. A. Williams (Editors), *Gums and Stabilisers for the Food Industry*, Vol. 3, Elsevier Applied Science, Barking, 1986, pp. 79–86.
47 D. W. Gammon, A. M. Stephen and S. C. Churms, *Carbohydr. Res.*, 158 (1986) 157.

Journal of Chromatography, 550 (1991) 539–547
Elsevier Science Publishers B.V., Amsterdam

CHROMSYMP. 2276

Multi-step procedure for the separation of vinyl chloride oligomers

J. V. DAWKINS* and M. J. FORREST[a]

Department of Chemistry, Loughborough University of Technology, Loughborough, Leicestershire LE11 3TU (UK)

and

M. J. SHEPHERD[b]

Ministry of Agriculture, Fisheries and Food, Food Science Division, Haldin House, Queen Street, Norwich NR2 4SX (UK)

ABSTRACT

A multi-stage scheme was developed for the separation of vinyl chloride (VC) oligomers. A low-molar-mass fraction was isolated from poly(vinyl chloride) by Soxhlet extraction with diethyl ether followed by fractional precipitation with pentane. The presence of VC oligomers up to the decamer was demonstrated by high-performance size-exclusion chromatography (HPSEC). Removal of polar impurities was effected by preparative adsorption liquid chromatography of the low-molar-mass fraction. Recycle HPSEC with repeated injections permitted the accumulation of fractions of VC trimer, tetramer and pentamer oligomers. Separations of isomers of VC tetramer and pentamer oligomers were performed by high-performance liquid chromatography.

INTRODUCTION

The chemical and molecular structure of poly(vinyl chloride) (PVC) has been investigated in some detail because the thermal stability of the polymer is lower than expected on the basis of its ideal structure $(CH_2CHCl)_x$. Work indicating the presence of anomalous structures such as branching, head-to-head addition, unsaturation and "labile chlorine" in PVC has been reviewed [1]. Explanations for these structural defects have been considered in terms of possible mechanisms occurring during the radical polymerization of vinyl chloride monomer (VC) [2,3]. Much information can be obtained from investigations of fractions of low molar mass in order to identify and quantify end groups and structural defects at branch points [4,5]. In addition, studies have been directed to the low-molar-mass fraction of PVC (including addi-

[a] Present address: RAPRA Technology Limited, Shawbury, Shrewsbury, Shropshire SY4 4NR, UK.
[b] Present address: Ministry of Agriculture, Fisheries and Food, Food Science Laboratory, Colney Lane, Norwich NR4 7UA, UK.

0021-9673/91/$03.50

tives and oligomers) because these components are potential migrants in plastics packaging [6].

It follows that efficient separation methods are required to isolate VC oligomers. Gilbert *et al.* [7] obtained low-molar-mass fractions of PVC by Soxhlet extraction followed by fractionation by gel filtration. The size distribution of components in these fractions was assessed by high-performance size-exclusion chromatography (HPSEC) using cross-linked polystyrene gels (particle size = 10 μm) having exclusion limits below 500 Å. Analysis of these low-molar-mass fractions by gas chromatography–mass spectrometry (GC–MS) [8] enabled the oligomer species from trimer to hexamer to be separated, with some evidence of the heptamer and octamer. From MS data obtained from hydrogenation studies on samples, each oligomeric species was postulated to exist in saturated and unsaturated forms, with each form itself occurring as a number of structural isomers. The total population of isomers was found to increase with increasing chain length. For any given oligomer the mass spectra of its isomers were very similar and no detailed structural information could be elucidated. It was apparent that other analytical techniques, such as nuclear magnetic resonance spectroscopy (NMR), would need to be employed to obtain these data. A separation scheme was devised [9] in which, by routine high-performance liquid chromatographic (HPLC) fractionation, 0.5 mg of a VC tetramer was isolated from a PVC polymer for ^{1}H NMR analysis. A partial structural characterization of the VC tetramer was achieved by this technique [10], the principle limitation being the small mass of oligomer available. A greater amount of each species had to be isolated if successful structural studies were to be performed using NMR. To this end, an alternate pumping recycle HPSEC technique [11] was used, which was capable of separating the VC oligomer species up to decamer present in a low-molar-mass fraction of PVC [12].

The object of this work was to improve and extend the separation scheme so that it would be possible to attempt a full structural characterization of each VC oligomer. Because of the requirements of NMR, the preferred separation scheme would be one that permitted the efficient collection of high-purity oligomer species. Another consideration was the inherent thermal instability of VC oligomers and so only chromatographic techniques that functioned at ambient temperatures were utilized and low-boiling-point solvents were used as eluents. The methods described in this paper are directed to VC oligomers up to the decamer with most emphasis on isolating those up to and including the pentamer.

EXPERIMENTAL

PVC polymer

The PVC polymer used was Lucovyl RB8010 with a *K* value (solution viscosity parameter used by PVC manufacturers) of 56. This was a mass-polymerized sample kindly provided by Atochem (Thatcham, UK).

Reagents

Diethyl ether (standard laboratory reagent grade), tetrahydrofuran (analytical-reagent grade), dichloromethane, hexane (95% *n*-hexane) and pentane (75% *n*-pentane) (all HPLC grade) were supplied by Fisons (Loughborough, UK). Methyl *tert.*-butyl ether (MTBE) (HPLC grade) was supplied by Fluka (Glossop, UK).

Low-molar-mass fractions of PVC

Low-molar-mass fractions were obtained from the PVC polymer by a two-stage process. Initially, the polymer (250 g) was extracted in a Soxhlet apparatus with diethyl ether for 20 h. At the end of an extraction the extract was filtered and then reduced to *ca.* 20 cm^3 in a rotary evaporator. A small portion of this mixture was dried in a vacuum oven at room temperature and then characterized by SEC with a 60 cm × 7.5 mm I.D. PL mixed gel (10-μm) column (Polymer Labs., Church Stretton, UK) in a Model 501 chromatograph (Waters Assoc. Hartford, UK) having a refractive index detector with tetrahydrofuran as mobile phase at a flow-rate of 1 cm^3 min^{-1}. The reduced extract was then added to 350 cm^3 of pentane at room temperature. The mixture was left for 20 min to ensure that the precipitation of the long-chain PVC was complete and then the mixture was filtered to leave a clear filtrate containing low-molar-mass PVC in solution. The dry low-molar-mass fraction was obtained by utilizing first a rotary evaporator and then a vacuum oven at room temperature.

Preparative adsorption liquid chromatography

The low-molar-mass PVC fraction was purified and further fractionated on a Merck Lobar Size B column (31 cm × 25 mm I.D.) containing LiChroprep Si 60 (40–63 μm) packing, supplied by Merck (Darmstadt, Germany). A Model 64 HPLC pump (Knauer, Berlin, Germany) was used in conjunction with a PU 4025 UV detector (Pye Unicam, Cambridge, UK) and a Rheodyne Model 7125 injection valve fitted with a 200-μl loop supplied by HPLC Technology (Macclesfield, UK). Aliquots (150 mg) of the low-molar-mass fraction were injected into the chromatograph and the fraction within the elution volume range 0–420 cm^3 was collected.

HPSEC

Individual oligomer species were separated from the low-molar-mass PVC fraction using an HPSEC system based on two 60 cm × 7.5 mm I.D. columns containing 5-μm, 50-Å PL gel (Polymer Labs.). The columns were used in conjunction with a Knauer Model 64 pump and a Knauer differential refractometer. An alternate pumping recycle system [12] was set up using a Rheodyne Model 7000 switching valve and the injection valve was a Rheodyne Model 7125, both supplied by HPLC Technology. The mobile phase dichloromethane was delivered at a rate of 1 cm^3 min^{-1}. A separation was performed by injecting a 10-mg sample and passing it with recycling through 480 cm of gel bed. Oligomers corresponding to resolved oligomer peaks were collected manually and the dry oligomer fractions were obtained using a vacuum oven at room temperature.

HPLC

Oligomers prepared by recycle HPSEC were separated into their isomeric forms by normal-phase HPLC. The chromatograph consisted of a Waters Model 6000A pump, a Pye Unicam PU 4025 detector operated at 200 nm and a 25 cm × 4.6 mm I.D. column containing Spherisorb S5W silica packing supplied by Phase Separations (Queensferry, UK). The mobile phase employed was hexane containing MTBE modifier (1.0–0.25%, depending on the oligomer being separated) at a flow-rate of 1 cm^3 min^{-1}. Routine fractionation of oligomers was carried out by injecting 2-mg aliquots

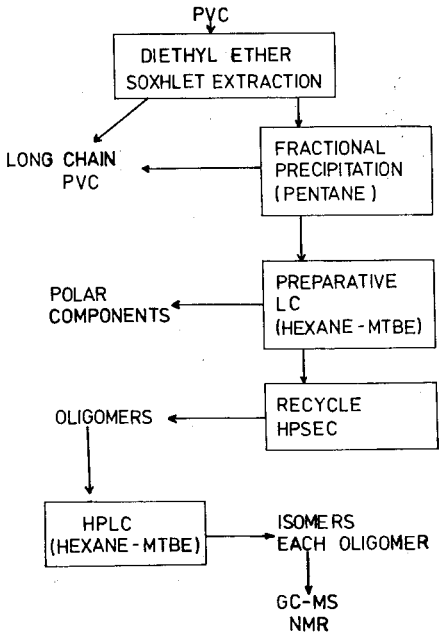

Fig. 1. Separation scheme.

and the fractions blown to dryness using nitrogen. A schematic illustration of the multi-stage procedure for the separation of VC oligomers from a PVC polymer is shown in Fig. 1.

GC–MS

GC–MS analysis of the various VC oligomer fractions was carried out using either a Carlo Erba Model 4160 gas chromatograph coupled to a VG Mass Labs Quadrupole 15-250 mass spectrometer or a gas chromatograph of the same type connected to a VG Mass Labs 7070 EQ mass spectrometer [7–10]. In each instance a Chrompack 25 m × 0.2 mm I.D. column coated with a 0.12-μm layer of CP-Sil 5CB was used. The flow-rate of the carrier gas (helium) was 1 ml min^{-1}. Separations were carried out under both isothermal and temperature-programmed conditions and the data obtained were processed using an LVG 11-250 data system.

RESULTS AND DISCUSSION

Extracting the Lucovyl RB8010 PVC polymer with diethyl ether gave an extract yield of 0.80%. When analysed by SEC this extract gave the molar-mass distribution shown in Fig. 2. The low-molar-mass fraction that was obtained from the filtrate after fractional precipitation of the diethyl ether extract with pentane constituted 25% by weight of the original. An HPSEC chromatogram of this fraction is shown in Fig. 3. The peaks due to VC oligomers have been assigned with regard to chain length, and

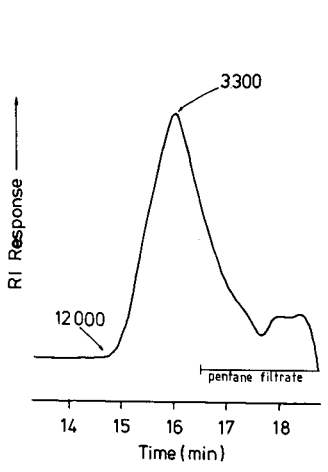

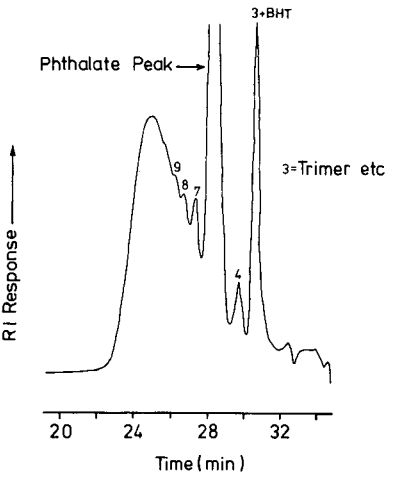

Fig. 2. SEC of diethyl ether Soxhlet extract. Molar mass data (g mol^{-1}) with reference to a calibration graph established with polystyrene standards.

Fig. 3. HPSEC of low-molar-mass fraction from pentane filtrate. Column, 120 cm PL gel (5 μm, 50 Å), eluted with dichloromethane at 1 ml min^{-1}.

peaks due to phthalate and 2,6-di-*tert.*-butyl-*p*-cresol (butylated hydroxytoluene; BHT) impurities are also indicated. It was possible to assign the oligomer peaks in Fig. 3 by using VC oligomers as calibrants because the pentamer to decamer oligomers had been prepared and described in a previous paper [12]. The phthalate and BHT impurities had been identified by GC–MS data.

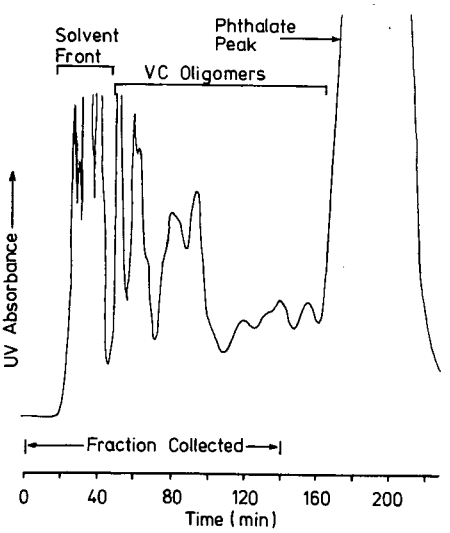

Fig. 4. Adsorption LC of low-molar-mass fraction from pentane filtrate. Mobile phase: hexane–MTBE (95:5) at 3 ml min^{-1}

Because some of the oligomer peaks in Fig. 3 were obscured by impurities, a further chromatographic technique was employed to purify the low-molar-mass fraction prior to HPSEC analysis. For this purpose a preparative adsorption liquid chromatographic system was employed. The chromatogram obtained for the low-molar-mass PVC fraction is shown in Fig. 4. It can be seen that the phthalate impurity and the oligomer fraction collected are well separated owing to the greater polarity, and hence longer retention time, of the phthalate. The amount of MTBE modifier in the mobile phase was set at 5% (v/v) to enable separations to be carried out in reasonable times whilst maintaining sufficient oligomer–phthalate resolution. It is clear from Fig. 4 that, in addition to removing more polar impurities, the purification stage also serves to reduce the amount of long-chain PVC in the fraction. The elution volume range designated in Fig. 4 for collection was derived by determining the volume required for all of the VC decamer isomers to elute from the column. As elution time is proportional to oligomer chain length, this ensured that none of the isomers of the oligomers of greatest interest, *i.e.*, up to and including the pentamer, were missed. By comparing an HPSEC trace for the purified low-molar-mass PVC fraction (Fig. 5) with Fig. 3, it is possible to see the reduction in the amount of long-chain PVC and the absence of the phthalate peak. The presence of the BHT peak is still evident in Fig. 5 and the failure of the adsorption chromatographic system to separate it from the VC oligomers could be due to its chemical structure, in which the *tert.*-butyl groups in the 2,6-substitution positions shield the hydroxyl group and so inhibit it from interacting with the column packing.

With the alternate pumping recycle technique [12], resolution of the VC oligomers was improved and the chromatogram obtained using 480 cm of gel bed is shown in Fig. 6, where the oligomer species from trimer to pentamer are well separated. These oligomers were of greatest interest because they have the greatest potential for migration from PVC. The absence of any discernible concentration of VC dimer is

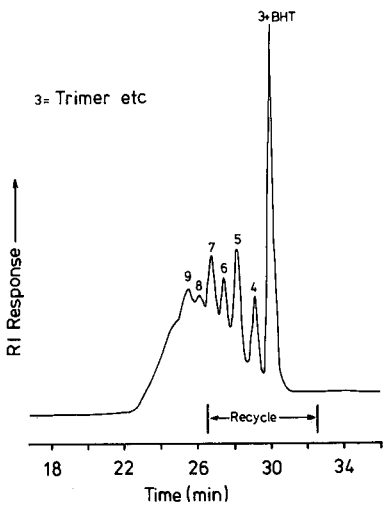

Fig. 5. HPSEC of low-molar-mass fraction from pentane filtrate after preparative adsorption LC. Column, 120 cm PL gel (5 μm, 50 Å), eluted with dichloromethane at 1 ml min^{-1}.

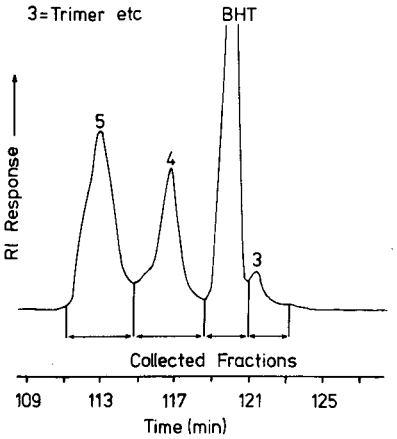

Fig. 6. HPSEC of low-molar-mass fraction from pentane filtrate after preparative adsorption LC. Column, 480 cm by recycle PL gel (5 μm, 50 Å), eluted with dichloromethane at 1 ml min^{-1}.

considered to be due to the monomer stripping process, in which the conditions are severe enough to remove the dimer species also. Amounts of the oligomers from trimer to pentamer were accumulated by fractionating the purified low-molar-mass PVC fraction on the HPSEC system by repeated injections and collecting the fractions designated in Fig. 6. The assignments of the oligomer peaks in Fig. 6, which had initially been performed by use of the VC oligomer standards, were confirmed by analysing each fraction by GC–MS and referring to data that had been published previously [8]. The data obtained confirmed the observation that each VC oligomer species exists as a number of structural isomers, the amount increasing with increasing chain length.

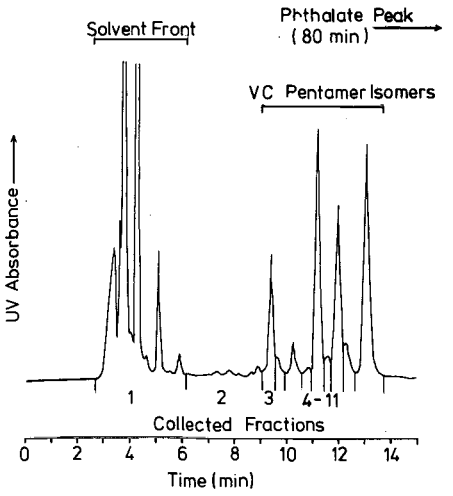

Fig. 7. HPLC of the VC pentamer fraction. Mobile phase: hexane–MTBE (99:1) at 1 ml min^{-1}.

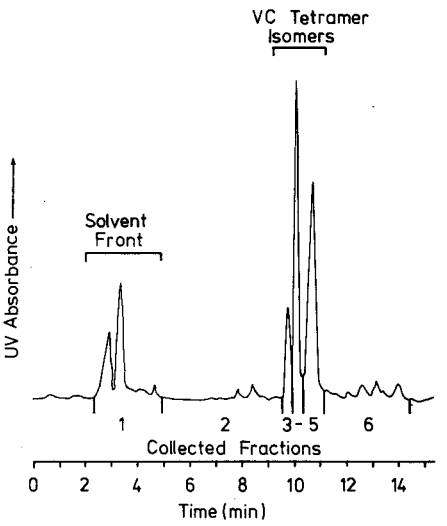

Fig. 8. HPLC of the VC tetramer fraction. Mobile phase: hexane–MTBE (99.75:0.25) at 1 ml min^{-1}.

The polyisomeric nature of the VC oligomers necessitated the development of a chromatographic technique for resolving each entity prior to an attempted structural chracterization by NMR. Such a combination of HPLC and ^{13}C NMR analysis has been reported for 2-vinylpyridine oligomers [13]. Liquid–solid chromatography has been used for isomer separation [14] and it was found that a normal-phase HPLC system based on a Spherisorb S5W silica column and a mobile phase consisting of hexane containing MTBE as a modifier was capable of resolving the isomeric forms of the VC oligomers. The chromatograms obtained for the pentamer and tetramer fractions are shown in Figs. 7 and 8. Only very small amounts of modifier were required to elute the oligomers from the column because of their relatively non-polar nature. Less modifier (0.25%, v/v) was used for the tetramer to optimize the isomer resolution.

The chromatograms were partitioned as shown in Figs. 7 and 8 and the collected fractions were analysed by GC–MS. From the data obtained the peaks within the fraction range 3–11 for the pentamer and 3–5 for the tetramer were found to be isomers of those respective oligomers. Two VC trimer isomers had been found by GC–MS analysis of the trimer HPSEC fraction but it was not possible to differentiate these from the solvent front when this fraction was analysed on the HPLC system. The degree of interaction between the trimers and the silica column is insufficient with the hexane–MTBE eluent. Having established which fractions present in Figs. 7 and 8 represented VC oligomer isomers, HPLC fractionation of the VC pentamer and tetramer fractions from HPSEC was carried out by repeated injections to accumulate a sufficient mass of each isomer for NMR analysis. The results of this spectroscopic study will be reported in a subsequent paper [15].

CONCLUSIONS

It has been demonstrated how, by a series of fractionation procedures utilizing a number of chromatographic techniques, relatively pure VC oligomer isomers can be isolated from a PVC polymer. The results show that, even for the VC oligomer pentamer, a large number of isomeric forms exist. By using this preparation scheme it is possible to accumulate a sufficient amount of each VC oligomer isomer to enable NMR to be employed as a characterization method. This development will enable data that were previously unobtainable to be collected and a clearer view of the structures of these oligomers to be formed.

ACKNOWLEDGEMENTS

The authors thank Dr. J. Gilbert of the Ministry of Agriculture, Fisheries and Food for his interest and encouragement, and MAFF for a grant to support the research performed at Loughborough University of Technology.

REFERENCES

1 A. A. Caraculacu, *Pure Appl. Chem.*, 53 (1981) 385.
2 T. Hjertberg and E. M. Sorvik, *J. Macromol. Sci. Chem.*, A17 (1982) 983.
3 M. F. Darricades-Llauro, A. Michel, A. Guyot, H. Waton, R. Petiaud and Q. T. Pham, *J. Macromol. Sci. Chem.*, A23 (1986) 221.
4 U. Schwenk, F. Cavagna, F. Lomker, I. Konig and H.Streitberger, *J. Appl. Polym. Sci.*, 23 (1979) 1589.
5 C. J. M. van den Heuvel and A. J. M. Weber, *Makromol. Chem.*, 184 (1983) 2261.
6 M. J. Shepherd, *Food Chem.*, 8 (1982) 129.
7 J. Gilbert, M. J. Shepherd and M. A. Wallwork, *J. Chromatogr.*, 193 (1980) 235.
8 J. Gilbert, M. J. Shepherd, J. R. Startin and M. A. Wallwork, *J. Chromatogr.*, 237 (1982) 249.
9 J. Gilbert, M. J. Shepherd and M. A. Wallwork, *J. Chromatogr.*, 320 (1985) 361.
10 J. Gilbert, M. J. Shepherd, M. A. Wallwork, C. Crews, J. R. Startin and J. C. Mitchell, *Eur. Polym. J.*, 21 (1985) 555.
11 R. A. Henry, S. H. Byrne and D. R. Hudson, *J. Chromatogr. Sci.*, 12 (1974) 197.
12 J. V. Dawkins, M. J. Forrest and M. J. Shepherd, *J. Liq. Chromatogr.*, 13 (1990) 3001.
13 S. S. Huang and T. E. Hogen-Esch, *J. Polym. Sci., Polym. Chem. Ed.*, 23 (1985) 1203.
14 L. R. Snyder and J. J. Kirkland, *Introduction to Modern Liquid Chromatography*, Wiley-Interscience, New York, 2nd ed., 1978, p. 356.
15 J. V. Dawkins, M. J. Forrest and M. J. Shepherd, in preparation.

Journal of Chromatography, 550 (1991) 549–558
Elsevier Science Publishers B.V., Amsterdam

CHROMSYMP. 2297

Separation and detection of oxidation products in Neurolite raw material

PETA A. RYAN*, BARBARA A. EWELS and JOSEPH L. GLAJCH
DuPont Merck Pharmaceutical Company, 331 Treble Cove Road, Bld 200-1, N. Billerica, MA 01862 (USA)

ABSTRACT

N,N'-1,2-Ethylenediylbis-L-cysteine diethyl ester (ECD) is a chiral compound and is a key component of Neurolite, a brain imaging agent. In order for the material to be used in the manufacture of Neurolite, it must meet optical rotation and other purity specifications. The optical rotation of ECD is affected by the presence of oxidation-related impurities of the parent material. Prior to this work, the optical rotation was used as a gross indication of these impurities. During product development, information regarding the impurity profile became necessary in order to understand and monitor ECD degradation. A gradient elution high-performance liquid chromatographic method compatible with liquid chromatography–mass spectrometry was developed and optimized using Drylab G software. System suitability of the method was assessed by adding L-methionine ethyl ester and acetophenone to the ECD standard as resolution markers. Comparison of the resolution between each marker and ECD with previous measures of resolution ensures sufficient zone capacity to resolve all potential impurities.

INTRODUCTION

Pharmaceutical quality and regulatory considerations have spurred the need to separate and identify potential impurities and degradation products in pharmaceuticals. As a result, high-performance liquid chromatography (HPLC) is becoming increasingly popular as in many instances the active ingredient and the impurities can be separated and determined using the same method. The past two decades have seen advances in both the theory and practice of HPLC which have allowed greater control and reproducibility of methods.

Concurrently, optimization theory has been developed and shown to be applicable to the development of all types of analytical methods. The optimization of HPLC methods has thus moved from a tedious and time-consuming exercise to one amenable to computer control and simulation. The role of computers in chromatographic method development has been reviewed [1–3]. One computer system for HPLC method development is DryLab, which has been described in detail [4]. DryLab is computer software which helps optimize an HPLC method using an approach that an experienced chromatographer would employ. It is based on the observation that changes in mobile phase concentration offer the greatest potential for separation improvements in HPLC. The program requires that the user supply retention times and peak identities for a given sample from three experimental runs in which only one

mobile phase variable is changed; the program will then pick the optimum mobile phase composition. Optimization of other separation variables, such as other mobile phase components and different columns, may be achieved with only a few additional experimental runs.

DryLab has been successfully applied to various real-life analytical problems [5–7]. DryLab G [8] is an extension of the DryLab software which permits the optimization of gradient HPLC parameters: gradient steepness and the initial and final percentages of each solvent. DryLab G was used to develop a method for detection of oxidation impurities in N,N'-1,2-ethylenediylbis-L-cysteine diethyl ester (ECD), a chiral compound.

An important aspect of method optimization is the definition of the goal of the method. For our purposes, the following were desired: adequate resolution between the major component (ECD) and observed degradation products; resolution (> 1.5) of all known impurities; minimized run time without sacrificing resolution; and rugged performance.

Gradient elution HPLC was chosen in order to resolve adequately all peaks of interest and to provide reasonable peak capacity. A large zone capacity will give the best chance of resolving all potential impurities. Although gradient elution was chosen as the initial method, a secondary goal was to develop an isocratic method if possible. The experimental design that was used permitted an extension to isocratic separation. The mobile phase components were picked for compatibility with liquid chromatography–mass spectrometry (LC–MS) to aid impurity identification. Minimum run time, although desired, was not critical to this method as it was designed for evaluation of only a few batches of raw material each year. Thus, analysis time could be sacrificed for greater resolving power. Finally, in order to ensure proper functioning of the method in various quality control laboratories, a system suitability assessment was developed.

EXPERIMENTAL

Instrumental

The reversed-phase gradient method was performed using two different HPLC instruments with UV detection at 210 nm: a Hewlett-Packard (Avondale, PA, USA) Model 1090L with a filter photometric detector and a Spectra-Physics (San Jose, CA, USA) Model SP8785 LC with a Model 1000S diode-array detector (Bioanalytical Systems, West Lafayette, IN, USA). Both instruments were connected to Hewlett-Packard Model 3392 integrators. The Spectra-Physics instrument was also connected to a Model CR/DS Flow-One beta radioactive flow detector (Radiomatic Instruments, Tampa, FL, USA). Separations were carried out on 25 cm × 0.46 cm I.D. Zorbax Rx columns and 1.25 cm × 0.4 cm Zorbax Rx guard cartridges (Mac Mod Analytical, Chadds Ford, PA, USA) with a flow-rate of 1.5 ml/min at room temperature. The total run time was 30 min, allowing for adequate equilibration of the column.

Chemicals

The mobile phase was a mixture of aqueous ammonium chloride (Fisher Scientific, Fairlawn, NJ, USA) and acetonitrile (Mallinckrodt, Paris, KY, USA). Deionized water was prepared with a Milli-Q water purification system (Millipore, Milford,

MA, USA). For LC–MS compatibility ammonium chloride was the buffer of choice. All solvents used for the gradients contained 0.1 *M* ammonium chloride, so that only the organic composition was varied over the gradient time. The dwell time for the system was determined to be 1.0 min according to procedures described [2].

ECD · 2 HCl was prepared according to published procedures [9,10]. [^{14}C]ECD was purchased from DuPont NEN (Boston, MA, USA). L-Methionine ethyl ester hydrochloride and acetophenone (Aldrich, Milwaukee, WI, USA) were used as received.

Computer software

The DryLab G software (LC Resources, Lafayette, CA, USA) was used on an IBM PS/2 Model 50 Z personal computer.

Experimental design

To facilitate the use of DryLab in optimization, and to aid in the identification of peaks, a 4 mg/ml solution of [^{14}C]ECD was used. The solution of [^{14}C]ECD was placed at room temperature for 24 h to form a large amount of oxidation products. Following injection of 25 μl of this [^{14}C]ECD solution a gradient was run from 20 to 90% acetonitrile for 20 min to determine the mobile phase strength required to elute all peaks of interest. The resulting chromatogram (Fig. 1) shows that no other peaks elute at acetonitrile concentrations above 50%. This indicates that there is no need to go above 50% acetonitrile in future optimization steps. The [^{14}C]ECD also contains impurities that are not found in the actual ECD raw material. These impurities are a result of the [^{14}C]ECD synthesis process, which is very different from that of the actual raw material, and were discounted in the optimization, as noted below. As it is easy to detect low levels of [^{14}C]ECD degradation products that might not have good UV absorbance, [^{14}C]ECD was used to ensure that all oxidation products were visible.

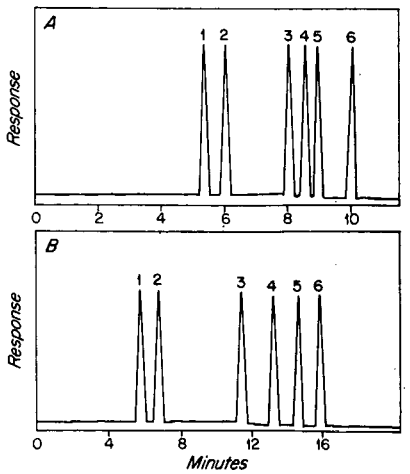

Fig. 1. Stimulated elutions using DryLab G. Chromatograms simulated using data from Table I. (A) 20–90% acetonitrile gradient in 20 min; (B) 20–50% acetonitrile gradient in 20 min.

RESULTS AND DISCUSSION

Optimization

In order to predict gradient elution times accurately data are required from at least two experimental runs which differ in gradient time. In this instance, a 20–50% acetonitrile gradient was run with gradient times of 10 of 60 min. The results from these runs are shown in Fig. 2 and Table I. The experimental conditions and retention data were entered into the computer to perform optimization on the gradient. Data from the experimental runs indicated that there are four peaks of interest, *i.e.*, ECD

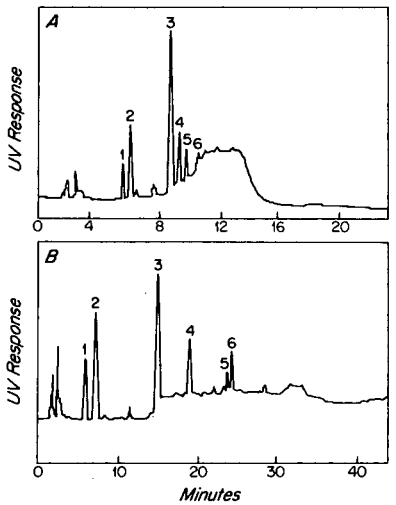

Fig. 2. Separation of oxidized [^{14}C]ECD material using gradient elution. Column, 25 × 0.46 I.D. cm Zorbax Rx; mobile phase gradient from 20 to 50% acetonitrile–aqueous ammonium chloride, with flow-rate 1.5 ml/min, temperature = 25°C and [^{14}C]ECD data from Table I. HPLC with gradient times of (A) 10 and (B) 60 min.

TABLE I

RETENTION TIMES OF PEAKS OF INTEREST

Peak No.	Retention time (min)	
	10-min run	60-min run
1	5.65	6.06
2	6.33	7.17
3[a]	8.59	14.78
4	9.22	18.75
5	9.69	21.84
6	10.79	23.10
Critical pair[b]	4 and 5 (R_s = 2.45)	5 and 6 (R_s = 2.02)

[a] ECD peak.

[b] The critical pair are the two closest eluting peaks for any given conditions.

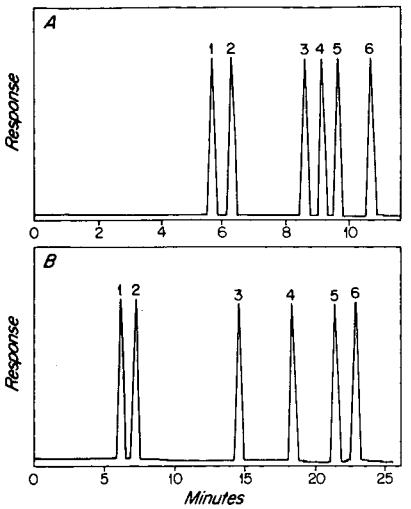

Fig. 3. Simulated elutions of oxidized [^{14}C]ECD material using gradient elution. Simulations using DryLab G from the data in Table I with gradient times of (A) 10 and (B) 60 min.

(peak 3) and three oxidation peaks (4, 5 and 6). In addition, two impurities were observed from the [^{14}C]ECD which were not found in the ECD raw material itself. The retention times of these six peaks were entered into DryLab as shown in Table I.

The computer program simulates a hypothetical picture for each change in run time or gradient step (Fig. 3). This information is used to predict the best conditions for adequate resolution of the critical pair. The first step is to change the run time using the same gradient. The program will calculate the average resolution, critical pairs and the retention time of the last-eluting peak. Snyder *et al.* [8] indicated that the accuracy between the actual and predicted retention time is ± 1–3% and 5–10% for resolution. Table II lists the calculated values as a function of changing the gradient time for 20–50% gradient.

The data show that the average resolution for each variation in gradient time is very good. Therefore, we need to examine each of the critical pairs more closely. Good separation of the ECD peak (3) and the three oxidation peaks (4, 5 and 6) is most important to this method. The first two peaks are of no consequence as they appear only in the batch of [^{14}C]ECD and not in actual ECD raw material. The gradient times between 7.3 and 16.6 min and from 30.3 to 62.6 min have critical pairs that include the three oxidation peaks (4, 5 and 6). Therefore, these gradient times are excluded from consideration. Between 17.7 and 24.6 min, the critical pair is 1 and 2, the two [^{14}C]ECD impurities. Therefore, the best gradient times on which to focus attention are between 17 and 25 min. A gradient time of 17 min was chosen as a compromise between best resolution of the known impurities, reasonable run time and excess resolving power to facilitate detection of other potential impurities.

The next step is to determine if any time can be saved at the beginning or end of the gradient by changing the gradient step. DryLab information led to a final choice of a 20–44.5% acetonitrile gradient. Fig. 4 shows the DryLab and the actual chromatogram using the optimized conditions. The predicted and actual retention times are

TABLE II

DRYLAB PREDICTIONS FOR A 20–50% ACETONITRILE GRADIENT WITH VARYING GRADIENT TIME

Gradient time (min)	Minimum R_s[a]	Critical band pair	Retention: last t_R (min)	k' (av.)[b]
7.3	1.89	4, 5	9.25	2.93
8.3	2.12	4, 5	9.86	3.20
9.5	2.35	4, 5	10.51	3.50
11.5	2.71	4, 5	11.56	4.00
12.3	2.83	4, 5	11.94	4.18
14.6	3.14	4, 5	12.92	4.66
15.6	3.26	4, 5	13.33	4.86
16.6	3.38	4, 5	13.74	5.08
17.7	3.44	1, 2	14.17	5.30
18.9	3.48	1, 2	14.60	5.52
20.2	3.52	1, 2	15.04	5.76
24.6	3.63	1, 2	16.42	6.51
30.3	3.49	5, 6	17.93	7.39
34.6	3.20	5, 6	18.91	7.99
40.5	2.86	5, 6	20.10	8.74
46.2	2.57	5, 6	21.10	9.40
52.6	2.29	5, 6	22.11	10.09
54.0	2.23	5, 6	21.80	9.88
61.6	1.96	5, 6	23.30	10.95

[a] R_s = resolution.

[b] k' (av.) = Average capacity factor.

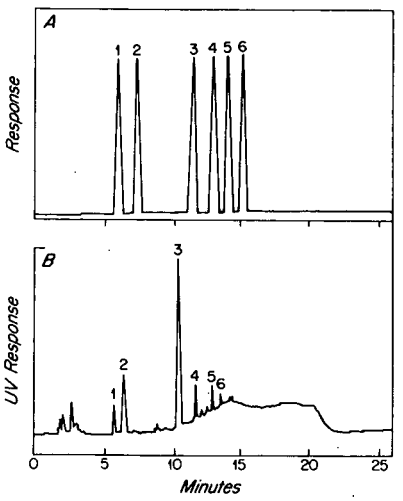

Fig. 4. Comparison of DryLab G prediction *vs.* actual gradient: Conditions as in Fig. 2, except gradient is from 20 to 44.5% acetonitrile in 17 min. (A) Simulated chromatogram; (B) actual chromatogram.

TABLE III

ACTUAL RETENTION TIMES *VS.* DRYLAB-PREDICTED RETENTION TIMES

Peak No.	Actual retention time (min)	Predicted retention time (min)	Difference (%)
1	5.65	5.89	−4.2
2	6.33	6.80	−7.9
3	10.23	11.16	−9.1
4	11.55	12.73	−10.2
5	12.76	13.86	−8.6
6	14.20	15.24	−7.3

given in Table III. The peak elution order was assumed to be constant throughout; the reasonable agreement between predicted and actual retention times indicates that this is a good assumption and that more stringent peak tracking methods are not required. The actual chromatogram in Fig. 4 contains the extra [^{14}C]ECD peaks and a baseline shift. By running a water blank with the gradient, it was determined that the shift in baseline and a very small blip at the void volume are due to the gradient.

System suitability

System suitability is used to ensure reproducibility and proper functioning of a method each time it is run. As resolution is the most important criterion of the method, two compounds are added to the ECD standard and are used as resolution markers. The compounds, L-methionine ethyl ester and acetophenone, have retention times that bracket the working range of the gradient. A straightforward calculation of resolution between each of these compounds and ECD ensures that the method is working properly.

To measure system suitability, five injections of an ECD standard containing the markers are used. Table IV gives the measured retention times of each component in the standard, and the measured resolution with respect to ECD.

Chromatography of impurities using the optimized method

This purity-indicating gradient method was developed to detect and resolve oxidation products that affect the optical rotation of the ECD · 2HCl raw material.

TABLE IV

RETENTION TIMES AND RESOLUTION OF MARKERS

n = 4; analyzed in 6 days.

Component	Retention time range (min)	Resolution (compared with ECD)
L-Methionine ethyl ester	2.6 ± 0.02	8.5 ± 0.77
ECD	6.7 ± 0.03	–
Acetophenone	12.9 ± 0.05	10.4 ± 1.55

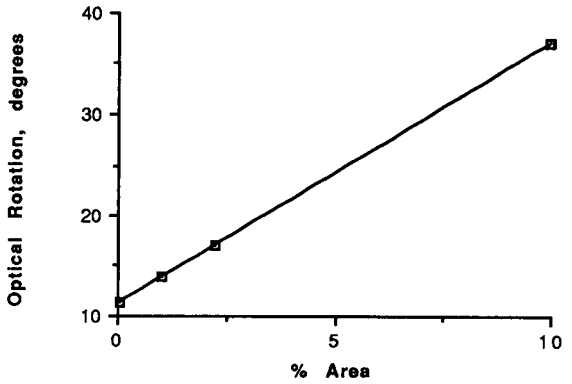

Fig. 5. Correlation of optical rotation and purity analysis of ECD. % Area = total area of impurities from Table V. The linear regression of the data shows a correlation of (optical rotation) = 11.2 + 2.6912x, with correlation coefficient = 1.000.

The raw material can be synthesized in high purity as the L,L-isomer, which has an optical rotation of +11°, and a chiral HPLC method has been developed to determine optical purity of the raw material [11]. Oxidation of the raw material will cause the optical rotation to increase. Three main oxidation impurities are typically seen, and the summed area of impurity peaks can be related to the percentage optical rotation as shown in Fig. 5 and Table V. The amount of oxidation impurities also increases with increasing age of the ECD solution. Efforts to isolate these oxidation products have been attempted without success owing to the complicated chemistry that can occur with dithiol–diamine materials. The oxidation products represent a very small amount of the original ECD · 2HCl, hence this technique is very sensitive to small changes in the quality of ECD · 2HCl.

We have also found excellent resolution for impurities other than those produced by oxidation. Fig. 6 shows the chromatography of a lactam formed by cyclization, a cleavage product (AECEE) and a thiazolidine impurity (EMT).

TABLE V

DETECTION OF OXIDATION PRODUCTS BASED ON OPTICAL ROTATION

Purity	Optical rotation (°)	Area of oxidation impurities (%)
High	11.3	0.03
Medium	13.9	1.01
Low	17.0	2.23
Low	37.0	9.94

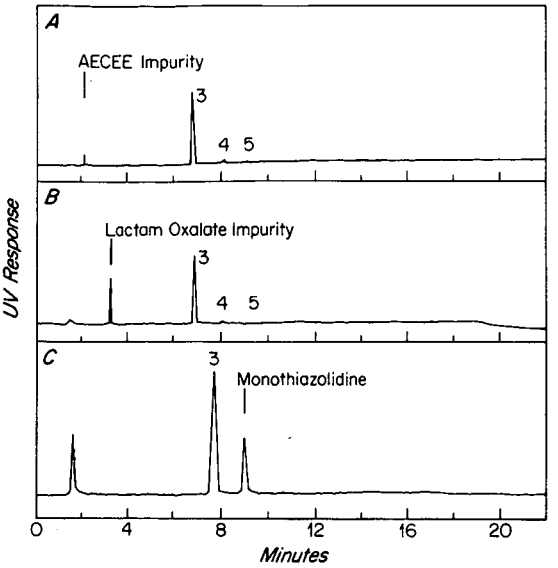

Fig. 6. Detection of impurities other than those produced by oxidation: (A) N-(2-aminoethyl)cysteine ethyl ester (AECEE), a cleavage product; (B) lactam oxalate formed by cyclization; (C) monothiazolidine (EMT). Peaks 3 is ECD and peaks 4 and 5 are two oxidation products.

CONCLUSION

In order for ECD to be used in the manufacture of Neurolite brain imaging agent, the material must meet optical rotation and purity specifications. As the optical rotation is affected by oxidation products, a method for the specific determination of the impurities was developed. A reversed-phase gradient was used to maximize the ability to find and eventually identify all oxidation products and also any potential impurities that may arise in the future. We were able to meet all our goals and reduce the development time with the use of DryLab. The resulting HPLC method is more specific than previous methods and provides excellent resolution of all potential impurities.

ACKNOWLEDGEMENTS

The authors are grateful to Lynne S. Mann for technical assistance and Neal E. Williams and Michelle E. Herrera-Foster for helpful discussions.

REFERENCES

1 J. L. Glajch and L. R. Snyder (Editors), *Computer-Assisted Method Development in Chromatography; J. Chromatogr.*, 485 (1989).
2 L. R. Snyder, J. L. Glajch and J. J. Kirkland, *Practical HPLC Method Development*, Wiley-Interscience, New York, 1988.
3 J. C. Berridge, *Techniques for the Automated Optimization of HPLC Separations*, Wiley-Interscience, New York, 1985.

4 L. R. Snyder, J. W. Dolan and D. C. Lommen, *J. Chromatogr.*, 485 (1989) 65.
5 R. G. Lehman and J. R. Miller, *J. Chromatogr.*, 485 (1989) 581.
6 D. J. Thompson and W. D. Ellenson, *J. Chromatogr.*, 485 (1989) 607.
7 J. D. Stuart, D. D. Lisi and L. R. Snyder, *J. Chromatogr.*, 485 (1989) 657.
8 L. R. Snyder, J. W. Dolan and D. C. Lommen, *J. Chromatogr.*, 485 (1989) 91.
9 P. Blondeau, C. Beerse and D. Gravel, *Can. J. Chem.*, 45 (1967) 49.
10 R. C. Walovitch, T. C. Hill, S. T. Garrity, E. H. Cheesman, B. A. Burgess, D. A. O'Leary, A. D. Watson, M. V. Ganey, R. A. Morgan and S. J. Williams, *J. Nucl. Med.*, 30 (1989) 1892.
11 J. M. Green, R. Jones, D. S. Edwards, J. L. Glajch and N. E. Williams, in preparation.

Journal of Chromatography, 550 (1991) 559–571
Elsevier Science Publishers B.V., Amsterdam

CHROMSYMP. 2229

Determination of free cyanide in gold cyanidation process liquors by ion-interaction chromatography with post-column derivatization

PETER A. FAGAN and PAUL R. HADDAD*

Department of Analytical Chemistry, The University of New South Wales, P.O. Box 1, Kensington, N.S.W. 2033 (Australia)

ABSTRACT

A chromatographic method is described for the determination of high levels of free cyanide in leach liquors encountered in the cyanidation process for the dissolution of gold from its ores. The method also offers simultaneous determination of metallo–cyanide complexes and thiocyanate, which are also present in the sample. A 10-μl aliquot of the sample is first separated by ion-interaction chromatography using a C_{18} column, 25% (v/v) aqueous acetonitrile containing 5 m*M* low-UV PIC A as mobile phase, and UV detection at 214 nm. Cyano complexes of Cu(I), Fe(II), Ag(I), Fe(III) and Au(I) are detected, together with thiocyanate. Linear calibrations were obtained over the concentration ranges in which these species are found in leach liquors. The free cyanide in the sample is eluted at the column void volume and is detected by absorbance at 500 nm [together with thiocyanate and the copper(I) cyano complex] after post-column reaction with N-chlorosuccinimide, barbituric acid and isonicotinic acid to form a polymethine dye. The calibration plot for cyanide was linear over the range 0–300 ppm and no interferences from 1000 ppm levels of common anions were identified, except for sulfide which can be tolerated only up to 500 ppm. Alternative chromatographic hardware configurations offering heart-cut of the cyanide fraction and subsequent ion-exclusion separation of cyanide from other anions are discussed. When applied to leach liquor samples taken from operating gold mines, the chromatographic method is shown to give clean chromatograms and to offer superior accuracy and precision to the conventional silver nitrate titrimetric procedure, especially in the presence of high levels of copper in the sample. On-line operation of the method at a throughput rate of 3 samples per hour is also described.

INTRODUCTION

The most widely used process for extracting gold from its ores involves leaching of the ore with cyanide in the presence of oxygen. Under these conditions, metallic gold is solubilized as the aurocyanide ion, according to the equation [1]:

$$4Au + 8CN^- + O_2 + 2H_2O \leftrightharpoons 4Au(CN)_2^- + 4OH^- \quad (1)$$

The aurocyanide is then recovered from the leach solution, usually by adsorption onto activated carbon. This process is known as carbon-in-pulp recovery and is favoured because of its simplicity and efficiency when applied to low-grade gold ores.

0021-9673/91/$03.50

The rate of dissolution of gold depends on many factors, such as the free cyanide concentration, the oxygen level, the pH of the leach liquor, the concentration of other cyanide consuming species, and the physical characteristics of the ore. However, the single most important of these factors is the free cyanide concentration, which must be monitored at frequent intervals in order to maintain efficient gold dissolution. The optimal free cyanide concentration varies with the nature of the ore and the leaching conditions used, but is usually within the approximate range of 50–300 ppm.

In addition to the free cyanide and the solubilized gold, a typical leach liquor also contains numerous other species produced by reaction of cyanide with components of the ore. These species include other metal cyanide complexes (especially those of iron and copper) and thiocyanate. Determination of the free cyanide in such leach liquors may be approached using titrimetric methods, spectrophotometric methods, or by the use of ion-selective electrodes. Many titrimetric methods exist but the most common approach is to titrate the sample with standard silver nitrate to form $[Ag(CN)_2]^-$, with a precipitate of $Ag[Ag(CN)_2]$ being formed at the end-point [2]. Alternatively, the end-point can be detected with a silver sensitive indicator, such as potassium iodide or 5-(4′-dimethylaminobenzylidene)rhodanine [3]. Potentiometric end-point detection is sometimes applied when the sample solution is coloured. Abundant spectrophotometric methods for free cyanide are available in the literature and can be subdivided broadly into those based on the König reaction [4] and those involving metal complex formation {such as the formation of the $[Ni(CN)_4]^{2-}$ complex [5]}. The König reaction, which converts cyanide to a polymethine dye, is the most widely used. Ion-selective electrodes of the solid-state [6] or membrane types [7] are also applicable to free cyanide determinations.

When applied to the routine monitoring of free cyanide in leach liquors, all of the above-mentioned analytical methods suffer from appreciable drawbacks. The spectrophotometric methods are prone to numerous interferences (such as sulfide and thiocyanate) which are likely to be present in the leach liquor, and do not have an appropriate linear calibration range for the concentration of cyanide typically encountered in such samples. The ion-selective electrode methods have the disadvantages of slow response, poor reproducibility and the requirement for sample dilution. The most rugged (and therefore the most frequently utilized) method is titration using rhodanine indicator, but this approach is very operator dependent, is not amenable to automation or on-line operation, and is also prone to interferences. Paramount amongst these interferences is the presence of copper cyanide complexes in the liquor. Copper(I) forms cyano complexes containing between 2 and 4 cyanide ions, with the most stable form being $[Cu(CN)_2]^-$ ($\log K_f = 23.9$ [8]). Copper cyano complexes with 3 or 4 cyanide ligands are formed at high concentrations of cyanide and a significant amount of the cyanide bound in these complexes is titratable with silver nitrate. Thus, routine titration procedures applied to copper-containing ores can yield erroneously high results for free cyanide unless care is taken to account for the level of copper in the leach liquor. Failure to make this correction can lead to a decrease in the rate of gold dissolution in the leaching process and ultimately, a reduction in gold recovery.

For some years, we have been studying the chromatographic behaviour of metallo-cyanide complexes and we have shown that most of the stable complexes can be separated by ion-interaction chromatography and detected by UV absorbance at 214 nm [9]. Moreover, we have also demonstrated that the cyano complexes of gold

(I), platinum(II) and palladium(II) can be concentrated on a suitable pre-column and then separated by ion-interaction chromatography to give detection limits of less than 1 ppb (μg/l) [10]. This approach has been applied to the determination of gold in carbon-in-pulp tailings solutions [11]. In the present paper, these studies are extended to include the determination of high levels of free cyanide in carbon-in-pulp leach liquors, without interference from labile metallo–cyanide complexes or other ionic components of the leach liquor, including thiocyanate. Furthermore, this method also permits simultaneous determination of metallo–cyanide complexes in the leach liquor, so that information on both the free and bound forms of cyanide can be obtained from a single analysis.

EXPERIMENTAL

Instrumentation

Ion-interaction system. All liquid chromatographic instrumentation used in this work was manufactured by Waters Chromatography Division of Millipore (Milford, MA, USA). The basic hardware comprised an ion-interaction chromatographic system, which was used to separate free cyanide from other constituents of leach liquor. This system consisted of a Model 510 pump, Model U6K injector, Model 441 fixed-wavelength absorbance detector operated at 214 nm, and a Model Baseline 810 data station. A Nova-Pak C_{18} column (150 × 4.6 mm I.D.) was used.

Post-column reaction system. The post-column reaction system for derivatization of free cyanide consisted of a Waters dual-pump post-column pumping system and two knitted open tubular reaction coils containing 40 cm and 30 m, respectively, of 0.22 mm I.D. PTFE tubing. Further details of this system are given later. The derivatized free cyanide was then passed to a Model 484 variable-wavelength absorbance detector operated at 500 nm. The output of this detector was recorded by the data station.

Hardware configurations. The basic ion-interaction system and the post-column reaction system were interfaced in several ways, as shown in Fig. 1. In the simplest case, shown in Fig. 1a, the effluent emerging from the UV detector in the ion-interaction system was passed directly into the post-column reactor (PCR). This approach will be referred to as a "tandem" system. The second approach (Fig. 1b) involved passing the effluent from the UV detector in the ion-interaction system through a 6-port rotary valve. This valve could direct the effluent either to waste or to the post-column reactor. In this way, a selected portion (or "cut") of the effluent could be transferred to the post-column reactor. A second Model 510 pump was employed to carry the sample to the post-column reactor. Rotation of the 6-port valve was accomplished by pneumatic pressure, under the control of the computer data station. This method will be referred to as a "cut" system. The third configuration (Fig. 1c) was identical to the "cut" system, except that a Millipore Waters Fast Fruit Juice ion-exclusion column (150 × 7.8 mm I.D.) was inserted prior to the post-column reactor as a means of separating free cyanide from any components co-eluted from the ion-interaction system. This approach will be referred to as a "coupled" system.

On-line system. On-line operation was employed in the latter stages of this work. This was accomplished by use of a Filtrate Master (Flow Measurement Services, Perth, Australia) filtration unit, which was inserted into a 500-l tank of carbon-

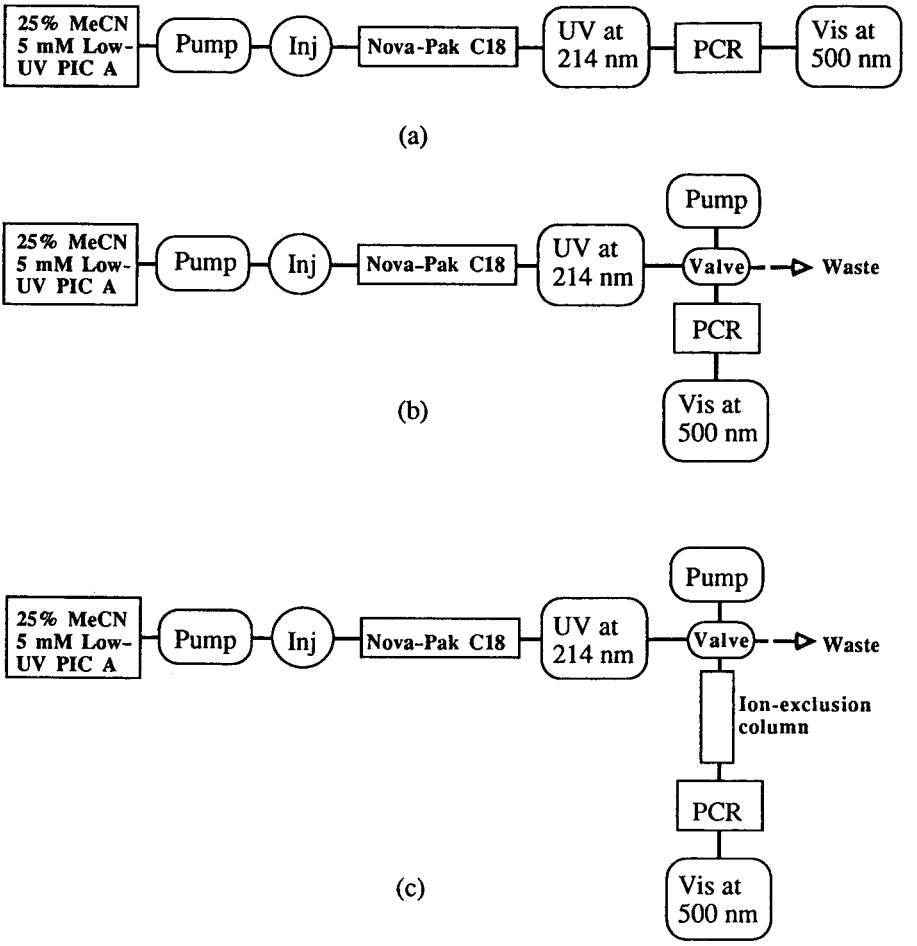

Fig. 1. Chromatographic hardware configurations used in this study. The post-column reactor is designated by PCR. (a) "Tandem" system, (b) "cut" system, (c) "coupled" system (MeCN = acetonitrile).

in-pulp leach liquor taken from an operating gold mine. The leach liquor was agitated using an electric motor connected to a suitable impeller. The filtrate from the Filtrate Master unit was pumped to a 10-μl sample loop connected across a 6-port high pressure rotary valve. This valve replaced the injector in the ion-interaction system. The position of the valve was controlled by the computer data station and rotation of the valve was achieved with pneumatic pressure. Filtered leach liquor was passed continuously through the 10-μl sample loop and the contents of the loop were injected into the chromatographic system, as required, by use of the appropriate valve position.

Reagents and procedures

All reagents used were of analytical-reagent grade. N-Chlorosuccinimide, succinimide, barbituric acid and isonicotinic acid were obtained from Aldrich (Mil-

waukee, WI, USA). Potassium aurocyanide was purchased from Johnson and Matthey Chemicals (London, UK), whilst potassium salts of the cyano complexes of Ag(I), Cu(I), Fe(II) and Fe(III) were synthesized according to published methods [12]. Chromatographic grade acetonitrile (UV cut-off 190 nm) was obtained from Millipore Waters. The mobile phase used in the ion-interaction chromatographic system comprised a 25% (v/v) aqueous solution of acetonitrile in 5 m*M* low UV PIC A, which was obtained from Millipore Waters. The carrier fluid used in the "cut" system shown in Fig. 1b was acetonitrile–water (25:75, v/v), and water served as the eluent for the ion-exclusion column used in the coupled system shown in Fig. 1c. All eluents were filtered through a 0.45-μm membrane filter and degassed in an ultrasonic bath prior to use. The flow-rate was 1 ml/min in all cases.

Two reagents were used in the post-column reactor, as shown in Fig. 2. The first reagent consisted of 0.1% (w/v) N-chlorosuccinimide and 1% (w/v) succinimide. A stock solution of 10% succinimide in water was prepared and the post-column reagent was prepared by dissolving 0.1 g of N-chlorosuccinimide in 10 ml of the succinimide stock solution, followed by dilution to 100 ml with water, in a volumetric flask. The reagent was prepared daily. The second post-column reagent consisted of 0.5% (w/v) isonicotinic acid and 0.25% (w/v) barbituric acid dissolved in dilute lithium hydroxide solution, after which the solution was buffered to pH 7.0 with phosphoric acid. Addition of the buffer was essential to maintain stability, and under the conditions described, the reagent was stable for 3 weeks. Both of the post-column reagents were filtered through a 0.45-μm membrane filter before use. The flow-rate of the N-chlorosuccinimide–succinimide reagent was 0.4 ml/min, and the same flow-rate was used for the isonicotinic acid–barbituric acid reagent. Further details on the post-column reactor are shown in Fig. 2.

RESULTS AND DISCUSSION

Selection of analytical methodology

The first step in the development of a chromatographic procedure for the determination of free cyanide in carbon-in-pulp leach liquors was to identify chromatographic conditions under which free cyanide could be separated from as many of the components of the leach liquor as possible. Coupled with this requirement was the desire to resolve those key components of the leach liquor which might yield important analytical information to the plant operator. We identified these key components as thiocyanate and the cyano complexes of silver(I), copper(I), iron(II), iron(III) and gold(I). From our previous experience with the separation of these complexes, and

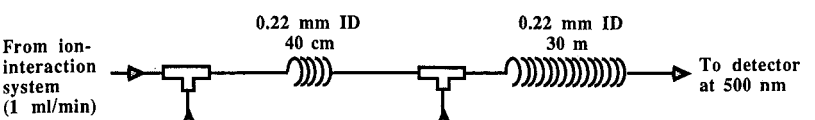

Fig. 2. Details of the post-column reactor used.

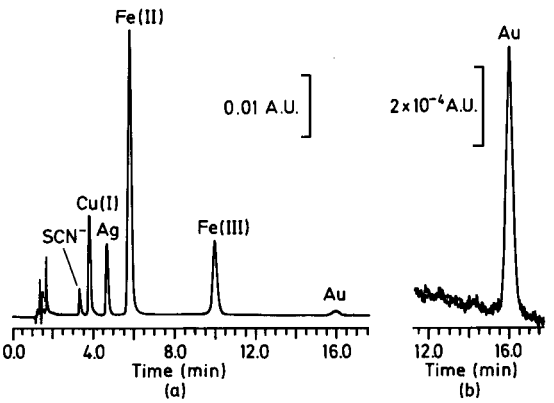

Fig. 3. Chromatogram obtained for the separation of free cyanide, thiocyanate and some metallo–cyano complexes by ion-interaction chromatography. Note that the free cyanide is not detected. Conditions: Waters Nova-Pak C_{18} column, with 25% (v/v) aqueous acetonitrile containing 5 m*M* low-UV PIC A as eluent at a flow-rate of 1 ml/min, with detection by UV absorbance at 214 nm. A 10-μl injection volume was used. Solute concentrations: SCN^- (3 ppm), cyano complexes of Cu(I) (1.5 ppm), Ag(I) (2 ppm), Fe(II) (2 ppm), Fe(III) (2 ppm) and Au(I) (1 ppm); CN^- (100 ppm). A higher scale expansion was used for (b) than for (a).

with the aid of a computer-assisted technique for selection of the optimal mobile phase composition, we found that 25% (w/v) acetonitrile in 5 m*M* low-UV PIC A was a suitable mobile phase. The separation achieved using this mobile phase with a Nova-Pak C_{18} column is shown in Fig. 3a. In this chromatogram, the concentrations of the species approximate those likely to be present in a carbon-in-pulp leach liquor. It can be seen that all components are well resolved and that the gold(I) peak can be quantified readily by appropriate scale expansion on the data system (Fig. 3b). Calibration plots constructed for all the species shown in Fig. 3 were linear up to the maximum concentrations tested, which were as follows: 300 ppm for thiocyanate and copper(I), 50 ppm for iron(II) and 20 ppm for iron(III), silver(I) and gold(I). It should be noted that these concentrations refer to the metal ions rather than to the complexes themselves.

The free cyanide eluted from the column is not detected at 214 nm, but collection and derivatization of mobile phase fractions revealed that this species was unretained on the column and was eluted at the void volume. It was therefore feasible that the small volume of mobile phase containing the free cyanide could be further analyzed to dermine the free cyanide concentration. To accomplish this, it was necessary to select appropriate analytical methodology to permit the determination of the eluted free cyanide in the presence of the mobile phase components and of any co-eluted components of the leach liquor. Moreover, any analytical technique used should be amenable to on-line operation so that the analysis could be automated. After consideration of these constraints, several possibilities existed, including the use of ion chromatography with conductometric or amperometric detection, and spectrophotometry using a flow-through reactor. We investigated the use of ion chromatography using anion-exchange columns, but this approach was abandoned because of interferences caused by acetonitrile and tetrabutylammonium ions (from the low-UV

PIC A). In addition, it was found that common inorganic anions present in the leach liquor, such as chloride and sulphate, were co-eluted with free cyanide on the ion-interaction system and these either eluted from the ion-exchange column at the same time as cyanide or were so strongly retained that excessive run times were necessary. On the other hand, a selective spectrophotometric reaction appeared more suitable, provided that any interfering species present in the free cyanide band could be removed. For this reason, we examined a wide range of spectrophotometric procedures for cyanide which could be adapted to a continuous flow system.

Chemistry of the post-column reaction

Many derivatisation reactions have been developed for the analysis of cyanide, with the single most common method involving variations of the König reaction [4]. These reactions were chosen for investigation in view of their high selectivity towards cyanide and because they have been utilized in continuous-flow, flow-injection and post-column reaction analysis systems [13,14].

The König reaction can be considered as three separate steps: (i) Chlorination (or bromination) of cyanide to give cyanogen chloride, a source of CN^+. (ii) Reaction of the CN^+ with pyridine or a pyridine derivative to produce a conjugated dialdehyde intermediate. (iii) Coupling of this aldehyde with one or two molecules of an aromatic amine or a compound containing reactive methylene protons to produce a conjugated, resonance stabilised polymethine dye [15,16].

Chlorination is preferred in a closed post-column reaction system since bromination requires the addition of arsenite to destroy the excess bromine which would otherwise prevent the formation of the dye [17]. The usual chlorination reagent is chloramine-T, but this reagent is not optimal for use in flow-through reactors because of the likelihood of precipitate formation. An alternative chlorination reagent, N-chlorosuccinimide [15], was found to be more suitable because its reaction product, succinimide, was soluble in water.

Pyridine and two of its derivatives, 4-methylpyridine (4-picoline) [18] and pyridine-4-carboxylic acid (isonicotinic acid) [19,20], have been used to form the dialdehyde. Pyridine has been used widely, but in view of the toxicity and unpleasant odours of pyridine and 4-picoline, we preferred to use isonicotinic acid, which is odourless and has minimal toxicity.

The most commonly used coupling reagent at present is barbituric acid [21], whilst others have included 3-methyl-1-phenyl-2-pyrazolin-5-one (pyrazolone) [22], *p*-phenylenediamine [23], benzidine [17], anthranilic acid [24], sulphanilic acid [25] and amsonic acid [26]. Benzidine is a carcinogen and *p*-phenylenediamine is a suspected carcinogen [27]. We have elected to use barbituric acid on the basis of toxicity considerations and ease of reagent preparation.

The reaction scheme for the derivatization of cyanide is shown in Fig. 4. N-Chlorosuccinimide (I) reacts with cyanide to produce cyanogen chloride and succinimide (II). The cyanogen chloride further reacts with isonicotinic acid (III) to give the intermediate product (IV) which hydrolyses to the dialdehyde (V). Barbituric acid (VI) condenses with the dialdehyde to produce a dye species (VII), which on standing condenses with a further molecule of barbituric acid to give a second polymethine dye (VIII). Several authors have noted that there are two distinct wavelengths of maximum absorbance associated with this reaction [19,20]. The first absorbance maximum

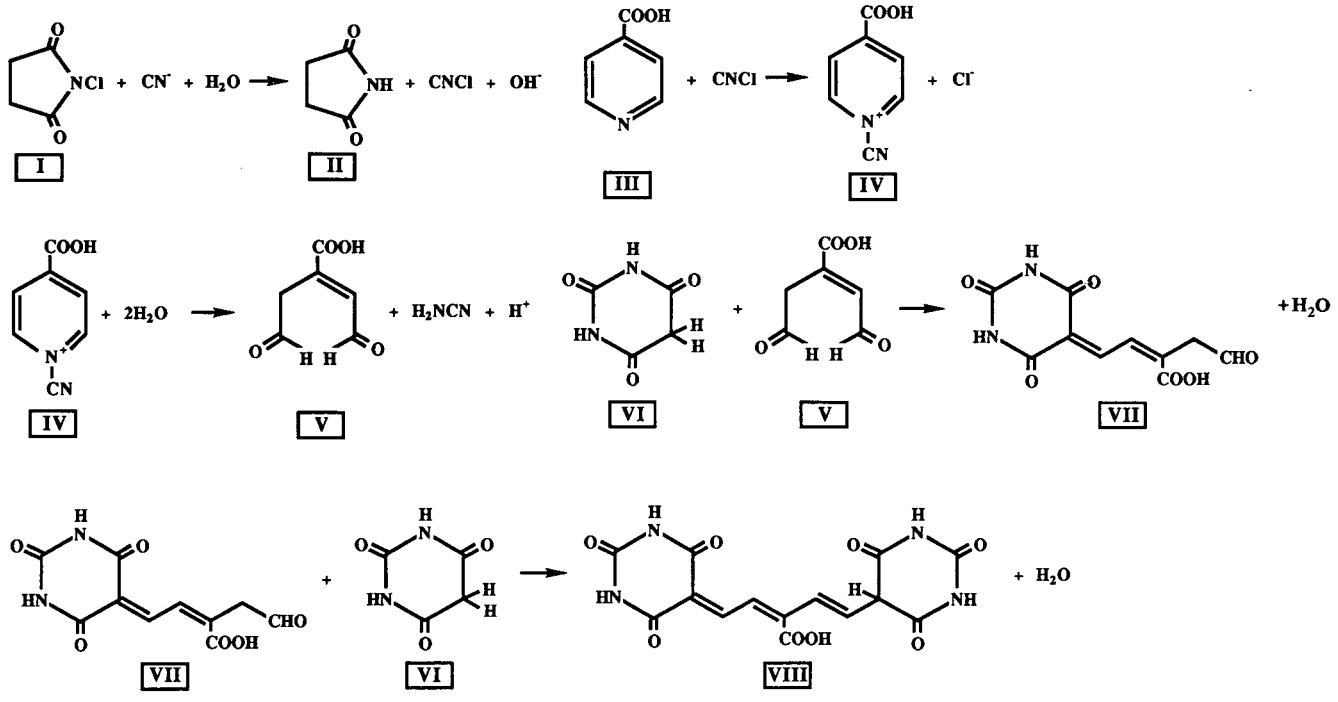

Fig. 4. Reaction scheme for the post-column derivatisation. See text for discussion. I = N-Chlorosuccinimide; II = succinimide; III = isonicotinic acid; IV = reaction intermediate; V = pent-2-enedial-3-carboxylic acid; VI = barbituric acid; VII = first dye species; VIII = second dye species.

appears rapidly at 525 nm and is due to the formation of the first dye species (VII). The second maximum occurs at 600 nm and is attained after approximately 15 min. This maximum is due to the formation of the polymethine dye (VIII) and is of greater magnitude than the first absorbance maximum. Under flow-through reaction conditions, the first maximum is the most useful because of its rapid formation and was therefore applied in this work.

The reaction conditions were then optimized to provide a suitable response to the range of cyanide concentrations expected in the samples to be analyzed. The detection wavelength was altered to 500 nm to reduce sensitivity and the isonicotinic acid and barbituric acid concentrations were varied until linearity of the cyanide calibration plots was achieved. The method was further modified by buffering the isonicotinic acid–barbituric acid reagent to pH 7.0 with phosphoric acid. This avoided the requirement to add a phosphate buffer as a post-column reagent (as used by Toida *et al.* [14]), improved the stability of this reagent, and provided a suitable pH for dye formation.

It was found that a gradual decrease in the absorbance of a derivatized 100 ppm cyanide standard in 10 m*M* lithium hydroxide was observed. This was attributed to instability of the N-chlorosuccinimide–succinimide reagent and could be prevented if this reagent was prepared freshly on a daily basis.

Evaluation of hardware configurations

As can be seen from Fig. 1, there are three possible ways in which the post-column reactor can be coupled to the ion-interaction chromatographic system. The "tandem" approach is the simplest, but has the disadvantage that all components of the leach liquor, including those which are co-eluted with free cyanide, are passed to the reactor. The use of a switching valve to select a desired portion of the free cyanide band (*i.e.*, the "cut" system shown in Fig. 1b) partly obviates this disadvantage but introduces the further problem of deciding which portion of the cyanide band should be passed to the post-column reactor. Full separation of the free cyanide from any co-eluted species can be achieved by passing the cut fraction through a suitable chromatographic column (*i.e.*, the "coupled" system shown in Fig. 1c), but again, the timing of the cut is critical. Preliminary experiments showed that free cyanide could be resolved from most common inorganic anions and all metallo–cyanide complexes which are weakly retained on the ion-interaction system by use of an ion-exclusion column with water as eluent. Under these conditions, the cyanide is present predominantly as undissociated hydrocyanic acid, which is moderately well retained on the ion-exclusion column used (Millipore Waters Fast Fruit Juice column). In contrast, all fully ionized inorganic species are unretained.

Chromatograms from injections of cyanide were obtained for each of the possible hardware configurations. Well-shaped peaks for the derivatized cyanide were observed in all cases. When the "coupled" system was employed, with water as eluent for the ion-exclusion column, cyanide was eluted at a retention time of 6.9 min. In comparison, fully ionized inorganic anions were eluted at the column void time (2.2 min), showing that these species were well resolved from the peak for free cyanide.

Calibration plots were constructed for each hardware configuration over the range 0–300 ppm of free cyanide, using 10-μl injections onto the ion-interaction chromatographic system. All hardware configurations yielded linear calibrations. Precision was less than 1% relative standard deviation (R.S.D.) for each system.

These results suggest that all three hardware configurations could be applied successfully to the determination of free cyanide in leach liquors. Clearly, the mechanical complexity of the system increases as one moves from the "tandem" to the "coupled" systems, but at the same time, the ability of the system to tolerate interferences increases. The choice between the hardware configurations is therefore dependent on the types of interferences observed in the particular post-column reaction employed.

Interferences

Known interferences in the König reaction used in this study include thiocyanate, labile metallo–cyanide complexes and sulfide. The first two of these yield positive interference by producing coloured reaction products which absorb at the detection wavelength, whilst sulfide gives negative interference by reacting with the oxidant. Under the chromatographic conditions used in the ion-interaction system, free cyanide is separated from both thiocyanate and $[Cu(CN)_4]^{3-}$, which is the only labile cyano complex likely to be present in appreciable concentrations in the samples analyzed. Common inorganic anions, including sulfide, are partially co-eluted with the free cyanide. The interference effects of these ions were examined by preparing 100-ppm cyanide standards containing 1000 ppm of each potential interferent. The peak area for free cyanide was altered by less than 1% for chloride, sulfate, nitrate, nitrite and phosphate, whilst sulfide caused a moderate interference (20%) at this level. A more detailed study of the interferences effects of sulfide was undertaken and showed that this interference is not evident for sulfide concentrations up to 500 ppm. Sulfide interference can be overcome using the "coupled" chromatographic system, but this was not considered necessary for the samples analyzed because the sulfide levels were below the interference threshold. Moreover, sulfide may be removed easily before analysis by treatment of the sample with lead acetate, followed by filtration.

The question of interference effects from $[Cu(CN)_4]^{3-}$ merits further examination. This species is likely to be present in samples which have significant copper content and also a high level of free cyanide (*e.g.* 50 ppm). Whilst the copper complex itself is separated from free cyanide, the dissociation equilibrium of this complex (see eqns. 2 and 3) will contribute some free cyanide to the solution:

$$[Cu(CN)_4]^{3-} \rightleftharpoons [Cu(CN)_3]^{2-} + CN^- \quad (2)$$

$$[Cu(CN)_3]^{2-} \rightleftharpoons [Cu(CN)_2]^- + CN^- \quad (3)$$

The equilibrium constant for eqn. 2 is $3.16 \cdot 10^{-2}$, whilst that for eqn. 3 is $5.01 \cdot 10^{-6}$ [8]. Injection of $[Cu(CN)_4]^{3-}$ should therefore produce a small peak for free cyanide, and this is observed in practice. When the level of free cyanide is high, as is the case for leach liquors, both of the above equilibria will be forced to the left. It would therefore be expected that a mixture of $[Cu(CN)_4]^{3-}$ and free cyanide should produce two peaks after the post-column reaction, the first being due to free cyanide and the second resulting from dissociation of the labile copper cyano complex in the post-column reactor. Again, this corresponds to the observed behaviour. A series of experiments was performed in which increasing amounts of $[Cu(CN)_4]^{3-}$ were added to solutions of 100 ppm and 500 ppm free cyanide and these solutions were injected. It

was found that the free cyanide peak height for the 100-ppm cyanide solution showed a small increase as the concentration of added copper was increased. Moreover, this increase was in approximate accordance with the calculated levels of free cyanide which would be produced from dissociation of the complex according to eqns. 2 and 3. However, there was virtually no change in the cyanide peak for the 500 ppm solutions, even when 300 ppm of $[Cu(CN)_4]^{3-}$ was added. This effect was due to suppression of the dissociation of the complex as a result of the high level of free cyanide. The chromatographic system used in this work should therefore provide a true measure of the free cyanide present in the sample, without interference from copper cyano complexes.

These interference studies suggest that the simplest hardware configuration, namely the "tandem" system, should be applicable to the analysis of many leach liquor samples. This configuration was therefore applied to a series of real samples and these analyses are discussed below.

Applications to the analysis of leach liquors

The proposed method was applied to a number of leach liquors taken from operating carbon-in-pulp processing plants. Chromatograms were obtained by direct injection of 10 μl of the filtered leach liquor and a typical chromatogram is shown in Fig. 5. Considering the complexity of the sample, the chromatogram is remarkably clean and permits ready quantification of the metallo–cyanide complexes, as well as free cyanide and thiocyanate. It will be noted that the chromatogram recorded after the post-column derivatisation reaction (Fig. 5c) shows peak for thiocyanate and $[Cu(CN)_4]^{3-}$, as well as for free cyanide. However, these components are well resolved from free cyanide and do not interfere.

A comparison of free cyanide values obtained by the proposed method and by titration with silver nitrate using the rhodanine indicator was undertaken. The results obtained for two particular samples are representative of this study and are shown in Table I. Sample A was low in copper (1.7 ppm) and there was very good agreement

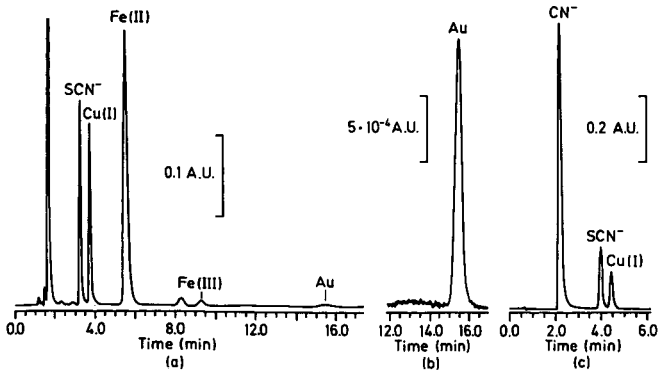

Fig. 5. Chromatogram obtained for a leach liquor. The sample injection volume was 10 μl. Chromatographic conditions as for Fig. 4; post-column reaction conditions as for Fig. 3. The "tandem" hardware configuration (Fig. 1a) was used. The output of the UV detector is shown in (a) and (b), whilst (c) shows absorbance at 500 nm after post-column reaction.

TABLE I

COMPARISON OF TITRIMETRIC AND CHROMATOGRAPHIC METHODS FOR THE DETERMINATION OF FREE CYANIDE IN LEACH LIQUORS

Sample	Copper content (ppm)	Free cyanide (ppm)			
		Titration method	Tandem system	Cut system	Coupled system
A	1.7	56.6	57.2	56.3	52.6
B	140	134	116	–	–

between the cyanide levels obtained by titration and those for the proposed method, using each of the hardware configurations. This agreement confirms the accuracy of the proposed method since the titrimetric method is known to be reliable when the level of copper is low. On the other hand, sample B contains 140 ppm of copper and it can be seen from Table I that the titrimetric method yielded a higher result for free cyanide than did the chromatographic method. This disparity can be attributed to interference of the copper cyano complex in the titrimetric procedure. Moreover, the precision of the titrimetric method for sample B was very poor (11% R.S.D.), whilst that for the chromatographic method was good (0.2% R.S.D.).

Limited experiments were carried out to show the feasibility of on-line operation of the chromatographic method. A filtration probe was inserted into the leach liquor and the filtrate emerging from this unit was found to be free of particulate material of diameter greater than 0.5 μm. This filtrate was therefore suitable for chromatographic analysis and was pumped directly to the sampling loop and thence to the liquid chromatograph. Analyses were performed at the rate of 3 samples per hour and excellent reproducibility was obtained for replicate chromatograms. These results suggest that the method can be adapted readily for on-line use, provided that the analytical hardware can be sited in relatively close proximity to the leach tank in order to prevent loss of cyanide transport of the sample to the instrument.

CONCLUSIONS

The proposed chromatographic method offers a simple approach to the simultaneous determination of free cyanide, metallo–cyanide complexes and thiocyanate in cyanidation leach liquor samples. No significant interferences were found with the derivatisation chemistry used in this work, but in the event that alternative post-column derivatisation reactions are preferred, it is possible to employ the coupled chromatographic system in order to further separate the free cyanide from potential interferences. Precision and accuracy of the chromatographic procedure are good and the method is amenable to on-line operation. A field trial of this system in a working gold processing plant is currently in progress.

ACKNOWLEDGEMENTS

Financial support from the Australian Research Council and Metana Minerals

is gratefully acknowledged. Patent applications on the technology described in this paper are pending.

REFERENCES

1 G. G. Stanley, *Extractive Metallurgy of Gold in South Africa, Vol. 2 (Monograph Series, M7)*, South African Institute of Mining and Metallurgy, Johannesburg, 1987.
2 W. J. Williams, *Handbook of Anion Determinations*, Butterworths, London, 1979, p. 73.
3 *Standard Methods for the Examination of Water and Wastewater*, American Public Health Association, Washington, DC, 16th ed., 1985.
4 W. König, *J. Prakt. Chem.*, 69 (1904) 105.
5 M. W. Scoggins, *Anal. Chem.*, 44 (1972) 1294.
6 M. S. Frant and J. W. Ross, *Science*, 154 (1966) 1553.
7 E. Pungor and K. Toth, *Analyst (London)*, 95 (1970) 1553.
8 A. G. Sharpe, *The Chemistry of the Cyano Complexes of the Transition Metals*, Academic Press, London, 1976.
9 D. F. Hilton and P. R. Haddad, *J. Chromatogr.*, 361 (1986) 141–150.
10 P. R. Haddad and N. E. Rochester, *Anal. Chem.*, 60 (1988) 536–540.
11 P. R. Haddad and N. E. Rochester, *J. Chromatogr.*, 439 (1988) 23–36.
12 J. C. Bailar (Editor), *Comprehensive Inorganic Chemistry*, Pergamon Press, Oxford, 1973.
13 T. Imanari, S. Tanabe and T. Toida, *Chem. Pharm. Bull.*, 30 (1982) 3800.
14 T. Toida, T. Togawa, S. Tanabe and T. Imanari, *J. Chromatogr.*, 308 (1984) 133.
15 J. L. Lambert, J. Ramasamy and J. V. Paukstells, *Anal. Chem.*, 47 (1975) 509.
16 R. B. Roy, *Int. Lab.*, Sept./Oct. (1988) 47.
17 J. L. Royer, J. E. Twichell and S. M. Muir, *Anal. Lett.*, 6 (1973) 619.
18 S. Nagashima, *Anal. Chim. Acta*, 91 (1977) 303.
19 S. Nagashima and T. Ozawa, *Int. J. Environ. Anal. Chem.*, 10 (1981) 99.
20 Z. Zhu and Z. Fang, *Anal. Chim. Acta.*, 198 (1987) 25.
21 A. Tanaka, K. Mashiba and T. Deguchi, *Anal. Chim. Acta*, 214 (1988) 259.
22 S. Nagashima, *Water Res.*, 17 (1983) 833.
23 R. W. Siergiej and N. D. Danielson, *J. Chromatogr. Sci.*, 21 (1983) 362.
24 S. Upadhyay and V. K. Gupta, *Analyst (London)*, 109 (1984) 1619.
25 S. Sunita and V. K. Gupta, *J. Ind. Chem. Soc.*, 64 (1987) 431.
26 E. Casassas, R. Rubio and G. Rauret, *Analyst (London)*, 109 (1984) 1159.
27 N. I. Sax and R. J. Lewis, *Dangerous Properties of Industrial Substances*, Van Nostrand Reinhold, New York, 7th ed., 1989.

Journal of Chromatography, 550 (1991) 573–584
Elsevier Science Publishers B.V., Amsterdam

CHROMSYMP. 2090

Chromatographic data for pharmacological classification of imidazol(in)e drugs

RENE GAMI-YILINKOU and ROMAN KALISZAN*
Department of Biopharmaceutics and Pharmacodynamics, Medical Academy of Gdańsk, Gen. J. Hallera 107, 80-416 Gdańsk (Poland)

ABSTRACT

A set of eighteen imidazol(in)e derivative drugs of various pharmacological activity were analysed under different high-performance liquid chromatographic (HPLC) conditions. Capacity factors were determined employing methanol–buffer eluents at seven volume ratios and at pH 10.9, 7.0 and 2.9. The use of an alkaline buffer was possible owing to the application of poly(butadiene)-coated alumina (PBCA) as the stationary phase. Two systems employing octadecylsilica (ODS) columns were applied, one operated at pH 7.0 and the other at pH 2.9. Capacity factors of the test solute drugs were determined in 21 chromatographic systems. All the data were subjected to chemometric analysis despite the fact that, except for the PBCA systems, only a limited range of linearity of the logarithm of capacity factor *versus* volume fraction of methanol in mobile phase was observed. The matrix of 21 × 18 capacity factors was statistically analysed by the principal component method. The first two principal components accounted for 80% of the variance in the capacity factors studied. The principal component object scores clearly separated the agents into groups in accordance with their pharmacological classification. It was concluded that diverse retention data can provide more information relevant to the bioactivity of solutes than just a one-dimensional hydrophobicity scale.

INTRODUCTION

Since Boyce and Milborrow [1] related thin-layer chromatographic (TLC) data to the biological activity of a series of solutes, chromatography has been extensively exploited by medicinal chemists for the determination of the physico-chemical properties of drugs [2]. The property of greatest importance for bioactivity is the lipophilicity (hydrophobicity) of an agent. Chromatography [in particular high-performance liquid chromatography (HPLC)] offers a convenient approach to hydrophobicity parameterization. Much effort has been devoted to the application of chromatography for this purpose. The most recent HPLC methods and procedures for hydrophobicity determination are reviewed elsewhere [3].

Certainly hydrophobicity is an important but by no means the exclusive structural property determining the pharmacological activity of chemical substances. Thus, the attempts by most workers to prepare "purely hydrophobic" chromatographic systems (or systems mimicking the 1-octanol–water partitioning processes) can be questioned. Dynamic processes of tissue penetration and drug–receptor interactions in a living system resemble the mass transfer and intermolecular

0021-9673/91/$03.50

interactions during chromatographic separation. One can therefore expect the chromatographic data to comprise more information relevant to bioactivity than just a one-dimensional hydrophobicity scale.

To derive a chromatographic measure of hydrophobicity one usually extrapolates logarithms of the capacity factor, $\log k'$, obtained in reversed-phase systems at several compositions of an organic–buffer eluent to 100% buffer as a mobile phase. In this way one assumes a linear relationship between $\log k'$ and the volume fraction of an organic modifier in a binary aqueous eluent. Such a relationship was suggested by Soczewiński and Wachtmeister [4]. Observed deviations from linearity were accounted for by the quadratic model proposed by Schoenmakers *et al.* [5]. However, Snyder *et al.* [6] demonstrated that over a limited range of compositions of a binary mobile phase the linear relationship can be used as a good approximation of the general quadratic equation. Although the range of linearity varies depending on the nature of the solute and the properties of the chromatographic system employed, the assumption of linearity generally works. Whatever the physical meaning of the extrapolated capacity factors (often different from those determined experimentally with 100% buffer as eluent), satisfactory correlations are usually reported between such extrapolated $\log k'_w$ data and the conventional hydrophobicity parameter, namely the logarithm of the 1-octanol–water partition coefficient, $\log P$.

If chromatography is to serve for hydrophobicity determination, then retention data that do not confirm the linear relationship between $\log k'$ and the volume fraction of organic modifier in the binary aqueous eluent, X_{org}, are discarded. Such discarded data are reproducible and vary with changes in the chromatographic systems, however. Hence they must comprise systematic information on properties of the solutes chromatographed. Bearing that in mind, we attempted to extract the systematic information concerning a set of test solutes by chemometric analysis of a complete table of retention data determined in various reversed-phase HPLC systems and not subjected to any preselection.

An interesting and challenging task was to relate the structural information provided by chromatography to the pharmacological properties of solutes. Having collected a representative set of imidazol(in)e drugs of different biological activity, we attempted to compare their established pharmacological classification with that resulting from chromatographic behaviour.

The imidazol(in)e test solutes considered here are circulatory drugs exerting their activity through the so-called adrenergic receptors of the α type. Some of the agents are known to bind preferentially to the α-1 subtype whereas the other have higher affinity to the α-2 subtype of adrenoceptor. After binding, some agents stimulate the receptor whereas the other inactivate it. Based on drug–receptor interactions, the imidazol(in)es considered may be classified as α-1 agonists, α-2 agonists, α-1 antagonists and α-2 antagonists. For the sake of this project we applied basically the classification scheme elaborated by Timmermans and van Zwieten [7]. Leaving aside the details not related to chromatography, one should note that the hydrophobicity of the agents does not allow their pharmacological classification [8,9].

EXPERIMENTAL

Materials

The series of eighteen drug solutes consisted of fifteen imidazoline, two imidazole and one thiazine derivatives. The following agents agents were chromatographed after dissolution in the mobile phase: cirazoline hydrochloride (a gift from Dr. J. Cavero, Synthelabo, Paris, France), detomidine hydrochloride and medetomidine hydrochloride (a gift from Dr. A. Karjalainen, Farmos-Group, Oulu, Finland), tiamenidine hydrochloride (a gift from Hoechst, Frankfurt, Germany), oxymetazoline hydrochloride (a gift from Schering, Bloomfield, IN, USA), lofexidine hydrochloride (a gift from Dr. H. Betzing, Nattermann, Cologne, Germany), phentolamine methanosulphate (Regitine; Ciba-Geigy, Basle, Switzerland), clonidine hydrochloride (Haemiton; Germed, Dresden, Germany), xylazine hydrochloride (Rotar; Spofa Prague, Czechoslovakia), moxonidine (a gift from Dr. B. I. Armah, BDF Research Labs., Hamburg, Germany), UK-14, 304 tartrate (a gift from Pfizer Central Research, Sandwich, UK), tramazoline hydrochloride (Rhinospray; a gift from Karl Thome, Biberach am Riess, Germany) and xylometazoline hydrochloride, tymazoline hydrochloride, naphazoline nitrate, antazoline hydrochloride, tetryzoline hydrochloride and tolazoline hydrochloride (Polfa, Warsaw, Poland).

A poly(butadiene)-coated alumina (PBCA) column was kindly supplied by Professor R. A. Hartwick (Rutgers University, Piscataway, NJ, USA). The column was 150 × 4.6 mm I.D., slurry packed with poly(butadiene)-coated Spherisorb A5Y using isopropanol as the slurry solvent and methanol as the packing solvent. The stationary phase was prepared according to the procedure of Schomburg and co-workers [10,11]. An ODS column (100 × 4.0 mm I.D., 5 μm particle size) was purchased from POCh (Lublin, Poland).

Universal buffer (Britton–Robinson buffer) was prepared at pH 2.9, 7.0 and 10.9. To obtain pH 2.9, 18.0 ml of 0.2 *M* NaOH were added to 100 ml of a solution of 0.04 *M* CH_3COOH, 0.04 *M* H_3PO_4 and 0.04 *M* H_3BO_3. To obtain pH 7.0 the corresponding volume of 0.2 *M* NaOH was 52.5 ml and to obtain pH 10.9 it was 82.5 ml.

Mobile phases were made by mixing the buffers with methanol (analytical-reagent grade, POCh) in the proportions 80:20, 70:3, 60:40, 50:50, 40:60, 30:70 and 20:80 (v/v). Following the recommendations of Minick and co-workers [12,13] for eluents used when working with the ODS column 0.25 ml of 1-octanol and 0.15 g of 1-dodecylamine were added to 100 ml of methanol. With the PBCA column the methanol used contained 0.25% of 1-octanol. Before use the eluents were left to stand overnight and then filtered through 0.45-μm nylon 66 filters.

Deuteromethanol (CH_3O^2H) was purchased from IBJ (Swierk/Otwock, Poland).

Methods

The chromatographic system (Altex Scientific, Berkeley, CA, USA) consisted of a single-piston reciprocating pump and a Model 157 UV detector operating at 254 nm. A Rheodyne (Cotati, CA, USA) Model 7410 injection valve fitted with a 20-μl sample loop was used. The flow-rate was 1 ml/min.

To determine the columns dead volumes, the approach [14] was applied

consisting in measuring the position of the peak of deuterated methanol with pure methanol as the eluent. Determinations of capacity factors, k', were made in duplicate at room temperature. In several systems studied the exclusion of solutes was observed as evidenced by negative values of k'. To accommodate such excluded solutes in our studies, we decided to consider the k' values instead of log k'. The capacity factors determined in the three chromatographic systems applied are given in Tables I–III.

In several instances we were unable to obtain measurable capacity factors. To overcome the problem of incompletenes of the capacity factor matrix, we estimated the mising data by linear extrapolation or interpolation of the log k' *vs.* X_{CH_3OH} relationship.

With the PBCA column and the ODS column operated at pH 7.0, the linear parts of the log k' *vs.* X_{CH_3OH} plot were extrapolated to 0% methanol in the eluent. The data thus obtained for individual solutes were designated log k'_w (PBCA) and log k'_w (ODS), respectively.

Statistical analysis

A matrix of capacity factors determined in $3 \times 7 = 21$ chromatographic systems for 18 drug solutes was subjected to statistical analysis by the principal component method [15]. A standard commercially available statistical package was employed.

The first principal component accounted for 60.5% and the second principal

TABLE I

CAPACITY FACTORS, k', OF IMIDAZOL(IN)E DRUGS DETERMINED ON POLY(BUTADIENE)-COATED ALUMINA WITH METHANOL–BUFFER OF pH 10.9 AS ELUENT WITH VARIOUS VOLUME FRACTIONS OF METHANOL, X_{CH_3OH}

Solute No.[a]	X_{CH_3OH} (v/v)						
	80	70	60	50	40	30	20
1	0.1666	0.6333	2.0416	3.6833	9.7500	9.4166	8.9166
2	0.1083	0.1666	0.6416	1.2500	3.1666	6.6326	7.2000
3	0.0251	0.0398	0.0635[b]	0.1000	0.3000	0.8367	0.7333
4	0.0219	0.0167	0.0917	0.4500	1.2500	3.4285	4.6666
5	0.1416	0.5000	1.1666	2.4833	5.9166	11.6938	10.6666
6	0.1166	0.0033	0.1833	0.6083	1.6583	3.9489	4.1166
7	0.0083	0.0333	0.1250	0.5333	1.7833	5.0204	5.5000
8	0.3250	0.5000	1.4000	2.4583	5.3330	11.6938	13.5833
9	0.5000	0.8000	2.1750	4.8083	11.5583	27.6734	24.5000
10	0.2426	0.3750	0.9750	1.5000	2.5666	4.9795	5.5000
11	0.4667	0.2000	0.5416	0.8500	1.8333	3.3469	3.0833
12	0.2000	0.2750	0.6666	0.8500	1.3666	2.7346	2.3330
13	0.0167	1.4666	4.4166	7.5000	14.8830	35.2200	47.5000
14	0.0333	0.1500	0.8500	2.2500	7.3833	16.2857	25.5000
15	0.0500	0.1333	0.3583	0.8333	2.3916	5.7346	6.6166
16	0.6000	0.8000	2.3589	5.8166	14.3330	37.7750	45.8333
17	−0.1500	−0.0833	−0.1416	−0.1000	0.1250	0.0000	0.0000
18	−0.1250	−0.1080	−0.1666	−0.1333	−0.1000	−0.0500	−0.1166

[a] Solutes are numbered as in Fig. 1.

[b] Interpolated data.

TABLE II

CAPACITY FACTORS, k', OF IMIDAZOL(IN)E DRUGS DETERMINED ON OCTADECYL-SILICA WITH METHANOL–BUFFER OF pH 7.0 AS ELUENT WITH VARIOUS VOLUME FRACTIONS OF METHANOL, X_{CH_3OH}

Solute No.[a]	X_{CH_3OH} (v/v)						
	80	70	60	50	40	30	20
1	3.6652	2.8330	2.2160	4.0830	8.8000	15.2545[b]	27.9660
2	4.3666	3.5000	2.9660	4.9500	6.0660	11.3830[b]	13.000
3	0.3660	0.6660	0.7500	1.0000	1.8500	3.7500	4.3333
4	0.6660	1.5830	2.4330	5.1660	15.0330	45.6600	113.470[b]
5	3.1666	2.0000	1.5000	3.3000	6.5830	19.5660	23.2660
6	1.6333	1.6660	1.6330	2.3000	4.5830	27.9330	2.6666
7	0.7333	1.8660	3.6660	7.4160	16.3900[b]	34.8600	2.7830
8	2.8333	2.7330	2.0830	3.0830	10.7160	31.3300	71.0700[b]
9	6.0000	3.0330	2.5830	4.7500	10.5000	26.8300	14.3500
10	3.6660	2.0000	0.0830	0.1660	3.6000	8.0660	6.0000
11	2.0000	1.3660	1.0830	1.6330	2.3330	6.0000	6.0333
12	3.2493	1.7830	1.3000	2.1660	2.0000	1.7160	3.0500
13	5.0000	2.5000	1.8330	3.2160	13.5000	27.5400[b]	74.1300[b]
14	2.6000	5.4600	4.7500	10.6330	16.9660	39.8100[b]	83.1763[b]
15	1.7498	2.2500	2.9160	5.0000	9.7500	12.4580[b]	15.1660
16	8.6333	5.0000	3.7500	8.0000	18.8330	25.7039	47.8630
17	0.5500	0.4500	0.5830	0.6660	1.1497	6.2488	3.4166
18	0.6000	0.5830	0.5414[b]	0.5000	0.6660	6.2488	1.4167

[a] Solutes are numbered as in Fig. 1.
[b] Extrapolated or interpolated data.

TABLE III

CAPACITY FACTORS, k', OF IMIDAZOL(IN)E DRUGS DETERMINED ON OCTADECYL-SILICA WITH METHANOL–BUFFER OF pH 2.9 AS ELUENT WITH VARIOUS VOLUME FRACTIONS OF METHANOL, X_{CH_3OH}

Solute No.[a]	X_{CH_3OH} (v/v)						
	80	70	60	50	40	30	20
1	2.4490[b]	1.7166	1.0357	0.7857	0.6070	0.0500	0.8750
2	2.0333	1.3333	1.0892	0.6428	0.7321	0.6785	0.5892
3	0.9666	0.6833	0.5714	0.3750	0.1562	0.1250	0.1785
4	2.3000	1.6000	0.8571	0.5535	0.7857	0.1750	0.8214
5	1.3333	1.0350	0.7500	0.3307	0.6071	0.5714	0.5731[b]
6	1.3333	1.1833	0.5000	0.4692	0.4107	0.3750	0.3928
7	2.2333	1.6666	1.1250	0.8750	1.0535	0.9285	1.0892
8	2.1333	1.4000	0.6250	0.6071	0.4821	0.4553[b]	0.4285
9	2.0000	1.6000	1.1250	0.8035	1.0000	1.0964[b]	1.2500
10	1.7000	1.2666	0.6071	0.5357	0.3750	0.2500	0.3928
11	1.0666	0.7000	0.5714	0.3928	0.2500	0.2500	0.2500
12	1.6333	1.1333	0.5714	0.4107	0.4285	0.4107	0.0714
13	1.6333	1.2166	0.7678	0.5714	0.4464	0.3214	0.3928[b]
14	2.6333	1.9666	1.4628	1.3035	1.5000	1.8214	1.8214
15	2.0000	1.1166	0.8214	0.4642	0.4464	0.4642	0.4285
16	2.6500	2.2166	1.5892	1.2321	1.5000	1.7321	2.0000
17	1.6330	1.0266	0.7500	0.4645	0.3393	0.3935	0.3571
18	1.0497	2.7327	0.4286	0.3750	0.3214	0.1607	0.1964

[a] Solutes are numbered as in Fig. 1.
[b] Extrapolated or interpolated data.

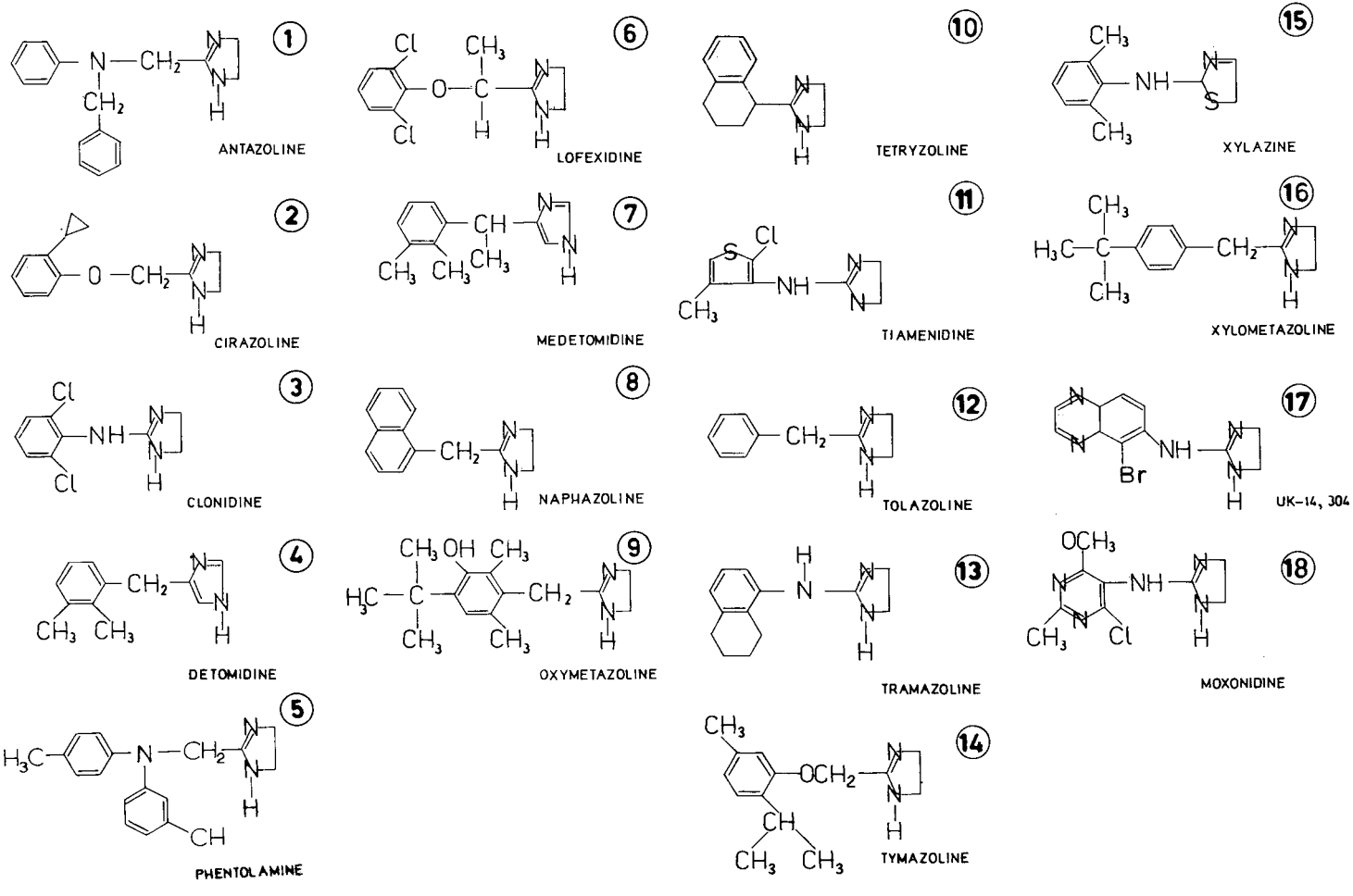

Fig. 1. Structural formulae of the imidazol(in)e derivative drugs studied.

component accounted for 18.9% of the variance in the capacity factors considered. The principal component scores by individual solutes were displayed graphically on the plane spanned by two principal component axes (Fig. 5).

In Fig. 4 the principal component loadings corresponding to the variations in column type and eluent composition are given.

RESULTS AND DISCUSSION

Structural formulae of the drug solutes are given in Fig. 1. There are no distinctive structural features (at least among the imidazoline subgroup) which would justify separation of the agents into classes. However, pharmacologically the drugs are ascribed to two main classes: those binding preferentially to α-1 adrenoceptor and others possessing a higher affinity to the α-2 adrenoceptor [7,16]. As a consequence of these differences, opposite circulatory effects are observed.

The relationship between capacity factors and volume fraction of methanol in the mobile phase can best be illustrated by means of semi-logarithmic plots. Such representative relationships are shown in Fig. 2. Using the poly(butadiene)-coated alumina column and a buffer of pH 10.9 a more or less linear dependence of log k' on

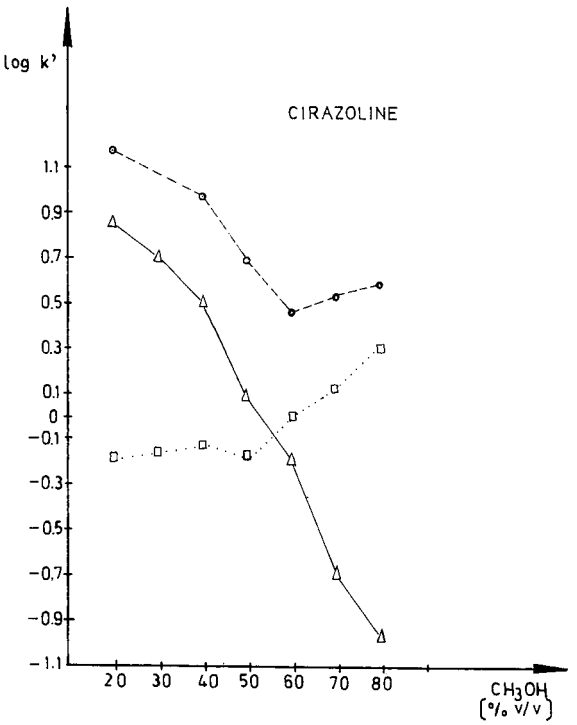

Fig. 2. Relationships between log k' and the volume fraction of methanol in mobile phase for cirazoline. Solid line, retention data determined on poly(butadiene)-coated alumina column operated at pH 10.9; broken line, data obtained on octadecylsilica column at pH 7.0; dotted line, data obtained on octadecylsilica at pH 2.9.

X_{CH_3OH} is obtained over the whole range of composition of the eluent studied. With the ODS column operated at pH 7.0, linearity is at best limited to the range of methanol content in the mobile phase from 20 to 60% (v/v). The results obtained demonstrate the unique advantages of PBCA for the chromatographic determination of the hydrophobicity of organic bases [17]. In the third system studied (ODS, methanol–buffer of pH 2.9), increasing retention of solutes (ionized) was observed with increasing amount of methanol in the mobile phase.

First we attempted to relate pharmacological activity to log k' corresponding to 100% buffer as a hypothetical eluent, log k'_w. Neither log k'_w determined on PBCA nor the corresponding parameter obtained from the system employing ODS at pH 7.0 allowed a reasonable pharmacological classification of the drugs studied (Fig. 3).

Assuming that the set of retention data obtained comprises information suitable for pharmacological classification of the solutes, we turned our attention to modern methods of data analysis. Multivariate methods of data analysis have been applied in chromatography since the early 1970s [18,19]. The reported studies were usually aimed at retention prediction [20,21] and/or explanation of the mechanism of chromatographic separations [22,23]. However, Wold and co-workers [24,25] reported multi-

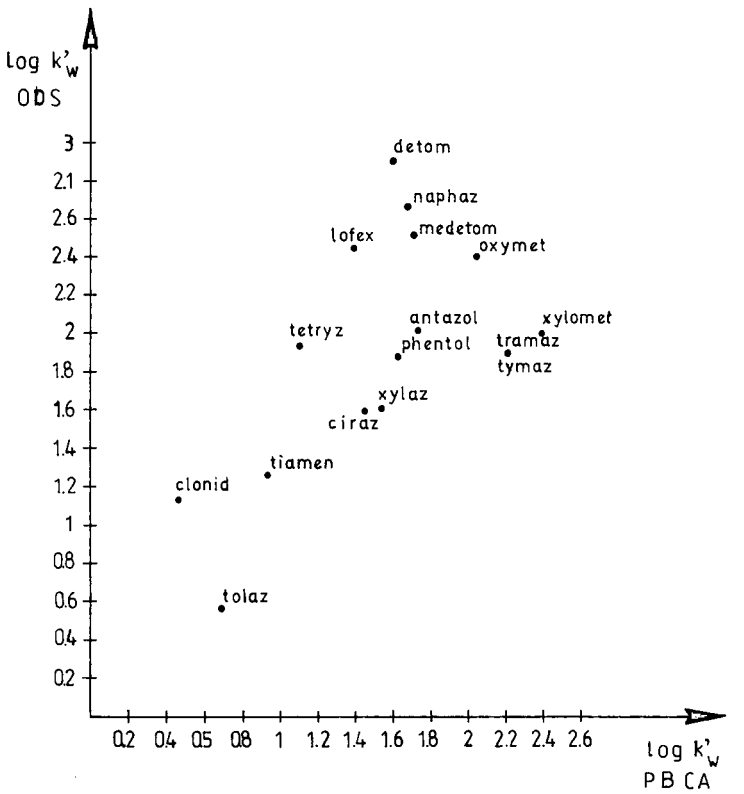

Fig. 3. Distribution of the imidazoline drugs on the plane determined by the logarithms of capacity factors extrapolated to pure buffer as the eluent. The respective retention data were obtained using the ODS (pH 7.0) and the PBCA (pH 10.9) columns.

variate parameterization of amino acid properties based on TLC data. The TLC data considered were R_F values determined in seven isocratic chromatographic systems (normal phase) differing with respect to the type of stationary phase and composition of the eluent. Principal component analysis of the data matrix comprising the R_F parameters, together with Van der Waals volume and molecular mass, resulted in two significant principal components. The principal components were shown to possess predictive capacity and explained about 70% of the variance reported in the literature data on the pharmacological activity of a series of oligopeptides. The differences in pharmacological activities considered by Wold and co-workers [24,25] were quantitative, *i.e.*, all the agents elicited the same effect but of varying magnitude. In selecting the solutes for this project we aimed at a qualitative differentiation of bioactive substances by means of diversified chromatographic data.

The principal component analysis of the retention data given in Tables I–III yielded two main factors accounting for about 80% of the variance in the HPLC capacity factors. Analysing the loadings of the two main principal components by the variables of the chromatographic analysis (Fig. 4), one can note that the first factor (PC1) is loaded mostly by retention data determined under acidic and neutral conditions. However, the input to PC1 by the k' values determined on PBCA with eluents containing higher proportions of water is also significant. Thus, PC1 may reflect a tendency of solutes to undergo hydration and ionizaton. The second principal component, PC2, is evidently loaded by capacity factors determined at pH 10.9 on the PBCA column. One can assume that PC2 reflects the hydrophobicity of non-ionized forms of the solutes. A conspicuous result is the high loading by the capacity factors determined with 70% methanol at pH 2.9 on the ODS column to the fourth principal component and also the marked loadings to the third principal component by the k' values from the 20 and 30% methanol (pH 7.0)–ODS systems and the 80% methanol

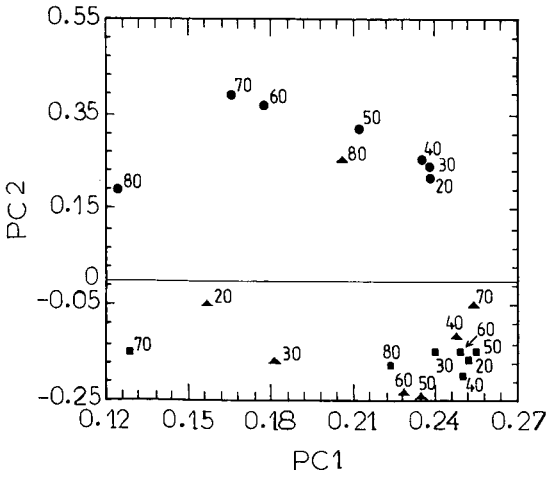

Fig. 4. Two-dimensional scatter plot of the loadings of the two first principal components, PC1 and PC2, by the variables of the chromatographic systems applied. Column: ●, PBCA operated at pH 10.9; ■, ODS operated at pH 2.9; ▲, ODS operated at pH 7.0. Numbers denote the volume percentage of methanol in the eluent.

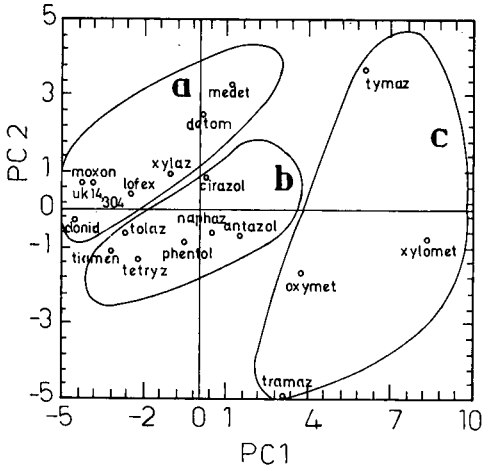

Fig. 5. Two-dimensional scatter plot of the scores by individual imidazol(in)es in the two first principal components, PC1 and PC2.

(pH 10.9)–PBCA system. It is difficult to speculate about the physical meaning of such observations, however.

For individual drug solutes, the principal component object scores were calculated. Thus, positions of the drugs on the plane spanned by two principal component axes could be displayed graphically (Fig. 5). The objects in Fig. 5 can be grouped into three clusters, a, b and c. Such a grouping due to retention behaviour correlates well with the established pharmacological classification of the solutes.

Pharmacology textbooks classify unequivocally the agents belonging to cluster a as selective agonists of α-2 adrenoceptor, whereas those belonging to cluster c are considered to be pure α-1 adrenoceptor agonists. A detailed pharmacological discussion of the results is inappropriate here, but it can be demonstrated that imidazolines belonging to cluster b possess affinity for both subtypes of the α adrenoceptor. For example, tolazoline and phentolamine block both α-1 and α-2 subtypes of adrenoceptor. Tolazoline is asumed to have a higher affinity to α-2 than α-1 adrenoceptor, whereas phentolamine blocks both receptors to the same extent [7,26]. This observation is in accordance with the relative positions of the two α adrenoceptor antagonists in Fig. 5. Tiamenidine is used clinically for to its α-2 adrenoceptor stimulating properties. Nevertheless, adverse effects of the drug can be ascribed to α-1 adrenoceptor stimulation [27]. Naphazoline and tetryzoline are usually classified among agonists of α-1 adrenoceptor. There is evidence that both agents react with α-2 adrenoceptors also, however [7,26,28].

The presence of cirazoline in cluster b appears unexpected as it has been considered to be a strong agonist of α-1 receptors. The positon of cirazoline can be rationalized however, in view of reports [29,30] that although an α-1 adrenoceptor agonist, it is at the same time an α-2 adrenoceptor antagonist. Also, the location of antazoline in cluster b seems reasonable. This agent, being an imidazoline derivative, does not belong to circulatory drugs acting via adrenoceptors but possesses

antihistamine properties instead. In independent experiments [31] we did not observe stimulation of either α-1 or α-2 adrenoceptors by antazoline, but the agent revealed antagonistic properties towards the receptors.

Systematic information extracted by principal component analysis from a set of retention data determined in various HPLC systems suffices for the differentiation of imidazol(in)e drugs in accordance with their pharmacological classification. This result demonstrates the usefulness of diversified chromatographic data for the characterization of solutes and thus for the prediction of their properties. By using multivariate methods of data analysis, the informative capacity of retention data so far neglected in retention–bioactivity relationship studies can be exploited. These neglected data (which reflect generally the ability of a solute to take part in specific intermolecular interactions with a stationary and/or mobile phase) can provide structural information that does not manifest itself within a set of capacity factors changing regularly with changes in chromatographic conditions. Provided that the data are reproducible, more reliable information on solute properties can be extracted the more diverse is the representative set of capacity factors considered. From the point of view of the application of chromatography in studies of quantitative structure–activity relationships (QSAR), it appears more productive to collect a representative set of diverse retention parameters than to concentrate all efforts on the determination of a chromatographic measure of hydrophobicity.

Leaving aside all the uncertainties and ambiguities accompanying hydrophobicity determinations (ionization, pH, ionic strength, reactions with buffer components, etc., in organic–aqueous solvents of varying composition), one cannot expect the one-dimensional hydrophobicity scale to comprise the bioactivity of various drugs. Certainly, the multi-dimensional structural characterization of agents based on their chromatographic retention in various systems appears more realistic.

ACKNOWLEDGEMENTS

This research was supported in part by the Polish Ministry of National Education's Fundamental Research Programme R.P.I.08. One of the authors (R.G.-Y.) acknowledges receipt of a scholarship from the Polish Ministry of Health and Social Welfare.

REFERENCES

1 C. B. C. Boyce and B. V. Milborrow, *Nature (London)*, 208 (1965) 537.
2 R. Kaliszan, *Quantitative Structure–Chromatographic Retention Relationships*, Wiley, New York, 1987, pp. 279–295.
3 R. Kaliszan, *Quant. Struct.–Act. Relat.*, 9 (1990) 80.
4 E. Soczewiński and C. A. Wachtmeister, *J. Chromatogr.*, 7 (1962) 311.
5 P. J. Schoenmakers, H. A. H. Billiet, R. Tijssen and L. de Galan, *J. Chromatogr.*, 149 (1978) 519.
6 L. R. Snyder, J. W. Dolan and J. R. Gant, *J. Chromatogr.*, 165 (1979) 3.
7 P. B. M. W. M. Timmermans and P. A. van Zwieten, *J. Med. Chem.*, 25 (1982) 1389.
8 P. B. M. W. M. Timmermans and P. A. van Zwieten, *Eur. J. Pharmacol.*, 54 (1977) 229.
9 A. de Jong and W. Soudijn, *Eur. J. Pharmacol.*, 69 (1981) 175.
10 U. Bien-Vogelsang, A. Deege, H. Figge, J. Köhler and G. Schomburg, *Chromatographia*, 19 (1984) 170.
11 G. Heinemann, J. Köhler and G. Schomburg, *Chromatographia*, 23 (1987) 435.
12 D. J. Minick, J. J. Sabatka and D. A. Brent, *J. Liq. Chromatogr.*, 10 (1987) 2565.

13 D. J. Minick, J. H. Frenz, M. A. Patrick and D. A. Brent, *J. Med. Chem.*, 31 (1988) 1923.
14 J. H. Knox and R. Kaliszan, *J. Chromatogr.*, 349 (1985) 211.
15 J. R. Llinas and J. M. Ruiz, in G. Vernin and M. Chanon (Editors), *Computer Aids to Chemistry*, Ellis Horwood, Chichester, 1986, pp. 200–256.
16 W. C. Bowman and M. J. Rand, *Textbook of Pharmacology*, Blackwell, Oxord, 2nd ed., 1980, pp. 11.31–11.32 and 23.47–23.49.
t7 R. Kaliszan, R. W. Blain and R. A. Hartwick, *Chromatographia*, 25 (1988) 5.
18 P. H. Weiner, C. J. Dack and D. G. Howery, *J. Chromatogr.*, 69 (1972) 249.
19 J. F. K. Huber, C. A. M. Meijers and J. A. R. J. Hulsman, *Anal. Chem.*, 44 (1972) 111.
20 B. Walczak, J. R. Chretien, M. Dreux, L. Morrin-Allory, M. Lafosse, K. Szymoniak and F. Membrey, *J. Chromatogr.*, 353 (1986) 123.
21 K. Szymoniak and J. Chretien, *J. Chromatogr.*, 404 (1987) 11.
22 R. Kaliszan, K. Osmiałowski, B. J. Bassler and R. A. Hartwick, *J. Chromatogr.*, 499 (1990) 333.
23 R. Kaliszan and K. Osmiałowski, *J. Chromatogr.*, 506 (1990) 3.
24 S. Wold, L. Eriksson, S. Hellberg, J. Jonsson, M. Sjöström, B. Skageberg and C. Wikstrom, *Can. J. Chem.*, 66 (1987) 1814.
25 L. Eriksson, J. Jonsson, M. Sjöström and S. Wold, *Quant. Struct.–Act. Relat.*, 7 (1988) 144.
26 G. M. Drew, *Eur. J. Pharmacol.*, 36 (1976) 313.
27 E. Lindner and J. Kaiser, *Arch. Int. Pharmacodyn.*, 211 (1974) 305.
28 R. J. Summers, B. Jarrott and W. J. Louis, *Eur. J. Pharmacol.*, 66 (1980) 233.
29 R. R. Ruffolo, Jr., and J. E. Waddel, *J. Pharmacol. Exp. Ther.*, 222 (1982) 29.
30 P. M. McDonough, G. T. Wetzel and J. H. Brown, *J. Pharmacol. Exp. Ther.*, 238 (1986) 612.
31 A. Radwańska and R. Kaliszan, in preparation.

Journal of Chromatography, 550 (1990) 585–594
Elsevier Science Publishers B.V., Amsterdam

CHROMSYMP. 2055

Use of Ce(IV) oxidizing agent for the derivatization of polycyclic aromatic hydrocarbons for liquid chromatography–electrochemical detection

J. R. MAZZEO and I. S. KRULL*
Department of Chemistry and The Barnett Institute (341 MU), Northeastern University, 360 Huntington Avenue, Boston, MA 02115 (USA)
and
P. T. KISSINGER
Department of Chemistry, Purdue University, West Lafayette, IN 47906 (USA)

ABSTRACT

Polycyclic aromatic hydrocarbons (PAHs) were oxidized with Ce(IV), and the resulting quinones were determined by reductive-mode liquid chromatography–electrochemical detection. This oxidation is a rapid, automatable step, involving addition of Ce(IV) reagent to the PAH sample and cleaning up the derivative with C_{18} solid-phase extraction. Using a C_{18} analytical column and a 2-propanol–phosphate buffer as the mobile phase, detection limits were in the ppb range for naphthalene, phenanthrene and anthracene, with linearity over 3–5 orders of magnitude. Method validation was performed by addition of the PAHs to tap water and determining the levels by reference to a calibration curve. The three PAHs can be simultaneously derivatized and determined under the same chromatographic conditions. Analysis of a motor-oil sample is also shown.

INTRODUCTION

Determination of polycyclic aromatic hydrocarbons (PAHs) is an area of great importance in environmental analysis. Both gas chromatography and liquid chromatography (LC) are methods of choice. In LC, reversed-phase separation followed by UV or fluorescence (FL) detection is most commonly used. PAHs exhibit high UV and FL sensitivity, and FL detection limits are in the sub-ppb[a] range. Multi-component analysis is easily achieved by reversed-phase chromatography. However, there exists a need for developing simple, rapid methods for individual PAHs which show carcinogenicity and mutagenicity [1].

One possibility for such analyses would be LC, combined with electrochemical detection (ED), a method which offers high selectivity and sensitivity. However, in aqueous media, most PAHs do not undergo any oxidation or reduction reactions at

[a] Throughout this article, the American billion (10^9) is meant.

0021-9673/91/$03.50

typical working electrode materials such as glassy carbon. The electrochemistry of PAHs has received a great deal of attention, particularly with regard to fundamental radical-ion chemistry. Electrochemical analysis of PAHs is usually performed in aprotic media. Single-electron additions and abstractions have been demonstrated in numerous papers, where electrochemistry was coupled to electron-spin resonance spectrometers [2–6]. This method has generally not been used for analytical purposes. There has been only one report describing the analysis of anthracene in non-aqueous LC–ED at a potential of +0.80 V *vs.* saturated calomel electrode (SCE) with a glassy carbon electrode [1]. Low-pmol detection limits were achievable for anthracene and aminoanthracene.

Here, we report the LC–ED analysis of Ce(IV)-oxidized PAHs. The final products from this oxidation step are quinones, which can be detected by reductive-mode LC–ED at mild potentials (*ca.* −0.40 V *vs.* Ag/AgCl) [7]. Ce(IV) is a powerful oxidizing reagent which has been used in organic synthesis to convert PAHs to quinones [8,12]. The mechanism of oxidation involves electron abstraction from the PAH by Ce(IV) to generate Ce(III) and a cation free radical, the latter being attacked by water molecules, to yield the final quinone product.

EXPERIMENTAL

Reagents

PAHs (anthracene, naphthalene, phenanthrene and pyrene), quinones (anthraquinone, 1,4-naphthoquinone and phenanthrenequinone), sodium phosphate (monobasic), sodium hydroxide, ceric ammonium nitrate (CAN) and nitric acid were purchased from a variety of sources, including Aldrich (Milwaukee, WI, USA), J. T. Baker (Phillipsburg, NJ, USA.), Pfaltz & Bauer (Flushing, NY, USA), Sigma (St. Louis, MO, USA) and Chem Service (West Chester, PA, USA). PAHs and quinones were purified by recrystallization from ethanol or tetrahydrofuran (THF). 2-Propanol and THF were OmniSolv grade from EM Science (Cherry Hill, NJ, USA). Water was deionized with a Nanopure system from Barnstead (Boston, MA, USA.). PAH standards were prepared in THF–water (50:50). The Ce(IV) reagent used for all derivatizations was 0.1 *M* CAN in 1.0 *M* HNO_3.

Apparatus

Cyclic voltammetry (CV) was performed using a Model CV-1B cyclic voltammograph from Bioanalytical Systems (BAS, West Lafayette, IN, USA). The working electrode was glassy carbon, with a Ag/AgCl reference and a Pt-wire auxiliary electrode. Cyclic voltammograms were recorded on a Hewlett-Packard (Palo Alto, CA, USA) XY recorder.

The LC system consisted of an LDC Constametric III pump (Riviera Beach, FL, USA), a Model 7010 injector with a 20-μl loop (Rheodyne, Cotati, CA, USA), a LiChrospher C_{18} 5 μm, 125 mm × 4.6 mm I.D. column (E. Merck, Darmstadt, Germany) and a BAS Model LC-4B amperometric detector with a glassy carbon working electrode, stainless-steel auxiliary and Ag/AgCl reference. The mobile phase was continuously kept under a He blanket. Data were recorded on a Göerz-Metrawatt (Vienna, Austria) Model SE120 strip-chart recorder. Peak heights were measured manually.

The mobile phase for oxidized PAH analysis was 2-propanol–0.05 *M* NaH_2PO_4 (30:70) (pH 6.5) [11]. The electrode was maintained at either −0.40 V for oxidized phenanthrene, naphthalene and pyrene analysis or at −0.60 V for oxidized anthracene.

PROCEDURE

Cyclic voltammetry

A 0.1% (w/v) solution of the PAHs (naphthalene, phenanthrene, pyrene or anthracene) was prepared in THF–water (50:50), and 5 ml of this were added to 5 ml of 0.1 *M* CAN in 1.0 *M* HNO_3. After 1 min reaction time, a cyclic voltammogram was recorded at a scan rate of 100 mV/s. Solutions (0.1%, w/v) of the quinones in THF–water (50:50) were prepared and 5 ml were added to 5 ml 1.0 *M* HNO_3. A cyclic voltammogram was recorded 1 min after addition.

Derivative clean-up for LC–ED work

A 1-ml volume of the analyte–Ce(IV) reaction mixture was applied to a preconditioned 1-ml C_{18} solid-phase extraction tube (Supelco, Bellefonte, PA, USA). Excess reagent was washed off with two 1-ml washings of deionized water. The derivative was eluted with 0.5 ml 2-propanol, and this solution was diluted with 0.5 ml deionized water prior to analysis.

Optimization and percent derivatization

A 0.001% (w/v) solution of naphthalene in THF–water (50:50) was used in the optimization study, and the peak height of the derivative was measured, under the chromatographic conditions stated above, as a function of various derivatization parameters. Volume ratio of analyte to Ce(IV) solution and reaction time were optimized in this way. Under optimized conditions, percent derivatizations were calculated for the PAHs by comparing the derivative peak with the peak of the quinone standard and taking into account the dilution of the analyte and the increased weight of the derivative compared to the analyte. The percent derivatizations are listed in Table I.

Detection limits and linearity

A stock solution of the PAHs (0.1%) was diluted and derivatized until no derivative peak could be seen by LC–ED. Detection limits and linearity are shown in Table I for each PAH.

TABLE I

PERCENT DERIVATIZATIONS, DETECTION LIMITS AND LINEARITY

Analyte	Percent derivatization, average ± S.D. ($n=3$)	Limit of detection (ppb)	Linear range (ppb)	r^2
Naphthalene	76.6 ± 3.6	5	10–10 000	0.9993
Phenanthrene	37.5 ± 1.1	50	50–100 000	0.9998
Anthracene	42.1 ± 1.2	50	50–100 000	1.0000

TABLE II

DETERMINATION OF PAHs ADDED TO TAP WATER

Sample	Concentration found (μg/l), average ± S.D. ($n=3$)	Actual	Relative error (%)
Naphthalene 1	30.4 ± 1.4	32.0	5.00
Naphthalene 2	16.7 ± 0.5	18.0	7.22
Naphthalene 3	75.1 ± 3.1	71.0	5.77
Phenanthrene 1	520 ± 4	520	0
Phenanthrene 2	342 ± 12	360	5.00
Phenanthrene 3	974 ± 5	920	5.87
Anthracene 1	522 ± 3	544	4.04
Anthracene 2	750 ± 2	732	2.46
Anthracene 3	257 ± 5	276	6.88

Single-blind spiking studies and application

Known amounts of the PAHs (naphthalene, phenanthrene or anthracene) were added to tap water. These solutions were diluted with an equal volume of THF and derivatized and analyzed using an external calibration plot, for which the standards were prepared in THF–water (50:50). The results are listed in Table II. Naphthalene, phenanthrene and anthracene were added at the 1-ppm level to tap water and also analyzed.

A sample of used motor oil from an automobile was also analyzed. A 1-ml volume of the motor oil was extracted with 10 ml of THF. The THF was diluted with 10 ml water and derivatized and analyzed by the described method. Naphthalene (naphthoquinone) and phenanthrene (phenanthrenequinone) were determined by using standard addition. The THF used for extraction of the motor oil contained 0, 50 and 100 ppm each of naphthalene and phenanthrene and these were analyzed. Also, known amounts of each of the two PAHs were added to the THF used for extraction and this was analyzed with the other samples. This procedure is based on a similar report in the literature [13]. Results are given in Table III.

TABLE III

ANALYSIS OF MOTOR OIL EXTRACT

Analyte	Native level (μg/ml), average ± S.D. ($n=3$)	Added level (μg/ml), average ± S.D. ($n=3$)	Actual	Relative error (%)
Naphthalene	77 ± 4	10 ± 0.1	11	9.1
Phenanthrene	25 ± 1	35 ± 0.4	33	6.1

RESULTS AND DISCUSSION

Cyclic voltammetry

For initial studies, cyclic voltammetry was used to determine if an electroactive derivative was formed with a Ce(IV)-oxidized PAH. The organic literature reports that Ce(IV) oxidation of PAHs leads to the formation of quinones [8–12], which are electrochemically reducible. In performing these initial studies, it became clear that the derivatization solvent greatly affected the rate of oxidation. In this regard, methanol and acetonitrile proved to be poor choices, as they complex with the Ce(IV), rendering it incapable of oxidizing the PAH. THF proved to work best as derivatization solvent. Thus, all studies were performed using THF–water (50:50) as the derivatization solvent.

Fig. 1 shows the cyclic voltammogram recorded for Ce(IV)-oxidized phenanthrene, as well as phenanthrenequinone at the same pH. The two are superimposable, lending evidence that the derivative of Ce(IV)-oxidized phenanthrene was phenanthrenequinone. A reversible reduction wave was seen at +0.35 V *vs.* Ag/AgCl, which phenanthrenequinone also showed. This was also the case for Ce(IV)-oxidized naphthalene, the cyclic voltammogram of which paralleled that for 1,4-naphthoquinone, and Ce(IV)-oxidized anthracene, whose cyclic voltammogram exactly

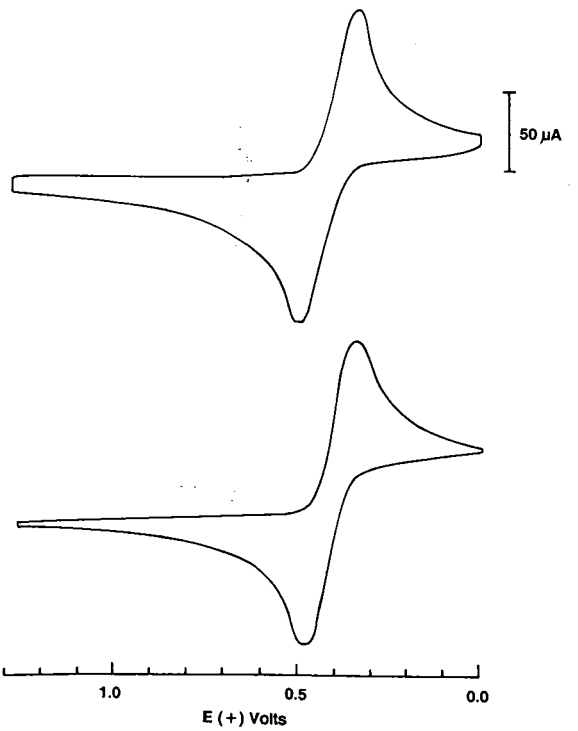

Fig. 1. CV of Ce(IV)-oxidized phenanthrene (top) and phenanthrenequinone (bottom), both in 1 *M* HNO_3. Glassy carbon working electrode, Pt auxiliary and Ag/AgCl reference electrode. 0.0 V to +1.3 V, 0.100 V/s scan rate, 50 μA sensitivity.

matched that for anthraquinone. These results were consistent with what the organic literature reported for oxidation products of PAHs [8–12]. There have been no literature reports of the oxidation products of pyrene. The cyclic voltammogram for Ce(IV)-oxidized pyrene showed the presence of more than one redox couple, suggestive of multiple derivatives. This was confirmed by LC–ED results.

Derivative clean-up for LC–ED work

In order to use the Ce(IV) oxidation procedure for LC–ED analysis of PAHs, it was necessary to clean up the derivative prior to injection. Injection of unreacted Ce(IV) ion to a high-performance liquid chromatographic column would lead to decreased column life, as well as a large solvent–matrix peak due to the Ce(IV) reducing at the electrode. Moreover, the reaction must be quenched so that further oxidation of the derivative does not occur. This was accomplished using a C_{18} solid-phase extraction step, which eliminated Ce(IV) and Ce(III) as well as HNO_3 from the final analysis solution.

Analysis of oxidized PAHs was performed using a mobile phase reported for the LC–ED determination of naphthoquinone, anthraquinone and phenanthrene quinone on a C_{18} column [7]. The same applied potentials used for analysis in the cited paper [7] were also used. Reduction of anthraquinone requires a lower applied potential (-0.60 V) than phenanthrenequinone and naphthoquinone (-0.40 V). The optimum potential for oxidized pyrene was determined to be -0.40 V. Unfortunately, this four-ring PAH gave multiple derivatization products, leading to poor sensitivity and non-linearity (Fig. 2). However, the ratio of the two main derivative peaks was constant over the range 1–100 ppm, which implies that this ratio could be used to confirm the presence of pyrene in a sample.

OPTIMIZATION AND PERCENT DERIVATIZATION

The derivatization was optimized for naphthalene, and the optimized conditions were used for all PAHs. The optimum volume ratio of analyte solution to Ce(IV) solution was determined to be 1.00 ml analyte to 0.75 ml 0.1 *M* CAN in 1.0 *M* HNO_3. The reaction time was seen to plateau at 1 min, with no change in percent conversion up to 1 h. For convenience, 1 min was chosen as the optimum reaction time. A temperature study was not performed. All reactions were performed at ambient temperature.

Percent derivatization was calculated as outlined under Experimental. The retention time was the same for the derivative as the quinone standard for all PAHs, further solidifying the belief that the derivative was the corresponding quinone. Table I summarizes percent derivatizations for all three PAHs. As expected, the highest value was for naphthalene, 80%, for which the derivatization was optimized. Phenanthrene (37%) and anthracene (43%) showed about half the percent derivatization as naphthalene. These values could be improved by separately optimizing the derivatization for each, athough not done here. Nevertheless, these percent derivatizations were analytically useful, as well as quite practical, given the fact that the reaction time was 1 min and only required a C_{18} clean-up step prior to analysis. Possible reasons for incompete conversion of naphthalene include further oxidation and losses during the C_{18} step.

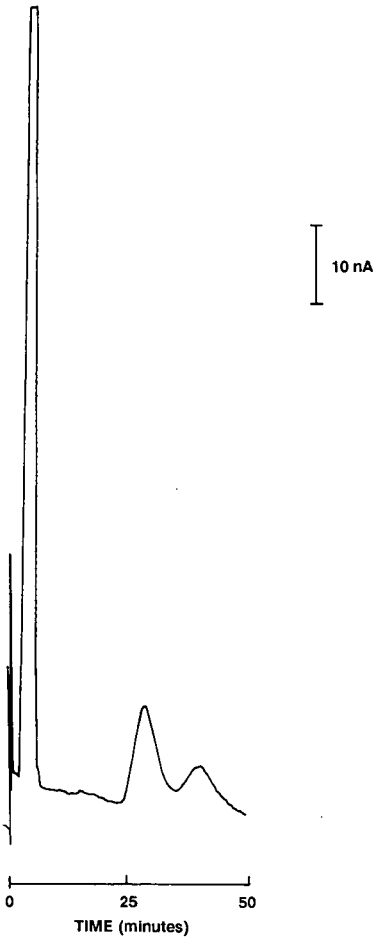

Fig. 2. Chromatogram of 10 ppm derivatized pyrene with electrochemical detection at potential −0.40 V *vs.* Ag/AgCl, 10 nA full scale (20 μl injection). LiChrospher C_{18} column, 5 μm, 125 × 4.6 mm I.D.; mobile phase, 2-propanol in 0.05 *M* NaH_2PO_4 (30:70) (pH 6.5); flow-rate, (pH 6.5); flow-rate, 1.0 ml/min.

Detection limits and linearity

Table I summarizes the detection limits and linearity for the oxidized PAHs. In all cases, the detection limits were in the ppb range, with the best, 5 ppb, for oxidized naphthalene. Linearity was at least three orders of magnitude in all cases. The detection limits were a bit high for typical LC–ED analysis. However, this work was performed in the reductive mode, where dissolved oxygen plays a major role in determining at what sensitivity level the detector could be effectively operated. It should be noted that if it were necessary to determine lower levels of analyte, pre-concentration during the C_{18} solid-phase extraction step could be employed.

Single-blind spiking study and application

In areas where an oil spill has occurred, high levels of PAHs can be found in the

surrounding area's water supply. Thus analysis of PAHs in tap water was chosen as a means to validate the method. Individual PAHs were added to tap water and analyzed using the described method. Table II summarizes the results. In all cases, percent relative errors (REs) were within 8%.

Fig. 3 shows a chromatogram of naphthalene, anthracene and phenanthrene added to tap water at the 1-ppm level and determined using the described method.

Fig. 4 shows chromatograms of underivatized and derivatized motor-oil extract. The two peaks present in the derivatized sample were determined to be naphthoquinone and phenanthrenequinone by retention time comparison. These presumably arose from naphthalene and phenanthrene in the motor oil extract. However, this would be difficult to prove conclusively, as Ce(IV) oxidation of naphthol or phenanthrol also leads to the quinone products. Thus, these peaks may be due to a combination of both the parent PAH and the PAH alcohol. Using standard addition, the levels of naphthalene and phenanthrene in the motor oil were determined to be 77

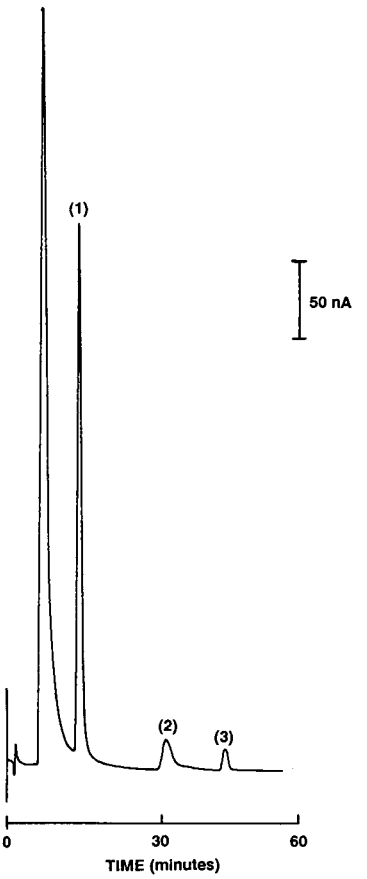

Fig. 3. Chromatogram of 1 ppm naphthalene (1), phenanthrene (2) and anthracene (3) in tap water. For conditions, see Fig. 2, except applied potential −0.60 V, 50 mA full scale.

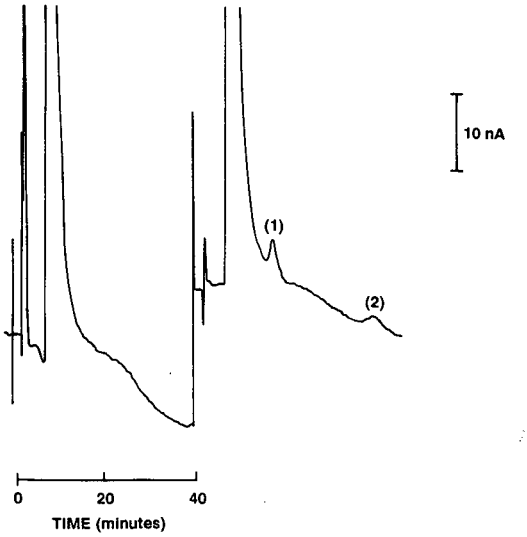

Fig. 4. Chromatogram of underivatized (left) and derivatized motor-oil extract. Peaks: 1 = naphthoquinone; 2 = phenanthrenequinone. Conditions as in Fig. 2.

μg/ml and 24 μg/ml, respectively. Analysis of fortified motor oil was also performed and subtracting out the values determined from the native oil, these added amounts were determined with 9% accuracy (Table III).

CONCLUSIONS

A rapid, simple procedure is described for the analysis of PAHs by LC–ED. Detection limits in the ppb range were attainable for all analytes, with linearity over several orders of magnitude. The approach has been shown valid for analysis of PAHs in tap water. High selectivity has been demonstrated through analysis of a motor-oil extract. The method has the potential for automation, and possesses the selectivity inherent in LC–ED.

The detection limits obtained with the described method (low-ppb) are orders of magnitude higher than what has been reported for LC with FL detection for these compounds (sub-ppb) [14]. It is clear that the described method offers no advantage over LC–FL in terms of detection limits. The advantage of the described method is the high selectivity which is obtainable, allowing an analyst to determine one or two PAHs present in a complex mixture. This was demonstrated with the analysis of a sample of used motor oil. It has been reported that LC–FL is not useful for determining one PAH present in a complex sample–matrix [14]. We believe that the described method may find utility for certain specific applications where one PAH must be determined in the presence of several. This selectivity can be gained by adjusting the applied potential or by adjusting derivatization conditions.

ACKNOWLEDGEMENTS

This research was supported by an unrestricted grant and materials donated to Northeastern University from Bioanalytical Systems, Inc. Additional funding was provided by an NIH Biomedical Research Support Grant to Northeastern University (RR07143), Department of Health and Human Resources (DHHS). Funding was also provided, over many years, by an unrestricted grant from Pfizer, Inc. (Groton, CT, USA). Spiking studies were performed with the assistance of A. J. Bourque, D. J. Magiera and M. E. Szulc. K. Bratin and L. Dou are thanked for their helpful discussions.

This is contribution No. 433 from The Barnett Institute of Chemical Analysis and Materials Science at Northeastern University.

REFERENCES

1 W. L. Caudill, M. V. Novotny and R. M. Wightman, *J. Chromatogr.*, 261 (1983) 415.
2 J. F. Coetzee, G. H. Kazi and J. C. Spurgeon, *Anal. Chem.*, 48 (1976) 2170.
3 J. Phelps, K. S. V. Santhanam and A. J. Bard, *J. Am. Chem. Soc.*, 89 (1967) 1752.
4 W. C. Niekam and M. M. Desmond, *J. Am. Chem. Soc.*, 86 (1964) 4811.
5 L. Jeftie and R. N. Adams, *J. Am. Chem. Soc.*, 92 (1970) 1332.
6 E. S. Pysh and N. C. Yang, *J. Am. Chem. Soc.*, 85 (1963) 2124.
7 D. S. Fluck, S. M. Rappaport, D. A. Eastmond and M. T. Smith, *Arch. Biochem. Biophys.*, 235 (1984) 351.
8 M. Periasam and M. V. Bhatt, *Synthesis*, (1977) 330.
9 T. L. Ho, T. W. Hall and C. M. Wong, *Synthesis*, (1973) 206.
10 G. Balanikas, N. Hussain, S. Amin and S. S. Hecht, *J. Org Chem.*, 53 (1988) 1007.
11 J. Skarzewski, *Tetrahedron*, 40 (1984) 4997.
12 T. L. Ho, *Synthesis*, (1973) 347.
13 P. J. A. Fowlie and T. L. Bulman, *Anal. Chem.*, 58 (1986) 721.
14 W. E May and S. A. Wise, *Anal. Chem.*, 56 (1984) 225.

Journal of Chromatography, 550 (1991) 595–601
Elsevier Science Publishers B.V., Amsterdam

CHROMSYMP. 2316

Confirmation of domoic acid in shellfish using butyl isothiocyanate and reversed-phase liquid chromatography

JAMES F. LAWRENCE* and CATHIE MÉNARD
Food Research Division, Bureau of Chemical Safety, Food Directorate, Health Protection Branch, Ottawa, Ontario K1A 0L2 (Canada)

ABSTRACT

A simple chemical confirmatory technique has been developed for domoic acid, a neurotoxic amino acid of marine origin. After extraction with water–methanol, the domoic acid-containing extract is analysed directly by reversed-phase liquid chromatography with UV absorption detection at 242 nm. For confirmation of positive results an aliquot of the extract is evaporated to dryness and reacted with butyl isothiocyanate to form a thiourea derivative which elutes later than underivatized domoic acid. No additional sample cleanup is required in order to carry out the derivatization for confirmation of domoic acid at the Canadian 20 μg/g guideline level in shellfish. In mussel extract, domoic acid was converted to the thiourea derivative with a yield of 86–91% compared to a pure standard carried through the same reaction. The detection limit for the derivative was about 5–10 μg/g of equivalent domoic acid in extracts of mussels, clams or oysters.

INTRODUCTION

Domoic acid is a neurotoxic amino acid which was found to be the cause of a large-scale human poisoning in Canada in 1987 resulting from the consumption of contaminated mussels [1–3]. Following this incident several high-performance liquid chromatographic (HPLC) methods were developed and reported in the literature [4–6]. In addition, several chemical confirmation methods for domoic acid have been reported [7,8]. They involved the use of UV-absorbing or fluorescent reagents to form derivatives of domoic acid followed by their separation and detection by liquid chromatography (LC). Because these reagents also reacted with proteinaceous coextractives that were present in the shellfish extracts, additional sample purification was required before the confirmatory tests could be carried out.

Domoic acid contains a chromophoric group which absorbs strongly enough at 242 nm to enable its direct detection in shellfish tissue at levels of 1 μg/g or less [5]. This is well below the guideline safety level of 20 μg/g suggested by Health and Welfare Canada. Thus, for regulatory purposes a confirmatory technique need only be as sensitive as the direct method. However, a useful feature of a confirmatory test for domoic acid would be to be able to carry out the derivatization reaction on the same extract without additional sample cleanup and using the same LC system with

0021-9673/91/$03.50

only a mobile phase change. None of the above confirmation reactions achieve both these requirements.

We report here a confirmatory method for domoic acid in shellfish tissue which involves reaction of the N–H moiety of domoic acid with butyl isothiocyanate to form a derivative which elutes later than domoic acid. Additional sample cleanup was found to be unnecessary at levels at or above the guideline level of 20 μg/g.

EXPERIMENTAL

Reagents

Solutions of domoic acid (National Research Council, ARL, Halifax, Canada) were prepared in twice deionized water (Milli-Q, Millipore, Bedford, MA, USA). Butyl isothiocyanate, 99% (Aldrich, USA) and triethylamine 99+% (Aldrich) were used as received. All other solvents and chemicals were HPLC- or analytical-grade materials. All solutions of standards, samples and reagents were refrigerated when not in use.

Apparatus

The LC system consisted of two pumps (Beckman Model 114M) with a gradient controller (Model 421A) and an injection port (Altex, Model 210) with a 20-μl loop. Separations were achieved with a Supelcosil LC-18 (15 cm × 4.6 mm I.D., 5 μm) reversed-phased column. Domoic acid and its butyl isothiocyanate (BITC) derivative were detected with a diode array UV absorption detector (Hewlett-Packard Model 1040 A) using 242 nm as the monitoring wavelength. The mobile phase consisted of a linear gradient of 15–80% (v/v) acetonitrile in water (adjusted to pH 2.5) over 20 min at a flow-rate of 1.0 ml/min. The column was then washed with 100% acetonitrile for 5 min then reequilibriated with 15% acetonitrile in water (pH 2.5) before the next injection.

Sample extraction

The extraction method employed has been described elsewhere [9]. A 5-g amount of homogenized shellfish tissue (Sorvall, USA) was mixed (vortex) with 5 ml of water in a 25-ml centrifuge tube for 1 min. Then 10 ml of methanol were added and the contents mixed (vortex) again for 1 min. The mixture was centrifuged and an aliquot of the clear supernatant was filtered through a 0.45-μm filter (Millex HV, Millipore) before injection into the LC system or derivatization. The PSP extraction procedure [6] was also employed for some samples and results compared to those from the water–methanol extraction method. Also, for comparison purposes, a 1-ml aliquot of the clear extract was cleaned up by employing a 1-ml phenylsulphonic acid strong cation-exchange solid-phase extraction (SPE) cartridge (Baker, USA) followed by a 1-ml octadecyl cartridge (Baker) exactly as described elsewhere [7]. Briefly, 1 ml of extract was added to a cation-exchange SPE cartridge which retained the domoic acid. The cartridge was washed with water then the domoic acid eluted with 0.5 *M* hydrochloric aicd. The acid extract was passed through a C_{18} SPE cartridge which retained the domoic acid. The C_{18} cartridge was then washed with water then the domoic acid eluted with 20% acetonitrile in water containing 1% acetic acid.

BITC Derivatization

The derivatization reagent was prepared fresh daily in a fume hood by mixing 200 μl of methanol with 50 μl triethylamine, 50 μl water and 20 μl butyl isothiocyanate in a small test-tube.

A 20-μl aliquot of sample extract was mixed with 20 μl of BITC reagent solution in a 1-ml reactivial. The contents were permitted to react for 20 min at room temperature with a gentle swirling of the tube after 10 min. The contents were then evaporated to dryness at 40°C with a stream of nitrogen for 15 min (to remove some of the excess reagent). The residue was dissolved in 0.5 ml of acetonitrile–water (15:85, v/v) and analysed by LC.

RESULTS AND DISCUSSION

Fig. 1 shows results for a standard solution of domoic acid before and after BITC derivatization. After reaction the domoic acid peak disappears and a derivative

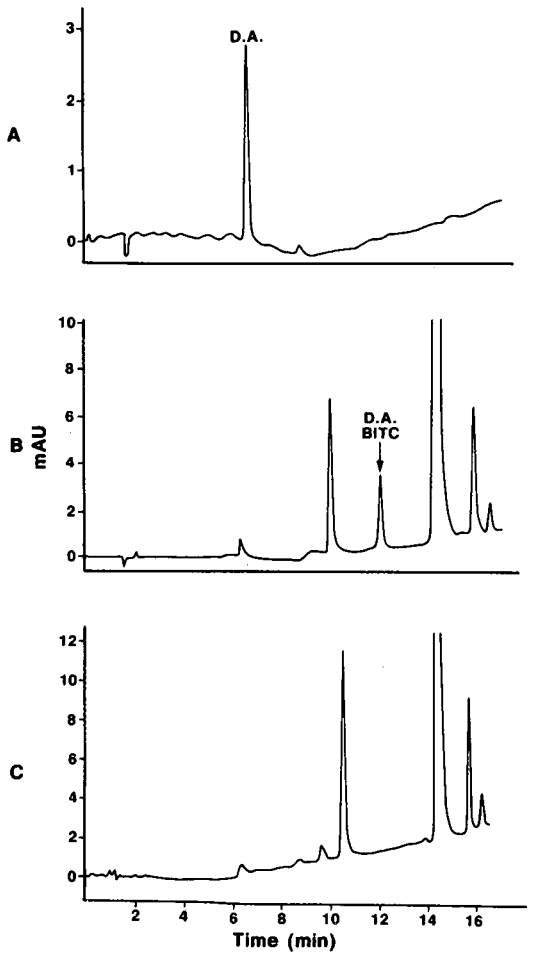

Fig. 1. Chromatograms of standard domoic acid (D.A.) before and after BITC derivatization: (A) 10 ng injected; (B) 10 ng equivalent domoic acid injected; and (C) blank reaction. Gradient conditions described in the text.

peak appears at a later retention time. The derivative peak was about 50% larger in surface area than underivatized domoic acid owing to its increased absorption due to the addition of the thiourea moiety to the molecule which also shifted the UV absorbance maximum to 246 from 242 nm for the underivatized domoic acid.

Fig. 2 compares results obtained for an extract of naturally contaminated mussels containing 538 μg/g domoic acid. The derivatized extract contains many more peaks due to reaction of proteinaceous coextractives with BITC to form products with increased UV absorption. However, the domoic acid derivative is separated and can be identified and quantitated in the extract. This was impossible to do using phenyl isothiocyanate (PITC) as a derivatization reagent [7] since the PITC derivatives of the coextractives completely prevented the detection of domoic acid even at the 500 μg/g level. Fig. 3 compares partial chromatograms of a reagent blank, an uncontaminated (blank) mussel and a mussel sample containing 92 μg/g and derivatized with BITC. The majority of peaks appearing in the chromatograms result from sample coextractives. No peak corresponding to derivatized domoic acid was found in the reagent blank nor the uncontaminated mussel sample.

For comparison purposes we applied the BITC derivatization reaction to extracts cleaned up using the two-cartridge SPE cleanup described earlier [7]. Fig. 4 shows results obtained with the same extract of a naturally contaminated mussel

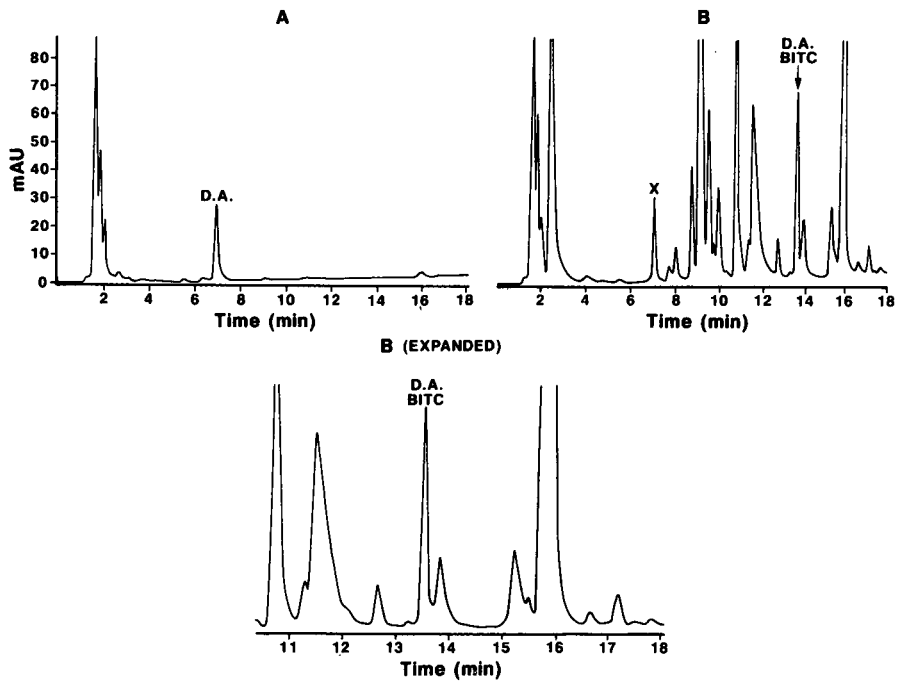

Fig. 2. Chromatograms of domoic acid in naturally contaminated mussel extract (538 μg/g), (A) before and (B) after BITC derivatization (lower chromatogram B expanded between 10–18 min for clarity). Conditions as in Fig. 1 except for a slight decrease in gradient rate. In both chromatograms, 0.2 mg of equivalent sample injected. X = Reagent peak.

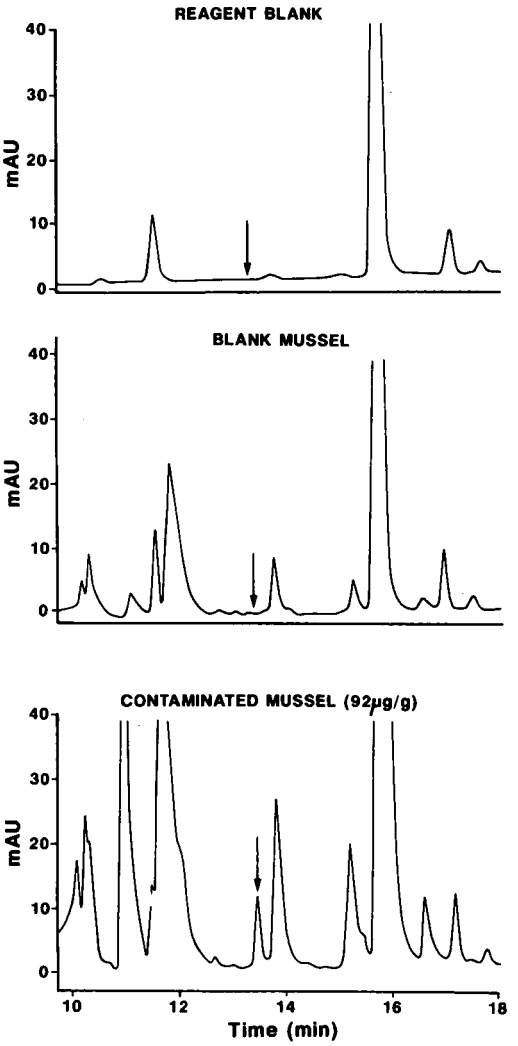

Fig. 3. Chromatograms obtained for a reagent blank, an uncontaminated (blank) mussel and a naturally contaminated mussel (92 μg/g) all after BITC derivatization. Equivalent of 0.2 mg of sample injected. Conditions as in Fig. 2.

sample (538 μg/g domoic acid) as illustrated in Fig. 1, before and after the SPE cleanup. The cleanup is particularly effective in removing coextractives resulting in a chromatogram which appears as clean as a derivatized domoic acid standard. Although the cleanup is rather selective for domoic acid, it is not really necessary for quantitation of BITC-domoic acid as is observed in the upper (A) chromatogram (uncleaned extract) of Fig. 4.

Fig. 5 compares chromatograms for an SPE cleaned-up and non-cleaned-up extract of uncontaminated mussel spiked with 22 μg/g domoic acid. Again the

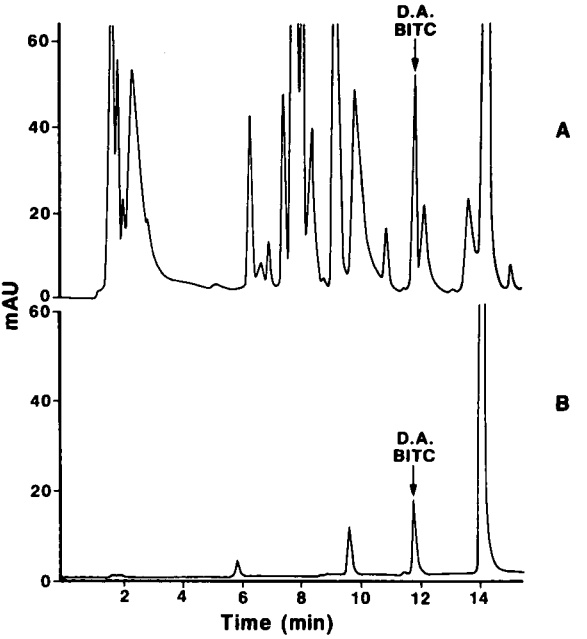

Fig. 4. Chromatograms of cleaned and uncleaned extracts of naturally contaminated mussels after BITC derivatization (538 μg/g). (A) Not cleaned, 0.2 mg of equivalent sample injected; (B) cleaned, 0.1 mg equivalent of sample injected. Conditions as in Fig. 1.

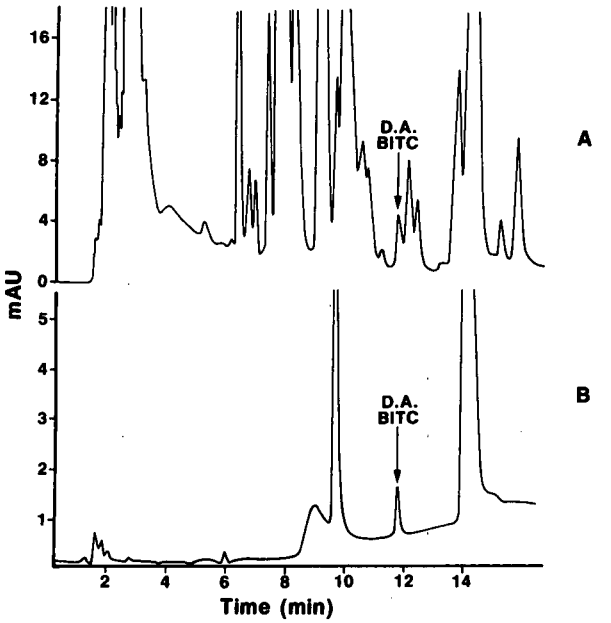

Fig. 5. Chromatograms of cleaned and uncleaned extracts of spiked mussels after BITC derivatization (22 μg/g). (A) Not cleaned, 0.2 mg of equivalent sample injected; (B) cleaned, 0.1 mg equivalent sample injected. Conditions as in Fig. 1.

cleaned-up extract yields a chromatogram similar to a standard. However, the clean-up is not necessary to quantitate domoic acid even at this level although it is a useful tool for additional confirmation puposes because of its good ability to selectively isolate domoic acid from the sample extracts. The small peak near 6 min in the chromatograms of the cleaned-up extracts in Figs. 4 and 5 is unreacted domoic acid which is not observed in the chromatograms of the non-cleaned-up extracts due to a reagent interference. The recovery of domoic acid through the SPE cleanup was about 80%.

The water-methanol extraction was found to be simpler and yielded higher recoveries of domoic acid compared to the acid extraction method. Also, although domoic acid could be confirmed by direct BITC derivatization of the acid extracts, the water–methanol extracts yielded cleaner chromatograms and higher yields of BITC derivative (86–91% yield at 22 μg/g for the water–methanol extraction and 64% yield at 45 μg/g for the acid extraction).

The BITC derivative of domoic acid was stable at 4°C for up to four days in actual derivatized shellfish extracts. This enables batch derivatizations to be performed on one day with HPLC analysis on the next.

The detection limit (3:1, signal-to-noise) for BITC–domoic acid in shellfish extracts was estimated to be about 5–10 μg/g under the conditions employed. This could be improved by employing the SPE cleanup and injecting more material into the LC system. However, for regulatory purposes at the 20 μg/g level, this is unnecessary.

The repeatability coefficient of variation of replicate BITC reactions ($n = 3$) for a spiked mussel extract (22 μg/g domoic acid) was 12% while for a naturally contaminated sample (28 μg/g domoic acid) it was 6%. The derivatization reaction provided linear results in extracts over the range of domoic acid concentrations studied (22–538 μg/g).

The method was successfully applied to the confirmation of domoic acid in fresh mussels, oysters and clams as well as canned pickled mussels. No interfering materials were found in any of these products.

REFERENCES

1 J. L. C. Wright, R. R. Boyd, A. S. W. De Frietas, M. Falk, R. A. Foxall, W. D. Jamieson, M. V. Laycock, A. W. McCulloch, A. G. McInnes, P. Odense, V. P. Pathak, M. A. Quilliam, M. A. Ragan, P. G. Sim, P. Thibault, J. A. Walter, M. Gilgan, D. J. A. Richard and D. Dewar, *Can. J. Chem.*, 67 (1989) 481.

2 M. A. Quilliam and J. L. C. Wright, *Anal. Chem.*, 61 (1989) 1053A.

3 R. F. Addison and J. E. Stewart, *Aquaculture*, 77 (1989) 263.

4 M. A. Quilliam, P. G. Sim, A. W. McCulloch and A. G. McInnes, *Int. J. Environ. Anal. Chem.*, 36 (1989) 139.

5 J. F. Lawrence, C. F. Charbonneau, C. Ménard, M. A. Quilliam and P. G. Sim, *J. Chromatogr.*,, 462 (1989) 349.

6 J. F. Lawrence, C. F. Charbonneau and C. Ménard, *J. Assoc. Off. Anal. Chem.*, 74 (1991) 68.

7 J. F. Lawrence, C. F. Charbonneau, B. D. Page and G. M. A. Lacroix, *J. Chromatogr.*, 462 (1989) 419.

8 R. Pocklington, J. E. Milley, S. S. Bates, C. J. Bird, A. S. W. DeFreitas and M. A. Quilliam, *Int. J. Environ. Anal. Chem.*, 38 (1990) 351.

9 M. W. Gilgan, B. G. Burns and G. J. Landry, presented at the *104th Annual Meeting of the Association of Official Analytical Chemists, New Orleans, 1990*, poster No. 3108.

Journal of Chromatography, 550 (1991) 603–607
Elsevier Science Publishers B.V., Amsterdam

CHROMSYMP. 2164

Determination of hydroxy and peroxy acid derivatives of uroporphyrin in the plasma of patients with congential erythropoietic porphyria by high-performance liquid chromatography

RONG GUO and C. K. LIM*
Division of Clinical Cell Biology, MRC Clinical Research Centre, Watford Road, Harrow, Middlesex HA1 3UJ (UK)

ABSTRACT

A reversed-phase high-performance liquid chromatographic method is described for the determination of hydroxy and peroxy acid derivatives of uroporphyrin in the plasma of patients with congenital erythropoietic porphyria. The porphyrins were extracted from the plasma with 20% trichloroacetic acid – dimethyl sulphoxide (1:1, v/v). The supernatant after centrifugation was chromatographed on a Hypersil-ODS column by gradient elution with 9% (v/v) acetonitrile in 1 *M* ammonium acetate buffer (pH 5.16) (solvent A) and 10% (v/v) acetonitrile in methanol (solvent B) as the gradient mixture. The method was also suitable for the preparative isolation of the porphyrins.

INTRODUCTION

We have previously isolated and characterized three hydroxy and one peroxy acid uroporphyrin I derivatives [1,2] in the urine of patients with congenital erythropoietic porphyria (CEP), namely *meso*-hydroxyuroporphyrin I, β-hydroxypropionic acid uroporphyrin I, hydroxyacetic acid uroporphyrin I and peroxyacetic acid uroporphyrin I (Fig. 1). CEP is a rare genetic disease inherited in the autosomal recessive trait. Patients with CEP characteristically excrete high concentrations of uroporphyrin I in the urine because of uroporphyrinogen III synthase deffect [3,4]. Uroporphyrin I also accumulates in the plasma and skin of these patients, resulting in multilating photo-induced skin lesions. As hydroxy and peroxy acid derivatives of uroporphyrins must be derived from uroporphyrin or uroporphyrinogen by as yet unknown oxidation mechanisms, the origin and distribution of these compounds were further investigated in the plasma of patients with CEP. This paper describes a reversed-phase high-performance liquid chromatographic (HPLC) method for the isolation and determination of hydroxy and peroxy acid derivatives of uroprophyrin in human plasma and reports for the first time the detection of these compounds in plasma of CEP patients.

0021-9673/91/$03.50

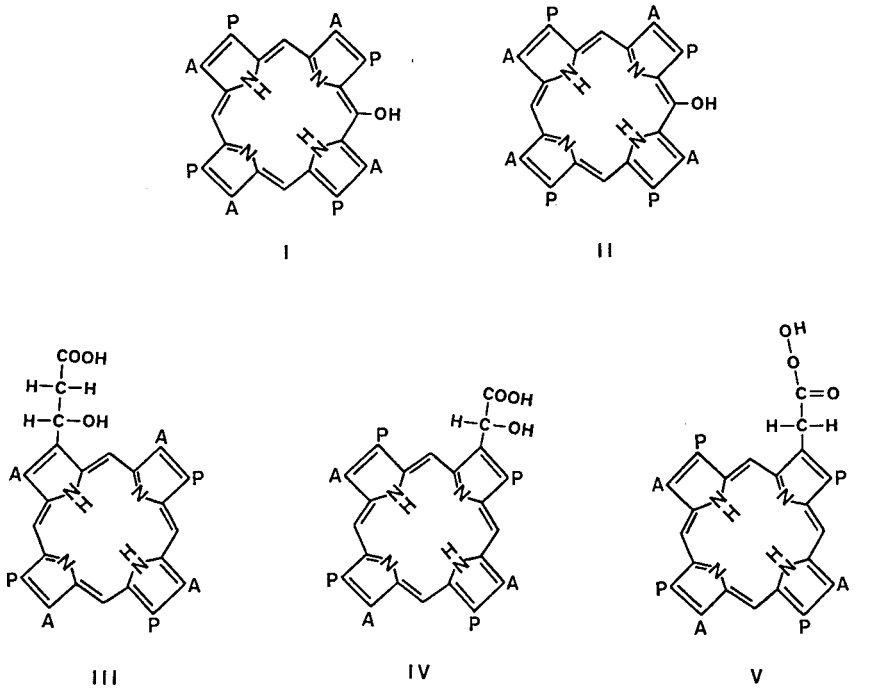

Fig. 1. Structures of hydroxy and peroxy acid derivatives of uroporphyrin. I, *meso*-Hydroxyuroporphyrin I; II, *meso*-hydroxyuroporphyrin III (only one of the four possible isomeric forms is shown); III, β-hydroxypropionic acid uroporphyrin I; IV, hydroxyacetic acid uroporphyrin I; V, peroxyacetic acid uroporphyrin I. A = Acetic acid and P = propionic acid.

EXPERIMENTAL

Materials and reagents

Ammonium acetate, glacial acetic acid, dimethyl sulphoxide (DMSO), trichloroacetic acid (TCA) and hydrochloric acid were of Analar grade from BDH (Poole, UK). Acetonitrile and methanol were of HPLC grade from Rathburn Chemicals (Walkerburn, UK). *meso*-Hydroxyuroporphyrin I and III were synthesized by the thallium(III) trifluoroacetate method [5], which has been adapted by us for the preparation of *meso*-hydroxyuroporphyrin [1], and β-hydroxypropionic acid uroporphyrin I and hydroxyacetic acid uroporphyrin I were isolated from CEP patients as described previously [1,2].

Extraction of porphyrins from plasma

Plasma (200 μl) from patients with CEP was vortex mixed for 1 min with 200 μl of 20% TCA–DMSO (1:1, v/v) and centriguged at 2000 *g* for 10 min. The supernatant was injected into the HPLC system.

For larger scale extraction, 15 ml of plasma were used. The plasma was vortex mixed with an equal volume of 20% TCA–DMSO (1:1, v/v). The supernatant after centrifugation was collected. The residue was again vortex mixed with 20% TCA–

DMSO (1:1, v/v) (5 ml), centrifuged and the supernatant collected. The pooled supernate was diluted 1:15 (v/v) with 0.5 *M* ammonium acetate buffer (pH 5.16) and loaded under suction into a C_{18} Bond-Elut sorbent extraction cartridge (Analytichem International, Habor City, CA, USA) that had been preconditioned by washing successively with methanol (2 ml) and 0.5 *M* ammonium acetate buffer (pH 5.16) (10 ml). The cartridge was washed with 3 ml of 0.5 *M* ammonium acetate buffer (pH 5.16) and the adsorbed porphyrins were eluted with 1-ml portions of 10% (v/v) acetonitrile in methanol until very little fluorescent was detected on the cartridge under a UV lamp. The eluate was pooled and then evaporated to dryness at 40°C under nitrogen. The residue was dissolved in 1 ml of 0.3 *M* hydrochloric acid for HPLC separation.

HPLC separation of uroporphyrin I and its hydroxylated derivatives in plasma extract

The HPLC system consisted of a Varian Associates (Walton-on-Thames, UK) Model 5000 pump and a Varian fluorescence detector with an excitation wavelength of 400 nm and a 580-nm cut-off filter for the emission. Samples (250 μl) were injected by a Rheodyne (Cotati, CA, USA) Model 7125 injection valve fitted with a 500-μl loop. The separation was carried out on a 25 cm × 5 mm I.D. Hypersil-ODS column (Shandon Scientific, Runcorn, UK) by gradient elution. The solvent mixtures were 9% (v/v) acetonitrile in 1 *M* ammonium acetate buffer (pH 5.16) (solvent A) and 10% (v/v) acetonitrile in methanol (solvent B). The elution programme was as follows: time 0 to 30 min, 0% solvent B (100% solvent A) to 90% solvent B (10% solvent A); time 30 to 40 min, isocratic elution at 90% solvent B; time 40.1 min, re-equilibrate column at 0% solvent B (100% solvent A). The flow-rate was 1 ml/min throughout.

For the preparative isolation of individual porphyrin, the peak was collected and pooled. The organic solvents were removed by evaporation under nitrogen. The porphyrin in the aqueous solution was then concentrated and recovered by the cartridge extraction technique described above.

RESULTS AND DISCUSSION

The chromatogram of porphyrins in the plasma of a patient with CEP is shown in Fig. 2. Of the eight peaks, six have been positively identified.

Peak 2 co-eluted with synthetic *meso*-hydroxyuroporphyrin I under all HPLC conditions. It is therefore probably *meso*-hydroxyuroporphyrin I (Fig. 1, structure I). This was confirmed by sodium amalgam reduction of the compound followed by aromatization with iodine, which eliminated the hydroxyl group to give uroporphyrin I [1].

Peak 3 was identified as *meso*-hydroxyuroporphyrin III (Fig. 1, structure II; there are four possible isomers of which only one is shown here) as it had a retention time identical with that of an authentic standard. The four *meso*-hydroxyuroporphyrin III isomers could not be resolved under the HPLC conditions used. Reduction of the compound followed by re-oxidation gave uroporphyrin III, confirming that the assignment was correct. The detection of *meso*-hydroxyuroporphyrin III in the plasma is interesting, as the compound had not been isolated from the urine of CEP patients despite the fact that uroporphyrin III excretion was also elevated, although this was not as high as uroporphyrin I. In the plasma, however, uroporphyrin III was barely detectable. Whether *meso*-hydroxyuroporphyrin III in its reduced form can

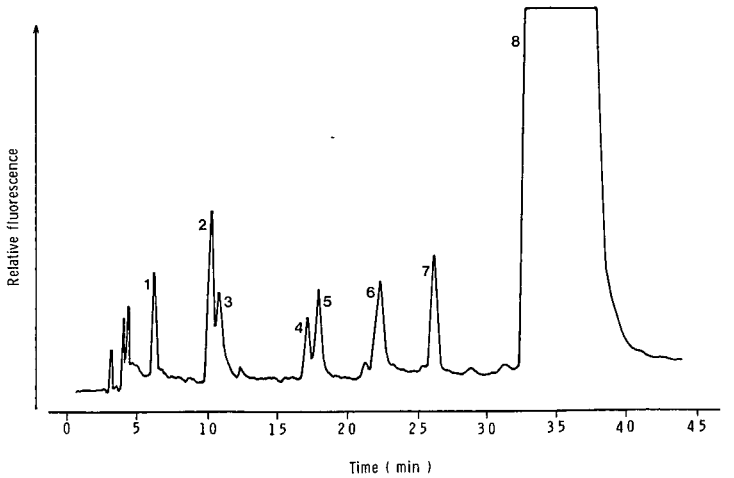

Fig. 2. Separation of porphyrins in the plasma of a patient with congenital erythropoietic porphyria. Peaks: 1, unidentified; 2, *meso*-hydroxyuroporphyrin I; 3, *meso*-hydroxyuroporphyrin III; 4, unidentified, 5, β-hydroxypropionic acid uroporphyrin I; 6, hydroxyacetic acid uroporphyrin I; 7, peroxyacetic acid uroporphyrin I; 8, uroporphyrin I.

give rise to uroporphyrinogen III *in vivo* is not known. If it can, then this could represent an alternative pathway to the biosynthesis of uroporphyrinogen III and hence haem.

Peak 5 was identical in chomatographic and chemical behaviour with that of the β-hydroxypropionic acid uroporphyrin I isolated from the urine of CEP patients [6] and was therefore assigned structure III in Fig. 1. This compound can be easily dehydrated by heating in dilute hydrochloric acid to give the monoacrylic derivative as the main product [6].

The chromatographic and chemical properties of peak 6 were identical with those of hydroxyacetic acid uroporphyrin I (Fig. 1, structure IV). This compound had also been isolated from the urine of CEP patients. On heating in dilute hydrochloric acid no dehydration product was formed [6], indicating that the hydroxyl group is attached to an acetic acid group and is therefore difficult to dehydrate. Some partial decarboxylation products were formed instead.

Peak 7 was peroxyacetic uroporphyrin I (Fig. 1, structure V). It had a characteristic greenish colour with a typical red porphyrin fluorescence under UV light. As with the same compound isolated from urine of CEP patients, it gave uroporphyrin I when treated with 0.1 *M* potassium or calcium hydroxide but was stable under acidic conditions [2]. It also co-eluted with the authentic standard under all HPLC conditions.

The presence of hydroxy and peroxy acid derivatives of uroporphyrins in the plasma of patients with CEP rules out of the possibility that they were formed in the kidney prior to excretion in the urine where they were originally isolated [1,2,6]. These compounds must be derived from uroporphyrin or uroporphyrinogen *in vivo* by unknown hydroxylation or oxidation processes which require further investigation.

Studies on the metabolism and the biological and toxicological importance of

these compounds are also needed. Hydroxylated and particularly peroxylated derivatives can easily generate free radicals which can lead to cell damage. The reduced forms (porphyrinogens) are structurally very similar to uroporphyrinogen III. They may therefore compete with or inhibit the decarboxylation of uroporphyrinogen III to coproporphyrinogen III by uroporphyrinogen decarboylase. It may be significant that we have found normal uroporphyrinogen decarboxylase activity in the red cells of patients with CEP while these patients always excrete elevated level of uroporphyrin III in the urine. Inhibition of uroporphyrinogen decarboxylase by any one or all of these compounds is a possible explanation.

Peaks 1 and 4 were not identified as these two compounds were not found in the urine of CEP patients and sufficient amounts have not been isolated for positive identification. Peak 8 was the large amount of uroporphyrin I present in the plasma of CEP patients.

REFERENCES

1 R. Guo, J. M. Rideout and C. K. Lim, *Biochem. J.*, 264 (1989) 293.
2 R. Guo, J. M. Rideout, W. Chai, A. M. Lawson and C. K. Lim, *Biomed. Chromatogr.*, 5 (1991) 53.
3 G. Romeo and E. Y. Levin, *Proc. Natl. Acad. Sci. USA*, 63 (1969) 856.
4 A. S. Gidari and R. D. Levere, *Semin. Hematol.*, 14 (1977) 145.
5 G. H. Barnett, M. F. Hudson, S. W. McCombie and K. M. Smith, *J. Chem. Soc., Perkin Trans. 1*, (1973) 691.
6 R. Guo, W. Chai, J. M. Rideout, A. M. Lawson and C. K. Lim, *Biomed. Chromatogr.*, 4 (1990) 141.

Journal of Chromatography, 550 (1991) 609–620
Elsevier Science Publishers B.V., Amsterdam

CHROMSYMP. 2083

Chemical class separation of coal liquids by high-performance liquid chromatography on a semi-preparative, phosphoric acid-modified amino-bonded-phase column

JOHN W. HAAS, III[a] and PETER C. UDEN*
Department of Chemistry, Lederle Graduate Research Tower A, University of Massachusetts, Amherst, MA 01003-0035 (USA)

ABSTRACT

A amino-bonded stationary phase, modified by treatment with phosphoric acid to form an amino phosphate, permits the high-performance liquid chromatographic separation of aliphatic, non-polar aromatic, neutral/acidic polar aromatic and basic polar aromatic hydrocarbon chemical classes. It was employed to fractionate coal liquid samples on a semi-preparative scale.

INTRODUCTION

Among fuel sources being investigated as alternatives to petroleum, coal-derived liquids have generated considerable interest because of the abundance and low cost of coal feedstock. Various sources and processing methods produce coal liquids with different chemical compositions. When evaluating the overall usefulness and acceptability of these various coal liquids as fuel sources, it is important to include measurements of utile energy content and health risk assessments using biological tests. The energy content of a fuel can often be determined using easily measured properties such as C/H ratios. However, biological testing to date has shown that in many instances only a few potent chemical compounds, present at trace levels in a coal liquid, account for most of the biological activity. Consequently, samples must be characterized extensively so that these species can be identified and determined. This task is made difficult, however, by the complexity of coal liquids; they are known to contain numerous hydrocarbons including aliphatics, "simple" aromatics (including benzene and polycyclic aromatics), alkyl- and other substituted aromatics, hydroaromatics and heterocyclics. Therefore, a combination of several high-resolution analytical methods is usually required to characterize fully a particular coal liquid sample.

Prefractionation can both simplify and reduce the number of high-resolution analyses needed to characterize a coal liquid thoroughly. Prefractionation by normal-

[a] Present address: Oak Ridge National Laboratory, Oak Ridge, TN 37832-6113, USA.

0021-9673/91/$03.50

phase high-performance liquid chromatography (HPLC) using silica, amino and amino–cyano columns has been reported [1–4]. All of the reported prefractionations, however, required the use of a back-flush in order to elute the aromatic fraction. Although the use of a back-flush is acceptable, a simplified prefractionation procedure that does not require the switching of valves in the middle of the chromatographic run would be of value. Also, the prefractionation steps reported achieved class separations of the aliphatic and aromatic fractions only. The separation of the aromatic fraction into the "simple" aromatics (including benzene and polycyclic aromatics), alkyl- and other substituted aromatics, hydroaromatics and heterocyclics was not accomplished.

In response to the limitations of existing polar bonded stationary phases and liquid–solid chromatographic (LSC) adsorbents, we recently developed a phosphoric acid-modified amino-bonded phase that, in a preliminary study, separated model compounds into aliphatic, non-polar aromatic, neutral/acidic polar aromatic and basic polar aromatic hydrocarbon chemical classes [5]. In the study described here, the phosphoric acid-modified column was investigated further and used to fractionate coal liquid samples on a semi-preparative scale.

EXPERIMENTAL

Reagents

Standard compounds were obtained from Aldrich (Milwaukee, WI, USA) and were used as received. HPLC-grade hexane and dichloromethane and 85% phosphoric acid were purchased from Fisher Scientific (Fair Lawn, NJ, USA). HPLC-grade isopropanol and glacial acetic acid were obtained from J. T. Baker (Phillipsburg, NJ, USA) and MCB Manufacturing Chemists (Cincinnati, OH, USA), respectively. All solvent mixtures were prepared volumetrically. The 10-μm Chromosorb LC-9 amino-bonded phase was from Manville Products (Denver, CO, USA).

Samples

The coal liquid and Illinois No. 6 heavy fuel oil (b.p. 435–900°F) was obtained from an H-coal pilot plant at Oak Ridge National Laboratory (Oak Ridge, TN, USA). Of primary interest to us was the hexane-soluble fraction of the SRC-II sample; the work reported here was part of an effort to develop methods to remove biologically active compounds from synthetic fuels. Thus, prior to HPLC fractionation, 10 g of the coal liquid were shaken with 10 ml of hexane and the asphaltene precipitate was removed by filtration. A spiked coal liquid sample was prepared by dissolving four standard compounds in a portion of the coal liquid–hexane mixture which had been diluted further (1:75) with hexane. The final concentrations of the four components were 50–150 mg/l in the spiked sample. Samples used for column recovery studies and as model polar hydrocarbons were individual standard compounds dissolved in hexane at concentrations of 75–200 mg/l. The mixture of standard *n*-alkanes was obtained from Supelco (Bellefonte, PA, USA).

High-performance liquid chromatography

HPLC was performed with an IBM Instruments (Wallingford, CT) Model 9533 ternary gradient chromatograph equipped with a fixed-wavelength (254 nm) UV ab-

sorbance detector and a 250-μl injection loop. The semi-preparative stainless-steel column (25 cm × 1 cm I.D.) was packed with 15 g of amino-bonded phase using isopropanol as both slurry and packing solvent [5]. The amino-bonded phase was modified with phosphoric acid by pumping 75 ml of 0.5% phosphoric acid in isopropanol solution through the column. The modified bonded phase, considered to consist primarily of ammonium phosphate groups [5], was then washed with 75 ml each of isopropanol and dichloromethane prior to equilibration with hexane.

The ternary solvent gradient program developed to separate model synthetic compounds [5] was modified for fractionation of the coal liquid samples. The complete solvent program is included in Table I and was also used for the recovery studies. The initial low flow-rate allowed a fraction to be collected from the beginning of the run until the first detectable species eluted from the column (at higher flow-rates it was difficult to change collection vessels before the second fraction began to elute into the vessel for the first fraction). The switch to 100% hexane after 35 min kept acetic acid out of the isopropanol fraction, from which it cannot be extracted. After 50 min, the flow-rate was again reduced because the pressure increased when 100% isopropanol was pumped through the column. The bonded phase was regenerated to full activity by pumping 0.5% phosphoric acid in isopropanol through the column for 5 min at the end of the chromatographic run. Coal liquid fractions or recovery standards were collected manually and concentrated by blowing nitrogen over the solutions as they were warmed on a hot-plate. Fractions containing acetic acid were extracted with 3 × 15 ml of distilled, dionized water and dried over sodium sulfate prior to concentration.

Gas chromatography

The coal liquid fractions and recovery standards were analyzed by GC using a Varian (Palo Alto, CA, USA) Model 2760 chromatograph equipped with a 22 m × 0.31 mm I.D. SE-52 capillary column and both flame ionization detection (FID) and

TABLE I

TERNARY HPLC MOBILE PHASE PROGRAM FOR THE SEMI-PREPARATIVE CHEMICAL CLASS FRACTIONATION OF COAL LIQUIDS USING A PHOSPHORIC ACID-MODIFIED AMINO-BONDED-PHASE COLUMN

Time (min)	Solvent	Flow-rate (ml/min)
0	100% hexane	2.00
8	100% hexane	5.00
20	100% hexane[a]	5.00
30	hexane–acetic acid (96.5:3.5)[b]	5.00
35	Switch to 100% hexane	5.00
40	100% hexane[a]	5.00
50	100% isopropanol[b]	3.50
65	Switch to 0.5% phosphoric acid in isopropanol	3.50
70	Switch to 100% isopropanol	3.50
80	100% isopropanol[a]	3.50
90	100% hexane[b]	5.00

[a] Begin a linear mobile phase gradient.
[b] End a linear mobile phase gradient.

nitrogen–phosphorus detection (NPD) were used. The column oven was programmed from 60 to 275°C at 8°C/min. Fractions were also analyzed with a Hewlett-Packard (Palo Alto, CA, USA) Model 5985 gas chromatographic-mass spectrometric (GC–MS) system employing the same GC column and temperature program. Electron impact ionization was used to obtain individual mass spectra, which were compared the NIH–EPA–MSDC mass spectral database using the GC–MS computer system.

RESULTS AND DISCUSSION

Recovery studies

Ideally, an HPLC prefractionation method should provide quantitative (100%) recovery of all sample components. In practice, bonded stationary phases normally give better recoveries than LSC adsorbents such as silica gel, silicic acid or alumina, which adsorb some polar compounds irreversibly. Recoveries from the phosphoric acid-modified amino bonded phase were determined for compounds representing some of the most abundant (*e.g.*, polycyclic aromatics) or bioactive (*e.g.*, amino aromatics) chemical classes found in coal liquids. The results are compared in Table II with those reported for low-pressure alumina and silicic acid columns [6]. Recoveries of non-polar aromatic hydrocarbons, neutral nitrogen-containing aromatic hydrocarbons and acidic hydroxy aromatic hydrocarbons from all three columns were nearly quantitative. The neutral alumina column provided better recoveries of the nitrogen-containing aromatic bases than did the two acidic columns. However, the modified amino-bonded phase yielded significantly higher recovery (72%) of the amino aromatic hydrocarbon 9-aminophenanthrene than did either the alumina adsorbent (57%) or the silicic acid adosrbent (39%). Overall, recoveries from the modified amino-bonded-phase column were excellent, comparing favorably with those obtained from the solid alumina and silicic acid adsorbents.

TABLE II

RECOVERIES OF MODEL COAL LIQUID COMPOUNDS FROM PHOSPHORIC ACID-MODIFIED AMINO, ALUMINA AND SILICIC ACID LC COLUMNS

Compound	Chemical class	Recovery (%)		
		Modified Amino	Alumina[a]	Silicic Acid[a]
Phenanthrene	Non-polar aromatic	99	98	–
1-Naphthol	Hydroxy aromatic	94	–	–
1-Acenaphthol	Hydroxy aromatic	–	85	–
Carbazole	Neutral nitrogen-containing aromatic	94	87	88
2-Methylindole	Neutral nitrogen-containing aromatic	82	–	–
Pyridine	Basic nitrogen-containing aromatic	84	–	–
Quinoline	Basic nitrogen-containing aromatic	–	100	81
Acridine	Basic nitrogen-containing aromatic	–	99	90
3-Aminofluoranthene	Amino aromatic	68	64	64
9-Aminophenanthrene	Amino aromatic	72	57	39

[a] Ref. 2.

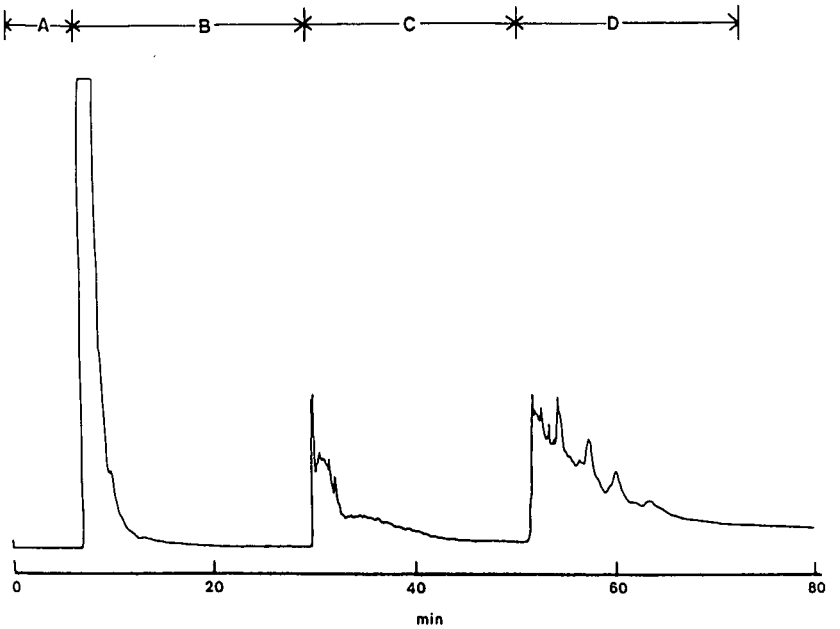

Fig. 1. Chemical class fractionation of hexane-treated Illinois No. 6 coal liquid on the semi-preparative, phosphoric acid-modified amino-bonded-phase HPLC column. Fractions: (A) non-polar aliphatics; (B) non-polar aromatics; (C) neutral/acidic polar hydrocarbons; (D) basic polar hydrocarbons.

HPLC fractionation of coal liquid samples

Three groups of peaks are observed in the chromatogram for the diluted coal liquid–hexane mixture (Fig. 1) and were collected as fractions B–D when the original hexane-soluble fraction (75 times more concentrated) was separated. A fourth fraction, A, expected to contain non-polar aliphatic hydrocarbons which are not detected at 254 nm, was collected from the beginning of the chromatographic run until the first peak was detected for fraction B.

Fig. 1 shows that fraction B, assigned to the non-polar aromatic hydrocarbon class, was eluted as a relatively narrow band with hexane. The compact elution profile was produced when a short equilibration with hexane was used prior to sample separation. Longer equilibrations (up to 1 h or more) removed residual isopropanol, water and phosphoric acid from the column and resulted in stronger adsorption and better resolution of components within the fraction. Thus, longer equilibrations can be used when "subfractionation" of the non-polar aromatic class is needed to facilitate the determination of single compounds. It has been demonstrated that polycyclic aromatics are separated by the modified amino-bonded phase according to the number of condensed rings in the range 2–5 [5]. This ring number-based separation is characteristic of polar stationary phases, including bonded phases and traditional LSC adsorbents, when non-polar solvents are used to separate parent and alkylated aromatic hydrocarbons [7–10]. Although these aromatics have been labelled "non-polar", they are in fact weakly polar and interacted enough with the polar stationary phase to elute after the aliphatic hydrocarbons, which were not retained at all on the

column. However, hydrocarbons substituted with polar functional groups, especially those capable of interacting with the polar stationary phase through strong hydrogen bonds, were retained on the column longer than the "non-polar" aromatics.

Fraction C was eluted from the HPLC column when acetic acid was added to the hexane mobile phase. Early in the gradient, increasing solvent strength caused polar species forming weak hydrogen bonds with the phosphate bonded phase groups (*e.g.*, neutral aromatics) to elute rapidly from the column after the non-polar aromatics. At higher concentrations of acetic acid, polar hydroxy aromatics and other acids capable of forming stronger hydrogen bonds with the stationary phase were displaced, leaving bases on the column. Because of their abundance in fossil fuels, only phenolic-type hydroxy aromatics were tested in our previous study [5]. In this study, however, it was confirmed with standard compounds that stronger acids such as aliphatic (*e.g.*, stearic) and aromatic (*e.g.*, benzoic) carboxylic acids were eluted in this fraction. Thus, the fraction can be classified more broadly as containing neutral aromatics and acidic hydrocarbons (both aliphatic and aromatic). It is also notable that the use of acetic acid in the mobile phase was critical for the selective elution of acids in fraction C. For example, when isopropanol (another strong hydrogenbonding solvent, but weaker than acetic acid) was added to the hexane mobile phase instead of acetic acid, the acids and bases eluted together [5]. Acetic acid's levelling effect on acids, strengthening of bases and strong competition for sites active for adsorbing acids could all have contributed to the preferential elution of the acids. The unique selectivity of acid-containing mobile phases employed with the modified amino-bonded-phase column is currently under further investigation.

The final acetic acid concentration, 3.5% in hexane, was not high enough to remove strongly adsorbed nitrogen-containing bases from the column. They were eluted in fraction D with a gradient to 100% isopropanol. The especially strong retention of the bases was presumably due to hydrogen bonds formed between the nitrogens of the bases and acidic hydroxyl protons of the phosphate stationary phase groups. It is well known that the strongest hydrogen bonds are formed between the most acidic proton donors and the most basic proton acceptors [11]. Further, it was confirmed with standard compounds such as 2-aminooctane that aliphatic bases eluted in this fraction along with the aromatic bases. Hence, fraction D can be assigned more generally to hydrocarbon bases.

The HPLC results provide some useful initial characterization of the hexane-soluble coal liquid sample. It is clear from Fig. 1 that the hexane-treated sample used in our study, similarly to a related whole oil which contained about 20% polar compounds [12], contained more non-polar aromatics than the more biologically active and less energetically useful polar aromatics. However, when a sample of whole oil was separated with the modified amino-bonded-phase column, the UV absorbances of fractions C and D increased relative to fraction B, indicating that the hexane dilution/precipitation procedure had enriched the non-polar hydrocarbon content of the fuel. More detailed HPLC characterization could be achieved if a variable-wavelength absorbance detector set near 200 nm or a refractive index detector was employed. Then the non-polar aliphatics would have been detected along with the aromatics, providing a non-polar aliphatic/aromatic hydrocarbon ratio which is one useful measure of energy content.

Support for the chemical assignments and retention mechanisms proposed

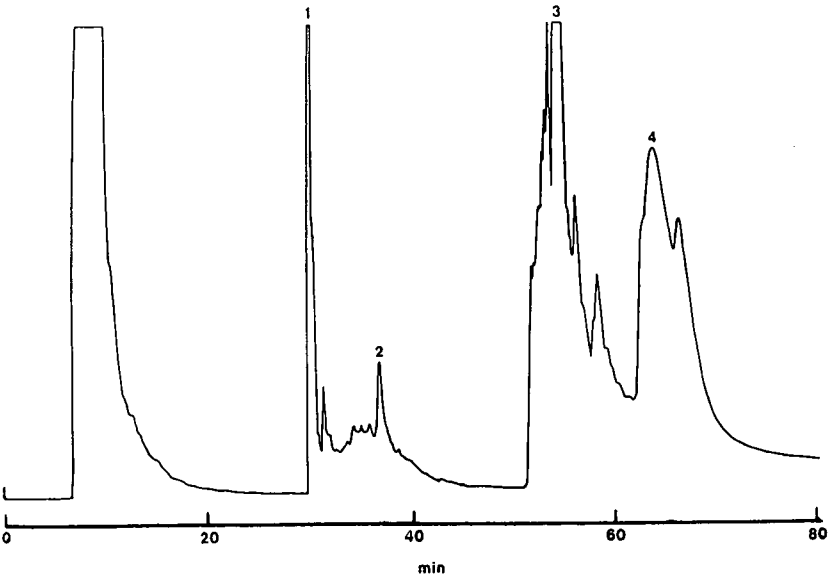

Fig. 2. Chemical class fractionation of hexane-treated Illinois No. 6 coal liquid hexane extract spiked with four model synthetic fuel compounds. Peak identities: (1) carbazole; (2) 1-naphthol; (3) phenanthridine; (4) 4-picoline.

above was obtained for the two polar fractions by spiking the hexane-soluble coal liquid fraction with four model compounds. The results (Fig. 2) indicate that the assignments were correct. Carbazole, a neutral nitrogen-containing compound, eluted early in the neutral/acidic polar hydrocarbon fraction C. Capable of forming a stronger hydrogen bond through its acidic hydroxyl group, 1-naphthol eluted later in the same fraction. Phenanthridine and 4-picoline are bases and eluted as expected in the basic polar hydrocarbon fraction D. Although both compounds were able to interact with the acidic phosphate groups of the stationary phase through a heterocyclic nitrogen, the hydrogen bond formed was stronger for 4-picoline, the stronger base (p^{K}_{a} = 6.02). Hence, it eluted after phenanthridine (pK_a = 5.58). The nitrogen in phenanthridine is also sterically hindered by its ring system, a factor which probably contributes to its weaker retention.

GC analysis of coal liquid fractions

GC and GC–MS analyses were used to confirm the chemical class assignments for the coal liquid fractions and demonstrate the usefullness of prefractionation when there is a need for individual compound identification. It may be noted that no evidence was seen of any GC column degradation and performance loss resulting from the presence in samples of phosphoric acid removed from the column.

Chromatograms for HPLC fractions A–C obtained with FID and NPD are presented in Fig. 3–5. The FID trace in Fig. 3 shows that fraction A contained an abundance of non-polar aliphatic hydrocarbons even though the fraction was not visible in the HPLC trace (Fig. 1). Appreciable amounts of n-C_{15}–C_{27} alkanes are

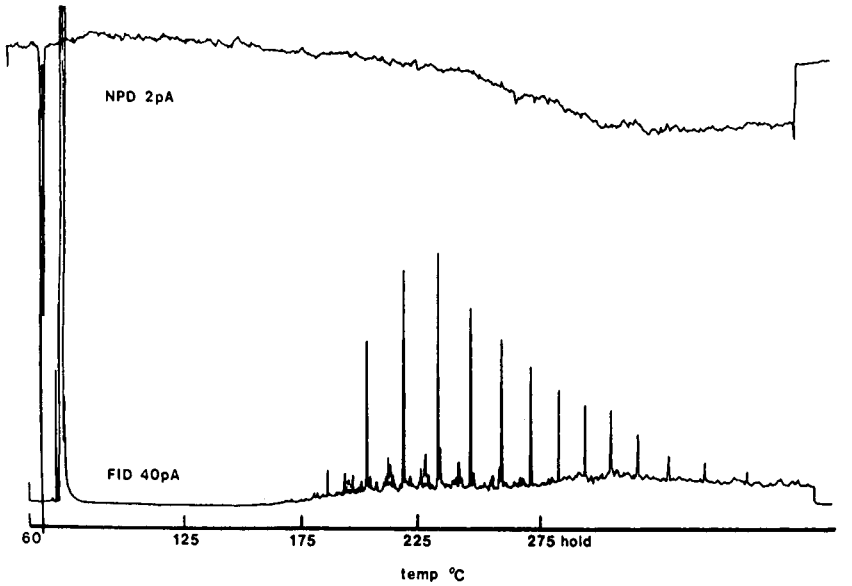

Fig. 3. Dual FID–NPD capillary gas chromatogram of the non-polar aliphatic hydrocarbon fraction A recovered from the HPLC separation of hexane-treated Illinois No. 6 coal liquid.

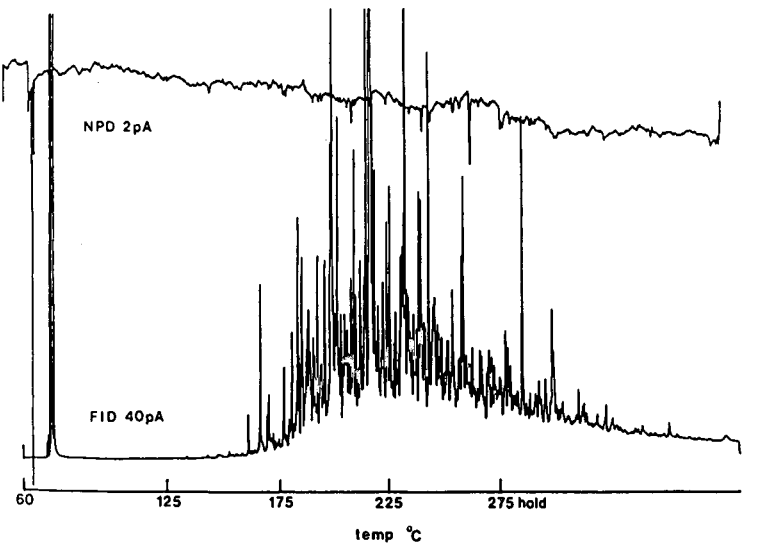

Fig. 4. Dual FID–NPD capillary gas chromatogram of the non-polar aromatic hydrocarbon fraction B recovered from the HPLC separation of hexane-treated Illinois No. 6 coal liquid.

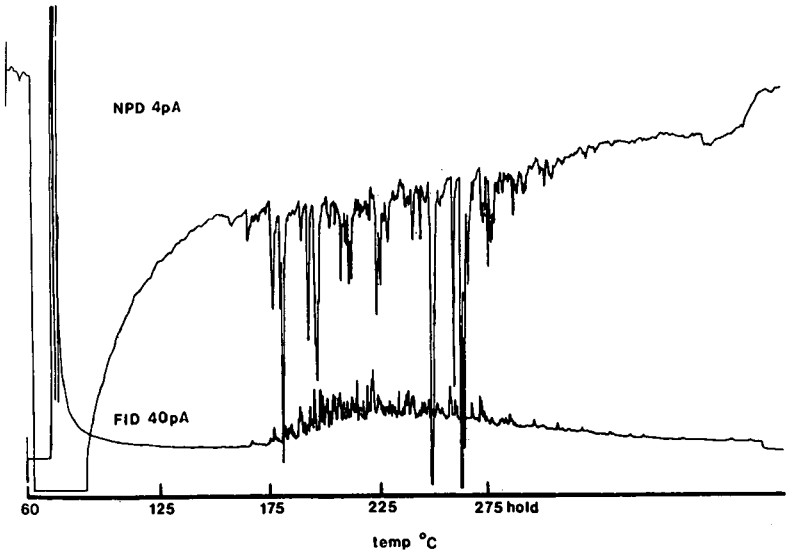

Fig. 5. Dual FID–NPD capillary gas chromatogram of the neutral/acidic polar hydrocarbon fraction C recovered from the HPLC separation of hexane-treated Illinois No. 6 coal liquid.

observed with the largest peak being at n-C_{17} (heptadecane). Peak identities were confirmed by comparing retention times and mass spectra with those for a standard mixture of normal aliphatic hydrocarbons. Lower molecular weight hydrocarbons, up to *ca.* C_{10}–C_{11}, were certainly lost during the concentration step. This was relatively unimportant, however, for this study, as they would elute prior to the alkanes which were observed. Only very small amounts of other compounds are evident in the FID trace. Mass spectra indicated that these species were primarily branched aliphatics, although most of the small peaks in the FID trace were below the MS detection limits. No aromatics were detected by MS. Further, using NPD no nitrogen-containing species were detected in this fraction. This is not surprising as any nitrogen-containing compound would probably have been polar enough to be retained more than the non-polar aliphatic or aromatic hydrocarbons.

Overall, the GC results for fraction A indicate that the HPLC separation of non-polar aliphatics from other hydrocarbons, most notably the non-polar aromatics, was efficient, allowing individual aliphatics to be easily determined without interference. This is not the case when whole coal liquids are analyzed by GC; the aliphatics are difficult to detect and determine in FID traces dominated by aromatic hydrocarbon peaks (see the discussion of fraction B below). Based on the strong FID responses for fraction A, it can be concluded that most of the valuable aliphatic hydrocarbon content of the SRC-II sample was maintained through the hexane dilution/precipitation procedure. This conclusion seems reasonable considering that non-polar aliphatic compounds such as octadecane are not retained on the HPLC column [5] (resulting in quantitative recovery) and are highly soluble in hexane. As discussed earlier, the use of a non-selective detector with the HPLC method would help to

confirm this conclusion by quantifying the non-polar aliphatic contents of dilute and whole oil comparison samples.

The second HPLC fraction, B, contained more gas chromatographable material (see Fig. 4) than did the other fractions. GC–MS analysis confirmed the predominance of unsubstituted and alkylated polycyclic aromatics in the fraction. These were the only species detected; the primary compounds indentified are included in Table III. The abundance of aromatics in the sample was consistent with previous analyses which indicated that non-polar aromatic compounds comprised about 47% of a similar whole oil sample [12]. The GC results were also consistent with the HPLC data which indicated that the non-polar aromatics were enriched relative to the polar compounds during hexane pretreatment of the whole oil. It is clear that hexane pretreatment did not reduce significantly the non-polar aromatic content relative to the whole coal liquid. The excellent recoveries of polycyclic aromatics such as phenanthrene (99%) from the HPLC columns and their generally favorable solubility in hexane support this conclusion.

TABLE III

SOME OF THE COMPOUNDS IDENTIFIED IN HPLC FRACTIONS B AND C OF HEXANE-TREATED ILLINOIS NO. 6 COAL LIQUID

HPLC fraction		Compound
(B)	Non-polar aromatic hydrocarbons	C_1-naphthalenes
		C_4-naphthalenes
		Anthracene/phenanthrene
		Fluoranthene/pyrene
(C)	Neutral/acidic polar hydrocarbons	Phenol
		Cresols
		C_2-phenols
		Carbazole

Fig. 4 also shows that the composition of fraction B was complicated and it would be difficult to determine many of the individual aromatic hydrocarbons. In this instance, the capability of the amino-bonded phase to provide ring number-based subfractions could be used to simplify subsequent GC analysis, including the identification and determination of biologically active compounds. A few nitrogen-containing species can be observed at trace levels in the NPD trace in Fig. 4. These species were probably neutral nitrogen-containing compounds in which the nitrogens were sterically hindered by alkyl groups or aromatic rings so that they were restricted from interacting with the stationary phase. However, the concentrations of these compounds were far below those of polycyclic aromatic hydrocarbons, and they could not be detected by MS.

The FID trace in Fig. 5 shows that HPLC fraction C contained many species at low concentrations. The low polar hydrocarbon levels were consistent with the HPLC results for hexane-treated and whole oil samples; this indicated that non-polar compounds were enriched relative to the polars compounds during hexane dilution/precipitation. This enrichment reflects the low solubility of polar compounds in hexane

and demonstrates that a simple precipitation scheme can be used to reduce the levels of undesirable polar compounds in synthetic fuels. GC–MS analysis confirmed the presence of neutral/acidic polar compounds in fraction C through identification of carbazole and various alkylated phenols (Table III). Non-polar aromatics were not detected, however, demonstrating that the separation of polar species from non-polar aromatics was efficient using the modified amino-bonded-phase column. These results illustrate again the merits of HPLC prefractionation, *i.e.*, GC analysis of the whole liquid would not have identified any of the polar compounds listed in Table III.

The NPD trace in Fig. 5 shows that many of the compounds in HPLC fraction C contained nitrogen, suggesting that all the neutral nitrogen-containing species, except the few observed in fraction B, were efficiently recovered and eluted in this fraction. The excellent recovery of carbazole (94%) from the modified amino-bonded phase supports this conclusion. Although the concentrations of the nitrogen-containing species were low and the hydroxy aromatics interfered with their analyses by GC–MS, there was no evidence that basic nitrogen compounds were present in the fraction. Specifically, selected ion monitoring was used to screen for amino compounds and heterocyclic nitrogen bases such as acridine but they were not detected. In a similar way to fraction B, subfractionation could be used to help identify and determine biologically active compounds in fraction C.

Finally, HPLC fraction D contained no material detectable by FID or NPD. From the GC results alone, one might conclude that there was little or no material in this fraction. However, this further demonstrates the usefulness of preliminary HPLC characterization, which clearly showed (Fig. 1) that a significant amount of material eluted in this fraction. Evidently, the simple addition of hexane did not precipitate all of the asphaltenes from the whole oil. Multiple polar functional groups and the high molecular weight of the species eluted in this fraction probably precluded analysis by GC. We are currently analyzing the fraction further using other high-resolution methods including HPLC and supercritical fluid chromatography, which are better suited for these types of compounds. Nevertheless, the absence of nitrogen-containing bases such as amino aromatics in the NPD trace indicates that these compounds, some of which are potent carcinogens that are normally present at low levels in coal liquids, were precipitated from the sample (to below the detection limits) during hexane pretreatment. Neutral nitrogen-containing compounds and various acids were also absent from this fraction, supporting the conclusion that they were efficiently eluted in fraction C.

CONCLUSIONS

An HPLC method employing a semi-preparative amino-bonded-phase column modified with phosphoric acid has been developed for the prefractionation of coal liquids. Separation of model compounds added to a coal liquid sample diluted with hexane and GC analysis of the HPLC fractions collected for a more concentrated coal liquid/hexane sample demonstrated that compounds were eluted according to chemical class with little or no overlap between classes. A mechanism based on hydrogen bonding can be used to explain the class separation. The HPLC results also supplied useful information about the effects of hexane pretreatment on the coal liquid and simplified subsequent GC analysis, allowing trace level species to be identified by MS.

The new method has several attractive features. First, the modification procedure is simple and rapid; many other potentially useful stationary phases could be produced as easily as the phosphoric acid-modified bonded phase using analogous acid–base chemistry. Second, the separation of hydrocarbon classes has been improved. The modified column uniquely separates the polar acids and bases into distinct fractions while demonstrating the same capability as other polar bonded phases for separating the non-polar hydrocarbon classes. Useful preliminary characterizations such as non-polar aliphatic/aromatic and polar/non-polar hydrocarbon ratios can be obtained for a variety of synfuel samples with the HPLC method and suitable non-selective detection. Third, the recovery of sample components is equal to or better than those reported for other stationary phases. This is an especially useful feature for preparative HPLC applications. Finally, the method could be scaled up to full preparative size and modified further (*e.g.*, by using a more gradual gradient program) to fractionate very complex samples more extensively, including synthetic and natural fuels or environmental samples requiring individual compound identification.

ACKNOWLEDGEMENTS

This study was supported in part by the US Department of Energy, Contract DE-AC02-077EV4320, and Manville Products. We thank Mark Italia and Charles Stewart for their assistance and S. B. Dave and Sidney Siggia for their continued interest in this work.

REFERENCES

1 F. Munari, A. Trisciani, G. Mapelli, S. Trestianu, K. Grob, Jr., and J. M. Colin, *J. High Resolut. Chromatogr. Chromatogr. Commun.*, 8 (1985) 601.
2 I. L. Davies, K. D. Bartle, G. E. Andrews and P. T. Williams, *J. Chromatogr. Sci.*, 26 (1988) 125.
3 G. Felix, E. Thoumazeau, J.-M. Colin and G. Vion, *J. Liq. Chromatogr.*, 19 (1987) 2115.
4 L. Szepesy, M. Horvath and K. Lakszner, *Chromatographia*, 19 (1984) 431.
5 J. W. Haas, III, W. F. Joyce, Y.-J. Shyu and P. C. Uden, *J. Chromatogr.*, 457 (1988) 215.
6 D. W. Later and M. L. Lee, in C. W. Wright, W. C. Weimer and W. D. Felix (Editors), *Advanced Techniques in Synthetic Fuels Analysis*, NTIS, Springfield, VA, 1983, p. 44.
7 J. Chmielowiec and A. E. George, *Anal. Chem.*, 52 (1980) 1154.
8 S. A. Wise, S. N. Chesler, H. S. Hertz, L. R. Hilpert and W. E. May, *Anal. Chem.*, 49 (1977) 2306.
9 M. Popl, V. Dolansky and J. Mostecky, *J. Chromatogr.*, 117 (1976) 117.
10 M. Popl, V. Dolansky and J. Mostecky, *J. Chromatogr.*, 91 (1974) 649.
11 L. R. Snyder and J. J. Kirkland, *Introduction to Modern Liquid Chromatography*, Wiley, New York, 1979, p. 257.
12 R. P. Khosah, *Ph. D. Dissertation*, University of Massachusetts, Amherst, MA, 1985.

Journal of Chromatography, 550 (1991) 621–628
Elsevier Science Publishers B.V., Amsterdam

CHROMSYMP. 2179

Chiral separation of ibutilide enantiomers by derivatization with 1-naphthyl isocyanate and high-performance liquid chromatography on a Pirkle column

C. L. HSU and R. R. WALTERS*
Drug Metabolism Research, The Upjohn Company, 301 Henrietta St., Kalamazoo, MI 49001 (USA)

ABSTRACT

The enantiomers of ibutilide fumarate, a new antiarrhythmic agent with a single secondary alcohol chiral center, were solid-phase extracted, derivatized with 1-naphthylisocyanate, and separated by high-performance liquid chromatography on a chiral Pirkle column (covalent 3,5-dinitrobenzoyl-D-phenylglycine stationary phase) with UV detection. Due to the strong interaction between the ibutilide derivatives and the stationary phase, a mobile phase containing 0.05% trifluoroacetic acid and 0.05% triethylamine in methanol was used. The assay was accurate to within 0.2% absolute error for samples ranging from primarily one enantiomer to racemic mixtures, measured as the percentage of peak area of one enantiomer relative to the total peak area of the two enantiomer peaks. The day-to-day reproducibility (standard deviation) ranged from ± 0.03% relative peak area for samples containing primarily one enantiomer to ± 0.2% for racemic mixtures. Accurate results over a wide range of enantiomer ratios were dependent on the method used to draw high-performance liquid chromatography peak baselines. The method was applied to racemization studies of ibutilide enantiomers in formulations and gastric fluid.

INTRODUCTION

Ibutilide fumarate, N-{4-[4-(ethylheptylamino)-1-hydroxybutyl]phenyl}methanesulfonamide, (*E*)-2-butenedioate (2:1 drug : salt, drug shown in Fig. 1), is a class III antiarrhythmic agent in clinical development. Previously, an achiral assay was developed for quantitating the racemate in formulations using reversed-phase high-performance liquid chromatography (HPLC) [1]. The method described here was developed for quantitating the enantiomers, (+)-ibutilide fumarate and (−)-ibutilide fumarate, in formulations. It was based on the reaction of the chiral hydroxy moiety of ibutilide with 1-naphthylisocyanate (NIC) (Fig. 1). The achiral NIC introduces a π-electron donating group which, along with the polarity of the carbamate functionality, interacts stereoselectively with a chiral stationary phase, covalent 3,5-dinitrobenzoyl-D-phenylglycine [2]. Other chiral alcohols and amines have been resolved by similar procedures or reciprocal procedures in which the compounds were derivatized with the 3,5-dinitrobenzoyl moiety and separated on naphthylene-derived stationary phases [3–8].

The important advantages of a procedure utilizing an achiral derivatizing agent include the identical physical properties of the derivatives of the two enantiomers,

0021-9673/91/$03.50

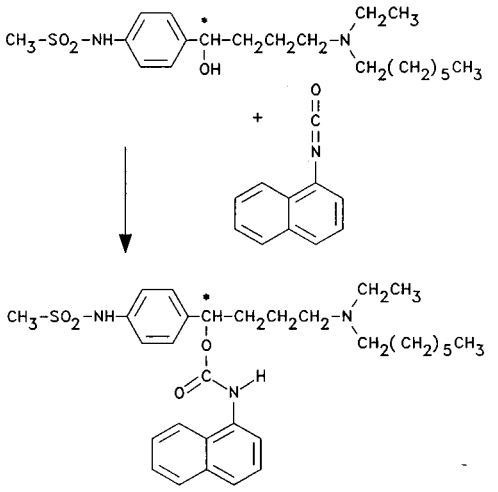

Fig. 1. Reaction of ibutilide with 1-naphthylisocyanate. The chiral center is marked with an asterisk.

which means that they will react at the same rate in an achiral medium and have identical optical properties, and elimination of any need to determine the chiral purity of the derivatizing agent. Therefore, relative enantiomer concentrations can be determined directly from the relative peak areas of the enantiomer derivatives after chromatographic separation and detection. The method was applied to *in vitro* racemization studies of ibutilide enantiomers in formulations and simulated gastric fluid.

EXPERIMENTAL

Materials

Ibutilide fumarate (racemic mixture and individual enantiomers) was synthesied by Upjohn (Kalamazoo, MI, USA). The NIC was from Regis (Morton Grove, IL, USA) and the sequanal quality trifluoroacetic acid (TFA) from Pierce (Rockford, IL, USA). Other reagents were of analytical grade and solvents were of HPLC or UV grade. The samples prepared for racemization testing were 0.25 mg/ml solutions of the individual enantiomers in 0.1% sorbic acid, 0.9% sodium chloride, or simulated gastric fluid (0.034 *M* sodium chloride adjusted to pH 1.8 with 1 *M* hydrochloric acid).

Apparatus

Solid-phase extraction (SPE) was performed using Bond-Elute C_{18} SPE columns containing 100 mg of stationary phase and a Vac-Elute solid-phase extraction manifold (Analytichem, Harbor City, CA, USA). The HPLC equipment consisted of a Beckman 114M solvent delivery module (San Ramon, CA, USA), a Perkin-Elmer ISS 100 autosampler with 100 μl loop (Norwalk, CT, USA), a Rexchrom covalent D-phenylglycine column, 25 cm × 4.6 mm I.D. with 10 μm packing (Regis), an ABI Spectroflow 783 UV detector (Ramsey, NJ, USA), and a Harris H1000 computer (Ft. Lauderdale, FL, USA) with custom interface and software (Upjohn) for data acquisition and analysis.

Procedure

A volume of sample containing approximately 0.25 mg of ibutilide was pipeted into a glass culture tube. If necessary, water was added to bring the volume to 0.5–1.0 ml. A 1-ml volume of buffer, 0.05 *M* NaH_2PO_4 containing 0.1% triethylamine (TEA), adjusted to pH 7.0 with sodium hydroxide, was added to each tube. Control samples containing variable ratios of (+)- and (−)-ibutilide were prepared in water with a total drug concentration of 0.25 mg/ml and similarly treated.

C_{18} SPE columns were attached to the vacuum manifold and activated with 1 ml of an acetone–acetonitrile–TEA solution (50:50:0.2, v/v/v), followed by 1 ml of water containing 0.1% TEA. The diluted samples were applied to the SPE columns, washed with 1 ml of water, dried for 3 min under maximum vacuum, washed with 0.3 ml hexane, and dried for an additional 10 min. Each SPE column was removed from the manifold and placed in a 75 × 10 mm glass culture tube. The ibutilide was eluted under gravity using 0.5 ml of the acetone–acetonitrile–TEA solution, with the last bed volume forced out with pressurized nitrogen.

A 50-μl aliquot of each solution was transferred to a glass autosampler vial. A 10-μl volume of 1.0% acetic acid in acetonitrile and 100 μl of 0.1% NIC in acetonitrile were added, and the reaction allowed to proceed for 10–15 min at room temperature. A 500-μl volume of mobile phase (methanol containing 0.05% TFA and 0.05% TEA by volume) was added to each vial to terminate the reaction.

The samples (100 μl) were injected and chromatographed isocratically at ambient temperature at a flow-rate of 1 ml/min and UV detection at 230 nm. Injections were typically performed at 32 min intervals. Peak area ratios were directly used as a measure of enantiomer ratios.

RESULTS AND DISCUSSION

Optimization of solid-phase extraction conditions

This inital step was used to extract the drug from an aqueous solution into an organic solvent so that derivitization could take place under anhydrous conditions. The samples were applied to C_{18} SPE columns after dilution of approximately 0.25 mg of ibutilide fumarate in an aqueous solution with a pH 7 buffer (0.05 *M* sodium phosphate) containing 0.1% TEA. The columns were washed with water to remove non-retained components, then dried briefly. Quantitative recoveries of ibutilide could be obtained after elution with either acetonitrile or acetone–acetonitrile–TEA (50:50:0.2, v/v). However, recovery was only 80% in the first 0.5 ml of eluent when acetonitrile was used, but quantitative when the latter solution was used. The TEA apparently served to elute the drug from polar sites on the column. An aliquot (50 μl) of the eluted solution of drug reacted quantitatively with NIC when either eluent was used. Varying the drying time prior to elution from 10 to 3 min of vacuum did not affect recovery nor the extent of reaction with NIC.

Derivatization conditions

Reactions of isocyanates are often catalyzed by acids or bases [9–12]. Therefore, catalysis by acetic acid or TEA was examined. The drug-containing extract consisted of 50 μl of acetone–acetonitrile–TEA (50:50:0.2). Experiments were performed in which 10 μl aliquots of acetic acid or TEA in acetonitrile were added, followed by 100

μl of 0.1% NIC in acetonitrile. Addition of 10 μl of 1% acetic acid was slightly more than what was required to neutralize the TEA in the extract. After reaction at room temperature for 15 min, the samples were diluted and chromatographed. There was a wide range (0–1% added acetic acid and 0–0.1% added TEA) over which the reaction appeared to give high yields (>96%). It was only in the presence of very high concentrations of acid or base that the reaction was diminished. No catalytic effect was observed compared to a reaction performed without any TEA or acetic acid present. Addition of 1% acetic acid was chosen for the final assay, in part because it had a slightly higher reaction yield than the other conditions and in part for stability reasons indicated below.

The effect of the concentration of NIC on the reaction yield was examined by derivatizing 50 μl eluates containing the enantiomers of ibutilide with 10 μl of 1% acetic acid in acetonitrile and 100 μl of various concentrations of NIC in acetonitrile (0.003–0.3%, v/v) for 15 min at room temperature. The reaction yield was high at or above 0.03% added NIC. Since NIC slowly degrades, 0.1% NIC (0.06% or 4.3 m*M* NIC in the final reaction mixture) was chosen for the final assay to ensure an adequate excess of the drivatizing agent.

The time course of the reaction of NIC with ibutilide was followed at temperatures of 0, 25 and 40°C using the standard conditions described above. After 15 min at 25 and 40°C the concentration of derivative reached a plateau and no unreacted drug remained. Reaction was much slower at 0°C and not complete even after 1 h. Therefore, room temperature derivatization for 15 min provided convenient conditions for the final assay procedure and the mild conditions minimized the possibility of racemization.

The conditions reported for the reaction of isocyanates with alcohols have varied from extreme, such as reaction in toluene at 80°C for 36 h, to mild, such as reaction in N,N-dimethylformamide at room temperature for 15 min [9–16] and the similar conditions reported here using acetonitrile. It has been suggested that polar organic solvents catalyze the reaction of phenyl isocyanate with amines in N,N-dimethylformamide [17]. Aliphatic alcohols were reported to react rapidly with phenyl isocyanate in N,N-dimethylformamide, acetonitrile, and dioxane [12].

The structure of the derivative (Fig. 1) was confirmed by fast atom bombardment mass spectrometry of collected chromatographic fractions. The protonated molecular ion at *m/z* 554 corresponded to the addition of one equivalent of NIC. An analogue containing the sulfonamide moiety but no hydroxyl group did not react with NIC, confirming that the site of derivatization of ibutilide was the hydroxyl group.

Chromatographic conditions

Pirkle columns are generally operated with mobile phases containing mixtures of hexane and isopropanol, sometimes with small amounts of other polar organic solvents as modifiers [2,7,8,18]. However, using isopropanol–hexane mixtures or even pure isopropanol as the mobile phase, the ibutilide–NIC derivative did not elute, probably because of strong interactions between the tertiary amine and the stationary phase. However, addition of TEA to the mobile phase did result in elution and chiral resolution, but the UV detector baseline drifted upward, suggesting a loss of stationary phase. Adding an excess of TFA in addition to the TEA appeared to stabilize the baseline and columns used under these conditions worked well for more than one year.

Various mobile phases were tested in order to optimize resolution and analysis time. The alcohols (methanol, ethanol and isopropanol) were the weakest solvents. Modifying retention with TFA–TEA (0.05–0.2% of each) worked best because the separation factor, α, remained constant (approximately 1.16) as the capacity factor, k', decreased, whereas with acetonitrile or tetrahydrofuran α always declined with k'. Methanol containing 0.05% TFA (6.7 m*M*) and 0.05% TEA (3.6 m*M*) was chosen as the mobile phase for the routine assay. Resolution was excellent (Fig. 2), although run times were moderately long (approximately 30 min). The elution order on a 3,5-dinitrobenzoyl-D-phenylglycine column was the (+)-ibutilide derivative followed by the (−)-ibutilide derivative. The absolute configuration of each enantiomer was not known.

Stability of derivatized samples

After reaction, the samples were diluted with 500 μl of mobile phase. Since analytical runs sometimes proceeded for 24 h or more, good stability of the derivatives in autosampler vials at room temperature was necessary. Initially, derivatization was performed without any added acetic acid, and the product was diluted with pure methanol. Thus, the final mixture was somewhat basic due to the TEA present in the eluate from the initial extraction. There was significant degradation of the product within a few hours and little remained after 26 h at room temperature (Fig. 3). Stability was better when the derivatization reaction was quenched with mobile phase containing an excess of TFA (middle tracing), and best (same chromatogram as when freshly prepared) when the reaction mixture contained an excess of acetic acid and the methanol used for dilution contained TFA (upper tracing). Samples prepared with acetic acid in the reaction mixture but diluted only with methanol also showed a slow loss of derivative. These results suggest that acetic acid in the reaction mixture prevented degradation from ocurring during the derivatization, while the TFA in the final sample solution enhanced the long-term stability of the derivative. Degradation of phenyl isocyanate derivatives of aliphatic alcohols has been observed in the presence of TEA [12].

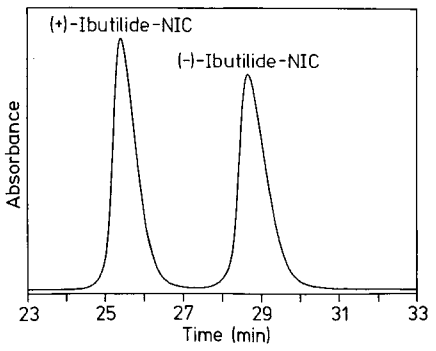

Fig. 2. Resolution of the enantiomers of ibutilide on a Pirkle column after derivatization with 1-naphthylisocyanate. Mobile phase: methanol containing 0.05% TFA and 0.05% TEA. Flow-rate: 1 ml/min. Detection: UV absorbance at 230 nm.

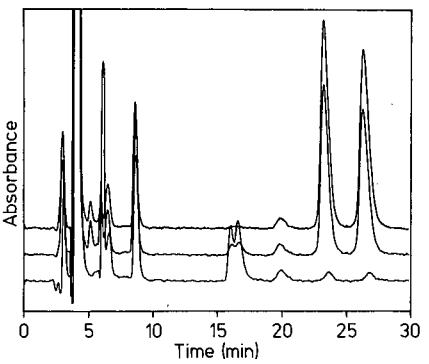

Fig. 3. Chromatograms of the NIC derivatives of ibutilide, approximately 26 h after preparation (stored at room temperature). Lower curve: a 50 μl extract containing ibutilide in acetone–acetonitrile–TEA (50:50:0.2, v/v/v) derivatized with 10 μl of acetonitrile and 100 μl of 0.1% NIC in acetonitrile, then diluted with 500 μl of methanol. Middle curve: same except for dilution with 0.05% TFA and 0.05% TEA in methanol. Upper curve: same as middle curve except that the 10 μl of acetonitrile contained 1% acetic acid. The enantiomer peaks eluted at 23–27 min. An unknown pair of peaks characteristic of degradation can be seen at a retention time of 16–17 min. The peaks at 3–9 and 20 min are from NIC and its impurities.

Effect of baseline drawing method

Although the resolution and peak shape of the derivatized enantiomers were good, difficulties were encountered when trying to quantitate a trace of one enantiomer in the presence of an excess of the other enantiomer. This common problem of trace analysis [19] is illustrated in Fig. 4 and was particularly acute when the (−)-enantiomer was present in trace quantities and eluted on the tail of the (+)-enantiomer. To ameliorate this problem, several different baseline drawing techniques were used (Fig. 4). Samples containing approximately 0.4% of the minor enantiomer or exactly 50% of each enantiomer were tested.

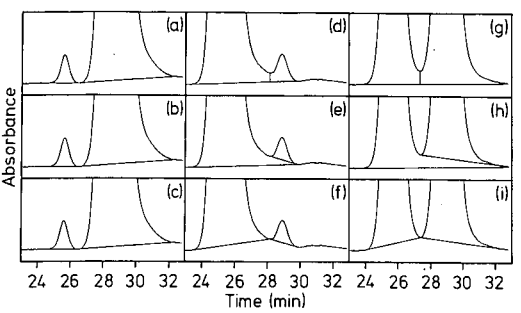

Fig. 4. Chromatograms showing baseline drawing methods for ibutilide enantiomer peaks ranging from 0.4% (+)-ibutilide (a–c) to racemic ibutilide (g–i) to 0.4% (−)-ibutilide (d–f). The perpendicular drop method was used for a, d and g. A tangent-skim of the smaller peak was used for b, e and h. A tangent-skim of both peaks was used for c, f and i. The large truncated peaks had peak heights of 0.27–0.59 absorbance units, while the small peaks had heights of 0.002–0.004 absorbance units.

All methods worked well when the (+)-enantiomer was present in trace amounts since it was totally resolved from the large (−)-enantiomer peak (Fig. 4a–c).

When the (−)-enantiomer was present in trace amount, the perpendicular drop method biased the results high by 0.2% for the (−)-enantiomer because part of the tail of the large peak was included in the small peak (Fig. 4d). Tangent-skimming both peaks or only the small peak worked well for trace amounts of the (−)-enantiomer (Fig. 4e and f). Another possibility would have been to use an L-phenylglycine column to reverse the elution order of the enantiomers.

The perpendicular drop method worked poorly for the racemic mixture since it truncated the tail of the first peak but not the second peak, giving a low result (0.3% error) for the percentage of the (+)-enantiomer (Fig. 4g). Tangent-skimming the second peak resulted in a 0.9% error in the opposite direction since the baseline of the first peak was extended too far (Fig. 4h). But by tangent-skimming both peaks (Fig. 4i), the error was only 0.1% (the second peak being slightly high). This appeared to be the best accuracy that could be obtained without using more sophisticated baseline drawing methods. Since tangent-skimming of both peaks worked well over a wide range of enantiomer ratios, it was chosen for routine use.

Accuracy and precision

The sample size (0.25 mg) chosen for the initial extraction gave peaks that were in the range of 0.3–1.0 absorbance unit full-scale, thus maximizing the signal-to-noise for samples containing only a trace of one enantiomer (Fig. 4).

Day-to-day reproducibility and accuracy were estimated from repeated analysis of control samples. The racemic control sample averaged 49.95% ± 0.20% (+)-ibutilide based on 15 assays on 5 days. Thus, the average error for this sample was 0.05%. The (+)-ibutilide control solution averaged 99.86% ± 0.03% (+)-ibutilide while the (−)-ibutilide control sample averaged 99.72% ± 0.03% (−)-ibutilide. The errors for these samples containing predominantly one enantiomer can not be stated exactly since they were not independently assayed, but were probably less than 0.05%, based on the purest enantiomer sample available. Errors for control samples prepared by mixing the enantiomers in varying ratios were typically less than 0.2% on any single

TABLE I

RACEMIZATION OF (+)- AND (−)-IBUTILIDE FUMARATE IN GASTRIC FLUID, SORBIC ACID AND SALINE

Sample	Conditions	Mean (%) (+)-ibutilide formed from (−)-ibutilide fumarate	Mean (%) (−)-ibutilide formed from (+)-ibutilide fumarate	Mean (%) increase in minor component
Gastric fluid	37°C, 24 h	9.73	9.30	9.5
0.1% Sorbic acid	4°C, 30 days	0.02	0.01	0.0
	30°C, 30 days	1.00	0.91	1.0
	40°C, 30 days	4.09	3.75	3.9
0.9% Sodium chloride	4°C, 30 days	−0.03	0.01	0.0
	30°C, 30 days	0.03	0.02	0.0
	40°C, 30 days	0.11	0.11	0.1

assay day. This accuracy and precision should be sufficient for most practical applications, such as the racemication studies described below.

Application to racemization studies

To evaluate possible racemization in formulations of various pHs and in the stomach prior to absorption, solutions of the ibutilide fumarate enantiomers (0.25 mg/ml) were prepared in the following matrices: simulated gastric fluid (0.034 *M* sodium chloride, adjusted to pH 1.8 with 1 *M* hydrochloric acid); 0.1% sorbic acid (pH 3.5); and 0.9% sodium chloride (pH 6.2.). The solutions were stored at controlled temperature. There was good agreement between the results from the individual enantiomers, as expected since the matrices were achiral (Table I). Ibutilide racemized slowly under most conditions but more rapidly in an acidic environment and at elevated temperature. The results from simulated gastric fluid suggest that only a small amount of racemization should occur in the stomach *in vivo* after oral dosing of the drug, assuming the gastric residence time is short.

ACKNOWLEDGEMENTS

The authors thank J. B. Hester and S. C. Perricone for their helpful discussions and for providing the enantiomer samples, I.A. O'Leary and J. J. Vrbanac for performing the mass spectrometry studies, and P. J. DeMulder and G. E. Amidon for performing the racemization studies.

REFERENCES

1 C. L. Hsu and R. R. Walters, Upjohn Co., unpublished results, 1988.
2 W. H. Pirkle, D. W. House and J. M. Finn, *J. Chromatogr.*, 192 (1980) 143–158.
3 W. H. Pirkle and J. E. McCune, *J. Liq. Chromatogr.*, 11 (1988) 2165–2173.
4 W. H. Pirkle and M. H. Hyun, *J. Org. Chem.*, 49 (1984) 3043–3046.
5 W. H. Pirkle, G. S. Mahler, T. C. Pochapsky and M. H. Hyun, *J. Chromatogr.*, 388 (1987) 307–314.
6 N. Oi and H. Kitahara, *J. Chromatogr.*, 265 (1983) 117–120.
7 Q. Yang, Z.-P. Sun and D.-K. Ling, *J. Chromatogr.*, 447 (1988) 208–211.
8 A. M. Dyas, A. F. Fell and M. L. Robinson, *Chirality*, 2 (1990) 120–123.
9 R. Wintersteiger and G. Wenninger-Weinzierl, *Fresenius' Z. Anal. Chem.*, 309 (1981) 201–208.
10 T. Ibuka, G.-N. Chu, T. Aoyagi, K. Kitada, T. Tsukida and F. Yoneda, *Chem. Pharm. Bull.*, 33 (1985) 451–453.
11 Y. Yamazaki and H. Maeda, *Agric. Biol. Chem.*, 50 (1986) 79–87.
12 B. Bjorkqvist and H. Tiovonen, *J. Chromatogr.*, 153 (1978) 265–270.
13 P. Michelsen, E. Aronsson, G. Odham and B. Akesson, *J. Chromatogr.*, 350 (1985) 417–426.
14 R. Wintersteiger, G. Wenninger-Weinzierl and W. Pacha, *J. Chromatogr.*, 237 (1982) 399–406.
15 K. M. Williams, *Clin. Pharmacol. Ther.*, 36 (1984) 817–823.
16 J. Gal, D. DeVito and T. W. Harper, *Drug Metab. Dispos.*, 9 1981) 557–560.
17 B. Bjorkqvist, *J. Chromatogr.*, 204 (1981) 109–114.
18 W. H. Pirkle and J. M. Finn, *J. Org. Chem.*, 46 (1981) 2935–2938.
19 J. A. Perry, J. D. Rateike and T. J. Szczerba, *J. Chromatogr.*, 389 (1987) 57–64.

Journal of Chromatography, 550 (1991) 629–638
Elsevier Science Publishers B.V., Amsterdam

CHROMSYMP. 2330

Separation of copolymers according to composition with special emphasis on the effect of block structure

G. GLÖCKNER

Department of Chemistry, Dresden University of Technology, Mommsenstrasse 13, O-8027 Dresden (Germany)

and

J. H. M. VAN DEN BERG

Analytical Development Department, Duphar B.V. Research Laboratories, P.O. Box 900, NL-1380 DA Weesp (Netherlands)

ABSTRACT

Block copolymers are a separate but important branch of copolymers. Like all copolymers, they are made of two (or more) different monomers, usually in a sequential manner. The characterization of block copolymers requires, among other things, the measurement of the precursor and other by-products. Gradient high-performance liquid chromatography, which has been used for the separation of statistical copolymers according to composition, can, under suitable conditions, also separate block copolymers with different molecular structures. This method has proved to be efficient even in cases where size-exclusion chromatography has failed. Block copolymers have longer retention times than statistical copolymers of the same composition. This is a result of the cooperative effect of adjacent repeat units.

INTRODUCTION

The objective of this paper is to review block copolymer synthesis and characterization methods, with an emphasis on the detection of homopolymer by-products.

BLOCK COPOLYMERS AND STATISTICAL COPOLYMERS

Copolymers are produced from at least two kinds of monomers. In the straightforward copolymerization of a binary mixture, the monomer reactivity ratios

$$r_A = k_{AA}/k_{AB} \quad (1)$$

$$r_B = k_{BB}/k_{BA} \quad (2)$$

govern the addition of either monomer A or B to the terminal A or B unit of a growing macromolecule.

Statistical copolymers usually consist of rather short sequences and can be described by the average sequence lengths

0021-9673/91/$03.50

$$L_A = 1 + r_A G \tag{3}$$

$$L_B = 1 + r_B/G \tag{4}$$

where $G = [A]/[B]$ is the molar ratio in the monomeric mixture.

Apart from systems with very high r values, or bipolymers with an extreme content of one of the monomers, the average sequence lengths of statistical copolymers are small in comparison with the degree of polymerization P. The lower limit is represented by alternating copolymers with $L_A = L_B = 1$, which are produced if $r_A = r_B = 0$ and $0 < G \ll \infty$.

A block copolymer is a copolymer in which the sequence lengths are of the same order of magnitude as P, *e.g.*, $L_A = L_B = P/2$ for a diblock copolymer with an equal molar content of the A and B units.

SYNTHESIS OF BLOCK COPOLYMERS

Block copolymers are produced in special reactions, usually in a sequential manner. In a sequential preparation, the A block of all the macromolecules is formed first, with the subsequent addition of the B block. Sequential copolymerization can be achieved by living polymerization of monomer A and (after the complete consumption of monomer A) continuation of the polymerization by the addition of monomer B. Diblock copolymers can be obtained by a termination reaction after the consumption of monomer B, whereas coupling reactions of the living A–B diblock copolymers can be used for the synthesis of A–B–A triblock copolymers.

A living polymerization reaction may be anionic or cationic in nature. Of these reactions, group transfer polymerization (GTP) [1–4] was found to be capable of producing polyacrylates or polymethacrylates with a narrow molecular weight distribution. As is common in proper living polymerizations, the molecular weight of the polymers (number average, M_n) obtained by GTP is controlled by the molar ratio of the monomer to the initiator. GTP was shown to yield binary block copolymers when two different kinds of monomer were fed successively [4,5].

If the addition of the second monomer causes deactivation of some of the precursor chains by side-reactions, the resulting block copolymer will be contaminated by a corresponding portion of precursor homopolymer. Coupling occurring as a side-reaction in the termination step of diblock copolymer synthesis also causes contamination of the desired product.

Block copolymers can also be obtained by free radical polymerization using, *e.g.*, multifunctional initiators. Using a polyester peroxide with five or six peroxide bridges within its backbone, commercial block copolymers were produced by polymerizing methyl methacrylate (MMA) at 65°C and, subsequently, styrene (S) at 75°C. The rather broad distribution in products of this kind, which is to be expected from the statistical processes of peroxide cleavage and chain termination, has been studied experimentally [6]. Block copolymers of vinyl acetate and styrene were also prepared by the stepwise decomposition of polymeric peroxides. The separation of three samples by gradient high-performance liquid chromatography (HPLC) and size-exclusion chromatography (SEC) revealed a broad distribution in chemical composition [7]. The molecular weight of fractions increased with vinyl acetate content.

The synthesis of block copolymers through free radical polymerization is also feasible by subjecting an initial homopolymer (poly-A) to mechanical stress in the presence of monomer B. Mechanical forces created by, *e.g.*, ball milling, mastication, or freezing and thawing of aqueous solutions may break the polymer chains. The segments are polymeric free radicals. The ends where the break occurred can, under favourable conditions and in the absence of radical-capturing agents, add units of monomer B by free radical polymerization, thus forming di- or triblock copolymers, AB or ABA, respectively.

Block copolymers can be obtained by transformation of a suitable end-group of a precursor polymer into a group capable of initiating another polymerization of a different monomer (with the incorporation of the precursor chain) or by the coupling of different kinds of prepolymers through mutually reactive end groups.

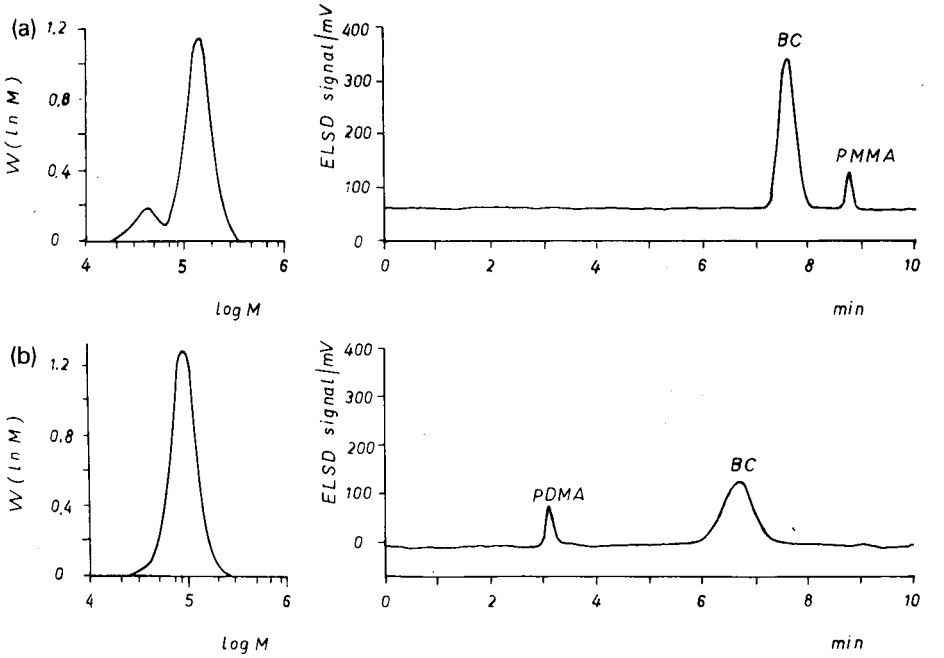

Fig. 1. (a) Block copolymer 9-16 (methyl methacrylate–decyl methacrylate, 36 mol% MMA, M_n = 155 500) containing 13.5% (w/w) PMMA precursor (M_n = 31 000). Left panel: molecular weight distribution (MDW) by SEC on a bank of two PS gel columns (TSK GMH6, 600 × 7.5 mm each, Toyo Soda, Tokyo Japan) with THF eluent, flow-rate 1 ml/min, injection volume 0.3 ml of a 1 g/l sample solution in THF, PMMA calibration. Right panel: gradient HPLC on a cyanide (CN) bonded phase column (60 × 4 mm, packed with Nucleosil 5 CN, $d_o \leqslant 5$ nm, $d_p = 5$ μm) at 40°C and 1 ml/min flow-rate; injection volume 5 μl of a 5 g/l solution in THF. Gradient: iso-octane–THF (1% constant for 1 min, followed by 1–81% within 8 min). Detection by evaporative light scattering detector (ELSD). Molecular weight of the whole sample (block copolymer + PMMA contaminant), 101 000. Experimental results from ref. 25. (b) Block copolymer 9-13 (decyl methacrylate–methyl methacrylate, 27.5 mol% MMA, M_n = 89 600) containing 10.6% (w/w) PDMA precursor (M_n = 76 700). Left panel: MWD by SEC, conditions as in (a). Right panel: gradient HPLC; for conditions see (a). Molecular weight of the whole sample (block copolymer + DMMA contaminant), 88 000. Experimental results from ref. 25. BC = Block copolymer.

DETECTION OF BY-PRODUCTS

The sequential synthesis of block copolymers allows the measurement of (1) the precursor molecular weight, *i.e.*, $M_{n,A}$ and $M_{w,A}$ (weight average) and (2) the molecular weight of the final product, *i.e.*, M_n and M_w. The ratio $M_{n,A}/M_n$ should equal the weight fraction of monomer A in the copolymer and also the weight fraction of monomer A in the monomeric feed. Deviations indicate side-reactions.

As a result of the limited accuracy of molecular weight measurements, agreement between experimental and calculated molecular weights cannot sufficiently prove the absence of side-reactions. The latter can be detected this way only if they occur to a relatively high degree.

A similarly pessimistic view holds for any other method which measures average values. Thus, separation techniques are required which are capable of discriminating between the actual block copolymer and possible by-products. Unfortunately, the familiar methods of fractionation by precipitation or dissolution are often not efficient enough for these difficult separations [8–11]. Density-gradient ultracentrifugation has been used for the estimation of homopolymer impurities in block copolymers [12,13].

SEC has often been used for revealing the presence of by-products [14–24]. Of course, a prerequisite is a sufficient difference in molecular weight between the unreacted precursor and the block copolymer. The left panel of Fig. 1 shows the results obtained by Müller *et al.* [25] which demonstrates success (Fig. 1a) or failure (Fig. 1b) of SEC investigations on different block copolymers of the monomer systems decyl methacrylate (DMA) and methyl methacrylate (MMA). The upper chromatogram (left panel of Fig. 1a) shows a small peak due to the polyMMA (PMMA) content of the sample, the block copolymer portion of which was eluted in a large peak. In this instance, SEC was successful. The lower chromatogram (left panel of Fig. 1b) shows only an unimodal SEC peak for a sample which consists of a block copolymer and a polyDMA (PDMA) homopolymer. In this instance, SEC failed to separate the two components.

CHROMATOGRAPHIC SEPARATION ACCORDING TO COMPOSITION

Methods for separation by chemical composition rather than by molecular weight should be better suited for the evaluation of by-products. Inagaki and coworkers used thin-layer chromatography (TLC) for the characterization of S–MMA [26–29] or S–butadiene (Bd) block copolymers [30]. Belenkii and Gankina [31] also performed TLC of S–MMA block polymers [31]. A paper by Gankina *et al.* [32] presents TLC analyses of poly(S–*b*–MMA), poly(S–*b*–Bd), poly(S–*b*–ethylene oxide), poly(S–*b*–acrylonitrile), poly(BG–*b*–S–*b*–BG), poly(MMA–*b*–BG) as well as poly(I–*b*–MS–*b*–I) and mentions poly(MMA–*b*–BMA), where *b* = block, BG = γ-benzyl glutamate, I = isoprene, MS = α-methylstyrene, and BMA = butyl methacrylate.

Gradient HPLC is well suited for separating statistical copolymers by composition [33–36] (for survey, see refs. 37,38,59). Gradient HPLC was also applied to block and statistical copolymers of styrene and *tert.*-butyl methacrylate (TBMA) [39].

Copolymers of S and MMA [34,40,41] or ethyl methacrylate [42] can be separated according to composition on polar columns, *e.g.*, packed with silica [34,40],

cross-linked poly(acrylonitrile) [41] or a nitrile bonded phase [42], through gradients increasing with eluent polarity, *e.g.*, iso-octane–tetrahydrofuran (THF). These chromatographic systems yielded retention times increasing with methacrylate content, *i.e.*, these separations of synthetic copolymers followed the principles of normal-phase separations. Attempts to separate the statistical copolymer S–TBMA in this manner have so far failed. Samples with a TBMA content between 24 and 86% (w/w) were, on a silica column, eluted in iso-octane–THF mixtures whose composition varied by less than 5% [39].

What was remarkable in this work was the fact that retention slightly decreased with increasing methacrylate ester unit content, the opposite of the behaviour of the corresponding copolymers with methyl or ethyl methacrylate units. This surprising effect indicated that *tert.*-butyl alcohol groups diminished the adsorption of –COO groups on silica to such an extent that the remaining interactions between the solute and stationary phase were due to the styrene units of the copolymer. Thus injections were repeated on a phenyl bonded phase column with a gradient methanol–THF, *i.e.*, employing a reversed-phase chromatographic system. This yielded a pronounced increase in retention with rising styrene content and a substantial gain in selectivity [39]. The combination of methanol–THF gradients with a C_{18} bonded phase column was also effective in separating S–TBMS copolymers.

GRADIENT HIGH-PERFORMANCE LIQUID CHROMATOGRAPHY FOR THE MOLECULAR SEPARATION OF BLOCK COPOLYMERS

The failure of familiar fractionation techniques [8–11] is due to the tendency of block copolymers to form micelles by association of the less solvated blocks when the solvent strength decreases. Hence, it is interesting to see if gradient HPLC is capable of separating block copolymers on a molecular level. The possibility of forming aggregates must not be ignored because, to obtain the correct retention, the solvent strength of the eluent may be low in gradient HPLC.

Of the S–TBMA block copolymers investigated, two samples [with 26 or 55% (w/w) TBMA containing 40 or 15% polystyrene precursor, respectively] eluted from the phenyl column in broad bands, whereas block copolymers containing 80 or 92% TBMA formed well shaped peaks. Mixtures of these samples with either polyS (PS) or polyTBMA (PTBMA) homopolymers yielded patterns which showed the admixture baseline separated from the block copolymer, the peak of which remained almost unchanged. The mixture of both copolymers also yielded two separate peaks without mutual interference. These results indicate a molecular separation [39].

Separation on a molecular level was found also by Augenstein and Müller [43] in the investigation of poly(DMA–*b*–MMA) samples on a cyanide bonded/phase column through gradients iso-octane–THF. Mixtures of two or three block copolymers yielded tracings which were simply the superimposition of individual chromatograms.

A quantitative determination was also carried out [43] by measured additions of PDMA homopolymer to a DMA–MMA block copolymer and integration of the PDMA signal. The block copolymer was obtained with a PDMA precursor and a monomer feed of 75:25 mol% DMA–MMA. The results from the measured addition of PDMA adhered to a linear calibration which was established by injections of

PDMA alone in the range 4–10 μg, thus indicating the separation of the PDMA homopolymer from the block copolymer. Subtracting the known addition of homopolymer from the amount calculated from the peak area, the content of PDMA precursor in the block copolymer was also determined with excellent reproducibility. The PDMA precursor was 10.6 ± 0.1% (w/w) (mean value of duplicate injections at five different levels of PDMA addition). The result, which was confirmed by repetition on a silica column, enabled the block yield to be calculated with similar precision.

The procedure marks a real advance in the characterization of block copolymers. The importance of this should be appreciated, because the block copolymer was that mentioned earlier, which showed an apparently monotonous SEC peak due to a precursor molecular weight amounting to 85.6% of the final molecular weight (89 000).

In contrast to these favourable results, a warning must be given against the association phenomena which may occur under other chromatographic conditions. Augenstein and Müller [43] observed the puzzling elution behaviour of DMA–MMA block copolymers under reversed-phase conditions with gradients of methanol–THF. This observation matches observation with a certain S–TBMA block copolymer on the addition of a PS homopolymer [44] where the PS molecular weight affected the type of associations formed.

PROLONGED RETENTION OF BLOCK COPOLYMERS

Under equivalent chromatographic conditions, block copolymers were retained longer than statistical copolymers of the same composition. This was found with S–TBMA samples [39] (Fig. 2a). A similar result can be deduced from the observations in a paper dealing with the separation by composition of S–Bd copolymers [45]. This was recently confirmed on the basis of a thorough investigation of DMA–MMA copolymers [25,43] (Fig. 2b) in which the excess retention of block copolymers was larger than with S–TBMA copolymers. This is due to the large difference in adsorption between MMA and DMA units in contrast to a more moderate difference between TBMA and S units.

The effect of block length on retention can be understood on the basis of a model [37] which takes into account the fact that polymers consist of repeat units which, on adsorption, form a "trains". For the adsorption of n repeat units with retention factor k'_u for each unit, the retention factor of the whole train becomes:

$$k'_{total} = (k'_u + 1)^n - 1 \tag{5}$$

With homopolymers, n is large, which has a significant effect on k'_{total}. Even k'_u values which only slightly exceed zero give rise to high k'_{total} data.

The diffent kinds of repeat units in copolymers will under given chromatographic conditions, be adsorbed differently. The consequences of this are diffent k'_u values for unlike constituting units. As, by eqn. 5, extremely small k'_u values suffice for k'_{total} data of the usual order ($2 \leqslant k'_{total} \leqslant 10$), the retention of copolymers will mainly be caused by the adsorption of only one kind of constituting unit. These units interact with a stationary phase under conditions where, for the chromatographically weaker units, k'_u is virtually zero.

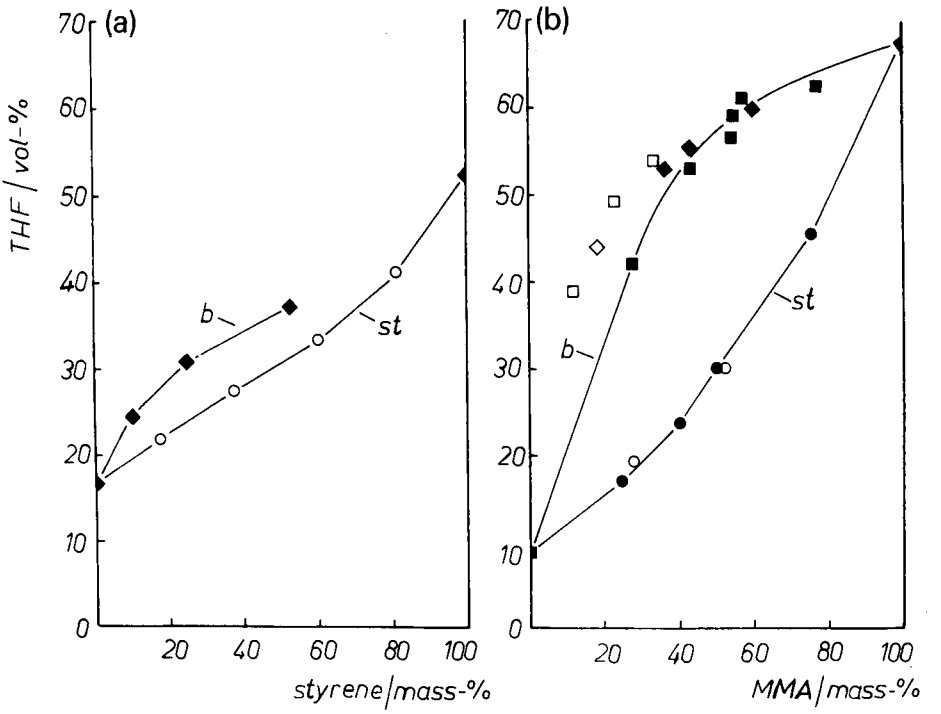

Fig. 2. (a) Elution characteristics of copolymers from styrene and *tert.*-butyl methacrylate of either statistical (○) or block architecture (◆). Phenyl bonded phase column (60 × 4 mm, $d_o \leqslant 5$ nm. $d_P = 7$ μm) at 50°C and 0.5 ml/min flow-rate; injection volume 40 μl (statistical) or 20 μl (block copolymers) of 0.4 g/l solutions in THF. Gradient, methanol–THF (10–70% within 12 min), UV signal at 254 nm. Data from ref. 39 (b) Elution characteristics of copolymers from methyl methacrylate and decyl methacrylate of either statistical (circles) or block architecture (squares). (●) Statistical copolymers from group transfer polymerization; (○) same, from free radical polymerization; (■) block copolymers from group transfer polymerization, precursor PDMA; (◆) same, precursor PMMA; (□) and (◇) same, but molecular weight ⩾ 160 000. CN bonded phase column (60 × 4 mm, packed with Nucleosil 5 CN, $d_o \leqslant 5$ nm, $d_P = 5$ μm) at 40°C and 1 ml/min flow-rate; injection volume 5 μl of a 5 g/l 1 min, followed by 1–81% within 8 min). Detection by evaporative light scattering detector. Data from ref. 43.

As a result of the small values of average sequence length in statistical copolymers the latter can, towards a stationary phase, expose only rather short trains of chromatographically active units, whereas block copolymers expose much longer trains. The larger number of consecutive repeat units in the latter give rise to a higher exponent n, which accounts for the stronger retention observed with block copolymers.

EFFECT OF MOLECULAR WEIGHT

The chromatographic behaviour of copolymers is determined by chemical composition and molecular weight. The latter effect can be described by:

$$\varphi_{NS} = A - B\,M^{-0.5} \tag{6}$$

where φ_{NS} is the volume fraction of the non-solvent (or weak eluent) at peak elution and A and B are constants. Originally stated for the effect of molecular weight on polymer solubility [46]. eqn. 6 was also found to be fulfilled by chromatographic results with excellent correlation, even under conditions where solubility is possibly not the predominant mechanism of retention [47–49]. Usually, the molecular weight effect on retention is small in comparison with the influence of copolymer composition. The parameter B is especially small when adsorption prevails and increases when solubility contributes substantially to retention. (For a discrimination between adsorption and solubility effects in polymer HPLC see, *e.g.*, ref. 50).

From eqn. 5 it was deduced that, under the given chromatographic conditions, the retention increases with the length of an adsorbed train. With block copolymers, the block length of chromatographically active units increases with the overall content in these units and the molecular weight of the polymer. Doubling of either of these values would double the number of the anchoring groups. This reasoning indicates that a molecular effect will be more pronounced in block copolymers than in statistical copolymers.

This has been reported by Augenstein and Müller [43], who measured a rather large value of $B = 40$ (see eqn. 6) for the MMA blocks in poly(DMA–*b*–MMA). They found that DMA–MMA block copolymers eluted earlier than PMMA homopolymers with a length similar to that of the MMA block in the copolymers. This indicates a "dragging" effect of the non-adsorbed DMA block on the adsorbed MMA block and demonstrates that, in contrast to low-molecular-weight adsorption, the interaction of polymer solutes with the mobile phase must not be ignored. Increasing the length of a dragging tail should increase its loosening effect. This expectation is in line with the slightly earlier elution of block copolymers of $M_n \approx 200\,000$, in comparison with other copolymers with the same PMMA block lengths but $M_n \approx 160\,000$. This exception aside, the common plot of eluent composition *versus* MMA block length for multifarious DMA–MMA block copolymers resembles a prediction of the critical elution theory [51–54].

ELUTION OF POLYMERS UNDER CRITICAL CONDITIONS

The critical elution conditions of polymers refer to a narrow intermediate state in the transition from SEC retention to retention due to adsorption. Here, at given eluent strength and temperature, the elution is independent of polymer molecular weight. This was first measured by Tennikov *et al.* [55] with PS standards on silica columns and confirmed by numerous other workers. For a survey, see ref. 56.

Among the features of critical elution is the important fact that oligomers can be separated exclusively by functionality when the elution conditions meet the critical conditions for the polymer chain [57]. Under these circumstances, the polymer portions of the molecules become "invisible". Theory predicts [54] that with block copolymers either of the constituting blocks may also become "invisible" under its critical conditions, which would allow the exclusive separation according to the length of the other blocks.

Critical conditions can be established on stationary phases, the pore size of which would also allow the SEC separation of the polymer under investigation. The results with poly(DMA–*b*–MMA) samples which showed retention (almost) exclu-

sively due to the MMA blocks were obtained on small-pore packings (pore diameter $d_o \approx 5$ nm). Thus, although similar in appearance, the observed effect is certainly not caused by critical elution of DMA blocks.

TLC experiments with poly(S–*b*–MMA) samples, where either the PS or the PMMA block is "invisible", have been performed by Gankina [58]. Under the critical conditions for the styrene block, the retention of the block copolymers increased with MMA block length due to the adsorption of the latter. Under critical conditions for the MMA block, the retention decreased with increasing size of the S block due to an SEC mechanism.

CONCLUSIONS

The paper has shown that reliable characterization of the by-products in block copolymers require separation methods. Gradient HPLC was found to be more efficient for this purpose than SEC or fractionations based on solubility differences.

REFERENCES

1 W. R. Hertler, D. Y Sogah, W. B. Farnham and T. V. Rajanbabu, *J. Am. Chem. Soc.*, 105 (1983) 5706.
2 M. A. Müller and M. Stickler, *Makromol. Chem., Rapid Commun.*, 7 (1987) 575.
3 P. Mai and A. H. E. Müller, *Makromol. Chem., Rapid Commun.* 8 (1987) 247.
4 D. Y. Sogah, W. R. Hertler, O. W. Webster and G. M. Cohen, *Macromolecules*, 20 (1987) 1473.
5 O. W. Webster, W. R. Hertler, D. Y Sogah, W. B. Farnham and T. V. Rajanbabu, *J. Macromol. Sci.*, A21 (1984) 943.
6 S. Mori, *J. Appl. Polym. Sci.*, 38 (1989) 95.
7 S. Mori, *J. Chromatogr.*, 503 (1990) 411.
8 R. J. Ceresa, *Block and Graft Copolymers*, Butterworths, London, 1962.
9 S. L. Aggarwal (Editor), *Block Copolymers, Proceedings of the American Chemical Society Symp., New York, 1969*, Plenum Press, New York, 1970.
10 R. J. Ceresa (Editor), *Block and Graft Copolymerization*, Wiley, London, 1973.
11 A. Noshay and J. E. McGrath, *Block Copolymers*, Academic Press, New York, 1977.
12 S. E. Bresler, L. M. Pyrkov and S. Ya. Frenkel, *Vysokomol. soedin.*, A2 (1960) 216.
13 J. Prud'homme and S. Bywater, *Polym. Prep., Am. Chem. Soc. Div. Polym. Chem.*, 10 (1969) 518.
14 J. J. Hermans, *Ber. Bunsenges, Physik. Chem.*, 70 (1966) 280.
15 D. G. Legrand, *J. Polym. Sci.*, 8 (1970) 195.
16 G. Price, A. G. Watson and M. T. Chow, *Polymer*, 13 (1972) 833.
17 L. J. Fetters, in R. J. Ceresa (Editor), *Block and Graft Copolymerization*, Wiley, London, 1973, Ch. 5, pp. 99–132.
18 F. J. Burgess, A. V. Cunliffe, J. V. Dawkins and D. H. Richards, *Polymer*, 18 (1977) 733.
19 V. V. Nesterov, V. D. Krasikov, L. D. Turkova, E. S. Gankina and B. G. Belenkii, *Vysokomol. Soedin.*, A20 (1978) 2320.
20 V. V. Nesterov, V. D. Krasikov, E. V. Chubarova and B. G. Belenkii, *Vysokomol. Soedin.*, A24 (1982) 1330.
21 V. V. Nesterov, L. V. Zamoiskaya, V. D. Krasikov and G. P. Matianova, *Vysokomol. Soedin.*, A25 (1983) 2561.
22 T. Bastelberger and H. Höcker, *Angew. Makromol. Chem.*, 125 (1984) 53.
23 H. Su, L. Yuan, Y. Ma, and L. Yu, Shiyou Huangong, 14 (1985) 288.
24 S. L. Malhotra, T. L. Bluhm and Y. Deslandes, *Eur. Polym. J.*, 22 (1986) 391.
25 M. A. Müller, M. Augenstein, E. Dumont and H. Pennewiss, *New Polym. Mat.*, in press.
26 F. Kamiyama, H. Matsuda and H. Inagaki, *Makromol. Chem.*, 125 (1969) 286.
27 F. Kamiyama, H. Inagaki and T. Kotaka, *Polym. J.*, 3 (1972) 470.
28 T. Kotaka, T. Uda, T. Tanaka and H. Inagaki, *Makromol. Chem.*, 176 (1975) 1273.
29 H. Inagaki, T. Kotaka and T.-I. Min, *Pure Appl. Chem.*, 46 (1976) 61.

30 N. Donkai, T. Miyamoto and H. Inagaki, *Polym. J.*, 7 (1975) 577.
31 B. G. Belenkii and E. S. Gankina, *J. Chromatogr.*, 141 (1977) 13.
32 E. S. Gankina, I. I. Efimova, J. J. Kever and B. G. Belenkii, *Talanta*, 34 (1987) 167.
33 S. Teramachi, A. Hasegawa, Y. Shima, M. Akatsuka and M. Nakajima, *Macromolecules*, 12 (1979) 992.
34 M. Danielewicz and M. Kubin, *J. Appl. Polym. Sci.*, 26 (1981) 951.
35 G. Glöckner, H. Kroschwitz and Ch. Meissner, *Acta Polym.*, 33 (1982)614.
36 M. Danielewicz, M. Kubin and S. Vozka, *J. Appl. Polym. Sci.*, 27 (1982) 3629.
37 G. Glöckner, *Adv. Polym. Sci.*, 79 (1986) 159.
38 G. Glöckner, in C. Booth and C. Price (Editors), *Comprehensive Polymer Science*, Vol. 1, Pergamon Press, Oxford, 1989, Ch. 16, pp. 313–337.
39 G. Glöckner and A. H. E. Müller, *J. Appl. Polym. Sci.* 38 (1989) 1761.
40 G. Glöckner and J. H. M. van den Berg, *J. Chromatogr.*, 352 (1986) 511.
41 Y. Tanaka, H. Sato and H. Takeuchi, *Polym. Prepr. Jpn.*, 33 (1984) 752.
42 G. Glöckner, M. Stickler and W. Wunderlich, *Fresenius Z. Anal. Chem.*, 328 (1987) 76.
43 M. Augenstein and M. A. Müller, *Makromol. Chem.*, 191 (1990) 2151.
44 G. Glöckner, unpublished results.
45 H. Sato, H. Takeuchi and Y. Tanaka, *Proceedings of the International Rubber Conference 85, Kyoto, October 1985*, 18 B15, pp. 596–601.
46 G. Glöckner, *Z. Physik. Chemie (Leipzig)*, 229 (1965) 98.
47 G. Glöckner, *Pure Appl. Chem.*, 55 (1983) 1553.
48 G. Glöckner, J. H. M. van den Berg, N. L. Meijerink, T. G. Scholte, in L. Kleintjens and P. Lemstra (Editors), *Intergration of Fundamental Polymer Science and Technology*, Elsevier, Barking, 1986, p. 85.
49 R. Schultz and H. Engelhardt, *Chromatographia*, 29 (1990) 205.
50 G. Glöckner, *J. Appl. Polym. Sci., Appl. Polym. Symp.*, 43 (1989) 39.
51 A. M. Skvortsov and A. A. Gorbunov, *Vysokomol. Soedin.*, A21 (1979) 333.
52 A. A. Gorbunov and A. M. Skvortsov, *Vysokomol. Soedin.*, A30 (1988) 3.
53 A. A. Gorbunov and A. M. Skvortsov, *Vysokomol. Soedin.*, A30 (1988) 453.
54 A. A. Gorbunov and A. M. Skvortsov, *Vysokomol. Soedin.*, A30 (1988) 895.
55 M. B. Tennikov, P. P. Nefedov, M. A. Lagareva and S. Ja. Frenkel, *Vysokomol. Soedin.*, A19 (1977) 657.
56 S. G. Entelis, V. V. Evreinov and A. V. Gorshkov, *Adv. Polym. Sci.*, 76 (1986) 129.
57 V. V. Evreinov, A. V. Gorshkov, T. N. Prudskova, V. V. Gur'yanova, A. V. Pavlov, A. Ya. Malkin and S. G. Entelis, *Polym. Bull.* 14 (1985) 131.
58 E. S. Gankina, personal communication, August 1989.
59 M. A. Quarry, M. A. Stadalius, T. H. Mourey, L. R. Snyder, *J. Chromatogr.*, 358 (1986) 1.

Journal of Chromatography, 550 (1991) 639–644
Elsevier Science Publishers B.V., Amsterdam

CHROMSYMP. 2235

Analysis of steroids

XLI[a]. Ion-pair high-performance liquid chromatographic separation of quaternary ammonium steroids on silica

M. GAZDAG*, M. BABJÁK, P. KEMENES-BAKOS and S. GÖRÖG
Chemical Works of Gedeon Richter Ltd., P.O. Box 27, H-1475 Budapest (Hungary)

ABSTRACT

A normal-phase ion-pair chromatographic system has been developed for the high-performance liquid chromatographic investigation of pipecuronium bromide (2β,16β-bis-(N'-dimethyl-1-piperazinyl)-3α,17β-diacetoxy-5α-androstane dibromide) and related quaternary ammonium steroids. The use of silica as the stationary phase and a 96:4 mixture of acetonitrile and water containing 0.1 mol/dm^3 sodium perchlorate as the eluent with detection at 213 nm enable the potential impurities as well as the hydrolytic and oxidative degradation products of pipecuronium bromide to be separated and detected down to the 0.01% level. The above system is also applicable to the high-performance liquid chromatographic investigation of other quaternary ammonium steroids (pancuronium bromide, vecuronium bromide).

INTRODUCTION

Three steroidal neuromuscular blocking agents are currently used in therapy: pancuronium bromide (Pavulon®; Organon, Oss, Netherlands), vecuronium bromide (Norcuron®; Organon) and pipecuronium bromide (Arduan®; Richter, Budapest, Hungary). These are 2β,16β-disubstituted quaternary ammonium derivatives of 3α,17β-diacetoxy-5α-androstane. In the case of the bis-quaternary pancuronium bromide and pipecuronium bromide the substituents are II and III, respectively, while in the mono-quaternary vecuronium bromide the substituents at positions 2 and 16 are I and II (Fig. 1).

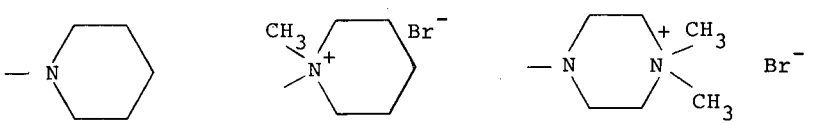

I II III

Fig. 1. Structures of the substituents of bis-quaternary pancuronium bromide (II) and pipecuronium bromide (III) and of the mono-quaternary vecuronium bromide at position 2 (I) and position 16 (II).

[a] For Part XL, see ref. 1.

0021-9673/91/$03.50

Only a few high-performance liquid chromatographic (HPLC) methods have been described in the literature for their separation and quantitative determination. Gazdag and co-workers [2,3] used silica as the stationary phase and a 43:43:14 mixture of acetonitrile, methanol and concentrated ammonia solution containing 0.1 *M* each of ammonium chloride and ammonium carbonate as the eluent for the batch analysis of pipecuronium bromide. This system enables the separation and quantification of pipecuronium bromide and its main impurities and degradation products [4]. A disadvantage is, however, the high ammonia and salt concentration of the eluent. The results obtained with this normal-phase hydrophobic interaction chromatographic system were superior to those obtained by the same authors [5] using various chemically bonded phases in reversed-phase hydrophobic interaction chromatographic systems.

For the determination of pancuronium bromide and vecuronium bromide in biological samples ion-pair chromatographic procedures have been described using iodide [6] or the highly fluorescent 9,10-dimethoxyantracene-2-sulphonate [7,8] as the ion-pairing reagents with pre- [6] or post-column [7,8] ion-pair extraction.

This paper describes a normal-phase HPLC system using neutral eluent containing sodium perchlorate as the ion-pairing reagent for the separation of quaternary ammonium steroids and their related impurities and degradation products.

EXPERIMENTAL

Apparatus

We used a Waters 600E multisolvent delivery system, a 990 photodiode array detector, a NEC/APC IV computer, a U6K variable-volume injector, a NEC CP6 pinwriter and a 990 plotter.

Chromatographic conditions

The column (250 × 4 mm I.D.) packed with SI 100, 5 μm, was purchased from Bio Separation Technologies (Budapest, Hungary). The UV detector was set to 213 nm. The separations were carried out at ambient temperature.

Various mixtures of acetonitrile and water (HPLC-grade purchased from Merck, Darmstadt, Germany) containing 0.1 mol/dm^3 sodium perchlorate (analytical reagent grade from Reanal, Budapest, Hungary) were used as the eluent at a flow-rate of 1 cm^3/min.

Test materials were injected in 20-μl samples of a 0.5% solution using the eluent as the solvent.

Samples

The three drugs were obtained from the manufacturers as listed in the introduction. The related steroids were synthesized by Dr. Z. Tuba (Chemical Works of Gedeon Richter).

RESULTS AND DISCUSSION

Aim of the study

The aim of the study described in this paper was to develop an HPLC system

suitable for purity testing of pipecuronium bromide bulk material, *i.e.* enabling the impurities and degradation products to be separated and quantified at the 0.01% level, and also for the assay of its formulations. It was also our aim that the eluent ensures the stability of both the sensitive ester-type test materials, the column and the HPLC equipment during the chromatographic run, *i.e.* that the use of alkaline eluents can be avoided.

The systems investigated were also checked for their applicability to the investigation of pancuronium and vecuronium bromides, but in these cases no detailed studies were carried out.

Selection of the ion-pair reagent

With their quaternary ammonium group(s) the test substances of this study are eminently suitable for the formation of ion pairs in neutral media with appropriate anions. This is the basis for a large variety of highly sensitive colorimetric and fluorimetric procedures for their determination mainly in biological samples [9] using various organic ion-pair forming agents. Many of them would also be suitable for the HPLC investigation with the great advantage of highly increasing the sensitivity of detection of the spectrophotometrically poorly active neuromuscular blocking agents [7,8]. To achieve this increase, however, an extraction step should be added to the procedure in order to separate the ion-pair complex from the bulk of the reagent. To avoid this we decided to select a simple inorganic anion: even the weak chromophores (tertiary and/or quaternary amino, as well as ester groups) provide sufficient sensitivity at short wavelengths to fulfil the aims of this study (ε_{215} of pipecuronium is 850).

Sodium perchlorate was selected as the ion pair-forming reagent. It has excellent spectral characteristics: it does not interfere with the estimation of the peaks of pipecuronium and related compounds. In addition, perchlorate anion is the strongest ion pair-forming inorganic anion: the logarithms of the extraction constants of the tetrabutylammonium ion pairs (organic phase: chloroform) in the order chloride, bromide, nitrate, iodide and perchlorate are -0.11, 1.29, 1.39, 3.01 and 3.48 [10].

A sodium perchlorate concentration of 0.1 mol/dm^3 was used throughout this study. The retention times of the investigated derivatives rapidly decrease with increasing concentrations of the ion pair-forming reagent up to about 0.05 mol/dm^3 and remain almost unchanged above 0.1 ml/dm^3, thus ensuring that the retention times will not be sensitive to minor changes in the reagent concentration around 0.1 *M*.

Optimization of the water/organic modifier ratio

The best results were obtained with the binary mixture of acetonitrile and water. The first important point to be taken into consideration is the relative position of the peak of the pipecuronium–perchlorate ion pair and that of the bromide ion, which is excluded from pipecuronium bromide by the stronger ion-pairing perchlorate ion and therefore migrates separately. The slopes of the increase of their capacity factors with increasing concentration of acetonitrile are different. Below about 70% of acetonitrile bromide is eluted first, then the elution order changes, but sufficient difference between their capacity factors can be obtained only at an acetonitrile concentration above 90%. This is important, as the majority of the potential impurities of pipecuronium bromide are eluted after the main peak and for this reason bromide should give the last peak if interference with the impurity peaks is intended to be avoided.

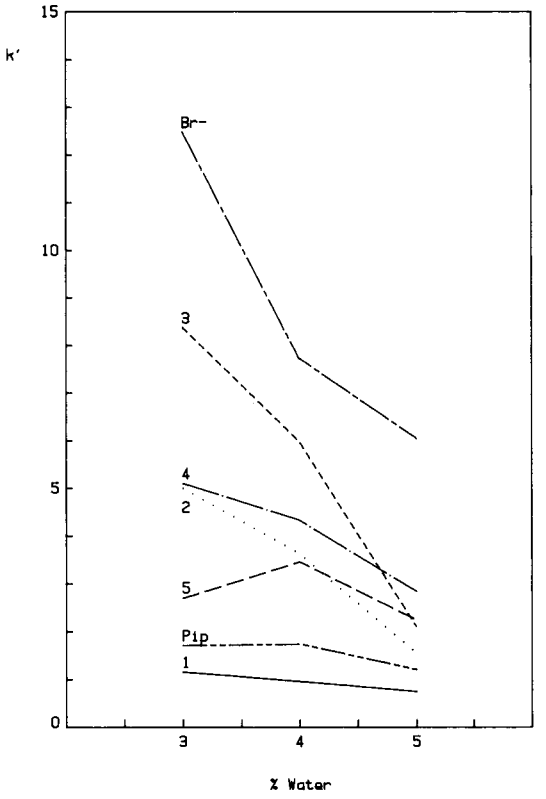

Fig. 2. Dependence of the capacity factor of pipecuronium (Pip) and its potential impurities on the water concentration in the eluent. For details, see Experimental.

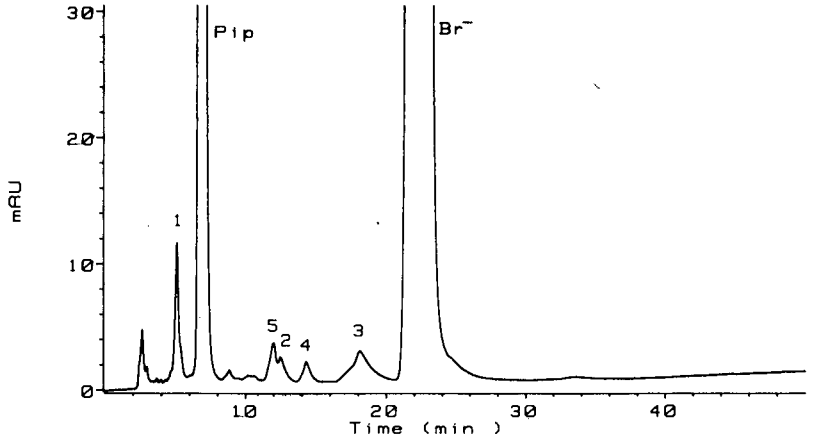

Fig. 3. Model chromatogram of pipecuronium bromide spiked with 0.1% of impurity 1 and 1% of each of impurities 2–5. Eluent, acetonitrile–water (96:4, v/v). For details see Experimental. The numbering of the impurities is summarized in Table I.

Fig. 2 shows that the critical range of water concentration is between 3 and 5% (v/v). An acetonitrile–water ratio of 96:4 has been selected for the separations.

Advantageous features of the proposed system

Fig. 3 shows the chromatogram of pipecuronium bromide spiked with 1% quantitites of the potential impurities and decomposition products. The relative quantity of impurity 1 was 0.1% only because, as a consequence of its enamine structure, its absorptivity at 213 nm is about ten-fold that of pipecuronium bromide and the other impurities. (The limit of detection for impurities 2–5 and 1 was 10 and 1 ng, respectively.)

The structures of the impurites are shown in Table I. Impurity 1 is an oxidative decomposition product. Impurities 2 and 3 are isomeric monoquaternary derivatives (partially methylated products), while 4 and 5 are the isomeric monoacetyl derivatives (partially acetylated products or hydrolytic decomposition products). The good sep-

TABLE I

STRUCTURES OF PIPECURONIUM BROMIDE AND ITS IMPURITIES

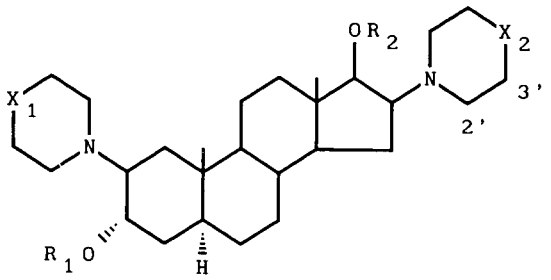

Compound	R_1	R_2	X_1	X_2
Pipecuronium bromide (Pip)	Ac	Ac	$=N^+(CH_3)_2BR^-$	$=N^+(CH_3)_2Br^-$
1	Ac	Ac	$=N^+(CH_3)_2Br^-$	$=N^+(CH_3)_2Br^-$ 2'3'-dehydro
2	Ac	Ac	$=N\text{-}CH_3$	$=N^+(CH_3)_2Br^-$
3	Ac	Ac	$=N^+(CH_3)_2Br^-$	$=N\text{-}CH_3$
4	H	Ac	$=N^+(CH_3)_2Br^-$	$=N^+(CH_3)_2Br^-$
5	Ac	H	$=N^+(CH_3)_2Br^-$	$=N^+(CH_3)_2Br^-$

TABLE II

CHROMATOGRAPHIC DATA FOR QUATERNARY AMMONIUM STEROID DRUGS AFTER SEPARATION AS ION PAIRS WITH PERCHLORATE ION

See Fig. 2 for the chromatographic conditions.

Compound	k'	H (mm)	Asymmetry factor
Vecuronium	0.55	0.073	0.94
Pancuronium	0.61	0.079	0.88
Pipecuronium	1.60	0.079	0.95
Bromide	7.81	–	–

aration of the two pairs of isomers is a remarkable feature of the selectivity of the system. The poor resolution of impurites 2 and 5 does not cause problems in the course of using this method for the analysis of batches of pipecuronium bromide since in practice only impurity 5 occurs.

As regards our desire to introduce a non-corrosive system the results can be demonstrated by the following data. About 300 chromatographic runs were carried out over a period of 3 months using the same column and with no problems in the pump systems either.

Although no detailed studies were carried out with pancuronium bromide and vecuronium bromide, the data in Table II indicate that the described method seems to be suitable for their HPLC investigation too.

Further results concerning the validation of the quantification of the individual impurities will be the subject of another publication.

REFERENCES

1 S. Görög, B. Herényi, Zs. Halmos, A. Georgakis, G. Balogh, É. Csizér and Z. Tuba, in S. Görög (Editor), *Advances in Steroid Analysis '90*, Akadémiai Kiadó, Budapest, 1991, pp. 000–000.
2 M. Gazdag, G. Szepesi, K. Varsányi-Riedl and Z. Tuba, in S. Görög (Editor), *Advances in Steroid Analysis '84*, Akadémiai Kiadó, Budapest, and Elsevier, Amsterdam, 1985, p. 431.
3 M. Gazdag, G. Szepesi, K. Varsányi-Riedl, Z. Végh and Zs. Pap-Sziklay, *J. Chromatogr.*, 328 (1985) 279.
4 G. Szepesi, M. Gazdag and K. Mihályfi, *J. Chromatogr.*, 464 (1989) 265.
5 M. Gazdag, K. Varsányi-Riedl and G. Szepesi, *J. Chromatogr.*, 347 (1985) 284.
6 J. E. Paanakkker and G. L. M. van de Laar, *J. Chromatogr.*, 183 (1980) 459.
7 J. H. Wolf, C. de Ruiter, U. A. Th. Brinkman and R. W. Frei, *J. Pharm. Biomed. Anal.*, 44 (1986) 523.
8 J. E. Paanakker, J. M. S. L. Thio, H. M. van den Wildenberg and F. M. Kaspersen, *J. Chromatogr.*, 421 (1987) 327.
9 S. Görög, *Quantitative Analysis of Steroids*, Akadémiai Kiadó, Budapest, and Elsevier, Amsterdam, 1983, pp. 429–431.
10 G. Schill, H. Ehrsson, J. Vessman and D. Westerlund, *Separation Methods for Drugs and Related Organic Compounds*, Swedish Pharmaceutical Press, Stockholm, 1984, p. 10.

Journal of Chromatography, 550 (1991) 645–656
Elsevier Science Publishers B.V., Amsterdam

CHROMSYMP. 2142

Mechanism of liquid adsorption chromatography in thin-layer chromatography with ternary mobile phases

B. OŚCIK-MENDYK
Faculty of Chemistry, Maria Curie-Sklodowska University, Pl. Marii Curie Sklodowskiej 3, 20-031 Lublin (Poland)

ABSTRACT

A model of the chromatographic process which takes into account molecular association in the mobile phase is discussed. This model is applied to the study of the association effects in liquid adsorption chromatography with ternary mobile phases. Jaroniec's equation was used to describe the molecular interactions in the systems investigated. The assumed model of the molecular mechanism of the chromatographic process significantly broadens the possibillity of interpretation of experimental chromatographic data.

INTRODUCTION

The optimum separation conditions of mixtures in liquid adsorption chromatography very often require application of mixed (multi-component) mobile phases. A great number of the mobile phase components used in the chromatographic separation process cause this process to become more complex. Physicochemical interpretation of experimental data in such chromatographic systems is difficult.

In our previous papers [1–3] a new method of presentation of the retention data obtained from systems with ternary mobile phases was described. It was stated that this method facilitated a complete interpretation of the process realized in such a system.

The process of liquid adsorption chromatography is determined by molecular interactions in the surface and mobile phases. Lately Jaroniec and co-workers [4–7] as well as Ościk-Mendyk and co-workers [8–10] have presented a simple model of the chromatography process mechanism and then verified it in thin-layer chromatography (TLC) and high-performance liquid chromatography (HPLC) systems. The investigations have until now shown the applicability of this model for interpretation of experimental retention data. It can be also concluded that the results of these investigations have not yet provided complete information relating to the molecular mechanism of the chromatographic process in real systems with a multi-component mobile phase.

0021-9673/91/$03.50

THEORETICAL

The chromatographic process in solid–liquid systems is determined by competitive adsorption of the chromatographed substance molecules and the components of a mobile phase. The adsorption phenomenon can be presented as the exchange reaction of the molecules of the chromatographic system components between surface and mobile phases. Molecular interactions in both phases, including interactions with the adsorbent surface, determine the results of such exchange. The strong specific interactions leading to the formation of molecular complexes (associates) in both phases play an especially important role. In many cases a model of the chromatographic process which assumes the existence of double associates in the mobile phase is sufficient to describe the properties of the chromatographic systems [11,12]. The strong localization effects of the test substance and solvent molecules during the adsorption process on silica gel or other oxide adsorbents cause the destruction of the associates in the surface phase. It can be assumed that in such systems only single molecules are adsorbed.

In liquid adsorption chromatography with binary and ternary mobile phases three most important types of associates can be distinguished: association of the molecules of the more polar mobile phase component (autoassociates of the 1–1 type); association of the chromatographed substance molecules and those of the more polar solvent (associates of the s–1 type); and association of both mobile phase components; (associates of the 1–2 and 1–3 types).

The non-specific interactions between the molecules of non-polar or weakly polar components of the mobile phase (components 2 and 3) can be ignored.

In the earlier investigations it was stated that only the first two types of association played a significant role in the chromatographic process. For such systems the equation describing the effect of the above specific molecular interactions on the retention parameter k'_s has been derived [4–7].

$$k'_s = K_{s1} q^{-1} \frac{y_1}{x_1} [1 + (C_1 - 2L_2)]^{-1} \tag{1}$$

where $k'_s = q^{-1} y_s / x_s$ is the capacity factor of the chromatographed substance; x_1, y_1 are the molar fractions of the most polar mobile phase component in the mobile and surface phase, respectively; x_s, y_s are the molar fractions of the chromatographed substance in the mobile and surface phases, respectively; q is a proportionality coefficient, characteristic of a given adsorbent and independent of the nature of the mobile phase; $K_{s1} = y_s x_1 / x_s y_1$ is the thermodynamic equilibrium constant of the phase exchange reaction between the molecules of the substance and of the more polar component of the mobile phase; $C_1 = x_{s-1} / x_s x_1$ is the equilibrium constant of formation of s–1 type bimolecular associates; x_{s-1} is the molar fraction of bimolecular associates of the s–1 type; $L_2 = x_{1-1} / x_1^2$ is the equilibrium constant of the formation of bimolecular associates of the 1–1 type (double autoassociates of the most polar mobile phase component); and x_{1-1} is the molar fraction of bimolecular associates of the 1–1 type.

In the theoretical considerations leading to eqn. 1, the model of the liquid adsorption chromatography process which introduces several simplifying assump-

tions was accepted [4]. Among others, the assumption of a very small concentration of the chromatographed substance in the chromatographic system considered was accepted. For this reason y_s and x_s are often neglected in theoretical considerations. Eqn. 1 can be written in the linear form [5–7]:

$$\frac{y_1}{k'_s x_1} = \alpha + \beta x_1 \tag{2}$$

where

$$\alpha = qK_{s1}^{-1} \text{ and } \quad \beta = q(C_1 - 2L_2)K_{s1}^{-1}$$

From the boundary conditions of the above equation α and β values can be calculated. These parameters are connected with the basic physicochemical factors determining the chromatographic process. The reciprocal of α is proportional to the adsorption equilibrium constant of a given chromatographed substance (K_{s1}). Numerical value of the ratio $\beta/\alpha = C_1 - 2L_2$ permits quantitative specification of the predominant association effects occurring in the mobile phase of the system investigated. These effects are expressed by the equilibrium constants C_1 and L_2 [8,9]. The positive value of β betokens that $C_1 > 2L_2$. In such a system, apart from adsorption expressed by the equilibrium constant K_{s1}, the second factor, association of s–1 type, has a predominant effect on the retention process. Negative β values betoken that autoassociation of most polar solvent molecules of a mobile phase (association of the 1–1 type) plays a significant role in the retention process. It can be said that $\beta = (C_1 - 2L_2)\alpha$ expresses the intensity of the association effect in the retention data of a given chromatographic system.

The relationships described by eqn. 2 include the experimental data relating to the chromatographic retention k'_s and adsorption of the more polar mobile phase component (y_1). In earlier papers [5–7] it has been stated that for a strongly polar solvent it can be assumed that $y_1 = 1.0$ in the whole concentration range of this solvent in the mobile phase. It has also been concluded that the linear relationship $1/k'_s x_1$ *vs.* x_1 for $x_1 \geq 0.5$ is identical with the relationship y_1/k'_s *vs.* x_1 taking into account the changes in y_1 values for $x_1 < 0.5$ [13,14]. It can be stated that for many systems with low concentrations of the most polar mobile phase component the conditions of the chromatographic process do not correspond to those of the assumed theoretical model. Thus, in the study of the chromatographic process we can use as a good approximation a simpler form of eqn. 2:

$$\frac{1}{k'_s x_1} = \alpha + \beta x_1 \tag{3}$$

Eqn. 3 permits description of the chromatographic process on the basis of the experimental retention data (k'_s) only. For binary mobile phases the equilibrium constants K_{s1}, C_1 and L_2 are the functions of the nature of mobile phase components and temperature. As all measurements were carried out at constant temperature the changes in numerical values of the above equilibrium constants depend only on the nature of mobile phase components and of the tested substances. The chromato-

graphic process becomes more complex with the increase in number of the mobile phase components. The description of the chromatographic process with a ternary mobile phase 1 + 2 + 3 (component 1 is the most polar) may also be based on eqn. 3. In this case one can assume that the ratio $r = x_2/x_3$ is constant. Changes in the value of r cause changes in α and β and thus changes in the equilibrium constants K_{s1}, C_1 and L_2. Analysis of the parameter changes of eqn. 3 due to the changes in r may allow complete interpretation of the chromatographic process mechanism in such a complicated systems. An attempt to carry out such an analysis for a few selected chromatographic systems with a ternary mobile phase is the main object of this paper.

The aim of study is to establish:

(1) Whether the proposed model can simplify the explanation of some physicochemical aspects of the molecular mechanism of the liquid adsorption chromatography process with a ternary mobile phase.

(2) How far eqn. 3 permits description of real chromatographic systems in complex conditions when a multi-component mobile phase is used.

(3) Whether the data obtained from eqn. 3 are realistic enough to have a definite physical meaning.

EXPERIMENTAL

The measurements were made at 293K using TLC. Silica gel 60H (Merck, Darmstadt, Germany) was used as the adsorbent. The components of mobile phases were: *n*-heptane, carbon tetrachloride, toluene, benzene, trichloroethylene, acetone and *n*-propanol. In all mixed mobile phases (binary and ternary) concentration of the more or most polar solvent was equal to 0.1, 0.3, 0.5, 0.7 and 0.9 of the molar fraction value. The criterion of polarity was solvent dipole moment (Table I). Naphthalene, *o*-nitrophenol, *o*-nitroaniline, fluorenone and isoquinoline were the test substances. Other details concerning the TLC measurements were described in the previous paper [9].

RESULTS AND DISCUSSION

The mechanism of the chromatographic process may be determined by molecular interactions of the 1–1 and s–1 types depending on the nature of the

TABLE I

DIPOLE MOMENTS AND CLASS, ACCORDING TO PIMENTEL AND McCLELLAN, OF MOBILE PHASE COMPONENTS

Solvent	Dipole moment (D)	Class
n-Heptane	0.00	N
Carbon tetrachloride	0.00	N
Benzene	0.00	N/B
Toluene	0.39	N/B
Trichloroethylene	0.94	A
n-Propanol	1.69	AB
Acetone	2.76	B

chromatographic system. In this connection interpretation of the experimental data was divided into two parts.

In the first part, chromatographic systems with ternary mobile phases containing two non-polar and one polar solvent from A, B or AB class according to the Pimentell and McClellan classification [15] were examined. Non-polar solvents differed in their physicochemical properties (carbon tetrachloride, benzene). Fig. 1 shows the mobile phase composition presented on Gibbs triangle. The vertex S_1 of this triangle corresponds to trichloroethylene (A), acetone (B) and *n*-propanol (AB), respectively. The analysis of the molecular mechanism was based on eqn. 3 for $x_1 \geq 0.5$ [13,14]. For such chosen concentrations of mobile phase components and because of the preadsorption process the demixing phenomenon may be ignored [16].

In each chromatographic system the measurements were made for five mixed phases according to the scheme presented in Fig. 1. From this scheme it can be seen that the measurements were made for two binary mobile phases, $S_1 + C_6H_6(S_2)$ and $S_1 + CCl_4(S_3)$ (systems 1 and 5 in Fig. 1), and for three ternary mobile phases, $S_1 + S_2 + S_3$. In the ternary mobile phase the ratio of mole fractions $r = x_{S_2}/x_{S_3}$ was constant and equal to 1/3, 1 and 3, respectively (systems 2, 3, and 4 in Fig. 1). The chromatographic measurements obtained for the selected substances are presented in Fig. 2 in the form of $1/k'_s x_1$ *vs.* x_1 relationships. Values of the eqn. 3 parameters obtained in three systems with different ternary mobile phases used are listed in Table II. Fig. 3 illustrates the changes of these parameters with the changes of r values. Complete interpretation of the results presented in Figs. 2 and 3 and Table II is based on the analysis of the changes of α and β in eqn. 3 with the changes of the mobile phase composition.

It can be seen that only negative values of β were obtained in the first part of the experiments. It can be stated that in these systems autoassociation of the molecules of polar mobile phase components (association of the 1–1 type) plays an important role in the chromatographic retention mechanism.

Values of $1/\alpha$ and their changes with the changes of the nature of the mobile phase depend, above all, on the properties of a polar component of mobile phase. Strong adsorption of *n*-propanol molecules on the silica gel surface leads to low adsorption of the chromatographed substance molecules. In this case numerical values of the equilibrium constant K_{s1} are very low and do not differ significantly from one

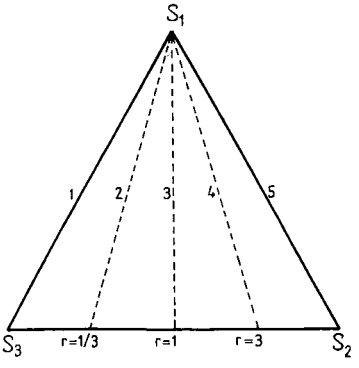

Fig. 1. Mobile phases used in the investigated systems. S_1 is the most polar solvent, S_2 and S_3 are non-polar or weakly polar solvents.

another. Variations of the mole fractions ratio of non-polar mobile phase components do not influence the value of $1/\alpha$, which increases slightly with the increase in benzene concentration in the mobile phase. This slight increase of $1/\alpha$ is observed mainly in the case of *o*-nitrophenol and *o*-nitroaniline. It can be said that the increase in benzene concentration in mobile phase causes the increase of the interactions between the molecules of *n*-propanol (AB) and benzene (N/B). In this connection both substances mentioned above adsorb strongly on the silica gel surface.

The numerical values of $1/\alpha$ are also low and decrease linearly with increasing benzene concentration in the mobile phase when acetone is used as a polar solvent (Figs. 2 and 3). Molecules of acetone can form autoassociates due to a very strong dipole moment (2.76 D). In this system benzene molecules can compete more strongly with the chromatographed substance molecules for active centres on the adsorbent surface. Thus, the greatest changes in $1/\alpha$ are again observed for *o*-nitrophenol and *o*-nitroaniline. The tendency of these substances to form intramolecular hydrogen bonds can also be taken into account. Apart from strong adsorption of *n*-propanol and acetone molecules, the association of the mobile phase components can also play a very important role in the chromatographic process. This can be confirmed from numerical values of β and β/α. For *n*-propanol, values of β/α are practically the same for all tested substances and do not change with the changes of the concentration of

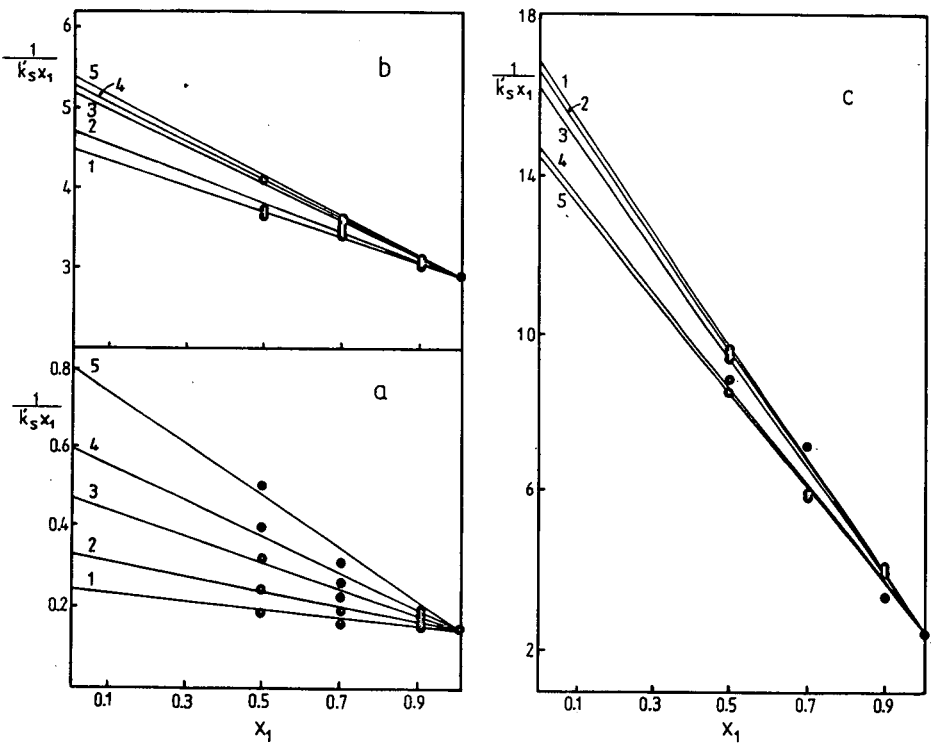

Fig. 2. $1/k'_s x_1$ *vs.* x_1 plotted for *o*-nitroaniline in (a) carbon tetrachloride–benzene–trichloroethylene, (b) carbon tetrachloride–benzene–acetone and (c) carbon tetrachloride–benzene–*n*-propanol. Numbers 1–5 indicate mobile phase compositions according to the scheme in Fig. 1.

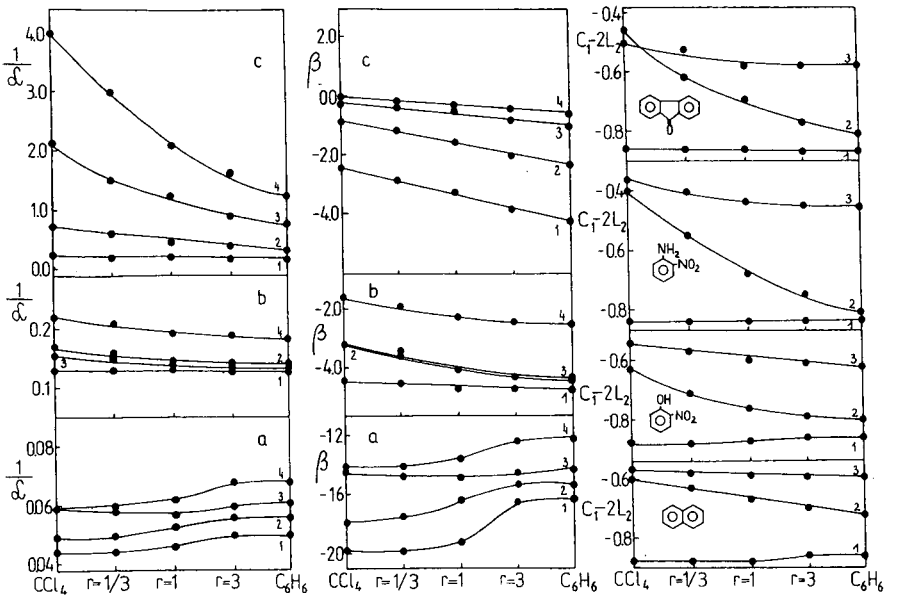

Fig. 3. Dependence of $1/\alpha$ (left panel) and β (centre panel) on different values of r for (1) naphthalene, (2) *o*-nitrophenol, (3) fluorenone and (4) *o*-nitroaniline in (a) carbon tetrachloride–benzene–*n*-propanol, (b) carbon tetrachloride–benzene–acetone and (c) carbon tetrachloride–benzene–trichloroethylene. Dependence of $C_1 - 2L_2$ values (right panel) on different values of r in (1) carbon tetrachloride–benzene–*n*-propanol, (2) carbon tetrachloride–benzene–acetone and (3) carbon tetrachloride–benzene–trichloroethylene.

non-polar mobile phase components. One can suppose that such results are determined mainly by strong autoassociation of molecules of a polar mobile phase component. In the system containing acetone, lower negative values of β/α depend, in great part, on the properties of the tested substance and on the concentration of non-polar mobile phase components (decrease with the increase of benzene concentration). Assuming a constant value of the equilibrium constant for the autoassociation of acetone molecules in a given system, the observed changes in $C_1 - 2L_2$ values may be due to the changes in solvation of the chromatographed substance only, *i.e.* to the changes in the equilibrium constant C_1 (Fig. 3).

The values of $1/\alpha$ depend on the properties of the chromatographed substances when trichloroethylene is used as a polar component of the mobile phase. For example, for fluorenone and *o*-nitroaniline high values of this parameter indicate a strong adsorption of these substances on the silica gel surface in comparison with that of *o*-nitrophenol and especially of naphthalene. The magnitude of the adsorption decreases significantly with increasing benzene concentration in the mobile phase. This is due to significantly lower adsorption of trichloroethylene molecules on the silica gel surface in comparison with the adsorption of *n*-propanol and acetone molecules. The adsorption of trichloroethylene on the silica gel surface is comparable to that of benzene. Great changes in the numerical values of β/α due to changes in concentration of non-polar mobile phase components illustrate the significant effect of molecular interactions in a mobile phase on the chromatographic process.

TABLE II

VALUES OF $1/\alpha$, β, AND $\beta/\alpha = C_1 - 2L_2$ OBTAINED FOR DIFFERENT MOBILE PHASE COMPOSITIONS

Mobile phase composition[a]	Naphthalene			*o*-Nitrophenol			*o*-Nitroaniline			Fluorenone		
	$1/\alpha$	β	$C_1 - 2L_2$	$1/\alpha$	β	$C_1 - 2L_2$	$1/\alpha$	β	$C_1 - 2L_2$	$1/\alpha$	β	$C_1 - 2L_2$
$S_1 + S_3$	0.25	−2.45	−0.60	0.74	−0.85	−0.63	4.00	−0.10	−0.40	2.17	−0.21	−0.46
$S_1 + r = 1/3$	0.22	−2.75	−0.62	0.59	−1.20	−0.71	3.03	−0.18	−0.55	1.54	−0.40	−0.62
$S_1 + r = 1.0$	0.20	−3.30	−0.67	0.48	−1.60	−0.76	2.13	−0.32	−0.68	1.25	−0.55	−0.69
$S_1 + r = 3.0$	0.18	−3.90	−0.70	0.39	−2.05	−0.79	1.67	−0.45	−0.75	0.91	−0.85	−0.77
$S_1 + S_2$	0.17	−4.30	−0.72	0.33	−2.40	−0.80	1.25	−0.65	−0.81	0.77	−1.05	−0.81
$S_1 + S_3$	0.13	−4.40	−0.57	0.17	−3.20	−0.54	0.22	−1.60	−0.36	0.16	−3.20	−0.50
$S_1 + r = 1/3$	0.13	−4.50	−0.58	0.16	−3.60	−0.57	0.21	−1.90	−0.40	0.15	−3.40	−0.52
$S_1 + r = 1.0$	0.13	−4.70	−0.59	0.15	−4.10	−0.60	0.19	−2.30	−0.44	0.14	−4.10	−0.55
$S_1 + r = 3.0$	0.13	−4.70	−0.59	0.14	−4.30	−0.61	0.19	−2.40	−0.45	0.14	−4.30	−0.58
$S_1 + S_2$	0.13	−4.70	−0.59	0.14	−4.40	−0.62	0.19	−2.50	−0.46	0.14	−4.30	−0.58
$S_1 + S_3$	0.04	−19.9	−0.88	0.05	−18.0	−0.88	0.06	−14.2	−0.84	0.06	−14.5	−0.86
$S_1 + r = 1/3$	0.04	−19.9	−0.88	0.05	−17.5	−0.88	0.06	−14.1	−0.84	0.06	−14.8	−0.86
$S_1 + r = 1.0$	0.05	−19.3	−0.88	0.05	−16.4	−0.87	0.06	−13.6	−0.84	0.06	−14.9	−0.86
$S_1 + r = 3.0$	0.05	−16.3	−0.86	0.06	−15.3	−0.86	0.07	−12.4	−0.84	0.06	−14.5	−0.87
$S_1 + S_2$	0.05	−16.3	−0.86	0.06	−15.3	−0.86	0.07	−12.2	−0.84	0.06	−14.2	−0.87

[a] S_1: trichloroethylene, acetone, and *n*-propanol, for top, middle and bottom group, respectively; S_2: benzene; S_3: carbon tetrachloride ($r = x_{S_2}/x_{S_3}$).

In the second part of our investigations chromatographic systems with ternary mobile phases of the composition acetone–*n*-heptane–toluene were used. Also, four chromatographed substances were used. The measurements were made in the same way as in the first part of our experiments. In ternary mobile phases the ratios of mole fractions ($r = x_{C_6H_5CH_3}/x_{C_7H_{16}}$) were constant and equal to 1/3, 1 and 3. Fig. 4 presents the results obtained for all compositions of a mobile phase, Table III lists the numerical values of eqn. 3 parameters for all substances and Fig. 5 illustrates the changes of these parameters with the changes in r values. Positive or negative values of β were obtained in the systems investigated. These values depend on the properties of the chromatographed substances and vary with changes of ternary mobile phase composition. Thus, according to the proposed model of the chromatographic process it can be stated that the results obtained for such systems indicate a very complex and differentiated effect of molecular interactions on the chromatographic process. This is due to significant differences in the properties of the individual mobile phase components: strong polar acetone, aromatic weakly polar toluene and non-polar saturated hydrocarbon *n*-heptane.

The values of $1/\alpha$ depend strongly on the composition of this ternary mobile phase. Weak interactions of *n*-heptane molecules with the silica gel surface mean that K_{s1} values in the acetone–*n*-heptane system are greatly differentiated depending on the properties of the substances chromatographed. Addition of toluene to such a system causes a rapid decrease of $1/\alpha$ (and thus the K_{s1} constant) because the toluene molecules participate in competitive adsorption on the adsorbent surface. In the acetone–toluene system the $1/\alpha$ values are low for all test substances and differ only slightly one from another (they are practically the same as in the acetone–benzene system).

The analysis of β and β/α values permits us to conclude that the effect of molecular interactions in a mobile phase on chromatographic retention is different

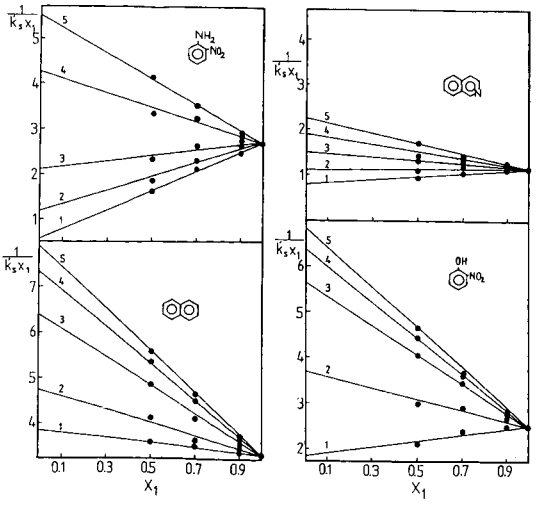

Fig. 4. $1/k'_s x_1$ *vs.* x_1 obtained in *n*-heptane–toluene–acetone.

TABLE III

VALUES OF $1/\alpha$, β, AND $\beta/\alpha = C_1 - 2L_2$ OBTAINED FOR DIFFERENT MOBILE PHASE COMPOSITIONS

Mobile phase composition[a]	Naphthalene			*o*-Nitrophenol			*o*-Nitroaniline			Fluorenone		
	$1/\alpha$	β	$C_1 - 2L_2$	$1/\alpha$	β	$C_1 - 2L_2$	$1/\alpha$	β	$C_1 - 2L_2$	$1/\alpha$	β	$C_1 - 2L_2$
$S_1 + S_3$	0.26	−0.55	−0.14	0.54	0.70	0.38	1.82	2.10	3.82	1.25	0.35	0.44
$S_1 + r = 1/3$	0.21	−1.50	−0.32	0.27	−1.20	−0.32	0.83	1.50	1.25	0.91	0.05	0.05
$S_1 + r = 1.0$	0.16	−3.15	−0.49	0.18	−3.20	−0.57	0.48	0.65	0.31	0.67	−0.40	−0.27
$S_1 + r = 3.0$	0.14	−4.00	−0.54	0.16	−3.85	−0.61	0.24	−1.55	−0.36	0.53	−0.80	−0.42
$S_1 + S_2$	0.13	−4.70	−0.59	0.15	−4.45	−0.65	0.18	−2.80	−0.51	0.44	−1.10	−0.49

[a] S_1: acetone; S_2: toluene; S_3: *n*-heptane ($r = x_{S_2}/x_{S_3}$).

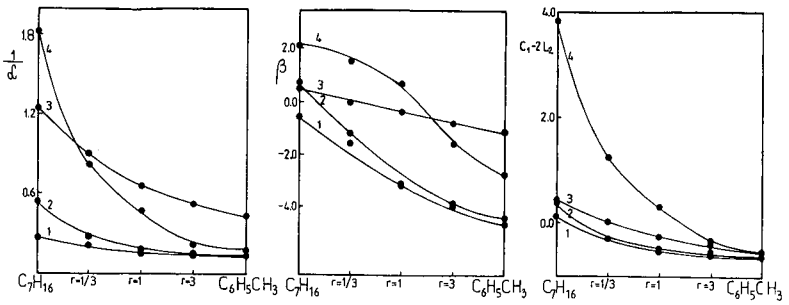

Fig. 5. Dependence of $1/\alpha$ (left), β (centre) and $C_1 - 2L_2$ (right) parameters on different values of r for (1) naphthalene, (2) *o*-nitrophenol, (3) isoquinoline and (4) *o*-nitroaniline in *n*-heptane–toluene–acetone.

from that in the first part of the study. For the acetone-*n*-heptane system and for ternary systems of high concentration of *n*-heptane the β values are positive for all substances except naphthalene. For higher concentrations of toluene the β values are negative. It can be supposed that non-active *n*-heptane molecules facilitate the formation of stable associates between the molecules of acetone and the substance chromatographed (associates of the s–1 type or polymolecular associates). The molecules of relatively active and weakly polar toluene significantly hinder this process and the increase of toluene concentration shifts the $C_1 - 2L_2$ value towards the autoassociation of acetone molecules.

CONCLUSIONS

The study of the mechanism of liquid adsorption chromatography with a ternary mobile phase made on the basis of eqn. 3 produced the following conclusions.

(1) The assumed model of the molecular mechanism of the investigated process significantly broadens the possibility of interpretation of experimental chromatographic data.

(2) The values obtained for the parameters in eqn. 3 allow quantitative evaluation of the molecular interactions determining the retention mechanism.

(3) The quantitative data resulting from this model and from eqn. 3 are realistic and relate to real values of physicochemical parameters characterizing a given chromatographic system.

(4) The widening of these investigations to include other chromatographic systems will produce a better understanding of a complicated retention process.

REFERENCES

1 B. Ościk-Mendyk and J. K. Różyło, *J. Chromatogr.*, 10 (1987) 1399.
2 B. Ościk-Mendyk, *J. Liq. Chromatogr.*, 12 (1989) 891.
3 M. Borówko and B. Ościk-Mendyk, *J. Liq. Chromatogr.*, 12 (1989) 2601.
4 M. Jaroniec and J. A. Jaroniec, *J. Chromatogr.*, 210 (1981) 130.
5 M. Jaroniec and J. A. Jaroniec, *J. Liq. Chromatogr.*, 4 (1981) 2121.
6 M. Jaroniec and J. A. Jaroniec, *J. Liq. Chromatogr.*, 7 (1984) 393.
7 M. Jaroniec, J. K. Różyło and J. Jaroniec, *Chem. Anal.*, 26 (1981) 623.
8 B. Ościk-Mendyk, J. K. Różyło and J. A. Jaroniec, *J. Liq. Chromatogr.*, 10 (1987) 2845.

9 B. Ościk-Mendyk and J. K. Różyło, *Chromatographia*, 25 (1988) 300.
10 B. Ościk-Mendyk, *Chromatographia*, 28 (1989) 151.
11 H. Wolff and A. Sandiakhy, *Fluid Phase Equilib.*, 7 (1981) 309.
12 J. Feenney and S. M. Walkner, *J. Chem. Soc.*, 66 (1966) 1148.
13 M. Jaroniec, J. K. Różyło, B. Ościk-Mendyk and J. A. Jaroniec, *J. Liq. Chromatogr.*, 5 (1982) 1033.
14 B. Ościk-Mendyk, *J. Planar Chromatogr.*, 3 (1990) 322.
15 G. C. Pimentel and A. L. McClellan, *The Hydrogen Bond*, Freeman, San Francisco, CA, 1960.
16 T. Wawrzynowicz and E. Soczewiński, *J. Chromatogr.*, 169 (1979) 191.

Journal of Chromatography, 550 (1991) 657–666
Elsevier Science Publishers B.V., Amsterdam

CHROMSYMP. 2245

Computer-assisted sample clean-up in liquid chromatography from thin-layer chromatographic data

A. M. SIOUFFI* and N. VOLPE
Laboratoire de Génie Chimique et Chimie Appliquée, Université Aix-Marseille 3, F-13397 Marseille Cedex 13 (France)

ABSTRACT

A method is presented where thin-layer chromatographic data with binary mixtures eluents are treated with NEMROD software in order to enhance the ΔR_F between two solutes. In this procedure it is possible to selectively retain one solute or one group of solutes with a change in solvent composition. The method has been succesfully applied to derivatives of phenols in both normal and reversed-phase systems and the only requirement is the capacity factor ranking.

INTRODUCTION

The ideal situation in liquid chromatography (LC) would be to directly inject the sample onto a chromatographic column and to obtain unambiguous separation of all solutes. Unfortunately this is not possible and in many cases sample pretreatment is required. For this purpose many strategies have been developed including liquid–liquid extraction, solid-phase extraction, column switching, etc. The topic is well documented in excellent book [1] and a recent review [2].

In many cases sample clean-up is performed either on-line or off-line with a cartridge of small dimensions. Samples are adsorbed onto the packing and a solvent is selected to retain the solutes of interest whilst the others are eluted. Conversely, appropriate choice of packing and solvent will retain the undesirable compounds and elute those of interest with the advantage of peak compression. Selection of suitable packing and solvent is usually carried out by trial and error or from knowledge of chromatographic behaviour. For example, hydrophobicity of a solute is commonly expressed as the logarithm of the partition coefficient (log P) between 1-octanol and water. Since the logarithm of the capacity factor (log k') obtained from reversed-phase liquid chromatography (RPLC) has been shown to have good correlation with the log P of several classes of chemicals, the value of k' in pure water (log k_w) can be deduced and can be effective in the designing of sample clean-up procedures [3]. On the other hand, knowledge of the polarity of the solutes permits maximization of the interactions with the packing in order to perform selective extractions.

These procedures are very selective but some drawbacks are obvious. For ex-

0021-9673/91/$03.50

ample, they may involve two immiscible solvents with the consequence of the required use of a third solvent and subsequent dilution of the solutes prior to injection in the analytical column. From the numerous data published in the literature it can be shown that extrapolation to 0% organic modifier in RPLC yields different values of $\log k_w$ depending on the nature of the organic modifier (methanol or acetonitrile) [4].

Two features caught our attention. (1) The performances of precolumns expressed as plate counts are not very high and can be compared to those obtained in classical thin-layer chromatography (TLC); large amounts of TLC data can be retrieved from the literature thus allowing the gathering of actual information on solute behavior. (2) From the optimization procedures advocated in high-performance liquid chromatography (HPLC) a slight change in solvent composition would dramatically change the selectivity. Thus it would be possible to enhance the selectivity by looking for the solvent composition which would produce the maximum difference in capacity factors, making it possible to separate and eliminate one solute (or one group of solutes) while keeping the others on the precolumn for a predicted time. In this paper we explore the feasibility of the concept and give some preliminary results.

THEORY

We shall first make some assumptions in order to restrict the domain. We shall only consider normal-phase (NP) and RP chromatography with binary eluents. We shall not consider mixtures of three to four solvents or ion-pairing chromatography. We shall consider that the sample can be chromatographed either isocratically or with gradient elution yielding a chromatogram in which peaks are ranked from first to last. This precludes trace analysis or sample overload. The aim will be to eliminate (or to keep) the first solute. Conversely we can eliminate all the peaks with the exception of the last one.

It has been demonstrated in TLC by Soczewinski and Golkiewicz [5,6] that in NP with a silica gel packing and a binary mobile phase consisting of an apolar diluent and a polar modifier that

$$R_M = \log [(1 - R_F)/R_F] = a_i \log X_s + b_i \tag{1}$$

where a and b are characteristics of a given solute i. In RP the utilization of the solubility parameter concept of Schoenmakers and co-workers [7,8] resulted in the quadratic equation

$$\log k' = a\varphi^2 + b\varphi + c \tag{2}$$

However numerous studies have established that the empirical relationship

$$\log k' = \log k_w - S\varphi \tag{3}$$

is valid within the range 20–80% of the volume of the organic modifier.

φ is the volume fraction of the strong solvent and k_w and S are constants that are characteristic of the strong solvent and solute respectively. For the sake of simplicity we shall write:

$$k' = (1 - R_F)/R_F \tag{4}$$

Since X_3 is similar to φ and $R_M = a_i \ln X_s + b_i$:

$$R_F = 1/[1 + \exp(a_i \ln X_s + b_i)] \quad (5)$$

The response function selected must be based on selectivity. A resolution criterion would be meaningless since information on spot widths is rather scarce in TLC and resolution is R_F-dependent with a given chromatographic system.

Separation between two components is expressed as:

$$\Delta R_{Fij} = R_{Fi} - R_{Fj} = 1/[1 + \exp(a_i \ln X_s + b_i)] - 1/[1 + \exp(a_j \ln X_s + b_j)] \quad (6)$$

We can select the mobile phase composition to maximize ΔR_F. It has been shown by Nurok and Richard [9] that plots of ΔR_F *versus* mobile phase composition of a binary eluent exhibits a maximum. We shall maximize the ΔR_F between the first (or the last) eluted solute and the others.

The procedure is as follows: since for a given X_s there will be different a_i and b_i values we have utilized a non-fractional two-level factorial design 2^k. Considering a pair of solutes we have a_i, b_i, a_j and b_j values, thus yielding a 2^4 factorial design. By fixing every a and b at + or − level, respectively, the matrix has 4 rows and 16 lines (see Table I). We are then able to construct the model matrix and determine the highest and lowest boundaries for a and b for every solute of the sample. The lowest values of a_i and b_i and the largest variation are determined. These yield the center of the variation domain for all a and b, and the steps within this variation. We chose to consider at the − level the values of a and b within the domain between the lowest boundary and the center of the domain. The X_s values are calculated which yield $\Delta R_{F\max}$ for the i, j pair of solutes. As many responses as are in the model matrix are obtained, and the NEMROD software calculates the coefficient of the model by multilinear regression.

TABLE I

EXPERIMENTAL MATRIX FOR THE NORMAL-PHASE MODEL

	X_1	X_2	X_3	X_4	a_i	b_i	a_j	b_j	X_s (computer)	$\Delta R_{F\max}$
1	−	−	−	−	−1.200	−1.819	−1.490	−2.395	0.53	0.07
2	+	−	−	−	−0.750	−1.727	−1.510	−1.980	0.08	0.33
3	−	+	−	−	−1.340	−1.243	−1.200	−1.819	0.02	0.20
4	+	+	−	−	−1.080	−0.253	−1.400	−2.395	0.44	0.45
5	−	−	+	−	−1.200	−1.819	−0.750	−1.727	0.07	0.20
6	+	−	+	−	−0.700	−1.543	−0.798	−1.814	0.63	0.05
7	−	+	+	−	−1.120	−1.658	−0.960	−1.704	0.10	0.09
8	+	+	+	−	−1.080	−0.253	−0.788	−1.814	0.23	0.46
9	−	−	−	+	−1.270	−0.737	−1.200	−1.819	0.33	0.30
10	+	−	−	+	−1.200	−1.819	−0.950	−1.727	0.08	0.11
11	−	+	−	+	−1.340	−1.243	−1.120	−1.658	0.21	0.18
12	+	+	−	+	−1.080	−0.253	−1.340	−1.243	0.80	0.23
13	−	−	+	+	−1.400	−2.395	−0.700	−1.543	0.05	0.23
14	+	−	+	+	−1.510	−1.985	−1.080	−0.253	0.61	0.36
15	−	+	+	+	−1.080	−0.253	−1.120	−1.658	0.44	0.34
16	+	+	+	+	−0.960	−1.704	−0.700	−1.543	0.04	0.11

NEMROD is able to work with either coded (or reduced) variables or with the actual variables. The reduced variable will be written as $a = (y - y_0)/c_y$ where y_0 is the value at the center of the domain and c_y is the step of variation.

RESULTS AND DISCUSSION

We shall consider some contaminants, especially the nitro and chloro derivatives of phenol (see Table II). From the TLC literature data we can consider either the NP or the RP mode. In Table II are the experimental a_i and b_i values from NP-TLC [10] with silica gel as stationary phase and heptane–ethyl acetate as solvent mixture.

To check the influence of a_i and b_i values on eqn. 6 it is necessary to have a knowledge of the different levels that a and b can attain. To this purpose a complete 2^4 factorial design has been constructed with yields a set of combinations a_i, b_i, a_j and b_j. From this factorial design, 16 pairs of compounds are characterized by their a_i, b_i values. A simple program permits the calculation of the responses from eqn. 6. The response is the value of X_s which permits the attainment of $\Delta R_{F\max}$. Plots of $\Delta R_{F\max}$ *versus* mobile phase composition are shown in Fig. 1. From Table II it is seen that variation of a is from -1.51 to -0.70 and b from -2.395 to -0.253. From these values the center of the variation domain is easily deduced and + and − levels are attributed.

Data from Table III are treated with NEMROD software. In this procedure an empirical model is postulated of the form $X_s = f(a_i, b_i, a_j, b_j)$. The mathematical form is a first- or second-order polynomial. NEMROD selects the model which yields the best statistical parameters (variance, covariance, etc.). From the NEMROD computation the highest quality is obtained, nevertheless, as is obvious particularly in TLC, experiments are often required to check the validity of the model.

TABLE II

CHARACTERISTIC VALUES OF CHLOROPHENOLS AND NITROPHENOLS ON SILICA GEL WITH BINARY MOBILE PHASE HEPTANE–ETHYL ACETATE

Solutes	Abbreviation	a	b	Levels a	Levels b
Phenol	Ph	−1.120	−1.663	−	−
2-Chlorophenol	2-CP	−0.750	−1.727	+	−
3-Chlorophenol	3-CP	−0.950	−1.795	+	−
4-Chlorophenol	4-CP	−1.200	−1.819	−	−
3,4-Chlorophenol	3,4-CP	−1,240	−1.865	−	−
3,5-Chlorophenol	3,5-CP	−0.700	−1.543	+	−
2,4-Chlorophenol	2,4-CP	−0.960	−1.704	+	−
2,4,6-Chlorophenol	2,4,6-CP	−0.798	−1.814	+	−
Pentachlorophenol	Penta-CP	−0.950	−1.727	+	−
4-Iodophenol	4.IP	−1.490	−2.395	−	−
4-Bromophenol	4-BrP	−1.400	−2.395	−	−
3-Nitrophenol	3-NtP	−1.510	−1.980	−	−
2-Nitrophenol	2-NtP	−1.080	−0.253	+	+
4-Nitrophenol	4-NtP	−1.340	−1.243	−	+
2,6-Nitrophenol	2,6-NtP	−1.270	−0.737	−	+

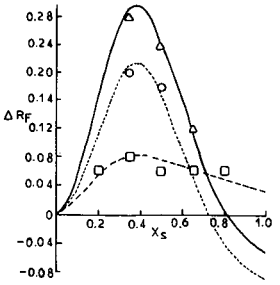

Fig. 1. Plots of $\Delta R_{F\max}$ *versus* X_s.

From the NEMROD results the best polynomial was:

$$X_s = X_0 + X_1\, a_i + X_2\, b_i + X_3\, a_j + X_4\, b_j$$

We must point out that it is possible to work with normalized reduced variables. In this case the comparison between the two procedures yielded the same results and the model with actual variables performed better (Table III). Selected values are as follows:

$X_0 = 0.71835$
$X_1 = 0.61186$
$X_2 = 0.02041$
$X_3 = -0.635537$
$X_4 = 0.193513$

Checking the model is necessary to make sure that estimated X_s values are identical to those from curves $\Delta R_{Fi,j} = f(X_s)$. We performed this checking with the "ideal" case (where $\Delta R_F < 0.3$), this 0.3 value was selected from experience since the maximization of ΔR_F is insufficient below 0.3.

TABLE III

COMPARISON OF RESPONSES OBTAINED BY PLOT OF ΔR_F AND MODELS FROM NORMALIZED REDUCED VALUES (nrv) AND FROM ACTUAL VALUES (ac)

Solute pair	X_s plot	X_s (nrv)	X_s (ac)	$\Delta R_{\max}$
2,6-NtP/2,4,6-CP	0.174	0.100	0.100	0.42
2,6-NtP/Penta-CP	0.226	0.180	0.200	0.34
2,6-NtP/3,5-CP	0.154	0.080	0.080	0.40
2-NtP/Penta-CP	0.320	0.320	0.320	0.38
2-NtP/2,4-CP	0.330	0.330	0.330	0.38
2-NtP/3,5-CP	0.208	0.200	0.200	0.42
2-NtP/2,6-NtP	1	0.720	0.720	0.10
2,6-NtP/4-NtP	0.560	0.480	0.540	0.10
4-NtP/3-NtP	0.430	0.450	0.450	0.14
Ph/4-CP	0.645	0.410	0.410	0.02
3,5-CP/2,4-CP	0.410	0.540	0.540	0.12

Fig. 2 shows the comparison between the response from the model and the first derivative of the $\Delta R_F = f(X_s)$ function. When the first derivative = 0 it represents the maximum of that function.

Discrepancies between responses were observed: (1) when X_s is outside the range 0.2–0.8, since beyond that range the experimental data do not fit a linear regression (an example is given in the first row of Table III, as $X_{s,model} = 0.1$ and $X_{s,plot}$ is 0.174); (2) when the ΔR_F difference is less than 0.1 (for example, of the phenol and 4-chlorophenol).

Application to NP chromatography

Nitrophenols (NtPs) and chlorophenols (Cps) with silica gel as stationary phase and heptane–ethyl acetate as mobile phase. From the mathematical model and the fixed contraints ($\Delta R_F > 0.1$ and $0.2 \leqslant X_s \leqslant 0.8$) we can consider a sample clean-up on 2-NtP and 2,6-NtP. From Table IV it looks obvious that these contaminants can be separated from chlorophenols and phenol. From the X_s values a stepwise procedure can be considered according to the wishes of the analyst. We can retain the 2-NtP ($k' = 4.42$) with a heptane–ethyl acetate (80:20, v/v) mobile phase and by consequence 3,5-CP and 2,4,6-CP would be eliminated ($k' = 0.65$ for both). By a simple change to a (67:33, v/v) solvent composition elimination of pentachlorophenol, 2,4-CP and 3-CP would be obtained ($k' =$ approximately 0.53). Of course the capacity factor of 2-NtP shifted from 4.42 to 2.57 but the gap is still large. In the third step with 54:46 (v/v) solvent composition phenol, 4-CP and 3,4-Cp are quickly eluted ($k' = 0.61$). Finally, 2-NtP is the only solute retained which can be eluted with pure ethyl acetate.

In the same way, it would be easy to separate 2,6-NtP from phenol, 3-CP, 4-CP, 3,4-CP, 2,4-CP and pentachlorophenol (Fig. 3) in a stepwise procedure.

Nitrophenols and chlorophenols with silica gel as stationary phase and a heptane–diisopropyl ether as mobile phase. In the above procedure we could not separate 4-NtP from the others. A careful change of the polar modifier will permit us to achieve this goal. A remarkable feature of the model elaborated from NEMROD computation is that it can be used with any NP system provided that a_i and b_i for the different polar modifier are available. Nevertheless it must be pointed out that some discrepancies may occur when silica gel of different activity is used as chromatographic packing. When care is taken to normalize the experiments the mathematical model performs very well. In our calculation we used data from Matyska and Soczewinski [10] which

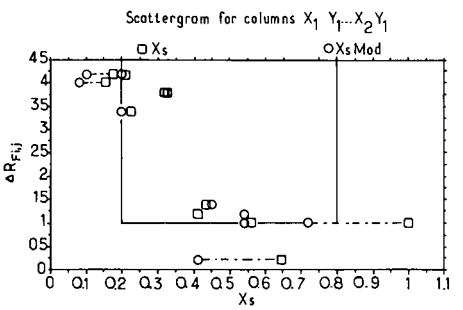

Fig. 2. Comparison of responses from the model and the first derivative of the $\Delta R_F = f(X_s)$ function.

TABLE IV

OPTIMAL MOBILE PHASE FOR SEPARATION OF CHLOROPHENOLS AND NITROPHENOLS

Solute pair	X_s (computer)	X_s (model)	$\Delta R_{F\ max}$
2-NtP/Ph	0.44	0.44	0.33
2-NtP/2-CP	0.22	0.19	0.22
2-NtP/3-CP	0.31	0.31	0.31
2-NtP/4-Cp	0.46	0.46	0.35
2-NtP/3,4-CP	0.47	0.46	0.36
2-NtP/3,5-CP	0.21	0.20	0.42
2-NtP/2,4-CP	0.33	0.33	0.37
2-NtP/2,4,6-CP	0.23	0.21	0.45
2-NtP/Penta-CP	0.32	0.32	0.38
2,6-NtP/Ph	0.3	0.32	0.27
2,6-NtP/2-CP	0.16	0.07	0.42
2,6-NtP/3-CP	0.22	0.18	0.35
2,6-NtP/4-CP	0.33	0.34	0.28
2,6-NtP/3,4-CP	0.34	0.35	0.28
2,6-NtP/2,4-CP	0.23	0.21	0.33
2,6-NtP/Penta-CP	0.22	0.20	0.34

are very coherent. It must be remembered that the above requirements are still valid (*i.e.* $0.2 \leqslant X_s \leqslant 0.8$ and $\Delta R_F > 0.3$). Table V shows both experimental and computational values. From these data it is possible to selectively retain 4-NtP from 2,4,6-CP, 3,5-CP and 2-Cp.

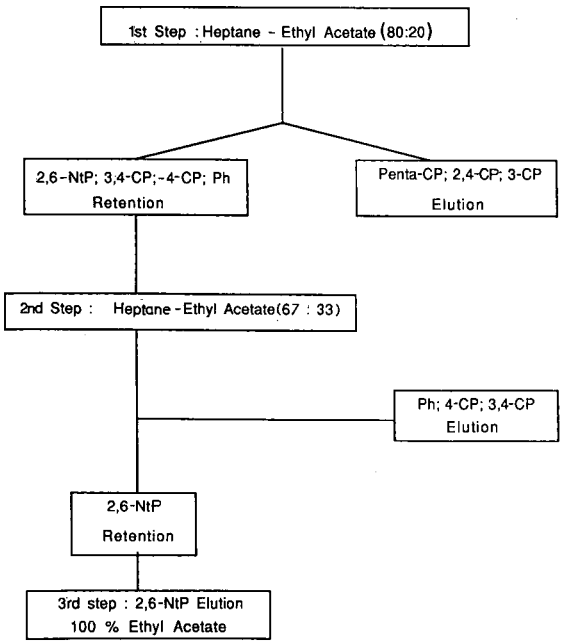

Fig. 3. Selective extraction of 2,6-NtP from a mixture of chlorophenols and nitrophenols.

TABLE V

EXTENDED MODEL FOR TREATMENT OF PARENT COMPOUNDS WITH A DIFFERENT POLAR MODIFIER

Solute pair	a_i	b_i	a_j	b_j	X_s (computer)	X_s (model)	ΔR_{Fmax}
4-NtP/2,4,6-CP	−1.150	−0.253	−0.960	−1.497	0.34	0.33	0.34
4-NtP/4-IP	−1.150	−0.253	−1.200	−0.944	0.67	0.59	0.17
4-NtP/4-BrP	−1.150	−0.253	−1.170	−1.51	0.57	0.53	0.22
4-NtP/3-NtP	−1.150	−0.253	−1.210	−0.760	0.78	0.63	0.12
4-NtP/Ph	−1.150	−0.253	−1.120	−1.013	0.54	0.53	0.19
4-NtP/2-CP	−1.150	−0.253	−0.760	−1.243	0.25	0.25	0.34
4-NtP/3-CP	−1.150	−0.253	−1.050	−1.174	0.44	0.45	0.24
4-NtP/4-CP	−1.150	−0.253	−1.020	−1.105	0.42	0.44	0.23
4-NtP/3,4-CP	−1.150	−0.253	−1.110	−1.105	0.51	0.50	0.22
4-NtP/3,5-CP	−1.150	−0.253	−1.140	−1.704	0.42	0.40	0.35
4-NtP/2,4-CP	−1.150	−0.253	−0.980	−1.106	0.39	0.42	0.24

Moreover, a careful selection of the mobile phase composition permits us to obtain two peaks: one for 4-NtP and the other of the three remaining chlorophenols which have not been separated ($k' = 2.23$ and 0.5, respectively).

In the above procedures we considered derivatives of phenol. We now attempt to separate some phenol derivatives from very different chemical species (Table VI). Conditions for application of the previous model are checked. 1-Naphthol is eluted whilst 2,6-NtP and 2-NtP are selectively retained. We note that isoquinoline can be separated from 8-methylquinoline. Phenol is eluted whilst isoquinoline is retained. Conversely it can be seen that for 1,2-HB–phenol a 8% difference in the mobile phase composition is found between the computed and actual values. This may be attributed to differences in plate activity since data from different origin are gathered.

Application to RP chromatography

Since selectivity observed with NP is very different from the selectivity observed in RP it would be valuable to consider the same solutes as in Table II with a reversed-

TABLE VI

EXTENDED MODEL FOR TREATMENT OF NON-PARENT COMPOUNDS WITH HEPTANE–ETHYL ACETATE

Solute pairs[a]	X_s (computer)	X_s (model)	ΔR_{Fmax}
IQ/8-MQ	0.27	0.31	0.31
2,6-NtP/1-NH	0.22	0.19	0.33
2-NtP/1-NH	0.31	0.32	0.38
1,2-HB/TH	0.27	0.17	0.40
1,2-HB/1-NH	0.30	0.19	0.52
IQ/Ph	0.39	0.41	0.30
1,2-HB/Ph	0.36	0.29	0.34
1,2-HB/Penta-CP	0.28	0.17	0.41

[a] IQ = isoquinoline; 8-MQ = 8-methylquinoline; 1-NH = 1-naphthol; 1,2-HB = 1,2-dihydroxybenzene.

TABLE VII

EXPERIMENTAL MATRIX FOR THE REVERSED-PHASE MODEL

For conditions see text.

	X_1	X_2	X_3	X_4	a_i	b_i	a_j	b_j	X_s	ΔR_{Fmax}
1	−	−	−	−	−3.506	−1.460	−3.625	−2.493	0.590	0.240
2	+	−	−	−	−3.625	−2.493	−3.229	−2.556	0.410	0.100
3	−	+	−	−	−3.898	−1.232	−3.625	−2.493	0.590	0.340
4	+	+	−	−	−3.356	−1.488	−3.506	−1.460	0.590	0.130
5	−	−	+	−	−3.375	−1.869	−3.625	−2.493	0.590	0.120
6	+	−	+	−	−3.245	−2.347	−3.223	−2.300	0.360	0.003
7	−	+	+	−	−3.588	−1.210	−3.101	−2.596	0.590	0.370
8	+	+	+	−	−3.356	−1.488	−3.457	−2.004	0.620	0.120
9	−	−	−	+	−3.625	−2.493	−3.616	−1.302	0.590	0.290
10	+	−	−	+	−3.761	−0.779	−3.101	−2.596	0.580	0.490
11	−	+	−	+	−3.761	−0.779	−3.588	−1.210	0.730	0.120
12	+	+	−	+	−3.637	−1.168	−3.356	−1.488	0.620	0.110
13	−	−	+	+	−3.616	−1.302	−3.588	−1.210	0.590	0.200
14	+	−	+	+	−3.506	−1.460	−3.101	−2.596	0.510	0.330
15	−	+	+	+	−4.119	−0.856	−3.356	−1.488	0.650	0.220
16	+	+	+	+	−3.356	−1.488	−3.387	−1.546	0.720	0.010

TABLE VIII

SELECTIVE EXTRACTION OF PENTA-CP OR 2,4,5-CP FROM A MIXTURE OF CHLOROPHENOL

Solute pair	X_s (computer)	X_s (model)	ΔR_{Fmax}
Penta-CP/2-CP	0.565	0.556	0.570
Penta-CP/3-CP	0.596	0.571	0.490
Penta-CP/4-CP	0.574	0.553	0.520
Penta-CP/2,3-CP	0.624	0.612	0.380
Penta-CP/2,4-CP	0.634	0.625	0.330
Penta-CP/2.5-CP	0.639	0.633	0.350
Penta-CP/2.6-CP	0.625	0.625	0.434
Penta-CP/3.4-CP	0.640	0.630	0.310
Penta-CP/3,5-CP	0.652	0.651	0.236
Penta-CP/2,3,4-CP	0.667	0.670	0.210
Penta-CP/2,3,5-CP	0.671	0.696	0.131
Penta-CP/2,3,6-CP	0.664	0.660	0.440
Penta-CP/2,4,5-CP	0.679	0.743	0.270
Penta-CP/3,4,5-CP	0.675	0.704	0.120
Penta-CP/2,3,4,5-CP	0.550	0.743	0.020
Penta-CP/2,3,5,6-CP	0.724	0.733	0.110
Penta-CP/3-BrP	0.603	0.586	0.430
Penta-CP/4-BrP	0.602	0.586	0.440
Penta-CP/2,4-BrP	0.650	0.650	0.220
2,4,5-CP/3,4-CP	0.600	0.611	0.170
2,4.5-CP/4-BrP	0.560	0.567	0.300
2,4.5-CP/3-BrP	0.560	0.567	0.300
2,4.5-CP/4-CP	0.530	0.530	0.382
2,4,5-CP/2,5-CP	0.610	0.614	0.190
2,4,5-CP/2,6-CP	0.590	0.606	0.290

phase system. The strategy for mathematical modeling is the same as above. Data were from the paper of Arai *et al.* [11]. Table VII displays both the experiment matrix and the responses, a first-order polynomial best fits the experimental data:

$$X_{sRP} = 0.686251 + 0.064745a_i + 0.115527b_i - 0.124439a_j + 0.059049b_j$$

We note the same features as previously observed, *i.e.* when $\Delta R_F \leqslant 0.1$ there is no correlation between the response given by plot of ΔR_F *versus* X_s and the response of the model.

It can be seen from Table VIII that the pentachlorophenol or the 2,4,5-CP is readily separated from all others.

A solid-phase extraction with same packing as advocated by Arai *et al.* [11] will permit selective retention of the pentachlorophenol with a mobile phase composition 37:63 (v/v) and will elute 2-CP, 3-CP, 4-CP, 2,3-CP, 2,4-CP, 2,5-CP, 2,6-CP, 3,4-CP, 4-bromophenol and 3-bromophenol.

CONCLUSIONS

This computer-assisted method exhibits some obvious advantages. The selection of optimal mobile phase composition for sample clean-up is effective. A large amount of TLC data is available and the model performs well with different organic modifiers in the mobile phase. The drawbacks are that secondary effects are not taken into account. We did not consider large differences in solute amounts, which will change retention according to the isotherm forms. This will be the subject of a forthcoming paper.

ACKNOWLEDGEMENTS

We are grateful to Dr. M. Matyska for helpful discussion. One of us (N.V.) is indebted to Parfums Christian Dior for a grant to support this work.

REFERENCES

1 R. W. Frei and K. Zech, in R. W. Frei and K. Zech (Editors), *Selective Sample Handling and Detection in High-Performance Liquid Chromatography*, Part A, Elsevier, Amsterdam, p. 1.
2 R. D. McDowall, *J. Chromatogr.*, 492 (1989) 3.
3 A. Betti, G. Lodi and S. Coppi, *J. Chromatogr.*, 513 (1990) 219.
4 A. Robbat, Jr. and T.-Y. Liu, *J. Chromatogr.*, 513 (1990) 117.
5 E. Soczewinski and W. Golkiewicz, *J. Chromatogr.*, 118 (1976) 91.
6 E. Soczewinski, *J. Chromatogr.*, 130 (1977) 23.
7 P. J. Schoenmakers, H. A. H. Billiet and L. de Galan, *J. Chromatogr.*, 205 (1981) 13.
8 P. J. Schoenmakers, A. C. J. H. Drouen, H. A. H. Billiet and L. de Galan, *Chromatographia*, 15 (1982) 688.
9 D. Nurok and M. J. Richard, *Anal. Chem.*, 53 (1981) 564.
10 M. Matyska and E. Soczewinski, *J. Planar. Chromatogr.*, 3 (1990) 144.
11 Y. Arai, M. Hirukawa and T. Hanai, *J. Liq. Chromatogr.*, 10 (1987) 635.

Journal of Chromatography, 550 (1991) 667–675
Elsevier Science Publishers B.V., Amsterdam

CHROMSYMP. 2212

Comparative investigation of the retention behaviour of nucleoside derivatives on alumina stationary phases in thin-layer chromatography and high-performance liquid chromatography

KLÁRA VALKÓ*, TIBOR CSERHÁTI and ESTHER FORGÁCS
Central Research Institute for Chemistry, Hungarian Academy of Sciences, P.O. Box 17, H-1525 Budapest (Hungary)

ABSTRACT

The retention of 21 natural and synthetic deoxyuridine derivatives was determined by high-performance liquid chromatography (HPLC) using an alumina column with water–2-propanol or dichloroethane–methanol mobile phases in various volume ratios. The log k' (capacity factor) values from HPLC were compared with the R_M [log $(1/R_E - 1)$] values determined by thin-layer chromatography (TLC) on alumina layers using water–2-propanol or dichloroethane–methanol mobile phases. The highest correlation coefficient (0.93) between the log k' values and the R_M values was obtained when dichloroethane–methanol–acetic acid (50:50:0.01) and 100% water were used as mobile phases both in TLC and HPLC, respectively. It was found that the retention of the nucleoside derivatives did not depend linearly on the concentration of the stronger component in the mobile phase. The length of the alkyl chain of the substituent at position 5 of the deoxyuridine has a negligible impact on the retention. The presence of the double and triple bounds in the substituent, however, significantly influenced the retention properties of the nucleosides on alumina layers. Principal component analysis proved that the reversed phase (water–2-propanol) and adsorption eluents (dichloroethane–methanol) show different selectivity.

INTRODUCTION

Alumina seems to be a promising substitute for silica in high-performance liquid chromatography (HPLC) due to its higher stability at extreme pH values [1]. Successful separations of some aromatic compounds [2], heroin derivatives [3], proteins [4] and various drugs [5] were achieved on alumina columns. When alumina was combined with anion-exchange columns, it was found to be a highly selective stationary phase for the preconcentration of sulphate from complex matrices [6]. Experiments were carried out to evaluate the synthetic procedures for the chemical modification of alumina for HPLC [7] and to compare the octadecyl-bonded alumina and silica for reversed-phase HPLC [8].

Due to its high versatility and simplicity thin-layer chromatography (TLC) can be used as a rapid pilot method in the search for HPLC separation conditions [9].

0021-9673/91/$03.50

However, the correlation between the retention in a TLC and HPLC system is not always good enough for the adequate prediction of HPLC parameters [10].

Synthetic nucleotides have many biological effects [11]; they can incorporate into DNA [12], resulting in the modification of some enzymatic processes [13]. Their incorporation rate into DNA depended on their hydrophobic and steric properties determined by chromatographic methods and the inductive effect of the substituents at position 5 of deoxyuridines also played an important role [14].

As the triphosphate group of nucleotides highly dominates their chromatographic properties, the retention behavior of the corresponding nucleoside derivatives were investigated on alumina stationary phase by TLC and HPLC in order to reveal the most important physico-chemical properties of the compounds governing their retention and the predictive power of TLC technique for HPLC.

EXPERIMENTAL

Alumina support of particle size 5 μm was produced by the research group of Dr. L. Zsembery at the Research Institute of the Hungarian Alumina Trust (Budapest, Hungary). A 15 cm × 4 mm I.D. column was filled in our laboratory with a Shandon analytical HPLC packing pump (Shandon Southern Products, Runcorn, UK). The HPLC equipment consisted of a Liquopump Model 312 (Labor MIM, Budapest, Hungary), a Cecil CE-212 spectrophotometer (Cambridge, UK) used as a detector, a Valco injector (Houston, TX, USA) with 20-μl sample loop, a Waters 740 integrator (Milford, MA, USA) or a Radelkisz Type OH-814/1 recorder (Radelkisz, Budapest, Hungary). The determination of the theoretical plate number was carried out as previously described [15]. The dead volume of the column was determined by injecting a 10% $NaNO_3$ solution. The nucleoside derivatives, deoxyuridine (**1**), 5-methyl-(**2**), 5-ethyl-(**3**), 5-*n*-propyl- (**4**), 5-butyl-(**5**), 5-hexyl- (**6**), 5-heptyl- (**7**), 5-octyl- (**8**), 5-vinyl- (**9**), 5-*E*-pentenyl- (**10**), 5-*E*-hexenyl- (**11**), 5-*E*-heptenyl- (**12**), 5-*E*-octenyl- (**13**), 5-propynyl- (**14**), 5-butynyl- (**15**), 5-pentynyl- (**16**), 5-hexynyl- (**17**), 5-heptynyl- (**18**), 5-octynyl- (**19**), 5-isopropyl- (**20**) and 5-bromovinyldeoxyuridine (**21**) were synthesized by the research group of Dr. J. Sági and described elsewhere [16–19]. The other chemicals were of HPLC purity. The nucleoside derivatives were dissolved separately in the eluents to give a concentration of 50 μg/ml. The retention of the nucleoside derivatives was determined in various eluent mixtures as water–2-propanol (0, 40, 50, 60, 70, 80 and 90%, v/v of 2- propanol) and dichloroethane–methanol (50, 60, 70, 80 and 90%, v/v of methanol). The effect of trifluoroacetic acid (TFA) concentration on the retention of nucleoside derivatives was investigated at 0.050, 0.025 and 0.01% (v/v) concentrations. The flow-rate was 0.8 ml/min. The detection wavelength was 260 nm. Each determination was carried out in triplicate. The calculation of the theoretical plate number and the log k' (capacity factor) values of the nucleoside derivatives were carried out as previously described [20].

DC-Fertigplatten Aluminiumoxid 60 F_{254} (Merck, Darmstadt, Germany) were used for TLC without any pretreatment. The nucleoside derivatives listed above were dissolved separately in methanol to give a concentration of 5 mg/ml, and 2 μl of each solution were spotted onto the plates. Dichloroethane–methanol–acetic acid (50:50:1) and water–2-propanol (1:9 and 85:15, v/v) were applied as eluents. After development the plates were dried at 105°C, and the nucleoside spots were detected via ultraviolet.

Each determination was run in quadruplicate. The R_M [log $(1/R_F\text{-}1)$] values were separately calculated for each eluent and nucleoside.

It was supposed that the main distinguishing mark between adsorption and reversed-phase chromatography for both TLC and HPLC is the relative polarity of the mobile and stationary phases, *i.e.* the stationary phase has to be more polar than the mobile phase in adsorption chromatography. This suggests that the chemical bonding of apolar substituents to the polar support is not a prerequisite for the reversed-phase separation mode. The validity of the hypothesis mentioned above was proved to be true for unimpregnated cellulose [21]. The application of the aqueous eluent systems may help in the elucidation of the relative polar or non-polar character of alumina compared to water–2-propanol mixtures.

To find the similarities and dissimilarities among various chromatographic systems and to assess the predictive power of TLC for HPLC, principal component analysis (PCA) was applied on the retention data [22]. The results of the PCA can give us information about the clustering of the variables according to their relationship and reveals possible backgrond variables which may have concrete physicochemical meaning, and in this way the number of variables can be decreased. The HPLC [water, water–2-propanol (1:9), dichloroethane–methanol–TFA (1:9:0.05 and 1:9:0.01)] and TLC [dichloroethane–methanol–acetic acid (50:50:0.01), water–2-propanol (1:9 and 85:15)] systems were taken as the variables during PCA. The log k' and R_M values of the nucleosides in the corresponding eluent system were taken as observations. As deoxyuridine was retained on the column in water it was excluded from the calculations. The PCA was carried out on the correlation matrix. The sum of the variance explained was set to 99.9%. The two-dimensional non-linear map of the obtained principal component loadings and variables was also calculated [23]. The iteration was carried out to the point where the difference between the maximum errors of the last two iterations was lower than 10^{-8}. The eluent systems or nucleosides showing similar retention characteristics are near to each other on the maps, whereas the eluent or compounds having opposite or very different retention behavior are widely separated.

The linear regression analysis between the chromatographic retention data was carried out using the Drugidea (Chemichro, Budapest, Hungary) software system.

RESULTS AND DISCUSSION

The log k' and R_M values obtained for the deoxyuridine and its derivatives in two HPLC and three TLC systems are listed in Table I. The correlation coefficients between the retention data obtained in various chromatographic systems are listed in Table II in a correlation matrix. It was surprising that the highest correlation coefficient (0.93) was obtained when log k' values with 100% water and R_M values with dichloroethane–methanol–acetic acic (50:50:0.01) were compared. In order to reveal some important physico-chemical characteristics governing the retention of the compounds on alumina, the hydrophobicity, electronic and steric parameters of the substituents at 5 position were taken from the compilation of Hansch and Leo [24]. The actual values for deoxyuridine derivatives have already been published [12]. The correlation study revealed that neither the hydrophobicity nor the molar refractivity (bulkiness of the substituent) play on important role in the retention. The Swain–

TABLE I

LOG k' VALUES AND THE MEAN $100R_M$ VALUES AND INDUCTIVE ELECTRONIC PARAMETER ($\mathcal{F}$) [12] OF THE INVESTIGATED DERIVATIVES

(I) log k' values obtained with 100% water as mobile phase; (II) log k' values obtained with methanol–dichloroethane–trifluoroacetic acid (90:10:0.05); (III) $100R_M$ values obtained with dichloroethane–methanol–acetic acid (50:50:0.01); (IV) $100R_M$ values obtained with water–2-propanol (1:9); (V) $100R_M$ values obtained with water–2-propanol (85:15); ($\mathcal{F}$) inductive electronic parameter of the 5 substituent.

Substituent	I	I	III	IV	V	$\mathcal{F}$
H	Inf.	Inf.	30	−1	start	0.00
Methyl	0.244	0.847	108	45	−29	−0.04
Ethyl	0.129	0.524	81	18	−33	−0.05
Propyl	0.222	0.284	80	11	−36	−0.06
Butyl	0.148	0.225	62	2	−40	−0.06
Hexyl	0.157	0.195	53	−5	−37	−0.06
Heptyl	0.140	0.109	47	−9	−31	−0.06
Octyl	0.177	0.085	39	−11	−9	−0.06
Vinyl	0.272	0.530	89	31	−30	0.07
E-Pentenyl	0.238	0.028	64	3	−34	0.03
E-Hexenyl	0.195	0.303	56	3	−29	0.03
E-Heptenyl	0.230	0.100	59	3	−38	0.03
E-Octenyl	0.219	0.254	43	−2	−4	0.03
Propynyl	0.746	0.234	167	114	−15	0.15
Butynyl	0.722	0.029	149	94	−15	0.15
Pentynyl	0.676	−0.253	154	85	−16	0.15
Hexynyl	0.678	0.000	164	91	−17	0.15
Heptynyl	0.685	0.885	146	77	−17	0.15
Octynyl	0.681	1.038	144	78	−20	0.15
Iso-propyl	0.023	0.364	64	−5	−39	−0.05
Bromovinyl	0.0254	0.480	112	25	−27	−

Loupton type [24] electronic parameter ($\mathcal{F}$) describing the strength of the inductive effect of the substituents at the 5 position showed significant correlation to the retention data. The correlation coefficients are shown also in Table II. It means that only the electronic properties are involved in the retention, and no partition phenomena take place even when hydro–organic mobile phases are used.

Each derivative showed unusual retention behavior on the alumina column. Their log k' value decreased between 0 and 40% of 2-propanol concentration in

TABLE II

MATRIX OF THE CORRELATION COEFFICIENTS BETWEEN THE DATA LISTED IN TABLE I

	I	II	III	IV	V	$\mathcal{F}$
I	1.00	0.72	0.93	0.84	0.64	0.93
II	0.72	1.00	0.74	0.57	0.60	0.64
III	0.93	0.74	1.00	0.84	0.44	0.84
IV	0.84	0.57	0.84	1.00	0.46	0.75
V	0.64	0.60	0.44	0.46	1.00	0.64
$\mathcal{F}$	0.93	0.64	0.84	0.75	0.64	1.00

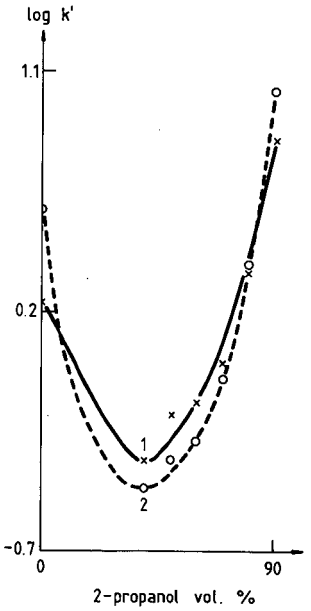

Fig. 1. Effect of 2-propanol concentration on the log k' value of 5-methyl- (1) and 5-octynyldeoxyuridine (2) in aqueous eluent systems.

aqueous systems according to the general rule of reversed-phase separation mode, reached a minimum and then increased again at higher 2-propanol concentrations (Fig. 1).

Opposite to our expectations, the nucleosides also showed anomalous retention behaviour in organic eluent systems (Fig. 2). The retention increased at higher methanol concentration, although methanol is a stronger eluent than dichloroethane. The

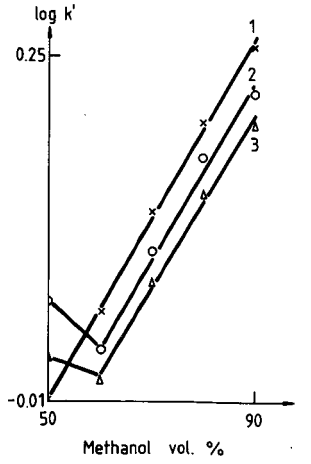

Fig. 2. Dependence of the log k' value of 5-ethyl- (1), 5-propyl- (2) and 5-butyldeoxyuridine (3) on the methanol concentration in the eluent (dichloroethane–methanol mixtures, containing 0.05%, v/v, TFA).

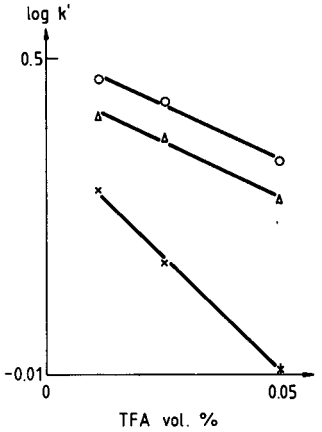

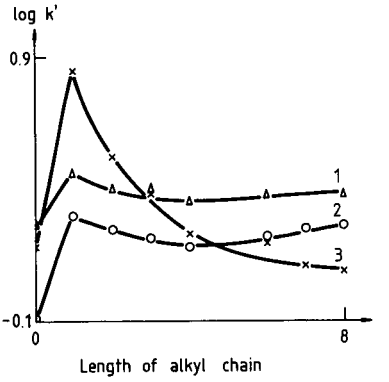

Fig. 3. Dependence of the log k' value of deoxyuridine (○), 5-methyl- (△) and 5-hexyldeoxyuridine (×) on the TFA concentration in the eluent (dichloroethane–methanol, 1:9, v/v).

Fig. 4. Dependence of the log k' values of some nucleosides on the length of saturated alkyl substituent. (1) Dichloroethane–methanol–TFA (1:9:0.01); (2) dichloroethane–methanol–TFA (1:9:0.05); (3) water–2-propanol (1:9).

retention decreased linearly with increasing concentration of TFA (Fig. 3) which proves the predominance of polar interactions between solute and support as outlined above. A strongly non-linear dependence of the retention on the length of alkyl substituents was observed (Fig. 4). The chromatographic behavior of deoxyuridine considerably deviates from that of the substituted ones. This is probably due to the fact that is has a higher capacity to form hydrogen bond with the alumina surface resulting in increased retention. The low dependency of retention on the length of

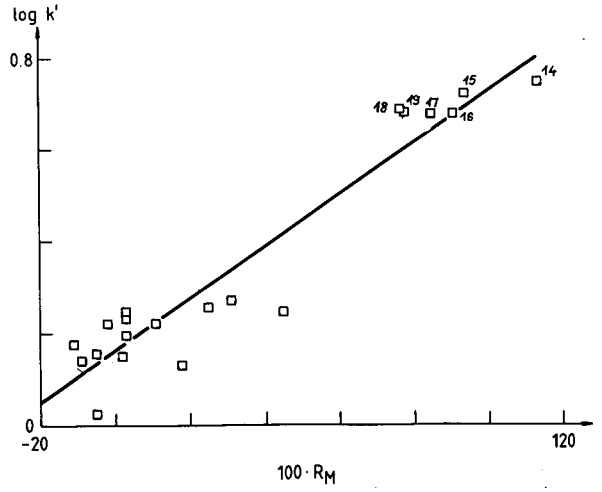

Fig. 5. Relationship between the log k' (eluent, water) and R_M (eluent, dichloroethane–methanol–acetic acid, 50:50:0.01) values of some nucleoside derivatives.

TABLE III

RELATIONSHIPS BETWEEN THE HPLC AND TLC RETENTION BEHAVIOR OF SOME NUCLEOSIDE DERIVATIVES AND RESULTS OF PRINCIPAL COMPONENT ANALYSIS

No. of principal component	Eigenvalue	Sum of variance explained (%)
1	3.69	56.69
2	1.03	71.43
3	1.01	85.89
4	0.61	94.64

Eluent	Principal component loading			
	No. of principal component			
	1	2	3	4
Water (HPLC)	0.96	0.03	−0.09	0.09
Water–2-propanol (1:9) (HPLC)	0.12	−0.31	0.93	−0.15
Dichloroethane–methanol–TFA (1:9:0.05) (HPLC)	0.83	0.22	0.09	−0.07
Dichloroethane–methanol–TFA (1:9:0.01) (HPLC)	−0.24	0.86	0.35	0.27
Dichloroethane–methanol–acetic acid (50:50:0.01) (TLC)	0.94	−0.18	0.02	0.27
Water–2-propanol (1:9) (TLC)	0.96	−0.03	0.01	0.23
Water–2-propanol (85:15) (TLC)	0.68	0.34	−0.08	−0.61

alkyl chain was a result of the fact that the alumina column under our experimental conditions is not suitable for the separation of these derivatives.

The correlations between HPLC and TLC systems were significant in some cases, as shown in Fig. 5, although the eluent systems were different. These relationships did not have any predictive value for the HPLC separation of the nucleosides.

The results of PCA are compiled in Table III. The first two components account for about 70% of the total variance. This means that two background variables include the majority of the information content of the seven eluent systems. It must be emphasized that the two hypothetical variables need not have any concrete physical meaning. The calculation only proves their mathematical possibility.

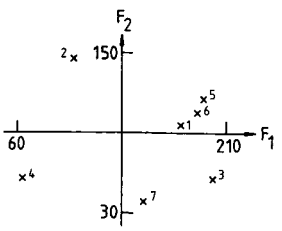

Fig. 6. Two-dimensional non-linear map of principal component loadings. Number of iterations: 97. Maximum error: $2.01 \cdot 10^{-2}$. (1) HPLC; eluent, water. (2) HPLC; eluent, water–2-propanol (1:9). (3) HPLC; eluent, dichloroethane–methanol–TFA (1:9:0.05). (4) HPLC; eluent, dichloroethane–methanol–TFA (1:9:0.01). (5) TLC; eluent, dichloroethane–methanol–acetic acid (50:50:0.01). (6) TLC; water–2-propanol (1:9). (7) TLC; water–2-propanol (85:15).

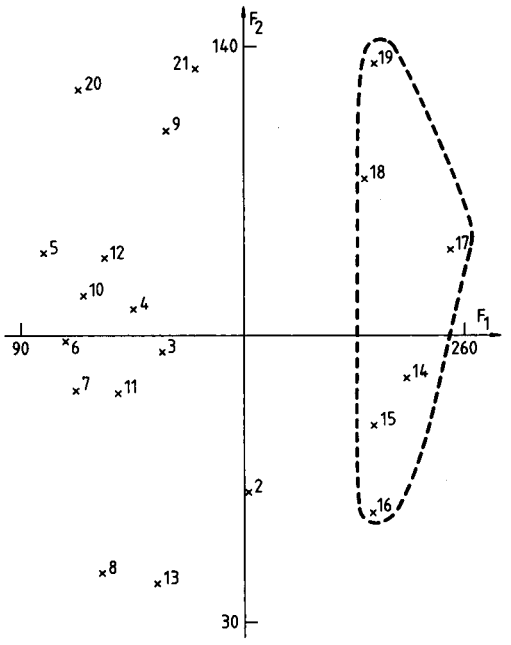

Fig. 7. Two-dimensional non-linear map of principal component variables. Number of iterations: 59 Maximum error: $3.16 \cdot 10^{-2}$. Number refer to nucleoside derivatives in Experimental. The compounds in the circle contained triple bond.

Neither the HPLC (points 1–4) nor the TLC systems (points 5–7) form separate clusters on the two-dimensional non-linear map of principal component loadings (Fig. 6). This results proves that the eluent composition has a higher impact on the retention characteristics then the type of chromatographic system. Each HPLC system is widely separated from the others, that is the separation capacity of the eluents is different. Points 1, 5 and 6 form a distinct cluster. However, this cluster contains very different chromatographic systems. The nucleoside derivatives having a triple bond in the alkyl chain form a loose cluster on the two-dimensional non-linear map of principal component variables (Fig. 7). It also proves that alumina stationary phase is sensitive to the π–π interactions, *i.e.* the inductive electronic properties with all of the investigated mobile phases. The length of the alkyl chain does not separate the compounds, *i.e.* the hydrophobic interactions are not important in the retention.

REFERENCES

1 R. Kaliszan, J. Petrusewitz, R. W. Blain and R. A. Hartwick, *J. Chromatogr.*, 458 (1988) 395.
2 K. K. Unger, W. Messer and K. F. Krebs, *J. Chromatogr.*, 149 (1978) 1.
3 C. J. C. M. Laurent, H. A. H. Billiet and L. de Galan, *J. Chromatogr.*, 285 (1984) 161.
4 C. J. C. M. Laurent, H. A. H. Billiet, L. de Galan, F. A. Buytenhuys and F. P. B. van de Maeden, *J. Chromatogr.*, 287 (1984) 45.
5 H. Lingeman, H. A. van Munster, J. H. Beyben, W. J. M. Underberg and A. Hulshoff, *J. Chromatogr.*, 352 (1986) 261.

6 W. Buchberger and K. Winsauer, *J. Chromatogr.*, 482 (1989) 401.
7 J. J. Pesek, *Chromatographia*, 28 (1989) 565.
8 J. E. Haky, S. Vemulapalli and L. F. Wieserman, *J. Chromatogr.*, 505 (1990) 307.
9 T. Cserháti and T. Bellay, *Acta Phytopathol. Entomol. Hung.*, 23 (1988) 257.
10 K. Valkó, S. Olajos and T. Cserháti, *J. Chromatogr.*, 499 (1990) 361.
11 E. de Clercq, *Methods Find. Exp. Clin. Pharmacol.*, 2 (1980) 253.
12 L. Ötvös, J. Sági, T. Kovács and R. T. Walker, *Nucleic Acid Res.*, 15 (1987) 1763.
13 J. Sági, A. Szabolcs, A. Szemzö and L. Ötvös, *Nucleic Acid Res.*, 4 (1977) 2767.
14 K. Valkó, T. Cserháti, I. Fellegvári, J. Sági and A. Szemzö, *J. Chromatogr.*, 506 (1990) 35.
15 T. Cserháti, *Chromatographia*, 29 (1990) 593.
16 A. Szabolcs, J. Sági and L. Ötvös, *J. Carbohydr. Nucleosides Nucleotides*, 2 (1975) 197.
17 J. T. Sági, A. Szemzö and L. Ötvös, *Nucleic Acid Res.*, 4 (1977) 2767.
18 L. Ötvös, J. Sági, T. Kovács, and R. T. Walker, *Nucleic Acid Res.*, 15 (1987) 1763.
19 L. Ötvös, J. Szécsi, J. Sági and T. Kovács, *Nucleic Acid Res. Symp. Ser.*, 18 (1987) 125.
20 L. R. Snyder and J. J. Kirkland, *Introduction to Modern Liquid Chromatography*, Wiley, New York, 1974, p. 29.
21 T. Cserháti, *Chromatographia*, 18 (1984) 18.
22 K. Mardia, J. T. Kent and J. M. Bibby, *Multivariate Analysis*, Academic Press, London, 1979, p. 213.
23 J. Sammon, Jr., *IEEE Trans. Comput.*, C18 (1969) 401.
24 C. Hansch and A. Leo, *Substituent Constants for Correlation Analysis in Chemistry and Biology*, Wiley, New York, 1989.

Journal of Chromatography, 550 (1991) 677–693
Elsevier Science Publishers B.V., Amsterdam

CHROMSYMP. 2282

Practical approach to high-speed counter-current chromatography

ALAIN BERTHOD
Laboratoire des Sciences Analytiques, Université de Lyon 1 (UA CNRS 0435, J.M. Mermet), 69622 Villeurbanne Cedex (France)

ABSTRACT

Counter-current chromatography (CCC) is mainly used in the preparative separation, extraction and purification of samples. CCC does not operate with a solid stationary phase. Two immiscible liquid phases are used. One is the liquid mobile phase and the other is the liquid stationary phase. Centrifugal fields are used to retain the liquid stationary phase while the mobile phase is pushed through it. The CCC "column" is often a continuous open tube, coiled on a spool which is rotated in a centrifuge. Most high-speed counter-current chromatographs are scheme IV Ito coil planet centrifuges. A practical CCC approach is reported in this paper. The user-adjustable parameters are divided into (i) configuration parameters and (ii) operating parameters. The configuration parameters are the tube internal diameter, the spool radius, the number of turns and the total internal apparatus volume. The operating parameters are three active parameters (mobile phase flow-rate, spool rotation speed and temperature) and two passive parameters (the stationary phase retention percentage and the driving pressure). The choice of solvents to be used as the biphasic liquid systems is critical. Tie lines in ternary phase diagrams are used to optimize the solvent choice with hexane–methanol–water and the chloroform–methanol–water systems. The effects of interdependent parameters on the CCC chromatograms are discussed and illustrated with examples. It is shown that a highly efficient counter-current chromatograph can have a poor resolving power if it cannot retain a sufficient amount of liquid stationary phase.

INTRODUCTION

More than 20 years ago, Ito and co-workers [1,2] initiated the development of modern counter-current chromatography (CCC). Today, this technique is mainly used in the preparative separation, extraction and purification of samples. CCC is a separation method which does not employ any solid stationary phase. Two immiscible liquid phases are used. The first is the mobile phase and the second is the stationary phase. The CCC "column" is usually a continuous open tube coiled on a spool which is rotated in a centrifuge. The centrifugal field holds the liquid stationary phase tightly so that the mobile phase can be pushed through it.

Ito and co-workers [3–6] developed numerous variations of the CCC technique, including locular, horizontal flow-through, droplet, helix, and coil planet centrifuge CCC. The publications of Ito and co-workers [3–6] and Conway [7] have described

0021-9673/91/$03.50

extensively the principle of hydrodynamic equilibrium in CCC, the various flow-through schemes, the distribution of centrifugal force vectors and the twist-free mechanism avoiding the use of a rotary seal.

From the various possible designs, Ito and co-workers [4–6] showed that scheme IV planetary motion was the arrangement which best held the liquid stationary phase and allowed the fastest and most efficient separation. Consequently, much of the commercially available high-speed CCC equipment derives from scheme IV coil planet centrifuge CCC. Such CCC devices are becoming very efficient and reliable, so that the use of CCC for preparative extraction and purification is rapidly spreading in academic and industrial laboratories. The growing interest for CCC is due to the following advantages of the technique: (a) a solid support is not required, which precludes any irreversible solute adsorption responsible for sample loss and damaged columns; (b) the direct introduction of crude liquid extracts can always be performed; and (c) a wide range of solvent systems can be used.

The aim of this paper is to present a practical approach to high-speed CCC. This paper discusses which parameters of the CCC system are important, how the adjustable parameters are related and the effects on the chromatogram. Special attention is given to the last cited advantage. The choice of suitable CCC solvent systems is so wide that it may be difficult to determine which system should be used in a given situation. Some physico-chemical properties of liquid systems will be used to facilitate the choice of the best liquid system required to obtain an acceptable separation.

BASIC COUNTER-CURRENT CHROMATOGRAPHY EQUATIONS

The equations used in CCC are very similar to the classical chromatographic equations. The basis retention equation is:

$$V_R = V_0 + (V_T - V_0)P \tag{1}$$

or

$$V_R = V_T + (P - 1)V_S$$

in which V_R is the retention volume, V_T is the internal volume of the apparatus, V_0 is the elution volume of an unretained solute of the volume of the mobile phase inside the apparatus and V_S is the stationary phase volume inside the apparatus; $V_T = V_0 + V_S$. P is the solute partition coefficient, *i.e.*, the ratio of the solute concentration in the stationary phase to the solute concentration in the mobile phase. For example, with an apparatus of 120 ml internal volume, equilibrated with a liquid system in such a way that 70 ml of stationary phase were trapped inside, with a 50-ml mobile phase moving through, the retention volume of a compound with a partition coefficient $P = 2$ is 190 ml. The retention time is 3 h 10 min at a 1 ml/min mobile phase flow-rate, or 45 min at 4 ml/min. When the partition coefficient is as high as 100, the retention volume is 7 l and the retention time is 24 h at 5 ml/min. The partition coefficient range which can actually be used is limited, as discussed later.

The solute capacity factor, k', is related to the partition coefficient, P, and to the phase ratio by:

$$k' = \frac{V_R - V_0}{V_0} = \frac{V_S}{V_0} P \tag{2}$$

The solute partition coefficient is directly proportional to the capacity factor, k'.

USER-ADJUSTABLE CHROMATOGRAPHIC PARAMETERS

The adjustable parameters vary according to the CCC apparatus used. They can be divided in two kinds of parameters. The configuration parameters are, in the case of the coil planet centrifuge CCC devices (P.C., Potomac, MD, USA; S.F.C.C., Neuilly-Plaisance, France; Pharma-Tech, Baltimore, MD, USA; Kromatron SEAB, Villejuif, France [8]), the internal diameter of the coiled tube, the spool radius, the number of turns (number of cartridges in the case of the Sanki device described recently [9], Sanki Lab., Sharon Hill, PA, USA), and the total internal volume of the apparatus. The operating parameters can be divided in active parameters, *i.e.*, the mobile phase flow-rate, the rotation speed and the operating temperature, and passive parameters, *i.e.*, the stationary phase retention percentage and the driving pressure. As these parameters are interdependent, it is important to have an idea of the effect of one change on the separation obtained.

Configuration parameters

The Ito coil planet centrifuge chromatographs contain one or several coiled plastic tube spools. Defining d_t (the internal diameter of a tube of length L), r (the spool radius), n (the number of turns) and V (the spool volume), the relationships between these parameters are:

$$n = \frac{L}{2\pi r}; \; V = \frac{\pi \, d_t^2 \, L}{4} \tag{3}$$

$$n = \frac{2 \, V}{\pi^2 \, d_t^2 \, r} \tag{4}$$

Introducing R, the spool gyration radius, Ito defined the β ratio as:

$$\beta = \frac{r}{R} \tag{5}$$

Eqn. 4 clearly shows that all configuration parameters are interdependent. The internal volume, V_T, depends on the square of the tube internal diameter (eqn. 3). The number of turns, n, is directly proportional to the tube length and inversely proportional to the spool radius.

Operating parameters

The operator can tune the active parameters and measure the passive parameters. The operating parameters, mobile phase flow-rate, rotating speed and percentage of stationary phase retention are intimately related. Fig. 1 illustrates the phase retention evolution *versus* flow-rate and rotation speed. The percentage of retention increases with rotation speed and decreases when the flow-rate increases. If the centrifugal field is higher, the stationary phase is held more tightly. A high flow-rate displaces more stationary phase. The amount of stationary phase retained is also depending on (a) the tube internal diameter, (b) the spool radius and (c) the liquid system used and the way it is used (upper or lower liquid phase mobile). The terminal of the rotating coil where all the objects tend to move is defined as the head. The other terminal is defined as the tail. For scheme IV coil planet centrifuge CCC, Ito [10] showed that with a sufficient rotation speed (>300 rpm), the maximum stationary phase retention was obtained under the following conditions: the heavy (lower) mobile phase must be pushed from the head to the tail through the light (upper) stationary phase. The light (upper) mobile phase must be pushed from the tail to the head if the stationary phase is the denser (lower) liquid. Unfortunately this useful rule is not valid in any instance. The rule is inverted when a very hydrophilic liquid system, such as *sec.*-butanol–water or *n*-butanol–acetic acid–water, is used [5,7,10].

The percentage of stationary phase retention also depends on the coiled tube internal diameter, d_t [11] and the injection conditions [4]. It is difficult to retain the stationary phase with a narrow-bore tube ($d_t < 0.9$ mm) [11]. Owing to solvent–wall interactions, the organic phase displaces the aqueous phase. The injection of concentrated solutions may also disturb the phase equilibrium inducing stationary phase loss. Ito [4] recommended the injection of large volumes (*e.g.*, 0.2 V_T) of concentrated solution dissolved in the stationary phase. These two effects show that the percentage of stationary phase retention depends largely on the liquid system used.

Temperature changes affect mainly the liquid system. A rise in temperature induces an increase in the mutual solubility of the phases, a decrease in liquid viscosity and a change in solute partition coefficients.

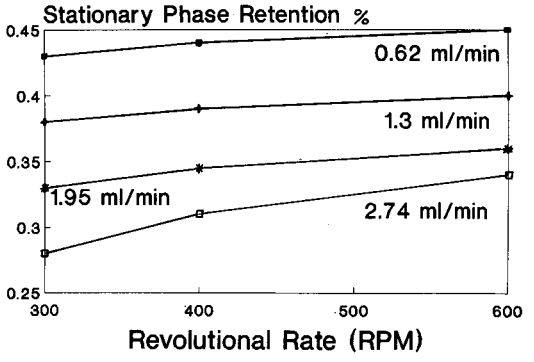

Fig. 1. Percentage retention of stationary phase *versus* the revolutional rate (rpm) for different flow-rates. Conditions: multilayer coil planet centrifuge CCC apparatus; liquid system, hexane–methanol–water; mobile phase, upper organic phase. Data from ref. 5.

BIPHASIC LIQUID SYSTEMS

In limited CCC applications two immiscible liquids are used. For example, octanol and water are used in the determination of the octanol–water partition coefficient [12]. In most other situations, the great advantage of CCC is the ability to use any liquid mixture that forms two phases. Water is a widely used liquid for its price, non-toxicity, ease of purification, availability and polar solvent properties. An apolar solvent forms the apolar phase and a third solvent, with an intermediate polarity, is used to adjust the solute partition coefficients. This looks easy; however, the possible compositions are boundless. The choice of solvents depends on the solutes to be separated. Once the solvents have been chosen, a knowledge of the ternary system is obtained using the ternary phase diagram.

Choice of solvent system

The range of liquid systems forming two immiscible layer is so wide that choice may be a problem. Furthermore, it is very difficult to find the partition coefficient of

TABLE I

BIPHASIC LIQUID SYSTEM USED IN CCC

The polarity index is the chromatographic elution strength on alumina, from ref. 15. (N) normal, lower phase mobile → input head, output tail; upper phase mobile → input tail, output head. (R) Reversed, lower phase mobile → input tail; upper phase mobile → input head.

Liquid	Polarity index	Liquid	Polarity index	Liquid	Polarity index	CCC mode
Hydrophobic						
n-Heptane	0.01	Chloroform	0.40	Water	>2	N
n-Heptane	0.01	Ethyl acetate	0.58	Methanol	0.95	N
				Water	>2	
n-Heptane	0.01	Chloroform	0.40	Acetonitrile	0.65	N
n-Hexane	0.01	Methanol	0.95	Water	>2	N
n-Hexane	0.01	Pentanol	0.61	Water	>2	N
n-Heptane	0.01	Acetic acid	1.00	Methanol	0.95	N
Toluene	0.29	Chloroform	0.40	Water	>2	N
Intermediate						
Dichloromethane	0.42	Methanol	0.95	Water	>2	N
Chloroform	0.40	Methanol	0.95	Water	>2	N
Chloroform	0.40	Acetic acid	1.00	Water	>2	N
Ethyl acetate	0.58	*n*-Butanol	0.72	Water	>2	N
		Acetonitrile	0.65			
Ethyl acetate	0.58	*n*-Propanol	0.82	Water	>2	N
Hydrophilic						
n-Butanol	0.72	Water	>2			N
n-Butanol	0.72	Methanol	0.95	Water	>2	R
n-Butanol	0.72	Acetic acid	1.00	Water	>2	R
n-Butanol	0.72	Pyridine	0.71	Water	>2	N
n-Butanol	0.72	*n*-Propanol	0.82	Water	>2	R
n-Pentanol	0.61	Methanol	0.95	Water	>2	R

a compound in the literature when more than two solvents are used. The data compiled by Wisniak and Tamir [13] is very helpful. Ito [4] classified some liquids systems as hydrophobic, intermediate and hydrophilic. The physico-chemical properties of the pure liquids are important. A low viscosity, high interfacial tension and high density difference are desirable. Ito and Conway [14] have shown that the settling time of the two solvent phases, *i.e.*, the time required for the hand-shake solvent mixture to be completely separated into two layers, provides a reliable numerical index for the hydrodynamic behaviour of the system in CCC. Table I lists some systems commonly used in CCC, along with a polarity index for the pure liquids and the CCC mode that should be used with the system.

A quick method of selecting a solvent system consists in checking the sample by thin-layer chromatography on silica or cellulose using the organic layer as the eluent [16,17]. As described by Hostettmann *et al.* [17], if the R_F values of the compounds to be separated are higher than 0.4, the less polar phase can be used as the mobile phase. For more polar substrates ($R_F < 0.4$), the more polar phase should be used as the mobile phase.

Ternary phase diagram

The ternary phase diagram of a three-liquid system fully characterizes the system at a given temperature. Unfortunately, few ternary phase diagram can be found in the

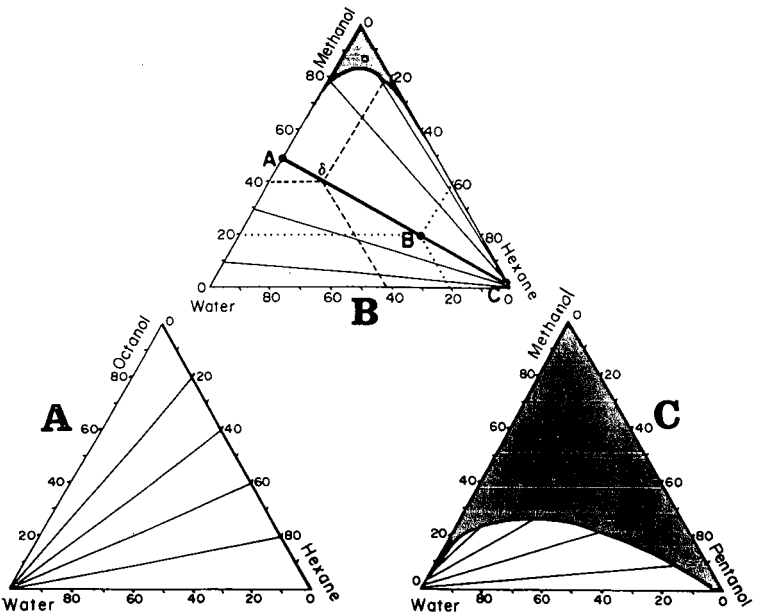

Fig. 2. (A) Hexane–octanol–water system; the organic upper layer is a mixture of hexane and octanol and the aqueous lower layer is essentially water. (B) Hexane–methanol–water system; the organic upper layer is mainly hexane; the aqueous lower layer is a methanol–water mixture. For points A, B, C and δ, see text. (C) Pentanol–methanol–water system, the pentanol–methanol upper layer can dissolve large amounts of water. The lower aqueous phase contains methanol and pentanol. This diagram is considerably modified by temperature changes. Dark areas, monophasic; open areas, biphasic with tie-lines. Temperature, 22°C.

literature [13,18,19]. To delineate a ternary phase diagram is easy but tedious work. Fig. 2 shows three recently obtained ternary phase diagrams [20]. The hexane–octanol–water system (Fig. 2A) has a very low mutual solubility between the aqueous and organic phase. With the hexane–methanol–water system (Fig. 2B), hexane is the main constituent of the organic phase. The aqueous phase is practically a water–methanol solution. A small monophasic area exists near the methanol apex. For the pentanol–methanol–water system (Fig. 2C), a large monophasic area exists. Water partitions between the two phases in the biphasic area. Small additions (<0.5%, w/w) of a fourth component do not significantly alter the phase diagram. For example, the addition of 0.1 *M* hydrochloric acid in water does not change the phase diagrams in Fig. 2. If four liquids are used to obtain the biphasic liquid system, it is possible to map a pseudo-ternary phase diagram by keeping the ratio of two liquids constant. One of the three diagram apexes will be, for example, methanol–water (50:50, w/w), and the two other apexes will represent the two other liquids. Temperature rises affect the mutual solubility of the liquids; usually, the monophasic area increases with temperature.

The tie-lines, which are indicated in the biphasic areas of Fig. 2, are extremely useful in CCC. They allow the quantity and composition of the two phases obtained when three liquids are mixed to be calculated. This is illustrated using the diagram for hexane–methanol–water (Fig. 2B). Point B in this diagram corresponds to the mass composition 60:20:20. For a 100-g preparation, 60 g of hexane are 91 ml (d_{hexane} = 0.660 g/cm^3), 20 g of methanol are 25.3 ml (d_{methanol} = 0.791 g/cm^3) and 20 g of water are 20 ml. The volume percentage ratio is: 66.8:18.5:14.7. This mixture is given in the CCC literature as hexane–methanol–water (18:5:4, v/v/v). The corresponding tie-line is drawn in bold. It gives the composition of the two phases that separate when mixture B is prepared. The aqueous phase, point A, has the mass composition methanol–water (49:51) (hexane, traces). The organic phase mass composition, point C, is hexane–methanol–water (99:0.9:0.1) [20]. Once the composition of A and C are known, the relative masses of A and C can be calculated using the lever rule:

$$\text{distance AB } (AB) \times \text{mass of A} = \text{distance BC } (BC) \times \text{mass of C} \tag{6}$$

and

$$\text{mass of A} + \text{mass of C} = \text{mass of B} \tag{7}$$

On Fig. 2B, $AB = 0.61AC$ and $BC = 0.39AC$. From eqns. 6 and 7 this becomes:

$$\frac{0.61\ \overline{AC}}{0.39\ \overline{AC}} = 1.56 = \frac{\text{mass of C}}{\text{mass of A}} = \frac{100 - \text{mass of A}}{\text{mass of A}}$$

which gives: mass of A = 39 g and mass of C = 61 g (or 61% of the initial mass mixture). The densities of the upper organic phase and the lower aqueous phase were 0.65 and 0.90 g/ml, respectively. This allows the calculation of the two volumes 93.8 and 43.3 ml for the upper and the lower phases, respectively.

Point δ (mass composition hexane–methanol–water, 18:40:42) belongs to the

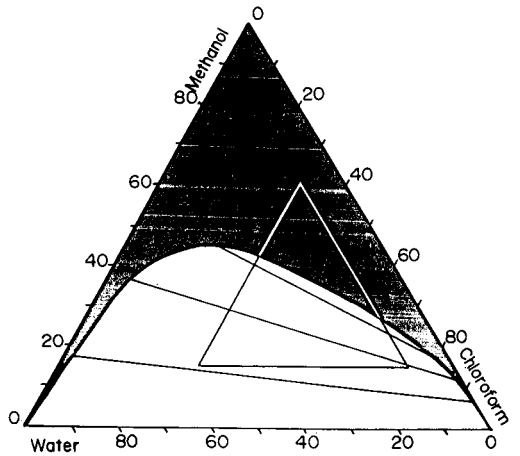

Fig. 3. Chloroform–methanol–water system with tie-lines. Methanol partitions between the lower organic phase and the upper aqueous phase. The inset triangle corresponds to Fig. 4. Temperature, 22°C.

same tie-line as point B (Fig. 2B). The mixture separates into two phases of composition A and C. Applying the lever rule for composition δ, the upper and lower phase volumes can be calculated as 27.2 and 91.4 ml, respectively (for a 100-g δ mixture). As the two phases separated from points B and δ have exactly the same composition, the optimum use of solvents is when composition B is prepared to use the lower aqueous phase as the stationary phase and the upper hexane phase as the mobile phase. Composition δ is prepared when the lower aqueous phase is the mobile phase.

Another important property of the tie-lines is that the longer the line, the greater the difference between the two liquid phases. The interfacial tension, density, viscosity and polarity difference increase with length of tie-line. The polarity difference between the upper and the lower phases explains the partition of a solute between the two phases. The tie-lines of Fig. 2A and B show little variations. The tie-lines of Fig. 2C have very different lengths. The popular CCC system chloroform–methanol–water (Fig. 3) also has tie-lines with variable lengths [21]. The solute partition coefficients depend on the length of the tie-line.

Liquid systems and partition coefficients

The separation power of CCC is based on small solute partition coefficient differences (eqn. 2). A change in the liquid composition induces various changes in the solute partition coefficients. Table II lists the partition coefficient for four compounds in various compositions of the Fig. 2B and Fig. 3 liquid systems. Compositions a to k are given in Fig. 4, which is an enlargement of the chloroform–methanol–water phase diagram (Fig. 3) with the tie-lines. The compositions listed in Table II do not indicate the relative polarity of the two phases obtained. Fig. 4 shows that the tie-lines delineate the polarity of the biphasic system. Composition a has the greatest polarity difference between the two phases (longest tie-line). The partition coefficients of the polar test solutes were 10 and 17. Composition k belongs to the shortest tie-line close to the biphasic area boundary (binodial line). It has the lowest polarity difference between

TABLE II

LIQUID SYSTEMS AND PARTITION COEFFICIENTS

System	No.	Volume composition			Mass percentage			Partition coefficient ($P_{org/aq}$)	
		$CHCl_3$	CH_3OH	H_2O	$CHCl_3$	CH_3OH	H_2O	DNP glucosaminc	PNP-α-D-glucopyr.
Chloroform–methanol–water[a]	a	13	7	8	58.3	16.9	24.8	10	17
	b	4	4	3	48.6	25.9	25.5	3.4	7.1
	c	5	9	7	34.7	33.2	32.1	3.1	6.3
	d	13	7	4	66.7	19.1	14.2	2.9	5.6
	e	5	6	4	44.5	29.4	25.1	2.6	4.4
	f	5	5	3	52.2	27.9	19.9	2.3	4.0
	g	43	37	20	56.4	25.9	17.7	2.1	3.5
	h	10	12	7	46.7	30.1	23.2	2.0	3.1
	i	7	13	8	36.2	35.5	28.3	1.9	2.9
	j	36	42	22	49.1	30.6	20.3	1.8	2.8
	k	5	10	6	35	37.4	27.6	1.7	2.7
		C_6H_6	CH_3OH	H_2O	C_6H_6	CH_3OH	H_2O	Promazine	Simazine
Hexane–methanol–water[b]	l	2	2	0	45.5	54.5	0	2.6	3.6
	m	2	2	1	33.8	40.6	25.6	2.0	5.0
	n	2	1	1	42.4	25.4	32.2	0.9	6.2
	o	2	1	2	32.1	19.2	48.7	0.3	1.6
	p	2	0	2	39.8	0	60.2	0.07	0.5

[a] Data from ref. 28.
[b] Data from ref. 27.

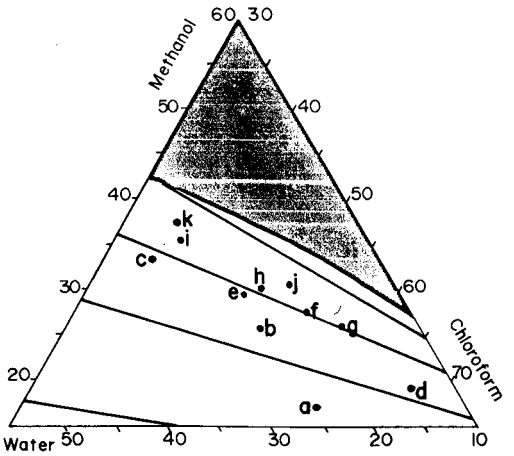

Fig. 4. Enlargement of the diagram chloroform–methanol–water with the tie-lines. Points a–k correspond to the compositions listed in Table II from ref. 28.

the phases. The partition coefficients of the two polar solutes were 1.7 and 2.7. Compositions f, g and h almost belong to the same tie-line. For these compositions, the partition coefficients are almost identical, *e.g.*, 2.3, 2.0 and 1.9, respectively, for dinitrophenylglycosamine, because all three separate in the same biphasic system. Only the relative phase volumes are different. Two points must be emphasized: (a) in different compositions belonging to the same tie-line, the solute partition coefficients do not change because the compositions of the separated phases do not change; and (b) the shorter the tie-line, the closer to unity the partition coefficient of all solutes. A tie-line of length zero is the critical limit of the monophasic area.

If the addition of electrolytes in the aqueous phase, such as acids, salts or buffers, does not significantly affect the ternary phase diagram, it can induce remarkable changes in the solute partition coefficients. The ionizable solutes are particularly sensitive to aqueous phase pH changes. Changes of several orders of magnitude with pH are commonly observed for the partition coefficients [4,5,7].

The partition coefficient of a given solute may be close to unity when that of another solute is very different, as illustrated by Table II, compositions l–p. The shortest tie-line of the diagram for hexane–methanol–water is the hexane–methanol binary mixture, with no water. Composition l belongs to that line. The partition coefficient for simazine was 3.6. It increased up to 6.2 when water was added up to 30%, v/v (composition n) and then decreased. This means that simazine has a greater affinity for the methanol–water solution than for the hexane-rich phase. However, this trend is reversed when the methanol content is low. Promazine has a high affinity for methanol. It is "pushed" into the hexane phase by increasing amounts of water (Table II). Note that with composition n, promazine partitions equally between the two phases ($P = 0.9$) and simazine has a high preference for the methanol–water phase ($P = 6.2$). Such a difference in partition coefficients will give a good CCC separation.

INFLUENCE OF VARIOUS PARAMETERS ON CHROMATOGRAMS

Configuration parameters, operating parameters and the liquid system used all have an important influence on the CCC separation. Obviously, if no stationary phase is retained, there is no chromatographic separation. Four different chromatographic merits are considered. These are: selectivity, efficiency, duration of analysis and loading capacity. Selectivity and efficiency both contribute to the chromatographic resolution. Duration of analysis and loading capacity both contribute to the chromatographic throughput.

Resolution

Selectivity is the ability of a chromatographic system to retain the components of a mixture differently. When the selectivity ratio $\alpha = k'_2/k'_1$ is higher than unity, compound 2 is separated from compound 1. The chromatographic efficiency is linked to the peak sharpness and is measured by the number of theoretical plates (N). A commonly used equation is: $N = (V_R/W_{0.6H})^2$, in which V_R is the retention volume and $W_{0.6H}$ is the peak width, expressed in volume, at 60% of the peak height. CCC efficiency depends on the number of turns of the coil [5], the way in which the solute injection was performed [22], the flow-rate and rotational speed [23], the temperature and the physico-chemical properties of the liquid system used (density, mutual solubility, interfacial tension and viscosity). These parameters act on the mechanical mixing quality which drives the kinetics of the solute exchange between the two liquid phases. The efficiency is directly related to the kinetics of the solute exchange between phases.

The resolution equation combines selectivity and efficiency:

$$R_s = \left(\frac{N^{\frac{1}{2}}}{2}\right)\left(\frac{k'_2 - k'_1}{k'_2 + k'_1 + 2}\right)$$

Using eqn. 2, R_s can be expressed as:

$$R_s = \frac{N^{\frac{1}{2}}}{2} \frac{P_2 - P_1}{P_2 + P_1 + 2\dfrac{V_0}{V_S}} \tag{8}$$

The baseline resolution is obtained when R_s is higher than 1.5. Fig. 5 shows the partition coefficient difference, $P_2 - P_1$, necessary to obtain a baseline resolution ($R_s = 1.5$) between compounds 1 and 2 plotted *versus* the CCC efficiency, N. A maximum separation power is obtained when $P_1 - P_2$ is at a minimum. This is obtained with a high efficiency and a maximum stationary phase retention (Fig. 5) [24,25]. In practice, an increase in efficiency up to *ca.* 800 plates produces an important gain in resolution. Also, a percentage of stationary phase retention of 65% (80 ml with the 125-ml volume apparatus used to draw Fig. 5) is satisfactory. Further improvements in efficiency or stationary phase retention above 800 plates and 65%, respectively, do not produce a dramatic gain in resolution.

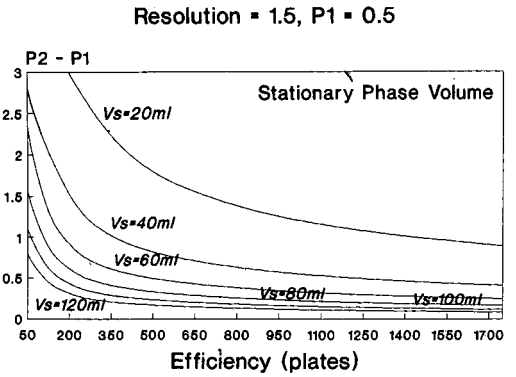

Fig. 5. Partition coefficient difference, $P_2 - P_1$, needed to obtain a baseline peak resolution ($R_s = 1.5$) *versus* the apparatus efficiency for different stationary phase retention volume. $V_T = 125$ ml; $V_0 = V_T - V_S$; $P_1 = 0.5$; eqn. 8.

Throughput

A high throughput is obtained when the loading capacity is high and the duration of separation is low. The loading capacity depends on the volume of stationary phase retained in the apparatus. The higher the internal volume, V_T, the higher the stationary phase volume that can be retained. An apparatus with a high loading capacity should be used with a long (L), large bore (d_t) tube to increase the spool volume (V, eqn. 3) and the internal volume (V_T). It should also have a small spool radius (r) to obtain a high turn number (n, eqn. 4) and a small gyration radius (R) to maximize the β ratio (eqn. 5) and to have an acceptable resolution capability [5,26].

The duration of separation depends on the mobile phase flow-rate and the highest partition coefficient (eqn. 1). The mobile phase flow-rate cannot be increased indefinitely for two reasons. (a) The stationary phase is washed off by a high flow-rate (Fig. 1) which significantly decreases the resolution power (Fig. 5). (b) The driving pressure, ΔP, increases with flow-rate and cannot pass a pressure limit of about 30 bar above which PTFE tubes rupture and leaks occur. The driving pressure is the sum of a hydrodynamic term (Darcy law) and a hydrostatic term [29].

$$\Delta P = \frac{64\eta LF}{\pi d_t^4} + n\Delta\rho\omega^2\Phi \tag{9}$$

ΔP is expressed in Pascals (N/m^2, 10^5 Pa = 1 bar). In the hydrodynamic terms of eqn. 9, η is the mobile phase viscosity [cP, $\times 0.001$ to take account of the units (cm^3) of the flow-rate] and F is the flow-rate (cm^3/s). In the hydrostatic term, $\Delta\rho$ is the density difference between the two liquid phases (g/cm^3), ω is the rotational speed (radian/s), Φ is a geometrical parameter (m^2) function of the β term, the rotor radius R and the spool radius r.

The separation duration depends on the solute partition coefficients and the stationary phase volume retained. Decreasing the V_S term in eqns. 1 or 2 decreases the solute retention volume V_R at the cost of the resolution which vanishes (Fig. 5 and eqn. 8). Once again, CCC parameters are intimately related. Fig. 6 recapitulates the

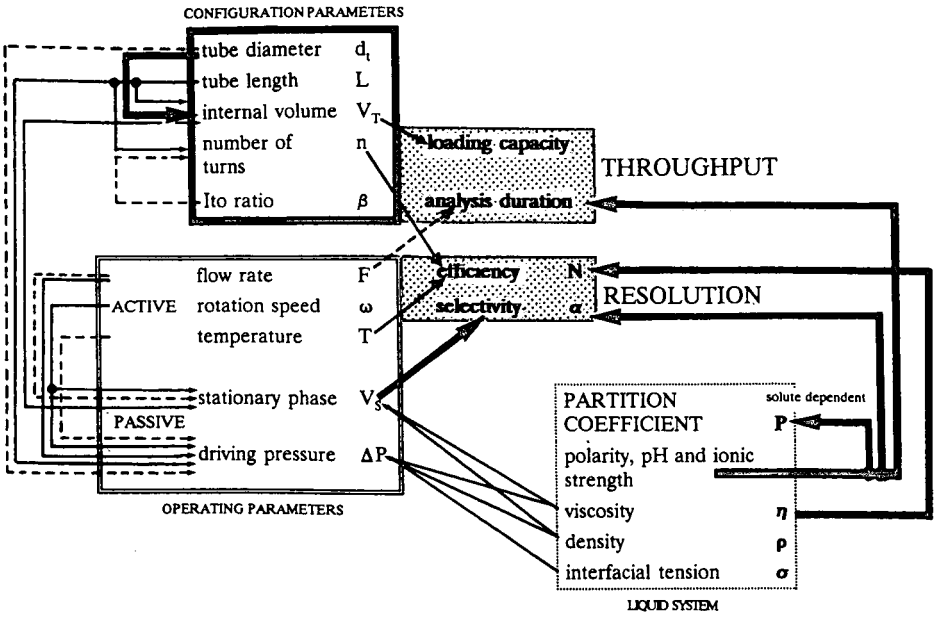

Fig. 6. Interconnections of the CCC parameters. Solid line indicates that an increase in the starting parameter increases the parameter to which it is connected. Broken line indicates that an increase in the starting parameter decreases the parameter to which it is connected. Thick line represents an important effect. P, the solute partition coefficient, depends on the way the system is used, $P_{org/aq} = 1/P_{aq/org}$. For symbols, see text.

relationships between the numerous parameters of CCC. The arrows join one parameter to another. The arrows with solid lines mean that an increase in the parameter at the start of the arrow induces an increase in the parameter to which it is connected. Arrows with broken lines mean the opposite: the connected parameter decreases. A thick line corresponds to a critical control. The liquid system is the most important in CCC optimization. The two key parameters are P, the solute partition coefficient, and V_S, the amount of stationary phase retained. P depends only on the liquid system and the solute. V_S depends on the configuration parameters, mainly V_T, on the operating parameters and on the liquid system. The optimization of a CCC separation may often need two different sets of apparatus. The first, with a low internal volume and a high efficiency, will sacrifice throughput for resolution. The liquid system can be rapidly optimized to adjust the solute partition coefficients and the resolution of separation. A large-volume CCC apparatus can then be used to obtain a high throughput.

EXAMPLES

To conclude this paper, some literature examples are discussed. Fig. 7 is an interesting example of the versatility of high-speed CCC. Fig. 7A–C shows three chromatograms of an extract of *Guttiferae* root bark obtained with the mobile phase

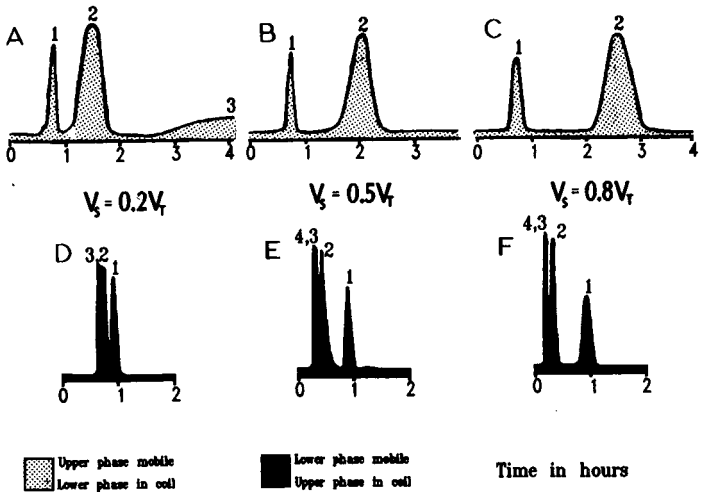

Fig. 7. Effect of V_S, the stationary phase volume, on the CCC chromatogram. The CCC apparatus retained 20% (A and D), 50% (B and E) and 80% (C and F) of the total apparatus volume in the coil. Apparatus: multilayer coil planet centrifuge CCC; compounds 1–4, anthranoid pigments; solvent system, hexane–acetonitrile–methanol (40:25:10, v/v/v); flow-rate, 4 ml/min; rotational speed, 700 rpm. From ref. 30.

consisting of the apolar upper phase of the waterless mixture hexane–acetonitrile–methanol (8:5:2, v/v/v) [30]. The stationary phase volume, V_S, was adjusted using two pumps running together. Fig. 7D–F shows the chromatograms obtained with the same sample and liquid system, but with the mobile phase as the lower polar phase. Table III lists the retention volumes of compounds 1 and 2 corresponding to the six chromatograms. The total volume of the apparatus, V_T, is 360 ml [30]. The partition coefficient of the solute can be calculated because the percentage of stationary phase is known and is indicated in Fig. 7 as a V_T percentage. Eqn. 1 allows the P value listed in

TABLE III

PARTITION COEFFICIENT DATA FOR FIG. 7

Abbreviations: lo. = lower phase in coil, upper phase mobile; up. = upper phase in coil, lower phase mobile. The aqueous/organic partition coefficients were calculated using: (1) for chromatograms A, B and C, $P = [(V_R - V_T)/V_S] + 1$; (2) for chromatograms D, E and F, $P = 1/\{[(V_R - V_T)/V_S] + 1\}$.

Fig. 7 chromatogram	Stationary phase	Retention volume (ml)		Partition coefficient with V_T = 360 ml		Partition coefficient with V_T = 195 ml	
		1	2	1	2	1	2
A	0.2 lo.	188	347	<0	0.82	0.82	4.8
B	0.5 lo.	186	480	0.03	1.65	0.90	3.9
C	0.8 lo.	173	613	0.35	1.88	0.86	3.7
D	0.2 up.	214	180	<0	<0	0.67	1.6
E	0.5 up.	216	110	5	<0	0.82	7.8
F	0.8 up.	221	77	1.9	58	0.86	4.1

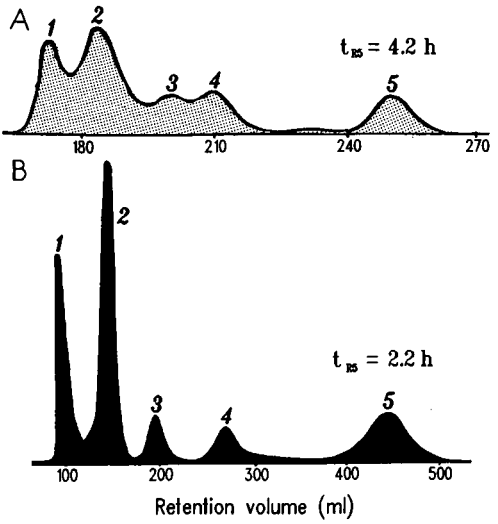

Fig. 8. CCC separation of the same sample (flavonoids) with the same liquid system [chloroform–methanol–water (4:3:2, v/v/v); mobile phase, lower organic phase] with two different apparatuses. Apparatus A: twelve-column horizontal flow-through coil planet centrifuge; V_T = 220 ml; V_S = 55 ml (25%); flow-rate: 1 ml/min; 300 rpm. Apparatus B: multilayer coil planet centrifuge; V_T = 300 ml; V_S = 255 ml (75%); flow-rate: 3.3 ml/min; 800 rpm. From ref. 24.

Table III as polar phase/hexane phase partition coefficients to be calculated. The P values for a compound are not constant. In some instances, the computation produced a negative P value which has no meaning. It was noted [30] that "the elution time of 1 was hardly affected by changing the stationary phase percentage in either the two modes". This behaviour is typical of a solute distributing equally in both phases (P close to unity). With this in mind, it was assumed that the apparatus volume V_T was inaccurate and it was estimated as V_T = 195 ml. Table III lists the corresponding P values of 0.85 ± 0.05, 4.2 ± 0.5 and *ca.* 20 for compounds 1, 2 and 3, respectively.

Fig. 8 shows two chromatograms obtained with the same sample and liquid

TABLE IV

EFFICIENCY AND RESOLUTION DATA FOR FIG. 8

For apparatus A: V_T = 200 ml; V_S = 0.25 V_T = 55 ml. For apparatus B: V_T = 300 ml; V_S = 0.75 V_T = 255 ml.

Fig. 8 peak No.	Apparatus A				Apparatus B			
	V_R (ml)	$P_{aq/org}$	N plates	R_S	V_R (ml)	$P_{aq/org}$	N plates	R_S
1	174	0.16	1100	–	100	0.21	500	–
2	186	0.38	1100	0.55	142	0.38	560	2.05
3	200	0.63	1200	0.63	196	0.59	530	1.84
4	213	0.87	1800	0.67	270	0.88	530	1.83
5	252	1.58	2400	2.05	450	1.59	500	2.80

system, but with two different counter-current chromatographs [24]. The CCC apparatus A that produced the Fig. 8A chromatogram was a horizontal coil planet centrifuge device. Fig. 8B was obtained with a multilayer coil planet centrifuge CCC apparatus B [24]. Table IV lists the retention volumes, partition coefficients, peak efficiencies and resolutions obtained for the five peaks separated from the vegetable extract sample. The first observation is that the throughput of the two sets of apparatus is very different. If A was able to separate the last solute (5) with 252 ml, it took 4.2 h because the flow-rate could not exceed 1 ml/min due to a poor 25% retention of the stationary phase. Apparatus B used 450 ml of aqueous mobile phase to elute compound 5, but it did so in only 2.2 h because the stationary phase was held tightly. A 3.3 ml/min flow-rate was possible with a 85% retention of the stationary phase. The partition coefficients of the five solutes are identical, within experimental error, whatever apparatus is used. They depend only on the liquid system (Fig. 6). Apparatus A has a higher efficiency, in the 1200 plate range, than apparatus B, which is two times less efficient. Apparatus A contains sixteen coiled columns connected serially, which was about 1850 turns, probably many more turns than apparatus B (not given) [24]. The two times higher efficiency of apparatus A is not obvious on Fig. 8. The B peaks look sharper because the volume scale is different and the origins are out of the figure. The resolution power of apparatus A is much lower than that of apparatus B. All the compounds separated using B were baseline-resolved ($R_s > 1.5$). The high stationary phase retention in B is responsible for its high resolution capability compared to A. In eqn. 8, the ratio $2V_0/V_S$ was 0.35 for B, and 6 for A. The two times better efficiency advantage of A could produce a 40% increase in resolution power at a constant percentage retention of the stationary phase. Unfortunately, the low retention of the stationary phase by A causes a very low selectivity (Fig. 6) and a low resolution power.

REFERENCES

1 Y. Ito, I. Aoki and E. Kimura, *Anal. Chem.*, 41 (1969) 1579.
2 Y. Ito and R. L. Bowman, *J. Chromatogr. Sci.*, 8 (1970) 315.
3 Y. Ito and W. D. Conway, *Anal. Chem.*, 56 (1984) 534A.
4 Y. Ito, *CRC Crit. Rev. Anal. Chem.*, 17 (1986) 65.
5 N. B. Mandava and Y. Ito (Editors), *Countercurrent Chromatography* (*Chromatographic Science Series*, Vol. 44), Marcel Dekker, New York, 1988.
6 Y. Ito, *Adv. Chromatogr.*, 24 (1984) 181.
7 W. D. Conway, *Countercurrent Chromatography*, VCH, Weinheim, 1990.
8 A. Berthod, *Chromatogr. Anal.*, Feb. (1990) 13.
9 A. Berthod and D. W. Armstrong, *J. Liq. Chromatogr.*, 11 (1988) 547.
10 Y. Ito, *J. Chromatogr.*, 301 (1984) 387.
11 R. J. Romanach and J. A. de Haseth, *J. Liq. Chromatogr.*, 11 (1988) 91.
12 A. Berthod, Y. I. Han and D. W. Armstrong, *J. Liq. Chromatogr.*, 11 (1988) 1441.
13 J. Wisniak and A. Tamir, *Liquid–Liquid Equilibrium and Extraction*, Elsevier, Amsterdam; Part A, 1980; Part B, 1981; Supplement 1, 1985; Supplement 2, 1987.
14 Y. Ito and W. D. Conway, *J. Chromatogr.*, 301 (1984) 405.
15 O. Mikes and R. Vespalec, in Z. Deyl, K. Macek and J. Janák (Editors), *Liquid Column Chromatography* (*Journal of Chromatography Library*, Vol. 3), Elsevier, Amsterdam, 1975, Ch. 10, p. 240.
16 Y. Ogihara, O. Inoue, H. Otsuka, K. Kawai, T. Tanimura and S. Shibata, *J. Chromatogr.*, 128 (1976) 218.
17 K. Hostettmann, M. Hostettmann and K. Nakanishi, *J. Chromatogr.*, 170 (1979) 355.
18 J. M. Sorensen and W. Arlt, *Liquid–Liquid Equilibrium Data Collection, Ternary Systems, Chemistry Data Series*, Dechema, Frankfurt, 1979.

19 A. W. Francis, *Liquid–Liquid Equilibriums*, Interscience, New York, 1963.
20 A. Berthod, J. D. Duncan and D. W. Armstrong, *J. Liq. Chromatogr.*, 11 (1988) 1171.
21 A. Foucault and K. Nakanishi, *J. Liq. Chromatogr.*, 12 (1989) 2587.
22 J. L. Sandlin and Y. Ito, *J. Liq. Chromatogr.*, 7 (1984) 323.
23 J. L. Sandlin and Y. Ito, *J. Liq. Chromatogr.*, 11 (1988) 55.
24 T. Y. Zhang, X. Hua, R. Xiao and S. Kong, *J. Liq. Chromatogr.*, 11 (1988) 233.
25 W. D. Conway and Y. Ito, *J. Liq. Chromatogr.*, 8 (1985) 2195.
26 Y. Ito, J. L. Sandlin and W. G. Bowers, *J. Chromatogr.*, 244 (1982) 247.
27 N. B. Mandava, Y. Ito and J. M. Ruth, *J. Liq. Chromatogr.*, 8 (1985) 2221.
28 W. D. Conway, R. L. Hammond and A. M. Sarlo, *J. Liq. Chromatogr.*, 11 (1988) 107.
29 A. Berthod and D. W. Armstrong, *J. Liq. Chromatogr.*, 11 (1988) 567.
30 I. Slacanin, A. Marston and K. Hostettmann, *J. Chromatogr.*, 482 (1989) 234.

Journal of Chromatography, 550 (1991) 695–704
Elsevier Science Publishers B.V., Amsterdam

CHROMSYMP. 2272

Protein separation with aqueous–aqueous polymer systems by two types of counter-current chromatographs

YOICHI SHIBUSAWA[a] and YOICHIRO ITO*

Laboratory of Biophysical Chemistry, National Heart, Lung, and Blood Institute, National Institutes of Health, Building 10, Room 7N322, Bethesda, MD 20892 (USA)

ABSTRACT

Two different types of counter-current chromatographs, the cross-axis coil planet centrifuge (*X*-axis CPC) and horizontal flow-through coil planet centrifuge (horizontal CPC), were evaluated for protein separation with an aqueous–aqueous two-phase polymer system. The sample solution, containing 10–200 mg each of cytochrome *c*, myoglobin, ovalbumin and hemoglobin in 2 ml of each phase was eluted with the lower phase.

In both instruments, the effects of the flow-rate, revolution speed, and parameter β (helical diameters of the multilayer coil) on the protein separation were investigated. The best results were obtained from the *X*-axis CPC operated at 750 rpm and a flow-rate of 2.0 ml/min using a multilayer coil with a small helical diameter (β = 0.25–0.60). Four protein samples were well resolved in less than 5 h.

INTRODUCTION

Counter-current chromatography (CCC) is a liquid–liquid partition chromatography utilizing no solid support matrix [1–3]. The stationary phase is retained in the column by the aid of a gravity or centrifugal force. The system eliminates all complications arising from the solid support. Consequently, the method is very useful for separation and purification of biopolymers such as proteins and nucleic acids, using aqueous–aqueous polymer phase systems [4,5]. Polymer phase systems have been introduced by Albertsson [6] for the partition of a variety of macromolecules and cell particles. However, high viscosity and low interfacial tension of polymer phase systems tend to delay phase separation and the operation of the conventional counter-current distribution apparatus becomes tedious and requires a long separation time. Recently some coil planet centrifuge (CPC) apparatus have been modified for performing CCC with polymer phase systems [7,8].

In this paper, the performance of two different CPC models, *i.e.*, the cross-axis coil planet centrifuge (X-axis CPC) and the horizontal coil planet centrifuge (horizontal CPC), were evaluated in the separation of four sample proteins including cytochrome

[a] Visiting scientist from Tokyo College of Pharmacy, 1432-1, Horinouchi, Hachioji, Tokyo, Japan.

0021-9673/91/$03.50

c, myoglobin, ovalbumin and hemoglobin with a two-phase polymer system composed of polyethylene glycol (PEG) 1000 and potassium phosphate. The partition coefficient (K) of these proteins were optimized by choosing a suitable pH of the potassium phosphate composition. The separations were performed by varying the chromatographic conditions such as the revolution speed, flow-rate and column dimensions.

EXPERIMENTAL

Apparatus

CCC separations were performed with two different CPC types, the improved cross-axis CPC (X-axis CPC) and the most recent model of the horizontal flow-through CPC, each producing a specific mode of planetary motion [8,9]. These two CCC centrifuges share a common feature in that the system permits continuous elution of the mobile phase through the rotating column without the use of the conventional rotary seal device which is a potential source of leakage and contamination [10].

The design of the X-axis CPC has been reported earlier [8]. The apparatus holds a pair of horizontal rotary shafts symmetrically, one on each side of the rotary frame, at a distance of 7.6 cm from the central axis of the centrifuge. A spool-shaped column holder is mounted on each rotary shaft at a lateral location 15 cm away from the midpoint. As reported earlier, this displacement of the column holder on the holder shaft is essential for providing stable retention of the polymer stationary phase against a high flow-rate of the mobile phase.

Each multilayer coil was prepared from 2.6 mm I.D. PTFE (polytetrafluoroethylene) tubing (Zeus Industrial Products, Raritan, NJ, USA) by winding it onto a 7.6 or 3.8 cm diameter holder forming multiple layers of left-handed coils between a pair of flanges spaced 5 cm apart. The larger columns consists of 6 layers of the coil with a 140-ml capacity and the smaller column of 8 layers of the coil with about a 125-ml capacity. In both columns all coiled layers were connected in series by bridging neighboring layers with narrow transfer tubes (0.85 mm I.D., PTFE) across the width of the column. Leak-free connections were made at each joint by using a short sheath of an intermediate-sized PTFE tube (1.6 mm I.D.) as an adaptor. A pair of columns mounted on the rotary frame was connected in series to make up a total capacity of about 280 ml in the larger column and 250 ml in the smaller column. Both inflow and outflow tubes exit together at the center of the top plate of the centrifuge case where they are tightly supported with silicone-rubber-padded clamps.

The horizontal CPC used in the present experiments is a modified version of the high-speed CCC centrifuge described previously [9]. The apparatus holds a set of three column holders symmetrically on the rotary frame at a distance of 10 cm from the central axis of the centrifuge. Each column holder is equipped with a planetary gear which interlocks to an identical stationary sun gear mounted around the central axis of the centrifuge. This gear arrangement produces a desired synchronous planetary motion of the holder, *i.e.*, rotation about its own axis and revolution around the centrifuge axis in the same direction at the same rate. Each column holder can be removed from the rotary frame by loosening a pair of screws on each bearing block.

The column holder was modified to form a composite coil assembly similar to

that in the eccentric CPC previously reported [11]. Each coil assembly consisted of a series of eight coil units which were prepared by winding a single piece of 1.6 mm I.D. PTFE tubing onto 12 cm long, 0.6 cm O.D. stainless–steel pipes forming double layers of coils. Each coil unit consists of about 75 helical turns with about a 9-ml capacity. Eight coil units were arranged around each holder in parallel to and at a distance of 3 cm from the holder axis. Three coil assemblies on the rotary frame were serially connected with flow tubes (0.85 mm I.D., PTFE) to make up the total capacity of about 220 ml. Each interconnection tube runs across the width of the rotary frame along the rotary tube support which was actively counter-rotated to prevent the flow tubes from twisting [9,12]. The inflow and outflow tubes (0.85 mm I.D., PTFE) were each tightly secured onto the side wall of the centrifuge using a pair of silicone-rubber-padded clamps.

Revolution speed of these centrifuges are regulated up to 1000 rpm with a speed control unit (Bodine Electric, Chicago, IL, USA). Dimensions of each column, including the number of layers, total capacity, range of parameter β (helical diameters of the multilayer coil), etc. are summarized in Table I.

Reagents

Polyethylene glycol (PEG) 1000 (mol.wt. = 1000), cytochrome *c* (horse heart), myoglobin (horse heart), ovalbumin (chicken egg) and hemoglobin (bovine) were purchased from Sigma (St. Louis, MO, USA). Anhydrous monobasic and dibasic potassium phosphates were obtained from J. T. Baker (Phillipsburg, NJ, USA). All these chemicals were of reagent grades.

TABLE I

TYPE OF APPARATUS AND DIMENSIONS OF THE SEPARATION COLUMNS USED IN THE PRESENT STUDY

Apparatus (planetary motion)	Coil holder		Type of column	Column			
	Diameter (cm)	Width (cm)		I.D. (mm)	Total length (m)	Total turns	Total capacity (ml)
X-axis CPC (Type XLL)	7.6	5.1	Coaxial multilayer 6 layers all left handed β^a = 0.50–1.00	2.6	53	156	280
	3.8	5.1	Coaxial multilayer 8 layers all left handed β = 0.25–0.60	2.6	47	208	250
Horizontal CPC (Type J)	0.6[b]	12.0	Eccentric double-layer 8 coil/holder right and left handed β = 0.3	1.6	109	2300	220

[a] $\beta = r/R$ where r is the distance from the holder axis to the coil and R, the distance from the holder axis to the central axis of the centrifuge.

[b] Diameter of stainless-steel pipe supporting the coil.

Preparation of polymer two-phase solvent systems and sample solution

The aqueous–aqueous polymer phase systems were prepared by dissolving 150 g of PEG 1000 and 150 g of anhydrous potassium phosphate in 900 g of distilled water. The solvent mixture was thoroughly equilibrated in a separatory funnel at room temperature, allowing the mixture to completely separate into two layers before use. The sample solution was prepared by dissolving 10–200 mg each of cytochrome *c*, myoglobin, ovalbumin and bovine hemoglobin in 4 ml of the two-phase system consisting of about equal volumes of each phase.

Measurement of partition coefficient (K) of protein samples

The partition coefficient of each protein sample was determined spectrophotometrically by a simple test tube procedure. About 2 ml of each phase was delivered in a test tube and about 1 mg of the sample was added. The contents were thoroughly mixed and allowed to settle at room temperature. After the clear two layers were formed, an aliquot (usually 1 ml) of each phase was pipetted and diluted with 2 ml of distilled water to determine the absorbance at 280 nm using a Zeiss PM6 spectrophotometer. The partition coefficient ($K = C_L/C_U$) was obtained by dividing the absorbance value of the lower phase by that of the upper phase.

CCC separation of proteins

For each separation, the coil was first completely filled with the stationary upper phase. This was followed by injection of the sample solution through the sample port. Then, the mobile phase was eluted through the coil at 0.5–4.0 ml/min while the apparatus was rotated at the desired rpm. The effluent from the outlet of the column was continuously monitored with an LKB Uvicord S (LKB Instruments, Uppsala, Sweden) at 280 nm and fractionated into test tubes (3 ml/tube) with an LKB Ultrorac fraction collector (LKB Instruments).

Analysis of fractions

An aliquot of each fraction was diluted with distilled water and the absorbance was determined at 280 nm with a Zeiss PM6 spectrophotometer.

RESULTS AND DISCUSSION

CCC is a liquid–liquid partition method which is based on difference in the partition coefficient of solutes. For achieving efficient separations of proteins, it is essential to optimize the partition coefficient of each component by selecting the proper composition of the polymer phase system used for separation. Fig. 1 shows the partition coefficient values ($K = C_L/C_U$) of four proteins plotted in a logarithmic scale against the ratio of monobasic and dibasic potassium phosphates in the polymer phase system. The partition coefficients of these proteins generally rise as the relative amount of monobasic potassium phosphate increases, apparently due to the pH shift toward the isoelectric points of the applied proteins. When the concentration of the monobasic to dibasic potassium phosphates exceeds a 1:1 ratio, however, the solvent mixture forms a single phase. An evenly scattered ideal distribution of the four partition coefficient values is observed in the solvent system composed of 12.5% (w/w) dibasic potassium phosphate and 12.5% (w/w) PEG 1000.

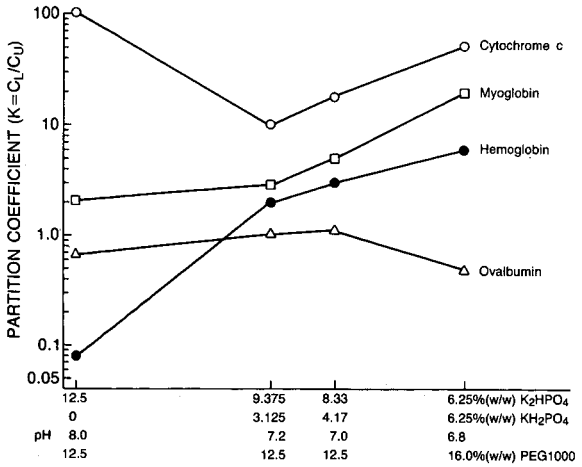

Fig. 1. Partition coefficients (K) of four protein samples in various polymer phase systems composed of PEG 1000 and potassium phosphate. K is the solute concentration in the lower phase divided by that in the upper phase.

Stationary phase retention

In the horizontal CPC, the effects of the revolution speed and flow-rate on the retention of the PEG-rich upper phase were investigated, using the lower phase as the mobile phase. As shown in Fig. 2A, the optimum condition for the retention of the stationary phase is 800 rpm. An increased revolution speed at 1000 rpm resulted in reduction of the retention volume probably due to emulsification caused by excessive mixing of the two phases. On the other hand, a reduced revolution speed down to 600 rpm gave lower retention apparently due to a lack of the centrifugal force field.

In Fig. 2B, the percentage retention for the stationary phase is plotted against the flow-rate at the optimum revolution speed of 800 rpm. It indicates that the retention of the stationary phase rapidly decreases with increased flow-rate. As the flow-

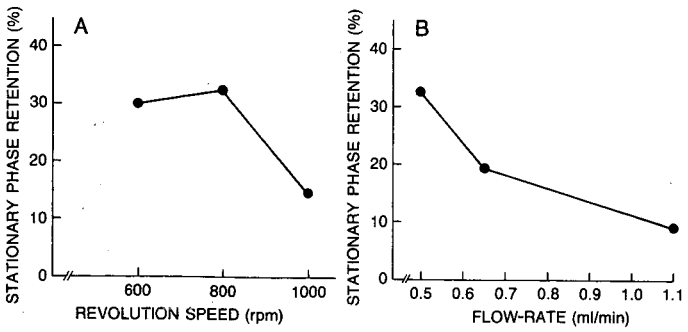

Fig. 2. Effects of revolution speed (A) and flow-rate (B) on the stationary phase retention in the horizontal CPC. (A) 1 ml/min flow-rate; (B) 800 rpm. See Table II for details.

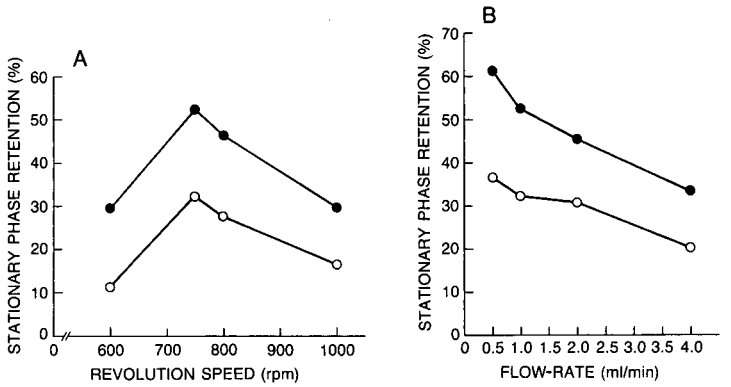

Fig. 3. Effects of revolution speed (A) and flow-rate (B) on the stationary phase retention in the X-axis CPC. (○) larger column (β = 0.50–1.00); (●) smaller column (β = 0.25–0.60); (A) 1 ml/min flow-rate; (B) 750 rpm. See Table III for details.

rate is increased from 0.5 to 1.1 ml/min, the stationary phase retention becomes about 1/4. The optimum operational conditions for the horizontal CPC are found at 800 rpm at a 0.5 ml/min flow-rate with the present aqueous–aqueous polymer phase system.

It has been reported that the present X-axis CPC has a unique capability of retaining a large amount of stationary phase for viscous, low interfacial tension solvent systems [8]. Fig. 3A and B similarly illustrate the effects of the revolution speed (A) and flow-rate (B) on the retention of the PEG-rich upper phase of a 12.5% (w/w) PEG 1000–12.5% (w/w) dibasic potassium phosphate system in the present X-axis CPC. In each diagram, open circles indicate the retention data obtained from the larger column (β = 0.50–1.00) and solid circles, those obtained from the smaller column (β = 0.25–0.60).

The effects of revolution speed on the stationary phase retention was studied by eluting the lower phase at a flow-rate of 1 ml/min. As shown in Fig. 3A, the retention sharply rises with the increased revolution speed from 600 to 750 rpm to reach the maximum level. Further increase of the revolution speed up to 1000 rpm results in a decline of the retention in a linear fashion. The two retention curves display similar shapes, while the retention in the smaller column always exceeds that in the larger column, as expected from the previous data with the organic–aqueous solvent systems [8].

Fig. 3B shows the effects of the flow-rate of the mobile phase on the retention of the stationary phase at a revolution speed of 750 rpm. In both columns, the retention decreases with an increased flow-rate from 0.5 to 4.0 ml/min. The retention level in the smaller column is much greater than that in the larger column. Even at a high flow-rate of 2.0 ml/min, the smaller column holds the stationary phase near 50% of the total column capacity, promising an efficient peak resolution of protein samples in a short elution time.

Separation of proteins with two different CPCs

In order to study effects of the revolution speed and flow-rate on the protein

TABLE II

PEAK RESOLUTION OF THREE PROTEINS OBTAINED BY HORIZONTAL CPC

cy = Cytochrome *c*; myo = myoglobin; ov = ovalbumin. Column capacity: 220 ml; $\beta = 0.3$.

Revolution speed (rpm)	Flow-rate (ml/min)	Peak resolution		Stationary phase retention (%)
		cy/myo	myo/ov	
600	0.5	1.63	0.43	29.8
800	0.5	2.22	0.43	32.6
1000	0.5	1.71	0.29	14.1
800	0.5	2.22	0.43	32.6
800	0.7	1.43	0.60	19.3
800	1.1	0.73	–	9.0

separation, a series of experimental runs was performed with a two-phase solvent system composed of 12.5% (w/w) PEG 1000 and 12.5% (w/w) dibasic potassium phosphate using the lower phase as the mobile phase. From the obtained chromatogram, partition efficiency was computed and expressed in terms of peak resolution, R_s, according to the conventional formula

$$R_s = 2(R_1 - R_2)/(W_1 + W_2) \quad (1)$$

where R_1 and R_2 are retention time or volume of two adjacent peaks, and W_1 and W_2, the peak width of the same peaks expressed in the same unit as R_1 and R_2. The results are summarized in Tables II and III, where R_s values between the first (cytochrome *c*) and second (myoglobin) peaks and between the second and third (ovalbumin) peaks are listed together with the percentage retention of the stationary phase obtained under various combinations of revolution speeds and flow-rates.

In the horizontal CPC (Table II), a fixed flow-rate of 0.5 ml/min produced the highest peak resolution at 800 rpm as shown in the top three rows. The shift of the revolution speed in either direction results in a lower R_s value. This loss of peak resolution may be secondary to the reduced stationary phase volume retained in the column since the percentage retention values appear to bear a somewhat significant correlation with the R_s values. At the optimum revolution speed of 800 rpm, the flow-rate was varied from 0.5 to 1.1 ml/min (bottom three rows in Table II). With one exception, the peak resolution decreases with an increased flow-rate and, again, R_s values between the first and second peaks show similar correlation with the percentage retention of the stationary phase.

These experimental results strongly suggest that, in the horizontal CPC, the retention level of the stationary phase may play a major role in governing the peak resolution of proteins within the applied experimental conditions.

Fig. 4 shows a chromatogram of the four proteins obtained by the horizontal CPC under the optimum operational conditions. The separation was performed at 800 rpm at a flow-rate of 0.65 ml/min using the lower phase as the mobile phase. The four components were eluted in the order of their partition coefficient values within 15 h. After the elution of cytochrome *c* ($K = 103.7$), myoglobin ($K = 2.08$), and

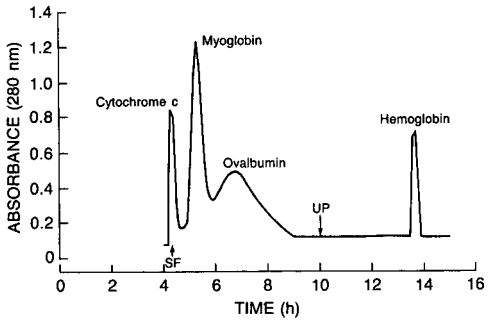

Fig. 4. Chromatogram of proteins obtained by the horizontal CPC. Experimental conditions: column: eccentric dual layer coil assemblies × 3, 1.6 mm I.D. PTFE, 220 ml capacity; sample: 10–200 mg of each protein in 4 ml solvent; solvent system: 12.5% (w/w) PEG 1000–12.5% (w/w) K_2HPO_4 in distilled water; mobile phase: lower phase; flow-rate: 0.65 ml/min; revolution: 800 rpm; SF = solvent front; UP = upper phase eluted in the reversed direction.

ovalbumin ($K = 0.63$), the PEG-rich upper phase was pumped into the column in the reversed direction to facilitate rapid elution of hemoglobin ($K = 0.08$) still remaining in the column. From the obtained chromatogram, the separation efficiency may be computed and expressed in terms of theoretical plate number using the conventional gas chromatographic formula.

$$N = (4R/W)^2 \tag{2}$$

where N denotes the theoretical plate number; R, the retention time or volume of the peak maximum; and W, the peak width expressed in the same unit as R. Using the above equation, the separation efficiency thus obtained for the third peak (ovalbumin) was $n = 50$, while the R_s between the second and the third peaks is 0.60.

The peak resolutions of proteins in the two different columns on the X-axis CPC have been studied under various experimental conditions, the results being summarized in Table III. In the smaller coil ($\beta = 0.25$–0.60), the effects of the revolution speed on the peak resolution were examined at a 1.0 ml/min flow-rate (top four rows). The maximum peak resolution was obtained at 750 rpm. The lower (600 rpm) or higher (1000 rpm) speed results in considerable decrease of peak resolution probably due to the lower stationary phase retention as observed in the horizontal CPC. At a 750 rpm revolution speed (5th–8th rows in Table III), an increase of the flow-rate up to 2 ml/min does not affect the peak resolution, despite a considerable decrease in stationary phase retention. However, further increase of the flow-rate at 4.0 ml/min results in a detrimental loss in the peak resolution probably due to a sharp decline in the retention level.

The effects of revolution speed on the peak resolution were similarly investigated in the larger column at a flow-rate of 1.0 ml/min (9th–12th rows in Table III). The results show that the R_s values between the first and second peaks (cy/myo) are rather insensitive to the revolution speed, while the best resolution between the second and third peaks (myo/ov) is found at 750 rpm associated with the highest retention level of the stationary phase as observed in the smaller column. At a constant revolution

TABLE III

PEAK RESOLUTION OF THREE PROTEINS OBTAINED BY X-AXIS CPC

cy = Cytochrome *c*; myo = myoglobin; ov = ovalbumin.

Column capacity (ml) β value	Revolution speed (rpm)	Flow-rate (ml/min)	Peak resolution		Stationary phase retention (%)
			cy/myo	myo/ov	
250 ml					
β = 0.25–0.60	600	1.0	1.59	0.56	29.1
	750	1.0	2.10	0.85	52.1
	800	1.0	1.88	0.51	46.4
	1000	1.0	1.75	0.45	29.6
	750	0.5	2.26	0.82	61.4
	750	1.0	2.10	0.85	52.1
	750	2.0	2.28	0.86	45.4
	750	4.0	1.01	–	33.5
280 ml					
β = 0.50–1.00	600	1.0	2.46	0.81	11.3
	750	1.0	2.29	0.90	32.3
	800	1.0	2.53	0.68	27.5
	1000	1.0	2.11	0.53	16.6
	750	0.5	3.35	0.99	36.6
	750	1.0	2.29	0.90	32.3
	750	2.0	1.73	–	30.9
	750	4.0	0.18	–	20.2

speed of 750 rpm, the lowest flow-rate of 0.5 ml/min yields the best peak resolution, while the highest flow-rate at 4.0 ml/min results in a serious loss of peak resolution apparently due to the low stationary phase retention.

Fig. 5 shows a chromatogram of the protein samples by the X-axis CPC using

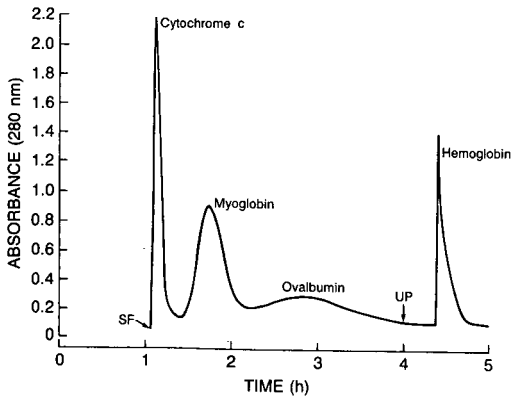

Fig. 5. Chromatogram of proteins obtained by the X-axis CPC. Experimental conditions: column: 2.6 mm I.D. PTFE multilayer coils × 2, β = 0.25–0.60, 250 ml capacity; sample: four proteins 10–200 mg each in 4 ml solvent; solvent system: 12.5% (w/w) PEG 1000–12.5% (w/w) K_2HPO_4 in distilled water; mobile phase: lower phase; flow-rate: 2 ml/min; revolution: 750 rpm; SF = solvent front; UP = upper phase eluted in the reverse direction.

the smaller column (β = 0.25–0.60). The separation was performed at 750 rpm and at a high flow-rate of 2 ml/min. All components were well resolved in less than 5 h. The hemoglobin with a low partition coefficient was collected from the column by applying the reversed elution as described earlier. The partition efficiencies computed from the chromatogram range from 550 TP (theoretical plates) for the first peak to 35 TP for the third peak, while R_s = 0.86 between the second and third peaks.

CONCLUSION

The peak resolution of the proteins is greatly influenced by the revolution speed and the flow-rate of the mobile phase in both horizontal and X-axis CPCs. The horizontal CPC was able to resolve the protein peaks at a low flow-rate of 0.5 ml/min in 15 h. In the X-axis CPC, the smaller column (β = 0.25–0.60) provided stable retention of the stationary phase against a high flow-rate of 2 ml/min, yielding a comparable separation of the proteins within 5 h. The results of the present studies succesfully demonstrate the capability of the two CCC instrument to perform protein separations with an aqueous–aqueous polymer phase system. The present methods will be useful in separation and purification of various biopolymers.

ACKNOWLEDGEMENT

The authors of this paper wish to thank Dr. Henry M. Fales for his assistance in reviewing this paper.

REFERENCES

1 Y. Ito and R. L. Bowman, *Science (Washington, D.C.)*, 167 (1970) 281.
2 W. D. Conway, *Countercurrent Chromatography: Apparatus, Theory and Applications*, VCH, New York, 1990.
3 Y. Ito, in N. B. Mandava and Y. Ito (Editors), *Principle and Instrumentation of Countercurrent Chromatography in Countercurrent Chromatography: Theory and Practice*, Marcel Dekker, New York, 1988, Ch. 3, p. 79.
4 I. A. Sutherland, D. Heywood-Waddington and Y. Ito, *J. Chromatogr.*, 384 (1987) 197.
5 Y. Ito and R. L. Bowman, *Science (Washington D.C.)*, 182 (1973) 391.
6 P. Å. Albertsson, *Partition of Cell Particles and Macromolecules*, Wiley-Interscience, New York, 1986.
7 Y. Ito and H. Oka, *J. Chromatogr.*, 457 (1988) 393.
8 Y. Ito, E. Kitazume, M. Bhatnagar and F. D. Trimple, *J. Chromatogr.*, 538 (1991) 59.
9 Y. Ito, E. Kitazume and J. L. Slemp, *J. Chromatogr.*, 538 (1991) 81.
10 Y. Ito, *CRC Crit. Rev. Anal. Chem.*, 17 (1986) 65.
11 J. L. Sandlin and Y. Ito, *J. Liq. Chromatogr.*, 11 (1988) 55.
12 Y. Ito, H. Oka and J. L. Slemp, *J. Chromatogr.*, 475 (1989) 219.

Journal of Chromatography, 550 (1991) 705–719
Elsevier Science Publishers B.V., Amsterdam

CHROMSYMP. 2293

Effect of sample viscosity in high-performance size-exclusion chromatography and its control

MARTIN CZOK[a], ANITA M. KATTI[b] and GEORGES GUIOCHON*

** Department of Chemistry, University of Tennessee, Knoxville, TN 37996-1600, and Division of Analytical Chemistry, Oak Ridge National Laboratory, Oak Ridge, TN (USA)*

ABSTRACT

When the sample viscosity greatly exceeds that of the mobile phase, flow instabilities occur, which lead to non-uniform flow in the radial direction. This "fingering" effect is usually greater with large-diameter than with micro-bore columns and may have worse effects in size-exclusion chromatography (SEC) than in any other chromatographic mode, as retention is shorter and dilution less important with SEC than with modes where retention is significant. This study suggests ways to reduce this viscosity effect. For example, this effect can be eliminated by controlling the concentration of a suitable mobile-phase additive which allows one to equate the viscosities of the eluent and the sample. Another possibility is to follow the sample with a plug of eluent, 0.3–0.5 column volumes wide, having a slightly higher viscosity than the sample. No spurious peaks are observed, as the plug acts as a wall prohibiting "fingering".

INTRODUCTION

Size-exclusion chromatography (SEC) is used as a preparative method that is able to separate and, thus, classify biopolymers according to their molecular size. It has the further advantages of (i) operating under very mild conditions where the biological activity of proteins can be conserved and (ii) permitting the complete elution of the entire sample with one single column volume of mobile phase [1,2]. This character would suggest applying SEC as a first fractionating step in the preparative purification of proteins. In practice, however, the amount of sample that can be applied to an SEC column is limited [3]. There are two reasons for this.

First, as for all the other retention mechanisms used in chromatography, there is an equilibrium isotherm relating the concentration of a given component in the mobile and the stationary phases, in this instance its concentration in the stagnant mobile phase inside the particles of the packing material. The equilibrium isotherm is related to the difference in Gibbs free energies of the component in the two liquid phases, a term dominated by the difference in the entropies of the solute in the bulk liquid and the liquid contained in the pores. These entropies are both functions of the

[a] Present address: Université de Paris-Sud, Centre d'Études Pharmaceutiques, Laboratoire de Chimie Analytique, Rue Jean-Baptiste Clement, 92290 Chatenay-Malabry, France.
[b] Present address: EI Chrom Industries, 8205 South Cass Avenue No. 107, Darien, IL, USA.

0021-9673/91/$03.50

concentration. Thus, like other modes of chromatography, SEC becomes non-linear at high concentrations.

Another phenomenon prevents or limits heavy column overloading. The viscosity of a polymer solution increases rapidly with the polymer concentration. The hydrodynamic behavior of a plug of a viscous solution moving along a packed bed in a less viscous stream is unstable. Local fluctuations of the packings permeability create perturbations of the rear of the plug which are unstable, increase exponentially and will generate fingering [4]. In such a case, the viscous plug separates into several smaller ones which propagate more or less independently. In the better case this enhances band broadening, whereas in the worse case the smaller plugs elute separately and the detector records a series of more or less well resolved bands. Although never analyzed in detail, this phenomenon has already been noticed and the difference in viscosity between the eluent and the sample bands has been blamed for excessive band broadening in attempts at performing high-concentration separations or purifications of high polymers or proteins [3,5,6]. Moore [5] reported that fingering appears when the product of the sample concentration, the sample intrinsic viscosity and the sample volume is higher than 0.05–0.10 ml.

The viscosity effect has been reported by Flodin [7]. Increasing the dextran concentration in a dilute sample of sodium chloride and hemoglobin resulted in increasingly tailing bands and in a marked decrease in the resolution. The resolution was little improved by a decrease in flow-rate. However, the effect was blamed on bed compression. Lambert [8] and Rudin [9] investigated the relationship between the retention volume and the sample concentration and attempted to derive corrections. This effect is observed at sample concentrations which are too low to promote fingering and is due to changes in the hydrodynamic volume of random polymer coils with concentration, changes caused in turn by a modification of the coil conformation. James and Ouano [10] studied the errors made in SEC measurements of the properties of polymers due to column overloading and found that their origin is in the sample viscosity. Emneus [11] avoided the band broadening effect due to fingering in the desalting of proteins by carrying out size exclusion in a batch mode. The sample is mixed with the dry packing and the highly viscous sample solution containing the proteins is separated by centrifugation from the packing containing only salt solution. Such a procedure is not chromatographic, however, and is unacceptable for difficult separations.

It has been recommended to keep the sample viscosity less than twice the mobile phase viscosity [1,12]. For proteins, it was suggested also that the sample concentration should not exceed 0.2% (w/w) or *ca.* 0.04 mg in a 20-μl sample loop for conventional analytical columns [1]. This figure is conservative and aims at avoiding other sources of difficulties also. A general method of reducing viscosity effects is to inject a larger, more dilute sample. However, there is a limit to the extent of volume overload that can be achieved this way before the resolution becomes too low for a useful purification.

As the separation mechanism is essentially entropic, it is not affected by temperature (provided that the size of the solute is not temperature dependent), whereas the sample viscosity decreases with increasing temperature. Insofar as the sample viscosity decreases faster than the solvent viscosity with increasing temperature, SEC separations are advantageously carried out near the upper temperature limit of the sample, the column packing or the equipment.

In an attempt to investigate the interplay of these high-concentration effects and to find some remedial action to improve the throughput of preparative SEC columns, we investigated the response of such a column to the injection of large volumes of high-concentration feed samples using different proteins. We also studied the influence of the viscosity of the eluent, which can be conveniently increased by adding glycerol whose small molecules have access to all the pores of the packing, but which is harmless towards the protein molecules and can easily be removed by dialysis.

EXPERIMENTAL

Columns

All chromatographic experiments were performed with a 25 cm × 4.6 mm I.D. SynChropak GPC 300 column (SynChrom, Lafayette, IN, USA) for high-performance size-exclusion chromatography of water-soluble polymers. According to the manufacturer, the average pore diameter of this material is *ca.* 300 Å and the average particle size is 5 μm. The total mobile phase hold-up volume of the column is 3.35 ml, as determined from the breakthrough time of uracil.

Chemicals

The samples used were uracil (Aldrich, Milwaukee, WI, USA), ovalbumin (from chicken egg and from turkey egg), bovine serum albumin and human hemoglobin. All proteins were purchased from Sigma (St. Louis, MO, USA). Glycerol was also obtained from Sigma.

Equipment

The chromatographic system consisted of two high-performance liquid chromatographic (HPLC) pumps (Model 302; Gilson, Middleton, WI, USA) controlled by a Gilson 621 Data Master and connected to an IBM PS/2 Model 50Z computer (IBM, Boca Raton, FL, USA). One or two six-port valves were used as sample injector or for solvent switching (Model 7510; Rheodyne, Cotati, CA, USA). Two variable-wavelength UV detectors (Spectroflow 757; ABI-Kratos, Ramsey, NJ, USA) were used; one, with a 1-mm path-length micro-cell, was set at 280 nm and the other, with an 8-mm cell, was set at 600 nm.

Detection

The elution of the protein mixture in the last experiment reported was monitored with two detectors in series, set at 280 and 600 nm, respectively. As hemoglobin absorbs in the visible range of the spectrum, it can be detected at 600 nm without interference from the colorless bovine serum albumin. At this wavelength, the absorption is low enough that a detector with a normal path length of 8 mm could be used. At 280 nm, both proteins absorb strongly (for this wavelength it was necessary to employ the micro-cell with a path length of only 1 mm). Hence it was possible to subtract the trace measured at 600 nm (multiplied by 1.3) from the one at 280 nm, isolating the contribution of serum albumin.

Viscosity measurement

For the determination of sample viscosities a Cannon-Fenske Routine Viscometer 50/286 was used (International Research Glassware, Kenilworth, NJ, USA). The kinematic viscosities of all the glycerol–water and ovalbumin–water solutions used were measured at 20°C. It was found that the viscosity of a 33% glycerol solution was 2.5 times that of water and that the dynamic viscosity of a 15% glycerol solution was approximately equal to that of a 140 mg/ml solution of ovalbumin. The viscosity of glycerol–water solutions increases less rapidly with increasing glycerol concentration than predicted by the classical logarithmic law ($\log \eta_{sol} = x_1 \log \eta_1 + x_2 \log \eta_2$, where x = mole fraction and η = dynamic viscosity), which is expected from a mixture of compounds able to be involved in many hydrogen bonds [13].

SEC experiments

The first experiments were made with water, a low-viscosity eluent (η = 1 cP at 20°C), as mobile phase. A flow-rate of 0.5 ml/min was selected. The eluent for the protein samples was phosphate buffer (pH 6.8) (0.2 mol/l in phosphate). For uracil (*ca.* 0.05 mg/ml) both the above-mentioned buffer and pure water were employed and the same results were obtained. For the experiments made using high-viscosity glycerol solutions in the aqueous buffer or large volumes of viscous samples, the flow-rate was lowered to 0.1 ml/min in order to decrease the column back-pressure and to take into account the influence of lower diffusion coefficients of the sample in the mobile phase on the column efficiency (*i.e.*, to operate the column at a nearly constant reduced velocity).

Optimization of operating procedures

Performance in chromatography is characterized by the column efficiency and the pressure required to move the mobile phase at the required flow velocity. The height equivalent to a theoretical plate, H, is given by the Knox equation [14]:

$$h = \frac{B}{v} + Av^{1/3} + Cv \tag{1}$$

where A, B and C are numerical coefficients, h is the reduced plate height ($h = H/d_p$), v the reduced velocity ($v = ud_p/D_m$), u the linear flow velocity, d_p the average packing-particle diameter and D_m the molecular diffusion coefficient of the solute in the mobile phase.

At constant mobile phase velocity, the reduced velocity is inversely proportional to the diffusion coefficient. This coefficient is related to the molecular characteristics of the solute and solvent. All correlation equations, and especially that derived by Young *et al.* [15], which gives very good results for globular proteins, show that the diffusion coefficient is inversely proportional to the eluent viscosity. Therefore, if we increase the viscosity of the mobile phase, for example by dissolving glycerol in the buffer normally used, we increase its viscosity, decrease the diffusion coefficients and increase the reduced velocity at constant mobile phase flow-rate. If we want to keep constant the reduced velocity to achieve the same column efficiency, we need to reduce the actual flow velocity [16].

Darcy's equation relates the mobile phase velocity to the column length, L, the inlet pressure, ΔP, and the specific permeability, $1/\phi$:

$$u = \frac{\Delta P d_p^2}{\phi \eta L} \tag{2}$$

Thus, at constant inlet pressure, the mobile phase velocity is also inversely proportional to the mobile phase viscosity. By keeping the inlet pressure constant when we change the mobile phase viscosity, we keep constant the reduced velocity and the column efficiency. The retention times and the cycle time increase and the production rate in preparative applications decreases in proportion to the actual mobile phase flow-rate.

RESULTS AND DISCUSSION

A series of experiments were first carried out with lysozyme and ovalbumin. As lysozyme carries a high positive charge at neutral pH, it reacts very sensitively to residual negative charges that are present on almost any silica-based stationary phase. Owing to cation-exchange interactions with the silanol groups on the silica surface, lysozyme was eluted after the dead time, with a retention factor of $k' = 0.2$ at low concentration. When the sample concentration was increased from 0.01 to 0.8 mg in the 20-μl sample injected, the retention volume of the band maximum decreased from 4.1 to 3.8 ml and the peak showed the tailing typical in overloaded elution chromatography [17]. The fact that lysozyme displays a moderate interaction with the column means that neutral molecules will show none.

The elution profile of ovalbumin displayed a different behavior (Fig. 1). When the amount injected was increased over a similar range, the position of the peak

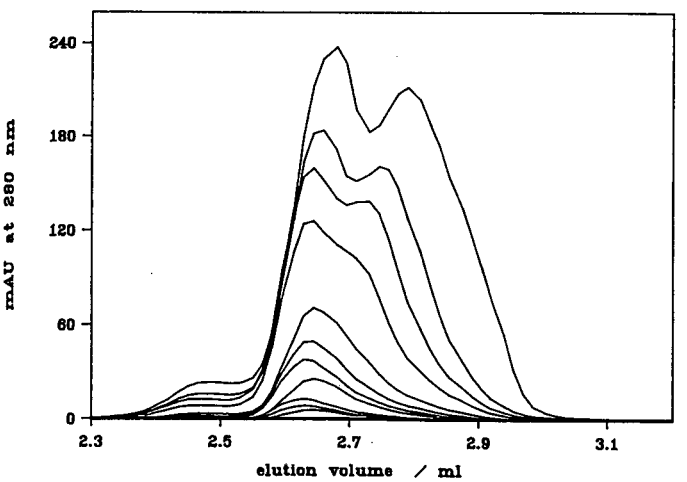

Fig. 1. Elution profiles of ovalbumin (chicken) at increasing concentrations. Sample amounts injected, 0.02–1.2 mg in 20 μl; flow-rate, 0.5 ml/min.

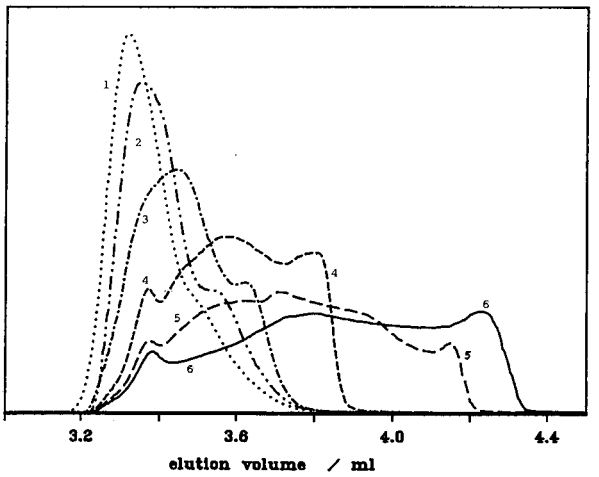

Fig. 2. Elution profiles of uracil solutions with varying glycerol content. Eluent, phosphate buffer; sample volume, 20 μl; flow-rate, 0.1 ml/min. Glycerol concentration: 1 = 0%; 2 = 10%; 3 = 17%; 4 = 33%; 5 = 50%; 6 = 67%.

maximum did not change significantly. However, a shoulder emerged towards higher retention times and grew into a second peak. This means that, although the main part of the sample molecules is eluted in the same manner as at low concentrations, an increasing fraction of the sample is retained in the column by some process. Also seen in Fig. 1 is a small shoulder preceding the main peak, but this is due to an impurity. It can be seen even at very low concentrations on the recorded chromatograms.

The following figures show an explanation for this effect, using a model system that can be manipulated more easily than a protein solution. Instead of ovalbumin solutions, we used as the sample uracil dissolved in the phosphate buffer with a variable concentration of glycerol. Uracil can be easily detected by its UV absorption, whereas the addition of glycerol allowed us flexibility in the choice of the viscosity of the sample solution within wide limits without changing the UV absorbance. As both uracil and glycerol are small molecules, the entire pore volume is accessible to them and they will not separate but will be eluted together with the total liquid volume (the total liquid volume or hold-up volume is the total volume of mobile phase in the column, contained both in the pores and between the particles of the packing).

Fig. 2 displays the chromatograms obtained when the glycerol content of the sample solution was gradually increased from 0 to 67%. The viscosities of the solutions were determined by viscosimetry. Whereas the viscosity of the most concentrated glycerol solution is about ten times that of water and therefore probably out of the range for practical samples, a solution of 33% had a relative viscosity, η/η_{H_2O}, of *ca.* 2.5. This solution was used primarily in the later experiments.

The dotted line (1) in Fig. 2 represents the chromatogram of uracil dissolved in the pure buffer. As the sample viscosity is raised by increasing the glycerol concentration (lines 2–6), an increasing fraction of the sample is spread out over up to three maxima occurring at higher retention times. In all instances, the first peak maximum remains at an elution volume of 3.35 ml, corresponding to the column total liquid

volume. This is the volume at which all the molecules that travel with the mobile phase velocity should appear. With the most viscous sample solutions, fingering of the mobile phase through the viscous sample plug takes place, the low-viscosity eluent being able to bypass part of the sample plug, leaving it behind. The effect increases with increasing viscosity of the sample plug. Only that portion of the sample that is diluted quickly will be carried with the mobile phase and arrive in the detector at the expected time. Although the effect is spectacular only at high sample viscosity, the band shape is already modified at low glycerol concentrations.

The chromatograms shown in Fig. 2 constitute an arbitrary selection from the different peak profiles found in numerous experiments. Even under identical conditions, two successive injections with the same amount of the same solution gave different chromatograms. It is not possible to reproduce the shape or exact location of the shoulders or maxima from one run to the other. This unpredictable behavior is another indication of the nature of the fingering process. Normally in chromatography, it is possible to apply the model of a "one-dimensional" column, assuming that the flow-rate and all concentrations are homogeneously distributed over the whole cross-section of the column. When fingering occurs, however, this is no longer true. In some parts of the column cross-section the mobile phase viscosity is lower and consequently the flow-rate is higher. As this is a self-amplifying process [4], the pattern for this distribution is inherently unpredictable. Consequently, this phenomenon should be relatively less important if a narrower column is used. We can also anticipate that in a large-diameter preparative column, major disturbances will take place on a scale still larger than reported in Figs. 1 and 2 [18,19]. Given the importance of the phenomenon observed, it is tempting to reverse the experiment and to inject a plug less viscous than the mobile phase.

In Fig. 3, the mobile phase contains 30% glycerol and the samples are either more or less viscous than the eluent. At the same time, the flow-rate was lowered to

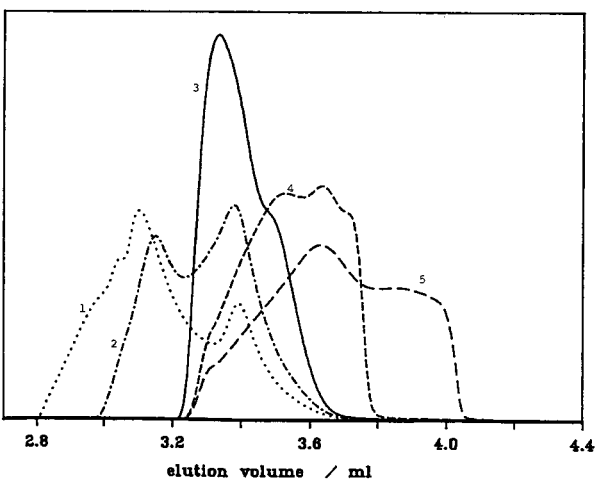

Fig. 3. Elution profiles of uracil solutions with varying glycerol content. Eluent, phosphate buffer with 33% glycerol; sample volume, 20 μl; flow-rate, 0.1 ml/min. Glycerol concentration: 1 = 0%; 2 = 17%; 3 = 33%; 4 = 50%; 5 = 67%.

0.1 ml/min, to lower the pressure drop and the reduced velocity of uracil. This more than compensates for the influence of the higher eluent viscosity, and hence for the lower diffusion coefficient of uracil in the eluent, on the column efficiency. The almost symmetrical peak in the center (3, solid line) belongs to the sample with a viscosity closest to that of the mobile phase. As the two solutions were prepared in different ways, the viscosities do not match perfectly, which leads to the appearance of a shoulder. When the viscosity increases we find elution profiles similar to those in Fig. 2.

On the other hand, when the viscosity of the sample is lower than that of the eluent, the elution band is again split into double peaks, but now this effect takes place on the band front. Part of the sample is eluted earlier than the original peak. In this instance, fingering of the sample front in the more viscous eluent occurs and it is the sample that is able to propagate along the column bed faster than the eluent. Then, the solute does not enter all the interparticle channels and does not have access to the entire packing inner porosity (see the figures in refs. 18 and 19). This leads to an effect similar to exclusion, with part of the mobile phase volume blocked by the more viscous eluent. Because of the random nature of fingering, the effect cannot be controlled and the details of the band profile are not reproducible.

The same result was obtained when a band of ovalbumin (140 mg/ml) was injected in a solution of glycerol (15%) with matching viscosity or in solutions of glycerol with higher (20%) or lower (10%) viscosities. The chromatograms obtained (not shown) exhibit a symmetrical band in the matching viscosity eluent, a bimodal band with a front eluted with a lower retention volume with the low-viscosity eluent and an important shoulder on the large retention volume side with the high viscosity eluent.

In all the experiments reported so far, the sample volume had been limited to 20 μl, the volume of the injector loop. In order to be able to vary the injection volume, a second HPLC pump was used, pumping the sample solution to the column. A switching valve determines which of the two streams would enter the column. At a flow-rate of 0.1 ml/min, it is easy to inject accurately volumes of 50 μl or larger. For Figs. 4–6, the aqueous buffer (viscosity 1 cP) or solutions at the intermediate concentration of 30% glycerol (viscosity 2.5 cP) were used as needed.

When increasing sample volumes are injected, the front of the peak does not change its position. It is always eluted at the column hold-up volume, whereas the rear of the band profile trails with increasing length (Fig. 4). We see that when we inject a sample plug more viscous than the eluent, the change from low to high viscosity still permits a stable front. However, while the sample plug moves through the column, the low-viscosity eluent following it penetrates the sample band through the formation and development of fingering. In this instance, the penetration depth is *ca.* 8 cm (Fig. 4). Only when the injection volume exceeds *ca.* 1 ml (about one third of the column dead volume) does the elution profile reach a plateau at the level of the injection concentration. In other words, it is necessary to inject a sample volume larger than 1 ml to prevent the eluent in the back of the plug from interfering with the front. As there is no retention in SEC, the front and rear boundaries should be symmetrical.

In order to separate more clearly the effects occurring at the front and at the rear of the sample band, a continuous plateau of the uracil sample solution was

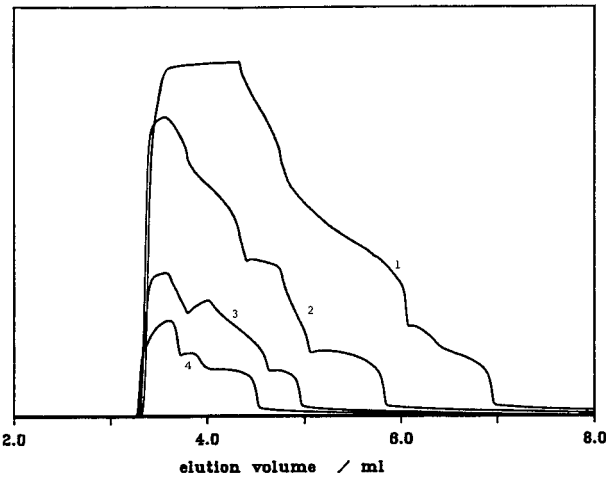

Fig. 4. Elution profiles of a viscous uracil solution, large-volume injections. Eluent, buffer; sample, 0.2–2 ml of a uracil solution containing 33% glycerol; flow-rate, 0.1 ml/min. Injection volume: 1 = 2.0; 2 = 1.0; 3 = 0.4; 4 = 0.2 ml.

delivered to the column by the second pump. Only after the plateau had reached the detector, *i.e.*, after a sample volume of 4 ml had been pumped, the valve was returned to its original position and the first pump resumed feeding pure eluent to the column. The results obtained are summarized in Fig. 5.

The bottom trace shows the plateau of a solution of uracil in pure water with water as eluent. The viscosities of both the eluent and the sample solution are equal and low. The only difference between the elution chromatogram of the plug and its injection profile is the rounding of the corners, owing to the axial dispersion in the

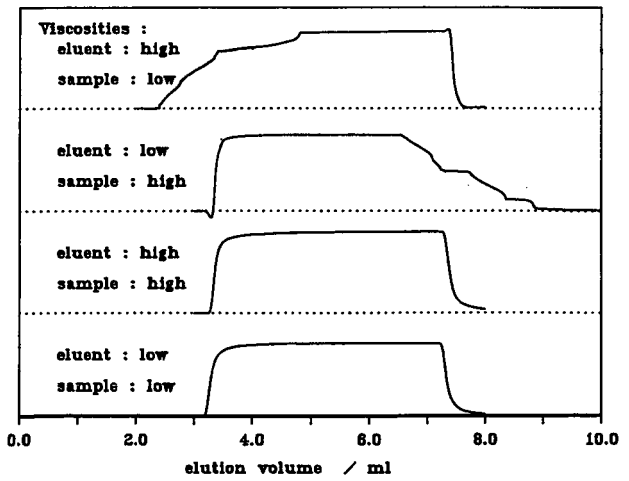

Fig. 5. Elution profiles of large rectangular plugs of uracil solutions of low or high viscosity (0 or 33% glycerol) injected into eluents of low or high viscosity. Volume of injection plug, 4 ml.

column and to the mass-transfer kinetics. When the viscosities of both sample and mobile phase solutions are high but are still equal, the second profile from the bottom in Fig. 5 is obtained. Both solutions contained 30% (v/v) of glycerol to raise their viscosity to about 2.5 times the value for pure water. As expected, this chromatogram differs from the bottom one only slightly and the differences are in the degree of band broadening. These results show that a high sample viscosity alone does not lead to any unusual effects, as long as the viscosity of the eluent and the mobile phase are equal.

The third trace from the bottom in Fig. 5 corresponds to the problematic case encountered in Figs. 1, 2 and 4. The eluent is pure water, while the uracil solution contains 30% of glycerol, as before. The front of the plateau looks almost the same as in the two lower traces. The small dip preceding the front is due to the response of the UV detector to the large change in the refractive index of the sample solution, which itself results from the high glycerol concentration added. This refractive index sensitivity of UV detectors is not unusual. It can also be seen when the sample plug contains only glycerol and no uracil. Instead of a well defined rear front, however, we find that the end of the plateau is eroded into a series of poorly defined steps. The onset of this decay occurs almost 1 ml before the expected end of the plateau, confirming our previous finding that the mobile phase which follows the viscous sample plug penetrates over such a distance (see Fig. 4).

Finally, the top chromatogram in Fig. 5 shows the fourth possible permutation of the relative viscosities of the two solutions: a sample of low viscosity is injected into an eluent of higher viscosity. Now the rear of the plateau has a well defined steep boundary. This demonstrates again that fingering arises only in the transition from a low viscosity to a higher one and not *vice versa*. As before, this step is accompanied by a small peak on the edge of the plateau, owing to the rapid change in the refractive index of the eluent. As already seen in Fig. 3 with the injections of low-viscosity, narrow-plug samples, part of the plateau moves faster than the eluent, bypassing the less accessible parts of the packed bed. The elution of the plateau begins too early, actually before the hold-up volume, illustrating again how a low-viscosity liquid can finger into a high-viscosity one.

In the practice of preparative liquid chromatography, the highly concentrated sample, for instance a protein solution, tends to be more viscous than the eluent which is normally the sample solvent. The previous figures have shown that in this instance the front of the injected plug remains stable, whereas its rear is eroded and broadened. Fingering can be prevented by raising the viscosity of the mobile phase and matching it to that of the sample. This may be inconvenient to achieve, as the viscosity of the sample must be known, and a too low or too high value will lead to unpredictably broadened peaks (see Fig. 3).

Although this procedure permits the achievement of conventionally shaped band profiles, it presents a significant drawback. Even when the viscosities are perfectly matched, the samples will experience more axial dispersion than when the column is operated at the same flow-rate but with a low-viscosity solvent. This is due to the slower diffusion rate caused by the high eluent viscosity. Increasing the solvent viscosity at constant mobile phase velocity in effect increases proportionally the reduced velocity at which the column is operated, and hence decreases its efficiency. Further, the column must be operated at an elevated back-pressure. Alternately, we

may elect to operate the column at the same reduced velocity, and hence at the same efficiency and inlet pressure as with the pure mobile phase. Then the actual flow-rate has to be lowered and the retention times and the cycle time are increased.

Another approach consists in stabilizing the rear boundary of the sample band. As the front needs no further protection, we can continue to use an eluent of low viscosity. However, the rear must be followed by a zone of high-viscosity mobile phase, for hydrodynamic stability. Immediately after the sample has been injected, it is followed by a plug of a more viscous solvent, *e.g.*, the buffered mobile phase containing an adequate amount of glycerol. This plug has to be at least as wide as the penetration depth of fingering, which is about 1 ml in our example. After the passage of an appropriate volume of viscous buffer we can return to the original eluent. It does not matter if the low-viscosity mobile phase "fingers" into the high-viscosity mobile phase plug.

Experimentally this set-up can be realized with two pumps and a switching valve that selects between the two alternating solvents and is placed upstream from the sample injector. Alternatively, one could use one pump for the main eluent and a sample injector with two loops in series, one for the sample and the other for the solvent plug. A flow scheme that permits independently loading of the two loops is through use of a ten-port valve.

Fig. 6 shows the chromatograms obtained for the injection of a 100-μl sample of a uracil solution in water containing 30% of glycerol, followed by plugs of the same viscosity with increasing volumes. For the sample alone a profile similar to those in Fig. 2 is obtained. When the sample is followed by another 100 μl of viscous eluent, the profile actually looks worse than before. Presumably, the two 100-μl bands behave as a single 200-μl injection band, which is penetrated just as easily by the following low-viscosity eluent stream. When the volume of the pusher is increased to

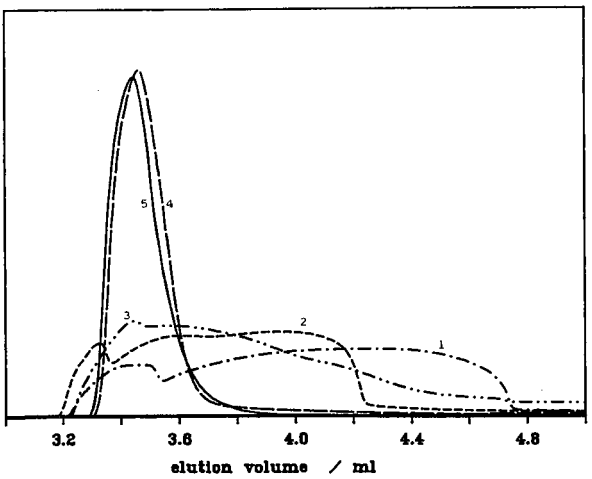

Fig. 6. Elution profiles of viscous uracil solutions. Eluent, buffer; sample, 100 μl of uracil solution containing 33% glycerol, followed by a variable volume plug of buffer with 33% glycerol. Width of viscous plug: 1 = none; 2 = 0.1; 3 = 0.4; 4 = 1.0; 5 = 2.0 ml.

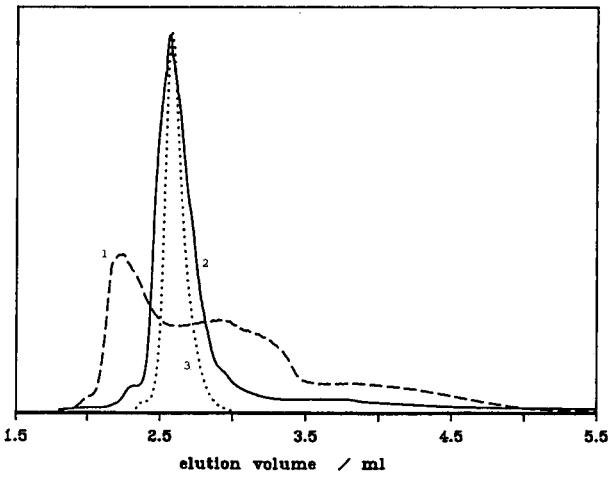

Fig. 7. Elution profiles of ovalbumin (turkey). Injection of low-concentration (expanded 15-fold, dotted line, 3), high-concentration (dashed line, 1) and high-concentration sample followed by a 1.4-ml viscous plug (solid line, 2). Concentrated sample, 2.8 mg in 20 μl; plug buffer with 15% glycerol.

400 μl, the band shape improves only slightly. However, as soon as the width of the plug reaches 1 ml, the sample peak appears narrow and almost symmetrical, very like the peak obtained for the injection of a matched viscosity sample in a high-viscosity stream of mobile phase (see Fig. 3). There is little change when the volume is increased further to 2 ml.

Now that the principle has been established with this model system, it is tested with a more realistic sample. Returning to the ovalbumin sample (*cf.*, Fig. 1), in-

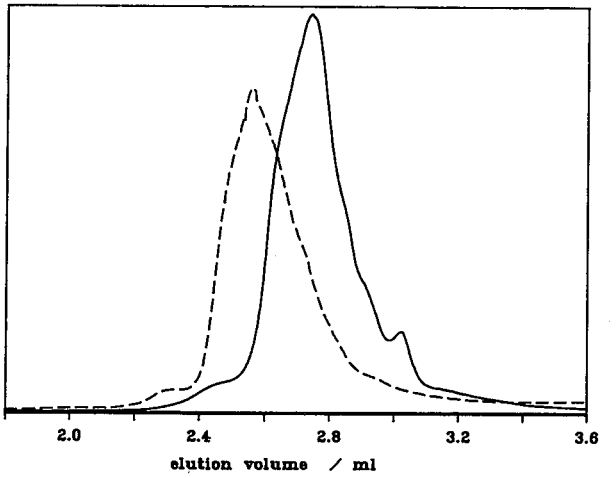

Fig. 8. Elution profiles of ovalbumin (turkey). Two ways to obtain narrow and symmetrical peaks: sample injected into eluent of matching viscosity (dashed line) or into pure buffer followed by a 2-ml plug of viscous buffer (solid line). Same sample as in Fig. 7; plug with 15% glycerol.

jections of a concentrated solution results in the elution profile shown in Fig. 7 with the dashed line (1). The first method for improving the shape of such a peak consists in matching the viscosity of the eluent with that of the sample. In this instance the sample viscosity was roughly equal to that of a 15% solution of glycerol. When chromatographed in this eluent, ovalbumin produced an almost symmetrical peak (solid line, 2). It is compared with the peak profile obtained at low concentration that has been expanded by a factor of 15, to the same peak height (dotted line, 3). The two peaks show the same symmetry, but the chromatogram taken with the high-viscosity eluent at the same mobile phase flow-rate displays significantly higher band broadening. The high-concentration band is almost twice as wide as the low-concentration band and the column efficiency is lower.

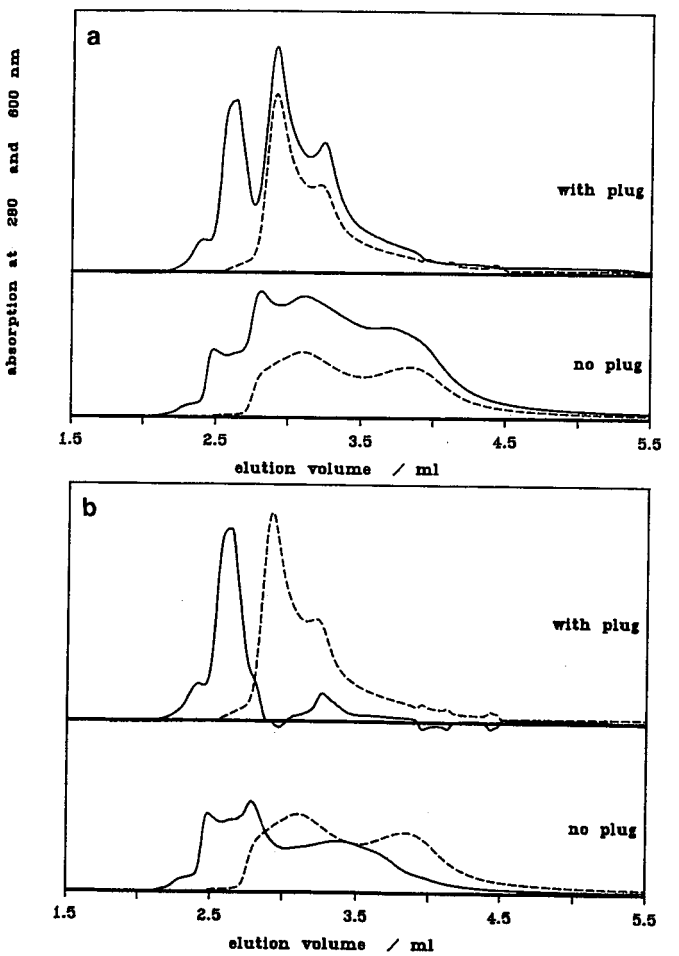

Fig. 9. Elution profiles of a mixture of bovine serum albumin and hemoglobin. Eluent, buffer; sample, 1.4 mg of each protein in 20 μl. Above: injection followed by 2-ml plug of buffer with 15% glycerol. Dashed lines, detector signal at 600 nm; solid lines, (a) signal at 280 nm and (b) difference between signals at 280 and 600 nm.

The result of the alternative procedure of following the injection of the sample by the injection of a viscous plug is shown in Fig. 8. When the protein sample band is followed by a 2-ml plug of the 15% glycerol solution, the peak shape obtained is equivalent or even narrower than that produced with an eluent of matching viscosity. In the experiments with uracil the sample band moved with the same velocity as the following plug, as both solutions contained only small molecules which have access to the entire inner porosity of the packing. Now, with the protein solution, the sample is partially excluded from the pore volume and leaves the viscous plug behind. Even though the protein and the glycerol molecules do not travel together any more, the front of the plug still has a stabilizing effect on the sample band.

Fig. 9 demonstrates the viscosity effect on a size-exclusion separation of the two proteins bovine serum albumin and hemoglobin and the improvement brought about by efficient control of this effect. For this study, two detectors were used; one set at 280 nm responds to both proteins and the other set at 600 nm responds only to hemoglobin. The chromatograms in Fig. 9a show the two detector signals. The chromatograms in Fig. 9b show the individual profiles of the two proteins. After calibration to determine the ratio of the detector responses for hemoglobin, the profile for bovine serum albumin is obtained by subtraction of the signal of the second detector from the signal of the first (in Fig. 9a). This procedure results in the chromatogram in Fig. 9b, containing the individual elution profiles of the two proteins.

The lower chromatograms in Fig. 9a and b show the elution profile obtained normally by injecting 20 μl of the concentrated protein in solution into a pure phosphate buffer. In the upper chromatogram, the injection was followed by a 2-ml plug of buffer containing 15% of glycerol. It is clear that for the lower chromatogram the separation is not sufficient. In contrast, when the injection was followed by a viscous plug (upper chromatograms), a satisfactory separation of the two protein components was achieved. The positive influence on the separation of the injection of a viscous plug after the sample is obvious.

CONCLUSIONS

When operating with high-viscosity samples, the least detrimental approach seems to be to follow the sample with a plug of mobile phase having a viscosity equal to or slightly higher than that of the sample. Glycerol appears to be a good mobile phase additive for this purpose, although low-molecular-weight carbohydrates (*e.g.*, sugar) could also be used. The band profile obtained is nearly identical with that of a very small plug. As the most important sample component moves faster than the unretained glycerol, the sample propagates in a low-viscosity mobile phase. Therefore, it is not necessary to decrease the mobile phase flow-rate in order to keep constant the reduced velocity of the main sample component as it would be if a high-viscosity eluent is used as the mobile phase.

ACKNOWLEDGEMENTS

We thank SynChrom (Lafayette, IN, USA) for the generous gift of the SynChropak GPC 300 column used in this study. This work was supported in part by grant CHE-8901382 from the National Science Foundation and by the cooperative

agreement between the University of Tennessee and the Oak Ridge National Laboratory.

REFERENCES

1 W. W. Yau, J. J. Kirkland and D. D. Bly, *Modern Size Exclusion Liquid Chromatography*, Wiley, New York, 1979.
2 H. Engelhardt, in F. Lottspeich, A. Henschen and K.-P. Hupe (Editors), *High Performance Liquid Chromatography in Protein and Peptide Chemistry*, Walter De Gruyter, Berlin, 1981, p. 55.
3 S. Yamamoto, M. Nomura and Y. Sano, *J. Chem. Eng. Jpn.*, 19 (1986) 227.
4 R. E. Collins, *Flow of Fluids Through Porous Materials*, Rheinhold, New York, 1961, pp. 196–200.
5 J. C. Moore, *J. Chromatogr. Sci.*, 19 (1982) 13.
6 J. C. Moore, *Sep. Sci.*, 5 (1970) 723.
7 P. Flodin, *J. Chromatogr.*, 5 (1961) 103.
8 A. Lambert, *Polymer*, 10 (1969) 213.
9 A. Rudin, *J. Polym. Sci., Part A-1*, 9 (1971) 2587.
10 P. M. James and A. C. Ouano, *J. Appl. Polym. Sci.*, 17 (1973) 1455.
11 N. I. Arne Emneus, *J. Chromatogr.*, 32 (1968) 243.
12 L. R. Snyder and J. J. Kirkland, *Introduction to Modern Liquid Chromatography*, Wiley, New York, 2nd ed., 1979, p. 507.
13 R. C. Reid, J. M. Prausnitz and B. E. Poling, *The Properties of Gases and Liquids*, McGraw-Hill, New York, 4th Ed., 1987.
14 J. H. Knox, *J. Chromatogr. Sci.*, 15 (1990) 352.
15 M. E. Young, P. A. Carroad and R. L. Bell, *Biotechnol. Bioeng.*, 22 (1980) 947.
16 G. Guiochon and M. Martin, *J. Chromatogr.*, 326 (1985) 3.
17 G. Guiochon, S. Golshan-Shirazi and A. Jaulmes, *Anal. Chem.*, 60 (1988) 1856.
18 P. G. Saffman and G. Taylor, *Proc. R. Soc. London, Ser. A*, 245 (1958) 312.
19 R. A. Greenkorn, *Flow Phenomena in Porous Media*, Marcel Dekker, New York, 1983, pp. 220–225.

Journal of Chromatography, 550 (1991) 721–739
Elsevier Science Publishers B.V., Amsterdam

CHROMSYMP. 2295

Hydrodynamic and size-exclusion chromatography of polymers on porous particles

G. STEGEMAN, J. C. KRAAK and H. POPPE*
Laboratory for Analytical Chemistry, University of Amsterdam, Nieuwe Achtergracht 166, 1018 WV Amsterdam (Netherlands)

ABSTRACT

When packed columns filled with porous particles are used for the separation of macromolecules, either size-exclusion chromatography (SEC), hydrodynamic chromatography (HDC) or a combination of the two determine the migration rate. A simple theoretical model, assuming a stagnant pore liquid, was developed to describe a molecular weight calibration graph, which includes both HDC and SEC. In the overall calibration graph, there is a transition from the HDC calibration region at higher molecular weights to an SEC region at lower molecular weights. The smoothness of the transition depends on the ratio of the particle diameter to the pore diameter.

INTRODUCTION

The current interest in high-resolution separation methods for macromolecules and colloidal particles has brought about a number of important new developments. Promising new separation techniques such as field flow fractionation (FFF) [1] and capillary zone electrophoresis (CZE) [2] have shown potential in the development stage and are now being introduced in analytical laboratories. The more mature separation technique size-exclusion chromatography (SEC) has been made applicable to ultra-high-molecular-weight polymers by the development of particles with very large pore sizes. Hydrodynamic chromatography (HDC) on non-porous particles has developed into an inexpensive, high-speed fractionation technique for the sub-micrometre range, applicable to synthetic polymers, colloidal particles and large molecules of biological origin [3]. Of the four separation techniques mentioned, HDC has received least attention up to now. However, recently there has been renewed interest in HDC owing to the availability of 1–3-μm non-porous particles [4,5].

In HDC macromolecules are separated on the basis of their size owing to the hydrodynamic effect [6–10]. This effect occurs in a non-uniform flow profile such as is present in the inter-particle space in packed columns or in open capillaries. The centre of mass of large molecules is excluded from the low-velocity flow regions near the wall. As a result, large molecules migrate with a higher mean velocity than smaller molecules that can approach the wall more closely. Whether this hydrodynamic effect will lead to significant differences in migration rate depends on the aspect ratio, λ, which is the

0021-9673/91/$03.50

ratio of the solute radius to the radius of the flow channels. When λ is very small, the selectivity for polymer separation is low. Typically for $\lambda = 0.005$ the velocity increase is only 1% compared with infinitely small molecules [10]. On the other hand, when λ exceeds a maximum value (in practice about 0.35 for random coil polymers in packed columns), polymer recovery decreases and solutes may eventually block the column. The available volume for separation is accordingly limited, in practice between *ca.* $0.75V_0$ and V_0 [3,5,10], where V_0 is the total mobile phase volume.

In order to obtain suitable values for λ, the diameter of the flow channels should be adapted to the effective diameter of the solutes that are to be separated. For packed columns this means that the particle diameter determines the molecular weight working range. Recently, the use of 1.4–2.7-μm non-porous particles allowed the separation of polymers in the molecular weight range 10^4–10^7 [5]. In principle, particle diameters can be reduced still further to the submicrometre range, but column preparation and pressure drop might then pose problems. For practical reasons it therefore seems unlikely that HDC can be applied to molecular weights below 10^4 in the near future.

SEC has many features in common with HDC, such as the elution order and the limited elution volume range. However, the solute size range in SEC traditionally comprises smaller macromolecules than in HDC. SEC has been most succesful for polymers up to molecular weights of 10^6. Recent developments in SEC have been directed towards raising the upper molecular weight limit through the development of very wide-pore particles.

As HDC and SEC are increasingly covering the same molecular weight range, a sound comparison of both techniques is desired. A comparison based on experimental results was carried out a decade ago by Yau and Kirkland [11]. From evaluation of performance parameters such as the dynamic range, the specific resolution, the discrimination factor and the peak capacity, it was concluded that HDC is inferior to SEC in most areas. Recent developments in HDC make a re-evaluation of these parameters desirable and show that a more theoretical approach, exploring the limits of both techniques, is needed.

In several studies it was shown that SEC for the higher molecular weight range can be optimized when small particles with relatively large pores are employed [12–14]. This means that the inter-particle channels become relatively small compared with the polymers in the SEC working range and HDC effects are already emerging. This combination of HDC and SEC will be treated in detail in this paper. A simple theoretical model for the migration in HDC–SEC will be compared with experimental results. Advantages, prospects and limitations of combined HDC–SEC are also discussed.

THEORY

Polymer migration in SEC

In SEC, a general equation is valid for the retention volume, V_r, of eluted polymers:

$$V_r = V_0 + K_{SEC}V_i \tag{1}$$

where V_0 is the volume of the inter-particle (mobile) solvent, K_{SEC} is the SEC exclusion coefficient and V_i is the (stagnant) intra-particle pore volume.

In order to find expressions for K_{SEC}, several theories have been developed, describing the migration rate of polymers in SEC. Nowadays general agreement exists that size separations in SEC can be fully explained on a steric basis. This reduces the problem of SEC modelling to that of finding the best description of the intra-particle pore structure. The most versatile theoretical models in that respect are developed by Van Kreveld and Van den Hoed [15] and Knox and Scott [16]. They represent the porous packing particles by a structure built up from randomly placed uniform spheres and random-sized touching spheres, respectively. The model of Van Kreveld and Van den Hoed can be compared with experimental results more easily and is therefore applied in this paper.

In the randomly placed uniform spheres model (RSM), the radius of the elementary solid spheres, R_s, is related to the pore fraction of the porous system ψ and the total surface area per unit volume of porous material, S, according to

$$R_s = -\frac{3\psi}{S}\ln\psi \tag{2}$$

The particle porosity (or pore fraction) ψ is defined as

$$\psi = \frac{V_i}{V_i + V_s} \tag{3}$$

where V_s is the volume of the support material. ψ may in practice easily be obtained from the pore volume per weight unit of dry packing material and the skeleton density.

For a polymer with an effective radius r_i the accessible pore fraction ψ' will be

$$\psi' = \psi\left(\frac{R_s + r_i}{R_s}\right)^3 \tag{4}$$

The SEC exclusion coefficient is subsequently obtained from

$$K_{SEC} = \frac{\psi'}{\psi} \tag{5}$$

For a linear random coil polymer in a good solvent the effective polymer radius, r_i, can be calculated from the radius of gyration, r_g. For polystyrenes in tetrahydrofuran (THF), used in this work, the relationship between r_g and the weight-average molecular weight, M_w, is known. For r_i we can write [15]

$$r_i = \tfrac{1}{2}\sqrt{\pi}r_g = 1.23 \cdot 10^{-5} M_w^{0.588}\ (\mu m) \tag{6}$$

Polymer migration in HDC

In HDC on non-porous particles, the migration rate can be expressed by a relative quantity τ_{HDC}:

$$\tau_{HDC} = \frac{v}{v_p} = \frac{V_r}{V_0} \tag{7}$$

where v and v_p are the solvent and polymer migration velocity, respectively. The value of v can be calculated from the breakthrough time of a non-interacting low-molecular-weight molecule (marker) and the column length. For non-porous particles, v is equal to the interstitial velocity v_0.

For the transport of a dilute solution of finite-sized polymers in a cylindrical tube, it is assumed that polymer–wall interactions are absent and that the Poiseuille flow profile is essentially unaffected by the presence of the polymers. For rigid macromolecules, able to sample the accessible radial positions several times during their residence in the tube, τ_{HDC} is related to the aspect ratio, λ, according to [17]

$$\tau_{HDC} = (1 + 2\lambda - C\lambda^2)^{-1} \tag{8}$$

where λ is the ratio of the effective polymer radius r_i to the tube radius. The parameter C includes several hydrodynamic effects such as rotation of the polymer. In the different theoretical models C ranges between 1 and 5.3 [17], depending on the assumptions made in the model and on the type of solute.

Eqn. 8, originally derived for capillary HDC, was also able to predict the migration rate in packed columns when the inter-particle flow channels were represented as a parallel bank of equi-sized capillaries. The equivalent capillary radius was calculated in terms of the hydraulic radius of the packed bed, R_0, and consequently $\lambda = r_i/R_0$ [4,5]. For monodisperse spherical particles R_0 can be calculated from the particle diameter, d_p, and the (inter-particle) bed porosity, ε [3]:

$$R_0 = \frac{d_p}{3} \cdot \frac{\varepsilon}{1 - \varepsilon} \tag{9}$$

where $\varepsilon = V_0/(V_0 + V_p)$, V_p being the volume occupied by particles. Although eqn. 9 has been used frequently in the literature on HDC, monodispersity of the chromatographic beads cannot be assumed in many instances. When a column is filled with different sized spherical particles, R_0 can be calculated from a more general expression:

$$R_0 = 2 \cdot \frac{V_0}{A_0} = 2 \cdot \frac{V_p}{A_0} \cdot \frac{\varepsilon}{1 - \varepsilon} = \frac{\bar{d}_p}{3} \cdot \frac{\varepsilon}{1 - \varepsilon} \tag{10}$$

where A_0 is the total wetted surface area of the non-porous particles and $\bar{d}_p$ is the mean effective particle diameter; $\bar{d}_p$ is defined as [18]

$$\bar{d}_p = \frac{\int_0^\infty d_p^3 f(d_p) \mathrm{d}(d_p)}{\int_0^\infty d_p^2 f(d_p) \mathrm{d}(d_p)} \tag{11}$$

where $f(d_p)d(d_p)$ is the number fraction of particles having radii in the range d_p to $d_p + d(d_p)$. Eqn. 11 can be evaluated numerically using data from an experimentally obtained particle size distribution.

Polymer migration in HDC–SEC

When pore diameters of the SEC support particles are relatively large compared with the particle diameter, HDC effects may become of importance for the largest polymers in the SEC calibration range. Additional exclusion from low-velocity streamlines in the inter-particle space is then superimposed on pore exclusion. In a combined HDC–SEC curve, the smallest molecules are separated on basis of an SEC mechanism, whereas the largest molecules show differing migration rates due to HDC effects. In the intermediate size range both SEC and HDC determine the migration rate

A fundamental description of simultaneous SEC and HDC may lead to complex expressions for the migration rate. We present here a simple treatment by assuming that the flow profile and polymer hydrodynamics are essentially the same for flow in a bed of non-porous and porous particles. A necessary condition for this approximation is the absence of significant flow inside the particles. The effect of pores on polymer migration will only be viewed on a steric basis.

In line with the formalism used in HDC on non-porous particles, we again want to express the migration rate by the ratio of the solvent migration velocity to the polymer migration velocity τ. An expression for τ should be more general than eqn. 8 by also including SEC.

For porous particles, solvent and polymer molecules are distributed over the accessible parts of the mobile liquid in the inter-particle space and the stagnant liquid in the pores with a distribution coefficient of unity. The solvent and polymer migration velocities are thus averaged over the mobile and stagnant liquid fractions of the column, available to the solvent and the polymer molecules, respectively. The solvent migration velocity can therefore be represented as

$$v = v_0 \cdot \frac{V_0}{V_0 + V_i} \tag{12}$$

An expression for the polymer migration velocity is more difficult because the column volume accessible to the centre of mass of a polymer is restricted by both pore exclusion and exclusion from the wall in the inter-particle flow channels. As a first approximation we assume that exclusion from the wall in the inter-particle flow channels occurs as if no pores were present (Fig. 1). This means that the centre of mass of polymers is either in the pores or in the mobile liquid at a distance r_i from the wall. In fact we introduce an imaginary exclusion layer of thickness r_i in front of every pore entrace. This forbidden zone has no physical meaning, but it enables us to represent the migration rate in the inter-particle mobile liquid by expressions developed for HDC on non-porous beads. According to eqn. 7, the mean interparticle polymer velocity is thus equal to v_0/τ_{HDC}. From this inter-particle velocity, the accessible inter-particle volume and the accessible pore volume, we can calculate the polymer migration velocity:

$$v_p = \frac{v_0}{\tau_{HDC}} \cdot \frac{K_{HDC}V_0}{K_{HDC}V_0 + K_{SEC}V_i} \tag{13}$$

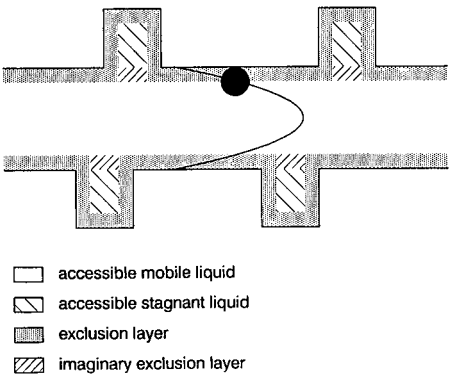

Fig. 1. Graphical clarification of the simple migration model for HDC–SEC.

where K_{HDC} is the fraction of the inter-particle volume that is accessible to the centre of mass of a polymer molecule. In the capillary model of the interstitial channels in a packed bed, we can write

$$K_{HDC} = \left(\frac{R_0 - r_i}{R_0}\right)^2 = (1 - \lambda)^2 \tag{14}$$

An expression for τ is found by combining eqns. 12, 13 and 14:

$$\tau = \tau_{HDC} \cdot \frac{V_0}{V_0 + V_i} + \tau_{HDC} \cdot \frac{K_{SEC} V_i}{(V_0 + V_i)(1 - \lambda)^2} \tag{15}$$

From this general expression for combined HDC–SEC, limiting forms are easily derived. For $\lambda = 0$ we arrive at an equation for pure SEC behaviour. For $V_i = 0$, HDC on non-porous particles is described. For $K_{SEC} = 0$, the migration behaviour is obtained for polymers being excluded from the pores.

Francis and McHugh [19] used a different approach to describe the migration rate in HDC–SEC by including force field effects and pore flow. In the limiting form for zero solute–wall interactions and zero pore flow, their general expression reduces to eqn. 15 except for the absence of the factor $(1 - \lambda)^2$. In practice, their expression will not give significantly different data, because the omitted factor is close to unity.

Refined migration model for HDC–SEC

The present migration model for HDC–SEC can be refined by permitting the presence of polymers between the pore entrance and $(R_0 - r_i)$ as shown in Fig. 2. Conserving simplicity, these partially pore-penetrated polymers are regarded as being in a stagnant liquid. Note that the velocity profile in the interstitial tube is still considered to be unchanged, leaving the migration of point molecules unaffected.

An expression for the volume of stagnant, partially penetrated polymers, $V_{0,s}$ is derived as follows. Rearrangement of eqn. 10 yields an expression for the outside surface area of the packing particles, A_0. A fraction of this surface constitutes pore

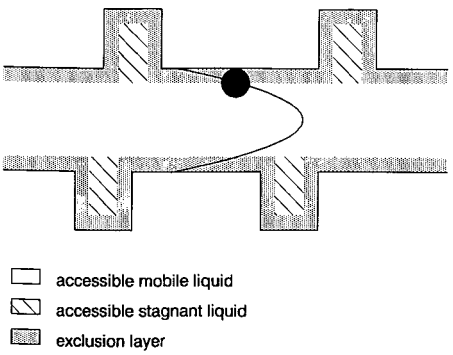

Fig. 2. Graphical clarification of the refined migration model for HDC–SEC.

entrances. We assume that this fraction is equal to ψ. Steric exclusion causes the cross-sectional pore area to be only partly accessible to the mass centre of polymers, the available part being approximately K_{SEC}. For $V_{0,s}$ we subsequently find

$$V_{0,s} = K_{SEC}\psi r_i A_0 = 2K_{SEC}\psi\lambda V_0 \tag{16}$$

The available volume in which polymers are stationary is the sum of $V_{0,s}$ and $K_{SEC}V_i$. An expression for τ can now be derived along the lines of the preceding migration model, yielding

$$\tau = \tau_{HDC} \cdot \frac{V_0}{V_0 + V_i} + \tau_{HDC} \cdot \frac{K_{SEC}(V_i + 2\psi\lambda V_0)}{(V_0 + V_i)(1 - \lambda)^2} \tag{17}$$

From eqn. 17, it is evident that the contribution from $V_{0,s}$ only becomes of importance

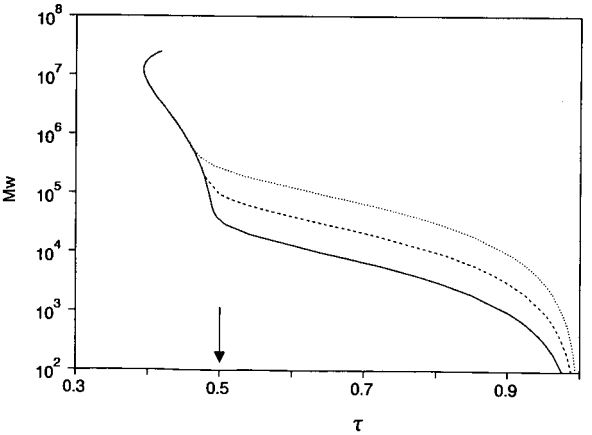

Fig. 3. Theoretical HDC–SEC calibration graphs for different pore radii. Curves are drawn for PS in THF according to eqn. 15. $d_p = 3\ \mu m$; $\varepsilon = 0.4$; $\psi = \frac{2}{3}$; R_p = (dotted line) 20 nm, (dashed line) 10 nm and (solid line) 5 nm. Arrow indicates τ value corresponding to the inter-particle space; $\tau = V_0/(V_0 + V_i)$.

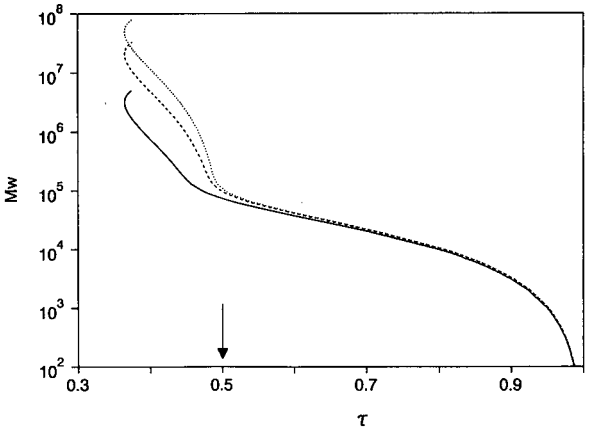

Fig. 4. Theoretical HDC–SEC calibration graphs for different particle diameters. R_p = 10 nm; d_p = (dotted line) 5 μm, (dashed line) 3 μm and (solid line) 1 μm. Other details as in Fig. 3.

for polymer sizes that are relatively large compared with the interstitial channels. In practice, $V_{0,s}$ may often be neglected, reducing eqn. 17 to eqn. 15.

Eqn. 15 was used to construct theoretical HDC–SEC calibration graphs in Figs. 3 and 4. The curves are drawn for polystyrenes in THF using eqn. 6 for the polymer radius. K_{SEC} was obtained employing the RSM model. For the polymer–solvent combination at hand, eqn. 8 for $C = 2.7$ gave good agreement with experimentally measured τ values on non-porous packing particles [5]. The assumptions made above on polymer hydrodynamics justify the use of this C value for polymer migration on porous particles also.

In Fig. 3, the effect of the pore radius on the calibration graph is shown for a constant d_p of 3 μm. For the smallest pore radius reflected, there is a clear distinction between the HDC and SEC calibration regions, although slight mutual overlapping is already present. On increasing the ratio of the pore radius to the particle diameter, R_p/d_p (*i.e.*, increasing the pore radius), the SEC and HDC region increasingly coincide. For the largest pore radius, it can be seen that HDC has a significant effect on the migration rate in the entire SEC molecular weight range.

The effect of the particle diameter for a fixed pore radius of 10 nm is represented in Fig. 4. Again, for the highest ratio R_p/d_p, the combined calibration graph shows the smoothest transition from the HDC region to a region dominated by SEC. For the 5-μm particles, the SEC and HDC regions appear fairly well separated. Calculations nevertheless show that HDC still has a notable influence on polymer migration near the exclusion limit. In order to eliminate these HDC effects, the R_p/d_p ratio should be further reduced. Only when this ratio is infinitely small is polymer separation due purely to a SEC mechanism. In that event, well known theoretical SEC calibration graphs appear, predicting coelution of all excluded polymers.

If eqn. 17 had been used instead of eqn. 15, the lower part of the calibration graph would have been shifted towards higher τ values. The largest shift in τ would have occurred for $\tau \approx 0.75$. However, this shift does not exceed an absolute value of 0.009 (or 1.2% relative), not even for the highest ratio R_p/d_p chosen. The use of eqn. 17 would therefore not have led to visibly distinct graphs.

Currently available SEC packing particles frequently reach R_p/d_p ratios such as those shown in Figs. 3 and 4. This means that nowadays many SEC calibration graphs are significantly affected by HDC effects. Indeed, in the literature chromatograms have appeared showing evident HDC effects [20,21], but these effects are mostly unnoticed or not understood. Such misinterpretations may lead to serious errors. Considerable errors may emerge when the SEC calibration graph is plotted as K_{SEC} *versus* log M_w. In that case V_0 needs to be determined, which is done by recording the elution volume of entirely excluded polymers. For these polymers, HDC effects are largest and the errors in V_0 (and in K_{SEC}) may be several percent [22]. In order to keep this HDC-induced error in V_0 within 1%, λ for an excluded polymer should not exceed 0.005 for $\varepsilon = 0.4$. For many popular SEC packing materials this condition cannot be fulfilled because the limiting λ value is already exceeded by polymers in the SEC dynamic range.

EXPERIMENTAL

Chemicals

Analytical-reagent grade THF and ethanol were obtained from Merck (Darmstadt, Germany). Prior to use these solvents were filtered through a 0.5-μm filter (Type FH; Millipore, Bedford, MA, USA).

Polystyrene standards (PS) with relative weight-average molecular weights, M_w, of $(0.5–2750) \cdot 10^3$ and polydispersities as indicated by the supplier, ranging from 1.04 to 1.18, were obtained from Merck. Polystyrenes with M_w from $300 \cdot 10^3$ to $20\ 150 \cdot 10^3$ and polydispersities from 1.03 to 1.30 were purchased from Macherey, Nagel & Co. (Düren, Germany). Two polystyrene fractions with polydispersities of 1.01 and M_w of $43.9 \cdot 10^3$ and $775 \cdot 10^3$ were obtained from Toyo Soda (Tokyo, Japan). Polystyrene sample solutions of 0.005–0.02% (w/w) were prepared in THF.

Equipment

Chromatographic experiments were carried out using conventional high-performance liquid chromatography equipment. Solvent was delivered by a high-pressure liquid pump (Spectroflow 400; ABI, Ramsey, NJ, USA). A pneumatically driven injection valve with a 0.5-μl internal sample loop (Model Ci4W; VICI, Houston, TX, USA) was modified for high-speed switching by means of an HSSA kit (VICI). A variable-wavelength UV detector (Spectroflow 757; ABI) was adapted for detection on fused-silica capillaries according to Tijssen *et al.* [23]. A 100 μm I.D. capillary, which was directly coupled to the column outlet, served as a low-volume detection cell. The capillary length between the column and the detection cell was *ca.* 10 cm. An integrator (Type 3390A; Hewlett-Packard, Avondale, PA, USA) and a potentiometric recorder (Kompensograph 3; Siemens, Karlsruhe, Germany) were used for signal registration.

Columns

Three columns of 316 stainless steel with dimensions 150 × 4.6 mm I.D. (Chrompack, Middelburg, Netherlands) were packed with 3-μm porous silica particles (Hypersil; Shandon Scientific, Astmoor, Runcorn, UK) following a previously described packing procedure [5]. Two stainless-steel columns, 300 × 7.5 mm I.D.,

TABLE I

HYPERSIL DATA

$\bar{d}_p$ (μm)[a]	$\bar{R}_p$ (nm)	A_{spec} (m^2/g)	$V_{i,spec}$ (ml/g)	ρ_s (g/ml)	ψ	R_s (nm)[b]
3.39	6.0	143	0.634[c] 0.605[d]	2.19	0.582[c] 0.570[d]	7.22[c] 7.15[d]

[a] According to eqn. 11.
[b] According to eqn. 2.
[c] Data of the specific pore volume is determined for $R_p \leqslant 33$ nm.
[d] Data of the specific pore volume is determined for $R_p \leqslant 17$ nm.

containing experimental 3-μm polymeric PLRP-S particles (cross-linked polystyrene–divinylbenzene) with 100 and 300 Å pores, respectively, were a kind gift from Polymer Laboratories (Church Stretton, Shropshire, UK).

In order to verify the theoretical model for HDC–SEC migration, data on the columns and the packing materials were required. The measurements needed were only performed for the silica material, as the polymeric material is not sufficiently rigid. Data on the Hypersil packing material and on one column are listed in Tables I and II.

In Table I the mean effective particle diameter, $\bar{d}_p$, was calculated using a particle size distribution, determined by means of light diffraction (Mastersizer 20; Malvern, Malvern, UK). The mean pore radius, $\bar{R}_p$, and the pore-size distribution were obtained from mercury intrusion (Porosimeter 4000; Carlo Erba, Milan, Italy). The specific surface area, A_{spec}, according to the BET method and the specific pore volume, $V_{i,spec}$, of the packing material were determined by means of nitrogen adsorption (Sorptomatic 1800; Carlo Erba). The skeleton density of the silica support, ρ_s, was determined using a multi-volume helium picnometer (Model 1305; Micromeritics, Norcross, GA, USA). The particle porosity, ψ, was calculated from the specific pore volume and the skeleton density. R_s was calculated from the RSM, where S was obtained from A_{spec}, ρ_s and ψ.

In Table II the hold-up volume of the column ($V_0 + V_i$) was determined by weighing the column filled with ethanol and water. The density of ethanol was obtained using a density meter (Model DMA 10; Paar, Graz, Austria). The volume of the silica support, V_s, was calculated from the weighed column contents of Hypersil and the skeleton density. V_i was determined from the specific pore volume and the weight of the packing material. V_0 was calculated from the hold-up volume and V_i. As

TABLE II

DATA ON ONE COLUMN FILLED WITH HYPERSIL PARTICLES

$V_0 + V_i$ (ml)	V_s (ml)	V_i (ml)	V_0 (ml)	ε
1.808	0.640	0.890[a] 0.850[b]	0.918[a] 0.958[b]	0.374[a] 0.391[vb]

[a,b] As [c,d] in Table I.

a final check, the volume of the empty column was determined from the weighing experiment with ethanol and water. This value (2.456 ml) agreed very well with the sum of ($V_i + V_0$) and V_s from Table II (2.448 ml). The latter value was used for the calculation of ε.

The determination of the specific pore volume proved difficult as there is no clear distinction between the largest intra-particle pores and the smallest inter-particle pores. From the nitrogen adsorption isotherm and the pore-size distribution we concluded that the most appropriate value for the specific pore volume is determined when pores with radii up to 33 nm are included. For reasons to be explained later, we include in Tables I and II the specific pore volume for $R_p \leqslant 17$ nm and consequently the recalculated values for V_i, V_0, ψ, ε and R_s.

RESULTS AND DISCUSSION

HDC–SEC calibration graphs

In order to plot an experimental HDC–SEC calibration graph, τ was determined for a number of polystyrenes with various molecular weights. For this the ratio of the polymer elution time and the elution time for toluene was calculated. This ratio was multiplied by a correction factor to account for partial pore exclusion of the finite-sized toluene molecules. This correction factor is the τ value for toluene when we standardize on the column hold-up volume as determined by weighing. From accurate measurements of the elution volume of toluene and from the column hold-up volume (Table II), we calculated $\tau = 0.9475$ for toluene.

Previous work [5] showed that the magnitude of τ for high-molecular-weight PS depends on the flow-rate. With decreasing flow-rate, the peak maximum shifts to larger apparent molecular weights, until a constant τ value is reached. This flow-rate-dependent migration behaviour is not accounted for in the simple HDC models, but it is evident that these interferences only occur at higher velocities. In order to eliminate flow effects, we were therefore forced to work at low flow-rates. The

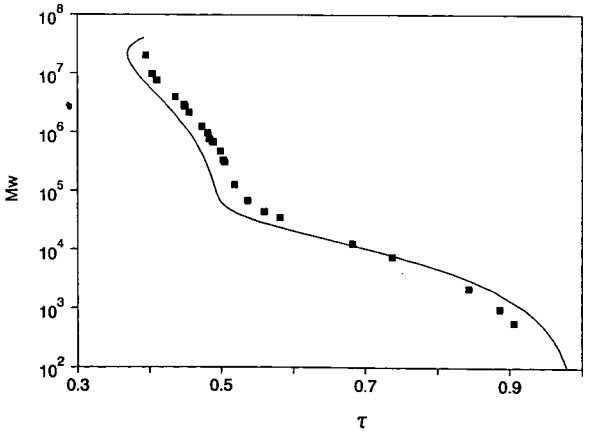

Fig. 5. Theoretical HDC–SEC calibration graph and experimental points for Hypersil packing particles. Details in the text and in Tables I and II ($V_{i,spec} = 0.634$ ml/g).

proper flow-rate settings were established by stepwise halving of the flow-rate until the decrease in τ was smaller than 0.001.

The theoretical calibration graph and the experimental points are presented in Fig. 5. The theoretical line was drawn according to eqn. 17, where K_{SEC} was calculated from the RSM model. From Tables I and II, we took the data that were calculated for a specific pore volume of 0.634 ml/g ($R_p \leqslant 33$ nm). From the graph it appears that the general shape of the experimental curve is predicted well by theory, although the fit is bad. For the entire HDC part, the theoretical line seems shifted to lower τ values compared with the experimental points. Such a parallel shift can, in our opinion, only be explained by a too large ratio V_i/V_0, caused by the uncertainty in the determination of the specific pore volume. We do not expect large errors in the determination of V_s and $V_0 + V_i$ (this is supported by the control measurement of $V_0 + V_i + V_s$).

When the specific pore volume is taken for pores up to 17 nm, we obtain a smaller V_i and consequently a smaller ratio V_i/V_0 (see Table II). The theoretical curve then shows a much better fit to the experimental points, as shown in Fig. 6. The agreement between theory and experimental points is fairly good, especially in the HDC part of the calibration graph. The experimental SEC curve shows a steeper gradient than the theoretical line. This is assumed to be a result of the pore-size distribution, which in the case of Hypersil cannot properly be accounted for by the RSM model. As was shown by Knox and Scott [16], the fit of the SEC part for Hypersil can be improved slightly when accounting for a range of pore sizes in the model. Such a modification makes the model complicated, whereas the improvement for the upper part of the SEC curve is only small.

As the validity of our simple HDC–SEC model hinges upon the fit of the curve near the SEC exclusion limit, Hypersil seems an unfortunate choice. A better fit of the SEC part can be expected for particles with a narrower pore-size distribution [16]. Moreover, for a narrow pore-size distribution, the migration model can be tested more accurately, because the specific pore volume is more reliably determined. Unfortunately, such particles are not easily available in a size range 1–3 μm.

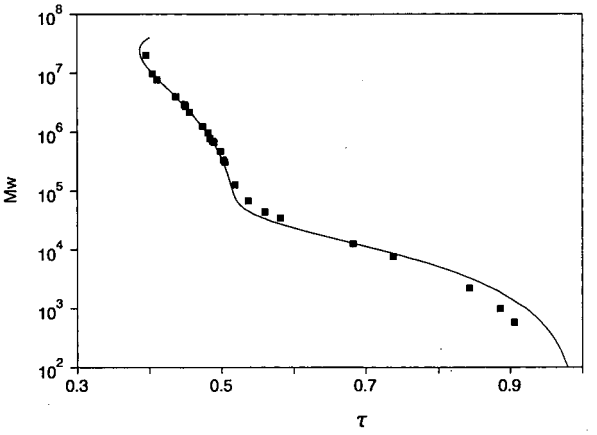

Fig. 6. Theoretical HDC–SEC calibration graph and experimental points for Hypersil packing particles. Details in the text and in Tables I and II ($V_{i,spec}$ = 0.605 ml/g).

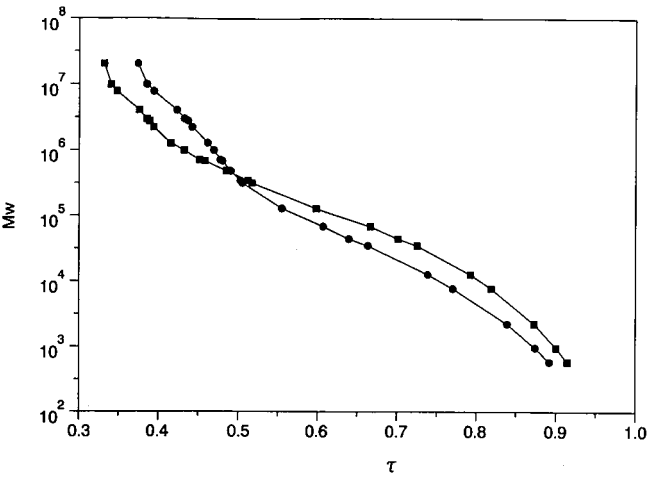

Fig. 7. Experimental HDC–SEC calibration graphs for polymeric packing particles (PL-RPS). $d_p = 3\ \mu m$; R_p = (●) 5 nm and (■) 15 nm.

Unlike the rigid silica particles, porous polymeric beads cannot be fully characterized to test our migration model. Therefore, HDC–SEC on these materials is treated more qualitatively. As for silica particles, polymeric SEC particles smaller than 5 μm are not commercially available. However, the gift of two columns packed with experimental PS–DVB particles, having pore radii of 5 and 15 nm, respectively, enabled us to construct an experimental calibration graph for 3-μm particles. These graphs, shown in Fig. 7, are not corrected for pore exclusion of the marker (toluene). Again we observe that the combined curves cover a large dynamic molecular weight range. Compared with the silica material the SEC and HDC part are even more difficult to distinguish, as a result of the broad pore-size distribution. The intermingling of the HDC and SEC curves is most obvious for the packing with the widest pores. For equal V_i/V_0 and equal R_0, we would expect the HDC parts to coincide for the two columns. The parallel shift of the HDC parts can only be explained by an unequal ratio V_i/V_0. Apparently, for the material with 15-nm pores, the particle porosity was highest or these particles were more densely packed.

Column efficiency

A generalized plate-height equation for packed-column HDC can be written as

$$H = \frac{2\gamma D_m}{v_0} + \frac{2\beta_1 d_p}{1 + \beta_2 (v_0 d_p / D_m)^p} \tag{18}$$

where D_m is the molecular diffusion coefficient, γ, β_1 and β_2 are constants and the exponent p has distinct values in the various plate-height models: Giddings [24], $p = -1$; Huber [25], $p = -\frac{1}{2}$; Horváth and Lin [26], $p = -\frac{1}{3}$. At high linear velocities, dispersion is determined solely by convective mixing (*i.e.*, the second term in eqn. 18) and reaches a constant value of $2\beta_1 d_p$. At lower velocities, the contribution

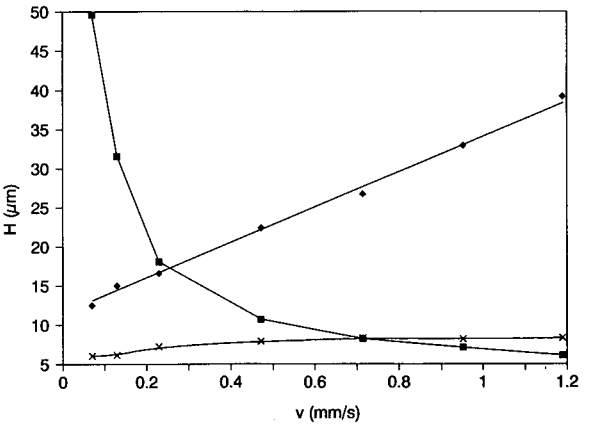

Fig. 8. Plate height *versus* solvent migration velocity on Hypersil packing particles. Solutes: (■) toluene, (◆) PS of M_w 43.9 · 10^3, (×) PS of M_w 775 · 10^3.

from longitudinal molecular diffusion (*i.e.*, the first term) may be significant, especially for fast-diffusing low-molecular-weight molecules.

In SEC, the plate-height equation contains an additional term accounting for resistance to mass transfer inside the particles [12,27]:

$$H = \frac{2\gamma D_m}{v_0} + \frac{2\beta_1 d_p}{1 + \beta_2 (v_0 d_p / D_m)^p} + \frac{V_0(V_r - V_0)d_p^2}{30 V_r^2 \gamma_s D_m} \cdot v_0 \qquad (19)$$

where γ_s is an obstructive factor for diffusion in the inner particle pores. For moderately high velocities the third term becomes the dominant plate–height term. In the high-velocity region where the analysis speed is greatest, plate heights in SEC thus far exceed those in HDC.

The different dispersion behaviours in HDC and SEC were verified experimentally for permeating and excluded solutes on a Hypersil column. The resulting curves of plate height *versus* solvent migration velocity are shown in Fig. 8. The solvent migration velocity instead of the inter-particle velocity was used because it could be calculated more accurately.

For toluene the plate height is mainly determined by longitudinal molecular diffusion, which is a result of the relatively high diffusion coefficient ($D_m = 2.66 \cdot 10^{-5}$ cm^2/s [28]). This causes H to decrease with increasing v whereas the minimum in the plate height curve is not yet reached at the highest solvent velocity in the graph. For PS of M_w 43.9 · 10^3, which is able to penetrate the intra-particle pores partly, longitudinal molecular diffusion is negligible ($D_m = 8.31 \cdot 10^{-7}$ cm^2/s [29]). The dominating plate-height contribution is the slow intra-particle mass transfer that causes H to increase in linear proportion to v. PS of M_w 775 · 10^3 ($D_m = 1.65 \cdot 10^{-7}$ cm^2/s [29]) is excluded from the pores. The plate height is exclusively determined by convective mixing and almost reaches a constant value at high velocities. In the investigated velocity range H is well below 9 μm.

The constant, low value for H in the HDC region shows that a large gain in

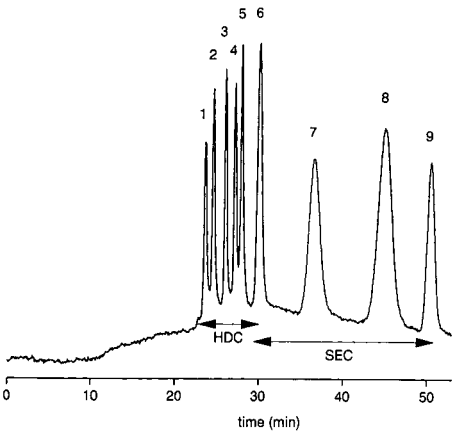

Fig. 9. HDC–SEC separation of polystyrenes on Hypersil particles. Column length = 45 cm (three columns coupled). Solutes: PS of M_w (1) $4000 \cdot 10^3$; (2) $2200 \cdot 10^3$, (3) $775 \cdot 10^3$; (4) $336 \cdot 10^3$; (5) $127 \cdot 10^3$; (6) $43.9 \cdot 10^3$; (7) $12.5 \cdot 10^3$; and (8) $2.2 \cdot 10^3$; and (9) toluene.

analysis time can be achieved at high v without sacrificing much efficiency. This provides important potential for high-speed separation of high-molecular-weight polymers. However, we shall meet an important proviso shortly, in terms of shear induced effects.

The dispersion and migration phenomena in HDC–SEC discussed so far are well illustrated by the separation of PS on Hypersil shown in Fig. 9. As can be seen, the combination of HDC and SEC yields a wide molecular weight dynamic range. In this instance the working range covers molecular weights from a few hundred to about $2 \cdot 10^7$, roughly the sum of the separate HDC and SEC ranges. When such a wide dynamic range is desired in SEC, a large pore-size distribution and consequently large particle diameters are required. However, the price that has to be paid for such an expanded dynamic range is a poorer column selectivity and larger plate heights, leading to poorer resolution. In combined HDC–SEC a large dynamic range is obtained while conserving high column selectivity and efficiency.

For the HDC–SEC columns in Fig. 9, a peak capacity of 66 was calculated [30] assuming a plate number of 75 000. From the chromatogram it appears that the number of fully resolved peaks is much lower. This can be explained by the polydispersity of the polymer samples, which largely determines the peak widths for most polymer fractions used [31]. In addition, for the calculation of the peak capacity we assumed a plate height of 6 μm for all polymer samples, which is certainly not true in the SEC region, as was shown by Fig. 8.

Effect of flow-rate

From the plate height–velocity curves in HDC–SEC, it appeared that high solvent migration velocities can be used without loss of column efficiency for the highest molecular weights. However, high flow-rates are often unfavourable for high-molecular-weight flexible polymers as shear degradation and deformation then become of importance.

In the literature on SEC, the subject of shear degradation has been treated frequently [32]. Although few experimental data on shear degradation have been published, it is well understood that one should be cautious not to use too high solvent velocities when analysing high-molecular-weight compounds. In HDC–SEC the avoidance of shear degradation restricts the solvent migration velocity even more than in SEC, because the molecular weights that can be determined are comparatively much higher.

Another effect of shear occurring at elevated flow-rates even before the limit of backbone breakage is reached is polymer deformation. When hydrodynamic forces are greater in magnitude than forces of chain relaxation arising from Brownian motion, the polymer chain is subjected to flow-induced stretching. The polymer diameter transverse to the direction of flow is then decreased, leading to higher τ values in HDC. Flow-rate-dependent data should be avoided whenever possible, so in HDC mobile phase velocities should be reduced to some critical value below which deformation is negligible.

Hoagland and Prud'homme [33,34] extensively studied shear-induced effects on polymer shape in HDC on non-porous particles. For partially hydrolysed polyacrylamide they found that the polymer size obtained from HDC decreased with flow-rate. Sample reinjection experiments at reduced flow-rates showed that degradation had not occurred. These results could be explained successfully by means of shear deformation using the Deborah number, *De*, the ratio of hydrodynamic forces to Brownian forces. They used the following expression for the Deborah number for flexible polymer chains in good solvents [33]:

$$De = k\left(\frac{\bar{v}}{d_p}\right)\frac{6.12\Phi\eta r_g^3}{RT} \tag{20}$$

where the constant k depends on the structure of the flow channels in the column, having an approximate nominal value $k = 6$ [35]. The superficial solvent velocity is $\bar{v}$, Φ is the Flory–Fox parameter (*ca.* $2.5 \cdot 10^{23}$ mol^{-1}), η is the solvent viscosity, r_g is the radius of gyration of the polymer at equilibrium, R is the gas constant and T is the temperature. At $De < 0.1$ molecular stretching can be considered insignificant and the polymer has its equilibrium diameter. At $De = 0.1$, there is an onset of deformation and at $De = 0.5$ a critical elongation rate is reached where coiled polymers are transformed into extended fibre-like chains [33].

For the experimental HDC–SEC calibration graph we were able to avoid flow-rate-dependent τ values by choosing sufficiently low flow velocities. For the Hypersil column some additional measurements of τ at higher flow-rates were carried out for PS of M_w $9800 \cdot 10^3$. According to eqn. 20, this polymer starts to deform at $\bar{v} = 0.033$ mm/s ($De = 0.1$), which corresponds to a solvent migration velocity $v = 0.044$ mm/s.

The results in Table III show an increase in τ with solvent velocity. This is in accordance with the coil-stretch theory and indicates shear deformation at higher velocities. At the highest flow-rate settings the chromatograms showed an apparent bimodal molecular weight distribution with two peak maxima. This is reflected in the table by two τ values in the last column. In order to check whether shear degradation had occurred, all eluted samples were collected and reinjected at the lowest flow-rate

TABLE III

EFFECT OF THE SOLVENT MIGRATION VELOCITY ON τ FOR PS OF M_w $9800 \cdot 10^3$

Column: Hypersil.

v (mm/s)	De^a	τ
0.031	0.089	0.427
0.059	0.13	0.427
0.073	0.16	0.435
0.14	0.32	0.451
0.29	0.65	0.464/0.499
0.58	1.3	0.481/0.602

[a] De = Deborah number according to eqn. 20.

setting. The τ values obtained were now equal to those for the original sample, demonstrating that shear degradation was not yet of importance in the selected flow-rate range. We cannot yet explain the double peaks at high velocities.

CONCLUSIONS

In the molecular weight calibration graph for porous packing particles with relatively wide pores there is a gradual transition from a region dominated by SEC to an HDC region. An experimentally obtained HDC–SEC calibration graph for porous silica particles was successfully described by a migration model where the inter-particle flow channels were represented as open tubes while the intra-particle structure was depicted by the random uniform spheres model. This model also showed that HDC already has a significant effect on polymer migration in many currently available SEC columns.

The advantages of combined HDC–SEC over separate operation are a higher peak capacity and an expanded molecular weight dynamic range.

In HDC (and in HDC–SEC) shear rates are sufficiently high to cause stress-induced changes in polymer conformation. This forms a serious restriction for the high-speed analysis of high-molecular-weight flexible polymers. Shear deformation of high-molecular-weight polystyrenes was demonstrated by an increase in τ with solvent velocity.

Further studies on HDC–SEC should be aimed at the development and testing of small monodisperse porous particles with a narrow pore-size distribution. The validity of the migration model remains to be tested for various d_p/R_p ratios. The assumed stagnancy of the pore liquid should be checked and possible effects of pore flow on migration and dispersion should be evaluated.

SYMBOLS

A_0 wetted surface area in a bed of non-porous particles
A_{spec} specific surface area

De	Deborah number
D_m	molecular diffusion coefficient
d_p	particle diameter
H	theoretical plate height
K_{HDC}	accessible fraction of the inter-particle space
K_{SEC}	accessible fraction of the intra-particle pores (SEC exclusion coefficient)
k	constant accounting for the structure of the flow channels in a packed column.
M_w	weight-average molecular weight
R	gas contant
R_0	hydraulic radius of the packed bed
R_p	pore radius
R_s	radius of an elementary solid sphere in the RSM
r_g	radius of gyration
r_i	effective polymer radius
S	surface area per unit volume of a porous system
T	absolute temperature
V_0	inter-particle solvent volume
$V_{0,s}$	volume containing stagnant partially penetrated polymers
V_i	intra-particle (pore) volume
$V_{i,spec}$	specific pore volume
V_p	volume occupied by particles ($= V_i + V_s$)
V_r	retention volume
V_s	volume of the solid support material
v	solvent migration velocity
$\bar{v}$	superficial solvent velocity
v_0	inter-particle solvent velocity
v_p	polymer migration velocity
$\beta_1,\beta_2,\gamma,\gamma_s$	constants in the plate-height equation
ε	bed porosity $= V_0/(V_0 + V_p)$
η	solvent viscosity
λ	aspect ratio, r_i/R_0
ρ_s	skeleton density of the solid support material
τ	relative migration rate in HDC–SEC
τ_{HDC}	relative migration rate in HDC
Φ	Flory–Fox parameter
ψ	pore fraction of porous particles (or particle porosity)
ψ'	pore fraction accessible to a finite-sized molecule

ACKNOWLEDGEMENTS

The authors thank Dr. F. P. Warner, Polymer Laboratories, for the kind gift of two packed columns. Mrs. Mittelmeijer-Hazeleger is thanked for characterizing the silica particles.

REFERENCES

1 W. G. Kuhr, *Anal. Chem.*, 62 (1990) 403R.
2 K. D. Caldwell, *Anal. Chem.*, 60 (1988) 959A.
3 A. J. McHugh, *CRC Crit. Rev. Anal. Chem.*, 15 (1984) 63.
4 J. C. Kraak, R. Oostervink, H. Poppe, U. Esser and K. K. Unger, *Chromatographia*, 27 (1989) 585.
5 G. Stegeman, R. Oostervink, J. C. Kraak, H. Poppe and K. K. Unger, *J. Chromatogr.*, 506 (1990) 547.
6 E. A. DiMarzio and C. M. Guttman, *J. Polym. Sci.*, 7 (1969) 267.
7 E. A. DiMarzio and C. M. Guttman, *Macromolecules*, 3 (1970) 131 and 681.
8 H. Small, *J. Colloid Interface Sci.*, 48 (1974) 147.
9 A. W. J. Brough, D. E. Hillmann and R. W. Perry, *J. Chromatogr.*, 208 (1981) 175.
10 D. C. Prieve and P. M. Hoysan, *J. Colloid Interface Sci.*, 64 (1978) 201.
11 W. W. Yau and J. J. Kirkland, *J. Chromatogr.*, 218 (1981) 217.
12 J. C. Giddings, *Adv. Chromatogr.*, 20 (1982) 217.
13 G. Guiochon and M. Martin, *J. Chromatogr.*, 326 (1985) 3.
14 H. Engelhardt and G. Ahr, *J. Chromatogr.*, 282 (1983) 385.
15 M. E. van Kreveld and N. van den Hoed, *J. Chromatogr.*, 83 (1973) 111.
16 J. H. Knox and H. P. Scott, *J. Chromatogr.*, 316 (1984) 333.
17 R. Tijssen, J. Bos and M. E. van Kreveld, *Anal. Chem.*, 58 (1986) 3036.
18 W. J. Beek and K. M. K. Muttzall, *Transport Phenomena*, Wiley, London, 1980, p. 119.
19 D. C. Francis and A. J. McHugh, *ACS Symp. Ser.*, No. 245 (1984) 3.
20 J. J. Kirkland, *J. Chromatogr.*, 125 (1976) 231.
21 J. H. Knox and F. McLennan, *J. Chromatogr.*, 185 (1979) 289.
22 G. Stegeman, J. C. Kraak and H. Poppe, in preparation.
23 R. Tijssen, J. P. A. Bleumer and M. E. van Kreveld, *J. Chromatogr.*, 260 (1983) 297.
24 J. C. Giddings, *J. Chromatogr.*, 5 (1961) 61.
25 J. F. K. Huber, *J. Chromatogr. Sci.*, 7 (1969) 85.
26 Cs. Horváth and H. Lin, *J. Chromatogr.*, 126 (1976) 401.
27 J. C. Giddings, L. M. Bowman, Jr., and M. N. Myers, *Macromolecules*, 10 (1977) 443.
28 R. C. Reid, J. M. Prausnitz and T. K. Sherwood, *The Properties of Gases and Liquids*, McGraw-Hill, New York, 3rd ed., 1977.
29 W. Mandema and H. Zeldenrust, *Polymer*, 18 (1977) 835.
30 E. Grushka, *Anal. Chem.*, 42 (1970) 1142.
31 J. H. Knox and F. McLennan, *Chromatographia*, 10 (1977) 75.
32 H. G. Barth and F. J. Carlin, Jr., *J. Liq. Chromatogr.*, 7 (1984) 1717.
33 D. A. Hoagland and R. K. Prud'homme, *Macromolecules*, 22 (1989) 775.
34 D. A. Hoagland and R. K. Prud'homme, *J. Appl. Polym. Sci.*, 36 (1988) 935.
35 W. M. Kulicke and R. Haas, *Ind. Eng. Chem., Fundam.*, 23 (1984) 308.

Journal of Chromatography, 550 (1991) 741–749
Elsevier Science Publishers B.V., Amsterdam

CHROMSYMP. 2154

Isolation of an interleukin 2-binding receptor from activated lymphocytes by high-performance immunoaffinity chromatography

TERRY M. PHILLIPS
Immunochemistry Laboratory, George Washington University Medical Center, Washington, DC 20037 (USA)

ABSTRACT

Isolation of a lymphokine-binding receptor, from activated lymphocyte membranes, can be achieved by high-performance immunoaffinity chromatography (HPIAC), using immobilized antibodies against human interleukin 2 (IL-2), as the ligand and natural IL-2 as the receptor probe. Activated lymphocytes were reacted with IL-2, sonically disrupted and their membranes solubilized, prior to passage through the HPIAC column. The IL-2 acted as an efficient receptor probe, which helped to maintain the integrity of the receptor during the isolation procedure and also acted as an attachment antigen for the immunoaffinity ligand. Recovery of the bound receptor was achieved by dissociation of the receptor–antigen–immobilized ligand complex by the action of chaotropic ions and collection of the released receptor from the column effluent during the elution phase of the separation.

INTRODUCTION

The structure of receptors on the membranes of activated lymphocytes is currently of great interest to molecular biologists, membrane biochemists and immunologists. The isolation of these receptors by conventional biochemical techniques is tedious and time consuming, following which the recovered receptor exhibits either decreased activity or no activity at all [1]. However, the isolation and recovery of membrane proteins can be effectively achieved by several different techniques, such as immunoprecipitation [2–5], ion-exchange chromatography [6], size-exclusion chromatography [6], lectin affinity chromatography [7,8], or immunoaffinity chromatography using antibodies, immobilized either directly to activated supports or bound to supports coated with specialized proteins, such as protein A and streptavidin [9–11].

Most cells possess receptors for exogenous growth factors, interaction with which leads to cytoplasmic signaling and cell proliferation. Interleukin 2 (IL-2) is a growth factor that is important in lymphocyte clonal expansion and regulation following antigenic stimulation. Recently, great interest has centered on isolating and

0021-9673/91/$03.50

characterizing IL-2-binding receptors, in an attempt to understand better their involvement in lymphocyte activation.

In this paper, a procedure is described for the isolation of a lymphocyte IL-2-binding receptor, using immobilized anti-human IL-2 antibodies and human IL-2 as the receptor probe.

EXPERIMENTAL

Materials

Solid glass beads (diameter 150–212 μm) and all laboratory chemicals were obtained from Sigma (St. Louis, MO, USA). 3-Aminopropyltriethoxysilane and 1,1′-carbonyldiimidazole were obtained from Aldrich (Milwaukee, WI, USA). Purified streptavidin was purchased as a lyophilized, pure product from Pierce (Rockford, IL, USA) and reconstituted in 50 m*M* sodium carbonate buffer (pH 9.0). Mouse immunoglobulin G_1 (IgG_1) monoclonal antibody (MAb) reactive with human IL-2 was obtained as a purified IgG preparation from benzyme (Cambridge, MA, USA) and purified natural human IL-2 was obtained from Collaborative Research (Bedford, MA, USA). Glass-lined, stainless-steel columns and column fittings were purchased from Alltech (Deerfield, IL, USA). Activated lymphocytes were obtained from consenting patients with systemic lupus erythematosus, seen at the Rheumatology Clinic at the George Washington University Medical Center.

Derivatization of glass beads

The glass beads were prepared as described by Babashak and Phillips [12]. The beads were washed by sedimentation in 0.1 *M* hydrochloric acid, followed by two washes in doubly distilled water. This removed manufactoring impurities from the bead surface, before preparing them for silanization and derivatization by placing 100 g of the washed beads in 500 ml of 0.1 *M* hydrochloric acid and gently sonicating for 25 min, followed by sedimentation in 1000-ml portions of 0.1 *M* hydrochloric acid. This process was repeated, using fresh acid solutions, until the acid supernatant became clear. The beads were then removed and air-dried, before refluxing them for 30 min in 500 ml of 1 *M* nitric acid, with constant agitation. The beads were recovered, air-dried and resuspended in 500 ml of 10% (v/v) 3-aminopropyltrietoxysilane dissolved in toluene. This suspension was gently refluxed for 16 h with constant agitation.

Following silanilization, the beads were recovered and washed twice in 500 ml of 95% methanol before being transferred to fresh 95% methanol and refluxed for 20 min, to remove the excess of silanizing agent. The beads were allowed to settle,washed three times in doubly glass-distilled water and air-dried prior to derivatization of the reactive side-groups.

The reactive carbonyldiimidazole (CDI) side-groups were attached to the bead surface by suspending the beads in 300 ml of dioxane and slowly adding 6 g of 1,1′-carbonyldiimidazole [13,14]. The mixture was placed in a 500-ml capped conical flask and incubated for 6 h at room temperature in an oscillating shaker. The beads were then recovered and thoroughly washed in dioxane by sedimentation and decantation before being air-dried and immediately coated with streptavidin.

Preparation of streptavidin-coated beads

A 100-g amount of the CDI-derivatized beads was suspended in 200 ml of doubly distilled water prior to the addition of 200 ml of 50 m*M* sodium carbonate buffer (pH 9.0) containing 5 g of streptavidin. The mixture was placed in a 500-ml capped conical flask and incubated for 18 h at 4°C in an oscillating shaker. Following this incubation, the beads were allowed to settle and washed ten times in 0.01 *M* sodium phosphate buffer (pH 7.4) by sedimentation and decantation. Attachment of the streptavidin to the beads was checked by incubating a 500-μl drop of the bead suspension, obtained after the last wash, with fluorescein-labelled biotin and examining the beads under a fluorescence microscope. Following satisfactory coating of the beads, they were sedimented, recovered and resuspended in 500 ml of 0.01 *M* sodium phosphate buffer (pH 7.4).

Biotinylation of monoclonal antibodies

The monoclonal anti-IL-2 antibody was biotinylated by using the hydrazine biotinylation technique described by O'Shannessy and Quarles [15]. This technique requires modification of the carbohydrate portion of the antibody by oxidation with periodate. Briefly, this was achieved by suspending the 100 mg of antibody in 10 ml of 0.1 *M* sodium acetate buffer (pH 5.0) and cooling to 4°C. A 10-ml volume of a 10 m*M* solution of cold sodium metaperiodate was added to the antibody before incubation for 20 min at 4°C in the dark. The reaction was stopped by adding 50 ml of 5% (w/v) ethylene glycol and dialyzing the solution against 0.01 *M* sodium phosphate (pH 7.4) for 18 h at 4°C, with five changes of the dialysate. The antibody was then removed from the dialysis tubing and placed in a capped glass tube. To this were added 10 ml of 0.01 *M* sodium phosphate buffer, (pH 7.4) containing 15 mg/ml of sodium cyanoborohydride and 25 mg/ml of biotin hydrazine, and the mixture was placed in a rotating mixer for 1 h at room temperature. The reaction was stopped by dialysis against 0.1 *M* sodium phosphate buffer (pH 7.4) overnight at 4°C.

Preparation of HPIAC column

The biotinylated MAb preparation was adjusted to 150 μg/ml in 0.1 *M* sodium phosphate buffer (pH 7.4) and 2 ml of this solution were added to 10 g of streptavidin-coated beads. The mixture was placed in a 15-ml capped tube and placed on an end-over-end mixer for 4 h at 4°C. The beads were then washed five times in 0.1 *M* sodium phosphate buffer (pH 7.4). Finally, the MAb-coated beads were slurry-packed into 100 × 4.6 mm I.D. glass-lined stainless-steel high-performance liquid chromatographic (HPLC) columns at 250 p.s.i., using a conventional pump-driven slurry packing apparatus.

Preparation of IL-2–IL-2-binding complex and isolation of lymphocyte membranes

Prior to disruption and solubilization of their membranes, active lymphocytes were isolated from whole blood by centrifugation at 400 *g* for 15 min in a Ficoll gradient [16]. The lymphocyte band was recovered and the cells were washed three times in RPMI 1640 medium and adjusted to $5 \cdot 10^6$ cells/ml. A 100-ng amount of human IL-2 was added to 1 ml of the cell suspension, incubated for 30 min at 37°C and the cells were recovered by centrifugation. The cells were washed twice in RPMI 1640 medium and sedimented by centrifugation at 800 *g* for 10 min. The cell pellet

was recovered, frozen and thawed three times and then sonicated for 2 min at maximum power. The sonicated pellet was resuspended in 2 ml of 0.1 *M* sodium phosphate buffer (pH 7.4) and the membrane fraction was isolated by centrifugation at 10 000 *g* for 30 min. The membrane-enriched supernatant was mixed with an equal volume of 1% (w/v) sodium deoxycholate and incubated for 30 min at room temperature. Finally, the solubilized membrane sample was centrifuged for 1 h at 10 000 *g* and the supernatant was applied to the immunoaffinity columns.

High-performance immunoaffinity chromatography

The MAb/bead-packed HPIAC column was installed in a Beckman (Palo Alto, CA, USA) Model 340 isocratic HPLC system equipped with a Model 112 pump, a Model 160 UV detector (set at 280 nm) and a Shimadzu (Columbia, MD, USA) C-R1B recording peak integrator. The elution profile was automatically controlled by a Model III OPG/S gradient controller (Autochrom, Milford, MA, USA). Samples (2.5 μg of protein) were introduced into the system by injection through an Altex 210 injection port, equipped with a 100-μl sample loop.

The column was isocratically developed in either 0.1 *M* sodium phosphate buffer (pH 7.4) with no additives, 0.1 *M* sodium phosphate buffer (pH 7.4) plus 0.5% of (w/v) sodium deoxycholate (a detergent which causes minimal effect on antibody–antigen interactions) or with 0.1 *M* sodium phosphate buffer (pH 7.4) to which 0.5% (w/v) of sodium deoxycholate and 0.1% (w/v) of polyvinylpolypyrrolidone (PVP) had been added. In all instances, the initial isocratic phase was maintained for 15 min at a flow-rate of 0.5 ml/min. Throughout the entire run, the column temperature was maintained at 4°C by a glass column jacket, attached to a recycling ice-bath. Following the initial 15-min run, during which the IL-2 of the II-2–IL-2-receptor complex bound to the immobilized antibody, an elution recovery phase was started. An elution gradient was developed by adding 0–2.5 *M* sodium thiocyanate to the running buffer over a further 15 min and maintaining the upper limit of the gradient for a further 5 min, before recycling the column. This was achieved by reversing the gradient until the column was returned to the initial running conditions. Fractions of 200 μl of the eluted material were collected in 500-μl Beckman microfuge tubes in a modified ISCO Cygnet fraction collector (ISCO, Lincoln, NB, USA) and dialyzed overnight at 4°C against 0.01 *M* sodium phosphate buffer (pH 7.4). Analysis of the isolated materials was performed by polyacrylamide gel electrophoresis (PAGE) on a 10–30% linear gradient gel containing 0.1% (w/v) sodium dodecyl sulfate (SDS). Following separation, the gels were fixed in methanol–acetic acid (4:1) and silver stained [17]. To establish the identity of the SDS-PAGE-isolated bands, the gel profiles were blotted to nitrocellulose membranes by the technique described by Towbin *et al.* [18]. The blotted membranes were stained with I^{125}-labelled human IL-2 by incubating them for 2 h in a solution of 0.1 *M* sodium phosphate, (pH 7.4) to which 1 ng/ml of radiolabelled IL-2 had previously been added. The membranes were washed five times in 0.1 *M* sodium phosphate buffer (pH 7.4) and the bound IL-2 probe was rendered visible by autoradiography.

Receptor binding studies

The functional ability of the immunoaffinity-isolated IL-2 receptor to bind its substrate was tested by incubating the HPIAC-isolated receptor isolated in the three

different buffers with I^{125}-labelled human IL-2 and plotting the binding efficiency against time [19]. Briefly, 5 ng of membrane protein from the immunoaffinity peak B, separated by the three buffer systems, were incubated at 37°C for 30 min with 500 fg of labelled IL-2. The IL-2 binding capacities of the three immunoaffinity-isolated membrane preparations were compared with the binding capacity of $1 \cdot 10^6$ intact lymphocytes, incubated with an identical amount of labelled IL-2.

RESULTS AND DISCUSSIONS

Analysis of over 200 batches of streptavidin-coated glass beads has shown that a 1-g batch of beads can be coated with between 0.76 and 1 mg of streptavidin. Once coated, the beads were able to bind between 120 and 185 μg of biotinylated antibody, which represents *ca.* 200 μg of bound antibody per column. Stability analysis showed that the columns could effectively be recycled between 20 and 30 times before the immobilized antibody became either detached or lost its activity. All columns remained stable for up to 6 months when stored at 4°C.

Fig. 1 shows a typical immunoaffinity chromatogram produced by passing the solubilized lymphocyte membrane preparation over the immobilized antibody. Three major peaks are produced, at 8 min (peak A), 23 min (peak B) and 25 min (peak C). SDS-PAGE of the starting materials and the contents of the three peaks revealed fifteen visible bands in the starting material and fourteen bands in peak A. Analysis of peak B demonstrated the presence of only one band at *ca.* 55 kilodalton, which is similar to that described for the IL-2 receptor isolated by other immunochemical techniques [20–22] and corresponded to the band missing from the profile of peak A (Fig. 2). Peak C contained a single band of *ca.* 15 kilodalton, which is similar to the molecular weight, estimated by the manufacturer, of the human IL-2 probe. Ligand-

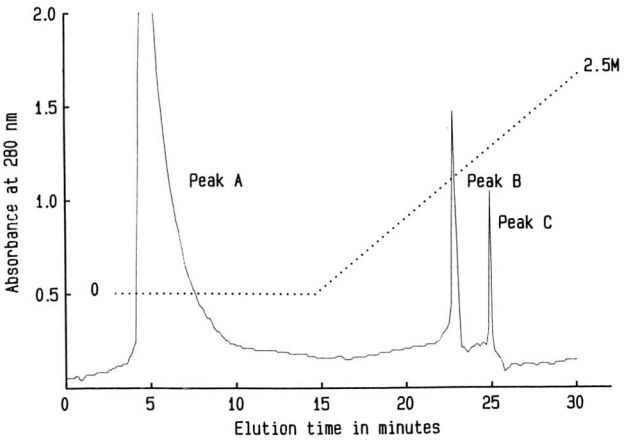

Fig. 1. HPIAC isolation of an IL-2 receptor from activated human lymphocytes using a 100 × 4.6 mm I.D. column, packed with anti-human IL-2 antibody, immobilized on streptavidin-coated glass beads. Peak A represents the unbound material, peak B contains the IL-2 receptor and peak C contains the IL-2 probe. The chromatogram was developed at 0.5 ml/min in 0.1 *M* sodium phosphate buffer–0.5% (w/v) sodium deoxycholate–0.1% (w/v) PVP buffer (pH 7.4). The elution profile was monitored at 280 nm with the detector set at 0.008 a.u.f.s. The dotted line represents the elution gradient.

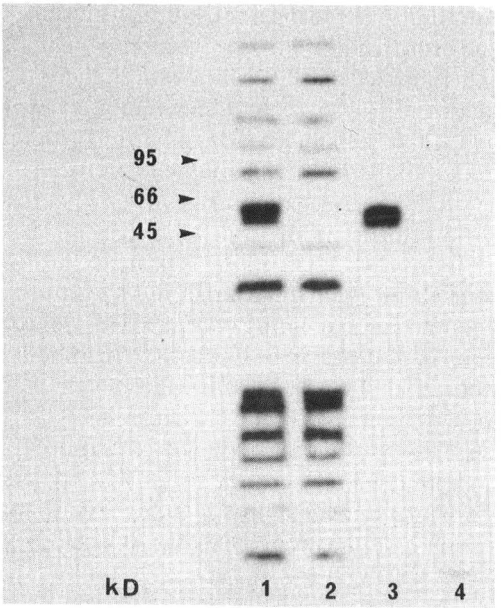

Fig. 2. SDS-PAGE of the immunoaffinity chromatographic peaks. Lane 1, 2 μg of starting cell membrane material; lane 2, unreactive membrane material from peak A of the immunoaffinity chromatogram; lane 3, material retained by the immobilized antibody and eluted in peak B of the chromatogram; lane 4, the material eluted in peak C of the chromatogram. Numbers above kD indicate reference molecular weights in kilodaltons, calculated from molecular weight standards.

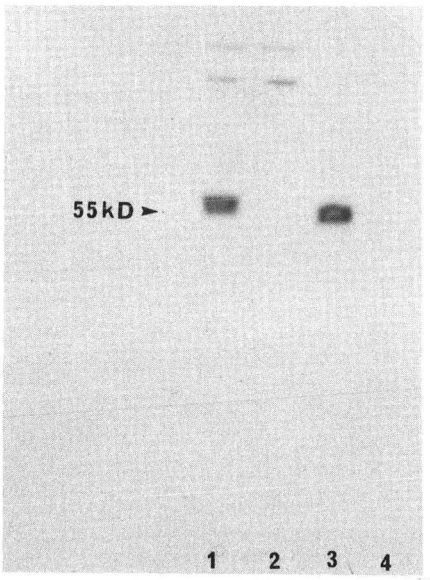

Fig. 3. IL-2 ligand blotting of the SDS-PAGE profiles shown in Fig. 2. Lane 1, starting membrane material; lane 2, peak A from the immunoaffinity chromatogram; lane 3, peak B from the immunoaffinity chromatogram; lane 4, peak C from the immunoaffinity chromatogram.

TABLE I

EFFECT OF HPIAC BUFFERS ON PROTEIN RECOVERY

Buffer	Starting material[a] (ng)	Peak A (ng)	Peak B (ng)	Peak C (ng)	Total recovery (%)
0.1 *M* NaH_2PO_4	2500	2219	61	22	92.1%
0.1 *M* NaH_2PO_4–0.5% deoxycholate	2500	2240	74	29	93.7%
0.1 *M* NaH_2PO_4–0.5% deoxycholate–0.1% PVP	2500	2259	87	31	95.1%

[a] Total protein content of the starting material, including the IL-2 probe, as measured by the BCA method (Pierce, Rockford, IL, USA).

staining of nitrocellulose blots of the SDS-PAGE profiles with radiolabelled IL-2 demonstrated strong binding to the 55 kilodalton band of the starting material and peak B. In addition, the ligand bound to an 85- and a 100-kilodalton band of both the starting material and peak A. No staining was observed in the 55-kilodalton range in peaks A or C (Fig. 3).

IL-2 binding studies demonstrated that the composition of the buffer used in the primary phase of the HPIAC isolation had an effect on the activity of the eluted receptor, even though little difference could be detected in the total protein recovered in each peak (Table I). The maximum IL-2 binding by intact cells took place at 60 min and all comparison measurements were taken at that time point. Taking the intact cell binding as a reference, it was found that the receptor isolated with the three different chromatographic buffers exhibited different binding capacities (Fig. 4). The receptor

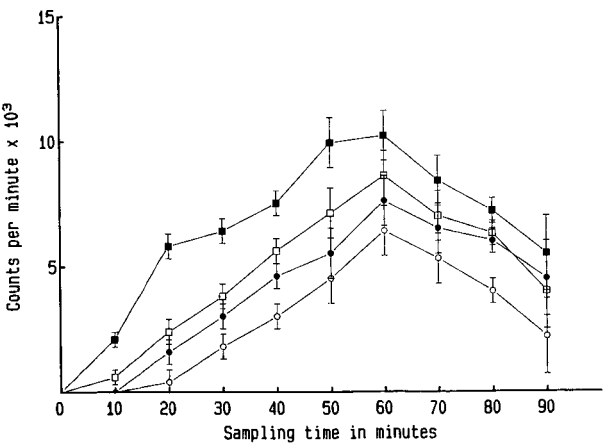

Fig. 4. Binding of radiolabelled IL-2 to HPIAC IL-2-isolated membrane receptor and intact cells. (○) Receptor isolated in 0.1 *M* sodium phosphate buffer (pH 7.4); (●) receptor isolated in 0.1 *M* sodium phosphate–0.5% (w/v) sodium deoxycholate buffer (pH 7.4); (□) receptor isolated in 0.1 *M* sodium phosphate–0.5% (w/v) sodium deoxycholate–0.1% (w/v) PVP buffer (pH 7.4); (■) intact lymphocytes. Points are the means of ten experiments ± the standard error of the mean.

isolated in 0.1 *M* sodium phosphate–0.5% (w/v) sodium deoxycholate–0.1% (w/v) PVP buffer (pH 7.4) retained the highest degree of binding activity, which equalled 85% of that shown by intact cells. The receptor isolated with 0.1 *M* sodium phosphate–0.5% (w/v) sodium deoxycholate buffer (pH 7.4) demonstrated a binding efficiency that was equal to 74% of the intact lymphocytes, while the receptor isolated in 0.1 *M* sodium phosphate buffer (pH 7.4) gave the lowest reactivity (63%).

Although HPIAC can isolate a receptor in less than 30 min, a significant amount of activity is lost during the process. It is unknown whether the loss of receptor function occurs during the initial binding of the receptor–substrate complex to the immobilized antibody or during the elution phase. Experiments with both acid and chaotropic elution have shown no difference in the activity of the recovered receptor and new elution agents are under investigation. It has been demonstrated that both acid and choatropic ions interfere with the tertiary structure of proteins [23], and perhaps these agents cause structural changes which a affect the binding capacity of the isolated receptor. However, sodium thiocyanate has been shown to be an effective elution agent for immunoaffinity procedures, especially membrane receptor [24,25], and has the added advantage that it does not appreciably damage the immunoaffinity support. Improved elution agents are required before HPIAC can achieve its full potential as the separation technique of choice for membrane receptor isolation.

CONCLUSIONS

Lymphocyte membrane receptors can be isolated by HPIAC using immobilized antibodies directed against the receptor substrate, which is used as a receptor probe. The technique is rapid and reasonably efficient, isolating receptors which retain 70–85% of their original binding efficiency in a form suitable for further biochemical or immunochemical analysis.

REFERENCES

1 S. Lapanje, *Physicochemical Aspects of Protein Denaturation*, Wiley, New York, 1978, p. 56.
2 R. A. Roth, B. Maddox, K. Y. Wong, R. L. Styne, G. V. Vliet, R. E. Humble and I. D. Goldfine, *Endocrinology*, 112 (1983) 1865.
3 J. C. Venter, *J. Biol. Chem.*, 258 (1983) 4842.
4 T. R. Malek, J. D. Ashwell, R. N. Germain, E. M. Shevach and J. Miller, *Immunol. Rev.*, 92 (1986) 81.
5 W. C. Greene, J. M. Depper, M. Kronke and W. J. Leonard, *Immunol. Rev.*, 92 (1986) 29.
6 J. L. Wittliff, *LC·GC*, 11 (1986) 1092.
7 J. W. Buckle and G. M. W. Cook, *Anal. Biochem.*, 165 (1986) 463.
8 D. Josic, W. Hofmann, R. Habermann and W. Reutter, *J. Chromatogr.*, 444 (1988) 29.
9 T. M. Phillips, in A. R. Kerlavage (Editor), *Receptor Biochemistry and Methodology*, Alan R. Liss, New York, 1989, p. 129.
10 T. M. Phillips and S. C. Frantz, *J. Chromatogr.*, 444 (1988) 13.
11 T. M. Phillips, S. C. Frantz and J. J. Chmielinska, *Biochromatography*, 3 (1988) 149.
12 J. V. Babashak and T. M. Phillips, *J. Chromatogr.*, 444 (1988) 21.
13 M. T. W. Hearn and E. L. Harris, *J. Chromatogr.*, 218 (1981) 509.
14 G. S. Bethell, J. S. Ayers, M. T. W. Hearn and W. S. Hancock, *J. Chromatogr.*, 219 (1981) 361.
15 D. J. O'Shannessy and R. H. Quarles, *J. Immunol. Methods*, 99 (1987) 153.
16 H. Wigzell, *Transplant. Rev.*, 5 (1970) 76.
17 A. Chrambach and D. Rodbard, in B. D. Hames and D. Rickwood (Editors), *Gel Electrophoresis of Proteins: a Practical Approach*, IRL Press, Washington, DC, 1981, p. 93.

18 H. Towbin, T. Staehelin and J. Gordon, *Proc. Natl. Acad. Sci. U.S.A.*, 76 (1979) 4350.
19 J. Haberman, C. R. Packhardt and P. C. Scriba, *Acta Endocrinol. (Copenhagen)*, 232 (1980) 135.
20 W. J. Leonard, J. M. Deppler, T. Uchiyama, K. A. Smith, T. A. Waldmann and W. C. Greene, *Nature (London)*, 300 (1982) 267.
21 L. A. Rubin, C. L. Kurman, W. E. Biddison, N. D. Goldman and D. L. Nelson, *Hybridoma*, 4 (1985) 91.
22 T. Diamantstein and H. Osawa, *Immunol. Rev.*, 92 (1986) 5.
23 E. Rouslahti, in E. Rouslahti (Editor), *Immunoadsorbents in Protein Purification*, University Press, Baltimore, 1976, p. 3.
24 V. Sica, G. A. Puca, A. M. Molinari, F. M. Buonaguro and F. Bresciani, *Biochemistry*, 19 (1980) 83.
25 T. M. Phillips, *Adv. Chromatogr.*, 29 (1989) 133.

Journal of Chromatography, 550 (1991) 751–764
Elsevier Science Publishers B.V., Amsterdam

CHROMSYMP. 2077

Cascade-mode multiaffinity chromatography

Fractionation of human serum proteins

JERKER PORATH* and PER HANSEN
Biochemical Separation Centre, Biomedical Center, Uppsala University, Box 577, S-751 23 Uppsala (Sweden)

ABSTRACT

The group-resolving power of cascade-mode multiaffinity column chromatography (CASMAC), was demonstrated with human serum as a model mixture. More than 99% of the serum proteins were adsorbed in the same high salt-containing buffer on a tandem column consisting of (1) immobilized Zn^{2+} on triscarboxymethyl diamine gel followed by (2) thiophilic (T) gel, (3) Zn^{2+} bound to the new tridentate chelating adsorbent dipicolylamine (DPA) agarose, (4) hexyl–thioether C_6-S agarose and (5) Ni^{2+}–DPA agarose. After the adsorption step the immobilized metal ion affinity gels were attached to the top of tandem columns of other adsorbents (T gel, Sephadex G-25 for desalting and Mono-Q) and the elution conditions were selected such that further group separation was achieved. High resolution, high recovery, easy manipulation and high capacity are characteristic features of the cascade process with these adsorbents. The advantage of CASMAC is particularly striking when, with a given number of adsorbents, the overall number of operations involving adsorption, desorption, washing, buffer change and substance concentration can be effectively minimized.

INTRODUCTION

Two main principles of separation have been developed and have become the most powerful tools for the isolation of biopolymers: chromatography and electrophoresis. Dr. Lloyd R. Snyder is one of the leading scientists who have made the most significant contributions in the field of liquid chromatography. In this paper, in his honor, we would like to pay him our homage by describing some developmental steps in another direction of liquid chromatography suited to the purification and isolation of biological substances. We stress the use of chemical affinities as important factors for separation.

The importance of separation methods, chromatography in particular, for progress in biochemical sciences can hardly be overestimated. Chromatographic materials are flooding the market, but most adsobents consist of variations on a few themes, many of them being ion exchangers with the same kind of simple ligands. Assessment of their relative merits is not an easy matter. The published methods have usually been selected by trial and error or accidently applied; only a few are based on a rational approach to the solution of a particular separation or isolation problem.

0021-9673/91/$03.50

There are two strategies for increasing the efficiency of chromatographic fractionation of a complex mixture: (1) to maximize the separation power in a bed of a given adsorbent or (2) to separate the components according to their affinities for a number of selected adsorbents, operating ideally according to different separation principles such as metal ion affinity or charge, supplemented, if necessary, by molecular size-descriminating methods. By use of rapid batch methods, Scopes and Porath [1] have recently shown how it is possible to screen a large number of different adsorbents in a sequential manner to produce a rational scheme for the fractionation of a number of enzymes in bacterial and yeast extracts.

To give this multiple affinity technique a high resolving power and ease of application, we suggest the use of sequential adsorption of material in tandem-coupled beds, each bed containing a different adsorbent. To increase further the resolution it is possible (1) to use selective elution or displacement from each bed separately or (2) to transfer the eluent to a new bed or a tandem column with a supplementary kind of affinity characteristics. The latter technique results in a cascade scheme of fractionation of the original mixture. This technique has been described previously by Porath [2] and Scopes [3]. In this paper such a cascade mode of fractionation will be exemplified by use of immobilized metal ion affinity (IMAC), hydrophobic, thiophilic interaction and ion-exchange chromatography as applied to human serum proteins.

EXPERIMENTAL

All chemicals were of analytical-reagent grade, obtained from commercial sources, and were used as purchased. Normal human serum was obtained from the blood bank at the University Hospital in Uppsala (Sweden). LC- and M-Partigen Immunodiffusion plates were purchased from Beringwerke (Marburg, Germany).

The triscarboxymethyldiamine (TED) gel, the hydrophobic C_6-S agarose and the thiophilic (T) agarose were synthesized as described previously by Porath and co-workers [4–6]. Sepharose 6B was activated with 1,4-butanediol diglycidyl ether, then treated with ethylene diamine followed by carboxymethylation with bromoacetic acid under alkaline conditions to produce the TED gel, with a nitrogen content of 920 μmol/g dry weight. The Zn^{2+}-loaded TED gel was found to contain 990 μmol/g dry weight. The hydrophobic C_6-S gel was synthesized from the 1,4-butanediol diglycidyl ether-activated Sepharose 6B by coupling hexanethiol in alkaline suspension under reducing condition. The T gel was obtained by treatment of Sepharose 6B with divinyl sulphone in carbonate buffer (pH 11.0) followed by coupling mercaptoethanol in sodium carbonate buffer (pH 9.0). The sulphur contents of the C_6-S agarose and T gel were 100 μmol/g and 8.1%, respectively, calculated on the dry adsorbents.

Dipicolylamine Sepharose 6B (DPA agarose)[a]

This new adsorbent was prepared as follows. Sepharose 6B (600 g) was washed thoroughly with deionized water and the excess water was removed on a glass filter under gentle suction. The moist gel was suspended in 120 ml of deionized water and 200 ml of 4 *M* NaOH containing 38 ml of epichlorohydrin and 1.72 g of $NaBH_4$. The suspension was stirred for 2 h. A 200-ml volume of 4 *M* NaOH and 200 ml of ep-

[a] Patent pending.

ichlorohydrin were added in portions of about 10 ml each for 3 h with adequate stirring. The stirring was continued overnight and the suspension was then washed thoroughly with deionized water. The moist activated gel was suspended in 600 ml of 1 *M* Na_2CO_3 containing 16.8 ml of picolylamine. The suspension was stirred for 48 h and then washed thoroughly with water and 1 *M* Na_2CO_3.

The picolylamine-coupled gel was suspended in 1.5 l of 1 *M* Na_2CO_3 (pH 12) and 1 l of ethylene glycol containing 40 g of picolyl chloride hydrochloride was slowly added. The suspension was coupled at 80°C in a water-bath for 6 h and was then cooled to room temperature overnight. The final dipicolylamine gel, DPA agarose, was thoroughly washed with water, 10% acetic acid and water again until neutral. The DPA agarose used had a nitrogen content of 590 μmol/g dry weight. The metal ion content of the Zn^{2+}- and Ni^{2+}-loaded gels was found to be 290 and 480 μmol/g dry weight, respectively.

Analytical procedures

The absorbance of the chromatographic fractions was measured at 280 nm with an Ultraspec II spectrophotometer (LKB, Bromma, Sweden). The analysis of the chromatographic fractions was performed by electrophoresis in slabs of 4–30% polyacrylamide gradient gel (PAA 4/30; Pharmacia, Uppsala, Sweden) according to the manufacturer's manual using a GE-2/4 gel electrophoresis apparatus with an EPS 500/400 electrophoresis power supply (Pharmacia). The electrophoresis buffer was 0.09 *M* Tris–0.08 *M* boric acid–0.0025 *M* Na_2EDTA (pH 8.4) and the running conditions were 150 V for 16 h. Fixing was performed with 10% sulphosalicylic acid solution for 30 min, staining with 0.02% Coomassie Brilliant Blue R-250–7% acetic acid in water overnight and destaining with 7% acetic acid overnight. Discontinuous sodium dodecyl sulphate–polyacrylamide gel electrophoresis (SDS-PAGE) (T = 12.2%, C = 1%)[a] was performed by using a gel electrophoresis apparatus from the BMC workshop (Biomedical Centre, Uppsala, Sweden) and the same power supply as above. The upper buffer was 0.040 *M* boric acid–0.41 *M* Tris–0.1% SDS (pH 8.64) and the lower buffer 0.42 *M* Tris (pH 9.18). The running conditions were 200 V for 5 h, the fixing conditions 50% methanol–7% acetic acid in water overnight, the staining conditions 0.05% Coomassie Brilliant Blue R-250 in the above fixing solution for 2–3 h and the destaining conditions were 10% methanol–10% acetic acid in water overnight. Identification and determination of protein concentration were performed by immunodiffusion using LC- and M-partigen immunodiffusion plates according to the manufacturer's manual.

Chromatography

The experiments were performed at room temperature using the Pharmacia FPLC system consisting of two P-500 pumps, an LCC-500 liquid chromatography controller, a Frac-100 fraction collector, a UV-1 single-path monitor and a Rec-482 two-channel recorder. Unless stated otherwise, the following buffers were used as eluents and will be referred to in abbreviated form throughout. Each buffer was de-aerated prior to use.

---

[a] C = g N,N'-methylenebisacrylamide (Bis)/%T; T = g acrylamide + g Bis per 100 ml of solution.

Buffer I (equilibration buffer): 50 m*M* sodium phosphate, 0.5 *M* in NaCl, 0.5 *M* in K_2SO_4 (pH 7.6).

Buffer II: buffer I, 0.1 *M* in imidazole.

Buffer III: 50 m*M* sodium phosphate (pH 7.6).

Buffer IV: 40% (v/v) ethylene glycol in buffer III.

Buffer V: 30% (v/v) 2-propanol in buffer III.

Buffer VI: 20 m*M* sodium phosphate (pH 8.0).

Buffer VII (final gradient buffer): buffer VI, 0–0.5 *M* in NaCl.

Immobilization of metal ions (Ni^{2+} and Zn^{2+}) was done as follows. A 4–5-g amount of the appropriate gel was thoroughly washed with deionized water over a glass filter. The gel was then transferred to a beaker containing 50 ml of a 20 m*M* metal ion solution. After *ca.* 15 min the gel was thoroughly washed with water over a glass filter to remove excess of and loosely bound metal ions. All gels (except Mono-Q, which is a prepacked column purchased from Pharmacia) were degassed prior to packing and packed at a constant flow-rate of 1 ml/min. The total gel volume was *ca.* 6 ml, except for the T and C_6-S gels, which were *ca.* ten and five times larger, respectively, to ensure the capacity needed for adsorption of immunoglobulins and albumin, respectively. The effect of human serum on the new adsorbent was then determined.

A column containing Zn^{2+}-DPA agarose was equilibrated with 50 m*M* sodium phosphate (pH 7.6), 0.5 *M* in NaCl, at a flow-rate of 0.5 ml/min. Human serum (1 ml) was applied and the chromatogram was developed with 0.5 *M* sodium acetate (pH 5.5), 0.5 *M* in NaCl, followed by 50 m*M* sodium phosphate (pH 7.6), 0.5 *M* in NaCl, 50 m*M* in imidazole. The fractions were read manually, pooled and further analysed by electrophoresis in polyacrylamide gradient gels. This procedure was repeated with Ni^{2+}-DPA agarose.

The beds were connected in tandem to produce a main-line tandem column consisting of the following beds in series: Zn^{2+}-TED agarose, T gel, Zn^{2+}-DPA agarose, C_6-S agarose and Ni^{2+}-DPA agarose (see Fig. 1 left). The tandem was equilibrated with five volumes of buffer I. The flow-rate was kept constant at 0.5 ml/min throughout the development of the chromatogram. The sample of human serum was equilibrated to buffer I by using a PD-10 column (1 ml of equilibrated human serum was found to have an absorbance $A_{280} \approx 42$). A 10-ml volume of human serum was applied to the column and the elution proceeded isocratically until the effluent adsorbance reached the baseline. The material passing through the train of beds without adsorption is denoted fraction A. The beds were disconnected and the adsorbed material was displaced from each bed separately, in some instances being transferred to the top of new "side-line" columns consisting in one instance of the T gel and in others of Sephadex G-25 followed by Mono Q. The following fractions were thus obtained (see Fig. 1).

Fraction B: the Zn^{2+}-TED agarose was connected in tandem to a T gel bed (6 ml). The material adsorbed on the Zn^{2+}-TED agarose was displaced with buffer II and allowed to pass into the T gel. These two columns were disconnected and the T gel bed was eluted as described previously [4], *i.e.*, using buffers III, IV and V in sequence.

Fraction C: the column containing T gel was developed as described previously [4].

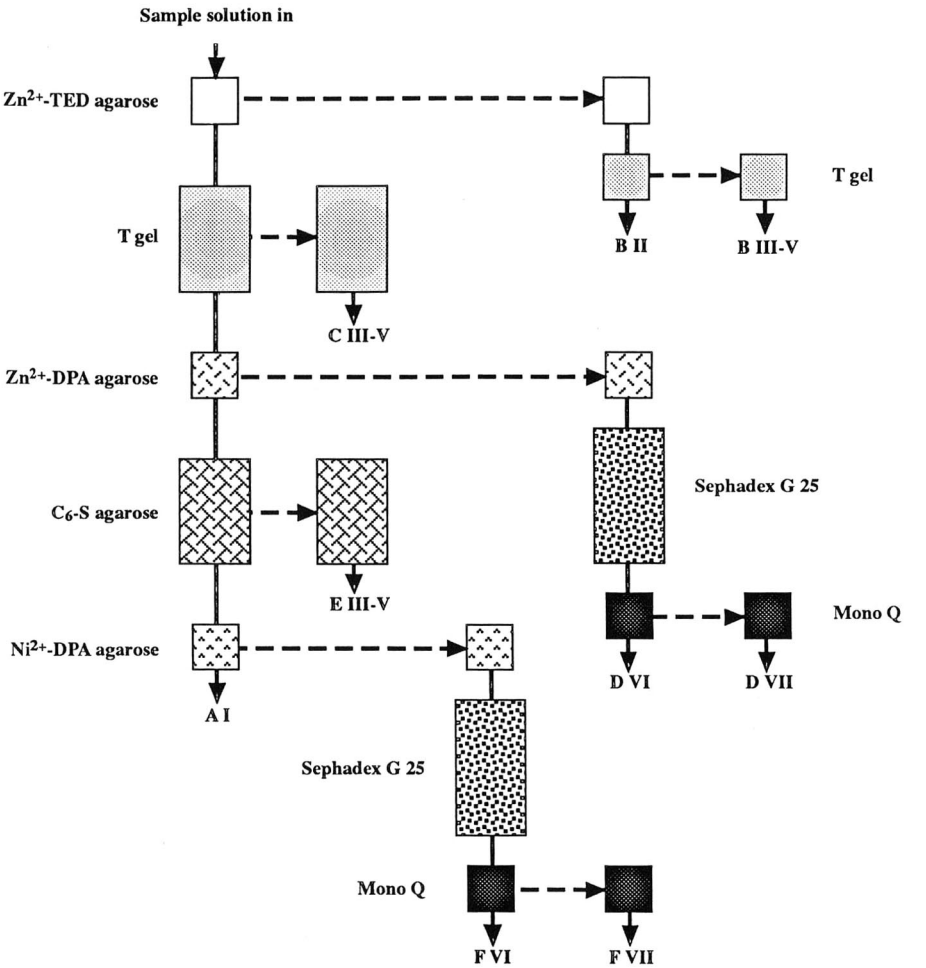

Fig. 1. Schematic diagram of the set-up of the tandem columns. The five columns to the left were connected in series at the start of the experiment. The columns were equilibrated with 50 m*M* sodium phosphate, 0.5 *M* in NaCl and 0.5 *M* in K_2SO_4 (pH 7.6) and 10 ml of human serum (equilibrated in the same buffer) were applied. The beds were washed until the A_{280} of the effluent reached the baseline. The beds were then disconnected and developed separately (see text). Solid arrows indicate liquid flow and dashed arrows indicate disconnection of a bed followed either by elution of adsorbed material directly or elution into a new tandem column. The letters and numbers refer to the fractions collected and the buffers used, respectively.

Fraction D: the adsorbed material on the Zn^{2+}-DPA agarose was displaced with buffer II into a Sephadex G-25 column (120 ml) equilibrated with buffer VI. The effluent was monitored continuously with a recording photometer and conductivity meter. The washing was stopped when the conductivity was increasing and A_{280} had decreased to the baseline. The Sephadex bed was disconnected. The desorbed material from the Zn^{2+}-DPA agarose gel, now in buffer VI, was transferred to a Mono-Q column, equilibrated with the same buffer. Isocratic elution proceeded until baseline

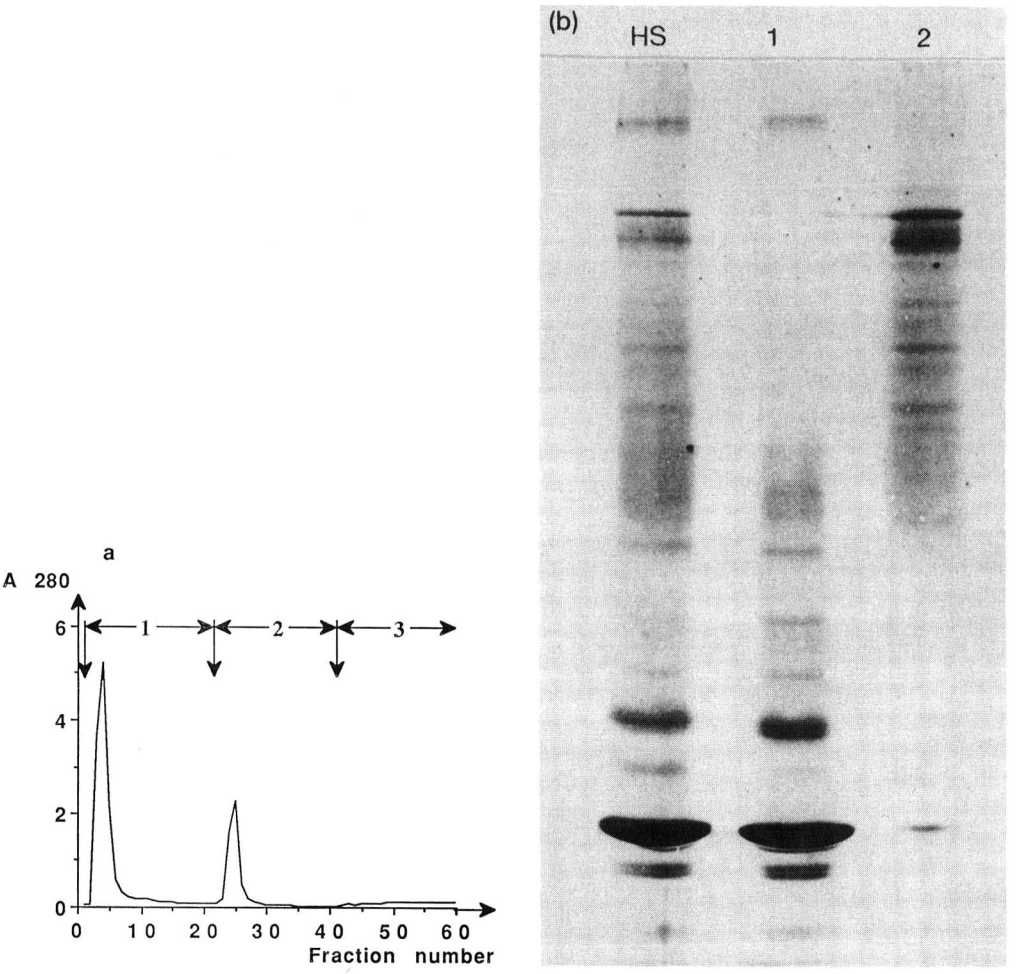

Fig. 2. (a) Chromatogram of Zn^{2+}-DPA agarose. A 1-ml volume of human serum was applied and the column was developed as follows: (1) 50 m*M* sodium phosphate, 0.5 *M* in NaCl (pH 7.6) (equilibration buffer); (2) 0.5 *M* sodium acetate, 0.5 *M* in NaCl (pH 5.5); (3) 0.5 *M* sodium acetate, 0.5 *M* in NaCl and 50 m*M* in imidazole (pH 5.5). (b) Electrophoresis of the peaks collected from the Zn^{2+}-DPA agarose. HS refers to human serum and 1 and 2 to peaks 1 and 2 in the chromatogram in (a).

adsorbance was reached. The Mono-Q bed in turn was disconnected and the adsorbed material in the bed separately eluted with a rising NaCl gradient using buffer VII.

Fraction E: the bed containing C_6-S agarose was developed as described previously [4], *i.e.*, using buffers III, IV and V.

Fraction F: the bed containing Ni^{2+}-DPA agarose was treated in the same way as the bed containing Zn^{2+}-DPA agarose.

RESULTS

Extensive experience in our laboratory has given us the necessary understanding of the properties of the adsorbents for the design of this kind of cascade chromatography. This includes careful matching of the metal ion, adsorbent and the mixture to be fractionated.

Effects of metal ion on human serum

The choice of metal ion to be loaded on the column is important. In our example, Zn^{2+} and Ni^{2+} show different adsorption properties. Thus, a Zn^{2+}-loaded DPA agarose adsorbs about 33% of applied serum proteins whereas a Ni^{2+}-loaded gel adsorbs about 96% (Figs. 2a and 3a). PAGE of the fractions from each chromatogram also reveals different adsorption properties. For example, the Ni^{2+}-DPA agarose adsorbs most of the albumin in human serum whereas Zn^{2+}-DPA agarose does not (Figs. 2b and 3b). α_2-Macroglobulin adsorbs very strongly to Ni^{2+}-DPA agarose (material in the strong band in the upper half of HS in Fig. 3b is not displaced by 50 m*M* imidazole), whereas Zn^{2+}-DPA agarose adsorbs α_2-macroglobulin more weakly. Material in the same band is displaced by buffer not containing imidazole (Fig. 2b).

Adsorption behaviour towards serum proteins of the tandem-coupled beds

For group separation of human serum proteins, we can now design an efficient strategy consisting of sequential adsorption in tandem-coupled beds as follows. Knowing that a Zn^{2+}-TED agarose adsorbs very little material from human serum, we place this gel first in the train of beds. The T gel adsorbs the majority of immunoglobulins and α_2-macroglobulins. It is placed second in the train ahead of the beds of DPA gel. The C_6-S gel adsorbs most of the albumin in human serum. The Ni^{2+}-DPA agarose adsorbs among other proteins albumin, which is not adsorbed by the corresponding Zn^{2+} gel. We therefore insert a bed of C_6-S gel between Zn^{2+} and Ni^{2+} beds of DPA gel to increase the separation efficiency of the last bed of the train (as indicated in the left part of Fig. 1). The arrangement of the side-line beds is also shown schematically in Fig. 1. The protein distribution in each fraction is shown in Table I. Fraction A, consisting of material passing the tandem column, contains less than 1% of the proteins in the sample.

Fig. 4 shows the composite chromatogram and Figs. 5 and 6 the diagrams from gel electrophoresis, gradient PAGE and discontinuous SDS-PAGE, respectively. The lower molecular weight limit for efficient analysis is M_r = 50 000 in Fig. 5 and 10 000 in Fig. 6. Two bands in Fig. 6 cannot be seen in Fig. 5 (the two lower bands in lane Da VII and E V). One of them corresponds to α_1-antitrypsin according to molecular weight and immunodiffusion, whereas the other component cannot be detected by immunodiffusion. It is probably κ- or λ-light chain of immunoglobulin. Some of the other bands in Figs. 5 and 6 can be correlated with the proteins listed in Table I.

DISCUSSION

Successful application of cascade chromatography requires a prior knowledge of the selectivity and capacity of the adsorbents and the relative proportions of the

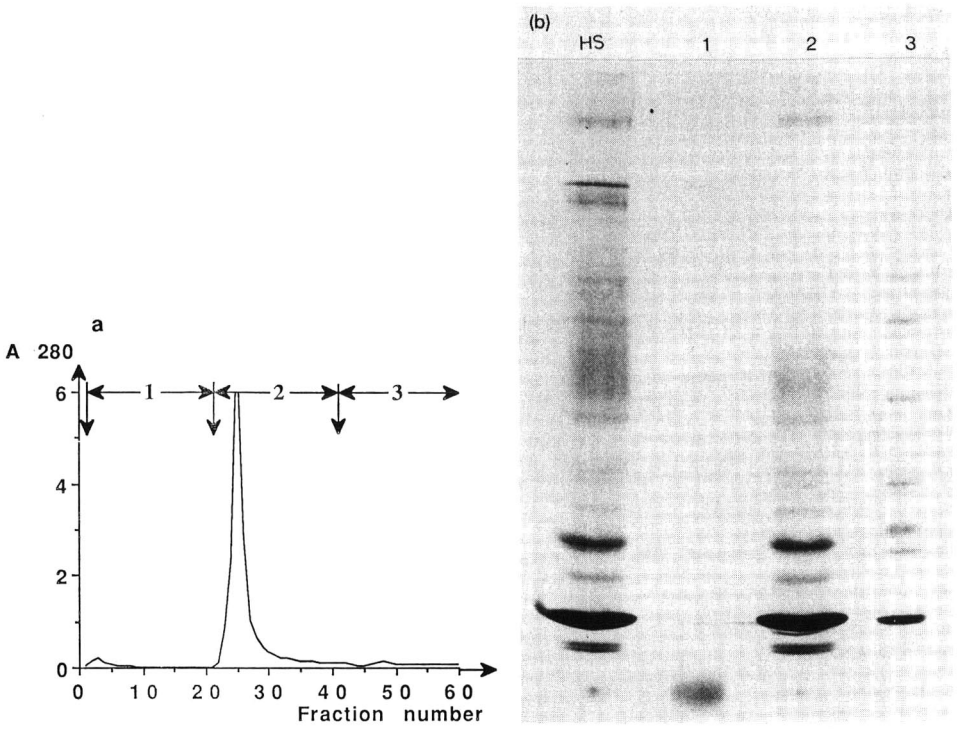

Fig. 3. (a) Chromatogram of Ni^{2+}-DPA agarose. A 1-ml volume of human serum was applied and the column was developed as follows: (1) 50 m*M* sodium phosphate, 0.5 *M* in NaCl (pH 7.6) (equilibration buffer); (2) 0.5 *M* sodium acetate, 0.5 *M* in NaCl (pH 5.5); (3) 0.5 *M* sodium acetate, 0.5 *M* in NaCl and 50 m*M* in imidazole (pH 5.5). (b) Electrophoresis of the peaks collected from the Ni^{2+}-DPA agarose. HS refers to human serum and 1, 2 and 3 to peaks 1, 2 and 3 in the chromatogram in (a).

various species in the mixture to be fractionated. Obviously, therefore, preliminary studies must be undertaken to optimize the efficiency of cascade chromatography whether the intention is the isolation of one, two or many of the components in the mixture. Once all the parameters are known, fractionation can be scaled up or down with retention of the resolving power.

One aim with the cascade technique is to minimize the number of operations. Adsorbents operating according to different affinity parameters should be used. In this study we selected (1) hydrophobic (C_6-S gel), (2) thiophilic (T gel) interactions, (3) size exclusion (Sephadex G-25 for buffer exchange), (4) electrostatic interaction (Mono-Q) and (5–7) three kinds of immobilized metal ion affinity (IMA). The use of IMA adsorbents is exploratory as we do not know *a priori* how the operations of the selected IMA gels complement or overlap each other.

IMA gels in conjunction with the other adsorbents permit a suitable selection of elution conditions and avoid extra buffer changes and separate concentration steps. For example (see Figs. 1 and 5 and Table I), fraction B adsorbed on the T gel is displaced by including imidazole in the buffer. By keeping the ionic strength high,

immunoglobulin M (IgM) is captured in the T bed but α_2-macroglobulin is allowed to pass.

The proteins adsorbed on the DPA gels can be further fractionated on an ion exchanger such as Mono-Q (Fig. 1), but this requires a buffer change. This can be accomplished by transferring the IMA gel to a penultimate Sephadex bed preceding an end bed of Mono-Q. The latter is disconnected after the proteins have just passed the Sephadex.

Albumin and immunoglobulin G (IgG) are the major components in serum and require larger beds for nearly complete adsorption than do the other proteins. If the amounts of gel are insufficient the proteins in question will, to a lesser or greater extent, pass the beds and contaminate fractions further down in the scheme. The T gel captures all IgG.

The major portion of the albumin (*ca.* 97%) is obtained in the C_6-S-adsorbed fraction (E) in almost pure form. The distribution in the other fractions may reflect

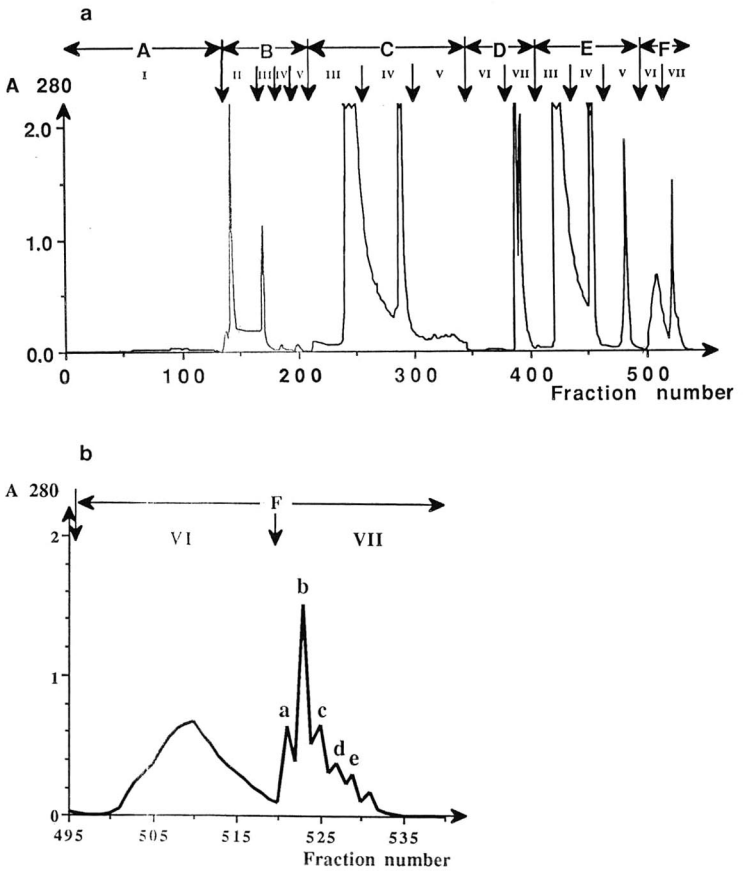

Fig. 4. (a) CASMAC chromatogram: A is the material passing the tandem columns, B is the material from the Zn^{2+}-TED gel, C the T gel, D the Zn^{2+}-DPA gel, E the C_6-S gel and F is the material from the development of the Ni^{2+}-DPA agarose. (b) Expanded part of (a).

TABLE I

AMOUNTS AND RECOVERIES OF SOME SERUM PROTEINS IN THE DIFFERENT FRACTIONS FROM THE DEVELOPMENT OF THE TANDEM COLUMNS

The components were determined using LC- or M-partigen immunodiffusion plates.

Subfraction	Serum protein (mg/l)													
	Albumin	α_2-Macroglobulin	α_1-Microglobulin	α_1-Antitrypsin	Transferrin	Ceruloplasmin	κ light chain	λ light chain	IgG	IgM	IgA	IgD	IgE	Recovery (%)
A I														0.6
B II		64												
B III	14	670							< 1					
B IV		13							0.02	5.7				6.6
B V		2.2								7.4				
C III	< 30	344				< 3	140	126	980		310			
C IV		< 14					56	77	780		64			40.1
C V							< 1.9	< 1.9	12		< 0.2			
Da VII	470			3.5			< 1.8	< 1.8			> 220			7.0
Db VII	385			< 1.8		440	< 1.8	< 1.8			124			
E III	16 000													
E IV	14 000													38.3
E V	49													
F VI					220									
Fa VII					65									
Fb VII			< 0.4	210	48						< 0.4			
Fc VII				55	< 1.0									5.6
Fd VII	< 5			105	≪ 2.6									
Fe VII	< 1.8			< 0.2										
Total														98.2

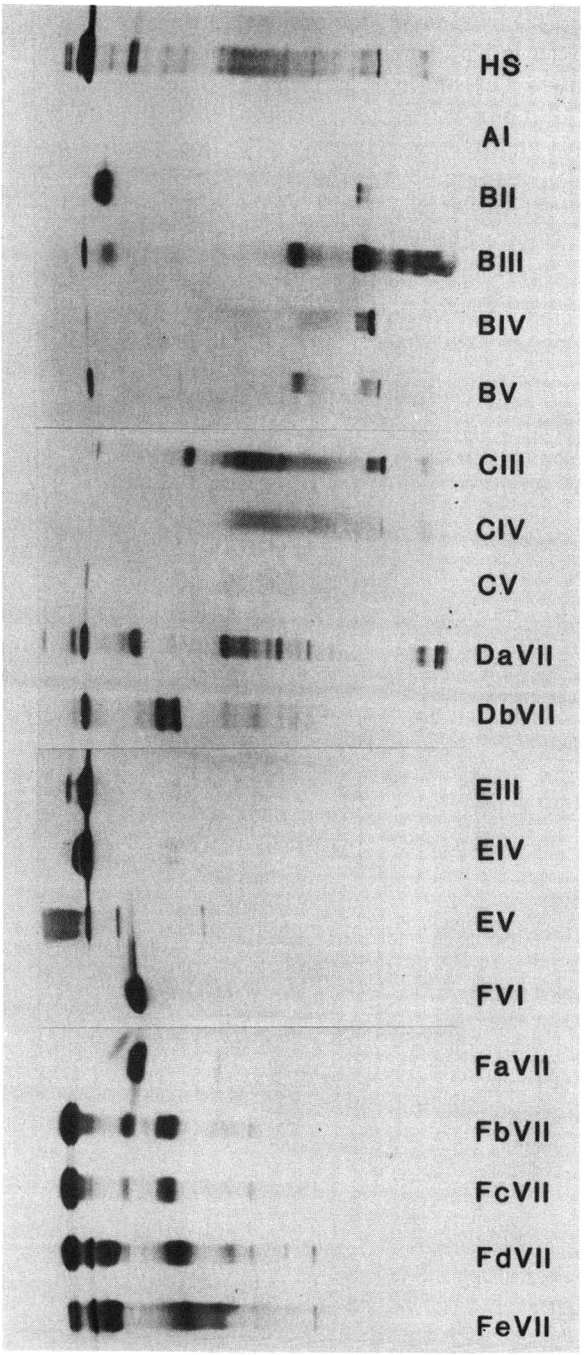

Fig. 5. Electrophoresis of the materials in the peaks collected from the chromatogram in Fig. 4a. Pharmacia PAA 4/30 polyacrylamide gradient gels were used.

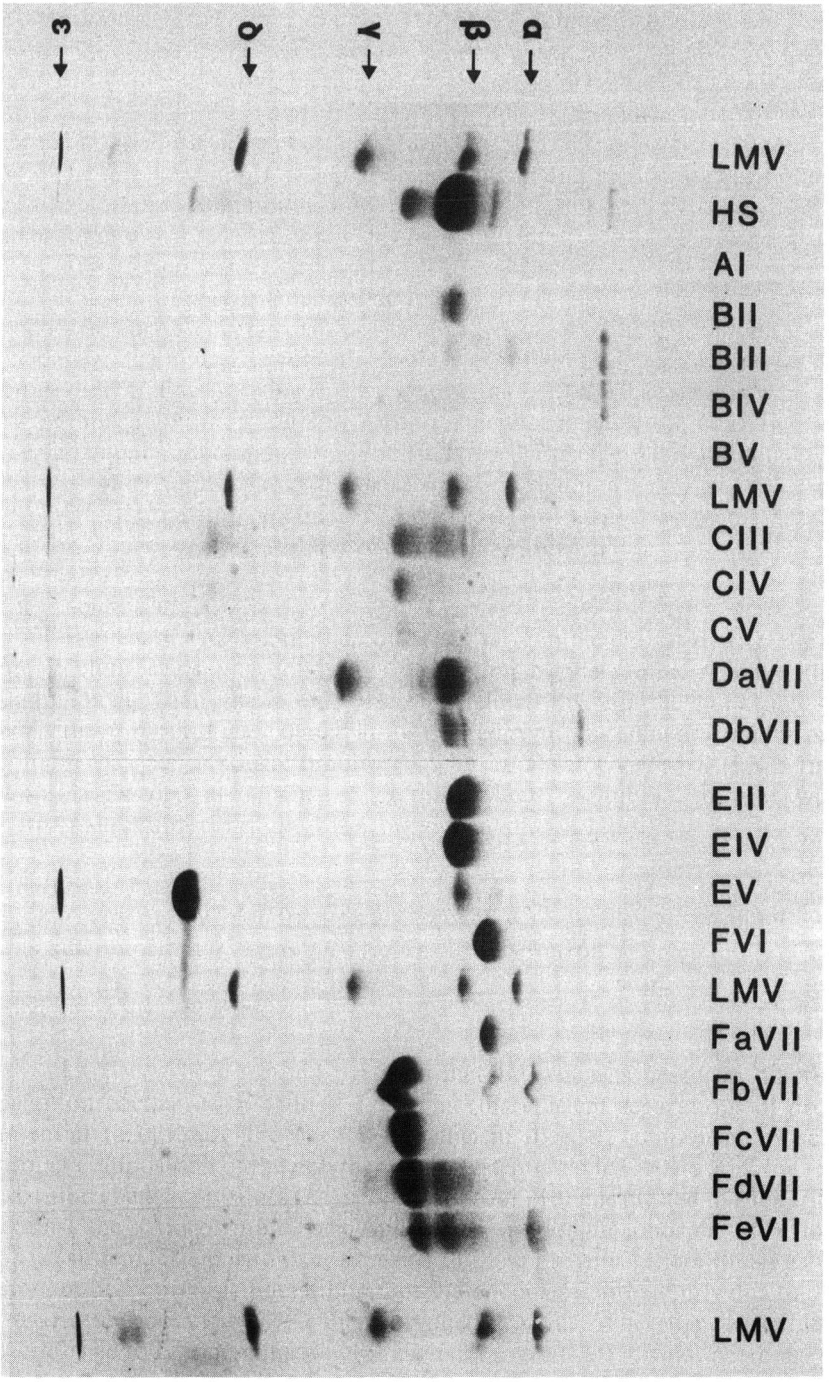

Fig. 6. Discontinuous SDS-PAGE of the materials in the peaks collected from the chromatogram in Fig. 4a. α = Phosphorylase *b* (M_r 94 000); β = bovine serum albumin (M_r 67 000); γ = ovalbumin (M_r 43 000); δ = carbonic anhydrase (M_r 29 000); ε = α-lactalbumin (M_r 14 400).

albumin heterogeneity. No albumin is found in fraction F, which proves that the C_6-S bed has sufficient capacity. The importance of proper bed order should be emphasized. If Ni^{2+}-DPA agarose had preceded the C_6-S gel, the albumin would have been distributed in both beds.

IgA has less affinity for the T gel than has IgG. Whereas the adsorption capacity is sufficient for the IgG (Fig. 1), it is not for IgA. The IgA that passes the T gel is captured in the Zn^{2+}-DPA bed where also all ceruloplasmin present in the serum is recovered together with some albumin. Transferrin and α_1-antitrypsin pass all the beds except the Ni^{2+}-DPA and they can subsequently be separated on Mono-Q.

CASMAC is a technique of general potential utility but its future success depends on the availability of a large number of selective adsorbents that can be applied generally to bioseparations. The number of possible combinations of chelate moieties and metal ions is enormous. IDA, TED and DPA are just some variants of the ligand part and Zn^{2+} and Ni^{2+} of the possible metal ions. However, a limited number of ligands with simple structures may serve most needs. In this paper some additional comments on the properties and use of DPA agarose may be justified.

Dipicolylamine (DPA), is a tridentate ligand like iminodiacetate (IDA) [7]. On binding a metal ion, an adsorption site is formed from DPA which may differ from IDA in its affinity for proteins. DPA possesses three nitrogen atoms for coordination whereas IDA has only one. Owing to the two carboxyls in IDA, the net charge of the adsorption site is lowered in the pH range 5–8 to a greater extent than for DPA. However, at the high ionic strength used in the experiments reported here, ionic attraction should be effectively suppressed. The π-electrons, the heteroaromatic nitrogen and the bulkiness of the pyridyl groups are all factors that should affect the affinity character of the DPA gel.

A DPA gel presumably has the structure

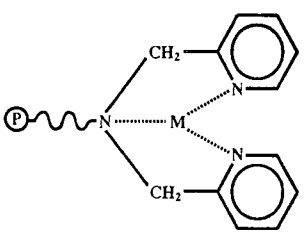

where P is the polymer matrix and M the metal ion. If, as is likely, Zn^{2+} and Ni^{2+} form hexacoordinate adsorption complexes, there should be three coordination sites per metal ion available for binding water or solutes. For steric reasons only one site on a protein will be bound, *e.g.*, an imidazole group from a histidine residue or, possibly, two oxygens from a phosphate group on a phosphoprotein.

Systematic stability studies of the immobilized metal ion complexes with the DPA ligand have not yet been undertaken. Therefore, in this study we deliberately avoided prewashing with weak chelators such as glycine. No overt signs of metal ion transfer have been discovered. Under the conditions used the metal ions are not bound in stoichiometric proportions to the fixed ligand; what that means remains to be established.

A comparison of the results shown in Figs. 2 and 3 with those obtained under

similar conditions for Zn^{2+}- and Ni^{2+}-IDA revealed both similarities and differences. The DPA gels seem to have broader selectivity and relatively higher capacity for human serum proteins. The structure–adsorption properties for tridentate liganded gels have to be studied in more detail.

The strength of protein interaction appears to be stronger with DPA than IDA. The protein adsorption capacity is of the same order (10–50 mg/ml gel bed). The metal ions can be easily removed from the adsorbents with a strong soluble chelator such as EDTA or by washing with acid.

The cascade adsorption procedures can be further extended and the separation power much improved by the introduction of gradient and affinity elution methods, *e.g.*, CASMAC can be combined with high-performance liquid chromatography by using the individual beds from the cascade as precolumns in the latter technique. It should also be possible to automate CASMAC. For large-scale, especially industrial, applications, batch operations in tanks is likely to be a preferred technique. This presumably requires the use of cheaper matrix materials such as cellulose, polyacrylates and hydrophilized silica.

ACKNOWLEDGEMENTS

We thank Professor John Law for valuable suggestions regarding the preparation of the manuscript and Ms. Karin Hellström and Mrs. Birgitta Hansson for technical assistance. This work was financially supported by the Swedish Board for Technical Development (STUF), an early grant from the Swedish Natural Science Research Council and the Erna and Victor Hasselblad Foundation.

REFERENCES

1 R. K. Scopes and J. Porath, *Bioseparation*, 1 (1990) 3.
2 J. Porath, *J. Chromatogr.*, 376 (1986) 331.
3 R. K. Scopes, *J. Chromatogr.*, 376 (1986) 131.
4 J. Porath and B. Olin, *Biochemistry*, 22 (1983) 1621.
5 F. Maisano, M. Belew and J. Porath, *J. Chromatogr.*, 321 (1985) 305.
6 J. Porath, F. Maisano and M. Belew, *FEBS Lett.*, 185 (1985) 306.
7 J. Porath, J. Carlsson, I. Olsson and G. Belfrage, *Nature (London)*, 258 (1975) 598.

Journal of Chromatography, 550 (1991) 765–774
Elsevier Science Publishers B.V., Amsterdam

CHROMSYMP. 2203

Separation of triacylglycerols by supercritical-fluid argentation chromatography

MUSTAFA DEMIRBÜKER and LARS G. BLOMBERG*
Department of Analytical Chemistry, University of Stockholm, Arrhenius Laboratory, 106 91 Stockholm (Sweden)

ABSTRACT

Microcolumns packed with a silica-based cation exchanger were used to separate triacylglycerols in vegetable oils. A supercritical mobile phase consisting of carbon dioxide, acetonitrile and isopropanol was used. Argentation chromatography results in separation according to the number of double bonds; in this work, separation was also obtained according to chain length and the nature of the double bonds. Full separation of molecular species of triacylglycerols in the investigated oils could be obtained after fractionation in reversed-phase liquid chromatography.

INTRODUCTION

Silver ion, or argentation, chromatography is a technique which has proved to be of great value in lipid analysis [1–5]. This method allows fractionation of triacylglycerols according to the number of double bonds they contain, and to some extent according to their geometrical configuration. The approach was first developed for thin-layer chromatography (TLC) [6]. Many attempts to adapt the technique to high-performance liquid chromatography (HPLC) have been made, these being for some time hampered by the lack of stable columns. However, it was shown by Christie and co-workers [7–9] that sufficient stability for use in HPCL could be achieved by using silica-based cation exchangers as support for the silver ions. In an earlier work, columns of this type were evaluated for group separation of triacylglycerols using supercritical fluids as the mobile phase (supercritical fluid chromatography, SFC) [10]. The chromatographic separation was performed on micropacked columns, and a supercritical mobile phase, consisting of carbon dioxide, 5.5% acetonitrile and 0.5% isopropanol, was used. Separation into groups according to the number of double bonds was sought, and the intention was to separate each group further by high-temperature gas chromatography (GC). However, such a system is not attractive for the analysis, since the recovery of highly unsaturated triacylglycerols with high-temperature GC [11,12] is uncertain. Another approach was taken by Takano and Kondoh [13], who used a two-dimensional liquid chromatography (LC) system for the separation of triacylglycerols. In that system, the sample first passes an argentation column and then a reversed-phase column. In the present work, another route

0021-9673/91/$03.50

was chosen for the separation of molecular species. Thus the vegetable oils were first fractionated according to the partition number by reversed-phase LC, and then separated further using microcolumn argentation SFC.

In this paper, it is shown that microcolumn argentation SFC can give separation of molecular species of triacylglycerols. This is an extension of our earlier results, in which separation into groups according to degree of unsaturation was achieved [10].

EXPERIMENTAL

The chromatographic system consisted of a Lee Scientific 600 Series SFC system and an Isco μLC-10 variable-wavelength absorbance detector. Detection was performed at 210 nm on a short length of 250 μm I.D. fused-silica tubing according to the method of Fields *et al.* [14]. The width of the slit on the detection capillary was about 1 mm. Fused-silica capillary tubing (Polymicro Technologies, Phoenix, AZ, U.S.A.), 11 μm I.D., was used as a restrictor in lengths of 20–25 cm.

Columns were prepared from fused-silica capillary tubing, 290 mm × 250 μm I.D. and 430 μm O.D. (Polymicro Technologies). All columns were packed with Nucleosil 5 SA (Macherey Nagel, Düren, Germany) and prepared as described previously [10]. After packing, the columns were washed, first with 400 μl of an aqueous solution of 10% ammonium nitrate and then with 400 μl of 0.1 *M* silver nitrate. Washing with ammonium nitrate was discontinued after preliminary experiments.

The mobile phase consisted of carbon dioxide–acetonitrile–isopropanol (92.8:6.5:0.7). The critical parameters were calculated from Lee Scientific software and ref. 15. The calculations indicated a critical temperature (T_c) of 62°C and a critical pressure (P_c) of 101 atm for the mixture. SFC-grade carbon dioxide (Scott Specialty Gases, Plumsteadville, PA, U.S.A.) was used. The mobile-phase mixture was prepared in the SFC pump as described previously [16]. Mobile phase velocity was 3.5 mm/s.

Reversed-phase HPLC was performed on columns, 250 mm × 10 mm, packed with Lichrosphere 100, RP 18, 5 μm (Merck), the mobile phase being HPLC-grade, degassed methanol–acetone (1:1).

Chromatographically purified oils, chromatographically purified (CPL) corn oil, CPL linseed oil, CPL palm oil, CPL soybean oil, CPL sunflower seed oil and standard substances (Larodan Fine Chemicals, Malmö, Sweden) were used. Solutes were dissolved in HPLC-grade pentane in concentrations of 30 mg/ml. Injection was performed with a split ratio of 1:1 and a time split of 0.2 s.

RESULTS AND DISCUSSION

Columns

Some columns were rinsed with ammonium nitrate before the treatment with silver nitrate. Such a rinsing was shown to be unnecessary, since no effect on the chromatographic properties was observed. Further, in some cases, plugging of the columns resulted. For the application of Ag^+, a large excess of reagent was applied, as it was believed this would lead to the highest yield. Relatively poor results were reported when using small amounts of silver nitrate for the impregnation [17]. Final-

ly, in order to provide a smooth change over from water to the relatively non-polar SFC mobile phase, the columns were rinsed with methanol after Ag^+ impregnation. However, observations made during the early stages of this work showed that such a rinsing could be omitted.

Mechanical column stability presented a problem in part I of this work [10], the columns often exploding when high pressure was applied. This problem was completely solved by the use of thick-walled fused silica capillary tubing, by which means a good stability was achieved. The columns could be used at temperatures up to 160°C. Moreover, under the conditions used in this work, the columns have now been used for more than one year without deterioration of the performance. It should be noted, however, that the injection of oxidizing substances may lead to the formation of silver oxide in the column.

Separation of vegetable oils

A series of chromatograms demonstrating the separation of vegetable oils is shown in Figs. 1–5. Note that the acyl groups are given in an arbitrary order and do not represent any specific positions within the triacylglycerol molecules. Two different pressure–temperature programmes were used, a relatively fast programme for oils containing highly unsaturated triacylglycerols, and a slow programme for oils having moderately unsaturated triacylglycerols. Peak identifications are tentative, and are based on comparisons with results from reversed-phase LC, from which the main components are known. Further, since the retention times obtained on an argentation column are very stable, the retention order can be mapped by comparison of the retention times of the main components of different oils. Moreover, peak identities have been further established by the separation of fractions obtained on reversed-phase LC. These fractions have been collected according to partition number, and

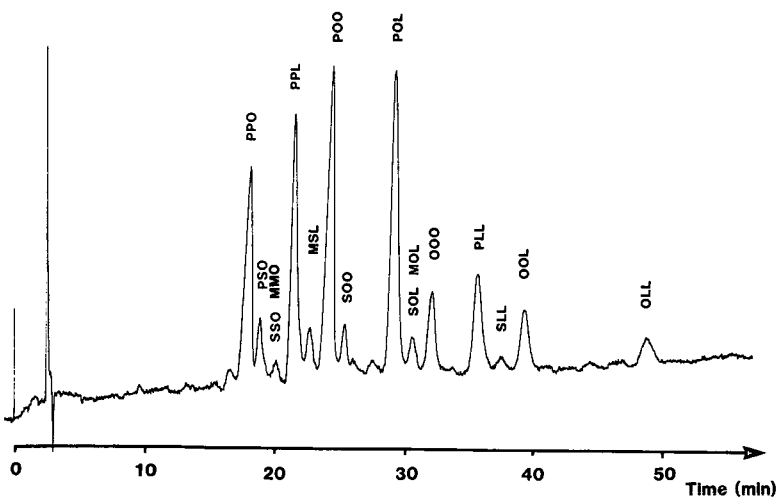

Fig. 1. Supercritical fluid chromatogram of palm oil. Injection at 95°C and 240 atm; after 2 min, programmed at −0.5°C/min to 75°C and 0.5 atm/min to 300 atm. UV detection at 210 nm. See the Experimental section for practical details and Table I for abbreviations.

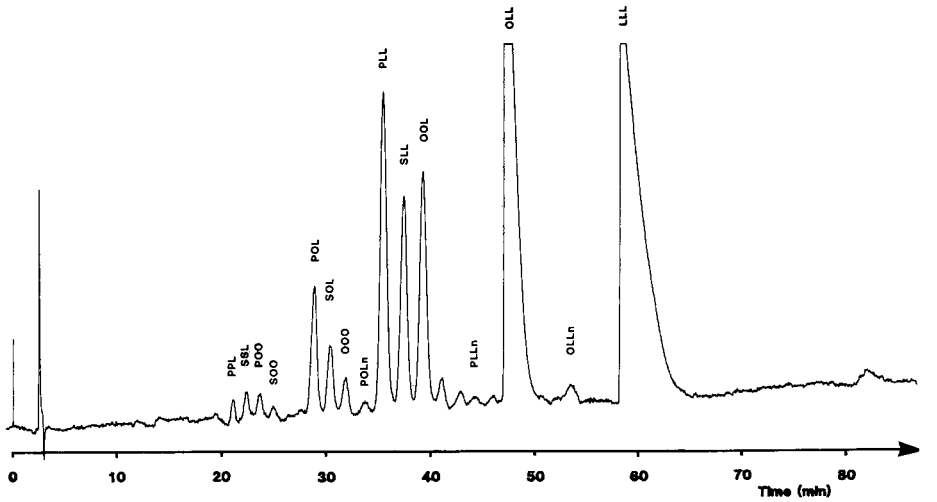

Fig. 2. Supercritical fluid chromatogram of sunflower seed oil. Conditions as in Fig. 1.

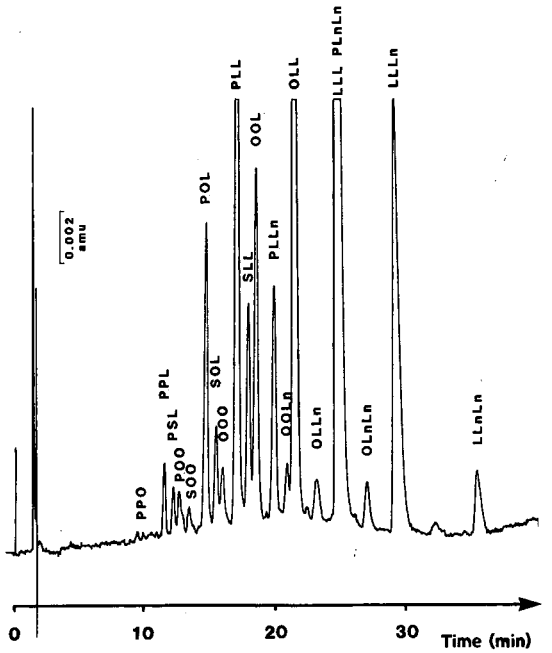

Fig. 3. Supercritical fluid chromatogram of soybean oil. Injection at 115°C and 260 atm; after 2 min, programmed at −1°C/min to 75°C and 1 atm/min to 300 atm. See Table I for abbreviations.

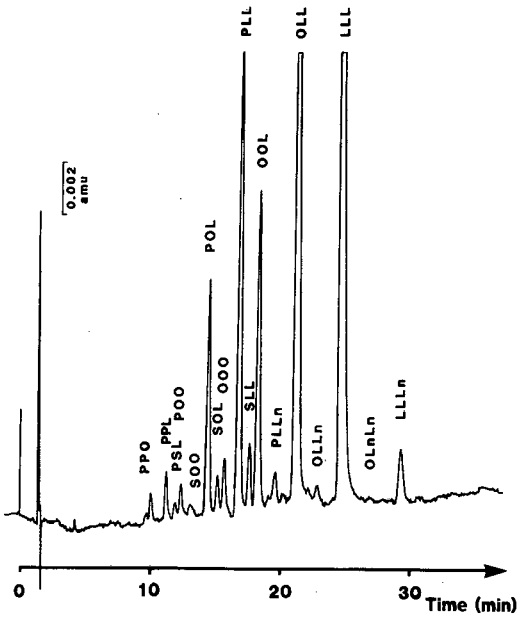

Fig. 4. Supercritical fluid chromatogram of corn oil. Conditions as in Fig. 3.

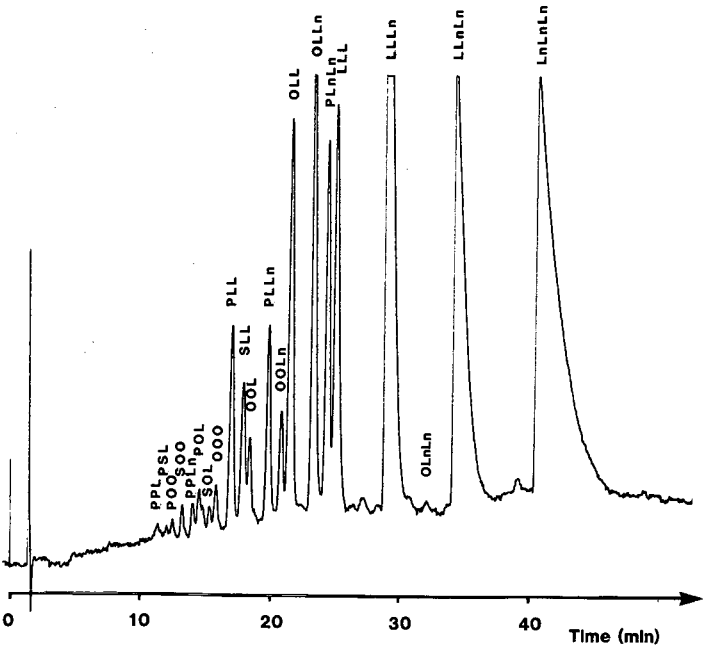

Fig. 5. Supercritical fluid chromatogram of linseed oil. Conditions as in Fig. 3.

thus each fraction contained a limited number of triacylglycerols, *e.g.* having partition number 46.

Separation of triacylglycerols in corn oil by means of SFC has been attempted on microcolumns packed with cyanopropyl-bonded silica [18]. However, the separation thus achieved was quite poor.

Separation of triacylglycerols

The ability of argentation TLC and HPLC to separate *trans* and *cis* isomers of unsaturated triacylglycerols is well recognized [3–5, 19,20]. The *cis* double bonds are thus retained more than *trans*. Such a separation was also achieved with microcolumn argentation SFC. An α value of 1.24 was thus obtained for the separation of 1,2,3-tri-[(*trans*)-9-octadecenoyl]glycerol and 1,2,3-[(*cis*)-9-octadecenoyl]glycerol under the conditions given in Fig. 1.

Elution of mono-, di- and triolein is shown in Fig. 6; it is evident that diolein complexes with Ag^+ to a lesser extent than triolein, while for mono-olein retention is determined mainly by residual silanol groups. Hammond and Irwin [4] reported longer retention times for diacylglycerols than for triacylglycerols when using silver nitrate-impregnated silica columns for HPLC. The silanol activity is obviously much higher in this type of silica than in silica which has been modified with cation-exchange moieties.

Separation of positional isomers, *e.g.* SOS from SSO (see Table I), was obtained by Smith *et al.* [21] using agentation HPLC. It was observed that the separation was favoured by a high silver content. The interaction between Ag^+ and double bonds increases with decreasing temperatures, and the separation of posi-

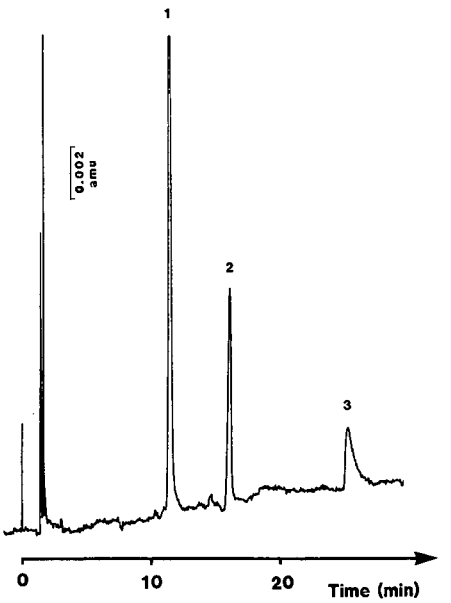

Fig. 6. Supercritical fluid chromatogram of mono-, di- and triacylglycerols. Conditions as in Fig. 3. Peaks: 1 = diolein; 2 = triolein, 3 = monoolein.

TABLE I

ABBREVIATION OF FATTY ACID MOIETIES

Fatty acid moiety	Abbreviation
Myristate	M
Palmitate	P
Stearate	S
Oleate	O
Linoleate	L
α-Linolenate	Ln

tional isomers was achieved at 6.8°C. However, a separation could also be obtained at 25°C [13]. Separation of positional isomers could not be achieved in this work, even when using subcritical conditions at 30°C.

Two-dimensional separations and elution orders

Although the argentation columns show a relatively high separation power, full separation of molecular species cannot be achieved. For example, in palm oil, the presence of myristate leads to many isomers (Fig. 1), and the presence of palmolein in olive oil results in separation problems. In Fig. 7 is shown the separation of a fraction of corn oil collected at partition number 46 from reversed-phase LC, and in Fig. 8 is shown the separation of the fraction having partition number 48.

Only slight separation of triacylglycerols according to chain length has been

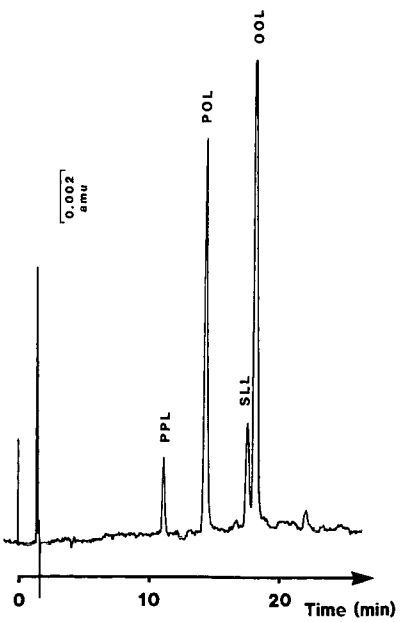

Fig. 7. Supercritical fluid chromatogram of a fraction of corn oil. Conditions as in Fig. 3. Fraction collected from reversed-phase LC at partition number 46.

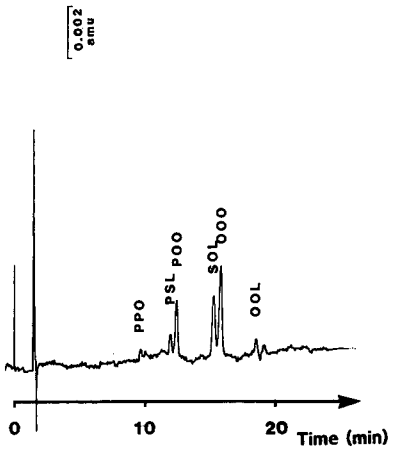

Fig. 8. Supercritical fluid chromatogram of a fraction of corn oil. Conditions as in Fig. 3. Fraction collected from reversed-phase LC at partition number 48.

obtained on silver-loaded silica in HPLC [4]. A notable chain length separation was obtained in this work: compare the difference in retention of POL and SOL (see Table I) in corn oil fractions (Figs. 7 and 8). Further, from the analysis of the fractions obtained from palm oil, an elution order — PPO, PSO, SSO, MMO — could be

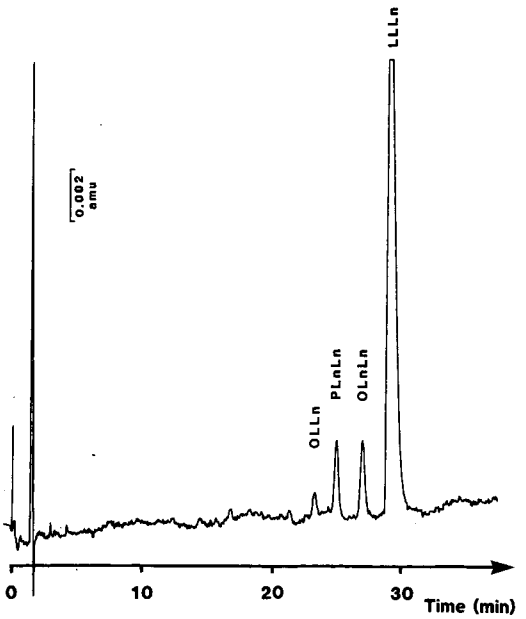

Fig. 9. Supercritical fluid chromatogram of a fraction of soybean oil. Conditions as in Fig. 3. Fraction collected from reversed-phase LC at partition number 40. The presence of OLLn is due to overlap between fractions.

established. Moreover, SOL and MOL were eluted at the same retention time. Depending on the aim of the analysis, such separations may be considered either as an advantage or as an unnecessary complication of the elution pattern.

A linoleic acid-containing triacylglycerol does not have a retention exactly equal to that of one containing two oleic acids [22]. In this work, the presence of one L-unit in the triacylglycerol results in lower retention than two O-units (compare PPL/POO and LLS/LOO in Fig. 1). The same elution order was shown for argentation LC by Hammond and Irvin [4], Aitzetmüller [3], and Takano and Kondoh [13]. Using an argentation TLC system, Gunstone and Padley [23] determined that LLS showed higher complexing powers than LOO. Similarly, as reported by Christie [8], LLS was shown to have a somewhat longer retention time than LOO. Further, as shown in this work, one α-linolenic acid unit gives a lower retention than three oleic acid units (compare the elution of PPLn and OOO in Fig. 5). A reversed elution order was reported by Christie [8]. The retention of α-linolenic-containing triacylglycerols is further demonstrated in Fig. 9, which shows separation of a fraction of soybean oil having partition number 40. Clearly, different mobile phase compositions may lead to different elution orders [5].

CONCLUSIONS

A technique for separation of molecular species of triacylglycerols was developed, and the retention characteristics of silver-modified cation-exchange columns in SFC were studied. Some separation according to chain length was found; triacylglycerols containing palmitin were thus eluted before those containing stearin. Unexpectedly, triacylglycerols containing myristin were found to be retained more than those containing stearin. The selectivity is thus different from what has been presented for argentation HPLC, where there is little or no chain-length separation. The separation of *cis* and *trans* isomers seems to be equal in HPLC and SFC. The separation of positional isomers has been reported for HPLC, but such separations could not be achieved with SFC. Further, some differences in elution orders were observed. The general resolving power of argentation SFC, as presented here is, however, higher than that achieved on argentation HPLC: compare the separation of linseed oil and sunflower seed oil in this work and in ref. 8. The improvement of the separations may be explained by the relatively high diffusion in supercritical media. Colum stability is of crucial importance, and it was excellent under the conditions applied. A high stability, in terms of silver ion leakage, was also reported for HPLC [8], however, the mobile phase should not contain polar solvents [24].

For SFC separation of triacylglycerols, the use of packed argentation columns makes a polar mobile phase modifier necessary. The flame ionization detector cannot be used in combination with such mobile phases, and we have thus resorted to detection with UV. The response is, at the wavelength used, proportional to the number of double bonds; saturated triacylglycerols could not be detected using this system. The use of a light-scattering detector would solve this problem. A further improvement of the system, leading to shorter analysis times, could be achieved by the introduction of gradient elution.

ACKNOWLEDGEMENTS

Magnus Bergkvist, LipidTeknik AB, Stockholm, is acknowledged for the fractionation of vegetable oils on reversed-phased LC. The work was kindly supported by Stiftelsen Karlshamns Forskning and the Swedish Natural Science Research Council.

REFERENCES

1 L. J. Morris, *J. Lipid Res.*, 7 (1966) 717.
2 C. Litchfield, *Analysis of Triglycerides*, Academic Press, New York, 1972.
3 K. Aitzetmüller, in H. Engelhardt (Editor), *Practice of High Performance Liquid Chromatography*, Springer, Berlin, 1986, p. 287.
4 E. W. Hammond and J. W. Irwin, in R. Macrae (Editor), *HPLC in Food Analysis*, Academic Press, London, 1988, p. 95.
5 W. W. Christie, *HPLC and Lipids*, Pergamon Press, Oxford, 1987.
6 L. J. Morris, *Chem. Ind. (London)*, (1962) 1238.
7 W. W. Christie, *J. High Resolut. Chromatogr. Chromatogr. Commun.*, 10 (1987) 148.
8 W. W. Christie, *J. Chromatogr.*, 454 (1988) 273.
9 W. W. Christie and G. H. McG. Breckenridge, *J. Chromatogr.*, 469 (1989) 261.
10 M. Demirbüker and L. G. Blomberg, *J. Chromatogr. Sci.*, 28 (1990) 67.
11 E. G. Hammond, *Trends Anal. Chem.*, 8 (1989) 308.
12 I. Hägglund, K. Janák, L. Blomberg, S. Claude and R. Tabacchi, in preparation.
13 S. Takano and Y. Kondoh, *J. Am. Oil Chem. Soc.*, 64 (1987) 380.
14 S. M. Fields, K. E. Markides and M. L. Lee, *Anal. Chem.*, 60 (1988) 802.
15 R. C. Reid, J. M. Prausnitz and B. E. Poling, *The Properties of Gases and Liquids*, McGraw-Hill, New York, 4th ed., 1987, Chapter 5 and Appendix A.
16 S. Schmidt, L. G. Blomberg and E. R. Campbell, *Chromatographia*, 25 (1988) 775.
17 F. Ulberth and E. Achs, *J. Chromatogr.*, 504 (1990) 202.
18 H.-C. K. Chang and L. T. Taylor, *J. Chromatogr. Sci.*, 28 (1990) 607.
19 W. W. Christie, *Gas Chromatography and Lipids*, The Oily Press, Ayr, 1989.
20 W. W. Christie, *Lipid Analysis*, Pergamon Press, Oxford, 2nd ed., 1982.
21 E. C. Smith, A. D. Jones and E. W. Hammond, *J. Chromatogr.*, 188 (1980) 205.
22 K. Aitzetmüller, *Chem. Ind. (London)*, (1988) 452.
23 F. D. Gunstone and F. B. Padley, *J. Am. Oil Chem. Soc.*, 42 (1965) 957.
24 N. U. Olsson, *Dissertation*, University of Stockholm, Stockholm, 1991.

Journal of Chromatography, 550 (1991) 775–785
Elsevier Science Publishers B.V., Amsterdam

CHROMSYMP. 2226

Review

Sorption isotherms in supercritical fluid chromatography

CLEMENT R. YONKER* and RICHARD D. SMITH
Chemical Methods and Separations Group, Chemical Sciences Department, Pacific Northwest Laboratory[a], *Richland, WA 99352 (USA)*

ABSTRACT

The continued and growing interest in supercritical fluid chromatography (SFC) has given rise to a need for a better understanding of the solute retention mechanism. One facet of research has aimed at a theoretical description of solute retention using equation of state models based on statistical mechanics and thermodynamic descriptions of the *P*, *V*, *T* relationship for a fluid. A second approach has involved studies of the physico-chemical interaction of the supercritical fluid with the solute molecule and the stationary phase. Solute retention in SFC has been demonstrated to be a dynamic process of intermolecular interactions between the solute and the fluid mobile phase and between the solute and the bonded polymeric stationary phase. This qualitative statement is supported by spectroscopic studies of solvent cluster formation about a solute molecule in a supercritical fluid, partial molar volume studies and isotherm measurements of the fluid in different stationary phases under various conditions in SFC. Progress made to date in determining the sorption isotherms of mobile phase components in SFC is reviewed.

CONTENTS

1. INTRODUCTION

The understanding of the solute retention mechanism in supercritical fluid chromatography (SFC), as in all chromatographic systems, is dependent on determining the complex interaction between multiple chemical processes. These physico-chemical processes involve the intermolecular interactions of the solute molecule with

[a] Operated for the US Department of Energy by Battelle Memorial Institute, under Contract DE-AC06-76RLO 1830.

0021-9673/91/$03.50

the mobile and stationary phases. Various methodologies have been used to study the mobile and stationary phases in SFC and many excellent papers have been published in these areas [1–8].

The understanding of the molecular dynamics of the retention process in the stationary phase hinges on the ability to study the interactions between the supercritical fluid and the bonded polymeric phase. The investigation of the sorption isotherms of the supercritical fluid mobile phase components in the stationary phase and their effect on solute retention will lead to a more complete understanding of the retention process in SFC.

There are numerous methodologies for the determination of adsorption isotherms in chromatographic systems. Conder and Young [9] presented an excellent discussion of these techniques for gas chromatography, but these methodologies are of equal importance for both liquid and supercritical fluid chromatography. Supercritical fluids present an interesting challenge because of the compressible nature of the solvent and the higher working pressures, but most methodologies are readily amenable to SFC.

The purpose of this paper is to review the progress in determining the sorption isotherms of mobile phase components in SFC and to discuss their relevance to the understanding of retention in SFC. This area is still in its infancy, but already some interesting results have been obtained.

2. METHODOLOGIES

In initial studies, Sie *et al.* [10] 25 years ago measured the solubility of near-critical and supercritical carbon dioxide in squalane and glycerol using a gas volumetric and titration method. These methodologies are better suited for bulk adsorption studies and do not lend themselves readily to *in situ* investigations on a chromatographic column.

In more recent work, Springston *et al.* [11] developed a chromatrographic technique to measure the swelling of bonded polymeric films used in modern capillary columns in a supercritical fluid. It is based on the change in elution time of a non-retained marker as the film thickness in the capillary varies. This hydrodynamic method of determining stationary phase swelling was used to investigate thick-film coatings in capillary SFC. The advantage of this technique lies in its ability for *in situ* measurements of stationary phase swelling in capillary SFC. Disadvantages of this method arise from practical constraints on film and column preparation and their resulting impact on the precision of such measurements.

Lochmüller and Mink [12,13] measured the adsorption isotherm of ethyl acetate, methanol and 1-hexanol on silica from supercritical carbon dioxide using the peak maxima method. In this chromatographic technique, the capacity factors of the peak maxima were determined for various solute concentrations injected into the column. The analysis of the chromatographic retention data can be used to obtain the sorption isotherm of the solute molecule [14]. The integration of the first-derivative plot in this technique could prove difficult in multi-component systems.

Janssen *et al.* [15] studied the adsorption isotherms of different supercritical fluid modifiers on octadecyl-modified silica using the breakthrough method. This technique involves the determination of the breakthrough profile of the solvent mod-

ifier from the chromatographic column. The stationary phase coverage of the modifier can then be easily determined as a function of pressure, temperature and fluid modifier concentration [16]. The ease of studying multiple simultaneous isotherms is questionable with this technique.

Selim and Strubinger [17,18], Yonker and Smith [19,20] and Parcher and co-workers [3,21–23] used tracer pulse chromatography to study the adsorption isotherms in SFC. The advantage of this technique is that multi-sorbate isotherms can be readily determined. The basic requirement for a solute is a detectable difference between itself and the background solvent. This is readily accomplished through the use of either mass isotopes or radioisotopes. There are several excellent discussions of tracer pulse chromatography in the literature, as applied to high-pressure gas chromatography, that describe the technique and theory [24–27].

3. DISCUSSION

The adsorption of high-pressure gases on solid surfaces under both near-critical and supercritical conditions has been studied since the early 1930s [28–31]. The work of Coolidge and Fornwalt [28] investigated the adsorption of carbon dioxide, nitrous oxide and silicon tetrafluoride on charcoal under various temperature and pressure conditions. Their results using a gravimetric technique based on the quartz spring balance showed S-shaped adsorption isotherms for carbon dioxide on charcoal. A successful fitting of the carbon dioxide adsorption data using the Polanyi treatment of multi-layer adsorption was completed.

The next high-pressure gas adsorption study was reported by Jones *et al.* [32], who investigated the adsorption of carbon dioxide and nitrogen on porous plugs of lamp black. Again a gravimetric technique was used. At 32°C, they reported a sharp maximum in the carbon dioxide adsorption data as the pressure increased. The pressure of this adsorption maximum was reported at 74 atm. Above this pressure the adsorption isotherm was seen to rapidly decrease.

When measuring adsorption isotherms, one either determines the absolute adsorption or the differential adsorption. Differential or Gibbs adsorption is defined as the excess solute present in a volume on the surface, beyond that which would be present owing to the normal density of the solute at that temperature and pressure. If measured at sufficiently high pressures, Gibbs adsorption isotherms always show a maximum. The simple explanation of this phenomenon is that as the background pressure increases, the density of the bulk solvent approaches that of the adsorbed solvent. This can continue until the bulk and adsorbed densities are equal; according to definition, at this point the adsorbed amount becomes zero. Therefore, high-pressure Gibbs adsorption isotherms must exhibit a maximum by definition, as reported by Jones *et al.* [32]. Menon's review [33,34] of high-pressure adsorption data further clarifies this point and demonstrates the difference between absolute and differential isotherm measurements for different systems.

Kobayashi and co-workers [35,36] described the high-pressure adsorption of methane and propane on silica gel (Porasil A) and the use of a chromatographic technique (tracer pulse chromatography) for the experimental study of these systems. The Gibbs adsorption isotherm obtained for methane on Porasil A first increased as a function of density and then decreased with continued increases in solvent density.

Values for the absolute adsorbed amount of methane and the density of the sorbate were determined from the Gibbs isotherms. This investigation was the first work employing tracer pulse chromatography on a chromatographic stationary phase.

Findenegg and co-workers [37,38] later studied the physical adsorption of krypton and propane on graphitized carbon black. The differential molar enthalpy of adsorption was derived from the temperature dependence of the Henry's law constant. Gibbs adsorption isotherms for supercritical fluids at the critical temperature were seen to pass through an adsorption maximum between $0.5\rho_c$ and the critical density, ρ_c.

The initial studies of high-pressure gas adsorption on solid surfaces demonstrated the important result of a maximum being reached in the Gibbs isotherm as a function of pressure. This adsorption maximum appeared to occur between a reduced density of 0.5 and 1.0. The use of tracer pulse chromatography for the determination of Gibbs adsorption isotherms demonstrated the applicability of this technique to SFC. In SFC, the chromatographic surface consists of a bonded polymer (capillary SFC) or a bonded hydrocarbon chain (packed-column SFC). The chromatographic stationary phase adds complexity to the sorption mechanism and increases the intermolecular dynamics between the fluid solvent and the stationary phase.

The initial work of Sie *et al.* [10] investigated the solubility of the supercritical fluid in a typical bulk stationary phase. This study demonstrated that supercritical carbon dioxide was soluble in a coated liquid stationary phase. The swelling of a bonded polymeric stationary phase in capillary SFC was demonstrated by Springston *et al.* [11] for SE-30 using supercritical butane and carbon dioxide. Butane expanded SE-30 to nearly three times its initial thickness, whereas the swelling observed with carbon dioxide was much less. These interactions between the fluid mobile phase and the stationary phase could alter the chromatographic retention mechanism for SFC.

Lochmüller and Mink [12,13] studied the adsorption isotherms of ethyl acetate, methanol and 1-hexanol on silica from supercritical carbon dioxide with the peak maxima method. Their results of fitting the adsorption isotherms to the Langmuir equation suggest monolayer adsorption for the fluid modifier. Modifier surface coverage was determined as a function of temperature at constant density and was seen to decrease with increasing temperature. The retention of substituted and unsubstituted aromatic solutes was determined in the presence of methanol modifier (0–1%, w/v) in supercritical carbon dioxide. For methoxynaphthalene and nitronaphthalene, the retention was lower than expected owing to competition between the solute and methanol for the active sites on the silica surface. For chloronaphthalene, the retention increased in the presence of methanol on the silica surface. This behavior was ascribed to either an increase in dispersive interactions with the modified silica surface because of covered active sites or lateral interactions between the solute molecule and the adsorbed methanol. The selectivity for a given solute pair was studied in the methanol-modified fluid, in which one solute molecule competed with methanol for the active sites on the silica surface and the other did not. The selectivity between these two solutes reached a maximum as a function of methanol modifier concentration (*ca.* 0.4%, w/v) and decreased with increasing methanol concentration. The relationship between surface site coverage and methanol modifier concentration controlled the change in selectivity for this system. 1-Hexanol was more effective in covering active sites on the silica surface because of its greater molecular surface area.

The retention data and adsorption data presented by Lochmüller and Mink [13] demonstrate that for certain solutes competitive solute–modifier active site adsorption occurs with silica in packed-column SFC.

The work of Janssen *et al.* [15] was similar to that of Lochmüller and Mink, except they studied an octadecyl-modified silica stationary phase. Various polar modifiers in supercritical carbon dioxide were investigated using the breakthrough method to determine the modifier surface coverage. The adsorption isotherms were fitted to a Langmuir-type adsorption equation and solute retention was based on a dual retention mechanism. Overall solute retention was considered to be a combination of selective interactions with the silanol surface sites and the chemically bonded surface. Retentions of various solutes were monitored as a function of modifier concentration, and their results were similar to those reported by Lochmüller and Mink [13]. The maximum amount of modifier sorbed on the surface was clearly correlated with molecular size and structure. Solute retention correlated with the amount of polar modifier adsorbed on the surface, leading to the conclusion that the modifier serves to deactivate residual silica surface sites in the chemically modified stationary phase. The interaction of the polar modifiers with the surface silanols was found to be important in altering the extent of the individual contributions to the dual retention mechanism.

Mass isotope tracer pulse chromatography (MITPC) has recently been applied to the investigation of the dynamic stationary phase sorption process for bound polymeric systems in SFC. Selim and Strubinger [17] first reported the use of MITPC for the study of sorption isotherms of supercritical *n*-pentane on SE-30 and SE-54 stationary phases in SFC. They reported a high solubility of *n*-pentane near its critical temperature in both the SE-54 and SE-30 stationary phases, which decreased with increasing pressure. A minimum in the adsorption isotherm was reported at a pressure of 650–700 p.s.i. for both stationary phase studies. At higher temperatures (250–300°C), the total amount of *n*-pentane sorbed into the stationary phases was appreciably lower than that measured at 220°C, and pressure had a minimal effect on the sorption behavior. The effect of film thickness of the stationary phase on sorption behavior was investigated at these higher temperatures. Enhanced sorption or solubility of the fluid in the thicker stationary phase was a general phenomenon seen under constant conditions.

Strubinger and Selim [18] also studied the isotherms of *n*-pentane in an SE-54 stationary phase using a mobile phase that contained various amounts of methanol as a polar modifier in supercritical *n*-pentane. The trends obtained were similar to those in their previous study using pure *n*-pentane as the supercritical fluid. The amount of sorbed *n*-pentane in the stationary phase decreased with increasing pressure and temperature. The presence of the polar modifier, methanol, had a slight effect on the amount of *n*-pentane sorbed into the stationary phase, the postulated reason for this effect being the direct interaction between methanol and any residual active sites on the capillary surface. The coverage of these sites by methanol changed the surface activity, making the surface less polar, which increased the amount of *n*-pentane sorbed into the stationary phase. They also proposed a thermal relaxation process as the possible mechanism through which the amount of *n*-pentane taken up by the stationary phase decreases with increasing temperature and pressure.

Yonker and Smith [20] studied the Gibbs adsorption isotherms of carbon diox-

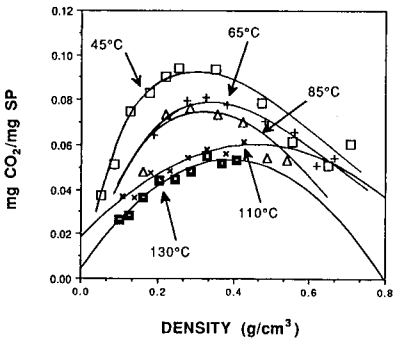

Fig. 1. Plot of mg adsorbate (CO_2) per mg of stationary phase (SP) *versus* bulk fluid density for temperatures of (□) 45, (+) 65, (△) 85, (×) 110 and (■) 130°C.

ide as a function of density on a bonded SE-54 stationary phase in capillary SFC. The results of these investigations are shown in Fig. 1. The Gibbs isotherms exhibit a maximum with density over a range of $0.5\rho_c < \rho < 1.0\rho_c$, where ρ_c, the critical density for carbon dioxide, is 0.468. This supports the findings of Findenegg and co-workers [37] in their studies of the adsorption of krypton on graphitized carbon black. As density (pressure) continues to increase the measured differential adsorption isotherms for carbon dioxide decrease. This effect arises as the density of the bulk solvent approaches the density of the adsorbed carbon dioxide. As the two densities approach one another, the differential adsorption isotherm for carbon dioxide on the surface approaches zero [32–34]. As the temperature increases, the excess amount of carbon dioxide sorbed in the stationary phase decreases. This result was comparable to that seen for *n*-pentane on SE-54 as reported by Selim and Strubinger [17,18]. The enthalpy of sorption of carbon dioxide in the polymeric stationary phase was determined to be *ca.* −4 kcal/mol (at a density of 0.23 g/ml) and −2.0 kcal/mol (at a density of 0.38 g/ml). The isosteric heats of adsorption (determined at constant volume) for propane, butane and acetone on graphitized carbon black were −5.6, −7.7 and −7.5 kcal/mol, respectively [39]. The isosteric heats of adsorption on graphite for propane and butane are −6.26 and −8.10 kcal/mol, respectively [40]. Findenegg and co-workers [37] reported an isosteric enthalpy for krypton on graphitized carbon black of −2.95 kcal/mol, whereas Ross *et al.* [40] reported a value of −3.20 kcal/mol. The enthalpy values reported by Yonker and Smith [20] compare favorably with the isosteric enthalpies in the literature for high-pressure adsorbate isotherms on solid surfaces.

Further work by Yonker and Smith [19] involved the study of the Gibbs adsorption isotherms of the polar fluid modifier 2-propanol in SE-54 as a function of temperature, density and modifier mole fraction. The general trend in the Gibbs isotherm data can be seen in Fig. 2. At each temperature studied, the amount of 2-propanol adsorbed into the stationary phase decreased with increasing density and converged to a limiting value. The temperature effect shown in fig. 2 is pronounced at the lower densities. The increase in temperature could contribute enough thermal energy to the system to begin to overcome the attractive interactions between 2-propanol and the stationary phase, thus contributing to the decrease in the amount of

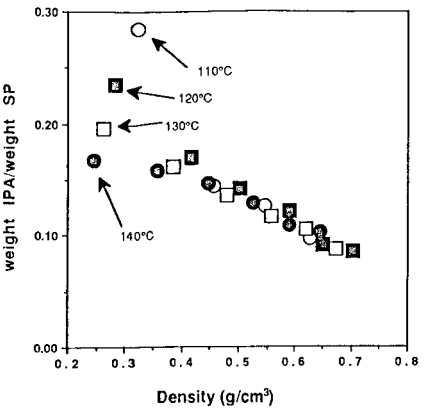

Fig. 2. Plot of weight of 2-propanol (IPA) per weight of stationary phase (SP) *versus* bulk fluid density for a constant mole fraction of 0.0258 2-propanol in CO_2 at (○) 110, (■) 120, (□) 130 and (●) 140°C.

2-propanol absorbed into the stationary phase as temperature increases. The 2-propanol was determined to be partitioning into the stationary phase based on the calculation of 2-propanol monolayer surface coverage relative to the amount of 2-propanol absorbed in the stationary phase, which was at least two orders of magnitude greater than that needed for monolayer coverage. In this study the authors demonstrated that the weight percentage of 2-propanol in the stationary phase was greater at lower bulk densities and decreased as the bulk density increased. A proposed explanation for this observation is the increase in solvent strength of the supercritical fluid as density increases. Similar results were observed in spectroscopic investigations of the local composition of the binary modifier in the cybotactic region of the probe molecule as a function of density for supercritical fluids [41]. The local composition of the binary modifier was found to be substantially enriched at lower pressures. The local composition of the modifier decreased and approached the bulk composition as density increased, reflecting the increasing solvent strength of the bulk fluid as density increased. At constant temperature, an increase in mole fraction of the polar modifier 2-propanol in the bulk fluid resulted in an increase in the amount of 2-propanol sorbed into the stationary phase. These results are shown in Fig. 3. The trend shown in Fig. 3 again demonstrates the effect of bulk solvent strength. At constant modifier mole fraction for lower bulk fluid densities, the polymeric stationary phase is a better solvent for 2-propanol than the supercritical fluid. As the bulk fluid density increases and its solvent strength increases, the amount of 2-propanol sorbed into the stationary phase concomitantly decreases.

Yonker and Smith [19] determined the enthalpy of sorption for 2-propanol into the polymeric stationary phase for densities of 0.35 and 0.40 g/cm^3. The heats of sorption for these densities at increasing mole fractions of 2-propanol in the bulk fluid (0.04–0.07) ranged from −3.5 to −4.7 kcal/mol and −2.8 to −3.8 kcal/mol, respectively. Again, these values are comparable to those reported by Ross *et al.* [40]. The heat of vaporization of 2-propanol is −9.5 kcal/mol at its boiling point of 82.2°C [42]. If 2-propanol were adsorbing in multi-layers on the stationary phase surface, then one might expect the heat of adsorption to approach the heat of vaporization. The

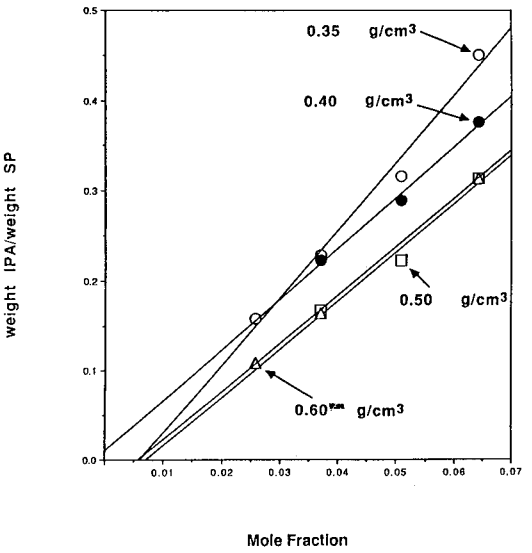

Fig. 3. Plot of weight of 2-propanol (IPA) per weight of stationary phase (SP) *versus* mole fraction of 2-propanol in the binary supercritical fluid at 140°C for bulk fluid densities of (○) 0.35, (●) 0.40, (□) 0.50 and (△) 0.60 g/cm^3.

measured experimental enthalpies reflect the intermolecular interaction between 2-propanol and the bound polymeric stationary phase. As the amount of 2-propanol sorbed into the stationary phase increases, the enthalpy of sorption for 2-propanol approaches the limiting value, the heat of vaporization.

Parcher and co-workers [3,21,22] studied the Gibbs adsorption isotherms of carbon dioxide on typical adsorbent materials used in packed-column SFC. These materials included silica and octadecyl-, cyano- and diol-modified silica. Their work demonstrated no major difference between the Gibbs adsorption isotherms for these four adsorbent materials. Multi-layer adsorption of carbon-dioxide above the critical pressure was observed independent of surface preparation. In packed-column SFC, the effect of the pressure drop down the length of the column must be taken into consideration. Parcher and Strubinger meticulouosly avoided any pressure drop in their columns during isotherm determination. The general trends seen in these isotherms were similar to those found in capillary SFC. At temperatures and pressures above the critical point, these workers reported that the amount of carbon dioxide sorbed decreased with increasing pressure at constant temperature and decreased with increasing temperature at constant density. Maxima in the Gibbs isotherms were seen near the critical pressure and temperature. The shape of the isotherm is due to the contribution of several interrelated factors, the high density of the adsorbate, temperatures close to the critical temperature and only the excess amount of carbon dioxide sorbed can be determined experimentally. A near-critical isotherm at 30°C showed the expected behavior at the vapor pressure for carbon dioxide (71.8 atm). A discontinuity was observed in the adsorption isotherm. Below this pressure, typical gas–solid adsorption behavior was noted; above this pressure, normal liquid–solid adsorption was encountered. Parcher and Strubinger attempted to calculate the abso-

lute adsorption isotherms based on the parameters of the specific surface area of the adsorbent and the thickness of the adsorbed layer. The accuracy of their results is limited by the assumed values of these parameters. These investigators also determined the effect of carbon dioxide adsorption in the stationary phase on the retention of benzene. At pressures below the critical pressure for carbon dioxide, benzene was highly retained on the surface at the temperatures investigated. As the pressure increased, the solute retention showed the expected exponential decrease with increasing density. At fixed pressure, the retention of benzene increased with temperature, which was postulated to occur as a result of the decreased sorption of carbon dioxide on the surface and the decreased density of the carbon dioxide mobile phase as temperature increases.

Parcher and co-workers [22,23] further studied the adsorption isotherms for supercritical carbon dioxide on an SE-30 bonded capillary column and the adsorption isotherms of a binary supercritical fluid composed of methanol in carbon dioxide on silica and octadecyl-bonded silica. They measured the specific volume of carbon dioxide in the polysiloxane bonded phase and showed that it increased with the concentration of carbon dioxide in the polymer. Further, the maxima determined in the adsorption isotherms as a function of density for supercritical carbon dioxide supported the earlier findings of Findenegg and co-workers [37] that the maxima occurred in the range $0.5\rho_c < \rho < \rho_c$. A comparison of carbon dioxide sorption between silica and octadecyl-modified silica showed that the bare silica adsorbed more carbon dioxide than the modified surface, the difference being the decrease in surface area on surface modification. A qualitative relationship between P_R^{max}/ρ^{max} (the reduced pressure at maximum adsorption/density at the adsorption maximum) *versus* reduced temperature was seen to be a common straight line for all systems studied. They also developed a similar qualitative relationship between the reduced maximum adsorption *versus* reduced temperature. This qualitative relationship is similar to the quantity discussed earlier by Menon [33], in which $P_{max} = P_c T_r^2$ is constant for all high-pressure adsorption studies (where P_{max} is the pressure of maximum adsorption and P_c and T_r are critical pressure and reduced temperature of the adsorbate, respectively).

The work of Parcher and co-workers [23] on the adsorption of binary supercritical fluid mobile phases on silica and octadecyl-modified silica represents an initial attempt to define the roles of temperature, pressure and composition on the retention mechanism in packed-column SFC. At the three temperatures investigated, the adsorption of carbon dioxide with methanol present was enhanced relative to the adsorption of pure carbon dioxide, and the adsorption maxima were shifted to higher densities. Therefore, in this system the adsorption process was interpreted to be a cooperative process. The amount of methanol adsorbed at 50°C increased with decreasing pressure as one approached the critical point. The composition of methanol in the stationary phase was much greater than that present in the bulk binary fluid. This result is similar to that reported earlier by Yonker and Smith [19] with an SE-54 stationary phase in capillary SFC. The amount of methanol adsorbed on the bare silica surface was greater than that on the modified surface owing to the greater number of polar adsorption sites.

The retention of two solutes were monitored during the adsorption isotherm studies and the general chromatographic trend in retention for supercritical fluids was

observed with increasing fluid density of the solutes. However, the addition of methanol to the mobile phase increased the retention of benzene at a fixed density on the octadecyl-bonded phase. The increased solvent strength of the mobile phase with methanol addition should decrease solute retention. Parcher and co-workers postulated that the increased retention was due to the following: (1) the adsorbed methanol increases the stationary phase volume while decreasing the mobile phase volume, which results in a net increase in the phase ratio for the separation; assuming a constant distribution coefficient, then solute retention will increase; (2) the distribution coefficients for the solutes may be greater in methanol than in either octadecane or liquid carbon dioxide; and (3) the increase in volume of the stationary phase with methanol leads directly to an increase in the distribution coefficient, if the solute molecule partitions directly into the sorbed phase.

4. CONCLUSIONS

The understanding of the retention mechanism in supercritical fluids is dependent on continuing efforts to investigate the dynamics of stationary phase solvation through the determination of the adsorption and absorption isotherms in both packed-column and capillary SFC. The physico-chemical interaction between the solute and the sorbed fluid in the stationary phase, as shown with MITPC studies and other techniques, directly impacts on retention in SFC. High-pressure adsorption processes have been studied for near-critical and supercritical fluids on both solid and polymeric surfaces. The classical methodologies are surpassed by the speed and flexibility of tracer pulse chromatographic techniques under such conditions. The ability to study simultaneously multiple adsorbates in one experiment is a distinct advantage of mass isotope tracer pulse chromatography. The determination of the exact extent of interaction between the fluid and the silica surface or the polymeric stationary phase still remains to be elucidated, but initial studies on sorption isotherms are beginning to address these questions. The understanding of the solute–sorbed fluid interactions and the extent of these interactions with fluid modifier concentration and bulk fluid density are necessary to obtain a greater insight into the retention mechanism in SFC. The studies reviewed here have attempted to understand the physico-chemical interactions involved during solute retention in SFC. The determination of adsorption isotherms in supercritical chromatography will contribute to the goal of understanding the retention mechanism in both SFC and LC. Further efforts are required to increase the ability to derive both qualitative and quantitative contributions of the intermolecular interactions in the solvated stationary phase and their effect on solute retention in SFC.

5. ACKNOWLEDGEMENTS

Work was supported by the Director, Office of Energy Research, Office of Basic Energy Sciences, Chemical Sciences Division of the US Department of Energy under Contract DE-AC06-76RLO 1830, and the US Army Research Office under Contract DAAL03-87-K-0042. The content of this paper does not necessarily reflect the position or the policy of the government, and no official endorsement should be inferred.

REFERENCES

1 D. E. Martire, *J. Chromatogr.*, 461 (1989) 165.
2 C. R. Yonker and R. D. Smith, *J. Phys. Chem.*, 92 (1988) 1664.
3 J. R. Strubinger and J. F. Parcher, *Anal. Chem.*, 61 (1989) 951.
4 E. P. Schmitz and E. Klesper, *J. High Resolut. Chromatogr. Chromatogr. Commun.*, 10 (1987) 519.
5 K. D. Bartle, A. A. Clifford, J. P. Kithinji and G. F. Shilstone, *J. Chem. Soc., Faraday Trans. 1*, 84 (1988) 4487.
6 P. J. Schoenmakers, L. G. M. Uunk and P. K. DeBokx, *J. Chromatogr.*, 459 (1988) 201.
7 T. A. Berger, *J. Chromatogr.*, 478 (1989) 311.
8 T. L. Chester, L. J. Burkes, T. E. Delaney, D. P. Innis, G. D. Owens and J. D. Pinkston, *ACS Symp. Ser.*, 366 (1988) 144.
9 J. R. Conder and C. L. Young, *Physicochemical Measurement by Gas Chromatography*, Wiley, New York, 1979, Ch. 9.
10 S. T. Sie, W. Van Beersum and G. W. Rijnders, *Sep. Sci.*, 1 (1966) 459.
11 S. R. Springston, P. David, J. Steger and M. Novotny, *Anal. Chem.*, 58 (1986) 997.
12 C. H. Lochmüller and L. P. Mink, *J. Chromatogr.*, 409 (1987) 55.
13 C. H. Lochmüller and L. P. Mink, *J. Chromatogr.*, 471 (1989) 357.
14 A. W. J. deJong, J. C. Kraak, H. Poppe and F. Nooitgedacht, *J. Chromatogr.*, 193 (1980) 181.
15 J. G. M. Janssen, P. J. Schoenmakers and C. A. Cramers, *J. High Resolut. Chromatogr. Chromatogr. Commun.*, 12 (1989) 645.
16 J. F. K. Huber and R. G. Gerritse, *J. Chromatogr.*, 58 (1971) 137.
17 M. I. Selim and J. R. Strubinger, *Fresenius' Z. Anal. Chem.*, 330 (1988) 246.
18 J. R. Strubinger and M. I. Selim, *J. Chromatogr. Sci.*, 26 (1988) 579.
19 C. R. Yonker and R. D. Smith, *Anal. Chem.*, 61 (1989) 1348.
20 C. R. Yonker and R. D. Smith, *J. Chromatogr.*, 505 (1990) 139.
21 J. F. Parcher and J. R. Strubinger, *J. Chromatogr.*, 479 (1989) 521.
22 J. R. Strubinger, H. Song and J. F. Parcher, *Anal. Chem.*, 63 (1991) 98.
23 J. R. Strubinger, H. Song and J. F. Parcher, *Anal. Chem.*, 63 (1991) 104.
24 D. L. Peterson and F. Helfferich, *J. Phys. Chem.*, 69 (1965) 1283.
25 F. Helfferich, *J. Chem. Educ.*, 41 (1964) 410.
26 D. L. Peterson, F. Helfferich and R. J. Carr, *AIChE J.*, 12 (1966) 903.
27 J. F. Parcher, *J. Chromatogr.*, 251 (1982) 281.
28 A. S. Coolidge and H. J. Fornwalt, *J. Am. Chem. Soc.*, 56 (1934) 561.
29 H. E. Morris and O. Maass, *Can. J. Res.*, 9 (1933) 240.
30 J. Edwards and O. Maass, *Can. J. Res.*, 12 (1935) 357.
31 J. Edwards and O. Maass, *Can. J. Res.*, B13 (1935) 133.
32 W. M. Jones, P. J. Isaac and D. Phillips, *Trans. Faraday Soc.*, 53 (1959) 1953.
33 P. G. Menon, *J. Phys. Chem.*, 72 (1968) 2695.
34 P. G. Menon, *Chem. Rev.*, 68 (1968) 277.
35 J. J. Haydel and R. Kobayoshi, *Ind. Eng. Chem., Fundam.*, 6 (1967) 546.
36 Y. Hou and R. Kobayoshi, *J. Chem. Phys.*, 54 (1971) 281.
37 S. Blümel, F. Köster and G. H. Findenegg, *J. Chem. Soc., Faraday Trans. 2, 78* (1982) 1753.
38 G. H. Findenegg and R. Loring, *J. Chem. Phys.*, 91 (1984) 3270.
39 J. F. Parcher, P. J. Lin and D. M. Johnson, *Anal. Chem.*, 58 (1986) 2207.
40 S. Ross, J. K. Saelens and J. P. Olivier, *J. Phys. Chem.*, 66 (1962) 696.
41 C. R. Yonker and R. D. Smith, *J. Phys. Chem.*, 92 (1988) 2374.
42 R. C. Reid, J. M. Prausnitz and T. K. Sherwood, *The Properties of Gases and Liquids*, McGraw-Hill, New York, 3rd ed., 1977, Appendix A.

Journal of Chromatography, 550 (1991) 787–797
Elsevier Science Publishers B.V., Amsterdam

CHROMSYMP. 2240

Comparison of power and exponential field programming in field-flow fractionation

P. STEPHEN WILLIAMS and J. CALVIN GIDDINGS*
Field-Flow Fractionation Research Center, Department of Chemistry, University of Utah, Salt Lake City, UT 84112 (USA)

ABSTRACT

Field programming in field-flow fractionation has the purpose of expanding the molecular weight or particle diameter range subject to a single analytical run. The two most widely used field programs are those in which the field strength decays with time according to an exponential function and a power function, respectively. The performances of these two programming functions are compared by obtaining limiting equations showing how retention time t_r, standard deviation in retention σ_t, and fractionating power F_d vary with particle diameter d. It is shown that uniform fractionating power (F_d independent of d) can be obtained with power programming but that in exponential programming F_d is always non-uniform, varying as $d^{-1/2}$. In exponential programming a linear relationship arises between t_r and log d. This particular relationship is impossible to realize in power programming but an alternative linear relationship can be obtained by plotting t_r *versus* $d^{1/3}$. These results are made more concrete by plotting and comparing field strength, relative field strength, F_d and t_r for specific programming cases.

INTRODUCTION

Field-flow fractionation (FFF) is a family of techniques whose many system and operating variables make the methodology adaptable to virtually all classes of macromolecular and particulate materials. Given a system geometry, a carrier liquid, a flow-rate and field type, the field strength becomes the most important remaining variable influencing retention and resolution. The field strength can be varied widely and almost instantly to accommodate the requirements of samples of different molecular weights and particle sizes. Further, when the sample contains molecules or particles covering a very broad range of molecular weights or diameters, it becomes advantageous to change the field strength as the run proceeds so that eluting species at different times are subjected to different average field strengths that encourage their adequate resolution and timely elution. This approach is termed field-programmed FFF.

Programming the field strength in FFF is analogous to, but simpler than, programming temperature or solvent strength in chromatography. All these programming methods are aimed at what Snyder [1] elegantly describes as the "general elution problem", the problem of adequately resolving the early components while avoiding the excessive elution time of the late components of wide ranging mixtures.

The programming of field strength as a tool for the optimized application of

0021-9673/91/$03.50

FFF to widely dispersed samples was first described by Yang *et al.* [2] in 1974. It was shown that different retention time relationships (describing retention time *versus* particle size) emerged for different programs (*i.e.*, different mathematical relationsips between field strength and time). Thus a variety of retention time relationships have been obtained for linear, parabolic, exponential, power and other programs based on the concepts and fundamental equations of the 1974 paper [3–10]. Of particular note, exponential decay programs (and modifications thereof) produce nearly linear relationships when the logarithm of particle diameter is plotted against time [5,6,8].

Despite the early accessibility to quantitative retention time relationships, the effect of programming and variations in programming on FFF resolution was not delineated in the initial studies, thus making the search for optimized programming difficult if not impossible. This void was filled in 1987 by a paper [8] defining fractionating power F (a kind of specific resolution applicable to continuous distributions of macromolecules and particles) and providing the general equations needed to compute F under different programming conditions. The equations were initially applied to exponential programming, showing that F decreases as particle diameter increases (*i.e.*, resolution is non-uniform, less for large than small particles) [8]. Subsequently, a new form of programming was developed having the characteristic that a constant fractionating power could be obtained over a large range of particle diameters or molecular weights [9]. The new programs were called power programs and their use was described as power programming.

The two most widely used classes of programs at present are exponential programs and power programs. Both program forms are used in commercial FFF instrumentation, with exponential programming utilized in the DuPont (Wilmington, DE, USA) sedimentation FFF system and power programming provided as part of both sedimentation FFF and thermal FFF instrumentation from FFF fractionation (Salt Lake City, UT, USA). These two programming approaches have different origins and specific objectives, although the broader objective in both cases is to realize the general advantages of programming first stated in the 1974 paper [2]. In particular, exponential programming was developed mainly to provide linear log (particle diameter) *versus* retention time plots and power programming has the specific purpose of yielding a uniform fractionating power for all particle sizes. In order to understand these two programming systems better, it is useful to ascertain if either programming form can assume the specific role of the other, or if these objectives are instead mutually exclusive. These and other comparative features of these two principal programming approaches will be examined in this paper.

Although we focus below on the dependence of retention time and fractionating power on particle diameter, the same basic mathematics are involved in relating these parameters to molecular weight when polymer analysis is being considered.

THEORETICAL RELATIONSHIPS

Exponential programming

The exponential program is described by the function

$$S = S_0 \exp\left(-\frac{t - t_1}{\tau'}\right) \tag{1}$$

where S is the field strength at time t (when $t \geqslant t_1$), S_0 is the initial field strength, t_1 is a period of constant initial field strength before the start of field decay and τ' is the field decay constant.

The specific objective of this program, as noted, is to obtain a linear relationship between retention time and the logarithm of particle size (see refs. 5 and 6). One presumed advantage of this lies in the relatively simple data manipulation required to obtain particle size distributions. This advantage has become less compelling, however, with the development of computer programs for the transformation from time to particle size and the capability to acquire particle size distribution curves for arbitrary field decay programs.

For the exponential decay program it may be shown (*e.g.*, refs. 8 and 11) that retention time, t_r, is given by

$$t_r = \tau' \ln \left[\frac{1}{2\lambda_0} (1 - B^{1/2}) \right] + t_1 \tag{2}$$

where λ_0 is the value of the retention parameter λ at the initial field strength and where

$$B \approx 1 - \frac{2t^0}{3\tau'} \tag{3}$$

Eqn. 2 is applicable for components significantly retained at the initial field strength (*i.e.*, $\lambda_0 \ll 1$). The above expression for B is a best approximation when $t_1 = \tau'$, which corresponds to the special case of time delayed exponential (TDE) decay utilized by Yau and Kirkland [5]. For the TDE program, eqn.2 reduces to

$$t_r = \tau' \ln \left[\frac{e}{2\lambda_0} (1 - B^{1/2}) \right] \tag{4}$$

where $e = 2.718282$ is the natural logarithmic base. For each subtechnique of FFF carried out in the normal mode of retention, λ is given by (see, for example, ref. 8)

$$\lambda = \frac{\Lambda}{Swd^n} \tag{5}$$

where w is the channel thickness, d is the particle diameter and n depends on the field type (*e.g.*, $n = 3$ for sedimentation FFF and $n = 1$ for flow FFF). The constant Λ is given by

$$\Lambda = \frac{kTd^n}{\phi} \tag{6}$$

where ϕ is the field–particle interaction parameter, which for sedimentation FFF is given by

$$\phi = \frac{\pi}{6} d^3 \Delta\rho \tag{7}$$

where $\Delta\rho$ is the density difference between the particles and the carrier fluid. The parameter Λ is independent of particle diameter for all FFF subtechniques.

It follows that for TDE programmed field decay,

$$\ln d = \frac{t_r}{n\tau'} - \frac{1}{n} \ln \left[\frac{eS_0 w}{2\Lambda} (1 - B^{1/2}) \right] \tag{8}$$

Thus, as first recognized by Yau and Kirkland [5], the theory predicts log–linear retention for TDE programming. Eqn. 8 shows that this relationship will hold for all normal mode separations subject to eqn. 5 under TDE programmed operation.

Assuming that B is given by eqn. 3 (which is a good approximation for significantly retained material), we can differentiate eqn. 8 with respect to d to obtain

$$\frac{dt_r}{dd} = \frac{n\tau'}{d} \tag{9}$$

It may be seen from eqn. 44 in ref. 8 that for significantly retained material (*i.e.*, material for which $\lambda_0 < \lambda_r \ll 1$), the standard deviation in retention time, σ_t, is given by

$$\sigma_t \approx \frac{12w}{D^{1/2} R_r} \left(\frac{\tau' \lambda_r^4}{4} \right)^{1/2} \tag{10}$$

where D is the particle diffusion coefficient, R_r is the retention ratio at the time t_r of elution and λ_r is the value of λ also at time t_r. Replacing R_r with $6\lambda_r$ (a good approximation for well retained material), we obtain

$$\sigma_t \approx w \left(\frac{\tau'}{D} \right)^{1/2} \lambda_r \tag{11}$$

Eqn. 47 in ref. 8 states that

$$\lambda_r = \frac{1}{2} (1 - B^{1/2}) \approx \frac{1}{2} \left[1 - \left(1 - \frac{2t^0}{3\tau'} \right)^{1/2} \right] \tag{12}$$

where the second form substitutes for B using eqn. 3. If $\tau' \gg t^0$, eqn. 12 reduces to

$$\lambda_r \approx \frac{t^0}{6\tau'} \tag{13}$$

Thus, for eqn. 11 we obtain

$$\sigma_t \approx \frac{wt^0}{6(\tau' D)^{1/2}} \tag{14}$$

The diameter-based fractionating power, F_d, is defined by [8]

$$F_d = \frac{d}{4\sigma_t} \cdot \frac{\mathrm{d}t_r}{\mathrm{d}d} \tag{15}$$

Therefore, for significantly retained material eluted under a TDE field decay program, we obtain (by the substitution of eqns. 9 and 14 into eqn. 15) the expression

$$F_d \approx d \cdot \frac{6(\tau' D)^{1/2}}{4wt^0} \cdot \frac{n\tau'}{d} \tag{16}$$

or equivalently

$$F_d \approx \frac{3n}{2w} (t^0 D)^{1/2} \left(\frac{\tau'}{t^0}\right)^{3/2} \tag{17}$$

Of the parameters in eqn. 17, only the particle diffusion coefficient D varies with particle diameter d. Specifically, the Stokes–Einstein equation shows that

$$D = \frac{kT}{3\pi\eta d} \tag{18}$$

where k is the Boltzman constant, T is the system absolute temperature and η is the carrier fluid viscosity. As D is inversely proportional to d, it follows that

$$F_d \propto d^{-1/2} \tag{19}$$

Eqn. 19 provides a very general relationship for the dependence of F_d on d for well retained spherical or near-spherical particles subject to TDE programming, or more generally for any programming governed by eqn. 1. This relationship shows that F_d inevitably varies with d in exponential programming. Hence there is no possible combination of parameters that will provide a constant fractionating power over a significant range of d with the use of the TDE field decay or related exponential programs. (For non-spherical particles, a constant F_d, defined relative to the effective spherical diameter by eqn. 15, is possible only if particles of all sizes have the same D, which requires the unlikely situation that particles of different effective spherical diameters must have the same Stokes diameter as found in eqn. 18.)

Power programming

The power program is described by the function [9]

$$S = S_0 \left(\frac{t_1 - t_a}{t - t_a}\right)^p \tag{20}$$

where S, S_0, t_1 and t are identically defined as for the exponential decay program, t_a is a program parameter with units of time and p is the program power. For a programmed decay it is necessary that $t_a < t_1$ and $p > 0$.

The objective of this program is to obtain constant fractionating power over a wide range of particle diameters for material eluted in the normal mode of FFF [9].

It was shown by Williams and Giddings [9] that retention time for elution under such a field decay program is given by

$$t_r \approx t^0 \left[\frac{(p+1)}{6\lambda_0} \left(\frac{t_1 - t_a}{t^0} \right)^p \right]^{\frac{1}{p+1}} + t_a \tag{21}$$

It was also shown that the approximation holds over a greater range of λ_0 when $t_a = -pt_1$. It follows from eqns. 21 and 5 that

$$t_r - t_a \propto d^{\left(\frac{n}{p+1}\right)} \tag{22}$$

Differentiating eqn. 21 with respect to d gives

$$\frac{dt_r}{dd} \approx \frac{nt^0}{(p+1)d} \left[\frac{(p+1)}{6\lambda_0} \left(\frac{t_1 - t_a}{t^0} \right)^p \right]^{\frac{1}{p+1}} \tag{23}$$

so that

$$\frac{dt_r}{dd} \propto d^{\left(\frac{n}{p+1} - 1\right)} \tag{24}$$

From eqn. 32 in ref. 9, it may be shown that for significantly retained material (*i.e.*, material for which $\lambda_0 < \lambda_r \ll 1$)

$$\sigma_t \approx \frac{12w}{D^{1/2} R_r} \left(\frac{t_r - t_a}{4p+1} \right)^{1/2} \lambda_r^2 \tag{25}$$

Substituting $6\lambda_r$ for R_r (good for well retained material), we have

$$\sigma_t \approx \frac{2w}{D^{1/2}} \left(\frac{t_r - t_a}{4p+1} \right)^{1/2} \lambda_r \tag{26}$$

and then replacing $(t_r - t_a)\lambda_r$ by $(p+1)t^0/6$ using eqn. 36 in ref. 9, we obtain

$$\sigma_t \approx \frac{2w}{D^{1/2}} \left[\frac{(p+1)t^0}{6(4p+1)} \right]^{1/2} \lambda_r^{1/2} \tag{27}$$

and finally, by using eqn. 43 in ref. 9 for λ_r, we are led to

$$\sigma_t \approx 2w \left[\frac{(p+1)t^0}{6(4p+1)D} \right]^{1/2} \left\{ \lambda_0 \left[\frac{(p+1)t^0}{6(t_1 - t_a)} \right]^p \right\}^{\frac{1}{2(p+1)}} \tag{28}$$

From the above equation together with eqns. 5 and 18 it follows that

$$\sigma_t \propto d^{\left(\frac{1}{2} - \frac{n}{2(p+1)}\right)} \tag{29}$$

Substituting eqns. 23 and 28 into the expression defining fractionating power, given by eqn. 15, and then rearranging gives

$$F_d \approx \frac{n}{48w}\left[\frac{6(4p+1)Dt^0}{(p+1)}\right]^{1/2}\left\{\frac{1}{\lambda_0}\left[\frac{6(t_1-t_a)}{(p+1)t^0}\right]^p\right\}^{\frac{3}{2(p+1)}} \tag{30}$$

From eqn. 30 in combination with eqns. 5 and 18, it is seen that

$$F_d \propto d^{\left(\frac{3n}{2(p+1)}-\frac{1}{2}\right)} \tag{31}$$

We observe from the above equations that for power programmed field decay there is always a power dependence predicted for $t_r - t_a$, dt_r/dd, σ_t and F_d on d for well retained components. Further, if p is set equal to $3n - 1$, that is, to 8 for sedimentation FFF and to 2 for flow FFF, then eqns. 22, 24, 29 and 31 reduce to

$$t_r - t_a \propto d^{1/3} \tag{32}$$

$$\frac{dt_r}{dd} \propto d^{-2/3} \tag{33}$$

$$\sigma_t \propto d^{1/3} \tag{34}$$

$$F_d \propto d^0 \tag{35}$$

The final expression, eqn. 35, shows that F_d is predicted to be independent of d. All of the power dependences are also observed to be independent of n. These dependences will therefore hold for all subtechniques of normal mode FFF (subject to eqn. 5) when field strength is power programmed using power p equal to $3n - 1$.

COMPARISON OF TYPICAL FIELD DECAY PROGRAMS

Consider Fig. 1 in ref. 9, in which a power program (with $p = 8$ and $t_a = -8t_1$) is plotted together with an exponential program for which $\tau' = (5/4)\,t_1$ (note that it was incorrectly stated in ref. 9 that $\tau' = t_1/4$ for this figure). We take this figure (with an appearance much like that of Fig. 1 shown here) as a starting point for our more extended comparison of the program types.

We shall consider the case of sedimentation FFF and assume typical experimental parameters, specifically $S_0 = 100$ gravities, $w = 0.025$ cm, $t^0 = 100$ s, $\Delta\rho = 1.5$ g/ml, $\eta = 0.01$ P and $T = 298$ K. We have shown in the previous discussion and earlier (see ref. 9) that for a power programmed field decay a value of 8 for p is expected to give rise to constant fractionating power for a wide range of significantly retained particle sizes. The time parameters t_1 and t_a (fixed at $-8t_1$) may be adjusted according to eqn. 57 in ref. 9 to give some desired level of constant fractionating power. For the experimental parameters stated above, we calculate that the values of 9.27 and -74.16 min are required for t_1 and t_a, respectively, to obtain $F_d = 5.0$. For the exponential decay program we retain $t_1 = 9.27$ min and set $\tau' = (5/4)\,t_1 = 11.59$ min in order to match the power program as closely as possible. The resultant field decay

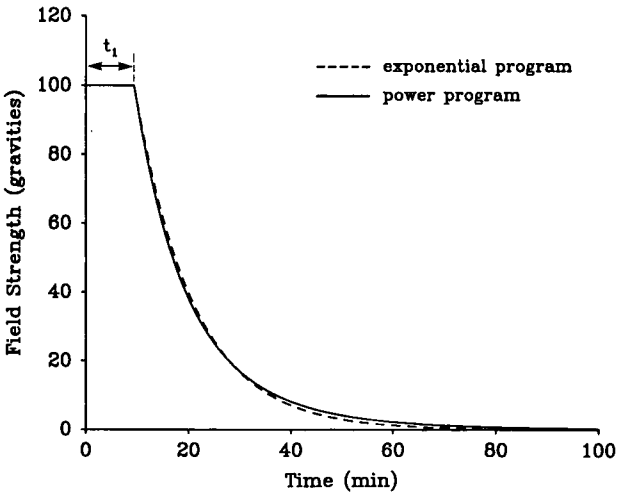

Fig. 1. Comparison of field strength decay for power and exponential programs.The programming parameters (see text) have been adjusted to give similar overall decay profiles.

programs are plotted together in Fig. 1 for elapsed times up to 100 min. The absolute difference between the curves is seen to be small over the full range of time shown. This comparison is deceptive, however. It is the relative difference in the programs that is of importance in comparing retention. The ratio of the field strengths (exponential/power) is plotted in Fig. 2. The exponential program is seen to decay more slowly at first but at an elapsed time of 28.5 min the two decay programs are again equal. With the further passage of time the exponential program decays more rapidly than the

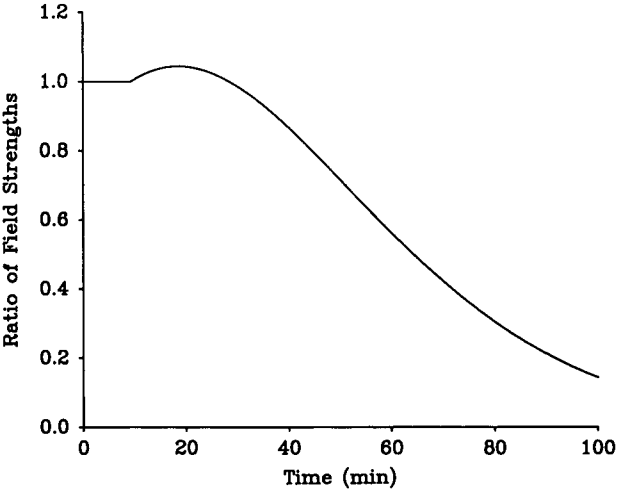

Fig. 2. Plot of the ratio of the field strength of the exponential decay program of Fig. 1 to the field strength of the power program shown in that figure.

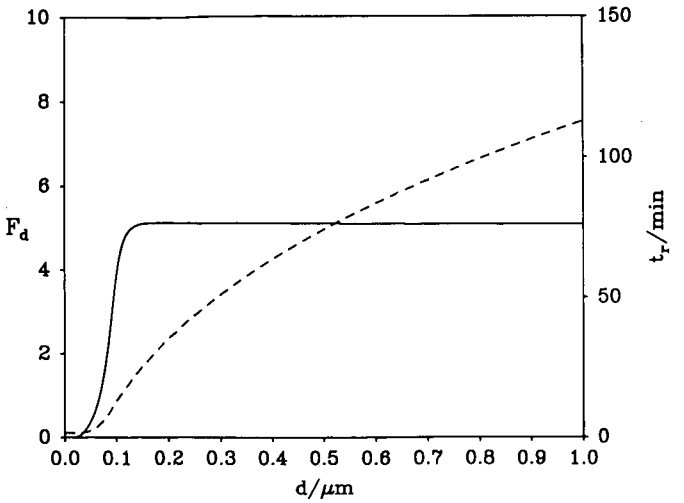

Fig. 3. Fractionating power F_d (solid line) and retention time t_r (dashed line) plotted as a function of particle diameter d for the power programming example described in the text.

power program, so that at a time of 64.2 min the field strength falls to half the strength of the power program, and at 100 min to one seventh of that of the power program.

Fig. 3 shows the variation of fractionating power (solid curve) and retention time (dashed curve) with particle diameter for the power program specified above and Fig. 4 the corresponding curves for the exponential example. The range of constant F_d (following an initial rise from $F_d = 0$) is apparent in Fig. 3 whereas F_d for significantly retained material (following a similar initial rise) is seen to decrease with $d^{-1/2}$ in Fig. 4, falling to a level of 3.7 for particles 1 μm in diameter. Note that retention times

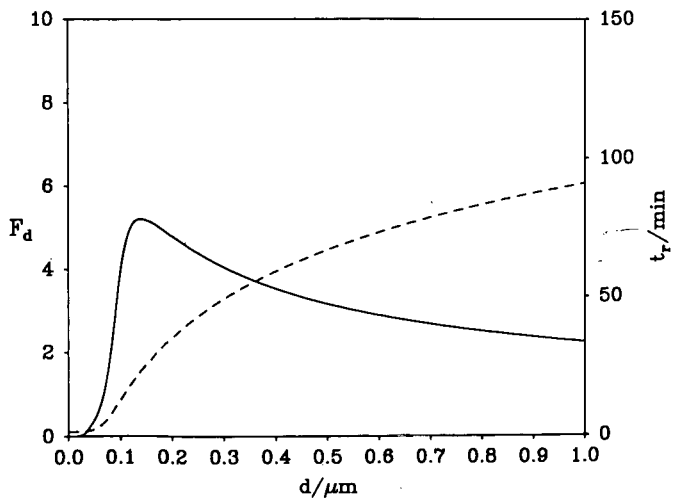

Fig. 4. Plot of the fractionating power (solid line) and the retention time (dashed line) against particle diameter for the exponential programming example described in the text.

for the larger components are lower for the exponential program chosen. This reflects the lower field strengths predicted with the passage of time for the exponential decay program and shows that the faster elution occurs at the expense of fractionating power.

It is clear from these examples that these two field decay programs, which superficially appear to be very similar, are actually different in relative terms and that the retention times and fractionating powers predicted for the two programs are consequently very different over a wide range of particle diameters.

CONCLUSIONS

The foregoing treatment shows that the fractionating power F_d of power programming can be made constant, independent of particle diameter d, by properly choosing the power p of the program, specifically $p = 3n - 1$, where n is defined by eqn. 5. The mathematics of programming, however, dictate that such a uniformity in fractionating power is not accessible through exponential (including time-delayed exponential) programming by any conceivable adjustment of parameters. Instead, F_d always decreases with increasing d through a dependence on $d^{-1/2}$. Power programming, by contrast, is sufficiently flexible that F_d can be made to depend on d, if desired, by choosing values of $p \neq 3n - 1$ in accordance with eqn. 31. Specifically, F_d can be made to increase or decrease with d (the choice depending on whether the highest resolution is needed for large or small particles) by setting $p < 3n - 1$ or $p > 3n - 1$, respectively. However, F_d cannot be made to decrease with d with a dependence as strong as that of the exponential program, $d^{-1/2}$, as this case corresponds to an infinitely high value for p (we note generally that F_d values in excess of those actually required for analysis have the disadvantage that they require more time than necessary for completion of the run).

Along with the constraints on F_d summarized above, there are similar constraints imposed by programming mathematics on the retention time (t_r)–diameter (d) relationships. For power programming, $t_r - t_a$ increases with some power of d (the power depending on the choice of p) in accordance with eqn. 22. This relationship cannot be converted into the log–linear relationship (see eqn. 8) characteristic of exponential programming. However, if a straight-line plot is desired for calibration purposes, a plot of $t_r - t_a$ (or simply t_r) *versus* $d^{n/p+1}$ is simple to construct and utilize. Similarly, a plot of log $(t_r - t_a)$ *versus* log d yields a straight line [a similar plot of log $(t_r - t_a)$ *versus* log (molecular weight, M) for polymers yields a straight line].

Various log–log plots in FFF more commonly yield straight calibration lines than any other type of plot; these plots, once established, can be readily used to obtain particle sizes or particle size distributions from experimental fractograms. In addition to power programming, where as we note a plot of log $(t_r - t_a)$ *versus* log d is linear (with slope 1/3 when $p = 3n - 1$), non-programmed FFF yields a straight line (again for well retained materials) of slope n when log t_r [or, more exactly, log $(t_r - t^0/3)$] [12] is plotted against log d. In both sedimentation/steric and flow/hyperlayer FFF, straight-line calibration plots are produced by plotting log t_r *versus* log d. An advantage of such log–log plots is that the slope is equal to the selectivity S_d, the percentage change in t_r for two particles differing in diameter by 1%.

Programs other than power and exponential (*e.g.*, linear and parabolic) have

their own unique F_d and t_r relationships [10]. Only the power program produces a uniform fractionating power across a wide range of d, but the other programs may prove useful in that they exhibit peak values of F_d that could be adjusted to focus on the most important constituents of a colloidal sample [10]. The possibilities for the flexible use of various programs to customize FFF separations to satisfy specific particle characterization holds considerable promise for future work.

ACKNOWLEDGEMENT

This work was supported by Public Health Service Grant GM10851-33 from the National Institutes of Health.

REFERENCES

1 L. R. Snyder, *Principles of Adsorption Chromatography*, Marcel Dekker, New York, 1968, ch. 2.
2 F. J. F. Yang, M. N. Myers and J. C. Giddings, *Anal. Chem.*, 46 (1974) 1924.
3 J. C. Giddings, L. K. Smith and M. N. Myers, *Anal. Chem.*, 48 (1976) 1587.
4 J. J. Kirkland, W. W. Yau, W. A. Doerner and J. W. Grant, *Anal. Chem.*, 52 (1980) 1944.
5 W. W. Yau and J. J. Kirkland, *Sep. Sci. Technol.*, 16 (1981) 577.
6 J. J. Kirkland, S. W. Rementer and W. W. Yau, *Anal. Chem.*, 53 (1981) 1730.
7 J. C. Giddings and K. D. Caldwell, *Anal. Chem.*, 56 (1984) 2093.
8 J. C. Giddings, P. S. Williams and R. Beckett, *Anal. Chem.*, 59 (1987) 28.
9 P. S. Williams and J. C. Giddings, *Anal. Chem.*, 59 (1987) 2038.
10 P. S. Williams, J. C. Giddings and R. Beckett, *J. Liq. Chromatogr.*, 10 (1987) 1961.
11 P. S. Williams, L. Kellner, R. Beckett and J. C. Giddings, *Analyst (London)*, 113 (1988) 1253.
12 J. C. Giddings, F. J. Yang and M. N. Myers, *Anal. Biochem.*, 81 (1977) 395.

Journal of Chromatography, 550 (1991) 799–809
Elsevier Science Publishers B.V., Amsterdam

CHROMSYMP. 2231

Quantitative particle-size distributions by sedimentation field-flow fractionation with densimeter detector[a]

J. J. KIRKLAND* and W. W. YAU
E. I. DuPont de Nemours and Company, Inc., Central Research and Development, Experimental Station, P.O. Box 80228, Wilmington, DE 19880-0228 (USA)

ABSTRACT

Certain colloidal samples pose problems in obtaining accurate transformation of turbidimetric detector signals in sedimentation field-flow fractionation (SdFFF) to the desired particle concentration output. A densimeter detector shows promise in eliminating these problems. This device responds to changes in the density of sample components in the channel eluent. Accurate concentrations of sample particles are available directly without the need for detector-response transformation. Displaying the required signal-to-noise sensitivity for inorganic colloids, the densimeter appears to be a useful alternative to the turbidimetric detector for many SdFFF applications.

INTRODUCTION

Sedimentation field-flow fractionation (SdFFF) is a superior method for determining the size and size distribution of colloids [1–6]. Particles of widely differing types in the range of *ca.* 10–10 000 nm can be accurately characterized with high precision without the need for standards or calibration [1,4,5].

SdFFF separations are performed in a thin, open channel that rotates within a centrifuge [7,8]. Because of an imposed centrifugal force, particles that are heavier than the liquid mobile phase settle radially outward against the accumulation wall of the channel. Build-up of particles next to this wall is resisted by normal diffusion in the opposite direction. Therefore, because of lower diffusion and higher sedimentation rates, larger and heavier particles are forced closer to the accumulation wall. These larger particles are intercepted by slower laminar-flow flow streams next to the wall. They are then eluted from the channel after smaller particles that are intercepted by higher flow stream velocities further from the wall.

The resulting SdFFF fractogram is a record of the elution of particles as a function of time. Earlier eluting peaks correspond to lighter and smaller particles, followed by particles of increasing mass or size. Data extracted from this fractogram

[a] Presented in part at the *Chromatography Award Symposium for Professor John Knox, American Chemical Society Meeting, Boston, MA, April 25, 1990.*

0021-9673/91/$03.50

permits the calculation of the particle size and particle-size distribution of the colloid sample [1,4,6].

Standards are not required for the SdFFF measurement, as the method is based on known physical first principles. The analytical precision is excellent because of high resolution [9]. Just as important, SdFFF is capable of handling samples with a wide range of particle sizes by utilizing programmed force-field methods, whereby the force field is decreased systematically during the experiment. Exponential decay of the centrifugal force field has been found to be a convenient method of programming. With this approach, a plot of retention time *versus* log (particle size) produces a linear plot for precise quantification [4].

Turbidimetric detection using a UV–visible photometer or spectrophotometer generally has been used for sensing particles as they elute from an SdFFF channel [1–3, 5–8]. This detection method is satisfactory for many particle size measurements. It usually provides adequate sensitivity, is readily available and is convenient to operate. However, the light-scattering principle involved in turbidimetry creates a problem in particle-size determination. Large particles scatter light much more effectively than small particles. Therefore, the response of the turbidimetric detector is very non-linear with particle size differences. This effect is illustrated in Fig. 1. This shows a family of plots of scattering efficiency, Q_{sca}, *versus* the parameter ρ, which is a complex function of spherical particle diameter, the relative refractive index of the particle and the suspending liquid and the reciprocal of the wavelength of the imping-

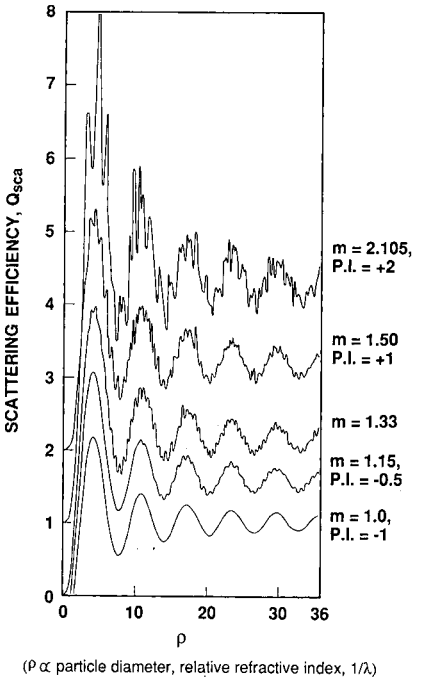

Fig. 1. Scattering efficiency plots for spherical particles. P.I. = plotting index; plotting scale change in scattering index units to simplify presentation. Adapted from ref. 10.

ing light. Here, $\rho = 2\pi d_p(m-1)/\lambda$, where d_p is the particle diameter, m is the relative refractive index ratio and λ is the wavelength of light in the medium. Plots are shown for various relative refractive index ratios, m (these plots are offset for ease of comparison). The initial steep portion of these plots represents the well known particle Rayleigh scattering regime. However, as ρ values increase (larger particles, higher refractive index, shorter wavelength), a complex "ringing" scattering function is found. The scattering function becomes extremely complex as the refractive index ratio m increases.

The complex scattering function shown in Fig. 1 greatly complicates the extraction of quantitative particle-size data from a turbidimetric detector output. Typically, this problem is handled by using computer software which transforms the turbidimetric detector output signal to true concentration values using the Mie scattering theory [11]. This approach generally provides good results, and so it is well suited and convenient for many applications.

However, experience has shown that turbidimetric detection is less desirable for measuring certain types of particles. Very small particles (*e.g.*, < 10 nm) are difficult to detect at useful concentrations because they scatter poorly. Decreasing the detector wavelength improves but often does not solve this problem. Another limitation is that the detector response to particles with high refractive indices is very difficult to convert accurately to concentration, as implied by the complex plots in Fig. 1. As a result, certain types of samples need a different type of detection to eliminate these problems, so that accurate particle-size information can be obtained.

This paper describes the application of a sensitive densimeter detector for determining particle size and particle-size distributions by SdFFF. This device, based on the mechanical oscillator method, directly measures particle concentration without any need for transforming the output signal. The detector also provides adequate sensitivity for inorganic colloids. Therefore, this device is a useful complement to turbidimetry in SdFFF particle-size measurements of colloidal materials.

EXPERIMENTAL

Apparatus and reagents

The SdFFF equipment used was the same as previously described [8,12]. A schematic diagram of the equipment is shown in Fig. 2. The densimeter detector was a Model DDS 70 (Anton Paar, Graz, Austria) prototype similar to that described by Trathnigg and Jorde [13]. The volume of the oscillator tube was 30 μl, and the total volume with the connecting tubing was 200 μl. This level of cell volume does not cause significant band broadening because of the relatively broad bands associated with SdFFF separations [3]. The temperature of the densimeter detector cell was maintained constant by placing it in a polyethylene bag located within a 20-l insulated foamed-polyethylene box filled with water. An inlet line of "crimped" 120 × 0.05 cm capillary tubing was loosely coiled around the detector cell within the bath to insure that the channel effluent entered the cell at the same temperature.

Colloid samples were obtained from DuPont. Scanning electron micrographs were obtained with a Model 840 instrument (Joel, Tokyo, Japan). Aerosol-OT was made from a 10% solution obtained from Fisher Scientific (Fair Lawn, NJ, USA). "Micro" detergent was obtained from Cole-Parmer Instrument (Chicago, IL, USA).

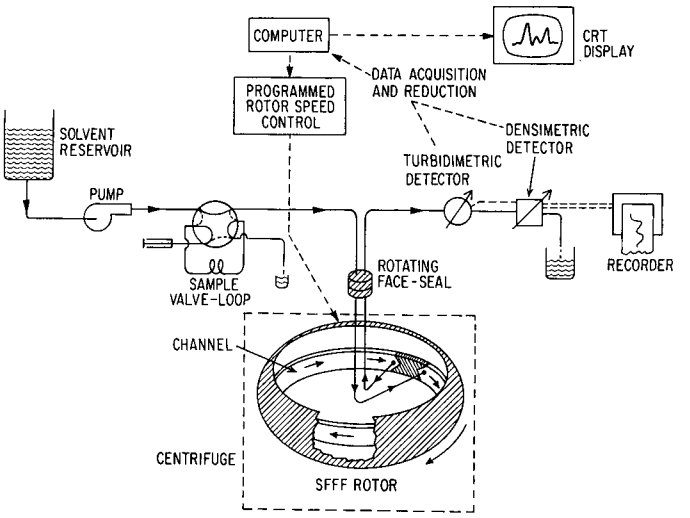

Fig. 2. Schematic diagram of sedimentation FFF apparatus with a densimeter detector.

Density detection

The basics of the densimeter detector using a mechanical oscillator were previously described by Trathnigg and Jorde [13]. The measuring cell contains an oscillating, U-shaped glass tube. Under optimum conditions, the oscillation period of this tube describes the density of its contents with precisions approaching 10^{-6} g/cm^3:

$$d = AT^2 - B \tag{1}$$

where d is the density of the material in the tube, T is the time period of the oscillation and A and B are constants for each cell. These constants are determined by a two-point calibration using water and air, or two solvents of widely different known densities. A density change Δd within the cell is then

$$\Delta d = A(T_2^2 - T_1^2) = A(T_2 - T_1)(T_2 + T_1) \tag{2}$$

where T_1 and T_2 are the initial and measuring time period of oscillations, respectively. For the small density changes measured in SdFFF,

$$T_2 + T_1 = 2T_0 \tag{3}$$

and

$$\Delta d = 2AT_0 dT \tag{4}$$

or, substituting eqn. 1,

$$\Delta d = 2(B + d_0)(\Delta T/T) \tag{5}$$

where dT or ΔT is the change in the oscillation time period and d_0 is the density of the mobile phase liquid.

Now, the period T_m is determined by counting the number N_b of periods T_b of a standard time base (a 10-MHz quartz oscillator) within a measuring interval t_m for a constant number N_m of periods T_m of the measuring cell:

$$t_m = N_m T_m = N_b T_b \tag{6}$$

Combining eqns. 5 and 6 gives

$$\Delta d = 2(B + d_0)(\Delta N_b / N_b) \tag{7}$$

The mobile phase volume V passing through the cell within each measuring interval at flow-rate F is

$$V = F N_b T_b \tag{8}$$

This volume contains a mass m_i of a solute i to be measured, and this will cause a density change:

$$\Delta d = c_i(1 - d_0 V_i^*) = a_i m_i / V \tag{9}$$

where $a_i = 1 - d_0 V_i^*$ and V_i^* is the volume for each specific measuring interval. Combining eqns. 7–9 gives

$$m_i = 2T_b(B + d_0)(F/a_i)x_i \tag{10}$$

where $x_i = (\Delta N_b)_i$; the digital response of the density detector is integrated over each measuring interval t_m to determine the mass of solute eluted with t_m. Integration of a peak is performed by summing x_i.

RESULTS AND DISCUSSION

The utility of the densimeter detector in the measurement of the particle-size distribution of colloids is illustrated in Fig. 3 for a silica sol sample. These data were obtained using the time-delay, exponential-decay force-field programming method (TDE-SFFF) that has been described previously [4]. The left hand panels in Fig. 3 show the "raw" turbidimetric detector *vs.* time output and the relative concentration *vs.* linear particle diameter plot. The latter was obtained by transforming the "raw" detector signal using software containing the Mie scattering correction method [11]. Panels on the right in Fig. 3 show data obtained with the densimeter detector on a separation identical with that performed with the turbidimetric detector. In this case, no transformation of the "raw" detector signal was required, because the output of the densimeter detector is linear with sample concentration. As shown by the data in the lower panels in Fig. 3, results for this silica sol sample are closely similar for the two different detectors.

Limitations of turbidimetric detection for measuring the particle-size distribu-

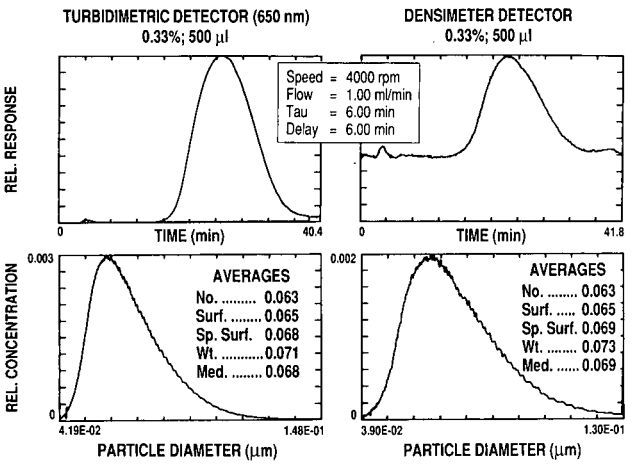

Fig. 3. Comparative detection for silica sol sample separated by TDE-SFFF. Mobile phase, 1 mM ammonia solution; ρ_S = 2.2 g/cm^3; $\Delta\rho$ = 1.2 g/cm^3; other operating parameters as shown.

tion of certain samples is illustrated in Fig. 4. The top panel shows the "raw" detector signal in a fractionation of a diamond dust sample. The middle panel represents the attempted transformation of the "raw" signal with the Mie scattering method to obtain the relative concentration or differential plot of concentration *vs.* particle size.

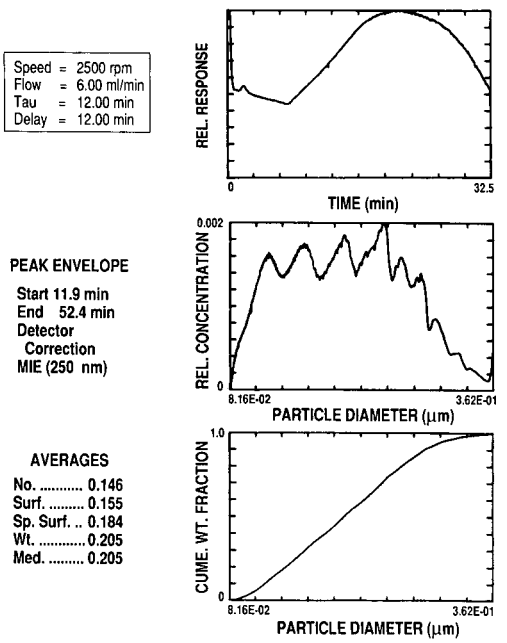

Fig. 4. TDE-SFFF of diamond dust with turbidimetric detection. Mobile phase, 0.2% "Micro" detergent; ρ_D = 3.51 g/cm^3; $\Delta\rho$ = 2.51 g/cm^3; detector, 250 nm; other operating parameters as shown.

The severe "ringing" effect seen in this plot is actually not characteristic of the sample, but results from errors in the transformation process. These errors arise from the very high refractive index of diamond and the relatively low wavelength (250 nm) used for the turbidimetric detection. These factors cause the scattering regime to be in a region that involves strong "ringing" or oscillations, as shown by the plots in Fig. 1. Small errors in refractive index, particle diameter or wavelength values for the transformation process then can create the type of "ringing" effect seen in the middle plot in Fig. 4, and also in the lower cumulative plot. This "ringing" effect also can cause errors in the calculation of particle diameters and particle-size averages for the samples.

As suggested by the plots in Fig. 1, increasing the wavelength of turbidimetric detection would place the scattering regime in a region where the "ringing" problem should be reduced. This is borne out by the data in the left-hand panel of Fig. 5. Here, the diamond dust sample now shows considerably less of the "ringing" effect in the differential plot when detection was performed at 700 nm, compared with 250 nm. Note that the calculated particle averages are smaller than those found at the higher detector wavelength.

Use of the densimeter detector for the diamond dust sample produced an unexpected bonus in measurement accuracy. The differential plot in the panel on the right in Fig. 5 shows a population of smaller particles that were not sensed by the turbidimetric detector under the conditions used. The reason for this is that the turbidimetric detector signal decreases as a fourth-power function of particle diameter (see Fig. 1). Again, transformation accuracy in turbidimetric detection is poor with very small particles. Note that the calculated averages with the densimeter detector are now significantly smaller, and in keeping with the manufacturer's claim of "1/8 μm" particles. In the scanning electron micrograph in Fig. 6, the presence of a population of <0.1 μm particles is apparent, in addition to particles <0.3 μm.

Comparison of turbidimetric and densimetric detection is also shown in Fig. 7

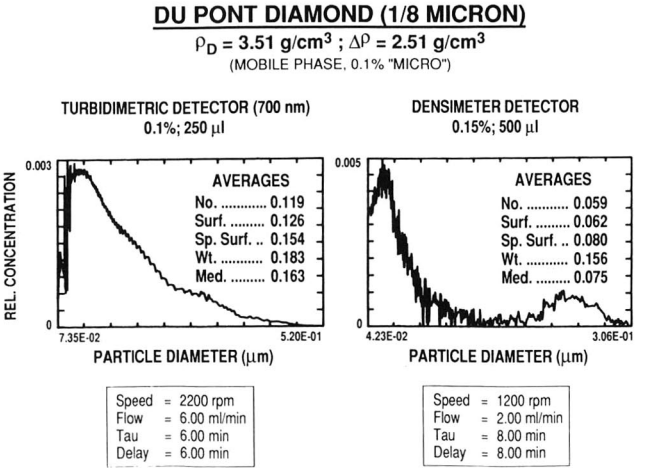

Fig. 5. Comparative detection with TDE-SFFF separation of diamond dust sample. Mobile phase, 0.1% "Micro" detergent; turbidimetric detection, 700 nm; other operating parameters as shown.

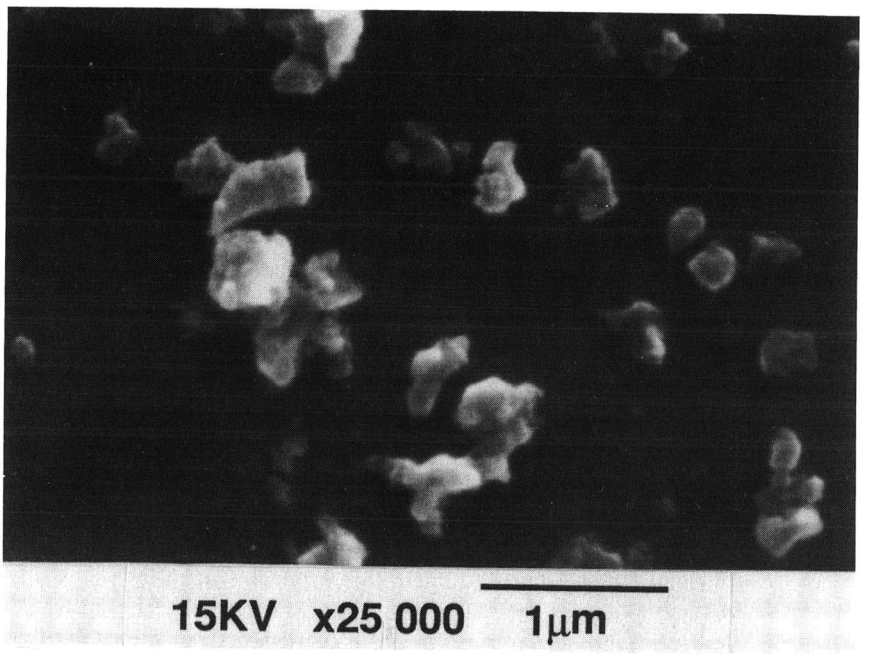

Fig. 6. Scanning electron micrograph of diamond dust particles.

in the particle-size distribution measurement of a chromium dioxide sample. "Raw" detector outputs and differential plots are shown for both detection systems. Excellent correlation was found for particle-size averages calculated for measurements with these detectors.

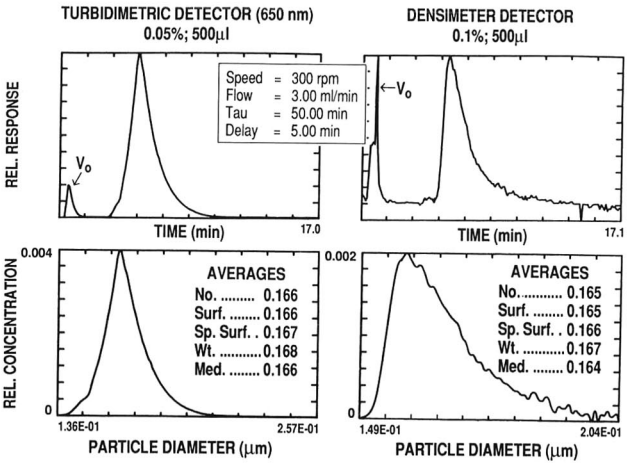

Fig. 7. TDE-SFFF of chromium dioxide. Mobile phase, 0.2% "Micro" detergent; $\rho_{CD} = 4.86$ g/cm^3; $\Delta\rho = 3.86$ g/cm^3; other operating parameters as shown.

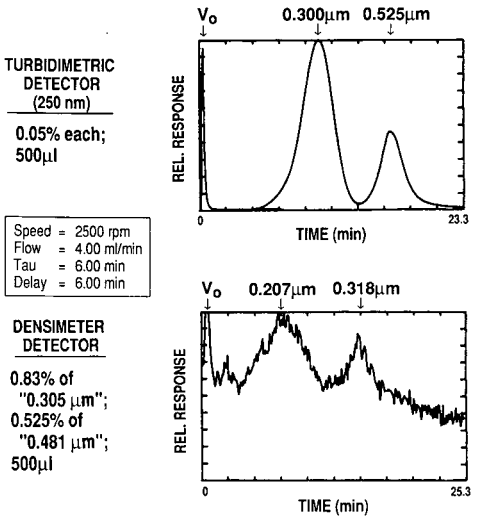

Fig. 8. Comparative detector sensitivity for polystyrene latex mixture. Mobile phase, 0.1% Aerosol-OT; ρ_{PS} = 1.05 g/cm^3; $\Delta\rho$ = 0.05 g/cm^3; other operating parameters as shown.

The main limitations of the densimetric detector in SdFFF applications involve inadequate sensitivity in instances where there are small differences in the densities of the particles and the mobile phase. The restriction is exemplified in Fig. 8 for the separation of two narrow-particle-size polystyrene latex standards (density of polystyrene = 1.05 g/cm^3; density of mobile phase = 1.00 g/cm^3; $\Delta\rho$ = 0.05 g/cm^3). The top graph shows the relative concentration *vs.* particle-size plot for the turbidimetric detector after transformation. The calculated values of 0.300 and 0.525 μm compare

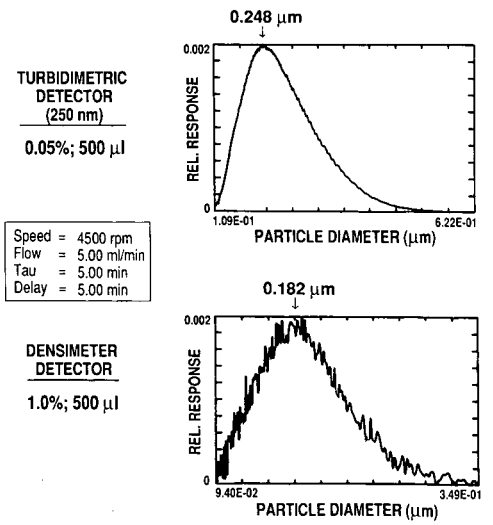

Fig. 9. Comparative detector sensitivity for experimental chloroprene latex. Mobile phase, 0.1% Aerosol-OT; ρ_N = 1.22 g/cm^3; $\Delta\rho$ = 0.22 g/cm^3; other operating parameters as shown.

with the supplier's values of 0.305 and 0.481 μm (the latter value is actually 0.535 $\pm$ 0.012 μm by independent measurements [14]). To obtain any recognizable signal with the densimeter detector (lower plate, Fig. 8), more than a 10-fold increase in sample concentration was required. Even at this high concentration, the detector signal was noisy. In this case, calculated values for particle sizes were significantly lower than actual, indicating that the channel was overloaded with sample. Overloading causes early elution of particles with resulting smaller than actual calculated values.

Organic polymer lattices with higher densities still do not give sufficient sensitivity with the densimeter detector to permit accurate analysis. This is illustrated by the data in Fig. 9 for a chloroprene (Neoprene) latex with a density of 1.22 g/cm^3 ($\Delta\rho$ = 0.22 g/cm^3). The top graph with the turbidimetric detector shows a peak-position particle diameter of 0.248 μm for this sample. With a 20-fold increase in sample amount, the densimeter detector signal (bottom plot) was still unacceptably noisy. The calculated particle-diameter value for the densimeter detector run was only about three quarters of that found with the turbidimetric detector, because of channel overloading.

CONCLUSIONS

The advantage of the densimeter in SdFFF analyses is that it is a universal detector needing no signal transformation for accurate particle-size distribution measurements. In its present form, the densimeter detector requires a density difference $\Delta\rho$ between the particle and the mobile phase of greater than 0.2 for adequate detection. Overloading the channel to compensate for inadequate signal-to-noise detector response results in particle-size measurements that are smaller than actual. Accurate particle-size distribution measurements are easily accomplished with densimetric detection if $\Delta\rho$ is greater than about 1.0. This means that this detector is well suited for measuring the particle size distributions of inorganic colloids by SdFFF, but has limited application for organic colloids that characteristically have lower densities.

The densimeter detector is sensitive to temperature, so the cell must be carefully thermostated. Incoming lines containing the channel effluent from the SdFFF should be thoroughly heat exchanged to minimize baseline upsets. As used in this study, the densimeter detector is essentially flow insensitive. This characteristic may make this device useful for flow programming in appropriate situations.

The densimeter detector used in this study has sufficient sensitivity for application in size-exclusion chromatography [13]. For general application in SdFFF for all types of colloids, an order of magnitude increase in sensitivity is needed, because of the significantly higher dilution of sample that occurs during the separation. Application of densimetric detection to thermal FFF and flow FFF would become highly attractive with increased sensitivity.

ACKNOWLEDGEMENTS

We thank W. H. Emerson for his assistance with the experiments and B. Trathnigg for his help in obtaining and setting up the densimeter instrument.

REFERENCES

1 J. C. Giddings, F. J. F. Yang and M. N. Myers, *Anal. Chem.*, 46 (1974) 1917.
2 F. J. Yang, M. N. Myers and J. C. Giddings, *J. Colloid Interface Sci.*, 60 (1977).
3 J. J. Kirkland, W. W. Yau, W. A. Doerner and J. W. Grant, *Anal. Chem.*, 52 (1980) 1944.
4 J. J. Kirkland, S. W. Rementer and W. W. Yau, *Anal. Chem.*, 53 (1981) 1730.
5 J. C. Giddings, K. D. Caldwell and H. K. Jones, *ACS Symp. Ser.*, 322 (1987) 215.
6 H. G. Mercus, Y. Mori and B. Scarlett, *Colloid Polym. Sci.*, 267 (1989) 1102.
7 J. C. Giddings, M. N. Myers, K. D. Caldwell and S. R. Fisher, *Methods Biochem. Anal.*, 26 (1980) 79.
8 J. J. Kirkland, C. H. Dilks, Jr. and W. W. Yau, *J. Chromatogr.*, 225 (1983) 225.
9 W. W. Yau and J. J. Kirkland, *Sep. Sci. Technol.*, 16 (1981) 577.
10 M. Kerker, *The Scattering of Light*, Academic Press, New York, 1969, p. 105.
11 G. Mie, *Ann. Phys.*, 25 (1908) 377.
12 J. J. Kirkland and W. W. Yau, *Anal. Chem.*, 55 (1983) 2165.
13 B. Trathnigg and C. Jorde, *J. Chromatogr.*, 241 (1982) 147.
14 W. W. Yau and J. J. Kirkland, *Anal. Chem.*, 56 (1984) 1461.

Journal of Chromatography, 550 (1991) 811–822
Elsevier Science Publishers B.V., Amsterdam

CHROMSYMP. 2248

High-performance displacement electrophoresis in 0.025- to 0.050-mm capillaries coated with a polymer to suppress adsorption and electroendosmosis

STELLAN HJERTÉN* and MARIANNE KIESSLING-JOHANSSON
Department of Biochemistry, University of Uppsala, Biomedical Center, P.O. Box 576, S-751 23 Uppsala (Sweden)

ABSTRACT

The risk of adsorption onto the walls of an electrophoresis tube increases with decreases in the bore of the tube and in the ionic strength (conductivity) of the buffers. It is therefore important to suppress adsorption in high-performance displacement electrophoresis where the diameter of the tube is often as narrow as 0.025 mm and the electrical conductivities are low (as they are in most displacement electrophoresis experiments at the steady state), for instance $10^{-4}\ \Omega^{-1}\ cm^{-1}$. This can be accomplished by coating the electrophoresis tube with a thin (preferably monomolecular) layer of a hydrophilic non-ionic polymer, which also eliminates electroendosmosis.

The narrow-bore tubes permit high field strengths without serious thermal zone broadening and therefore have the advantage of affording fast runs with high resolution (displacement electrophoresis often gives lower thermal zone broadening at a given field strength than does zone electrophoresis, because the average conductivity in the former method is usually lower than the conductivity in the latter). An analysis of serum proteins at a field strength of 860 V/cm took about 10 min. In the presence of continuous spacers the resolution increased dramatically: human serum could be resolved into about 30 components. Twelve nucleotides were separated within 10 min.

Displacement electrophoresis in coated tubes gives reproducible electropherograms, which makes the method suitable for clinical analyses, exemplified by a study of serum from a patient with multiple myeloma.

The zone broadening is considered with regard to diffusion, Joule heat and adsorption. The terms displacement electrophoresis and isotachophoresis are discussed.

INTRODUCTION

A common diameter of the electrophoresis tube in displacement electrophoresis (isotachophoresis) experiments is 0.2 mm. Theoretically, it is an advantage to use even smaller diameters, since the thermal zone deformation is proportional to $(dF)^2$, where d is the diameter of the tube and F is the field strength [1] (if d is decreased the field strength can be increased proportionally to get the same zone deformation). Another advantage of high field strengths is that the automatic zone-sharpening characteristic of displacement electrophoresis is more pronounced the higher is the field strength (broadening caused by diffusion is thus of less importance). Displace-

0021-9673/91/$03.50

ment electrophoresis experiments should therefore be conducted at high field strengths to give high resolution and short analysis times, but not so high that the thermal zone deformation becomes the dominating cause of zone broadening.

There are, consequently, theoretical reasons why one should try to decrease the diameter of the electrophoresis tubes. However, a reduction in tube diameter means, in practice an increased risk of adsorption onto the tube wall of the solutes to be separated. Only if the adsorption can be virtually eliminated can one take advantage of diameters as small as 0.025–0.050 mm. The purpose of this paper is to investigate whether the method successfully used to suppress adsorption in zone electrophoresis (*i.e.* coating the inside of the electrophoresis tube with a hydrophilic polymer, which also eliminates electroendosmosis) [2] is applicable in displacement electrophoresis experiments in tubes with these small bores.

Most of the experiments described here in have been presented at two recent symposia [3,4].

MATERIALS AND METHODS

Normal human serum was from the University Hospital in Uppsala, Sweden, and serum of a multiple myeloma patient from the Department of Neurology, University of Pécs, Hungary. Acrylamide, potassium persulphate, N,N,N′,N′-tetramethylethylenediamine (TEMED), agarose (zero = m_r), tris(hydroxymethyl)aminomethane (Tris) and the carrier ampholytes Bio-Lyte were obtained from Bio-Rad Laboratories, Richmond, CA, USA. γ-Methacryloxypropyltrimethoxysilane (Bind-Silane) was purchased from Pharmacia, Uppsala, Sweden, and the fused-silica tubing (inside diameters, 0.025–0.05 mm; lengths, 290–360 mm) from Scientic Glass Engineering, Ringwood, Australia.

The coating of the tubes was performed as described in ref. 2 with minor modifications. A 15-μl sample of Bind-Silane was mixed with 0.5 ml of 50% ethanol (pH 3.6). The 4% (w/v) acrylamide solution contained 0.8 μl of TEMED and 2 mg of ammonium persulphate per ml solution. The tubes were treated twice with Bind-Silane and once with the acrylamide solution. Excess polymerized non-bound acrylamide was displaced from the capillary tube with the aid of a high-performance liquid chromatography (HPLC) pump. The coupling between the tube and the pump was accomplished with standard HPLC connectors.

In all displacement electrophoresis experiments for the separation of serum proteins we employed the following buffer system: leading buffer, 0.01 *M* HCl adjusted to pH 8.3 with solid Tris [5]; terminating buffer, 0.1 *M* β-alanine adjusted to pH 9.2 with solid barium hydroxide. Barium ions precipitate bicarbonate formed by uptake of atmospheric carbon dioxide [5,6]. A 0.01 *M* HCl solution adjusted to pH 3.9 with solid β-alanine served as leading buffer for the separation of nucleotides and 0.01 *M* caproic acid (pH about 3.7) as terminator. In all experiments the anode vessel contained the leading and the cathode vessel the terminating solution. Coated electrophoresis tubes were filled (with the aid of water suction) with leading and non-coated tubes with terminating buffer. A 30-mm length of buffer was sucked off from one end of the tube. The opposite end was dipped into the sample solution, which by capillary forces entered the tube within about 20 s. The starting zone thus had a length of 30 mm.

The sample end of the tube was pressed into a 3% agarose gel prepared in the terminator. A 1 to 2-mm gel plug thus closed the tube and prevented hydrodynamic flow in the tube during the run.

The on-tube detector was a modified Zeiss spectrophotometer (Model M4 QIII). The proteins were recorded at 280 and the nucleotides at 254 nm. The 30-kV power supply was purchased from Glassman, Whitehouse Station, NY, USA. The electrophoretic migration distance up to the UV detector was 30 mm shorter than the length of the tube.

EXPERIMENTS AND RESULTS

Displacement electrophoresis in polymer-coated and non-coated capillaries

The experiment was performed at a voltage of 10 kV in a 340 × 0.025 mm I.D. fused-silica tube coated with linear polyacrylamide. As sample we used normal human serum diluted 6:1 with 0.7 *M* β-alanine titrated with solid barium hydroxide to pH 9.2. The electropherogram is presented in Fig. 1a. To test the stability of the coating the experiment was repeated every fourth day during a period of twenty days. Between the runs the tube was filled with the terminator (pH 9.2). No differences in the appearance of the electropherograms were observed.

The experiment was then repeated in a non-coated tube. Since non-coated tubes have a cathodic electroendosmotic velocity which is larger than the anodic electrophoretic velocity of the solutes, these will be transported toward the cathode. The non-coated tubes were therefore filled with terminator. The tube end with the 30-mm sample was in contact with the leading solution in the anode vessel. The cathodic vessel contained the terminating solution. The protein pattern obtained in a non-coated tube is shown in Fig. 1b. The zones in this figure are broader and less concentrated than those in Fig. 1a, indicating that a polymer coating suppresses disturbances caused by adsorption or/and electroendosmosis.

Displacement electrophoresis in polymer-coated capillaries of different diameters

The experiment presented in Fig. 1a was repeated with the difference that the diameter of the capillary tube was 0.05 mm instead of 0.025 mm. The electropherogram (Fig. 2) was similar to that shown in Fig. 1a.

Displacement electrophoresis in polymer-coated capillaries at different field strengths

The experimental conditions were the same as those in the experiment shown in Fig. 1a, but the voltage was increased to 30 kV (= 860 V/cm). The serum pattern (Fig. 3) resembled that in Fig. 1a, *i.e.* a field strength of 860 V/cm can be used for tubes with an inner diameter of 0.025 mm without loss of resolution.

Displacement electrophoresis in polymer-coated capillaries in the presence of discrete spacers

The sample was prepared by mixing 80 μl of normal human serum with 10 μl of 0.7 *M* β-alanine (titrated to pH 9.2 with solid barium hydroxide) and 10 μl of 0.1 *M* β-alanine (pH 9.2) containing 0.119 mg of glycylglycine, 0.026 mg of asparagine, 0.024 mg of threonine and 0.015 mg of glycine [7]. The peptide and the amino acids served as discrete spacers; their final concentrations in the applied sample were 9, 2, 2 and 2 m*M*, respectively. The protein pattern is shown in Fig. 4.

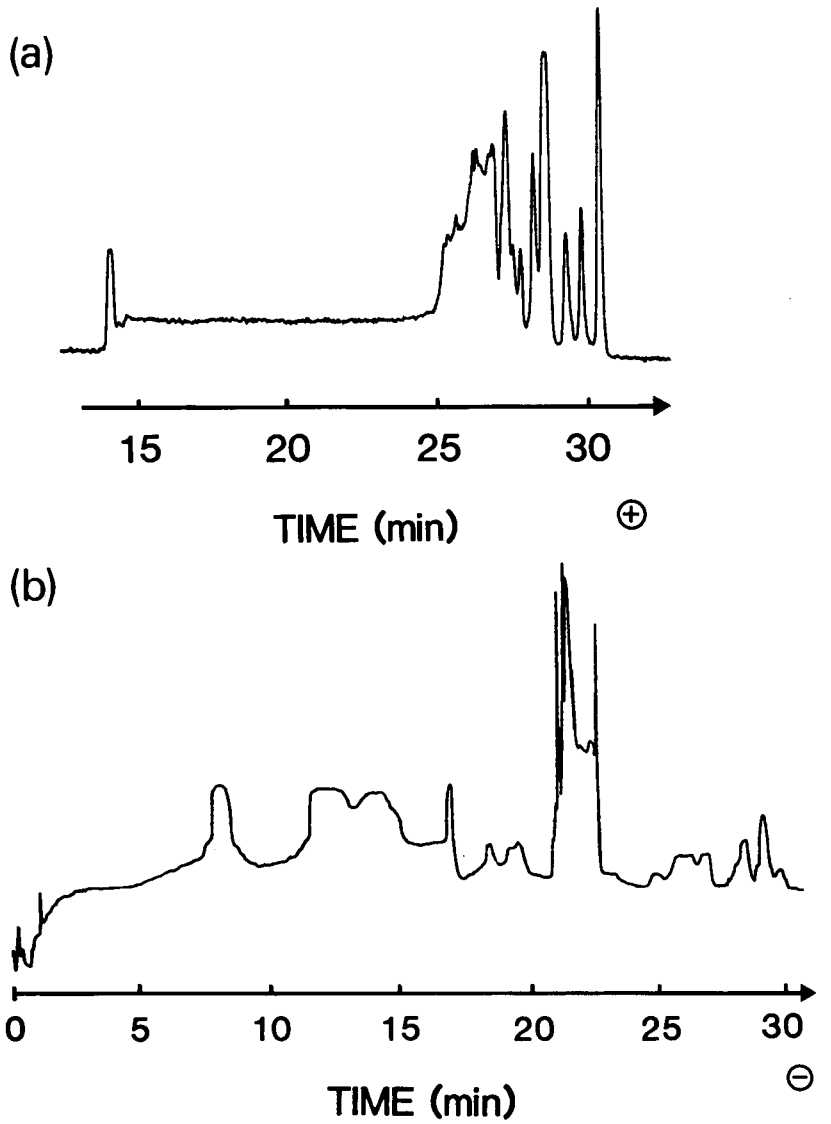

Fig. 1. High-performance displacement electrophoresis of human serum in polymer-coated (a) and non-coated (b) capillaries. Sample volume: 15 nl (= 30 mm). 0.01 *M* HCl adjusted to pH 8.3 with Tris served as anolyte (leading solution) and 0.1 *M* β-alanine titrated to pH 9.2 with barium hydroxide as catholyte (terminator). The electrophoresis tube was filled with leading solution in (a) and terminator in (b). Dimensions of the electrophoresis tubes: 340 × 0.025 mm I.D. Voltage: 10 kV. Detection wavelength: 280 nm. Anodic migration in (a), cathodic in (b) caused by electroendosmosis. The zones are narrower in (a) than in (b) because of suppression of adsorption or/and the absence of electroendosmosis.

Displacement electrophoresis in polymer-coated capillaries in the presence of continuous spacers

A 168-μl portion of 0.7 *M* β-alanine, pH 9.2, was mixed with 60 μl of Bio-Lyte 3/10. The pH was adjusted to 9 by the addition of 7 μl of 1 *M* NaOH. A 15-μl aliquot

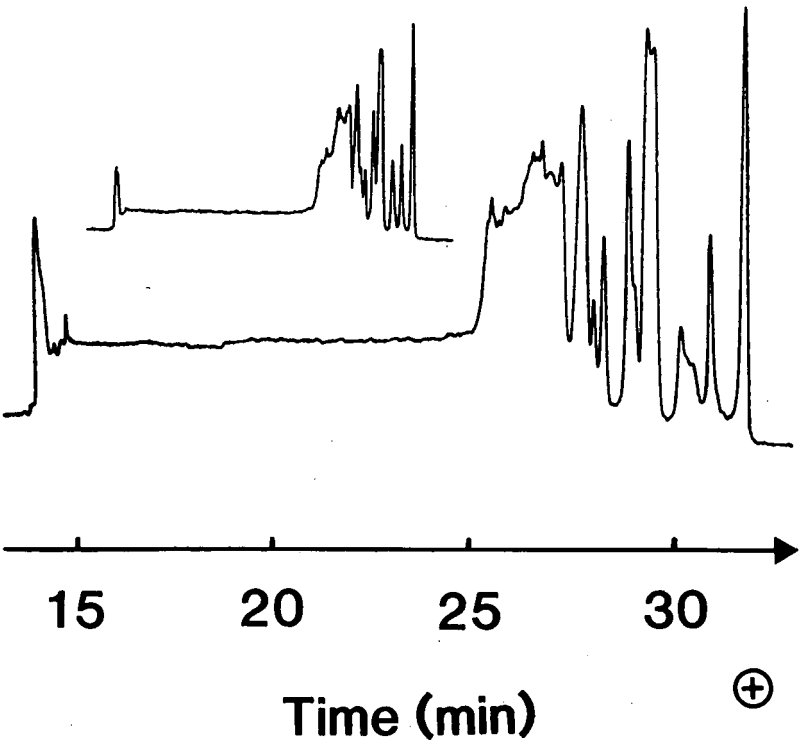

Fig. 2. High-performance displacement electrophoresis of human serum in polymer-coated capillaries of different diameters. Sample volume: 59 nl (= 30 mm). Anolyte, catholyte, voltage and wavelength are similar to those in the experiment shown in Fig. 1a. Dimensions of the electrophoresis tube: 350 × 0.05 mm I.D. A comparison with Fig. 1a (inserted) indicates that one can decrease the diameter of the capillary down to at least 0.025 mm without loss of resolution.

of this solution was mixed with 80 μl of normal human serum. A displacement electrophoresis of this sample gave the pattern in Fig. 5. A comparison with Fig. 2 shows the increased resolution achieved in the presence of spacers, Bio-Lyte (Svendsen and Rose [8] were the first to use carrier ampholytes for isoelectric focusing as spacers in displacement electrophoresis). Alternative conditions for displacement electrophoresis of serum proteins in the presence of such spacers are given in an early publication on free capillary electrophoresis [9]; see also ref. 10.

Displacement electrophoresis in polymer-coated capillaries of serum from a patient with multiple myeloma

The run was performed essentially as described for the experiment in Fig. 1a. The electropherogram (Fig. 6) differs chiefly from that in Fig. 2 in that it has a larger slowly migrating zone, corresponding to an increased concentration of immunoglobulins [11].

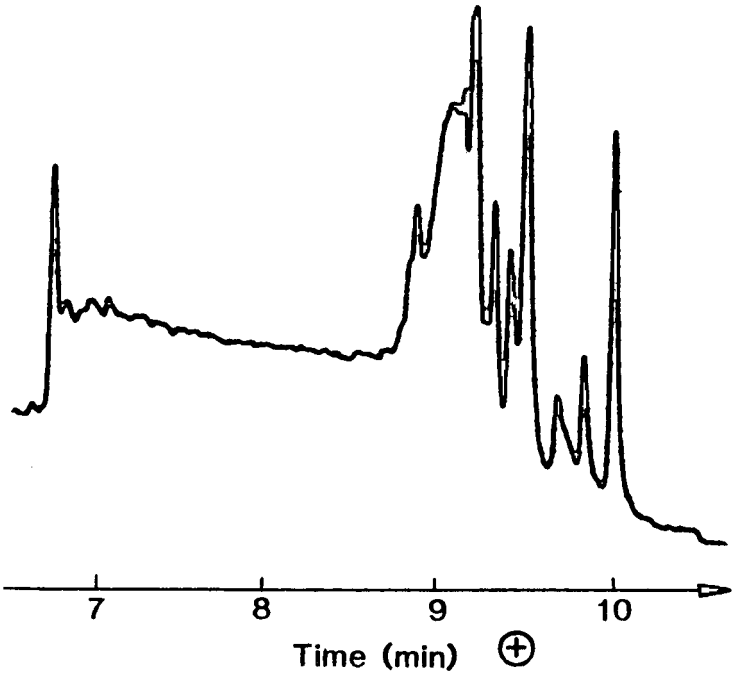

Fig. 3. High-performance displacement electrophoresis of human serum on polymer-coated capillaries at increased field strength. Sample volume: 15 nl (= 30 mm). Anolyte, catholyte and wavelength are similar to those in Fig. 1a. Voltage: 30 kV. Dimensions of the electrophoresis tube: 350 × 0.025 mm I.D. A comparison between Figs. 1a and 3 shows that one can use at least 30 kV (maximum voltage of the power supply) without loss of resolution and that there is a good correlation between field strength and run time.

Displacement electrophoresis of nucleotides in a polymer-coated capillary

Sample of 1 mg of each of the nucleotides AMP, ADP, ATP, CMP, CDP, CTP, GMP, GDP, GTP, UMP, UDP and UTP were dissolved in 200 μl of water, and 30 μl of 0.07 *M* caproic acid was added [11]. The starting zone had a length of 2 mm. The separation pattern is shown in Fig. 7.

Thermal zone broadening

The Joule heat generated in an electrophoresis experiment gives rise to a temperature difference between the axis of the electrophoresis tube and its inner wall. The solute molecules therefore migrate faster at the axis than at the wall. Eqn. 73 in ref. 1 was used to calculate the percentage difference in these migration velocities as a function of the square of the field strength for different radii of the electrophoresis tube (Fig. 8). This equation is only approximately valid for the displacement electrophoresis experiments described in the present paper (for instance, the capillaries have an outer polyimide coating and are not liquid-cooled), but still gives an idea as to how the field strength and the capillary radius affect the zone broadening.

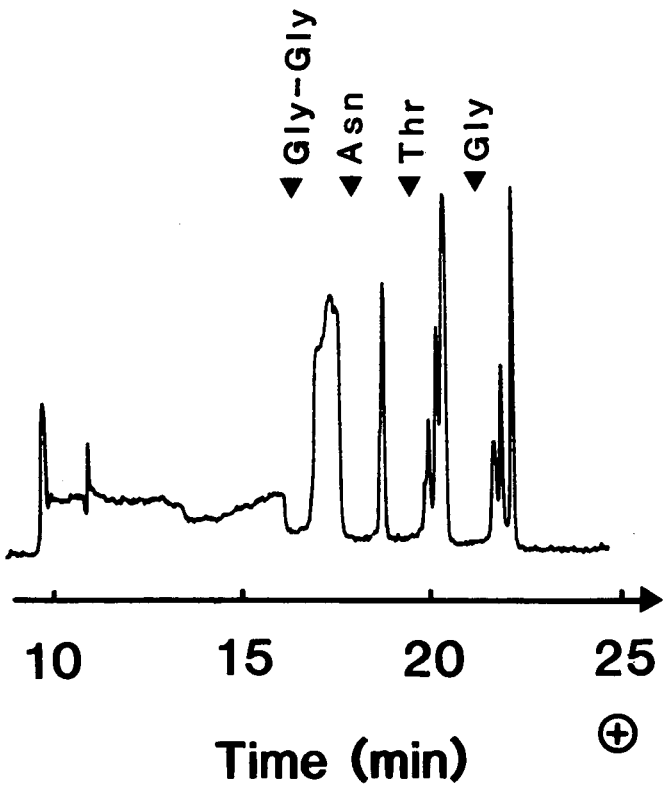

Fig. 4. High-performance displacement electrophoresis of human serum in a polymer-coated capillary in the presence of discrete spacers. Sample volume: 15 nl (= 30 mm). Anolyte, catholyte, voltage and wavelength are similar to those in Fig. 1a. Dimensions of the electrophoresis tube: 320 × 0.025 mm I.D. The spacers have negligible absorption at 280 nm, the wavelength used for detection.

DISCUSSION

The importance of correct nomenclature

Since the following equation applies to all methods based on electrophoresis, chromatography and centrifugation, any separation method within one of these three techniques has a counterpart within the other two [12,13].

$$c_j^{\alpha} v_j^{\alpha} - c_j^{\beta} v_j^{\beta} = v^{\alpha\beta} (c_j^{\alpha} - c_j^{\beta}) \quad (1)$$

where α and β are two phases separated by a moving boundary, which migrates with the velocity $v^{\alpha\beta}$; c_j^{α} and v_j^{α} are the concentration and the velocity, respectively, of the ion j in the α phase (c_j^{β} and v_j^{β} refer to the β phase). For instance, there must accordingly exist a method which is the electrophoretic counterpart of displacement chromatography and it is natural to give this method an analogous name, *i.e.* displacement electrophoresis —a term preferred and used by one of the pioneers in this field, A. J.

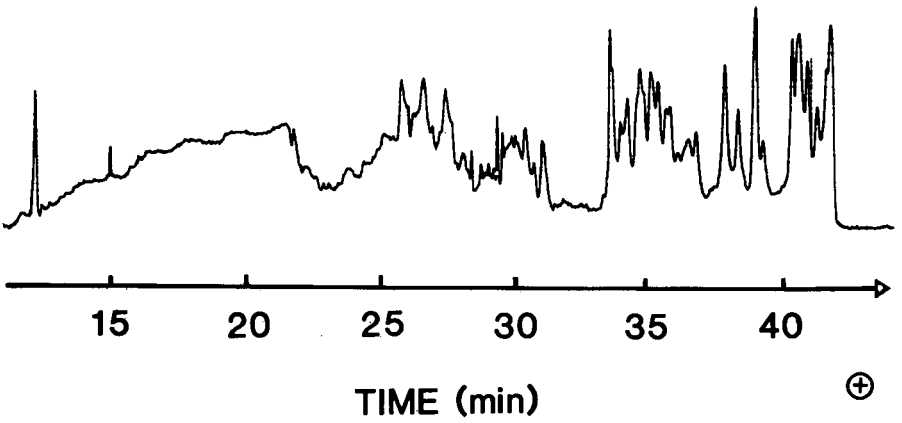

Fig. 5. High-performance displacement electrophoresis of human serum in polymer-coated capillaries in the presence of continuous spacers. Spacers: Bio-Lyte 3/10. Sample volume: 59 nl (= 30 mm). Anolyte, catholyte, voltage and wavelength are similar to those in Fig. 1a. Dimensions of the electrophoresis tube: 350 × 0.05 mm I.D. A comparison with Fig. 2 shows that the presence of continuous spacers increases the resolution considerably.

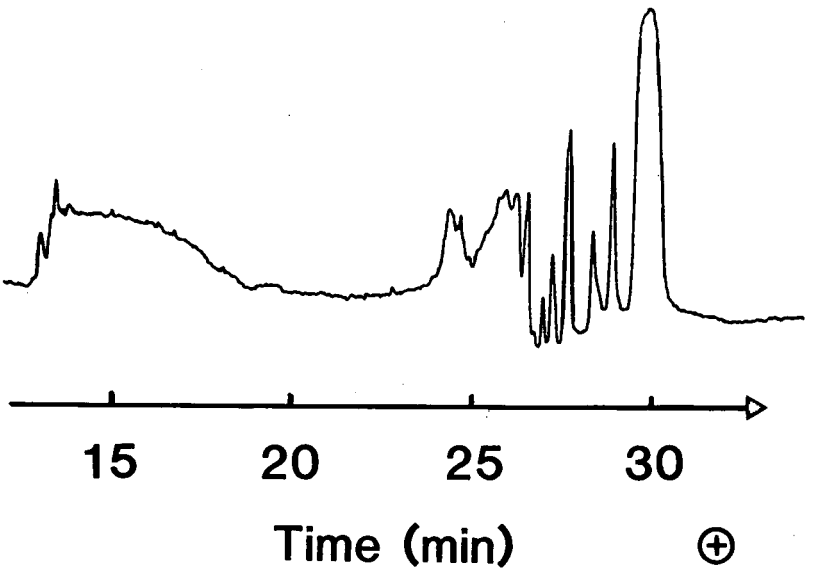

Fig. 6. High-performance displacement electrophoresis of a multiple myeloma serum in a polymer-coated capillary. Sample volume: 59 nl (= 30 mm). Anolyte, catholyte, voltage and wavelength are similar to those in Fig. 1a. Dimensions of the electrophoresis tube: 340 × 0.05 mm I.D. A comparison with Fig. 2, where serum from a healthy person was used, shows that multiple myeloma patients have an elevated level of immunoglobulins (the last zone).

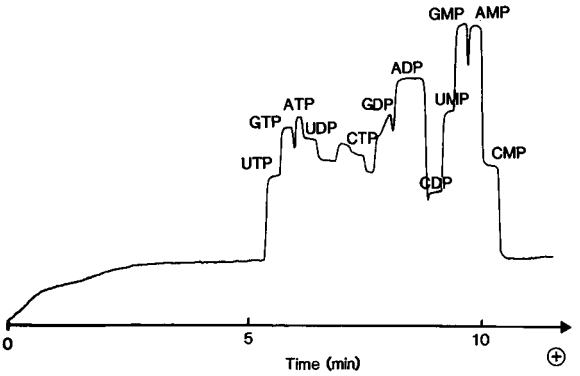

Fig. 7. High-performance displacement electrophoresis of nucleotides in a polymer-coated capillary. Sample volume: 4 nl (= 2 mm). Anolyte: 0.01 *M* HCl adjusted to pH 3.9 with solid β-alanine. Catholyte: 0.01 *M* caproic acid. Dimensions of the electrophoresis tube: 290 × 0.05 mm I.D. Voltage: 10 kV. Detection wavelength: 254 nm. The analysis time is about fourfold shorter than that obtained in commercial equipment with a non-coated 0.2-mm capillary.

P. Martin [14,15] and employed by Everaerts in his thesis [16]. One can expect these analogous methods to have analogous separation mechanisms and to be described by analogous equations. This is, in fact, true: in both methods the width of a zone is proportional to the amount of the solute in the zone; and the solute concentration in the zone is independent of its concentration in the applied sample but is characteristic of the solute and can be used to identify it. Furthermore, the leading and terminating solutions in displacement electrophoresis correspond to the equilibration and displacing buffers, respectively, in displacement chromatography. The two methods also give similar separation patterns: a step-formed diagram when the solute concentrations are measured in suitable units.

From the above considerations it might be evident that all analogous separation methods should be given analogous notations, since this stresses the analogy and facilitates theoretical understanding of the separation mechanisms, and thereby rational utilization of the methods. For this reason we prefer the term displacement electrophoresis to isotachophoresis.

It is very likely that progress in separation science has been delayed —and therefore also that in life sciences— because the existence of a common equation for electrophoresis, chromatography and centrifugation —and the consequences of it— have not until recently been emphasized [12,13]. For instance, isoelectric focusing in natural pH gradients was described in 1961 [17], but the first paper on the chromatographic counterpart, chromatofocusing, was not published until 1978 [18]. Seventeen years is too long for the introduction of the analogous chromatographic method. Another example of a consequence of ignorance of eqn. 1 is that indirect detection in chromatography was not utilized [19] until many years following introduction of this detection method in electrophoresis [1].

Factors causing zone broadening

In zone electrophoresis the following factors affect the width of a zone: diffusion; Joule heat; adsorption; and pH and conductivity differences between the solute

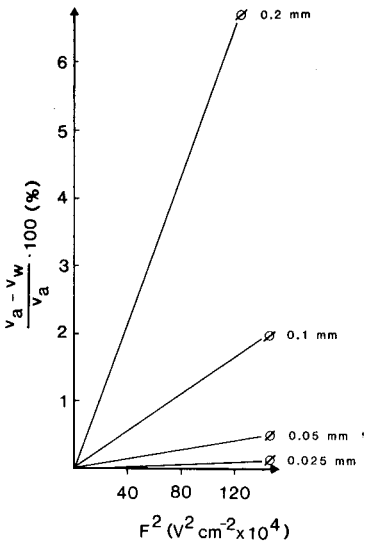

Fig. 8. Rough estimation of thermal zone broadening as a function of the square of the field strength, F (V/cm), for different tube diameters (Ø). v_a and v_w are the electrophoretic migration velocities at the axis and the wall of the electrophoresis tube, respectively. Eqn. 73 in ref. 1 was used with obvious modifications for the calculation of the zone braodening. The following parameter values were employed: a constant, B = 2400 K, electrical conductivity, $\kappa = 4.8 \cdot 10^{-4}\ \Omega^{-1}\ cm^{-1}$, thermal condctivity, $\lambda = 6.0 \cdot 10^{-3}\ J\ s^{-1}\ cm^{-1}\ K^{-1}$, T = 295 K. The figure, illustrating the importance of using narrow-bore tubes to suppress thermal zone broadening, permits an estimation of the zone broadening at different field strengths and for varying diameters of the electrophoresis tube.

zone and the surrounding buffer (for a detailed treatment, see ref. 13). In displacement electrophoresis the conductivity difference causes not broadening but rather zone sharpening, which decreases the disturbing influence of diffusion. For proteins, with their low diffusion constants, the diffusional zone broadening in displacement electrophoresis is therefore often negligible at high field strength. The adsorption, which may be very disturbing in uncoated tubes, particularly for proteins with their multipoint attachment to the tube wall [20], is often more pronounced in displacement electrophoresis than in zone electrophoresis. One reason is that a displacement electrophoresis must be conducted in the absence of a carrier buffer and therefore the conductivity (ionic strength) is lower, with attendant increase in the risk of adsorption (electrostatic interaction). That the adsorption is very disturbing in uncoated tubes of the small diameters used in this study is evident not only from a comparison of Fig. 1a and b, but also from our observation that the electropherogram in Fig. 1b was far from reproducible (often no proteins passed the detector). The difficulty in avoiding adsorption of proteins onto uncoated tubes in zone electrophoresis also is obvious from investigations by Lauer and McManigill [21] and many others.

Since the ionic strength is low in displacement electrophoresis, one can use very high field strengths without significant thermal zone broadening. However, zone broadening induced by reversible adsorption increases with the field strength [13,22], so one cannot expect in displacement electrophoresis high resolution at high field

strengths in uncoated tubes, although the automatic zone sharpening in displacement electrophoresis decreases the adsorptive zone broadening.

In uncoated quartz tubes the solutes are transported much faster by electroendosmosis than by electrophoresis. Uncoated tubes must, accordingly, be longer than coated tubes (for a given electrophoretic migration distance). Uncoated tubes therefore have the drawback that they require a higher voltage for a given field strength, with attendant risk of increased noise caused by electrical shock (current leakage). One should also recall that the longer the transport distance, the greater is the zone broadening caused by adorption.

Electroendosmosis can also be suppressed by addition of a hydrophilic polymer to the buffer [23]. This technique, which is often used in displacement electrophoresis, will also suppress adsorption. However, a thin coating on the tube itself is more efficient and does not increase the viscosity of the bulk of the buffer (an increase in viscosity decreases the migration velocities of the solutes, *i.e.* increases the analysis time).

Some proteins are not soluble at low ionic strengths and therefore have a tendency to precipitate in displacement electrophoresis [24], which may explain the small variations observed among some of the electropherograms presented herein. The precipitation may be suppressed or eliminated if the experiments are performed in the presence of ethylene glycol or a neutral detergent [24].

The conductivity used for the plot in Fig. 8 corresponds roughly to the average value of that in the experiment shown in Fig. 3. It is evident from Fig. 8 that the field strength used in this experiment (860 V/cm) gives a thermal zone broadening of only 0.06% (capillary diameter, 0.025 mm). For the experiment illustrated in Fig. 2 (field strength, 285 V/cm; capillary diameter, 0.050 mm) the corresponding figure is 0.03%. The electrophoretic migration distance was in both experiments about 320 mm. The thermal zone broadening was, accordingly, $320 \times 0.06/100 = 0.19$ mm and $320 \times 0.03/100 = 0.10$ mm, respectively, *i.e.*, almost negligible, which is in agreement with the observation that the resolution in Figs. 2 and 3 is about the same. Fig. 8 also shows that a capillary diameter of 0.2 mm —a common diameter in most equipment for displacement electrophoresis— gives a thermal zone broadening of 4 and 0.5% at the above field strengths, respectively, corresponding to 13 and 1.6 mm broadening for a 320-mm migration distance. This comparison illustrates the importance of reducing the diameter of the electrophoresis tube, provided that the adsorption and electroendosmosis can be eliminated, for instance, with a polymer coating as described herein (see also refs. 2, 13 and 25).

ACKNOWLEDGEMENTS

This investigation was financially supported by the Swedish Natural Science Research Council and the Carl Trygger and the Knut and Alice Wallenberg Foundations.

REFERENCES

1 S. Hjertén, *Chromatogr. Rev.*, 9 (1967) 122–219.
2 S. Hjertén, *J. Chromatrogr.*, 347 (1985) 191–198.

3 *First International Symposium on High-Performance Capillary Electrophoresis, Boston, MA, April 10–12, 1989, Abstract No. 105.*
4 *Thirteenth International Symposium on Column Liquid Chromatography, Stockholm, June 25–30, 1989, Abstract No. 156.*
5 G. Johansson, L.-G. Öfverstedt and S. Hjertén, *Anal. Biochem.*, 166 (1987) 267–275.
6 M. Bier, R. M. Cuddeback and A. Kopwillem, *J. Chromatogr.*, 132 (1977) 437–450.
7 A. Kopwillem, W. G. Merriman, R. M. Cuddeback, A. J. K. Smotha and M. Bier, *J. Chromatogr.*, 118 (1976) 35–46.
8 P. J. Svendsen and C. Rose, *Sci. Tools*, 17 (1970) 13–17.
9 S. Hjertén, in H. Peeters (Editor), *Protides of the Biological Fluids*, Pergamon Press, Oxford, 1975, pp. 669–672.
10 T. Manabe, H. Yamamoto and T. Okuyama, *Electrophoresis*, 10 (1989) 172–177.
11 *Isotachophoresis*, LKB-Produkter AB, Bromma, 1978.
12 S. Hjertén, *Nucleosides & Nucleotides*, 9 (1990) 319–330.
13 S. Hjertén, *Electrophoresis*, 11 (1990) 665.
14 F. Hampson and A. J. P. Martin, *J. Chromatogr.*, 174 (1979) 61–74.
15 A. J. P. Martin and F. M. Everaerts, *Anal. Chim. Acta*, 38 (1967) 233.
16 F. M. Everaerts, Thesis, University of Technology, Eindhoven, 1968.
17 H. Svensson, *Acta Chem. Scand.*, 15 (1961) 325.
18 L. A. A. E. Sluyterman and O. Elgersema, *J. Chromatogr.*, 150 (1978) 17.
19 N. Parris, *Anal. Biochem.*, 100 (1979) 260.
20 S. Hjertén, J.-L. Liao and K. Yao, *J. Chromatogr.*, 387 (1987) 127–138.
21 H. H. Lauer and D. McManigill, *Anal. Chem.*, 58 (1986) 166–170.
22 R. J. Wieme, in E. Heftmann (Editor), *Chromatography, A Laboratory Handbook of Chromatographic and Electrophoretic Methods*, Van Nostrand Reinhold, New York, 1975, pp. 228–281.
23 S. Hjertén, *Ark. Kemi*, 13 (1958) 151–152.
24 G. Johansson, L.-G. Öfverstedt and S. Hjertén, *Anal. Biochem.*, 166 (1987) 267–275.
25 S. Hjertén, in P. D. Grossmann and J. Colburn (Editors), *Guidebook to Capillary Electrophoresis*, Academic Press, New York, 1991, in press.

Journal of Chromatography, 550 (1991) 823–830
Elsevier Science Publishers B.V., Amsterdam

CHROMSYMP. 2076

High-performance capillary electrophoresis of proteins

Sodium dodecyl sulphate–polyacrylamide gel-filled capillary column for the determination of recombinant biotechnology-derived proteins

KIYOSHI TSUJI

Control Biotechnology, Pharmaceutical Product Control Division, The Upjohn Company, Kalamazoo, MI 49001 (USA)

ABSTRACT

Fused-silica capillary columns were filled with sodium dodecyl sulfate–polyacrylamide gel and the column effluent was monitored at 214 nm using a commercially available high-performance capillary electrophoresis (HPCE) instrument to separate and rapidly quantify recombinant biotechnology-derived proteins. An excellent linear relationship ($r > 0.999$) exists between the peak migration time and the molecular weights of reference proteins in the range 10 000–100 000 and 40 000–200 000 dalton by use of the capillary columns filled with acrylamide gel at a T composition of 5% and 3%, respectively. The relative standard deviation (R.S.D.) of the peak migration time is *ca.* 1%. Theoretical plates of $5 \cdot 10^5$–$1 \cdot 10^6$ per metre are routinely being obtained. Calibration graphs of peak area *versus* weight of recombinant biotechnology-derived proteins are linear ($r > 0.999$) and the proteins may be quantified with an R.S.D. of *ca.* 3–7%. As little as 50 nmol of a protein may be quantified and an impurity peak of molecular weight *ca.* 1500 less than that of the parent compound (*ca.* 60 000 dalton) may be differentiated by HPCE with a gel-filled capillary column.

INTRODUCTION

Biotechnology-derived proteins are posing a considerable challenge to analytical chemistry as the separation efficiencies of high-performance liquid chromatography (HPLC) for these proteins are far less than those of lower molecular weight compounds [1]. Electrophoresis, especially polyacrylamide gel (PAG) electrophoresis, is an indispensable technique for the separation of proteins based on their apparent molecular weights. In spite of impressive advances made in recent years [1], electrophoresis still represents a collection of labor-intensive and time consuming techniques and is not readily automatable. Casting of a gel, application of samples, electrophoresis and staining of gels are time-consuming tasks prone to irreproducibility and quantification by means of an optical scanning apparatus is often sub-optimum.

Recent developments in the commercialization of high-performance capillary

0021-9673/91/$03.50

electrophoresis (HPCE) instruments for capillary zone electrophoresis (CZE) [2–5] have made it possible to exploit potential of sodium dodecyl sulfate (SDS)-PAG-filled capillary columns for the analysis of recombinant biotechnology-derived protein with promises of rapid and automated analysis of multiple samples and improved reproducibility and quantification. Although several U.S. patents have been issued for the preparation of gel-filled capillary columns [6–8], mainly for nucleotide analysis [9–12], no such column has been made commercially available. Cohen and Karger [13] applied gel-filled capillaries to the electrophoresis of peptides and proteins, but no quantitative data were presented.

This paper describes the preparation of SDS-PAG-filled capillary columns and the application of such columns to the electrophoretic separation and quantification of recombinant biotechnology-derived proteins using a commercially available HPCE instrument.

EXPERIMENTAL

HPCE instrumentation

A P/ACE System 2000 HPCE instrument (Beckman, Palo Alto, CA, U.S.A.) was used to obtain analytical data. A Model 270A Capillary Electrophoresis System (Applied Biosystems, Foster City, CA, U.S.A.) was used to develop and evaluate the SDS-PAG composition for the longevity and performance of gel-filled capillary columns (GFC).

Each HPCE-GFC run involves a 10-s electrokinetic injection (-2.5 kV) of a protein sample into a GFC and monitoring compounds migrating in the column effluent at 214 nm. The temperature in a column cartridge was maintained at 25°C and an electrophoretic run was conducted at -2.0 to -3.0 kV (-83 to -130 V/cm, 12 μA) with a running buffer. The area under the protein peak was integrated by means of a program in a VAX mainframe computer.

Reagents

Phosphate-buffered saline (PBS), sample solubilization buffer (SSB) and running buffer solution were made from stock reagent solutions [1]. An acrylamide stock solution containing 30% acrylamide and 0.8% bisacrylamide was obtained from Enprotech (Hyde Park, MA, U.S.A.).

Acrylamide buffer solution [1,14] contained either 5.1% T and 2.6% C or 3.1% T and 2.6% C with 375 m*M* Tris (pH 8.8), 3.2 m*M* SDS and 2.35 *M* ethylene glycol. The percentage of T and C in the acrylamide gel solution was calculated using the equations

$$\text{T (\%)} = \text{acrylamide (g)} + \text{bisacrylamide (g) per 100 ml of solvent}$$

$$\text{C (\%)} = \frac{\text{bisacrylamide (g)} \cdot 100}{\text{bisacrylamide (g)} + \text{acrylamide (g)}}$$

The presence of ethylene glycol in the gel formulation as well as in the running buffer minimizes the formation of bubbles during electrophoresis and thus significantly improves the longevity of the GFC. The acrylamide buffer solution was

deaerated by sparging with dry helium for 60 s. Appropriate amounts of ammonium peroxodisulfate solution (Bio-Rad Labs., Richmond, CA, U.S.A.) and N,N,N′,N′-tetramethylethylenediamine (TEMED) solution (Bio-Rad Labs.) were then added to the acrylamide buffer solution to initiate slow polymerization.

PBS contains 150 m*M* NaCl, 2.8 m*M* NaH_2PO_4 and 7.8 m*M* Na_2HPO_4 and 4X SSB consists of 62.5 m*M* Tris (pH 6.8) and 12.8 m*M* SDS. The running buffer contains 300 m*M* Tris (pH 8.8), 3.2 m*M* SDS and ethylene glycol. Just prior to an electrophoretic run, the running buffer is deaerated by sonication under vacuum.

Preparation of gel-filled capillaries (GFC)

A roll of fused-silica capillary tubing (50 μm I.D., 375 μm O.D.) was obtained from Polymicro Technologies (Phoenix, AZ, U.S.A.). Capillaries were cut to a few centimeters longer than the final column length of 24 cm and a detector window was created at *ca.* 2 cm longer than the effective column length of 7 cm by removing the polyimide coating with a polyimide stripper (Model S200, Polymicro).

The inner surface of the capillaries was first treated with 2 *M* H_2SO_4 by heating at 200°C for 15 min to prepare the surface for later attachment of bifunctional groups. A bifunctional reagent, γ-(acryloxypropyl)methyldichlorosilane (Petrarch Systems, Bristol, PA, U.S.A.), 9 m*M* in toluene, was attached to the capillaries by reaction at 100°C for 10 min. The bifunctional reagent silanizes the inner glass surface to minimize adsorption of protein and covalently bonds the polyacrylamide gel to the capillary wall [15,16]. Polyethylene tubing (0.38 mm I.D., 1.09 mm O.D.) (Clay Adams, Parsippany, NJ, U.S.A.) was connected to the capillary and a micro-syringe pump was used (Hamilton, Reno, NV, U.S.A.) to facilitate column rinsing and filling.

After the capillary had been treated with the bifunctional reagent, new polyethylene tubing was attached to both ends of the capillary. Just prior to the initiation of the polymerization of the gel, the columns were rinsed and the inner, silanized capillary surfaces wetted with dry methanol. The column was then filled with water. Wetting the inner, silanized surface is an essential operation in order to consistently obtain air-bubble-free, well packed columns.

Just prior to each rinsing and filling operation, *ca.* 0.5 cm of the polyethylene tubing was cut from the inlet side to minimize the introduction and trapping of air bubbles in the capillary. Immediately after the capillary had been filled with the acrylamide gel solution, the polyethylene tubings attached to both ends of the columns were cramped tightly with hemostatic forceps (VWR Scientific, Chicago, IL, U.S.A.). The gel-filled capillary columns thus prepared were left to stand vertically at room temperature for 48–72 h. The idea is to cure the column and to allow fluid, induced by shrinkage of the gel, to migrate to an upper end of the column. The top end of the column is then cleared to remove the fluid. The gel-filled capillary column was installed in a capillary column cartridge (Beckman) and stored by immersion of both ends of the capillary in the running buffer. Just prior to an electrophoretic run, both ends of the capillary column were cut squarely so as to have lengths of 7.0 cm (inlet) and 17 cm (outlet) from the detection window. The column was conditioned at − 50 V/cm for 60 min.

Separation of proteins

Both the high- and low-molecular-weight reference protein standard solutions

(Bio-Rad Labs.) used contained a mixture of proteins: hen egg white lysozyme (molecular weight 14 400 dalton), soybean trypsin inhibitor (21 500), bovine carbonic anhydrase (31 000), hen egg white ovalbumin (45 000), bovine serum albumin (BSA) (66 200), rabbit muscle phosphorylase *b* (97 400), *Escherichia coli* β-galactosidase (116 250) and myosin (200 000). Samples of recombinant biotechnology-derived protein used were manufactured by Upjohn (Kalamazoo, MI, U.S.A.). They are (1) soluble CD_4 (molecular weight 20 395 dalton), which contains 183 amino acids, and (2) soluble CD_4-PE (molecular weight 59 187 dalton), which consists of 545 amino acids and contains the domains I and II of the CD_4 molecule [17] and the domains II and III of the *Pseudomonas* exotoxin A [18]. Protein samples were diluted in PBS to an appropriate concentration and made up to a final volume of 20 μl with 4X SSB. The protein samples were heated at 55 ± 5°C for 10 min to denature them.

RESULTS AND DISCUSSION

Longevity of gel-filled capillary columns

Without the additive, ethylene glycol, an SDS-PAG-filled capillary column forms bubbles within a few minutes and the flow of electric current ceases. The presence of ethylene glycol in SDS-PAG at a level of 1.8–2.7 *M* significantly improves the longevity of the GFC. For example, one column lasted over 2 weeks of continuous electrophoresis and another quantified over 300 protein samples. The column performance gradually deteriorates, however, after *ca.* 40 sample analyses. Below a 1.8 *M* ethylene glycol concentration, the lifetime of a GFC is short and ethylene

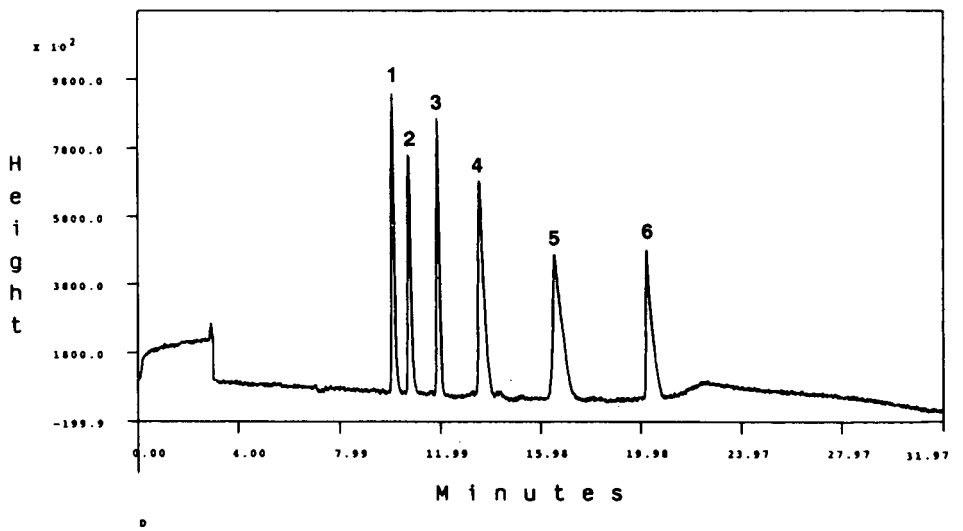

Fig. 1. Separation of molecular weight reference standards by HPCE-GFC as monitored at 214 nm. Conditions: −83 V/cm; 12 μA; column temperature, 25°C; migration distance, 7 cm; fused-silica capillary, 75 μm I.D.; running buffer, 375 m*M* Tris (pH 8.8)–0.1% SDS–ethylene glycol. Molecular weight standards used: 1 = lysozyme (mol. wt. 14 400 dalton); 2 = trypsin inhibitor (21 500); 3 = carbonic anhydrase (31 000); 4 = ovalbumin (45 000); 5 = BSA (66 200); 6 = phosphorylase *b* (97 400).

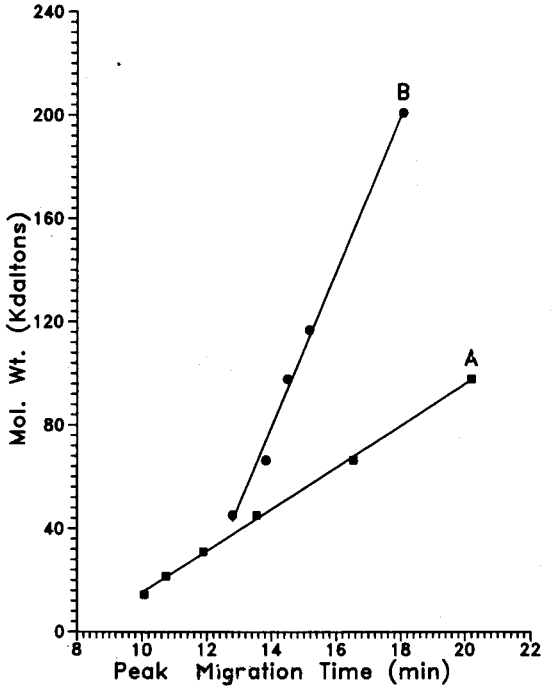

Fig. 2. Molecular weight calibration graphs (line A, 5% T; line B, 3% T) for HPCE-GFC indicating the existence of a linear relationship ($r > 0.999$) between peak migration time and molecular weight. Molecular weight standards used: lysozyme, trypsin inhibitor, carbonic anhydrase, ovalbumin, bovine serum albumin, phosphorylase *b*, β-galactosidase and myosin. Conditions: −83 V/cm; 12 μA; column temperature, 25°C; migration distance, 7 cm; fused-silica capillary, 75 μm I.D.; running buffer, 375 m*M* Tris (pH 8.8)–0.1% SDS–ethylene glycol.

glycol concentrations over 2.7 *M* results in a very soft gel with a significant loss of peak resolution. The running buffer may contain over 4 *M* ethylene glycol with no loss of theoretical plates. However, the SDS-PAG composition developed for capillary electrophoresis is not the ultimate one. The lifetime of a column is still not predictable. Frequently, a tiny bubble forms at the detector window, resulting in significant deterioration of the column performance even though no loss of current flowing through the column can be detected. During a prolonged HPCE-GFC run, the gel becomes extremely soft and fluid due to Joule heating and soft/fluid gel tends to drip out of the capillary column. Fluidity is especially pronounced with the gel of 3% T composition.

Wetting of the inner surface of the silanized capillary column with methanol has been a key factor contributing to dependable and consistent preparation of GFCs.

Molecular weight reference standards

Capillary columns filled with SDS-PAG of 5% and 3% T composition may be used to determine the apparent molecular weights of proteins, ranging from 10 000 to 100 000 and 40 000 to 200 000 dalton, respectively. A typical HPCE-GFC electropherogram indicating the separation of molecular weight reference protein standards

TABLE I

PRECISION OF THE PEAK MIGRATION TIME FOR MOLECULAR WEIGHT PROTEIN STANDARDS

Run No.	Peak migration time (min) for proteins A–F[a]					
	A	B	C	D	E	F
1	14.82	15.68	17.28	20.00	25.81	29.78
2	14.44	15.75	17.42	20.18	25.48	30.18
3	14.52	15.88	17.55	20.41	25.90	30.73
4	14.65	16.00	17.63	20.59	26.12	31.06
5	14.41	15.74	17.41	20.22	25.60	30.30
6	14.23	15.55	17.20	20.02	25.38	30.84
R.S.D. (%)	1.4	0.99	0.92	1.1	1.1	1.6

[a] Proteins: A = lysozyme (mol. wt. 14 400 dalton); B = trypsin inhibitor (21 500); C = carbonic anhydrase (31 000); D = ovalbumin (45 000); E = BSA (66 200); F = phosphorylase *b* (97 400).

using an SDS-PAG (5% T) filled capillary is shown in Fig. 1. The existence of a linear relationship ($r > 0.999$) was noted when the peak migration time was plotted against the molecular weights of the protein standards (Fig. 2).

The precision of the protein peak migration time was determined by repeated injection of the protein reference molecular weight standard solution containing lysozyme, trypsin inhibitor, carbonic anhydrase, ovalbumin, BSA and phosphorylase b. The relative standard deviation of the peak migration time ranged from 0.92 to 1.6% (Table I).

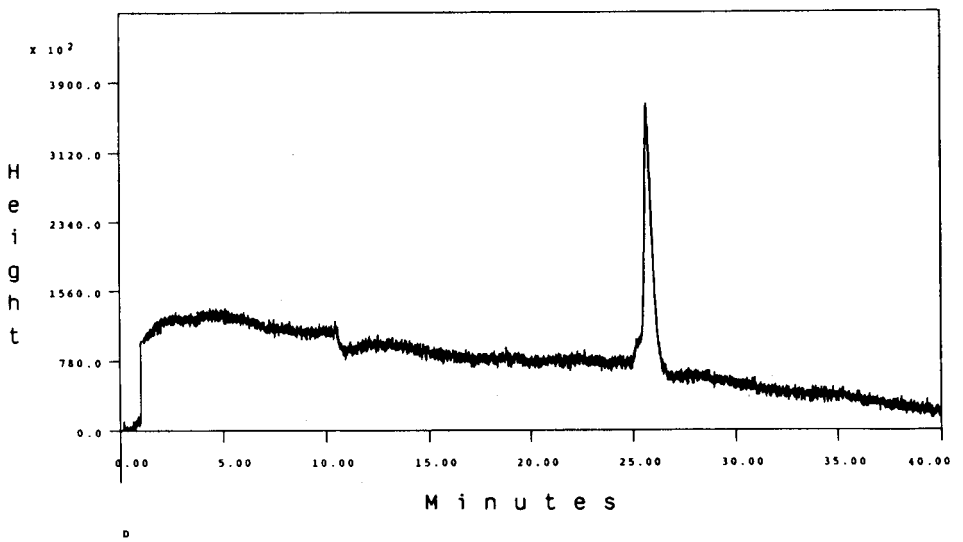

Fig. 3. HPCE-GFC separation of a recombinant biotechnology-derived protein (soluble CD_4-PE) as monitored at 214 nm. Conditions: −83 V/cm; 12 μA; column temperature, 25°C; migration distance, 7 cm; fused-silica capillary, 75 μm I.D.; running buffer, 375 m*M* Tris (pH 8.8)–0.1% SDS–ethylene glycol.

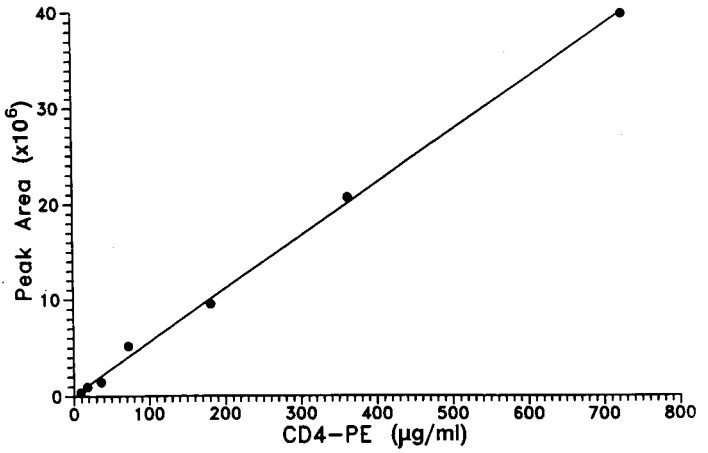

Fig. 4. Calibration curve for the determination of soluble CD_4-PE, indicating the existence of a linear relationship ($r > 0.999$) between the weight of sCD_4-PE and the peak area as monitored at 214 nm. Conditions: −83 V/cm; 12 µA; column temperature, 25°C; migration distance, 7 cm; fused-silica capillary, 75 µm I.D.; running buffer, 375 m*M* Tris (pH 8.8)–0.1% SDS.

Determination of recombinant biotechnology-derived proteins

A typical electropherogram of a recombinant biotechnology-derived protein, soluble CD_4-PE is shown in Fig. 3. HPCE-GFC detected the presence of a dimer in a sample of sCD_4 (data not shown) and demonstrated the capability of detecting an impurity peak with a molecular weight *ca.* 1500 less than that of the parent compound of *ca.* 60 000 dalton in a sample of sCD_4-PE (Fig. 3).

The ability of HPCE-GFC to quantify proteins was examined. The calibration curve for sCD_4-PE is linear ($r > 0.999$) in the range 10–725 µg/ml protein (Fig. 4). The line intersected the *x*-axis at near zero, indicating minimum adsorption of the protein on the column wall. The calibration curve for sCD_4 is also linear ($r > 0.999$) between 20 and 2000 µg/ml protein (data not shown). A linear assay range of two orders of magnitude of protein concentration has thus been demonstrated. The detector became saturated at sCD_4 concentrations above 3 mg/ml. As little as 50 nmol of pro-

TABLE II

PRECISION OF HPCE-GFC FOR THE ASSAY OF sCD_4-PE

Run No.	Peak migration time (min)	Peak area
1	15.77	7 220 000
2	15.87	7 761 000
3	15.93	7 172 000
4	15.97	7 405 000
5	16.02	7 578 000
6	16.08	7 774 000
7	16.07	7 196 000
R.S.D. (%)	0.70	3.53

teins may be quantified by HPCE-GFC. This relatively high sensitivity of HPCE-GFC to protein samples was obtained by monitoring the migration of the proteins at 214 nm.

The precision for the assay of a biotechnology-derived protein, sCD_4-PE, was evaluated by repeated injection of samples. The relative standard deviation (R.S.D.) of the peak migration time was less than 1% and that for the assay of the protein is *ca.* 3.5% (Table II). The precision for the HPCE-GFC assay of CD_4 is similar (data not shown). In order to improve the precision of the assay, an increase in the electrokinetic injection time and/or protein concentration was attempted. However, the R.S.D. of the assays stubbornly remained between 3 and 7%. Inclusion of an internal standard may be needed to further improve the precision of the assay. As the instrument has no provision for cooling the samples, an increase in temperature of the protein sample solution was observed during a long HPCE-GFC run, such as an overnight run. The questionable stability of proteins and the potential for adsorption of protein onto the plastic sample cup (Beckman) under such adverse HPCE-GFC running conditions may be a factor to be recognized for development of the assay method. Efforts are being made to improve the precision of the HPCE-GFC assay of proteins.

CONCLUSION

HPCE-GFC has been demonstrated to be capable of separating and determining the apparent molecular weights of impurities and of quantifying recombinant biotechnology-derived proteins in a relatively short time. Hence HPCE-GFC may become an indispensable tool for monitoring protein purification processes and for determining the stability characteristics of a pharmaceutical product containing a recombinant biotechnology-derived protein.

REFERENCES

1 F. M. Ausubel, R. Brent, R. E. Kingston, D. D. Moore, J. G. Seidman, J. A. Smith and K. Struhl (Editors), *Current Protocols in Molecular Biology*, Vol. 2, Wiley, New York, 1990, pp. 10.05–10.17.5.
2 R. A. Wallingford and A. G. Ewing, *Adv. Chromatogr.*, 29 (1989) 1–76.
3 F. E. P. Mikkers, F. M. Everearts and Th. P. E. M. Verheggen, *J. Chromatogr.*, 169 (1979) 11–20.
4 J. W. Jorgenson and K. D. Lukacs, *Science (Washington, D.C.)*, 222 (1983) 266–272.
5 B. L. Karger, A. S. Cohen and A. Guttman, *J. Chromatogr.*, 492 (1989) 585–614.
6 P. F. Bente and J. Myerson (Hewlett-Packard), *U.S. Pat.*, 4 810 456 (1989).
7 B. L. Karger, *U.S. Pat.*, 4 865 707 (1989).
8 B. L. Karger and A. Cohen, *U. S. Pat.*, 4 865 706 (1989).
9 H. Drossman, J. A. Luckey, A. J. Kostichka, J. O'Cunha and L. M. Smith, *Anal. Chem.*, 62 (1990) 900–903.
10 A. S. Cohen, D. R. Najarian, A. Paulus, A. Guttman, J. A. Smith and B. L. Karger, *Proc. Natl. Acad. Sci. U.S.A.*, 85 (1988) 9660–9663.
11 A. Guttman, A. S. Cohen, D. N. Heiger and B. L. Karger, *Anal. Chem.*, 62 (1990) 137–141.
12 H. Swerdlow and R. Gesteland, *Nucleic Acids Res.*, 18 (1990) 1415–1419.
13 A. S. Cohen and B. L. Karger, *J. Chromatogr.*, 397 (1987) 409–417.
14 U. K. Laemmli, *Nature (London)*, 227 (1970) 680–685.
15 V. Neuhoff, *Electrophoresis*, 5 (1984) 251.
16 *Isoelectric Focusing, Principles and Methods*, Pharmacia, Uppsala, 1982, pp. 47–49.
17 R. L. Garlick, R. J. Kirshner, F. M. Eckenrode, W. G. Tarpley and C. Tomich, *AIDS Res. Hum. Retroviruses*, 6 (1990) 465–479.
18 V. K. Chaudhary, T. Mizukami, T. R. Fuerst, D. J. FitzGerald, B. Moss, I. Pastan and E. A. Berger, *Nature (London)*, 335 (1988) 369–372.

Journal of Chromatography, 550 (1991) 831–837
Elsevier Science Publishers B.V., Amsterdam

CHROMSYMP. 2221

Axial-beam absorbance detection for capillary electrophoresis

JOHN A. TAYLOR and EDWARD S. YEUNG*
Ames Laboratory–USDOE and Department of Chemistry, Iowa State University, Ames, IA 50011 (USA)

ABSTRACT

A novel approach to absorbance detection has been demonstrated for capillary electrophoresis utilizing an incident light beam directed along the capillary axis. The resulting absorption path length is roughly equal to the width of the sample bands present. This represents a 60-fold improvement in analytical path length over conventional on-column absorbance detectors without any loss of separation efficiency. The method can be used with completely aqueous buffer systems or those containing organic modifiers, and is applicable to both fused-silica and PTFE capillaries.

INTRODUCTION

The spread of capillary electrophoresis (CE) applications in recent years has led to the development of many detection schemes, each with its own degree of selectivity and sensitivity to fit a specific purpose. Two characteristics have allowed absorbance detection to earn its place among the most popular of these techniques. First, if the proper incident wavelengths are chosen (*e.g.*, the ultraviolet region), this one detector can be used for almost every class of organic compound. Second, this technique usually does not require sample derivatization or special buffer considerations.

Ultra-high separation efficiencies and low mass detection limits, which have become the main attraction of CE, require that detector volumes be small, thus favoring on-column detectors. By convention, on-column absorbance detection in CE has been carried out with the incident light beam directed perpendicular to the capillary walls [1–3]. While some of these designs have demonstrated reasonable detection limits owing to high light source stability, they are seriously hindered by short absorption path lengths. Diffusion processes along the axis of a CE column keep the minimum band width attainable to about 3 mm [4,5]. If, instead of the standard configuration, one directs the light beam along the capillary, then the entire 3-mm band width becomes the absorption path length. In a 50-μm capillary, given the same source stability, a 60-fold improvement in detection limits could be obtained with no loss of separation efficiency.

Increasing analytical path lengths by directing the incident light beam along the axis of a capillary cell is not a new idea. Fuwa and co-workers [6–8] obtained analytical path lengths in excess of 1 m in glass and polymer capillaries. Axial absorbance

0021-9673/91/$03.50

detection has also been demonstrated for smaller capillaries incorporating open-tubular liquid chromatography [9]. In that application, a laser beam was focused into one end of a 10-μm fused-silica capillary using a single-element lens. With the proper choice of solvents (*i.e.*, solvents having a greater refractive index than that of fused silica), light entering the capillary is transmitted by total internal reflection at the interface between the solution and the capillary wall. At the capillary exit, light is collected with a microscope objective and imaged onto either a photomultiplier tube or a photodiode.

This research involves the application of the axial-beam technique to detection in CE. Two strategies have been studied. The first of these takes advantage of the partial internal reflectance at the water/fused-silica interface to propagate light along the capillary axis. The second utilizes polymers of low refractive index and buffer systems with organic modifiers to bring about total internal reflectance.

EXPERIMENTAL

Axial detection system

Fig. 1 shows a schematic diagram for axial detection. The light source was a 10-mW, 632-nm He–Ne laser (GLG5261, NEC, Mountain Valley, CA, USA). The beam was directed through two mirrors on pivoting mounts (2 × 2 in.; Newport, Fountain Valley, CA, USA) and focused using a 2.5-cm focal-length lens (KPX076; Newport) mounted on a three-dimensional translational stage. Both the front and rear cells were constructed from Plexiglas blocks with channels bored in a three-dimensional "T-shape" to allow introduction of the capillary, indicent light beam, electrode wire and liquid buffer. These cells contained windows fabricated from mi-

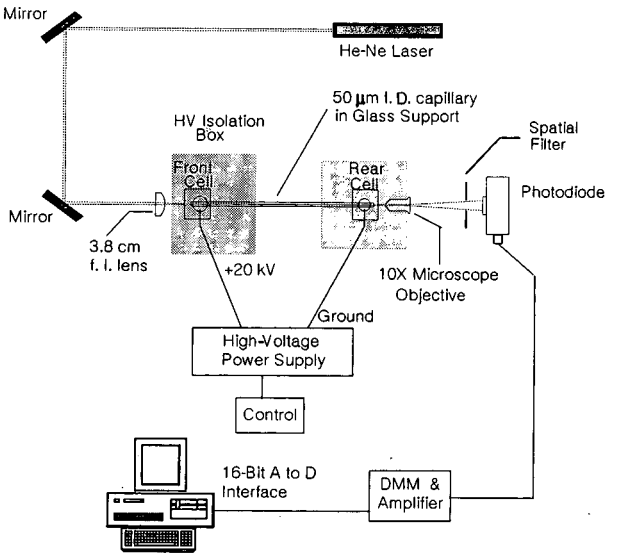

Fig. 1. Schematic diagram of axial absorbance detection in CE. The dotted lines indicate the path of the laser beam. A to D = Analog-to-digital; DMM = digital multimeter; f.l. = focal length; HV = high-voltage.

croscope slides and were sealed on all sides except the top with epoxy (Devcon, 5-min). The capillary was mounted in a glass support (borosilicate glass tubing, 25 cm × 5 mm O.D., × 1 mm I.D.) by gluing at both ends and through three evenly spaced holes drilled perpendicular to the length of the tube. This support was used to maintain rigidity and straightness.

Light emitted from the capillary exit was collected with a 10× microscope objective (BM2888, 16 mm, Bausch and Lomb, Rochester, NY, USA) and focused onto a spatial filter (size ranging from 1 to 10 mm depending on the distance between the objective and the filter). The resulting beam intensity was converted to an electrical signal via a photomultiplier tube (R928; Hamamatsu, Middlesex, NJ, USA) or a photodiode (1 cm^2 area, S179004N; Hamamatsu) and amplified through a digital multimeter (160B; Keithley Instruments, Cleveland, OH, USA). Data collection and analysis were accomplished using an IBM AT computer with a 16-bit analog-to-digital conversion board (2827; Data Translation, Marlboro, MA, USA). A smoothing algorithm [10] was applied to sequential data files, providing an effective time constant compatible with the injection peak widths.

Beam profile measurements

Intensity profiles at the exit of the capillary were measured by focusing the exiting light through the 10× microscope objective onto a white background at the location of the spatial aperture. Images were then recorded using a CCD camera (Series 200; Photometrics, Tucson, AZ, USA) through a 90-mm macro lens (Tamron, Tokyo, Japan) and converted to 50 × 50 matrices of pixel intensities.

Electrophoresis

The separation of bromocresol green and bromothymol blue was carried out in a fused-silica capillary (75 μm I.D., 150 μm O.D.; Polymicro Technologies, Phoenix, AZ, USA) and in a PTFE capillary (50 μm I.D., 150 μm O.D.; Zeus Industrial Products, Raritan, NJ, USA). The power supply, PS/MJ30PO400-11 (Glassman, Whitehouse Station, NJ, USA) was operated at +20 kV applied across two chromel electrodes positioned at the ends of the capillary (capillary exit at ground). Electrokinetic injection was accomplished by placing a sample solution in the front cell, activating the power supply momentarily, then flushing the front cell with running buffer prior to the separation.

Buffers and reagents

For electrophoresis in the fused-silica capillary, the running buffer consisted of 10 m*M* disodium phosphate (certified ACS grade; Fisher, Fair Lawn, NJ, USA), adjusted to pH 7.5 using phosphoric acid. When the PTFE capillary was used, the buffer was 10 m*M* disodium phosphate and 50 m*M* sodium dodecyl sulfate (Sigma, St. Louis, MO, USA) in 50% (v/v) ethylene glycol (Fisher, purified grade), adjusted to pH 7.6. All buffers were degassed by applying vacuum while the buffer bottle was agitated in an ultrasonic bath. Bromocresol green and bromothymol blue were obtained from J. T. Baker (Phillipsburg, NJ, USA).

RESULTS AND DISCUSSION

Partial internal reflectance

An advantage of this mode of axial absorbance detection for CE is that it can be carried out using the same aqueous buffer solutions and fused-silica capillary as in standard absorbance detection. According to Lei *et al.* [7], the total intensity of light transmitted through a long glass capillary cell containing water consists of light rays taking many paths through the capillary center or through the walls. The secret of obtaining a useful analytical signal from the light emitted at the exit of a very small capillary (less than 100 μm I.D.) is to separate wall-propagated light from center-propagated light. This was accomplished by imaging the exiting light beam on a spatial filter using a microscope objective. An important difference between the present work and the published results for liquid chromatographic detection [9] is evident. In the latter instance, much smaller diameter capillaries (approaching 5 μm) are needed to provide highly efficient separations. The smaller tubes are not suitable for transmitting light by partical internal reflectance because of the ratio of the cross-sectional areas of the liquid *versus* the walls is too small to allow proper discrimination. On the other hand, CE works well in capillaries up to 75 μm, and partial internal reflectance can be implemented.

An intensity profile at the exit end of the capillary, as seen at the spatial filter, is shown in Fig. 2. The peak of intensity at the middle of the image represents light propagated through the capillary center while the ring of intensity around the outside represents wall-propagated light. Interference modes within the small bore of the tube are probably responsible for the nodes seen in the center peak. This mode structure changes with heat build-up along the capillary or fluctuations in the refractive index of the buffer. Evidence for the complete spatial separation of wall- and center-propagated light can be seen when the capillary is filled with an opaque dye solution. In this instance, only the outer ring of intensity remained in the image. An aperture size for the spatial filter was chosen so as to allow only the center peak to pass on to the photomultiplier or photodiode, thus excluding wall-propagated light from the signal.

Fig. 3 is a sample electropherogram incorporating partial internal reflectance axial absorption detection. On injection of the sample, the transmitted intensity drops to a low level owing to the combined absorption of both sample components. This level is maintained as the samples migrate within the column, even though they are physically being separated by electrophoresis. The separation of bromocresol green and bromothymol blue is indicated by two sharp rises in intensity, each representing a loss in absorbance due to the elution of the individual compounds. Bromothymol

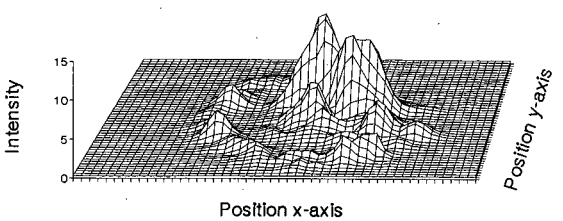

Fig. 2. Intensity profile at the exit end of a fused-silica capillary. Capillary I.D. 75 μm, O.D. 150 μm.

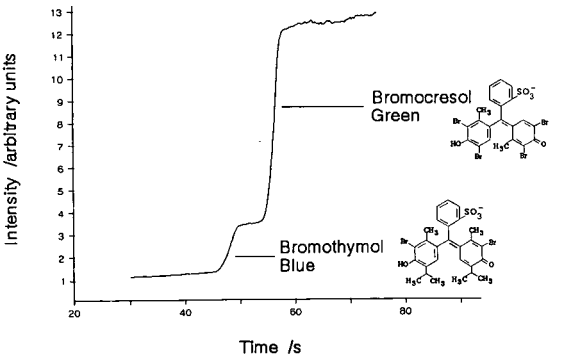

Fig. 3. Separation of bromothymol blue and bromocresol green. The separation took place in a fused-silica capillary (75 μm I.D.). Buffer, 10 mM phosphate adjusted to pH 7.5; analyte concentration, $2 \cdot 10^{-5}$ M each; applied potential +20 kV; electrokinetic injection time, 2.5 s. A data smoothing routine was applied with an effective time constant of 2.5 s.

blue elutes first, owing to its higher pK_a value and consequently lower degree of ionization and lower affinity for the positive electrode. The "integrating" nature of this electropherogram results in lower detection limits because the absorbance of the entire length of each analyte band is measured continuously from the beginning of the run until elution [11]. As has been shown previously, this type of integral electropherogram (chromatogram) preserves all the information in a normal electopherogram, such as elution time, peak area and peak width. In fact, the first-derivative plot of these data produces the normal electropherogram [9].

Total internal reflectance

Total internal reflectance allows efficient transmission of light along the liquid-filled core of the capillary, analogous to an optical fiber. When this phenomenon is applied to axial detection, two distinct advantages are seen. The first advantage arises from the fact that all the light rays impinging on the capillary, within a certain cone of acceptance, are completely internally reflected. The results are less noise associated with small capillary vibrations in the electric field and greater reproducibility of measured absorbances. A second advantage is that as very little loss of light occurs, longer capillaries (in excess of 1 m) in conjunction with higher applied potential can be used for greater electrophoretic resolution.

The condition for total internal reflectance is that the refractive index of the liquid filling the capillary must be greater than the refractive index of the capillary itself. PTFE has a refractive index in the range 1.35–1.38 [8] and has been well characterized in zone electrophoresis [12]. Although the refractive index of water is only 1.33 [13], much less than that PTFE, organic modifiers [14] can be added to the buffer to raise the refractive index above 1.38 and may actually enhance electrophoretic resolution. We chose ethylene glycol as an additive because of its high refractive index enhancement per unit concentration added. The liquid medium naturally must remain ionic for proper electrophoresis.

Fig. 4 shows that the same two test compounds can be separated in the ethylene

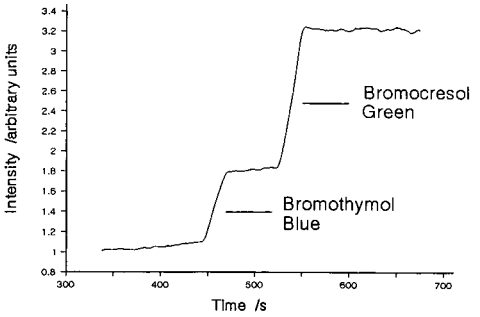

Fig. 4. Electropherogram of bromothymol blue and bromocresol green separated in a PTFE capillary (50 μm I.D.). Buffer, 50% (v/v) ethylene glycol–10 mM phosphate–50 mM SDS adjusted to pH 7.6; bromothymol blue concentration, $5 \cdot 10^{-5}$ M; bromocresol green concentration, $2 \cdot 10^{-5}$ M; applied potential, +20 kV; injection time, 20 s. The effective time constant was 20 s.

glycol–water-based buffer. The key ingredient in the separation buffer is 50 mM sodium dodecyl sulfate (SDS) [15]. Our explanation of the role of SDS is as follows: the presence of the organic modifier favors ion-pair formation for the two test compounds. These ion pairs tend to interact with the PTFE capillary, causing band smearing. SDS micelles provide a moving organic phase which carries the analyte ion pairs along and gives each of the compounds a distinct mobility based on its affinity for the micellar phase. SDS ions also adsorb to the PTFE walls, producing a zeta potential and generating electroosmotic flow similar to that seen in silica capillaries. The evidence for enhanced electroosmotic flow is that, in the presence of SDS analyte flow is directed toward the cathode, whereas in its absence this flow is directed toward the anode.

Detection limits

The main source of noise limiting the signal-to-noise ratio of the transmitted light beam is capillary vibration. These effects of capillary vibration have been discussed earlier [9], and in the present instance vibration arises from electrostatic motion in the very large applied potential field. With the PTFE capillary glued onto a glass support and by applying a digital smoothing routine [10] with an effective time constant of about 5 s, the signal-to-noise (S/N) ratio measured over 20 s (one peak width) is 600 for the transmitted beam. This gives an absorbance limit of detection (ALOD at $S/N = 3$) of $2 \cdot 10^{-3}$.

In order to compare our results with the performance of the common cross-beam absorbance detector, we must use a criterion that is independent of the molar absorptivity of the analyte. This can be accomplished by using the ratio of the absorbance limit of detection to the absorbance path length (ALOD/b). For a typical cross-beam system [16], the ALOD was $5 \cdot 10^{-4}$, resulting in ALOD/$b = 1 \cdot 10^{-2}$/mm for a 50-μm capillary. Our system exhibits an ALOD/b of $7 \cdot 10^{-4}$/mm, a 15-fold improvement over the cross-beam arrangement. It is also important to note that if the capillary diameter is decreased further, such as in the case when reduced Joule heating is needed to maintain a high separation efficiency, there will be a proportionate increase in this improvement factor. Note that we are comparing an integral electrophe-

rogram with the standard electropherogram. As pointed out earlier [11], integration of standard electropherograms is not always possible because of drifting baselines.

In summary, we have shown that an axial-beam absorption detection mode is feasible for CE. Even though a laser is used here for ease of coupling to the capillary tube, there is no reason why a conventional light source cannot be used. For example, the commercial absorption detectors for CE are already capable of collimating light from a xenon lamp to illuminate 25–75-μm capillaries. If the capillary can be held rigidly, then the higher stability of conventional light sources can even translate into better detectability. As discussed earlier [9], the present detection mode has a limited dynamic range at high concentrations because of depletion of transmitted light, but the lower concentration range is extended because of better detectability.

ACKNOWLEDGEMENTS

The authors thank L. Koutny for operating the CCD camera. The Ames Laboratory is operated by Iowa State University for the US Department of Energy under Contract No. W-7405-Eng-82. This work was supported by the Director of Energy Research, Office of Health and Environmental Research.

REFERENCES

1 S. Hjerten, *J. Chromatogr.*, 347 (1985) 191.
2 Y. Walbroel and J. W. Jorgenson, *J. Chromatogr.*, 315 (1984) 135.
3 Z. Prusik, V. Kasicka, S. Stanek, G. Kuncova, M. Hayer and J. Vrkoc, *J. Chromatogr.*, 390 (1987) 87.
4 X. Huang, W. F. Coleman and R. N. Zare, *J. Chromatogr.*, 480 (1989) 101.
5 W. G. Kuhr, *Anal. Chem.*, 62 (1990) 404R.
6 K. Fuwa, W. Lei and K. Fujiwara, *Anal. Chem.*, 56 (1984) 1640.
7 W. Lei, K. Fujiwara and K. Fuwa, *Anal. Chem.*, 55 (1983) 951.
8 K.-I. Tsunoda, A. Nomura, J. Yamada and S. Nishi, *Appl. Spectrosc.*, 44 (1990) 163.
9 X. Xi and E. S. Yeung, *Anal. Chem.*, 62 (1990) 1580.
10 A. Savitzky and M. J. E. Golay, *Anal. Chem.*, 36 (1964) 1627.
11 R. E. Synovec and E. S. Yeung, *Anal. Chem.*, 57 (1985) 2162.
12 K. D. Lukacs and J. W. Jorgenson, *J. High Resolut. Chromatogr. Chromatogr. Commun.*, 8 (1985) 407.
13 R. C. Weast, M. J. Astle and W. H. Beyer (Editors), *CRC Handbook of Chemistry and Physics*, CRC Press, Boca Raton, FL, 65th ed., 1984, p. E-357.
14 S. Fujiwara and S. Honda, *Anal. Chem.*, 59 (1987) 487.
15 S. Terabe, K. Otsuka and T. Ando, *Anal. Chem.*, 57 (1985) 834.
16 N. J. Dovichi, F. Zarrin, T. G. Nolan and D. J. Bornhop, *Spectrochim. Acta, Part B*, 43 (1988) 639.

Author Index

Chemical Sensor Technology Volume 2

edited by T. Seiyama, *Kyushu University, Fukuoka, Japan*

Chemical Sensor Technology is a series of annual reviews reporting the latest progress in research and technology, both basic and applied, regarding chemical sensors. Chemical sensors continue to grow rapidly in importance encompassing a broad spectrum of technologies covering safety, pollution, fuel economy, medical engineering and industrial processes. Various types of chemical sensors have been devised for detection and monitoring of chemical substances in gases, solutions and organisms, and much work is being done to produce sensitive, selective, reliable and inexpensive sensors.

The subjects chosen for this second volume have been carefully selected by the international editorial board to cover new, important progress in this fast-developing field. With contributions from many prominent researchers working at the frontiers of the chemical sensor field, the book provides up-to-date information and inspiration to all readers.

1990 304 pages
US$ 174.25 / Dfl. 340.00
ISBN 0-444-98784-3
Exclusive sales rights in Japan: Kodansha Ltd., Tokyo

ELSEVIER

P.O. Box 211, 1000 AE Amsterdam, The Netherlands

P.O. Box 882, Madison Square Station, New York, NY 10159, USA

Also available...

Volume 1

1988 xvi + 250 pages
US$ 146.25 / Dfl. 285.00
ISBN 0-444-98901-3
Exclusive sales rights in Japan: Kodansha Ltd., Tokyo

PUBLICATION SCHEDULE FOR 1991

Journal of Chromatography and Journal of Chromatography, Biomedical Applications

MONTH	D 1990–F 1991	M	A	M	J	J	A	S	
Journal of Chromatography	Vols. 535–539	540/1 + 2 541/1 + 2 542/1	542/2 543/1	543/2 544/1 + 2 545/1	545/2 546/1 + 2 547/1 + 2	548/1 + 2 549/1 + 2 550/1 + 2	552/1 + 2 553/1 + 2 554/1 + 2 555/1 + 2	556/1 + 2	This publication schedule for further issues will be published later.
Cumulative Indexes, Vols. 501–550							551/1 + 2		
Bibliography Section		560/1			560/2			561/1	
Biomedical Applications	Vols. 562, 563	564/1	564/2 565/1 + 2	566/1 566/2	567/1	567/2 568/1	568/2	569/1 + 2	

INFORMATION FOR AUTHORS

(Detailed *Instructions to Authors* were published in Vol. 522, pp. 351–354. A free reprint can be obtained by application to the publisher, Elsevier Science Publishers B.V., P.O. Box 330, 1000 AH Amsterdam, The Netherlands.)

Types of Contributions. The following types of papers are published in the *Journal of Chromatography* and the section on *Biomedical Applications:* Regular research papers (Full-length papers), Review articles and Short Communications. Short Communmications are usually descriptions of short investigations, or they can report minor technical improvements of previously published procedures; they reflect the same quality of research as Full-length papers, but should preferably not exceed six printed pages. For Review articles, see inside front cover under Submission of Papers.

Submission. Every paper must be accompanied by a letter from the senior author, stating that he/she is submitting the paper for publication in the *Journal of Chromatography*.

Manuscripts. Manuscripts should be typed in double spacing on consecutively numbered pages of uniform size. The manuscript should be preceded by a sheet of manuscript paper carrying the title of the paper and the name and full postal address of the person to whom the proofs are to be sent. As a rule, papers should be divided into sections, headed by a caption (*e.g.*, Abstract, Introduction, Experimental, Results, Discussion, etc.). All illustrations, photographs, tables, etc., should be on separate sheets.

Introduction. Every paper must have a concise introduction mentioning what has been done before on the topic described, and stating clearly what is new in the paper now submitted.

Abstract. All articles should have an abstract of 50–100 words which clearly and briefly indicates what is new, different and significant.

Illustrations. The figures should be submitted in a form suitable for reproduction, drawn in Indian ink on drawing or tracing paper. Each illustration should have a legend, all the *legends* being typed (with double spacing) together on a *separate sheet*. If structures are given in the text, the original drawings should be supplied. Coloured illustrations are reproduced at the author's expense, the cost being determined by the number of pages and by the number of colours needed. The written permission of the author and publisher must be obtained for the use of any figure already published. Its source must be indicated in the legend.

References. References should be numbered in the order in which they are cited in the text, and listed in numerical sequence on a separate sheet at the end of the article. Please check a recent issue for the layout of the reference list. Abbreviations for the titles of journals should follow the system used by *Chemical Abstracts*. Articles not yet published should be given as "in press" (journal should be specified), "submitted for publication" (journal should be specified), "in preparation" or "personal communication".

Dispatch. Before sending the manuscript to the Editor please check that the envelope contains four copies of the paper complete with references, legends and figures. One of the sets of figures must be the originals suitable for direct reproduction. Please also ensure that permission to publish has been obtained from your institute.

Proofs. One set of proofs will be sent to the author to be carefully checked for printer's errors. Corrections must be restricted to instances in which the proof is at variance with the manuscript. "Extra corrections" will be inserted at the author's expense.

Reprints. Fifty reprints of Full-length papers and Short Communications will be supplied free of charge. Additional reprints can be ordered by the authors. An order form containing price quotations will be sent to the authors together with the proofs of their article.

Advertisements. Advertisement rates are available from the publisher on request. The Editors of the journal accept no responsibility for the contents of the advertisements.